AIRCRAFT ENGINE NOISE AND SONIC BOOM

Advisory Group for Aerospace Research and Development
Paris, France

May 1969

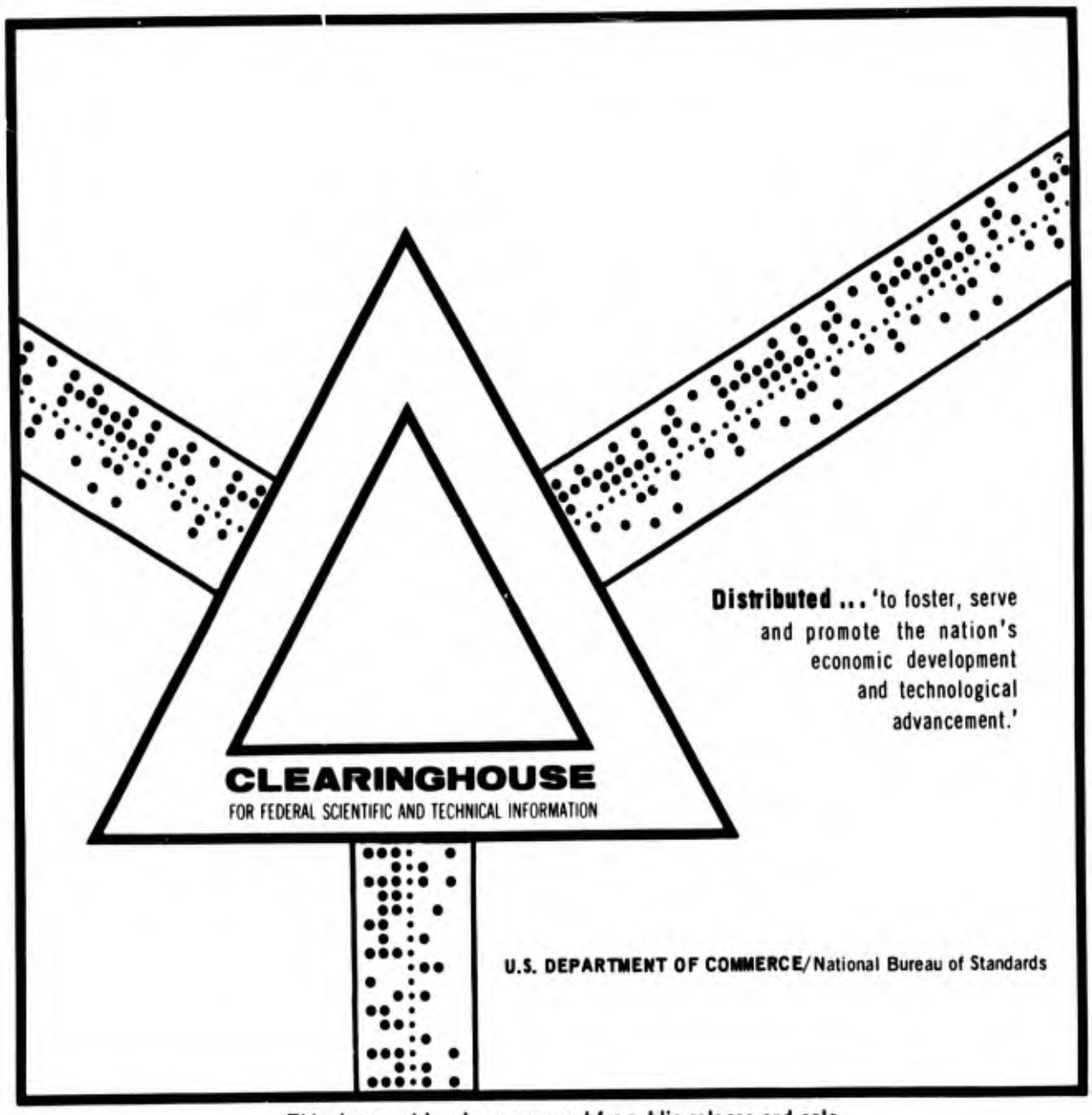

AGARD CONFERENCE PROCEEDINGS No. 42

AGARD

ADVISORY GROUP FOR AEROSPACE RESEARCH & DEVELOPMENT

7 RUE ANCELLE 92 NEUILLY SUR-SEINE FRANCE

Aircraft Engine Noise and Sonic Boom

★

MAY 1969

NORTH ATLANTIC TREATY ORGANIZATION

INITIAL DISTRIBUTION IS LIMITED
FOR ADDITIONAL COPIES SEE BACK COVER

AGARD Conference Proceedings No.42

NORTH ATLANTIC TREATY ORGANIZATION

ADVISORY GROUP FOR AEROSPACE RESEARCH AND DEVELOPMENT

(ORGANISATION DU TRAITE DE L'ATLANTIQUE NORD)

AIRCRAFT ENGINE NOISE AND SONIC BOOM

Papers presented at the Fluid Dynamics Panel and Propulsion and Energetics Panel (33rd) Joint Meeting held at the Institut Franco-Allemand de Recherches, Saint-Louis, France, 27-30 May 1969.

The material in this publication has been produced directly from copy supplied by each author.

534.830:629.735:
533.6.011.72

Printed by Technical Editing and Reproduction Ltd
Harford House, 7–9 Charlotte St, London, W.1

AGARD FLUID DYNAMICS PANEL

PANEL CHAIRMAN	Professor R.N.Cox, The City University, London, UK.
PANEL DEPUTY CHAIRMAN	Professor W.R. Sears, Cornell University, Ithaca, US.

AGARD PROPULSION AND ENERGETICS PANEL

PANEL CHAIRMAN	Professor A.Ferri, New York University, US.
PANEL DEPUTY CHAIRMAN	Dr C.T.Hewson, Rolls-Royce Ltd., UK.

PROGRAMME COMMITTEE FOR JOINT FDP/PEP (33rd) MEETING

Mr A.Auriol (FDP), Institut Franco-Allemand de St. Louis, France. (Chairman)
Dr C.T.Hewson (PEP), Rolls-Royce Ltd., UK. (Vice-Chairman)
Professor R.N.Cox (FDP), The City University, London, UK.
Professor D.Dini (PEP), University of Pisa, Italy.
Professor A.Ferri (PEP), New York University, US.
Professor A.Naumann (FDP), Technische Hochschule, Aachen, Germany.
Professor W.C.Nelson (FDP), University of Michigan, US.
Professor P.Ruden (PEP), Industrieanlagen Betriebsgesellschaft, Munich, Germany.
Professor W.R.Sears (FDP), Cornell University, Ithaca, US.
Dr J.Seddon (FDP), Ministry of Technology, London, UK.
Mr J.Surugue (PEP), Office National d'Etudes et de Recherches Aérospatiales, Châtillon-sous-Bagneux, France.

FDP EXECUTIVE
Dr R.Barth

PEP EXECUTIVE
Dr R.P.Hagerty

FOREWORD

The noise of modern aircraft and the sonic boom of future supersonic carriers pose important problems. Considerable effort has been devoted in recent years to studying the generation, propagation and effects of aircraft engine noise and sonic boom, with the final aim of developing means to minimise them.

Late in 1967, therefore, the AGARD Fluid Dynamics and Propulsion and Energetics Panels decided that it would be timely to organize in Spring 1969 a joint meeting on "Aircraft Engine Noise and Sonic Boom", at which broadly the PEP would be responsible for presentations dealing with problems of engine noise and the FDP for presentations relating to sonic boom. The meeting was planned to present the theory, techniques and results of the most-up-to-date work, covering the state-of-the-art in both the aerodynamic and propulsion areas of the field, and thus to provide guidance for further research and development.

Of the thirty-four programmed papers, five were review papers devoted respectively to the physics of noise, some legal problems relating to sonic boom, airport design and operation for minimising exposure to noise, the effects of aircraft noise and sonic boom on ground structures, and human response to sonic booms. The remaining papers dealt with specialized aspects, theoretical and experimental, of aircraft engine noise or sonic boom, and were grouped appropriately in the meeting programme.

Papers from six NATO countries were included in the programme.

CONTENTS

THE PHYSICS OF AERODYNAMIC NOISE

BY

G.M. LILLEY *

UNIVERSITY OF SOUTHAMPTON

* Head of Department of Aeronautics
and Astronautics

SUMMARY

The theory of Aerodynamic Noise was formulated by Lighthill in 1953. Its application to the theory of noise from turbulent jets was made by Lighthill, Ffowcs Williams, Ribner and others. The theory of the noise from rotating machinery such as propeller and compressor noise can be developed along similar lines by the introduction of suitable source terms in Lighthill's general formulation. Thus in all aerodynamic noise problems the far field pressure distribution is found as a solution of the wave equation with a right hand side forcing function. This applies to flow fields at both subsonic and supersonic speeds.

The present paper not only sets out the unified theory of aerodynamic noise involving random disturbances in the flow, but also shows how the theory can include the analysis of the pressure fields from bodies travelling through otherwise undisturbed air at subsonic and supersonic speeds, and therefore includes the theoretical background for the treatment of the sonic boom problem for generalised aircraft motions.

2. Introduction

Aircraft noise will in the near future be subject to rigid control in the form of Noise Certification in relation to subsonic transport aircraft operating into and out of conventional airports. Legislation with respect to aircraft noise from other types of aircraft such as V/STOL and supersonic aircraft will almost certainly follow. Legislation with respect to ground over flights of supersonic aircraft will almost certainly be discussed within a reasonable time.

All these movements to control aircraft and engine noise reflect back on us and demand that we exert and exploit our scientific understanding of the aerodynamic noise to the full, and with great urgency, in order to guide the development of noise attenuation schemes by control of the main noise generating mechanisms. The problem is, of course, not just one for the acoustic scientist or engineer but has repercussions throughout every branch of engine and airframe design. In addition acoustic control by itself is meaningless unless it can achieve its aims with no influence on the aircraft performance and hence on its operating economics, and this we know to our cost is not a reality. Thus noise control and engine and aircraft performance must proceed together and, as experience has shown, aircraft operating techniques do indeed by themselves alone offer possibilities for ground noise control, although, in conjunction with noise suppressors, lies the solution to our task. The one dominant question that has still to be answered, because of the complex interaction between noise control and aircraft performance and aircraft economics, is by how much has aircraft noise to be lowered. This is in itself a gigantic pyscho-human - sociological problem and demands attention to detailed study of the role of aviation in society. The range of problems in this sphere is vast and includes the whole financial cost to the community in its demand for quiet aircraft. The cost must include that of land zoning near airports, noise control of buildings as well as the cost to the aircraft operator, which is indirectly borne by the community in the seat price paid by the air traveller. These closely woven problems can indeed lead to the production of an answer but that answer will be a function of the level set for human annoyance, and the relation between any aircraft noise nuisance and other noise nuisances of our time. Here lies one of the great imponderables. What we need to know, and to know quickly, is what level and character of noise is judged to be annoying and how far these limiting characteristics change with time, when the characteristics of the noise are known and recognised. These remarks apply to that of the sonic boom as well.

The futility of studying any one of these problems in isolation is thraught with danger and an attack on a broad front is of vital importance. However the problem facing us does not even begin to make sense unless we fully understand the sources of noise we are dealing with. Much progress has been made in studying the physics of aerodynamic noise but even today many aspects of this vast subject remain a complete mystery and the areas in which detailed understanding has been obtained are few indeed. Aerodynamic noise problems associated with turbulent flow fields are difficult to study and present great challenges to the theoretical worker and the experimentalist. Aerodynamic noise problems giving rise to discrete tones present in general sufficient identification of the sound to enable rapid progress to be made in understanding the physical nature of the source and its control. However in most aerodynamic noise work turbulence introduces itself either as the dominant noise generator or acts to distort the noise wave form as it propagates through turbulence. (We are continuously reminded that noise is unwanted sound and the natural state of the environment is turbulent).

The problems that arise in aviation physical acoustics include:

(a) jet noise at sub and supersonic speeds including shock cell noise and wake noise.
(b) compressor fan and turbine noise
(c) combustion noise
(d) boundary layer radiated noise and turbulent wall pressure fluctuations including structural response
(e) radiated noise from cavity flows and from separated flows in general
(f) engine/airframe interaction effects
(g) propeller and helicopter rotor noise
(h) ground attenuation and atmospheric absorption
(i) propagation of noise in the presence of wind and temperature shear and turbulence
(j) propagation of noise in ducts with and without acoustic splitters and absorbent linings
(k) characteristics of cabin noise
(l) sonic boom generation including the effects of variable flight conditions
(m) shock wave-turbulence interaction

Many of these problems as named could be subject to further breakdown and, as stated above, present problems in all branches of engine-airframe study. From this list I have purposely excluded all reference to the excitation of structures exposed to noise radiation and problems of acoustic fatigue.

In this paper I wish to explore the connecting links with some of these problems notably that of jet noise and the sonic boom without attempting in anyway to review, both the extensive and detailed progress that has been made so far and the detailed comparison between theoretical and experimental results.

3. Theory of Aerodynamic Noise

Aerodynamic noise is associated with the unsteady flow of a compressible fluid. If the unsteadiness is confined to a volume of fluid immersed within an extensive region of fluid at rest, noise generated by the unsteadiness is propagated outwards into the ambient fluid at the speed of sound.

The unsteadiness in the fluid inside a volume V, bounded by a surface S, (Fig. 1) could be the result of an aircraft flying through V along a certain trajectory, in which case the volume V would embrace the fluid surrounding the flight trajectory and would extend outwards to those regions in which the disturbance velocity, due to the aircraft motion, had fallen to a negligible level. At this distance from the flight trajectory the disturbance velocity field would be entirely due to the outward propagation of sound. The field outside V is, however, not necessarily at rest. It will possess the general motions of the atmosphere and must therefore include both wind and temperature stratification both vertically and horizontally which in turn involve turbulent motions. This problem, that of aircraft motion, can therefore be divided up into a source problem, in which the aircraft lift and volume is represented by a distribution of sources, or multipoles, and a propagation problem in which the sound waves generated within or near the boundaries of the source region suffer refraction, absorption and dispersion as a result of their interaction with the atmospheric field. At subsonic flight speeds the pressure disturbance in the aircraft's distant field is a regular function of time, apart from the influence of atmospheric turbulence, at a given observation point as the aircraft sweeps past overhead. At supersupersonic flight speeds disturbances no longer travel far in front of the aircraft except at the time, when after a period of supersonic flying, the aircraft returns to subsonic flight speeds. Under supersonic flight conditions sound waves generated at different times along the flight trajectory coalesce, and shock waves are formed resulting in the sonic boom as heard at ground level. The generation of shock waves, albeit weak shock waves, in the far field of the aeroplane introduce significant non-linear acoustic ray distortion but in theoretical work useful solutions are obtained in which, following Whitham, a complete linear solution to the problem is first obtained, and then only the distant sound field is adjusted to allow for the finite disturbance field associated with this sound field. Allowances can be made for all the various atmospheric effects previously referred to but the role of atmospheric turbulence in distorting the wave pattern remains more or less an unsolved problem.

The introduction of the linear approximation to the acoustic field of an aircraft in motion arises from the fact that when the atmospheric scale height is very large compared with the aircraft's dimensions, the entropy disturbance arising from the aircraft's motion can be neglected to first order. Thus to a first order approximation the disturbance created by an aircraft in motion at both subsonic and supersonic speeds may be regarded as isentropic. In the case of an aircraft flying through an atmosphere at rest, but allowing for the variation of temperature and pressure with height, the linearised form of the equation for the pressure disturbance is

$$\frac{\partial^2 p}{\partial t^2} - a_0^2 \nabla^2 p + \left(\gamma g - \frac{da_0^2}{dz}\right)\frac{\partial p}{\partial z} = \rho_0 a_0^2 \left(\frac{DM}{Dt} - \nabla \cdot \underline{F}\right) \qquad (1)$$

where p is the perturbation pressure.

a_0 is the ambient speed of sound (assumed to be a function of z only

where z is measured vertically downwards)

ρ_0 is the ambient air density.

ρM and $\rho \underline{F}$ are the distribution of mass and force sources, respectively, per unit volume, representing the aircraft geometry its aerodynamic forces.

Other terms have their usual significance.

The disturbance pressure, p, leads to an acoustic disturbance velocity $v/\rho_o a_o$ in the direction normal to the wavefront. Thus sound is propagated not at the ambient speed of sound a_o but at the speed $a_o + \frac{\gamma+1}{2} v$, and the non-linear distortion of the acoustic field, and the production of shock waves, can be evaluated. This non-linear problem can however be easily dealt with by the introduction of an effective ray tube area function A, which is a function of the distance travelled along the sound ray, the flight trajectory, and the variation in the atmospheric density and temperature with altitude as well as the variation in wind velocity with altitude. If further a set of curvilinear orthogonal co-ordinates (x) are introduced with origin at the intersection of a given sound ray and the wave surface, Λ = constant, associated with, say, the noise of the aircraft (and measuring x_1 along a normal to the wave surface, Fig. 2, the problem reduces to a solution of the non-linear Burgers' equation

$$W \frac{\partial W}{\partial x_1} + \frac{\partial W}{\partial \lambda} = 0 \qquad (2)$$

where viscous effects are neglected and

$$W = vA$$

$$\lambda = \int^{\Lambda} \frac{\gamma+1}{2A} d\Lambda$$

Further distortion of the wave form by atmospheric viscous and turbulence interaction introduce extra terms in Burgers' equation.

In the absence of the non-linear convective distortion, associated with the term

$$W \frac{\partial W}{\partial x_1}$$

, Burgers' equation shows that W = constant along a given ray and the disturbance pressure or velocity are inversely proportional to A. The effect of convective distortion, involving steepening of the wavefront, leads to the introduction of shock waves. In a simple case the pressure signature in the aircraft's distant field reduces to the form of a simple N-wave. For aircraft in accelerated motion the resulting shock wave pattern suffers considerable modification and indeed the simple theory described above breaks down. This results from the effective ray tube area function tending to zero as a point of focus of the shock waves is approached. The reduction in A leads to an augmentation of the shock waves and the increased strength of the sonic boom under these flight conditions is referred to as the super boom. The theory up to the point where A tends to zero is simply an application of geometrical acoustics associated with the given motion of a multipole source field. However as A tends to zero the changes in the flow field are no longer small over the effective acoustic wavelength and geometric acoustics fail in giving an adequate representation to this problem. In this domain diffraction theory must be applied and in such an approach the effective ray tube area always remains finite. The complications in the description of shock waves approaching a point of focus and in emerging from the focus impose many difficulties in a theoretical treatment of the problem and similar difficulties are not entirely absent in measurements of this phenomenon.

So far I have considered a fairly simplified picture of the sonic boom problem associated with aircraft in motion at supersonic speeds. Some may argue that what I have described is not aerodynamic noise but I respectfully maintain that in terms of my definition of aerodynamic noise, aircraft in motion through the atmosphere presents just as much a problem of aerodynamic noise as the case, I will now consider, of noise due to turbulence. We will see that the essential difference lies in the differences in the description of the sources rather than in any major modifications to the physical description of the two problems.

In the theory of aerodynamic noise due to turbulence, Lighthill found that the unsteadiness in the flow could be replaced by an equivalent set of acoustic sources of strength

$$A(\underline{x},t) = \frac{\partial^2 T_{ij}}{\partial x_i \partial x_j}$$ per unit volume

immersed in a uniform medium at rest in which the speed of sound is everywhere constant and

equal to a_o. In this model the sources move but not the fluid. The stress tensor, T_{ij}, includes all source effects as well as refraction and scattering within the flow and includes also both viscous and entropy fluctuations in the flow. The resulting equation for the radiation of sound from within a turbulent flow field is

$$\frac{\partial^2 \rho}{\partial t^2} - a_o^2 \nabla^2 \rho = A(\underline{x},t) \tag{3}$$

with

$$T_{ij} = \rho u_i u_j + (p - \rho a_o^2)\delta_{ij} - \tau_{ij} \tag{4}$$

where τ_{ij} is the viscous stress tensor.

If there are fluctuations in mass sources, Q, heat sources E, and body forces $\underline{X}$,

then

$$A(\underline{x},t) = \frac{\partial^2 T_{ij}}{\partial x_i \partial x_j} - \operatorname{div}(\rho \underline{X}) + \frac{\partial Q}{\partial t} \tag{5}$$

while $\nabla^2(p - \rho a_o^2)$ will include the heat source term E. These terms are, reading from right to left, representative of monopoles, dipoles and quadrupoles respectively.

We now see that if we allow for the variations in the atmosphere when considering the propagation of the sound rays outside the region of turbulent flow the problems of aerodynamic noise arising from turbulence and that associated with the sonic boom, are similar and both are represented by the solution of the wave equation associated with a certain multipole source distribution. In many turbulent flow problems however shock waves in the external flow are absent whereas it is only when these are present that the problem of aircraft as opposed to engine noise is important.

4. A Unified Treatment of Aerodynamic Noise Problems

A solution is required to Lighthill's wave equation for a turbulent flow

$$\Box^2 \rho = A(\underline{x},t) \tag{6}$$

where

$$\Box^2 \equiv \frac{\partial^2}{\partial t^2} - a_o^2 \nabla^2$$

and

$$A(\underline{x},t) = \frac{\partial^2 T_{ij}}{\partial x_i \partial x_j} \tag{7}$$

Let us assume that the turbulence is being convected but the convection speed does not remain constant along the convection path. For simplicity we will assume the convection path is a straight line but this will not be a necessary restriction to this formulation.

Consider (Fig. 3) the pulse waves as in a sonic boom problem which are generated at a point P, having co-ordinates $\underline{y}$ relative to a fixed set of axes, at a time (τ) and which are received at a point Q, having co-ordinates $\underline{x}$ relative to the same fixed set of axes, at a time (t).

Therefore in terms of the space-time function $\Gamma(P,\tau\,;\,Q,\,t)$ we find that pulse waves are described by

$$\Gamma = 0 \tag{8}$$

where

$$\Gamma(P,\tau\,;\,Q,t) = (t-\tau)^2 - |PQ|^2/a_o^2 \tag{9}$$

$PQ \equiv |\underline{x} - \underline{y}|$ is the distance from $\underline{P}$ to $\underline{Q}$ but for many purposes, including the case where a_o is not uniform, it is more convenient to write (9) in the form

$$\Gamma = (t-\tau)^2 - \left(\int_{\underline{P}}^{\underline{Q}} \frac{d\sigma}{a_0}\right)^2 \qquad (10)$$

where $d\sigma$ is an element of the 'ray' from $\underline{P}$ to $\underline{Q}$.

In terms of the function Γ the solution of (6) given by Guiraud [1] is,

$$\rho(\underline{Q},t) = \frac{1}{2\pi a_0^3} \iiint d\underline{\eta} \sum_{n=1}^{n=N} \frac{A(\underline{\eta},\tau_n)}{\left|\Gamma_\tau(\underline{\eta},\tau_n;\underline{Q},t)\right|} \qquad (11)$$

where

$$\Gamma(\underline{P},\tau_n;\underline{Q},t) = 0 \qquad (12)$$

and τ_n are the n = 1 to n = N roots of equations (12).

Also $\underline{\eta}$ is a set of moving axes moving with the sources.

From (9) we find

$$\frac{\Gamma_\tau}{2} = (\tau - t) + \frac{|PQ|}{a_0}\left(\underline{V}\cdot\underline{e}/a_0\right) \qquad (13)$$

where $\frac{d\underline{P}}{d\tau} = \underline{V}$ and $\underline{e}$ is the direction of the ray from $\underline{P}$ to $\underline{Q}$.

Hence provided that $\Gamma_\tau \neq 0$

$$\frac{\Gamma_\tau}{2}\left(\Gamma = 0\right) = \left(\frac{\underline{V}\cdot\underline{e}}{a_0} - 1\right)\frac{|PQ|}{a_0} \qquad (14)$$

where $|\underline{V}|/a_0 = M$ the local 'acoustic' Mach number, the Mach number based on the uniform speed of sound in the region <u>outside</u> the turbulence.

When the motion is <u>uniform</u> there is only one root satisfying (12) and this is

$$\tau = t - |PQ|/a_0 \qquad (15)$$

so that with (14) and (15) the solution of (11) becomes

$$\rho(\underline{Q},t) = \frac{1}{4\pi a_0^2} \iiint \frac{d\underline{\eta}\; A\left(\underline{\eta}, t - |PQ|/a_0\right)}{|PQ|\;\left|\underline{M}\cdot\underline{e} - 1\right|} \qquad (16)$$

where the denominator can be written

$$R = \left|1 - M\cos\theta\right| \Big/ |\underline{y} - \underline{\eta}|$$

since $\underline{e}$ makes an angle θ with the direction of motion along or parallel to $\underline{e}_1$.

Now $$d\underline{\eta} = d\underline{y} - a_0 \underline{M}\, d\tau$$

so that $\left(\frac{\partial}{\partial \eta_i}\right)_\tau = \left(\frac{\partial}{\partial y_i}\right)_\tau$ when $\underline{M}$ is a function of τ only.

Thus the value of $A(\eta, t^*)$ in (16) is given by

$$A(\eta,t^*) = \frac{\partial^2}{\partial \eta_i \partial \eta_j} T_{ij}(\eta, t^*) \qquad \text{when } \underline{M} \text{ is uniform} \qquad (17)$$

where the differentiation with respect to the η_i's is performed with

$t^* = t - |x-y|/a_o$ = constant. Further on specifying that T_{ij} and its derivatives vanish beyond some finite distance surrounding the domain of turbulence, and making use of the divergence theorem we find

$$\rho(\underline{Q},t) = \frac{1}{4\pi a_o^2} \frac{\partial^2}{\partial x_i \partial x_j} \iiint d\underline{\eta} \; \frac{T_{ij}(\underline{\eta}, t^*)}{R} \qquad (18)$$

which is Lighthill's result. Thus the solution of the wave equation in the form given by equation (11) has, in the case of uniform motion of the sources, led to the identical result found earlier by Lighthill. We reiterate however that the solution given by (16) or in its equivalent form (18) is not correct when $\Gamma = \Gamma_\tau = 0$ and this case will be treated in some detail in what follows.

We note from (14) that when $\Gamma_\tau = 0$, with $\Gamma = 0$,

$$\frac{\underline{e}\cdot\underline{V}}{a_o} = 1$$

or, $M \cos\theta = 1.$ (19)

Thus for all subsonic 'acoustic' Mach numbers $\Gamma_\tau \neq 0$ and the solution to (6) given by (16) is satisfactory for the case of uniform motion of the sources, or, what is more correct, fluctuate randomly in a moving co-ordinate system, which itself is in uniform motion.

In passing we note when the sources are at rest

$$|\Gamma_\tau(\Gamma=0)| = 2\int_{\underline{P}}^{\underline{Q}} \frac{d\sigma}{a_o} = \frac{2|\underline{x}-\underline{y}|}{a_o} \qquad (20)$$

or

$$\rho(\underline{Q},t) = \frac{1}{4\pi a_o^2} \iiint \frac{d\underline{y}}{|\underline{x}-\underline{y}|} \frac{\partial^2 T_{ij}(\underline{y}, t^*)}{\partial y_i \partial y_j} \qquad (21)$$

the well known retarded time solution of the wave equation.

We now turn to the solution of (6) when $\Gamma_\tau = 0$ and where the solution is required in the region around $\Gamma = \Gamma_\tau = 0$. First we note that when $\Gamma = 0$ we have a pulse wave at $\underline{Q}$ generated at a time earlier at $\underline{P}$. When both Γ and $\Gamma_\tau = 0$ we have the condition for an envelope of pulse waves at $\underline{Q}$ which is the condition for Mach waves to appear at $\underline{Q}$. If we go further and find the result of putting $\Gamma = \Gamma_\tau = \Gamma_{\tau\tau} = 0$ we find that this is the condition for the generation of a caustic associated with the focussing of rays in unsteady motion or a non-uniform environment. However for the moment we will assume $\Gamma_{\tau\tau}$ is finite.

Let, as before

$$\Gamma = (t-\tau)^2 - \left(\int_{\underline{P}}^{\underline{Q}} \frac{d\sigma}{a_o}\right)^2$$

Consider the pulse waves passing the distant point $\underline{Q}$, outside the domain of generation, at time t associated with the point of generation $\underline{P}$ ($\underline{y}$) at time τ_o. The corresponding point in the moving co-ordinates is $\underline{\eta}_o$.

Such pulse waves are governed by

$$\Gamma = \Gamma(\underline{\eta}_o, \tau_o ; \underline{Q}, t) = 0 \qquad (22)$$

For a Mach wave to appear at $\underline{Q}$

$$\Gamma_\tau(\underline{\eta}_o, \tau_o ; \underline{Q}, t) = 0 \qquad (23)$$

Let $\tau_o = \tau^*$ define the time off generation of pulse and Mach waves which reach $\underline{Q}^*$ and t^*.

Then

$$\Gamma(\underline{z}_o, \tau^*; \underline{Q}^*, t^*) = \Gamma_\tau(\underline{z}_o, \tau^*; \underline{Q}^*, t^*) = 0 \tag{24}$$

while $\Gamma(\underline{z}_o, \tau_o; \underline{Q}, t) = 0$ denotes a neighbouring point at which pulse waves, but not Mach waves, appear. (see Fig. 4).

Let τ_o be nearly but not exactly equal to zero then we can replace Γ by the following approximation

$$\Gamma = \tfrac{1}{2}\,\Gamma_{\tau^*\tau^*}(\tau-\tau_o)^2 + \Delta\tau\,\Gamma_{\tau^*\tau_o}(\tau-\tau_o) + L(\underline{z}\cdot\underline{z}_o) \tag{25}$$

on writing

$$\Gamma_\tau(\underline{z}_o, \tau_o; \underline{Q}, t) = \Delta\tau\,\Gamma_{\tau\tau}(\underline{z}_o, \tau^*; \underline{Q}^*, t^*) \tag{26}$$

and

$$L(\underline{z}-\underline{z}_o) \equiv (z_i - z_{oi})\,\Gamma_{z_i^*} \tag{27}$$

where the derivatives are all evaluated at $\underline{z} = \underline{z}_o$, $\tau = \tau^*$, $Q = Q^*$, $t = t^*$.

Terms in $\Gamma_{z_i^*\tau^*}$ can be neglected since as will be shown later they are order $a_o|\tau-\tau_o|/\sigma^*$ relative to L, which is a magnitude very small compared to unity when $\underline{Q}^*$ is in the far field.

But $\Gamma = 0$ for pulse waves so

$$\tfrac{1}{2}(\tau-\tau_o)^2\,\Gamma_{\tau^*\tau^*} + \Delta\tau(\tau-\tau_o)\,\Gamma_{\tau^*\tau_o} + L = 0 \tag{28}$$

while

$$\Gamma_\tau = (\tau-\tau_o)\,\Gamma_{\tau^*\tau_o} + \Delta\tau\,\Gamma_{\tau^*\tau^*} \tag{29}$$

If following Guiraud [1], who solves the related problem near a caustic, we put

$$X = \frac{-2L}{\Delta\tau^2\,\Gamma_{\tau^*\tau_o}} \quad ; \quad Y = \frac{\Gamma_\tau}{\Delta\tau\,\Gamma_{\tau^*\tau^*}} \quad ; \quad Z = \frac{\tau-\tau_o}{\Delta\tau}$$

then

$$Z^2 + 2Z - X = 0 \tag{30}$$

and

$$Y = Z + 1 \tag{31}$$

The solution is

$$Y = \pm\sqrt{(X+1)} \tag{32}$$

and

$$Z = -1 \pm \sqrt{(X+1)} \tag{33}$$

In what follows we put

$$G_i(X) = |Y_i(X)|^{-1} \tag{34}$$

or

$$G_1(X) = G_2(X) = 1/\sqrt{(X+1)} \tag{35}$$

Since $Y = \Gamma_\tau / \Delta\tau\,\Gamma_{\tau^*\tau^*}$

$$|\Gamma_{\tau_i}|^{-1} = \frac{G_i(X)}{|\Delta\tau\,\Gamma_{\tau^*\tau_o}|} \tag{36}$$

In the neighbourhood of a Mach wave $\Delta\tau \to 0$ and $X \to \infty$, so that in this region

$$\gamma_i = \pm\sqrt{\chi} \tag{37}$$

with $$\left|\Gamma_{\gamma_i}\right|^{-1} = 1\Big/\left(\sqrt{\chi}\,\left|\Delta\tau\,\Gamma_{\tau^*\tau^*}\right|\right) \tag{38}$$

Also from $\zeta = \frac{\tau-\tau_0}{\Delta\tau}$ we find

$$(\gamma_i - \tau_0) = \Delta\tau\left(-1 \pm \sqrt{(\chi+1)}\right)$$

$$\sim \pm\,\Delta\tau\sqrt{\chi} \quad \text{as} \quad \Delta\tau \to 0. \tag{39}$$

The value of L is found as follows. From the defining relation for Γ

$$\Gamma_{\gamma_1^*} = \frac{2\sigma^*}{a_0^2}\,\underline{\theta}\cdot\underline{e}_1 \;;\; \Gamma_{\gamma_2^*} = \frac{2\sigma^*}{a_0^2}\,\underline{\theta}\cdot\underline{e}_2 \;;\; \Gamma_{\gamma_3^*} = \frac{2\sigma^*}{a_0^2}\,\underline{\theta}\cdot\underline{e}_3 \tag{40}$$

where $\underline{\theta}\cdot\underline{e}_1 = \frac{1}{M^*}$ since $\Gamma_\tau = 0$ associated with a Mach wave.

Thus $$L = \frac{2\sigma^*}{a_0^2 M^*}\left[(\gamma_1 - \gamma_{0_1}) + (\gamma_2 - \gamma_{0_2})\,\underline{\theta}\cdot\underline{e}_2 M^* + (\gamma_3 - \gamma_{0_3})\,\underline{\theta}\cdot\underline{e}_3 M^*\right] \tag{41}$$

and on writing

$$\gamma_1^* = \gamma_1 + (\gamma_2 - \gamma_{0_2})\,\underline{\theta}\cdot\underline{e}_2 M^* + (\gamma_3 - \gamma_{0_3})\,\underline{\theta}\cdot\underline{e}_3 M^* \tag{42}$$

we find

$$\chi = \frac{4\,\sigma^*\,(\gamma_{0_1} - \gamma_1^*)}{a_0^2\,M^*\,\Delta\tau^2\,\Gamma_{\tau^*\tau^*}} \tag{43}$$

and

$$\left|\Gamma_{\gamma_n}\right|^{-1} = \frac{1}{2}\sqrt{a_0^2 M^*\Big/\left(\sigma^*\left|\gamma_{0_1} - \gamma_1^*\right|\left|\Gamma_{\tau^*\tau^*}\right|\right)} \tag{44}$$

where * denotes conditions at the source corresponding to the generation of both pulse and Mach waves.

When a_0 is constant

$$\frac{\Gamma_{\tau\tau}}{2} = 1 - M^{*2} + \sigma^*\,\underline{\gamma}^*\cdot\underline{\theta}\Big/a_0^2 \tag{45}$$

where the acceleration $\underline{\gamma}(\tau) = \dfrac{d\underline{V}}{d\tau}$

On substitution of (44) and (45) into (11) noting that there are two roots, (39), having the same modulus, we find on the Mach wave

$$\rho^*(Q,t) = \frac{1}{4\pi a_0^2}\left(M^*/2\right)^{1/2}\iiint \frac{d\underline{\eta}\;\dfrac{\partial^2 T_{ij}}{\partial\gamma_i\,\partial\gamma_j}\left(\underline{\eta},\ \tau^* \pm \dfrac{2\,\sigma^*\,(\gamma_1 - \gamma_1^*)}{a_0 M^*\,\Gamma_{\tau^*\tau^*}}\right)}{\sqrt{|\underline{\eta}-\underline{y}|}\sqrt{|\gamma_1 - \gamma_1^*|}\sqrt{\left((1-M^{*2}) + |\underline{\eta}-\underline{y}|\,\underline{\gamma}^*\cdot\underline{\theta}/a_0^2\right)}} \tag{46}$$

But $\tau_n = \tau^* \pm 2\sqrt{\dfrac{\sigma^*(\eta_1 - \eta_1^*)}{a_0^2 M^2 \Gamma_{\tau^*\tau_n}}}$ on the Mach wave

so that $$\frac{a_0(\tau_n - \tau^*)}{\sigma^*} = \pm \sqrt{\frac{2(\eta_1 - \eta_1^*)}{\sigma^*}} \Big/ \sqrt{M^2 \int \left(1 - M^{*2} + \sigma^* \frac{\underline{\gamma}^* \cdot \underline{\theta}}{a_0^2}\right)}$$

and is small compared with unity when in the far field the size of the source region is small compared with σ^*.

Figure 5 shows the position of the sources at τ_1 and τ_2 which emit disturbances and which are received simultaneously at (Q,t). As (Q,t) approaches (Q^*, t^*) so τ_2 and τ_1 lie equispaced about τ .

In place of (41) we can write

$$L = \frac{2\sigma^*}{a_0^2}\left(\eta_1' - \eta_{01}'\right)$$

where $\underset{\sim}{\eta}'$ is a new co-ordinate system with η_1' parallel to $\underline{P}\,\underline{Q}^*$. Thus on the Mach wave

$$\rho^*(\underline{Q}^*, t^*) = \frac{1}{4\pi a_0^2} \frac{1}{\sqrt{2|s-y|}\sqrt{(1 - M^{*2}) + \frac{|s-y|}{a_0^2}\underline{\gamma}^* \cdot \underline{\theta}}} \cdot \iiint d\underset{\sim}{\eta}' \frac{\partial^2 T_{ij}}{\partial \eta_i' \partial \eta_j'}\left(\underset{\sim}{\eta}', \frac{2\tau^*}{a_0}\sqrt{\frac{\sigma^*|\eta_1' - \eta_1'|}{M^2 \Gamma_{\tau^*\tau_n}}}\right) \Big/ \sqrt{|\eta_1' - \eta_1'|} \tag{47}$$

where the integration is along the direction of the rays in the source region and is therefore perpendicular to the rays. Since the retarded time differences between τ_1 and τ_2 can be neglected

$$\rho^*(\underline{Q}^*, t^*) = \frac{\sqrt{2}}{4\pi a_0^2} \frac{1}{\sqrt{|s-y|}\sqrt{(1 - M^{*2}) + \frac{\sigma^* \underline{\gamma}^* \cdot \underline{\theta}}{a_0^2}}} \cdot \iiint \frac{d\underset{\sim}{\eta}' \frac{\partial^2 T_{ij}}{\partial \eta_i' \eta_j'}\left(\underset{\sim}{\eta}', \tau^*\right)}{\sqrt{|\eta_1' - \eta_1'|}} \tag{48}$$

The integration is over all values of η_1' in the source region and the distribution of pressure is found by varying η_{01}' .

This important result for the density fluctuation in the direction of Mach wave emission can be extended to other angles. The result is

$$\rho = \frac{2\sqrt{2}}{4\pi a_0^2} \iiint \frac{d\underset{\sim}{\eta}' \frac{\partial^2 T_{ij}}{\partial \eta_i' \partial \eta_j'}}{|PQ|\sqrt{(M\cos\theta - 1)^2 + 4(\eta_1' - \eta_1')\left(\frac{\underline{\gamma} \cdot \underline{\theta}}{a_0^2} - \frac{M^2 - 1}{|PQ|}\right)}} \tag{44}$$

and indicates a smooth transition from that pertaining to Mach wave emission from that associated with the normal Doppler factor ($M\cos\Theta - 1$).

Our result agrees with that obtained independently by Ffowcs Williams and Hawkings [2] in a recent paper. In fact the result above is one of a number of important results obtained by the above authors who have considered in detail the formulation of the acoustic radiation from regions in which the boundary surface moves and which includes the case of moving surfaces in the flow across which discontinuities in fluid velocity occur. The above result for the perturbation density is valid for both subsonic and supersonic convection speeds provided discontinuities in T_{ij} do not arise within the volume of flow. If we replace

$$4(\gamma_1' - \gamma_1')\left(\frac{\underline{\gamma}\cdot\underline{\theta}}{a_0^2} - \frac{M^2-1}{|PQ|}\right) \quad \text{by} \quad b^2M^2$$

we recover the result given by Lighthill [3] Ffowcs Williams [4] and Ribner [5]. The importance of non-uniform convection velocity over the life-time of an eddy appears to be worthy of further study especially in and around the directions of Mach wave emission.

The order of magnitude of the square of the density perturbation is easily found if T_{ij} is of order $\rho_1 a_0^2 M^2$ and the turbulence scale is typically ℓ. It follows that on the Mach wave

$$\overline{\rho^2} \sim \frac{1}{8\pi^2}\left(\frac{\ell\,\rho_1^2\,M^4}{r^2\left|\frac{\underline{\gamma}\cdot\underline{\theta}}{a_0^2} - \frac{M^2-1}{r}\right|}\right) \qquad (50)$$

In the absence of acceleration

$$\overline{\rho^2} \sim \frac{1}{8\pi^2}\left[\rho_1^2\,\frac{\ell}{r}\left(\frac{M^4}{M^2-1}\right)\right] \qquad (51)$$

showing that the Mach wave decay falls like $\frac{1}{r}$ whereas at other angles the decay follows the inverse square law. These results were also obtained by Ffowcs Williams and Hawkings who point out that for a confined distribution at sources M^2-1 would be replaced by $\sqrt{(M^2-1)}$.

Having established that sonic boom theory can aid the development of the theory of other problems in aerodynamic noise we note the possibility of the development of caustics in the Mach wave radiation from jets and the estimation of the perturbation edensity on the caustic using the results of Guiraud.

Further the introduction of non-linear effects together with the effects of atmospheric distortion as well as flow field distortion on the sound ray pattern can all be treated in a manner analogous to the treatment of these problems in sonic boom theory.

5. Concluding Remarks

This brief introductory note shows that the broad features of aerodynamic noise theory in problems as diverse as the sonic boom and jet noise have much in common such as with respect to the effects of source convection. These problems however differ in one important feature in that whereas the source (multipole) strength distribution for an aircraft travelling at supersonic speeds can be evaluated from the geometry and forces on the aircraft, the source strength distribution in turbulent flow problems relies heavily on their experimental determination. Other major differences are that the aircraft surfaces are rigid to all intents and purposes during flight while turbulence has no fixed boundaries.

Although progress can be made in the understanding of any aerodynamic noise problem by the accumulation of noise measurements in the radiated field the deep understanding of the distribution of the equivalent acoustic sources and their strengths can only be established by detailed probing of the unsteady flow in the source region. In the jet noise problem the accumulated experimental data on the structure of the turbulent shear layer in all flight conditions is very sparse indeed even though the average bulk properties of these flows are known and can be calculated. For instance, in the case of a fan blade subjected to interaction with a turbulent flow field it is surprising how little is known of the fluctuating forces and their spectrum, and this is a dominant problem in all work non the noise from turbofan propulsive and lifting fan engines.

In many cases of aerodynamic noise a lack of detailed understanding of the flow unsteadiness producing the radiated noise will not preclude the development of noise attenuating devices.

However the full potential of any noise suppressor, and bearing in mind the need to limit the performance penalty involved, can only be derived when the strength and distribution of the equivalent acoustic sources is known. The theory of aerodynamic noise is still in its infancy even though many important and basic results have already been derived. It provides and will continue to provide a basic framework on which the experimentalist can build and explore those features of aerodynamic noise which the theoretician finds almost impossible, without guidance from experimental results, to develop.

6. References

1. Guiraud, J.P. — Remarques sur le bruit balistique au Voisinage d'une Caustique. La Recherche Aerospatiale No. 98 (1964)

2. Ffowcs Williams, J.E. Hawkings, D.L. — Sound Generation by Turbulence and Surfaces in Arbitrary Motion. Proc. Roy. Soc. Trans. (A) Vol. (1969)

3. Lighthill, M.J. — The Bakerian Lecture 1961 Sound Generated Aerodynamically Proc. Roy. Soc. A267 147 - 182 (1962)

4. Ffowcs Williams, J.E. — The Noise from Turbulence Convected at High Speed Phil. Trans A255 p.469 - 503 (1963)

5. Ribner, H.S. — The Generation of Sound by Turbulent Jets. Adv. in Appl. Mech. Vol. 8 (1964).

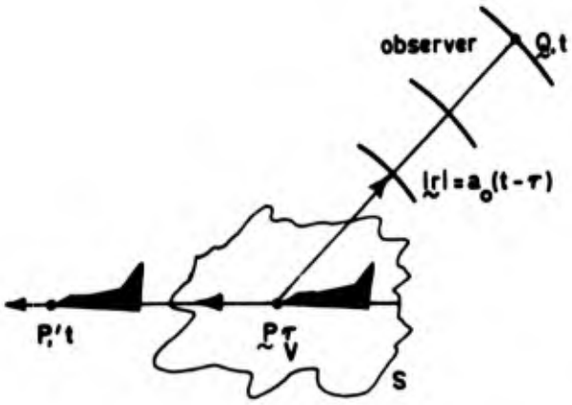

Fig.1

Aerodynamic Noise Emission and Reception

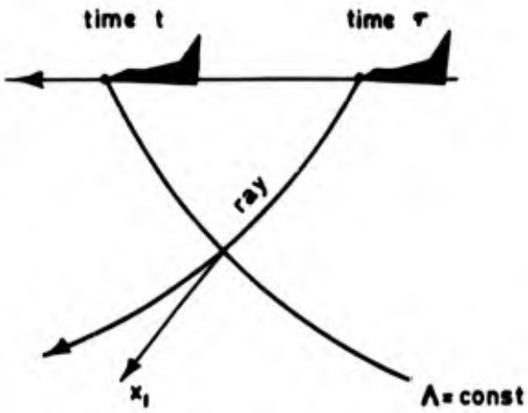

Fig.2

Diagram of Rays and Wave-Fronts from an Aircraft in Supersonic Motion in a Non-Homogeneous Atmosphere

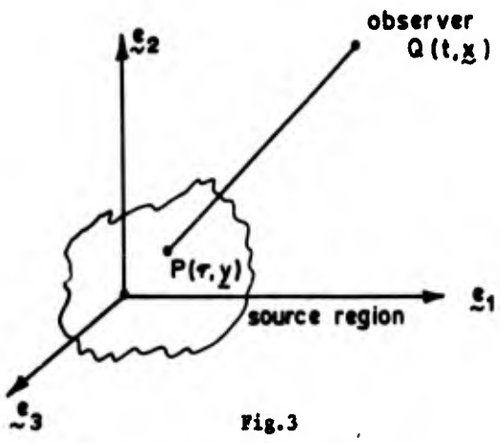

Fig.3

Aerodynamic Noise - Notation

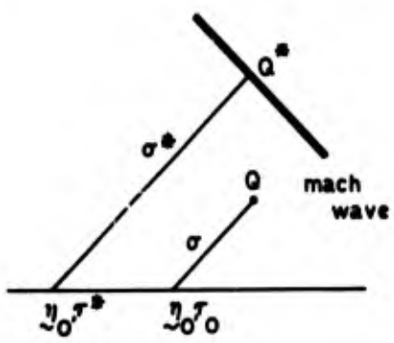

Fig.4

Source Location for Far-Field Region Neighbouring a Mach Wave

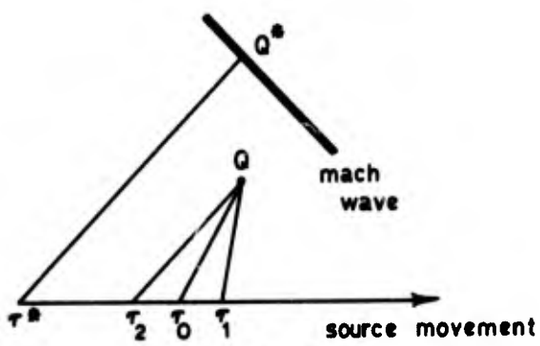

Fig.5

Source Location for Far-Field Point Near to a Mach Wave

A BRIEF LEGAL HISTORY OF THE SONIC BOOM IN AMERICA

By

J. P. and E. R. G. Taylor

Note:

The contents of this paper are solely the responsibility of its authors, not of the organizations for which they work.

SUMMARY

Leading world air carriers are now making detailed plans involving commercial supersonic transports (SST's). The legal consequences of such flights may well turn out to be as complex, in their own way, as the development of the aircraft itself. This new form of rapid transportation will develop a body of law to cope with its special problems. Decisions of the courts can well determine the degree to which SST's will be able to fulfill their potential in the conduct of world commerce during the critical decades ahead.

Legal precedents already established in connection with military supersonic flight operations bear on the disposition of one of the important potential problems of commercial travel at supersonic speeds -- sonic boom damage claims. American jurisprudence does provide some guidelines of consequential liability and responsibility within partially defined ranges.

In this paper sonic booms and their effects on man and his structures are examined through material available from administrative claims and court cases. Several recent Congressional actions and early response thereto by the Department of Transportation, and Federal Aviation Administration insofar as the sonic boom is concerned, are briefly described.

Recent rapid progress of science and engineering in such fields as transportation, communications and medicine has brought about and will continue to create novel problems to which, in time, civilization in its legal processes has and, hopefully, will continue to accommodate.

A BRIEF LEGAL HISTORY OF THE SONIC BOOM IN AMERICA

"Soon shall thy arm, unconquered steam! afar
Drag the slow barge, or drive the rapid car;
Or on wide-waving wings expanded bear
The flying chariot through the field of air."

--Erasmus Darwin, "The Botanic Garden" - 1791

"For I dipt into the future, far as human eye could see,
Saw the Vision of the world, and all the wonder that would be;
Saw the heavens fill with commerce, argosies of magic sails,
Pilots of the purple twilight, dropping down with costly bales."

--Alfred Tennyson, "Locksley Hall" - 1842

Introduction: Poets of the 18th and 19th centuries, having known neither Bleriot nor the brothers Wright, projected our 20th century jets in "argosies of magic sails" and "wide waving wings" of "flying chariots." Their eloquence scarcely foresaw the many aviation based problems of engineering, psychology, physiology, and law that concern us today. After almost six decades of flight, aviation law, for example, finding its way through admiralty, statutory, the several national laws, international law, and law affecting surface transportation, has indeed "soared into a different realm than any that has gone before." (Chicago & Southern Air Lines v. Waterman SS Corp., (USSC, 1948), 68 S. Ct. 431).

Justinian's Roman law phrase of cujus est solum ejus est usque ad coelum et ad inferiors (to whomsoever the soil belongs, he owns also to the sky and to the depths) was adopted into English law by Lord Coke in his 1832 Institutes and restated by Blackstone and Kent in their Commentaries. The phrase res ipsa loquitur (the thing speaks for itself) was early utilized in the now century old Rylands v. Fletcher doctrine. In essence this doctrine states that if a person has anything likely to do mischief if it escapes, he keeps it in at his peril or is liable for all damages that are the natural consequence of its escape. Thus, the 1815 Pickering v. Rudd British case concluded that an aeronaut was liable for trespass, a conclusion based on the analogy that any overhang over another's property could be a trespass.

Anglo-American concepts of common law tort, contract liability regarding operator, manufacturer, bailee or injured party, expanded by statutory law on utilization of airspace, acquisition of land for airports and zoning regulations led to some necessary accommodation, on the basis of public policy, between aircraft operation and private rights.

The New York state decision in Guille v. Swan (N.Y. Sup. Ct., 1822; 1 Avi.1) involved a suit by a landowner for damages to his garden caused by an aeronaut in a free balloon; the latter was held responsible for the physical trespass of persons in the garden in which he had inadvertantly landed in that he should have foreseen that a curious crowd would follow the balloon, investigate and assist. But by the early 20th century, U. S. courts were using such phrases as: "The upper air is a natural heritage common to all of the people..." (Johnson v. Curtiss NE Airplane, (D.C., Minn., 1923) 1 Avi. 61); that surface owners have rights and may be compensated for nuisance but not every overflight is a trespass as "...absolute ownership of private property may to some extent be limited and curtailed in a greater public interest..." (Swetland v. Curtiss Airport, (41 F 2d 929 (D.C., N.D., Ohio, 1932); 55 F2nd 201, (6th CCA, 1932); that the "landowner no more possesses a vertical control of all the air above him than a shore owner possesses horizontal control of all the sea before him. The air is too precious as an open highway to permit it to be 'owned' to the exclusion or embarrassment of air navigation by surface landlords who could put it to little use." (NW Airlines v. Minn. (USSC, 1944) 322 US 292,303); and that "The air, like the sea, is by its nature incapable of private ownership except insofar as one may actually use it." (Hinman v. Pacific Air Transport Corp. 84 F. (2d) 755,758 (CAA 9th, 1936); USSC denied cert. 300 US 655 (1936)). However, the 1944 Chicago Convention, to which the U.S. acceeded and is a party, states in Article 1 that "...every State has complete and exclusive sovereignty over the airspace above its territory."

Change is the life-blood of the law; increased speed has long been one of the magic touchstones by which new forms of transportation have found wide acceptance. Now, however, in this period of growing individual expectation, increasing public interest in clean air, pure water, and freedom from manmade noise may well cause changes in future forms of transport considered unthinkable even a decade or two ago. Scientific developments in aeronautics, astronautics, organ transplants, birth control, floridation, etc., all create problems both in jurisprudence and morality, but the essential of justice remains accommodation of interest to serve the common weal.

Since the law can sometimes be slow in its response to rapid change, the orderly and rapid development of commercial aviation over the last half century called for the establishment of national bodies to set forth requirements of and effect certification, accreditation and standards; international agreements

on routes and rates; and treaties such as those on liability for passengers and luggage (Warsaw, 1929 (TIAS 876)), overflights and landings (Chicago, 1944 (TIAS 1591)), and surface damage (Rome, 1933 and 1952). Indeed commercial aviation has by now become one of the great forces at work in the world to bring about a common set of rules and agreements by means of which nations, states and municipalities can better enjoy and profit from those "wide waving wings of flying chariots" foreseen so long ago.

But now, commercial supersonic flight, tomorrow's reality, brings with it additional problems operationally and, in time, possibly, legally, in such diverse directions as airport facilities, air traffic control, scheduling, crew salaries, and areas of special concern, such as high altitude radiation, clear air turbulence, vapor trail condensation and sonic boom. These factors in turn can have an impact on adequate safety, equitable rates, viable insurance, economical operation and public acceptance which are of primary interest to the airline operator and also attract the special attention of the civil aviation regulatory agencies and Congress. In America these matters tend to become involved in varying degrees in the legislative, administrative, and judicial processes. Of the problems which are in apparent part of the supersonic transport (SST) operation, the sonic boom has at times received more attention from mass communication media in the States than any other single problem.

THE SONIC BOOM: We are all familiar with the charming analogy that Joshua of the Old Testament created and recorded the first sonic boom. Captain Charles Yeager, piloting the Bell XS-1 at Edwards Air Force Base on 14 October 1947, became the first man to exceed purposely the speed of sound in level flight in an aircraft instrumented for the purpose, and thereby produced the first pre-planned sonic (actually supersonic) boom. This is the N-shaped pressure signature on the ground of the approximately conical bow and stern shock waves that any body moving supersonically produces in atmospheric flight. In subsonic flight pressure waves propagate outward in all directions from a moving body; approaching the speed of sound, the body overtakes its own disturbances; above the speed of sound, the body travels faster than its own pressure waves and a cone of disturbance fronts forms with the nose of the body at the apex of a cone. In the case of an airplane other local shocks may also be formed at the several transition points of airframe and engine. As the distance from the aircraft moving supersonically increases significantly these local shock waves coalesce into two shock fronts, bow and tail, producing an N-shape wave. Hence, a structure or person at ground level can be subjected to two abrupt pressure discontinuities and, on occasion, two distinct booms may be heard. The boom can extend 20 to 30 miles laterally on each side from the flight track if the aircraft is flying supersonically at a sufficiently high altitude.

The first formally recorded boom incident in America is believed to have occurred during 1950 test dives by a jet fighter when a ground radar operator noted an explosive like noise after each dive and the sound was correlated with supersonic flight. Although physical principles of production of shock waves by a body moving in air were well known, it had not been generally anticipated that the shock wave formed at high altitude would reach the ground with such intensity as to cause a plainly audible signal.

As we are now learning, local meteorological conditions can significantly affect sonic boom N-wave shape and maximum overpressures reached at ground level. Such conditions include differences in seasonal and diurnal temperatures, air mass relative humidity and dust particle content, speed and direction of wind at various altitudes, and more particularly, temperature inversions, low altitude mechanically induced turbulence and the rate of change of wind shear between different air masses can cause deflection and distortion in the classical N-wave shape. Several design parameters also affect the sonic boom: e.g., aircraft shape, weight, altitude, speed and maneuverability are particularly important. Although the phenomenon has been the subject of much study in laboratory and field experiments, over the last decade, at the cost of a considerable outlay of time, talent and money, there is still much that must be learned before the final textbook version of the sonic boom in all its variations can be written.

A popular American reaction developed over the years is that the sonic boom must have destructive consequences. Much publicity has been given the more spectacular although generally inadvertant type of sonic boom. In 1957 Marine Major John Glenn, later Project Mercury Astronaut, during a record making cross-country supersonic jet flight, reduced altitude over the mid-west for refueling, creating a boom. LIFE magazine (29 July 1957) included a picture of a collapsed ceiling of a Terra Haute, Indiana, house, which, it was claimed, resulted from the generation of this boom. Low level accidental sonic booms are infrequent but not impossible, despite constant vigilence. On June 9, 1966, over Washington Court House, Ohio, an F-4 with an apparently faulty Mach indicator barely exceeded the speed of sound at about 1,000 feet above the ground without the pilot being aware of it; result: over 300 complaints and 200 claims. In June, 1968, the pilot of a USAF F-105 fighter aircraft over the U. S. Air Force Academy at Colorado Springs, Colorado, cut in his afterburner a second or two too soon to increase his power output for fast climbout and in so doing went above Mach 1, causing a sonic boom at an altitude of approximately 150 feet above the ground.

Some $50,000 in damage resulted, mainly to a glass walled dormitory and physical injury of generally minor nature caused by flying glass splinters. Although such unusual incidents are certainly not contemplated with the commercial SST, it is this type of extreme case which has helped to form a public viewpoint on the sonic boom in America.

Since all supersonic flight in America can be traced to military operations whose consequences are controlled by special statutes, military sonic boom experience can only portend for its civil aviation counterpart; nevertheless, a review of such experience, administrative and judicial, may prove helpful in understanding current trends in sonic boom jurisprudence in America.

ADMINISTRATIVE SETTLEMENT of sonic boom claims in America generally stems from Federal legislation which permits a claimant to be paid for damages under the Military Claims Act when the damages were caused by "non-combat" activities of the military forces and under the Foreign Claims Act for damages caused by U. S. military forces abroad. Negligence is not specifically necessary; the crux is causation by military aircraft and consequential, proven damages.

Originally sonic boom claims were considered and paid on the basis of an evaluation of what damage a military claims officer working alone or with the assistance of an engineer estimated that a sonic boom caused by a military aircraft could have been expected to have caused. By now almost two decades of practical experience in the sonic boom claims field have been reinforced by a study of the results of a considerable body of controlled sonic boom field tests over a number of countryside and metropolitan areas. Aeronautical, structural, acoustical, medical and other experts, utilizing the best available instrumentation, have checked in varying degrees the effect of sonic booms on human response, structures and animals by employing military aircraft ranging in size from small supersonic fighters to the out-sized B-70.

In the administrative claims procedure used by the United States Air Force (USAF), certain requirements are basic to settlement. Initially it must be established that there was in fact a sonic boom propagated by an instrumentality of the government. Glass damage may be favorably considered if investigation indicates that it occurred coincident with a sonic boom; at present a USAF claims procedure states that damage to concrete block must be accompanied by glass damage. It must also be established that the damage is not inconsistent in type, location and nature with that caused by sonic booms previously studied.

By now a considerable amount of money has been paid by the U. S. Government to settle claims of damages to property caused by sonic booms. Between 1 July 1956 and 30 June 1968, 38,831 claims were submitted to the USAF for all types of sonic boom damage involving a total of $22,539,000; of these 14,006 claims were approved in whole or in part in an amount of $1,517,000. This is an approval rate of about 36% of claims submitted. In 1956, 36 claims were presented to the USAF for a total of $12,000; of these 21 were paid for $2,000. By 1968 the great increase in USAF supersonic flying resulted in 3,402 claims presented for a total of $2,565,000; of these it is estimated that some 1,391 were paid involving a total of approximately $191,000. Of the paid claims about 65% were for glass damage; 21% for plaster; 8% for fallen objects such as bric-a-brac; and 6% for miscellaneous. (USAF JAG data bank)

Instructions to the USAF authorities charged with responsibility for claims investigation and payment state that military aircraft flying under normal operating conditions do not cause the following damage and such claims are not payable, so no investigation is required: cracked concrete driveways, walks, patios, basements, retaining walls, brick or stone chimneys, mortar joints, automobile glass, TV safety screens, TV picture tubes, stereo components, water closets, commodes, or broken seals in thermopane windows. These USAF instructions also state that claims for glass damages in residential or commercial glass doors or windows may be caused by sonic booms and may be payable for replacement cost but not for improvement or enrichment.

The USAF also considers that sound plaster properly placed will not ordinarily be cracked by sonic booms from aircraft flying supersonically under normal operating conditions; such claims must be investigated by qualified engineers who estimate overpressures involved, study other complaints in the area, determine the aggravation of plaster cracks caused by the boom and the like. When plaster damage has been determined to have, in fact, been aggravated by a sonic boom for which the USAF has responsibility, payment is limited to 50% of the reasonable cost of repair of the cracked plaster, including reasonable cost of repainting and related repairs. This percentage is a maximum and a lesser amount may be appropriate.

In the nature of human reactions mysterious damage of unknown or unexplained origin is sometimes blamed on the sonic boom if the occurrence or discovery is within the same general time span; thus, the military sonic boom has been blamed for such unlikely events as shifting bedrock, withered gardens, dried up wells, and severely cracked irrigation ditches. In addition to utilization of the services of an engineering expert to ascertain the cause of damage, the USAF investigator must identify the aircraft or the causal factor as of USAF origin. As an investigative aid, the USAF in

October 1967, directed that all USAF supersonic flights were to be conducted at above 30,000 feet over land and above 10,000 feet over water areas; that a sonic boom may be intentionally generated below these altitudes only in specific instances and that USAF and National Guard pilots who fly supersonically keep sonic boom logs whose entries are transmitted at frequent intervals to a Central Sonic Boom Repository in the Pentagon at USAF Headquarters. The data in the Repository is computerized and available for interrogation by properly authorized USAF personnel. This administrative aid has proved most helpful. In general, then, the Department of Air Force, and to a lesser extent, the Department of Navy, have developed a time tested system for processing sonic boom claims.

In those cases where the claimant is not satisfied when notified of the disposition of his claim, he may choose to institute suit against the Government. Generally prior to such court action, the party claimant has attempted administrative settlement and declined to accept the amount offered, or been denied recovery because the type of damage is not that contemplated in the terms of the phenomenon; e.g., there was no military aircraft known to have been flying supersonically overhead at the time the damage was said to have happened, or, rarely, because the supersonic aircraft was still in the custody, control and operation of the contractor-manufacturer prior to being turned over to the federal government and military authorities.

COURT ACTIONS have generally been brought under the terms of the Federal Tort Claims Act, permitting recovery against the Government through a limited waiver of its sovereign immunity, for negligent or wrongful act of its employees or agents, acting in the scope of employment. At this point it may be useful to state that American tort law, liability for wrong, is based on standard principles of justice, stemming from the French "vous avez tort," "you are wrong." It is the civil wrong for which compensation is demanded. Justice Holmes of the Supreme Court stated the elements as a finding of "who hit the boy in the eye with the stone," indicating the requirements of proper parties of wronged and wrongdoer, method or causation and resultant damage.

To establish a judicial claim, experts, qualified and accepted by both parties and the judge must present evidence by required legal standards. Expert opinion must be based upon specialized knowledge, experience and/or training; if not, it is as speculative or conjectural as that of a layman and the expression of opinion is then founded on reducing possible choices to the most probable. (Hartman v. U.S., (USDC, CD, Calif., 31 Oct. 1967) Civil No. 62-760F).

In a practical sense because of the diversity of citizenship of the parties involved, federal courts have been utilized to try sonic boom cases. In a word, federal courts follow procedures prescribed by law and are grouped into ten circuits, which are persuasively, but not required to be, in conformity with decisions of the other circuits, at least until the U. S. Supreme Court decides to and acts on the subject matter, thus providing the law which all must follow. To one unacquainted with its detailed workings, this complexity of judicial affairs may at first seem difficult to follow but in due course all suits can be resolved within the existing judicial framework. In general, legal suits involving a sonic boom do not come before the courts unless the claimant is dissatisfied with the disposition of his administrative claim, and he seeks judicial redress.

Since courts are interpreters rather than innovators of the law, and since applicable clarifying legislation often follows rather than precedes points at issue in the courts, the judicial system in rendering substantial and rational court judgments within the terms of existing legislation may arrive at different interpretations in its several jurisdictions on the same general issue. Following are several sonic boom cases involving different courts which illustrate this point.

Sonic Boom Cases - Structures: At an air show at Oklahoma City's Will Rogers Field on 3 September 1956, certain USAF and U. S. Navy supersonic flights, made according to specified and preplanned flight patterns, resulted in supersonic dives with the focal point of the booms being the intersection of the runways. During a practice session the week before the show, one low level supersonic flight broke some glass in the airfield terminal building and did other damage. An insurance company had contracted in writing with the Government (US) to pay all damages caused by breaking the "sound barrier," whether caused by negligence or otherwise. The plaintiff (Lloyds of London v. Blair and USA (10th CCA, 1958) 262 F(2d) 211; 6 Avi. 17,232) claimed structural damage; some 300 other home owners intervened in the case for their own damage claims in amounts from $25.00 to $3,973.00. Although the U. S. admitted the activity the court held for the U. S. on the basis it was improper to join a tort action against the U. S. with a contract action against the insurer.

On January 4, 1958 a barn was destroyed by fire in Alabama; the owner (and other witnesses) heard two loud sounds in the nature of explosions, a few seconds apart. The owner got off a bed, put on his shoes, went out, saw the barn, 50' away, burning, looked up, saw an aircraft at 600'-1200' in altitude and the circle and star on its wings (Cook v. U.S. (DC, Ala. 1958) 163 F. Supp. 784). There was no evidence a U. S. agent was the operator of the aircraft, no evidence what caused the explosions that destroyed the barn or that the aircraft caused the explosions, or, assuming

it did, how it caused them. The court held that there was no res ipsa loquitur; i.e., that the concomitance of events and the sighting of the aircraft did not, in the absence of other evidence, imply the aircraft caused the barn to burn and fall.

In another case (Brown v. U. S. (DC, Mass, 1964) 230 F. Supp. 774) the U. S. admitted that its employees in the scope of their employment did exceed the speed of sound in the Boston area on 3 November 1959, but denied any negligence in their actions; the plaintiff failed to recover his suit for $6,754 damages.

Mr. Sanders (Sanders v. Fireman's Fund Ins. Co., 1912, Bedford Co., Tenn., June 1967) asked $2,770 from his insurer for damages by "several jet aircraft" flying at supersonic speed on 22 June 1960, and the jury trial resulted in his favor. The pleading, the lawyer's phraseology in the complaint is of interest:

> "...extensive damage to plaintiff's aforesaid dwelling house; that at said time and place the exterior walls of said dwelling house shook and trembled and cracked due to the aforesaid pressure wave created by the aircraft exerting the force directionally, pushing against the said exterior walls on the side from which they approached and pulling said walls on the side the aircraft receded; that the aforesaid shaking, trembling and cracking of the exterior walls of the said dwelling house was directly and solely caused by the speed of the aircraft passing overhead..."

On 17 November 1956 a jet aircraft allegedly executed a sonic boom over Hico, Texas, that reportedly knocked dishes from shelves in the area and broke them. An insurance company witness categorically stated that "a sonic boom of sufficient intensity can cause structural damage to a building." In the same town another building owner asked the full amount of his $3,000 insurance policy for destruction of his 1954, two-year-old frame and metal warehouse, used for storing lumber, with a 7-8 boxcar load capacity; there was no visible evidence that it was unsafe or had deteriorated in any manner prior to loss. It was alleged that the aircraft flight was at supersonic speeds, creating disturbances, shock waves and compression waves which "unseated the girders beneath the building and capsized it." A finding against the plaintiff was reversed on appeal (J. E. Alexander v. Fireman's Ins. Co., 317 SW 2d 752, 5 Avi. 18,218; 328 SE 2d 350, 6 Avi. 17,711; rehearing denied 5 November 1959). One interesting aspect of the case involved the insurance company which argued that the policy covering damage by aircraft comprehended only falling aircraft or objects falling from aircraft and that the sonic boom was not an explosion in the other terms of the policy. The court held that such a policy containing words "shall include..." were not words of limitation but of enlargement and the policy did not limit recovery thereunder to falling aircraft or objects therefrom; "...since plaintiff alleged a loss occasioned by aircraft, he is entitled to recover if he can prove that he has a loss which was proximately caused by aircraft..."

A valid claim for sonic boom damage, in an agreed amount, is generally capable of administrative settlement and, if disputed, a court action by the injured party, on occasion can result unfavorably for him. One such case (McMurray v. US (DC, Mo., 1968) 286 Fed. Supp. 701; 10 Avi. 18,114) was brought under the Federal Tort Claims Act for damages allegedly caused by USAF aircraft operating at supersonic speeds in the vicinity of Kansas City, Missouri, during July-September 1962. The court held the U.S. not liable and that the flights, in accordance with USAF regulations within prescribed corridors, were authorized in the "discretionary function or duty on the part of a federal agency or an employee of the government."

One case which goes extensively into matters of substance and utilizes the lore of controlled testing data, although with the judgment contrary to the technical evidence submitted (Neher v. US 265 Fed. Supp. 210 (USDC, Minn., 1967), 10 Avi. 17,271) involved an apartment building, 8-10 miles west of the center line of a corridor used by B-58 aircraft from Indiana making some 49 flights over the Minneapolis - St. Paul area between 5 April and 6 August 1962. The plaintiff-owner asked $10,000 damages, the property differential before and after the sonic booms occurred; repair estimates and USAF engineering evaluation indicated pre-boom cracks and an offer of administrative settlement was made in the amount of $750. Parenthetically, the court held the USAF negligent, and therefore liable to suit, in designating this metropolitan area as a supersonic corridor when it could have used uninhabited or sparsely populated areas or bodies of water for overflight, inasmuch as radar tracking equipment could have been located anywhere, due to its mobility. The court quoted testimony of an expert witness knowledgeable of the U. S. Government White Sands Test program that data taken during this test had established that:

> "(1) structures work elastically under a sonic boom pressure, returning to their original shape after the pressure subsides, rather than having any type of permanent set; (2) that the threshold level of pressure for plaster cracks and glass breakage was ten pounds per square foot, except that predamaged glass might crack at six or seven pounds per square foot..."

Utilizing these premises the court rejected part of the claim for structural damage, holding that

"since sonic booms do not cause permanent set, any squeakiness attributable to the booms would have occurred immediately," rather, such an effect was due to "the normal cycle of expansion and contraction due to temperature changes and repeated traffic over the years." However, the court did award a $750 judgment (perhaps influenced by the fact that this was the initial offer of administrative settlement) and stated that it was:

> "...unable to accept the expert opinion that the booms did not cause plaster damage and glass breakage.
>
> "...Perhaps the most compelling influence on this Court's rejection of the expert opinion regarding plaster and glass damage is the apparent distinction between cause and effect as viewed by scientists and legal causation. Although Dr. Wiggins and the various test reports acknowledge the triggering and accelerating effect of sonic booms, from a scientific standpoint these do not seem to be considered a cause. For example, in discussing a window broken by a boom of very great strength...the window did not break because of excessive pressure per se, 'but because the window, which was opened at the time, was slammed by the boom and the slamming broke the window. Throughout the reports...this type of approach to cause and effect is apparent. But this type of cause is not the same as proximate cause, which is the efficient cause, or the one which necessarily sets in operation the factors which accomplish the damage. Applying this test, I conclude that the sonic booms did cause plaster and glass damage to plaintiff's building." (10 Avi. 17,271, 17,276)

However, another court did accept the uncontradicted expert testimony of the same Dr. Wiggins. Several homeowners (Lorick et al, v, US (DC, SC, 1967) 267 F. Supp. 96; 10 Avi. 17,412) with relatively new houses, alleged hairline cracks in brick and mortar, bathroom tile, concrete foundation, and damage to a pond and damsite, as a result of three military aircraft flying sub-sonically on 20 July 1963, at about 200-300 feet above ground so that their markings were clearly visible. At the time of overflight an explosive sound was heard. No glass breakage was alleged. The expert testimony included statements that such traffic would produce noise and rattling, but no damage; that the human being is sensitive to some vibrations to which structure is not; and that "the lowest threshold of damage to a building from a sonic boom is the shattering or breaking of glass windows and the causing of bric-a-brac...to fall." It was concluded that such pressure would not produce cracks in concrete block or exterior wall and that the cracks in the pond were probably caused by dry weather resulting in shrinking of soils in the damsite. There was a failure to prove causal connection between overflights and property damage.

Several cases of structural damage resulting from the FAA-USAF Oklahoma City sonic boom test program of 1,253 flights during the six month period 3 February to 30 July 1964 have aroused special interest. From the inception of the tests, the U.S. position was to pay for any damage administratively and from the inception of litigation, to pay for any damage which could be shown was a result of the program. Therefore, the U.S. did not judicially assert defenses normally available to it under the Federal Tort Claims Act, but limited argument to causation, and, if causation be found, to the amount of damages. One class action, on behalf of residents and property owners (Bennett v, U.S. (DC, WD, Okla., dismissed 29 Aug. 1965) 266 F. Supp. 627, 10 Avi. 17,410) claimed that the U.S. had taken a temporary avigation easement over their property and that of all the residents of Oklahoma City and asked unspecified monetary compensation. Another class action (Gravelle v, U.S. (USDC, WD, Okla. 14 April 1967) heard on appeal, 10th CCA, 19 Nov. 1968) for structural damage, on behalf of 97 property owners, who made individual judicial claims in amounts from about $100 to $9,000+ for a total of $123,257, continues in litigation after a judgment favorable to the property owners, on appeal by the U.S. Almost all of these individuals had filed administrative claims with the USAF which were denied on the grounds that the facts did not substantiate sonic boom as a cause of damage. Another suit (Liberty Bldg. Corp. v, U.S. (USDC, WD, Okla.)) alleging damage to a building and glass breakage in the amount of $5,439 as a result of these tests, is being delayed pending the results of the Gravelle case. In two other federal court cases from the Oklahoma City tests, decided by jury, two opposite results obtained. One (Smith v, Valley Forge Ins. Co. & U.S. (USDC, Okla., 17 Feb., 1967)) asked damages in the amount of $40,000; the issue was whether cracks in masonry walls of a house was due to sonic boom activity and whether it was in the terms of an insurance contract. There was a thorough defense with comprehensive, detailed explanation of sonic booms, over-pressures, how created, energy involved, soil mechanics and effect of booms on structures and buildings in the Oklahoma City area. The plaintiff testified that the cracks did not exist prior to the start of the tests but developed during the course of it. The jury was unconvinced by the expert, chose to believe the plaintiff and awarded him $10,000. In a parallel case (Beckham v, Hartford Fire Ins. Co. (USDC, WD, Okla., 21 June 1967)) the only issue was causation. Damage, alleged in the amount of $18,984 was essentially the same type: massive cracking of foundation, cracks in brick veneer, plaster cracks, roof damage and broken glass, but the jury verdict was in favor of the U.S. on the evidentiary conclusion (after hearing the same expert witness as in Smith) that the damage claimed resulted from weathering, aging, expansion and contraction of soil and possibly earthquake tremors in the early 1950's.

A recent carefully considered case (U.S. v. Hartman (DC, Calif. 1967) Civil No. 62-730, 31 Oct., 1967) for structural damage was decided for the U.S. on failure of the plaintiff "to prove causation, negligence or government connection with the sonic booms." The structure was a 35-year old stucco house in Hollywood; the owners heard and felt sonic booms which were, in fact, recorded on a California Institute of Technology micro-barograph, in Pasadena, several miles distant. The owners reported seeing the "smoke trail" of the aircraft and the court calculated, on the basis of meteorological data and the fact that since the width of the sonic boom trail or carpet is about 2-1/2 times the altitude of the plane, with a 20 mile lateral spread, the altitude of the aircraft was about 40,000 feet. The damage to the house, apparent from photographs and the judge's personal examination, included a two-inch separation of a porch, cracks in concrete steps and interior ceilings, cracks in interior concrete floors and broken windows. The court could have disposed of the case on the failure to establish that it was a U.S. aircraft; however, it concluded that the damages were the result of natural forces, progressive and continuous, before and after the boom. Adhering to engineering findings and utilizing the results of a decade of sonic boom research, the court held that the nature of the damage could not have been caused by a sonic boom as "concrete is too strong a material to be damaged by sonic booms, and...no damage to concrete had occurred in any test program." In its findings of fact, the court stated:

> "7. The overpressures resulting from the sonic booms in question were about one pound per square foot.
>
> "8. A sonic boom can cause damage to a structure. However, not all booms can cause all types of damage. Sonic booms of certain magnitudes are capable of causing certain types of damage. Different structural elements have different thresholds of damage. The threshold for glass is lowest, with higher overpressures being required to cause cracks in plaster, movement of bric-a-brac or loose objects, cracks in gypsum board ('sheetrock'), or damage to other stronger materials.
>
> The threshold for sonic boom damage represents the level at which incipient damage occurs, and to cause more than, for example, an extension of an existing crack, significantly higher over-pressures are required. The type of material which is damaged is also highly significant when considering whether the cause of the damage was sonic boom. For example, in all the scientific sonic boom test programs the government has conducted, no damage to concrete has occurred, regardless of the magnitude of the sonic boom.
>
> The scientific research relating to structural response to sonic boom has shown the threshold for all materials to be in excess of five pounds per square foot. Glass damage has a minimum threshold of about 7.9 psf per square foot, with 6.5 psf being the lowest level at which an existing crack in glass has been extended. The threshold for extending existing cracks in stucco, bathroom tile, or sheetrock is about 7.9 psf. The threshold for incipient plaster damage on various types of lath is about 10 psf. These threshold figures for the slightest damage when compared with the one psf figure and the gross damage involved in this case show that sonic boom could not have caused the damage in question.
>
> The type of damage which sonic boom is capable of causing is of a limited nature. The damage occurs, if at all, simultaneous with the boom. Damage occurring after or continuing after a sonic boom has no causal relationship with the boom. The cracks which sonic boom can cause are small, hardly discernable, hairline cracks. If a crack is larger than this, sonic boom is disproved as a possible cause."

SONIC BOOM CASES: HUMAN: There have been relatively few cases of actual physical injury adjudicated as a result of sonic boom activity. Of these few, the most prevalent are those of individuals injured by falling or flying objects or glass splinters. The occasional claims for hearing loss, nervousness or shock, without some physical contact, have not been favorably considered by the USAF. Between July 1966 and March 1968, ten such claims were processed by the USAF for a total amount of $261,000; of this amount one single claim for $200,000 was disapproved. Of the ten only three were paid in a total amount of $1,850.74 and two of the three involved persons cut by glass broken as a result of a sonic boom. It is Air Force experience to date that approximately 1 in 1,000 claims presented is for personal injury, with an approval rate of about 6%.

Mrs. Adeline Huslander (Huslander v. U.S. (USCD, WD, NY, 1964) 234 F. Supp. 1,004; 9 Avi. 17,288) was kneeling on the floor of her home in Elmira, New York on 13 January 196. when a sonic boom allegedly broke a window pane near her, causing her personal injury. Her demand was denied administratively and she sued under the Federal Tort Claims Act, again losing on the ground that the supersonic flights were within the discretionary function or duty exemption of the Act, as the USAF aircraft interceptor supersonic flights were simulating wartime defensive situations for training purposes. The court added that

> "...while this decision points up the necessity for alternative means of honoring valid claims against the Government, it also avoids a quagmire of varying results under the Federal Tort Claims Act which is dependent upon local law."

During the Oklahoma City tests a plaintiff alleged that he cut himself with a razor while shaving during a sonic boom occurrence; that shock waves damaged property and affected health and well being; that under state law the flights were a continuing trespass and public nuisance; that the tests offended due process and violated constitutional rights. The defendant U.S. Government denial included a statement that such claims were compensable and could be satisfied in monetary damages. The state court granted plaintiff a temporary injunction against the tests; this was vacated on removal of the case to a federal court; on an expedited appeal, the matter was returned to the lower federal court for testimony on the evidence (Coxsey v. Hallaby (CCA, 10th, 17 July 1964) 334 F. (2d) 286). The appellate judge added that "Speaking generally, the public must submit to inconvenience and discomfiture caused by legitimate governmental activities which do not offend constitutional requirements." (at 287). On rehearing, plaintiff failed to prevail (Coxsey v. Hallaby (DC, Okla., 6 Aug 1964) 231 F. Supp. 978). The court held that the FAA was authorized by statute (49 USC Sec 1353(b)) to conduct tests on improved aircraft, such as the SST; that the statute was not "unreasonable, arbitrary or capricious;" and that the means (i.e., tests) had "real and substantial relation to the object sought to be obtained;" and that there was no denial of due process. The judge stated that sonic booms had not caused physical or mental harm to the plaintiff or others, and

> "...Furthermore, this testimony established that tests neither did, nor could, aggravate or precipitate any pre-existing or latent physical, mental, psychological or neurological condition of these residents." (at 980)

The opinion concluded that there was a lack of jurisdiction as the government had not consented to suit; even had the court had jurisdiction the plaintiff failed to establish personal physical damage or other irreparable injury but had an adequate remedy at law and no right to equitable relief.

Other Oklahoma City cases included: an allegation that the plaintiffs were being used as unwilling guinea pigs in the tests in violation of Constitutional rights and that the booms impaired the hearing of a child and aggravated an existing inner ear condition of the father (Bussey v. Hallaby (USDC, WD, Okla. filed 14 Feb 1964; dismissed 28 March 1964)); a request that tests be enjoined as they caused damage to the plaintiff's home and health (Lashley v. FAA & Dept. USAF (USDC, WD, Okla) filed 27 Feb 1964; dismissed 13 March 1964); and another attempt by Mr. Bussey, having failed to have the tests stopped, asking monetary damages in the amount of $101,250 alleging he and his daughter had sustained profound mental and physical damages as a result of the booms, losing a second time for failure to plead the proper party (Bussey v. Lyndon Baines Johnson, President, U.S. (USDC, WD, Okla, filed 12 June 1964; dismissed 15 Aug 1964). None of these three latter cases were heard on the merits nor was there consideration of the issue of actual physical harm to the individuals. In America in the field of community problems an equity suit for injunctive relief has sometimes been used rather than the filing of a legal action for monetary damage.

Arousal from sleep, particularly with daytime sleepers, causing insufficient rest and relaxation leading to reduced efficiency, health and well being has been of increasing concern in connection with the possibility of frequent sonic booms. Of special interest is the possible startle reaction of noise as it relates to such activities as the operating surgeon, the munition hand loader, or the girder-striding construction worker. Based on present evidence, sonic booms generated by commercial supersonic aircraft flying in accordance with preplanned flight profiles are unlikely to cause any direct damage to human hearing. Considerable field testing has been accomplished on the effects of certain limits of sonic booms on human reaction, but more work needs to be done to determine sonic boom thresholds of human annoyance.

From trends in the aircraft noise abatement field, courts may in the future draw analogies for use in sonic boom litigation. The following three cases serve as examples.

A California Superior Court (New York Times, 2 July 1968) ruled invalid a Santa Monica (near Los Angeles) city ordinance barring jet aircraft takeoffs between 11 p.m. and 7 a.m. without special permission. These conglomerate (232 families) jet noise suits totaling $12.5 million against the city are to be processed on the sole basis of property damage claims (Aviation Daily, 23 Oct 1968, p. 282).

Another clue to possible future handling of sonic boom claims may be seen in a related noise problem of surface transportation. The New York Court of Appeals in a decision (Ira and Dorothy Dennison v. New York, Judge Keating presiding, New York Times, 2 July 1968, pp. 37 and 70), not otherwise prevailing in other jurisdictions, awarded a $37,000 judgment to a property owner of a colonial home in a remote wooded, essentially resort lake area of the state, not for loss of privacy, seclusion or view, but solely for traffic noise from the construction of a nearby freeway interchange. The state, presumably, will appeal. Accommodation is the major clue and premise here; it remains a community problem without definable criterion, save public interest.

Also, of possible import to future sonic boom suits is a case favorable to aviation operators and airport owners which, essentially, held invalid a 1964 Unnecessary Noise Ordinance of the City of Hempstead, Long Island, aimed at jet aircraft from Kennedy International Airport; the 150,000+ residents of Hempstead live within three miles of the airport. After 4,000 pages of testimony, affidavits and exhibits (American Airlines, Inc., Port of New York Authority, Ruby et al v. Town of Hempstead (USDC, ED, NY, 1967) 272 F. Supp. 226, 10 Avi. 17,337) the District Court held (30 June 1967) the airlines entitled to a preliminary injunction against enforcement of town ordinance stating:

> "...air transport, and particularly long distance air transport, is not an optional alternative to ground and water transport but is indispensable." (10 Avi. 17,337, 17,338-9) and "The dimensions of the noise problem cannot be minimized. It is, however, one of the manifold of environmental problems that press on a society in which the pace of industrialization steadily outstrips the capacity to deal with its modification of the total environment of urban and suburban existence. Perhaps the aircraft noise problem differs in that it appears to be unavoidable, in the present stage of technical development, and not a consequence of the failure to take feasible precautions or to provide practical remedies." (10 Avi. 17,337 at 17,339).

It was held that the ordinance was not an exercise of landowners rights or concepts of trespass or nuisance but an exertion of police power. The order granting the preliminary injunction was affirmed 17 July 1968 (American Airlines, Inc. et al v. Hempstead (2nd CCA, 1968) 398 F. (2d) 369; 10 Avi. 18,029); the U. S. Supreme Court denied certiorari (New York Times, 14 January 1969).

Reasonableness and relativity are the key. Favorable to airline operators is the language in the Neher case, mentioned earlier, in regard to structural damage. In regard to noise annoyance the court stated:

> "...plaintiff's complaint is not that the aircraft invaded her property, but that they generated noises, shocks and vibrations which did descend upon the building. Without a physical invasion by low and frequent flights directly and immediately interfering with the use and enjoyment of the land, these annoyances are not compensable under the Fifth Amendment...(Citing earlier cases...) the court indicated that the interference with plaintiff's property was consequential damages and not a taking. Further, the court said sound waves, shock waves, and smoke pervade property neighboring that on which they have their source but the disturbance caused thereby is only a neighborhood inconvenience..." (Neher v. U.S. (USDC, Dist. Minn. 1967) 265 F. Supp. 210).

Although many additional cases involving disposition of damage suits due to other forms of transportation noise could be cited, these cases, briefly described, demonstrate clearly the need for the sonic boom legal specialist to analyze and weigh the points at issue and the decisions rendered by the courts in parallel legal fields if he is to foresee possible trends in the disposition of cases involving possible sonic boom damage.

LEGAL PORTENTS: Space limitations preclude any further delineation of sonic boom and related aircraft noise cases involving individuals, communities, structures and animals, etc., useful and interesting as these are to a comprehensive understanding of sonic boom legal trends in America. There is another facet of the problem, however, which must be at least touched upon because of its longer term impact on the law. Because public interest and reaction to more effective guidance and control of the transportation system as a whole was steadily increasing, the U. S. Congress enacted, and the President approved, legislation in October 1966 creating the Department of Transportation. Among other things, the general provisions of this legislation defined the duties of the Secretary of the Department and charged him with a responsibility to..."promcte and undertake research and development relating to transportation, including noise abatement, with particular attention to aircraft noise..." (PL 89-670; 80 Stat. 933 (Sec 4(a))). The Department has interpreted aircraft noise to include the sonic boom. Supersonic flight time (now in excess of 400,000 supersonic engine hours) is also a small but important fraction of the total U.S. Military aircraft flying hours logged since 1956.

As Congressmen and Senators continued to hear more and more often from their constituents on the impact of jet aircraft noise around the larger commercial airports of the nation, the need for additional legislative action became more apparent. Following public hearings in the summer of 1968, the House of Representatives, by unanimous vote, and the Senate, by a large majority, sent to the President for signature legislation (PL 90-411; 82 Stat. 395) which amended the Federal Aviation Act of 1958 in part as follows:

> "Control and Abatement of Aircraft Noise and Sonic Boom
> "SEC. 611 (a) In order to afford present and future relief and protection to the public from unnecessary aircraft noise and sonic boom, the Administrator of the Federal Aviation Administration, after consultation with the Secretary of Transportation, shall prescribe and amend standards for the measurement of aircraft noise and sonic boom and shall prescribe and amend such rules and regulations as he may find necessary to provide for the control and abatement of aircraft noise and sonic boom, including the application of such standards, rules, and regulations in the issuance, amendment, modification, suspension, or revocation of any certificate authorized by this title."

Since enactment, the Department of Transportation (DOT) and the FAA have mounted a considerable effort to comply with the law.

Since today's proposed legislation can become tomorrow's law, it is of special interest to note what Federal legislators have recently proposed which could have direct impact on sonic boom law of the future or indirectly could effect such law through legislative impact on the commercial supersonic

transport program itself. Indicative of the tenor of the times are several bills which have been introduced into "the hopper" of the current session of Congress (1st Session, 91st Congress), the following bills are the same or similar to earlier bills, introduced but not acted on, during the last Congressional session. Because of their potential significance, key sections of these bills are quoted below although no attempt will be made to cover all points or provisions of these bills. On 27 January 1969 Mr. Brown of California introduced H.R.4565 into the House, "A bill to establish a sonic boom damage fund to provide payment of damages caused by sonic booms. The bill to be known as the "Sonic Boom Damage Recovery Act," was referred to the House Committee on the Judiciary. The bill states in part:

> "SEC.2. The Congress hereby finds that the Nation is entering into a new era of aviation development of profound significance, the era of supersonic aircraft. Recognizing the lessons of the past from the unexpectedly rapid growth of subsonic aircraft and the environmental and noise problems thereby created, the Congress finds that it is necessary to provide adequate means for the recovery of damages for personal injury or death and for injury or loss of property caused by sonic boom. It is additionally the hope of Congress that legislation providing for recovery of damages for injuries and losses caused by sonic boom will also serve as an incentive to those entrusted with the final development of supersonic aircraft to incorporate such engineering features as may be available to reduce the incidence of sonic boom and thereby prevent undue noise and boom problems in populated areas..."
> and
> "SEC.4.(a) If there is any injury or loss of property, or any personal injury or death, caused by a sonic boom resulting from the operation of any aircraft within the United States, money damages shall be paid to any claimant in an equal to the money damages which would be payable to such claimant if such injury, loss, or death had been caused by a negligent or wrongful act or omission of the owner or operator of the aircraft at the place where the injury (including an injury resulting in death) or loss occurred. Such compensation shall be paid out of the sonic boom damage fund provided for by section 6 of this Act..."
> and
> "SEC.5.(a) Payments. The owner or operator (including any government other than the United States) of every supersonic civil aircraft which -
> (1) carries persons or property (including mail) for compensation or hire, or
> (2) is operated in the conduct or furtherance of any business or vocation
> within the United States or between any place in the United States and any place outside thereof shall pay to the United States, with respect to the operation of such aircraft within the United States, for deposit in the fund, the amount determined pursuant to subsection (c)."

This bill then describes how the sonic boom damage fund is to be created, maintained, managed and safeguarded.

On 7 February 1969 Mr. Javits of New York, on behalf of himself and other Senators, introduced S.942 in the Senate, "A Bill to amend the Federal Aviation Act of 1958 in order to provide for regulation of public exposure to sonic booms by certain aircraft over the United States." The bill which was referred to the Senate Committee on Commerce states in part:

> "Regulation of Sonic Booms. The Administrator (FAA) shall (1) prohibit nonmilitary aircraft, singly or in any combination thereof, from being operated over the United States (including territories and possessions thereof) in such a way as to produce sonic booms, but such prohibition shall not apply to aircraft used in the investigation and study herein authorized; (2) conduct a full and complete investigation and study for the purpose of determining what exposures to sonic booms (amount and frequency) are detrimental to the health and welfare of any persons,..."

The bill then calls for the Administrator, Federal Aviation Administration, to consult with several other interested Cabinet members, the Administrator of NASA and the President of the National Academy of Sciences and to carry out an investigation and study for the purpose of submitting a preliminary report to Congress in one year and a final report in two years after enactment.

Regardless of future Congressional action on these bills, their very existence is noteworthy particularly in view of the recent Federal legislation creating a Department of Transportation (one of whose specific responsibilities is to "promote and undertake research and development relating to transportation including noise abatement, with particular attention to aircraft noise,") and the more recent specific law concerned with "Control and Abatement of Aircraft Noise and Sonic Boom." The Congress is clearly demonstrating a real and continuing concern in the potential impact of the boom.

For many years prior to the Congressional actions described above had transpired, the FAA, NASA, and the USAF had worked cooperatively in seeking to understand the sonic boom and its impact on people, animals and structures. Although much useful information had been obtained as a result of continued research and field experiments, studies by the National Academy of Sciences Committee on SST-Sonic Boom, the Department of Transportation's Interagency Noise Abatement Program, the Federal Aviation Administration's office of Noise Abatement and other groups in 1967 and 1968 were used by DOT/FAA to establish an intensive three-year sonic boom research program involving a total of $6,525,000 (Congressional Record, 11 July 1968, S8530). Of this total the FAA Fiscal Year 1969 program planning called for an expenditure of $2,025,000 for several new projects (ibid). This amount is in addition to important sonic boom research being conducted in NASA laboratories and several significant University sonic boom research efforts funded by NASA.

The results of earlier, current, and proposed sonic boom research should go far in providing a sound basis for DOT/FAA to comply with its Congressional edict to "...prescribe and amend standards for the measurement of...sonic boom and...prescribe and amend such rules and regulations as... necessary to provide for the control and abatement of...sonic boom..." (82 Stat. 395 (Sec. 611 (a))). In fact it is to be hoped that sonic boom research efforts of interested nations can continue to be fully and freely exchanged as is being so ably accomplished by this Joint Panel meeting of AGARD if standards of measurement and control and abatement of the sonic boom when finally accomplished are to be generally acceptable worldwide.

SUMMARY: In brief, this paper has attempted to provide some background on the sonic boom in the United States; a summary of the administrative history; procedures and guidelines used by the USAF in its handling of large numbers of sonic boom claims; a series of court cases resulting from sonic booms generated by military aircraft to provide an indication of judicial trends; the continuing interest of Congress in the sonic boom; and a recent action taken by DOT/FAA that should lead to improved data on which rules and regulations pertaining to the sonic boom can be based. Space does not permit consideration of all the other factors which will also determine in part the impact of the sonic boom on the future of commercial supersonic flight over the United States.

In closing, I trust this paper clarifies how the Courts in the United States attempt to render substantial and rational judgments on military sonic boom experience and its legal consequences, administrative and judicial, within the terms of existing legislation, at least, until such time as the legislative process accommodates the public interest in new ways. As public awareness of noise and its impact on society grows, transportation systems on which the public depends must attain acceptable noise levels in their operation or suffer the inevitable results of an aroused public consciousness.

BLANK PAGE

AIRPORT DESIGN AND OPERATION FOR MINIMUM NOISE EXPOSURE

by

Isaac H. Hoover
Office of Noise Abatement

and

Donald G. Cochran
Airports Service
Federal Aviation Administration
Washington, D.C.

Summary

Regulatory action in a number of countries and standards in the International Civil Aviation Organization (ICAO) will result in significantly reduced maximum noise levels for new aircraft entering the world's air carrier fleets. Modifications to many of the existing aircraft can be made to significantly reduce their noise output within the next few years. Alleviation of the aircraft noise problem requires that new airport designs and modifications to existing airports be tailored to take maximum advantage of the potential noise reductions soon to become available. This paper examines the expected noise exposures to be generated by commercial aircraft operating in the next decade and reviews significant considerations in the location of new airports, the land requirements of existing and new airports as a function of the type service, and airport design in terms of runways and necessary support facilities to minimize noise exposure. The potential of existing and developing operational practices and restrictions to minimize noise are assessed. Finally, the forecasting of aircraft noise exposure near airports and its relationship to the development of compatible land use programs and public relations/education programs are discussed.

AIRPORT DESIGN AND OPERATION FOR MINIMUM NOISE EXPOSURE

I. INTRODUCTION

The rapid growth of air commerce in the United States since the end of World War II, and in many other countries as well, has resulted in the development of strong public reaction to the increasing noise exposure near busier airports. The market growth rate has outpaced the development of new airport capacity and attempts to develop needed capacity are frequently inhibited by public fear of and opposition to the noise exposure which normally follows the construction of new runways and/or airports.

Under current United States judicial decisions, a landowner in the vicinity of an airport may recover compensation for interference with the reasonable use of his property caused by aircraft noise. In the case of social costs, however, they are generally neither recognized nor reimbursed and that inequity is a root cause of the noise problem which has developed near most major commercial airports in the world today. Social costs are not measurable in dollars and consequently difficult to reimburse.

Engine noise reduction technology is advancing rapidly and offers, for the first time, the promise of practical and significant reductions in areas affected by noise. This paper first examines the noise reduction potential available through technology and operating procedures. It then relates the remaining or residual noise exposure to the design and operation of airports to show how the undesirable social impact of civil aircraft can be minimized.

The discussion in this paper is based on a number of fundamental premises:

a. That modern societies have come to recognize the social and economic benefits of commercial air transportation as essential, rather than merely desirable.

b. That flight vehicles which provide such transportation presently adversely affect the environment around airports with noise and soot, inflicting social and, sometimes, economic costs on communities near airports.

c. That noise exposure should be reduced to the practical minimum because it both degrades our environment and inhibits the development of new airport capacity necessary to accommodate the rapidly expanding demand for air transport.

d. That if economic or social costs must be imposed on an airport's neighbor so that the benefits of air commerce may be made available to the entire metropolitan area served by the airport, and to the aviation system, in general, then those costs should, in some manner, be recognized and reimbursed. (In the United States, the courts have placed liability for aircraft noise on the airport operator who,

in determining the type of service to be provided, brings the noise to the nearby communities and effectively determines what the noise levels and total noise exposure in those communities will be).

II. NOISE LEVELS

Ten years ago, a revolution in commercial air transportation began with the widespread introduction of turbojet powered civil aircraft. At about the same time, turbo-propeller aircraft were introduced, but the passenger preference for the jets with their faster, smoother, and quieter ride was soon evident. The jets, though quieter inside than propeller aircraft, generally created considerably higher noise levels during flight operations around airports and during maintenance activities on the ground. Vast sums were spent on the development of suppressors to achieve large reductions in the jet exhaust noise without imposing large performance losses, but the manufacturers were, in general, unsuccessful in both instances.

Low bypass ratio turbofan engines soon replaced the pure turbojet engines on new production aircraft, because they offered greater efficiency and, in most cases, slightly lower noise levels, particularly on takeoff. The jet exhaust noise was reduced some, but the fan generated more noise at the front of the engine than had the earlier compressors. In general, acoustical treatment and jet exhaust suppressors were not used on those engines even though such devices were occasionally developed and, at least in one case, offered to airlines as a sales option.

In the past five years, noise reduction technology has developed at an impressive pace. During the same period, engine technology advanced to the point where large high bypass engines are being developed to power a complete new generation of larger, more efficient aircraft. Those aircraft, which will supplement the existing fleet and replace certain elements of that fleet, offer the potential of significantly reduced noise levels during all flight and ground operations. The noise reductions will come primarily from three sources: (1) reductions in the jet exhaust noise; (2) reductions in fan inlet and exhaust noise through detail design; and, (3) reductions in remaining turbo-machinery noise through extensive use of acoustical treatment in the nacelle inlet and fan ducts, in the engine fan section, and possibly in the tailpipe area.

Aircraft noise certification standards being developed in the United States and a number of other countries will assure that the lowest levels practicably attainable will be achieved. Action in the International Civil Aviation Organization (ICAO) is expected to follow and result in the development of compatible international noise certification criteria. There will, of course, be a cost associated with achievement of the lowest practicable noise levels; however, the new high bypass ratio engines represent such an improvement that the "quiet propulsion systems" should still be 20 percent more efficient than their predecessors.

Future Subsonic Aircraft

Noise certification plans under consideration in the Unites States, the United Kingdom, and France, define three measurement points at which specified noise limits should be met: (1) 1.0 nautical miles

from the runway threshold on approach; (2) 0.25 nautical miles to the side of the runway centerline during takeoff; and (3) 3.5 nautical miles from the start of the takeoff roll under the takeoff flight path (Figure 1)

Figure 2 shows the maximum noise limits as a function of certificated gross weight proposed by the Federal Aviation Administration for adoption in the United States (Reference 1). The maximum noise levels decrease from 108 EPNdB as aircraft decrease in size from 600,000 pounds certificated takeoff weight to lower values at the lower cutoff certificated weight of 75,000 pounds.

The decreasing levels reflect the reduced thrust requirements for the smaller aircraft as well as the reduced number of engines and the resulting increase in takeoff performance capability.

In showing compliance with certification criteria, the maximum values must not be exceeded under a difficult combination of circumstances (maximum takeoff weight, hot day, no wind), so the average takeoff noise levels should be lower in actual day-to-day scheduled operations.

The unit of noise used throughout this paper is the "Effective Perceived Noise Decibel" (EPNdB) as defined in "Aircraft Noise Evaluation," Federal Aviation Administration Report No. FAA-NO-68-34, September 1968 (Reference 2). This unit is recommended as the most appropriate unit for evaluation during noise certification of new aircraft. It has also been used as the basis for calculating Noise Exposure Forecasts-NEFs (cumulative noise exposure) in the United States.

Present Subsonic Aircraft

The existing air carrier fleet for which data under the conditions specified in the proposed United States noise certification rule (Reference 1) are available, create noise levels as shown in the upper shaded bands of Figures 3 and 4. The crosses represent approximate noise levels of a few popular executive jets used in the United States. The maximum noise levels proposed in the rule are also plotted for reference. Very little reliable data on sideline noise values under the conditions specified in the rule exists.

Present Subsonic Aircraft Modified

During the past three years, intensive research and development has been conducted in the United States on acoustical treatment which could be installed in engines and nacelles to absorb part of the turbo-machinery noise before it is emitted from the aircraft. This effort has been unusually rewarding, particularly in relation to the absorption of the most annoying pure tones generated by turbofan engines. A National Aeronautics and Space Administration (NASA) sponsored flight demonstration program, using a Douglas DC-8 with modest acoustical treatment in the nacelles and a Boeing 707 with considerably more treatment, successfully demonstrated the effectiveness of such treatment in flight. The lower shaded bands on Figures 3 and 4 represent the levels to which the existing turbofan powered fleet could be reduced if efficient acoustically treated nacelles were installed on those aircraft.

Studies of achievable noise reductions, the servicability of acoustical treatment, and the impact of acoustically treated nacelles on operational efficiency and operating economics are underway at the present time. If it is determined that the installation of acoustically treated nacelles on the existing air carrier fleet is technically practicable, economically reasonable, appropriate to the particular type, and in the public interest, the Federal Aviation Administration will propose rulemaking action to require such modification to the United States air carrier fleet on the fastest practical schedule. Estimates of the time required for a complete fleet retrofit program indicate that such a program could be completed by the end of calendar year 1973. It is recognized that pure turbojet powered transports are not amenable to such large noise reductions short of both reengining and the addition of new acoustically treated nacelles. Modifications of that magnitude on airframes nearing the end of their useful life are generally considered impractical.

Future Supersonic Transports

Developers of all supersonic transport aircraft are faced with two critical problems - range and noise. All supersonic transports in the foreseeable future will generate high noise levels during the initial takeoff operation when afterburning thrust is used. It is expected that the maximum noise levels proposed for subsonic transports at a .25 nautical mile sideline distance will extend to approximately one nautical mile for supersonic transports. Prior to over-flying noise sensitive areas, they will be required to make thrust reductions which will result in large reductions in the jet exhaust velocity and resulting noise levels. All supersonic transports have controllable inlets which provide the potential for "choked" (sonic velocity) flow to control forward radiated noise on approach and after thrust reduction on takeoff.

The difficult decision that the supersonic transport designer must face is that of whether or not to put a horizontal tail on the aircraft. A tail carries the disadvantage of a drag penalty in cruise thereby intensifying the range problem which is critical for all supersonic transports. The horizontal tail, however, offers the designer the distinct advantage of being able to balance aerodynamic moments, thereby permitting the installation of high lift devices on the leading and trailing edge of the wing. The resulting improvement in low speed aerodynamic performance permits supersonic transports with horizontal tails to achieve approximately the same approach and takeoff flyover noise levels as proposed for subsonic transports in Reference 1.

There is little doubt but that supersonic transports will be restricted to those airports where their noise characteristics are acceptable. The developers are then left with the difficult choice of increasing the number of airports they can serve (and their potential market) by achieving lower noise levels and paying a price in range, or achieving the longest range possible (to develop a larger potential market) and pay a price in being restricted to service at a smaller number of airports in any geographical area.

Figure 5 shows the approximate 105 PNdB takeoff noise contour for the United States prototype SST using the engine presently being developed under a Federal Aviation Administration contract. The dashed line represents the 105 PNdB contour for subsonic intercontinental Boeing 707. Based on data furnished by the developers of the Concorde, that aircraft's 105 PNdB contour is expected to fall slightly inside the SST contour except that it would not close at 3.5 miles but would have a trail extending in the direction of the takeoff similar to that of the Boeing 707. Developers of the Concorde and the United States SST have aggressive noise reduction programs underway in an attempt to reduce the noise levels of their aircraft and production versions may possibly demonstrate smaller contours.

Military Aircraft

Military aircraft sometimes share use of airfields with civil aircraft but more frequently are operated from exclusively military airfields. The noise characteristics of some operational United States military aircraft are depicted in the Technical Report "Land Use Planning Relating To Aircraft Noise" (Reference 4). Noise levels for more modern aircraft would have to be obtained from the military services which use the particular types for which data is desired. It should be noted that low noise levels are not a design objective for which operational penalties are paid on most aircraft in military inventories.

VTOL and STOL Aircraft

Large vertical and short takeoff and landing aircraft will someday come into widespread use, particularly for short range service (less than 500 miles) in areas of high population density if their designers can produce aircraft that are safe, have high cruise speeds, reasonable operating costs, and noise characteristics that will be accepted by neighbors of small "city center" airports from which they must operate. The noise requirements for such aircraft have not been established; however, it is obvious that verti-port or STOL-port noise requirements must be sufficiently strict that VTOL and STOL aircraft will impose no significant increment of noise exposure when operated into and from airports served by conventional air carrier aircraft (Reference 3).

Intensive evaluation of a number of STOL configurations using various propulsion cycles has been underway for the last few years in Europe and the United States. It appears that smaller, quieter propeller-driven aircraft should be able to operate from STOL-ports build over railroad yards and along certain rivers without exposing the noise sensitive neighbors to unacceptable levels of noise. However, even the quietest larger aircraft (100 to 150 passengers) driven by propellers would probably be restricted to those STOL ports having relatively large areas around them insensitive to noise. Configurations without propellers generally appear to be approximately 10 EPNdB noisier than those with propellers (on the logarithmic scale used to measure and evaluate noise, a reduction of 10 dB requires that approximately 90 percent of the noise energy be eliminated).

III. NOISE EXPOSURE FORECASTING

The development of new airports or new or extended runways on existing airports requires that the cumulative (total) noise exposure from projected operations be defined if the noise pollution resulting from the new development is to be identified and minimized. A number of adequate and very similar systems for describing noise exposure have developed in the United States and Western European countries (Composite Noise Rating-CNR; Noise Number Index-NNI; Q-Rating; Noise Exposure Forecast-NEF; etc.). The United States is in the process of transitioning from use of the Composite Noise Rating (Reference 4) to the Noise Exposure Forecast (Reference 5) system which is conceptionally identical but incorporates three improvements: (1) the EPNdB replaced the PNdB as the unit for describing a single flight noise exposure; (2) the total exposure from all operations and the penalty for night operations is calculated in smaller increments; and (3) the numerical scale is changed to avoid confusion between single flight noise level rating and the cumulative noise exposure ratings. Additionally, the interpretation of Noise Exposure Forecasts in terms of compatible land uses is being signigicantly improved to provide a more useful tool for the development of zoning and land use or land conversion plans. We have also found the Noise Exposure Forecast a useful tool in evaluating the effectiveness of proposed operational procedures, hardware changes, and regulations (Reference 6).

The Noise Exposure Forecast is usually plotted in a series of at least five contours of equal noise exposure, five units apart around the runways for which traffic is projected. There is a tolerance on the accuracy of the contour lines but, in general, they portray a fairly reliable picture of gradually decreasing noise exposure as they are crossed going away from the runways (Figure 6). Given a situation where an average airport was surrounded by level terrain on which an average mixture of residences were populated by average people with average living habits in their area which has average weather conditions, etc.; it might be fair to say that the critical zone in which people should not live is bounded by the 40 Noise Exposure Forecast contour and the noise affected area was bounded by the 30 Noise Exposure Forecast contour. Naturally, that hypothetical situation does not exist anywhere and, in real life, a number of significant factors are present which require adjustments to or selection of different contours when developing land use (zoning) plans and planning suitable airport boundaries.

Terrain near airports frequently slopes, occasionally has topographical features which can focus or shield sound, or has large areas of water which affect sound transmission. General weather conditions can vary frequently or seasonally and specific conditions such as temperature, humidity, winds, inversions, etc., effect noise exposure. The sound attenuation qualities at residences vary considerably with the type of construction, whether they are multiple or single family dwellings, and other features such as air conditioning.

People also vary considerably in health, patterns of living, activities, individual sensitivity to noise, affluence, and other factors which effect their reaction to noise. The most annoying characteristics of aircraft noise, however, seem to nearly always be interference with communication

(face-to-face, telephone, radio, television, etc.) and interference with sleep. There are, of course, many noise sensitive uses of land near airports other than residential.

Factors which complicate the interpretation of Noise Exposure Forecasts in terms of compatible land uses and public reaction are mentioned to make it clear that all airports require individual analysis if meaningful land use programs are to be developed.

Type Service

An early step in development of any airport is the determination of the type and amount of service that will eventually be offered from the airport at that point in the future for which plans are being made. For noise purposes, the most useful definition of type service is in terms of flight length. This is because the flight length generally determines the performance characteristics of the aircraft which will determine the distance exposed to high noise levels (the distance at which a suitable altitude is reached for thrust reduction after takeoff). Short flights (less than 600 nautical miles) are generally served from at least 6,000 foot runways by two or three engine aircraft which can reach a 1,000 foot altitude above the runway approximately 2.5 miles from the start of takeoff roll. Intermediate range flights (600 to 2,000 nautical miles) are generally served from at least 8,000 foot runways by three or four engine aircraft which can reach a 1,000 foot altitude in approximately 3.0 miles. Long range flights (2,000 to 4,000 nautical miles) are generally made from at least 10,000 foot runways by four engine aircraft which require approximately 3.5 miles to reach a 1,000 foot altitude. Four engine aircraft in extreme range service (greater than 4,000 nautical miles) generally operate from runways at least 12,000 feet in length and require approximately 4.0 miles to reach a 1,000 foot altitude in hot weather.

The importance of determining the type of service to be offered rests with the fact that a significant decrease in noise level occurs at that point where a takeoff thrust reduction is made, whereas all other changes in noise level occur very gradually. This suggests that point as a logical dividing line in any land use or zoning plan since a step from very high takeoff power noise levels to lower climb power noise levels occurs. A "rule of thumb" sometimes used in the United States is that a suitable altitude for thrust reduction will be reached at approximately twice the runway length (or twice the balanced field length for any particular aircraft, as appropriate).

Supersonic Transports

Supersonic transport aircraft require individual analysis and attention. It is expected that the first generation supersonic transports will serve a relatively small number of large international airports. During full power takeoff and initial climb operations, they are expected to expose areas a mile to the side to noise levels undesirable in residential neighborhoods. Those aircraft having high lift devices on the wings can comfortably operate within the 3.5 mile distance previously listed for long range flights. Highly swept delta winged aircraft without high lift devices, however, must achieve higher speeds for reasonably quiet and efficient climbing flight.

Therefore, greater distance (preferably more than 4.0 miles) should be identified for noise compatibility if hot weather supersonic transport operations are contemplated. The longer the distance at full thrust, the lower the noise levels will be following thrust reduction.

Supersonic transports will force one other consideration that has generally been ignored in the past; that of possible hazard from single exposures to very high noise levels near or under the takeoff flight path. During the takeoff run and shortly after lift-off when the aircraft are climbing at full thrust, all first generation supersonic transports are expected to generate very high noise levels at close distances. It will be necessary to restrict people without adequate protection from such exposure; therefore, such areas will have to be identified. Generally speaking, these areas can be confined within the boundary of the airport.

Operational Procedures

Operational procedures can vary the pattern of noise exposure on the ground and can frequently make a significant reduction in the area within noise exposure contour. The most commonly used procedure after preferential runways have been employed to minimize noise exposure over populated areas is the takeoff thrust reduction (Figure 7). A modest thrust reduction (to that required to maintain approximately a six percent climb gradient) at the edge of the noise sensitive area, but not before reaching a safe altitude, generally results in significant noise level reductions under the flight path without increasing the total area within a noise contour. The reduced thrust should be maintained until the aircraft is clear of the noise sensitive areas or has attained an altitude where reapplication of climb power will not result in the creation of unacceptable noise levels on the ground. Greater thrust reductions can produce slightly lower noise levels immediately following the cut, but result in long extensions to the noise affected area and higher noise levels further from the airport. Turbofan powered aircraft with dominant fan noise characteristics sometimes achieve little noise reduction directly under the flight path but do cause significant reductions one-half mile or more to the side where the high frequency fan noise has been attenuated by the atmosphere.

Takeoff procedures can be optimized for maximum noise reduction at any airport; however, a proliferation of procedures does not enhance the safety of operations and, at most airports, "standard" noise abatement takeoff procedures can be used with very little decrease in effectiveness.

The quietest operation comes from achieving the highest possible altitude, a "clean airplane" (landing gear and flaps retracted) and minimum thrust; however, the close proximity of residential communities frequently prevents the attainment of either a clean airplane or significant altitude.

On approach, noise is minimized by using the steepest glide slope that can be safely utilized to minimize thrust requirement and keep as much altitude as possible. Using minimum flap settings also reduces thrust requirements but causes a slight increase in landing runway length requirements.

A concept of minimum noise approach called the bent glide slope or two-segment approach is presently being evaluated in the United States and shows considerable promise. In this procedure, the inbound aircraft maintains a higher altitude than normal and intercepts a synthetic five or six degree initial glide slope (derived from altitude and distance by an onboard computer) at from 3,000 to 5,000 feet. At approximately a 1,000 foot altitude (three miles from the runway threshold), the final (conventional) two and one-half to three degree glide slope is intercepted and followed thereafter (Figure 8). The procedure can significantly reduce areas affected by approach noise greater than three miles from the airport and still be compatible with minimum visibility operations.

IV. AIRPORT DESIGN CONSIDERATIONS

Present technology does not indicate that the noise associated with aircraft can be eliminated entirely, although it can be reduced significantly. Unfortunately, the residual noise will undoubtedly be bothersome to some airport neighbors. With the foregoing in mind, there appear to be two alternatives in locating new airports; they are (1) locate the airport where there are no neighbors, or (2) locate the airport so that it has the type of neighbors who are not bothered by the aircraft noise. With respect to existing airports, there are also some modifications that can be made within the airport boundaries that can partially alleviate existing aircraft noise problems.

Airport Location

When locating a new airport to serve a metropolitan complex, it is extremely important that the airport be located for the convenience of the flying public using the facility. Unfortunately, most airport sites cannot provide both convenience and a lack of neighbors. Therefore, airport planners are usually faced with the problem of locating the airport in a manner that will provide a balance of the following:

a. Convenience to users

b. Availability of airspace

c. Economy of acquisition and construction

d. Noise compatibility with neighbors

Airport Configuration

The location of runways, holding aprons and maintenance facilities can have a major effect on noise annoyance in the airport environment. Whether developing a new airport or expanding an existing one, runway alignment is a critical factor for both maximum utility and control of aircraft noise. Runways should be aligned insofar as possible (1) to provide aircraft with the most favorable wind conditions, and (2) to avoid noise sensitive areas with approach and departure paths. Selective runway alignment can minimize problems from noise in the potentially most noise sensitive areas adjacent to the airport.

Placement of holding aprons and alignment of holding aircraft must also be considered. Noise can be selectively directed to areas having the least impact from noise. Likewise, aircraft maintenance and engine testing areas should be located well within the interior portions of an airport so that noise effects will be minimized for airport neighbors. Although improvements can be made by airport configuration, it must be recognized that airport design cannot be the total answer in controlling the effects of noise. For example, noise generated at an airport during the day may not be objectionable while the same noise at night may cause serious complaints from airport neighbors. In this case, operational control rather than airport design may provide the solution.

Land Requirements

To effectively perform the function for which it is created, an airport must include adequate land for both present and future airport development and airport protection purposes. Land for airport protection purposes includes the land necessary to provide close-in aircraft approach and departure protection and land to act as a buffer for noise control purposes between the airport and its neighbors. Land for development purposes is normally controlled by airport ownership. Land for airport protection purposes may be controlled by: (1) ownership; (2) easements; and (3) zoning. These are dealt with in greater detail as part of Land Use Programs.

V. AIRPORT OPERATIONAL CONTROLS

An airport operator has several potential means of controlling noise through operational restrictions. These include controls on flight operations and controls on ground operations.

Flight Operations

Three principal controls potentially available to the airport operator are:

a. Limitations on the amount of aircraft noise permitted in the takeoff and landing paths related to the airport;

b. Night curfews; and,

c. Limitations on classes of aircraft utilizing the airport.

These limitations, when exercised, are done so on the basis of "landlord rights" or contractual authority, or both. They are not exercised at many airports, however, because of either legal authority questions or political policy decisions.

The establishment of noise limitations for takeoff and landing carries with it a related commitment for monitoring and enforcement. The location of points at which noise is monitored, the levels established, and the availability of effective enforcement determine very precisely the minimum noise performance characteristics that must be possessed by aircraft operating from that location. Maximum range limitations and sometimes maximum weight limitations can be used in the same manner to control aircraft performance, but with less preciseness than specific noise limits.

At a few airports in the United States, the use of night curfews has proved to be an effective way of reducing public reaction to noise since sleep interference is a primary source of noise complaints. Night curfews can work very effectively at commuter type airports offering short range airline service, particularly if there is a nearby non noise sensitive airport that can serve as an alternate when scheduled flights are running late. Such curfews, however, impose a very significant, and sometimes prohibitive, penalty on long range operations, particularly if the flights cover several time zones. Night restrictions at both ends of a heavily travelled route like the North Atlantic would cause very severe scheduling problems for the airlines who base their economics on a high utilization rate.

Figures 3 and 4 indicate the noise levels generated by different classes of aircraft and the potential reductions available by restricting the type of service to, for example, two and three engine aircraft.

Ground Operations

Airport neighbors sometimes find ground running of engines at high power more bothersome than flight operations, because of the indefinite and relatively long time periods involved. In contrast with flight operations, changing noise levels and a doppler effect give an indication to the listener that the noise will soon stop. The airport operator has a number of effective tools to control the noise problem from ground operations, particularly the night operations which generate the strongest reaction. In the United States, the use of carefully selected locations for runups with the aircraft pointed in a specific direction have been used. Restrictions on the hours of operation are also effective but pose a hardship on airlines who normally must perform maintenance during the most sensitive night-time hours. Effective noise suppressors are also available.

The establishment of a relatively low noise level not to be exceeded at the airport boundary (comparable to industrial noise standards existing in many city codes) is probably the most reasonable type of restriction with which to get compliance, particularly if there is some variation in the noise level with the time of day and if there is some remote location on the airport where full power runups may be made at any time of the day or night. With specific noise levels at the airport boundary, carriers with considerable scheduled maintenance can acquire portable sound suppressors and take advantage of shielding from topographical features or structures so that maintenance runups may be conducted at their normal maintenance site, whereas smaller or unscheduled maintenance operations might be more economically conducted using a remote site or waiting until a time period when higher noise levels were permitted.

VI. LAND USE PROGRAMS

Aviation provides services to society in the form of security, economic benefits, direct social benefits, and a host of intangible benefits. Aviation also imposes costs on society. These take such forms as noise, vibration and soot, generally classed as environmental degradation; and fear, which is psychologically associated with aircraft noise. Aviation can and will thrive so long as the benefits to society outweigh the costs to society, providing that a significant burden is not placed on that minority of people near airports who must pay, without compensation of some sort, the pre-

dominant portion of the social costs. With the benefits more widely distributed but the costs borne by a small minority of the people, equity demands that those costs be minimized. As noted earlier, technology should be fully exploited to minimize the environmental degradation at the source (the airplane); but even after completion of those efforts, there will still remain large areas on the ground exposed to high undesirable levels. The purpose of land use programs is to achieve a state of compatibility between the noise exposure in such areas and the manner in which the land is used.

Many attempts have been made to define human reaction to noise under a great number of circumstances and uses of land which are compatible with frequently occurring high noise levels. In the United States, such efforts are continuing and useful refinements are being developed but, as explained in the section titled "Noise Exposure Forecasting," many variables are involved and the definition of compatible land uses near an airport will always require individual attention and analysis. Some of the potential methods of land use control are through: (1) purchase for direct airport use or conversion to a compatible use; (2) avigation easements, under some circumstances; (3) zoning, under some circumstances; and (4) building code applications.

Ownership of Land

Public ownership of land is the most positive method of providing space between noise generating areas on airports and surrounding noise sensitive areas such as residential developments.

Such publicly owned land may be acquired for future airport expansion or for other public purposes. If for airport development, it can be utilized in the interim for agriculture, recreation or aviation related activities. If acquired for buffer purposes, it may also be used for agricultural, recreational and aviation purposes, or for industrial uses that are non sensitive to aircraft noise. Highways, parking lots, railroads, and other non sensitive uses should also be encouraged.

At existing airports in built-up areas, land conversion programs may be a suitable method to obtain compatible land use. For this method to work, the use of the land may be converted to a purpose which is both noise compatible and of a higher economic value than the existing one. For example, low cost, low grade housing might be replaced by industrial warehouses, manufacturing facilities, etc.

There are many financial, legal, and social obstacles to such a program, not least among which are the local legal and fiscal restraints which inhibit the availability of public funds to acquire the property for conversion. Nevertheless, the rapidly developing requirements for business and industrial property near major airports should permit residents who object to their noise exposure to sell and relocate without suffering any economic penalty in the transaction.

Avigation Easements

A method for controlling land use short of outright purchase is the acquisition of an avigation easement. This is the purchase of the right for aircraft to fly over a property without recourse by the property owner against either the aircraft or airport operator. This method has been used both by United States, military, and civil authorities. It has serious drawbacks, however, since the United States courts have held that the property owner can recover from the easement holder if the character of use of the airport has changed substantially. For instance, easements purchased when piston engine airplanes were using an airport were held unenforceable when jets later used it. And likewise, when heavy bombers replaced fighters at an airbase, the easements had to be purchased again. The net result is that easements may, in the long run, cost more than outright purchase unless legal ways are found to purchase greater protection.

Zoning

Zoning, in general, falls into two distinct categories. One is a "police" type zoning, which is based upon safety. A typical example is zoning to limit the height of tall buildings, towers, or other structures which penetrate the flight path of aircraft taking off or approaching an airport. These are generally upheld by the courts except where the property is so close to the airport that the effect of such a zoning law is to prohibit almost any practical economic use of the property.

The other type of zoning is an "economic use" type of land use zoning. It normally protects residential areas from encroachment by industry and business. In a few cases, it protects industry and business from residential encroachment. It is the latter type of zoning that is desired near airports. It is practically unattainable if the area is already built up with homes or apartments. It is even difficult to obtain for new airports if the land developers wish to promote residential development, and they have more politically persuasive powers than does the aviation interests. This problem is even greater when one political jurisdiction owns the airport and the surrounding property is in other political jurisdictions as is frequently the case at major airports serving large cities.

In addition to the purchase of land most seriously affected by aircraft noise, both types zoning - height restrictions and compatible land use - should be acquired near airports whenever possible.

Compatibility in Peripheral Areas

Noise decreases very gradually as the distance from the airport increases; therefore, there will be large areas subjected to undesirable noise levels (outside the critically affected areas) where residential areas do or will, in the future, exist. Acoustical insulation can provide considerable attenuation of noise inside residences; therefore, building codes can be used effectively to minimize the impact of the noise environment. The same building qualities which provide thermal insulation are usually effective for acoustical insulation and vice versa; therefore, the cost of improved acoustical qualities can be shared with other benefits. The financing of improvements in the acoustical attenuation of residences subject to high noise exposure would be materially assisted by programs to recognize and

reimburse the social costs of aircraft noise whether through direct "token payments" or reductions in taxes in proportion to the total noise exposure. However, it must be stressed that in the more critically affected areas, any actions taken in respect to non-compatible uses should, in some way, contribute toward the eventual conversion of that land to noise compatible usage.

VII. EDUCATION/PUBLIC RELATIONS

Education and communications are important factors in establishing and maintaining a state of tolerant compatibility between an airport and its neighbors, both in terms of helping those who can, to adapt to the noise exposure, and for those who cannot, to recognize that fact and relocate to a more acceptable environment. This will remain true so long as the noise exposure is so great as to interfere with some portion of the daily activities of those neighbors. For the foreseeable future, there appears to be little doubt that such noise exposure levels will exist around major airports, even if the existing fleet is modified to reduce its noise output, and the new generation of quieter aircraft now being developed, are substituted for the noisier vehicles in use today. Therefore, it is desirable that major airports maintain an active program of public relations and education to keep the nearby communities aware of a number of important factors relating to the airport and its operation.

Among the important areas to be accurately and factually reported through the news media, schools, speeches, participation in civic groups, newsletters, etc., are:

a. The social and economic benefits that aviation provide to the community - If a direct link between the citizen's welfare and the role of air transportation and the operation of the airport can be identified, this is extremely desirable; however, the value of the airport to the total community is also an important factor.

b. Maintenance of an up-to-date history of past operations, a description of present operations and resulting total noise exposure, as well as projections of future operations and noise exposure - New or extended runways change noise exposures, and land use planners should have as long a lead time as possible to account for significant changes.

c. The steps that have been taken and are being taken to minimize noise exposure over noise sensitive areas, and the reasons why other actions are impractical or of no benefit - Useful steps normally include preferential runway systems, minimum noise departure and arrival routes, noise abatement takeoff and approach procedures, operational restrictions, maintenance or ground operation restrictions, construction on the airport, land acquisition, etc.

d. The compliance with noise reduction requirements and results of noise monitoring if such systems are used.

e. The state of technology in noise reduction - Hopes for future improvement are valuable but false hope is very detrimental (Confidence that the airport operator, the airlines, and the government recognize the impact of aircraft noise on airport neighbors and that everything practical is being done to reduce noise exposure safely is an important factor in public acceptance of the "necessary noise").

Experience in the United States has shown that an honest candid relationship between an airport operator and aviation interests and the airport neighbors will go a long way toward creating an atmosphere in which necessary noise is accepted with minimum complaint by neighborhoods near airports as long as they understand that they are listening only to necessary noise and that all unnecessary noise has been eliminated or is in the process of being eliminated.

VIII. CONCLUSION

There is little question but that air transportation significantly contributes to the well-being of the majority of the population in the United States and throughout the world, whether or not they have ever flown. While its rapid growth to meet an ever increasing demand for services over the last decade or so has brought many benefits, both tangible and intangible, so too has it brought certain unwanted side effects not least of which has been intrusive and objectional levels of noise. We have seen that the noise problem has grown to such a magnitude that there is a real potential for inhibiting a continued flow of national and international air transportation benefits. In fact, at many major airports, air commerce has already felt some negative impact from the aircraft noise problem. We have also seen that technology exists, and continues to advance, in the area of aircraft noise alleviation. Considering all relevant factors, it is obvious that a concerted effort must be made now to apply every practical aircraft noise alleviation method both to the vehicle and on the ground if we are to insure the continued orderly growth of air commerce and its contribution to the social and economic betterment of mankind.

LIST OF REFERENCES

1. "Noise Standards: Aircraft Type Certification," Notice of Proposed Rulemaking (NPRM 69-1), January 11, 1969

2. W. C. Sperry, "Aircraft Noise Evaluation," Report No. FAA-NO-68-34, September 1968

3. "Conference On STOL Transport Aircraft Noise Certification," Report No. FAA-NO-69-1, January 30, 1969

4. Bolt, Beranek and Newman, Inc., "Land Use Planning Relating To Aircraft Noise," October 1964

5. Bolt, Beranek and Newman, Inc., "Noise Exposure Forecast Methodology And Contours For 29 Airports For 1967, 1970, And 1975," Contract No. FA68WA-1900, summer 1969

6. Dwight E. Bishop and Richard D. Horonjeff, Bolt, Beranek and Newman, Inc., "Noise Exposure Forecast Contour Interpretations Of Aircraft Noise Tradeoff Studies," FAA-NO-69-2, February 1969

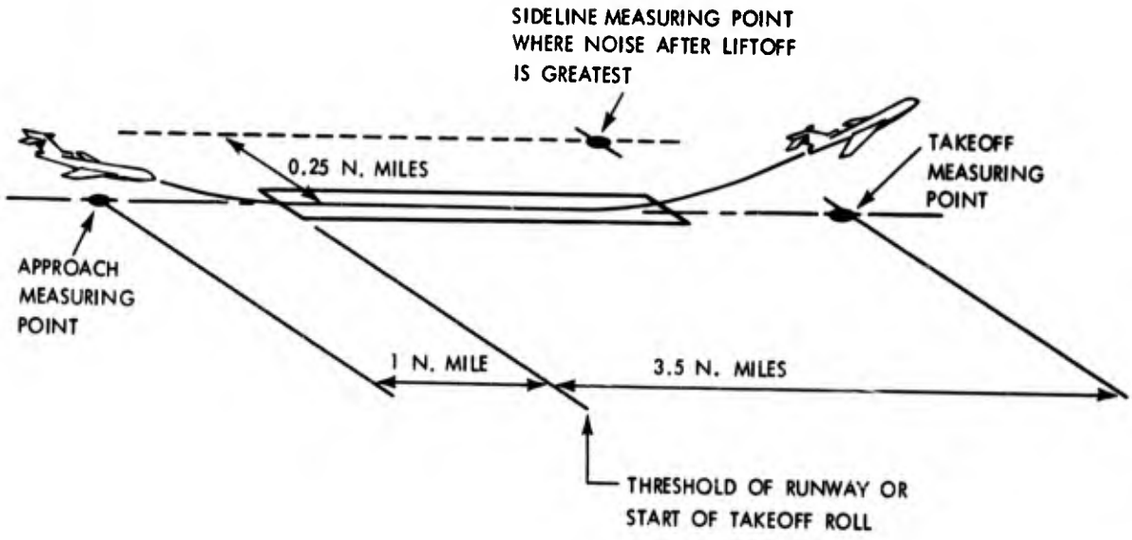

NOISE MEASURING POINTS FOR AIRPLANE TYPE CERTIFICATION

FIGURE 1

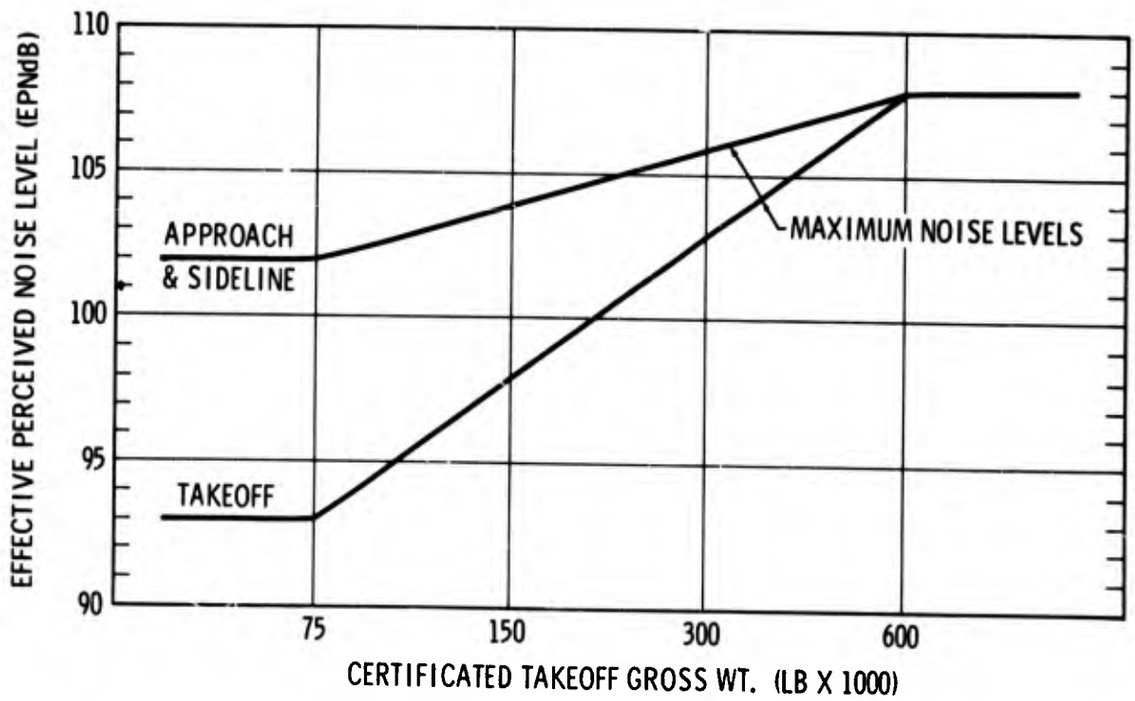

FAA PROPOSED MAXIMUM NOISE LIMITS FOR CERTIFICATION

FIGURE 2

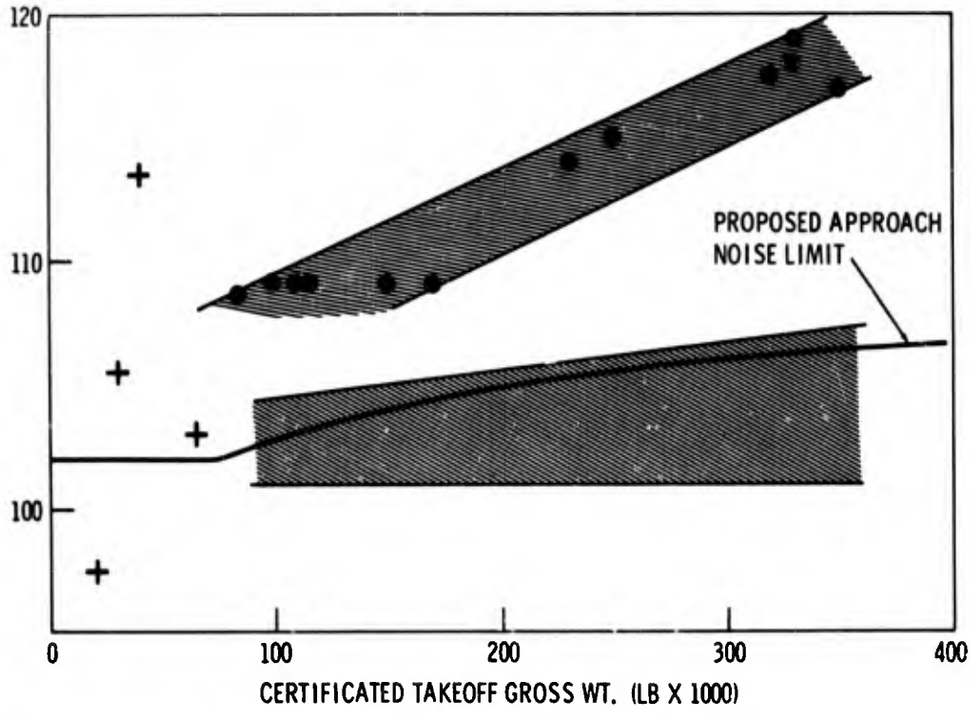

APPROACH NOISE LEVELS - PRESENT AIRCRAFT
(1.0 N. MILES ON 3° GLIDE SLOPE)

FIGURE 3

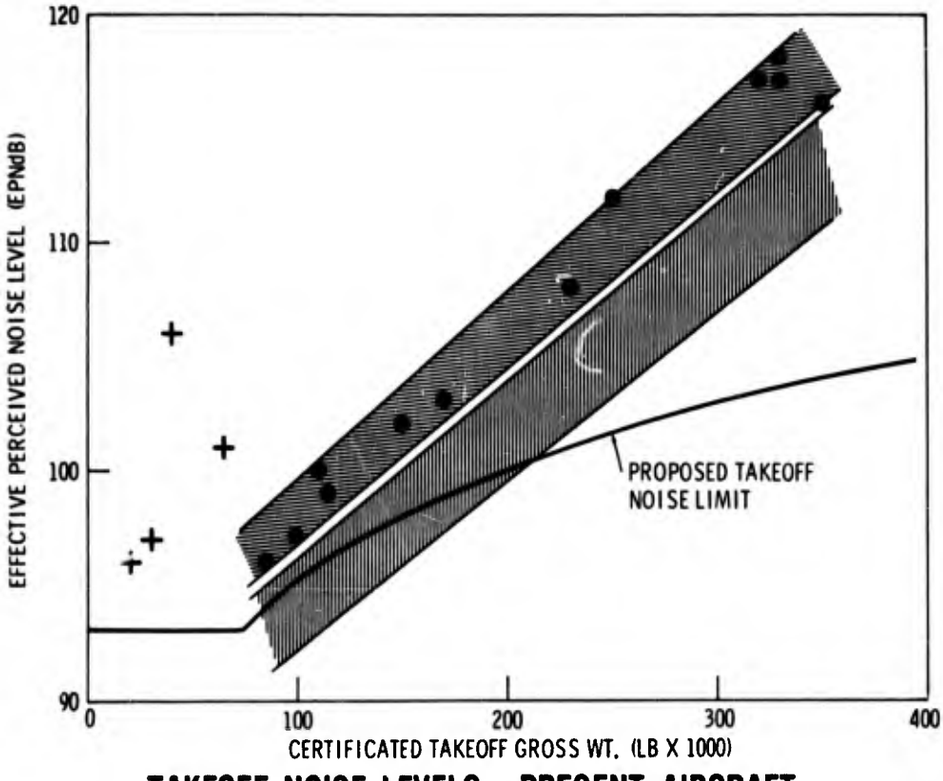

TAKEOFF NOISE LEVELS - PRESENT AIRCRAFT
(3.5 N. MILES 6% CLIMB @ 1000 FT.)

FIGURE 4

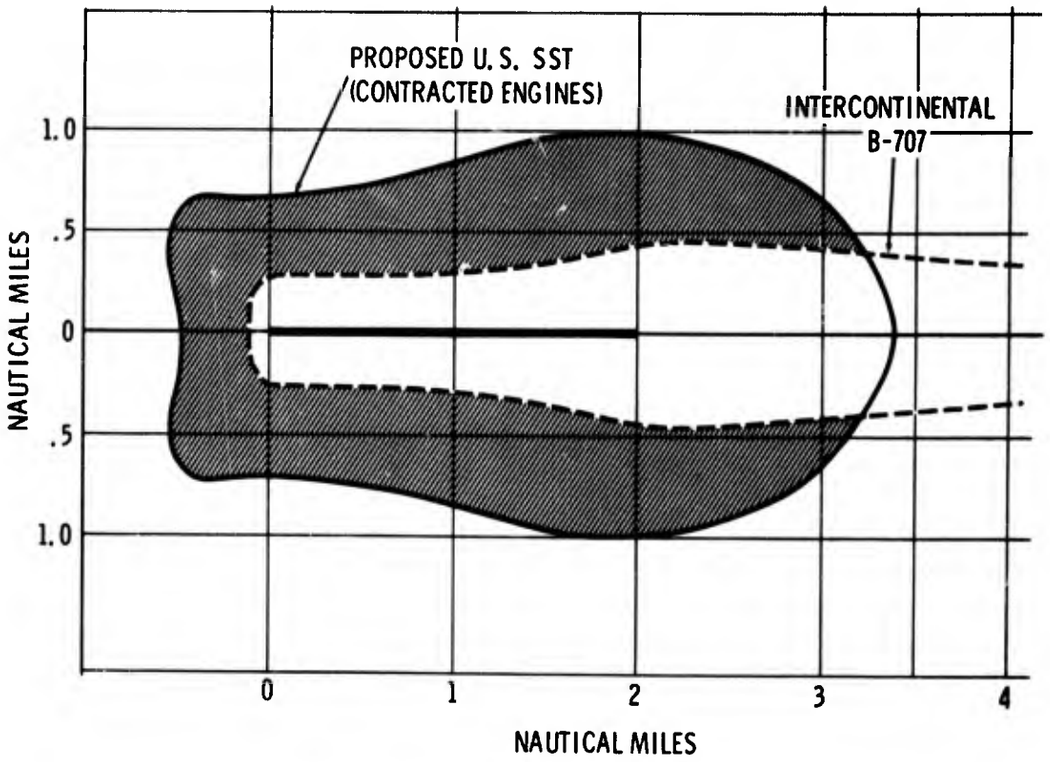

105 PNdB TAKEOFF NOISE CONTOURS

FIGURE 5

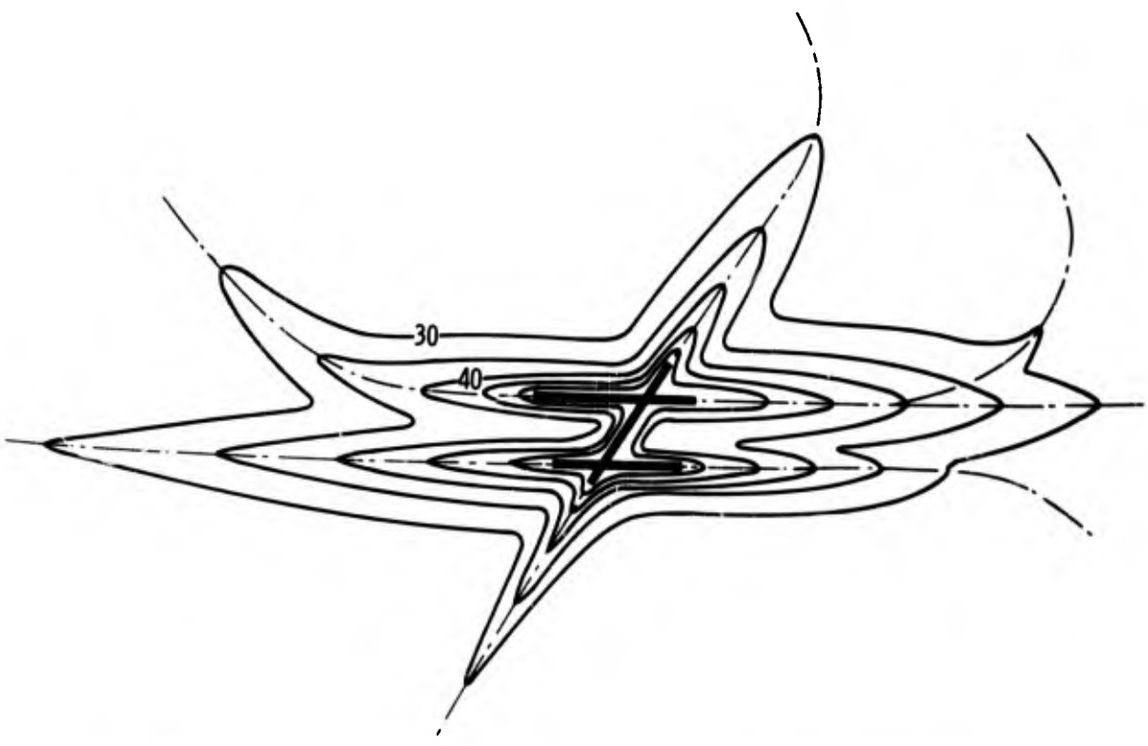

NOISE EXPOSURE FORECAST (HYPOTHETICAL AIRPORT)

FIGURE 6

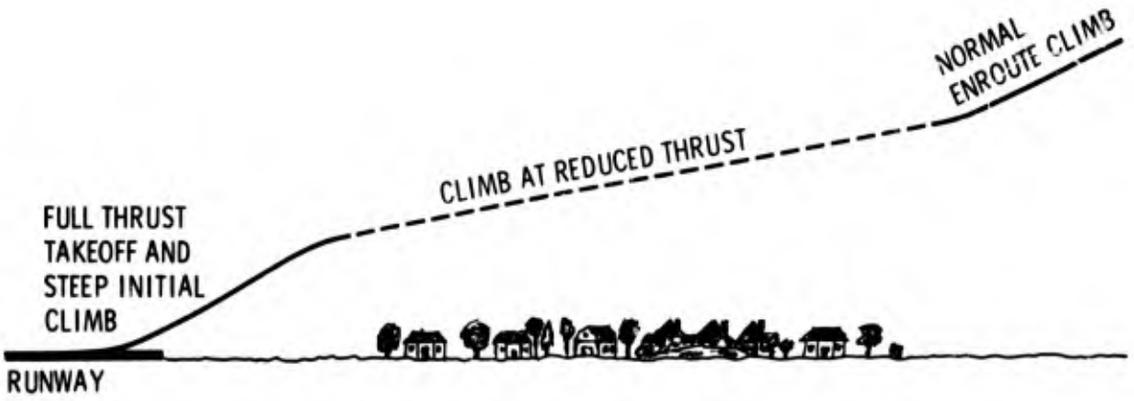

NOISE ABATEMENT TAKEOFF PROCEDURE

FIGURE 7

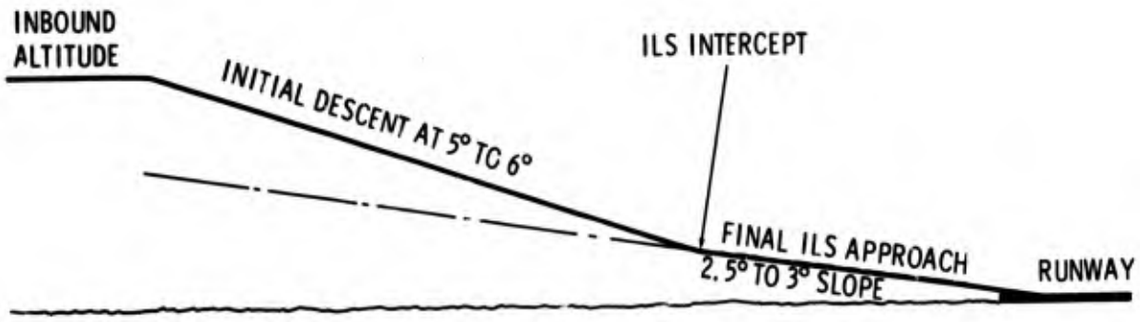

TWO SEGMENT NOISE ABATEMENT APPROACH PROCEDURE

FIGURE 8

PROBABILITY OF AIRCRAFT NOISE AND SONIC BOOM INDUCED BUILDING DAMAGES

by

Dr-Ing Gunter Weber

Technical University,
Hanover, Germany

Summary.

Buildings are calculated for certain static deadloads and payloads, prescripted by buidling standards. Aircraft noise and sonic booms are transient supplement loads, neglected in calculation. Scope of this paper is the evaluation of the ratio of calculated static main stresses to dynamic supplement stresses induced by aircraft noise and sonic booms.

Aircraft noise with sound pressure levels from 81 dB to 92 dB produced stresses up to $\sigma = 0{,}8$ kp/cm^2 in glass panes of a multistory building allowable stresses in glass panes $\sigma = 300$ kp/cm^2.

For an old church and a residential structure excitations producing limit stresses were calculated and compared with overpressures measured in booms. Boom generated supplement stresses in primary parts of buildings will reach less than 1% of allowable stresses, in roofs less than 10%, in glass panes up to 50%, unfavourable circumstances presupposed.

Damages therefore will follow a certain order:
Primary structures like walls staircases etc. only could be influenced if before parts of the roof would be damaged. Tiles on the roof would crack before purlins and rafters would reach their stress limit. Glass panes would break before damage on roofs would happen. Unsound plaster with adhesive strength approaching zero would fall of at first. Damages on primary structures of buildings are till now known and are not to be expected.

Buildings are calculated for certain static deadloads and payloads prescripted by building standards. Aircraft noise and sonic booms are transient supplement loads, which are not considered in the calculation of buildings. Scope of this paper is the evaluation of the ratio of calculated static main stresses to dynamic supplement stresses induced by aircraft noise and sonic booms. Aircraft noise induced effects to panes of glass installed in a multistory building will be regarded first and than the response of buildings and their parts to sonic booms will be theoretically explained in their main features, to show within which limitations predictions of the effects of sonic booms to buildings and their parts are available. These considerations will be completed by the results of the structural response of a residential structure and a granary located on a training area near Meppen during a testing program consisting of twenty-five controlled sonic booms.

Aircraft noise damages of glass panes installed in a multistory spinning-mill were claimed to be caused by aircraft noise. The building located in the flying lane of a Bundeswehr-air-base was passed over in about 150 m by aircrafts of the type starfighter F 104 after starting and before landing. For objektive information sound measurements and in connection with these strain measurements on the glass panes were suggested. The evaluation of the sound records picked up a few centimeters ahead the glass panes of the third floor of the building shows a wide-band noise with a chief area between 200 and 2000 c/s. (See Fig. 1). Sound pressure levels between 81 dB and 92 dB were recorded and maximum sound pressures from 3 µbar to 11 µbar, in one case 20 µbar measured ahead the window, that means an oscillating pressure from $\Delta p = \pm 0{,}2$ kp/m^2. The wind design load prescripted by German standards of buildings is for normal buildings from 8 to 20 m in altitude $w = 1{,}2 \cdot 80 = 96$ kp/m^2, about 500 times that of the aircraft noise.

Buildings and glass panes normally have natural frequences in the range from 2 to 80 c/s. In this range the appropriate sound pressure attains only 1/20 to 1/40 of the total sound pressure. Thinkable resonance effects are therefore not of importance. By push or knock against the windows the following natural frequences were excitated:

Panes in	Window in concrete frame	14,7 Hz
" "	" " " "	62,5 "
	" " steel-frame	22,4 "
	" " " "	59,0 "

The measuring of aircraft noise induced strains on the glass panes was possible only during the breaks of the workshop. The spinning machines in operation excited strains 4 - 6 times greater as the aircraft noise induced stresses in the panes from $\sigma = 0{,}4 - 0{,}8$ kp/cm^2. Normally recommanded design allowables are $\sigma = 300$ kp/cm^2, static breakdown stresses are about $\sigma = 900$ kp/cm^2. The magnitude of stresses obtained in this test was only a small promille of the allowable stresses. Aircraft noise induced damages of the panes of this building were to deny. There was no damage on glass panes in one of any neighbouring houses and there is no damage on glass panes to expect by aircraft noise of this kind.

Aircraft noise is with regard to buildings a slowly increasing and decreasing process, sonic boom is a very abrupt starting and stopping process. The response of buildings and their parts to static and slowly changing loads is only determined by the rigidity of the construction, The response to transient loads like sonic boom is essentially influenced by the masses of the construction and the elasticity of the ground below the building. The total movement of buildings in reaction to transient loads is composed from three partial movements: a) The house rotates as a stiff body on the elastic ground, b) the house oscillates on the rigid thought ground as a bending beam with one end clamped, one end free, c) the house oscillates on the rigid thought ground without bending in shear oscillations. All three partial oscillations have different periods, which are shorter than the total rotary bending shear period T. (See Fig. 2).

In regard to this system natural period T, the rise time τ of boom overpressure is very short. When the ratio of step rise time to system natural period approaches zero and the overpressure than would stay constant, the step would approach the simple rectangular step in shape and the amplification of the response in regard to static loads of equal size would approach the upper extreme of 2, damping neglected. If τ/T, pulse duration to system natural period is less than 1/4, the pulse shape is of little consequence in almost all cases and the system response can be determined to a fair approximation by use of the simple impulse theorie. If τ/T is larger than 1/2, the pulse shape may be of great significance. Fig. 3 shows correlating excitations and responses of systems with only one degree of freedom.

Till now only step-type excitations without change in sign were considered full-cycle pulses [force-time integral = 0] may have duplicated effects related to half cycle pulses. So a rectangular full-cycle impulse with $2\tau/T = 1$ has amplitudes up to the factor 4 related to static loads of equal size. (See Fig. 3c). Single full-cycle impulses with other shapes have factors less than 4, f.e. full-cycle-sinusoidal pulses 3,14, full-cycle triangular pulses with vertical front and vertical ending 2,12. This last one is a good approximation to the shape of some sonic boom pulses. Full-cycle excitations with with 1/2 $2\tau/T$ 1 provoke deflections in the direction of the force with negative sign. In connection with sonic boom the pulse shape might be of great importance: Booms with very high sound pressure but very short excitation times relative to the system natural period will excite people by the loudness, but buildings will give only little response, proportional to the hatched area in Fig. 3c, not to Δp. A blynk cartridge might have the same loudness, as a sonic boom, but ist has not the same effects to buildings.

When the ratio $2\tau/T$ pulse duration to system natural period is a known quantity and static pressing stresses in the walls are given facts, maximum pulse forces generating oscillating stresses of equal size as the static pressing stresses, could be calculated, see table 1. The static pressing stresses - $\sigma = 2{,}1$ kp/cm^2 - in the walls of the house - will be either duplicated or just compensated by these pulse generated oscillating stresses. The summarized pressing stresses in the walls of the church and of the residential construction don't trespass $\sigma = 6$ kp/cm^2. According to German standards of buildings pressing stresses in the walls of $\sigma = 12$ kp/cm^2 and more would be allowable. Compared with the calculated overpressures necessary for duplicating the static stresses in the walls, from $\Delta p = 55$ mbar up to several thousend mbar, the overpressures measured in sonic booms, between $\Delta p = 0{,}1$ mbar to $\Delta p = 1$ mbar, in special cases up to about 6 mbar, are small quantities.

Recently in several cases the assertion was made, that damages in buildings would be generated by boom induced seismic waves. For the two buildings under regard, the church and the residential construction, amplitudes of an excitation by two full-cycle sinusoidal pulses where calculated, so that no tensil stresses in the walls of the church and no tensil stresses greater than $\sigma = 0{,}1$ kp/cm^2 in the walls of the residential construction would be induced. The so calculated amplitudes in the area of the church tower foundation were = 0,11 cm, in the area of the side-wall foundation = 0,05 cm in vertical direction for a ratio $2\tau/T = 1$ pulse duration to system natural period. For the foundation of the residential construction the calculated amplitude was = 0,069 cm. These calculated amplitudes seem to be very small quantities, but compared with boom generated seismic amplitudes measured on the surface of the earth, the calculated amplitudes are extreemly high. The boom induced additional stresses in the walls and in the foundation, which might even be a more delicate question, don't exceed one persent of the allowable stresses. Boom induced damages on structural elements like walls and foundation are not to except.

Unfortunately the ratio of boom induced oscillating stresses to static design stresses will be less favourable in other parts of buildings. Parts of great square dimensions with little masses of their own, not precharged by other parts are designed only for small maximum loads, f.e. roofs and especially glass panes.

Tiled roofs are designed for dead weight, wind load and/or snowload. All three loads have simular dimensions, about $p = 75 - 100$ kp/m^2 in roofs of residential buildings. The allowable stresses in wooden rafters are about $\sigma = 80 - 110$ kp/m^2, only one third of these stresses are used by dead weight. Sonic boom overpressure usually acts on roofs only charged by dead load, not charged by wind and/or snowloads, on roofs with 2/3 of the allowable stresses stored. Unfavourable ratio $2\tau/T$ 1 presupposed, a simple full cycle triangular pulse with vertical rise and ending with an amplitude of $\Delta p = 1$ mbar could induce additional stresses of about $\sigma = 6$ kp/cm^2, about 7,0% of the allowable stresses in wooden structures. [1 mbar 10,2 kp/m^2, an amplification-factor of about 2,1, prescripted design, windload for usual buildings from 8 - 20 m in altitude $w = 1{,}2 \cdot 80 = 96$ kp/m^2, means 4,7 mbar 96 kp/m^2. σ_w 80/3 = 27 kp/cm^2; 1 mbar 80/3·4,7 5,7 kp/cm^2].

These additional stresses are no more to be neglegted against stresses generated by static loads, but a sufficient margin of safety is left in calculation even in structural elements with fully used design stresses to tolerate additional stresses of this size. Tiled roofs with mortar filled joints are sometimes too inflexible to follow oscillating movements with stresses within limits without crackings in the mortar. This means no loss in stability but in tighness against driftsnow.

Glass panes usually are designed only for windload, not for deadload or snowload. According to standards the design windload for buildings up to 8 m in altitude is $w = 1{,}2 \cdot 50 = 60$ kp/m^2, from 8 - 20 m in altitude $w = 1{,}2 \cdot 80 = 96$ kp/m^2. Glass panes designed just for the 60 kp/m^2 windload could reach their design stress

limit by a single full-cycle triangular pulse with vertical rise and ending of 60/2,1·10,2 = 2,8 mbar overpressure, with the ratio $2\tau/T = 0{,}875$ presumed. A pulse with an amplitude of only 1 mbar could induce additional stresses of about 36% of the allowable stresses. Recommanded for the calculation of thickness of panes are safety factors of 2,5 and more and the allowable design stress limit is only $\sigma = 300$ kp/cm², the average breaking stress for short time loads from tests was $\sigma = 590$ kp/cm². Therefore design wind loads and sonic booms may coincide without harm for panes. In case of cumulation of unfavourable circumstances breaking of panes accidentally cannot be excludet. These conditions might be: Excitation of panes of minor quality with suitable system natural periods, uncorrectly installed panes, excitation by more than one pulse by reflections or double bangs from accelerated flights, accelerated flights in lower altitudes.

From all damages claimed to be caused by sonic booms cracked plaster ist most numerous. Special static tests with plaster have shown the factors significant for the adhesive strength. Sound plaster was determinated by adhesive strength greater than $\sigma = 1$ kp/cm², plaster with adhesive strength below $\sigma = 0{,}2$ kp/cm² was classified as not sufficient, but adhesive strengths below $\sigma = 0{,}05$ kp/cm² were even in the test not very rarely. The variation of the atmospheric pressure by sonic booms is usually less than one millibar or less than $\sigma = 0{,}001$ kp/cm². Sound plaster, prepared according to code of practise will not be damaged by sonic booms. But the adhesive strength of plaster decreases in the course of time and minimum adhesive strength is not prescripted by standards. Sonic booms could cause loosened plaster to peel of.

These theoretical considerations were completed by the results of the structural response of one small residential structure and one granary in the testing area near Meppen during a testing programm consisting of 25 controlled sonic booms. In connection with structural response measurements, overpressure and wave lenghts of the sonic booms at three fixed stations where recorded. The roof of the granary with a base of 48 x 12,5 m was comparable in size to roofs of churches. A total of eleven pickups measuring velocity amplitudes were available for the granary, the locations of the instruments are to be seen in Fig. 4. For the testing program favourable were two circumstances: There were excitations of the roof with two full-cycle pulses, generated by two aircrafts in unaccellerated flights in altitudes of 9000 m, velocity 1,4 Mach, distance about 6 m, and the ratio $2\tau/T$ pulse duration to system natural period of the roof was about 0,9. Double pulses caused approximately double amplitudes of the roof with maximum amplitudes of about $\delta = 0{,}15$ mm in vertical direction, measured on a rafter. The booms produced additional stresses in the rafters up to about $\sigma = 4$ kp/cm². Fig. 5 shows a record of the boom induced velocity amplitudes of the roof, the first trace beeing a microphone response. This microphone was mounted plane with the roof covering tiles on the north slope of the roof. Another microphone was mounted ahead a window of the residential building, a third one on earth level on free field.

These shock wave measurements of the 25 booms showed pressure amplitudes from $\Delta p = 0{,}1$ up to $\Delta p = 0{,}95$ mbar, with pulse durations from $2\tau = 0{,}09$ sec to $2\tau = 0{,}16$ sec. The time-history of the pulses was approximately of N-form in most of the cases, but sometimes great divergences happened without visible reason.

Locations of instruments in the residential structure were a rafter, a window sill of a first floor window and the middle of the living room floor for velocity measuring instruments and a strain gage on the glass pane of the living room window. By pushing the window the natural frequence of the pane was determined to f=41c/s, or a period of $T = 0{,}0024$ sec. The boom induced stresses in the glass pane went up to $\sigma = 2$ kp/cm², [allowable stresses $\sigma = 300$ kp/cm²]. Amplitudes of the rafter of this building were smaller than those of the granary roof. All strains and stresses recorded in this program correspond with the theoretical considerations and are comparable with the results of other test programs, f.e. the American test program of Oklahoma-City.

Review of all calculated and measured overpressure values and the calculated and measured structural response indicates that the levels of stress produced in structural elements of primary structure can be considered negligible. The additional stresses will be less than 1% of the allowable stresses. In rafters of roofs additional stresses up to less than 10% would be possible under unfavourable circumstances and in glass panes up to about 50%. Sound plaster will not be influenced by sonic booms, but if the adhesive strength decreases to zero, no prediction can be made.
Evaluation of alleged damage from sonic booms therefore is faciliated by the fact that damage would follow a certain order: Damage in structural elements like walls, floors, staircases are only to be expected if tiles on the roofs and most of the panes of glass had been broken before and parts of loosened plaster are dissolved. Damages of this dimensions are till now not known and are not to expect. What happens is cracking of unsound plaster and falling out of mortar from roofs.

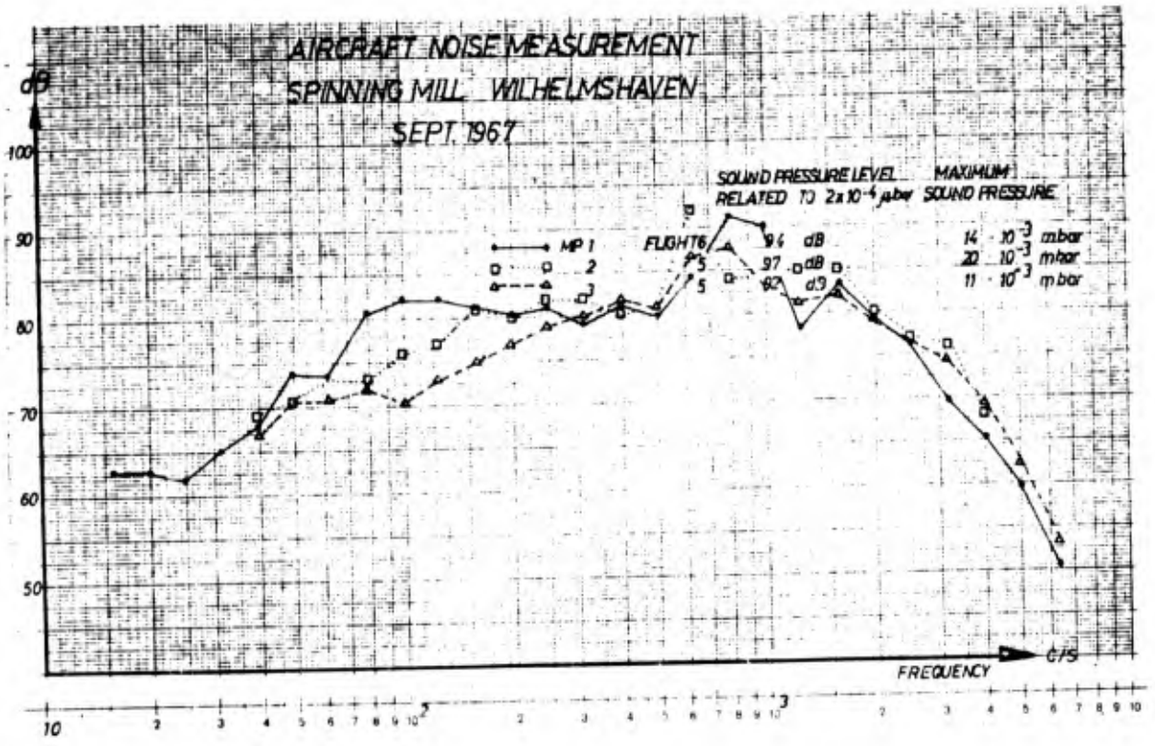

Fig. 1 Aircraft noise, Wilhelmshaven

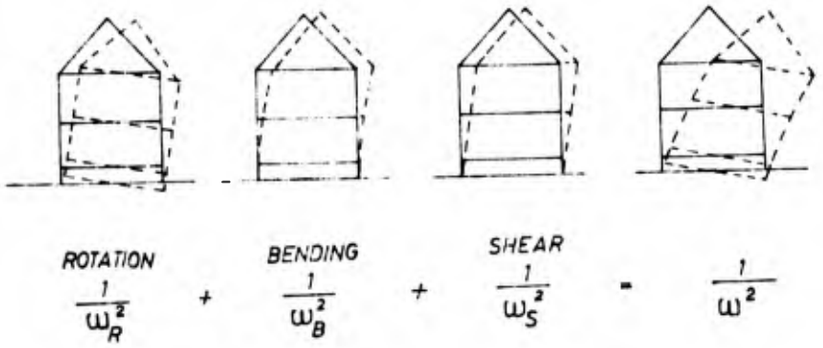

Fig. 2 Movements of buildings

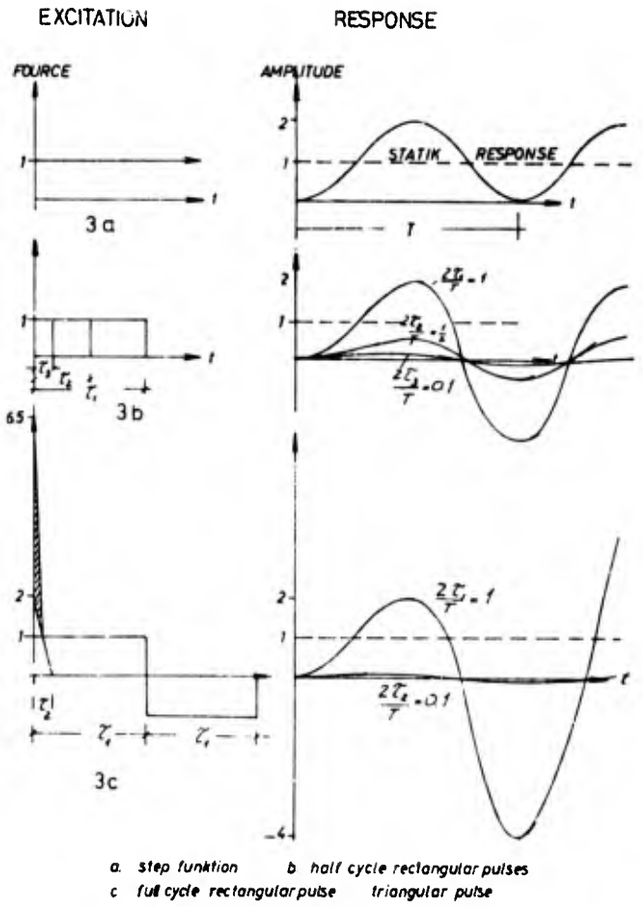

Fig.3 Excitation and response

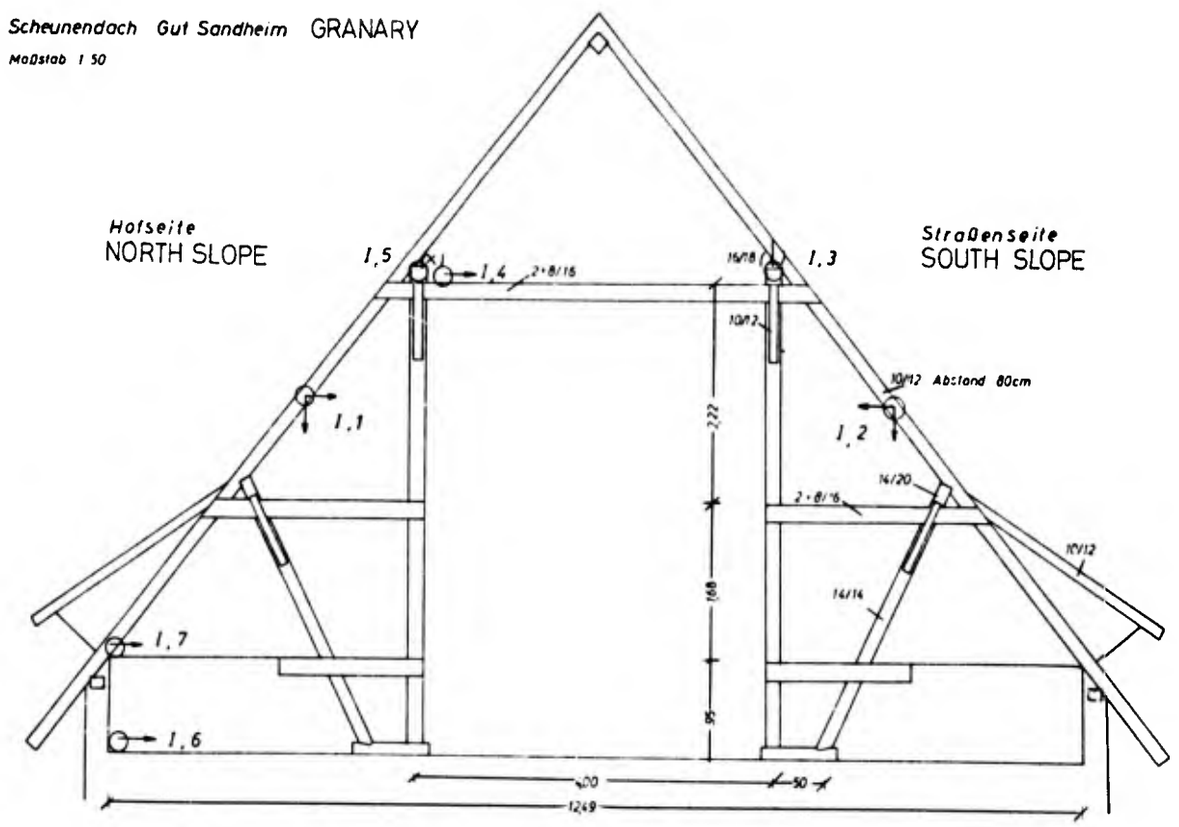

Fig.4 Granary roof construction - locations of instruments

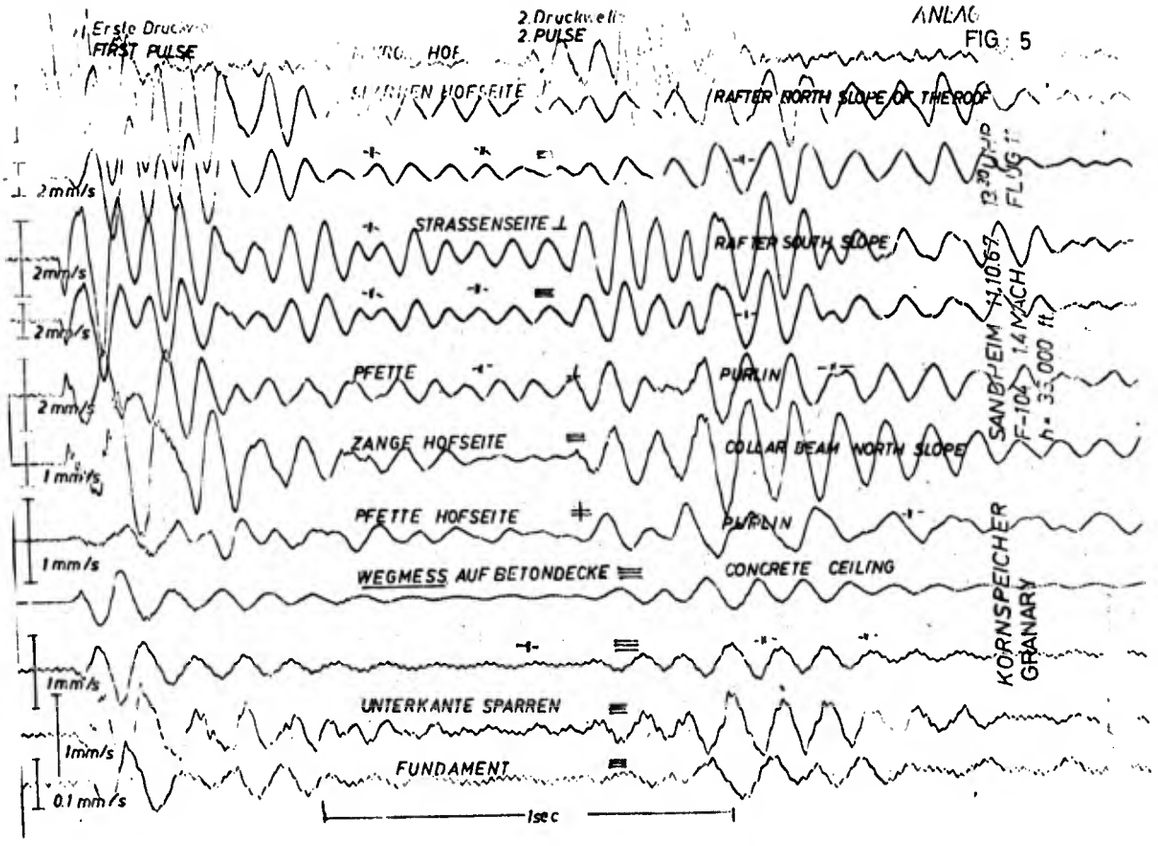

Fig.5 Roof of a granary - recorded oscillations

	CHURCH [Auf dem Schönenberg]				RESIDENTIAL STRUCTURE		
	TOWER AREA		SIDE WALLS				
	bending	rotation	bending	rotation	bending	rotation	shear
SYSTEM NATURAL PERIOD T [sec]	0.39	0.41	0.17	0.42	0.044 – 0.039	0.11 – 0.07	0.09 – 0.072
	0.56		0.45		0.15 – 0.10		
N-wave duration 0.08 sec AMPLIFCATION FACTOR	0.13		0.188		1.42 – 2.05		
PRESSURE AMPLITUDE [mbar] necessary to duplicate statik pressure in the walls	2080	3560	527	600	1.44 – 99		
N-wave duration 0.3 sec AMPLIFICATION FACTOR	1.5		1.83				
mbar	186	292	54.5	522			
Seismic waves sinusoidal AMPLITUDES necessary [c.m] to duplicate static pressure in the walls Two full cycles T/T = 1	↔ 0.11 ↕ 0.38	↕ 0.62	↔ 0.055 ↕ 0.085				
Three " " "					↕ 0.077 – 0.096		

Table 1

HUMAN RESPONSE TO SONIC BOOMS

by

Dr H.E. von Gierke and Dr C.W.Nixon

Aerospace Medical Research Laboratory,
Wright-Patterson Air Force Base, Ohio

Summary

This paper reviews the results of the various observations, overflight programs, experimental field and laboratory tests, which form the basis for present day estimates regarding the acceptability of sonic booms by man. The loudness and annoyance of individual booms and their dependence on the boom overpressure and pressure time function as well as the complex reaction of individuals, groups and cities exposed to sonic booms of varied magnitude and frequency are discussed. The few experiments available proving that even sonic booms of the maximum intensity presently feasible cannot produce any direct medical injury are described. Based on the integrated body of results of recent physiological, psychoacoustic, behavioral and sociological studies in various countries, estimates of the effects and acceptability of regular, frequent supersonic commercial overland flight schedules are presented and discussed in terms of aircraft noise pollution in general and of potential certification of aircraft with respect to noise and sonic boom.

HUMAN RESPONSE TO SONIC BOOMS

Dr. H. E. von Gierke*
Dr. C. W. Nixon**
Aerospace Medical Research Laboratory
Wright-Patterson Air Force Base, Ohio

Introduction

In this period of time prior to the commercial supersonic transport era widespread concern exists about the possible undesirable effects on people of repeated sonic boom exposures. Many experimental programs and observations of human response to sonic booms have been conducted in an attempt to estimate the nature and extent of these projected exposures. Based upon the integrated body of results from physiological, psychological and sociological response programs conducted in various nations in recent years estimates have been made of the acceptability of frequent, regular commercial supersonic flights over populated areas. In this report, laboratory, field and community studies concerned primarily with human response activity which were conducted in France, the United Kingdom and the United States are reviewed and considered in terms of present foundations for criteria for sonic boom acceptability. Although emphasis and interest in sonic boom research over the last 5 years has been primarily dictated by the prospect of commercial supersonic transport operation, military requirements are in need of the same data even if not with the same urgency and all-addressing importance. After all, sonic booms in increasing numbers have been an attribute of military training flights for almost 20 years and all experience gained today with respect to personal reaction, community reaction and potential damage to structures was obtained with military aircraft. Even without a commercial SST in sight the assignment of areas for supersonic tests and training flights makes knowledge of the effects of sonic booms on people and the capability to predict the boom environments and human responses to them mandatory. The same way as in the airport - community noise problem area, where military noise research preceded the present large scale international effort in this area, military sonic boom research has formed the foundation for the present efforts in support of civilian aviation and has remained in most countries an essential part of them. Therefore, the data to be presented are useful to and essential for both types of requirements.

Human response to sonic boom in the community is exceedingly complex, involving the physical stimulus, the immediate environment, the ambient noise conditions, the experiences, attitudes and opinions of those exposed as well as various factors not related directly to the stimulus. Consequently the possibility of formulating a completely satisfactory method for reliably estimating the repsonses of individuals and communities to operational sonic boom exposures on the basis of the physical stimulus alone is recognized as ambitious and perhaps unattainable at this time. Nevertheless, knowledge gained from various observations, overflight programs, experimental laboratory and field studies of noise and sonic boom effects on people does form a basis for present day estimates of the acceptability of sonic booms by man.

Although large gaps exist in technical knowledge regarding this matter guidance is needed today, and is in fact overdue, for authorities responsible for certification, regulation and operation of supersonic vehicles, for rendering legal judgments and for general planning purposes. The urgency of the need for measures to allow populations to be protected from possible adverse effects of overexposure to sonic booms, dictates that provisional recommendations and guidelines be established now and continually refined as our technical understanding is increased by future research efforts and experience. In the following the methods and results of laboratory, controlled field studies and uncontrolled overflight field studies on individual subjects, groups and communities are briefly reviewed (Figure 1). The last section gives the best present day yardstick for estimating sonic boom acceptability taking all experimental evidence and experience into account.

Laboratory Studies

In the laboratory study of sonic boom the physical stimulus as well as other important parameters may be controlled to a degree unattainable in any other investigative situation considered. Within these constraints knowledge has been provided regarding effects of stimulus characteristics on subjective psychological responses such as loudness or noisiness, comparative judgments of sonic boom and aircraft noise, and some physiological responses including startle.

1. Loudness and Annoyance Judgment

It is well known that the loudness and annoyance of an impulse type noise such as the sonic boom are directly related to its energy spectral density function and qualitatively successful attempts have been made to calculate these attributes from the boom pressure time function (19).

* Chief, Biodynamics and Bionics Division

** Chief, Biological Acoustics Branch

However, since no generally accepted method for these calculations exists laboratory judgment tests were conducted to confirm in detail variations in loudness and annoyance with the boom signature.

The perceived loudness or annoyance of sonic booms is primarily related to components of the pressure-time-history of the event, i.e., the peak pressure and rise time (15,20). Peak overpressure is the most obvious contributor to loudness for in general, the higher the peak pressure the greater is the judged loudness of the boom. Annoyance or loudness is increased as rise time is decreased. A decrease in rise time from 10 ms to 1 ms (Figure 2) corresponds to a 13 dB increase in loudness.

The presence of a peak factor which extends the rise time of a specific signature, with the remainder of the signature unchanged, increases the positive peak overpressure and the corresponding judged relative loudness. As shown in Figure 3 the peak factor alone increased the loudness by 4 dB and 8 dB relative to the standard reference signature. Relative annoyance and loudness are generally unaffected by N-wave signature durations. Figure 4 displays signature durations ranging from 100 ms to 500 ms for which the annoyance or loudness was reported as essentially the same. The relationships between sonic boom signature characteristics and subjective judgments of loudness or annoyance are reasonably well established.

2. Comparative Judgments of Booms vs Aircraft Noise

Methods for estimating the community acceptability of aircraft noise exposure are in use today, therefore, to study the acceptability of sonic booms relative to these established aircraft noise control guidelines is a logical approach to the sonic boom question. Although it is recognized that the experience of a sonic boom exposure is vastly different from that of aircraft noise, both from the standpoint of the stimulus characteristics and the nature of the exposure situation, quite good agreement in judgment tests has been found in the laboratory as well as in field studies to be discussed.

Pearson & Kryter (13) found (Figure 5) that a simulated indoor sonic boom of 1.7 psf was judged equally acceptable as a subsonic aircraft noise of 113 PNdB. Broadbent and Robinson (4) report findings that are almost identical to these 1.7 psf and 113 PNdB values. The present level of acceptability of noise around airports in terms of perceived noisiness is about 100 to 110 CNR* (outdoors) and this includes the wide range accounting for variations in time of day, number of exposures and the like, which are not considered in the laboratory sonic boom judgments. If a direct extrapolation was appropriate, the level of the 1.7 psf boom (113 PNdB) would exceed the range of acceptability as defined by the aircraft noise control guidelines.

The two major sonic boom exposure situations experienced by residents in a community are the indoor and the outdoor exposures. The outdoor exposure is nominally a clean signal or N-wave with a rapid initial rise time. The indoor sonic boom exposure is quite different because it is affected by the response characteristics of the building, i.e., cavity resonances of the rooms and mechanical excitation of the main building modes. Indoor booms are lower in magnitude, longer in duration, have slower rise times and visably vibrate objects within the building which generate rattling and other noises. Indoor sonic boom exposures, with the additional visual, vibratory and acoustic cues, are clearly less acceptable than those experienced out of doors. This well recognized difference between the acceptability of exposures to the same sonic boom stimulus indoor vs outdoor is demonstrated in Figure 5. The 1.7 psf sonic boom heard outdoors was judged equally as acceptable as a 94 PNdB aircraft noise. The large difference of 19 PNdB between the same sonic boom heard indoors and outdoors emphasizes the importance of recognizing the significantly greater unacceptability of indoor boom exposures.

3. Physiological Responses

Physiological responses of humans to sonic boom and other impulsive acoustic stimuli have been considered in the laboratory in the form of startle, effects on the auditory system and sleep interference. Although data are meagre in many areas and additional research is desirable some conclusions may be reached relative to the human auditory system and other immediate direct effects of sonic boom exposure.

a. Startle was investigated during a psychomotor tracking task in which the subjects were exposed to simulated sonic booms (9). Myographic responses (EMG's) taken from the contralateral (to tracking arm) trapezius muscle were the criterion measures. Subject groups experienced different amounts of sonic boom exposure prior to the initiation of their task performance. The experimental design for the study of startle response to simulated sonic booms is summarized in Figure 6. Group 1 began the tracking task in the initial test phase with simultaneous boom exposure while Group 4 tracked only during the final test session having experienced three boom sessions earlier. Startle responses to sonic booms, as measured by an increase in skeletal muscle tension, did occur. Figure 7 displays the mean differences in the electro-myograms between the measures recorded before and during the boom exposures. The mean-difference myographic responses

*Composite Noise Rating (CNR) is a procedure whereby physical measures of noise are adjusted to take into account number of occurrences, time of day of occurrences, spectra and intensity of the noise to provide a rating number which allows a meaningful interpretation of effects of the noise on human behavior.

appear directly related to the boom exposures as evidenced by their relative absence from the control group data. Some adaptation in this muscular startle response may be observed as a decrease in the mean difference values with successive sessions, however, after the four sessions (36 booms) the EMGs were still greater than those recorded by the control group. An extrapolation of these data, based on the assumption of a continued linear growth rate with successive sessions, would suggest that Groups 1, 2 and 3 would reach the Control level mean difference values around sessions 7 to 9. It would be of particular interest to pursue this response behavior until adaption stabalizes either at or somewhere above the Control Group level of response. Incidentally, the tracking performance was not significantly influenced by the boom exposures.

b. The human auditory system is adapted to respond to very small fluctuations in pressure and as such may be considered the human mechanism most sensitive to sonic boom type acoustic impulses. In a recent laboratory (1) study 91 subjects (12 females) were exposed to an impulsive acoustic stimulus with a positive peak pressure level of 168 to 170 dB, a median rise time of about 5 msec and a median duration of about 20 msecs. This acoustic exposure was very similar in signature and overpressure level to the intense near field sonic booms generated by a fighter type aircraft at very low altitude. Otological and audiometric examination of the subjects exposed to this laboratory stimulus revealed no adverse effects on the tympanic membrane or on auditory acuity. The sonic boom type acoustic impulses of 168-169 dB, were shown to be safe for the participating subjects, thus indicating a very wide margin of safety for community populations which experience nominal sonic booms of about 130 dB or so.

Rice and Coles (14), measured temporary threshold shift (TTS) for subjects exposed to simulated sonic booms produced by special explosive charges. Resulting TTS suggested that exposure to a sonic boom type N-Wave of 17 psf (152 dB) would not constitute an acoustic hazard and that exposures considerably greater than this can be safely tolerated. It was concluded that the sonic boom can be disregarded as a threat to the auditory system.

c. Lucas and Kryter have reported preliminary results of a study of effects of simulated sonic booms on sleep. Their laboratory consists of a furnished bedroom to which is attached a sonic boom simulator (Figure 8). Indoor booms of varying magnitudes and with good realism are generated inside the room. Two subjects slept in the test room each night of the study and their Electro-encephalograms (EEG's) were monitored continuously to reveal the sleep patterns experienced by the subjects and changes which occurred in these patterns due to the simulated sonic booms. The subjects were instructed to close a signal switch located on their bed if they awakened for any reason at all during the night. This "awakening response measure" was the only subjective behavior observed during the sleep interference study. Subjects were exposed during various stages of sleep to simulated indoor booms of 0.6, 0.8, 1.6 and 2.1 psf and the EEG and awakening response behavior were analyzed. Some of the major findings indicate that (1) sleep interference by booms is to some extent dependent on the individual, (2) significantly more awakening occurred with booms of 1.6 and 2.1 psf magnitudes (Stage 2 sleep) than from booms of lesser intensity, (3) some adaptation to booms of 0.6 and 0.8 psf occurred during stage 2 sleep (Figure 9), but adaptation to the 1.6 and 2.1 psf booms was not found and (4) awakening was about the same for all booms during the REM sleep stage. This last finding is significant for it suggests that booms of very low intensity level will be sufficient to awaken sleepers in the REM stage of sleep.

Laboratory studies have demonstrated (1) that loudness or annoyance is directly related to particular characteristics of the sonic boom signature, (2) that the acceptability of sonic booms can be related to the acceptability of subsonic aircraft noise with some degree of success, (3) that muscle startle response to sonic boom did occur as did partial adaptation in successive exposures, (4) that the human auditory system was not adversely affected by single impulsive stimuli of much greater intensities than are ever expected for sonic booms in communities and (5) that sleep interference and adaptation were observed for booms below 1.0 psf but not for booms in excess of 1.0 psf.

Field Studies (Controlled)

Experimental field studies have been conducted in the United States and the United Kingdom to further demonstrate the reactions of people to the sonic boom. Generally, aircraft in supersonic flight generate programmed sonic booms exposing personnel participating in the programs as well as panels of observers selected to provide subjective judgments of the exposures on some sort of a statistical basis. One type of field study has investigated comparative magnitude judgments of the sonic booms relative to subsonic jet aircraft flyover noise while another type, involving very high level sonic booms, has examined observable direct physiological response behavior or possible injury of man.

1. Loudness - Annoyance

The comparative loudness or annoyance of sonic booms vs subsonic jet aircraft flyover noise work is well represented by the UK Project Westminster (19) and the US Edwards AFB Program (6). In Project Westminster two juries of observers were exposed, both indoors and outdoors, to sonic booms from military aircraft, explosive bangs, a subsonic jet aircraft flyover noise and indoors to an occasional door slam. Of particular interest is the comparative judgment findings shown in Figure 10. A sonic boom of 1.7 psf was judged equally annoying as a flyover noise of 110 PNdB heard indoors. This finding is surprisingly close to that reported in the laboratory comparative judgment studies wherein 1.7 psf was judged equivalent to 113 PNdB aircraft noise. As a matter of added interest, it was reported that the door slams were judged 29% more annoying than

any of the sonic booms experienced in the study.

The Edwards AFB study, utilizing the same general jury type approach as that used in Westminster, measured the relative acceptability of sonic booms and noise from various types of aircraft employing the psychophysical technique of paired-comparison judgments. Observations were made both indoors and outdoors at the specially constructed test site. Individuals with prior experience with aircraft noise and sonic boom, those with little and those with no prior experience were included among the observers.

A major finding of these experiments was the clearcut difference in subjective judgments of annoyance as a function of the prior experience of the subjects with noise and sonic boom exposure. As shown in Figure 11, for indoor booms, individuals with prior experience (Edwards) judged the B-58 nominal sonic boom of 1.69 psf equally acceptable with a subsonic jet aircraft noise of 109 PNdB. Those with little experience (Redlands) judged the same boom equal to 118 PNdB aircraft noise and those with no experience (Fontana) equal to 119 PNdB noise. The same relationships hold for the outdoor listening conditions. In addition, the 1.69 psf sonic boom was rated as "just acceptable" to "unacceptable" by 27% of the Edwards subjects and by 40% of the others.

It is clear from the field and the laboratory study that comparative judgments of the annoyance or acceptability of sonic boom and aircraft flyover noise have been made with reasonably good reliability and in this sense have some validity for estimating relative acceptability of sonic booms. However, it must be reemphasized that relationships between laboratory judgments of annoyance and the annoyance actually experienced during everyday living have not been established.

2. High Level Sonic Booms

In the United States various programs have been conducted primarily for military purposes during which personnel were exposed to very intense sonic booms, several orders of magnitude greater than what would ever occur in a community. In one study, personnel experienced sonic booms at a maximum peak overpressure level of 120 psf (10), while in another the maximum sonic boom exposure of the experimenters was 144 psf (12). Although no biomedical monitoring by electronic means was accomplished the observations of individuals experienced in noise exposure were carefully reviewed. Transient tinnitus and fullness in the ears were reported by the observers exposed to the very intense booms. No aural pain was reported for sonic booms of up to 144 psf. Neither temporary nor permanent effects on auditory acuity were subjectively reported or observed.

During a study at White Sands (16), no significant temporary shift in hearing levels was observed after days of exposure to an average of 30 sonic booms daily ranging in overpressure from 2 to 24 psf. In general, no adverse effects of the very intense sonic boom exposures on any human function were observed. As stated earlier relative to the laboratory study of impulsive (sonic boom) type noises, the margin of safety for community exposures to sonic booms is very wide and the probability of direct damage to the human auditory or other physiological system under those conditions is essentially non-existent.

Controlled field study results are in good agreement with the laboratory findings enumerated above. In addition, the significance of prior exposure to sonic boom and noise in affecting judgments of annoyance or loudness was clearly demonstrated.

Field Studies (Uncontrolled)

The community survey approach to the sonic boom problem investigates the attitudes, opinions and reactions of individuals exposed to sonic booms during their day-to-day living activities. This approach has been taken in specific programs in France, in the United Kingdom and in the United States. The paradigm of these studies consists of exposures of whole communities to sonic booms generated by aircraft flying supersonic over the designated populated areas, of the measurement or calculation of sonic boom magnitude occurring within the community and of assessment of the community response by various means.

1. United States

The first extensive survey of community reactions to sonic booms in the US was conducted in St. Louis (11) where the population was repeatedly exposed to sonic booms ranging in overpressures up to 3.1 psf. Results were obtained from personal interviews in more than 1,000 households, analyses of complaint files and of alleged damage evaluations. About 90% of the community experienced some interference with ordinary living activities, 35% were annoyed and 10 percent had considered complaint action. This study served as a basis for and was followed approximately 2 years later by the Oklahoma City study.

The Oklahoma City (3) program is considered by many to be the most comprehensive experiment to date on sonic boom exposure of a large community over a relatively long period of time. Eight sonic booms per day (total of 1,253) were programmed at overpressure levels of from 1.5 to 2.0 psf and personal interviews were completed with 3,000 families three times each, during the six month program. Results of this program were quite extensive and were obtained from personal interview, from complaint files, and claim actions all of which were related in the analysis to the sonic boom pressure measurements.

Responses of residents of the Oklahoma City area were quite similar and in good agreement with the findings in the St. Louis program. Interference, annoyance and complaint activity were generally the same. Community adaptation to the boom could not be determined because the intensity of the stimulus was gradually increased at various times during the program. Annoyance was strongly related to believed or expected damage to personal property. At the end of six months, about one fourth of the residents felt they could not learn to live with or accept eight sonic booms daily.

Of the many conclusions to be drawn from this study, one relating to complaint activity is considered vitally significant. This may be observed in Figure 12, which is a chronological history of the complaints and alleged incidents of damage to property received at the Complaint Center during the program. In general, the curves represent the high initial response expected at the introduction of overflights to a community and some degree of adaptation with time and continuation of the same stimulus exposure. One of the most significant aspects of these curves consists of the irregularities or peaks which appear thereon and the factors which caused or contributed to them.

Each of the peaks can be related to some event or incident which received widespread coverage via the local news media and which in almost all instances was independent of the stimulus. This means that the community reactions as reflected by the peaks on these curves were not directly related to the sonic boom but were strongly influenced by factors other than the stimulus. This finding is not encouraging for one who wishes to estimate reactions to sonic boom based solely on the physical stimulus.

The numerous facets of this study serve (1) to emphasize that the problem of community exposure to sonic boom is very complicated and (2) to offer a considerable basis for interpretation.

A community survey was conducted at Edwards AFB in 1966 which permitted the comparison of attitudes from 793 persons toward sonic boom exposures prior to and during a special test period of boom activity increased over that usually experienced by the residents. Prior to the test the exposure was 4 to 8 booms per day at a mean overpressure level of 1.2 psf. During the tests (a one month period) 289 booms were generated at a mean overpressure level of 1.7 psf.

More than 50% of the respondents had experienced the 4-8 boom exposure schedule for over a year. Some adaptation to sonic boom exposure is believed possible when one is exposed regularly on a daily basis to sonic booms since 60% found the boom more acceptable after being regularly exposed to it before the tests. Ten booms per day at an overpressure level of 1.7 psf less than acceptable for these respondents as it was for Oklahoma City residents.

2. United Kingdom

A number of community programs have been conducted in the United Kingdom (UK) in which the impulsive stimuli were in some cases sonic booms from supersonic aircraft and in others pressure waves from explosive charges. Exercise Crackerjack (17) exposed people to sonic booms and explosive bangs at intensities of from 1.0 to 2.0 psf. Among the findings it was concluded that explosive bangs closely resembled sonic booms but were more annoying than the booms after subjects become familiar with them. Explosive bangs were judged to be adequate stimuli for future studies of sonic boom effects on people.

Project Yellow Hammer (18) was a more extensive community program, which used explosive charges as the basic impulsive stimuli. A small community of less than 300 residents was exposed to explosive bangs ranging from 0.5 psf to 7.5 psf on an exposure schedule of from 8 to 72 booms per day (Figure 13). The standard program called for 24 bangs daily during the working hours at an overpressure level of 2.6 psf. Residents were interviewed weekly to determine the extent of their annoyance with the booms heard during the previous week. In general, it was found that annoyance decreased with familiarity with the bangs and this appears particularly significant because the overpressure level of the bangs remained at about 2 to 2.5 psf during this time.

As clearly shown in Figure 14, the percentages of both those persons considerably annoyed and those persons less annoyed (at all) decreased as the program progressed from the first thru the fourteenth week. The considerably annoyed group appeared to decrease only about five percent from about 17% to 12% whereas the other group decreased about 33% from about 53% to 20%. The two sharp peaks of approximately equal magnitude appearing for each group at the 10th and 14th weeks correspond to a 3-fold increase in the number of booms and an increase in the overpressure by a factor of 2 in that order. This is interpreted as indicating that the annoyance generated by increasing the number of booms per day by a factor of three was essentially equivalent to that resulting from a doubling of the standard overpressure of 2.6 psf. The community reflected some adaptation to the repeated sonic boom exposures, however the community was considered not to be a noise sensitive community.

3. France

In 1965, approximately 2,300 personal interviews were conducted in eastern (Strasbourg area) and southwestern (Bordeaux area) France to assess community responses to military aircraft flying supersonic over those regions and to estimate projected acceptability of future booms to the

citizens (5). No data on the physical stimulus, number of booms, prior exposure of individuals and the like, were available. Among the results it was found that (1) interference with daily living activities was about the same as in St. Louis and Oklahoma City, but a higher percentage of respondents felt they could not live with 10 booms per day, (2) expectation of property damage and personal injury were significant factors in annoyance, (3) reaction to general noise was unrelated to reaction to the sonic boom, and (4) the response "no" was given to the proposal that an Oklahoma City type study be conducted in France. Observations of the behavior of residents and attitude surveys during community studies have contributed to an increased understanding of the sonic boom problem.

Present Suggested Criteria For Acceptability

Based upon an integration of the community overflight experiments with experimental field and laboratory studies, past experience and observations, the question of criteria for acceptability of sonic booms in the community may be approached.

The sonic boom continues to influence the design, economy and planned operation of commercial supersonic aircraft and is a major consideration in military programs involving aircraft flying at supersonic speeds over populated areas. Although many factors influence human response to sonic boom, the peak overpressure value of the physical stimulus has been the basic characteristic associated with measures and estimations of human reactions. Interim estimations of effects of sonic booms on people and expected community reactions considered only ground overpressure as the relevant factor. A present proposed extension of the Composite Noise Rating (CNR) method of estimating effects of aircraft noise exposures on communities (7) to include estimates of effects of sonic booms considers in addition to peak overpressure, the frequency of the boom occurrences and other variables. Major objections to such an extrapolation are recognized. However, some support is derived from the fact that data from laboratory, field and community response studies are consistent with each other.

Composite noise rating (CNR) is a method of relating the undesirable aspects of noise exposure to response behavior of people by means of calculations based on the characteristics of the noise exposure. The calculation provides a number (CNR) for the noise which is related to the expected behavior of a population exposed to the noise. These methods are well established for various habitual noise environs and especially for noise associated with aircraft operations. This rating method is based primarily upon the magnitude of the noise exposure, the duration of the individual exposure, the number of occurrences and the time of day. Another method, Noise Exposure Forecast (NEF) procedures, define the undesirable aspects of aircraft noise in the same general manner as the CNR, however, the NEF includes additional corrections for duration and for the presence of discrete frequencies in the exposure (2). Reactions of people in communities exposed to aircraft noise environments of different CNR's do correspond to the predicted behavior, confirming the validity of the procedure for aircraft noise evaluations (Figure 15).

The experimental field and laboratory studies revealed that even though the sonic boom is a vastly different acoustic stimulus from aircraft noise, its loudness or annoyance can be reliably judged relative to the noise. Equally as important is the fact that annoyance with sonic boom exposures is strongly influenced if not determined by the magnitude and frequency of occurrence of the boom, as it is for noise. Intuitively, since basic factors contributing to annoyance with the signal are the same for noise and sonic boom, the CNR might be considered as a tentative present criteria for acceptability of sonic booms as well.

Immediately, objections to this consideration may be stated in terms of the differences in durations of the various types of signals, the absence of startle with aircraft noise, significantly greater presence of vibrations and rattlings of dwelling contents with sonic booms, the presence of believed damage to property and of the fact that sufficient evidence is not presently available to fully substantiate such a proposal. These are rather formidible arguments which cannot be ignored and a more positive conclusion will require additional information either for or against such a consideration.

Kryter (8) extrapolates composite noise ratings for sonic booms, accepting the equation that a sonic boom of 1.9 psf (population has adapted over the years) will be subjectively equal to a subsonic aircraft noise of 110 PNdB. On this basis, one boom per day would provide a CNR of 98 and the CNR would increase with greater frequencies of occurrence of the boom. In general, sonic booms of 1.9 psf occurring at a rate of 2-3 or more daily would result in CNR's of 100 and more which would indicate sporadic to vigorous, widespread complaints and appeals to authorities by exposed communities.

Possible supersonic commercial overland flight schedules anticipated when the British-French Concorde and the US SST are fully operational are shown in Figure 16. Such schedules, depending on routing, could expose 35 to 65 million people to 10-20 booms daily ranging in overpressure from 1.3 to 2.1 psf. According to the extrapolation made earlier, vigorous, widespread complaints could be expected from the population under the flight path and from many persons at a lateral distance or at least 12.5 miles from the flight path. Political and legal action against the boom from the SST would appear to be assured.

A level of acceptability of sonic boom exposure in the community has not been established. The wide variations in stimuli, immediate environs and response behavior due to socio-psychological factors suggest that the concept of a range of acceptability or unacceptability indicating minimum

and maximum acceptability is perhaps more appropriate than a single value guideline. The minimum acceptability values could describe those sonic booms to which no adverse response would occur and the remainder of the range would describe degree of unacceptability. Regardless of the form of such data, judgments will be required by individual users of the information, i.e., those responsible for aircraft certification, planning, etc., according to the manner in which they wish to apply it or in other words, according to the degree of unacceptability to be experienced. Although acquisition of additional technical knowledge is both necessary and desirable the establishment of community exposure criteria is not solely dependent on new research data. Whenever efforts are initiated to establish such criteria, decisions will still be required as to the exposure parameters to be incorporated and the number of people to be exposed.

Summary

Human response to sonic boom has been reviewed primarily in terms of possible physiological and psychological responses as found in experimental field and laboratory studies and community survey programs.

1. The probability of immediate direct physiological injury to persons exposed to sonic booms in the community is essentially zero. Long term effects on health of repeated daily exposures to sonic booms has not been investigated.

2. Startle occurs in response to the sonic boom and some adaptation is observed with repeated exposures. However, the extent to which adaptation of startle to the boom may occur is undetermined. Typical transient changes in respiration, heart rate, etc., might be expected to accompany startle, however, this does not imply that the exposed is being harmed in any way.

3. Sleep interference from night time booms, which may be a major determinant of public reaction, was observed for simulated sonic booms in excess of 1.0 psf for which adaptation did not occur during the test period. All sonic booms in that study were adequate stimuli for awakening subjects during their REM state of sleep. Possible long term effects on sleep of repeated nightly exposure to sonic booms are not known.

4. Comparative judgments of the relative annoyance of sonic booms and aircraft noise are in good agreement and form a basis for considering the acceptability of sonic boom exposures (primarily during day time) in terms of Composite Noise Rating.

5. A level of acceptability of sonic boom exposures in the community has not been determined. Determination of the exposure level below which no adverse response occurs would be desirable.

6. Sonic booms from fully operational SST schedules of present configuration vehicles flying over the US several flights per route per day, in terms of current estimates of the overpressures they would generate, would likely result in widespread action against the boom and its source. Night-time operation would make this action considerably stronger. There is evidence that reactions in European countries would not be very different.

7. Although physical parameters of the sonic boom signature important to annoyance or loudness have been identified, a standard procedure for measuring and describing the sonic boom is not agreed upon and in use. Positive peak overpressure is widely described as a less than satisfactory measure but still remains the primary measure found almost universally in the scientific and technical community to physically describe the exposure experience. Energy spectral density includes more of the relevant information than peak pressure alone.

Although basic human behavior and community response to the sonic boom is not expected to drastically change with time, different factors motivating the attitudes and opinions that result in response behavior may develop in the future. It is possible that human responses measured today may differ somewhat from those recorded in the next eight to ten years. It would be expected that acceptability might increase slightly with adaptation over a few years, however, it cannot be determined at this time whether such a change would have any appreciable effect on the overall community response.

Finally, it must be considered that introduction of the sonic boom from commercial SST operation constitutes a new phenomenon in aircraft noise and environmental pollution in general: probably never before has a technological development exposed with one step such a large number and large percentage of the general population to such an increase in disturbing acoustic stimuli. The new phenomenon would be such that it would be virtually impossible for people to escape the sonic boom and avoid boom exposed areas similar to the way some people avoid noise polluted areas in our major cities today. The sonic boom from SST operation would probably not make the environment more noisy than the environment many people have to tolerate today in the vicinity of airports; the main difference will be that instead of a small minority a large percentage of the population will be exposed almost without escape to this new noise.

In spite of all research and predictive capability the final decision as to what boom environment people will be willing to tolerate cannot be made until the real environment will surround their daily living. Therefore, a decision to fly over water and not over land is wise for it will introduce the new environment as slowly and controlled as possible gathering experience which can be used to modify the situation without undue harm to technological progress, economy and first of all human health and happiness.

REFERENCES

1. Authors' data to be published.

2. Bishop, Dwight E. and Horonjeff, Richard D., "Procedures for Developing Noise Exposure Forecast Areas for Aircraft Flight Operations," Aircraft Development Service, FAA DS-67-10, August 1967.

3. Borsky, P. N., "Community Reactions to Sonic Booms in the Oklahoma City Area," National Opinion Research Centre, AMRL-TR-65-37 (1965).

4. Broadbent, D. E. and Robinson, D. W., "Subjective Assessment of the Relative Annoyance of Simulated Sonic Bangs and Aircraft Noise," J. Sound Vib., 1-2, 162 (1964).

5. de Brisson, Med. Lt Col, "Opinion Study on the Sonic Bang," RAE Library Translation No. 1159 (1966).

6. Kryter, Karl D., "Sonic Boom Experiments at Edwards Air Force Base," NSBEO-1-67, 28 July 1967.

7. Kryter, Karl D., "Concepts of Perceived Noisiness, Their Implementation and Application," JASA, Vol. 43, No. 2, February 1968.

8. Kryter, Karl D., "Sonic Booms From Supersonic Transport," Science, Vol. 163, 24 January 1969.

9. Lukas, J. S. and Kryter, K. D., "A Preliminary Study of the Awakening and Startle Effects of Simulated Sonic Booms," SRI Final Report, Contract NAS 1-6193 (1968).

10. Maglieri, D. J., Huckel, Vera and Parrott, Tony L., "Ground Measurements of Shock-Wave Pressure for Fighter Airplanes Flying at Very Low Altitudes and Comments on Associated Response Phenomena," NASA TN D-3443, Langley Station, Hampton, Virginia, July 1966.

11. Nixon, C. W. and Hubbard, H. H., "Results of USAF-NASA-FAA Flight Program to Study Community Responses to Sonic Booms in the Greater St. Louis Area," NASA TN D-2705 (1965).

12. Nixon, C. W., Hille, H. K., Sommer, H. C. and Guild, E., Lt Col, USAF, "Sonic Booms Resulting From Extremely Low-Altitude Supersonic Flight: Measurements and Observations on Houses, Livestock and People," AMRL-TR-68-52, October 1968.

13. Pearsons, K. S. and Kryter, K. D., "Laboratory Tests of Subjective Reactions to Sonic Boom," NASA CR-187 March 1965.

14. Rice, C. G. and Coles, R. R. A., "Auditory Hazards From Sonic Booms?" International Audiology, VII, No. 1, March 1968.

15. Shepherd, L. J. and Sutherland, W. W., "Relative Annoyance and Loudness Judgments of Various Simulated Sonic Boom Waveforms," NASA CR NAS-1-6193 Subcontract B-87017-US.

16. Sonic Boom Structural Response Test Program, White Sands Missile Range, New Mexico, SST-65-4, Federal Aviation Agency, Washington, D.C., March 17, 1965.

17. Warren, C. H. E., "A Preliminary Analysis of the Results of Exercise Crackerjack and Their Relevance to Supersonic Transport Aircraft," RAE TN No. Aero 2789. ARC 23273.

18. Webb, D. R. B., and Warren, C. H. E., "An Investigation of the Effects of Bangs on the Subjective Reaction of a Community," J. Sound Vib. 6-3, 375 (1967).

19. Webb, O. R. B., and Warren, C. H. E., "Physical Characteristics of the Sonic Bangs and Other Events at Exercise Westminster, RAE TR65248 (1965).

20. Zepler, E. and Harel, J. R. P., "The Loudness of Sonic Booms and Other Impulsive Sounds," J. Sound Vib. 2-3, 249 (1965).

LIST OF FIGURES

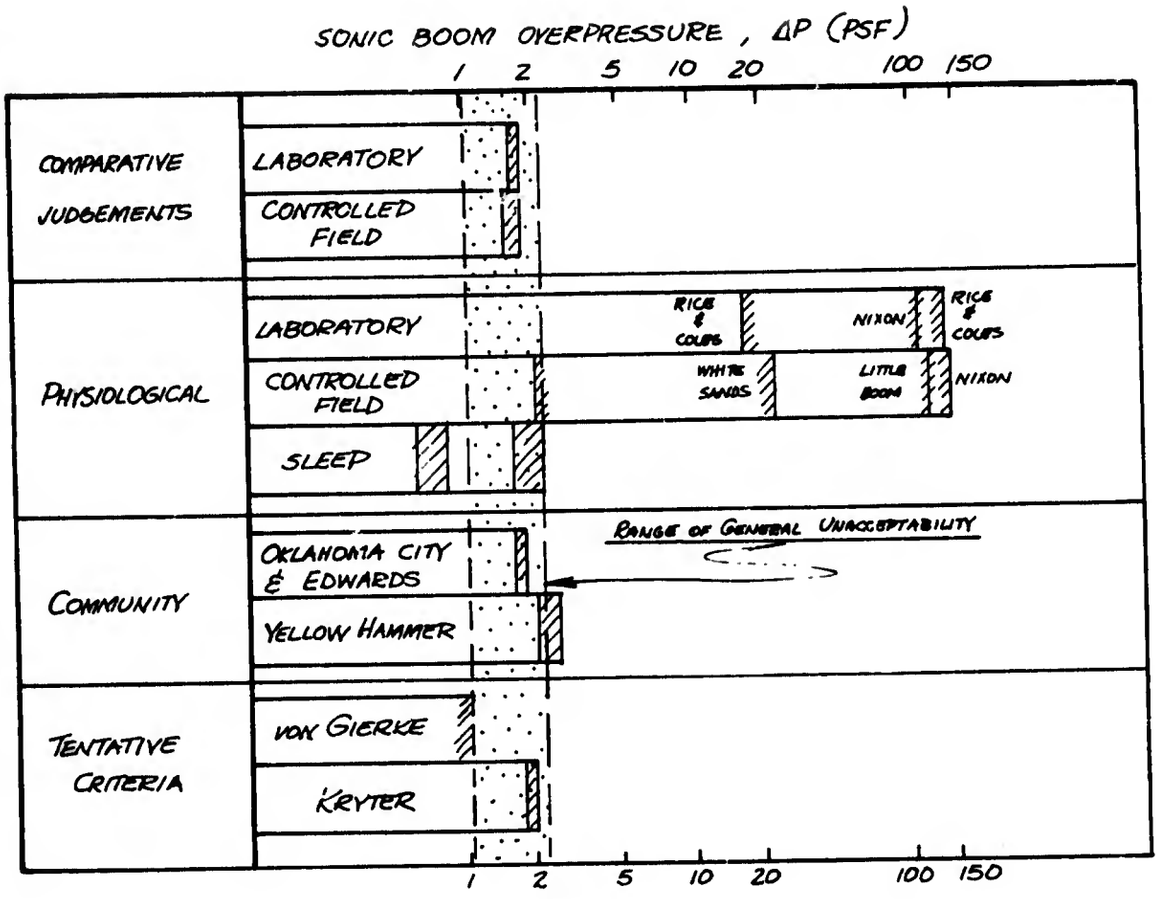

Fig. 1

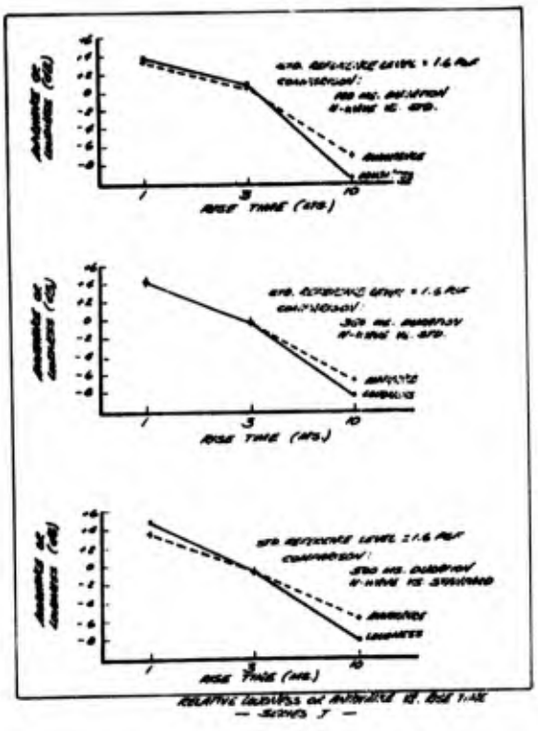

Fig. 2

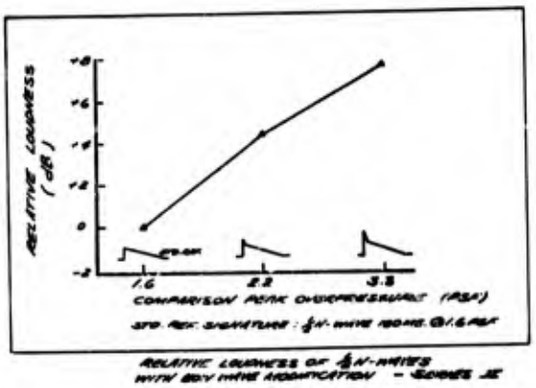

Fig. 3

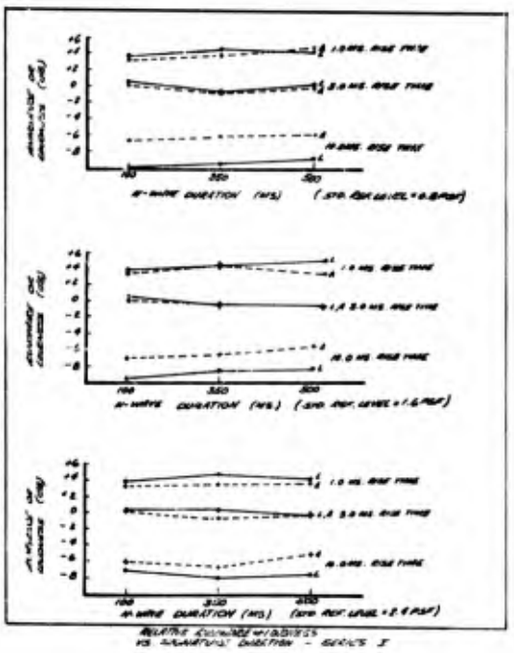

Fig. 4

RESULTS TO DATE

(NOTE - ALL PHYSICAL MEASURES AS THOUGH MADE OUTDOORS)

L

SUBSONIC AIRCRAFT

P&K (N=20) BOOM	NOISE EQUAL TO BOOM	
1.7 psf	INDOORS	OUTDOORS
	113 PNdB	94 PNdB

B&R (N=87) BOOM	NOISE EQUAL TO BOOM	
1.7 psf	INDOORS	OUTDOORS
	107-113 PNdb	

2. LOUDNESS AND ANNOYANCE OF OUTDOOR BOOM PREDICTABLE FROM SPECTRUM AND CALCULATED LOUDNESS OR PERCEIVED NOISE LEVELS

Fig. 5

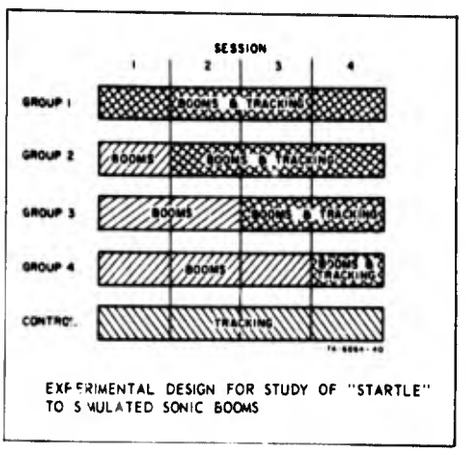

EXPERIMENTAL DESIGN FOR STUDY OF "STARTLE" TO SIMULATED SONIC BOOMS

Fig. 6

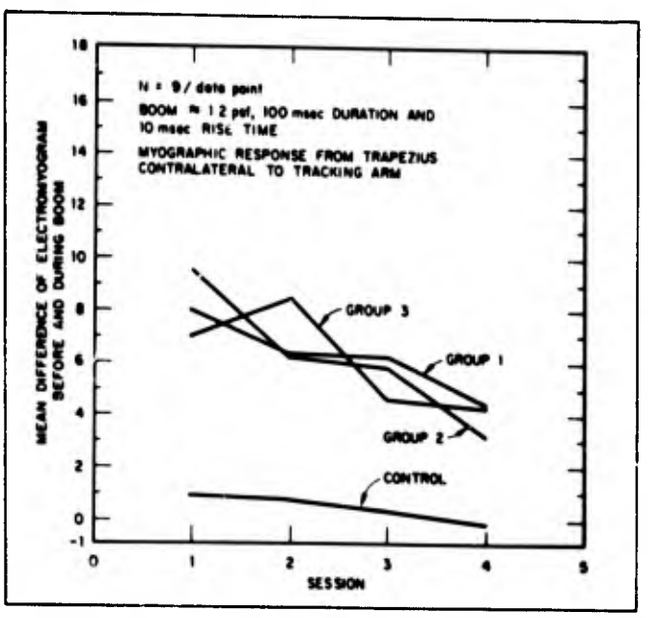

Fig. 7

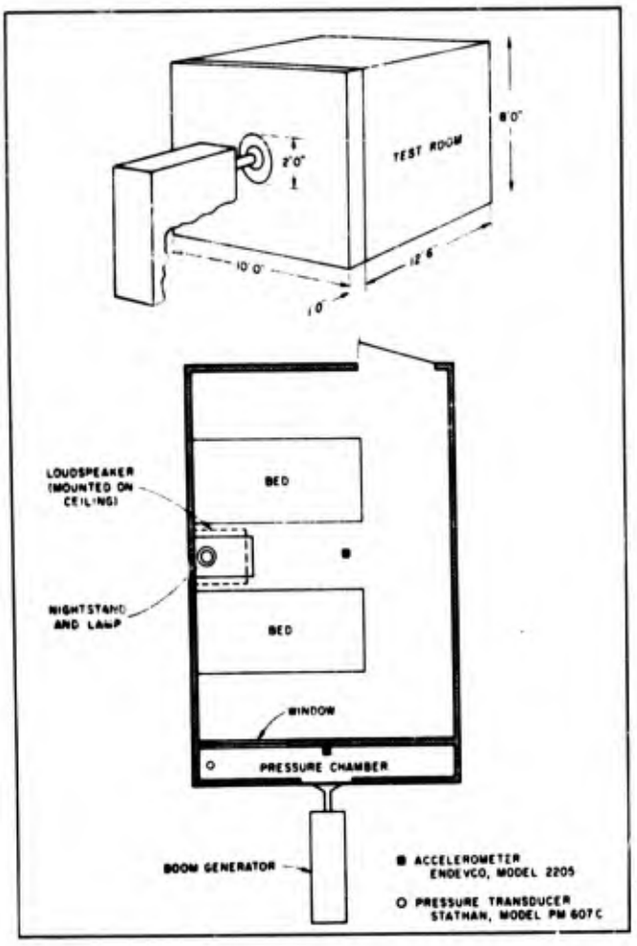

Fig. 8

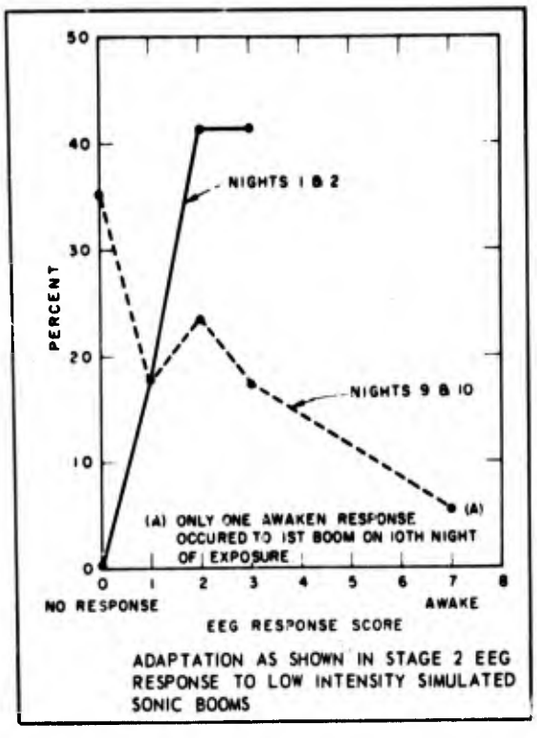

Fig. 9

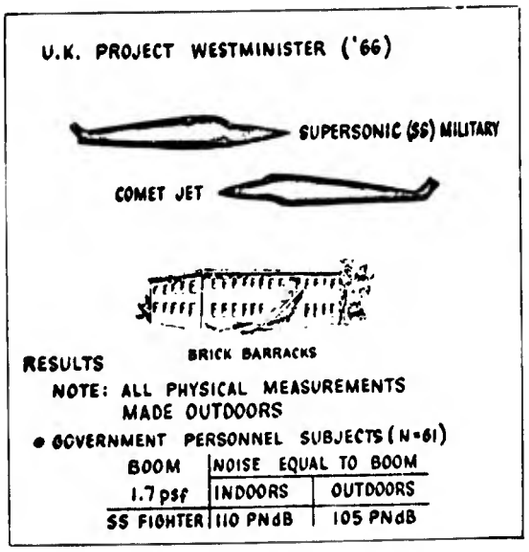

Fig. 10

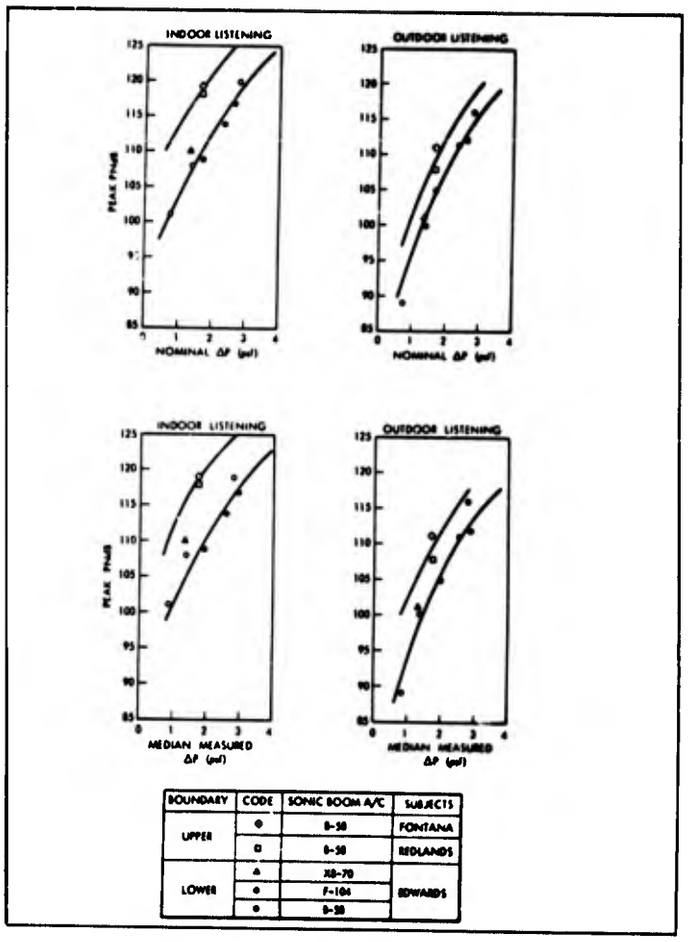
INDOOR LISTENING
OUTDOOR LISTENING
PEAK PNdB
NOMINAL ΔP (psf)
INDOOR LISTENING
OUTDOOR LISTENING
PEAK PNdB
MEDIAN MEASURED ΔP (psf)
MEDIAN MEASURED ΔP (psf)
BOUNDARY
CODE
SONIC BOOM A/C
SUBJECTS
UPPER
B-58
FONTANA
B-58
REDLANDS
LOWER
XB-70
EDWARDS
F-104
B-58

Fig. 11

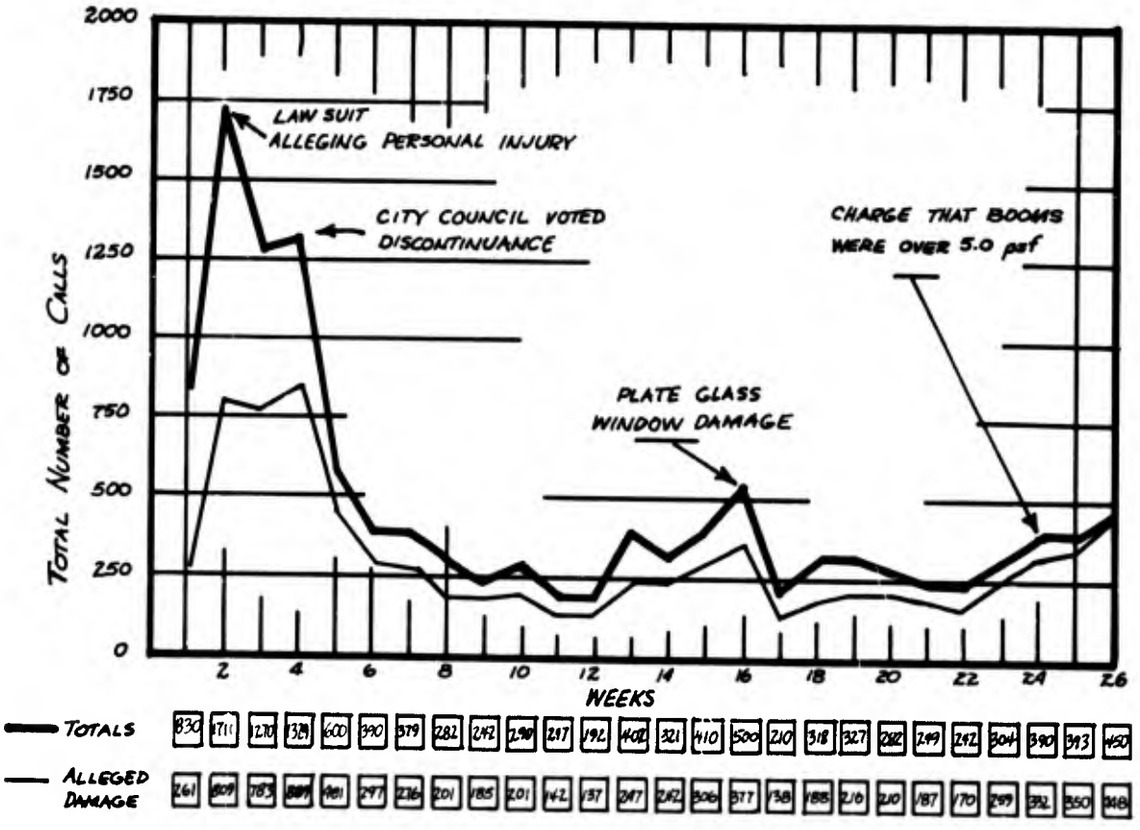
TOTAL NUMBER OF CALLS
2000
1750
1500
1250
1000
750
500
250
0
LAW SUIT ALLEGING PERSONAL INJURY
CITY COUNCIL VOTED DISCONTINUANCE
CHARGE THAT BOOMS WERE OVER 5.0 psf
PLATE GLASS WINDOW DAMAGE
2
4
6
8
10
12
14
16
18
20
22
24
26
WEEKS
TOTALS
830 711 1270 1328 600 990 979 1282 1242 1298 1217 1192 1402 1321 1410 1500 1210 1318 1327 1282 1299 1242 1304 1390 1393 1450
ALLEGED DAMAGE
1261 1009 1785 1889 981 1297 1236 1201 1185 1201 1142 1137 1247 1242 1306 1377 1358 1388 1210 1210 1187 1170 1299 1392 1350 1348

Fig. 12

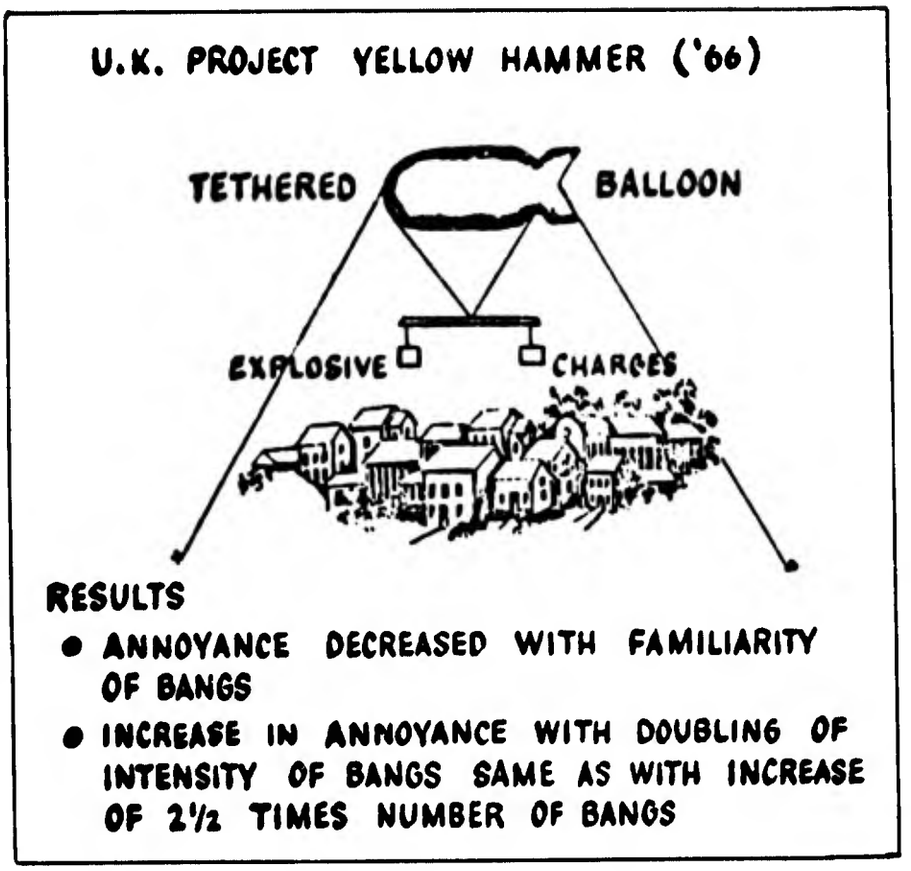

Fig. 13

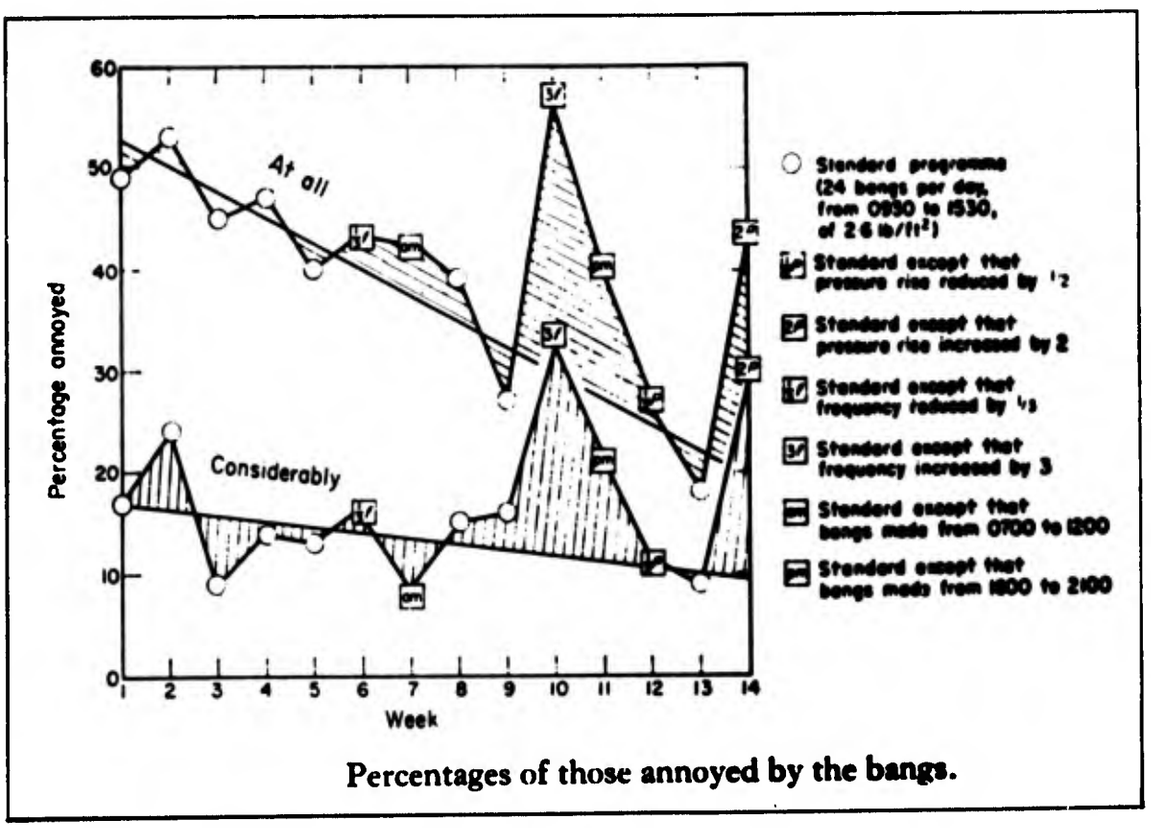

Percentages of those annoyed by the bangs.

Fig. 14

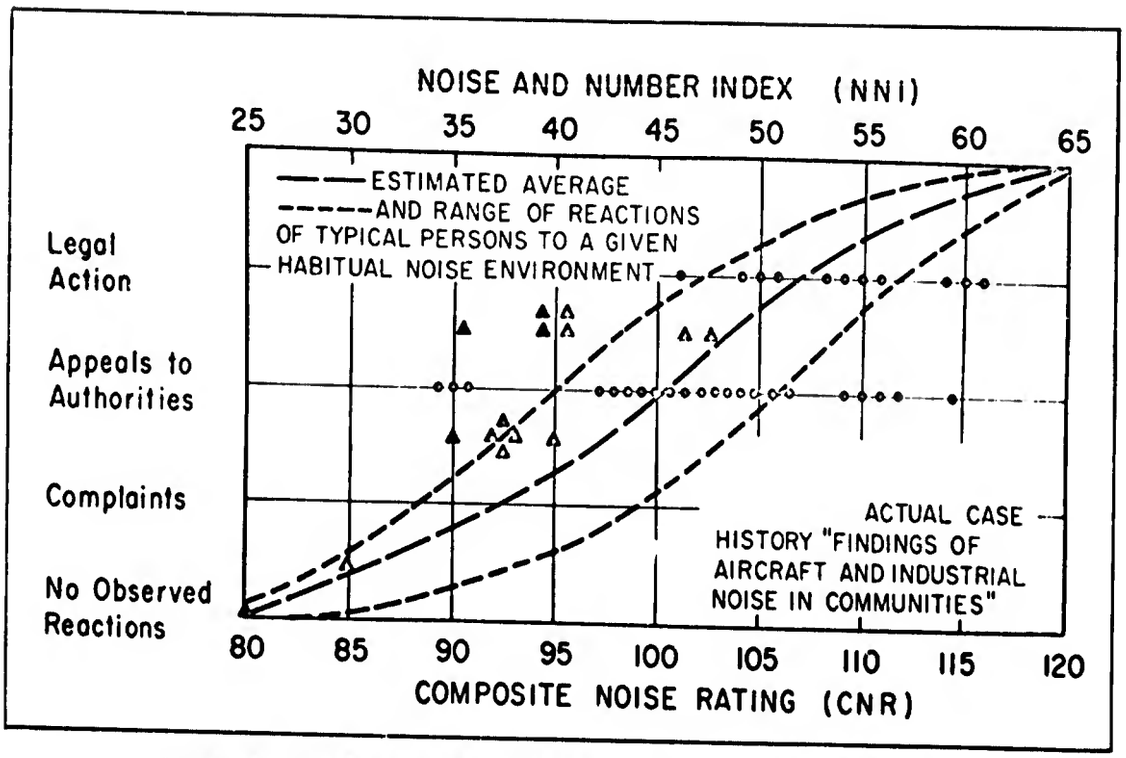

GENERAL RELATION BETWEEN COMMUNITY RESPONSE TO AIRCRAFT OR OTHER NOISES AND COMPOSITE NOISE RATING OR NOISE AND NUMBER INDEX.

Fig. 15

SUMMARY OF SONIC BOOM PROBLEM AND RESEARCH CONCLUSIONS

POSSIBLE OVERLAND SST OPERATIONS

1. MEDIAN BOOM INTENSITIES		UNDER FLIGHT PATH		12.5 MILES TO SIDE OF FLIGHT PATH	
		TRANSSONIC	CRUISE	TRANSSONIC	CRUISE
	BOEING	2.1 psf (est)	1.8 psf (est)	1.6 psf (est)	1.3 psf (est)
	CONCORDE	2.0 psf (est)	1.9 psf (est)	1.5 psf (est)	1.4 psf (est)

2. 50% OF LONG HAUL U.S. AIR TRAVEL ON SST WOULD PRESENT 10-20 BOOMS PER DAY TO:
   a. GREAT CIRCLE ROUTES
      65.5 MILLION PEOPLE (WITHIN 25 MILE BOOM PATH)
   b. CIRCUITOUS ROUTES
      35 MILLION PEOPLE (WITHIN 25 MILE BOOM PATH)

Fig. 16

BLANK PAGE

TURBOFAN ENGINE NOISE - MECHANISMS AND CONTROL

by

Colin G. Gordon

Bolt Beranek and Newman Inc.

SUMMARY

At the exhaust flow velocities typical of current turbofan engines, a number of source mechanisms for broadband noise generation can be postulated. These sources exist within the engine and act in addition to the more classical sources of jet noise that arise in the turbulent exhaust stream.

Data are presented from laboratory studies that illustrate the importance and suggest the parametric dependence of some of these sources. These sources seem to play a particularly significant role in the turbine and fan exhaust ducts of an engine--a role which may be augmented, rather than diminished by current techniques of engine quieting.

There is much to be learned about these sources before their significance in current and projected engine designs can be properly understood. Part of this understanding may derive from careful and systematic studies of current vehicles. Some ideas are suggested for such a study.

SYMBOLS

c	speed of sound
D	diameter of pipe
$\tilde{F}$	fluctuating-force amplitude
f	frequency
f_o	constant having dimensions of frequency
I	acoustic intensity
k	constant
$k(s)$, $k'(s)$	spectrum-shape constants
S	Strouhal number
U	flow velocity
U_c	constricted-flow velocity
W	radiated power
Δp	pressure drop across obstruction
δ	geometric thickness of wake
ρ	gas density

IT HAS LONG BEEN RECOGNIZED that the noise of turbulent mixing in the exhaust of a jet engine is not the only significant source of engine noise. Past measurements on turbojet vehicles operating at low power setting appear to indicate a change in source characteristic that can be accounted for by postulating source mechanisms within the engine itself. Such mechanisms seem reasonable in light of current aerodynamic noise theory and can be associated with flow through compressor and turbine blading, with combustion processes and with the simple flow of turbulent gases through the engine ducting.

The advent of the turbofan vehicle has brought with it an intensification of those parameters that seem to favour internally generated sound; a reduction of typical operating flow velocities; increase in the intensity of flow turbulence; increase in the extent of solid surfaces within the vehicle. Yet these "new" mechanisms of aerodynamic noise generation are not properly understood and the engine designer is not able to predict, with any surety, the sound output of a new design or to develop, with confidence, noise suppression devices for existing vehicles.

There is a very significant step between recognizing a new area of noise generation and devising and developing the analytical and engineering tools to cope with it. This truism is compounded by the complexity and adverse environment of an engine; an engine does not serve as an ideal device for fundamental studies. It is possible, however, to model some of these mechanisms in the laboratory using specially designed air jets. The experiment described in this paper consisted, in essence, of a stationary flow obstruction inserted into an air jet carrying subsonic air flow. The intent was to model schematically, a turbofan vehicle--low speed flow, high in-duct turbulence and extensive discontinuous surfaces.

Much of the content of this paper has been reported elsewhere (1,2,3,4). New data from an extension to this study (5) have recently become available however. These data have an influence on the conclusions drawn.

SOURCES OF AERODYNAMIC NOISE

The three most fundamental sources of subsonic aerodynamic noise that can be elicited from aerodynamic noise theory are respectively the monopole, the dipole and the quadrupole. These sources have been discussed analytically in detail elsewhere (6,7,8), and it will suffice here to present a simple physical interpretation of these sources as they might relate to the experimental system, shown schematically in Fig. 1.

The aerodynamic monopole source is generated by a net perturbation of the volume flow across the exit plane of the jet pipe. The simple convection of turbulence across the plane is not, necessarily, in itself sufficient since no net volume flow fluctuation might arise. What is required is, perhaps, flow of large scale turbulence across the plane or the presence of instability in the rate of flow into the jet pipe system--caused, for instance, by combustion instability in the engine. It can be shown analytically that the intensity of acoustic radiation (I) from the monopole source has the parametric dependence

$$I \sim \rho U^4/c^3 \qquad (1)$$

where ρ is the fluid density, U the mean flow velocity and c the speed of sound (9). The aerodynamic monopole thus displays a dependence upon the fourth power of flow velocity.

The aerodynamic dipole derives from the fluctuating lift- and drag-forces generated when turbulence impinges on a surface or when turbulence is shed by a surface. It can be shown, analytically, that the acoustic radiation from dipole sources has the parametric dependence

$$I \sim \rho U^6/c^3 \qquad (2)$$

The aerodynamic dipole thus displays a dependence upon the sixth power of flow velocity. There are obviously many opportunities for dipole-like noise to be generated within an engine: wake shedding by, and wake impingement on, stator and rotor blading, flow of heavy turbulence past surface discontinuities in ducting, turbulence shedding at the exit lip of the jet pipe, and so forth. One might suppose also that the presence of net flow perturbation through the system (which leads to monopole radiation) would also cause perturbation of the net thrust and thus dipole sound in addition.

The final source of present interest, the aerodynamic quadrupole, derives from the turbulent mixing that occurs in a wake or in the free exhaust of a jet. The radiation efficiency is related to the scale of the turbulence. Net flow perturbation is not required and no surfaces are needed. The acoustic intensity for quadrupole sound can be shown to vary as

$$I \sim \rho U^8 / c^5 \qquad (3)$$

Thus a quadrupole displays a dependence upon the eighth power of flow velocity. The quadrupole sources in the exhaust jet dominate the sound of commercial turbojet engines at high subsonic flow speeds. Part of the purpose of the present paper is to query the role played by the quadrupole source in the current generation of turbofan vehicles.

EXPERIMENT

The experiment was designed to study the noise radiation from a jet exhaust when a flow obstruction was placed in the jet pipe some distance upstream from the exit plane. A flow obstruction, it was felt, would simulate the turbulence generating propensities of stationary and moving surfaces associated with the compressor (and fan) within an engine, and with discontinuities in the internal geometry of the exhaust ducting. Since the experiment was limited to subsonic flow conditions, it was felt that the study was especially relevant to the turbofan engine of high bypass ratio. It is with particular regard to this vehicle that our discussions are directed.

A most important design requirement for the experiment was that a high degree of measurement accuracy be obtained, so that the different source mechanisms could be identified on the basis of the measured velocity exponents.

A schematic of the experimental arrangement is shown in Fig. 2. Air from the airflow apparatus was passed via a sound attenuating muffler to a 6"-diameter pipe which penetrated the wall of the anechoic measurement chamber. This pipe then decreased in diameter to the diameter of the experimental jet, generally two inches. The airflow in the pipe was measured by a pitot static tube some distance upstream from the test section which carried the flow disturbance. The pipe was constructed in such a way that the flow obstruction could be readily inserted and removed. The distance of the obstruction from the exit plane could also be changed. Throughout most of the experiments the obstruction was located three pipe diameters (6 in.) from the exit plane. The total length of jet pipe (following the transition) was some 36 inches. Thus fully developed pipe turbulence was established before the obstruction location.

The sound field in the anechoic chamber was scanned in a single (horizontal) plane centered on the pipe exit. A simple traverse for each flow condition was used, the overall noise signal being recorded on magnetic tape. The reduction of this data into octave bands of frequency was made later. A graphic computer technique was used to compute the radiated sound power. In the preliminary studies (1,2,3) efforts were directed towards establishing dependence between the level and spectrum of the radiated noise, on the one hand, and the steady flow parameters and system geometry, on the other. In a more recent extension to this work (5) the flow obstruction was instrumented with force transducers to allow a direct correlation between the radiated sound and the fluctuating forces on the obstruction.

OVERALL RADIATED SOUND POWER

In the preliminary studies, attention was focussed on the "overall" sound power (measured over the entire frequency range) radiated by the system. The principal findings in this regard can be summarized as follows.

The level of the overall radiated sound power from a plain unobstructed jet is shown in Fig. 3 as a function of the exit-plane velocity. Results are shown for three separate experiments made over a four-month period. These demonstrate the high order of repeatability made possible by the experimental equipment. The plain pipe radiation shows an eighth-power-of-velocity dependence at the higher velocities, tending, however, to a sixth-power dependence as the velocity decreases. The eighth-power dependence is identified with free jet turbulence and agrees closely with theoretical predictions (solid line in Fig. 3) based on constants determined experimentally by Fitzpatrick and Lee (10). The sixth-power dependence may be identified with dipole noise generated at the exit lip of the pipe. It is suggested that this "lip noise" is fundamental to the noise generating characteristics of jet flow. More will be said about this later.

When a flow obstruction is inserted into the pipe, the radiated power increases as shown in Fig. 4 and a sixth-power of velocity becomes established over the total operating flow range.

This result is typical in that a sixth-power-of-velocity law was consistently and accurately observed throughout the studies for most cases in which the pipe flow was obstructed. If this velocity exponent is assumed to be indicative of an aerodynamic dipole mechanism within the pipe, at least two possible locations for the noise sources can be postulated. These locations are:

a) on, or close to, the flow obstruction, associated with turbulence generation, or
b) at the exit plane, associated with the interaction of the highly turbulent wake with the exit lip.

Fig. 5 shows the result of an experiment in which an acoustic muffler was placed immediately downstream from the spoiler. The purpose of the muffler was to attenuate the acoustic energy propagating downstream from the obstruction without influencing, sensibly, the form of the downstream turbulence. The data in Fig. 5 indicate that the sources of obstruction-generated sound must be located in the vicinity of the obstruction rather than at the exit lip. In a second experiment, the muffler was replaced by flow straighteners which attenuated the downstream propagating turbulence without significantly interrupting the acoustic propagation path. The same conclusion was reached; the sources of obstruction-generated sound are located on, or close to, the surface of the obstruction.

Sound power data for three different obstruction geometries are presented in Fig. 6. The data are presented as a function of exit plane velocity. While each geometry displays a dependence upon the sixth-power-of-velocity, a very considerable scatter occurs between the data of one geometry and another. Exit plane velocity is apparently not a good correlating parameter for obstruction-generated sound.

When, however, these same data are plotted against the pressure drop that occurs across the flow obstruction, the degree of correlation is excellent as shown in Fig. 7. The sound power from a pipe-immersed obstruction can, apparently, be expressed in terms of the third power of the pressure drop across it. The dimensions of the spoiler seem to be of little importance.

A DIPOLE MODEL OF OBSTRUCTION-GENERATED SOUND

The result demonstrated in Fig. 7 was found to hold for a wide variety of obstruction geometries and sizes. It seemed that herein lay the basis for a prediction scheme for obstruction-generated sound. A physical model was needed to provide a basis for a prediction formula.

The observed dependence of obstruction sound upon the sixth power of flow velocity is a strong indication that the source mechanism is the aerodynamic dipole. It is thus related to the fluctuating force field exerted by the flow on the obstruction.

Consider the jet pipe schematic of Fig. 8. Airflow passing along the pipe is constricted as it passes the flow obstruction. The flow then expands to form a highly turbulent wake behind the obstruction. The process of vortex shedding by the obstruction causes fluctuations in the drag and lift forces exerted on it. These fluctuating forces form the dipole source of sound.

The power radiated from a fluctuating force field in a free-field acoustic environment is given by

$$W \sim \tilde{F}^2 f^2 \tag{4}$$

where $\tilde{F}$ is the amplitude and f the characteristic frequency of the force. For this model Eq. (4) is assumed to be valid even in the confines of the pipe. Furthermore, the drag forces, rather than the lift forces, are assumed to be primarily responsible for the radiation.

The characteristic frequency of vortex shedding from the obstruction is given by the quotient of the constricted velocity U_c and the geometric thickness of the wake δ. If constant proportionality between the steady and fluctuating drag components is assumed, then the fluctuating force field can be expressed by the product of the constricted velocity pressure $\frac{1}{2}\rho U_c^2$ and the area of the wake. Thus, the expression for radiated power can be derived as

$$W = \frac{k\Delta p^3 D^2}{\rho^2 c^3} \tag{5}$$

where Δp is the pressure drop across the obstruction, D is the diameter of the pipe and ρ and c are, respectively, the density and speed of sound of the air, and k is a constant. Eq. (5) is identical in form with that developed by Yudin (11) some years ago, from studies of air-duct elements (related to low-velocity ventilating

systems). This equation is observed to provide a good degree of overall-power data correlation in the present study. For this study the value of k (for overall power) has been observed to lie close to 2.5×10^{-4}.

FREQUENCY SPECTRUM

The result of the dipole model has been found to describe quite accurately the overall noise radiation from many different obstruction configurations. Its correctness as a physical model is less certain, however, when the frequency spectrum of the obstruction-generated sound is examined.

The octave-band spectrum for a typical obstruction geometry, normalized in accordance with the dipole-model formula of Eq. (5), is presented in Fig. 9. Conforming with usual practice, the normalizing frequency is the Strouhal number. In the present study the Strouhal number is based on the constricted velocity U_c and the geometric thickness δ of the wake. The data collapse is quite good at low Strouhal numbers. It is less complete at high Strouhal numbers.

The same data, however, take the form shown in Fig. 10 when the normalizing formula is modified to

$$W = k'(s)\frac{\Delta p^3 D^2}{\rho c^3}\left[1 + (f/f_o)^2\right] \qquad (6)$$

where f is the center frequency of the band, k'(s) is the spectrum-shape constant and f_o is a constant having the dimensions of frequency (4,000 Hz for the example cited). The degree of data collapse is quite excellent and Eq. (6) has been applied, equally successfully, to spectrum data for several different flow obstructions. In each case the final range of data scatter lay within ±2 dB.

The first term of Eq. (6) is identical to Eq. (5) and, as such, is derivable from the dipole model described previously. The second term, however, has an additional frequency-squared term. For aerodynamic noise mechanisms, frequency is proportional to velocity and thus the second term has the velocity dependence of a quadrupole source. It would appear, therefore, that both dipole and quadrupole source mechanisms are involved, the dipole dominating at frequencies below f_o and the quadrupole at frequencies above f_o. Both mechanisms appear under the same spectrum shape constant k'(s) thus implying a strong interrelation between the two (12).

In a recent paper (4), an alternative physical model was suggested to explain these data. This model was based on the theoretical observation (13) that the enclosure of aerodynamic sound sources within an infinitely long pipe should have a quite drastic effect upon their radiation efficiency at frequencies below the acoustic cutoff frequency of the pipe. Specifically, the enclosed quadrupole should exhibit the velocity dependence of the dipole source (U^6), and the dipole source the dependence of the monopole source (U^4). Above the cutoff frequency the sources should revert to their free-field behavior. It was therefore postulated that the measured data might relate entirely to quadrupole-like sources; that the dipole model of obstruction-generated sound was conceptually in error.

In these same discussions, however, it was recognized that when the pipe is truncated and only the energy radiated through exit plane up the pipe is considered the effect of "end-reflection" must be included in the analysis. Analytically it can be shown that below acoustic cutoff frequency end-reflection should entirely negate the increased radiation efficiency caused by source enclosure--i.e., the enclosed source should exhibit the same velocity dependence (if not the same level) as the free-field source. It was suggested however that, in the experimental system, the exit plane flow velocities were sufficiently high to inhibit end-reflection.

RECENT OBSERVATIONS

It would now appear that this alternative model is wrong. In a recently completed extension to this study (5) Heller et al observed a close correlation between the noise radiation and the measured dynamic drag force on the flow obstruction. It seems clear from these studies that the dominant sources in the lower frequency range are truly dipole in character. In these same studies the question of source enclosure within a pipe was looked at both analytically and experimentally using an acoustic (non-aerodynamic) source. It was found that the close immersion of the source within the pipe did increase the radiation efficiency by an inverse frequency-squared term, and that this effect was almost exactly cancelled by a corresponding frequency-squared term in the exit plane transmissibility.

It is therefore concluded that the dominant source of obstruction-generated sound is dipole in character deriving from perturbation of drag forces on the obstruction caused by incoming turbulence, when this is heavy, and by shed turbulence when the inflow is relatively smooth. A significant secondary source, however, is formed by quadrupole radiators in the turbulent mixing region immediately downstream from the obstruction. The quadrupole radiation dominates the sound field above some constant frequency f_o which is related to the dimensions of the system (14). Both quadrupole and dipole sources appear to have a characteristic Strouhal number of about 0.2, based on the thickness of the obstruction (the wake thickness) and on the constricted flow velocity past the obstruction.

With regard to the unobstructed air jet, the experiments suggest that dipole noise, associated with the shedding of turbulence at the exit lip, dominates (on an overall frequency basis) the quadrupole noise of the free jet turbulence at exit plane velocities below about 700 ft/sec. Possibly the transition occurs at still higher velocities when the in-pipe turbulence level is high. The data also suggest that the characteristic frequency of lip noise is influenced by the external geometry of the jet pipe, insofar as this geometry influences the scale of eddy shedding.

At no point in the study were data observed indicative of aerodynamic monopole sources. It is concluded therefore that, within the constraints of the experiment, the aerodynamic monopole does not play a role in obstruction-generated sound.

REAL ENGINE SYSTEMS

These findings have implicit relevance to the noise of real engine systems, particularly the high bypass ratio turbofan engine:

a) The experimental findings suggest, for instance, that classical jet noise very easily becomes subservient to internal engine sources when tail pipe velocities are reduced. Even in the absence of internal engine sources, lip noise plays a significant role. This role might be augmented by current methods of jet noise suppression.

b) The formulae of Eqs. (5) and (6) stress the role played by pressure losses in a system. Many current and projected noise suppression devices (duct liners, etc.) impose significant pressure losses. Thus their use may not be entirely beneficial.

c) Compressor and fan noise studies have long recognized the significance of the aerodynamic dipole both as a discrete tone (blade interaction) generator and as a broadband noise (vortex shedding) generator. The role played by quadrupole sources in the wakes of fixed and rotating blading has not, however, been discussed.

d) The presence of significant sources of broadband noise radiation within an engine may cause jet noise prediction schemes to significantly under-estimate the extent of exhaust noise. This would be particularly so for "in-flight" predictions, since internal engine sources are not sensitive to forward flight velocity.

These and other open questions on the mechanisms and locations of broadband engine noise sources suggest a very pressing need for careful and systematic studies on real engine systems. Such studies must try to accurately measure the dependence between the radiated noise and the gas flow parameters. Attempts must be made to identify and separate externally generated sources from internally generated sound. The experiment should cover as wide a range of the engine operating parameters as possible and engine modifications should be contemplated that would alter the balance between one source and another. By such methods one might, for example, identify and measure monopole noise associated with the combustion process.

REFERENCES

(1) Gordon, C. G. and Maidanik, G.: "Influence of Upstream Flow Discontinuities on the Acoustic Power Radiated by a Model Air Jet", NASA CR679, 1967.

(2) Gordon, C. G.: "Spoiler-Generated Flow Noise. I. The Experiment", J. Acoust. Soc. Am. 43, 1041-1048, 1968.

(3) Gordon, C. G.: "Spoiler-Generated Flow Noise. II. Results", J. Acoust. Soc. Am. 45, 214-223, 1969.

(4) Gordon, C.G.: "A Study of Exhaust Noise As It Relates to The Turbofan Engine". Progress of NASA Research Relating to Noise Alleviation of Large Subsonic Jet Aircraft - NASA SP-189, 1968.

(5) Heller, H. H., Widnall, S.E. and Gordon, C.G.: "Correlation of Fluctuating Forces with The Sound Radiation from Rigid Flow Spoilers". BBN Rpt. No. 1734 submitted to NASA, Langley, Virginia, Oct. 1968.

(6) Lighthill, M. J.: "Sound Generated Aerodynamically". The Bakerian Lecture, Proc. Roy. Soc. A267, 147-182, 1962.

(7) Ribner, H. S.: "On Spectra and Directivity of Jet Noise". Adv. in Appl. Mech., Vol. VII, Acad. Press, 1964.

(8) Ffowcs Williams, J. E.: "Jet Noise at Very Low and Very High Speed". Paper presented at AFOSR-UTIAS Symposium on Aerodynamic Noise, Toronto, 1968.

(9) The intensity relations are expressed in terms of steady rather than fluctuating flow components. It is generally true that the ratio of the unsteady to steady components is independent of flow speed.

(10) Fitzpatrick, H. M. and Lee, R.: "Measurements of Noise Radiated by Subsonic Air Jets". Rpt. No. 835, David Taylor Model Basin, Navy Dept., 1952.

(11) Yudin, E. Ya.: "The Acoustic Power of the Noise Created by Airduct Elements". Sov. Phys. - Acoust. 1, 383-398, 1955.

(12) It would appear, in fact, that the spectrum shape constant for the quadrupole source mechanism is proportional to $S^2k'(s)$, i.e., the quadrupole spectrum shape is simply tilted by about 6 dB/octave.

(13) Davies, H. G. and Ffowcs Williams, J. E.: "Aerodynamic Sound Generation in a Pipe". J. Fluid Mech. 32, 765-778, 1968.

(14) The dependence of f_o upon the dimensions of the pipe-obstruction system is not yet clear. It is suggested at this time that f_o is inversely related to the thickness of the flow obstruction (i.e., the wake thickness).

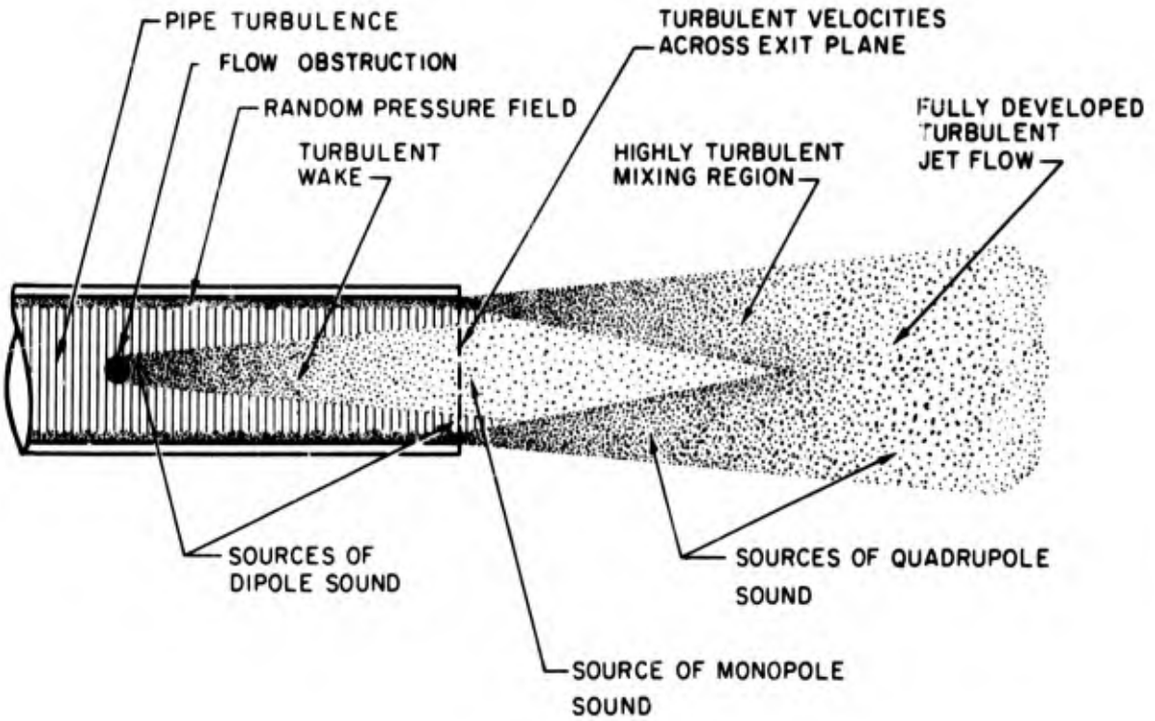

Fig. 1 Aerodynamic noise sources in turbulent jet flow

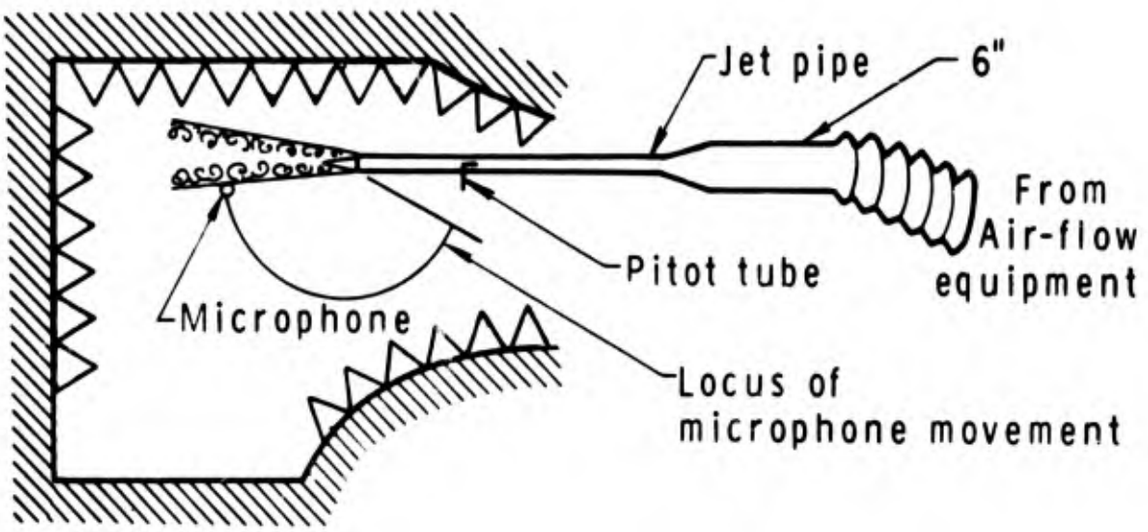

Fig. 2 Experimental arrangement

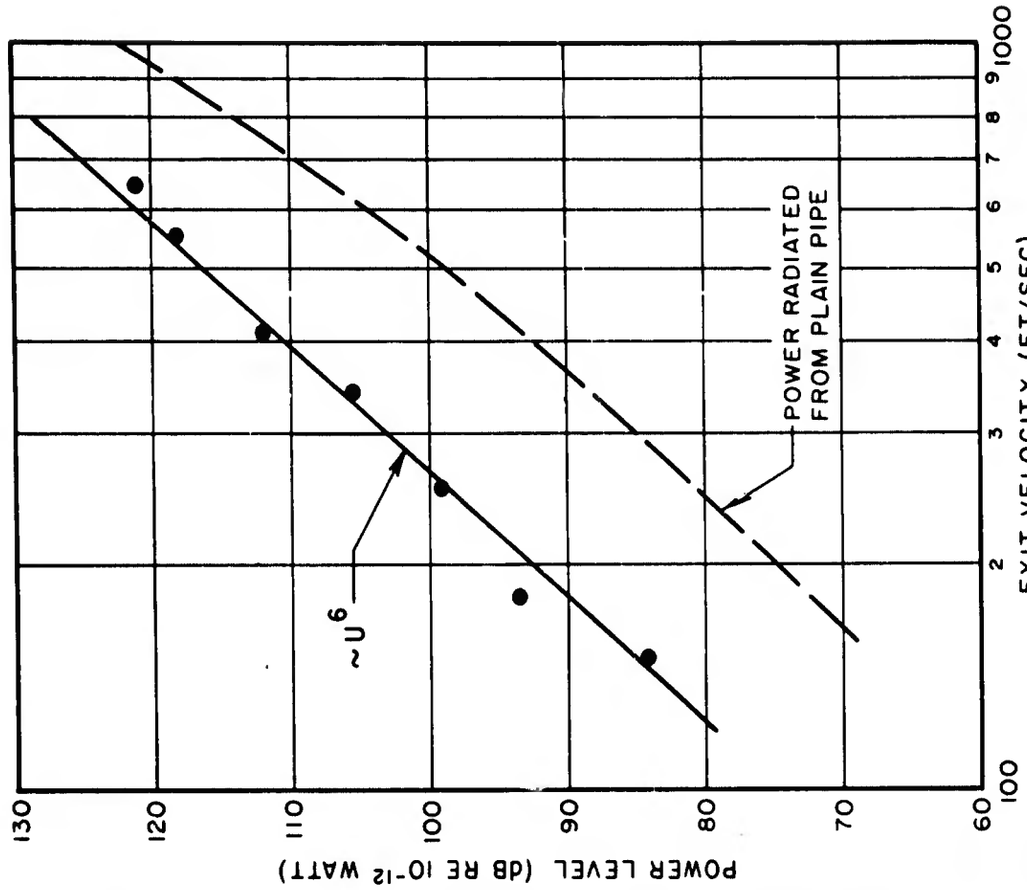

Fig.4 Effect of flow obstruction on sound power

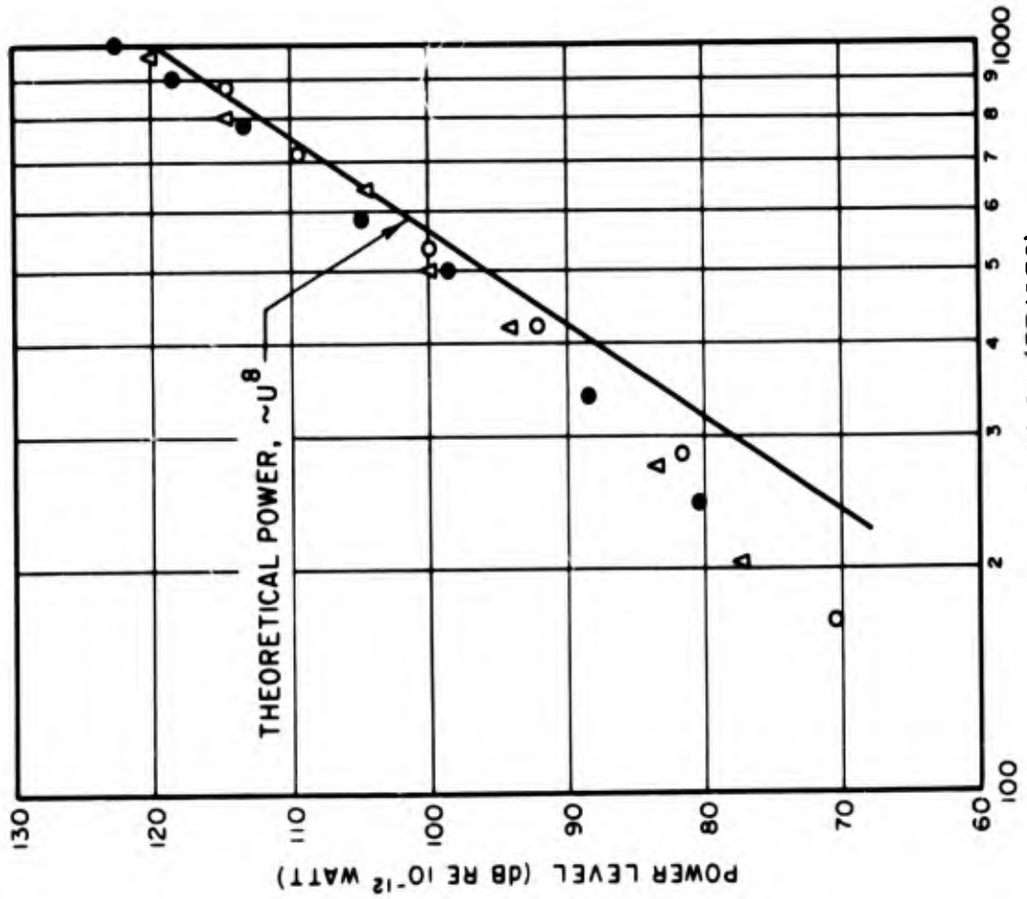

Fig.3 Total sound power with no flow obstruction

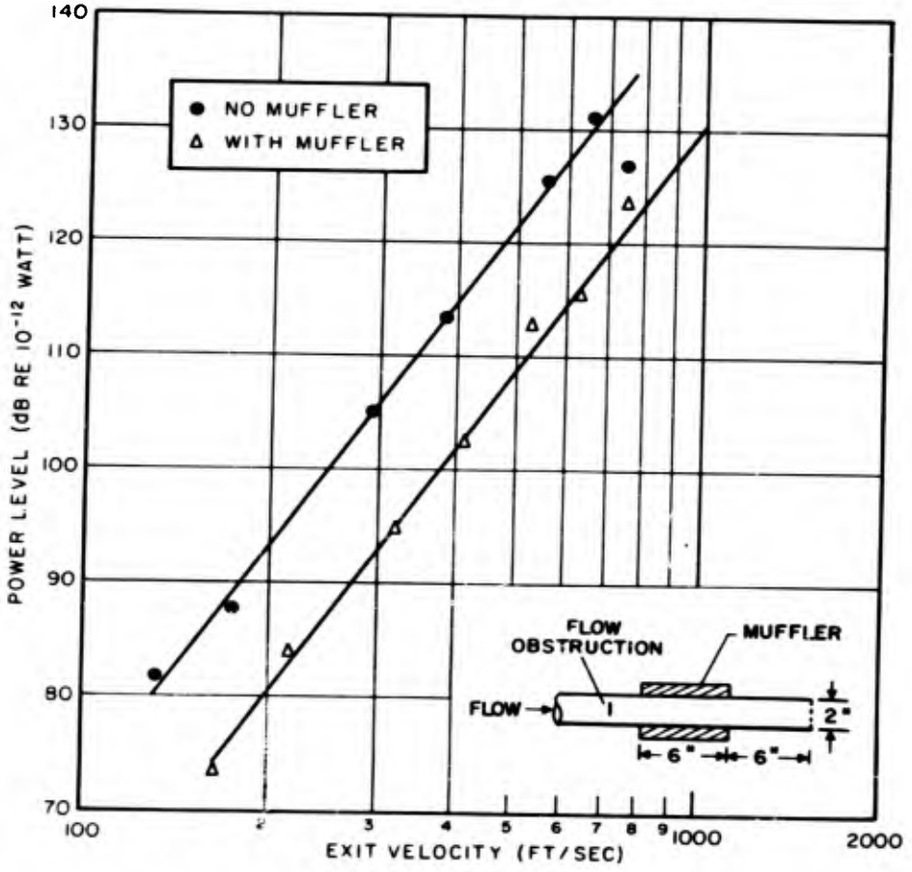

Fig. 5 Determining location of flow-obstruction generated sound

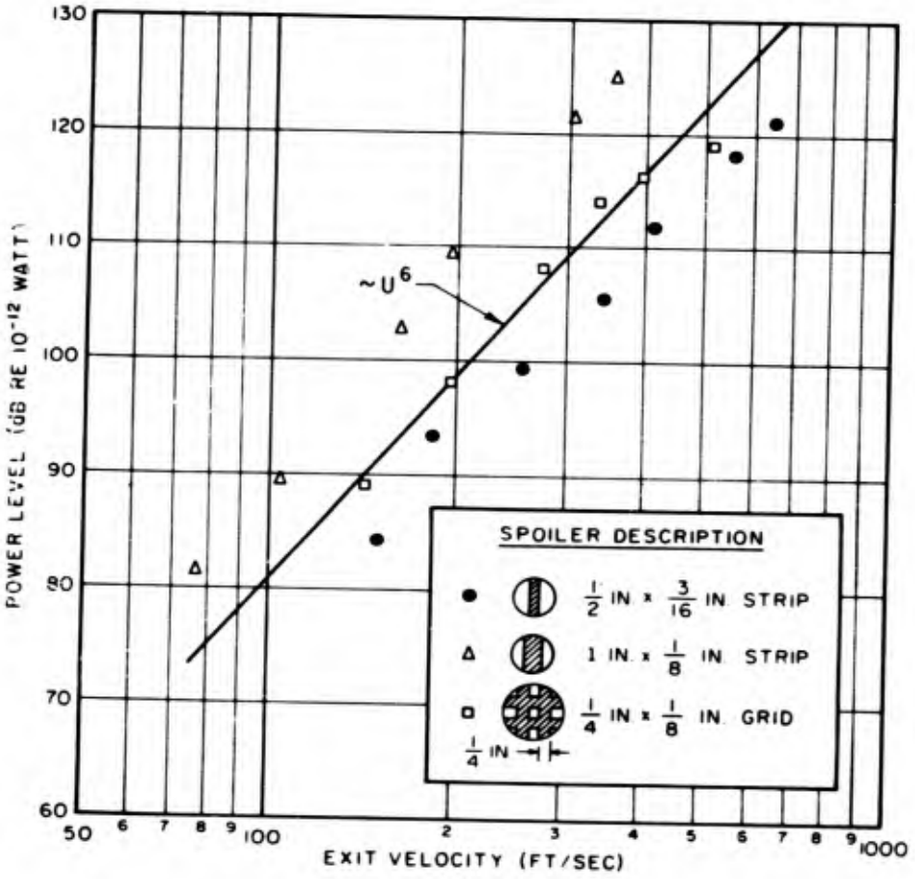

Fig. 6 Influence of different geometries of flow obstruction upon total radiated sound

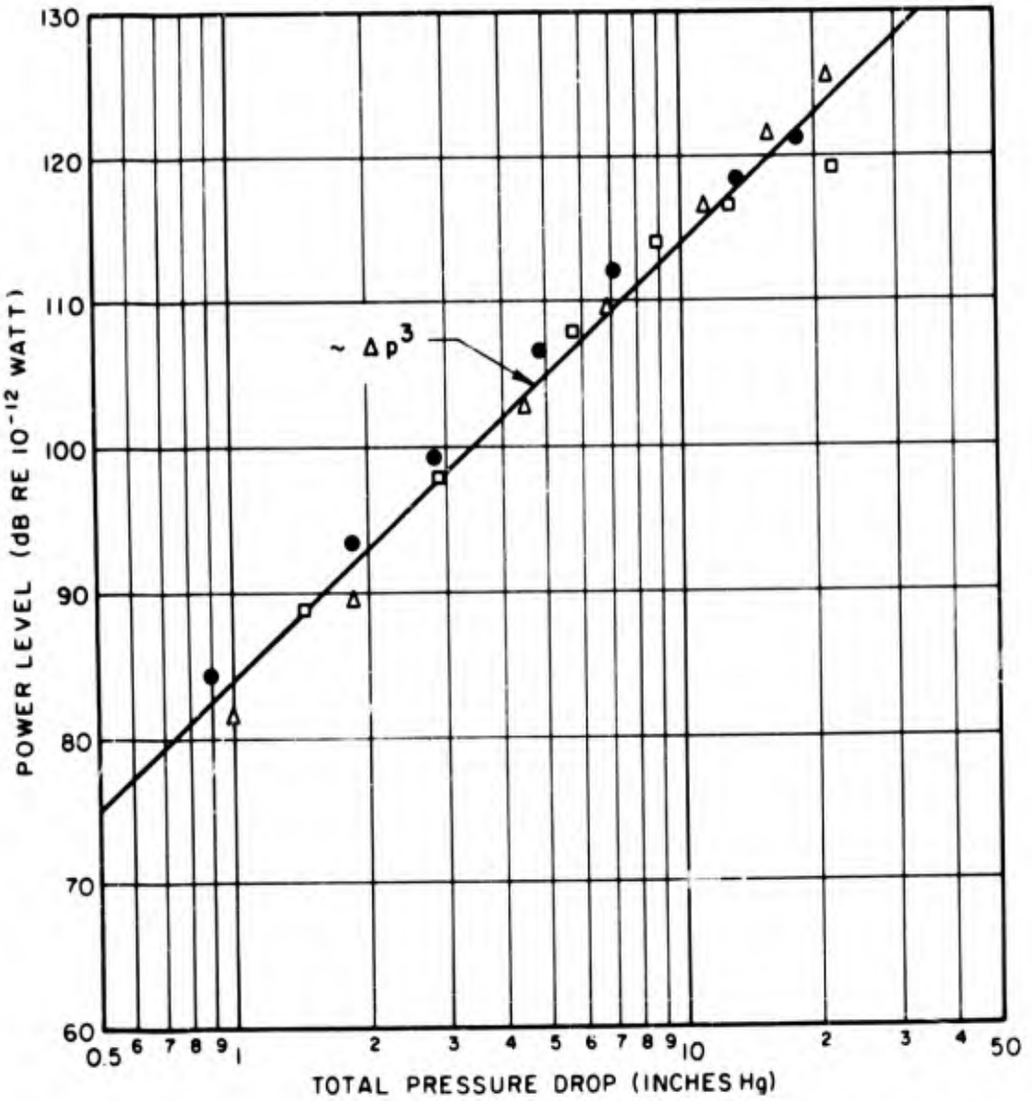

Fig.7 Use of pressure drop as correlating parameter - (for data of Fig.6)

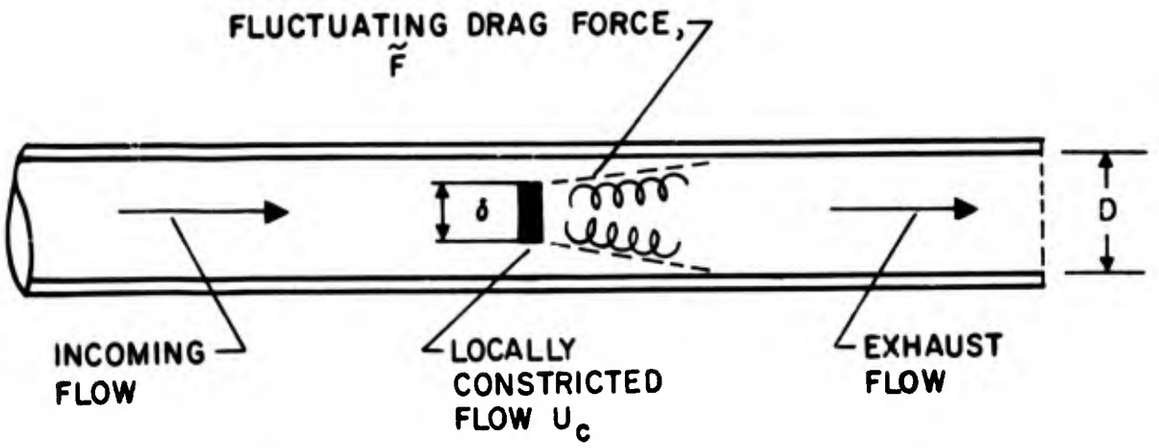

Fig.8 Free-field dipole model of obstruction-generated sound

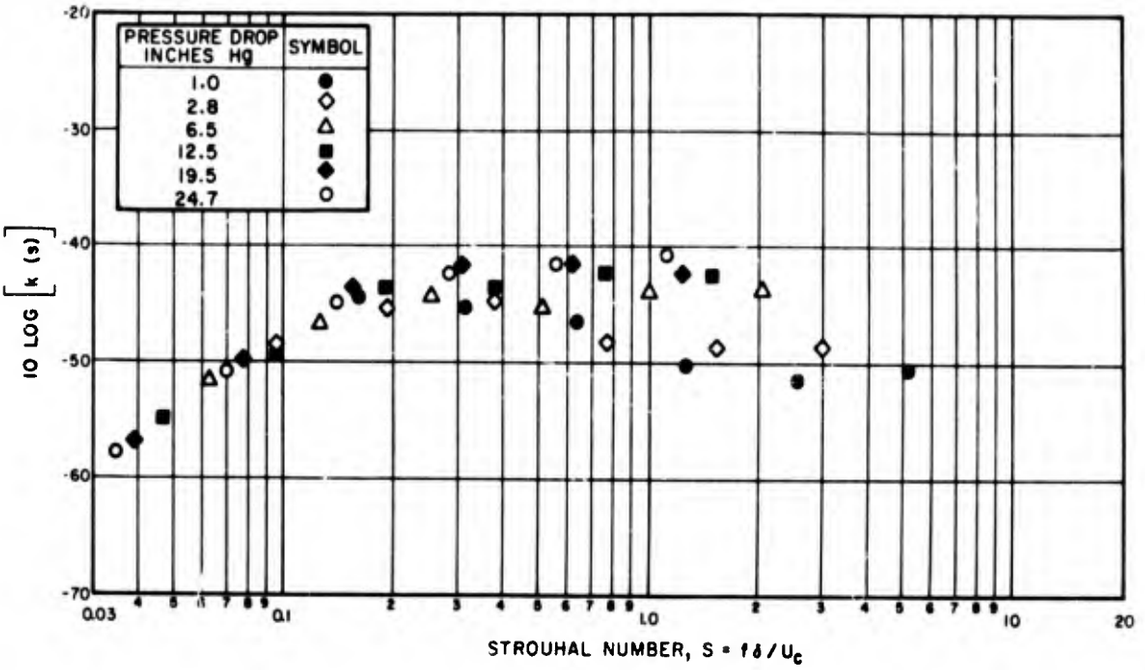

Fig. 9 Typical octave-band spectrum normalized on basis of dipole model

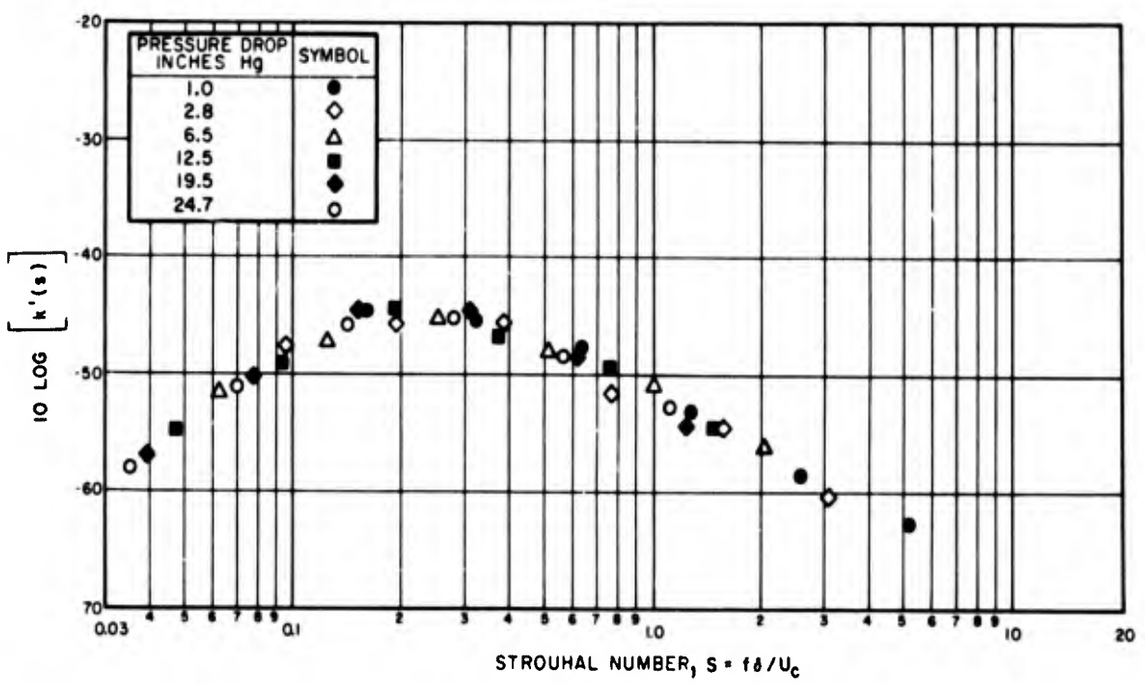

Fig. 10 Octave-band spectrum renormalized for improved collapse

BLANK PAGE

NOISE ASSOCIATED WITH SHOCK WAVES IN SUPERSONIC JETS

by

D. L. MARTLEW

MINISTRY OF TECHNOLOGY
NATIONAL GAS TURBINE ESTABLISHMENT
PYESTOCK, FARNBOROUGH,
HANTS, ENGLAND

SUMMARY

Current methods for predicting the field of noise around a jet are not adequate to explain observations of high noise levels in directions at large angles to supercritical jets in motion. Experiments on static jets in the anechoic chamber at N.G.T.E. suggest that part, at least, of this "forward throw" of noise may be due to the presence of a regular shock cell structure in the jet. Noise fields are compared for jets with and without shock cells and similarities are pointed out between the phenomenon of jet screech due to shock cell oscillation and the forward throw of broad band noise. Limited tests with a plug nozzle show that this type produces less forward noise, probably owing to differences in the shock system which is of small extent and irregular in comparison with that of a convergent nozzle.

It is concluded that the elimination of the shock cell pattern could reduce jet noise forward of the nozzle by 10 dB.

LIST OF SYMBOLS

A_j	fully expanded jet area
D	nozzle throat diameter
Fmax	frequency for peak sound pressure level
K	constant
L	length of shock cell
Po	ambient static pressure
Pt	jet total pressure
R	applied pressure ratio
Rc	critical pressure ratio
V_j	fully expanded jet velocity
ρ_j	fully expanded jet density
θ	angle to direction of jet discharge

THE STRUCTURE OF incorrectly-expanded supersonic jets has been understood in general terms for many years. In the most usual practical case the flow from a nozzle, blown at a higher pressure ratio than it can expand internally, has to undergo a sudden supersonic expansion on emerging. The internal reflections of this expansion from the free boundaries of the jet cause a re-compression culminating in a shock wave which returns the flow to an underexpanded state, not dissimilar to that at the nozzle throat (Figure 1). Further cycles of overexpansion and re-compression result in the familar pattern of shock cells which extends downstream until mixing of the jet with its surroundings causes it to lose its identity.

Powell (1) was the first to draw attention to the significance of the shock cell system in connection with the noise of jets. He showed that instability in the cells could occur whereby a disturbance convected or propagated downstream through the shock cells causes the emission of acoustic waves. These, propagating past the exit of the nozzle act on the emerging jet to cause new disturbances. Intense discrete frequency noise, sometimes known as screech, is caused by this closed resonant loop of events. Many workers have examined the phenomenon, usually on a model scale, and its dependence on an acoustic feedback process is indisputable. Many of the individual processes within the loop are still far from clear, particularly the nature of the disturbances within the jet and the nature of their interaction with the shocks by which the sound waves are generated. It is possible to predict with some certainty the frequency of shock cell oscillation since this depends primarily on geometric factors. The amplitude of the oscillation, or the sound pressure level of the radiated tones, however, defy prediction since the gain or damping of the various processes within the loop cannot at present be anticipated. Shock cell oscillation remained an aerodynamic and acoustical curiosity until it was identified a few years ago as a cause of fatigue in jet aircraft structures. Hay (2,3), for instance, shows how structural excitation, caused by jet screech, has been the cause of skin cracks in a subsonic airliner.

While the problems of shock cell oscillation have received considerable attention the characteristics of the broad band noise from jets containing shock cells have largely gone unrecognised. Hay (3), for example, points out an area where present knowledge of jet noise is inadequate, namely that sound pressure levels at large angles forward of the direction of the jet tends to be underestimated under flight conditions. It is important to be able to calculate the distribution of noise from about 20° to the jet axis through to about 30° to the intake axis in order to be able to estimate the correct time for reducing power during a noise abatement take-off. This need will become far more exacting when limits of Effective Perceived Noise Level have to be met under the rules of noise certification. Hay quotes examples where both model jets and actual aircraft show a considerable amount of forward throw of noise and this is attributed to the effects of forward motion of the nozzle.

In the present paper it will be shown that a certain amount of forward throw of broad band noise can be caused by the presence of shock cells, although it may not be sufficient to account for the whole of the forward throw referred to above. It will be shown, however, that a considerable improvement in jet noise may be obtained if the regular pattern of shock cells can be removed.

CHARACTERISTICS OF JET SCREECH

The broad band noise associated with the presence of shock cells has certain features in common with the jet screech which results when the cells oscillate. It is appropriate first, therefore, to review briefly some of the characteristics of jet screech.

The frequency of shock cell oscillation varies inversely with the length of the shock cells. This length increases as pressure ratio increases and Powell (1) determined empirically that

$$\frac{L}{D} = K(R - Rc)^{\frac{1}{2}} \qquad \ldots.(1)$$

this relationship is in some degree an over-simplification but is generally agreed to provide a useful working rule.

The acoustic waves are emitted from several sources along the jet and these do not generally coincide with the positions of the shock waves. Typically, but not always, the cell system oscillates from side to side, or spirally in the case of an axisymmetric jet, and the sound waves are emitted alternately from each side. Figure 2 is a shadowgraph picture of a two-dimensional jet taken at N.G.T.E. and it shows clearly how several sources emit sound waves with such a phase relationship that the upstream moving waves from each source coincide. The acoustic radiation is highly directional. At the fundamental frequency of the oscillation it is directed preferentially in the upstream or forward direction. It is also directed downstream but is often difficult to detect in the peak jet noise. The sound is directed sideways at twice the fundamental frequency. Higher harmonics can frequently be observed. Figure 3 is due to Powell (4) who explained this directionality by assuming a number of suitably phased monopole sources emitting sound waves at the frequency at which disturbances pass downstream, and at higher harmonics.

THE EXPERIMENT

The present tests were performed in the anechoic jet noise laboratory at N.G.T.E. This is depicted in Figure 4, and has a working volume 17 ft (5 m) square by 15 ft (4.5 m) high. The model jet discharges vertically through the opening in the roof. Free entry for air entrained

by the jet is assured by openings around the chamber. Internal surfaces are rendered anechoic by a lining of 2 ft (0.6 m) glass fibre wedges.

The major part of the results presented in this paper were obtained from the conical convergent nozzle illustrated in Figure 5. This had a throat of 2.5 in. (6.35 cm) diameter approached by a conical contraction having a half angle of 12°. This nozzle was representative of those fitted to current subsonic aircraft. Total pressure was measured upstream of the nozzle and the applied pressure ratio was determined from this. A combustion system burning hydrogen enabled the air temperature to be raised as required.

Acoustic measurements were made with a $\frac{1}{2}$ in. Bruel and Kjaer condenser microphone and cathode follower. A traversing arm enabled the microphone to be moved around an arc of 7 ft 3 in. (2.2 m) radius centred on the nozzle exit. The signals were recorded on a Nagra III BH tape recorder and analysed into 5 per cent bandwidths on a Muirhead K101 automatic recording wave analyser. Calibrations were made with a pistonphone and by applying signals of known frequency and level to the electrical system.

The measurements extended over the following ranges:

Pressure ratio 1.85, 2.5, 3.1 and 3.4
Temperature 20°C to 900°C
Angles to jet axis 30° to 150°

RESULTS

In many cases the measured spectra contained one or more discrete tones resulting from shock cell oscillation. Where this occurred the 5 per cent spectra were adjusted to remove the tones. The band levels were then combined to give the overall sound pressure levels of the broad band noise and these were normalised by subtracting 10 $\log_{10} \rho_j^2 A_j$. The results are shown plotted against the logarithm of the fully-expanded jet velocity in Figure 6 for angles to the jet axis of 30°, 90° and 150°.

Figure 6a, relating to what is roughly the angle for peak jet noise shows that over most of the range of velocities the levels for all pressure ratios fall close to the line predicted by the jet noise study due to Coles (5). The few points at the lowest jet velocities lie somewhat below Coles' curve although they are well within the scatter of his experimental points. Possibly, since the combustion system was not alight, they represent the effect of a smooth inlet flow. Turning to Figure 6b, it is seen that the points for the noise at 90° fall into two groups. For a pressure ratio of 1.85, i.e. for a subsonic jet free of shocks, they lie on a line following a V_j^8 law. The remaining supersonic points lie clearly above this line indicating an excess of noise of about 7 dB. Figure 6c shows this feature to be even more marked at 150°. Once again the subsonic points follow a V_j^8 law while the supersonic ones lie generally together, up to 10 dB above. This extra noise is probably due to a mechanism other than turbulent mixing and it should therefore be a function of other variables than V_j alone. Nevertheless the simple presentation of Figure 6 serves to show the considerable difference that exists between subsonic and supersonic noise levels. In Figure 7 these differences are shown in terms of field shape and the forward throw of the noise of supersonic jets is evident.

When this additional component of noise, apparently due to the presence of shock cells, is present the broad band spectrum has a quite distinctive shape, whether or not shock cell oscillation is present. Figure 8a shows the normalised 5 per cent bandwidth levels observed at a typical condition of $\log_{10} V_j = 3.2$. The spectrum shape at 30° is the familiar one for peak jet noise and is more or less independent of pressure ratio. Turning now to Figure 8b, for 90°, it is seen that the spectrum for the subsonic jet is once more of a normal form. The supersonic jets are, however, characterised by a considerable increase in high frequency noise which comes in quite sharply around a frequency which appears to decrease as pressure ratio rises. In Figure 8c, for 150°, the same features are observed, only the frequencies at which the jump in level occurs are rather lower than at 90°.

These spectral characteristics suggest that a mechanism other than that of mixing noise is at work when shocks are present in the jet. The sound levels at the lower frequencies are apparently governed by the noise of the jet mixing process while at and above a certain frequency the dominant noise appears to be associated with the shock waves. The way in which this peak frequency varies with jet conditions is reminiscent of shock cell oscillation, decreasing in frequency as pressure ratio increases and radiating at higher frequencies to the side of the jet than upstream. It is thus natural to suppose that the broad band shock associated noise involves part of the cycle of events which combine in shock cell oscillation but without the loop being closed. It will be supposed, then, that disturbances at the lip of the nozzle are amplified in the mixing region while being convected downstream at a velocity between that of the jet and that of its surroundings. These disturbances pass the shock waves in succession causing the emission of a series of acoustic waves from sources associated with, but not necessarily at, each shock. These will be observed at 90° at the frequency of passage while at forward angles the observed frequency will be lowered owing to a Doppler shift as the position of the radiating source moves downstream. The broad band nature of the observed spectra above this frequency must be explained as the result of an irregular series of disturbances passing through the shock system.

Measurements of shock cell lengths on the present nozzle suggest the relation

$$L = 0.236\,(R - Ro)^{\frac{1}{2}} \qquad \ldots.(2)$$

for the cell length in feet, averaged over the first five cells. These observations were made with a cold jet but it has been confirmed experimentally that the relation will hold for elevated temperatures because the shock cell structure is mainly dependent on supersonic quantities which are functions of pressure ratio only.

In Figure 9 the frequency of peak sound pressure level for the supersonic jets is plotted against $V_j + 0.236\,(R - Rc)^{\frac{1}{2}}$. Clearly, although there is considerable scatter, a proportional relation is approximately true. The slope of the mean line for 90° is 0.7 and this implies that, if the simple mechanism postulated above is correct, the disturbances causing the noise are carried downstream at about 0.7 of the jet velocity. This is of a reasonable order when compared, for instance, with jet screech observations (2) where a value of 0.625 is successfully used. The conclusion seems justified, then, that the extra high frequency noise observed from jets containing shock cell systems is due to disturbances convected through the regularly spaced shock waves.

PLUG NOZZLES

Observations of the shock associated noise of nozzles having markedly different shock structures would be valuable in confirming the ideas set out above. In the limit, convergent-divergent nozzles free of shocks at supercritical design pressure ratios would be expected to show an absence of the high frequency broad band noise. At the time of writing such convergent-divergent nozzles were not available for noise testing.

A few measurements were made, however, with the plug nozzle shown in Figure 10. This model could not be run with heated air so the tests were limited in range. The field shapes observed are compared with those of the cold tests on the conical nozzle in Figure 11. It is apparent that at subsonic jet conditions (p.r. = 1.85) both nozzles have the same field shape. At the intermediate supersonic condition (p.r. = 2.5) the plug gives considerably less noise at 90° and 150° than the conical but at the higher pressure (p.r. = 3.4) the plug shows the same forward throw as the conical. The plug nozzle, incidentally, is quieter by 1½ to 3 dB than the conical in the peak direction.

The shock structure with the plug nozzle is very different from that in the supersonic jet of the conical nozzle, as is shown in Figure 12. This example is for a pressure ratio of 2.5 where the absence of shock noise is most marked; probably due to the irregular system of small shocks attached to the centrebody. At the pressure ratio of 3.4 visualisation tests showed that a free shock cell system was forming downstream of the tip of the plug and this is accompanied by shock noise. The spectrum then also shows the characteristic high frequency components.

CONCLUSIONS

Model scale tests have shown that supersonic jets containing shock cells can radiate a considerable amount of broad band high frequency noise sideways and forwards. This noise appears to be due to disturbances in the jet mixing region being convected through the regularly spaced series of shocks. At large angles to the jet direction the sound pressure level can be as much as 10 dB above that for a shock-free jet. Much more investigation is needed to establish the full range of the effect and to completely understand its mechanisms.

At full scale this noise mechanism could have important implications. For aircraft where jet noise in the forward direction is not masked by compressor or fan noise the levels observed as the machine approaches an observer could be 10 PNdB above those which could be achieved with nozzles designed to eliminate the regular shock cell pattern. Limited observations with a plug nozzle suggest that this type might considerably reduce shock associated noise, as might other nozzles which prevent the formation of regular shock cells.

ACKNOWLEDGEMENT

The author wishes to acknowledge the work of Mr. J. A. Gardiner and Mr. G. J. Bates who carried out the experimental programme.

REFERENCES

No.	Author(s)	Title, etc.
1	A. Powell	On the mechanism of choked jet noise Proc. Roy. Soc. B.66, 1953
2	J. A. Hay E. G. Rose	In-flight shock cell noise British Aircraft Corporation Paper presented at British Acoustical Society meeting on "Sonically induced vibration of structures" January 1969

REFERENCES (cont'd)

No.	Author(s)	Title, etc.
3	J. A. Hay	The estimation of jet engine noise British Aircraft Corporation Paper presented at the Anglo-French Symposium on "Aeronautical Acoustics", Toulouse March 1968
4	A. Powell	On the noise emanating from a two-dimensional jet above the critical pressure Aeronautical Quarterly, Vol. 4, p. 103 1953
5	G. M. Coles	Estimating jet noise Aeronautical Quarterly, Vol. 14, p.1-16 1963

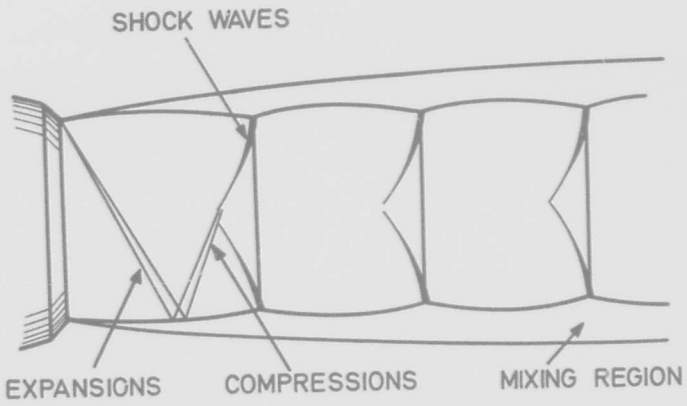

FIG. 1 SHOCK CELL STRUCTURE

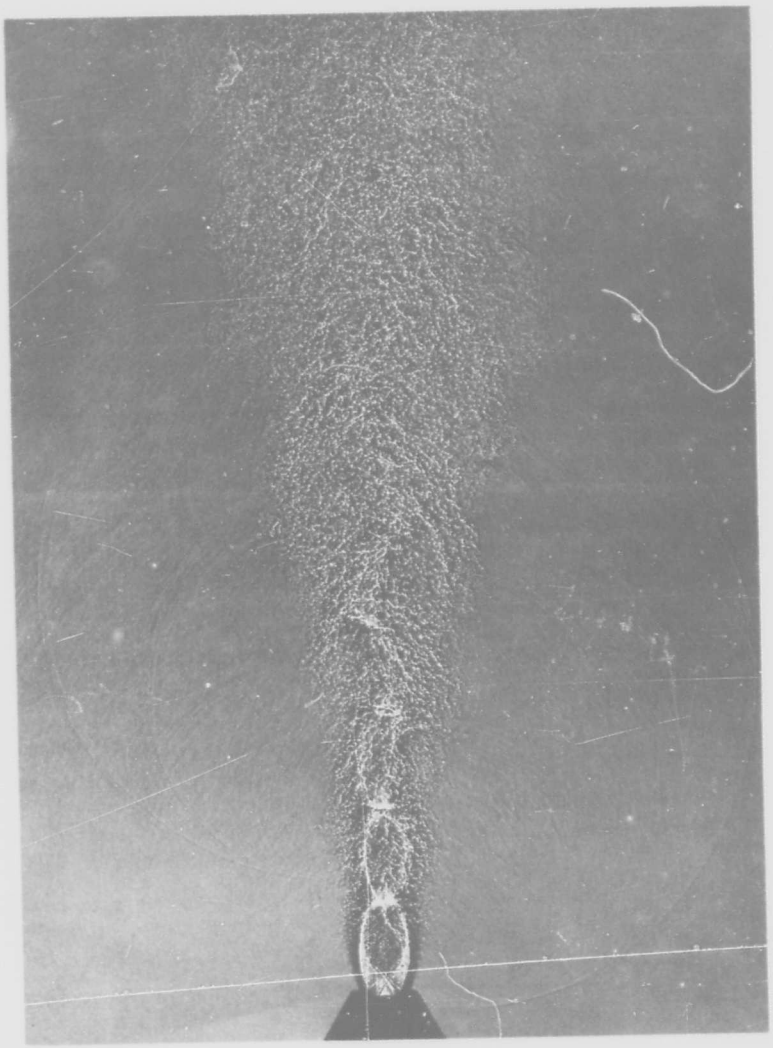

FIG 2 SHADOWGRAPH OF OSCILLATING JET

FIG 3 SHOCK CELL OSCILLATION - DIRECTIONAL PATTERNS

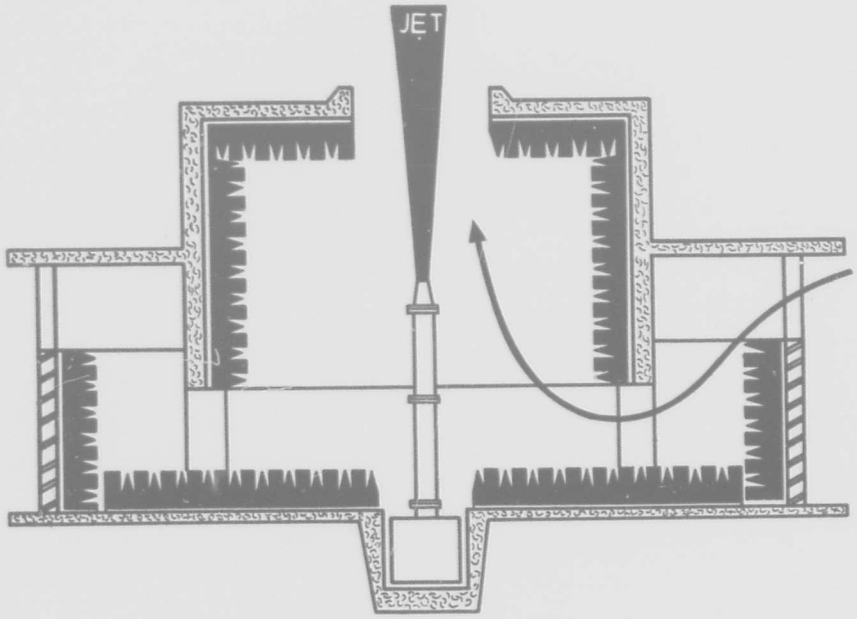

FIG. 4 ANECHOIC CHAMBER - SECTION

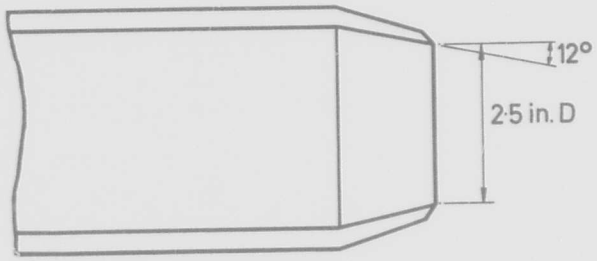

FIG. 5 CONICAL NOZZLE

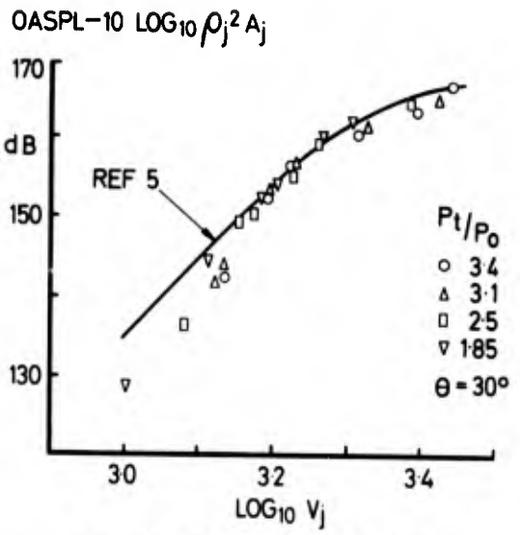

FIG. 6a OASPL vs LOG_{10} V_j

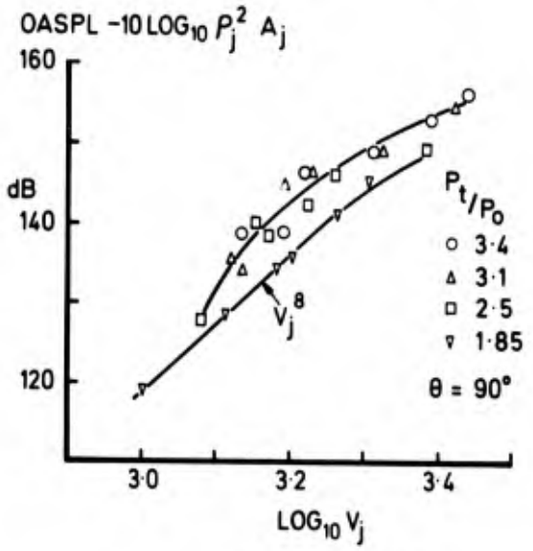

FIG. 6b OASPL vs LOG_{10} V_j

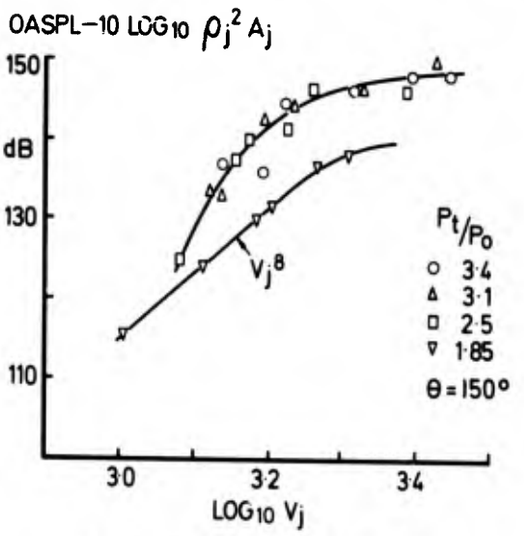

FIG. 6c OASPL vs LOG_{10} V_j

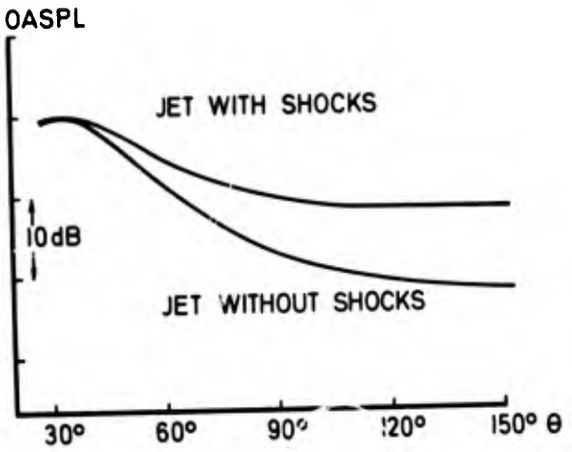

FIG.7 EFFECT OF SHOCKS ON FIELD SHAPE

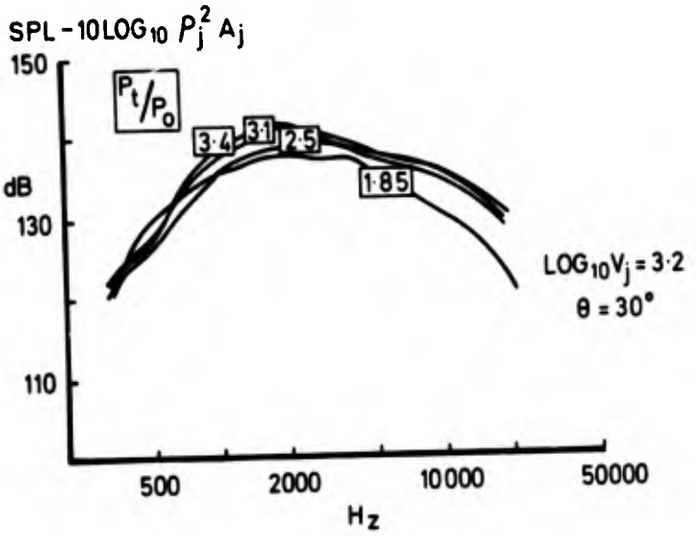

FIG. 8a 5% BANDWIDTH SPECTRA

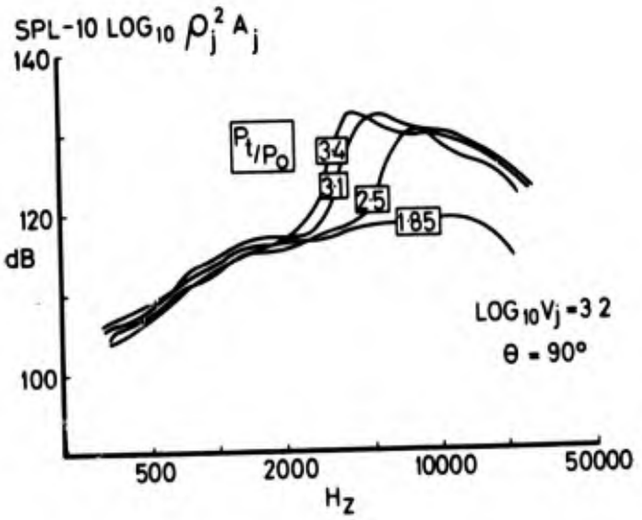

FIG. 8b 5% BANDWIDTH SPECTRA

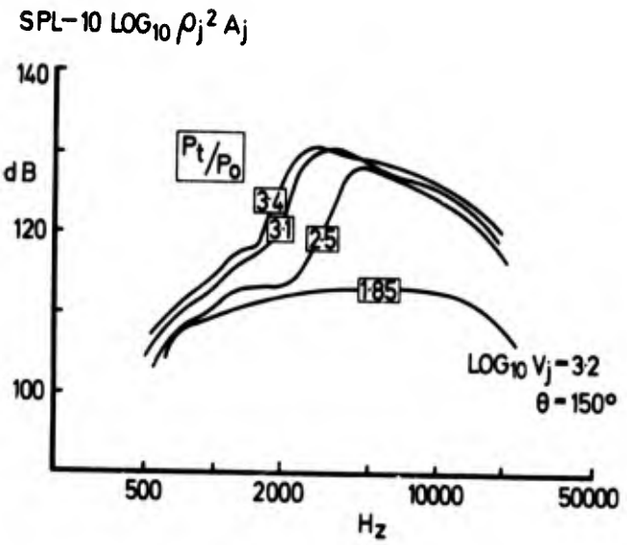

FIG 8c 5% BANDWIDTH SPECTRA

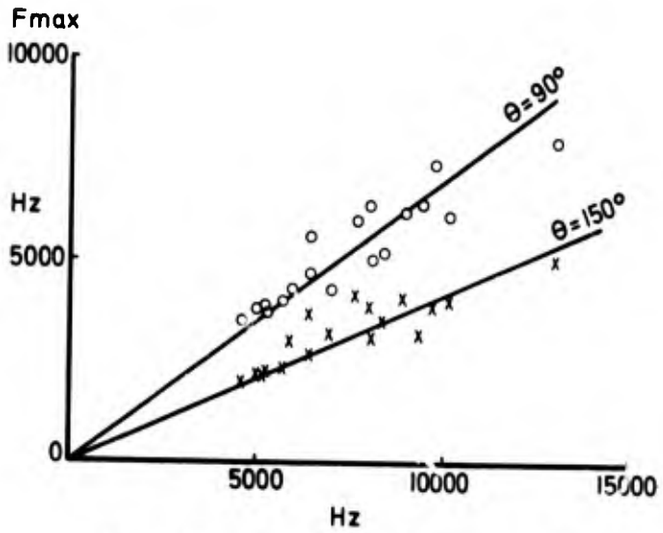

FIG. 9 Fmax vs $V_j \div 0{\cdot}236(R-Rc)^{\frac{1}{2}}$

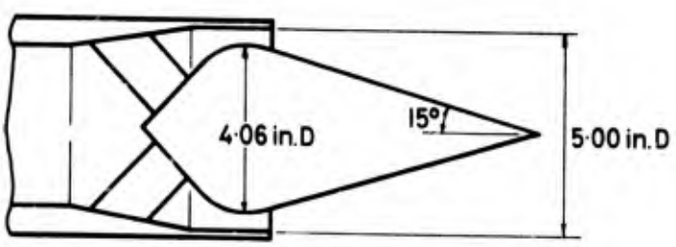

FIG. 10 PLUG NOZZLE

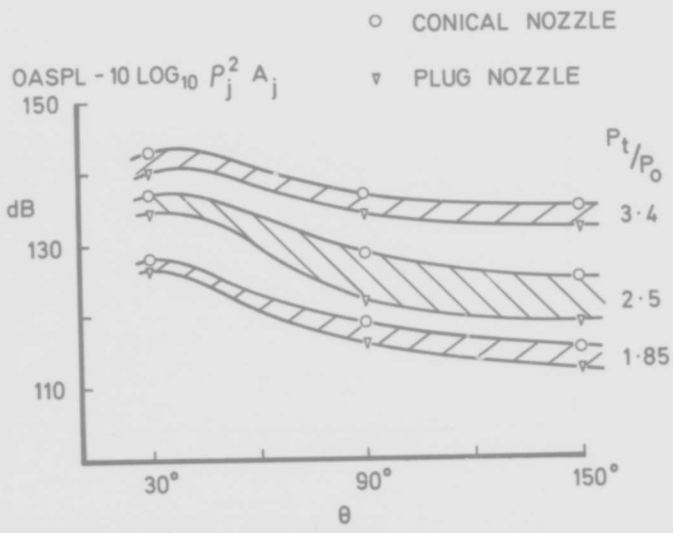

FIG. 11 PLUG AND CONICAL NOZZLE FIELD SHAPES

FIG 12 SHOCK WAVES ON PLUG NOZZLE

JET NOISE FROM MOVING AIRCRAFT

JOHN E. FFOWCS WILLIAMS

DEPARTMENT OF MATHEMATICS,

IMPERIAL COLLEGE,

LONDON S.W.7.

Equation 1.29 of reference (1) on the noise from turbulence convected at high speed is an exact equation for the mean square density radiated to large distances from turbulence that is stationary in time in a frame of reference moving with a velocity $a_o\underline{N}$ relative to the air at rest. The acoustic intensity at a distant observation point $\underline{x}$ will vary with observation time, t, because the source region as a whole is in motion with velocity $a_o\underline{N}$. This region is moving with the aircraft. The intensity $I(\underline{x},t)$ is $a_oB(\underline{x},t,o)/\rho_o$ in the notation of the paper so that:

$$I(\underline{x},t) = \frac{|1 + N\cos\phi|^{-1}\,|1 - M\cos\theta|^{-5}}{16\pi^2\rho_o r^2 a_o^5}\int_V\int_V \frac{\partial^4}{\partial\tau^4} P_r(\underline{\eta},\underline{\lambda},\tau^*)\,d\underline{\lambda}\,d\underline{\eta} \qquad 1.0$$

$$\tau^* = \frac{\lambda_r}{a_o(1-M\cos\theta)} \qquad 1.1$$

$$P_r(\underline{\eta},\underline{\lambda},\tau) = \overline{T_{rr}(\underline{\eta},o)T_{rr}(\underline{\eta}+\underline{\lambda}+a_o(\underline{M}+\underline{N})\tau,\tau)} \qquad 1.2$$

$$T_{rr} = \rho u_r^2 + p - a_o^2\rho - \overline{(\rho u_r^2 + p - a_o^2\rho)} \qquad 1.3$$

The meaning of the symbols in this equation are as follows and the geometry of the model is illustrated in Figure 1. ϕ is the angle at which the sound ray leaves the source at the time and place of emission measured from the direction of aircraft flight, $\underline{N}$. The velocity $a_o\underline{M}$ is a constant which can at this stage be regarded as arbitrary the equations being invariant to the choice of $\underline{M}$. θ is the angle at which the sound ray leaves the source at the emission time measured from the direction of $\underline{M}$. ρ_o and a_o are respectively the mean density and sound speed in the uniform environment of the source. r is the distance travelled by a sound ray from the moment it leaves the source to its arrival at $\underline{x}$. T_{rr} is the particular element of Lighthill's stresss tensor responsible for sound radiated in a particular direction, the direction going from point of emission to $\underline{x}$, a direction signified by the suffix r (repetition of r does not imply tensor summation). p, ρ and $\underline{u}$ are the actual pressure, density and velocity in the flow which is assumed a stationary function of time in a reference frame moving with velocity $a_o\underline{N}$. Coordinates in this reference frame are $\underline{\eta}$ so that the origin of $\underline{\eta}$ moves with the aircraft, and the volume integration over $\underline{\eta}$ is over the entire source region, which is the entire jet exhaust. $P_r(\underline{\eta},\underline{\lambda},\tau)$ is the cross correlation of T_{rr} expressed in a space separation coordinate moving with velocity $a_o(\underline{M}+\underline{N})$ relative to the aircraft, or with a velocity $a_o\underline{M}$ relative to the static environment in the opposite direction to that of aircraft motion. $\underline{\lambda}$ is the separation variable in this second moving frame and the $\underline{\lambda}$ integration is to be performed over all the volume surrounding $\underline{\eta}$ where there is a significant correlation of T_{rr} with the value at $\underline{\eta}$. The object of introducing this second reference frame is that turbulent eddies tend to travel several eddy lengths in a coherent lifetime in the direction of the jet flow. We will choose the value of $a_o\underline{M}$ to be the eddy convection speed which we shall assume constant for any one eddy, so that $\underline{M} = \underline{M}(\underline{\eta})$ may if desirable be treated as a function of eddy location in the flow. $P_r(\underline{\eta},\underline{\lambda},\tau)$ is consequently the moving axis stress tensor cross correlation, and since the turbulence is not homogeneous in general, it will be a non-trivial function of eddy position.

Equation 1.0 then represents a very complete specification of the sound field with a minimum of approximation. For completeness these are listed again. 1) Those non radiating parts of the density field that fall off more rapidly than r^{-2} are ignored. 2) Viscous stresses have been ignored. 3) An eddy has been assumed to have a well defined convection velocity $a_o\underline{M}$ relative to the outside environment.

To make further progress in the evaluation of 1.0 we must either have measured data of P_r or we must model it in some way. In fact, the latter approach is the only sensible way to progress since the function depends on seven independent variables so that the labour of specifying it experimentally is prohibitive.

Also the function has a high order zero to counter the singular coefficient $|1 - M \cos \theta|^{-5}$ at the Mach wave condition and this must be tackled analytically. It seems that the most plausible assumption we can make about the form of the correlation function is enough to greatly simplify the expression. That assumption is based on the fact that we have no reason to expect the correlation to have fundamentally different decay properties depending on which direction the separation vector $\underline{\lambda}$ is increased, or for that matter whether it is a mixture of space and time separations. The scale may well be different in these particular coordinate directions, but we will assume that the scale is the only property that depends on the coordinates individually. That is we assume that by suitable scaling of axes we can find a coordinate system in which the correlation function is isotropic in space-time. This assumption allows us to rewrite equation 1.0 in a way devoid of any residual effect of retarded time and also devoid of any singularity (unless the aircraft travels supersonically - the singularity then corresponding to the sonic boom). This equivalence is proved in the appendix. We have then as a starting point for scale evaluation the expression

$$I(\underline{x},t) = \frac{|1 + N \cos \phi|^{-1}}{16\pi^2 \rho_o r^2 a_o^5} \int_V \frac{\int_v \frac{\partial^4}{\partial \tau^4} P_r(\eta,\underline{\lambda},\tau=o)\,d\underline{\lambda}}{\{(1 - M \cos \theta)^2 + b_1 M^2(\cos^2\theta + b_2^2 \sin^2\theta)\}^{5/2}} d\underline{\eta} \qquad 1.4$$

I will now go on to describe the type of analysis that can be done on this equation by applying it to a particular model, but in doing so would emphasise that the equation is more general than the model and could be applied to several other models if they were more appropriate to real flow. The model I take is as follows 1) I will assume that all eddies travel at the same speed irrespective of the position they occupy in the jet, and will assume that speed to be 0.6 times the relative speed of the jet and ambient fluid.

$$M = 0.6 \left\{ \frac{Uj}{a_o} - N \right\} \qquad 1.6$$

Uj is the jet exit speed relative to the aircraft.

2) I will assume that the ratio $b_1^2 = 0.3$ and that b_2^2 is 0.1.

These values of the numbers are the ones that seem appropriate from the experimental survey of the turbulent velocity level in a low Mach number jet reported in reference 2. For lack of anything more appropriate these can serve as a guide line. This experimental survey also justifies the use of a single valued eddy convection speed in as much as the convection velocity is fairly slowly changing over the region of most intense turbulence. With these assumptions equation 1.4 can be written.

$$I(\underline{x},t) = F(\underline{x},\underline{N},\underline{M}) \int_V S_r(\underline{\eta})\,d\underline{\eta} \qquad 1.7$$

where S_r is now a measure of the sound output to the particular position $\underline{x}$ produced per unit volume of the exhaust flow,

$$S_r(\underline{\eta}) = \int_V \frac{\partial^4}{\partial \tau^4} Pr(\underline{\eta},\underline{\lambda},\tau = 0)\,d\underline{\lambda} \qquad 1.8$$

and $F(\underline{x},\underline{N},\underline{M})$ contains the main effect of forward speed, eddy convection and position. It contains all the directional effects if the turbulence is isotropic since S_r is then independent of direction.

$$F(\underline{x},\underline{N},\underline{M}) = \frac{|1 + N \cos \phi|^{-1}}{16\pi^2 \rho_o r^2 a_o^5} \left\{(1-M \cos \theta)^2 + 0.3\, M^2(\cos^2 \theta + 0.15 \sin^2\theta)\right\}^{-\frac{5}{2}} \qquad 1.9$$

On this model, the maximum radiation from an isotropic source does not propagate at the Mach angle, but at a direction making a slightly greater angle with the jet axis. In fact the Maximum polar angle is at

$$\theta m = \cos^{-1}\left\{\frac{0.77}{M}\right\} \qquad 1.10$$

The estimate of the source strength per unit volume and its integral over the source volume has been left till last because this involves the assumptions most difficult to justify in the high speed jet problem. A more realistic model may well be forthcoming and that could be incorporated into the analysis at this stage. So far only ratios of scales have been used and they might well be less susceptible to error than the absolute values which have now to be estimated.

The usual analysis goes as follows. We will assume that the source strength is essentially locally determined by three parameters at any one position $\underline{\eta}$. These parameters are the local density the local characteristic velocity (measured relative to the ambient air - that being the reference frame for the analysis ie. it is the frame from which u_i is measured) and the characteristic local length scale of the turbulence. These we could refer to as $\rho^*(\underline{\eta}), U^*(\underline{\eta})$, and $L^*(\underline{\eta})$ respectively. By pure dimensional analysis then

$$S_r = K^* \rho^{*a} U^{*8} L^{*-1} \qquad 1.11$$

where K^* is a constant and other parameters are functions of $\underline{\eta}$, position relative to the moving aircraft, only.

The integration of this quantity over the source volume η can conveniently be carried out in two stages. First, the volume integral can be split into an area integral across the plane of the jet, η_1, and an integral over axial distance η_1.

$$\int_V S_r(\underline{\eta}) d\underline{\eta} = \int_{\substack{\text{axial} \\ \text{distance}}} \int_{\substack{\text{cross-sectional} \\ \text{area}}} K^* \rho^{*a} u^{*8} L^{*-1} d\underline{\eta}_1 \, d\eta_1 \qquad 1.12$$

Now if we assume the source region to be an annular shear layer surrounding the cone of an axially symmetric jet, the characteristic values are functions of axial, η_1, and radial, η_2, positions only. Further if we assume a geometrically similar flow, the shear layer expanding conically, then the asterisked functions can be determined in terms of the ratio $(\eta_2 - D/2)/(\eta_1 \sigma_0)$, $\frac{\sigma_0 \eta_1}{\sigma}$, the overall characteristic density (ρ_0 or ρ_j) and the overall characteristic velocity across the shear layer $(U_j - U_0)$. D is the jet exit diameter, η_1 is measured from the jet orifice, U_j is the jet exit velocity relative to the nozzle and U_0 the aircraft forward speed.

$$\rho^*(\underline{\eta}) = (\rho_0 + \rho_j) f_\rho \left(\frac{\eta_2 - D/2}{\frac{\sigma_0}{\sigma} \eta_1} \right) \qquad 1.13$$

$$U^*(\underline{\eta}) = (U_j - U_0) f_u \left(\frac{\eta_2 - \frac{D}{2}}{\frac{\sigma_0}{\sigma} \eta_1} \right) \qquad 1.14$$

$$L^*(\underline{\eta}) = \frac{\sigma_0}{\sigma} \eta_1 f_L \left(\frac{\eta_2 - D/2}{\frac{\sigma_0}{\sigma} \eta_1} \right) \qquad 1.15$$

The length of the mixing region is σD with $U_0 \neq 0$, but is $\sigma_0 D$ when $U_0 = 0$.

The area integral in 1.12 can then be set in polar coordinates by writing

$$\int d\underline{\eta} = \int_0^\infty 2\pi \eta_2 d\eta_2 \qquad 1.16$$

and equation 1.12 can be written

$$\int_V S_r(\underline{\eta}) \, d\underline{\eta} = Q \int_0^{\sigma D} \left\{ A + B \frac{\eta_1 \sigma_0}{D\sigma} \right\} d\eta_1 \qquad 1.17$$

where

$$Q = \pi K^* D (\rho_0 + \rho_j)^a (U_j - U_0)^8 \qquad 1.18$$

$$A = \int_{-\infty}^{\infty} G(f) df \qquad 1.19$$

$$B = 2\int_{-\infty}^{\infty} \mathcal{Y} G(\mathcal{Y})\, d\mathcal{Y} \qquad 1.20$$

and $$G(\mathcal{Y}) = f_{\mathcal{Y}}^{8}(\mathcal{Y}) f_u^{8}(\mathcal{Y}) f_L^{-1}(\mathcal{Y}) \qquad 1.21$$

The integrals on the normalised radial direction, $\mathcal{Y}$, have been taken between infinite limits on the assumption that the source strength is zero outside the shear layer and the shear layer has not yet grown to envelop the laminar cone. The axial position at which the shear layers meet on the axis is $\eta_1 = \sigma D$ which is the limit of η_1 integration permitted by this simple model.

Now $\mathcal{Y} = 0$ marks the radial position in the jet corresponding to the extension into the flow of the nozzle periphery. $\mathcal{Y} < 0$ is the section within this nozzle radius. It is clear from 1.21 that the function G, which is a non-dimensional measure of how much sound is produced by unit volume of turbulence as a function of radial position is a positive definite quantity. If G is symmetric about $\mathcal{Y} = 0$, i.e. the shear layer properties are symmetric about the radial position corresponding to the nozzle exit, then B which is a moment of G is zero. This is the property usually assumed in dimensional analysis and is essential to the deduction that sound output per unit length of jet is a constant - as is clear from 1.17 when B = 0. However, it is rather unlikely that B is in fact zero so that it is pertinent to enquire into its likely magnitude. This is easily obtained from equation 1.20 to be:

$$B = 2\epsilon A \qquad 1.22$$

where ϵ is the distance on a $\mathcal{Y}$ scale of the ''centroid'' of G out from the position $\mathcal{Y} = 0$. Bradshaw, Ferris and Johnson, reference 3, observe the shear layer of a static jet to be growing in such a way that $\epsilon = +0.02$. We can use this value as a guide line. According to equation 1.17.

$$\int_v S_r(\underline{\eta})\, d\underline{\eta} = AQ \int_0^{\sigma D} \left\{1 + \frac{2\epsilon\eta_1\sigma_0}{\sigma D}\right\} d\eta_1 \qquad 1.23$$

$$= AQ\sigma D\,(1 + \epsilon\sigma_0) \qquad 1.24$$

from which we see that the sound output per unit length of jet actually increases slightly with axial distance downstream but, if $\epsilon = +2\%$ by only 20% in the mixing region of a subsonic jet. This effect may be important in supersonic jets which are flows with a much longer length of mixing region. If the mixing region is σD in length, then the usually neglected term, $2\epsilon\eta_1\sigma_0/D\sigma$, amounts to $2\epsilon\sigma_0$ at the downstream extremity of the mixing zone. With $\epsilon = 2\%$ this is a correction to the usual analysis of $+ 4\delta_0\%$ on the sound output per unit length and a correction of $+ 2\delta_0\%$ on the total output of the mixing region.

All that remains to complete the analysis is to estimate the value of σ, the length of the mixing zone measured in nozzle diameters. This clearly varies as a function of aircraft forward speed U_0 according to Squire and Trouncer in proportion to $U_j/(U_j - U_0)$. If we use this result we can combine equations 1.18, 1.24 and 1.7 to produce an estimate for the sound radiated by a well behaved annular mixing region of a jet in flight.

$$I(\underline{x},t) = \frac{K(\rho_0 + \rho_j)^2 (U_j - U_0)^7 U_j}{\rho_0 a_0^5} \frac{D^2}{r^2}\,(1 + \epsilon\sigma_0)\, E(\underline{x},\underline{N},\underline{M}) \qquad 1.25$$

where K is a constant and

$$E(\underline{x},\underline{N},\underline{M}) = |1 + N\cos\phi|^{-1}\left\{(1 - M\cos\theta)^2 + 0.3M^2(\cos^2\theta + 0.1\sin^2\theta)\right\}^{-\frac{5}{2}},$$

$$N = U_0/a_0, \quad M = 0.6[U_j - U_0]/a_0 \qquad 1.26$$

σ_0 is the length of the mixing zone of a static jet at speed U_j measured in diameters.

APPENDIX

Consider the integral S

$$S = \int_V \frac{\partial^4}{\partial \tau^4} P_r \left(\underline{\eta}, \underline{\lambda}, \tau = \frac{\lambda_r}{a_o(1-M\cos\theta)}\right) d\underline{\lambda} \qquad A1$$

Rescale space variables by scale factors α_i to make P_r as isotropic in space as possible.

$$z_i = \alpha_{(i)}\lambda_i \qquad A2$$

$$P_r(\underline{\eta}, \underline{\lambda}, \tau) = P(\underline{\eta}, \underline{z}, \tau) \qquad A3$$

Now make P as isotropic as possible in space time by rescaling time variable

$$\gamma = \beta M a_o \tau \qquad A4$$

$$P(\underline{\eta}, \underline{z}, \tau) = I(\underline{\eta}, \underline{z}, \gamma) = I(\underline{\eta}, \underline{\xi}) \qquad A5$$

where I is the isotropic space time correlation as a function of the four vector separation variable $\underline{\xi}$

$$\underline{\xi} = (\underline{z}, \gamma) \qquad A6$$

$$\frac{\partial}{\partial \tau} = \frac{\partial \gamma}{\partial \tau} \cdot \frac{\partial}{\partial \gamma} = \beta M a_o \frac{\partial}{\partial \gamma} \qquad A7$$

$$d\underline{\lambda} = d\underline{z}\,(\alpha_1\alpha_2\alpha_3)^{-1} \qquad A8$$

so that:

$$S = \int_V \frac{(\beta M a_o)^4}{\alpha_1\alpha_2\alpha_3} \cdot \frac{\partial^4}{\partial \gamma^4} I\left(\underline{\eta}, \underline{z}, \gamma = \frac{\beta M(\frac{z_1}{\alpha_1}\cos\theta + \frac{z_2}{\alpha_2}\sin\theta)}{(1 - M\cos\theta)}\right) d\underline{z} \qquad A9$$

The $\underline{z}$ coordinates, which can be chosen arbitrarily, have been set in such a way that:

$$\lambda_r = \lambda_1\cos\theta + \lambda_2\sin\theta \qquad A10$$

A9 can be rewritten as an integral of a generalised function

$$S = \frac{(\beta M a_o)^4}{\alpha_1\alpha_2\alpha_3} \int_{V,\gamma} \frac{\partial^4}{\partial \gamma^4} I(\underline{\eta}, \underline{z}, \gamma)\, \delta\left(\gamma - \frac{\beta M(\frac{z_1}{\alpha_1}\cos\theta + \frac{z_2}{\alpha_2}\sin\theta)}{(1-M\cos\theta)}\right) d\underline{\xi} \qquad A11$$

$$S = \frac{(\beta M a_o)^4}{\alpha_1\alpha_2\alpha_3} \int_{V,\gamma} I(\underline{\eta}, \underline{z}, \gamma) \frac{\partial^4}{\partial \gamma^4} \delta\left(\gamma - \frac{\beta M(\frac{z_1}{\alpha_1}\cos\theta + \frac{z_2}{\alpha_2}\sin\theta)}{(1 - M\cos\theta)}\right) d\underline{\xi} \qquad A12$$

$$S = \frac{(\beta M a_o)^4}{\alpha_1\alpha_2\alpha_3} \left| 1 + \frac{\beta^2 M^2 (\frac{\cos^2\theta}{\alpha_1^2} + \frac{\sin^2\theta}{\alpha_2^2})}{(1 - M\cos\theta)^2} \right|^{-5} \int_V \frac{\partial^4}{\partial \gamma^4} I(\underline{\eta}, \underline{z}, 0) d\underline{z} \qquad A13$$

At this stage we can reverse all the scaling operations to express this result in term of the original variables in A1.

$$S = \frac{|1 - M\cos\theta|^5}{\left\{(1-M\cos\theta)^2 + \frac{\beta^2 M^2}{\alpha_1^2}(\cos^2\theta + \frac{\alpha_1^2}{\alpha_2^2}\sin^2\theta)\right\}^{5/2}} \int_V \frac{\partial^4}{\partial \tau^4} P_r(\underline{\eta}, \underline{\lambda}, \tau = 0) d\underline{\lambda} \qquad A14$$

Now the ratio β/α_1 is the integral length scale of the eddy in the direction of convection divided by the distance travelled by the eddy in a moving axis integral time scale i.e. $\frac{\alpha_1}{\beta}$ is the distance travelled by an eddy in its coherent lifetime measured in eddy lengths. The ratio α_1/α_2 is the ratio of eddy scale in the direction perpendicular to the direction of travel (but in the plane of the observer at $\underline{x}$ and the vector $\underline{M}$) divided by the longitudinal length scale. If any eddy is elongated in the direction of convection α_1/α_2 is less than unity but is equal to unity for a spherical eddy. The eddy scale in a direction perpendicular to the convection and radiation directions does not feature directly in the equations - though it influences the volumetric scale.

On writing the ratios

$$\beta/\alpha_1 = b_1 \quad \text{and} \quad \alpha_1/\alpha_2 = b_2, \qquad \text{A15}$$

A14 can be used to re-express equation 1.0 in a more easily interpreted form

$$I(\underline{x},t) = \frac{|1 + N\cos\phi|^{-1}\iiint \frac{\partial^4}{\partial\tau^4} P_r(\underline{\eta},\underline{\lambda},\tau = 0)\,d\underline{\lambda}\,d\underline{\eta}}{16\pi^2\rho_o r^2 a_o^5\left\{(1-M\cos\Theta)^2 + b_1^2M^2(\cos^2\Theta+b_2^2\sin^2\Theta)\right\}^{5/2}}$$

Acknowledgment: This work was carried out in conjunction with the Bristol Engine Division of Rolls-Royce.

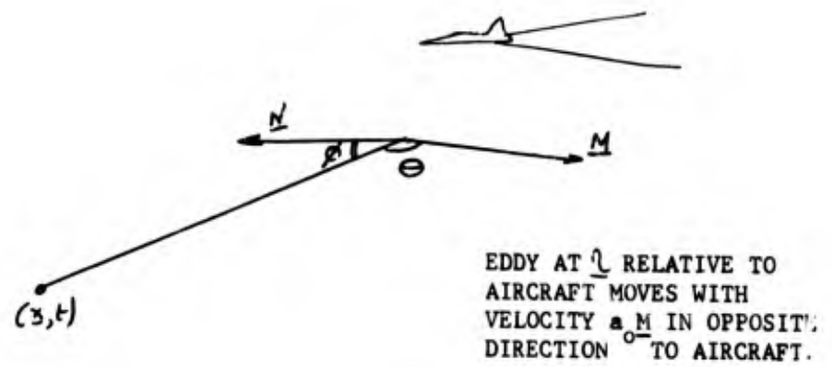

FIG.1

References

(1) Ffowcs Williams, J. E., 1963.
Phil.Trans.Roy.Soc.A.1061,255.

(2) Davies, P. O. A. L., Fisher, M. J. and Barratt, M., 1963.
J. Fluid.Mech.15.

(3) Bradshaw, P., Ferris, D. H. and Johnston, R. F., 1964.
J.Fluid Mech.19.

DETERMINATION DU CHAMP SONORE PRODUIT PAR L'EVOLUTION DES AVIONS A REACTION

par M. KOBRYNSKI

Office National d'Etudes et de Recherches Aérospatiales
29, avenue de la Division Leclerc
92 - CHATILLON-sous-BAGNEUX
(France)

0

0 0

S O M M A I R E

La relation entre le champ total de pression sonore émis par un jet de révolution stationnaire et le champ sonore provenant du même jet mobile, observé en un point fixe au sol, est étudiée en faisant intervenir dans l'équation généralisée du niveau de pression sonore globale locale dont on rappelle la forme, un nouvel indice de convection dérivé de l'expression de Ribner

$$\left[(1-M_c\cos\theta)^2+\alpha^2 M_c^2\right]^{5/2}\ (1+\cos^4\theta)$$

La nouvelle équation confirme les résultats antérieurs dans la direction du rayonnement acoustique maximal θ_M et améliore la prévision du bruit dans les autres directions.

L'influence de la vitesse de vol sur l'émission sonore dans un large éventail d'angles (20° - 160° par rapport à l'axe du jet) est mise en évidence; on en déduit la relation entre l'effet de convection des tourbillons dans les jets stationnaire et mobile et la variation de puissance acoustique produite par l'entraînement du jet dans l'atmosphère.

Les résultats de l'étude analytique, confirmés par de nombreuses vérifications expérimentales, ont montré que dans les angles différents de θ_M la vitesse relative n'est pas le paramètre significatif à retenir pour déterminer les niveaux de pression sonore globale locale.

E R R A T A

Au lieu de	Lire
éqon 2 $W = K\,\dfrac{\rho_j^2\, S V_j^8 \left(1-\frac{V_e}{V_j}\right)^4}{\rho_a\, C_a^{-5}}$	$W = K\,\dfrac{\rho_j^2 S V_j^8 \left(1-\frac{V_e}{V_j}\right)^4}{\rho_a\, C_a^5}$
en bas de la page 9.1 $M_j = V_e/C_a$	$M_v = V_e/C_a$
éqon 8 $\left[(1-M_c\cos\theta)^2+\left(\dfrac{\omega_s \ell}{\pi C_a}\right)^2\right]$	$\left[(1-M_c\cos\theta)^2+\left(\dfrac{\omega_s \ell}{\sqrt{\pi}\, C_a}\right)^2\right]^{-5/2}$
éqon 11 $\alpha = \dfrac{\omega_s \ell}{\pi V_c}$	$\alpha = \dfrac{\omega_s \ell}{\sqrt{\pi}\, V_c}$
éqon 14 $\alpha_v = \dfrac{\omega_v \ell}{\pi V_c\left(1+\frac{M_v}{2M_c}\right)}$	$\alpha_v = \dfrac{\omega_v \ell}{\sqrt{\pi}\, V_c\left(1+\frac{M_v}{2M_c}\right)}$
milieu de la page 9-3 $(1+M_c\cos\theta)^{-1}$	$(1+M_v\cos\theta)^{-1}$
éqon 29 $\left\{\dfrac{\left[1-M_c\left(1-\frac{M_v}{2M_c}\right)\cos\theta_M\right]+\alpha_s^2 M_c^2\left(1+\frac{M_v}{2M_c}\right)^2}{(1-M_c\cos\theta_M)^2+\alpha_s^2 M_c^2}\right\}^{5/2}\left(1-\dfrac{M_v}{2M_c}\right)^4 \simeq 1$	$\left\{\dfrac{\left[1-M_c\left(1-\frac{M_v}{2M_c}\right)\cos\theta_M\right]^2+\alpha_s^2 M_c^2\left(1+\frac{M_v}{2M_c}\right)^2}{(1-M_c\cos\theta_M)^2+\alpha_s^2 M_c^2}\right\}^{5/2}\left(1-\dfrac{M_v}{2M_c}\right)^4 \simeq 1$
milieu de la page 9-5 dans cette direction seulement	dans cette direction singulière

LE CALCUL PREVISIONNEL du bruit d'un avion , au stade du projet de celui-ci, est devenu une nécessité, tant pour étudier des trajectoires optimales que pour satisfaire aux conditions de certification acoustique; le champ de pression sonore au sol doit donc être connu en fonction des paramètres des moteurs et du vol, et pendant la durée de l'évolution de l'avion, en amplitude et spectre, afin de déterminer par exemple le niveau de gêne en PNdB effectifs.

Une méthode de calcul prévisionnel du champ sonore produit par les jets de révolution stationnaires et mobiles a été exposée dans des travaux antérieurs, en limitant d'abord ce calcul à la direction de rayonnement acoustique maximal [1], puis en l'étendant à un large éventail d'angles, de 20° à 160° par rapport à l'axe du jet [2].

Cette méthode de calcul du bruit des turboréacteurs à flux direct, fonctionnant en régime sec ou avec post-combustion, est reprise et complétée, dans ce travail, en particulier en faisant intervenir une nouvelle forme du facteur de convection des tourbillons dans le jet.

1.- RAPPEL DES RESULTATS ANTERIEURS [1,2]

Soient α l'angle de montée d'un avion à réaction (figure 1), i son incidence, β le calage des réacteurs, θ l'angle formé entre l'axe du jet et le rayon sonore dirigé vers un point d'observation O et ψ l'angle entre le rayon sonore et l'horizontale. Ces angles sont reliés par :

$$\theta = \pi - (\psi + \alpha + \beta + i) \qquad (1)$$

En prenant pour origine du temps le passage de l'avion à la verticale du point O , on peut déterminer la position de l'avion à l'instant d'émission du son reçu en O et le temps de cette émission, en fonction de l'altitude du passage en O , de la vitesse de l'avion et des angles précédents. La variation des niveaux sonores enregistrés en fonction du temps peut alors être rapportée à l'angle θ , comme indiqué sur la figure 2.

Nous nous proposons de déterminer au point O ou en un point pris sur la perpendiculaire à la trace, les niveaux sonores globaux et par bandes de fréquences émis par le jet en fonction de l'angle θ , de 20 à 160°, et notamment les niveaux sonores associés à l'angle du rayonnement acoustique maximal θ_M. Bien entendu, le calcul permet d'obtenir aussi le champ sonore produit par les jets stationnaires.

Le calcul du niveau sonore fait intervenir d'abord la puissance acoustique engendrée par le jet, dont l'expression générale est

$$W = K \frac{\rho_j^2 S V_j^8 \left(1 - \frac{V_e}{V_j}\right)^4}{\rho_a c_a^{-5}} \qquad (2)$$

où ρ_j est la densité volumique des gaz du jet détendu, ρ_a celle de l'air ambiant, V_j la vitesse des gaz éjectés à travers la surface S , c_a la célérité du son dans l'air ambiant et V_e la vitesse d'entraînement de l'avion. Le coefficient K est égal à $1{,}8.10^{-4}$ [1] . De cette puissance, on déduit le niveau moyen spatial (source supposée isotrope) sur une sphère de référence, dont le rayon R_o a été choisi de 30 m, centrée sur la buse du réacteur, puis le niveau de pression sonore globale N_θ en un point, caractérisé par l'angle θ , la directivité étant donnée par le facteur de convection. Le résultat obtenu est introduit ensuite dans le calcul des niveaux de pression sonore associés aux bandes de fréquences (par octave par exemple) en faisant intervenir les courbes du spectre acoustique généralisé, caractéristiques des directions considérées (voir paragraphe 4). Ces niveaux sonores, calculés pour R_o = 30 m, sont enfin corrigés en leur appliquant les atténuations géométriques et moléculaires correspondant aux longueurs des rayons sonores considérés.

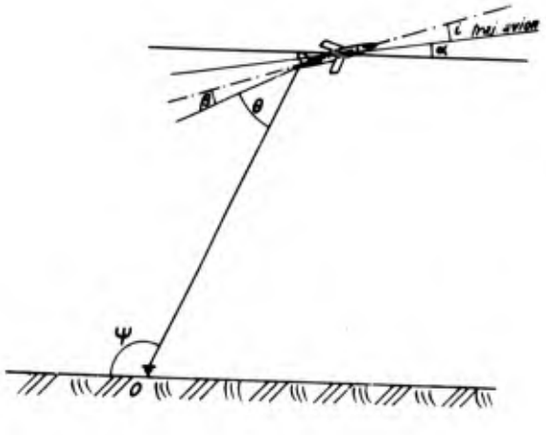

Fig. 1
Trajectoire de l'avion en vol.
Angles considérés.

L'expression de N_θ est (équation 14, référence 2)

$$N_\theta = 10 \log_{10} \frac{\rho_j^2 S M_c^8 \left(1 - \frac{M_v}{2M_c}\right)^4}{\left[1 - M_c \left(1 - \frac{M_v}{2M_c}\right) \cos\theta\right]^\eta} + C \qquad (3)$$

Dans cette équation M_c est le nombre de Mach de convection des tourbillons dans le jet $\left(M_c = \frac{1}{2}\frac{V_j}{c_a}\right)$, $M_j = V_e/c_a$ est le nombre de Mach de vol, et l'exposant η du facteur de convection est déterminé par la formule expérimentale $\eta = 16 M_c / (6M_c^3 + 1)$

A la distance de référence $R_o = 30\,m$ la constante cumulative C prend la valeur 138 dB pour les jets stationnaires et 140 dB pour les jets en vol. La validité du facteur de convection de l'équation (3) est limitée aux

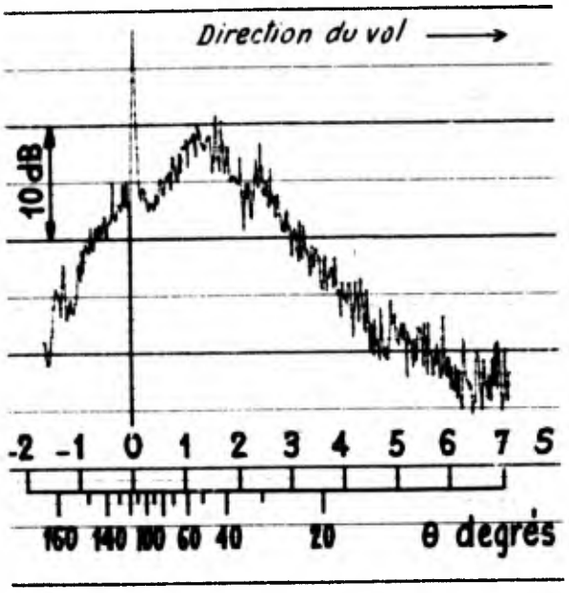

Fig. 2
Avions à réaction en vol. Variation du niveau de pression sonore globale linéaire sur la trace en fonction du temps ou de l'angle.

angles $\theta > \theta_M$ où θ_M est l'angle de rayonnement acoustique maximal, donné par la relation expérimentale

$$\theta_M = 24\, M_c + 18 \qquad (4)$$

Toutefois, en remarquant que les courbes de variation des niveaux sonores globaux polaires sont symétriques, avec une approximation satisfaisante, de part et d'autre de θ_M dans l'intervalle angulaire $\pm$ 20°, intervalle suffisant dans nos calculs on peut adopter pour chaque angle $\theta < \theta_M$ la valeur θ' de l'angle symétrique de θ par rapport à θ_M soit

$$\theta' = 2\theta_M - \theta \qquad (5)$$

Dans l'expression (3) donnant la valeur de N_θ, le dénominateur est le facteur de convection d'une forme dérivée de celle donnée par Lighthill [3], avec une modification expérimentale de l'exposant. Nous nous proposons dans ce travail de déterminer un nouveau facteur de convection basé sur une expression plus élaborée, proposée par Ribner.

2.- FACTEUR DE CONVECTION

2.1.- JETS STATIONNAIRES - On sait depuis les travaux de Lighthill [3] et de Ffowcs-Williams [4] que pour un jet stationnaire de faible nombre de Mach la distribution directionnelle de l'intensité sonore suit les lois d'émission des quadruplets aérodynamiques entraînés dans le jet avec une vitesse de convection $V_c = M_c\, C_a$ Le facteur de convection obtenu est de la forme

$$\left(1 - M_c \cos\theta\right)^{-5} \qquad (6)$$

Il est bien évident que l'amplification annoncée par ce facteur ne peut croître indéfiniment avec M_c et devenir infinie pour

$$M_c \cos\theta = 1 \qquad (7)$$

C'est pourquoi, pour satisfaire les valeurs expérimentales, nous avons remplacé l'exposant - 5 de (6) par l'exposant variable η ; de plus, pour diverses raisons et tenant compte de (7), la validité du facteur de convection ainsi exprimé était limitée aux angles θ compris dans l'intervalle

$$\arccos 1/M_c > \theta \geq \theta_M$$

Les études postérieures effectuées par Ffowcs-Williams [5] et Ribner [6] ont conduit à une expression modifiée du facteur de convection qui élimine la singularité (7) :

$$\left[\left(1 - M_c \cos\theta\right)^2 + \left(\frac{\omega_s\, \ell}{\pi C_a}\right)^2\right] \qquad (8)$$

où ω_s est une pulsation caractéristique de la turbulence du jet stationnaire et ℓ le rayon de corrélation, ou ℓ^3 le "volume efficace du tourbillon" de rayonnement cohérent (le nouveau terme $\frac{\omega \ell}{\pi C_a}$ est le paramètre de Damkohler).

Considérant que l'orientation priviligiée des systèmes des quadruplets dans le jet introduit le facteur [6]

$$1 + \frac{\cos^4\theta + \cos^2\theta}{2} \simeq 1 + \cos^4\theta \qquad (9)$$

le facteur de directivité globale du bruit est donné par [6]

$$\left[\left(1 - M_c \cos\theta\right)^2 + \alpha^2 M_c^2\right]^{-5/2} \left(1 + \cos^4\theta\right) \qquad (10)$$

$$\text{avec} \qquad \alpha = \frac{\omega_s\, \ell}{\pi V_c} \qquad (11)$$

La comparaison de l'expression (10) avec la distribution polaire expérimentale des niveaux de pression sonore globale des jets stationnaires nous a conduits par itérations à une expression de α_s^2 donnée avec une bonne approximation par

$$\alpha_s^2 = 0{,}45\, \frac{1}{M_c^2} + 0{,}75\, \frac{\log M_c}{M_c} \qquad (12)$$

valeur retenue dans la suite des calculs.

2.2.- JETS MOBILES - Par rapport à l'atmosphère, lieu de propagation des ondes sonores, le nombre de Mach de convection est

$$M_c - \frac{1}{2} M_v \tag{13}$$

Appelons α_v le coefficient (11) relatif au jet en vol, et soit ω_v la pulsation caractéristique associé à la turbulence de ce jet.

Par ailleurs, dans le système des coordonnées mobiles, liées au jet, que nous devons adopter ici, la vitesse de convection devient $V_c\left(1+\frac{M_v}{2M_c}\right)$. En admettant que le rayon de corrélation reste inchangé, on peut écrire :

$$\alpha_v = \frac{\omega_v \ell}{\pi V_c \left(1+\frac{M_v}{2M_c}\right)} \tag{14}$$

Le rapport entre les pulsations caractéristiques associées à la turbulence des jets stationnaires ω_s et mobiles ω_v est donné par

$$\frac{\omega_v}{\omega_s} = \left(1+\frac{M_v}{2M_c}\right)^2 \quad pour \quad \frac{M}{2M_c} < 0,3 \tag{15}$$

comme nous l'avons déjà montré (voir référence 1). De (14), (15) et (11), il vient :

$$\alpha_v = \alpha_s \left(1+\frac{M_v}{2M_c}\right) \tag{16}$$

En combinant (10) (13) et (16) et en remarquant que dans une direction donnée le rayonnement acoustique provenant des jets est réduit à celui des tourbillons dont l'émission arrive simultanément, le facteur de réduction étant $(1+M_c\cos\theta)^{-1}$ déterminé par Ff. Williams [4] par des considérations purement géométriques, on peut écrire que l'intensité directionnelle du bruit des jets mobiles est donnée par :

$$\left\{\left[1-M_c\left(1-\frac{M_v}{2M_c}\right)\cos\theta\right]^2 + \alpha_s^2 M_c^2\left(1+\frac{M_v}{2M_c}\right)^2\right\}^{-5/2} (1+M_v\cos\theta)^{-1}(1+\cos^4\theta) \tag{17}$$

ou α_s^2 est donné par (12)

Cette expression valable aux angles $\theta \geq \theta_M$, θ_M étant déterminé par la formule (4), se réduit à (10) pour $M_v = 0$.

Aux angles $\theta < \theta_M$, les conditions d'emploi de cette expression sont précisées au paragraphe 1.

3.- NIVEAUX DE PRESSION SONORE GLOBALE POLAIRE

3.1.- JETS STATIONNAIRES - La méthode de calcul des niveaux de pression sonore globale polaire produit par les jets stationnaires N_θ comporte les étapes suivantes :

- déterminer la puissance acoustique émise à partir des caractéristiques thermodynamiques du jet.
- calculer la pression sonore moyenne spatiale en champ lointain (pression produite par la répartition isotrope de cette puissance)
- faire intervenir l'amplification de cette pression en fonction de l'angle θ, décrite par le facteur de convection.

La puissance acoustique globale émise par les jets stationnaires W_s est donnée par la formule (2) avec $V_e = 0$. En champ libre la valeur quadratique moyenne de la pression sonore à la distance R est

$$\overline{p^2} = \frac{\rho_0 C_a W_s}{4\pi R^2} \tag{18}$$

Le niveau de pression sonore moyenne spatiale $\langle N_m \rangle$ est donné d'après (18) et (2) et avec nos notations

$$\langle N_m \rangle = 10 \log_{10} \rho_j^2 S M_c^8 + C_1 \tag{19}$$

ou C_1 est une constante cumulative qui vaut 141 dB en champ libre, à la distance $R = R_0 = 30\,m$

Nous avons admis que la source sonore et le point d'observation sont situés tous les deux dans le milieu indéfini et de plus, que la distance entre la source et le point considéré est grande par rapport à la longueur d'onde de la fréquence la plus basse mesurée et par rapport à la dimension caractéristique de la source elle-même (condition du champ acoustique lointain). En fait, les mesures sont effectuées près du sol, et la présence du sol, plus ou moins réfléchissant, perturbe la propagation des ondes sonores entre la source et le récepteur; le spectre acoustique reçu est modifié en raison de l'interférence entre les rayons sonores.

L'étude montre que l'effet du sol se manifeste par un accroissement du niveau sonore global pouvant varier de 3 dB à 6 dB. En considérant les conditions rencontrées en pratique, nous retenons la valeur de 3 dB, généralement admise.

Dans ces conditions, la constante cumulative C_2 aura pour valeur $C_1 + 3 = 144\ dB$, et incluant l'effet du sol, l'équation (19) s'écrit

$$< N_m >_s = 10 \log_{10} \rho_j^2\ S M_c^8 + C_2 \qquad (20)$$

pour $R_0 = 30\ m.$

Introduisons à présent dans (20) la combinaison des facteurs d'amplification de l'intensité sonore dus à la vitesse de convection des tourbillons dans le jet et à l'orientation priviligiée des quadruplets, exprimés par (10), nous obtenons le niveau sonore global local polaire :

$$N_{\theta_s} = 10 \log_{10} \frac{\rho_j^2\ S M_c^8\ (1 + \cos^4\theta)}{\left[(1 - M_c \cos\theta)^2 + \alpha_s^2\ M_c^2\right]^{5/2}} + C_2 \qquad (21)$$

où α^2 est remplacé par α_s^2 déterminé par (12)

Notons que le niveau de pression sonore local <u>linéaire</u> est donné par

$$N_{\theta_s} + 10 \log_{10} \frac{\sin^2\theta}{\cos^2(\alpha + i + \beta)} \qquad (22)$$

$\alpha, i, \beta,$ étant définis au paragraphe 1.

3.2.- <u>JETS MOBILES</u> - Le calcul des niveaux de pression sonore globale polaire produite par les jets mobiles sera effectué d'abord en un point défini dans le système de références lié au jet, puis dans un système de références lié à l'atmosphère supposée immobile, ou au sol.

Soit $N^*_{\theta_v}$ le niveau sonore N_{θ_v} dans le premier système de références.

Comme pour le jet stationnaire, le calcul de $N^*_{\theta_v}$ fait intervenir la puissance acoustique exprimée par (2), le niveau de pression sonore moyenne spatiale du jet mobile $< N_m >_v$ en champ libre qui d'après (19), vaut :

$$< N_m >_v = 10 \log_{10}\ \rho_j^2\ S M_c^8 \left(1 - \frac{M_v}{2 M_c}\right)^4 + C_1 \qquad (23)$$

ou C_1 est la constante cumulative du jet stationnaire et enfin l'amplification de l'intensité sonore due à la vitesse de convection et d'autres causes exprimée par (17).

Tous calculs faits, et en incluant dans la constante l'effet de sol, nous obtenons l'expression analytique :

$$N^*_{\theta_v} = 10 \log_{10} \frac{\rho_j^2\ S M_c^8 \left(1 - \frac{M_v}{2 M_c}\right)^4 (1 + \cos^4\theta)}{\left\{\left[1 - M_c \left(1 - \frac{M_v}{2 M_c}\right)\cos\theta\right]^2 + \alpha_s^2 M_c^2 \left(1 + \frac{M_v}{2 M_c}\right)^2\right\}^{5/2} (1 + M_v \cos\theta)} + C_2 \qquad (24)$$

Dans cette équation α_s^2 est donné par (12) et $C_2 = 144\ dB$ pour $R_0 = 30\ m.$

Notons que, comme pour le jet stationnaire, les angles intervenant dans l'indice de convection seront déterminés par la formule (5) pour $\theta < \theta_M$, θ_M étant donné par (4).

L'équation (24) indique le niveau sonore global <u>émis</u> par le jet mobile (axes liés à l'avion en vol). Cependant, le niveau sonore <u>mesuré</u> (axes liés au sol) dépend de la variation du rayon sonore R en raison de l'atténuation géométrique et moléculaire du bruit (α dB par m.).

De plus, il faut faire intervenir la largeur de la bande passante dans laquelle travaille l'analyseur, d'où la nécessité d'introduire dans (24) des corrections dues à l'effet Doppler.

Soit, en effet f_{ev} une fréquence caractéristique émise par le jet en vol telle qu'elle serait mesurée en un point de l'espace rapporté aux coordonnées mobiles, liées à l'avion. Au point rapporté aux coordonnées fixes, la fréquence mesurée sera la fréquence apparente f_a transformée de f_{ev} par l'effet Doppler, soit

$$f_{ev}/f_a = 1 + M_v \cos\theta \tag{25}$$

Si Δf_i est la largeur normalisée des bandes de fréquence mesurées dans l'intervalle i l'intensité sonore correspondante a été émise dans une bande de largeur $\Delta f_i (1 + M_v \cos\theta)$. Il s'ensuit une correction des niveaux sonores donnée par $10 \log_{10} (1 + M_v \cos\theta)$

Dans ces conditions, si N_{θ_v} est le niveau sonore global local reçu en point fixe au sol la distance R.

$$N_{\theta_v} = N^*_{\theta_v} + 10 \log_{10} (1 + M_v \cos\theta) - 20 \log \frac{R}{R_0} - a (R - R_0) \tag{26}$$

ou $N^*_{\theta_v}$, déterminé par (24), est le niveau sonore global polaire émis à la distance R_0

Le coefficient a étant fonction de la fréquence, le calcul du terme $a (R - R_0)$ nécessite la connaissance du spectre acoustique associé à $N^*_{\theta_v}$. Ce spectre est déterminé suivant la méthode décrite au paragraphe 4.

La forme générale de l'expression donnant N_{θ_v} étant précisée, posons pour simplifier $R = R_0$ En combinant les équations (26) et (24), il vient

$$N_{\theta_v} = 10 \log_{10} \frac{\rho_j^2 S M_c^8 \left(1 - \frac{M_v}{2M_c}\right)^4 (1 + \cos^4\theta)}{\left\{\left[1 - M_c \left(1 - \frac{M_v}{2M_c}\right) \cos\theta\right]^2 + \alpha_s^2 M_c^2 \left(1 + \frac{M_v}{2M_c}\right)^2\right\}^{5/2}} + C_2 \tag{27}$$

Pour $M_v = 0$ on retrouve l'équation (21) donnant le niveau N_{θ_s} du jet stationnaire.

3.3.- <u>EFFET DE LA VITESSE D'ENTRAINEMENT DU JET SUR LE CHAMP SONORE</u> - La réduction des niveaux sonores suivant la direction θ produite par le nombre de Mach de vol, est mise en évidence en combinant les équations (27) et (21). Nous obtenons :

$$N_{\theta_s} - N_{\theta_v} = 10 \log_{10} \frac{\left\{\left[1 - M_c \left(1 - \frac{M_v}{2M_c}\right) \cos\theta\right]^2 + \alpha_s^2 M_c^2 \left(1 + \frac{M_v}{2M_c}\right)^2\right\}^{5/2}}{\left[(1 - M_c \cos\theta)^2 + \alpha_s^2 M_c^2\right]^{5/2} \left(1 - \frac{M_v}{2M_c}\right)^4} \tag{28}$$

La solution numérique de cette expression, effectuée en attribuant aux nombre de Mach M_c et M_v de nombreuses valeurs discrètes, a montré que dans la direction du rayonnement acoustique maximal θ_M , déterminé par (4), et <u>dans cette direction seulement</u>, on peut écrire avec une bonne approximation

$$\left\{\frac{\left[1 - M_c \left(1 - \frac{M_v}{2M_c}\right) \cos\theta_M\right] + \alpha_s^2 M_c^2 \left(1 + \frac{M_v}{2M_c}\right)^2}{(1 - M_c \cos\theta_M)^2 + \alpha_s^2 M_c^2}\right\}^{5/2} \left(1 - \frac{M_v}{2M_c}\right)^4 \simeq 1 \tag{29}$$

c'est-à-dire que dans la direction θ_M , le rapport des facteurs de convection des jets stationnaire et mobile est approximativement égal au facteur de réduction de la puissance acoustique dû à la mobilité du jet $\left(1 - \frac{M_v}{2M_c}\right)^{-4}$

Dès lors, en remplaçant le facteur de convection de (27) par sa valeur particulière tirée de l'équation (29), nous obtenons une expression approchée du niveau de pression sonore globale <u>maximale</u> polaire du jet mobile N_{θ_M}, qui est

$$N_{\theta_M} = 10 \log_{10} \frac{\rho_j^2 S \left(M_c - \frac{1}{2} M_v\right)^8 (1 + \cos^4\theta)}{\left[(1 - M_c \cos\theta_M)^2 + \alpha_s^2 M_c^2\right]^{5/2}} + C_2$$

Ce résultat rapproché de l'équation (21), relative au jet stationnaire, montre que dans la direction θ_M le niveau de pression sonore maximale globale polaire produite par le jet mobile peut être déterminé, soit par l'équation (27), soit par l'équation (21) dans laquelle figure la vitesse relative du jet. Ceci montre que dans la direction du bruit maximal et dans cette seule direction, la vitesse relative peut être prise comme paramètre pour le calcul des niveaux sonores des jets en vol.

3.4.- VERIFICATIONS EXPERIMENTALES DE L'EQUATION (27) - Nous avons effectué un grand nombre de mesures du bruit émis par les avions à réaction de différents types (MIRAGE IV, CARAVELLE stade I, GLOSTER, METEOR, FOUGA MAGISTER) au point fixe et en vol.

Dans ce travail, les données expérimentales déjà exploitées dans [1, 2] sont complétées par des résultats plus récents.

La comparaison entre les niveaux sonores mesurés et calculés demanderait en toute rigueur l'introduction d'une correction pour tenir compte de l'effet de sol, qui est calculable dans le cas d'un plan parfaitement réfléchissant [7]. Cette hypothèse de réflexion ne peut être retenue dans le cas de nos expériences, c'est pourquoi aucune correction n'a été apportée aux niveaux mesurés globaux ou par octave.

Les vérifications expérimentales de l'équation (27) ont été faites pour les jets stationnaires ($M_V = 0$) et en vol à différents angles θ mesurés à partir de l'angle θ_M , de 20 en 20 degrés, soit θ_M , $\theta_M + 20°$, ----, $\theta_M + 100°$ et $\theta_M - 20°$

Dans les deux cas, les niveaux sonores globaux polaires sont ramenés à $R_0 = 30\ m$ en faisant intervenir les atténuations géométrique et moléculaire, les corrections adoptées étant celles de SAE [8], puis normalisées par le terme $10 \log_{10} \rho_j^2 S$ et enfin, dans le cas des jets groupés, corrigés par le terme 5 log(jet stationnaire) ou $10 \log_{10} n$ (jet en vol), n étant le nombre des turboréacteurs équipant l'avion.

Notons que les niveaux sonores des avions en vol ont été déterminés à partir des courbes de variation des niveaux sonores linéaires enregistrés en un point fixe et de la distance des avions à ce point au moment d'émission sonore. De plus, ces niveaux sonores ont été corrigés par la formule (28) qui représente l'effet de la vitesse d'entraînement du jet mobile, en vue de comparer les résultats obtenus avec les résultats relatifs aux jets stationnaires.

3.4.1.- JETS STATIONNAIRES - La comparaison entre les résultats des mesures et des calculs est mise en évidence, pour chacun des angles θ adoptés, sur les figures 3 à 9. Sur ces figures, les niveaux sonores globaux polaires des jets stationnaires sont repérés par des × et chacune des courbes a été calculée par l'équation (27) pour $M_V = 0$ aux valeurs de θ spécifiées plus haut.

Notons que suivant la direction $\theta_M - 20°$, l'angle θ du facteur de convection a été remplacé par l'angle θ' déterminé par la formule (5).

Nous constatons que pour toutes les directions considérées, l'accord entre l'expérience et la théorie est satisfaisant.

3.4.2.- JETS MOBILES - La comparaison entre les niveaux sonores globaux normalisés des jets en vol exprimés par $N_\theta + \Delta N_{\theta_V} - 10 \log_{10} \rho_j^2 S$, et les courbes théoriques données par l'équation (27) pour $M_V = 0$ est visible sur les figures 3 à 9 (repérés par des points).

Cette comparaison a montré que la correction due à la vitesse d'entraînement du jet donnée par la formule (28) est bien vérifiée uniquement aux angles θ compris entre $\theta_M - 20°$ et $\theta_M + 40°$ (figure 3, 4, 5 et 9), soit pour $\theta < \pi/2$.

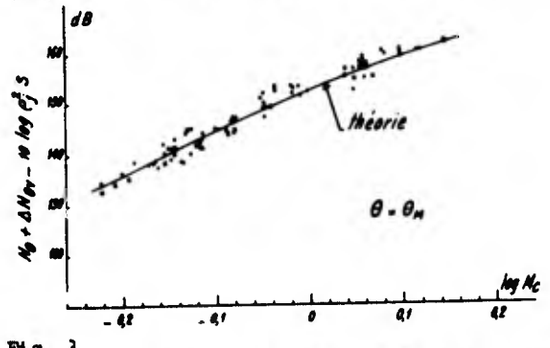

Fig. 3
Niveaux de pression sonore globale polaire des avions au point fixe (repérés par des ×), et en vol, repérés par des •) dans la direction pour R_0 = 30 m. Courbe théorique pour $\theta = \theta_M$

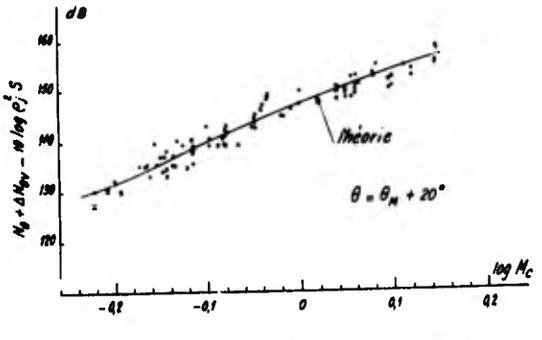

Fig. 4
Niveaux de pression sonore globale polaire polaire des avions dans la direction $\theta = \theta_M + 20°$ mesurés et calculés.

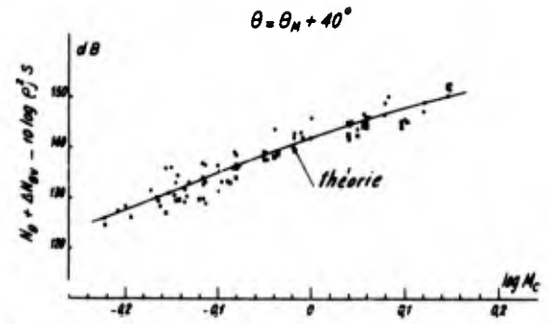

Fig. 5
Niveaux de pression sonore globale polaire des avions dans la direction $\theta = \theta_M + 40°$ mesurés et calculés

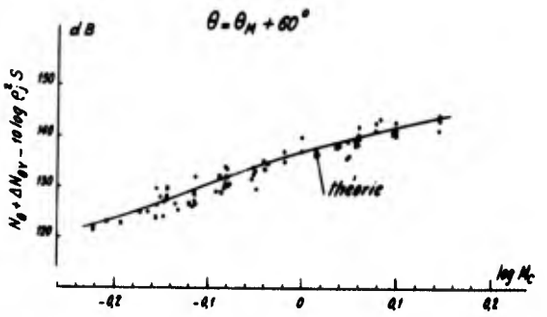

Fig. 6
Niveaux de pression sonore globale polaire des avions dans la direction $\theta = \theta_M + 100°$ mesurés et calculés.

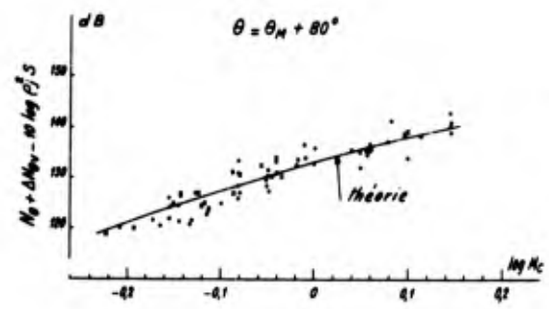

Fig. 7
Niveaux de pression sonore globale polaire des avions dans la direction $\theta = \theta_M + 60°$ mesurés et calculés.

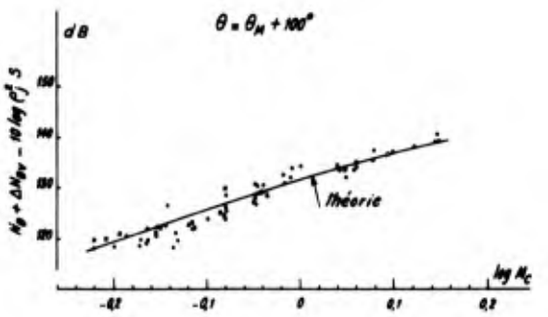

Fig. 8
Niveaux de pression sonore globale polaire dans la direction $\theta = \theta_M - 20°$ mesurés et calculés.

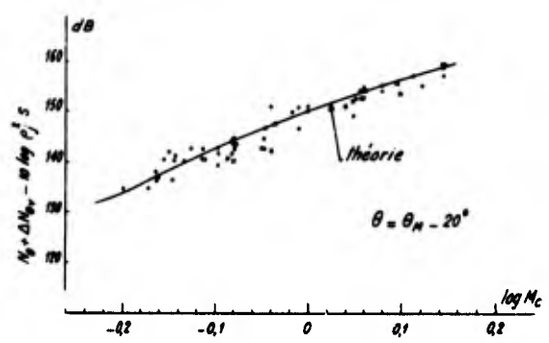

Fig. 9
Niveaux de pression sonore globale polaire des avions dans la direction $\theta = \theta_M + 80°$ mesurés et calculés.

Par contre, pour l'intervalle angulaire défini par $\pi/2 < \theta < \pi$, (figures 6 à 8), et pour $M_c > 0,9$ environ, l'accord entre les niveaux sonores globaux normalisés des jets en vol et l'équation (27) pour $M_v = 0$ est meilleur en exprimant la réduction des niveaux sonores due au nombre de Mach de vol M_v, ΔN_{θ_v}, par :

$$\Delta N_{\theta_v} = 10 \log_{10} \frac{\left\{\left[1 - M_c\left(1 - \frac{M_v}{2M_c}\right)\cos\theta\right]^2 + \alpha_s^2 M_c^2 \left(1 + \frac{M_v}{2M_c}\right)^2\right\}^{\gamma} (1+\cos^4\theta)^{\frac{\gamma}{2}(K-\frac{2}{\gamma})}}{\left[(1 - M_c\cos\theta)^2 + \alpha_c^2 M_c^2\right]^{\frac{\gamma}{2}} \left(1 - \frac{M_v}{2M_c}\right)^4} \qquad (30)$$

où l'exposant γ, primitivement égal à $5/2$, est une fonction de M_v de θ et probablement aussi du rapport de pressions (EPR) et où $\delta(i-j)$ est le symbole de Kronecker ($\delta = 1$ pour $i = j$, $\delta = 0$ dans les autres cas).

Une étude est en cours en vue de préciser la relation entre γ, M_v et θ . Provisoirement, nous avons adopté pour les angles $\theta \geq (\theta_M + 60°)$ la valeur de γ donnée par l'expression de la forme

$$\gamma = \frac{3}{2} - \frac{2}{\pi} \operatorname{arc\,tg} (10 M_v - 3) \tag{31}$$

Puisque la valeur de l'exposant du facteur de convection est caractéristique de la nature de la source aérodynamique, il semble que pour les jets en vol et aux angles θ supérieurs à 90° environ, les sources sonores prépondérantes ont des caractéristiques directionnelles non de quadruplets, mais de sources d'ordre 1 et 0. Cela semble confirmé par la courbe de variation du niveau sonore linéaire (fig. 2) qui, aux angles considérés, montre un premier maximum qui serait dû aux sources d'ordre 0 et 1, puis le second maximum classique attribué aux sources quadripolaires.

3.5.- FORME FINALE DE L'EXPRESSION DES NIVEAUX DE PRESSION SONORE GLOBALE POLAIRE - D'après ce qui précède, l'équation donnant le niveau de pression sonore globale polaire locale produite par les jets stationnaires et en vol peut prendre la forme finale suivante

$$N_\theta = 10 \log_{10} \frac{\rho_j^2 S M_c^8 \left(1 - \frac{M_v}{2M_c}\right)^4 \left(1 + \cos^4\theta\right)^{\delta(\gamma - 5/2)}}{\left\{\left[1 - M_c \left(1 - \frac{M_v}{2M_c}\right) \cos\theta_1\right]^2 + \alpha_s^2 M_c^2 \left(1 + \frac{M_v}{2M_c}\right)^2\right\}^\gamma} + C_2 \tag{32}$$

où α_s^2 est déterminé par la formule (12) et avec $C_2 = 144$ dB à la distance de référence $R_0 = 30$ m.

L'angle θ_1 est égal à θ si $\theta_M \leq \theta < \pi$, θ_M étant déterminé par (4); pour $\theta < \theta_M$, θ_1 est donné par (5).

Pour le jet stationnaire $\gamma = \frac{5}{2}$

Pour le jet en vol et pour $M_c > 0{,}9$:

si $\theta < \frac{\pi}{2}$ $\quad \gamma = \frac{5}{2}$

$\theta = \frac{\pi}{2}$ $\quad \gamma = 2 - \frac{1}{\pi} \operatorname{arc\,tg} (10 M_v - 4)$

$\theta > \frac{\pi}{2}$, $\gamma = \frac{3}{2} - \frac{2}{\pi} \operatorname{arc\,tg} (10 M_v - 4)$

Si $M_c < 0{,}9$, $\gamma = 5/2$

Les niveaux de pression sonore globale linéaire (sur la ligne parallèle à l'axe du jet, à 30 m de celui-ci) sont donnés par l'équation (22).

4.- NIVEAUX DE PRESSION SONORE POLAIRE LOCALE PAR BANDES DE FREQUENCES

Le calcul des niveaux sonores polaires associés à la bande de fréquence i , $N_{\theta i}$, est effectuée suivant la méthode décrite dans [2] qui fait intervenir le spectre généralisé de pression sonore dans les directions considérées, ainsi que le niveau sonore global N_θ . Nous allons en rappeler les grandes lignes.

Si ψ (f) est la densité spectrale de la puissance acoustique dont la valeur globale est P , nous pouvons écrire

$$P = \int_0^\infty \psi(f)\, df$$

Adoptons la relation de similitude : $f \alpha \frac{V}{L}$ ou V est une vitesse caractéristique du jet et L une dimension caractéristique de celui-ci.

Dans le champ acoustique lointain, si $\overline{p^2}$ est la valeur quadratique moyenne de la pression

sonore locale, l'équation précédente prend la forme

$$\int_0^\infty \left[\frac{V}{L}\,\frac{\overline{p^2}(Z,\theta,f)}{\overline{p^2}\,(Z,\theta)}\right]\frac{L}{V}\,df = 1\ ,$$

où Z est la distance entre la source sonore et le point d'observation.

Les relations de similitude

- $L \propto D$, D étant le diamètre du jet dans le plan de sortie des gaz
- $V \propto V_j$
- ainsi que les équations (15) et (25), conduisent à la détermination du nombre de Strouhal du jet en vol :

$$S_n = \frac{(1+M_v\cos\theta)D}{\left(1+\frac{V_e}{V_j}\right)^2 V_j}\ f_a$$

qui pour $M_v = 0$ se réduit à sa forme classique

$$S_n = \frac{D}{V_j}\ f_{es} \tag{33}$$

Dans ces équations f_a et f_{es} indiquent la même fréquence centrale des bandes de fréquences normalisées.

De son côté, le niveau de densité spectrale adimensionnelle de pression sonore émise par les jets stationnaires ($M_v = 0$) et en vol, est :

$$K_i = N_{fi}\left[N_\theta - 10\log_{10}\frac{\left(1+\frac{V_e}{V_j}\right)^2 V_j}{(1+M_v\cos\theta)D}\right] \tag{34}$$

tenant compte de (15) et de la correction due à l'effet Doppler intervenant aussi sur l'intensité (voir § 3).

Dans cette expression N_{f_i} est le niveau sonore spectral déterminé par

$$N_{fi} = N_{\theta i} - 10\log \Delta f_i \tag{35}$$

où Δf_i est l'intervalle des fréquences associé à la bande de fréquence i .

Les niveaux sonores spectraux, provenant des différents avions au point fixe et en vol et déterminés au sol suivant différents angles θ ont été exprimés dans le système des coordonnées ayant pour abscisses (33) et pour ordonnées (34).

Cette vérification expérimentale a montré [2] que les spectres acoustiques locaux ainsi généralisés admettent bien avec une approximation satisfaisante une courbe moyenne caractéristique de la direction considérée.

Pour les angles θ variant de 20° depuis 20° jusqu'au 160° ces courbes moyennes sont représentées sur la figure 10.

Revenant au calcul des niveaux de pression sonore associés aux bandes des fréquences, $N_{\theta i}$ nous obtenons, en remplaçant dans (34) N_{f_i} par son expression donnée par (35)

$$N_{\theta i} = N_\theta - 10\log_{10}\frac{\left(1+\frac{V_e}{V_j}\right)^2 V_j}{(1+M_v\cos\theta)D} + 10\log_{10}\Delta f_i + K_i$$

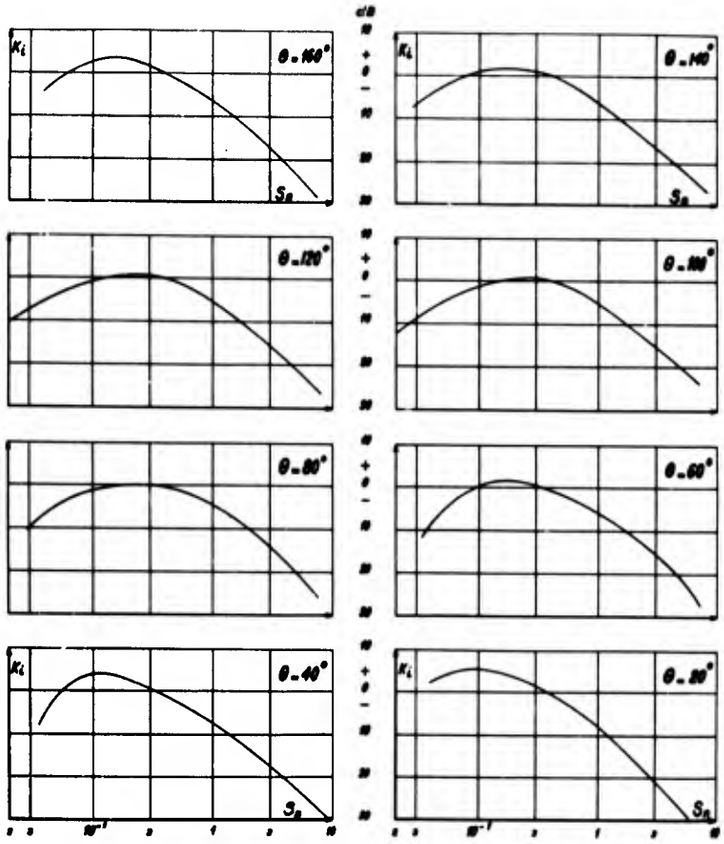

Spectre généralisé pour divers angles θ. *fig.10*

Dans cette formule N_θ est déterminé par l'équation (32) et K_i positif ou négatif est lu sur l'ordonnée de la courbe du spectre généralisé (fig. 10) afférente à l'angle θ considéré.

5.- CONCLUSION

Le calcul du champ total de pression sonore au sol produit par l'évolution des avions à réaction est effectué par une méthode qui fait intervenir les caractéristiques thermodynamiques du jet, la vitesse d'entraînement de celui-ci, V_e , ainsi que les spectres acoustiques généralisés afférents aux directions considérées.

Cette méthode, vérifiée par l'expérience pour les jets de révolution issus des turboréacteurs à flux direct, de rapports de pression subcritique et légèrement supercritique et pour les valeurs du paramètre aérodynamique V_e / V_j inférieures à 0,3, a confirmé les résultats antérieurs dans la direction du rayonnement acoustique maximal et a amélioré la prévision du bruit aux angles supérieurs à 90°.

Un des principaux résultats de cette étude analytique est la mise en évidence de l'importance du paramètre V_e / V_j , dans le calcul du champ sonore émis par les jets mobiles.

Par ailleurs, cet effet de la vitesse d'entraînement du jet se manifeste par une modification des caractéristiques directionnelles du bruit par rapport aux jets stationnaires aux angles supérieurs à 90°, qu'il semble possible d'attribuer à la prépondérance des sources aérodynamiques d'ordre 0 et 1.

Nous avons cherché à représenter cette modification, qui est une amplification notable du bruit de spectre continu vers l'avant de l'avion (non imputable au compresseur), par une expression convenable, expérimentale et provisoire, de l'exposant qui affecte le facteur de convection, en fonction du nombre de Mach de vol. Cet exposant, pour $\theta > 90°$, est en fait fonction de nombreux paramètres : rapport de pression, nombre de Mach, angle θ , etc ...

REFERENCES

[1] KOBRYNSKI M. - Sur le calcul du spectre de pression sonore maximale émis par les jets stationnaires et en vol.
Note Technique ONERA n° 108 (1967)
Sur la puissance acoustique émise par les jets coaxiaux subsoniques
C.R. Académie des Sciences, série A, p. 255 - 258 (24 janvier 1966)

[2] KOBRYNSKI M. - Méthode générale de calcul du champ de pression sonore émis par les jets stationnaires ou mobiles.
Symposium sur le bruit d'origine aérodynamique, Toronto, 20-21 mai 1968.
Sur une généralisation de la représentation de la densité spectrale de l'énergie acoustique émise par les jets de révolution..
C.R. Académie des Sciences, série B p. 370 - 373 (12 février 1968)

[3] LIGHTHILL M.J. - On sound generated aerodynamically - I General theory
Proc. Roy. Soc. A 211 (1952)

[4] FFOWCS WILLIAMS J.E. Some Thoughts on the Effects of Aircraft Motion and Eddy Convection on the Noise from Air Jets
Univ. of Southampton Dept. of Aero/Astre, U.S.A. rep. 155 (1960)

[5] FFOWCS WILLIAMS J.E - The noise from turbulence convected at high speed. Phil. Trans. Roy. Soc. London - série A, 255 (1963)

[6] RIBNER H.S. - The generation of Sound by turbulent jets
Advances in App. mec. vol. 8 (1964)

[7] HOWES L.M. - Ground reflexion of jet noise NASA T.R. R-35 (1959)

[8] - - Jet noise prediction S.A.E. Air 876

ETUDE DES INTERFERENCES ACOUSTIQUES PAR REFLEXION. APPLICATION AUX SPECTRES DE PRESSION ACOUSTIQUE DES JETS.

par

P. THOMAS

SNECMA

(Paris - France)

SOMMAIRE

Les mesures de champs sonores de turboréacteurs se font habituellement en présence d'un sol et les spectres de pression acoustique mesurés sont alors perturbés par des phénomènes de réflexion complexes qui rendent leur exploitation difficile.

La SNECMA ayant réalisé une installation d'essais pour mesures du bruit des turboréacteurs (conforme à une recommandation de l'Organisation Internationale de Normalisation qui préconise que les mesures se fassent au-dessus d'une aire bétonnée), une étude théorique et expérimentale des problèmes de réflexion a été entreprise.

Les résultats présentés concernent principalement l'influence des réflexions sur les spectres de pression acoustique des jets.

Les expressions des indices de réflexion qui résultent de la présence d'un plan réfléchissant ou partiellement absorbant sont présentées.

Toutefois, l'hypothèse de source ponctuelle qui peut, sous certaines conditions, être retenue pour des mesures dans le champ acoustique lointain, ne l'est plus lorsque le jet est à faible distance du sol. Pour ces cas particuliers, une théorie des réflexions qui fait intervenir une distribution de sources élémentaires indépendantes est développée. Une étude expérimentale en chambre sourde, sur des jets de maquettes et principalement avec des réflecteurs parfaits, a permis de confirmer les relations théoriques établies.

SYMBOLES UTILISES

p, p' = pression acoustique

ω = pulsation

f = fréquence

f_i = fréquence centrale d'une bande d'analyse $f_i = \sqrt{f_a . f_b}$

f_a, f_b = fréquences de coupures d'une bande de largeur $\Delta f = f_b - f_a$

λ = longueur d'onde

λ_i = longueur d'onde de la fréquence centrale

C = célérité du son

$\overline{(\ )}$ = valeur moyenne

$\overline{(\ )}^2$ = valeur quadratique moyenne

τ = retard

t = temps

N = niveau de pression sonore en dB

R = rapport entre la valeur quadratique moyenne du signal résultant et celle du signal direct

$\Delta N = 10 \log_{10} (R)$: indice de réflexion (différence entre le niveau mesuré en présence du plan et le niveau mesuré en champ libre)

h = hauteur de la source au-dessus du plan réflecteur

h' = hauteur du récepteur au-dessus du plan réflecteur

r = distance source-récepteur

r' = longueur du trajet suivi par le signal réfléchi

r_1 = projection du rayon direct sur le plan réfléchissant

Z = paramètre géométrique ($Z = r'/r$)

Δr = différence de marche géométrique du signal direct et du signal réfléchi

α = paramètre définissant le mode d'analyse spectrale $= \pi \Delta f / f_i$

β = paramètre définissant le mode d'analyse spectrale $= 2\pi \sqrt{1 + (\Delta f / 2 f_i)^2}$

Q = coefficient de réflexion complexe

$|Q|$ = module du coefficient de réflexion

δ = argument du coefficient de réflexion

C_τ = coefficient d'autocorrélation de p (t)

$W(f)$ = densité spectrale

W_0 = valeur de la densité spectrale d'un bruit blanc

D = diamètre de la section d'éjection

U_j = vitesse d'éjection du jet

L = distance axiale d'une source sonore par rapport au plan d'éjection

θ = angle formé par la direction d'émission sonore et l'axe du jet

U = vitesse instantanée dans la zone de mélange

PAR SUITE DE LA COMPLEXITE DES LOIS qui régissent l'émission acoustique des jets, seuls de nombreux résultats expérimentaux permettent de justifier les hypothèses introduites dans les études théoriques. Mais cette justification expérimentale ne peut se faire de manière valable que si l'on a su mesurer les caractéristiques acoustiques de ces jets dans des conditions idéales parmi lesquelles celles de champ libre sont de loin les plus importantes.

Or s'il est relativement aisé de se placer dans de telles conditions au cours d'études expérimentales sur maquettes (mesures en chambre sourde ou en plein air à une hauteur suffisante au-dessus du sol), il est pratiquement impossible d'éviter la proximité du sol lors de mesures acoustiques faites autour de turboréacteurs. Qu'il s'agisse de mesures autour de moteurs au point fixe ou d'avions en vol, il est rarement possible de trouver une aire d'essais à caractéristiques uniformes et bien connues. Dans la majorité des cas, les mesures se font en bordure d'une piste d'aérodrome, au-dessus d'un sol herbeux ou d'un terrain mixte (mi-herbeux, mi-bétonné).

Les spectres de pression acoustique mesurés dans ces conditions subissent alors des perturbations produites par des phénomènes de réflexion complexes qui sont influencés par la nature du sol et la disposition relative de la source et du récepteur. Une illustration des allures obtenues est fournie par les figures 1 et 2. Sur la figure 1 sont représentés les spectres d'un turboréacteur ATAR mesurés à hauteur constante au-dessus d'un sol herbeux et à trois distances différentes du moteur, dans la direction d'émission sonore maximale du jet. Par leurs allures caractéristiques, les spectres, représentés à la figure 2 et correspondant à des mesures effectuées au cours d'un survol d'avion, montrent que de telles mesures n'échappent pas aux perturbations produites par les réflexions au sol.

Ces exemples montrent la nécessité d'une méthode de correction permettant de tenir compte des phénomènes d'interférences résultant des réflexions par une surface réfléchissante ou partiellement absorbante. Après un rappel des relations qui traduisent les facteurs de correction à appliquer aux analyses spectrales du bruit d'une source ponctuelle, nous examinerons dans ce document les possibilités d'application des expressions obtenues aux mesures du bruit des jets des turboréacteurs.

Toutefois, la SNECMA ayant réalisé à Istres, une installation d'essais qui permet d'effectuer des mesures acoustiques autour de turboréacteurs conformément à la recommandation de l'I.S.O. (c'est-à-dire en présence d'une aire bétonnée), l'étude théorique et expérimentale a été plus particulièrement orientée vers de telles conditions de mesures. Des exemples de corrections appliquées à des spectres de pression acoustique enregistrés sur cette installation montrent qu'il est possible de restituer de façon satisfaisante les allures des spectres de champ libre.

RAPPEL DES RELATIONS APPLICABLES AUX CAS D'EMISSION DE BRUIT PAR UNE SOURCE PONCTUELLE

HYPOTHESES - Les approches théoriques du problème d'interférences acoustiques par réflexion sur un plan analysées par différents auteurs (références (1), (2), (3)), ne seront pas développées dans ce chapitre. Nous rappellerons toutefois les hypothèses nécessaires à l'établissement des relations fondamentales qui seront citées ci-dessous.

La source sonore, ponctuelle, est supposée émettre un bruit aléatoire stationnaire qui satisfait l'hypothèse ergodique.

Le récepteur est considéré dans le champ lointain de la source, c'est-à-dire à une distance grande comparée aux longueurs d'ondes du bruit émis. Les spectres conservent alors leur forme au cours de la propagation car chacune des composantes obéit à la loi de l'inverse du carré de la distance à la source (à condition toutefois de négliger les phénomènes d'absorption atmosphérique particulièrement sensibles aux fréquences élevées).

L'atmosphère dans laquelle se propagent les ondes sonores est supposée isotherme, immobile et homogène.

Les irrégularités de surface du plan réflecteur étant supposées petites devant les longueurs d'ondes, la réflexion peut être considérée comme spéculaire, ce qui conduit à adopter le concept d'une source image symétrique de la source réelle par rapport au plan réflecteur.

La schématisation du problème est illustrée par la figure 3.

RELATIONS FONDAMENTALES DANS LE CAS D'UN REFLECTEUR PARFAIT - Si le plan est parfaitement réfléchissant, le rapport de la pression quadratique moyenne résultante à la pression quadratique moyenne qui aurait été mesurée en champ libre est donné par :

$$R = 1 + \frac{1}{Z^2} + \frac{2}{Z} C_\tau \qquad (1)$$

Dans cette relation, Z est un paramètre géométrique exprimant le rapport des trajets des rayons direct et réfléchi ($Z = r'/r$)

C_τ est la fonction d'autocorrélation normée ou coefficient d'autocorrélation, lié à la densité spectrale $W(f)$ de la pression acoustique $p(t)$ par la relation :

$$C_\tau = \frac{\int_0^\infty W(f) \cos. 2\pi\tau f \, df}{\int_0^\infty W(f) df} \qquad (2)$$

Cette équation montre que pour un bruit à densité spectrale de puissance donnée, le coefficient d'autocorrélation est défini par une relation dans laquelle apparaissent les limites d'intégration, c'est-à-dire les fréquences limites du domaine de fréquences considéré et le retard τ résultant de la différence de marche $\left(\tau = \frac{\Delta r}{C} = \frac{r' - r}{C}\right)$

Si f_a et f_b sont les fréquences de coupure des bandes du mode d'analyse spectrale choisi et si on suppose que les filtres utilisés sont idéaux, l'expression de C_τ devient :

$$C_\tau = \frac{\int_{f_a}^{f_b} W(f) \cos. 2\pi\tau f \, df}{\int_{f_a}^{f_b} W(f) df} \qquad (3)$$

Dans le cas particulier d'une émission de bruit blanc, on aboutit alors aux expressions suivantes du rapport des pressions quadratiques moyennes :

- bruit blanc, analyse à largeur de bande Δf constante :

$$R = 1 + \frac{1}{Z^2} + \frac{2}{Z} \cdot \frac{\sin.\left(\pi \frac{\Delta r}{C} \Delta f\right)}{\pi \frac{\Delta r}{C} \Delta f} \cos.\left(2\pi \frac{\Delta r}{\lambda_i}\right) \qquad (4)$$

(λ_i : longueur d'onde de la fréquence centrale f_i - $\Delta f = f_b - f_a$).

- bruit blanc - analyse à pourcentage de bande constant :

$$R = 1 + \frac{1}{Z^2} + \frac{2}{Z} \cdot \frac{\sin.\left(\alpha \frac{\Delta r}{\lambda_i}\right)}{\alpha \frac{\Delta r}{\lambda_i}} \cos.\left(\beta \frac{\Delta r}{\lambda_i}\right) \qquad (5)$$

En posant : $\alpha = 2\pi \frac{\Delta f}{2 f_i}$

$\beta = 2\pi \sqrt{1 + \left(\frac{\Delta f}{2 f_i}\right)^2}$

} paramètres déterminant le mode d'analyse choisi.

Le mode d'analyse étant choisi, nous pouvons représenter cette fonction (équation (5)) en fonction de $\Delta r/\lambda_i$ pour différentes valeurs du paramètre géométrique Z.

En fait nous représenterons toujours l'indice de réflexion $\Delta N = 10 \log(R)$

La figure 4 illustre l'évolution de ΔN en fonction de $\Delta r/\lambda_i$ dans le cas d'une analyse par 1/3 d'octaves et par octaves, le paramètre géométrique Z étant supposé voisin de 1. Cette valeur correspond pratiquement à la majorité des cas de mesures dans le champ acoustique lointain.

RELATIONS FONDAMENTALES DANS LE CAS D'UNE SURFACE PARTIELLEMENT ABSORBANTE - Nous supposerons que le plan partiellement absorbant est caractérisé, pour une incidence donnée, par un coefficient de réflexion, fonction de la fréquence :

$$Q(f) = |Q_f| e^{j\delta_f} \qquad (6)$$

Le spectre de puissance de la pression résultante en présence du plan peut s'exprimer par :

$$W(f)\left|1+\frac{Q(f)}{Z}e^{-2j\pi\tau f}\right|^2 \qquad (7)$$

L'expression de la pression quadratique moyenne résultante dans une bande de largeur f_a, f_b s'écrira alors :

$$\overline{P^2}=\int_{f_a}^{f_b} W(f)\left|1+\frac{Q(f)}{Z}e^{-2j\pi\tau f}\right|^2 df$$

D'où le rapport des pressions quadratiques moyennes :

$$R=\frac{\int_{f_a}^{f_b} W(f)\left|1+\frac{Q(f)}{Z}e^{-2j\pi\tau f}\right|^2 df}{\int_{f_a}^{f_b} W(f)\,df} \qquad (8)$$

Dans le cas d'une émission de bruit blanc, nous aurons la relation :

$$R=\frac{\int_{f_a}^{f_b}\left[1+2\frac{|Q(f)|}{Z}\cos.(2\pi\tau f-\delta_f)+\left(\frac{|Q(f)|}{Z}\right)^2\right]df}{f_b-f_a} \qquad (9)$$

Nous pouvons remarquer qu'en supposant $|Q(f)|$ et δ_f constants dans la bande d'analyse (f_a,f_b), la valeur considérée pouvant être celle correspondant à la fréquence centrale f_1, nous obtenons l'expression suivante du rapport des pressions quadratiques moyennes :

$$R=1+\left(\frac{|Q_i|}{Z}\right)^2+2\frac{|Q_i|}{Z}\cdot\frac{\int_{f_a}^{f_b}\cos.(2\pi\tau f-\delta_i)\,df}{f_b-f_a} \qquad (10)$$

En fonction du type d'analyse choisi, cette expression pourra prendre les formes suivantes :

- bruit blanc, analyse à largeur de bande constante :

$$R=1+\left(\frac{|Q_i|}{Z}\right)^2+2\frac{|Q_i|}{Z}\cdot\frac{\sin.\left(\pi\frac{\Delta r}{C}\Delta f\right)}{\pi\frac{\Delta r}{C}\Delta f}\cos.\left(2\pi\frac{\Delta r}{\lambda_i}-\delta_i\right) \qquad (11)$$

- bruit blanc, analyse à pourcentage de bande constant :

$$R=1+\left(\frac{|Q_i|}{Z}\right)^2+2\frac{|Q_i|}{Z}\cdot\frac{\sin.\left(\alpha\frac{\Delta r}{\lambda_i}\right)}{\alpha\frac{\Delta r}{\lambda_i}}\cos.\left(\beta\frac{\Delta r}{\lambda_i}-\delta_i\right) \qquad (12)$$

La figure 5 représente les indices de réflexion calculés à l'aide de l'éq. (12) dans le cas d'une analyse par octaves et par 1/3 d'octaves. Les courbes tracées correspondent aux conditions suivantes : $|Q_i|/Z=0{,}5$; $\delta_i=-\pi/2$

APPLICATION THEORIQUE AU BRUIT DES JETS

Les relations que nous venons de rappeler ont nécessité certaines hypothèses qui ont été énoncées au début du chapitre précédent. La condition supplémentaire d'émission de bruit blanc a, dans chacun des cas examinés, permis d'obtenir des expressions relativement simples. Nous examinerons, dans ce chapitre, les possibilités d'application des relations obtenues à la source sonore que constitue un jet. Dans ce but, nous ferons un bref rappel des caractéristiques de l'émission acoustique des jets, qui sont susceptibles de modifier les hypothèses admises :

- distribution des sources sonores dans le jet

- allures des densités spectrales de pression acoustique dans le champ lointain.

EXAMEN DE CES CARACTERISTIQUES - Si nous nous reportons au schéma classique d'un jet gazeux s'échappant d'un orifice dans l'atmosphère au repos (figure 6), nous distinguons trois zones principales

zone A : cône isovitesses

zone B : zone de mélange périphérique à forte turbulence produite par l'entraînement de l'air ambiant

zone C : zone située en aval du cône isovitesses où le mélange est pleinement établi.

Depuis les travaux de Powell (4) basés sur la théorie de Lighthill, on admet généralement que les zones B et C (zones émissives de bruit) peuvent être découpées en tranches perpendiculaires à l'axe du jet et que chacune de ces tranches émet une fréquence bien déterminée. Des mesures de spectres le long de jets ont permis de justifier cette schématisation. Le graphique A de la figure 6 présente ainsi quelques valeurs mesurées de la position axiale des sources sonores en fonction du nombre de Strouhal($S = fD/U_j$) qui sont valables pour des jets subcritiques ou légèrement supercritiques. Des études expérimentales de localisation effectuées plus récemment ont montré que, dans le cas de jets à nombre de Mach élevé, les distances axiales pouvaient atteindre des valeurs nettement plus grandes que celles présentées sur ce graphique.

Les densités spectrales de la pression acoustique dans le champ lointain d'un jet sont fonction de l'azimuth du point de mesure par rapport à l'axe de ce jet. Les allures moyennes mesurées à deux azimuths dont l'un correspond à l'émission sonore maximale sont représentées en fonction du nombre de Strouhal sur le graphique B de la figure 6. On peut remarquer que les pentes de ces densités spectrales varient avec l'azimuth et que les valeurs maximales (+ 2 pour les basses fréquences, -3 pour les hautes fréquences) correspondent à l'angle θ_{max}. Nous résumerons ces quelques rappels, suffisants pour l'étude que nous nous sommes fixée, en disant que l'on peut assimiler la zone émissive d'un jet à une succession de couronnes juxtaposées ayant pour diamètre moyen le diamètre de la tuyère et une longueur totale de plusieurs diamètres. Ces couronnes émettent chacune sur une fréquence déterminée par les dimensions et les caractéristiques du jet et, dans le champ sonore lointain, la densité spectrale de pression acoustique possède une pente variant de + 2 pour les basses fréquences à -3 pour les hautes fréquences. A partir de cette schématisation, nous avons examiné le problème particulier des interférences du bruit d'un jet lorsque la mesure est effectuée au-dessus d'un plan réflecteur.

INFLUENCE DE LA FORME DES COURBES DE DENSITE SPECTRALE SUR L'INDICE DE REFLEXION - Les expressions du coefficient d'autocorrélation rappelées au chapitre précédent (Eq. (2) et Eq. (3)) montrent que la densité spectrale $W(f)$ intervient dans le calcul de l'indice de réflexion.

Les densités spectrales du bruit d'un jet ayant une évolution continue, nous avons examiné les deux points suivants dans l'hypothèse provisoire que le jet est assimilable à une source ponctuelle :

- influence de la forme de la densité spectrale sur l'indice de réflexion en niveau global

- influence de la pente de la densité spectrale sur l'évolution du coefficient d'autocorrélation pour les 2 types d'analyse courants : 1/3 d'octaves et octaves.

Sur la figure 7 sont représentées à nouveau les densités spectrales de la figure 6 correspondant aux azimuths θ_{max} et $\theta_{max} + 60°$ et une approximation de ces densités supposées pouvoir s'exprimer par une relation de la forme :

$$\frac{\left(\frac{fD}{U_j}\right)}{\left(\frac{fD}{U_j}\right)_{max}} \cdot e^{1 - \frac{\frac{fD}{U_j}}{\left(\frac{fD}{U_j}\right)_{max}}} \qquad (13)$$

Pour un réflecteur supposé parfait, l'indice de réflexion en niveau global peut alors s'écrire :

$$\Delta Ng = 10 \log \left[1 + \frac{1}{Z^2} + \frac{2}{Z} \cdot \frac{1 - \left(2\pi \frac{\Delta r}{\lambda_{max.}}\right)^2}{\left[1 + \left(2\pi \frac{\Delta r}{\lambda_{max.}}\right)^2\right]^2} \right] \qquad (14)$$

λ_{max} : longueur d'onde correspondant à la valeur maximale de la densité spectrale. Nous avons donc représenté sur la même figure l'évolution de ΔN_g en fonction de $\Delta r/\lambda_{max}$ pour la valeur Z $\neq$ 1 valable dans la majorité des cas pratiques. Sur le même graphique, nous avons tracé la droite horizontale à + 3 dB qui est applicable, dans les mêmes conditions de mesure, à une source émettant du bruit blanc. Ces courbes sont pratiquement confondues dès que $\Delta r/\lambda_{max.}$ est supérieur à 0,1.

L'influence de la pente de la densité spectrale sur le coefficient d'autocorrélation dans une bande d'analyse par 1/3 d'octaves ou par octaves est illustrée par la figure 8. Ces graphiques mettent en évidence qu'une pente variant de + 2 à -2 n'intervient pas dans le cas d'une analyse par 1/3 d'octaves et qu'elle peut être négligée dans une analyse par octaves. En fait, cette propriété reste encore valable avec une bonne approximation lorsque la pente est égale à $\pm$ 3.

Ces propriétés nous permettent donc d'appliquer l'hypothèse d'un bruit blanc dans les estimations des phénomènes d'interférences par réflexion du bruit de jets.

INFLUENCE DES DIMENSIONS DE LA SOURCE SONORE QUE CONSTITUE UN JET - Nous examinerons maintenant l'influence des dimensions finies de la source sonore que constitue un jet. Cet examen permettra ainsi de définir dans quelles limites l'hypothèse simplificatrice d'une source ponctuelle centrée dans le plan d'éjection est acceptable, compte tenu de la distribution des sources sonores rappelée précédemment. Si nous considérons une source élémentaire située dans la zone de mélange, le calcul de la différence de marche, effectué en ramenant fictivement cette source au centre de la tuyère, est entaché d'une erreur. Nous avons donc essayé d'estimer cette erreur en considérant :

- l'influence de la distribution axiale des sources élémentaires en supposant celles-ci placées sur l'axe du jet.

- l'influence de la répartition périphérique de ces sources élémentaires.

Dans le premier cas, un calcul simple montre que l'écart relatif sur la différence de marche qui peut résulter de l'hypothèse citée ci-dessus s'écrit :

$$\frac{\delta(\Delta r)}{\Delta r} \approx \left(1 - \frac{1}{Z}\right) \frac{L}{r} \left(\frac{L}{2r} - \cos\theta\right) \qquad (15)$$

L = distance d'une source élémentaire au plan d'éjection (voir schéma de la figure 6). Nous pouvons en conclure que dans toutes les mesures de bruit effectuées dans le champ lointain d'un jet et pour lesquelles Z $\neq$ 1, il est possible de négliger, dans le calcul des phénomènes de réflexion, la distribution axiale des sources et considérer que l'émission acoustique s'effectue dans le plan d'éjection.

Puisque l'émission acoustique est surtout très intense dans la zone de mélange entourant le cône isovitesse et compte tenu du résultat précédent, nous pouvons donc admettre que le jet est assimilable à une distribution annulaire de sources au niveau des lèvres de la tuyère. Lorsque nous supposons l'émission acoustique concentrée au centre de la tuyère, nous déplaçons fictivement les sources sonores élémentaires d'une quantité D/2. Or un déplacement parallèle au plan réflecteur étant assimilable à un déplacement axial sera par conséquent négligeable. Les sources sonores peuvent alors être supposées distribuées suivant le diamètre vertical de la tuyère et cette nouvelle disposition nous amène à examiner l'écart relatif sur la différence de marche résultant de l'écart relatif sur la hauteur d'une source élémentaire. Le passage aux différences finies d'un simple calcul d'erreur nous conduit à la relation :

$$\frac{\delta(\Delta r)}{\Delta r} = \frac{1}{2}\left(\frac{Z+1}{Z}\right)\frac{\delta h}{h} \qquad (16)$$

Cette relation montre que, contrairement au cas où nous avions une répartition axiale, l'écart relatif sur la hauteur entraînera dans la majorité des cas de mesures (Z voisin de 1) un écart relatif identique sur la différence de marche.

Etant donné que cet écart relatif sur la hauteur peut devenir important lorsque les mesures de bruit de jet sont effectuées autour de turboréacteurs au point fixe,

nous avons essayé d'envisager une théorie des phénomènes d'interférences tenant compte d'une répartition de sources dans le plan de la tuyère.

INTERFERENCES ACOUSTIQUES DANS LE CAS DE "n" SOURCES INDEPENDANTES - Cette nouvelle approche du problème d'interférences du bruit d'un jet nous amène à supposer que les sources sont indépendantes. Or la relation étroite qui existe entre l'émission acoustique et la turbulence nous permet de considérer que si l'espacement entre deux sources consécutives est supérieur à la longueur maximale de corrélation périphérique, cette hypothèse est satisfaite. Les longueurs de corrélation périphérique étant très faibles comparées aux longueurs de corrélation longitudinale, la valeur maximale de cette dernière constituera une limite inférieure extrême d'espacement entre sources. Or les résultats de mesures de corrélation effectuées par différents auteurs ont montré que :

$$\omega \mathcal{L} \approx 1{,}7 \sqrt{\overline{U'^2}}$$

ω = pulsation type émise par un volume turbulent cohérent

$\mathcal{L}$ = longueur de corrélation

U' = fluctuation de vitesse

L'expérience montre d'autre part que $\sqrt{\overline{U'^2}}_{max} \neq 0{,}15\, U_j$ et on peut donc en déduire que la valeur maximale de $\mathcal{L}$ est donnée par :

$$\mathcal{L}_{max} \approx 0{,}04 \frac{U_j}{f}$$

ou, en introduisant le nombre de Strouhal $S = \frac{f.D}{U_j}$:

$$\mathcal{L}_{max} \approx 0{,}04 \frac{D}{S}$$

Les espacements entre sources que nous considèrerons dans ce paragraphe satisferont cette condition d'indépendance.

Soit donc une source sonore constituée par n sources élémentaires indépendantes. Dans ce cas, posons que $p_k(t)$ sont les fonctions représentant les signaux envoyés directement par ces sources élémentaires suivant le trajet r_k et $p'(t-\tau_\ell)$ ceux suivant r'_ℓ :

$r_k(r_\ell)$ = trajet de l'onde directe issue de la source $S_k(s_\ell)$

$r'_k(r'_\ell)$ = trajet de l'onde réfléchie issue de la source $S_k(s_\ell)$

En supposant que :

$$p(t) = \sum_{k=1}^{k=n} p_k(t) \qquad (17)$$

on peut écrire la pression quadratique moyenne en champ libre :

$$\overline{[p(t)]^2} = \sum_{k=1}^{k=n} \overline{[p_k(t)]^2} \qquad (18)$$

Car tous les termes croisés sont nuls par suite de l'hypothèse d'indépendance des sources.

Si nous sommes en présence d'un plan réflecteur parfait, nous écrirons que la pression résultante en un point de réception sera :

$$P(t,\tau_\ell) = \sum_{k=1}^{k=n} p_k(t) + \sum_{\ell=1}^{\ell=n} \frac{1}{Z_\ell} p_\ell(t-\tau_\ell) \qquad (19)$$

avec $Z_\ell = \frac{r'_\ell}{r_\ell}$ et en posant $p'(t-\tau_\ell) = \frac{1}{Z_\ell} p_\ell(t-\tau_\ell)$

En fait les variations de hauteur ou de distance résultant de la répartition des sources n'entraînent que de faibles variations de Z. Dans l'Eq. (19), nous pouvons par conséquent considérer la valeur moyenne de Z et écrire :

$$P(t,\tau_\ell) = \sum_{k=1}^{k=n} p_k(t) + \frac{1}{Z} \sum_{\ell=1}^{\ell=n} p_\ell(t-\tau_\ell) \tag{20}$$

La pression quadratique moyenne s'écrira :

$$\overline{[P(t,\tau_\ell)]^2} = \overline{[p(t)]^2} + \frac{1}{Z^2}\overline{\left[\sum_{\ell=1}^{\ell=n} p_\ell(t-\tau)\right]^2} + \frac{2}{Z}\overline{\sum_k \sum_\ell p_k(t).p_\ell(t-\tau_\ell)} \tag{21}$$

Si nous admettons toujours l'hypothèse d'indépendance et de stationnarité du bruit émis, nous aurons :

$$\overline{\left[\sum_\ell p_\ell(t-\tau_\ell)\right]^2} = \sum_\ell \overline{[p_\ell(t-\tau_\ell)]^2} = \overline{[p(t)]^2} \tag{22}$$

Dans la double sommation, tous les termes pour lesquels $k \neq \ell$ sont nuls (hypothèse d'indépendance) et on peut écrire que :

$$\sum_K \sum_\ell \overline{p_k(t).p_\ell(t-\tau_\ell)} = \sum_K \overline{p_k(t).p_k(t-\tau_k)} \tag{23}$$

Le rapport de la pression quadratique moyenne mesurée en présence du plan (Eq.(21)) à la pression quadratique moyenne mesurée en champ libre $\overline{[p(t)]^2}$ s'écrit par conséquent :

$$R = 1 + \frac{1}{Z^2} + \frac{2}{Z} \cdot \frac{\sum_{k=1}^{k=n} \overline{p_k(t).p_k(t-\tau_k)}}{\overline{[p(t)]^2}} \tag{24}$$

Mais si les sources sont supposées de forces égales : $\overline{[p(t)]^2} \approx n\overline{[p_k(t)]^2}$,

nous écrirons que :

$$\frac{\sum_{k=1}^{k=n} \overline{p_k(t).p_k(t-\tau_k)}}{\overline{[p(t)]^2}} = \frac{1}{n}\sum_{k=1}^{k=n}\left(\frac{\overline{p_k(t).p_k(t-\tau_k)}}{\overline{[p_k(t)]^2}}\right) \tag{25}$$

Cette expression fait apparaître le coefficient d'autocorrélation élémentaire :

$$C_{\tau_k} = \frac{\overline{p_k(t).p(t-\tau_k)}}{\overline{[p_k(t)]^2}}$$

L'Eq. (24) devient donc :

$$R = 1 + \frac{1}{Z^2} + \frac{2}{Z} \cdot \frac{1}{n}\sum_{k=1}^{k=n} C_{\tau_k} \tag{26}$$

En considérant le cas où le bruit émis est blanc et l'analyse à pourcentage de bande constant, nous aurons :

$$R = 1 + \frac{1}{Z^2} + \frac{2}{Z} \cdot \frac{1}{n} \sum_{k=1}^{k=n} \left[\frac{\sin\left(\alpha \cdot \frac{\Delta r_k}{\lambda_i}\right)}{\alpha \cdot \frac{\Delta r_k}{\lambda_i}} \cos\left(\beta \cdot \frac{\Delta r_k}{\lambda_i}\right) \right] \qquad (27)$$

Afin de définir l'espacement maximal acceptable entre sources prises en considération dans le calcul du coefficient d'autocorrélation moyen, nous avons calculé ce coefficient en prenant deux sources ponctuelles espacées d'une distance d et situées à une hauteur moyenne "h_m". Les résultats de ces calculs ont montré que si le rapport $d/_{hm}$ est approximativement égal à 0,1, nous avons un écart relatif sur le coefficient d'autocorrélation inférieur à cette valeur. On peut donc en conclure que si le rapport du diamètre de la tuyère à la hauteur du centre de celle-ci au-dessus du plan est supérieur à 10%, il est nécessaire d'envisager une répartition de sources élémentaires, le nombre minimal de celles-ci étant déterminé par la quantité $d/_{hm} \approx 0,1$. Il faut, toutefois, rappeler que l'espacement d ainsi obtenu doit satisfaire le critère d'indépendance examiné auparavant.

A titre d'illustration, nous avons représenté sur la figure 9 l'évolution de l'indice de réflexion pour une analyse par 1/3 d'octaves calculé en supposant deux rapports de diamètre de tuyère sur hauteur moyenne : $D/_h = 0,2$, $D/_h = 0,4$. Nous avons également tracé sur ce graphique la courbe valable pour une source ponctuelle.

ETUDES EXPERIMENTALES

DISPOSITIF ET METHODE EXPERIMENTALE - Le but immédiat de l'étude entreprise étant la détermination des indices de réflexion à appliquer aux spectres mesurés autour de turboréacteurs au-dessus de l'aire bétonnée du banc d'Istres, l'étude expérimentale a été principalement orientée vers la réflexion du bruit de jet sur un réflecteur parfait.

Pour mener à bien cette vérification expérimentale, il était nécessaire de mettre en oeuvre un dispositif d'essais qui permette à la fois la mesure des spectres d'un jet en champ libre et en présence d'une surface réfléchissante. Cet impératif excluait évidemment la possibilité d'une étude directe sur turboréacteur.

L'étude expérimentale a donc été menée sur un jet de maquette de tuyère convergente, dans la chambre sourde du Centre d'Essais des Propulseurs à Saclay. Aux conditions de champ libre ainsi satisfaites s'ajoutaient d'autres avantages, à savoir une stabilité temporelle des conditions d'éjection du jet, une atmosphère ambiante calme et isotherme.

L'un des montages d'essais utilisés est représenté sur la figure 10. Le plan réflecteur était constitué par des plaques métalliques en alliage léger fixées sur un cadre. Le bruit aérodynamique étudié était celui d'un jet de maquette de tuyère convergente, montée sur un poste d'essais et alimentée sous des conditions génératrices constantes. Les mesures acoustiques ont été réalisées avec une chaîne d'enregistrement classique et les spectres analysés par tiers d'octaves et par octaves dans la plage de fréquence 200 - 40.000 Hz.

Le mode opératoire comportait l'enregistrement, pour chaque géométrie expérimentale (caractérisée par les paramètres h, h', r_1 et θ), des spectres de pression acoustique du jet en champ libre et en présence du plan réfléchissant. Ces deux mesures ne pouvant être simultanées, des essais préliminaires ont permis de vérifier le caractère parfaitement stationnaire et reproductible des spectres.

QUELQUES RESULTATS EXPERIMENTAUX - Les résultats expérimentaux que nous présenterons ci-dessous sont relatifs à des analyses par bandes de tiers d'octaves. Ce type d'analyse est en effet le plus couramment utilisé dans l'étude des bruits à spectre continu car, tout en étant rapide, il fournit en général suffisamment de renseignements sur l'allure des spectres étudiés. Nous nous limiterons à la présentation de résultats relatifs à Z très voisin de 1. Cette valeur limite couvre la majorité des cas pratiques de mesures dans le champ acoustique lointain de turboréacteurs (mesures au point fixe ou mesures en vol). La figure 11 présente des résultats relatifs à des mesures de réflexions effectuées à trois azimuths différents (θ = 30°, 60°, 90°). Cette étude à différents azimuths nous a paru indispensable puisqu'elle permettait de modifier les allures des spectres de la pression acoustique considérée et de vérifier ainsi l'hypothèse de bruit blanc admise au cours de l'étude théorique. En même temps elle confirmait l'existence d'une courbe de correction unique applicable au bruit d'un jet. Les résultats montrent un accord satisfaisant entre les mesures et la courbe théorique.

Afin d'examiner si le paramètre Z est suffisant pour caractériser la géométrie de mesure, nous avons fait varier certaines grandeurs géométriques tout en maintenant la valeur de Z constante. La figure 12 représente ainsi des valeurs de ΔN mesurées à l'azimuth $\theta = 30°$ dans des configurations où $Z \neq 1$ mais où la hauteur du récepteur était variable ($h' = h/2$, $h' = h$ et $h' = 3h$). Aucun écart systématique n'a été relevé.

La vérification expérimentale de l'hypothèse d'une répartition de sources, qui est nécessaire au calcul de réflexion lorsque la source sonore a des dimensions non négligeables devant la hauteur moyenne, a fait l'objet d'une série de mesures particulières. Quelques valeurs obtenues au cours de ces mesures sont représentées sur les figures 13 et 14. Deux couples de conditions d'alimentation de la tuyère ont été étudiés ($P_j/P_a = 1,8$, $T_j = 750°K$ - $P_j/P_a = 3$, $T_j = 1050°K$).

Les résultats de la figure 13, correspondant à une configuration telle que $D/h = 0,2$, montrent une concordance assez bonne entre les valeurs mesurées et la courbe théorique calculée en considérant trois sources indépendantes placées sur l'axe vertical de la tuyère : une au centre, les deux autres étant diamétralement opposées. La figure 14 représente des résultats de mesures effectuées pour les deux cas de fonctionnement cités précédemment mais relatifs à une géométrie telle que $D/h = 0,4$. Tandis que les valeurs enregistrées dans le cas d'un jet subcritique correspondent assez bien à la courbe théorique calculée en considérant 5 sources indépendantes régulièrement espacées sur le diamètre vertical de la tuyère, les écarts de niveaux mesurés lorsque le jet est supercritique divergent nettement. Il semble donc que dans certaines configurations proches du plan, il y ait une influence assez marquée du rapport de détente et que les phénomènes de réflexion soient alors altérés. Ce cas particulier fait actuellement l'objet d'études complémentaires.

CONCLUSIONS

Ce document a permis de rappeler les relations fondamentales qui expriment les facteurs de correction des phénomènes de réflexion à appliquer aux mesures acoustiques, lorsque celles-ci sont effectuées en présence d'un plan réflecteur. Ces expressions nécessitent certaines hypothèses et deux de celles-ci ont été particulièrement examinées afin de définir les possibilités d'application à la source sonore que constitue un jet :

- hypothèse de bruit blanc

- hypothèse de source ponctuelle.

Etant donnée la faible influence de la pente de la densité spectrale sur le coefficient d'autocorrélation lorsque les analyses de bruit sont effectuées par tiers d'octaves ou même par octaves, les allures expérimentales des spectres de pression acoustique des jets ont permis de retenir la condition simplificatrice de bruit blanc pour ces types d'analyse.

Dans certaines conditions particulières de mesures (faibles valeurs de la différence de marche géométrique), la forme des spectres du bruit de jets intervient sur l'écart de niveau global existant entre la mesure en présence d'un plan et la mesure en champ libre. Toutefois dans la majorité des cas de mesures pratiques au-dessus d'un réflecteur parfait, cet écart peut varier de 2 à 5 dB (la valeur théorique correspondante, si l'on suppose que le jet émet un bruit blanc, serait de 3 dB).

Par suite des dimensions de la zone d'émission acoustique d'un jet, l'examen de la validité de l'hypothèse d'une source ponctuelle a abouti aux conclusions suivantes:

- dans les cas habituels de mesures dans le champ acoustique lointain, la distribution axiale des sources sonores d'un jet peut être négligée

- dans ces mêmes conditions de mesures, le rapport du diamètre de la tuyère à la hauteur moyenne peut devenir un paramètre significatif supplémentaire lorsque le moteur est au point fixe. Il est alors possible d'exprimer les facteurs de correction en considérant que le bruit émis provient de sources élémentaires distribuées suivant le diamètre vertical de la section d'éjection.

L'étude expérimentale a confirmé la validité des relations établies pour une telle distribution, dans l'hypothèse d'un plan parfaitement réfléchissant. Cette étude a également montré que, si le jet est très près de la surface et alimenté sous certaines conditions génératrices, les phénomènes d'interférences sont altérés. Ce problème est actuellement à l'étude mais il semble déjà que pour les rapports de détente élevés, une hauteur minimale du bord inférieur de la tuyère soit nécessaire à l'application des relations présentées. D'autres points particuliers tels que la rugosité du plan réflecteur ou l'hétérogénéité de l'atmosphère seraient certainement à considérer pour compléter ces résultats.

Malgré ces remarques, les spectres représentés à la figure 15 (qui correspondent à des mesures effectuées autour d'un turboréacteur ATAR sur l'installation d'Istres et qui ont été corrigés des réflexions)montrent que dans des conditions de mesure correctes, on peut espérer, par la méthode proposée, une approche plus réaliste des caractéristiques acoustiques de champ libre des jets.

REFERENCES

(1) Howes, W.L.:
Ground Reflection of Jet Noise
NASA Technical Report R 35 (1959)

(2) Franken, P.A.:
A Theoretical Analysis of the Field of a Random Noise Source Above an Infinite Plane
NACA TN 3557

(3) Hoch, R. et Thomas, P.:
Influence des réflexions sur les spectres de pression acoustique des jets
1er Colloque d'Acoustique Aéronautique (Toulouse 1968)

(4) Powell, A.:
On the Generation of Noise by Turbulent Jets
ASME Paper, n° 59 AY53 (1959)

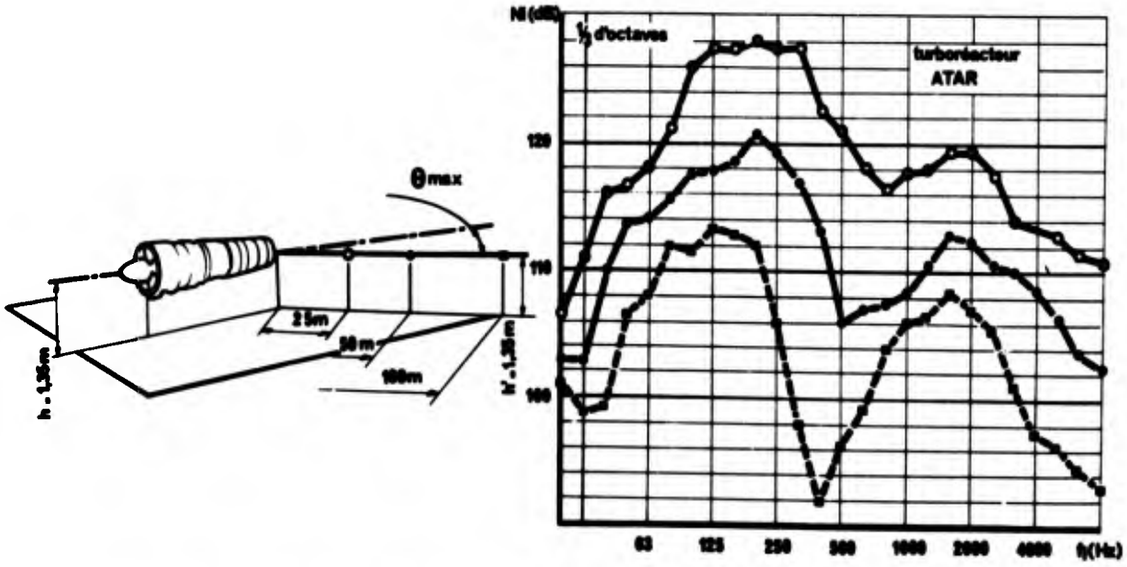

1 Spectres de jet mesurés en présence d'un sol herbeux (distance variable)

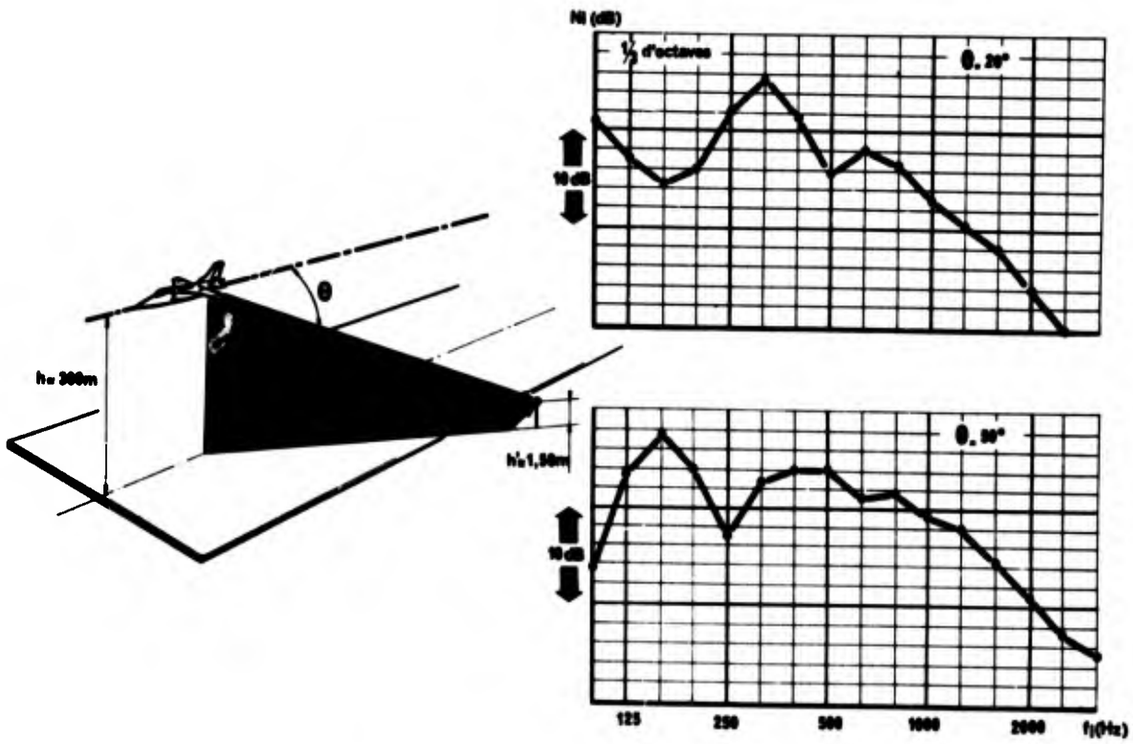

2 Spectres de jet mesurés lors d'un survol

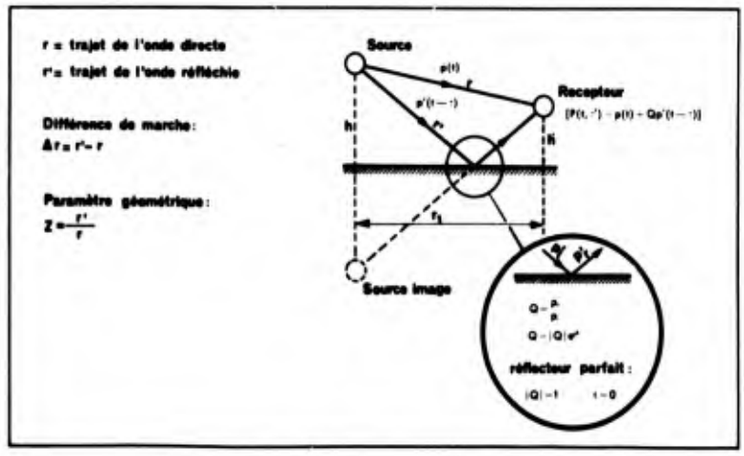

3 Schématisation du problème

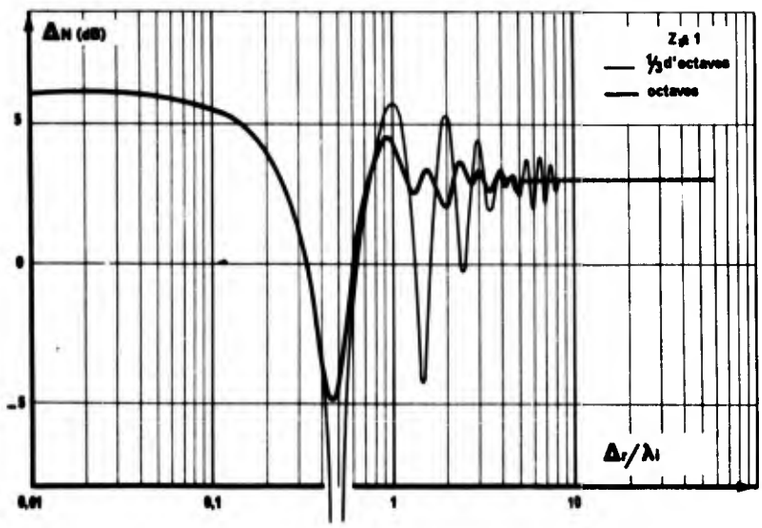

4 Indices de réflexion (plan réflecteur parfait)

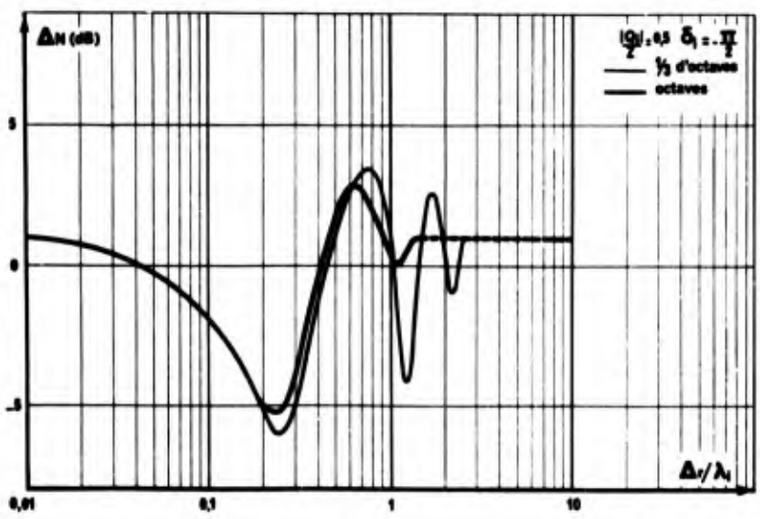

5 Indices de réflexion (plan partiellement absorbant)

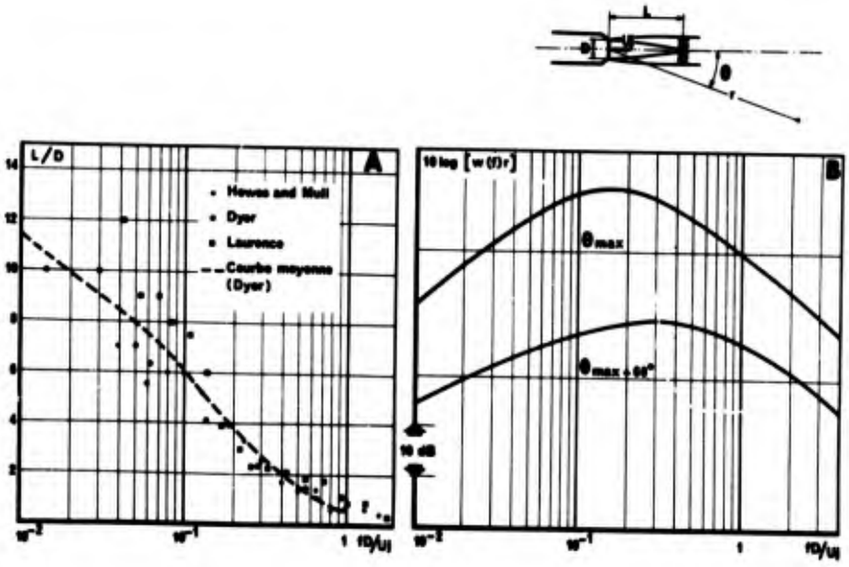

6 Caractéristiques de l'émission acoustique d'un jet

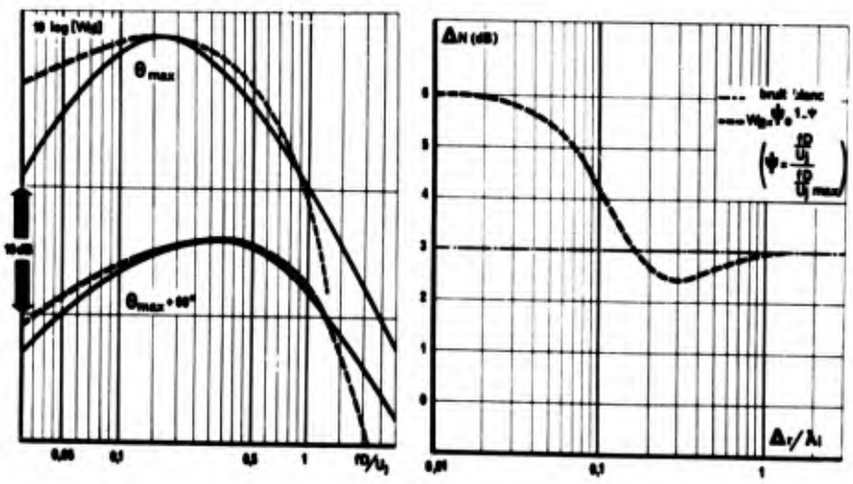

7 Influence de la forme du spectre sur l'indice de réflexion en niveau global

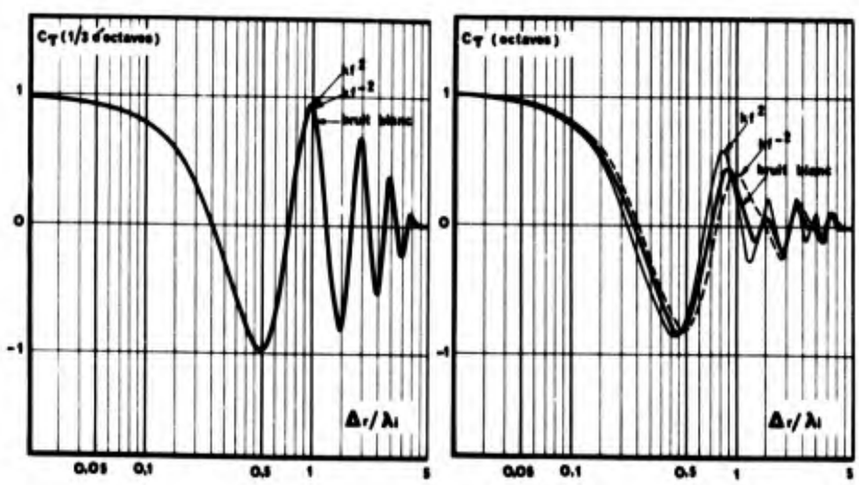

8 Influence de la pente spectrale sur le coefficient d'autocorrélation

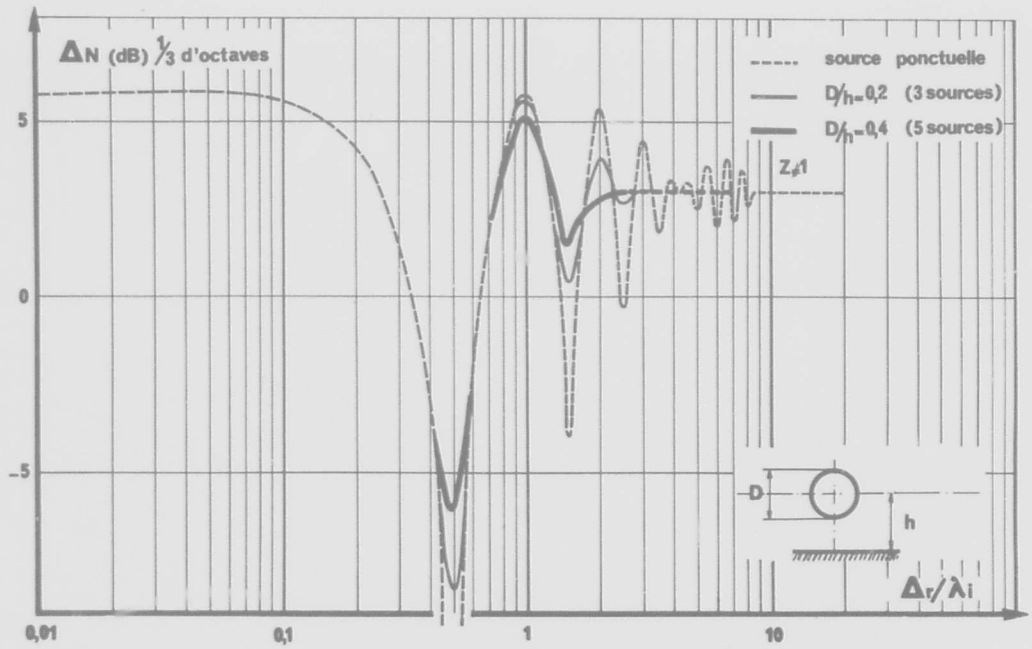

9 Influence du paramètre $D/_h$ sur l'indice de réflexion (réflecteur parfait)

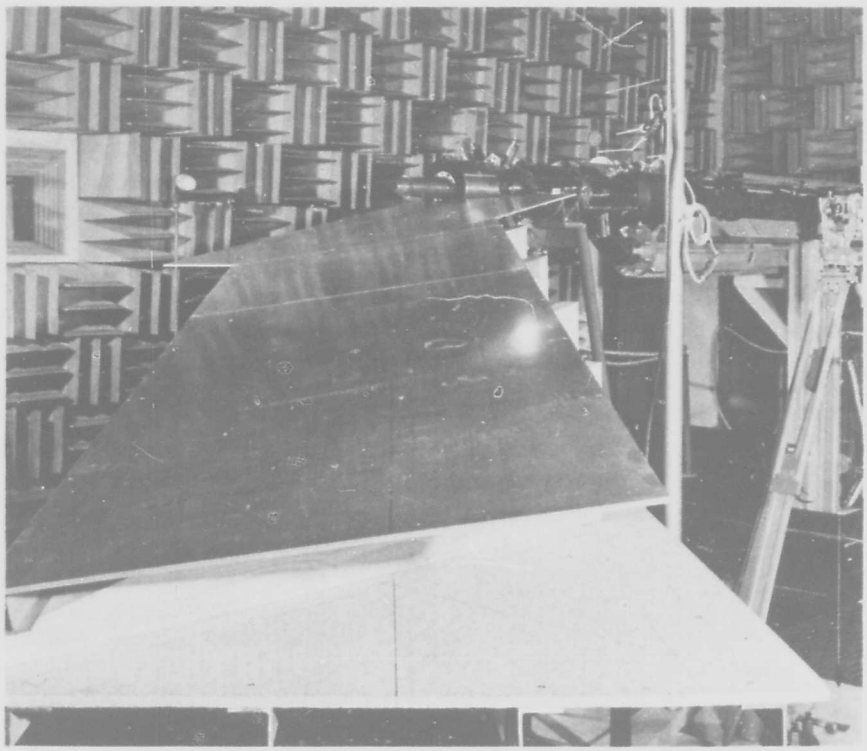

10 Dispositif d'essais en chambre sourde

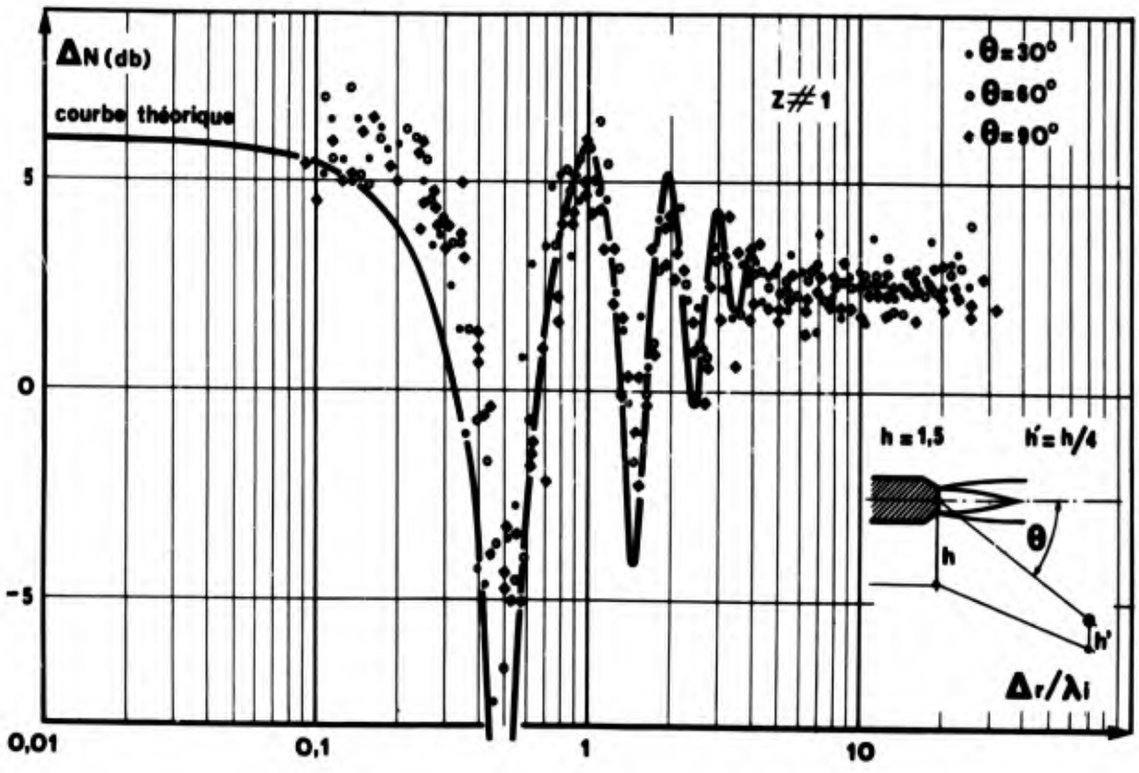

11 Résultats d'essais avec source ponctuelle (azimuth variable)

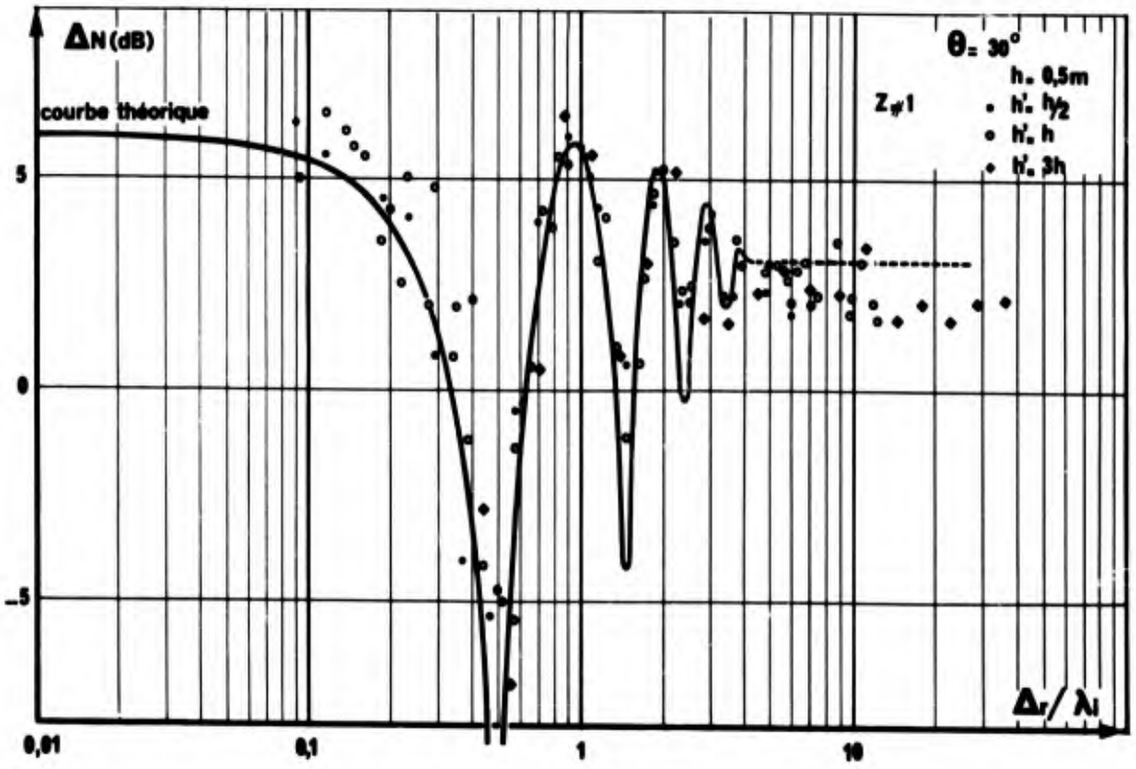

12 Résultats d'essais avec source ponctuelle (hauteur du récepteur variable)

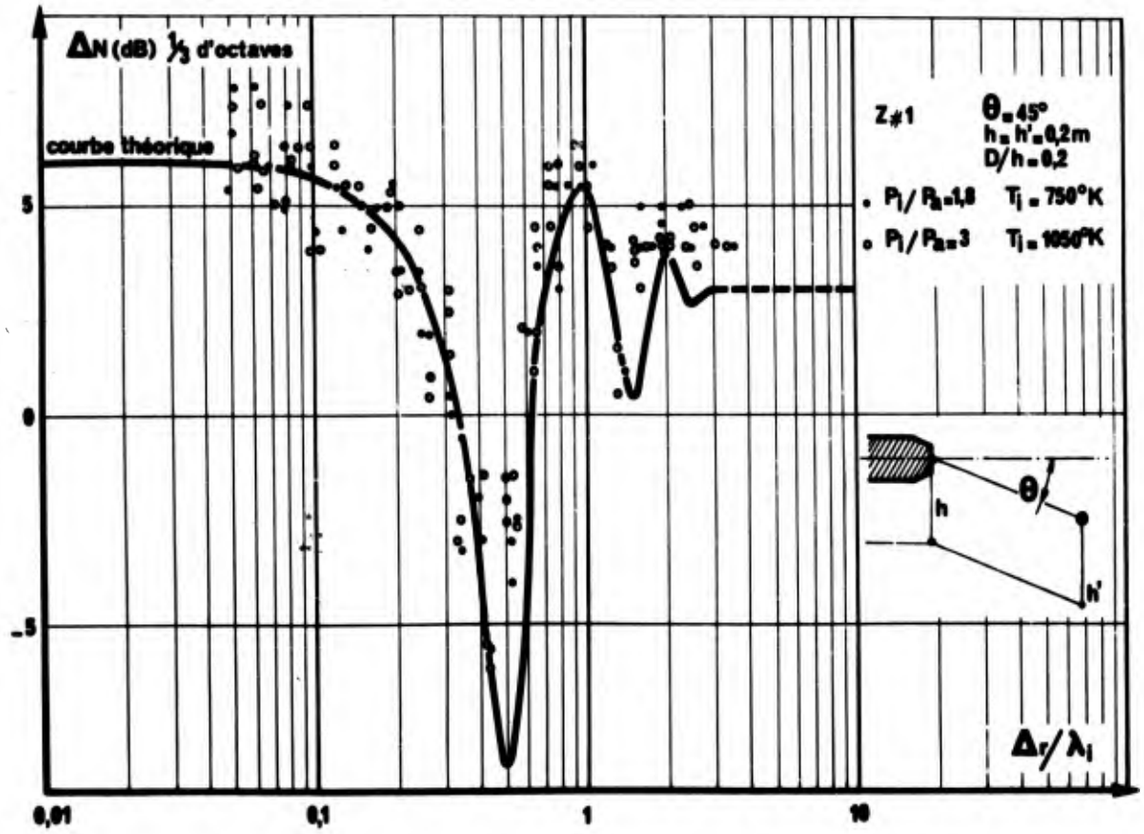

13 Résultats d'essais avec source de dimensions non négligeables devant la hauteur

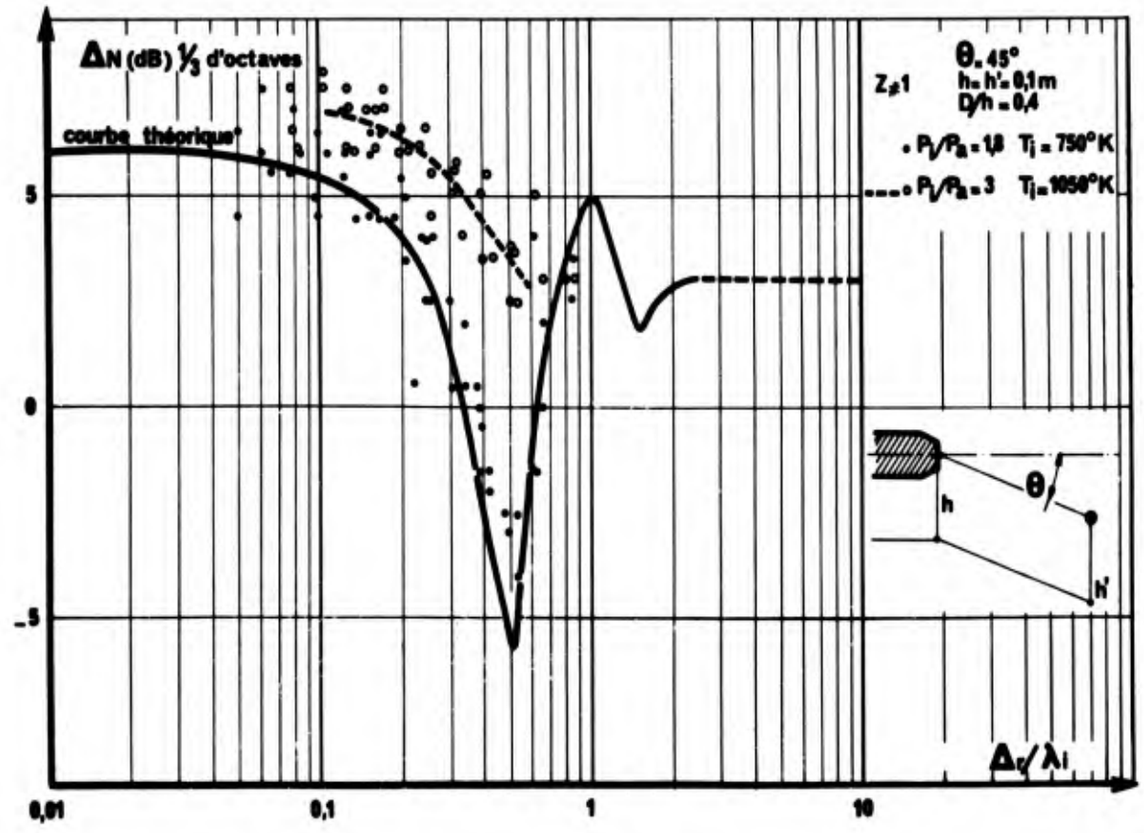

14 Résultats d'essais pour différentes conditions génératrices

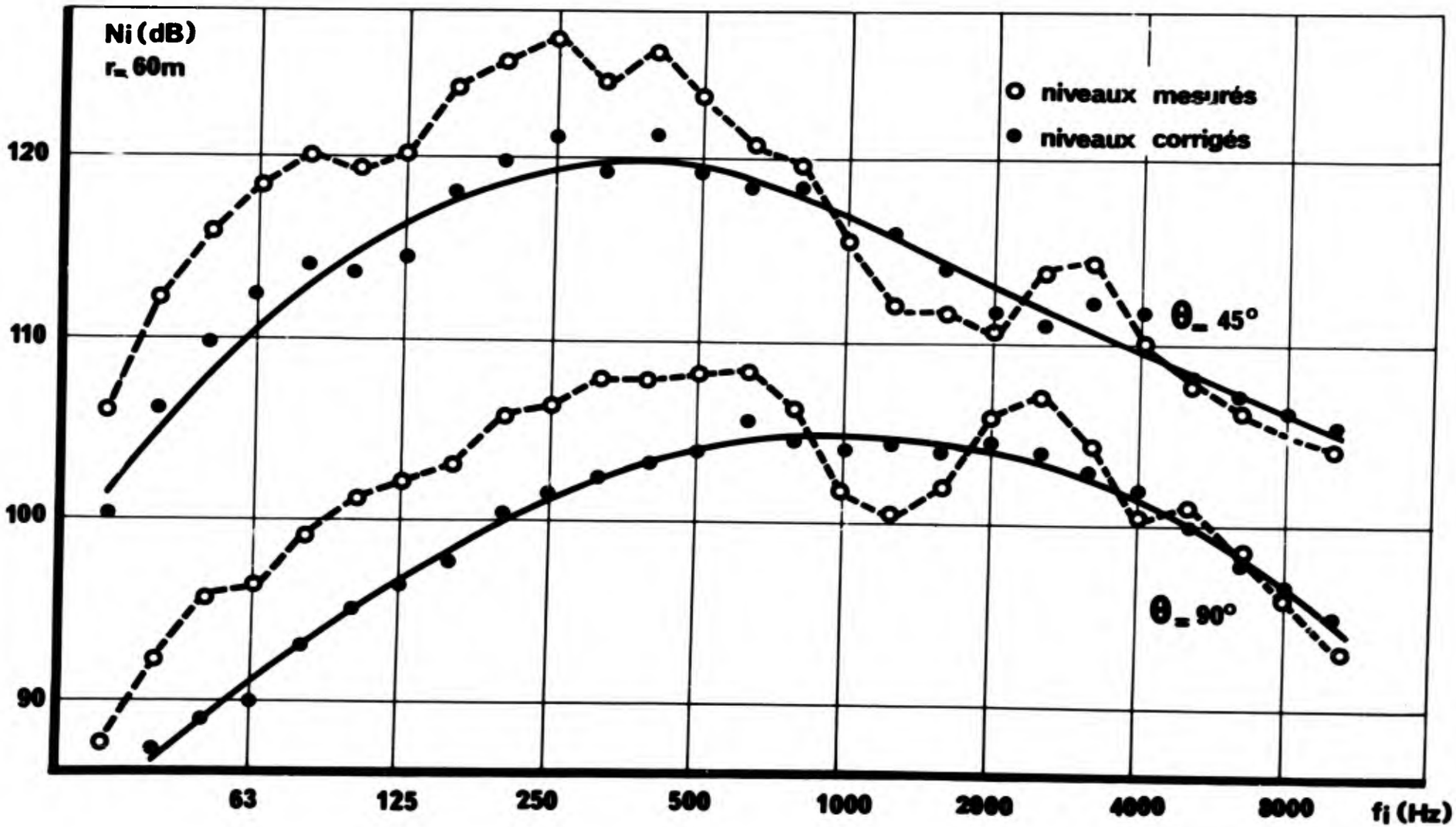

15 Exemples de restitution de spectres de champ libre.

BLANK PAGE

SONIC BOOM OF BODIES OF REVOLUTION

by

K.Oswatitsch

DVL - Aachen

Summary

This paper briefly outlines recent work on the sonic boom problem done at the DVLR-Institute of Theoretical Gasdynamics. The problems treated with the aid of an analytic method of characteristics are:

1. Sonic boom generated by inclined and non-inclined bodies of revolution moving at a constant supersonic speed

2. Sonic boom generated by a non-inclined body of revolution moving at an increasing or decreasing transonic speed

3. Influence of the isothermal stratification of the atmosphere on the sonic boom

It turns out that the widely used asymptotic formulas are unsatisfactory at altitudes of practical importance.

Sonic Boom of Bodies of Revolution

K. OSWATITSCH+

DVL - Aachen

1. Introduction

In the following we will report about our collaborators' computations dealing with the formation and decay of shocks on axisymmetric bodies. In particular we will discuss the steady supersonic flow over a body parallel to the flow or at an angle of attack, the accelerated or decelerated body near Mach Number one, and finally the influence of an isothermally stratified atmosphere.

The restriction to axisymmetric bodies is due to our present limitation in work- and computing capacity but not the analytic method of characteristics. At the moment we are extending our computations to simple wing-geometries.

The present results allow certain conclusions with regard to the effect of wings and wing-body combinations at large distances, although according to our experience one has to be careful in extrapolating to "large distances". It is quite possible that at the flying heights in question the shocks on the airplane do not form a single front- and tail-shock of circular cross section fast enough to justify the simple model of conical shocks due to lift and drag. Here seem to be certain possibilities for reducing the sonic boom.

The method of computation can be indicated only in its simplest form. It is treated in the given references and has been simplified even up to the present time.

2. Outline of the Method

As an illustration of the method we will use plane, steady, supersonic flow. One of the first papers in this area was published by C.C. Lin [1]. With W, θ and M being the velocity, direction of the velocity vector and Mach Number respectively we introduce the velocity function

$$(1) \qquad Ch(W) = \int \sqrt{M^2 - 1}\ \frac{dW}{W} .$$

Then we obtain from the gasdynamic equation together with the equation of irrotationality the well known equation of compatibility

$$(2) \qquad \frac{\partial Ch(W)}{\partial \xi} + \frac{\partial \theta}{\partial \xi} = 0; \quad \frac{\partial Ch(W)}{\partial \eta} - \frac{\partial \theta}{\partial \eta} = 0.$$

Here ξ = constant and η = constant denote the left- and right-running Mach lines respectively.

If we introduce the new independent variables x_o, y_o by the linear transformation

$$(3) \qquad \xi = x_o - y_o \cot \alpha_o; \quad \eta = x_o + y_o \cot \alpha_o$$

we obtain the following system of equations:

$$(4) \qquad \begin{aligned} &- \frac{\partial Ch(W)}{\partial x_o} + \operatorname{tg} \alpha_o \frac{\partial \theta}{\partial y_o} = 0 ; \qquad - (M_o^2 - 1) \frac{\partial u_1}{\partial x} + \frac{\partial v_1}{\partial y} = 0 ; \\ &\operatorname{tg} \alpha_o \frac{\partial Ch(W)}{\partial y_o} - \frac{\partial \theta}{\partial x_o} = 0 ; \qquad \frac{\partial u_1}{\partial y} - \frac{\partial v_1}{\partial x} = 0 . \end{aligned}$$

The exact system (left) is compared with the linearized equations of the Ackeret theory (right). With

$$(5) \qquad \cot \alpha_o = \sqrt{M_o^2 - 1}$$

+ Head of the Institute of Theoretical Gasdynamics, DVL Aachen

and taking

$$(6) \qquad \sqrt{M_o^2 - 1}\; u_1 = Ch(W); \quad \theta = v_1; \; x_o = x; \; y_o = y$$

it is easy to show that the Ackeret system coincides with the exact system. The two systems (4) differ in the following. While the left system is exact and can be written in a linear form only by introducing new variables (especially the characteristic coordinates x_o, y_o) the right system is linearized already in the flow plane causing the Mach lines to "freeze" at a value $\pm\, \alpha_o$. In the latter case it is impossible for Mach lines to converge or diverge; therefore, shocks and Prandtl-Meyer expansions cannot appear. In our method we use in addition to the physical plane (x,y), the characteristic plane (x_o,y_o) where the Mach lines are straight according to equation (3).

The boundary - and initial conditions must be transformed into the corresponding ones for the x_o,y_o - plane. This way W and θ are found as functions of x_o and y_o or ξ and η. x and y are easily determined from the well known differential equations for the physical characteristics

$$(7) \qquad \frac{\partial y}{\partial \eta} = tg\,(\alpha + \theta)\,\frac{\partial x}{\partial \xi}\;; \quad \frac{\partial y}{\partial \xi} = tg\,(-\alpha + \theta)\frac{\partial x}{\partial \xi}$$

since the Mach angle α and the velocity W are known.
Fig. 1 shows the flow over a wedge in the physical and characteristic plane. The bow shock appears as a region of overlapping of the characteristic plane in the physical plane.

According to a new formulation of our collaborator Kluwick [2] one obtains the inclination of the shock for weak disturbances from equation (7) of the Mach lines by taking the arithmetic mean of Mach angle and flow angle immediately before and after the shock. This instantly gives the strength of the sonic boom. An exact transformation into linear equations is possible only for plane, steady, supersonic flow and for plane, unsteady waves. In all other cases one has to assume "weak disturbances". However, under this assumption we may linearize in the characteristic space [3]. Shocks are obtained as regions of overlapping in the flow plane. The boundary conditions and the computation of spatial Mach surfaces cause certain difficulties, the solution of which will be presented together with the results.

3. The Steady Flight of an Axisymmetric Body

The axisymmetric body at zero angle of attack was computed by W. Schneider [4] using the method described before. As an example he chose a parabolic body of revolution. At very large distances his solution may be compared with the explicit formula of Whitham [5] and gives complete agreement. The explicit formula of Whitham is often called Whitham Formula in the literature. However, in general front- and tail-shock hit the ground before this explicit formula becomes valid. In deriving this explicit formula it is assumed that the characteristics running into the shock originate from the immediate neighborhood of the neutral Mach line of the body. Fig. 2 shows the error in the pressure jump, made by the above assumption, for the characteristic running into the shock. Thus, the result according to the Whitham Formula turns out to be a little too unfavorable.

For the axisymmetric body at an angle of attack one has to notice that the axis of the undisturbed Mach cone does not coincide with the axis of the body. This distinction, which was neglected in the theory of Tsien [6], is unessential for the pressure distribution on the body but is important for the position and strength of the bow shock. Also for the computation of supersonic flow over circular cones at a small angle of attack, see for example Z. Kopal [7], a perturbation theory about the flow over a cone at zero angle of attack has been used. But this is not permissible near the bow shock. The relevant computations according to our analytic theory of characteristics have been performed by our collaborator P. Niederdrenk [8]. Fig. 3 shows the results for the circular cone. For the small lift-drag ratios in the case of an axisymmetric body of about

$$(8) \qquad C_L/C_D = 1/10$$

the change of the shock strength due to the angle of attack is only small. The shock strength on the leeward side is diminished while the shock strength on the windward side is increased by a small amount. The angle of attack has a substantially larger effect on the pressure- and velocity-distribution at the body than on the pressure- and velocity-distribution at the bow shock, since the effect of the angle of attack decays with a higher power of the quotient of thickness over radial distance from the body than the effect of the thickness. In general Niederdrenk obtained for the

bang the following relation

$$(9) \qquad \frac{\Delta p}{p_o} = \sqrt{1 - tg\ \varepsilon \cot \alpha_\infty \cot \beta}\ \left(\frac{\Delta p}{p_o}\right)_{\varepsilon = 0} .$$

Here $\left(\frac{\Delta p}{p_o}\right)_{\varepsilon=0}$ is the pressure jump across the shock at the same distance but at zero angle of attack, i.e., $\varepsilon=0$. On the leeward side $\cos \beta = 1$, while on the windward side $\cos \beta = -1$. According to the assumption of weak disturbances we have $tg\ \varepsilon \cot \alpha_\infty << 1$.

4. Influence of Atmospheric Stratification

The isothermal atmospheric stratification has no effect on geometrical acoustics since the speed of sound remains constant for constant temperature. The decay of shocks, however, is influenced by stratification. Already E. Schrödinger [9] pointed out that the particle amplitude in a plane wave propagating in the direction of stratification must change like the square root of the local density. This follows from the conservation of wave momentum. Due to the smaller disturbance the overlapping in the shock below the flying object is not as wide as for a homogeneous atmosphere. This introduces an error function into the formula for the shock. A similar effect appears for any stratification, but the isothermal stratification is the easiest to compute. R. Stuff [10] developed the theory for arbitrary flight direction even for accelerated and decelerated flight. Here we reproduce only his results for the horizontal, steady, supersonic flight. Fig. 5 shows the ratio of the pressure jump Δp in the shock over the local, heightdependent static pressure p_o. According to this, the pressure disturbance on the ground is reduced due to the increasing density. Hence the decline of particle motion with increasing density has a favorable effect on the shock. θ indicates the plane in which the shock wave propagates. In the vertical plane below the flying object θ equals 0^o, while in the horizontal plane containing the trajectory of the flying object θ equals 90^o.

5. The Wave Propagation in Space as an Acoustic Problem

Already the comparison of the systems of equations (4) shows that the linearity of the equations is not a distinctive mark of our analytic method of characteristics compared with the linearization in the physical space. The latter method, which originally was adopted from acoustics and is marked by a "frozen Mach cone", will be called "acoustic approximation" from now on. The first step in our method always corresponds mathematically to the solution of an acoustic problem in the characteristic space. Therefore, it is important to understand the acoustic solution. As an example, we treat here the decelerated flight of the tip of a body during the transition from supersonic to subsonic speed, Fig. 5. The explanation of the acoustic problem has been given by L. Prandtl [11] . The flight Mach Number $M_p = 1$ has been transposed to the origin. Hence the trajectory of the tip for deceleration in the plane $y = 0$ is flatter than the generators of the Mach cone for $t < 0$ and steeper for $t > 0$. The Mach surface behind which the disturbance starts (i.e., the "acoustic bow wave") can be found as the enveloping surface of all Mach cones which have their tips on the trajectory. The contact lines of the enveloping surface with the Mach cones are the so-called bi-characteristics. One has to proceed along these in order to determine the Mach surface. Hence, in our case the acoustic bow wave is a regular surface, the generators of which are the bi-characteristics.

At the origin, the flight Mach Number becomes smaller than one; the acoustic bow wave runs ahead of the tip of the body. Therefore, at the origin one observes at a moment t = constant a detached bow wave. On the other hand, for $M_p > 1$ the bow wave is attached. At a certain instant t = constant, one can observe in the immediate vicinity of the tip the quasi-steady picture which belongs to the Mach Number M_p. In this acoustic approximation the detachment occurs at $M_p = 1$.

6. Deceleration and Acceleration in the Framework of the Analytic Theory of Characteristics

As for the simple plane, steady, supersonic flow the solution must be found first in the characteristic space. The disturbances in the form of an increase in pressure behind the acoustic bow wave lead to an overlapping in the physical space. But overlapping always gives a shock. The theory was worked out by our collaborator R. Stuff [12] .

Essentially since we are interested only in the shocks and their immediate neighborhood, the computation is limited to the vicinity of those acoustic Mach surfaces which in the characteristic space form the acoustic front- and tail-wave. One works with the bi-characteristics which generate these Mach surfaces and the corresponding normal surfaces. Integration along bi-characteristics is typical for all problems with more than two independent variables (i.e., problems which describe phenomena in physical spaces). For two independent variables, for example x_o and y_o, which

describe phenomena in physical planes, the bi-characteristics are identical with the Mach lines.

The bi-characteristics are already of importance for the acoustic theory in space. Therefore, out of the boundary conditions result additional typical problems in the theory of characteristics. For example the bow shock becomes unattached already at a Mach Number $M_{sep} > 1$. Since the flow at the tip can be treated as quasi-steady, M_{sep} is the steady flow Mach Number for the corresponding cone at which the shock becomes unattached. At that location at which the trajectory of the tip of the body corresponds to the Mach Number M_{sep}, the inclination of the trajectory jumps from a supersonic to a subsonic inclination in the characteristic space (Fig. 6); that is, from an inclination which lies outside the Mach cone to one which lies on the inside. For the attached bow shock the trajectory is the same in the characteristic and the physical space. The inclination of the trajectory in the x_o, y_o, t_o-space after detachment, which for the time being is unknown, can be determined from the condition that the trajectory in the physical space has no kink. With that the solution of the problem can be found. Fig. 7 shows the process of detachment on an infinitely long decelerated circular cone. With increasing time an intermediate zone with an unattached shock grows linearly. In this zone the flow is conical only in time, while in the remaining domain it is also conical in space. Hence, the transition from an attached shock to a detached normal shock does not take place through a continuous change in the inclination of the shock but through the appearance and growth of the intermediate zone.

Fig. 8 depicts R. Stuff's computation of the front- and tail shock for a decelerated sharp nosed body of revolution of a thickness ratio $\tau = 0.0488$. The front- and tail-shock detach when the body passes below $M = 1.5$. Corresponding to the actual condition the acceleration parameter has been chosen extremely small, namely

$$(10) \qquad B = \frac{b\ell}{c_o^2} = -10^{-3}.$$

Here b is the effective acceleration, ℓ the length of the flying object, and c_o the speed of sound. Fig. 9 shows a snapshot of a sharp nosed body of revolution accelerated near sonic speed, which demonstrates a close relationship with the picture L. Prandtl [11] gives. However, Prandtl uses Mach lines whereas we have weak shocks in Fig. 9.

Finally, in Fig. 10 we compare the jump in pressure across the bow wave for the steady flight with that for accelerated and decelerated flight. The bow waves become unattached when the body flies with Mach Number 1.5. Again the acceleration parameter which has been chosen is very small (i.e., $B = \pm 10^{-3}$). This corresponds to an actual acceleration of approximately 5^m/sec., if we take the body length as 20m and the speed fo sound as 330^m/sec. In these unsteady problems one can identify always a quasi-steady effect together with an acceleration effect. But the latter is not important yet for the range covered in the figure. The acceleration influences the strength of the sonic boom with increasing distance. Fig. 11 depicts the front- and tail-wave during the transition of the sonic speed. In this case, the direction of propagation coincides with the straight trajectory of the flying object. In the cut t = constant these shocks appear behind the body since the body has passed the shocks already.

7. Conclusion

In this survey we considered only those contributions of our collaborators which deal with bodies of revolution. We refer to the list given at the end for additional references dealing with the sonic boom on wings and for unsteady wave propagation.

References

[1] Lin, C.C. — On a Perturbation Theory Based on the Method of Characteristics
J. Math. and Phys. 33 (1954), 117 - 134

[2] Kluwick — (in preparation)

[3] Oswatitsch, K. — Das Ausbreiten von Wellen endlicher Amplitude
Z. f. Flugw. 10 (1962), 13o - 138

[4] Schneider, W. — Analytische Berechnung achsensymmetrischer Überschallströmungen mit Stößen
DVL Report 275 (1963)

[5] Whitham, G.B. — The Flow Pattern of a Supersonic Projectile
Comm. Pure and Appl. Mech. (1952), 3o1 - 348

[6] Tsien, H.S. — Supersonic Flow over an inclined Body of Revolution
J. Aeronaut. Sci. 12 (1938), 691 - 695

[7] Kopal, Z. — Tables of Supersonic Flow around Cones
Mass. Institute of Technology, Cambridge, Rep. 1 (1947)

[8] Niederdrenk, P. — Berechnung der Überschallströmung um angestellte Rotationskörper mit Hilfe eines analytischen Charakteristikenverfahrens
DLR Research Report (in preparation)

[9] Schrödinger, E. — Zur Akustik der Atmosphäre
Phys. Z. 18 (1917), 445 - 453

[10] Stuff, R. — Die Theorie der Knallausbreitung in einer geschichteten Atmosphäre
(To be published in Z. f. Flugw.)

[11] Prandtl, L. — Über Knallausbreitung bei rasch bewegten Körpern
(Lecture given at the Deutsche Akademie Luftfahrtforschung 1938) Ges. Abhandlungen
Springer Verlag (1962), 1o59 - 1o7o

[12] Stuff, R. — Analytische Berechnung von Verdichtungsstößen beschleunigter oder verzögerter Rotationskörper
DLR Research Report 68 - 62

[13] Schneider, W. — Die Ausbreitung räumlicher Stoßwellen in ein ruhendes Medium
ZAMP 18 (1967), 66 - 78

[14] Schneider, W. — Über die Ausbreitung des Mündungsknalles
DVL Report 667
DLR-FB 67 - 5o, Juli 1967

[15] Sun, E.Y.C. — Vergleich der Behandlung des Dickenproblems eines Deltaflügels mit Schallvorderkanten mit der Theorie der schallnahen Strömung
ZAMM Special publication GAMM Meeting 46 (1966), T219 - T22o

[16] Sun, E.Y.C. — Die Kopfwelle an einem nichtangestellten Deltaflügel in stationärer Überschallströmung beim Übergang von Unterschall- zu Überschallvorderkanten
J. de Mécanique
Vol. 7, Nr. 4, (1968)

[17] Oswatitsch, K. — Ausbreitungsprobleme
ZAMM 45, (1965), 485 - 498

[18] Oswatitsch, K. — Analytische Berechnung von Charakteristikenflächen bei Strömungsvorgängen
DLR-FB 65-62 (1965)

[19] Frohn, A. — Theorie der schwach gestörten Überschallströmung um kegelige Flügel mit Kantenumströmung
(Thesis at the Institute of Technology Aachen), 1969

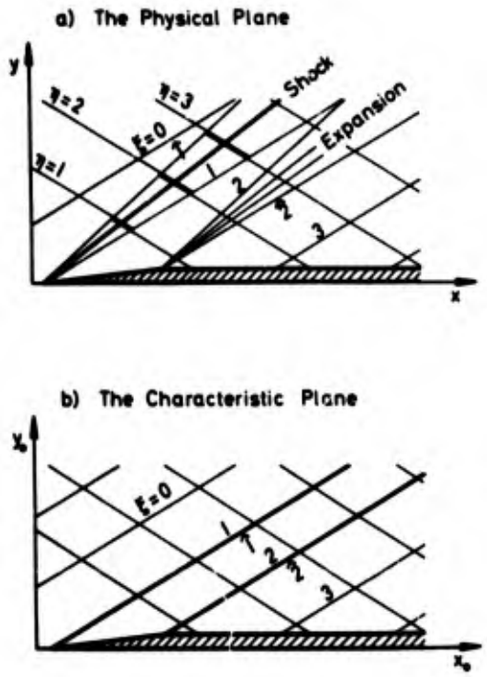

Figure 1: Characteristic- and Physical Plane

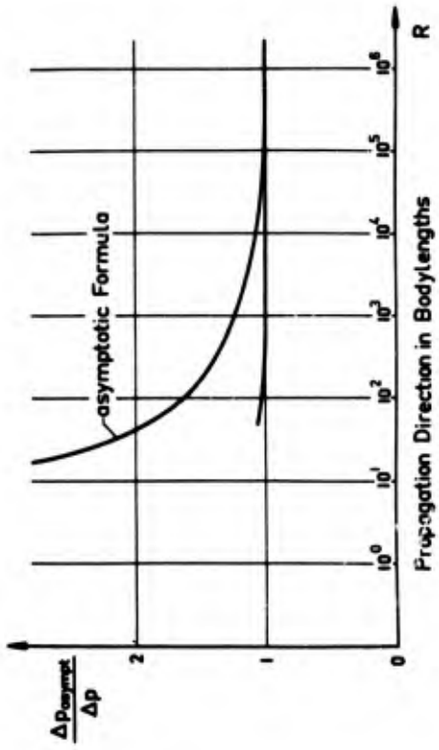

Figure 2: Pressure Jump in Propagation Direction

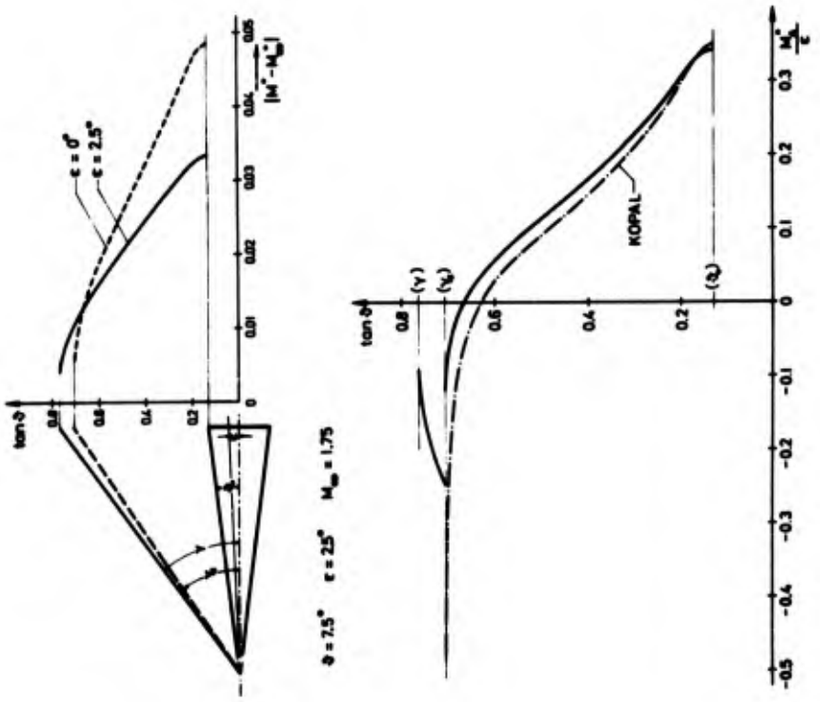

Figure 3: Velocity Perturbation Due to a Cone at an Angle of Attack Refered to the Critical Velocity of Sound

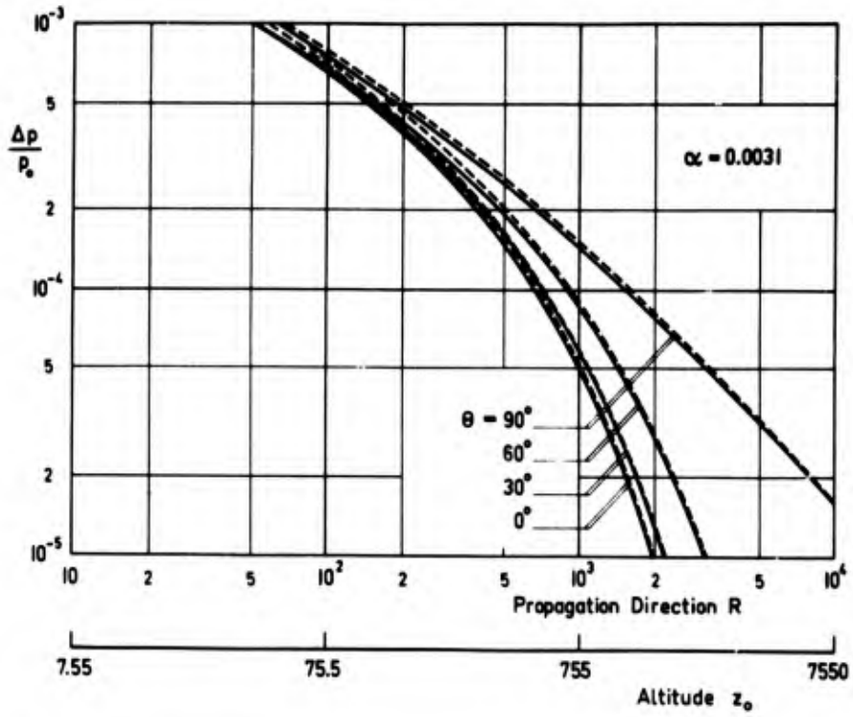

Figure 4: Pressure Jump across a Shock Wave in the Isothermal Atmosphere

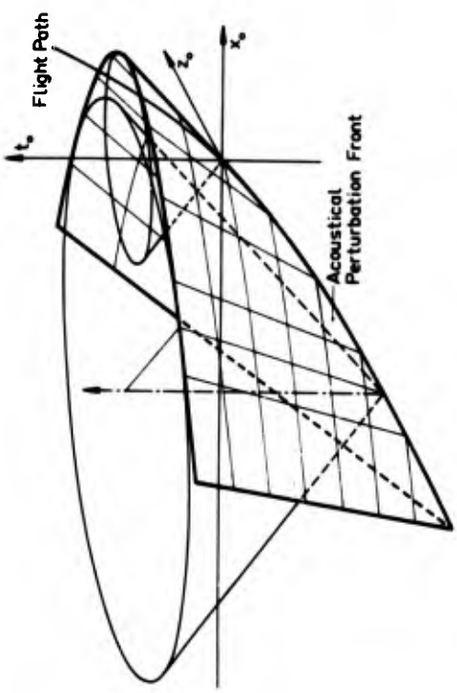

Figure 5: The Acoustical Perturbation Front

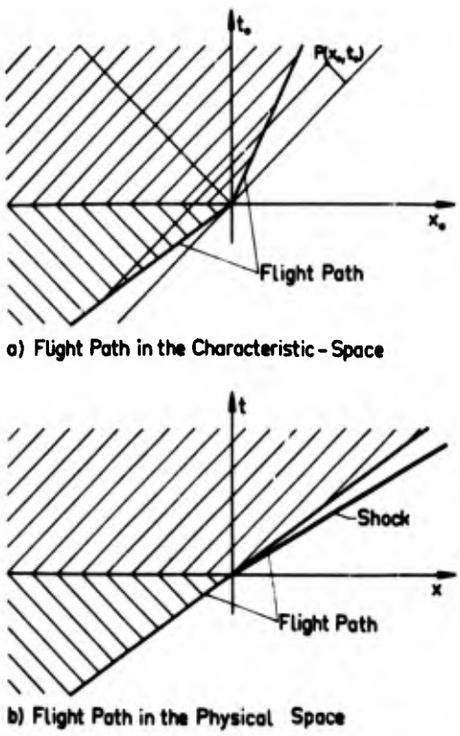

Figure 6: Flight Paths in Characteristic- and Physical Space

Figure 7: The Detaching Front Shock at Different Times

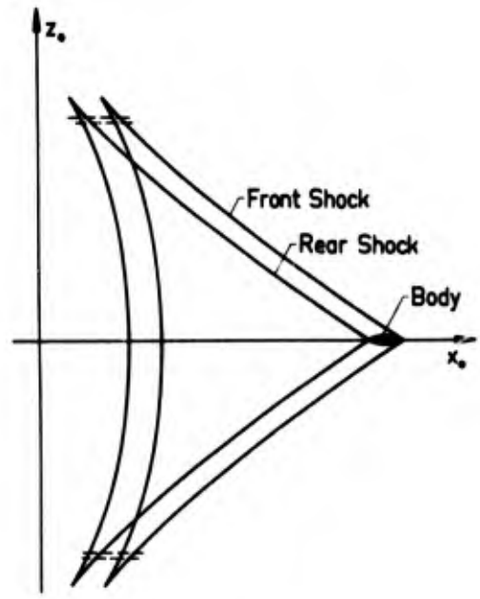

Figure 9: Configuration of the Shocks in the Accelerated Case

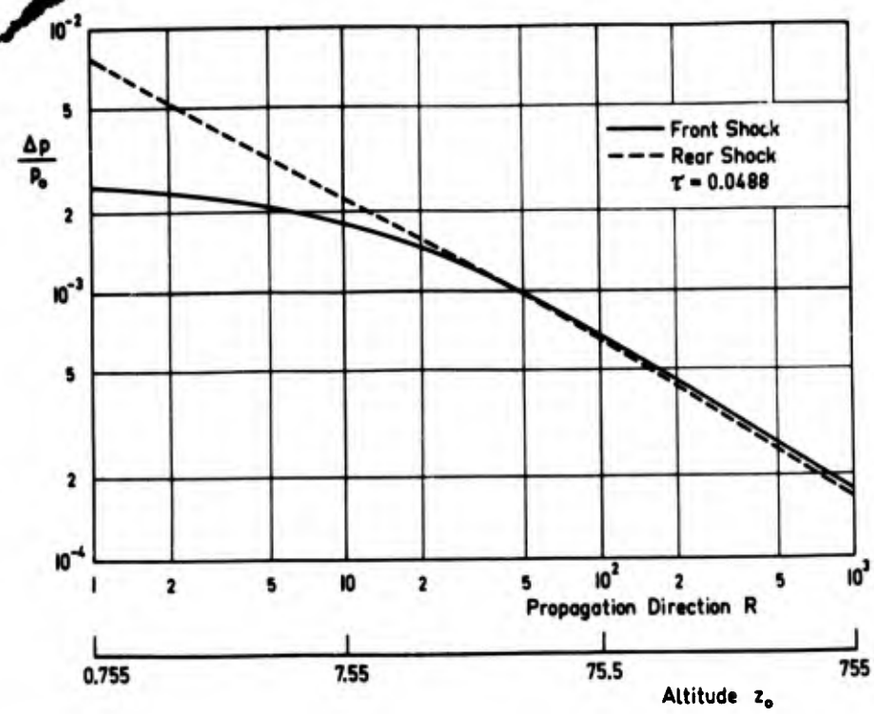

Figure 8: Pressure Jumps across the Shock Waves of a Decelerated Body in a Homogenous Atmosphere

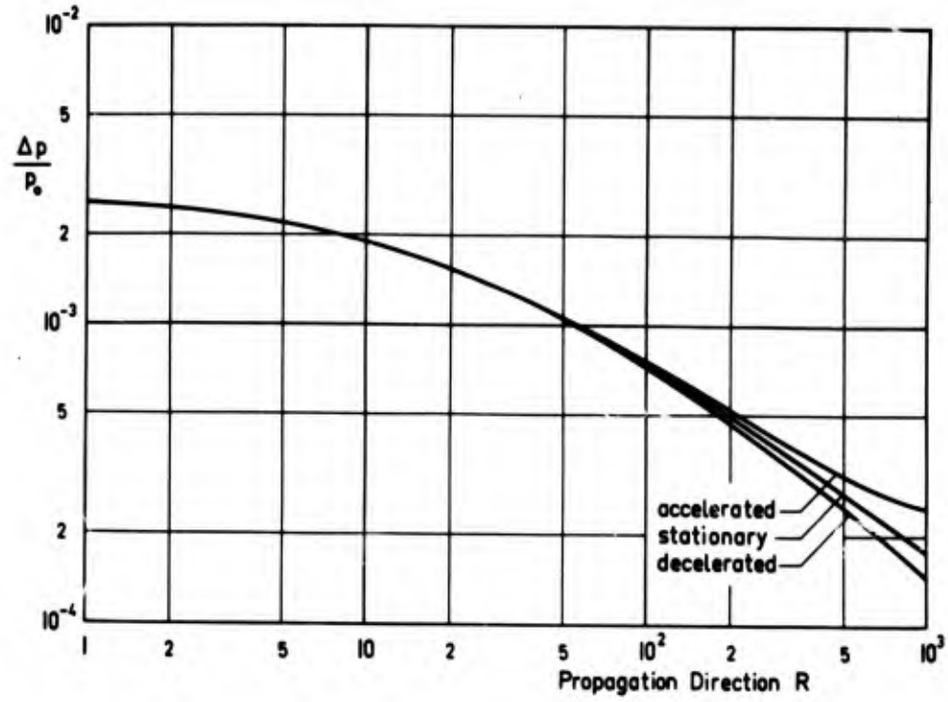

Figure 10: Front Shocks in the Accelerated, Stationary and Decelerated Case

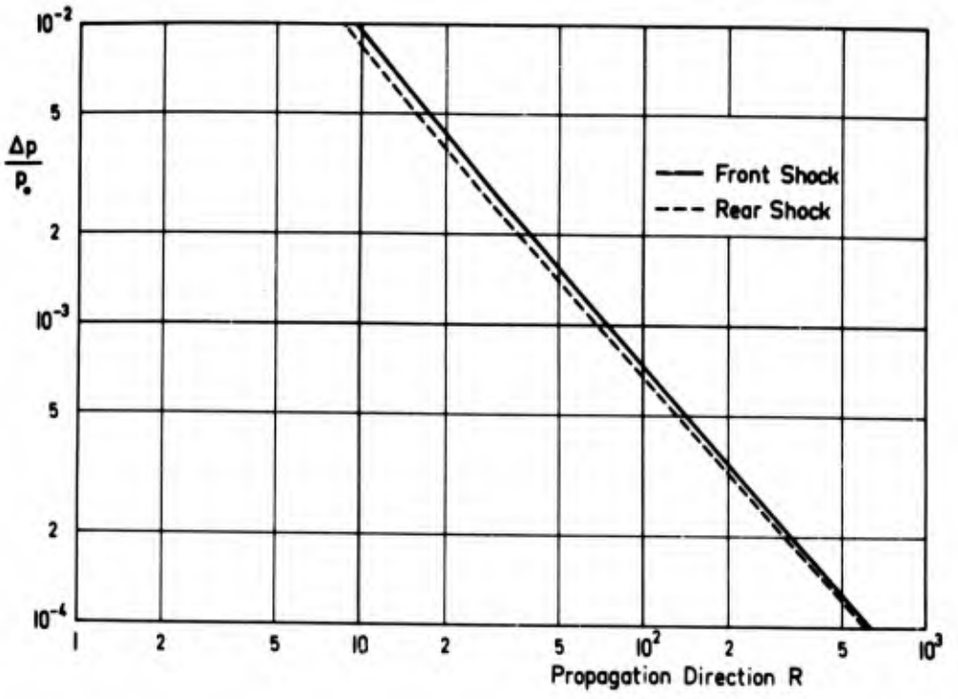

Figure 11: Front and Rear Shock of an Accelerated Body near Mach Number 1

BLANK PAGE

FOCALISATION DANS LES ONDES COURTES NON LINEAIRES
APPLICATION AU BRUIT BALISTIQUE DE FOCALISATION

par

Jean-Pierre GUIRAUD (*)

O.N.E.R.A. (France)

(*) Collaborateur extérieur
Professeur à la Faculté des Sciences d'ORSAY

SOMMAIRE

De même que la théorie du boom supersonique constitue une application de la théorie non linéaire des ondes courtes, de même et sans beaucoup plus de difficulté le boom de focalisation n'est qu'une application de la théorie générale des phénomènes de focalisation dans les ondes courtes.

FOCUSSING EFFECTS IN NON LINEAR SHORT WAVES
APPLICATION TO THE FOCUSSING SUPERSONIC BOOM

ABSTRACT

The supersonic boom theory may be considered as an application of the non linear theory of short waves, and in the same way and whithout real more difficulty the focussing boom theory appears to be an application of the general theory of focussing phenomena in short waves.

Le bang supersonique doit son origine à un phénomène complexe de propagation par ondes et résulte de la compétition de plusieurs phénomènes élémentaires : (i) accumulation des perturbations dans le voisinage de certaines surfaces d'ondes ; (ii) raidissement des signaux par effet non linéaire ; (iii) dispersion et diffusion des ondes par effet dissipatif de la viscosité et de la conductibilité thermique.

Le phénomène de propagation peut être décrit mathématiquement par un système d'équations de conservation :

$$(1) \qquad \frac{\partial U}{\partial t} + \frac{\partial \phi_k(U)}{\partial x_k} = 0 .$$

On désigne par U un vecteur à 5 composantes, soit :

$$(2) \qquad U : \{ \rho , \rho s , \rho u_1 , \rho u_2 , \rho u_3 \} ,$$

alors que l'on désigne par ϕ_k, pour chaque indice k allant de 1 à 3, un autre vecteur à 5 composantes, soit :

$$(3) \qquad \phi_k : \{ \rho u_k , \rho s u_k , \rho u_1 u_k + p\delta_{1k} , \rho u_2 u_k + p\delta_{2k} , \rho u_3 u_k + p\delta_{3k} \} .$$

Les notations sont assez usuelles : les x_k sont les composantes du vecteur (position) les indices muets comme dans (1) donnent lieu à sommation, ρ désigne la masse volumique, s désigne l'entropie spécifique et p désigne la pression ; enfin δ_{ij} est le symbole de KRONECKER, alors que les u_k sont les composantes du vecteur vitesse $\underline{u}$.

Le phénomène d'accumulation des perturbations est bien connu des ingénieurs, en relation avec le bang supersonique, et, en particulier, on sait très bien localiser dans l'espace-temps le phénomène en question (Fig. I). Celui-ci se traduit par le fait que, si un signal est en quelque sorte "piégé" à un certain instant entre deux surfaces voisines, il reste, à tout instant ultérieur, "piégé" dans un train d'ondes, c'est-à-dire entre deux surfaces qui se déduisent des deux premières par un phénomène de propagation, un peu au sens de l'optique géométrique. Le phénomène mécanique est ainsi étroitement lié au phénomène purement géométrique de propagation conformément au principe de HUYGENS. Il y a plus, non seulement le signal se trouve piégé dans un train d'ondes qui voyage, dans notre cas particulier, avec la célérité du son relativement à l'atmosphère au repos, mais encore il se trouve fortement "piégé" dans les tubes de rayons sonores qui servent de support au phénomène de propagation. Un exemple très simple (Fig. 2) illustre abondamment ce fait : soit une perturbation sonore qui se trouve localisée, à l'instant t_1 , sous forme de train d'ondes divergent, dans une couronne sphérique Σ_{t_1} , de très faible largeur ; on constate alors, qu'ultérieurement, cette même perturbation se trouve, à l'instant t_2 , localisée dans une couronne Σ_{t_2} qui se déduit de la première par propagation avec la célérité du son le long des rayons. Il y a plus : on peut même mettre les deux couronnes en correspondance par les rayons sonores et l'on peut reconnaître la même perturbation, éventuellement atténuée en amplitude, mais non déformée (en première approximation), dans des éléments des deux trains d'ondes qui se correspondent.

Il n'est pas bien difficile de reconnaître les lois qui régissent ce processus sur le système (I). Commençons par introduire trois matrices 5 x 5, soit A_k , telles que l'on ait :

$$(4) \qquad d\phi_k = A_k \, dU ,$$

il est alors clair que le système prend la forme

$$(5) \qquad \frac{\partial U}{\partial t} + A_k(U) \frac{\partial U}{\partial x_k} = 0 ,$$

et nous remarquons au passage que les matrices A_k dépendent de U, le système initial étant non linéaire ; donnons-nous ensuite une représentation d'un train d'ondes à l'aide d'une fonction $F(x_1, x_2, x_3, t)$ sous la forme

$$\text{Train d'ondes} : \quad \alpha < F < \beta$$

et représentons un signal piégé dans le train par

$$(6) \qquad U = \tilde{U}(F ; x_1 , x_2 , x_3 , t) ,$$

avec la convention que U est très faible en dehors du train d'ondes, ou très voisin d'une solution particulière remarquable U_0 , dont il s'écarte notablement dans le train. Par substitution de (6)

dans (5), nous obtenons :

$$(7)\qquad \boxed{\left(\frac{\partial F}{\partial t}\,1+\frac{\partial F}{\partial x_\kappa}\,A_\kappa\right)\frac{\partial \tilde U}{\partial F}}+\frac{\partial \tilde U}{\partial t}+A_\kappa\frac{\partial \tilde U}{\partial x_\kappa}=0,$$

où 1 désigne la matrice (5 x 5) diagonale unité. Si la perturbation est réellement piégée dans le train d'ondes, c'est que l'on a

$$(8)\qquad \left|\frac{\partial \tilde U}{\partial t}\right|\ll\left|\frac{\partial F}{\partial t}\,\frac{\partial \tilde U}{\partial F}\right|\quad,\quad\left|\frac{\partial \tilde U}{\partial x_\kappa}\right|\ll\left|\frac{\partial F}{\partial x_\kappa}\,\frac{\partial \tilde U}{\partial F}\right|\ ,$$

de telle sorte que, mieux le piégeage est réalisé, et plus l'on s'approche de la situation pour laquelle la fonction $\tilde U(F)$, qui n'est autre que la signature de la perturbation, s'approche d'une solution du système :

$$(9)\qquad \left(\frac{\partial F}{\partial t}\,1+A_\kappa\frac{\partial F}{\partial x_\kappa}\right)\frac{\partial \tilde U}{\partial F}=0\ .$$

De cette équation toute simple, on peut tirer deux conséquences importantes qui se laissent interpréter physiquement dans notre cas particulier, caractérisé par (2) et (3). Introduisons d'abord le concept de vitesse de propagation normale, expliqué sur la figure 3, en écrivant :

$$(10)\qquad \frac{\partial F}{\partial t}=-\lambda w\quad,\quad\frac{\partial F}{\partial x_\kappa}=\lambda n_\kappa\ ,$$

de telle sorte que les n_κ soient les composantes du vecteur unitaire $\underline{n}$ normal à F = Const. L'équation (8) s'écrit alors :

$$(11)\qquad \left(n_\kappa A_\kappa-w\,1\right)\frac{\partial \tilde U}{\partial F}=0,$$

et il apparaît que les deux conclusions annoncées plus haut sont les suivantes :

(12)
(i) w est valeur propre de la matrice $n_\kappa A_\kappa$
(ii) $\dfrac{\partial \tilde U}{\partial F}$ est vecteur propre, à droite, de la même matrice.

Examinons d'abord l'application de (10) au cas particulier que nous avons en vue. Si nous éliminons les solutions qui correspondent aux ondes d'entropie, nous avons :

(13)
(i) $(n_\kappa u_\kappa-w)^2=c^2$
(ii) $\dfrac{\partial \tilde U}{\partial F}=\text{Const}\left\{\rho(w-n_\kappa u_\kappa)\ ,\ 0\ ,\ cn_1\ ,\ cn_2\ ,\ cn_3\right\}$,

en désignant par c la célérité du son. La condition (i) exprime que chaque surface d'onde dans le train se déplace, normalement à elle-même, avec la célérité locale du son, relativement au gaz ; la condition (ii) qui peut s'écrire :

$$(14)\qquad \frac{\partial \tilde U}{\partial F}=a\,R(\tilde U)\ ,$$

où a désigne un scalaire dépendant éventuellement de F et où R désigne le vecteur propre à droite convenablement normalisé, apparaît comme un système différentiel ordinaire* assurant la détermination de $\tilde U$ comme fonction de F.

Remarquons que (9) est l'équation à laquelle on aurait abouti si l'on avait recherché une solution exacte de (I), ayant la forme U = U (F). De telles solutions sont bien connues en dynamique des gaz sous le nom d'ondes simples et l'on peut énoncer : si une perturbation est fortement piégée dans un train d'ondes, la signature de cette perturbation est, localement, celle d'une onde simple. Dans une onde simple au sens strict, la perturbation reste constante lorsque l'on se déplace sur une onde F = Const. Lorsqu'il s'agit d'une perturbation qui n'est pas rigoureusement une onde simple mais qui est seulement fortement piégée dans un train d'ondes, il y a lieu de s'attendre à ce que la signature varie en amplitude et en forme d'un instant-point à l'autre sur une onde F = Const. La seule chose que l'on demande est que cette variation soit relativement lente, comparée à la variation de U relativement à F. Le problème capital de la théorie des ondes courtes concerne la prévision de cette évolution de la signature lorsqu'on parcourt une onde, c'est-à-dire lorsque l'on suit le train d'ondes dans sa propagation.

---

*En fait, il faut prendre en compte simultanément les deux conditions (12).

La théorie des ondes courtes a surtout été développée pour les équations et les systèmes linéaires et, dans ce domaine, elle a une longue et brillante histoire. C'est qu'en effet, le passage de l'optique physique à l'optique géométrique d'une part, le passage de la mécanique quantique à la mécanique classique d'autre part, relèvent précisément de la théorie des ondes courtes. Récemment, sous l'impulsion des travaux de WHITHAM [1], la théorie des ondes courtes a été reprise et employée dans le domaine des ondes dispersives non linéaires, dont les ondes de gravité, les ondes de la magnétodynamique des fluides et les ondes dans les plasmas fournissent de vastes champs d'application [2]. La structure des équations change d'un phénomène physique à l'autre, mais l'idée est toujours à peu près la même. Le système d'équations représentant le phénomène physique considéré est supposé posséder une solution particulière $U = U(F)$ se présentant sous la forme d'une onde progressive comme indiqué sur la figure 4 a. S'il s'agit d'ondes de gravité, la solution en question peut être une onde solitaire ou une onde périodique. En fait, la solution en question dépend de paramètres $\xi_1, \xi_2, \ldots \xi_N$, soit :

$$U = U(F; \xi_1, \xi_2, \ldots \xi_N) \,. \tag{15}$$

Dans le cas d'une onde solitaire en eau peu profonde, par exemple, les paramètres dont il s'agit sont ceux qui définissent la direction de progression de l'onde et son amplitude. Appelons onde élémentaire une solution telle que (15) ; on peut avoir l'idée qu'une situation en apparence très complexe est peut-être analysable en termes d'ondes élémentaires, en ce sens que le phénomène est peut-être approximativement représentable par une onde élémentaire du type (15), mais dont les paramètres sont lentement variables d'un instant point à l'autre. La figure 4 b montre une onde solitaire (progressive), analogue à celle de la figure 4 a, mais dont l'amplitude est modulée. C'est un peu la situation que l'on rencontre dans le phénomène des battements. Le problème capital de la théorie des ondes courtes consiste alors à former le système d'équations qui régit l'évolution spatio-temporelle des paramètres.

Revenons à (6) et (7) en supposant que les matrices A_k soient indépendantes de U ; alors, le vecteur R qui figure dans (14) est bien déterminé (après avoir été convenablement normalisé) et l'on a manifestement :

$$\tilde{U} = a(F; x_1, x_2, x_3, t)\, R(x_1, x_2, x_3, t), \tag{16}$$

la fonction $a(F)$ étant lentement variable d'un instant point à l'autre et largement arbitraire. Notons que, si les matrices A_k ne sont pas constantes mais varient lentement, le vecteur R varie lentement également. Sans entrer dans les détails de la théorie, nous pouvons voir fort simplement quel est le mécanisme qui règle l'évolution de la fonction d'amplitude a. Considérons à cet effet le vecteur propre à gauche L associé au vecteur propre à droite R, c'est-à-dire tel que l'on ait :

$$(n_\kappa A_\kappa - w1)R = 0 \quad , \quad L(n_\kappa A_\kappa - w1) = 0 \,, \tag{17}$$

et revenons à l'équation (7) pour la multiplier scalairement par L. Les termes encadrés donnent un résultat nul, en raison de (17), et il reste une équation :

$$LR\frac{\partial a}{\partial t} + LA_\kappa R\frac{\partial a}{\partial x_\kappa} + a\left(L\frac{\partial R}{\partial t} + LA_\kappa\frac{\partial R}{\partial x_\kappa}\right) = 0 \,, \tag{18}$$

qui est susceptible d'une interprétation très imagée. Un raisonnement que nous ne ferons pas ici montre en effet que l'on a :

$$LR\, V_\kappa = LA_\kappa R \,, \tag{19}$$

les V_κ étant les composantes d'un vecteur $\underline{V}$, qui n'est autre que le vecteur vitesse de propagation de l'onde en suivant un rayon, c'est-à-dire ce que l'on appelle un rayon sonore en acoustique. Il apparaît donc que (18) est en fait une équation différentielle ordinaire :

$$\frac{da}{dt} + \rho\, a = 0 \tag{20}$$

régissant l'évolution de a le long d'un rayon. Ainsi, la signature conserve-t-elle, à une affinité près, une forme invariable au cours de l'évolution, seule son amplitude changeant au cours de la progression le long du rayon.

Pour passer à la théorie du boom supersonique, il faut prendre en compte le caractère faiblement non linéaire des équations, c'est-à-dire la faible variation des A_k avec U. Nous disons que la variation est faible parce que les perturbations sont petites. Les vecteurs R et L sont relatifs aux valeurs des A_k à amplitude nulle.

Il est alors clair que le vecteur L n'annule pas exactement les termes encadrés dans (7) et l'équation (20) doit être remplacée par :

$$\frac{\partial a}{\partial t} + \Gamma a \frac{\partial a}{\partial x_1} + k a = 0, \tag{21}$$

où Γ est un coefficient purement numérique si l'on s'arrange pour que a ait les dimensions d'une vitesse. Notons que x_1 désigne la distance à l'onde centrale du train, soit F = 0, comptée à t = Const et normalement à l'onde. Ceci est rappelé sur la figure 5. On peut donner de Γ une expression explicite dès que l'on connaît la variation des A_κ en fonction de U. Il est sans doute plus intéressant de saisir la signification physique du second terme dans (21). Revenons à (7), compte tenu de (10), nous obtenons :

$$L R \left\{ n_\kappa V_\kappa - W \right\} \frac{\partial \tilde{U}}{\partial F} + L \frac{\partial \tilde{U}}{\partial t} + L A_\kappa \frac{\partial \tilde{U}}{\partial x_\kappa} = 0, \tag{22}$$

et nous remarquons qu'à amplitude nulle, l'on a :

$$\left(n_\kappa V_\kappa \right)_{a=0} = W, \tag{23}$$

de telle sorte que Γa représente la variation de vitesse de propagation normale de l'onde lorsque l'amplitude passe de la valeur nulle à la valeur a. En dynamique des gaz Γ vaut $(\gamma+1)/2$, si γ désigne le rapport des chaleurs spécifiques.

Si simple que puisse paraître la théorie ci-dessus sous sa forme synthétique, son élaboration a une longue histoire, même si l'on met de côté tous les travaux consacrés à l'optique et à l'électromagnétisme. On peut considérer que la première ébauche d'utilisation de la théorie des ondes courtes en aérodynamique linéaire remonte à la règle des aires supersoniques de HAYES [3]. L'analogie entre l'optique géométrique et la structure et l'évolution des discontinuités (ou chocs acoustiques) en acoustique linéaire a été exploitée par KELLER [4]. La signature en N associée au vol supersonique a été découverte par WHITHAM [5] dans deux articles fondamentaux qui ont ouvert la voie aux très nombreux travaux concernant le boom supersonique. Le lien avec la théorie générale des ondes courtes ne s'est pourtant dégagé que très lentement. KRISTIANOVICH et WHITHAM [6] ont reconnu le caractère très général de l'équation (21), en relation avec la phase finale de la propagation du système de chocs engendré par une explosion. Il semble que HAYES [7] ait reconnu assez tôt le rôle joué par l'opérateur $\frac{\partial}{\partial t} + \Gamma a \frac{\partial}{\partial x_1}$. Le concept d'ondes courtes est sous-jacent aux idées développées par LIGHTHILL [8] dans un mémoire remarquable. Toutefois, LIGHTHILL ne met pas en oeuvre le formalisme de la théorie des ondes courtes et il détermine le coefficient k par l'application d'une règle de conservation du flux d'énergie acoustique associée à un tube de rayons sonores. L'application de cette règle soulève des difficultés dans le cas le plus général d'une atmosphère non homogène, non stationnaire avec vent. En revanche, LIGHTHILL prend en compte les effets dissipatifs par modification de l'équation (21) et son remplacement par une pseudo équation de BURGERS :

$$\frac{\partial a}{\partial t} + \Gamma a \frac{\partial a}{\partial x_1} + k a = \nu_e \frac{\partial^2 a}{\partial x_1^2}, \tag{24}$$

où ν_e est un coefficient de viscosité effectif dont LIGHTHILL donne l'expression. En fait, le formalisme de la théorie des ondes courtes est absolument nécessaire pour obtenir une évaluation correcte de k en atmosphère non homogène avec vent. C'est ainsi que l'expression donnée par FRIEDMAN, KANE et SIGALLA [9] est incorrecte. Le formalisme de la théorie des ondes courtes apparaît comme tel dans les travaux de GOUBKIN, RIJOV et GUIRAUD [10] qui donnent des expressions correctes pour k, le cas le plus général ayant été traité par GUIRAUD. Mais, ces divers auteurs n'ayant pas reconnu la structure profonde du formalisme, leurs analyses sont inutilement et singulièrement compliquées par la prise en compte de détails spécifiques liés au cas particulier des équations de la dynamique des gaz et qui masquent la belle simplicité de l'édifice. Celle-ci a été effectivement reconnue par GUIRAUD [11], qui a également montré comment l'équation (24) peut se déduire des équations de NAVIER-STOKES si l'on emploie le formalisme de la théorie des ondes courtes. Notons ici l'interprétation suivante de l'équation (20) : l'évolution de a est correctement prédite par la théorie linéaire à condition de convenir que cette évolution se fait en suivant une onde telle qu'elle se propage compte tenu des effets non linéaires. Cette règle a été découverte par WHITHAM [5] dès le début et elle paraît constituer une application de la technique de perturbations connue sous le nom de méthode PLK parce qu'elle fut créée par POINCARE, qu'elle fut exploitée en aérodynamique par LIGHTHILL et que KUO en a donné une présentation systématique. Une application directe de cette technique au cas du boom supersonique a été présentée par GUIRAUD [12], avec comme résultat, justifié au prix d'estimations laborieuses effectuées sur une formule de représentation, une représentation approchée identique à celle que l'on peut obtenir à partir de la théorie des ondes courtes. Une démonstration directe et beaucoup plus simple de ce résultat a été donnée par OSWATITSCH [13] dans le cas des écoulements plans non stationnaires. Revenons au coefficient k pour préciser que HAYES à la suite de GARRETT [14] a réussi à en relier la valeur à un principe de conservation du flux d'énergie associé à un tube de rayons sonores, donnant ainsi une démonstration rigoureuse du principe heuristique dont LIGHTHILL avait fait le point de départ de son analyse. GUIRAUD [12] a donné de ce résultat une démonstration très simple utilisant la structure profonde du formalisme de la théorie des ondes courtes et une propriété sans doute peu connue des équations de la dynamique des gaz, savoir

le fait qu'elles sont symétrisables. Partons des équations de l'acoustique en atmosphère non homogène sous la forme :

$$\frac{\partial U}{\partial t} + A_\kappa \frac{\partial U}{\partial x_\kappa} + \frac{\partial A_\kappa}{\partial x_\kappa} U = 0 \,, \tag{25}$$

nous obtenons pour la valeur de k l'expression :

$$k = L \frac{\partial R}{\partial t} + L A_\kappa \frac{\partial R}{\partial x_\kappa} + L \frac{\partial A_\kappa}{\partial x_\kappa} R \,. \tag{26}$$

Remarquons alors que l'on peut établir, selon un raisonnement que nous ne ferons pas ici, et qui utilise la symétrisabilité des équations de la dynamique des gaz, les relations suivantes :

$$L\,dR = (dL)R \,, \quad L A_\kappa\, dR = (dL) A_\kappa R \,; \tag{27}$$

il est clair que (26) devient donc :

$$k = \frac{1}{2} \frac{\partial}{\partial x_\kappa} (L A_\kappa R) + \frac{1}{2} L \frac{\partial A_\kappa}{\partial x_\kappa} R \,, \tag{28}$$

car l'on peut toujours choisir la normalisation de R et L de telle sorte que L R = I. Revenons à l'équation (25) et multiplions la par V, lié à U comme L l'est à R, il vient une équation :

$$\frac{\partial}{\partial t}\left(\frac{1}{2} VU\right) + \frac{\partial}{\partial x_\kappa}\left(\frac{1}{2} V A_\kappa U\right) + \frac{1}{2} V \frac{\partial A_\kappa}{\partial x_\kappa} U = 0 \,, \tag{29}$$

qui peut être considérée comme traduisant un bilan énergétique. Supposons alors que U et, corrélativement V ait une structure d'ondes courtes, puis intégrons par rapport à F sur un intervalle contenant toute la partie significative du train d'ondes ; il vient ainsi la relation :

$$\frac{\partial}{\partial t}\left(\int_\alpha^\beta \frac{1}{2} VU\, dF\right) + \frac{\partial}{\partial x_k}\left(\int_\alpha^\beta \frac{1}{2} V A_\kappa U\, dF\right) + \frac{1}{2}\int_\alpha^\beta V \frac{\partial A_\kappa}{\partial x_\kappa} U\, dF = 0 \,, \tag{30}$$

qui conduit directement à (20) si l'on substitue :

$$U = a(F) R \,, \quad V = a(F) L \,. \tag{31}$$

Nous voulons maintenant discuter les questions de focalisation, si importantes pour la prévision du boom supersonique, à la lumière de la théorie des ondes courtes. Nous supposerons, pour simplifier l'exposé, que les matrices A_k ne dépendent que de U, et nous examinerons successivement le phénomène de focalisation dans les ondes courtes linéaires d'abord, puis dans les ondes courtes non linéaires ensuite. Revenons à l'équation (20) et remarquons que l'expression de k peut se mettre sous la forme :

$$k = \frac{1}{2} \frac{\partial V_\kappa}{\partial x_\kappa} \,, \tag{32}$$

si l'on tient compte de (27), du fait que les A_k sont constants et de (19). On peut, dans ce cas particulier assez simple, donner de l'expression de k une interprétation géométrique soulignant l'intervention du phénomène de focalisation. Comme les A_k sont constants, les rayons sont rectilignes et une onde se représente paramétriquement sous la forme :

$$\begin{cases} t = t_0 + \sigma \,, \\ \underline{x} = \underline{x}_0 + \sigma \underline{V}(\underline{n}) \,. \end{cases} \tag{33}$$

La figure 6 illustre cette construction géométrique. Notons que $\underline{n}$ est le vecteur unitaire normal à la surface d'onde et que sa direction se conserve le long d'un rayon. Il faut comprendre que, si l'on veut obtenir, à l'aide de (33), une onde, $\underline{X}_0$ doit dépendre de deux paramètres et décrire une surface dont $\underline{n}$ est le vecteur unitaire de la normale. Les formules (33) définissent ce que l'on appelle en géométrie une congruence de droites, c'est-à-dire une famille de droites dépendant de deux paramètres. Sur chacune de ces droites, il y a deux et seulement deux points focaux $\underline{X}_P$ et $\underline{X}_Q$. Soit t_p et t_q les instants où l'onde arrive en ces points, un raisonnement que nous ne reproduirons pas permet d'établir la relation :

$$k = \frac{1}{2} \frac{t_p + t_q - 2t}{(t - t_p)(t_q - t)} \,, \qquad (t_p < t_q) \,, \tag{34}$$

de telle sorte que la relation d'évolution devient :

$$\frac{da}{dt} + \frac{1}{2} \frac{t_p + t_q - 2t}{(t - t_p)(t_q - t)} a = 0 \,, \qquad t_p < t < t_q \tag{35}$$

Cette équation présente une singularité en $t = t_P$ et $t = t_Q$, et ne saurait donc régler l'évolution de a que pour t strictement compris entre t_P et t_Q. En fait, la solution de (35) est :

$$a^2 (t - t_P)(t_Q - t) = f(x_1) \quad , \quad t_P < t < t_Q \, , \tag{36}$$

la fonction $f(x_1)$ dépendant du rayon considéré. En théorie du boom supersonique, le point focal P est sur la trajectoire de l'avion, comme l'indique la figure 7, alors que le point focal Q est le point de contact du rayon sonore avec la caustique, lieu des arêtes de rebroussement des conoïdes de Mach. La détermination de la fonction $f(x_1)$ dans (36) s'effectue en appliquant la règle des aires supersoniques qui donne le comportement du train d'ondes au voisinage de P. Au voisinage du second point focal Q, l'amplitude a augmente indéfiniment et cela interdit de traverser le point focal en question. A supposer que l'on sache effectuer une étude locale dans le voisinage du point Q et que cette étude locale révèle que la solution émergeant au-delà de Q est à nouveau un train d'ondes courtes, l'équation (35) peut alors à nouveau être appliquée au-delà de Q pour conduire à

$$a^2 (t - t_P)(t - t_Q) = g(x_1) \quad , \quad t_P < t_Q < t \, , \tag{37}$$

avec une fonction $g(x_1)$ qui diffère de $f(x_1)$. L'un des problèmes fondamentaux de la théorie du phénomène de focalisation consiste précisément à déterminer la signature de sortie connaissant la signature d'entrée.

Avant d'aborder le problème de la focalisation proprement dit, on peut obtenir des renseignements intéressants en essayant d'améliorer la représentation (6), par exemple en écrivant :

$$U = \tilde{U}_1 (\bar{F} \, ; x_1, x_2, x_3, t) + \varepsilon \, \tilde{U}_2 (\bar{F} \, ; x_1, x_2, x_3, t) + \cdots \quad , \; F = \varepsilon \bar{F} . \tag{38}$$

Nous supposons ici que F est identifié avec la distance que nous avons appelée x_1 précédemment, notamment en relation avec la figure 5. On notera que la présence du petit paramètre ε caractérise le fait que la largeur du train d'ondes est négligeable en comparaison de la distance entre points focaux P et Q. Substituons (38) dans (7) et tenons compte du fait que U vérifie (9), il vient

$$(n_\kappa A_\kappa - w 1) \frac{\partial \tilde{U}_2}{\partial F} + \frac{\partial \tilde{U}_1}{\partial t} + A_\kappa \frac{\partial \tilde{U}_1}{\partial x_\kappa} = 0 . \tag{39}$$

Comme w est valeur propre de la matrice $n_\kappa A_\kappa$, l'équation (39) ne détermine $\partial \tilde{U}_2 / \partial F$ que si une condition de compatibilité est satisfaite, mais il se trouve que cette condition est précisément celle qui conduit à l'équation d'évolution (20), de telle sorte qu'elle est automatiquement satisfaite et que (39) est résoluble par rapport à $\partial \tilde{U}_2 / \partial F$, d'une manière non unique d'ailleurs, deux solutions différant par un vecteur proportionnel à U_1. Nous nous intéressons ici au comportement de $\tilde{U}_2$ dans le voisinage du point focal Q. Il est utile, à cet effet, d'introduire un système de coordonnées lié à la caustique. Conformément au schéma de la figure 8, appelons $\underline{X}^*$ le (vecteur position du) point de contact du rayon avec la caustique, appelons t^* l'instant où l'onde F = 0 atteint ce point et désignons par $\underline{X}_\Sigma$ le point courant sur le rayon, nous avons :

$$t = t^* - \sigma \quad , \quad \underline{X}_\Sigma = \underline{X}^* - \sigma \underline{V}^* \, , \tag{40}$$

et il faut se souvenir que t^* et $\underline{x}^*$ dépendent de deux paramètres a_1 et a_2, et que le vecteur $\underline{V}^*$ dépend du vecteur unitaire $\underline{n}^*$, normal à l'onde, lequel se conserve le long du rayon. Un point déterminé de l'espace, en un instant déterminé, est complètement caractérisé par sa projection $\underline{X}_\Sigma$ et par sa distance à l'onde, soit x_1. Nous ne ferons pas ici le travail de géométrie différentielle qui consiste à effectuer, dans le système (5), le changement de coordonnées*

$$(x_1, x_2, x_3, t) \Longrightarrow (a_1, a_2, \sigma, x_1) . \tag{41}$$

Il nous faut pourtant expliquer quelques notations absolument indispensables. Il y a d'abord la définition des vecteurs unitaires $\underline{e}_1^*$ et $\underline{e}_2^*$ qui résulte de :

$$d\underline{x}^* = H_1^* \underline{e}_1^* \, da_1 + H_2^* \underline{e}_2^* \, da_2 \, ; \tag{42}$$

---

*Noter que x_1 n'a pas la même signification des deux côtés de (41)

il y a ensuite le fait que a_1 reste constant le long de l'arête de rebroussement de l'onde qui focalise sur la caustique et que les courbes $a_2 = Const$ sont tangentes aux rayons. Tout ceci est illustré sur la figure 9. Le changement de coordonnées (41) est singulier en $\sigma = 0$ et c'est précisément cette singularité qui nous intéresse ; il suffit même de prendre en compte le terme le plus singulier, soit :

$$(43)\quad \frac{\partial}{\partial t} \sim - \underline{V}^* \cdot \underline{D} \quad , \quad \underline{V} \sim \frac{H_1^*}{V^*} \frac{\underline{e}_2^* \wedge \underline{n}^*}{\frac{\partial \underline{V}^*}{\partial a_1} \cdot (\underline{e}_2^* \wedge \underline{n}^*)} \frac{1}{\sigma} \frac{\partial}{\partial \sigma} = \underline{D} \quad .$$

Revenons alors à l'équation (39) et notons $\underline{A}$ la matrice vectorielle dont les A_κ sont les composantes, il vient :

$$(44)\quad \left(\underline{A} \cdot \underline{n}^* - w^* 1\right) \frac{\partial \tilde{U}_2}{\partial \bar{x}_1} + \frac{H_1^*}{V^*} \frac{1}{\frac{\partial \underline{V}^*}{\partial a_1} \cdot (\underline{e}_2^* \wedge \underline{n}^*)} \left\{ \underline{A} \cdot (\underline{e}_2^* \wedge \underline{n}^*) - \underline{V}^* \cdot (\underline{e}_2^* \wedge \underline{n}^*) 1 \right\} \frac{1}{\sigma} \frac{\partial \tilde{U}}{\partial \sigma} = 0,$$

de telle sorte qu'au voisinage de la caustique, la représentation du train d'ondes est la suivante :

$$(45)\quad U = \frac{f(\bar{x}_1)}{\sigma^{1/2}} R_1 + \varepsilon \frac{g(\bar{x}_1)}{\varepsilon \sigma^{5/2}} \frac{H_1^*}{V^* \frac{\partial \underline{V}^*}{\partial a_1} \cdot (\underline{e}_2^* \wedge \underline{n}^*)} R_2 + O(\varepsilon^2) \quad , \quad f + g' = 0 \quad , \quad x_1 = \varepsilon \bar{x}_1 ;$$

en convenant de noter R_1 ce que nous avons noté R précédemment et de noter R_2 une solution particulière de :

$$(46)\quad \left(\underline{A} \cdot \underline{n}^* - w^* 1\right) R_2 + \left\{ \underline{A} \cdot (\underline{e}_1^* \wedge \underline{n}^*) - \underline{V}^* \cdot (\underline{e}_2^* \wedge \underline{n}^*) \, 1 \right\} R_1 = 0 .$$

Il apparaît que le second terme dans (45), qui est en principe $0(\varepsilon)$ et qui est donc négligeable hors focalisation, présente une singularité beaucoup plus élevée sur la caustique que ne l'est celle du premier terme. Cette simple observation indique pleinement que la représentation sous forme d'ondes courtes ne saurait être valable au voisinage de la focalisation.

BUCHAL et KELLER [15] ont discuté le phénomène de focalisation associé à l'équation d'HELMOLTZ ; ils ont montré que l'étendue du domaine intéressé par la focalisation était $0(\varepsilon^{1/3})$ comme indiqué sur la figure 10, que l'amplitude correspondante était $0(\varepsilon^{-1/6})$ et que la représentation de la solution s'effectuait en termes de la fonction d'AIRY. En fait, l'ensemble de ces conclusions présente un caractère très général et nous pouvons les retrouver ici. Supposons que l'étendue du domaine intéressé soit $0(\varepsilon^{2\alpha})$ avec α indéterminé, posons

$$(47)\quad \sigma = \varepsilon^{2\alpha} \hat{\sigma} \quad , \quad U = \varepsilon^{-\alpha} \hat{u} R_1 + \varepsilon^{1-5\alpha} \hat{v} R_2 + \dots \quad ,$$

nous voyons que la nouvelle représentation se racoordera à l'ancienne pourvu que l'on ait :

$$(48)\quad \lim_{\hat{\sigma} \to \infty} \hat{\sigma}^{1/2} \hat{u} = f(\bar{x}_1) \quad , \quad \lim_{\hat{\sigma} \to \infty} \hat{\sigma}^{5/2} \hat{v} = A^* g(\bar{x}_1) \quad ,$$

en notant

$$(49)\quad A^* = \frac{H_1^*}{V^* \frac{\partial \underline{V}^*}{\partial a_1} \cdot (\underline{e}_2^* \wedge \underline{n}^*)} .$$

Pour nous convaincre que (47) est la bonne représentation au voisinage de la caustique, nous pouvons partir du fait qu'après le changement de variables (41), et en ne conservant que les termes dominants, le système (5) devient*

$$(50)\quad \left(\underline{n}^* \cdot \underline{A} - w^* 1\right) \frac{\partial \tilde{U}}{\partial F} + \varepsilon A^* \left\{ (\underline{e}_2^* \wedge \underline{n}^*) \cdot \underline{A} - \underline{V}^* \cdot (\underline{e}_2^* \wedge \underline{n}^*) 1 \right\} \frac{1}{\sigma} \frac{\partial \tilde{U}}{\partial \sigma} = 0,$$

mais cela n'est pas suffisant car les deux termes de cette relation sont annulés séparément et identiquement par le vecteur propre L. Il y a donc lieu de rechercher quels sont, après changement de variables, les termes significatifs de l'équation scalaire

$$(51)\quad L \frac{\partial \tilde{U}}{\partial t} + L A_\kappa \frac{\partial \tilde{U}}{\partial x_\kappa} = 0 .$$

---

*On notera que la condition de compatibilité $L\left\{ \underline{A} \cdot (\underline{e}_2^* \wedge \underline{n}^*) - \underline{V}^* \cdot (\underline{e}_2^* \wedge \underline{n}^*) 1 \right\} R_2 = 0$ est automatiquement satisfaite.

Il est clair que l'on a

$$(52)\qquad \left(L\frac{\partial}{\partial t}+LA_K\frac{\partial}{\partial x_K}\right)\left(\varepsilon^{-\alpha}\hat{u}\,R_1\right)\sim-\varepsilon^{-3\alpha}\left(\frac{\partial\hat{u}}{\partial\hat{\sigma}}+\frac{\hat{u}}{2\hat{\sigma}}\right)R_1\ ,$$

au moins dans le cas symétrisable, car il suffit de se reporter à (35). Ensuite, conformément à (43), l'on a

$$(53)\qquad \left(L\frac{\partial}{\partial t}+LA_K\frac{\partial}{\partial x_K}\right)\left(\varepsilon^{1-5\alpha}\hat{v}\,R_2\right)\sim\varepsilon^{1-9\alpha}\,\kappa^*\mathcal{A}^*\,\frac{1}{\hat{\sigma}}\frac{\partial\hat{v}}{\partial\hat{\sigma}}\ ,$$

avec

$$(54)\qquad \kappa^*=L\left(\left[\underline{e}_2^*\wedge\underline{n}^*\right]\cdot\underline{A}\right)R_2-\underline{V}^*\cdot\left[\underline{e}_2^*\wedge\underline{n}^*\right]L\,R_2\ .$$

Finalement, pour que la description soit cohérente, on est amené à choisir

$$(55)\qquad 1-9\alpha=3\alpha\quad\Longrightarrow\quad\alpha=\frac{1}{6}\ ,$$

et l'on obtient, pour $\hat{u}$ et $\hat{v}$, un système d'équations aux dérivées partielles

$$(56)\qquad \frac{\partial\hat{v}}{\partial\hat{x}_1}=\mathcal{A}^*\frac{1}{\hat{\sigma}}\frac{\partial\hat{u}}{\partial\hat{\sigma}}\ ,\qquad \frac{\partial\hat{u}}{\partial\hat{\sigma}}+\frac{\hat{u}}{2\hat{\sigma}}=\kappa^*\mathcal{A}^*\frac{1}{\hat{\sigma}}\frac{\partial\hat{v}}{\partial\hat{\sigma}}\ .$$

Il est remarquable que le système d'équations décrivant la focalisation soit aussi simple et surtout que sa structure dépende aussi peu de la structure du système initial, c'est-à-dire du phénomène physique étudié. Celui-ci n'intervient que dans l'explicitation des coefficients $\mathcal{A}^*$ et κ^* , et aussi, mais à un autre niveau, par les vecteurs R_1 et R_2 .

L'application au boom supersonique ne présente aucune difficulté. On trouve que R_1 est caractéristique d'une onde plane isentropique, normale à $\underline{n}^*$, et que R_2 est caractéristique d'un écoulement à pression et entropie nulles, dont le vecteur vitesse est normal à la caustique ; on trouve aussi que K^* est égal à l'unité ; enfin, l'expression de $\mathcal{A}^*$ est un peu complexe et se trouve être explicitée par GUIRAUD [10] (comparer la présente équation (56) avec (119) du mémoire cité).

L'élimination de $\hat{v}$ entre les deux équations (56) conduit à une équation unique portant sur $\hat{u}$, soit

$$(57)\qquad \frac{\partial}{\partial\hat{\sigma}}\left(\frac{\partial\hat{u}}{\partial\hat{\sigma}}+\frac{\hat{u}}{2\hat{\sigma}}\right)=\kappa^*\,\mathcal{A}^*\frac{1}{\hat{\sigma}}\frac{\partial}{\partial\hat{\sigma}}\left(\frac{\mathcal{A}^*}{\hat{\sigma}}\,\frac{\partial\hat{u}}{\partial\hat{\sigma}}\right).$$

Il s'avère que cette équation peut se ramener à une équation de TRICOMI. Il suffit à cet effet de poser :

$$(58)\qquad \zeta=\hat{\sigma}\left(8\kappa^*\mathcal{A}^{*2}\right)^{2/3}\ ,\qquad \xi=\hat{x}_1+\frac{\hat{\sigma}^3}{12\kappa^*\mathcal{A}^{*2}}\ ,\qquad \hat{u}=u$$

pour obtenir

$$(59)\qquad \zeta\frac{\partial^2u}{\partial\xi^2}-\frac{\partial^2u}{\partial\zeta^2}=0.$$

On vérifie sans difficulté que ξ représente une abscisse curviligne le long des courbes tracées sur la caustique qui sont tangentes aux rayons et que ζ représente la distance à la caustique, comptée normalement avec une unité convenable, ζ étant positif du côté qui est balayé par les ondes et négatif du côté dont l'accès est interdit aux ondes. La figure 10 illustre cette géométrie.

GUIRAUD [10] a construit la solution de (56) qui satisfait aux conditions (48) et nous ne reprendrons pas ici cette discussion. Pour terminer, nous voulons simplement discuter brièvement l'intervention des effets non linéaires. Ceux-ci se font sentir d'une part par l'opérateur de convection non linéaire $\Gamma a\frac{\partial}{\partial x_1}$, c'est-à-dire par la substitution

$$(60)\qquad \frac{\partial}{\partial\sigma}\quad\Longrightarrow\quad\frac{\partial}{\partial\sigma}-\Gamma a\frac{\partial}{\partial x_1}\ ,$$

dans l'équation qui provient de la condition de compatibilité, d'autre part par le fait que le petit paramètre ε caractérise non seulement la largeur du train d'ondes, mais aussi l'amplitude des perturbations, de sorte qu'il convient de remplacer (47) par

$$(61)\qquad \sigma=\varepsilon^{2\alpha}\hat{\sigma}\ ,\qquad U=\varepsilon^{1-\alpha}\,\hat{u}\,R_1+\varepsilon^{3-5\alpha}\,\hat{v}\,R_2+\cdots\ ,\qquad (\alpha=1/6)\ ,$$

de telle sorte que, compte tenu de $x_1 = \varepsilon \bar{x}_1$, il vient

$$\frac{\partial}{\partial \sigma} - \Gamma a \frac{\partial}{\partial x_1} \sim \varepsilon^{-\ell\alpha} \frac{\partial}{\partial \hat{\sigma}} - \Gamma \varepsilon^{-\alpha} \hat{u} \frac{\partial}{\partial \bar{x}_1},$$

et que le terme de convection non linéaire est négligeable en première approximation. Le phénomène de focalisation est toujours, essentiellement, un phénomène linéaire.

En réalité, lorsque le train d'ondes courtes qui approche de la caustique est associé à un phénomène physique non linéaire, il a en général une signature en N plus ou moins prononcée mais comportant, en tout cas, des discontinuités qui conduisent à des singularités dans la solution du système (5§). Ces singularités ont été discutées par GUIRAUD [10] et elles ne peuvent être levées que par une étude locale. Le terme non linéaire joue cette fois un rôle capital et l'équation que l'on est conduit à résoudre peut s'identifier comme cela a été montré par VECKEN [16], avec l'équation des écoulements irrotationnels stationnaires transsoniques à deux dimensions. Les progrès ultérieurs passent vraisemblablement par une étude numérique et tout ce que l'on sait faire est de formuler une règle de similitude que l'on trouvera explicitée dans [10]. Cette règle a été retrouvée par THERY, LECOMTE et REGGIANI [17] en employant une méthode souvent utilisée en dynamique des gaz. Puisque les singularités de la description linéaire se placent le long des caractéristiques de l'équation de TRICOMI qui sont les prolongements des chocs de la signature en N, les auteurs précédents proposent de suivre l'évolution de ces chocs sans tenir compte du reste du phénomène ; ils y arrivent en appliquant une règle formulée initialement par WHITHAM et qui consiste à appliquer le long du choc la relation différentielle qui est valable le long d'une caractéristique. Cette technique a donné de bons résultats dans de nombreux cas, mais il est douteux qu'elle soit réellement applicable avec sûreté jusqu'à la focalisation. Il faut dire qu'elle permet de chiffrer numériquement la règle de similitude mentionnée plus haut ce que ne permet de faire aucune méthode rigoureuse à l'heure actuelle.

o o

o

- R E F E R E N C E S -

[1] WHITHAM a consacré toute une série de mémoires à cette question, par exemple :
Proc. Roy. Soc. A, N° 1393, Vol. 283, p. 238, 1965. Voir aussi la réf. 2.

[2] Tout un symposium a été consacré aux ondes dispersives non linéaires.
Proc. Roy. Soc. N° 1456, Vol. 299, 1967.

[3] Thèse Caltech 1947, également Tech. Rep. Amer. Aviat. Inc, AL-222 ; difficilement accessible.

[4] Journ. Appl. Physics, Vol. 25, N° 8, p. 938.

[5] Proc. Roy. Soc. A, Vol. 201, p. 89 et Comm. Pure Appl. Math., Vol. 5, N° 3, p. 338, 1952.

[6] KRISTIANOVICH, PMM, Vol. 20, N° 5, p. 599.
WHITHAM, Journ. Fluid Mechanics, Vol. I, N° 3, p. 290, 1956.

[7] Journ. Aero. Soc., Vol. 21, N° 14, p. 721, 1954.

[8] Article dans SURVEYS IN MECHANICS, Edité par DAVIES. Volume Jubilaire de G.I. TAYLOR, OXFORD 1956.

[9] A.I.A.A. Journal, Vol. I, N° 6, p. 1327, 1963.

[10] GOUBKIN, PMM, Vol. 22, N° 4, p. 561, 1968 ;
RIJOV, A.I.A.A. Journal supplement, Vol. I, N° 12, p. 2011, 1963 ;
GUIRAUD, Journal de Mécanique, Vol. 4, N° 2, p. 215, 1965.

[11] Communication au colloque Franco-Allemand sur le bang des avions supersoniques, SAINT-LOUIS, 18-20 octobre 1967. T.P. ONERA N° 521.

[12] ONERA, N.T. 79 ; résumé dans ICAS 3 STOCKHOLM, sept. 1962, édité par SPARTAN BOOKS.

[13] Archiwum Mechanici Stosowanej, Vol. 14, N° 3-4, p. 621, 1962.

[14] GARRETT, Proc. Roy. Soc. A, 299, p. 26, 1967
HAYES, Phys. Fluids, Vol. 11, N° 8, p. 1654, 1968.

[15] Comm. Pure. Appl. Math., Vol. 13, N° 1, p. 85, 1960.

[16] Communication personnelle.

[17] Communication personnelle.

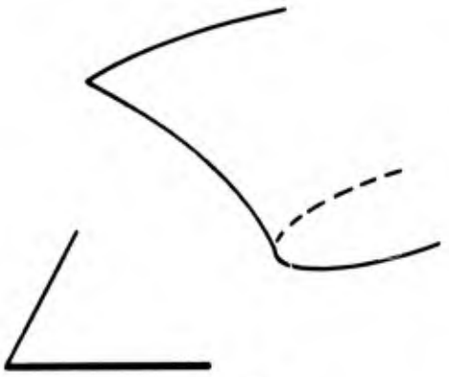

FIG. 1_

montrant un conoide de Mach et sa trace sur le sol.

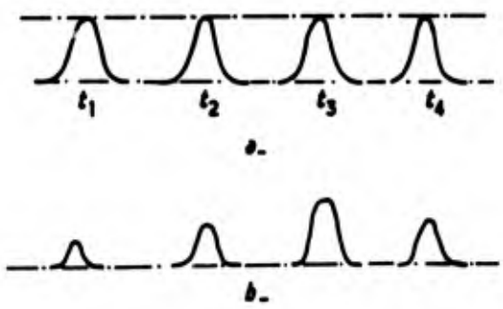

FIG. 4_

montrant une onde progressive d'amplitude constante a, ou modulée b.

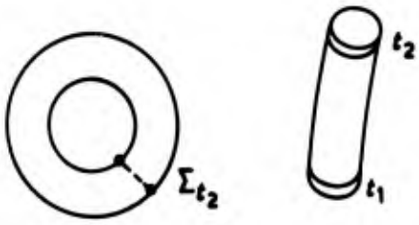

FIG.2_

montrant un train d'ondes sphériques courtes à deux instants successifs et les volumes découpés par un tube de rayons sonores.

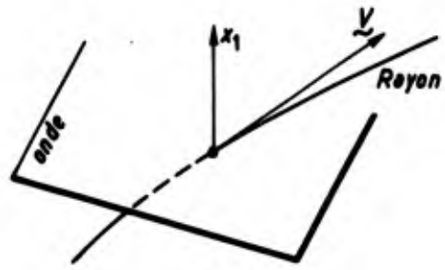

FIG.5_

surface d'onde, rayon, vitesse de propagation $\underset{\sim}{V}$ et distance à l'onde x_1 .

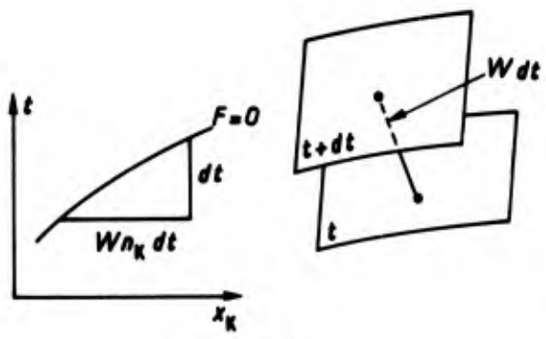

FIG. 3_

illustrant la définition de la vitesse de propagation normale w.

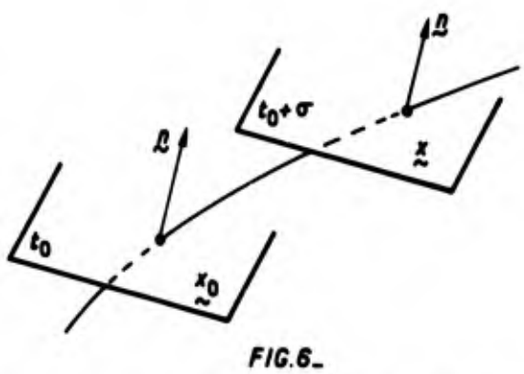

FIG.6_

illustrant la propagation le long des rayons.

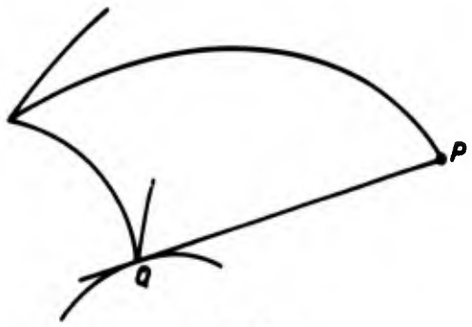

FIG. 7_

illustrant la signification des points focaux dans le cas du boom supersonique

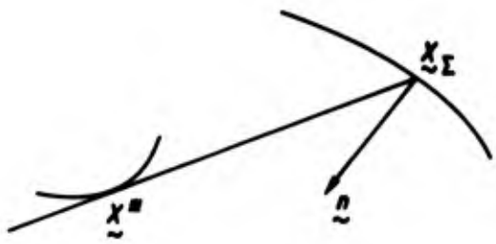

FIG. 8_

illustrant le système de coordonnées lié à la caustique.

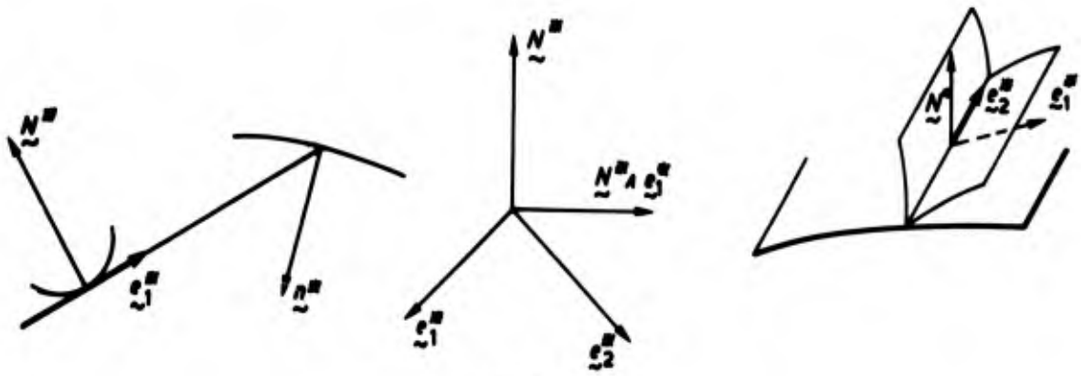

FIG. 9_

explicitant diverses notations.

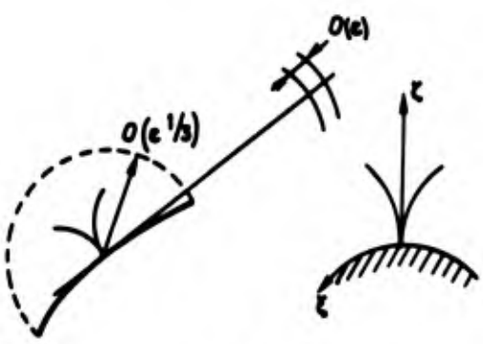

FIG. 10_

géométrie de la focalisation.

REFRACTION ATMOSPHERIQUE ET REFLEXION AU SOL DES BANGS

par

C. Thery

Institut franco-allemand de recherches de St-Louis

REFRACTION ATMOSPHERIQUE ET REFLEXION AU SOL DES BANGS

par C. THERY

Institut franco-allemand de recherches de St-Louis

Position du problème

On sait que les méthodes d'étude développées par Whitham, Rao, Friedman ([1], [2], [3]) permettent de calculer la perturbation de pression émise par un avion donné en vol supersonique dans une atmosphère homogène ou non homogène, pour un vol stationnaire ou accéléré. Ces méthodes cependant cessent d'être applicables au voisinage des surfaces caustiques sur lesquelles l'onde se réfléchit totalement. Ces surfaces, enveloppes des rayons sonores caractéristiques, sont en effet singulières et les théories précédentes y prédisent une intensité infinie de l'onde.

Une analyse du phénomène ayant lieu au voisinage de la caustique est due à Guiraud ([4]). Elle décrit la déformation progressive de l'onde à mesure que l'on se rapproche de la caustique; elle laisse cependant subsister sur la caustique et pour l'onde réfléchie, une singularité aux fronts d'ondes avant et arrière pour lesquels les surpressions demeurent infinies, le reste du signal étant fini. Elle fournit une loi de similitude permettant de rendre compte de l'influence qu'auront les différents paramètres géométriques et physiques sur l'intensité de l'onde au niveau de la caustique. Elle n'apporte cependant pas de solution complète au problème posé, une constante demeurant indéterminée.

Nous avons tenté une approche de ce même problème ([6] à [8]), par une voie assez différente et ne s'appliquant bien qu'à des cas relativement simples. La méthode employée est une méthode de caractéristiques que l'on a appliquée successivement aux cas stationnaires de la réfraction d'une onde échelon dans une atmosphère bidimensionnelle et de la réfraction d'une onde en N dans une atmosphère ayant une symétrie de révolution autour de la trajectoire de l'avion. Le procédé de calcul utilisé permet de suivre de proche en proche la réfraction de l'onde tant que l'écoulement derrière celle-ci demeure supersonique. Il ne permet donc pas de suivre l'évolution de l'intensité de l'onde jusqu'au point où elle s'évanouit mais son intensité étant faible il est possible d'en approcher d'assez près. Comme on s'intéresse surtout au signal qui sera perçu au sol, il faut compléter l'étude de la réfraction atmosphérique par celle de la réflexion au sol de l'onde qui dans des conditions proches de la focalisation se trouve être presque rasante ([5]).

Réfraction atmosphérique des ondes de faible intensité : Onde échelon.

Dans un premier calcul nous avons étudié la réfraction d'une onde de choc échelon, stationnaire, dans un milieu à gradient vertical de vitesse du son. Cette forme d'onde a été choisie de manière à ce que, tout au moins en première approximation, les perturbations ne soient transmises que suivant un seul système de caractéristiques; la configuration du phénomène de réfraction est alors simple (voir fig. 1 a), le choc incident se réfracte sur chaque couche d'atmosphère donnant naissance à un faisceau d'ondes de compression ou de détente réfléchi et à un choc transmis. En appliquant les relations à travers le choc d'une part et d'autre part celle liant la déviation de l'écoulement au saut de pression à travers un faisceau d'onde simple, on obtient la relation différentielle suivante qui lie l'intensité de l'onde à son incidence

$$\left[-\frac{\sqrt{1-\lambda y}\,\sqrt{x^2-y(1-\lambda y)}}{(1-y)\,\sqrt{1+(1-\lambda)y}} + x \right] dy = y\,\frac{1-\lambda y-x^2}{1+x^2}\,dx \qquad (1)$$

.../...

avec $y = 1 - \frac{a_0^2}{v_0^2 \cos^2\varphi} = \frac{(p_1 - p_0)/p_0}{2\gamma/(\gamma+1) + (p_1 - p_0)/p_0}$, $x = \operatorname{tg}\varphi$, φ complément de l'angle d'incidence, $\lambda = 2/(\gamma+1)$.

A cette relation il faut joindre la relation qui lie intensité de l'onde et incidence à l'altitude :

$$\frac{a_0^2(h)}{v_0^2} = \frac{1-y}{1+x^2} \quad ; \qquad (2)$$

(1) ne faisant intervenir que les seules intensité et incidence de l'onde, on constate que, pour une onde d'intensité et d'incidence initiales données, l'effet de la réfraction de l'onde sur son intensité finale demeurera le même quelle que soit la répartition du gradient de température pourvu que le saut de température à travers la couche d'atmosphère traversée demeure le même.

L'expression différentielle (1) n'est définie que pour $x^2 - y(1 - \lambda y) \geq 0$, condition qui exprime que l'écoulement est supersonique de part et d'autre du choc; les conditions critiques (écoulement sonique derrière le choc) sont données par $x^2 - y(1 - \lambda y) = 0$ ou pour les chocs de très faible intensité par $\varphi_c \simeq \sqrt{\frac{\gamma+1}{2\gamma}} \sqrt{\frac{p_1 - p_0}{p_0}}$.

(1) peut être intégrée numériquement et on obtient un faisceau de courbes intégrales qui peuvent être paramétrées en fonction de la vitesse du son à l'aide de (2) ou en altitude si la loi $a_0 = a_0(h)$ est donnée.

La solution générale de (1) est donnée figure 2. Les courbes intégrales présentent toutes le même aspect : lorsqu'on suit une telle courbe dans le sens des incidences croissantes (φ décroissant, vitesse du son croissante, altitude décroissante) l'intensité de l'onde décroît, passe par un minimum pour une incidence voisine de $\frac{\pi}{4}$ x) puis croît jusqu'à l'incidence critique. Pour les ondes de très faible intensité, telles que les bangs, le minimum est très plat et l'intensité de l'onde ne varie sensiblement que pour les incidences très faibles (qui ne nous intéressent pas ici : avions extrêmement rapides) et pour les incidences voisines de 90° pour lesquelles un net renforcement est observé

$\left(\frac{\Delta p_c}{\Delta p(\frac{\pi}{4})} \simeq 4 \text{ ou } 4{,}5\right)$ (voir figure 3 : solution pour les ondes de faible intensité).

Suivant le domaine d'incidence dans lequel on se place, on peut chercher pour les ondes de faible intensité ($y \ll 1$) des solutions approchées (leur contrôle numérique est excellent) de l'équation différentielle. Ainsi loin de la focalisation (x non petit) on obtient :

$$y \simeq c^{te}\,\frac{1+x^2}{2x} \quad \text{ou} \quad \frac{\Delta p}{p_0} \simeq \frac{k}{\sqrt{\sin 2\varphi}} \qquad (3)$$

Au voisinage des conditions critiques (x^2 et y petits) on obtient :

$$\frac{c^{te}}{x^5} \simeq \left[1 + \frac{2}{3}\sqrt{1 - \frac{y}{x^2}}\right]^3 \left[1 - \sqrt{1 - \frac{y}{x^2}}\right]^2 . \qquad (4)$$

La relation (3) est intéressante car c'est celle que fournit l'application de la théorie acoustique.

La relation (4) permet de décrire l'évolution de l'intensité de l'onde au voisinage de la focalisation (étude du comportement asymptotique) et de comparer son intensité à l'altitude critique à celle qu'elle a assez loin de la focalisation (renforcement à l'altitude critique).

.../...

---

x) pour les ondes de faible intensité.

Dans cette dernière optique, (4) peut se récrire $\left(\frac{y_c}{y}\right)^{5/2} \simeq \frac{125}{108} \times y^{-1/2}$ avec la condition $y \ll x^2 \ll 1$. Comme $\varphi \simeq \frac{s_f - s}{R}$, $y \simeq \frac{\gamma+1}{2\gamma} \frac{\Delta p}{p}$ ($s_f - s$ distance curviligne comptée sur le rayon sonore, 1/R courbure relative du rayon sonore et de la caustique, ici rayon de courbure du rayon sonore (voir figure 4)), ceci peut encore s'écrire $\frac{\Delta p(s_c)}{\Delta p(s)} \simeq \left(\frac{25}{18}\right)^{3/5} \left(\frac{\gamma}{\gamma+1}\right)^{1/5} \left(\frac{s_f - s}{R}\right)^{2/5} \left(\frac{\Delta p(s)}{P_0}\right)^{-1/5}$ (5)
avec les conditions suivantes $s_f - s_c \ll s_f - s \ll R$.

Cette formule est intéressante car elle présente une grande analogie avec la loi de similitude présentée par Guiraud qui moyennant une légère transformation s'écrit

$$\frac{\Delta p(s_f)}{\Delta p(s)} = c^{te} \cdot \left(\frac{\gamma}{\gamma+1}\right)^{1/5} \left(\frac{s_f - s}{R}\right)^{2/5} \left(\frac{\Delta p(s)}{P_0}\right)^{-1/5} \quad . \qquad (6)$$

La constante étant une constante universelle à déterminer.

Les seconds membres de (5) et (6) sont identiques à la constante numérique près. Par contre, le premier membre concerne dans la première expression le renforcement à l'altitude critique et dans la seconde le renforcement à la focalisation. Si on considère que au voisinage des conditions critiques les chocs incident et réfléchi sur la caustique pourraient présenter une configuration en y (figure 1a), la constante numérique calculée dans l'expression (5) devrait fournir un ordre de grandeur et plus précisément une borne inférieure de la valeur de la constante indéterminée de la relation (6).

Etant donné par ailleurs que dans l'analyse faite par Guiraud du comportement du phénomène au voisinage de la caustique, il était prévu une singularité pour l'onde sur la caustique, on demeurait hésitant quant à la validité de la loi de similitude fournie par Guiraud, obtenue il est vrai à partir de considérations quelque peu différentes. L'analogie du résultat obtenu dans ce cas particulier avec celui obtenu de manière très générale par Guiraud paraît donc précieuse.

On pourrait également comparer le comportement asymptotique que prévoit la relation (4) avec celui que prévoit Guiraud mais ce travail n'a pas été fait encore.

La formule d'approximation (5) n'est valable que pour $y \ll x^2 \ll 1$ donc en pratique pour des surpressions dans l'onde extrêmement faibles. On peut donc se demander si les intensités habituelles des bangs ($\frac{\Delta p}{P_0} \simeq 0{,}5.10^{-3}$) ne sont pas trop grandes pour que on leur puisse appliquer valablement l'approximation obtenue. On a donc reporté sur le graphique 5 les valeurs du rapport $(\Delta p(s_c)/p_0)$ en fonction de $(\Delta p_{min}/p_0)$ et de $(\frac{\Delta p(\gamma=0,2)}{P_0})$; on voit que la loi (5) est satisfaite dans un domaine de surpression qui couvre très largement celui des intensités habituelles des bangs. Quant à la proportionnalité à $\left(\frac{\Delta p}{P_0}\right)^{-1/5}$, elle semble se vérifier même quand l'écart d'incidence qui sert de référence cesse d'être petit.

Enfin, nous avons vu que la méthode employée n'est pas absolument rigoureuse puisqu'elle néglige l'effet des réflexions secondaires. Cependant, il est aisé de contrôler la validité des résultats obtenus en effectuant des calculs de contrôle à l'aide d'une méthode de caractéristiques sans approximation (voir figure 1b). Une telle comparaison est faite figure 6. Les intensités à la focalisation obtenues sont identiques. Les altitudes critiques diffèrent très légèrement.

.../...

Ce travail peut être complété de diverses manières, en particulier, par l'étude de l'action d'un vent longitudinal ou de celle de la pesanteur. L'expression différentielle obtenue dans ce dernier cas qui lie l'intensité du choc (y) et son incidence (x) est plus complexe. La loi de variation de la température avec l'altitude y figure explicitement et les effets de la température et de la gravitation s'y trouvent couplés. Cependant, dès que l'on considère des ondes de choc de faible intensité cette complexité disparaît. Ainsi on peut montrer que ces deux effets se séparent et on obtient avec une très bonne approximation

$$\frac{\Delta p(h)}{\Delta p(h_0)} \simeq K_G \cdot K_{T,W}$$

K_G : facteur de renforcement dû au seul effet de la gravitation, $K_G \simeq \sqrt{\frac{p(h)}{p(h_0)}}$,

$K_{T,W}$: facteur de renforcement dû aux seuls effets de la température et du vent longitudinal (par exemple, par un vent nul $K_{T,W} \simeq \sqrt{\frac{\sin 2\varphi_0}{\sin 2\varphi}}$ loin de l'altitude critique).

On donne figure 7 la solution générale obtenue pour une atmosphère pesante.

Au voisinage de l'altitude critique la loi de variation de l'intensité des chocs faibles avec l'incidence de l'onde est la même que celle obtenue pour une atmosphère non pesante et elle est donnée par (4).

Etude de la réfraction d'une onde en N dans une atmosphère de révolution.

L'étude précédente est simple et conduit à des formules explicites qui permettent de décrire le comportement de l'onde à la fois loin de la caustique et près de celle-ci. Mais, elle ne met en évidence ni l'effet de l'expansion de l'onde ni celui de la forme particulière en N de l'onde (rattrapage des chocs par les détentes); c'est pourquoi on a complété cette étude par celle de la réfraction d'une onde en N dans une atmosphère inhomogène à symétrie de révolution autour de la trajectoire supposée de l'avion.

La technique de calcul employée est toujours une méthode de caractéristiques (figure 1b) et le traitement est purement numérique. Les principaux résultats sont regroupés dans les figures 8 à 12.

L'étude en atmosphère homogène met en évidence l'effet couplé de l'affaiblissement de l'onde dû à l'interaction des chocs avec les détentes qui le suivent ou le précèdent et de l'expansion. Pour les chocs de très faible intensité (bien moindre que celle du bang), seul ce dernier effet subsiste et la surpression varie alors comme la racine carrée de la distance à la trajectoire. Pour des ondes plus intenses l'amortissement de l'onde est plus important, ainsi pour des ondes d'intensité voisine de celles des bangs l'évolution de l'intensité de l'onde avec l'altitude est voisine de celle que permet de prévoir la loi en $h^{-3/4}$ généralement retenue. L'étude en atmosphère isotherme montre que l'effet de la pesanteur est de faire varier les surpressions dans l'onde comme la racine carrée de la pression locale. L'étude en atmosphère isobare permet de mettre en évidence l'effet de la seule température, de contrôler loin de la focalisation les prévisions de la théorie acoustique et près de la focalisation la validité des lois (5) et (6) que l'on avait établi lors de l'étude du cas précédent (voir figure 13). Enfin, les divers effets se trouvent regroupés dans l'étude de la réfraction des ondes en N dans une atmosphère de type standard.

La théorie acoustique indiquant que le problème du bang peut être traité par tranche comme un problème de révolution, le phénomène de focalisation étant local, les résultats présentés doivent être très proches de ceux que fourniraient l'étude du cas réel (tridimensionnel) sous trace. En changeant la valeur du gradient de température et la distance sur laquelle s'effectue l'étude, on devrait pouvoir rendre compte des phénomènes se produisant hors trace.

.../...

En résumé, cette étude permet de décrire le phénomène dans un cas déjà assez représentatif du cas réel et de contrôler la validité des résultats établis dans l'étude d'un cas plus simple.

Etude de cas plus généraux :

Le principal problème à résoudre demeure celui des focalisations. Le contrôle que l'on a effectué dans les cas précédents de la loi générale de similitude présentée par Guiraud semble autoriser son emploi pour le traitement du cas général, un ordre de grandeur de la constante universelle indéterminée de (6) étant fournie par celle de (5). De cette manière, on peut montrer, par exemple, que le renforcement d'intensité de l'onde à la focalisation en cas de vol en palier accéléré pour des accélérations réalistes de l'avion ($\gamma \simeq 0{,}3 m/s^2$, $\gamma = 1 m/s^2$) est très voisin de celui que l'on obtient dans le cas du vol stationnaire à vitesse égale à la vitesse du son au sol. (Comparaison des courbures relatives des rayons sonores et de la caustique dans chacun des cas: calcul à partir de la théorie acoustique (voir 9)). Ce dernier cas ayant été traité, on peut donc connaître l'intensité du bang à attendre dans le premier.

D'autre part, il doit être possible de montrer que la loi de comportement asymptotique (4) (dans laquelle x serait remplacé par $\frac{S_f - S}{R}$) reste applicable. Si cela était effectivement le cas, il serait alors également possible de déterminer sur quelle étendue le phénomène de focalisation demeure sensible et quelle sera dans ce domaine l'évolution des surpressions. On peut noter à ce propos que cette étendue mesurée horizontalement dans le cas du palier accéléré semble devoir être d'autant plus importante que l'accélération sera plus faible.

Réflexion au sol

Pour compléter cette étude puisque le problème du bang se pose surtout par suite de l'effet qu'il peut avoir au sol, il faut étudier sa réflexion sur celui-ci.

On peut montrer que la réflexion des ondes de choc de faible intensité est régulière et conduit à un doublement de l'intensité de l'onde dans un très large domaine d'incidence. Cependant, pour les incidences presque rasantes certaines singularités se produisent : au voisinage de la limite de réflexion régulière, le coefficient de réflexion croît rapidement pour atteindre 3. Dans le domaine étroit de la réflexion irrégulière, le coefficient de réflexion varie très rapidement pour atteindre la valeur 1 pour l'incidence rasante (voir figure 14); or, dans les cas de focalisation par palier accéléré, l'onde se présente au sol sous une incidence presque rasante, on peut donc s'attendre alors à observer des effets anormaux dus à la réflexion qui parfois provoqueront un renforcement supplémentaire. Pour fixer les idées, remarquons que pour un vol horizontal à 11 000 m accéléré à raison de = 0, 3 m/s^2 l'onde à la focalisation se présente au sol avec une incidence déjà située dans le domaine de la réflexion régulière (coefficient de réflexion de l'ordre de 2, 1 ou 2, 2 suivant l'intensité de l'onde).

Contrôle expérimental

Les résultats présentés ici sont en accord qualitatif et quantitatif avec les résultats des essais en vol organisés par le CEV lors des expériences Jéricho.

La réflexion des ondes de choc a pu être étudiée en laboratoire (tube à choc); par contre, les tentatives d'étude expérimentale de la réfraction en atmosphère inhomogène d'ondes échelon, délicate à mener, n'ont pas été jusqu'ici très concluantes.

Nous remercions MM. GUIRAUD, AURIOL, WECKEN pour l'aide qu'il nous ont apportée dans ce travail.

BIBLIOGRAPHIE

[1] WHITHAM G.B. — The flow pattern of a supersonic projectile Comm. pure and applied Math vol. 5 n°3 pp 301-348) (1952)

[2] RAO — Supersonic bangs. Parts I and II. Aero. Quart. Vol. 7 Part. I pp 21-44. Part. II pp 135-155 (1956)

[3] FRIEDMAN KANE SIGALLA — Effects of atmosphere and aircraft motions on the location and intensity of a sonic boom. AIAA Vol. 6 p. 1327 (1963)

[4] J.P. GUIRAUD — Acoustique géométrique, bruit balistique des avions supersoniques et focalisation. Journal de mécanique. Vol. 4 n°2 pp 215-267 (1965)

[5] A. AURIOL J.B. NOYERE C. THERY — Réflexion des ondes de choc de faible intensité. Note ISL T 20/65

[6] A. AURIOL et coll. — Réfraction des ondes de choc aériennes. Parties I, II, III, IV Notes et Notices ISL : T 14/66, T 29/66, T 44/66, N 11/68.

[7] C. THERY C. ROTHEA — Réfraction d'une onde de choc en N de faible intensité dans une atmosphère de révolution : Résultats de calcul. Note ISL : T 48/68.

[8] C. THERY C. LECOMTE F. REGGIANI — Remarques concernant les renforcements du bang des avions supersoniques au voisinage des zones de focalisation. Note ISL T 51/68.

[9] J.C. WANNER — Le bang supersonique. 1er colloque d'aérodynamique appliquée de l'AFITAE (Nov. 64) ou compte rendu du colloque sur le bang des avions supersoniques et leurs effets - Saint-Louis 18-20 octobre 1967. Rapport ISL : 11/67.

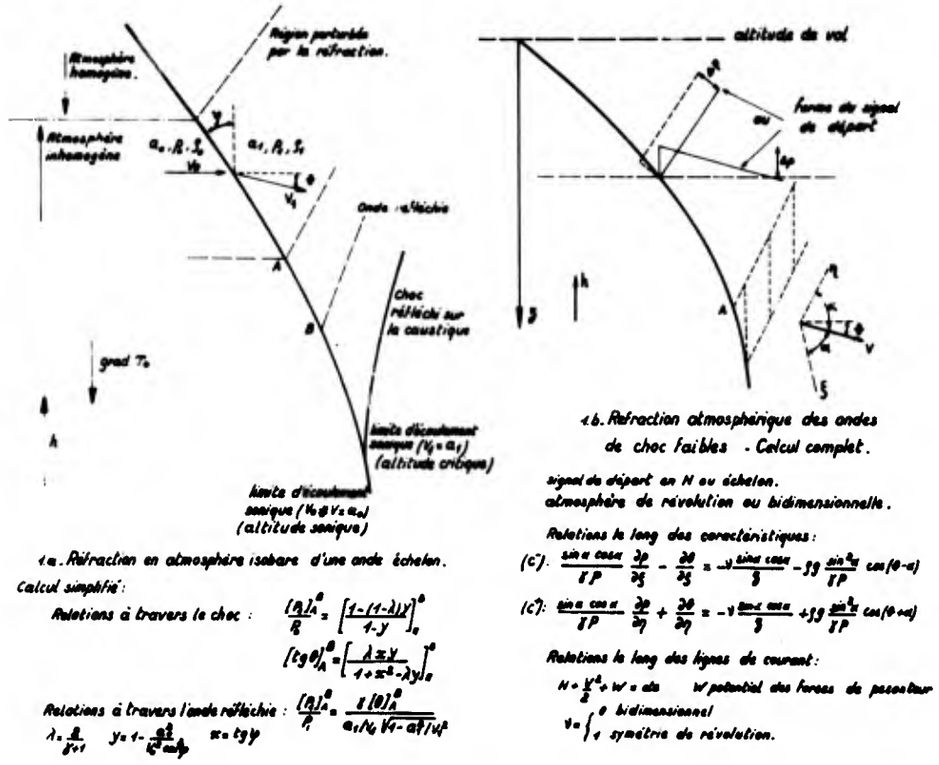

1 a. Réfraction en atmosphère isobare d'une onde échelon.
Calcul simplifié :
Relations à travers le choc :
Relations à travers l'onde réfléchie :

1 b. Réfraction atmosphérique des ondes de choc faibles - Calcul complet.

Figure 1 — Principe des méthodes d'étude de la réfraction employées

1 a : Méthode simplifiée
1 b : Méthode complète (atmosphère bidimensionnelle ou de révolution avec ou sans pesanteur).

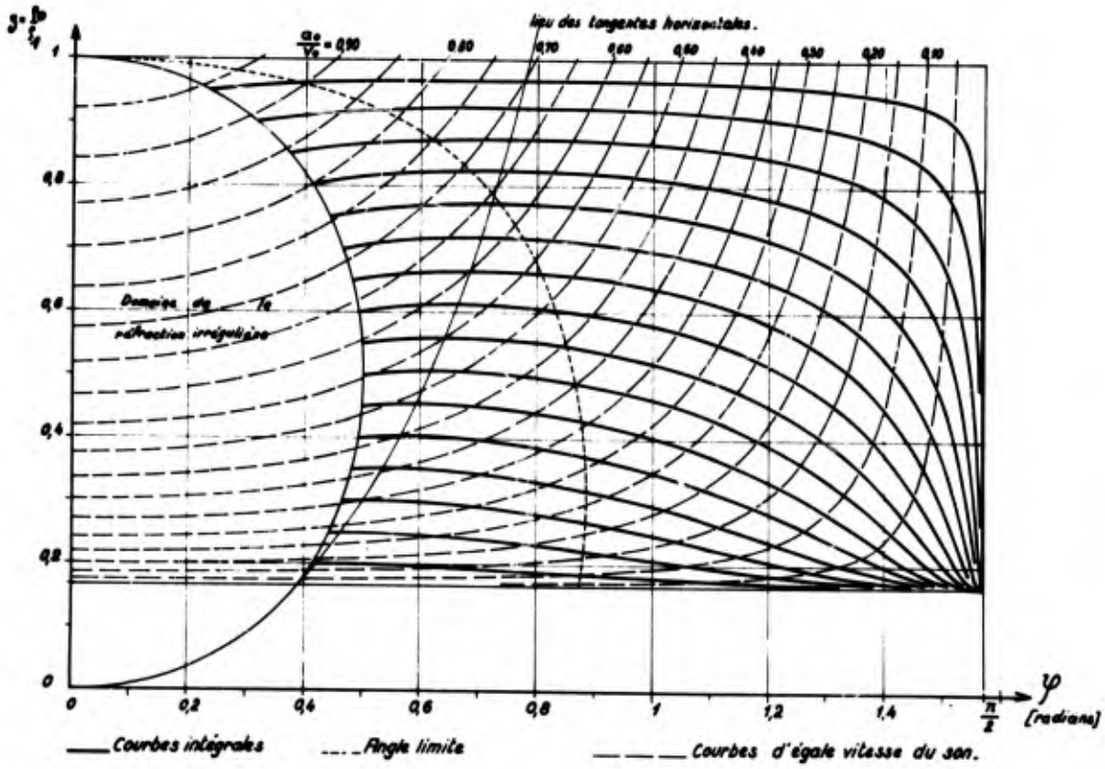

Figure 2 — Réfraction d'une onde échelon - atmosphère isobare : Solution générale de l'équation (1) $\left(z = \frac{\rho_0}{\rho_1} = 1 - \lambda y\right)$.

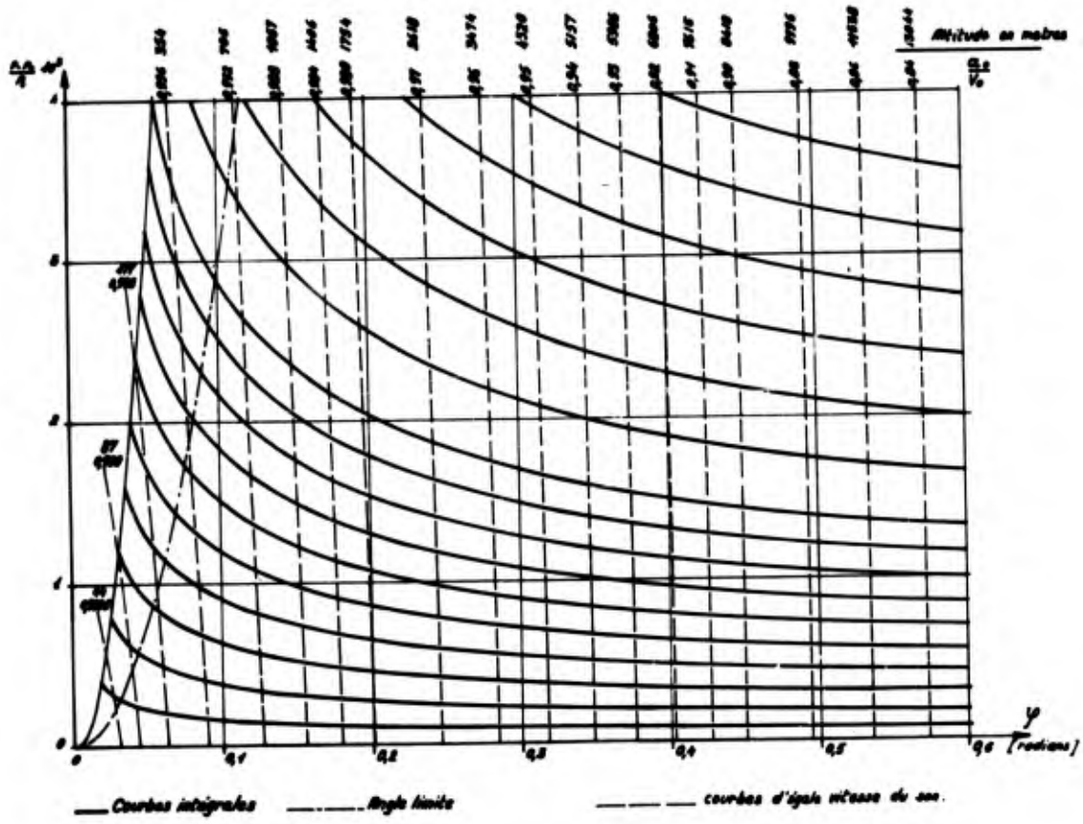

Figure 3 Réfraction d'une onde échelon - atmosphère isobare : Solution de l'équation (1) pour les ondes de faible intensité.
Les altitudes repérées correspondent à $V_o = a_{sol}$ et à la loi de température de l'atmosphère standard.

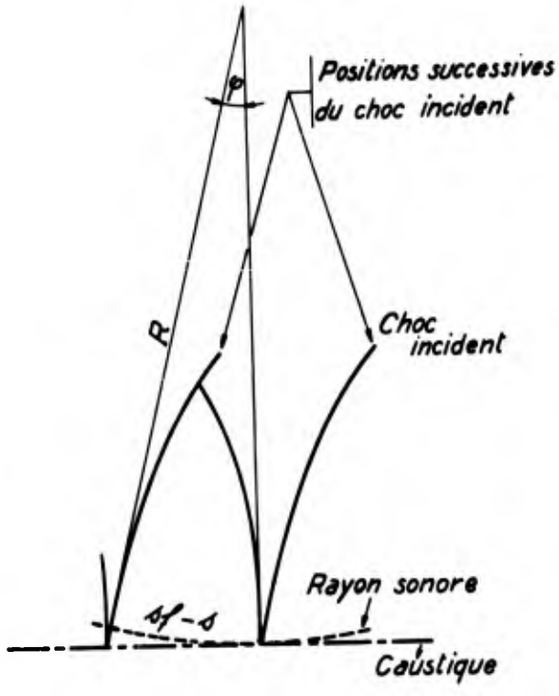

Figure 4 Acoustique géométrique : Relation entre courbure du rayon sonore et co-incidence.

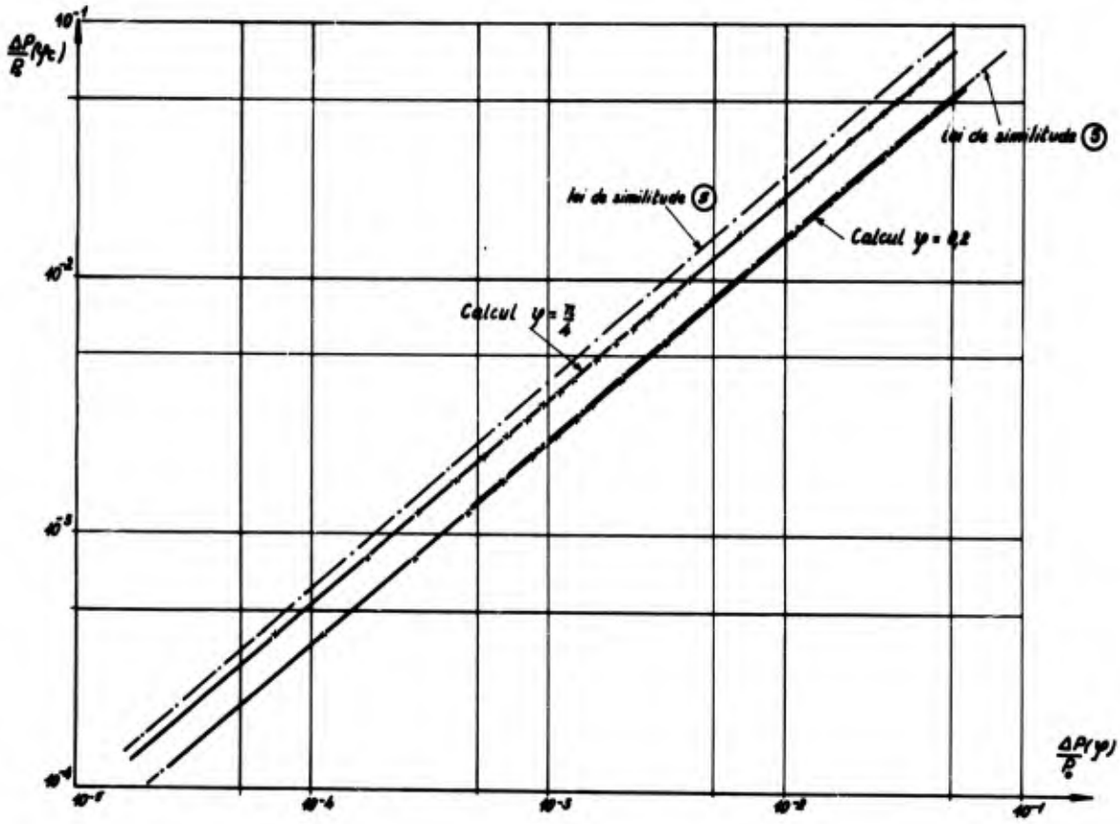

Figure 5 Réfraction d'une onde échelon -atmosphère isobare : Evolution de la surpression critique en fonction de la surpression assez loin des conditions de focalisation; comparaison avec la loi de similitude (5).

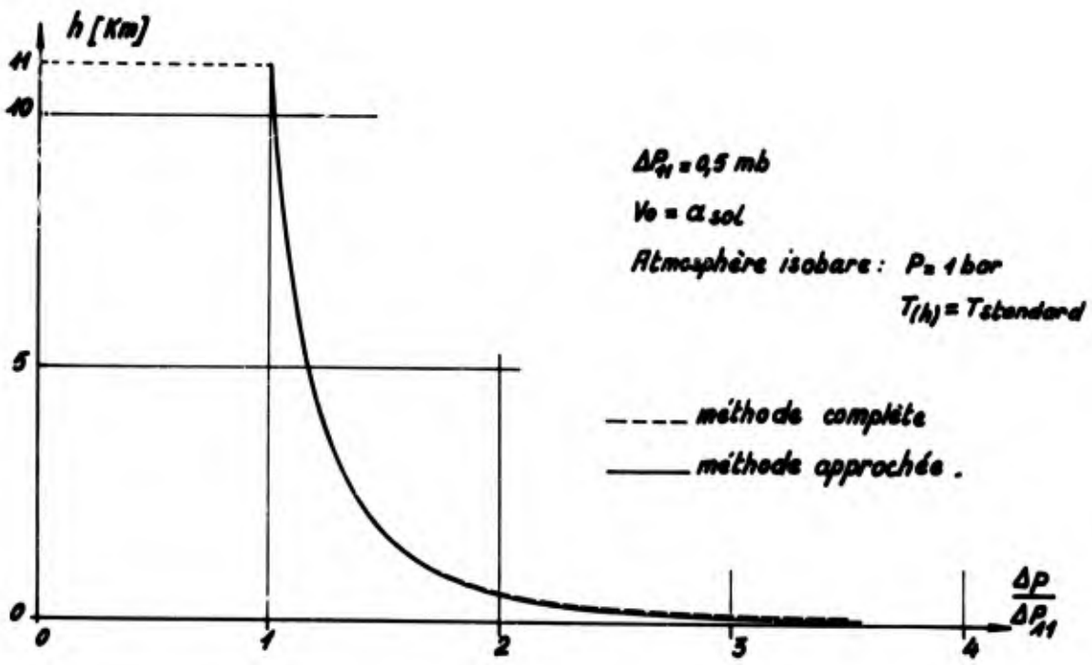

Figure 6 Réfraction d'une onde échelon -atmosphère isobare
Comparaison entre méthodes approchée et complète.

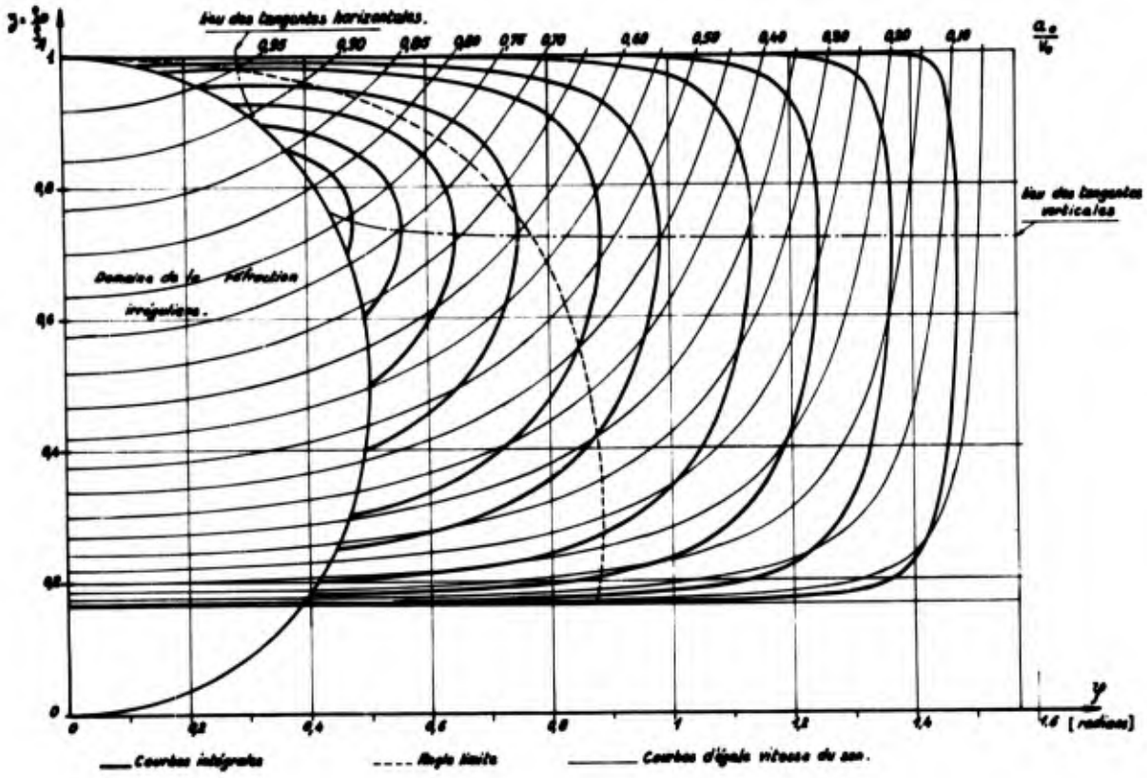

Figure 7 Réfraction d'une onde échelon - atmosphère pesante : solution générale pour une atmosphère standard.

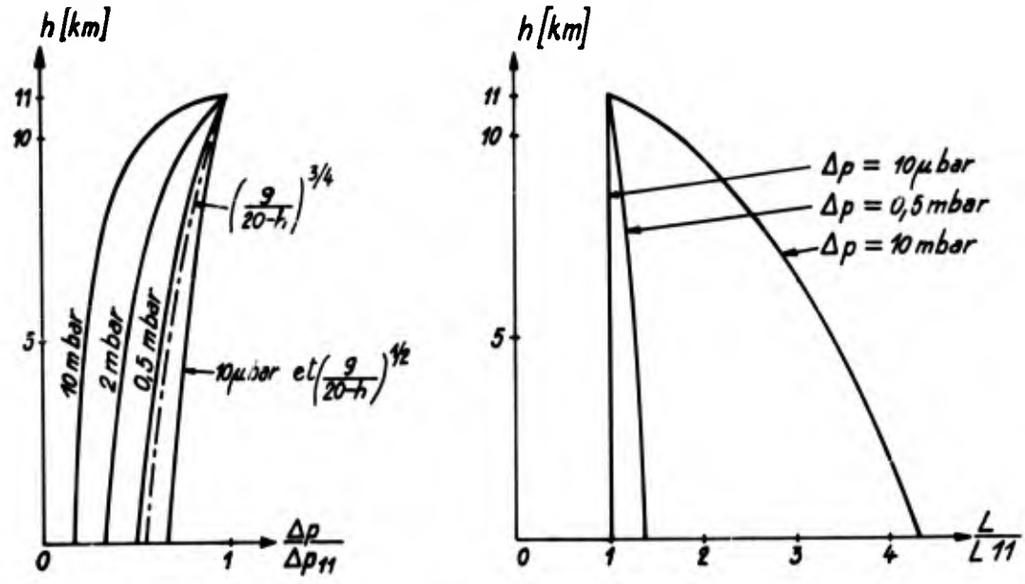

Evolution de l'intensité et de la demi-longueur d'onde du N avec l'altitude
Atmosphère homogène

Figure 8 Onde en N - atmosphère de révolution
Réfraction en atmosphère homogène
Evolution de l'intensité et de la 1/2 longueur d'onde de l'onde avec l'altitude
$p = p_{std}\ (h = 11000)$, $T = T_{std}\ (h = 11000)$, $M = 1{,}15$ et $2{,}30$.

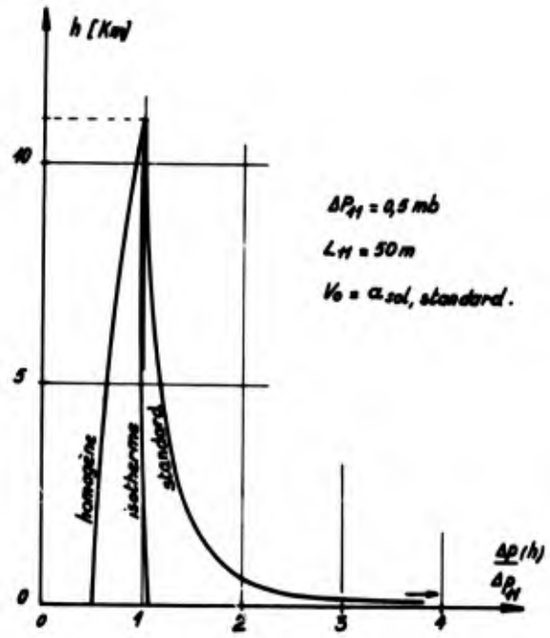

Figure 9 — Onde en N - atmosphère de révolution
Réfraction dans des atmosphères homogène, isotherme, standard : Comparaison entre l'évolution des intensités.
Atmosphère homogène $p = p_{std}$ $(h = 11000)$, $T = T_{std}$ $(h = 11000)$
Atmosphère isotherme $p(h) = p_{std}$, $T = T_{std}$ $(h = 11000)$.

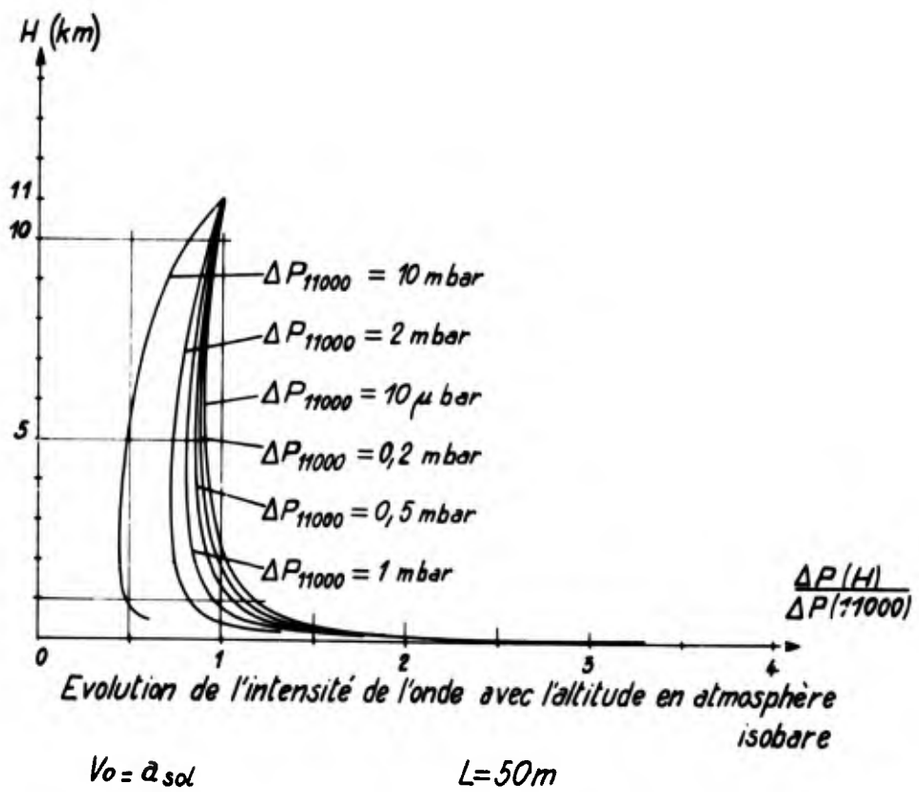

Figure 10 — Onde en N - atmosphère de révolution
Réfraction dans une atmosphère isobare
Evolution de l'intensité de l'onde avec l'altitude pour diverses intensités de l'onde incidente.
P = 1 bar; $T(h) = T_{std}$.

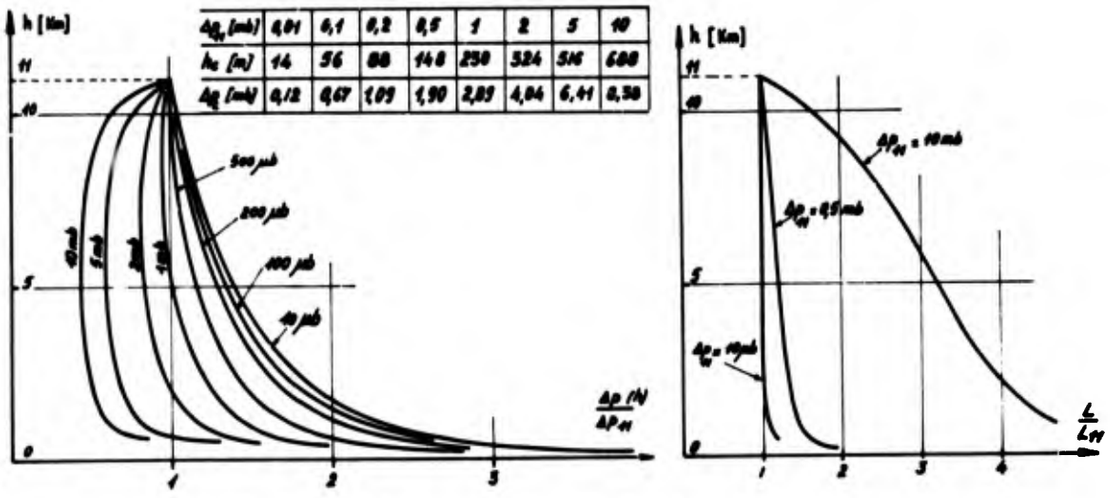

Δp_M [mb]	0,01	0,1	0,2	0,5	1	2	5	10
h_M [m]	14	56	88	148	230	324	516	688
Δp [mb]	0,12	0,67	1,09	1,90	2,89	4,84	6,41	8,38

Evolution de l'intensité et de la demi-longueur d'onde du N avec l'altitude. Atmosphère standard.

L_M : demi longueur d'onde du N à 11000 m: 69 m. $\nu_0 = a_{sol}$

Figure 11 — Onde en N - atmosphère de révolution
Réfraction dans une atmosphère standard
Evolution de l'intensité de l'onde et de la demi-longueur d'onde avec l'altitude.

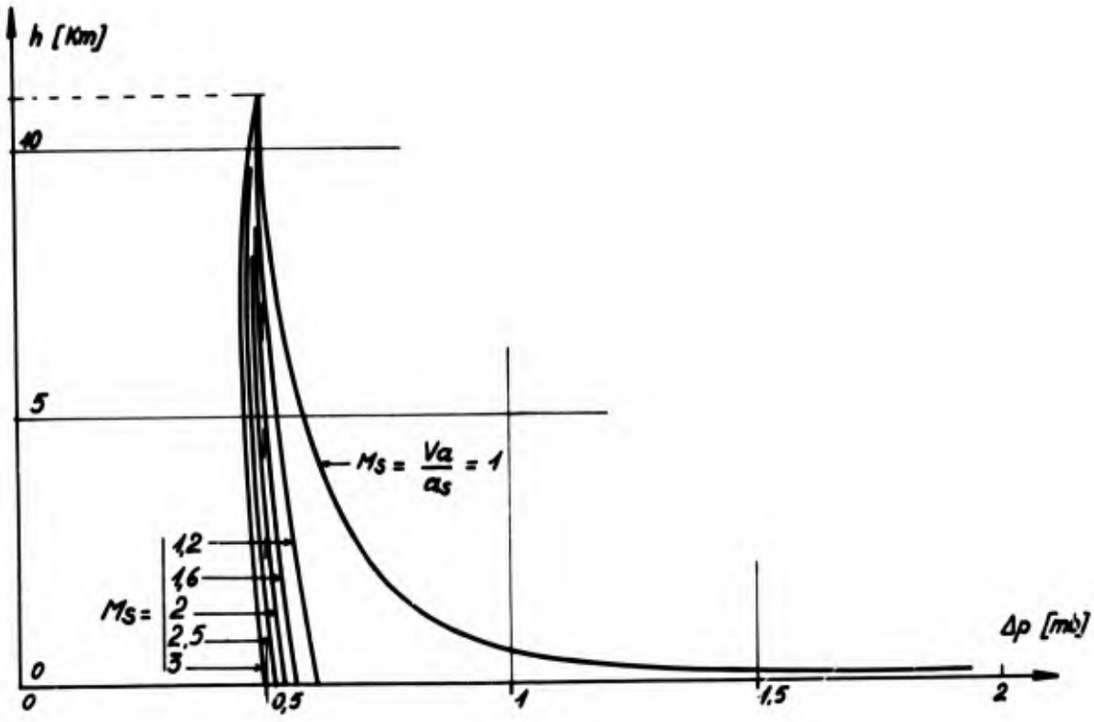

Intensité à 11000 m : Δp = 0,5 mb. *Atmosphère standard.*
demi-longueur d'onde à 11000 m : 50 m.

Figure 12 — Onde en N - atmosphère de révolution
Réfraction dans une atmosphère standard
Evolution de l'intensité de l'onde avec l'altitude pour diverses incidences de l'onde.

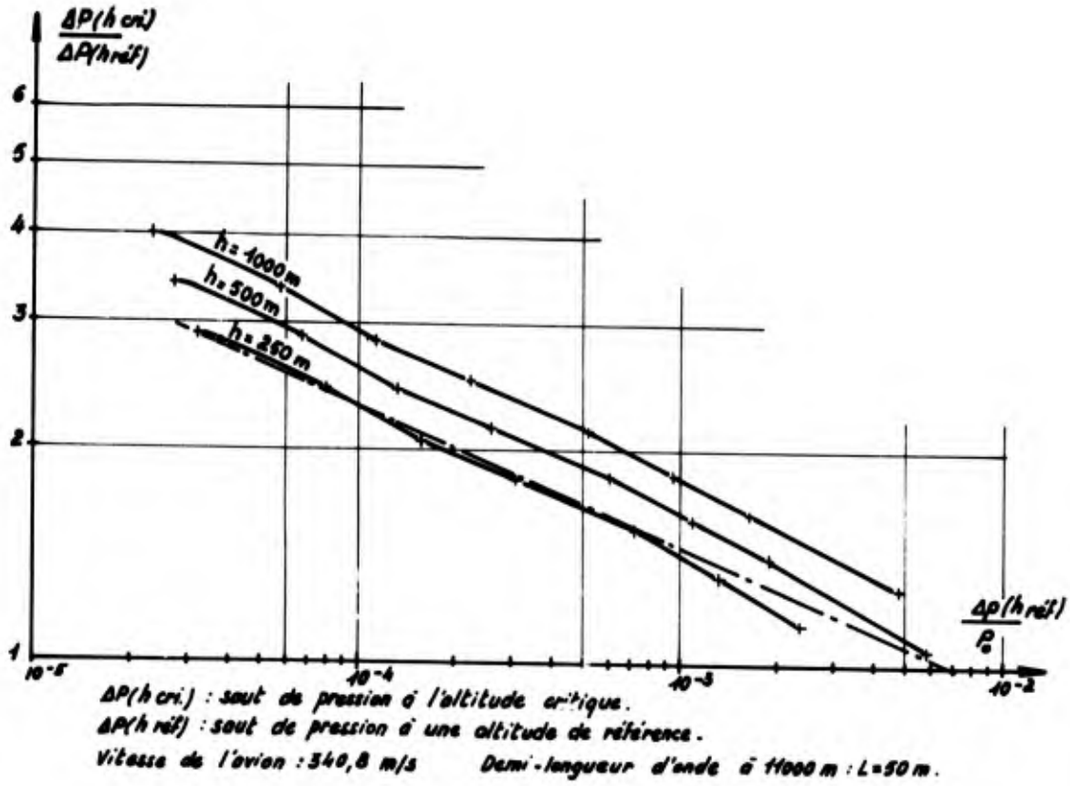

Figure 13 Onde en N - atmosphère de révolution
- Réfraction dans une atmosphère isobare
- Comparaison entre intensités à l'altitude critique calculée et prévue par (5).

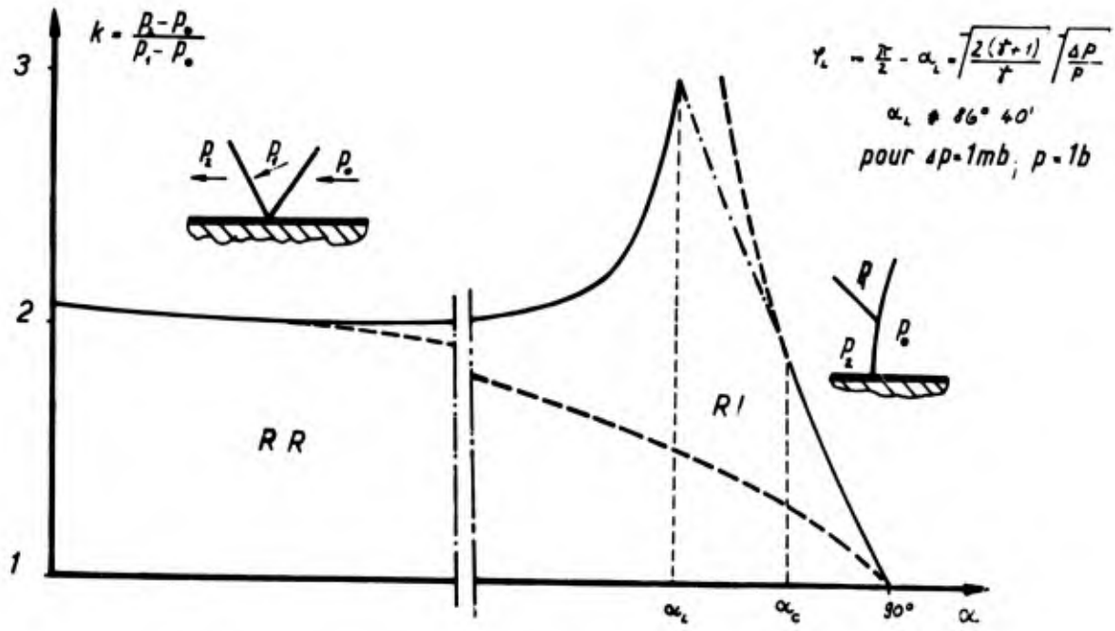

Figure 14 Réflexion des ondes de choc de faible intensité
Allure générale de la variation du coefficient de réflexion avec l'incidence.

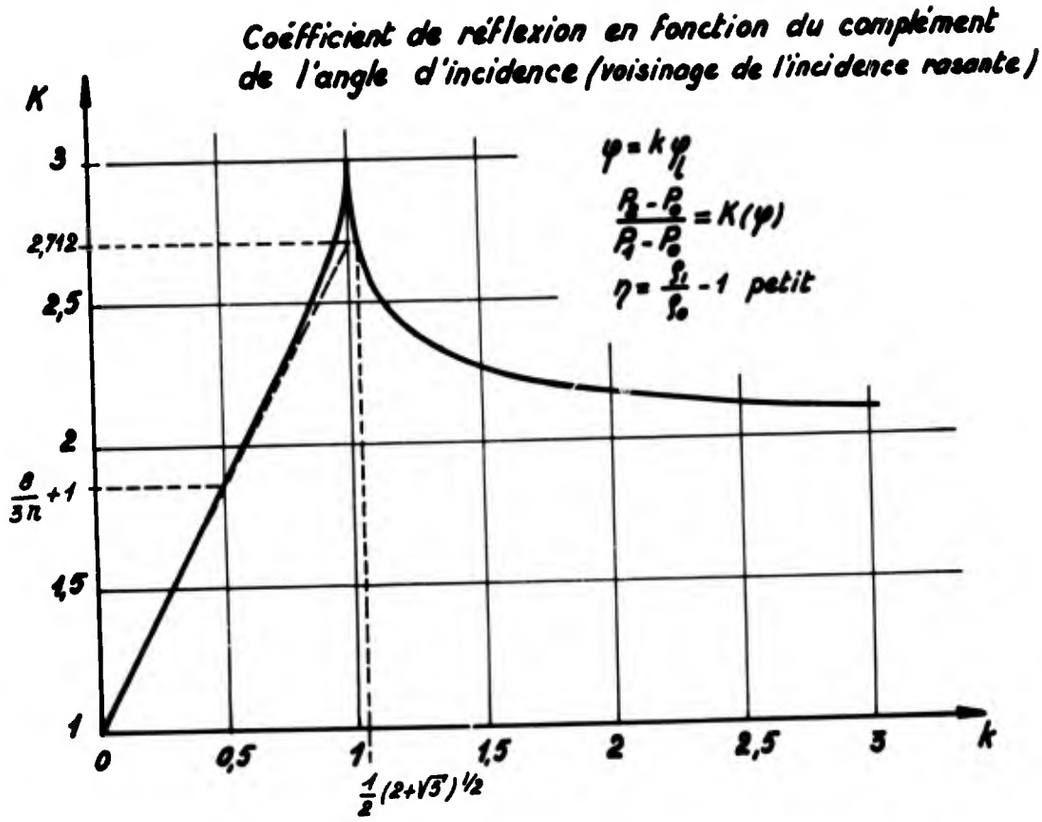

Figure 15 Réflexion des ondes de choc de faible intensité
Variation du coefficient de réflexion avec l'incidence
pour les incidences presque rasantes.

ESSAIS MIRAGE IV

par

M. I. C. Wanner

Service Technique de l'Aeronautique
Paris, France

BLANK PAGE

- ESSAIS MIRAGE IV -

1. OBJECTIF POURSUIVI.

On peut maintenant considérer que nos connaissances, tant théoriques qu'expérimentales, en matière de bang produit par un avion en vol rectiligne uniforme sont suffisantes pour permettre une bonne prévision du phénomène ; il reste bien entendu à préciser la nature et le mode d'action des différents paramètres influant sur la dispersion, statistiquement connue, des résultats.

Il n'en va pas de même pour les différents cas de focalisation provoqués par les évolutions de l'avion. Les théories se révèlent encore incapables de prévoir l'amplitude absolue de phénomène et la faible étendue des zones intéressées en rend l'étude expérimentale difficile.

Le Groupe de Travail chargé de l'étude du bang en tant que phénomène physique (propagation et amplitude), composé de représentants du Centre d'Essais en Vol et du Service Technique Aéronautique a donc décidé d'orienter les recherches expérimentales sur le phénomène de focalisation tout en faisant poursuivre les études théoriques à l'ONERA et à l'Institut Franco Allemand de St Louis.

2. METHODES ET MOYENS D'ESSAI - PROGRAMME.

La zone intéressée par le phénomène étant étroite et sa position étant délicate à prévoir, une zone de mesure la plus grande possible avec des points de mesure les plus serrés possible est hautement désirable. Il faut noter que la zone de focalisation se détermine facilement en théorie lorsque l'on connait les caractéristiques de la trajectoire et celles de l'atmosphère. Sur le plan pratique apparaissent très rapidement deux difficultés :

a) Il est très difficile de connaître correctement l'atmosphère à l'instant de l'essai et dans tout le volume intéressé par la propagation de la nappe de choc venant focaliser au sol.

b) Même en admettant connue parfaitement l'atmosphère et calculée en conséquence la trajectoire conduisant à la focalisation sur la zone de mesure, il est difficile de guider l'avion de façon à respecter cette trajectoire (position et vitesse) avec une précision suffisante.

D'un autre côté la zone intéressée par le phénomène est étroite, de l'ordre de grandeur de l'épaisseur de la nappe de choc elle-même (en ce qui concerne la focalisation proprement dite : il y a donc intérêt à serrer au maximum les points de mesure.)

Le nombre total de points de mesure étant nécessairement limité, un compromis s'impose entre l'étendue de la zone de mesure et l'écartement des points de mesure.

Nous avons donc été conduit à la solution suivante : un axe de 3 km constitué par une ligne de 28 microphones et deux zones de contrôle à 1,5 km de chaque extrémité de l'axe. La figure 1 montre la disposition retenue et donne les principales caractéristiques du matériel utilisé.

L'objectif essentiel de l'OPERATION JERICHO-VIRAGE était de mesurer le coefficient d'amplification en focalisation par virage au cours de vols spéciaux qui correspondaient à une utilisation normale des avions militaires mais dont les résultats pouvaient être en principe extrapolables aux avions civils supersoniques (altitudes voisines de 36.000 ft). Cette condition de focalisation conduit en effet à un phénomène de focalisation qui se déplace en suivant la trajectoire de l'avion ; il est donc relativement facile de faire couper l'axe de mesure par cette ligne de focalisation, ce qui explique que l'on ait retenu cette méthode en priorité.

.../...

Comme il était de toute façon nécessaire de faire une accélération transonique avant les essais en virage, nous avons également tenté de capter ce type de focalisation bien que la technique de guidage soit plus délicate (la partie de trajectoire intéressée se situe, pour une accélération à 36000 ft, à 35 km environ, en avant de l'axe de mesure).

3. RESULTATS OBTENUS POUR LES FOCALISATIONS EN ACCELERATION RECTILIGNE.

3.1. La figure 2 rappelle la façon dont naît la nappe de choc au cours de l'accélération rectiligne de l'avion : au cours des essais nous nous sommes efforcés de placer la pseudo-parabole, lieu des points de focalisation, de telle sorte que son axe soit confondu avec l'axe de mesure et que son sommet soit situé dans l'intervalle de 3 km réservé aux mesures.

La figure 3 donne un exemple type d'enregistrement du phénomène sur les 28 microphones de l'axe de mesure. La focalisation proprement dite s'est produite au voisinage du premier micro de l'axe (micro n°11) (les micros numérotés de 1 à 10 sont les micros BK placés au milieu de l'axe). On peut y distinguer les formes caractéristiques de la signature dans les quatre cas intéressant :

- la focalisation proprement dite (ou du moins en un point très proche de la focalisation) (micro 11)
- le début de séparation des deux nappes avant et arrière : la signature est alors très voisine d'une addition des signatures des nappes avant et arrière (micros 12 à 19),
- l'onde avant dont la signature est le N classique,
- l'onde arrière dont la signature présente une certaine analogie avec celle d'un signal en N après filtrage des basses fréquences (ce filtrage n'est pas dû à la chaîne de mesure puisque le N de l'onde avant est enregistré correctement).

Sur cette planche qui permet d'étudier la séparation des deux ondes, ne figure pas le cinquième cas intéressant c'est-à-dire la forme du signal avant la focalisation. En avant du point de focalisation, il n'y a pas à proprement parler de "bang" : les perturbations émises par l'avion parviennent au sol dans l'ordre de leur émission et par conséquent ne forment pas d'onde de choc ; néanmoins, la vitesse de l'avion dans la zone d'émission est très proche de la vitesse du son et les perturbations parviennent au sol très groupées ; la signature en avant du point de focalisation ne présente donc pas de front raide et sa forme est d'allure sinusoïdale sans "saut" ni variation brutale de pente. Il n'empêche que ce signal se traduit pour les observateurs par un bruit que l'oreille ne parvient pas en général à distinguer du véritable bang. Ce phénomène a été gênant au cours des essais car les observateurs répartis sur le terrain pour faciliter le "réglage du tir" se sont révélés incapables de se situer par rapport à la focalisation.

La figure 4 résume ces diverses formes de la signature en situant les microphones par rapport à la ligne de focalisation. L'origine des temps de l'enregistrement correspondant à chaque micro est décalée de façon à aligner tous les signaux en N de l'onde avant.

Ce décalage est très généralement nécessaire (surtout dans le cas de la focalisation par accélération rectiligne où les ondes de choc se déplacent dans le sens de l'axe) ; sur la figure 3, on peut constater par exemple que l'axe a été balayé en un peu moins de 9 secondes, alors que la "largeur" de la signature est de l'ordre de 0,15 s. Sur la plupart des figures qui suivent, nous avons donc effectué ce décalage : nous ne le signalerons plus.

3.2. Ces différentes formes de signature se retrouvent dans la plupart des enregistrements. Nous avons pu néanmoins observer quelques phénomènes particuliers comme par exemple celui donné figure 5. Dans la zone de séparation des deux nappes avant et arrière après focalisation, on constate une deuxième focalisation sur la nappe avant identifiée par la forme caractéristique de la signature d'une part et par la séparation d'une deuxième nappe auxiliaire d'autre part. Cette deuxième focalisation peut être due soit à un effet atmosphérique (le profil du vent étant assez perturbé), soit à une courbure de la trajectoire dans le plan vertical (la tenue d'altitude fut assez mauvaise dans la zone où était engendrée la nappe focalisant sur l'axe).

.../...

Au cours de l'expérimentation JERICHO-FOCALISATION (1966) où furent étudiés les phénomènes de focalisation en accélération rectiligne à basse altitude (2000 ft) on a pu également observer des signatures de focalisation différentes de celles rencontrées au cours de JERICHO-VIRAGE.

Sur la figure 6 on peut constater une focalisation du front arrière de la nappe focalisante deux cents mètres environ avant la focalisation du front avant. On observera également sur cette figure la forme du signal en avant de la zone de focalisation. L'amplitude de la pointe de focalisation est de 25 millibars environ (50 psf) (n'oublions pas que nous sommes à très basse altitude). Le signal avant la focalisation a une amplitude maximale de l'ordre de 5 millibars (10 psf) : ce n'est pas un "bang" mais les observateurs sont bien incapables de distinguer ce signal d'un bang réel ! La focalisation séparée des fronts avant et arrières de l'onde peut s'expliquer par le fait que les deux caustiques correspondant aux nappes avant et arrière sont décalée dans les deux cas (haute et basse altitudes) et que, de plus, en champ proche, les deux caustiques ne sont pas parallèles : la focalisation se produit en effet à basse altitude à un nombre de Mach voisin de 1.
Une illustration très approximative de ce phénomène est donnée en fig. 7.

Bien que, dans les 2 expérimentations citées, l'avion utilisé était différent (Mirage III à basse altitude), il est intéressant de comparer également la forme des signatures dans les deux cas d'accélération haute et basse altitudes. Indépendamment des amplitudes on peut constater (voir figure 8) que la pointe de surpression est beaucoup plus aigue dans le cas basse altitude (les deux enregistrements ont été effectués avec les mêmes types de capteur). Cette différence de forme de signature est générale (du moins pour les quelques cas, de l'ordre d'une dizaine, dans chaque expérimentation). A cette occasion on peut se demander si le coefficient d'amplification défini comme il est précisé plus loin (cf paragraphe 3.3.) et dans lequel intervient l'amplitude maximale du signal, est vraiment significatif.

3.3. Quels ont été dans ces conditions les résultats obtenus en ce qui concerne le coefficient d'amplification ?
Il nous faut tout d'abord définir le coefficient d'amplification.

Soit ΔP_f la valeur maximale de la surpression mesurée au point de focalisation. L'élément d'onde de choc, arrivant au point de focalisation F, a été engendré lorsque l'avion passait en un point P avec un vecteur vitesse $\vec{V}$. Soit ΔP_{ref} la valeur maximale de la surpression que l'on aurait pu mesurer au même point F pour un élément de choc émis au même point P, par le même avion animé d'un mouvement rectiligne uniforme à vitesse $\vec{V}$ ayant traversé la même atmosphère. Le coefficient d'amplification est alors :

$$f = \frac{\Delta P_f}{\Delta P_{ref}}$$

Les mesures effectuées au cours des essais nous fournissent l'évolution du ΔP le long de l'axe de mesure. La figure 9 donne ces résultats pour deux cas de focalisation l'un à basse altitude (600 m) l'autre à haute altitude (11000)

La valeur maximale observée n'est pas ΔP_f car la focalisation proprement dite a beaucoup de chance de se produire entre deux points de mesure (éloignés de 100 m) : l'essai nous fournit donc une estimation par défaut de ΔP_f.

D'un autre côté la valeur moyenne des ΔP mesurés après la focalisation (dans la partie de l'axe de mesure où ΔP est sensiblement constant) fournit une bonne approximation de ΔP_{ref} ; en toute rigueur le bang arrivant 1 km environ après la focalisation n'a pas été émis au nombre de Mach de focalisation, mais à un Mach très légèrement supérieur ; les écarts qui en résultent sont de toute façon négligeables devant la dispersion des mesures dues en particulier aux effets atmosphériques.

Dans ces conditions les valeurs maximales de ΔP_f rencontrées au cours des essais JERICHO-FOCALISATION et JERICHO-VIRAGE ont été :

- Vol basse altitude - 600 m (≠ 2000 ft) - accélération 3 m/s2 (≠ 9 ft/s2)
  ΔP_f = 28 mb (≠ 56 psf)

.../...

- Vol haute altitude - 11000 m (≠ 36000 ft) - accélération 1 m/s2 (≠ 3 ft/s2)
  ΔP_f = 3,3 mb (≠ 6,6 Psf)

Les valeurs de ΔP_{ref} correspondant à ces deux cas de vol étant respectivement de 5,5 mb (11 Psf) et 0,65 mb (≠ 1,2 Psf) les coefficients d'amplification sont dans les deux cas voisins de 5.

Au cours des douze focalisations réussies à basse altitude et des cinq focalisations réussies à haute altitude nous avons mesuré des valeurs de ΔP_f inférieures aux valeurs données ci-dessus. Il serait cependant illusoire de prendre la moyenne de ces résultats pour obtenir une évaluation du coefficient d'amplification ; n'oublions pas en effet que les valeurs de ΔP_f mesurées ne sont que des estimations par défaut de ΔP_f réel (focalisation entre deux points de mesure).

Nous retiendrons donc une valeur voisine de 5 comme coefficient d'amplification.

Il nous faut noter enfin que la théorie de Guiraud conduit à des valeurs de f voisines dans les deux cas étudiés (basse altitude grande accélération et haute altitude faible accélération).

4. RESULTATS OBTENUS POUR LES FOCALISATIONS EN VIRAGE.

4.1. La figure 10 rappelle la forme de la trace au sol de la nappe de choc lors d'un virage permanent. Le point de rebroussement de la Trace, c'est-à-dire le point de focalisation, décrit un cercle de même centre que la trajectoire mais de rayon plus faible. Sur la figure 11, nous donnons la forme de la trace au sol de la nappe de choc au cours de l'évolution en palier constituée par une ligne droite et un virage circulaire. A l'instant q1 aucune des trois branches de la trace ne coupe l'axe de mesure. A l'instant q2, les nappes 1 - 2 et 3 coupent l'axe ; les nappes 2 et 3 ont été émises pendant le virage, leur point commun est le rebroussement de focalisation, la nappe 1 a été émise pendant la partie rectiligne de la trajectoire.

Sur l'axe de mesure on voit donc apparaître successivement :

- un bang normal émis en palier rectiligne
- un bang de focalisation (précédé d'une perturbation qui n'est pas un choc mais une évolution rapide et continue de la pression comme dans le cas de la focalisation en accélération). Ce bang se dédouble (nappes 2 et 3).
- dans certains cas on peut observer le croisement des deux nappes 2 et 1.

Au cours de nos expériences, la trajectoire avion était située de telle sorte par rapport à l'axe de mesure que nous n'avons pas observé le rebroussement entre les nappes 1 et 3, rebroussement provoqué par la mise en virage elle-même.

4.2. La figure 12 donne un exemple de focalisation avec séparation des deux nappes 2 et 3. La tangente au rebroussement est sensiblement parallèle à l'axe de mesure si bien que tous les microphones sont atteints par la nappe avant presque au même instant (on remarquera que nous n'avons pas eu à décaler les origines des temps pour chacun des enregistrements).

La figure 13 donne une vue d'ensemble du phénomène tel que nous l'avons décrit ci-dessus : focalisation, séparation des deux bangs (nappes 2 et 3), bang de palier rectiligne (nappe 1), et en bas à gauche intersection des nappes 1 et 2 entre les microphones 25 et 27.

Ces deux cas représentent une bonne illustration de la théorie, les signatures sont régulières et l'on retrouve les caractéristiques habituelles des divers cas : focalisation, nappe avant, nappe arrière ; la signature du bang émis en trajectoire rectiligne est assez affaiblie car nous sommes sur la partie latérale de la nappe non loin du point de coupure.

4.3. Nous avons par contre rencontré un certain nombre de phénomènes de distorsion des signatures qu'une analyse plus fine des résultats peut attribuer soit à des perturbations atmosphériques soit à des évolutions de l'avion autour de la trajectoire idéale. A titre d'exemple on peut obeerver sur la figure 14 une amplification importante de la signature de la nappe

.../...

avant sur le micro 8 (ceci n'est sûrement pas dû à la mesure car l'on peut voir apparaître et disparaître le phénomène sur les micros voisins en ce qui concerne la nappe avant, alors que les enregistrements de la nappe arrière montrent une constance très nette de l'amplitude). La signature sur le micro 8 ressemble à une signature de focalisation mais l'on n'observe pas la séparation d'une nappe arrière auxiliaire comme c'était le cas figure 5.

Sur la figure 15 nous avons donné l'exemple de signatures très perturbées, en avant de la focalisation (micro 24) on observe une perturbation de pression très tourmentée avec des discontinuités qui ressemblent bien à des chocs ; en outre la séparation des deux nappes est très perturbée. Sur le micro 28 où les deux nappes sont séparées déjà de 0,30 s environ on ne voit aucun retour au zéro de la surpression. Nous avons joint les courbes d'évolution de la température du vent (en grandeur et direction) ainsi qu'un état de la nébulosité. Il est évident que l'atmosphère était loin d'être calme ce jour-là (variation de 20 m/s sur la force du vent et changement de 90° de sa direction entre le sol et l'altitude de vol) ; ces altérations de la signature sont sans doute à attribuer à cet état de l'atmosphère.

4.4. Pour les 27 cas enregistrés, obtenus au cours de vols dans des conditions de trajectoire très voisines (même rayon de virage, facteur de charge voisin de 2 et nombre de Mach constant voisin de 1,7) nous avons obtenu les résultats suivants :

Pour ΔP_{ref} nous avons pris la valeur 0,85 mb ($\neq$ 1,7 Psf) correspondant d'une part à la moyenne des valeurs hors focalisation et d'autre part à la valeur moyenne des mesures effectuées par ailleurs en vol rectiligne à même Mach, cette valeur est également celle fournie par la théorie de Whitham.

Dans ces conditions la valeur maximale mesurée de f est de 5,1, la valeur minimale de 1,40 (2 valeurs entre 4 et 5 ; 5 valeurs entre 3 et 4 ; 9 valeurs entre 2 et 3 ; 10 valeurs entre 1, 4 et 2).

Compte tenu des remarques faites déjà au sujet de la mesure de ΔP_f, nous pouvons en déduire ici encore que le coefficient d'amplification f est de l'ordre de 5.

5. VERIFICATION DE LA THEORIE DE PROPAGATION.

Les calculs de la propagation ont été effectués en se basant sur la loi de réfraction des rayons caractéristiques en atmosphère avec vent

$$\frac{a}{\cos\varphi} + V_v = C^{te}$$

où a est la vitesse du son à l'altitude Z, φ l'angle de la normale à la surface d'onde à l'altitude de Z, Vv la composante de la vitesse du vent sur le plan vertical tangent au rayon caractéristique au point d'émission. Cette formule suppose la propagation acoustique des perturbations (perturbations suffisamment faibles pour que l'atmosphère puisse être considérée comme revenue à son état initial après passage de la perturbation) ; elle suppose d'autre part qu'il n'existe pas de composante verticale du vent (une démonstration de cette formule est donnée dans l'ouvrage cité en référence 6).

Les calculs étaient effectués sur CAB.500 et IBM 1800 avec le programme STROUM mis au point entre STAé et CEV-ISTRES.

Pour chaque cas de focalisation, la trace au sol théorique et la position du point de focalisation ont été calculées, compte tenu de la trajectoire réelle de l'avion en supposant l'atmosphère standard puis en utilisant les sondages de température et de vent effectués à l'occasion de l'essai.

La trajectoire de l'avion était déterminée par poursuite de l'avion au radar Super Cotal. Les grandeur et direction du vent étaient déterminées également au radar Super Cotal par ballon lâché peu de temps avant ou après l'essai. La température était relevée par les enregistreurs de bord de l'avion au cours de la montée à l'altitude d'essai (et recoupement avec les sondages effectués par les services locaux de la Météorologie).

.../...

Les écarts entre les points calculés et les points mesurés (en atmosphère standard et en atmosphère réelle) sont donnés figure 16. Nous avons également joint à ces graphiques les droites de Henry correspondantes qui permettent de déterminer la moyenne et l'écart quadratique moyen des résultats.

Ainsi dans le cas de l'atmosphère standard on obtient une valeur moyenne de l'écart de 280 m avec un σ de 810 m.

Dans le cas de l'atmosphère réelle ces valeurs sont nettement améliorées : valeur moyenne 60 m et σ de 450 m.

Ces résultats sont valables pour les focalisations par virage.

En ce qui concerne les focalisations par accélération rectiligne les résultats sont moins bons ; ceci est dû au fait que les trajectoires suivies par les rayons caractéristiques sont très longues (de l'ordre de 35 km) et que les rayons arrivent au sol sous un angle presque rasant : de faibles écarts sur le vent, la température, le nombre de Mach provoquent de grandes variations du point d'impact au sol.

Les résultats sont les suivants : sur les cinq cas réussis, l'écart minimum entre théorie et expérience est de 200 m, l'écart maximum de 2400 m. Ceci confirme d'ailleurs les difficultés rencontrées pour "placer" la focalisation sur l'axe de mesure.

6. EXPERIMENTATION FUTURE : OPERATION JERICHO-CARTON.

Les deux expérimentations JERICHO-FOCALISATION et JERICHO-VIRAGE ont permis, nous le pensons, de conclure en ce qui concerne le phénomène de focalisation.

Mais le phénomène de focalisation est-il le plus important que l'on risque de rencontrer au cours d'un vol ? L'examen de la figure 11 montre que la mise en virage conduit à la formation de deux rebroussements. Nous n'avons observé, au cours de JERICHO-VIRAGE, que le rebroussement correspondant à la focalisation de virage (rebroussement entre nappes 2 et 3). Tout porte à croire que l'autre rebroussement dû à la mise en virage (entre nappes 1 et 3) ne conduit pas à des coefficients d'amplification différents de ce que nous avons mesuré. Il nous reste cependant à le vérifier. En outre que se passe-t-il lorsque les deux rebroussements sont confondus ou très voisins (naissance de la nappe 3 entre les rebroussements). N'observons nous pas une superfocalisation en ce point ?

L'objectif de l'opération JERICHO-CARTON est donc de répondre à ces deux interrogations. Mais il ne faut pas se cacher la difficulté expérimentale due à la précision nécessaire de la visée : le nom même donné à l'expérimentation résume bien le problème.

7. CONCLUSIONS.

Les expérimentations JERICHO-FOCALISATION et JERICHO-VIRAGE ont permis de montrer que le coefficient d'amplification en focalisation dans les conditions suivantes :

Altitude 600 m (2000 ft) - Accélération rectiligne 3 m/s2 (9 ft/s2)
Altitude 11000 m (36000 ft) - Accélération rectiligne 1 m/s2 (3 ft/s2)
Virage 11000 m (36000 ft) - Mach 1,7 - Facteur de charge 2.

est de l'ordre de 5. Cette valeur est beaucoup plus importante que ce que laissait attendre les premiers résultats expérimentaux obtenus jusqu'à présent.

BIBLIOGRAPHIE

1 - J.P. GUIRAUD - Sur le bruit provoqué au sol par le vol des avionssupersoniques C.R. Académie des Sciences. Paris 253 (1) - 1961 - 67.9

2 - J.P. GUIRAUD - Sur la valeur de l'intensité, au voisinage d'une caustique, du bruit balistique produit par le vol supersonique. C.R. Académie des Sciences. Paris 256 - (8) 18.2.1963 - 1669 - 1671

3 - J.P. GUIRAUD - Remarques sur le bruit balistique au voisinage d'une caustique. La Recherche Aérospatiale - Janvier - Février 1964 - 3.13

4 - J.C. WANNER - Le bang supersonique. Journal de la Société des Ingénieurs de l'Automobile - Août - Septembre 1965 (423-430)

5 - J.C. WANNER - Le bang supersonique. Technique et Sciences Aéronautiques et Spatiales (Association Française des Ingénieurs et Techniciens de l'Aéronautique et de l'Espace) n°6 - 1966.

6 - DE MAISTRE - THERY - VALLEE - VIVIER - WANNER -
- Bang sonique - Théorie et expérimentation du phénomène de focalisation (Association Technique Maritime et Aéronautique - Session 1969).

7 - J. VALLEE - Rapport d'étude C.E.V. n°277 - Etude expérimentale des focalisations de bang sonique engendrées par le vol supersonique en accélération rectiligne ou en virage d'un avion Mirage IV à l'altitude de 11000 m. Opération Jericho-Virage. Mai 1969

8 - J. VALLEE - Rapport d'étude C.E.V. n°272 - Mesure de l'intensité des bangs soniques engendrés par un avion volant en palier accéléré supersonique - Opération Jericho-Focalisation. Octobre 1967

9 - A. AURIOL - C. THERY - J.B. NOYERE -
- Réflexion des ondes de choc de faible intensité - N.T./I.S.L./20/65

10 - A. AURIOL - C. THERY - J.B. NOYERE - C. ROTHEA - LAURENT -
- Réfraction des ondes de choc aériennes - N.T./I.S.L./14/66 - 29/66 - 44/66 - 11/68 -

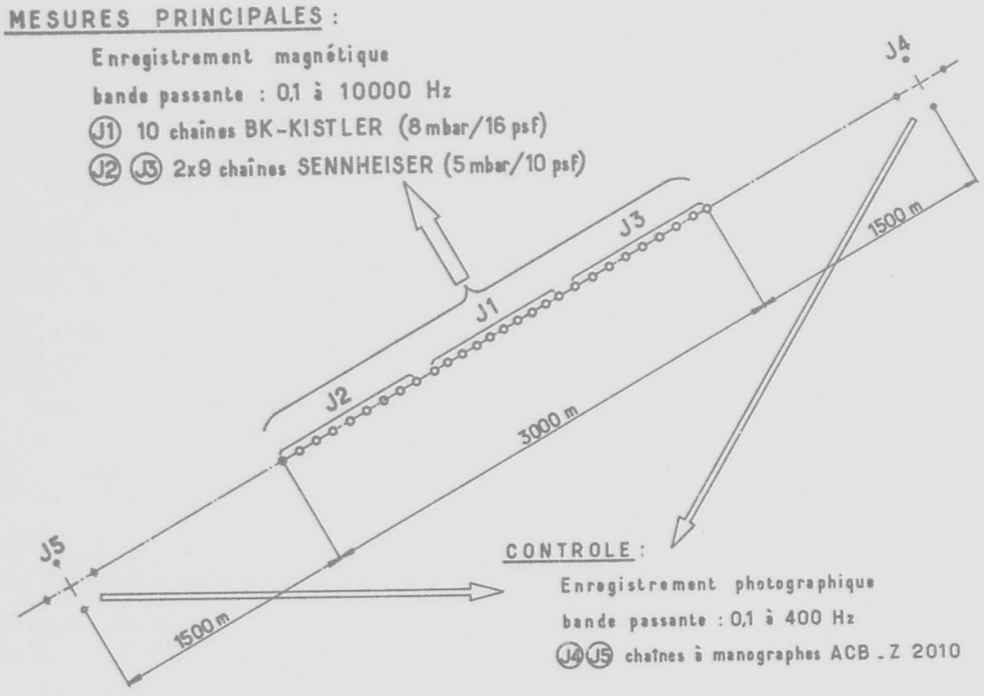

Fig. 1 Schéma d'implantation de l'axe de mesure JERICHO

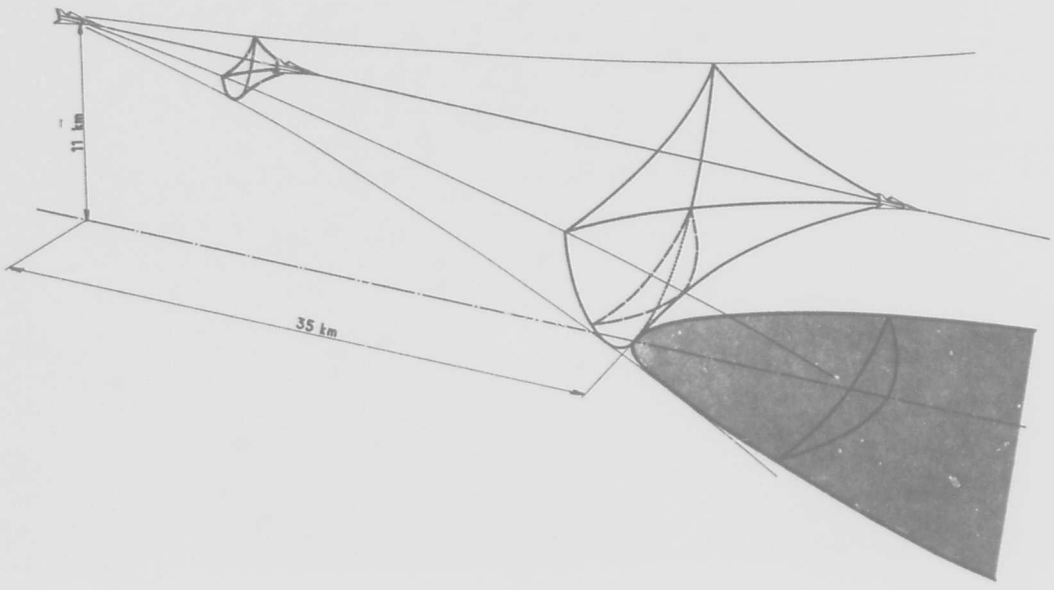

Fig. 2 Focalisation par accélération rectiligne

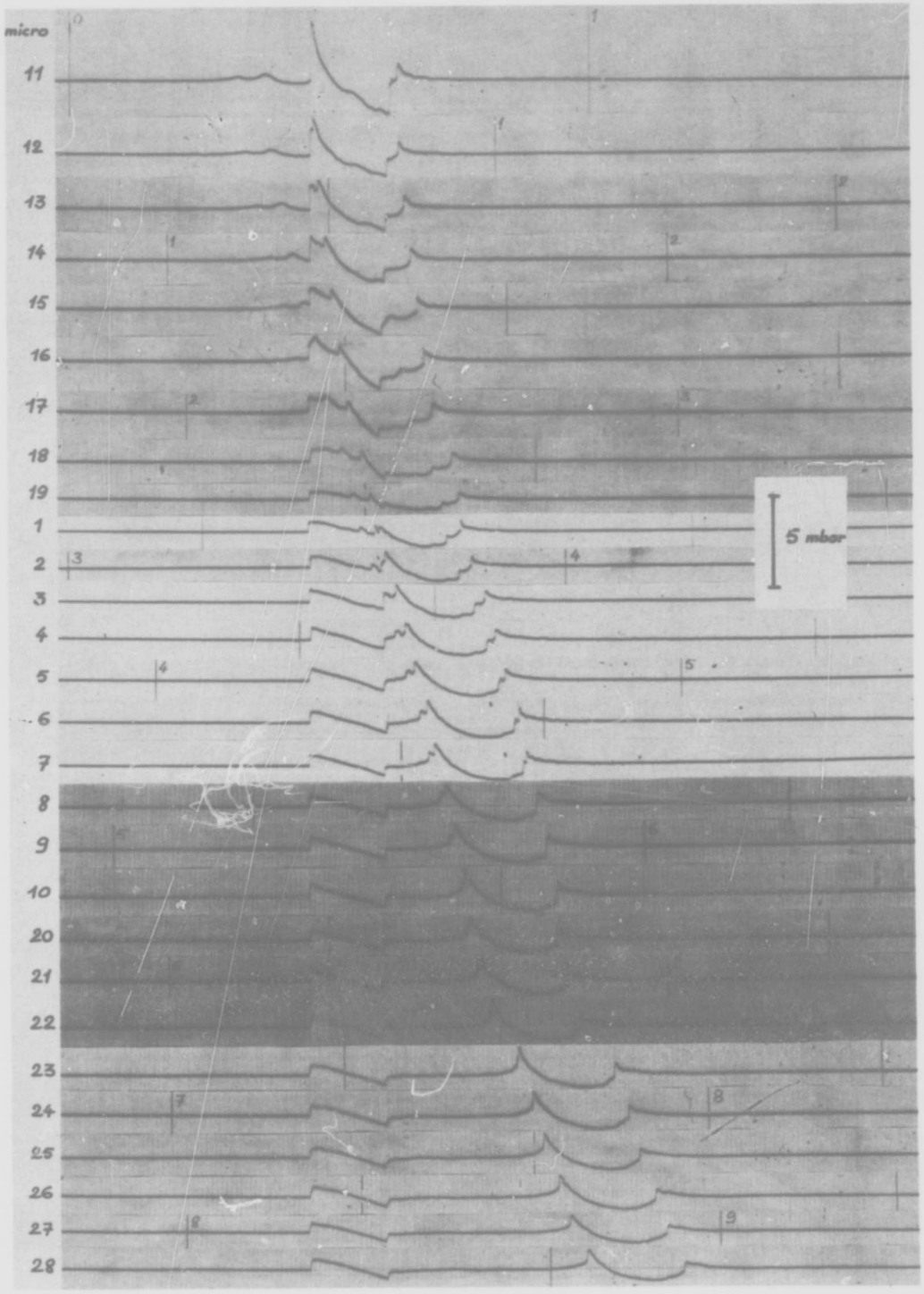

Fig. 3 Exemple d'enregistrement d'une focalisation par accélération rectiligne

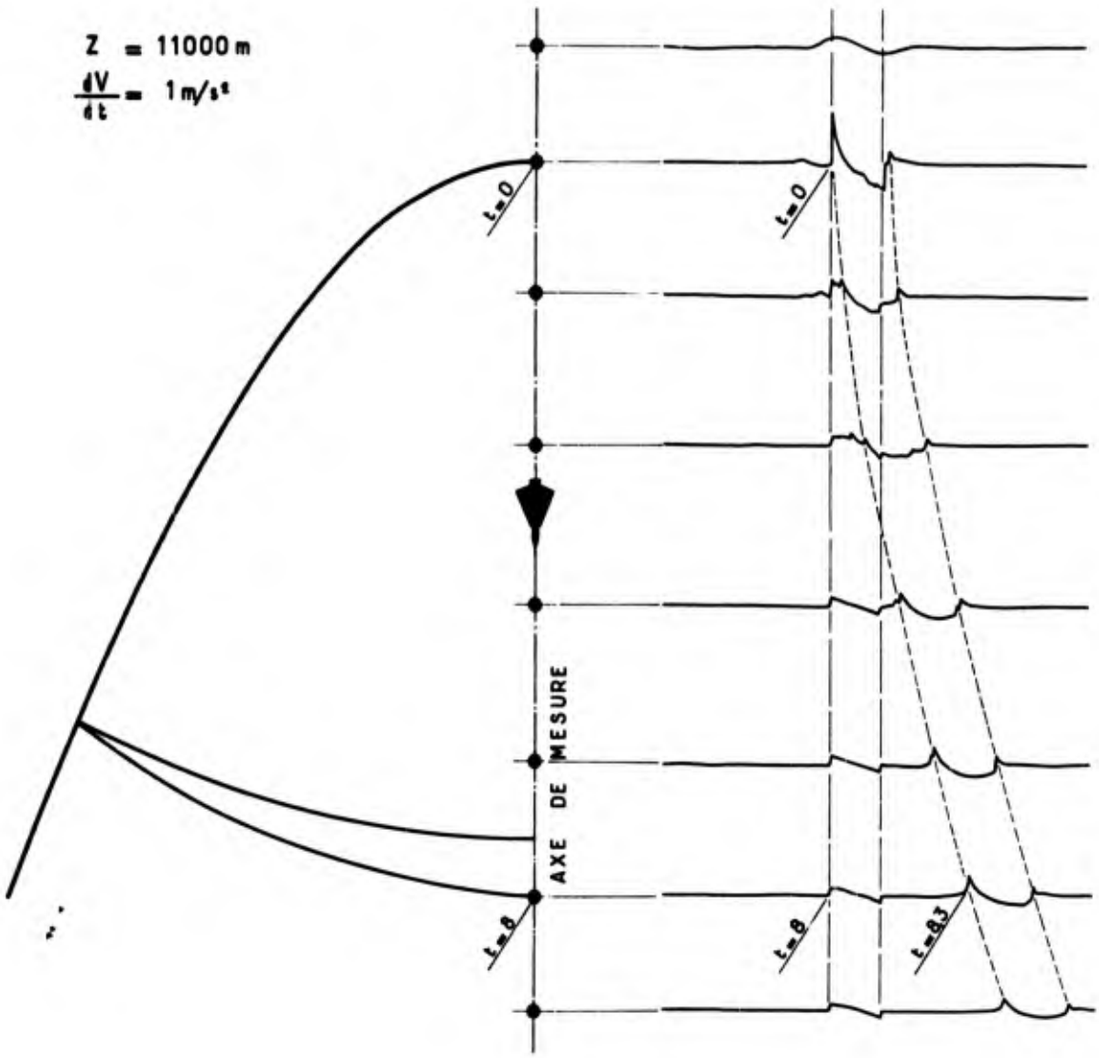

Fig. 4 Enregistrement type d'une focalisation par accélération rectiligne mesurée sous la trajectoire de l'avion

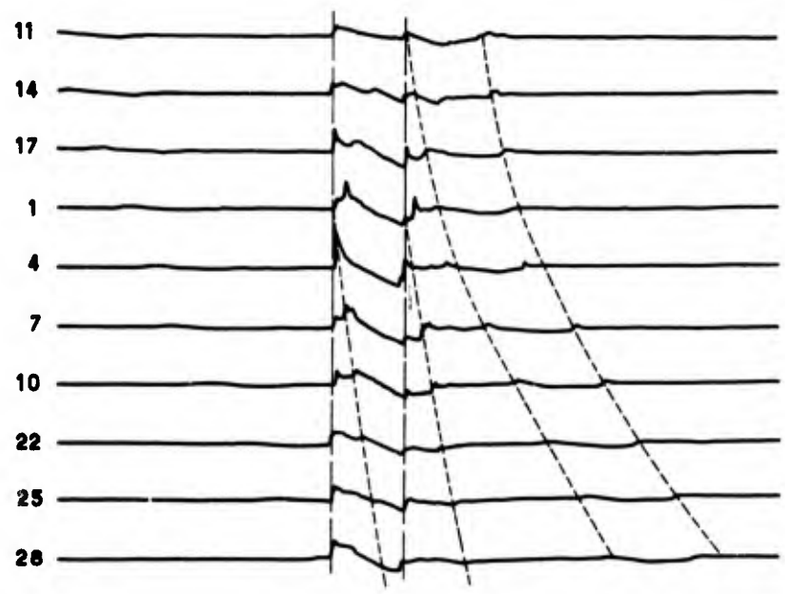

Fig. 5 Cas complexe de focalisation par accélération rectiligne

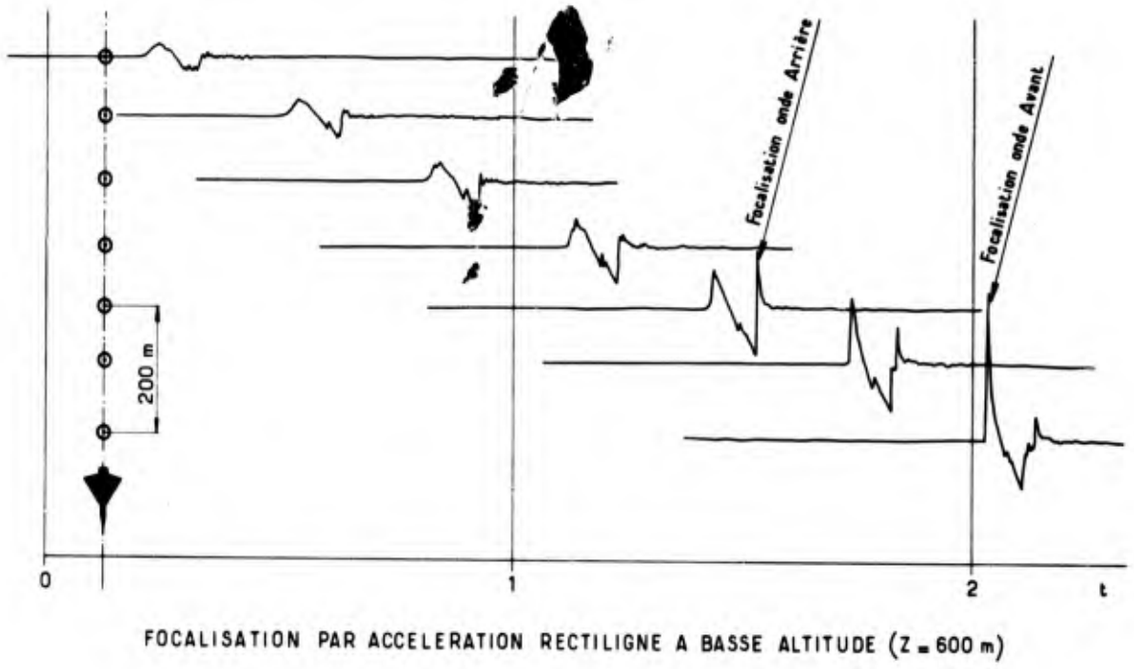

FOCALISATION PAR ACCELERATION RECTILIGNE A BASSE ALTITUDE (Z = 600 m)

Fig. 6 Focalisations distinctes des fronts avant et arrière du bang sonique

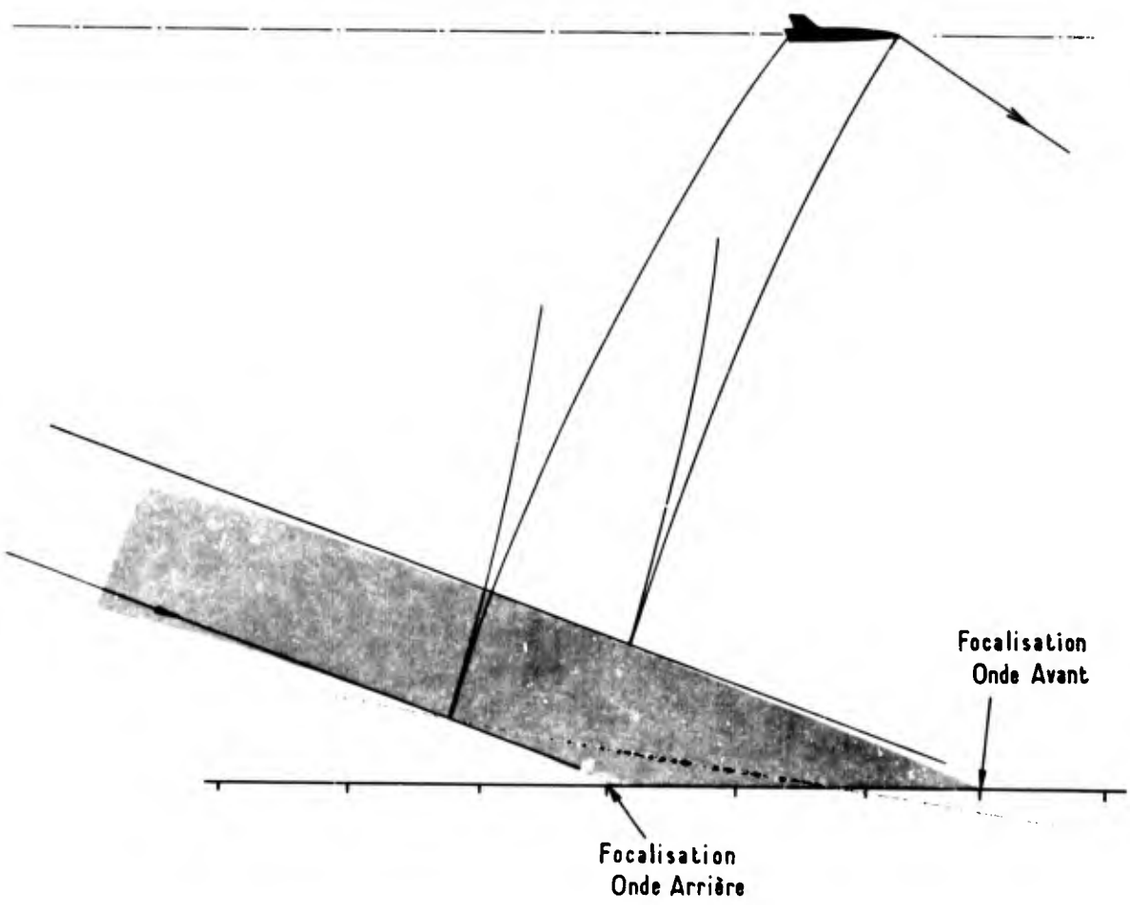

Fig. 7 Caustiques relatives aux fronts avant et arrière

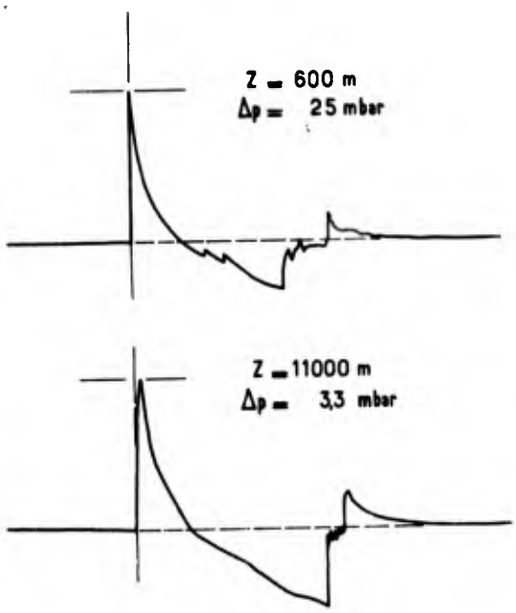

Fig.8 Comparaison des signatures de focalisation par accélération rectiligne à basse et haute altitude

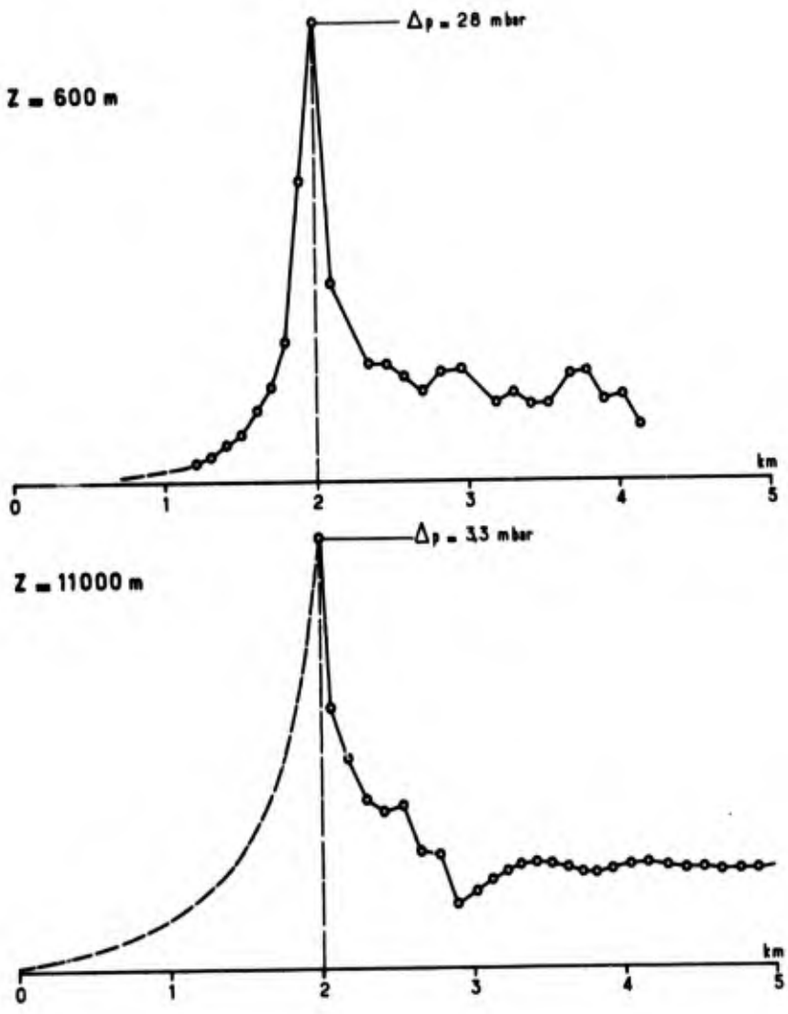

Fig.9 Evolution type du Δp en focalisation par accélération rectiligne sous la trajectoire de l'avion

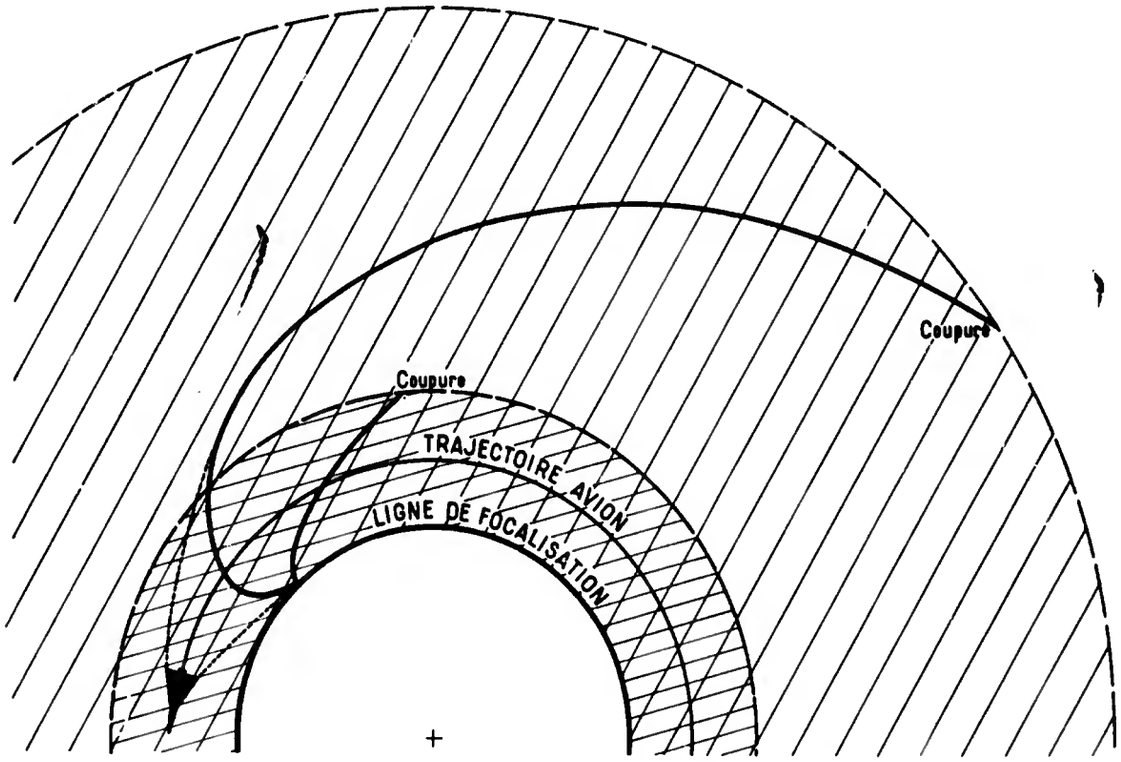

Fig. 10 Focalisation par virage uniforme

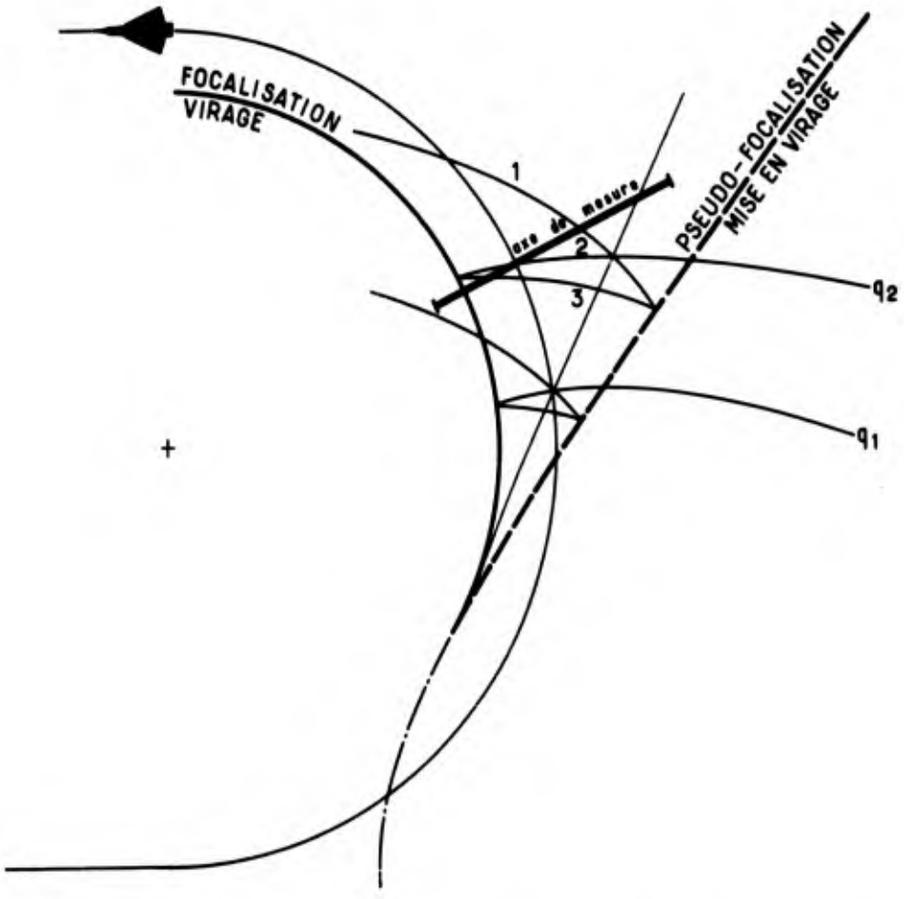

Fig. 11 Focalisation par mise en virage uniforme après une trajectoire rectiligne

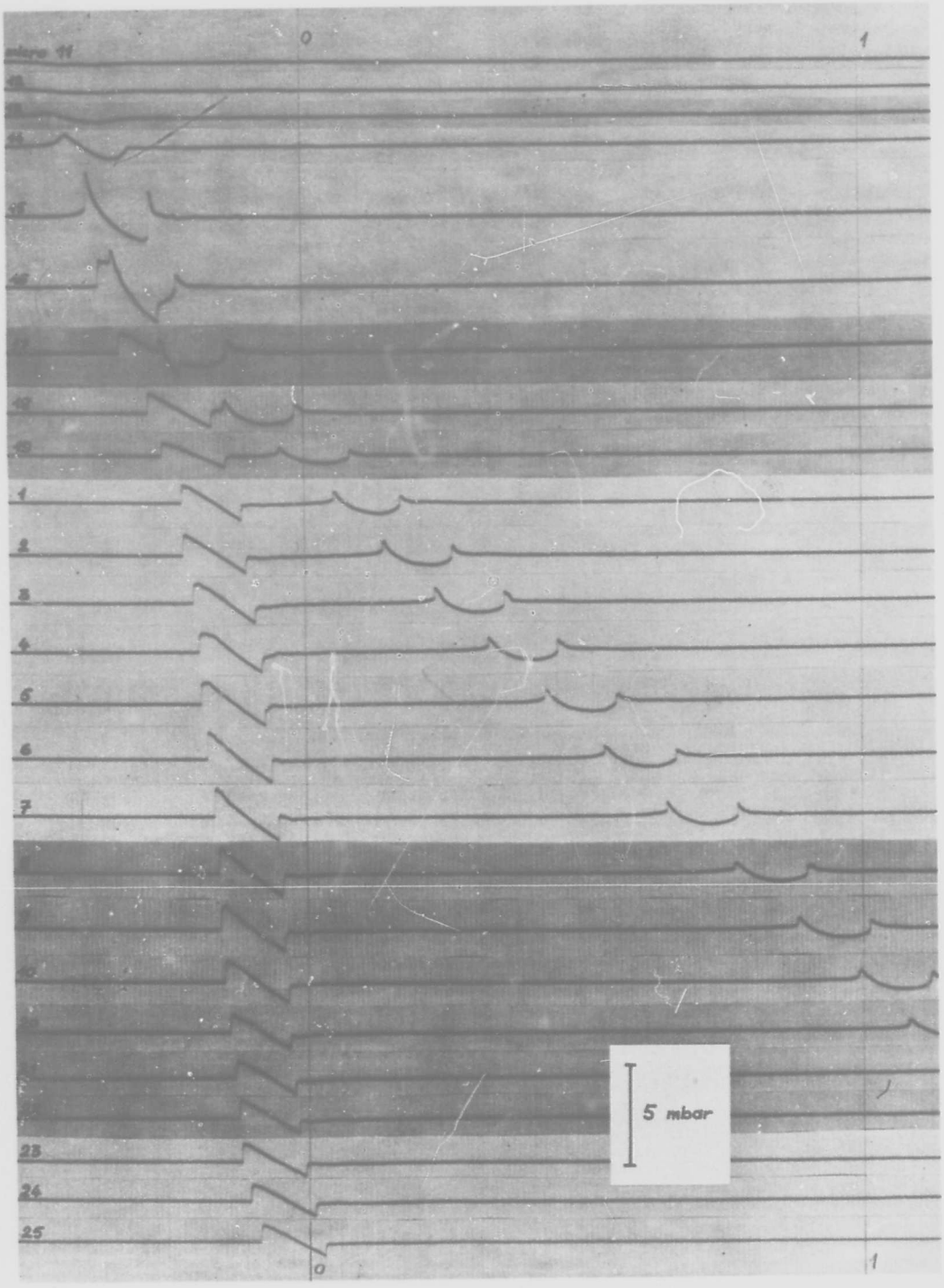

Fig. 12 Exemple type de focalisation par virage

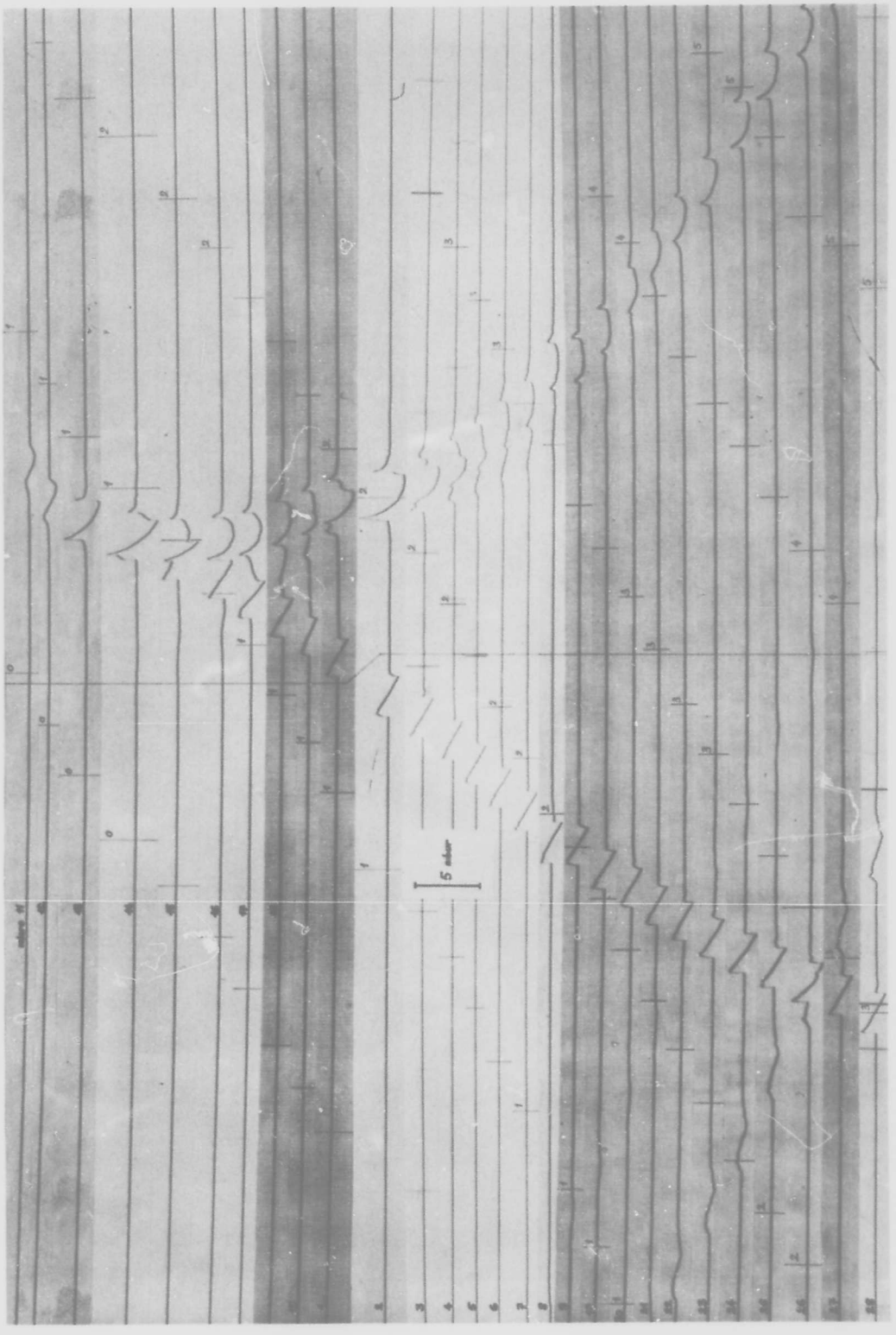

Fig. 13 Passage sur l'axe de mesure des 3 ondes caractéristiques d'une focalisation par mise en virage

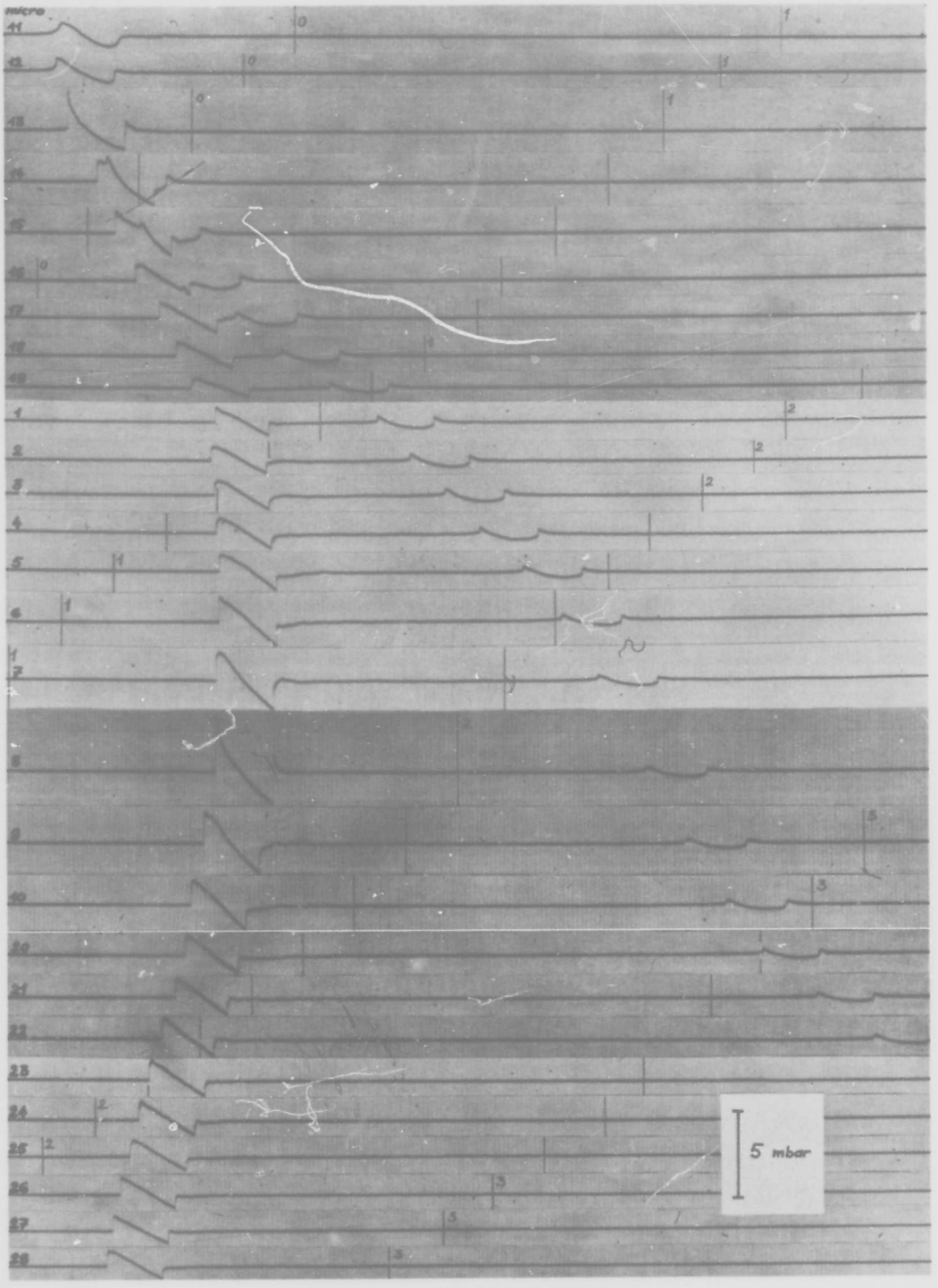

Fig. 14 Amplification parasite de la signature de l'onde avant dans une focalisation par virage

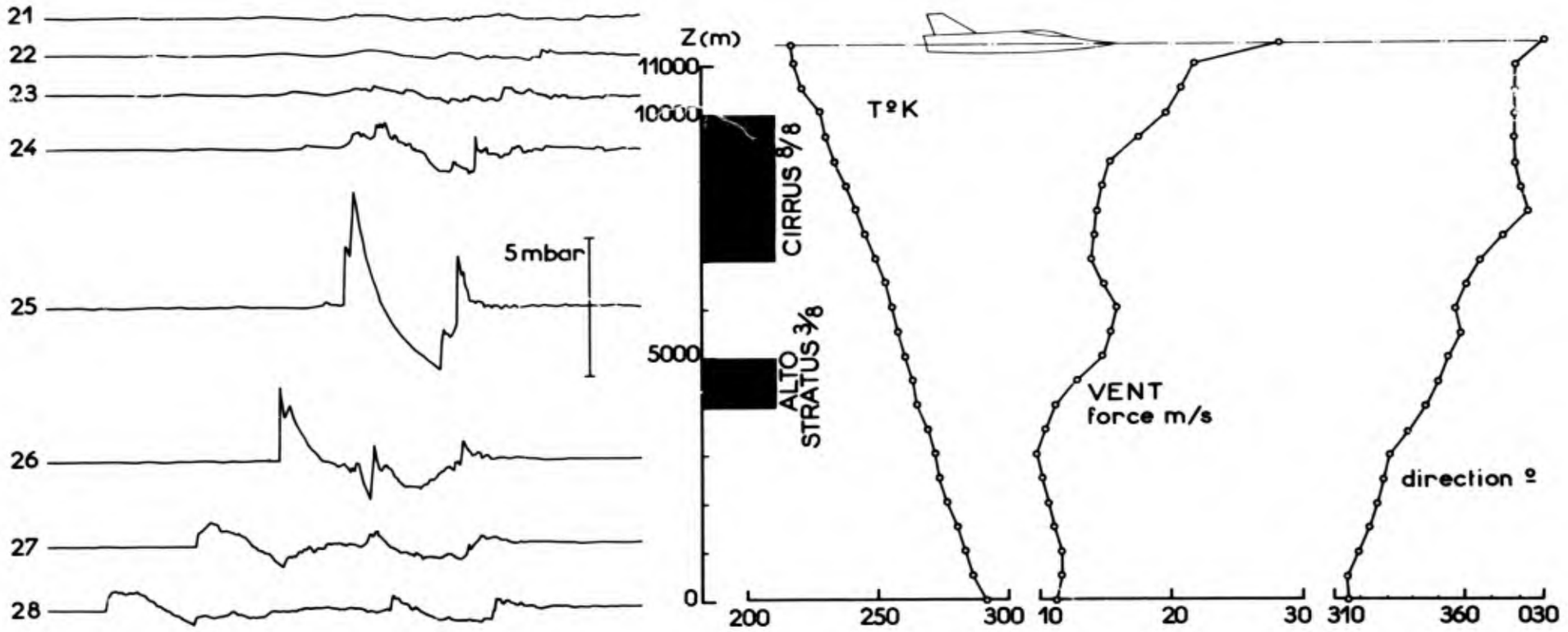

Fig. 15 Effet des perturbations atmosphériques sur les signatures en focalisation par virage

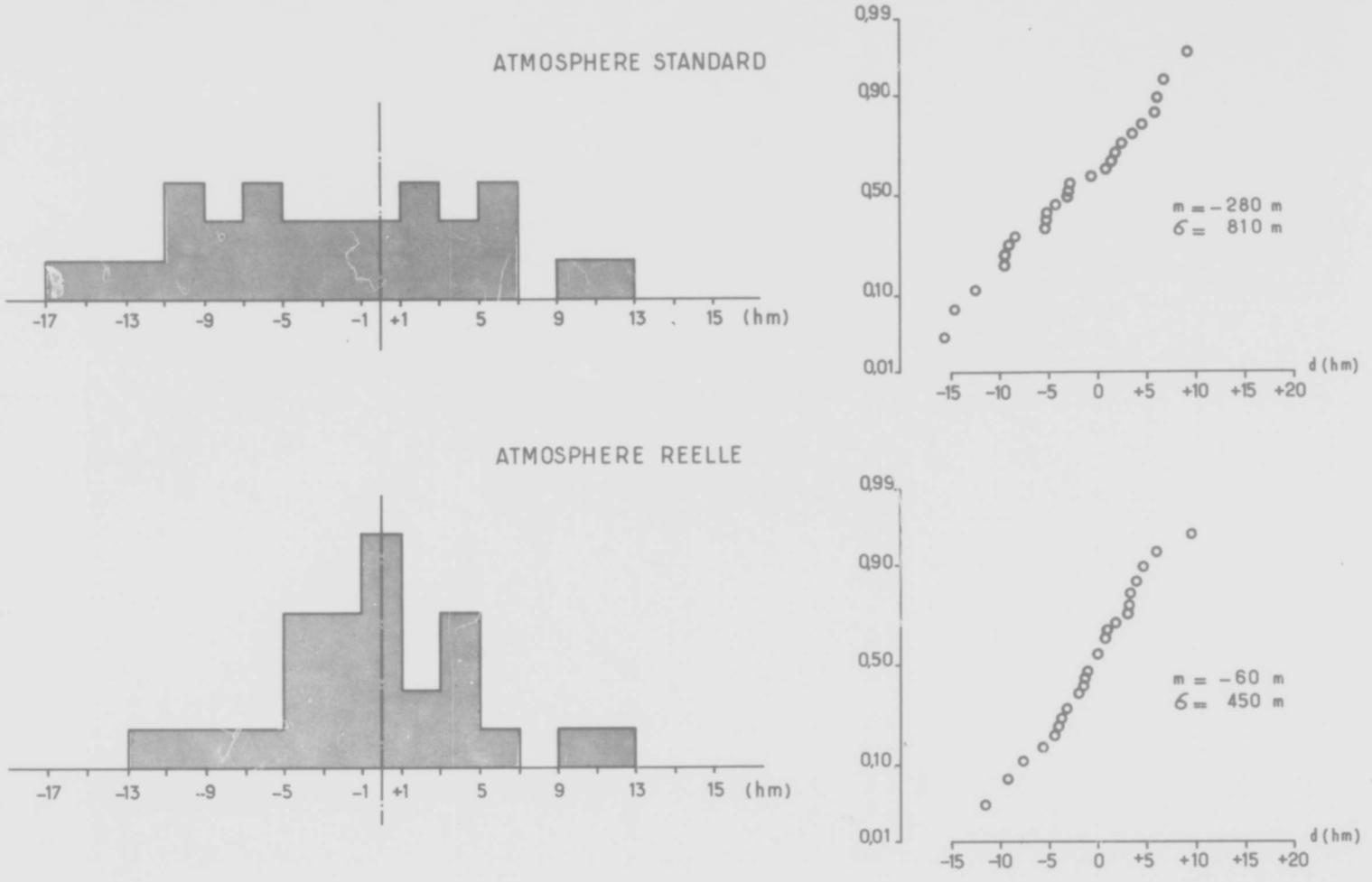

Fig. 16 Comparaison entre focalisation calculée et focalisation mesurée.
Dispersion des résultats

SURVEY OF UNITED STATES SONIC BOOM OVERFLIGHT EXPERIMENTATION

by

Dr. John O. Powers, J. M. Sands
Office of Noise Abatement
Federal Aviation Administration
Washington, D. C.

and

Domenic J. Maglieri
Langley Research Center
National Aeronautics and Space Administration
Hampton, Va.

BLANK PAGE

SURVEY OF UNITED STATES SONIC BOOM OVERFLIGHT EXPERIMENTATION

I. INTRODUCTION

For 22 years man has had the capability of maintaining steady state flight at speeds faster than the speed of sound. For almost as many years, continuing programs of supersonic overflight experimentation have been conducted to improve our knowledge and understanding of the sonic boom, a phenomena which is inescapably associated with supersonic flight. Several survey papers exist, for example, References 1 through 3, which have reviewed the chronology and the significant findings from overflight experimentation. The present paper will utilize much of the material previously presented in those references; however, it is the authors' intent to add new and recent material which will, in effect, update the previous papers. In addition, some recent developments in the claims and legal activity associated with this experimentation permit us to obtain an up-to-date view of the legal and social costs associated with the test programs. Other recent developments in the field of sonic boom overpressure measuring instrumentation and in the theoretical methods of signature prediction are included. These developments are expected to facilitate future sonic boom overflight studies and will enhance our ability to theoretically interpret the resulting experimental findings.

II. CHRONOLOGICAL REVIEW

A graphical summary of the United States sonic overflight research is presented in Figure 1. This figure is an adaptation of a similar figure used by Nixon in Reference 3. The figure has been arranged to indicate the areas of emphasis during the specific overflight programs. The shading indicates programs directed at understanding the flow phenomena related to the process of sonic boom generation and propagation, programs directed towards investigations of structural interactions with sonic boom, programs directed towards psychoacoustic investigations, and finally, programs designed to improve our understanding of the interaction of the sonic boom with the earth's atmosphere. From the figure, it is observed that the initial programs were related primarily to military investigations and dealt to a large extent with the problem of sonic boom generation and propagation. The reason for this was that the initial sonic booms were generally accidental, generated by military aircraft, and accordingly, it was desirable to determine the conditions associated with the generation of sonic booms. As a result, the military agencies found that it was possible to avoid sonic boom accidents by the conduct of training missions over sparsely populated areas and by having the aircraft fly at sufficiently high altitudes thereby minimizing the effects of sonic booms on the ground observer. The next period in the overflight research during the latter 1950's represented the initiation of active participation by the National Aeronautics and Space Administration in investigations of a phenomenon associated with sonic booms. This research was more general in nature and primarily directed at evaluating the influence of aircraft operational parameters such as gross weight, Mach number, and altitude on the sonic boom overpressure magnitude.

In 1960, the projects "Little Boom" and "Big Boom" were conducted at the Nellis Air Force Base. These studies were directed towards the evaluation of the feasibility of using the sonic boom as a weapon

and as such provided an excellent opportunity to study potential structural damage and physiological reactions in the presence of extreme sonic boom overpressures. The greatest overpressure reached in this series of tests was approximately 120 lbs. per square foot which was the largest overpressure recorded to that date. After these tests, the overflight programs were influenced by considerations of the development of a commercial supersonic transport. In particular, it is noted that the flight experiments over St. Louis, Oklahoma City, and finally at the Edwards Air Force Base were conducted to evaluate the psychoacoustic reaction of community groups to repeated supersonic overflights. More recent flights, including the series which terminated in 1967, were conducted at Edwards AFB. These tests were highlighted by the inclusion of the XB-70 aircraft, which is the largest American supersonic aircraft flying today. The current experimentation in the Pendleton, Oregon, area is utilizing target of opportunity flights of military aircraft to evaluate the atmospheric effects on sonic booms.

III. SONIC BOOM GENERATION AND PROPAGATION

Sonic booms experienced by a ground observer are the manifestation of the aerodynamic flow field about a body traveling at supersonic speeds. In an idealized uniform atmosphere, the sonic boom felt at the ground would be a result of the geometric spreading of the acoustic energy of the supersonic flow field. In the real atmosphere, the sonic boom signature is changed by atmospheric temperature gradients, influenced by the wind profile, and altered by propagation through turbulent air masses. The overflight studies directed at understanding the physics of sonic boom generation and propagation have contributed considerable insight into the mechanisms involved. Many of the overflight studies have resulted in quantitative evaluations of the mechanisms, however, some of the mechanisms are understood only in a qualitative manner.

a. Signature Characteristics. Typical signatures measured during overflight programs are shown in Figure 2. It is noted that regardless of the aircraft size, the signatures in general can be categorized as "peaked," "normal," or "rounded." It is interesting to observe that for these signatures, the deviations from a smooth N wave related to the bow shock and the tail wave are similar. This fact was pointed out by Kane and Palmer in Reference 4 and was postulated as a basis for contributing the entire distortion of the signature to propagation through atmospheric inhomogeneities. The signatures shown in the figure for the F-104, B-58, and the XB-70 aircraft were respectively roughly 100, 200, and 300 milliseconds in duration. Among people involved in sonic boom experimentation, it is the general concensus that the rounded signature shape is markedly more acceptable from a psychoacoustic standpoint than the peaked signature shape. In Figure 3, representative N wave traces are presented for the SR-71 aircraft which is capable of supersonic flight in altitudes in excess of 70,000 feet. These signatures show the increase in signature duration with increased altitude and also indicate a tendency for the initial shock wave to exhibit a finite rise time before reaching the peak overpressure. It is of interest that the trace for an altitude in excess of 70,000 feet retains the character of a finite rise time signature in spite of the long propagation path. This could be interpreted as a tendency for the signatures to reach an asymptotic form at some intermediate altitude without further advance or sharpening prior to reaching the ground.

b. Flow Field Measurements. The flow fields related to the B-58 and the XB-70 bomber aircraft have been explored by a unique experimental technique. This technique consists of flying an F-106 or F-104 probe aircraft both above and below the bomber aircraft and measuring the pressure variation at different relative positions of the two aircraft. The results of flight tests made using the XB-70 aircraft are shown in Figure 4. At the locations 2,000 feet above and below the XB-70, the flow field is observed to be closely related to the detailed geometry of the aircraft. The marked differences between the pressure field above and below the aircraft are attributed to the lift contribution of the aircraft. The probe measurements made 5,000 feet below the aircraft show the tendency for the individual waves of the flow field to coalesce at more remote distances from the aircraft. The signature length, which is in the order of two to three times the aircraft length at ground level, is observed to approach the far-field N wave shape with the exception of one intermediate shock. This intermediate shock would probably tend to coalesce with the bow shock for greater altitudes of the generating aircraft.

c. Altitude Effects. The results of experimental overflights with F-104 and F-105 aircraft during programs at Nellis AFB in 1960 and Edwards AFB in 1961 show graphically, Figure 5, the effect of increased altitude on the sonic boom signature shapes. During this program, the 120 psf overpressures were measured. These measurements and the measured overpressures of 144 psf reported in Reference 5 are probably the largest overpressures from sonic booms that have been recorded by man. The computational procedures of Carlson and Middleton (Reference 6) predict reasonably accurately the location and magnitude of the majority of the shocks in Figure 5. The atmospheric propagation for that computation was accounted for by the method of Friedman, Kane, and Sigalla, Reference 7. This technique effectively consists of utilizing a multiplying factor to increase the signature overpressure computed under the assumption of uniform atmospheric conditions. One point to be observed is the tendency, at the higher altitude and Mach numbers, for the tail wave to be theoretically estimated at a location aft of the experimentally realized value. This characteristic has been observed in other calculations of high altitude or higher Mach number results and will be discussed further in section VII. The effect of altitude on overpressure and impulse for the B-58 and F-104 aircraft is shown in Figure 6. The comparison with the theoretically expected altitude variation indicated on the figure shows reasonably good agreement with the measurements for the operational range investigated. The increase in overpressure and impulse associated with the larger aircraft is clearly indicated in the figure. It is noted that these values are currently being experienced as the result of routine military operations. A similar plot of the variation of peak overpressure with altitude is presented for the SR-71 aircraft in Figure 7. At present, the calculated sonic boom characteristics and altitude values of this aircraft are not available to the general public. The plot does indicate, however, that by comparison with the B-58 aircraft, which is similar in size and weight, that no unanticipated trends were experienced. On the figure, each symbol represents an individual mission with the solid symbols representing the average measurements from a large number of microphones. There is a slightly discernible trend in the measurements taken during the summertime, and this variation is attributed to the less quiescent atmospheric conditions that exist at that time of the year.

d. Lateral spread. The prediction of the spread of the sonic boom carpet is generally well defined and the procedures have been experimentally confirmed. As a rough rule of thumb, the total lateral spread in miles may be related to the aircraft altitude in thousands of feet. For example, in Figure 8 the lateral spread of the B-70 sonic boom track when generated at altitudes of 37 and 60,000 feet is roughly in the order of 35 and 60 miles respectively. While the character of the lateral spread is well predicted, it is seen that there is some difficulty in predicting the actual point of lateral cut-off. This characteristic is observed again in Figure 9 for flights of the SR-71 aircraft. In Figure 10, the actual signature traces at varying lateral distances from the ground track are given for the SR-71 aircraft at an altitude in excess of 70,000 feet. It is seen that as the distance from the flight track increases, the signatures tend to become rounded with an increased rise time. At the distance of 26.8 n.mi. from the flight track, which is very near to lateral cut-off, the sonic boom signature tends to degenerate into an approximate sine wave.

e. Wavefront Ground Intersection. The data presented in the previous section on the lateral spread of the overpressures has been time correlated utilizing radar tracking data to define airplane position. From the time correlation of the measurements it was then possible to define the shockwave ground intersection shown in Figure 11. As was anticipated, the intersection of the aircraft's Mach cone with the ground approximately forms a hyperbola. Using the calculation method of Reference 8, ground intersections were estimated using both a homogeneous and the actual atmosphere. The calculations utilizing the homogeneous atmosphere tend to intersect the ground track three to four miles behind the calculations made with the actual atmosphere. This is attributed to the lack of refraction of the acoustic ray paths in the absence of atmospheric temperature gradients. The agreement with the calculations using the actual atmosphere and the experimental data is considered to be quite satisfactory. It is interesting to note that the aircraft is approximately 20 miles beyond the point on the ground at which the boom is observed.

f. Atmospheric Effects. Investigations of the atmospheric effects on sonic boom signatures are considered of primary current importance. Accordingly, in the present meeting, a paper by Angell, Herbert, and Hass (Reference 9) will explore this subject in some depth. It is, however, considered desirable in the present survey to include for completeness some representative results which were significant in pointing up the importance of the problem of sonic boom atmospheric interactions. The pressure signatures presented in Figure 12 were measured by flights over a linear microphone array with microphones spaced at 200 foot intervals. The recorded waveforms in the distance of the 800 foot array vary from sharply peaked signatures to extremely rounded signatures with maximum overpressures differing by a factor as great as three. Since these measurements were taken under moderately turbulent atmospheric conditions, it was hypothesized that the rapid signature variation was associated with inhomogeneities in the atmosphere. To isolate the segments of the atmosphere which contributed to the distortion of the sonic boom signature, measurements were made by the technique indicated on Figure 13. The "blimp," which had a microphone mounted in a manner to minimize interference with the sonic boom measurements, was flown at altitudes up to 2,000 feet.

Accordingly, it was able to penetrate fairly deeply into the upper reaches of the earth's boundary layer and sonic boom signatures were measured which had passed only through a small segment of the earth's boundary layer. The incident shockwaves were often observed to be sharp, undistorted N waves whereas the reflected shocks which traversed the earth's boundary layer to the ground and returned to the blimp were considerably distorted. These measurements tend to indicate that the majority of the distortion occurs in the lower altitude turbulent air masses even though on occasions the incident waves at the blimp level did indicate some distortion. A recent scattering mechanism has been proposed by Crow (Reference 10) which offers great potential in defining the mechanism of sonic boom atmospheric interaction. However, further experimentation is believed to be necessary to quantitatively substantiate the scattering theory.

g. Aircraft Maneuvers. The subject of amplification of sonic boom overpressures due to aircraft maneuvers has been investigated for many years. Attempts have been made to measure the maneuver amplification factors for turning maneuvers, linear accelerations, and porpoising maneuvers. The very excellent experimental work of the French in projects "Focalization" and "Jericho" and the procedures developed by Guireaud are described in the present conference (References 11 and 12). In an early Edwards AFB test program, a series of linear accelerating maneuvers was made and the experimental overpressure measurements taken along the ground track are shown in Figure 14. In this figure, the results from three independent flights have been normalized to the zero distance along the ground track. As noted on the schematic sketches, the ground zero point occurs at the location where the superboom first touches the ground. Further down the track, the sonic boom separates into two separate shock waves with the trailing shock resulting in weaker overpressures because it was generated at an earlier point in time and hence experienced more distance attenuation. In this series of accelerated flights, the maximum amplification of the sonic boom overpressure was approximately three times the value of the unamplified sonic boom. It is interesting to note that acoustic ray tracing techniques have been utilized to predict the location of the superboom and have, in many cases, been accurate within three miles.

A second motion of the aircraft, namely, a propoising flight, was studied to determine if this type of motion could be a contributor to the variation of signatures along a linear ray as indicated in Figure 12. In this test, a series of flights at an altitude of 35,000 feet and Mach number of 1.5 were made with an F-106 aircraft. As is shown in Figure 15, the motion of the aircraft produced a plus and minus 0.5g normal acceleration. The period of the motion was one second which corresponds to wave lengths of approximately 1600 feet. Attempts were made to correlate the experimental overpressure variations with the wave length of the aircraft motion to see if the perturbations about the flight track resulted in corresponding shockwave perturbations which would be propagated to the ground. It was not possible from this data to obtain correlations with any preferred wave length. When the root mean square overpressure difference was plotted as a function of separation distances between two measuring microphones, it was found that the data for steady and porpoising overflights essentially coincided.

While this might imply that variations of the overpressure made from these flights could be essentially contributed to atmospheric effects, some recent computations indicate that the variations may be due to the porpoising motion. Accordingly, it is believed that more theoretical and experimental investigations of this phenomenon would be desirable.

h. Statistical Variability of Peak Overpressures. The large number of experimental overpressure measurements facilitates the statistical presentation of the peak overpressure variation. For example, in Figure 16, measurements made on the XB-70 aircraft are shown on a log normal probability plot. Otherwise expressed, the probability of the measured value exceeding or being less than the calculated overpressure is presented. A straight line through the data points indicates that the overpressures measured form logarithmically a normal or Gaussian distribution. Also observable on this type of a plot is the fact that the variations of plus or minus one standard deviation lie between the probability of .16 and .84. Extending this to two standard deviations would include 95.5% of all data presented. In Figure 16, the striking difference between data taken in the summertime and in the winter months is indicated. A much greater variability is noted during the summer months when the atmosphere is inclined to be less stable. A similar plot of wintertime variability for three different aircrafts, (the XB-70, the B-58, and the F-104), is shown in Figure 17. While these aircraft are considerably different in size, it is observed that the probability curves are essentially similar indicating that aircraft size is not a strong factor in the statistical variability of overpressure measurements.

The statistical variability of the sonic boom bow wave rise time normalized by peak overpressure value is presented for the SR-71 aircraft in Figure 18. Rise time was measured as the time from the onset of the bow shock overpressure rise to the time of the maximum overpressure. The overpressure values used to normalize the rise time data were generally on the order of one psf and therefore the histogram essentially represents the distribution of rise time values. It is observed that the most frequently occurring value of the rise time is approximately 10 milliseconds. The longer rise time values were associated with the rounded wave forms and shorter rise times are associated with peaked wave forms. An additional presentation of the normalized rise time is presented in Figure 19. This presentation attempts to explore the effects of flight conditions or specifically of altitude on the SR-71 rise time. The data symbols represent the average of a large number of flights taken within ± 3 n.mi. of the ground track and the vertical extent of the lines indicates the scatter in the experimental data. While it is difficult to specify absolute trends from data with such large scatter, it is possible to observe that there is a tendency for the rise time to be larger at the higher altitudes. A possible explanation of this trend may be related to the development of the age variable of the signal and its approach to an asymptotic limit but a more probable explanation is related to atmospheric effects. Beyond the asymptotic limit, further sharpening of the signature is not probable and correspondingly, atmospheric scattering may effectively thicken the shock front. Irrespective of the cause, the tendency for the SR-71 aircraft to produce signatures with a finite rise time continues to be demon-

strated by recent overflight measurements made in Pendleton, Oregon. Since increased rise time is considered to be a favorable characteristic from subjective response considerations, these data will be examined in detail to explore the parameters contributing to this favorable signature characteristic.

IV. SONIC BOOM EFFECTS ON ENVIRONMENT

Since the sonic boom is a rapid transient pressure pulse, it is apparent that it may have the potential of producing adverse physical and psychological effects on people, animals, and structures. Accordingly, a large number of the overflight studies were directed at evaluating these potential effects and at attempting to quantitatively relate the magnitudes of structural and psychoacoustic interactions to the characteristics of sonic boom signatures. The tests previously mentioned to evaluate the feasibility of using the sonic boom as a weapon produced essentially negative results and the balance of the overflight testing was directed at the general acceptability of overland supersonic flight in terms of psychoacoustic reactions and potential structural damage.

a. Structural Effects. The character of the transient structural loading is indicated in Figure 20. The aircraft is approaching the building from left to right and initially there is a racking load followed by a period during which the positive pressure pulse engulfs the building. This inward pressure loading is quickly reversed as the negative portion of the pressure pulse passes over the building and then finally as the tailwave passes the building receives a second racking load. The response of a building to a typical sonic boom stimuli is shown in Figure 21. The sonic boom signature illustrated in this figure is of the "spikey" character with the peak overpressure just slightly under 1.5 psf and a duration of approximately 100 milliseconds. From the measurements made inside of the house, it is observed that the overpressure levels are considerably reduced and that the wave form is markedly altered. The curve labeled "Noise" represents measurements made with a filter which passed acoustic signals in the audible range. The amplitude of this signal is an order of magnitude lower than the internal pressure pulse. A lower curve labled "acceleration" indicates the vibrations of the floor which would be sensed directly or through the furniture in the room. This characteristic is a direct response to both the outside pressure pulse and the inside pressure oscillations. Because of the comparatively favorable psychoacoustical evaluation of finite rise time sonic boom signatures when heard outdoors, it is considered desirable to evaluate the response of building structures to these signatures to determine if the structural characteristics of the building offset the desirable characteristics of the signature on the indoor observers.

During the overflight program at Edwards Air Force Base, it was possible to evaluate the effects of sonic booms of considerably different duration on the acceleration of walls of one- and two-story houses. The results of the wall acceleration measurements are shown in Figure 22 and are given for overpressures up to 4.4 lbs. per square foot. While the three different aircraft used had signature durations of one, two, and three hundred milliseconds, it is difficult from the figure to discern difference responses for

the different aircraft. It is also observed that at the maximum overpressures experienced in these tests, the wall accelerations were considerably below the value set as a criteria for structural damage.

b. Subjective Reactions. A major feature of the recent Edwards AFB tests was that of measuring the psychoacoustic reactions of subjects to sonic boom overflights. These reactions were evaluated in terms of a more familiar noise; namely, the noise of aircraft flyovers. Subjects were selected from nearby communities and were exposed in random order to pairs of subsonic aircraft flyovers and sonic booms generated by different aircraft at different overpressure levels. The evaluated experimental data is presented in Figure 23 where the large shaded area represents not only experimental scatter, but the difference between the subjective reactions of subjects located inside houses and subjects located out-of-doors. The lower boundary of the shaded region was generally related to indoor subjective response. This type of comparison is somewhat limited in value because weighting factors with respect to durations and pure tones of the flyover noise were not included and the sonic boom signatures were not weighted in terms of signature rise time which is known to result in a relative reduction of the sonic boom annoyance level.

c. Seismic Effects. It has been postulated that the effects of the sonic boom on ground-induced motion might be an area for concern. Accordingly, ground-induced motions resulting from overflights by fighter and bomber aircraft have been measured in terms of the three components of the ground acceleration. Measurement of the ground particle velocity presented as a function of time is given in Figure 24. This pressure wave resulted from the sonic boom produced by a B-58 aircraft and the theoretically anticipated values are indicated by the dashed curve. The highest values of the particle velocity are associated with the passage of the bow and tail shockwave and are the expected motion of an elastic surface under a transient load. The superimposed lower-amplitude higher-frequency variations on the time history record are due in part to the Rayleigh wave phenomena. A large number of ground particle velocity measurements are presented in Figure 25 as a function of sonic boom overpressure. It is noted that the maximum particle velocity is in the order of 250 microns per second. This value is less than one percent of the damage threshold criteria now recommended by the U. S. Bureau of Mines. Otherwise expressed, earthquake damage is considered to be associated with particle velocities approximately 100 times the values indicated in Figure 25.

d. Effects on Other Aircraft. In the 1963 Edwards overflight program, the question of possible shockwave effects from a supersonic aircraft as it passes over a small subsonic aircraft was investigated. Several light aircraft were instrumented for accelerations and were overflown by the sonic boom generating aircraft which generated sonic booms from one to 16 psf. Accelerations of the instrumented aircraft were also measured when it was parked on the ground and during maneuvered flights. Typical results of the sonic booms on the light aircraft are shown in Figure 26. Normal accelerations experienced by the aircraft on the ground are observed to be approximately 0.3 g's whereas the aircraft in cruise experienced an appreciably smaller acceleration. By comparison, the accelerations

when taxiing over a rough runway or in air turbulence are both shown on the figure and the latter accelerations are greater than those experienced during the sonic boom overflights. One observer in a Comanche aircraft noted that the 16 psf sonic boom was heard in cruise flight as a muffled sound and that the only visible effect on the aircraft was a slight movement of the window. He was attempting to observe the wing surface for possible oil canning but was unable to detect any distortion due to the passage of shock-wave. It is generally concluded as a result of these tests that sonic booms do not constitute a hazard for other aircraft in flight or on the ground.

V. COSTS OF SONIC BOOM EXPERIMENTATION

The United States' active envolvement in sonic boom research has provided significant insight into the legal and social costs of this type of experimentation. Four extensive test programs which were conducted in a field community environment will be considered in this section in terms of their economic aspects as measured by the associated costs and, when appropriate, damage claims. Specifically, these experiments are the (1) St. Louis Community Response Study, (2) Oklahoma City, Oklahoma, Public Reaction Study, (3) Structural Reaction Program, White Sands Missile Range, New Mexico, and (4) Sonic Boom Experiments at Edwards Air Force Base, California.

a. St. Louis Community Response Study

The St. Louis program was conducted during the period July 1, 1969, through January 31, 1962, with the United States Air Force, National Aeronautics and Space Administration, and the Federal Aviation Administration participating. This program utilized B-58 and F-106 aircraft to generate a total of seventy-six (76) booms, over a seven-month period, with a maximum overpressure of 3.1 psf and an average of 2.0 psf. Since this was basically a military training operation rather than a sonic boom research program, overpressure and valid claims data was obtainable only during an 11 day period. During this period, overpressures from 16 booms were recorded and 165 damage claims were investigated by professional engineers. The community response personal interview studies consisted of a total of 1,145 initial interviews followed by a re-interview of the respondents at a later date. The approximate cost of obtaining the overpressure, damage, and public reaction data was $100,000.00. The cost for aircraft operations is not included since the training character of the program made it difficult to delineate the purely research costs. The final number of damage claims filed as a result of the program was 1,624 for a value of $366,019.00, of which, 825 claims were approved by the USAF for a cost of $58,648.00.

b. Oklahoma City Public Reaction Study

The Oklahoma City Program was initiated on February 3, 1964, and terminated on July 31, 1964. The program was a joint effort of the USAF, NASA, and FAA, and was under the immediate direction

of the FAA's Supersonic Transport Development Office. FAA performed the planning, direction, and management function and established most of the operational requirements. NASA participation was primarily technical including structural instrumentation and overpressure detection. The USAF provided aircraft support and adjudication and payment of claims for all sonic boom damage in the Oklahoma City Study area.

The public reaction was obtained through the establishment of a telephone complaint center and periodic public opinion polls accomplished by the National Opinion Research Center of the University of Chicago. Structural reaction to the sonic boom was evaluated by a local engineering firm, Andrews Associates, Inc., which investigated the response of several test houses. Additional scientific support was provided by Oklahoma State University. The Remmert Adjustment Company of Oklahoma City, acting under contract to the FAA, received all alleged damage and complaint telephone calls, conducted investigations of claims, and forwarded their findings and recommendations to the Judge Advocate General's Office, Tinker Air Force Base, Oklahoma City. This office then accomplished final adjudication and claims payment subject to normal review and appeal procedures standard with the United States Air Force.

The overall operational aspects of the Oklahoma City program are summarized in Table I.

TABLE I

Oklahoma City Operational Aspects

Beginning Date	February 3, 1964
Termination Date	July 30, 1964
Total Scheduled Supersonic Flights	1394
Total Flights Cancelled	141
Total Flights Completed	1253
Scheduled Flights Per Day	8
Standard Flight Schedule	7:00 a.m. 7:20 a.m. 9:00 a.m. 9:20 a.m. 11:00 a.m. 11:20 a.m. 1:00 p.m. 1:20 p.m.
Scheduled Overpressures	1.3, 1.5, and 2.0 psf

In initiating the study program, there was a gradual build-up to the sonic boom overpressure objectives. At the start of the program, there was only one flight per day with a scheduled overpressure of one psf. This was increased slowly to a schedule of eight flights per day at one psf and then to eight flights at a scheduled overpressure of 1.5 psf. This operational level was reached after approximately three weeks. Then there was a similar increase from

1.5 psf to two psf which was accomplished in a manner to ensure controlled transition. The aircraft utilized in the program were the F-101, F-104, F-106, and the B-58. During the 26 weeks of the program, 15,452 telephone calls and letters were received by the complaint center; of these, 9,732 alleged damage. Four thousand nine hundred and one damage claims were filed for a value of $2,492,577; of these, 289 were approved for $19,355.00. Also as a result of this test program, seven lawsuits were filed against the United States and the Government was joined as a third party defendant by insurance companies in two other actions. Three of the cases against the United States were filed while the test program was in progress seeking injunctions to stop the program. The remaining cases sought compensation for property damage allegedly caused by the sonic booms.

The three injunction suits seeking to halt the program were dismissed and the program continued without interruption. In the remaining six cases, which seek compensation for alleged damages, the disposition is as follows: (1) The Government has successfully defended three suits totaling $101,268,984.00, (2) the plaintiffs have received compensation in two suits totaling $133,257.00, and (3) one suit for $5,439.00 is awaiting trial.

The total cost of this program including aircraft support and payment of claims was $1,039,657.00.

c. White Sands Missile Range

The Structural Reaction Program was conducted during the period November 18, 1964, through February 15, 1965. This program was designed to determine structural response characteristics for overpressures ranging from 2.0 to 28.0 psf and cumulative structural effects from repeated boom resulting from flights at a frequency of 30 per day. This study, conducted at the White Sands Missile Range, New Mexico, consisted of two phases. The first phase began on November 18 and ran through December 15, 1964, and generated a total of 615 sonic booms. The nominal overpressure ranged from 2.0 psf through 16.0 psf progressing at scheduled increments of 2.0 psf. Thirty flights were scheduled for each overpressure level. The second phase began January 15, 1965, and ended February 15, 1965. A total of 879 booms were generated during this period. The cumulative effect of sonic boom was explored by exposing structures to 680 sonic booms at a nominal overpressure of 5.0 psf. A total of 76 flights were conducted to obtain data on the effects of focusing of sonic booms due to aircraft maneuvers.

Sixteen types of structures were included in the test, seven of which were built specifically for this program. Five types of plaster, interior finishings and a variety of commercial glass installations were studied during the two phases. Prior to program initiation, a thorough engineering inspection was conducted for each structure to establish a state of repair and overall condition. Daily inspections were conducted at 30 minute intervals on each of the structures by a 22-man engineering team.

Subsidiary test objectives included the determination of the effect of sonic booms on the hatchability of chicken eggs; human hearing impairment or adverse physiological effects caused by

sonic boom at high overpressure levels; and sonic boom characteristics associated with aircraft maneuvers. The total cost of this program including construction of test structures and aircraft support was $511,100.00.

d. Edwards Air Force Base

The Sonic Boom Experiments at Edwards Air Force Base, California, were a joint effort under the management of the USAF, funded by the FAA with the NASA, ESSA, and USDA participating. The general objectives of these experiments were:

1. To measure the judgments of the relative acceptability of sonic booms and noise of various intensities from various types of aircraft.

2. To determine the response of "typical" house structures to sonic booms having different signature characteristics.

3. To obtain detailed measures of sonic boom signatures as functions of the type of aircraft, mode of operation, and the atmosphere through which the wave was propagated.

4. To observe the response of animals to the sonic booms.

The aircraft used during this program were the XB-70, SR-71, YF-12, B-58, F-104, F-111, KC-135, WC-135B, and Cessna 150. A total of 367 supersonic flights and 261 subsonic flights were accomplished. A detailed breakdown of the flights appears on the following table.

TABLE II

Edwards Experiment
Number of Overflights by Aircraft Type

SUPERSONIC		SUBSONIC	
YF-12	2	KC-135	99
SR-71	34	WC-135B	119
XB-70	20	BLIMP	6
B-58	169	C-131B	19
F-104	124	Cessna-150	18
F-106	18		
TOTAL	367	TOTAL	261

The total cost of this program, including the salaries of the observers, construction of test houses, claims, and aircraft support was $2,151.00.00.

The costs of the four research programs is summarized in Table III. The programs are listed in order of increased complexity of the test objectives. As is to be expected, the cost of sonic boom overflight experiments increased as a function of the diversity of the experiment and as a result of using advanced aircraft.

TABLE III

Sonic Boom Research Costs
($ in thousands)

St. Louis	$158.6
White Sands Project	$511.1
Oklahoma City Project	$1,039.7
Edwards AFB	$2,151.0
TOTAL	$3,860.1

VI. RECENT OVERPRESSURE INSTRUMENTATION DEVELOPMENTS

The instrumentation used to measure the sonic boom overpressures described in Sections III and IV was the culmination of many years of effort because of the special character of the sonic boom measurement problem. The spectrum of the sonic boom N wave contains appreciable energy at frequencies in the order of 0.1 Hz up to several thousands Hz and hence standard instrumentation was not adequate without extensive modifications. The development of this instrumentation is described by Hilton and Newman in Reference 13. Generally, the microphones used as the measurement systems were required to have essentially flat frequency response from nearly d.c. to the upper frequency range. In all of these recording systems, it was necessary to have experimenters in attendance to ensure continual operation and proper functioning of recording equipment.

Recently, a means of obtaining random sonic boom overflight data from unattended recording equipment has been developed. The instrument is referred to as a transient data recorder (TDR) and is currently being used in the Pendleton atmospheric program indicated on Figure 1. A picture of the transient data recorder is shown in Figure 27. The operation of the measurement equipment has been described in detail by Power in Reference 14. The recorder is self-contained and microphones are located at distances up to 500 feet from the recorder. There are three microphone pickups used with each recorder and upon arrival of a sonic boom, one of the three microphones acting on an overpressure threshold sensor activates the equipment for each of the three acoustic data channels. The recorder utilizes three equally spaced record heads on a cylindrical drum which continuously rotates inside an open loop of tape. When the signal on the threshold mike exceeds a predetermined value, a recording commences and continues for 1.6 seconds. After the recording interval the recorded tape is transferred to a storage reel while a new tape is positioned from a supply reel. By this mode of operation, the tape is advanced only during the actual recording of a signature and the expenditure of

large amounts of magnetic tape while waiting for a sonic boom is avoided. As a result of this feature at least 800 independent events may be recorded on a single reel of tape. A typical TDR recording of an N wave is shown in Figure 28. It is observed that at the end of the recording period, a calibration signal is imposed giving both the amplitude of the sonic boom overpressure and the duration which is derived from a 100ms, 50Hz square wave signal. In addition to this, the date and time of day are also recorded. The transient data recorder with 99 pickup microphones is currently being used in the atmospheric effects test program at Pendleton, Ore. They have been arranged in both a checkerboard array and in a two-mile linear array. Because these recorders can operate unattended, it is possible to utilize random military overflights as the source of the sonic boom generating aircraft and the need for special overflights is avoided.

VII. RECENT DEVELOPMENTS IN SIGNATURE PREDICTION

The basis of most sonic boom signature prediction methods relies on the developments by G. P. Whitham described in Reference 15 and supplemented by the procedures of Hayes (Reference 16). These two basic works have provided the foundation for a quasy-linear theory which can define the sonic booms of lifting aircraft configurations in a uniform atmosphere at some distance from the aircraft. Before these theoretical methods could be utilized to calculate signatures for comparison with the experimental overflight measurements described in Section III, it was necessary to develop procedures for calculating the propagation of the sonic boom from the aircraft to the ground through real atmospheres. One of the early methods for computing the propagation of sonic booms through real atmospheres was described by Kane and Palmer in Reference 4. That method was modified by Friedman as described in Reference 17 and also by Kane in Reference 18.

In view of the complexity of these highly numerical techniques, it was difficult to make direct comparisons and resolve differences that accrued from utilizing the different programs. Accordingly, a study was undertaken by Hayes and others under contract to the NASA to clarify the confusion existing in the area of sonic boom propagation theories. This contract effort culminated in the development of a sonic boom propagation technique and computer program described in Reference 19. The procedure is based on linear geometric acoustics and uses an age variable to define the non-linear effects on the shape of the sonic boom pressure signatures. By so doing, the results can be computed in the form of complete signatures, independent of far-field assumptions necessary in other techniques. As a result, it is possible through the use of the new program to observe the progression of the signature shape development with distance from the aircraft in steady flight, as a function of aircraft maneuvers and with standard or non-standard real atmospheric effects.

a. Atmospheric Overpressure Corrections

A recent investigation (Reference 20), by Haefeli, has utilized the new method to evaluate the effects of different atmospheric conditions and aircraft maneuvers. One result of these calculations is shown in Figure 29. In that figure, the Mach number effects on the overpressure for an F-104 aircraft are presented in

terms of $\Delta p / \Delta p_{standard}$ where the standard value is that for a Mach number of 1.25. On the figure, the overpressure variation with Mach number in a uniform atmosphere without winds is shown as the lower curve. The value in a standard atmosphere without winds is also compared with the results obtained by applying the correction factor, K_A, to uniform atmosphere curve by the method described in Reference 4. It is shown that over the Mach number range indicated and for this specific aircraft the Reference 4 technique gave peak overpressure values which were essentially consistent with those of the Reference 19 method. Also presented on this figure are calculations of the sonic boom in the presence of the high altitude wind shear profile. Examination of the ray tube areas for this calculation indicated that at a Mach number of 1.3 focusing occurred just above the ground level. This is a result of the large wind decrement between aircraft altitude and the ground and yields the very large overpressure ratios.

b. While the new computational procedure compared well with the procedure of Reference 4 in the calculation of peak overpressures, the computations shown in Figure 30 demonstrate an area of potential refinement by the Reference 19 technique. In Section III.c., it was mentioned that theoretical methods previously used overestimate the signature length. In Figure 30, a comparison between the signature length computed by the two techniques is shown as a function of Mach number in terms of the signature length parameter $L_{signature}/L_{airplane}$. For the two representative aircraft chosen, namely the F-104 and the SCAT 15-F, it is seen that the computations using the uniform atmosphere, K_A, tends to give increasingly longer signature lengths as a function of Mach number than the lengths computed by the new Reference 19 method. In fact, the new procedure gives signatures which are as much as 20 percent shorter than those computed by the previous method. This result is consistent with much experimental data particularly at the higher Mach numbers.

c. <u>Signature Aging</u>

The most salient difference between the new method and the previous methods may be explained in terms of the amount of signature distortion which is governed by an age variable, τ . The age variable is an integral which is proportional to the distance from the aircraft and inversely proportional to the square root of the product of the atmospheric density times the ray tube area; i.e.,

$$\tau \propto \int (\rho A)^{-\frac{1}{2}} dz$$

This age variable represents the cumulation of the weak non-linear effects which result in the formation and merging of shock waves. In this Figure 31, the effects of signal aging are shown for a standard atmosphere and are compared with results obtained from a uniform atmosphere calculation. Also shown are the ray tube area variations with altitude. It is observed during the propagation from 80,000 feet to the ground, that the ray tube areas are essentially linear with altitude and tend to deviate slightly at the lower altitudes because of the increased density. A

significant difference, however, is noted in the age variable which for the standard atmospheric calculation tends to an asymptotic limit. In fact, the value of the age variable at approximately one atmospheric scale height (i.e., in this case, 50,000 feet), below the aircraft in a uniform atmosphere is approximately equal to the asymptotic value of the age variable in the standard atmosphere. This indicates that the asymptotic age in the real atmosphere has a finite limit and signature distortion need not continue in all cases to the classic N wave. In the uniform atmosphere, however, the age variable increases without limit and the asymptotic solution always yields an N wave. From a practical standpoint, this implies that "F" functions which are designed to produce unique signature characteristics, such as the finite rise time signatures, may in fact propagate to the asymptotic form and then proceed to the ground without further distortion.

d. Maneuver Calculations

As was mentioned previously, the ARAP Program permits the inclusion of any type of maneuvers in all planes and will yield the ground shock intersection patterns and signature shapes. Since it is based on acoustic theory, however, it will predict the location of focalization but not the magnitude of the overpressures.

An additional fact that has been developed in the Reference 20 calculations is that the changes in overpressure due to an aircraft's maneuvers may be a strong function of the aircraft's characteristics. This was observed in calculations using two different aircraft, (and hence two different "F" functions), which executed the same maneuver but experienced amplification factors differing by as much as 100%. This is illustrated by the results presented in Figure 32 which shows the change in overpressure during a pushover for the F-104 and the SCAT 15-F. For the F-104, the leading shock is much stronger in the pushover, $n_L = -0.5$, than in level flight, whereas for the SCAT 15-F, the leading shocks are nearly the same. For both aircraft the shapes of the signatures are affected greatly by the pushover which in turn is an indication of the sensitivity of the ray tube area to the rate of change of flight path angle. It must be pointed out that computation of maneuver characteristics can only be as reliable as the input data. This means that the "F" function must be continuously variable as a function of many parameters, such as: Mach number, load factor, angle of attack, etc. In the calculation to date, the "F" function variations have been accommodated by simplifying assumptions in lieu of a procedure for rapidly developing a multiplicity of "F" functions. Accordingly, this fact should be recognized as a limitation of the theoretical sonic boom prediction methods.

VIII. SUMMARY

The sonic boom overflight programs described in the preceding sections have generated a broad knowledge and understanding of the basic fundamentals of sonic boom generation, propagation, and

physical effects on structures. The majority of the operational and maneuver related sonic boom characteristics are sufficiently well defined to preclude any unexpected results due to the overflight of supersonic aircraft. Further information is needed to identify the interactions of sonic boom with atmospheric inhomogeneities and to define psychoacoustic acceptability. One area which appears promising is the utilization of the recent knowledge of signature aging to design acceptable signatures, most probably signatures with long rise times, or what has been referred to as "bangless booms,".

LIST OF REFERENCES

1. John O. Powers and Domenic J. Maglieri, "A Survey of Sonic Boom Experiments," prepared for the 1968 Aviation and Space Conference of the American Society of Mechanical Engineers, June 16-19, 1968.

2. Johnny M. Sands, "Sonic Boom Research (1956 - 1968)", prepared November 1968.

3. C. W. Nixon, "Sonic Boom, People and SST Operation: A Status Report," Aerospace Med. 36, 170(A) (1965).

4. Edward J. Kane and Thomas Y. Palmer, "Meteorological Aspects of the Sonic Boom," Contract Report prepared for the Federal Aviation Administration by The Boeing Company, September 1964.

5. C. W. Nixon, H. K. Hille, H. C. Sommer, "Sonic Booms Resulting from Extremely Low-Altitude Supersonic Flight: Measurements and Observations on Houses, Livestock and People," Wright-Patterson Air Force Base, Ohio, October 1968.

6. Wilbur D. Middleton and Harry W. Carlson, "A Numerical Method for Calculating Near-Field Sonic-Boom Pressure Signatures," NASA Technical Note TN D-3082, November 1965.

7. Manfred P. Friedman (Massachusetts Institute of Technology), Edward J. Kane and Armand Sigalla (The Boeing Company), "Effects of Atmosphere and Aircraft Motion on the Location and Intensity of a Sonic Boom," as published in the AIAA Journal, June 1963.

8. Donald L. Lansing and Domenic J. Maglieri, "Comparison of Measured and Calculated Sonic-Boom Ground Patterns due to Several Different Aircraft Maneuvers," NASA Technical Note TN D-2730, April 1965.

9. K. Angell, G. A. Herbert and W. A. Hass, "A Preliminary Study of the Atmospheric Effects on the Sonic Boom," Environmental Science Services Administration, presented at AGARD Meeting, Saint-Louis, France, May 1969.

10. S. Crow, "Distortion of Sonic Bangs by Atmospheric Turbulence," National Physical Laboratory, NPL AERO Report 1260, London, March 1968.

11. J. P. Guiraud, O.N.E.R.A., "Focusing in Non Linear Short Waves - Application to Ballistic Focusing Noise," presented at AGARD Meeting, Saint-Louis, France, May 1969.

12. I. C. Wanner, Serv. de l'Aeronautique/EG, Paris, "Mirage IV - Flight Tests," presented at AGARD Meeting, Saint-Louis, France, May 1969.

13. David A. Hilton and James W. Newman, Jr., "Instrumentation Techniques for Measurement of Sonic-Boom Signatures," as published in the Journal of the Acoustical Society of America, November 1965.

14. Joseph K. Power, "An Investigation of Sonic Boom Simulator Techniques and Measurement Devices," prepared for the University of Tennessee Space Institute, December 1968.

15. G. B. Whitham, "The Flow Pattern of a Supersonic Projectile," Comm. on Pure & Applied Math, Vol. V, 301-348 (1952), University of Manchester, England (now at New York University.)

16. Hayes, W. D., "Linearized Supersonic Flow," Thesis, Calif. Inst. of Tech., 1947. Also North Amer. Aviation, Inc., Report No. AL-222, 1947.

17. Manfred P. Friedman, "A Description of a Computer Program for the Study of Atmospheric Effects on Sonic Booms," prepared under contract by Massachusetts Institute of Technology for National Aeronautics and Space Administration, NASA CR-157, February 1965.

18. E. J. Kane, "Propagation of Sonic Boom Through a Nonuniform Atmosphere," The Boeing Company, D6-8979.

19. Wallace D. Hayes, Rudolph C. Haefeli, and H. E. Kulsrud, "Sonic Boom Propagation in a Stratified Atmosphere, with Computer Program," prepared under contract to National Aeronautics and Space Administration by Aeronautical Research Associates of Princeton, Inc., Princeton, New Jersey, NASA CR 1299.

20. Rudolph C. Haefeli, "Effects of Atmosphere, Wind, and Aircraft Maneuvers on Sonic Boom Signatures," prepared under contract to National Aeronautics and Space Administration by Aeronautical Research Associates of Princeton, Inc., Princeton, New Jersey.

LOCATION OF STUDY	PARTICIPATING AGENCIES
WPAFB	USAF
WPAFB-EDWARDS	USAF
WPAFB-EDWARDS	USAF
EDWARDS AFB	NASA
EGLIN AFB	USAF/USA
WALLOPS STATION	NASA
WALLOPS STATION	NASA
WPAFB	USAF
NELLIS AFB	USAF/NASA
EDWARDS AFB	USAF/NASA/FAA
ST. LOUIS	USAF/NASA/FAA
X COUNTRY SPEED RUN B-58	USAF
WALLOPS STATION	USAF/NASA/USN/FAA
EDWARDS AFB	USAF/NASA/USN/FAA
OKLAHOMA CITY	USAF/NASA/FAA
WHITE SANDS	USAF/FAA
EDWARDS AFB	NASA
CHICAGO	USAF/NASA
WALLOPS STATION	USAF/NASA/USN
JTF-2 (TONAPAH)	USAF
EDWARDS AFB (B-70)	NASA/USAF
PENDLETON, ORE.	FAA/ESSA

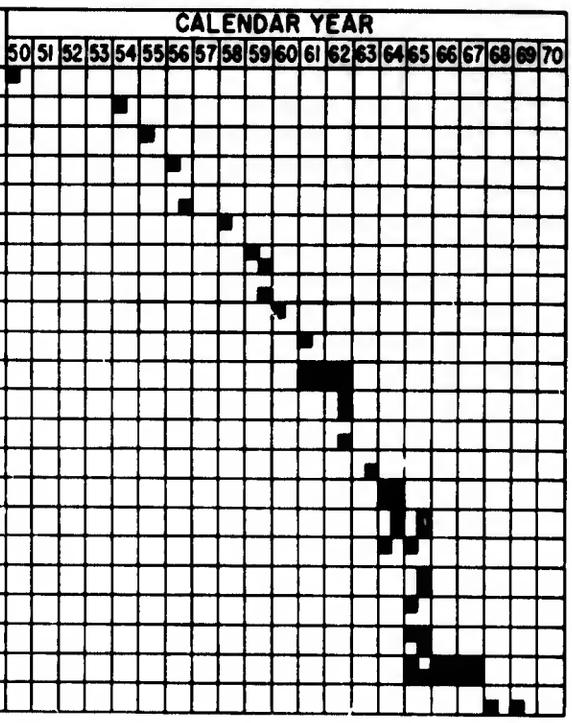

Fig.1 Chronology of US sonic-boom research

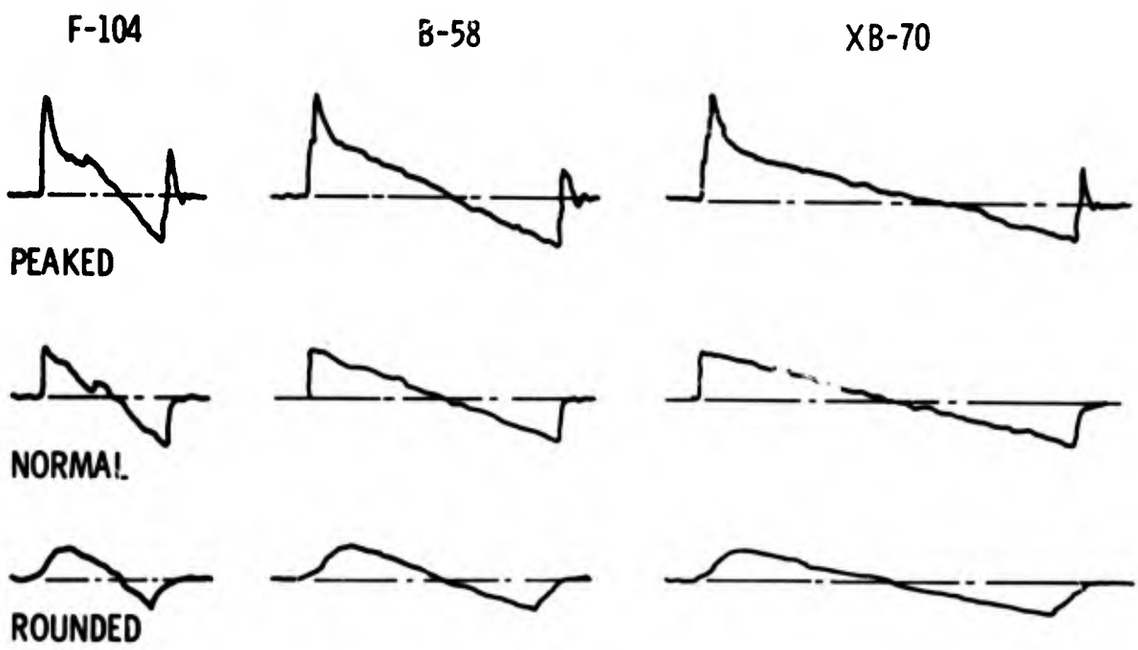

Fig.2 Sonic boom signatures

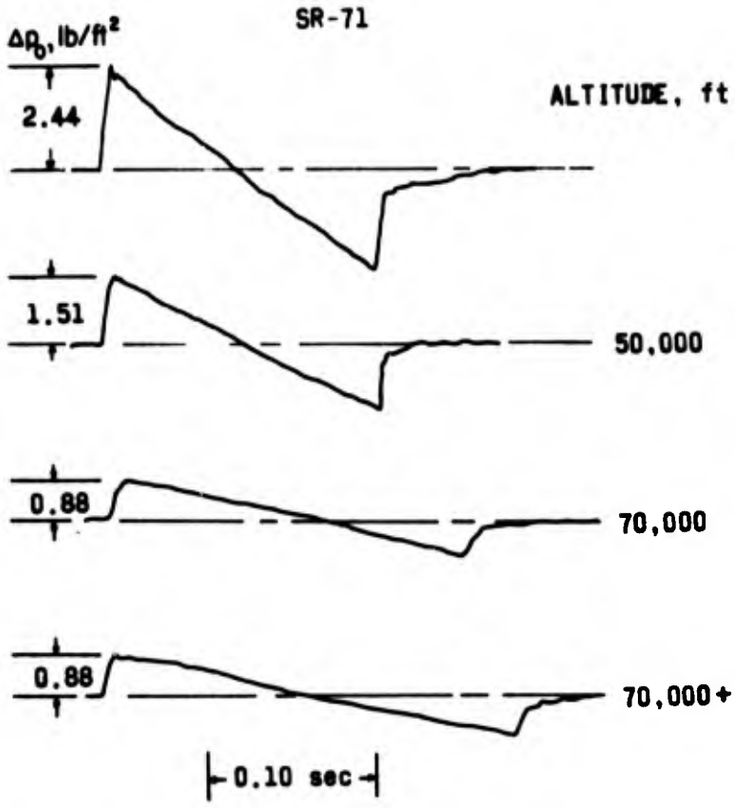

Fig.3 Variation of signature with altitude

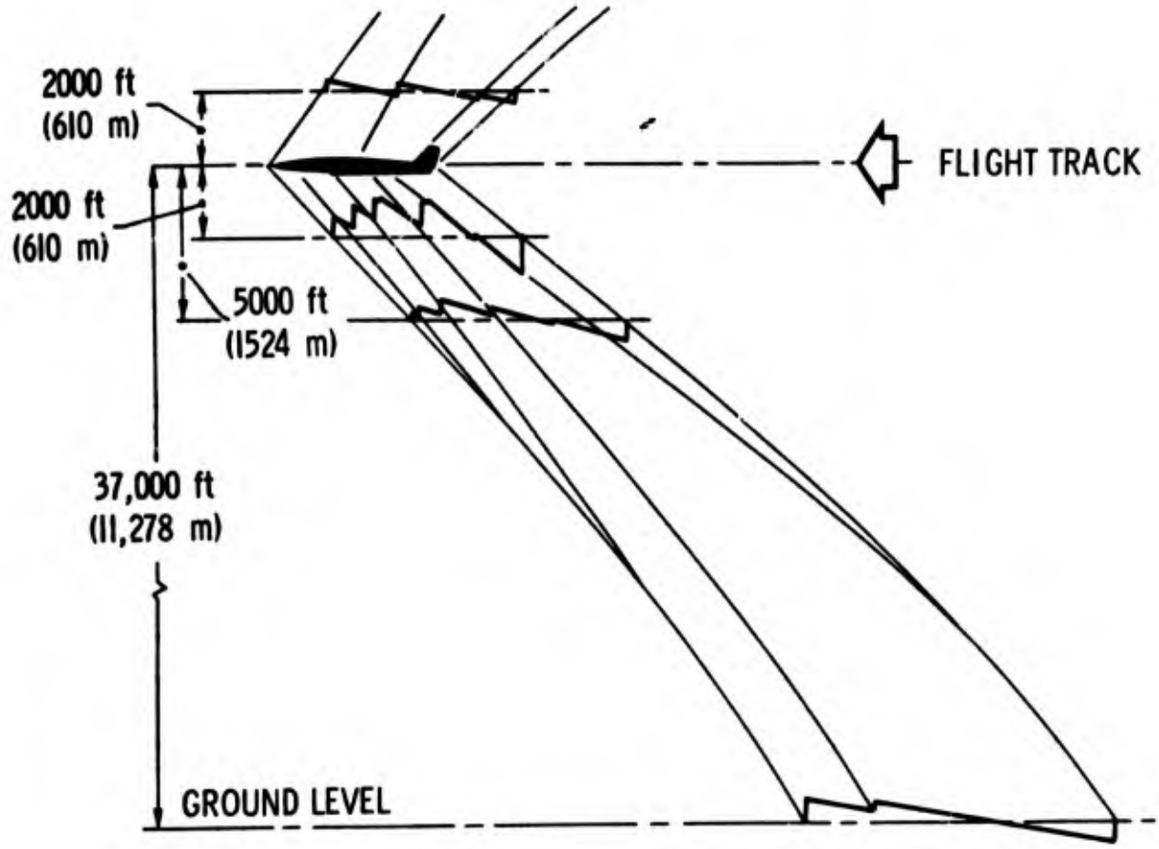

Fig.4 Flow field measurements of large aircraft

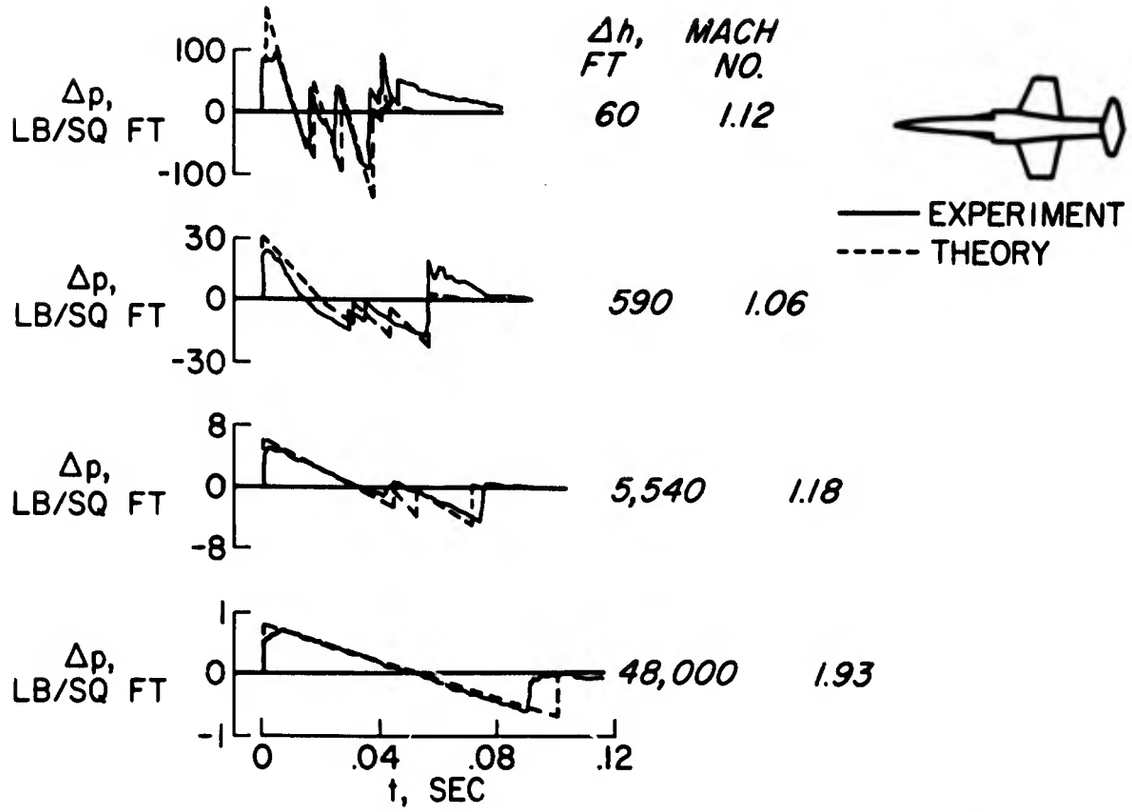

Fig.5 Comparison of theory with flight signatures

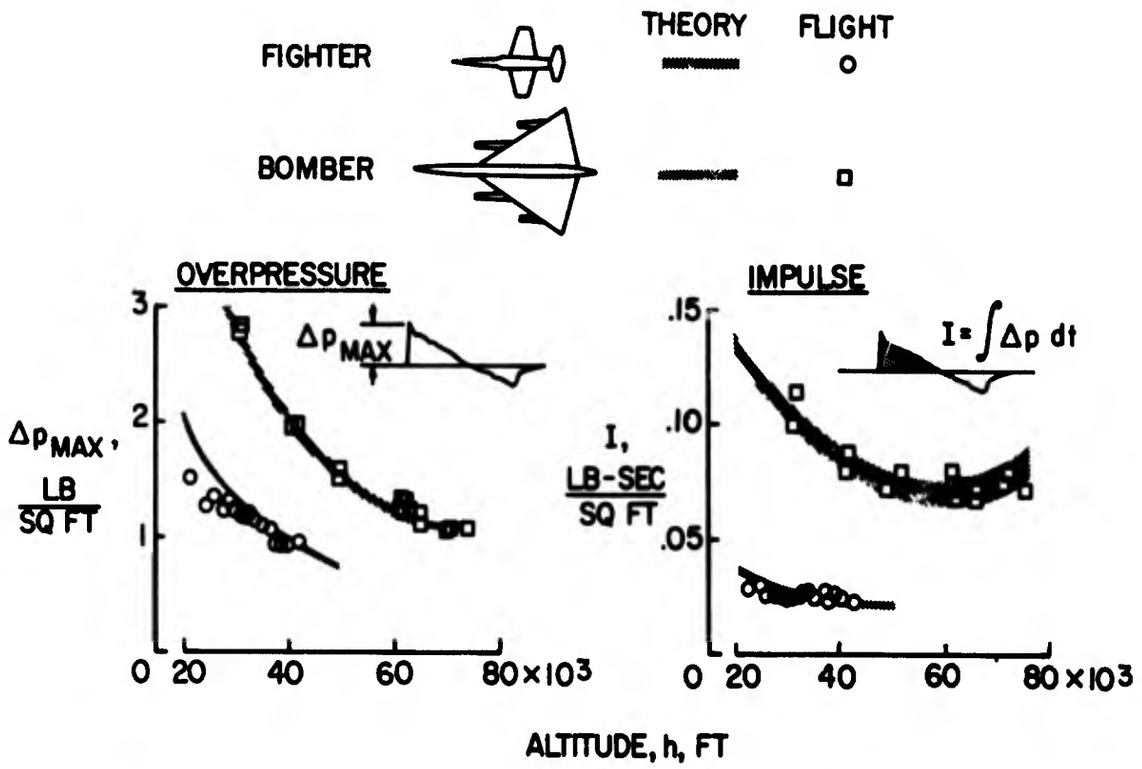

Fig.6 Comparison of theoretical and flight data

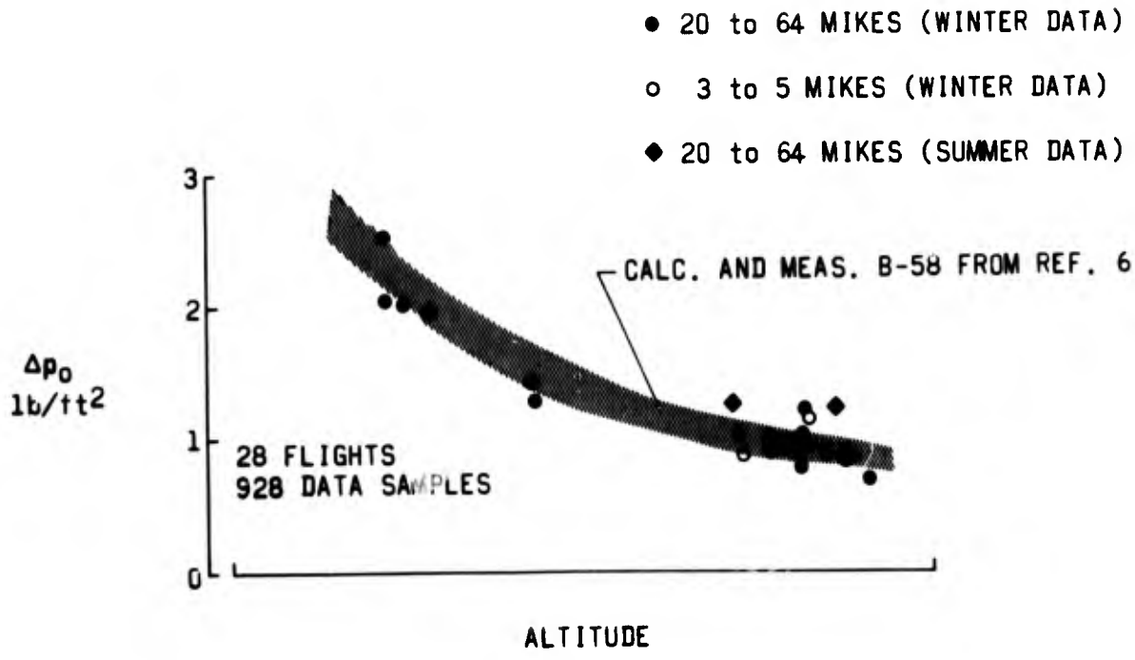

Fig.7 SR-71 ground track overpressures

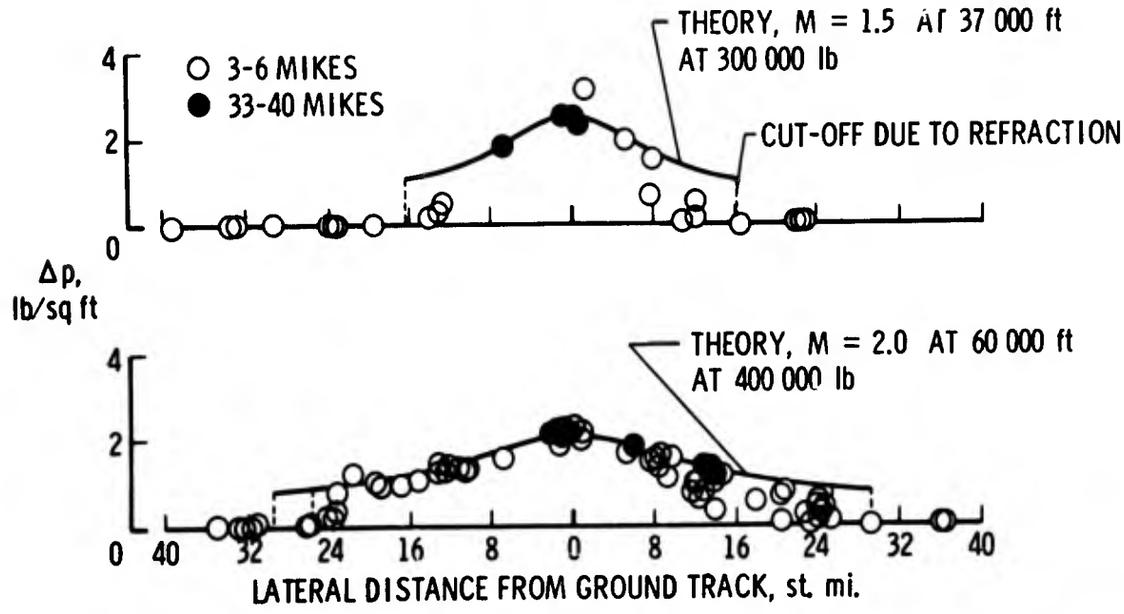

Fig.8 Lateral spread patterns - XB-70

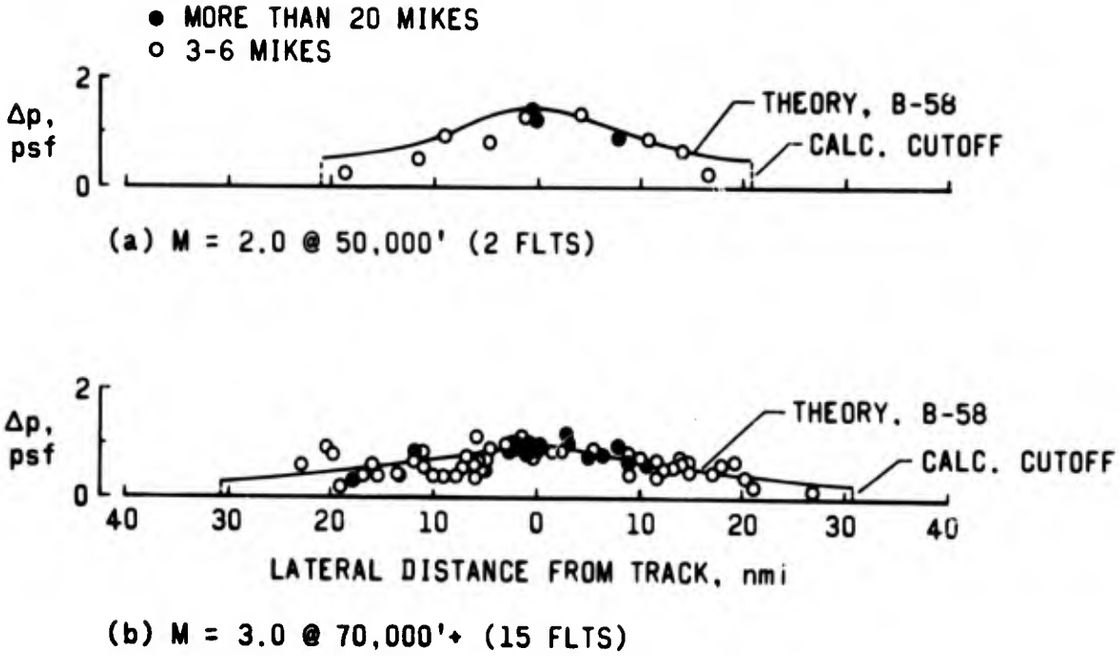

Fig.9 SR-71 lateral spread overpressure EAFB

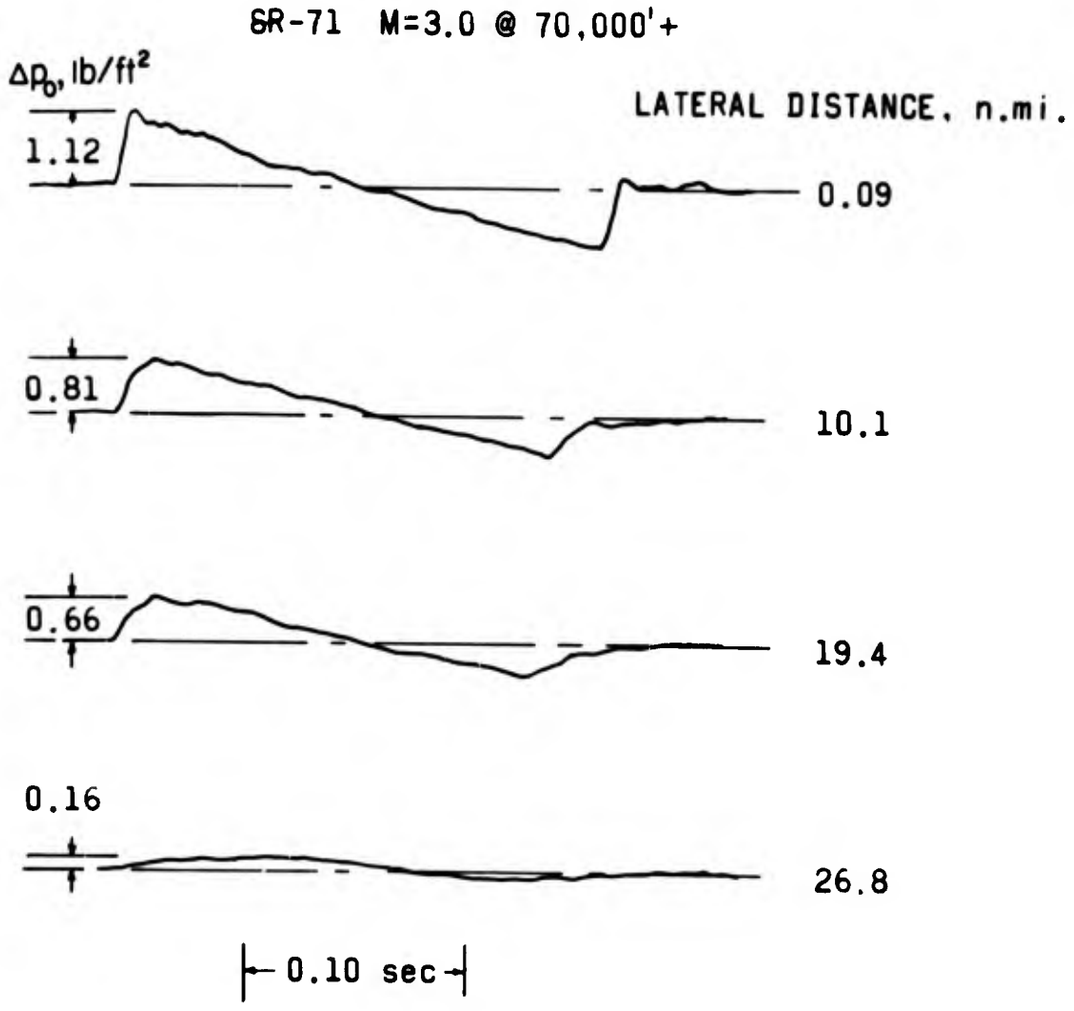

Fig.10 Variation of signature with lateral distance

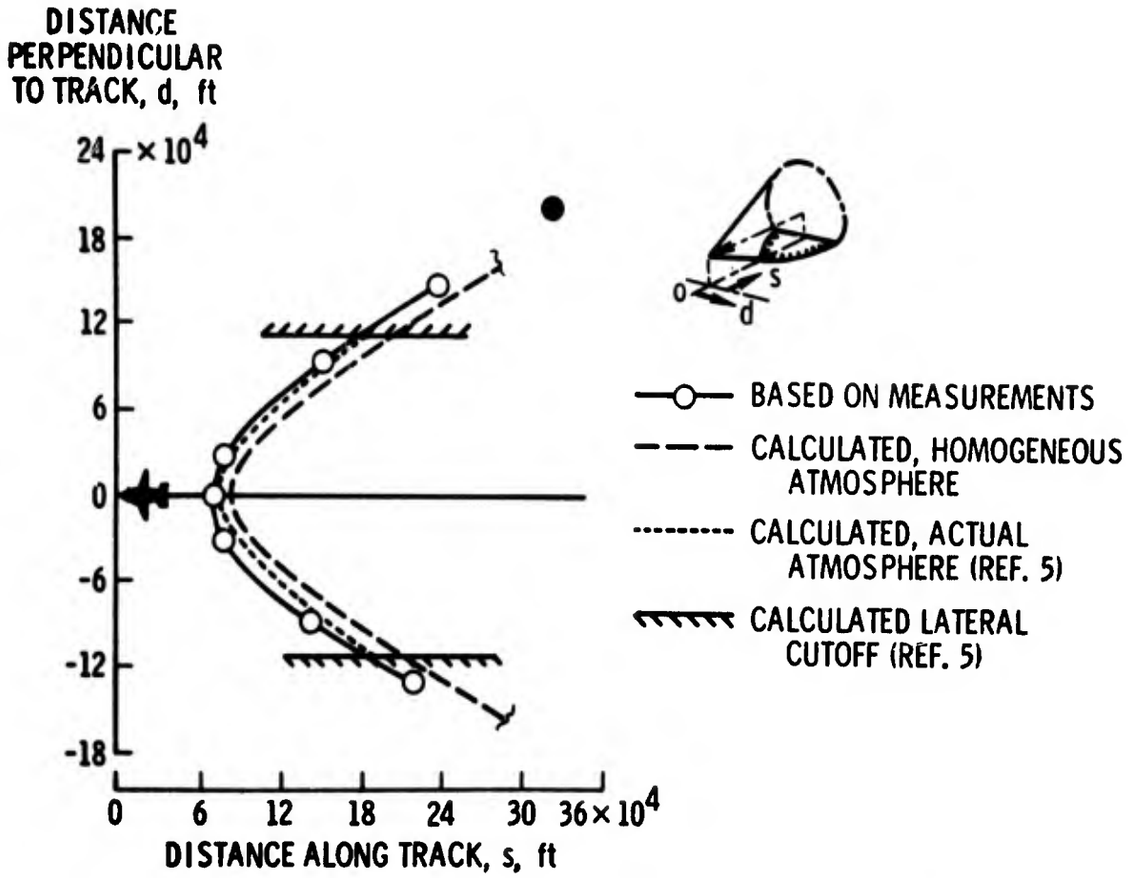

Fig. 11 Bow shock wave ground intersection patterns

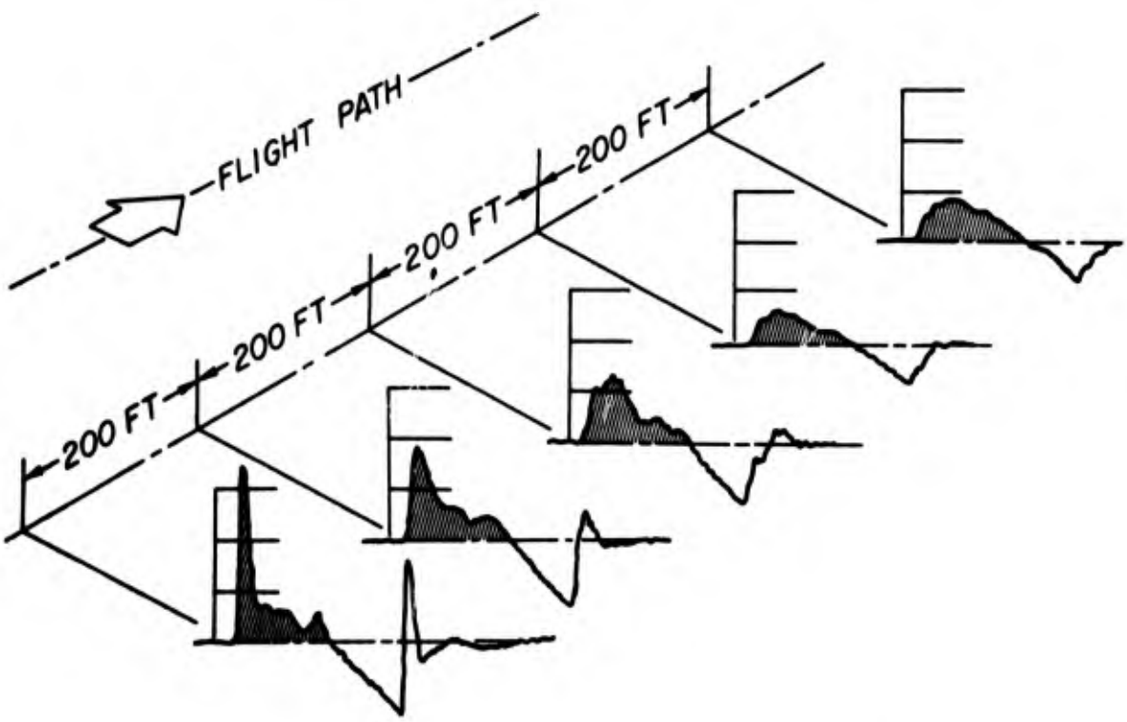

Fig. 12 Effect of atmosphere on pressure signature

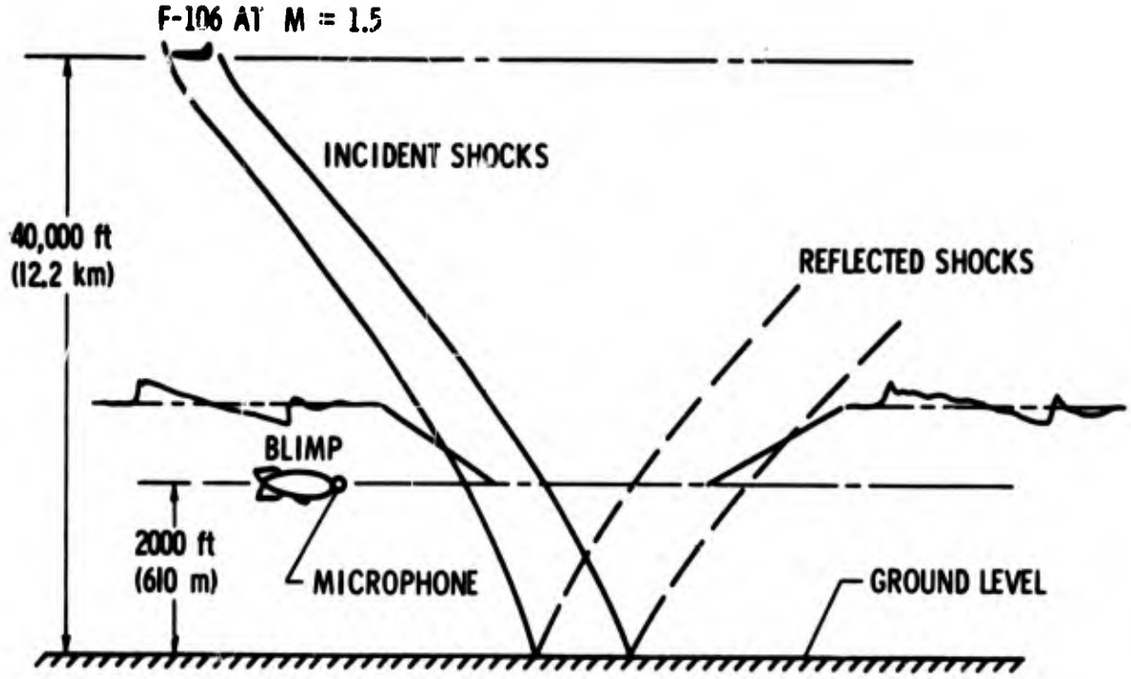

Fig.13 Airship measurements

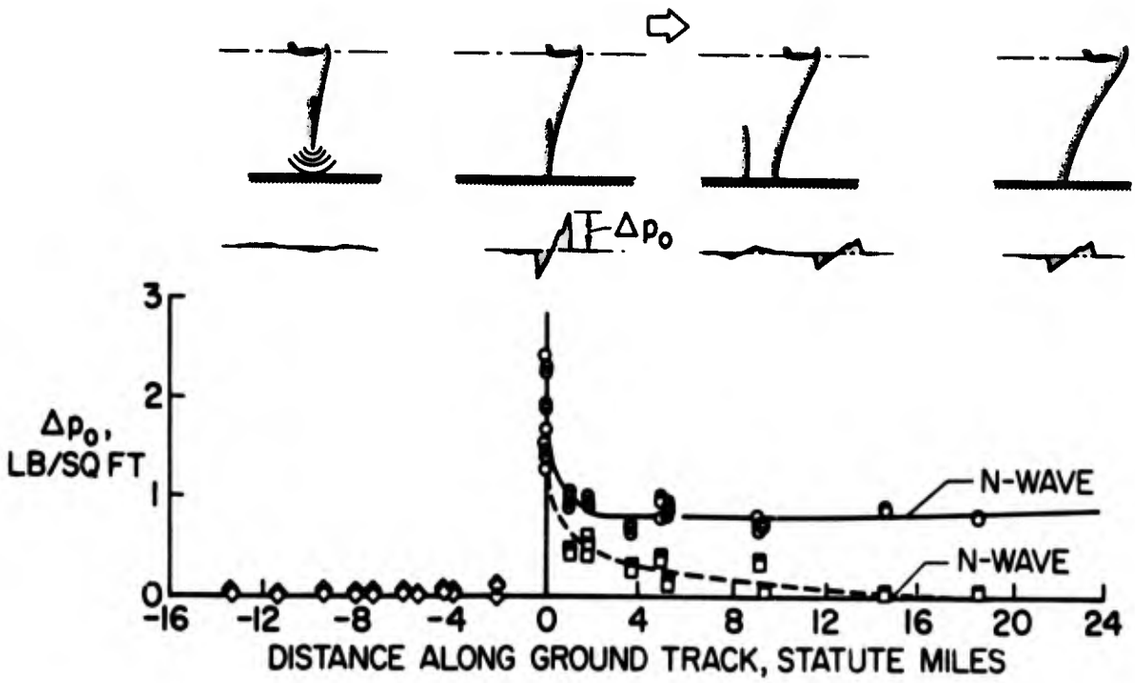

Fig.14 Ground pressures for accelerated flight

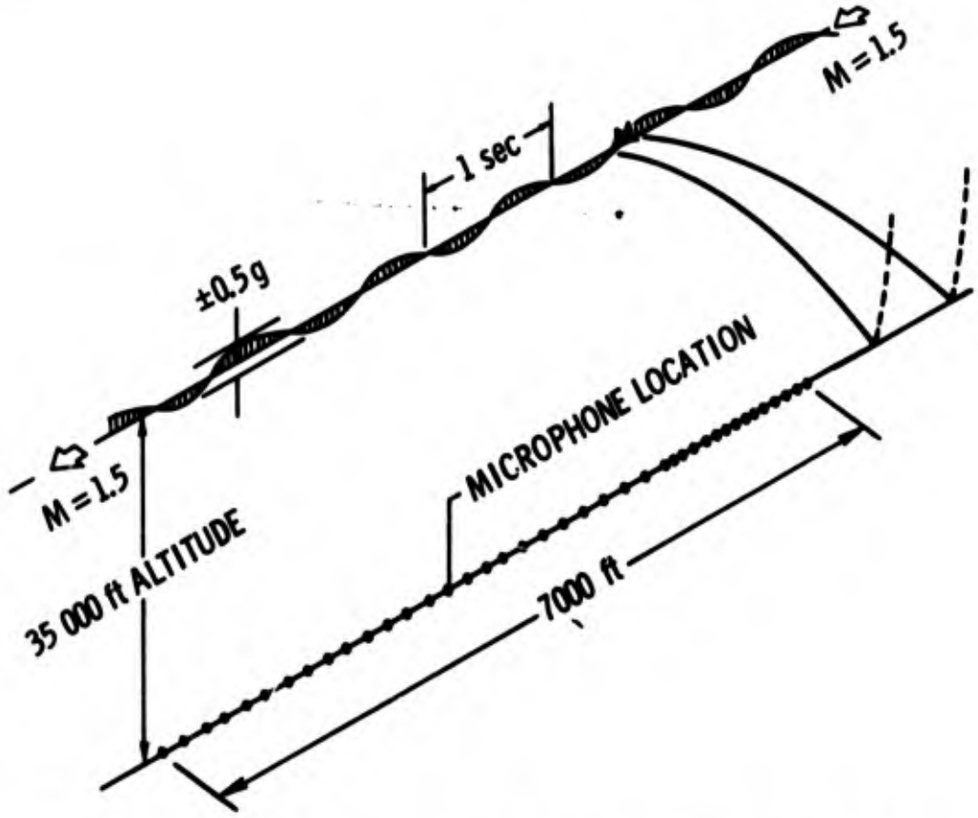

Fig. 15 Setup for studying airplane motion effects

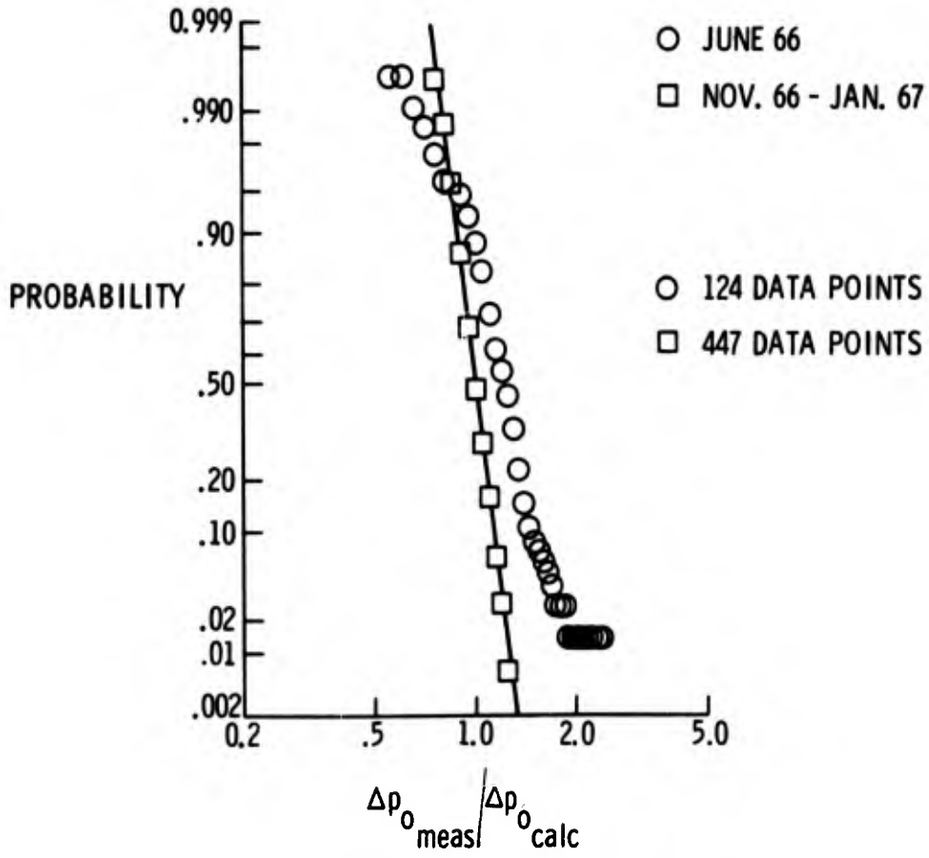

Fig. 16 Probability distributions - XB-70

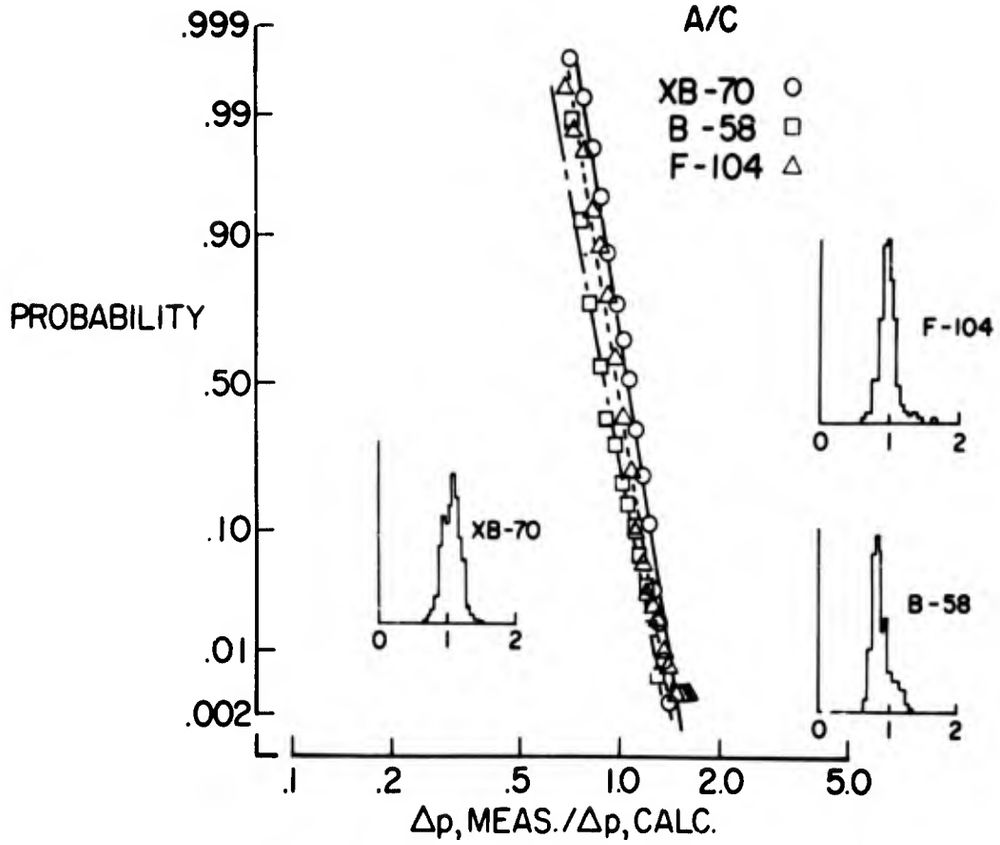

Fig.17 Probability data for three aircraft

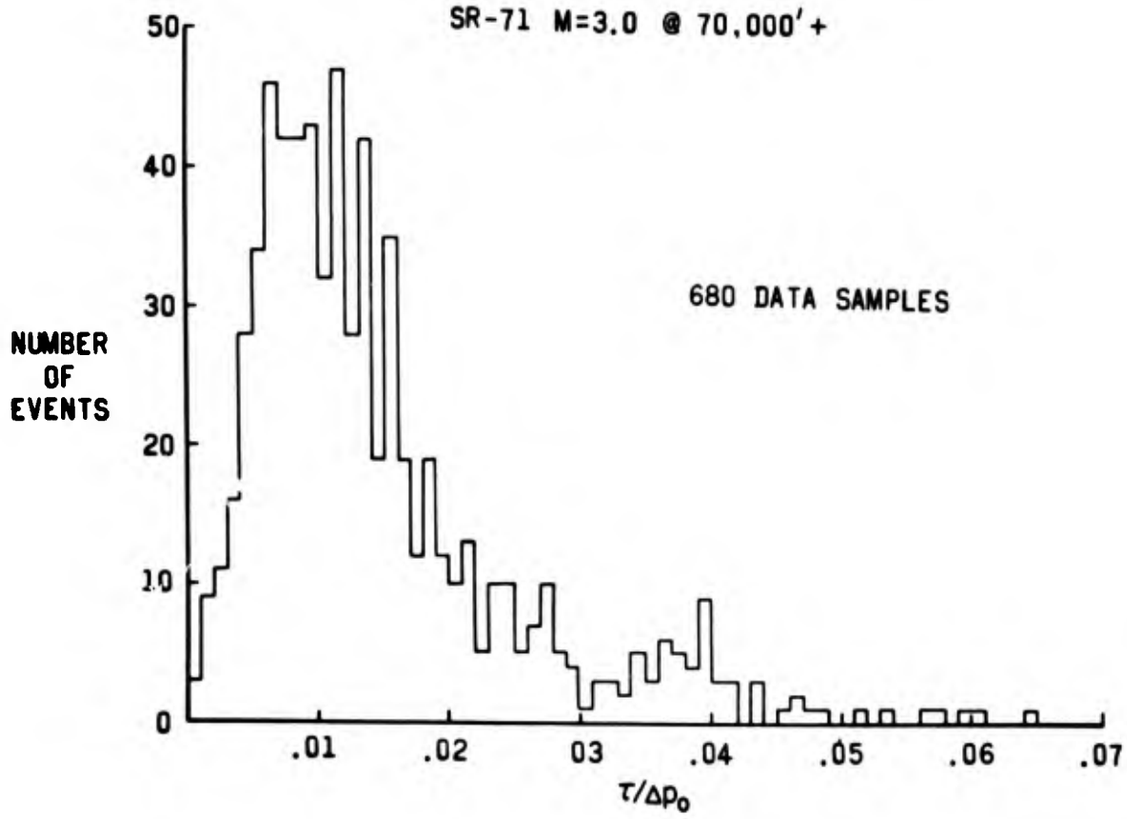

Fig.18 Variation of rise times

SR-71

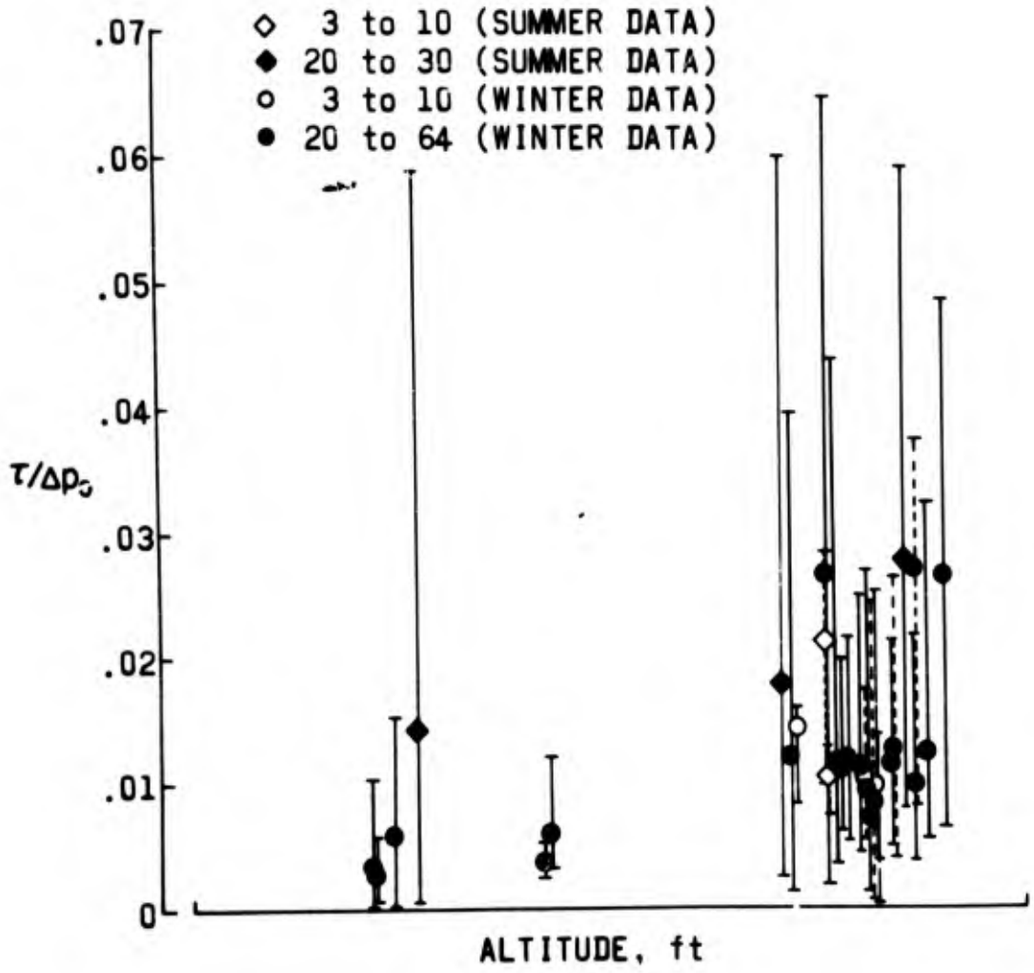

Fig.19 Effects of altitude

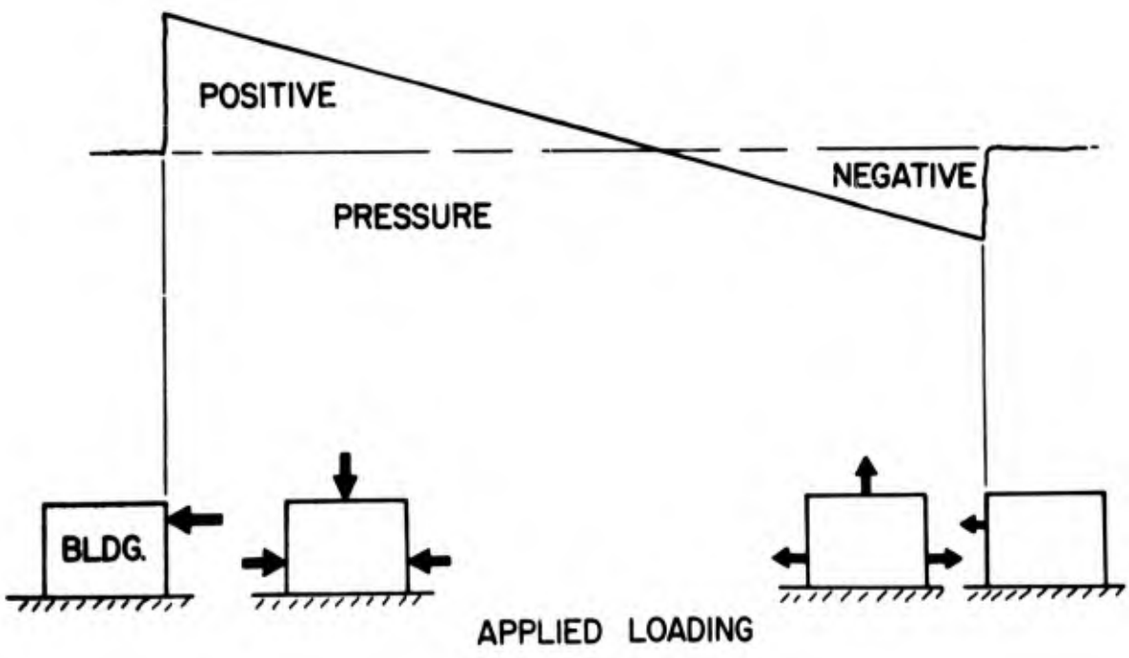

Fig.20 Sequence of loading

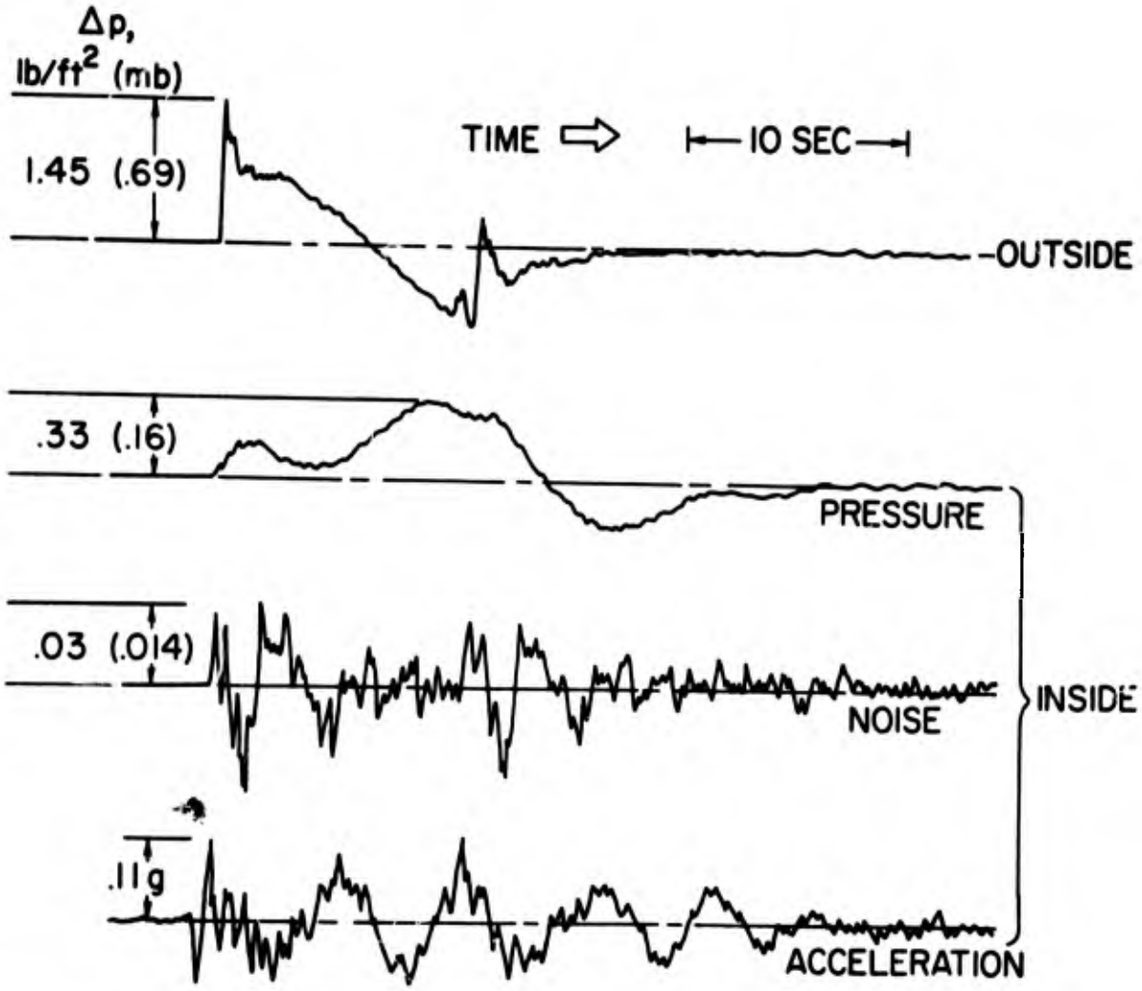

Fig.21 Sonic boom stimuli

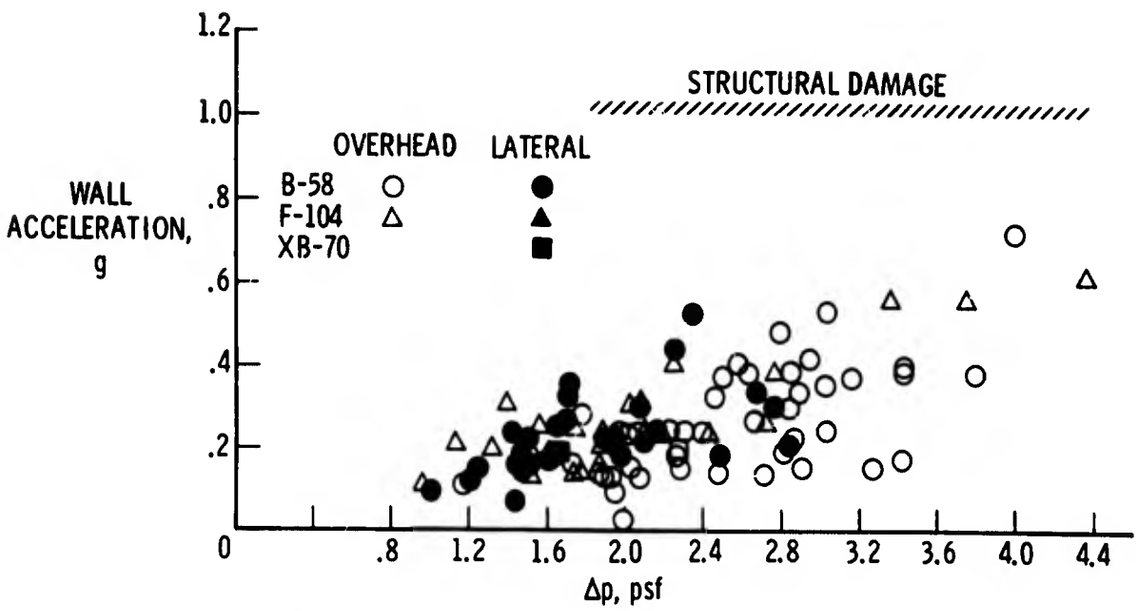

Fig.22 Building wall vibration amplitude as a function of overpressure

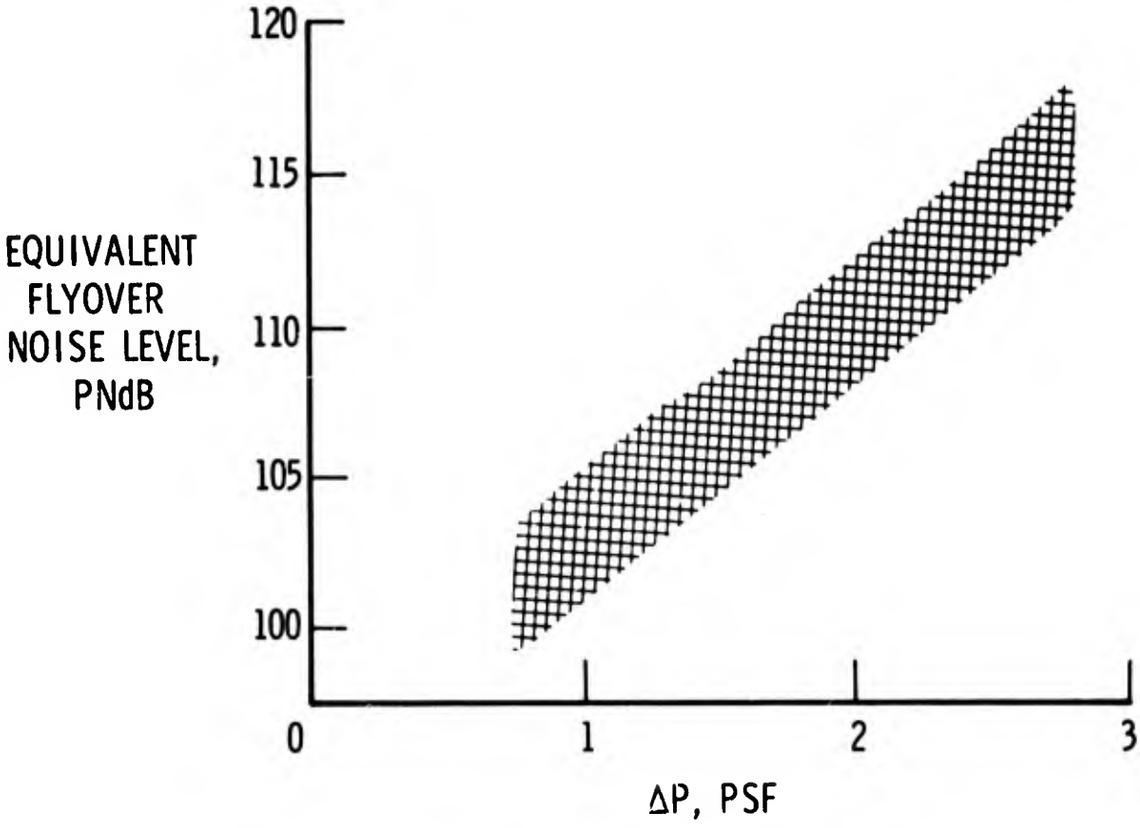

Fig.23 Subjective reactions

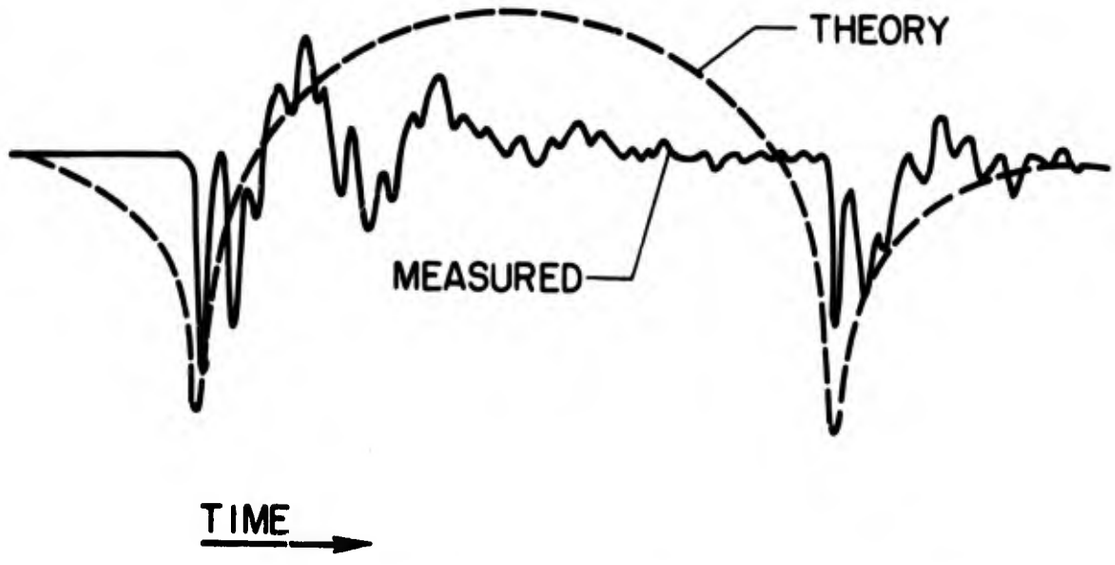

Fig.24 Sonic boom induced ground motions. Ground particle velocity

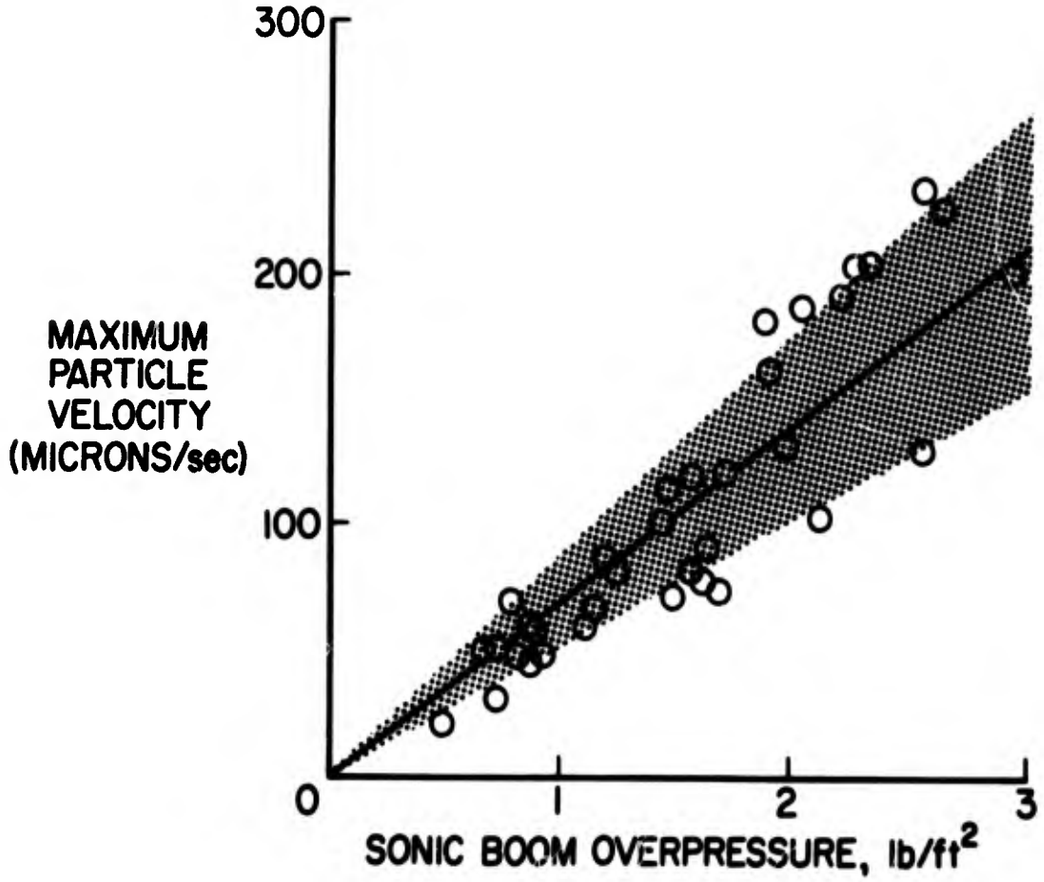

Fig.25 Sonic boom induced ground motions. Maximum particle velocity

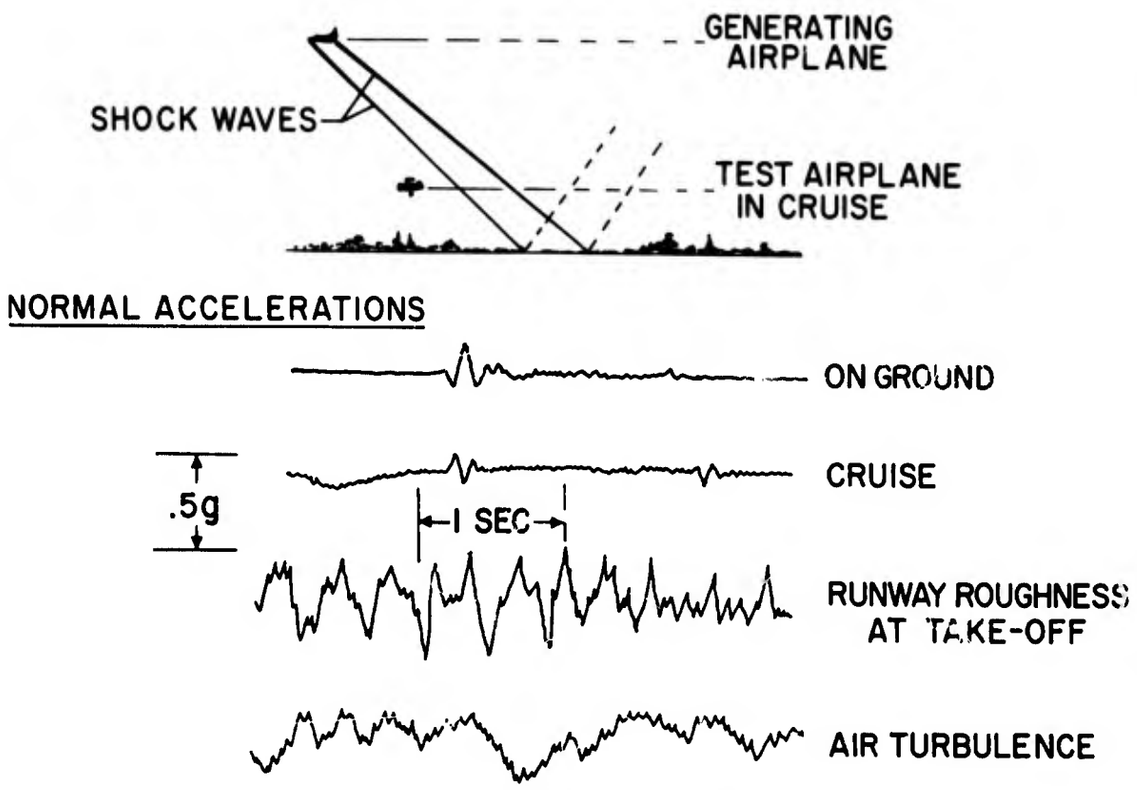

Fig.26 Sonic-boom effects on light airplanes

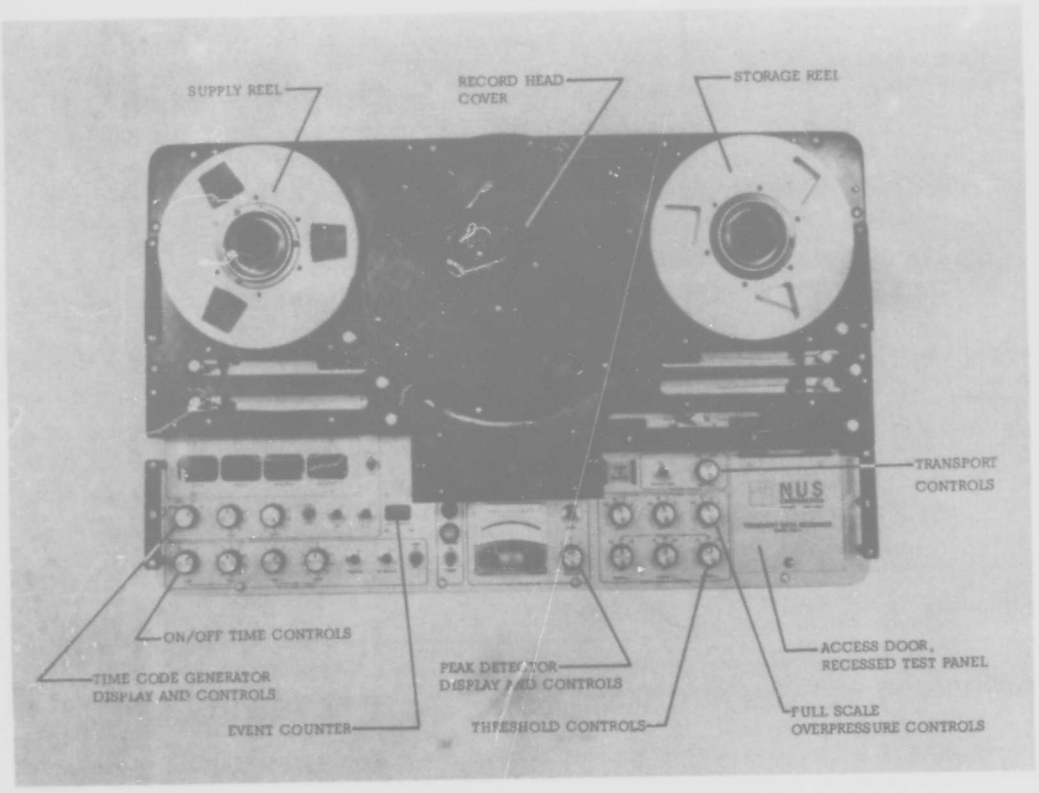

Fig.27 Transient Data Recorder, top view

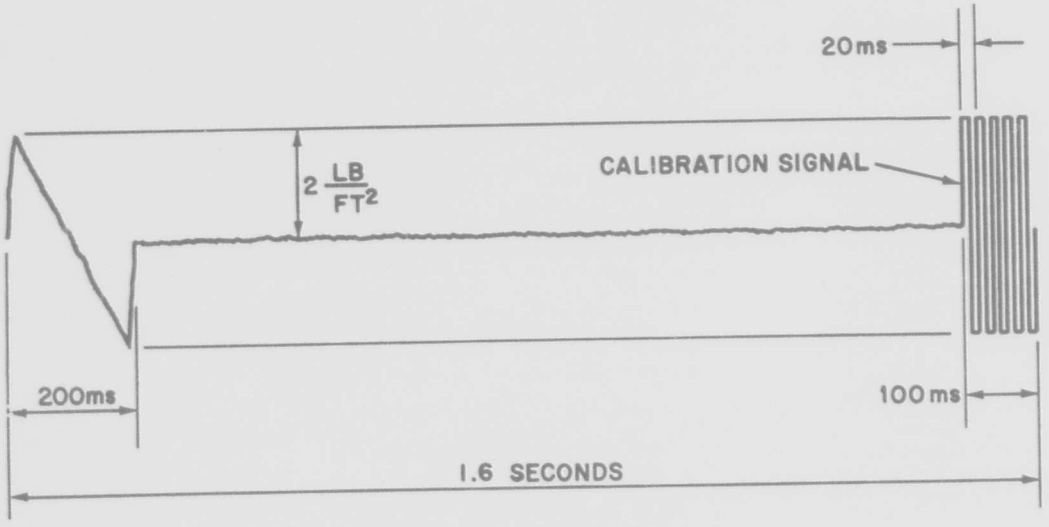

Fig.28 Typical TDR recording of N-wave

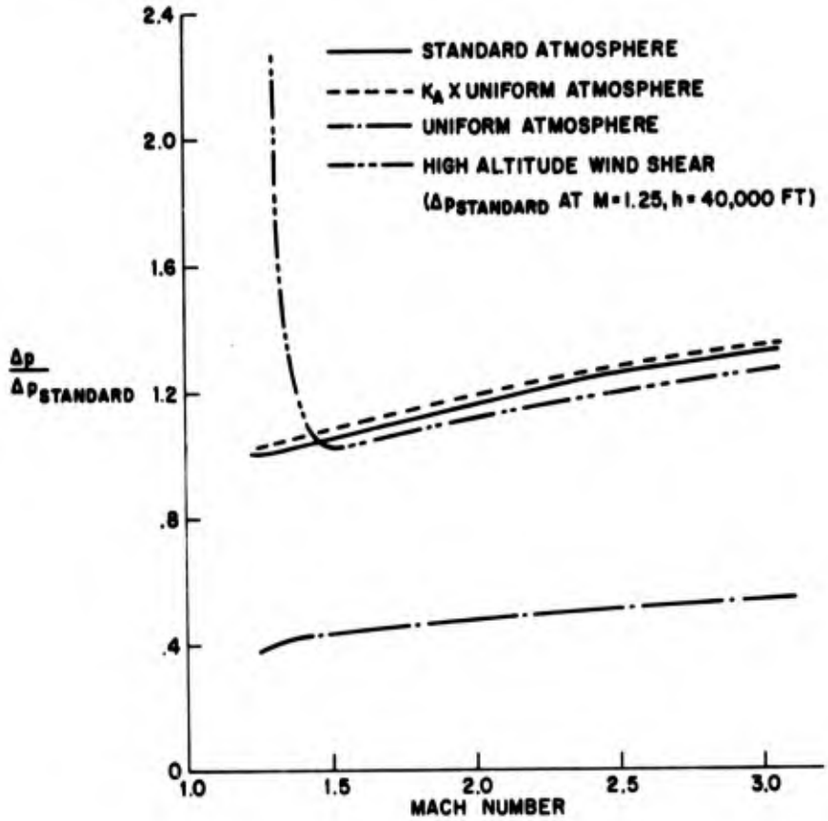

Fig.29 Mach number effects on overpressure ratios: F-104

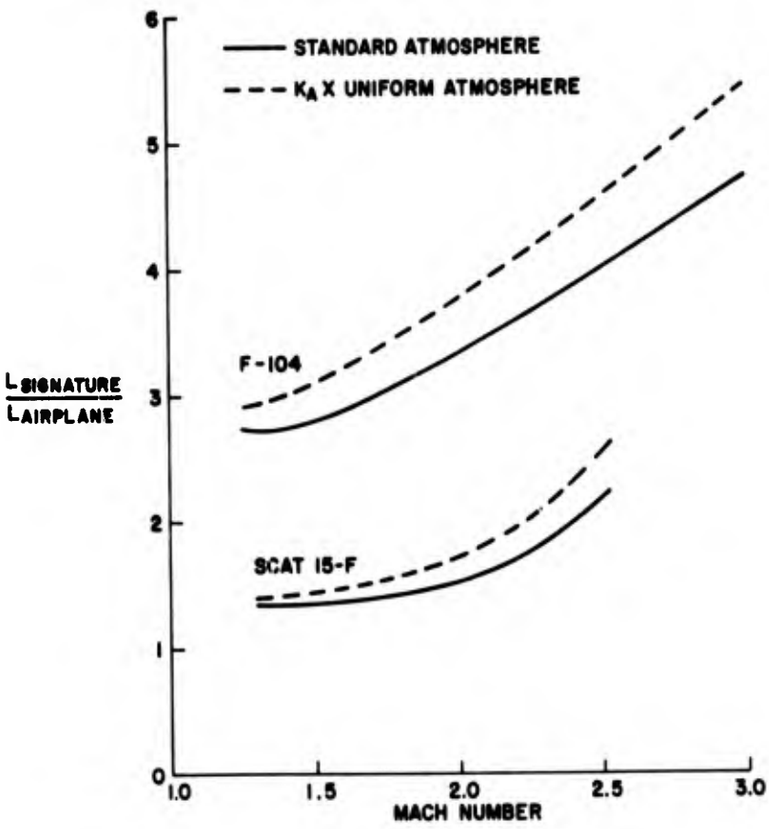

Fig.30 Mach number effects on signature length

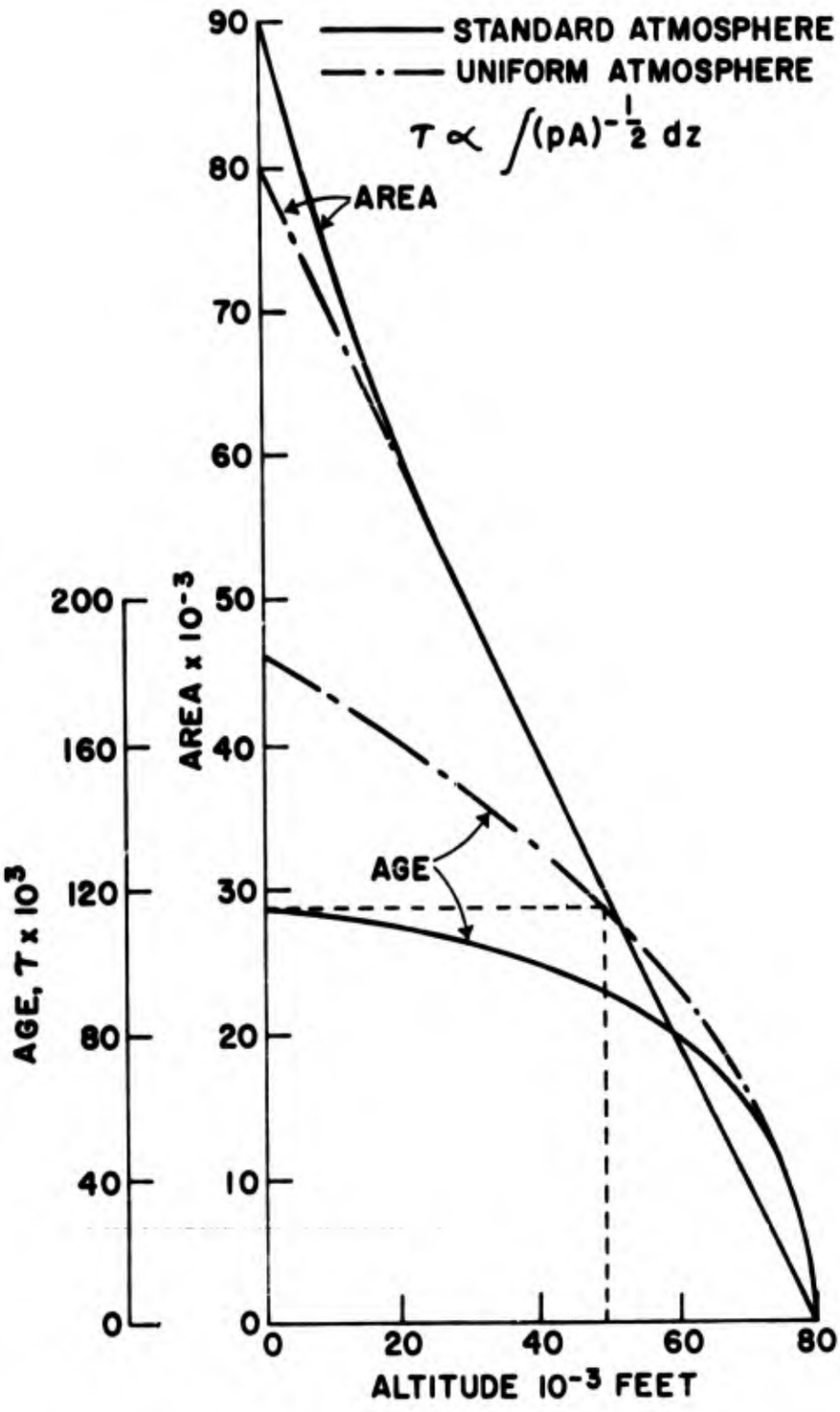

Fig.31 Variation of ray tube area and age variable with altitude

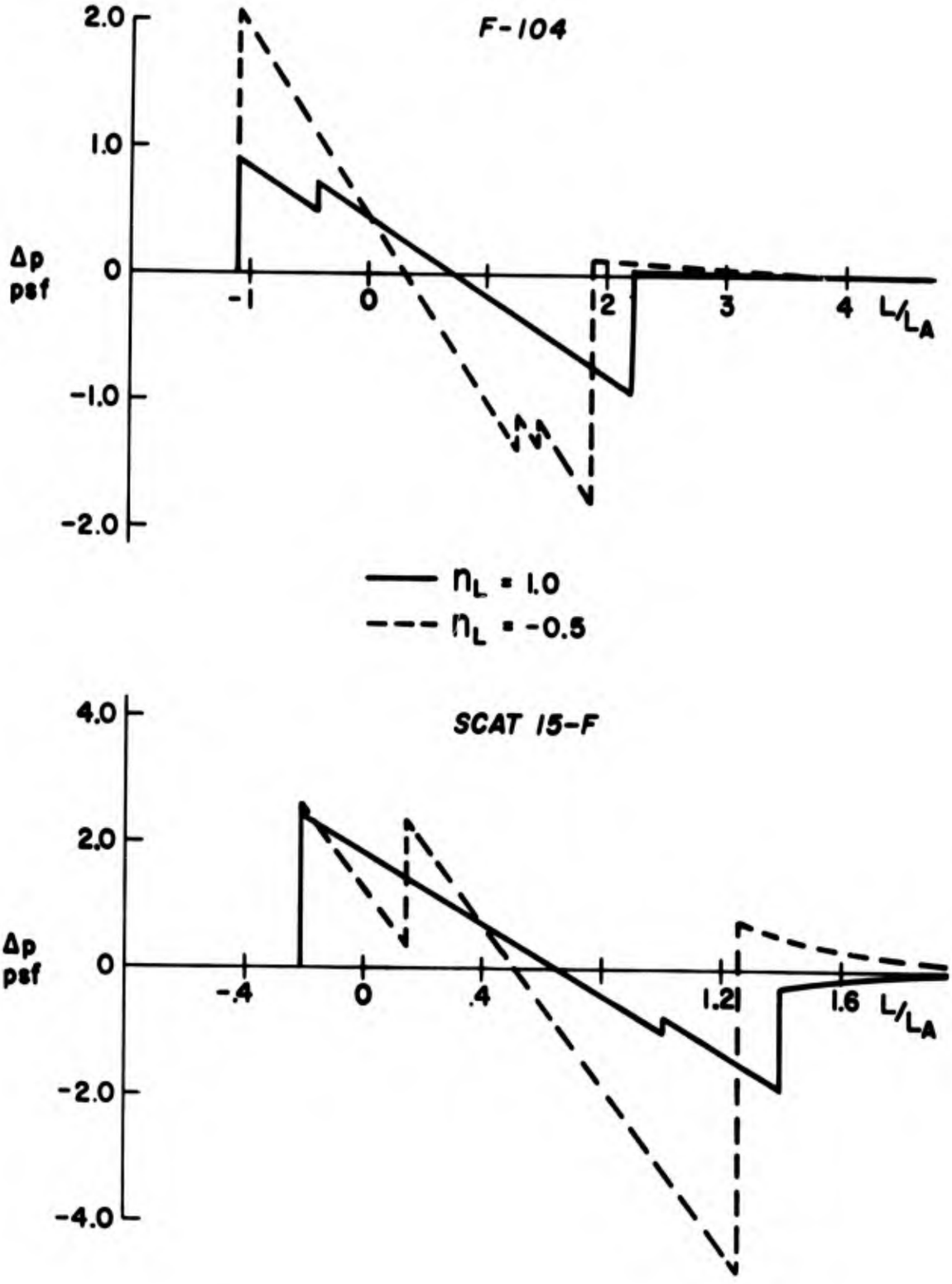

Fig. 32 Signatures for pushover maneuver and level flight at M = 2.0

BLANK PAGE

AN ANALYSIS OF DEVICES FOR REDUCING SONIC BOOM

Sin-I Cheng* and Arnold Goldburg**
Boeing Scientific Research Laboratories
Seattle, Washington

* Professor, Department of Aerospace and Mechanical Sciences, Princeton University, Princeton, New Jersey. Consultant - Boeing Scientific Research Laboratories, Seattle, Washington

** Head, Flight Sciences Laboratory, Boeing Scientific Research Laboratories, Seattle, Washington

SUMMARY

Techniques to apply electro-kinetic forces and to add thermal energy to the flow field around a supersonic transport have been proposed to alter the shock configuration and thereby to reduce sonic boom. Two questions are discussed in this paper.

1. Are the techniques for reducing the boom physically valid?

2. For those techniques which are valid, are the weight requirements for the electrical equipment within payload capability?

For the first question, it is found that the concepts advanced so far for the aerodynamic interactions are deficient in that an intensive interaction in more than one spatial dimension between the electric discharge or combustion over the nose and wing and the incoming supersonic flow will lead to a detached bow shock, not the attached shock of weak family claimed in the proposed schemes. Under these circumstances, both the boom and the drag are increased.

The second question of the specific power consumption (S.P.C.) is investigated. The estimate of the thrust generation and electric power required by the discharge is based on the analysis of a one-dimensional model which includes the key physical processes of the electric discharge. The S.P.C. is found to be of the order of 1 watt per dyne of the redistributed pressure force of the oncoming air around the supersonic airplane, (or 1/2 megawatt per pound force). New cathode materials or ingenious cathode configurations can reduce the S.P.C. at most by a factor of 10. Consider the supersonic transport at 65,000 ft (20 km) cruising altitude and at M = 2.7. For a 10% reduction of the strength of the leading shock, with possibly a 10% reduction of boom intensity, electric power of the order of a thousand megawatts is required. At the specific weight of 1 lb. (or 1/2 kg) per kilowatt of electric power, the electric equipment is beyond payload capability.

The conclusions reached are: The electro-aerodynamic and combustion techniques currently proposed are conceptually deficient. While some configurations, to be proposed in the future, of the electro-aerodynamic devices may prove to be conceptually valid, they are technically not feasible. Efforts for reduction of boom intensity should concentrate on the development of detailed optimization of the aerodynamic design of the airplane.

I. Introduction

Sonic Boom (or sonic bang) refers to the pressure distribution at the ground level produced by an airplane in Supersonic Flight. In the absence of any upstream propagating signals, upon the arrival of the airplane in the air space, the air is forced to deflect suddenly through shock waves to conform to the airplane contour. A complicated wave system around the airplane results as is sketched in Fig. 1. It is this wave system that produces pressure variation on the airplane surface that supports the airplane weight and acts against the engine thrust. The waves interact extensively and decay fairly rapidly with distance away from the airplane. This pressure field is very complex and is influenced by the airplane configuration. As the waves decay with lateral distance from the airplane, the details of the near pressure field gradually disappear and the boom generally emerges in the asymptotic form of an N-wave; also shown in Fig. 1. Theoretical studies[1]-[4] have revealed the qualitative dependence of such decaying waves. The boom of an airplane depends primarily on its "effective volume" and may be roughly divided into two parts: that due to the airplane volume at zero lift and that due to the angle of attack of the airplane in producing lift. The two components of the ground level boom may be referred to as the volume boom, Δp_V, and the lift boom, Δp_L, given respectively as

$$\Delta p_v = k_v (p_a\, p_o)^{1/2}\ (M^2 - 1)^{1/8}\ \frac{d}{\ell_v^{1/4}} \cdot \frac{1}{h^{3/4}} \tag{1a}$$

$$\Delta p_L = k_L\, p_o^{1/2}\ \frac{(M^2 - 1)^{3/8}}{M} \cdot \frac{W^{1/2}}{\ell_L^{1/4}}\ \frac{1}{h^{3/4}} \tag{1b}$$

K_V and K_L are shape factors of order 0.5 to 1.0 and vary slowly with changes in shape. p_a and p_o are the atmospheric pressure at flight altitude and at ground level respectively. The airplane is assumed to be cruising at altitude h at Mach number M. d is the characteristic diameter of the airplane volume and W is the weight of the airplane. Both components decay as the quarter power of the relevant length scale in the flight direction: ℓ_v may be taken as the overall length of the airplane while ℓ_L should be taken as the characteristic length of the lifting surface. Δp_V decays as 1/2 power of p_a at flight altitude h while Δp_L is independent of p_a. With the atmospheric pressure decaying exponentially with increasing altitude, Δp_V decays much more rapidly than Δp_L as h increases. Thus, at low altitudes, Δp_V dominates. However, at the cruising altitudes of commercial supersonic transport Δp_L becomes the larger component although Δp_V remains significant (Fig. 2). Under these circumstances, the reduction of the lift boom, Δp_L, is of primary concern.

By increasing the scale lengths ℓ_v and ℓ_L, the boom will be reduced according to the 1/4 power law. These scale lengths can be increased by extending the airplane structure. This is generally deemed undesirable from a structural point of view due to the obvious increase of the airplane weight. Any possibility of effectively increasing these scale lengths without additional structure is clearly of great interest. Thus the concept of creating a "phantom" airplane of increased length over the physical dimensions has been proposed for boom reduction. It must be noted that a physical extension of the length of the airplane by affixing a long spike in front of it will produce little effect on the boom without a significant redistribution of the lift and volume from the airplane onto the spike. In the limit, a spike of zero thickness and great length attached to the airplane nose would have no effect on the boom although the length of the airplane may be much increased. Under the circumstances, neither ℓ_v nor ℓ_L would be increased by the spike with K_v and k_L unchanged for the original volume and lift distribution over the given scale lengths. If one prefers to adopt an extended length as ℓ_v and ℓ_L, then both k_v and k_L must be correspondingly reduced due to the different distributions. The boom can be proportionally reduced according to the increase of the length scale only to the extent that the lift and the volume are actually redistributed along the axis so as to keep k_v and k_L unchanged. This is the crux of the similtude argument.

The determination of the optimum distributions of airplane volume and lift for minimum values of the propationality constants k_v and K_L has been the subject of extensive aerodynamic studies[5]-[9] Difficult and tedious as such studies may be, they will point to the correct direction of designing airplanes with lower boom. Even without a careful analysis of the aerodynamic situation, it is obvious that if the leading shock wave could be replaced by a very long series of isentropic compression waves or by a succession of weaker shock waves, the airplane drag and boom would be simultaneously reduced. Such progress towards boom reduction might be accomplished with carefully designed compression ramps with the associated weight penalty of the ramp structure. Now, if the air could be so deflected and compressed gradually, prior to the arrival of the supersonic airplane, without the use of physical ramps, reduction of the sonic boom might be expected in the form of smaller k_v and K_L without the weight penalty of the ramps. The above considerations give rise to the early warning concepts, the underlying principle of which does not appear to be completely different from that of the concept of the phantom airplane of extended scale lengths.

Alternately, if the exhaust gas from the jet engine could be cooled significantly while maintaining the engine thrust, the reduction of the effective volume of the exhaust jet would reduce k_v and therefore the volume boom.[10] Or, if one could increase the lift curve slope $dC_L/d\alpha$ or the lift drag ratio L/D of the airplane, the constant K_L and hence, the lift boom Δp_L would be reduced. A great variety of schemes may be proposed to operate on one or several of the basic ideas described above. Although the physical identity of the annoying or objectionable aspects of the sonic boom are not firmly established, it is believed[14] that the reduction of the peak pressure rise and of the time of rise are among the most significant factors. In this sense, any schemes enumerated

above for reducing Δp and widening the compression region may be considered as possibly leading to devices for reducing the sonic boom. For each such device, two questions must be faced: one, is the scheme conceptually correct in that a boom reduction would result; and two, is the scheme technically feasible and economically justifiable?

II. Aerodynamic Interaction

The suggested devices for boom reduction involve the coupling of thermal energy[10,11] or electrokinetic forces[12,13] to the conservation laws of mass and momentum. Cahn and Andrew[12] demonstrated (Fig. 3a) that a corona discharge over the nose leads to a thick, diffused or scattered shock layer over the nose and conjectured about a slower pressure rise and a weaker leading shock. The idea of extending the compression region into the undisturbed air upstream of the airplane is pursued by the proposal of direct injection of electrostatic charges from the nose (Fig. 3b). In each case, the effective length of the airplane was to be increased by the upstream penetration of the charged particles. The deflection and compression of the undisturbed air was to be visualized as the response of air to the early warning carried by the ionized particles. The early warning can also be achieved by other means. Energy additions to the undisturbed air may be achieved by focusing light of various frequencies or the more exotic laser beam. Chemical energy may be released from fuel injected upstream in the form of external combustion. Since the nose region is at higher pressure than downstream locations, the energy released there may in part be recovered through a guided expansion as in the form of useful thrust. Thus external combustion was proposed not only as a boom reduction device but with the added benefit of auxiliary thrust generation.[11] All these schemes presumed that an extended region of upstream compression would a priori weaken the leading shock and increase the effective length scale, both contributing to boom reduction.

The first question is now considered: are these schemes conceptually correct? When disturbances in the form of heat and/or of momentum addition are introduced at some point on or along the upstream axis (or plane of symmetry), there cannot be a purely isentropic or a shock free flow in the nose region ahead of the solid boundary. The hypothetical configuration of two (or more) detached straight shocks (Fig. 4a) deflecting the upstream supersonic flow in two (or more) steps to conform to the required flow deflection at the nose is not compatible with the mass continuity relation near the axis and hence cannot occur; a vacuum would be required.

When the fluid motion is continuous through the axial region, the lateral velocity component, v, the streamline deflection angle δ and the streamline curvature κ must vanish on the axis and are odd functions of the distance from the axis. The lateral motion may be the result of the action of lateral force or of the expansion of gas volume under heat addition, for example. The streamlines in the upper half plane must be concave to conform, at least in part, to the deflection of the wedge or cone surface. The centrifugal force due to these curved streamlines is sustained by a pressure gradient across the streamlines. The pressure field is set up by a curved shock just upstream of the disturbance. The cross stream momentum balance is

$$\kappa\rho q^2 = -\frac{\partial p}{\partial n} + f_n \tag{2}$$

where ρq^2 is the local dynamic head of the flow with local curvature $\kappa>0$. The distance normal to the curved streamline is designated by η and f_n is the component of the body force acting on the fluid in the normal direction.

Consider the case of heat addition with $f_n = 0$. Let the curved shock be defined by $y_s\ (x_s)$ where the origin $x_s = y_s = 0$ coincides with the intersection of the curved shock on the axis. Immediately behind the shock, we have

$$\kappa\rho q^2 = -\frac{\partial p}{\partial n} = -\rho q \cdot \frac{\partial p}{\partial \psi}$$

$$= \frac{pq}{p_\infty q_\infty}\left(\frac{dp}{d\delta}\right)_s \left(\frac{d\delta}{dy_s}\right)_s > 0 \tag{3}$$

Here ψ is the Stokes, or the planar stream function, δ is the streamline deflection angle and subscript s indicates qualities evaluated along the shock wave. For $y_s \geq o$, the symmetry requires

$$\delta = \left(\frac{d\delta}{dy}\right)_s \cdot y_s + \cdots\cdots\cdots \geq 0 \tag{4}$$

$$\kappa = \left(\frac{d\kappa}{dy}\right)_s \cdot y_s + \cdots\cdots\cdots \geq 0 \tag{5}$$

The equality sign holds when $y_s = 0$ on the axis. With ρq and $\rho_\infty q_\infty$ both finite and positive, we conclude that along the shock

$$\left(\frac{dp}{d\delta}\right)_s = -\rho_\infty q_\infty \cdot q \cdot y_s \left(\frac{d\kappa}{dy}\right)_s \Big/ \left(\frac{d\delta}{dy}\right)_s \leq 0 \tag{6}$$

Now, for planar shock, the pressure-deflection polar diagram (p-δ) is shown in Fig. 16-4d. With $(dp/d\delta)_s \leq 0$, the local planar shock elements of the curved shock in the vicinity of the axis must be of the strong family as shown in sketch Fig. 16-2c, starting with a normal shock (transition O-N Fig. 16-4d) on the axis. The configuration of curved shock with weak family elements forming a cusped peak on the axis (Fig. 16-4b) is dynamically unstable[15] although kinematically consistent. The reason for this is that the dynamic force balance requires that the pressure decrease parabolically with distance from the axis while the cusped weak shock family would produce a pressure field increasing from the axis. The bow shock, (Fig. 16-4c) with a normal shock across the axis, can be the only result. This gives a subsonic region between the shock and the nose at a pressure considerably higher than the pressure produced by an attached shock of weak family over the sharp nose. The higher air pressure behind the bow shock considerably decreases the penetration distance of the disturbance so that it is within the stand off distance of the bow shock wave.

In the case of electric discharge over the nose, the electro-aerodynamic interaction provides a lateral force on the stream in the subsonic region at elevated pressure behind the bow shock. The resultant lateral force is, however, of higher order immediately behind the shock since the bow shock itself is the initial response of the uniform supersonic flow to downstream disturbances. The general pattern of strong aerodynamic interaction between the uniform supersonic flow and some downstream disturbance remains unchanged, no matter whether the downstream disturbance of the various boom reduction devices is of the nature of heat, momentum or mass addition. A sketch of the flow field between the bow wave and a wedge nose charged as anode (or cathode) is shown in Fig. 16-5.

The detached bow shock wave is much stronger than the oblique shock attached to the nose and will lead to a higher peak pressure rise of the N-wave in the far field. It will also produce higher drag on the airplane, and most likely lower lift. The loss of lift is inferred from Fig. 16-4d, since the pressure difference on a wedge surface at an angle of attack α as might be produced by shocks of strong family is not only of smaller magnitude but of opposite sign as that produced by shocks of weak family. The loss of lift and the increase of drag produced by the shocks of strong family would further increase the boom and lead to serious deterioration of the performance of the airplane.

The external combustion scheme patented by Schoppe[11] is similar to a forward facing ramjet. The boom is to be reduced in an undisclosed way and subsequent exhaust expansion of the heated gas is to compensate to some extent for the drag created by the bow shock However, there is the added expense of a significant increase of the volume boom.[10] Further under the cruise condition, the main engines are not operating at maximum thrust so that the fuel for the external combustion can be used much more effectively if burned in the primary engines. The auxiliary thrust of the external combustion scheme does not offset the several boom increasing factors of heat addition.

Plausible schemes of boom reduction should avoid the detached bow shock over the nose or the leading edge of the airplane. However, detached waves in the downstream portion of the airplane flow field are not serious in boom production. In fact, strong shock waves in the midfield may be desirable in the sense that the effect of devices to increase the local pressure will be additionally magnified by the strong shock interactions. If the optimum lift distribution for a given airplane is known from aerodynamic studies, but the airplane configuration departs from this optimum due to other design constraints, redistribution of the lift by either electro-aerodynamic or thermal devices may be accomplished to approach this optimum. The redistribution would be at the expense of electric power or chemical fuel instead of structural changes. Accordingly, we next examine how effectively electric discharge may be utilized in this manner for reducing the boom of a given airplane.

III. Stream Thrust Generation by Gaseous Discharge

Electric discharge in moving air modifies the flow field through momentum and energy exchange between the ionized and the neutral particles of air.[16] It will cause changes in the general pattern of the supersonic flow as was discussed in the previous section, even if the center line is replaced by a straight solid boundary (inviscid or viscous). Approximations are required to make an analytical estimate on the pressure change produced and the power expenditure required of the electric discharge in the complex flow field downstream of the curved shock. A one dimensional model in which the electric field E is parallel to the flow velocity u is adopted here. This one dimensional configuration is the most favorable for the momentum exchange between the ionized particles and the air to produce a change of the air pressure. The various physical processes important in electric discharge are represented phenomenologically within the continuum framework. The phenomenological representation is convenient since we wish to apply our result to various modes of electric discharge in which different physical processes dominate respectively. This approach is also necessary because the information concerning the details of the fundamental physical processes of electric discharge are numerous, varied and unevenly known. The strongest assumption made to facilitate analysis is the neglect of diffusion of the ionized particles. While the lateral diffusion can be consistently neglected in a one dimensional model, the longitudinal diffusion is known to be important in some interesting phenomena of the detailed structure of the electric discharge. We believe, however, that the neglect of diffusion tends to overestimate the thrust generation and underestimate the power expenditure and such an assumption is therefore in favor of the proposed schemes. Such errors will reinforce rather than defeat our conclusion of the very poor performance of the proposed devices. Of lesser importance, the change of the global temperature of the discharge medium is also neglected. Other minor simplifications are adopted along the way to facilitate the analysis.

The governing differential equations are:

$$\begin{cases} j_+ = \sigma_+(V_{d+} + u) & (>0) \end{cases} \tag{5}$$

$$\begin{cases} j_- = \sigma_-(V_{d-} - u) & (>0) \end{cases} \tag{6}$$

$$\begin{cases} \frac{d}{dx} j_+ = \alpha j_- + \beta j_+ + \lambda \end{cases} \tag{7}$$

$$\begin{cases} \frac{d}{dx}(-j_-) = \alpha j_- + \beta j_+ + \lambda \end{cases} \tag{8}$$

$$\frac{1}{4\pi} \frac{d}{dx} E = (\sigma_+ - \sigma_-) = \frac{j_+}{U+V_{d+}} - \frac{j_-}{V_{d-}-u} \tag{9}$$

$$\begin{cases} \rho u \frac{du}{dx} + \frac{dp}{dx} = E\sigma_+ - kE\sigma_- = f_i \\ \qquad = E(\sigma_+ - \sigma_-) + (1-k) E\sigma_- \end{cases} \tag{10}$$

$$\begin{cases} \frac{d}{dx}(\rho u) = 0 \end{cases} \tag{11}$$

The first pair of equations (5 & 6) relates the convective currents $j_\pm$ to the convective velocities ($V_{d\pm} \pm u$) and the charge densities $\sigma_\pm$ for ions (+) and electrons (-) respectively, where V_d is the drift velocity of the respective particle. The second pair of equations (7 & 8) represents particle conservation for each species under the assumption that singly charged ions and electrons are created in pairs with no other charged particles present. α and β are ionization constants due to electron or ion encounters and λ is that due to external sources, assuming that electrons and ions are always created in pairs. The Poisson equation (9) relates the electrostatic field and the charge densities. The last pair of equations (10 & 11) expresses the global conservation of momentum and mass. Here ions are assumed to transfer all the momentum acquired from the electric field in excess of what is required to maintain the local drift velocity V_{d+} to the neutrals. An efficiency factor k is introduced for the electrons. This is due to the large number of inelastic collisions that occur for the electrons. If k = 1, the electrons are taken as equally effective in momentum transfer as ions and the neutral gas would experience a force only when there is local net charge. We shall refer to this portion of the momentum transfer as the electric pressure effect. If k = 0, the electrons are considered as incapable of transferring momentum. The momentum transfer to neutral gas due to ions alone is known as the "Electric Wind".[17] We shall refer to the net momentum transfer due to the difference (1-k) in the capability of electrons and ions in momentum transport as the electric wind effect.

The drift velocities are taken from Ref. 18 as the correlations of experimental data:

$$\begin{cases} V_{d_+} = b_+ \times 10^5 \, (E/p) & \text{for } E/p \ll 1 \text{ esu field/torr} \\ V_{d_+} = a_+ \times 10^5 \, (E/p)^{1/2} & \sim 1 \text{ esu field/torr} \end{cases}$$

$$\begin{cases} V_{d_-} = b_- \times 10^9 \, (E/p)^{1/2} & \ll 10^{-1} \text{ esu field/torr} \\ V_{d_-} = a_- \times 10^9 \, (E/p) & \gtrsim 10^{-1} \text{ esu field/torr} \end{cases}$$

The constants $a_\pm$ and $b_\pm$ are of O(1) for most gases. For air $a_+ = 1.7$ and $a_- = 1.4$. The electron ionization constant α is given likewise as a semi-empirical relation:

$$\alpha(x) = Ap \exp\left[-Bp/E(x) \right]$$

where B corresponds to ionization energy and is about 1.22 esu field/torr for air. A is the saturation constant about 15 cm^{-1} $torr^{-1}$ for air. Other ionization constants may be expressed likewise but generally much smaller than α.

The electric equations (5-9) may be uncoupled from the momentum and mass conservation equations (10) and (11) since u/V_{d+} and u/V_{d-} are generally much less than unity. Even if u/V_{d+} may not be too small, a perturbation procedure can be set up to correct for small but significant values of u/V_{d+}.[16] Thus, equations (5-9) can be solved first independently for the five unknowns $\sigma_\pm$, $j_\pm$ and E. The boundary conditions on the electrodes are:

On the anode x=0 $\qquad \sigma_+(o) = j_+(o) = 0$ (15)

On the cathode x=d $\qquad j_-(d) = \gamma j_+(d) = \int_o^d \delta j_-(x)dx$ (16)

where γ is the cathode emission coefficient due to ion incidence and δ is the emission coefficient due to various processes in the discharge depending on electron concentration. Two overall boundary conditions are the voltage drop across the electrode

$$\Delta\bar{V} = \int_0^d (-E)\ dx < 0 \tag{17}$$

and the global current density

$$J_o = j_+ + j_- \tag{18}$$

The solution of the system of equations (5-9) depends critically on the overall cathode emission parameter ω/α defined as:

$$\frac{\omega}{\alpha} \gtrsim \frac{\gamma + \beta/\alpha + \delta/\alpha}{1 + \gamma + \frac{\delta}{\alpha}(1 - \frac{\beta}{\alpha})} \quad \cdots\cdots \tag{19}$$

For dark and normal glow discharges, the overall current intensity J_o is small $\lesssim 10^{-6}$ amp/cm^2 and the cathode remains cool. ω/α is of the order of $10^{-2} \sim 10^{-3}$, varying slightly with E/p. In abnormal glow discharges, and in discharges with hot cathode, ω/α may be 0 (10^{-1}).

The five electric quantities, $\sigma_\pm$, $j_\pm$ and E have been solved in terms of the coefficients α and ω/α and are given in Ref. 16 in dimensionless form. The results relevant to this discussion are taken from Ref. 16 and shown here in Figs. 16-6 and 16-7.

When $\sigma_\pm$, $j_\pm$ and E are determined the momentum equation 10 can be integrated from the anode, x = 0, to the station x to give

$$\frac{1}{B^2p^2}\left[p(x) + \rho u^2(x) - \frac{E^2(x)}{8\pi}\right] - \frac{1}{B^2p^2}\left[p_o + \rho_o u_o^2 - \frac{E_o^2}{8\pi}\right]$$

$$= \frac{J_o}{p^2} \cdot p \int_0^x (1-k)\ dx \cdot 10^{-8} \tag{20}$$

The quantity $(p + \rho^2)$ is often referred to as the stream thrust in one dimensional gas dynamics. The additional term in the stream thrust, $E^2/8\pi$, is the energy density of the electric field per unit volume, which may be interpreted as the mechanical force per unit area, i.e., the electric pressure. The integral term on the left hand side of (20) represents the deficiency of momentum transfer by electrons, i.e., the "electric wind" effect. It is necessary to express the electric wind term as an integral because the variation of the number densities of ions and electrons and the variation of the electric field in the discharge region are drastic. The relative effectiveness of electrons in transferring momentum to the neutrals is also incorporated in equation (20).

In this equation (20) the positive x direction is from the anode (x=0) to the cathode(x=d>0) with air flowing with velocity u in the positive x direction. If the air flows from the cathode (x=0) to the anode (x=d), a negative sign should be added to both f_i and to the space charge equation. Under the circumstances, the sign of the electric wind term in equation (20) will be changed provided that we understand that the integral from (x=0) to x means the integral from the cathode (x=0) to some positive value x in the stream.

Equation (19) is written in a form where the local electric pressure $E^2/8\pi$ may be considered as part of the stream thrust. For the case k = 1, with electrons transferring momentum as effectively as ions, the one dimensional model simply states that the total stream thrust $(p + \rho u^2 - E^2/8\pi)$ remains constant and the local static pressure rises and falls directly with the variations in the electric pressure $E^2/8\pi$ and the momentum flux of the stream $(\rho u \cdot u)$. The local static pressure will be increased by the value of the local electric pressure $E^2/8\pi$ so that the total stream thrust $(p + \rho u^2 - E^2/8\pi)$ remains unchanged with or without the electric field. The total stream thrust is modified only by the electric wind effect. This is a consequence of the assumption made in the one dimensional analysis that both u/V_{d+} and u/V_{d-} <<1 in the discharge region so that the electric properties are not affected by the flow of the neutrals.

If the air motion, u, is directed away from a nonpermeable anode surface, with boundary condition $u_o = 0$, the static pressure on the anode will be increased by the anode field $E^2_o/8\pi$, but decreased by the electric wind. If the inter-electrode distance is large enough, the electric wind term may eventually lower the static pressure when

$$p \cdot d \int_0^1 (1-k)\ d\ (\frac{x}{d}) \gtrsim 0(10^2) \text{ cm. torr}$$

At 60 to 65 kilo ft. altitude, p ~ 30mm. Hg. The condition of lower static pressure on the anode surface may then be obtained if the positive column extends several centimeters away from the anode surface. If the air motion is directed away from a cathode surface, the electric wind serves to increase the static pressure over the cathode in addition to the cathode electric pressure, which

in general is substantially larger than the electric pressure at the anode.

The electric wind term, besides depending upon the effective inter-electrode distance,

$$p \cdot d \int_0^1 (1-k)\, d\left(\frac{x}{d}\right)$$

is directly proportional to the reduced discharge current density, J_o/p^2. Smaller overall voltage drops will maintain the same J_o/p^2 in a given gas discharge for smaller inter-electrode distances. In general, both the cathode and the anode regions are much smaller in physical extent than the positive column. The magnitude of the electric wind effect at a given static pressure, p, is primarily determined by the current density J_o and the length of the discharge. If we maintain the reduced current density J_o/p^2 constant, a discharge with shorter positive column with a smaller overall voltage drop will consume less power. The discharge phenomena near the electrodes do not change substantially, even if the positive column is nearly eliminated; and in which case, the electric wind term is negligible and we have the case of minimum power requirement.

To maintain such a steady discharge in air at several mm. Hg pressure, without a positive column, the overall voltage drop is only slightly above 300 volts; i.e., the normal cathode fall, since the anode drop is generally small. When appropriate values of the constants for air are adopted, numerical results from equation (20) and Figs. 16-6 and 16-7 show that the maximum change in the stream thrust $(p + \rho u^2)$ for these conditions takes place at about 10 dynes per watt of electric power input evaluated as: $J_o (\bar{V}_d - \bar{V}_o) = J_o |\Delta \bar{V}|$. If the electrodes are further apart, the voltage drop must be increased to maintain the current density and produce the electric wind. There will develop a positive column in which the E field is fairly low and uniform. The electric wind effect will then contribute to the change of the stream thrust at the expense of additional electric power roughly, again from equation (20) and Figs. 16-6 and 16-7, at 1 dyne/watt. The electric wind process taking place within the positive column is much less efficient than the processes in the cathode and the anode in changing the stream thrust.

In an attempt to modify the lift distribution of an airplane, planar electrodes may be distributed over the lifting surface. In the immediate vicinity of such planar electrodes, the situation is essentially one dimensional normal to the electrode locally. The significant deviation from one dimensionality lies in the less efficient positive column. Hence, the quantitative estimate of the specific power consumption based on the one dimensional analysis are the most optimistic for electro-aerodynamic interaction.

IV. Specific Power Consumption for Boom Reduction

The electric discharge in the downstream flow field between two planar electrodes on the lifting or volume surface will be considered as produced by placing fictitious cathodes (or anodes) somewhere in the stream facing the electrodes on the airplane surface. The change of the stream thrust in the flow field would then be due to (1) the anode (or cathode) electric pressure $E^2/8\pi$ and (2) the portion of the electric wind term extending into the stream. When the proper sign is taken in equation (20) under the different circumstances, the change of the stream thrust in the positive column to the electrode on the airplane surface can be obtained. The electric power expenditure to achieve the change of stream thrust under this hypothetical situation would be no less than that required for maintaining the entire discharge region, excluding the fictitious cathode (or the anode) fall. Thus, the electric power required to maintain an electric discharge over a cm^2 of the airplane surface to produce a change of 1 dyne/cm^2 of the stream thrust in the flow field or of 1 dyne/cm^2 of stagnation pressure on the electrode will be of the order of 1 to 10^{-1} watt/cm^2 / dyne/cm^2 as given in the one dimensional analysis.

At an airplane cruising altitude of about 65,000 ft. with a cruising Mach number of M_∞=2.7 and 5° initial deflection of the external stream at the leading edge, a 10% change of the pressure rise across an attached oblique straight leading shock would mean a change of the stream thrust of 3.4×10^3 dynes/cm^2 (7.5 lb/ft^2). Regardless of how this is achieved, the electric power needed to accomplish this 10% change of leading edge shock pressure rise per square cm. of shock frontal area would be 0.34 to 3.4×10^3 kw or 0.3 to 3 mega-watts per square foot of frontal area of the modified shock. Conservatively, the shock should be weakened over one-tenth of the chord length to produce a meaningful reduction of the boom. If such is to be accomplished for a commercial supersonic air transport, purely through an electro-aerodynamic device, the electric power requirement on board the airplane is of the order of thousands of mega-watts. Clearly, at the present technology level for power equipment of 4 to 5 pounds per kilowatt, electrical equipment of the order of million of pounds is beyond payload capability.

One may raise the following questions concerning the general validity of the previous inference. (1) Might other modes of electric discharges be more efficient than dark or glow discharges? (2) Would it be possible to reduce significantly the power required by varying the different physical parameters or materials governing the electric discharge in air? The results of the analysis in Reference 16 was given in a dimensionless form through various phenomenological constants. The practical ranges of values of these constants will deny this possibility as is explained below.

To maintain an electric discharge in air without a hot cathode, the overall voltage drop must be larger than the 300 volts cathode fall. The only means for reducing the power expenditure in the

absence of the less efficient electric wind effect is to reduce the discharge current density J_o while maintaining the dimensionless parameter J* of current density a constant. The magnitude of J* determines the level of stream thrust change in the discharge by means of electric pressure over the electrodes.

From equation 20, reference (16) and Figs. 16-6 and 16-7, we have,

$$\frac{J_o}{p^2} \times 10^{-5} = \frac{J^*}{4\pi} a_+ A B^{3/2} \Big/ \left[\ln \frac{\alpha}{\omega} - 1\right] \qquad (21)$$

A small discharge current density J_o will result if a_+, A, and B are reduced and α/ω is increased. From equations (20) and (21) we have that both stream thrust and current density are proportional to p^2. Thus the power expenditure to produce unit change of stream thrust is not affected by the air pressure within reasonable ranges.

Now a_+ is the mobility constant of the positive ion in the discharge. A and B are the characteristic constants of ionization of the gas by electrons. They have fixed values for air, given with equations (2) and (12), within the experimental errors of the data. In fact the ranges of variations of these phenomenological constants for most gases (molecular or rare) are limited to within the order of magnitude. The remaining parameter α/ω is the only one which may vary considerably for various choices of electrode material and cathode operating conditions. In fact, the latter determines to a large extent the mode of operation of the electric discharge.

Equation (21) shows that smaller values of ω/α (therefore, smaller cathode emission) mean smaller discharge current density. Thus, under conditions when electric discharge through a gas is relatively difficult to initiate and sustain, that is, when artificial stimulation of cathode emission by "external" means is almost required at very low discharge current density of much less than 10^{-6} amp/cm^2, the effective parameter α/ω is large. The value of α/ω in these cases may be as much as 10^3 or more depending on various circumstances, but largely upon cathode materials and cathode conditions. For the normal glow discharge, where the photo emission from the cathode due to the photons generated within the gas discharge becomes significant $\alpha/\omega \sim 100$ to 10.

For more intense discharges at still higher current densities, the glow discharge becomes abnormal and the thermal emission from the cathode becomes significant, with α/ω of 0(10) or less. Under these circumstances, the theoretical treatment given in Ref. 16 fails progressively. As equation (21) shows, J_o becomes infinitely large when $\alpha/\omega \to e = 2.718$. This is the mathematical indication of the failure of the physical model adopted when arc discharge conditions are approached. The transition to a fully established arc discharge is usually not a smooth process. The cathode fall diminishes rapidly and the cathode emission becomes almost entirely thermionic.

An apparently steady and fully established arc discharge between planar electrodes is not really steady. The current density J_o is very large but remains finite of the order of several amp/mm^2 and is confined in a very small cross-sectional area. The cathode fall is small and the cathode field is less than the anode field. The diffusion loss in the positive column dominates. The analysis in Ref. 16 does not apply for the arc discharge. Experimental results for the arc discharge and the results of a recent analysis based on a diffusion dominant model, (Ref. 19), give for the magnitude of the specific power expenditure 1 dyne/watt, which is the same value as for the other discharge processes.

It is clear that the most efficient self-sustaining electric discharge that requires the least electric power for producing a given change of thrust is the Townsend discharge of very small current density of orders 10^{-6} amp/cm^2 or 10^{-3} amp/ft^2 or less. The Corona discharge and the brilliant glow discharges produce larger current density and larger change of stream thrust but at the expense of larger electric power per unit change of stream thrust.

The second question relates to electrode geometry and materials. The value of α/ω varies considerably for various choices of electrode material but not to the extent described above for the different types of discharges. Since a larger value of α/ω corresponds to a smaller cathode emission, the more efficient discharge would be more difficult to initiate and more difficult to maintain and would produce very little change in stream thrust because of the small current density. In any case, equation (21) shows that the effect of α/ω in determining J_o enters as a logarithm. The reduction in discharge current density and power expenditure cannot be changed by an order of magnitude under any circumstances. The electric power requirement is fixed at the order of $\sim$1 watt to produce a change of stream thrust of 1 dyne over a cm^2 of shock frontal area.

V. Summary and Conclusion

We have explored and examined various schemes for reducing sonic boom of a supersonic airplane. The shock repellant concept, the concept of creating a phantom plane and the concept of early warning are similar in principle. They could be implemented by electrical, optical or chemical devices. These concepts are, however, aerodynamically unsound since their presumed model of weak aerodynamic interaction cannot be realized. In the absence of a solid boundary on the axis, weak aerodynamic interaction would lead to flow fields not compatible with the conservation laws. Under the actual strong interaction, a detached bow shock wave would result. Devices based on the above concepts for boom reduction would, instead, intensify the boom and increase the drag of the airplane.

Calculations based on aerodynamic theory indicate that the dominant component of the boom of a cruising commercial supersonic air transport is due to lift. The reduction of the sonic boom could be more advantageously sought from the redistribution of the lift, rather than volume, along the longitudinal axis of the airplane to approach some optimal conditions. Electro-aerodynamic devices could be employed to accomplish such redistribution. However, the power expenditure required is of the order of 1 watt/cm^2 to change the stream thrust or the flow pressure by 1 dyne/cm^2, regardless of the circumstances of the electric discharge. If such electro-aerodynamic device should be used solely to reduce the boom of a commercial supersonic transport through a 10% reduction of the strength of the leading shock, thousands of mega-watts of electric power are required on board the airplane. The electric equipment alone is three orders of magnitude beyond total payload capability.

It is therefore concluded that low boom characteristics are most likely achieved through effective aerodynamic design concepts as against external additions of heat or momentum to the flow field.

References

1. W. D. Hayes, Brief Review of the Basic Sonic Boom Theory. Sonic Boom Research, NASA SP-147 (1967).

2. Sonic Boom, A Review of Current Knowledge and Developments, Boeing Document D6A10598-1, The Boeing Company, Seattle, Washington, January 1967.

3. G. B. Whitham, The Flow Pattern of a Supersonic Projectile, Communications in Pure and Applied Mathematics, V, 301-348 (1952). _____, On the Propagation of Weak Shock Waves, J. Fluid Mech., 1, 290-318 (1955).

4. Report on Generation and Propagation of Sonic Boom, Committee on SST Sonic Boom, National Academy of Sciences, National Research Council, October 1967.

5. L. B. Jones, Lower Bounds for Sonic Bangs, J. Roy. Aero. Soc. 65, 433-436 (1961).

6. F. E. McClean and B. L. Shrout, Design Methods for Minimization of Sonic Boom Pressure Field Disturbances, J. Acoust. Soc. 39, (1966).

7. A. R. George, Reduction of Sonic Boom by Azimuthal Redistribution of Overpressure, AIAA Paper 68-159 (1968).

8. Sonic Boom Research, NASA SP-147, A. R. Seebass, Ed. (1967).

9. Second Conference on Sonic Boom Research, NASA SP-180, I. R. Schwartz, Ed. (1968).

10. Ibid.; Reduction of Sonic Boom Attributed to Lift, E. L. Resler, 99-106.

11. F. Schoppe, External Combustion Stato-Jet Engine, Patent No. 2,995,317, August 8, 1961. U. S. Patent Office, Washington, D.C.; also announcement entitled Method for Reduction of Sonic Boom submitted by the Law Office of George Eric Rosden, Washington, D.C., Summer 1966.

12. M. S. Cahn and G. M. Andrew, Electro-aerodynamics in Supersonic Flow, Preprint No. 68-24, AIAA Sixth Annual Meeting, N.Y., January 1968.

13. Langley Research Center, Hampton, Va., Report of Electro-aerodynamic Research for Reduction of Sonic Boom, New York Times, June 28, 1968.

14. H. H. Hubbard, Sonic Boom Effects on People and Structures, Sonic Boom Research, 65-76, NASA SP-147 (1967).

15. H. W. Liepmann and A. Roshko, Elements of Gas Dynamics, J. Wiley, New York (1957).

16. Sin-I Cheng, Glow Discharge as an Advanced Propulsion Device, ARS J. 32 1910-1916, December 1962.

17. L. B. Loeb, Basic Processes of Gaseous Electronics, Berkeley, University of California Press, (1955).

18. A. Von Engel, Ionized Gases, Oxford Clarendon Press, London, 1955 (first edition).

19. A. N. Chester, Experimental Measurements of Gas Pumping in an Argon Discharge, Phys. Rev. 169, No. 1, 184-193 (May 1968).

20. R. Greenberg, Laminar Mixing of Two Streams in a Pressure Gradient, M.I.T. Aerophysics Lab. Tech. Rept. 117 (Feb. 1966).

21. Private Communication, via the Boeing Scientific Research Laboratories, Seattle, Washington.

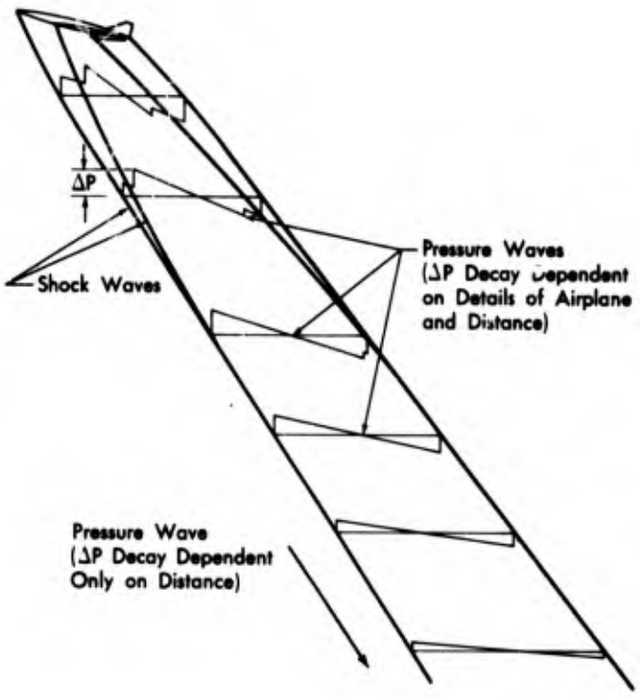

Fig. 16-1. Decay of shock waves.

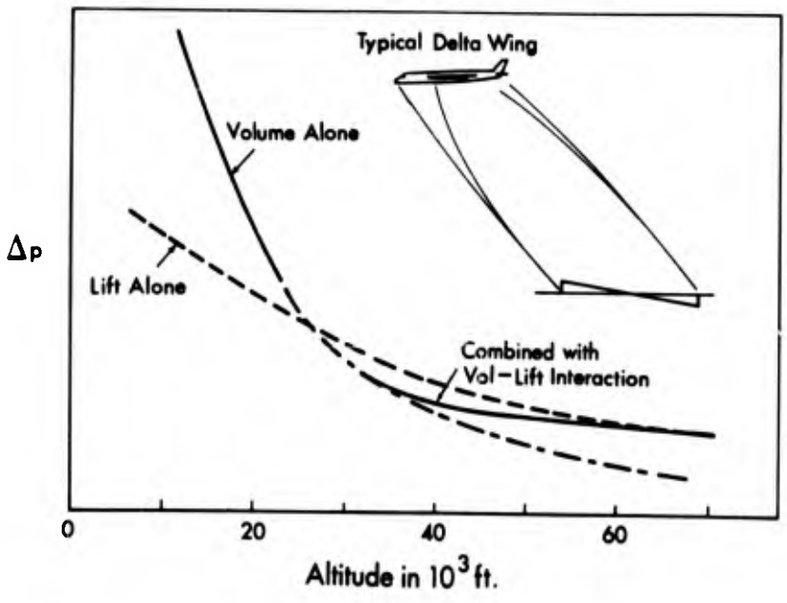

Fig. 16-2. Relative Significance of Lift and Volume Boom.

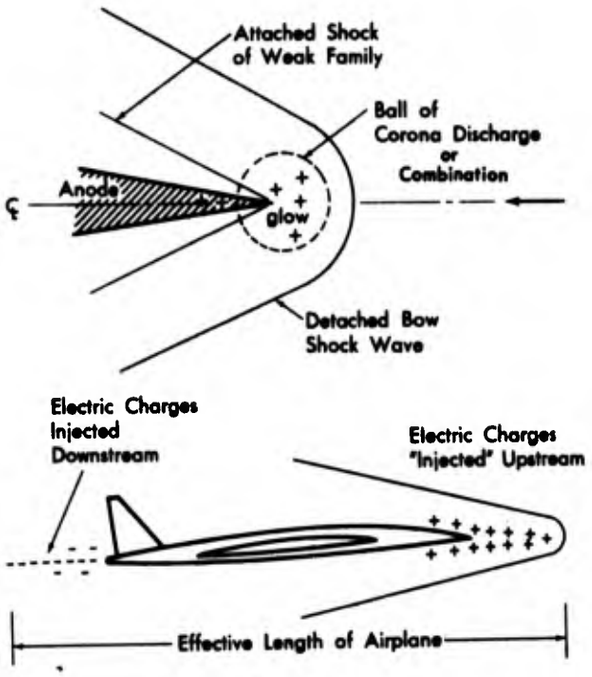

Fig. 16-3. Schematic Drawing of Proposed Electroaerodynamic Devices.

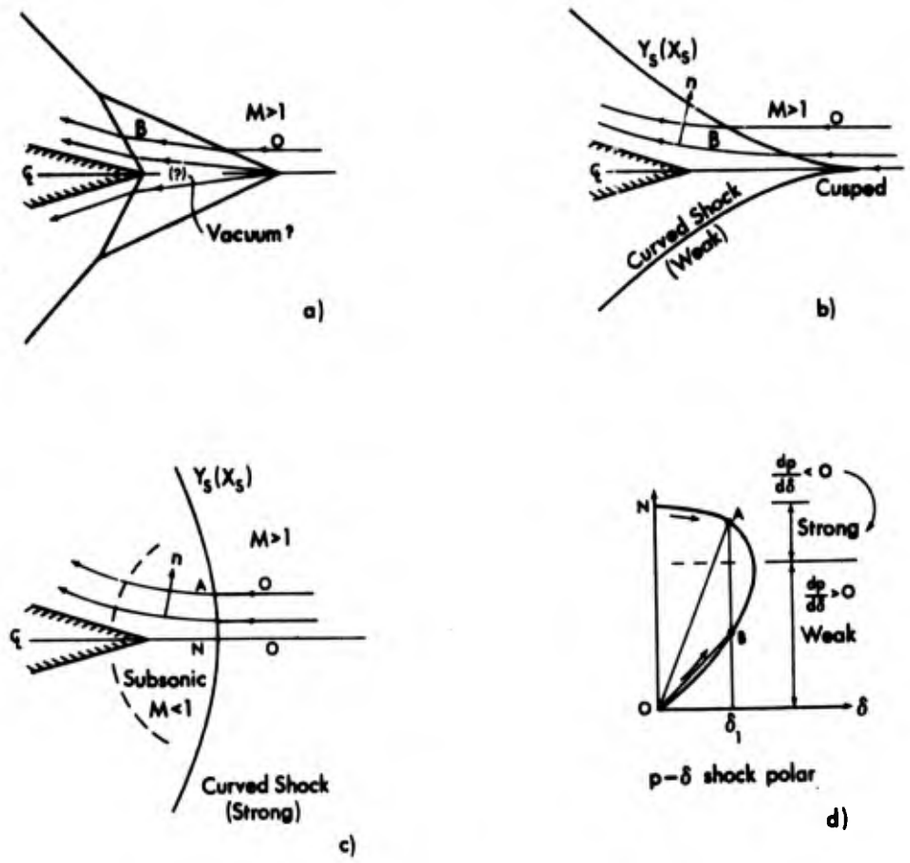

Fig. 16-4. Patterns of Aerodynamic Interaction. $x_s = y_s = 0$ coincides with the intersection of the curved shock on the axis, figs. b and c.

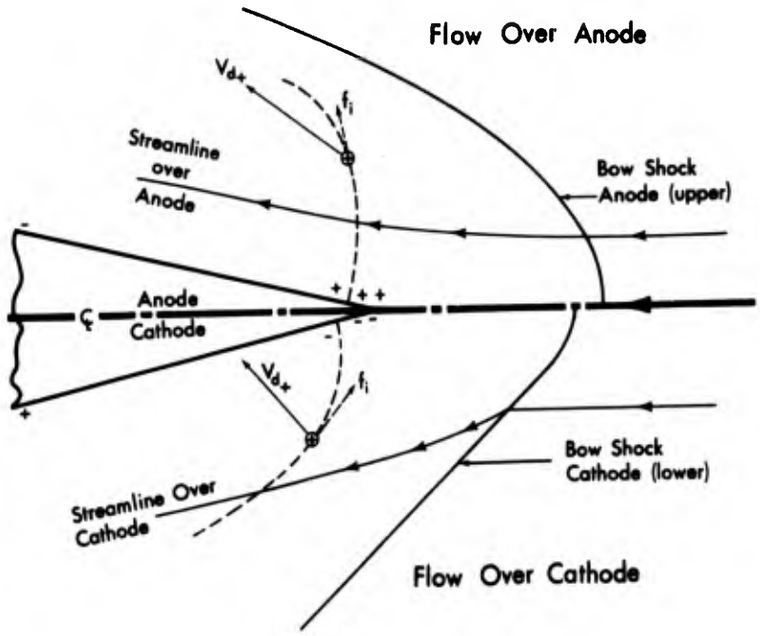

Fig. 16-5. Flow over anode or cathode.

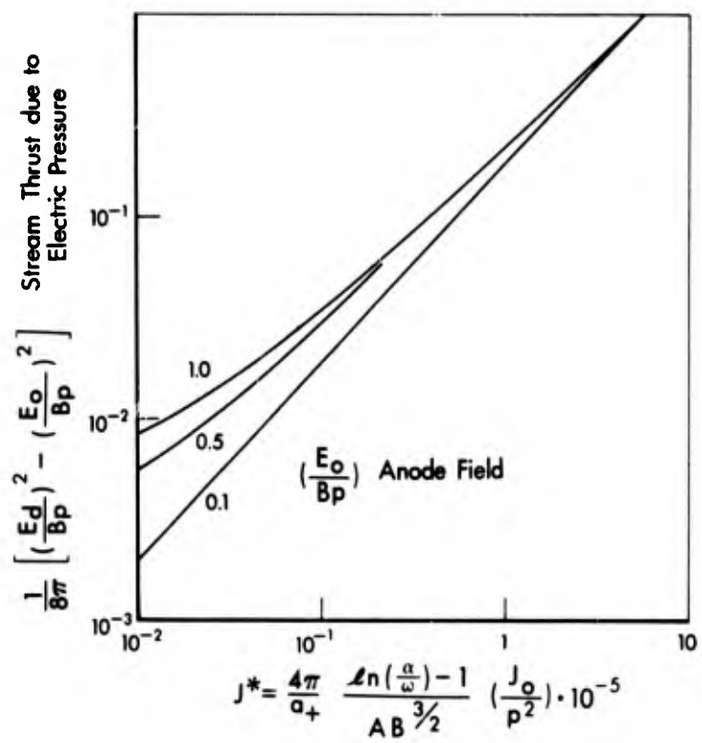

Fig. 16-6. Change of Stream Thrust vs. Dimensionless Discharge Current Parameter J*.

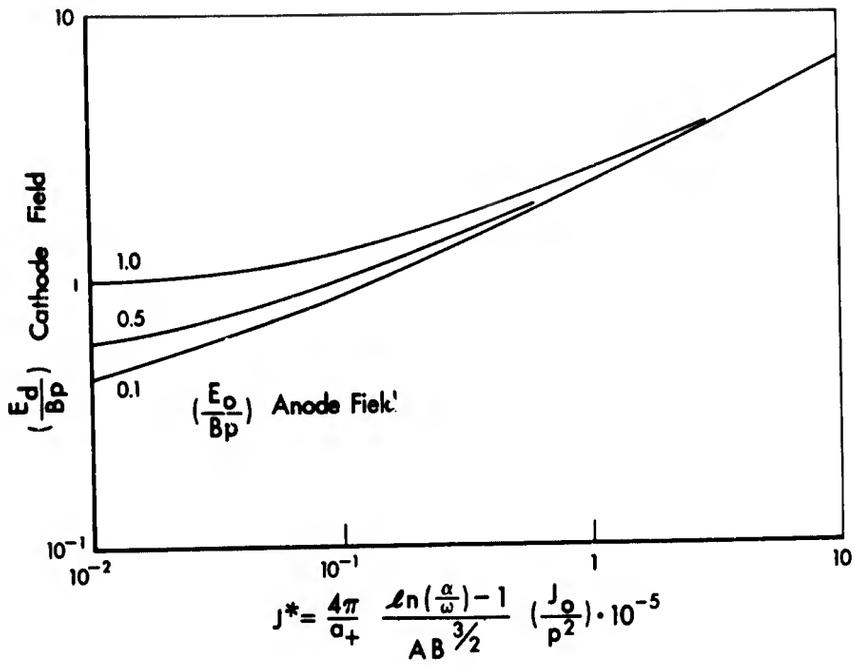

Fig. 16-7. Cathode and Anode Field vs. J*.

THE DEVELOPMENT OF ACOUSTIC ABSORBERS FOR TURBOFAN ENGINES

C.J. Webber

Project Engineer - Noise,
Rolls-Royce Limited,
Hucknall Aerodrome,
Near Nottingham,
ENGLAND.

SUMMARY

Recent proposals by the F.A.A. for legislation on maximum noise levels from aircraft emphasise the need for reduction in the noise radiated from engines. High bypass ratio engine noise is dominated by the fan and turbine sources. Noise from these components may be reduced by the application of absorbent liners to the engine ducts. The design of such liners for optimum acoustic performance requires experimental data on the behaviour of absorbent systems in a representative environment. A description is given of a high sound presence level impedance tube, and a large scale absorption flow facility, developed by Rolls-Royce for this purpose. Some results for typical liner designs obtained in these rigs are presented and discussed.

THE NEED FOR ACOUSTIC ABSORBERS

The need for a reduction in the aircraft noise nuisance is becoming increasingly widely recognised, by the public, by industry, and by governments. The first firm steps towards legislation requiring lower levels from aircraft around airports have been taken by the F.A.A. in issuing their Notice of Proposed Rule Making, in January of this year. The proposed rules do not deal at the present with existing aircraft, but their effect is best illustrated by a comparison between the proposed maximum allowed levels, and the noise levels observed from present day aircraft, shown in FIGURE 1. This shows the typical flyover levels produced by a range of aircraft with unsilenced engines, measured at 3½ nautical miles from the start of the take off run.

It is clear that the proposed legislation demands real progress both in the advancement of noise reduction technology, and in the immediate application of the silencing methods already under development. It is also clear that the new levels have been strongly influenced by the reduction in noise generation associated with the trend towards higher bypass ratios for propulsion of subsonic transport aircraft. Increasing by-pass ratio implies not only lower overall noise levels at constant thrust, but also a change in the relative importance of the individual sources contributing to the overall noise. FIGURE 2 illustrates the change by presenting the component noise source levels for engines of by-pass ratio 0, 1.5, & 5. These represent roughly the long range transport engines of 1960-64, 1964-70, and 1970-1980. The increasing significance of engine blading noise in general, and fan noise in particular, as by-pass ratio is increased, is apparent. Several engines of low or zero by-pass ratio have been in service for some time with jet noise suppressors of a common basic type, but there are no engines in general service yet with suppressors of a common basic type, but there are no engines in general service yet with suppressors designed to reduce fan or compressor noise.

The potential reduction in overall noise level, during take off, obtainable by complete suppression of the three major sources of rearward noise; jet, turbine, and fan is shown in FIGURE 3. If we could achieve effectively total suppression of fan noise on a typical engine of 5:1 by-pass ratio, we should obtain a reduction in overall noise level of about 6 PNdB. If in addition we were able to get rid of all significant turbine noise, we would obtain a further reduction of about 6.5 PNdB. That is, a total reduction of about 12.5 PNdB in rearward overall take-off noise is possible in such an engine by treatment of noise sources within the engine, without attention to the externally generated noise produced by the propulsive jets. The major engine manufacturers are making considerable efforts to reduce the noise generated by the engine blading, but once the design cycle of an engine has been determined by a compromise among the many competing economic and technical factors, the most readily applicable way of achieving further noise reduction is by fitting noise absorbent linings to the engine ducting.

THE DESIGN PROBLEM

The task of the noise suppression engineer in this case is to design duct liners which will modify the engine noise spectrum at specified distances and thrust levels in such a way that the maximum reduction in perceived noise is obtained. This is illustrated in FIGURE 4. The variables at his disposal, within the constraints imposed by performance and weight considerations, are the disposition and area of the liners, and the detailed design of the liners themselves. In its simplest form, the objective is to produce the maximum value of peak attenuation (dB_p), and to vary the frequency of peak attenuation (f_p) so as to obtain the greatest possible reduction in perceived noise. This may involve variations in f_p along a duct in order to increase the bandwidth of attenuation.

At the time when the high by-pass ratio engines for the new 3 & 4 engined transport aircraft were designed, there was no generally available and reliable method, either theoretical or empirical, by which suitable absorbent linings could be designed, or their performance predicted. Rolls-Royce had therefore, in common with other engine manufacturers, to undertake an experimental programme designed to provide the data on which successful designs could be used, and to develop sufficient understanding of the physical processes involved to allow reasonably accurate prediction of their acoustic performance. During this programme we have used and developed some test apparatus which will be briefly described in this paper.

The acoustic behaviour of an absorbent system can be described in a simple form by the expression for the acoustic impedance Z, which is the complex ratio of the r.m.s. pressure p to the r.m.s. particle velocity v, both measured at the surface of the absorber.

$$\text{or} \qquad Z = R + iX$$

Where R = resistive component
X = reactive component

In practical applications R is largely a function of the properties of the absorbent material, in a given environment, and is of greatest significance in determining the maximum attenuation; while X is largely controlled by the properties of the cavity behind the liner. The problem of predicting the acoustic performance of a noise suppression system is principally that of predicting the acoustic impedance of the system under environmental conditions.

On the basis that the acoustic impedance of an absorbent liner in a fan or turbine would be strongly influenced by:-

1. The environmental sound pressure level.
2. Boundary layer pressure fluctuations.

and further that the attenuation obtained from linings with a given environmental impedance would be affected by :-

1. The distribution of acoustic energy amongst the propagating modes.
2. The separation between the treated walls of the duct.
3. The length of liner in the direction of flow.
4. The axial mean air flow Mach Number.
5. Velocity and temperature gradients within the duct.

we have used and developed several types of test apparatus to study these effects.

D.C. FLOW RESISTANCE

The simplest test which gives information on the acoustic behaviour of liner materials is the determination of the steady flow resistance. The apparatus is illustrated diagramatically in FIGURE 5, and the value of flow resistance obtained is indicative of, but not in general identical to, the resistive component of the liner impedance for alternating flows. Test results (FIGURE 5) indicate that for most liner materials the flow resistance increases linearly with velocity. This observation is consistent with the view that the flow resistance is made up of a constant viscous drag component, and a form drag component varying with the first power of velocity. Perforated materials, having a larger characteristic pore size than fibrous materials, exhibit in general a lower viscous component, the velocity dependence being a function of the porosity.

HIGH INTENSITY IMPEDANCE MEASUREMENT

A flow resistance test gives us some information of the variation in the resistive component of the acoustic impedance over a range of steady flow velocities, but it does not throw light upon the reactive component. Both parts of the impedance may be determined in a standing wave, or impedance tube; but in the generally available form this is limited to a maximum sound pressure level at the material surface of about 120 dB. Typical maximum pressure levels in a fan duct close to the blades are of the order of 165 dB. To allow measurements to be made at representative sound pressure levels, the standing wave tube shown diagramatically in FIGURE 6 has been developed.

The apparatus is similar in principle to the standard low intensity standing wave tube, but incorporates four driver units. These are of electrodynamic type rated at 100 watts each, mounted at the ends of four ducts of 1" square cross section placed axi-symmetrically above the basic tube test section. The four driver tubes are smoothly joined and the area exponentially reduced to the 1.3" diameter test section. An $\frac{1}{4}$ inch condenser microphone is mounted on a long adaptor which is remotely actuated along the axis of the tube. The maximum sound pressure levels obtainable range from 173 dB at 1.25 KHz to 160 dB at 6.3 KHz. A photograph of the apparatus is given on FIGURE 7.

Typical variations of the resistive and reactive components with frequency for a fibrous material mounted over a 1 inch cavity measured in this apparatus are plotted in FIGURE 8 for values of sound pressure level of 120, 150 & 160 dB. It is seen that the resistive component, whilst fairly constant over the frequency range of interest, is sensitive to the sound pressure level, as would have been expected from the steady flow resistance tests. The relationship between the resistive component, at a fixed frequency of 2 KHz, and sound pressure level for this lining is shown in FIGURE 9, which supports the roughly linear behaviour deduced from FIGURE 5. The corresponding results for a perforated liner FIGURE 10 shows similar trends.

A convenient way of expressing the relative acoustic efficiency of materials determined in the standing wave tube is the normal incidence absorption coefficient.

$\alpha_N = \frac{4R}{(R+1)^2+X^2}$ This is defined as the ratio of the acoustic energy absorbed by the material to that incident upon it. Typical variations of α_N with frequency and S.P.L. are in FIGURES 11 & 12. In a given environment the peak (resonant or X = 0) absorption value is determined by the resistive component of the absorber i.e. a function of the lining material, and the frequency at which peak absorption occurs is largely determined by the reactance of the absorber, i.e. a function of the backing cavity dimensions.

An important conclusion drawn from the result of tests in the high intensity standing wave tube was that in order to obtain the desired lining impedance (approximately the local characteristic of air) at the sound pressure levels found inside engine ducts, linings must be fitted which display considerably lower flow resistance measured at low sound pressure levels, Also, the rate of change of resistance with sound pressure level was found to be an important design factor for a lining material, since it influences the extent to which the lining will depart from optimum acoustic performance at off-design speeds.

FLOW RIG

In order to explore the variables, other than high sound pressure level, which are likely to affect the attenuation obtained from a duct lining, a flow rig is necessary. We are using the facility shown in FIGURE 13. This has available two test ducts, having cross sectional dimensions of 16" x 30", & 16" x 47" with maximum lengths of lining in the direction of flow of 80" & 40".

Absorbent linings may be attached to the larger walls of the ducts in adjacent removable flat panels giving a maximum separation between treated surfaces of 16". Flow velocities of up to .6 Mach No. are obtainable in the ducts, with maximum overall sound pressure levels of 157 dB. In the cold duct the maximum air temperature is about 55°C, whilst in the hot it can be varied from 300°C to 450°C.

The source of air for these ducts is a large B.S.100 turbo-fan engine of by-pass ratio one. The by-pass air and turbine exhaust stream can be passed either through the test ducts or discharged into a muffler as indicated in FIGURE 14 which shows the flow diagram for a test on a cold duct lining. A sound insulating wall has been built around the entire engine to screen from the measurement area all noise except that emerging from the test duct. The design of the facility was strongly influenced by a wish to reproduce as closely as possible, the conditions existing within the ducting of the type of engine for which linings were to be developed, while allowing the maximum flexibility for basic investigations. By fixing the cold duct width at 16 inches, the ratio of wall separation to characteristic wavelength of a full size engine has been reproduced and a sufficiently high duct aspect ratio has been obtained to allow it to be treated with fair validity as a limiting case of a thin annular duct.

Measurements are taken by a polar array of microphones around the duct exit at 40 feet radius, the $\frac{1}{3}$ octave levels being integrated to obtain comparative radiated powers between runs at identical flow conditions with a hard walled duct and with the lining under test. The semi-free field measurement technique is dictated by the difficulty of constructing an adequately ventilated reverberant chamber for both cold and hot tests. It has the advantage of allowing assessment of the directivity changes associated with particular silencer designs.

The in-duct spectra measured upstream of the test ducts are quite representative (FIGURE 15) of those occurring in the fan and turbine ducts of current high by-pass ratio engines. Cross-duct velocity profiles and boundary layer thicknesses are also typical of engine values. These conditions give the advantage of allowing rapid preliminary assessments of the suitability of liner designs for these applications.

EFFECTS OF FLOW

A simple procedure which has been used in the prediction of the acoustic performance of liner designs is to determine approximately, or to estimate from other data, the sound pressure level in the engine duct at the design condition. This value is then used to establish a point on a curve of flow resistance against velocity, from which is derived the resistance necessary to give the design impedance at the environmental conditions. The appropriate resonant frequency is obtained by choice of the backing cavity depth, on the assumption that the reactance of the liner itself is not a sensitive variable.

A sample of the results obtained on the flow rig shows that such a procedure can be seriously mis-leading. FIGURE 16 shows comparative attenuation spectra for two types of liner tested at .4 Mach No. at 30°C at 40 inch panel length. The two liner materials are a fibre metal of nominal flow resistance 25 c.g.s. rayls (at .2 m/sec), and a perforated sheet .015" thick .095" diameter holes at 20% porosity. Both liners are backed by a cavity one inch deep, subdivided into $\frac{3}{4}$" hexagonal cells.

These two liners show under representative environmental conditions similar maximum attenuation and bandwidth, although their flow resistances measured under steady flow conditions analogous to the measured environmental sound pressure level are quite different; being 33 rayls & 3.5 rayls respectively. The use of such a design method as outlined above is apparently of limited value when considering a wide range of liner materials. The implied A.C. resistance obtained from D.C. flow resistance measurements and that obtained in the high intensity impedance tube are in good agreement. It is apparent therefore, that the alternating flow regimes through the fine pores of the fibre metal liner and the relatively large holes of the perforated liner are sufficiently different in a representative environment to require measurement of the r.m.s. velocity at the liner surface to define the operating point on the resistance v. sound pressure level graph.

In order to find the actual acoustic resistance and reactance in a representative environment, point measurements of pressure, using small area microphones, and of velocity, using hot wire anemometers, will be made at the lining surface in the flow facility. Data from representative lining designs can then be used to provide reliable values of environmental resistance and reactance to allow accurate prediction of the performance of absorbent liners in real engine situations from simple laboratory determined data.

F.A.A. Proposed Noise Limits

3½ N.M Take-off Flyover

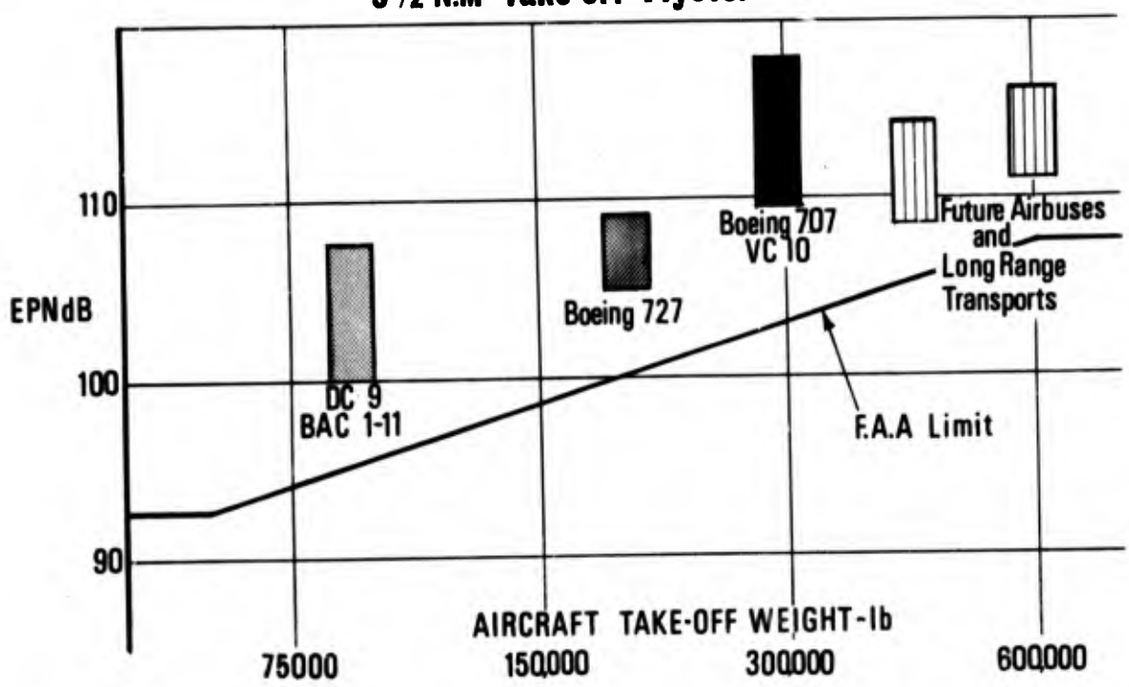

Fig.1

Component Noise Levels - Variation with By Pass Ratio

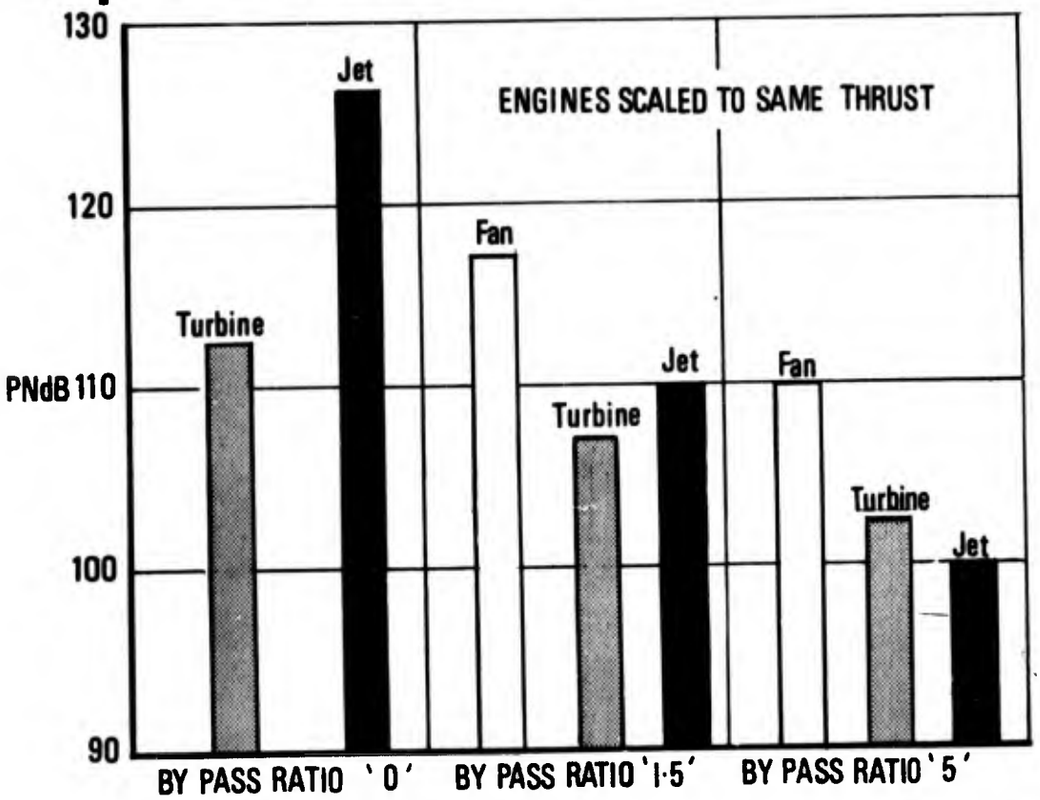

Fig.2

Effect of Component Suppression

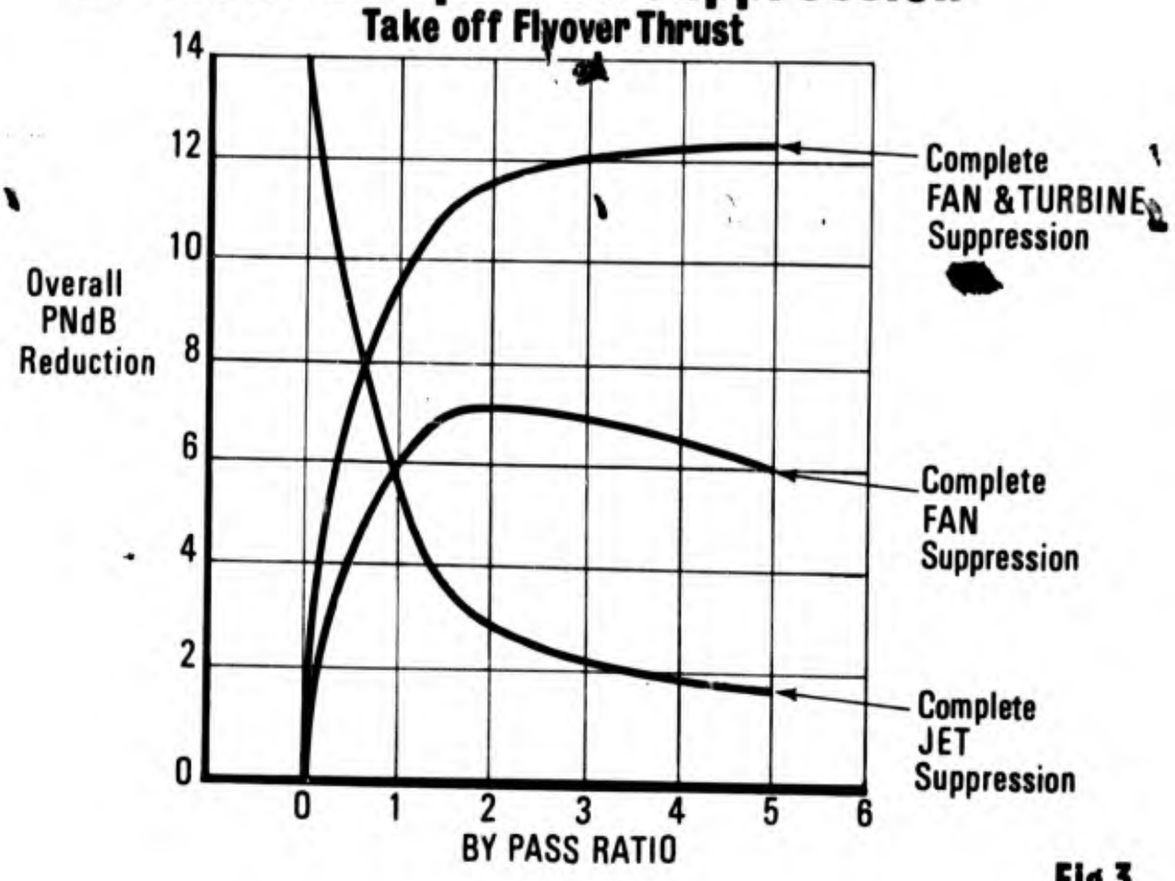

Fig.3

Effective Design of Acoustic Linings

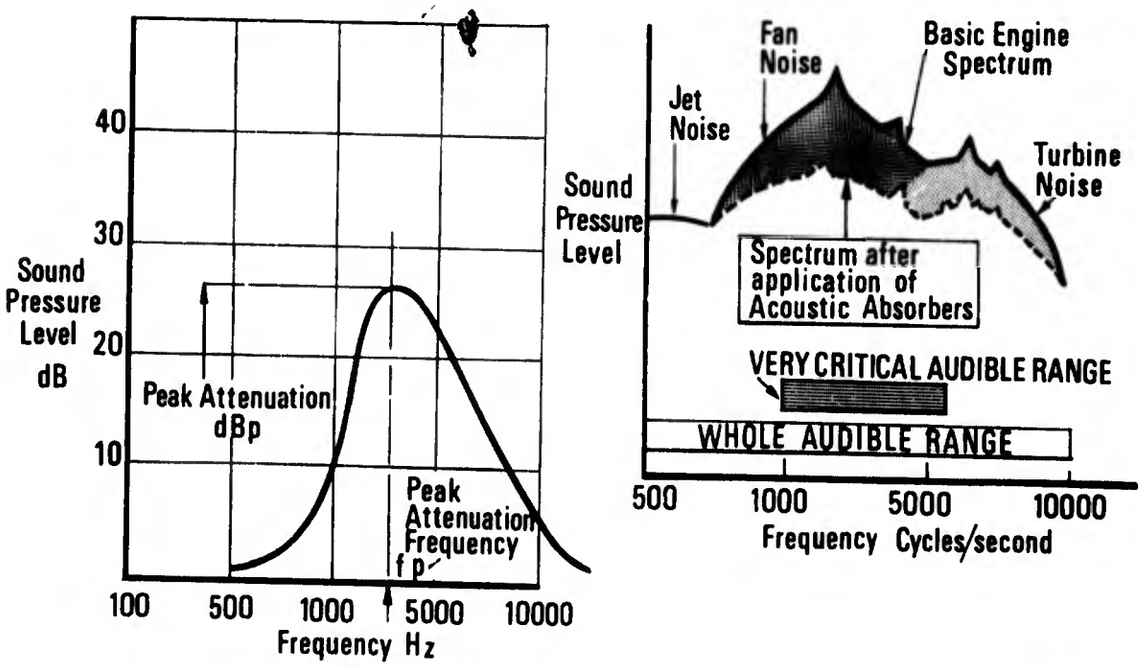

Fig.4

Acoustic Flow Resistance

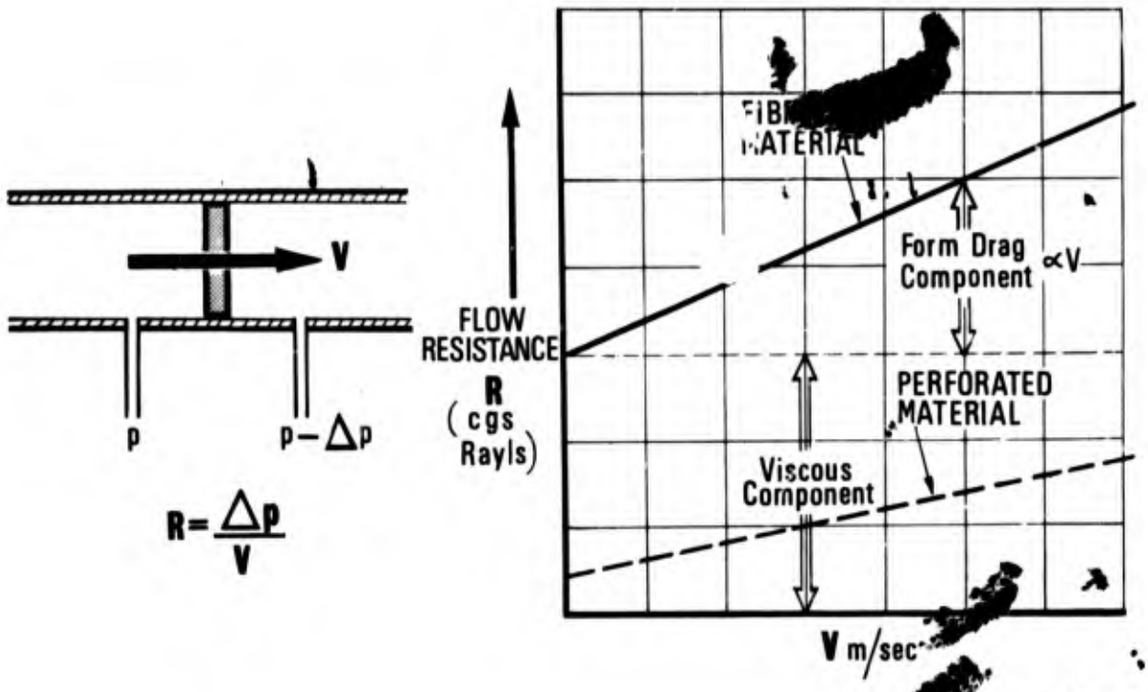

Fig. 5

High Intensity Standing Wave Tube

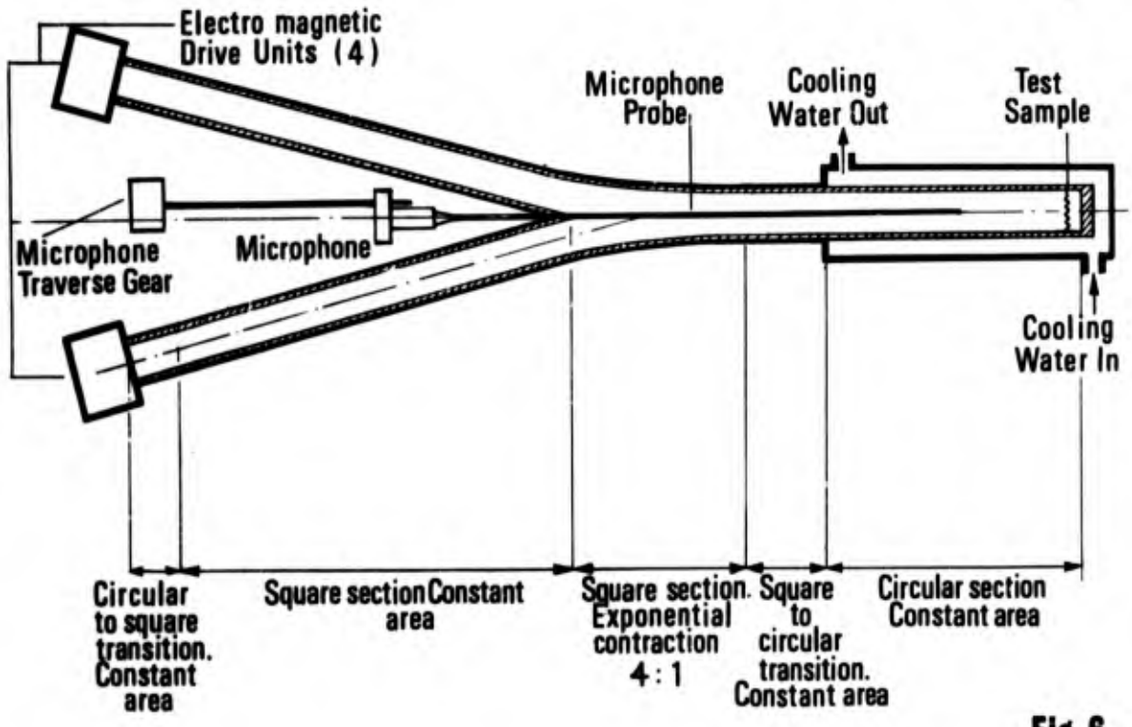

Fig. 6

High Intensity Impedance Tube

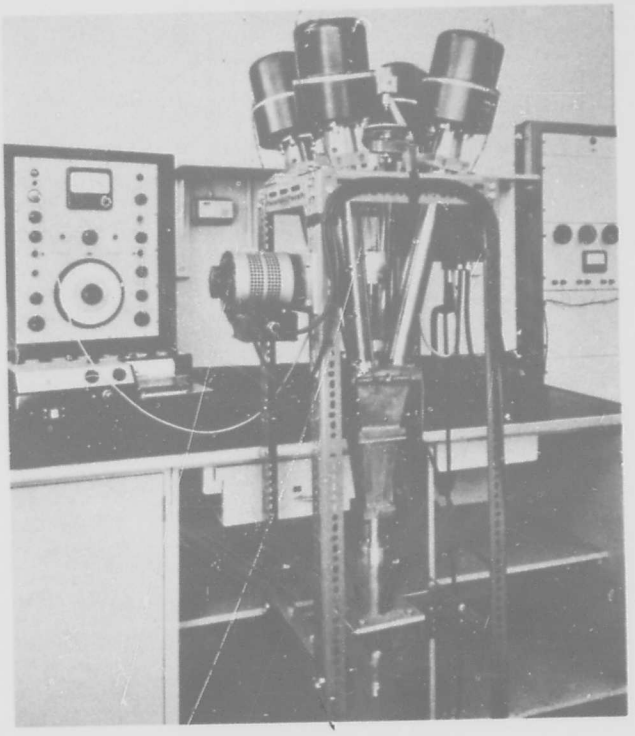

Fig. 7

Variation of Acoustic Impedance

FIBREMETAL

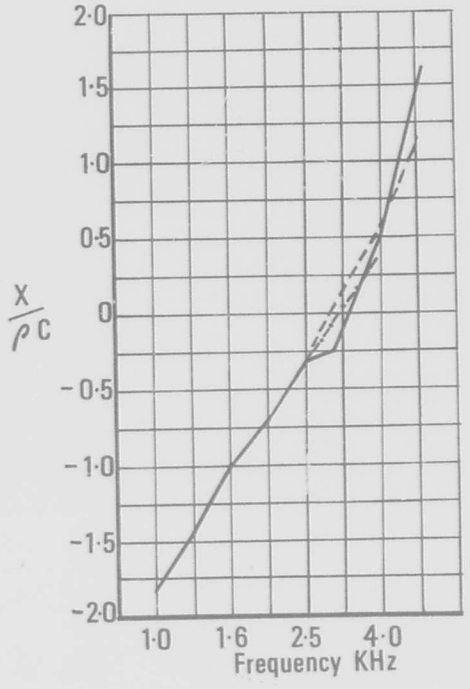

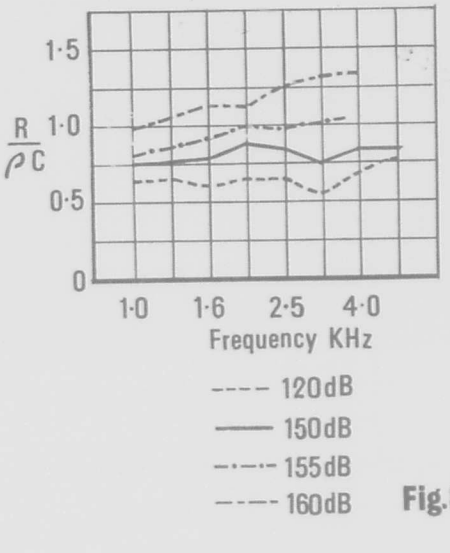

Fig. 8

Variation of Resistance with S.P.L (Constant Frequency 2 KHz)

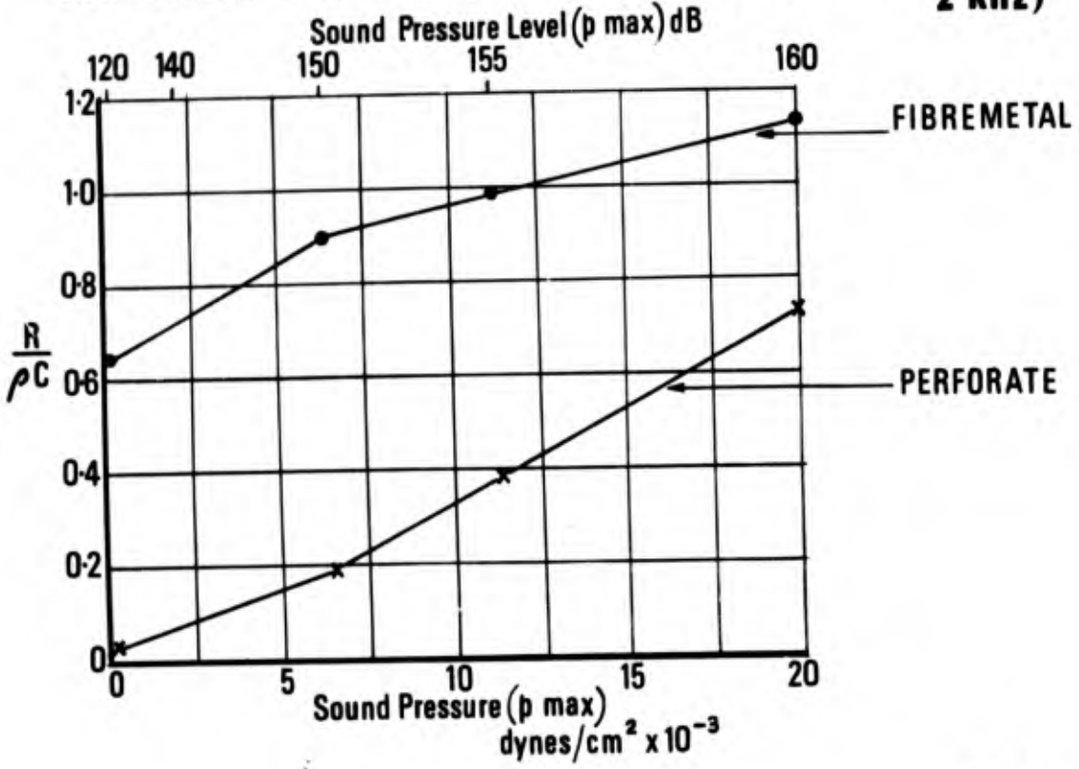

Fig.9

Variation of Acoustic Impedance

PERFORATE

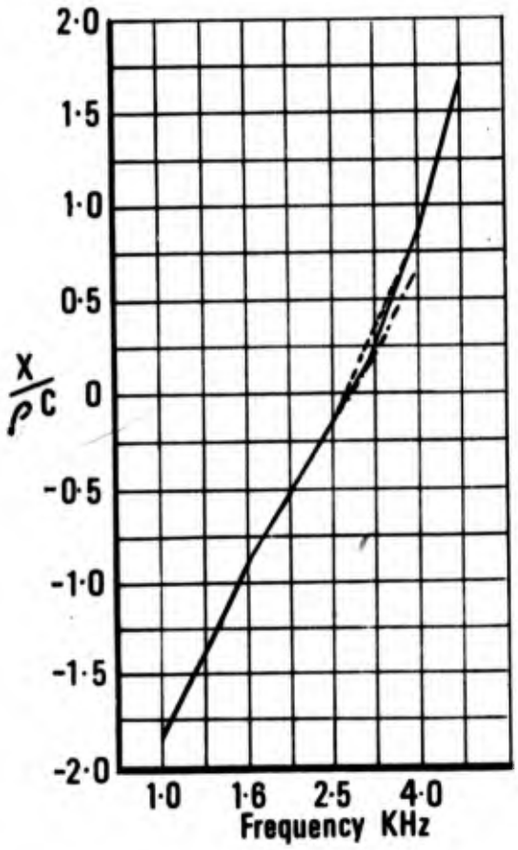

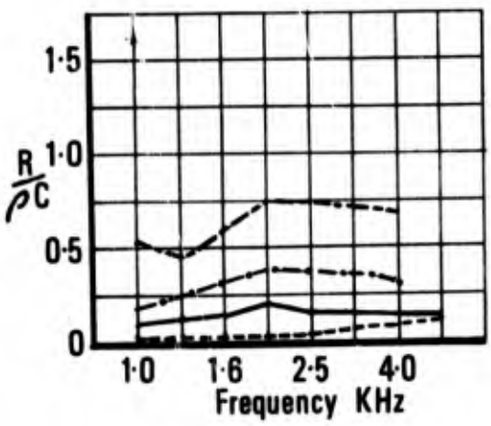

----- 120dB
——— 150dB
·—·—· 155dB
-·—·- 160dB

Fig. 10

Variation of Absorption Coefficient with S.P.L

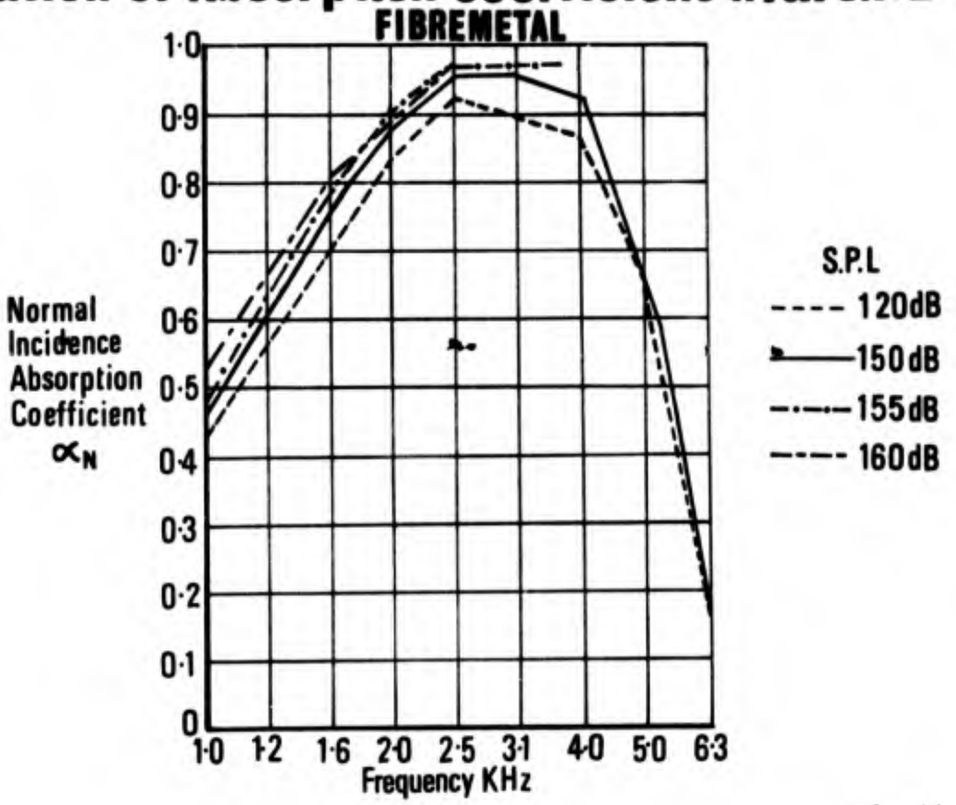

Fig. 11

Variation of Absorption Coefficient with S.P.L

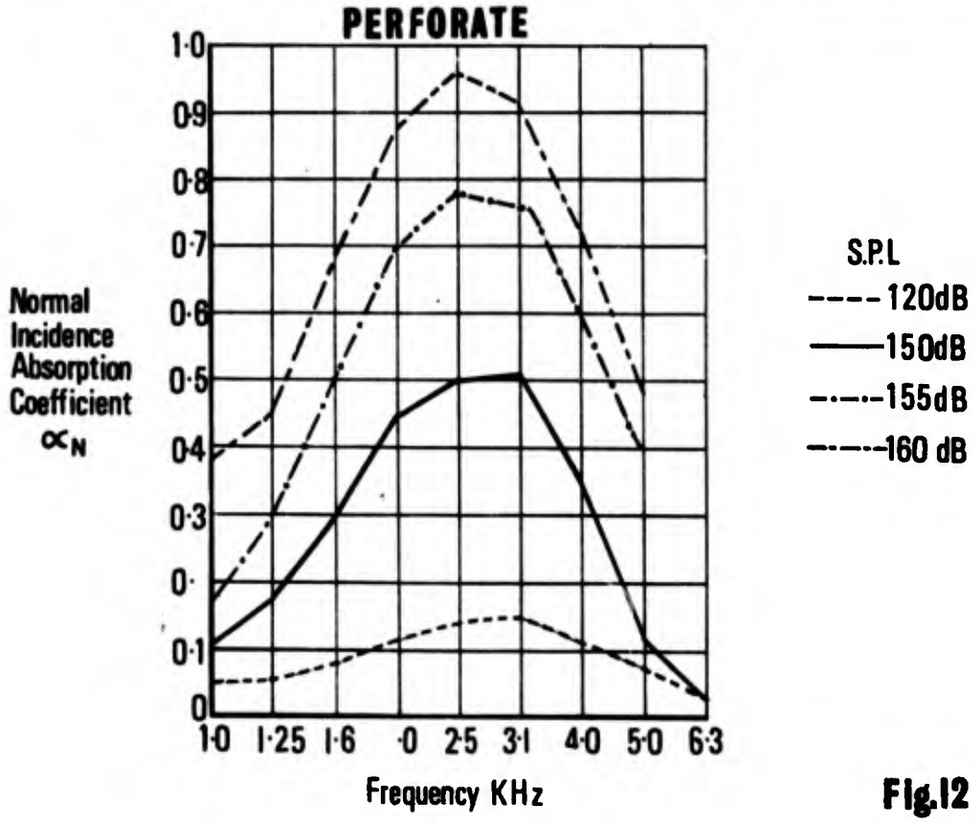

Fig.12

Large Scale Absorption Flow Facility

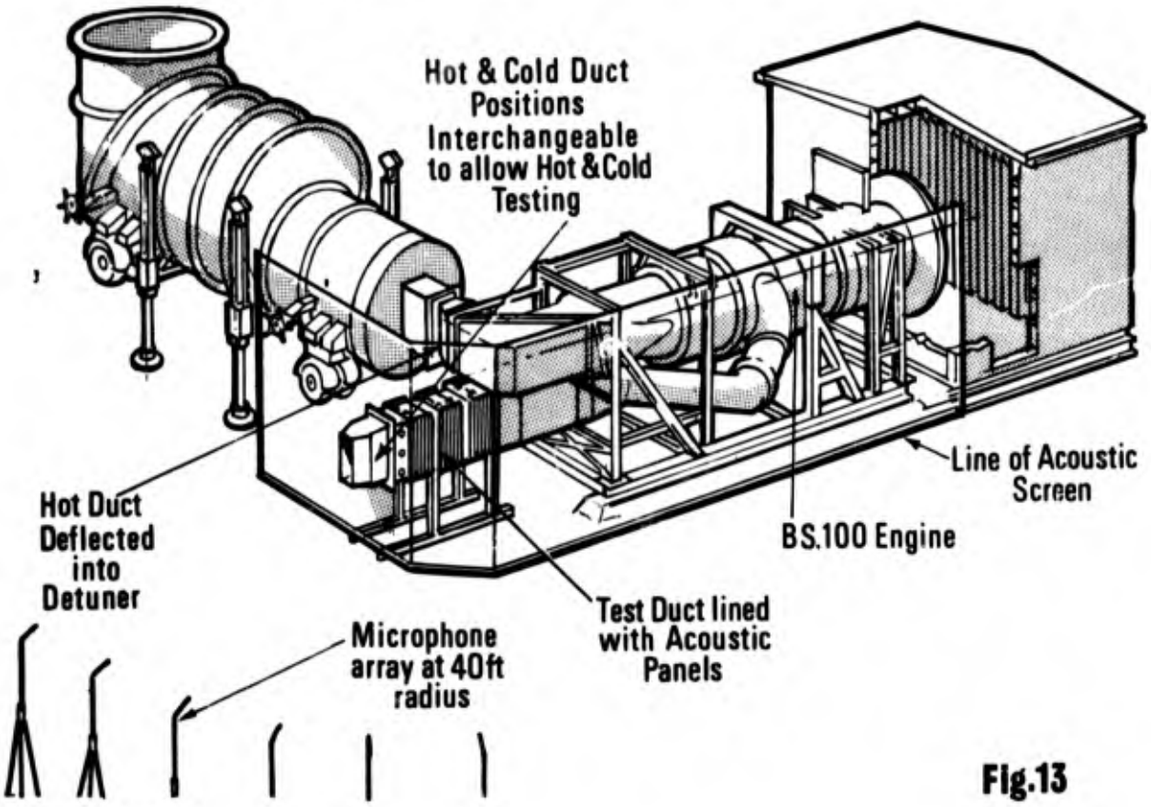

Fig.13

Large Scale Absorption Flow Facility

(Flow Diagram)

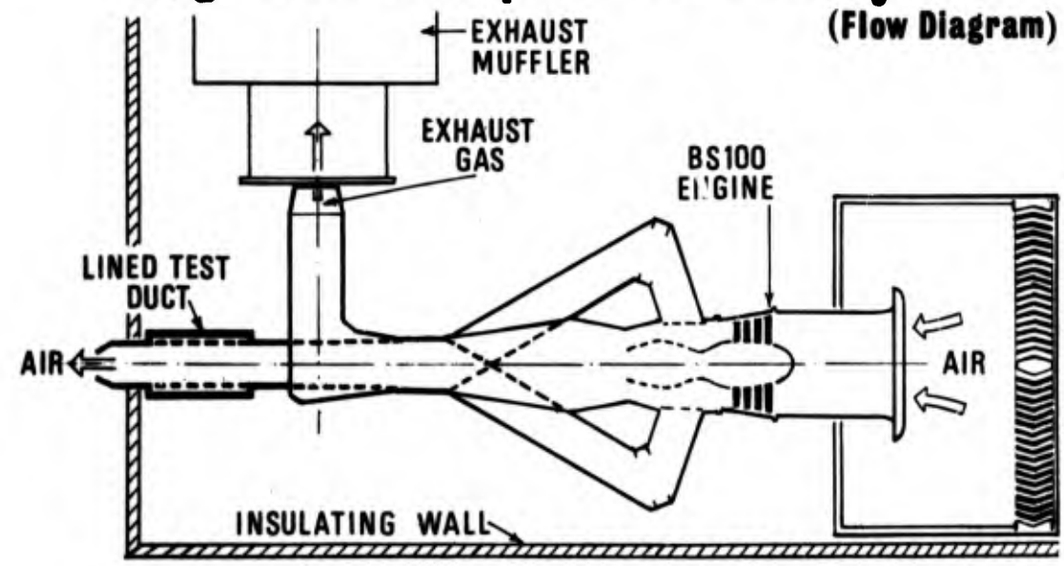

MICROPHONES at 40' RADIUS

○ Flow indicated for COLD DUCT TESTS

● For tests on HOT EXHAUST LINERS cold flow is led to muffler, and hot flow exhausts through smaller duct into measuring area.

Fig.14

Cold Test Duct Velocity Profiles

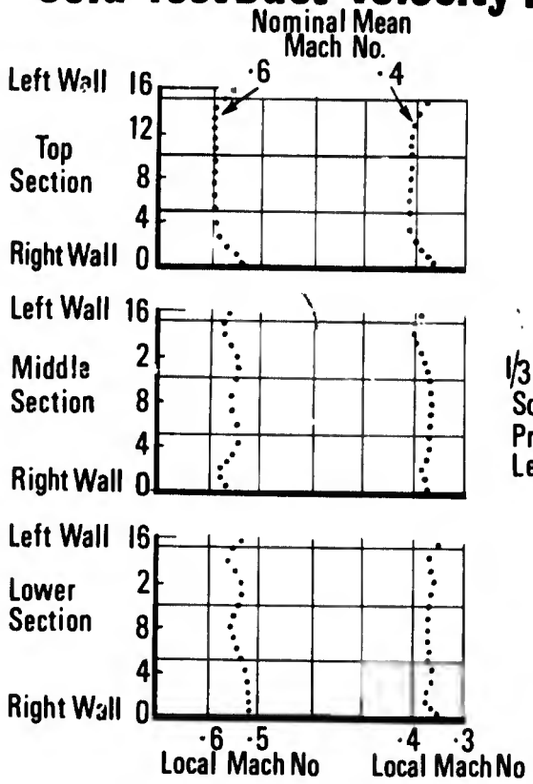

Spectra at Entry to Test Section (COLD)

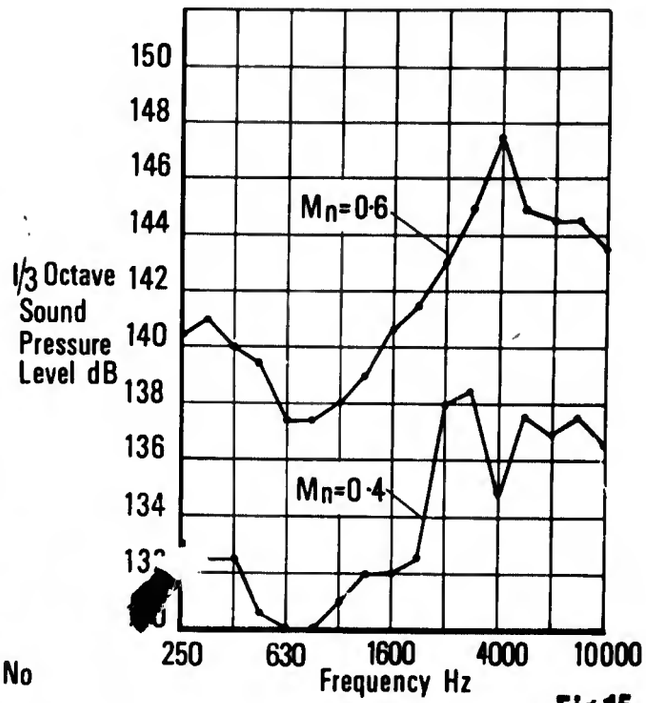

Fig.15

Measured Attenuation Spectra

0·4 MACH No. COLD FLOW

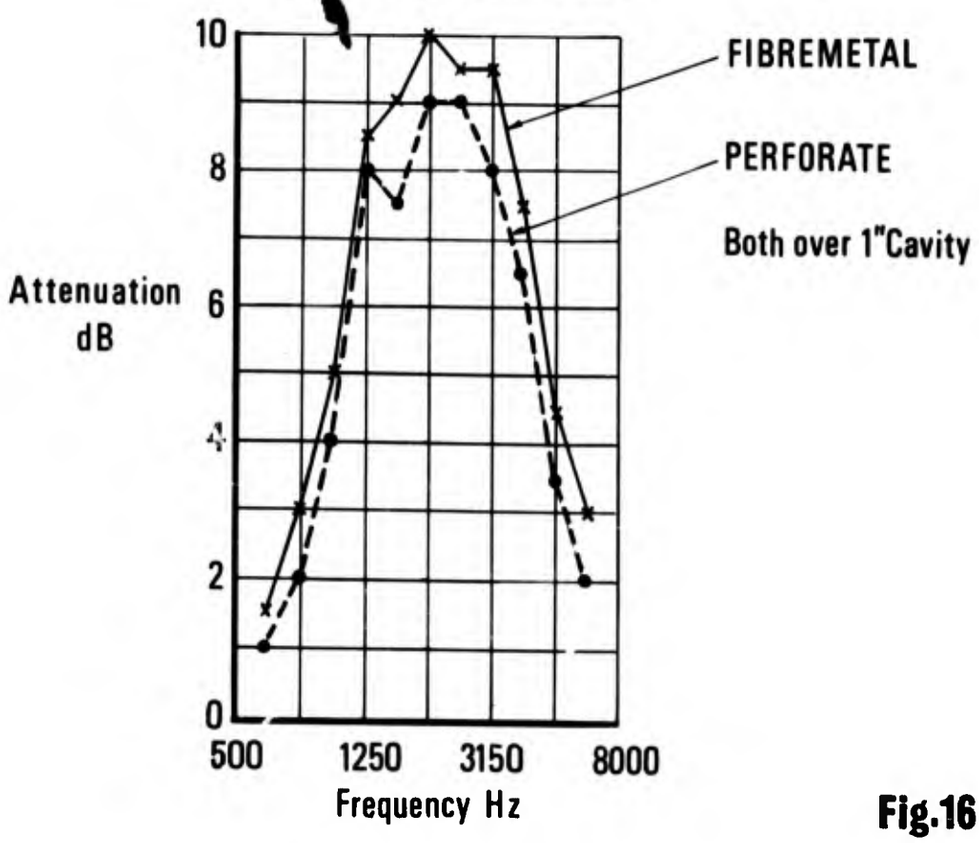

Fig.16

BLANK PAGE

AIRCRAFT ENGINE NOISE MEASUREMENT TECHNIQUES, FACILITIES, AND TEST RESULTS

Dr. William R. Morgan
Manager, Quiet Engine Program
Advanced Technology Programs Department
Aircraft Engine Group
General Electric Company
Cincinnati, Ohio 45215

Dr. Spiridon N. Suciu
Manager, Design Technology Operation
Aircraft Engine Group
General Electric Company
Cincinnati, Ohio 45215

SUMMARY

This paper describes three basic phases of acoustic testing and analysis work necessary to advance the state of the art of quiet engine designs which, in turn, contribute to the reduction of noise emanating from aircraft. The paper provides a description of types of laboratory test equipment and some important, early results that may be obtained from such equipment; far field (open field) acoustic ground test facilities and test results; and finally, flight test facilities and flight results.

Throughout the paper emphasis is placed on the importance of specifying the noise requirements early (and carrying out early substantiating tests) so that the engine will incorporate the basic features necessary to achieve the specified noise levels at a minimum penalty in performance, weight, cost, and reliability. Also, the need is spelled out for an analytical effort closely integrated with, and parallel to, the experimental work to gain an understanding of the basic mechanisms of noise generation and suppression and to develop reliable prediction methods for system tradeoff studies and future noise level projections.

AIRCRAFT ENGINE ACOUSTIC DESIGNERS ARE CONSTANTLY CONFRONTED with the task of predicting engine flyover noise for a given aircraft application during preliminary design phases of the engine. This is as it should be, for the acoustic requirements should be integrated into the propulsion system design as are other important requirements (such as powerplant weight and specific fuel consumption). Until recently, however, the state of the art of acoustic design did not permit an accurate assessment of the acoustic characteristics of preliminary designs for wide variations of such parameters as jet velocities, pressure ratios, and bypass ratios (in the case of fan engines). By necessity, the acoustic designers resorted to elemental scaling rules, empirical scaling laws, and past measurements from full scale engines that on the surface appeared to be acoustically similar (but in fact quite frequently turned out to be acoustically dissimilar). The necessity for reaching further back into the engine design features to determine the acoustic characteristics becomes obvious. To this end, one must devise laboratory experiments, augmented by analysis, that will tend to develop the acoustic characteristics early in the development of the propulsion system. These experiments must then be followed by full scale engine static far field acoustic tests to verify or improve the laboratory correlations, and finally flight tests are required to obtain the resultant acoustic characteristics of a particular engine design. All along the engine development path (and particularly from the flight test results) it is necessary to "feedback" information to each phase of the acoustics program to update and improve the noise prediction methodology.

To expound on this noise prediction methodology, this paper describes some facilities and test equipment and provides typical test results, for each of the three basic acoustic development phases: Acoustic Laboratory Tests; Full Scale Far Field Static Acoustic Tests; and Flight Tests.

ACOUSTIC LABORATORY TEST FACILITIES

Figure 1 illustrates a test set-up that enables evaluation of some of the acoustic characteristics of fans/compressors. Such evaluations can be carried out early in the engine development program (along with the fan/compressor aero evaluations). Illustrated by the Figure are traverse planes for acoustic probes that can provide information relative to the axial and radial distribution of the noise emanating from both the front and discharge sides of the fan/compressor. The type of data that typically can be obtained from such tests is illustrated by Figure 2. From this Figure one can clearly identify the fundamental blade passing frequency (and harmonics). Analysis and integration of these types of data can lead to such information as: the radial distribution of the sound energy in the duct; maximum sound pressure level at any point in the duct; axial mode of decay of the energy; and integrated total sound power from the front and aft end of the fan/compressor.

An important factor relative to this type of test is that measurements are taken close to the noise generating sources. This fact enables one to seek out and reduce the generation mechanisms -- explore such factors as blade/vane ratio and spacing as well as aerodynamic factors as they relate to noise generation. Coupled with adequate theoretical analysis, data from such tests can improve prediction techniques. For example, Figure 3 illustrates the comparison of theoretical predictions and measured test results for two different rotor configurations. Without the benefit of an extensive source measurement program the prediction technique would not have been developed to the degree indicated by the good agreement of the predicted and measured results.

Another important aspect of aircraft engine noise reduction that can be quite effectively pursued by laboratory type experiments is noise reduction by acoustic treatment. Initial development phases of acoustic treatment can be carried out by use of a standing wave test apparatus (impedance tube). This equipment is illustrated by Figure 4. Basic acoustic properties, such as the acoustic treatment resistance and reactive components of the acoustic impedance, and normal incidence absorption coefficients, can be obtained by use of this equipment. Also, the effect of sound pressure level on the absorptive properties of the treatment can be determined. The particular apparatus illustrated has a frequency range of 0.5 to 6.3 KHz. Noise from the generators travels down the tube, through an exponential horn, and is incident upon a 4" by 4" test sample located in the sample holder at the left of the Figure. With the six noise sources operating, sound pressure levels of the order of 160 dB for selected frequencies, and 140 dB over the entire frequency range, can be obtained at the sample.

Typical results from the impedance tube are illustrated by Figures 5 and 6. Figure 5 provides the reactive and resistive components of a honeycomb type acoustic treatment. Altering these components by altering the physical characteristics of the treatment enables one to tune the treatment material for absorption at selected frequencies that are predominant in the spectra of noise from a given engine design. Figure 6 illustrates the design potential by plotting experimentally obtained absorption characteristics of a treatment material tuned for a single frequency and those for a second material designed to have two peak frequencies and a broader range of good absorption characteristics.

Although of significant value, impedance tube test results are not sufficient to formulate a good acoustic treatment design, even though the engine noise spectral characteristics are known. In actual aircraft engine applications, the flow effect over the treatment alters the absorption characteristics. Laboratory tests to account for this factor may be performed by treatment duct flow test equipment such as is illustrated by Figure 7. The equipment design is such that the aerodynamic conditions, for either the inlet or discharge of engines, can be simulated. The noise source generator can be located either upstream or downstream to simulate flow either in

the direction of, or against, the direction of noise propagation. With this apparatus, sound levels of the order of 160 dB can be obtained. Microphone probes are employed ahead of and after the treatment to measure the degradation of sound (sound transmission loss) due to the presence of the treatment. Typical of the results that one might obtain are those illustrated by Figure 8. The Figure illustrates the effect on transmission loss as a function of Mach number for a single geometry and single type of treatment. From these data it is axiomatic that properly designed treatment (tuned for desired frequencies) must account for flow effects. Analysis of the type of data illustrated by Figure 8 also can be used to direct refinements of the treatment design, which in turn could be reevaluated on the impedance tube apparatus.

Other laboratory type acoustic development apparatuses that provide the opportunity for early, inexpensive evaluation of acoustic design concepts are portable research compressors. Examples of uses of these types of equipment are illustrated by Figures 9 and 10. The 15 inch compressor shown by Figure 9 is configured to evaluate the effect of blade/vane ratio and vane wake effect on noise generation. For the particular test set-up illustrated, the original inlet guide vanes that were designed for the compressor have been removed and sets of rods of circular cross section were substituted for the vanes. The number and size of the rods are easily varied to provide different blade/vane combinations. Sound pressure levels are measured in the duct at each of three radial probe positions, by microphone. The microphone probes terminate in a ρc coil mounted on top of the compressor. Figure 10 illustrates a 26 inch research compressor set up to evaluate a given sound absorption treatment configuration. For this particular test the compressor has been moved to an outdoor area (open field) and both probe microphones and far field microphones used to record the test data.

FULL SCALE FAR FIELD STATIC TEST FACILITIES

Figure 11 is an aerial view of an open field (far field) acoustic test facility sufficiently well equipped to provide excellent far field acoustic evaluations of both full scale aircraft engines and large size fans/compressors. At the left of the Figure is a test pad for mounting full scale engines. Microphones are located around this test pad every 10° for an arc of 180° at a distance of 250 feet. Far field acoustic evaluations have been made on both turbojet and turbofan engines using this test facility. A typical installation of a fan engine mounted in this facility for acoustic evaluation is illustrated by Figure 12.

A second acoustic test pad, suitable for acoustic evaluation of fans/compressors, is illustrated at the center of Figure 11. Fans/compressors mounted on this pad are shaft driven through coupling to a 15,000 horsepower gas turbine (LM1500). This arrangement is unique in that it permits independent far field evaluation of the acoustic characteristics of rotating machinery, separated from the effects of relatively hot core jet velocities that would be involved with the total engine. The inlet and exhaust to the gas turbine drive for this facility is well baffled and heavily treated with acoustic treatment so as to adequately muffle any noise from this source.

The control room (visible in the background of Figure 11) for both of these acoustic test pads contains all the usual measuring and monitoring equipment that would be found in any normal test cell set-up. In addition, however, acoustic recording provisions to record 25 FM channels and 3 AM channels on a one inch magnetic tape are also available.

Figure 13 illustrates a 36 inch fan being readied for installation on the fan/compressor far field acoustic test pad. The Figure shows the fan with the aft cowl duct removed. This vehicle was designed such that the fluid flowpaths of the fan were fabricated to allow testing with or without various lengths and amounts of acoustic treatment. Prior to testing the fan without treatment, predictions of sideline perceived noise levels were made, based on previous laboratory type experimental work and analytical correlations. A comparison of the predicted and experimental results is illustrated by Figure 14. Also shown on the Figure are the measured sideline PNdB reduction produced by placing acoustic treatment in the fan flow path cowling. Significant noise reduction is obtained over the entire operating range of the fan.

Acoustic treatment can be designed to be effective in reducing fan noise over a wide frequency range as illustrated in Figure 15. The multiple pure tones (which are a harmonic series with the initial tone at the once-per-rev frequency of the fan) are radiated most strongly into the forward quadrant. The two narrowband spectra at the top of Figure 15 are reproduced from a forward quadrant far field measurement location with and without inlet suppression on the cowl wall. The effectiveness of the treatment is obviously reducing the highest MPT components by 16 dB. The one-third octave band spectra at the bottom of the Figure illustrates the suppression bandwidth as measured in the aft quadrant at two engine power settings. The treatment in the aft ducting suppresses not only the fundamental blade passing frequency but also the fan broadband noise.

A final important feature of a fan engine suppression system is the capability of "balancing" the aft and forward radiated noise. The experimental results of Figure 16 shows that the sideline perceived noise level peaks can be made equal with the proper installation of inlet and exhaust duct treatment, an important consideration when designing for minimum peak flyover noise.

FLIGHT TEST FACILITIES

Of the many acoustic flight tests performed by General Electric at various locations throughout the United States, one of the more unique acoustic flight test set-ups was established, and the test performed, by General Electric's Flight Test Operation at Edwards Air Force Base in California. The series of flight tests were performed specifically to determine the ground to flight engine acoustic correlations for the Convair 990 (CJ805-23 fanjet engine), Falcon (CF700 fanjet engine), and B52 test vehicle (TF39 fanjet engine). The flight test set-up for this series of tests is illustrated by Figure 17. The extensive array of microphones is illustrated by the Figure. For this test set-up, radar tracking was employed to identify the space relationship of the aircraft relative to the microphone field at any given time, and the signals synchronized with the acoustic tape recorders. Flights for the three aircraft were performed at various altitudes, flight speeds, and engine power settings. Figure 18 illustrates a Convair 990 flyby during one of the acoustic test series. Ground noise tests of these aircraft were also performed prior to the flight tests.

One type of result from these tests is illustrated by Figure 19, showing the comparison of ground and flight measurements for the Convair 990 (CJ805-23 engine). There, of course, were many other interesting results, including some humidity absorption data based upon similar flybys at different altitudes.

Flight test set-ups need not be nearly as elaborate as [illegible] described to obtai[illegible]nificant results. For example, a single line of microphone[illegible] the flight [illegible] use of cameras synchronized with the recording system to determine the [illegible] of the aircraft with the microphone field has successfully been employed. A [illegible]ound to flight correlation with this type of test set-up is illustrated by Figure 20. To formulate this plot static ground test noise data was stored in a digital computer. The aircraft was then flown by digital computer and the noise level and specific "tent" noise characteristic predicted as a function of time. The actual experimental data from the flyover tests were then also plotted. The agreement is fair. The important point is, however, that any significant discrepancies in the comparison should be "fed back" into the static ground test noise development phase and into the prediction math model, and reasons for the discrepancies developed.

CONCLUDING REMARKS

The fundamental procedures for developing aircraft engine acoustic characteristics and for formulating noise prediction methods are not basically dissimilar to the procedures for developing performance characteristics and formulating prediction methods for other of the aircraft engine components (for example, compressor performance characteristics). In fact the same basic facilities may often be employed (virtually simultaneously) to do both. As with other engine components, the acoustic development quite frequently should start with fundamental laboratory type tests based upon specifications as a consequence of the preliminary engine design (including acoustic design considerations). It is then quite natural to follow through with acoustic cell tests, full scale acoustic static tests, and finally acoustic flight tests, with adjustments in the acoustic design as the engine progresses through the normal development cycle.

It has been said that, in the past, aircraft engines have been designed and developed and then attempts made "to make them quiet". This is not to say that the desire "to design them quiet" was not always present, but it is more likely that neither the theoretical and experimental technology nor the necessary facilities were available to carry out the task at a level sufficiently sophisticated to obtain the desired "quiet" results. Based upon need, a rapid growth has taken place in both aircraft engine acoustic technology and in the acquisition of good acoustic test facilities to carry out the necessary acoustic development along with the development of the other components of the engine system.

Results to date are encouraging from the standpoint of being able to significantly reduce the noise levels caused by turbomachinery sources emanating from aircraft engines. However, the degree to which these features should be incorporated into operational systems will depend upon a combination of economic, social, and political considerations. A sizeable effort which is international in scope, is being directed towards making a judicious compromise between these factors and much work remains to be done before such deliberations can be concluded.

The facilities, programs, and methods of the type described herein will provide a significant part of the input necessary to achieve this end.

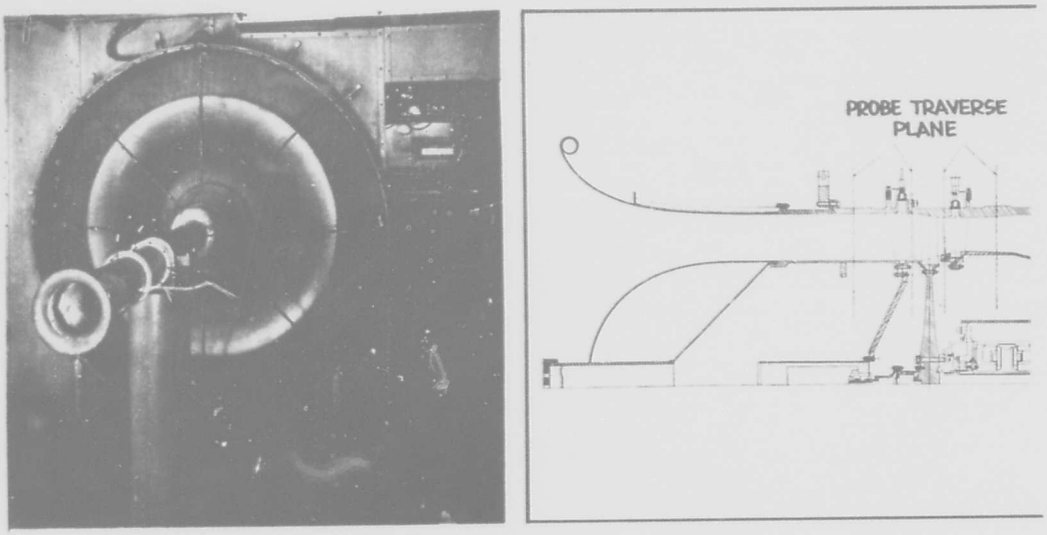

Figure 1 - Fan/Compressor Acoustic Test Facility

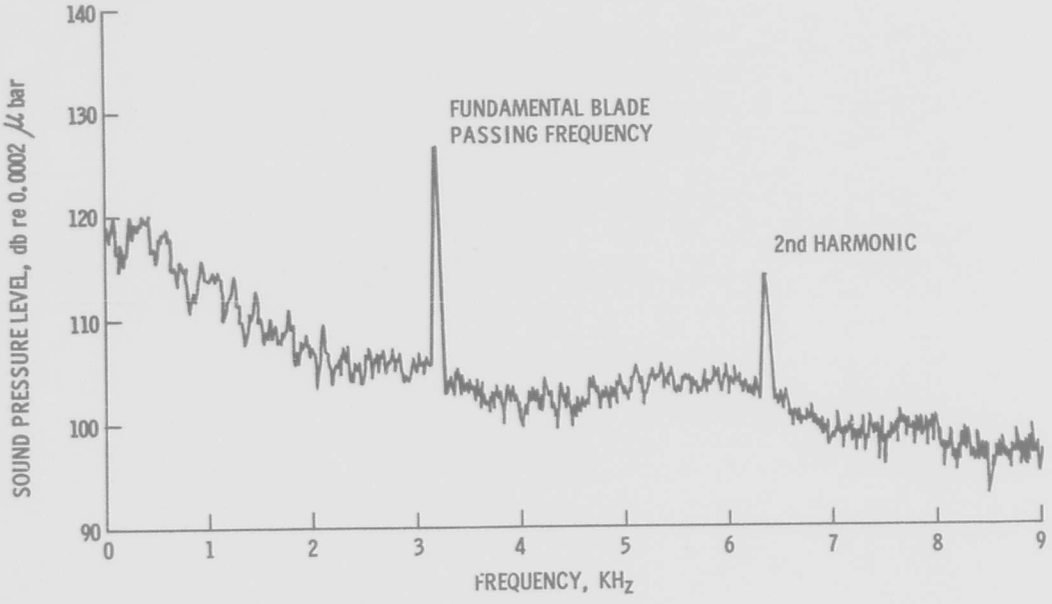

Figure 2 - Typical Spectra, Measured Near Fan Face By Acoustic Probe

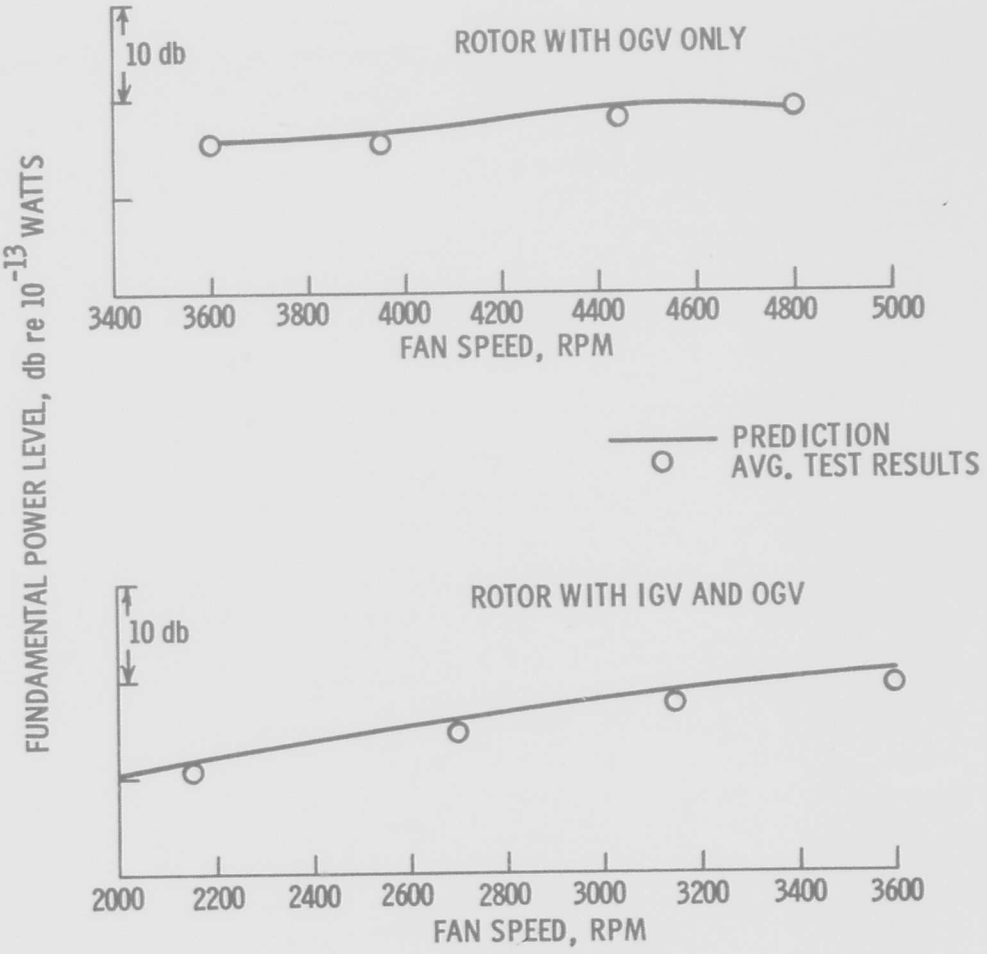

Figure 3 - Comparison of Predicted and Measured Results for Two Rotor Configurations

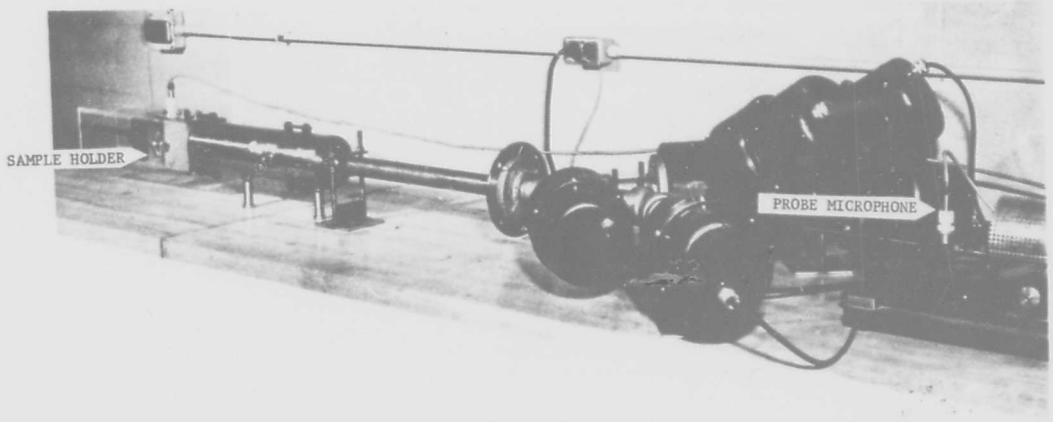

Figure 4 - High Intensity Standing Wave Tube with Six Drivers

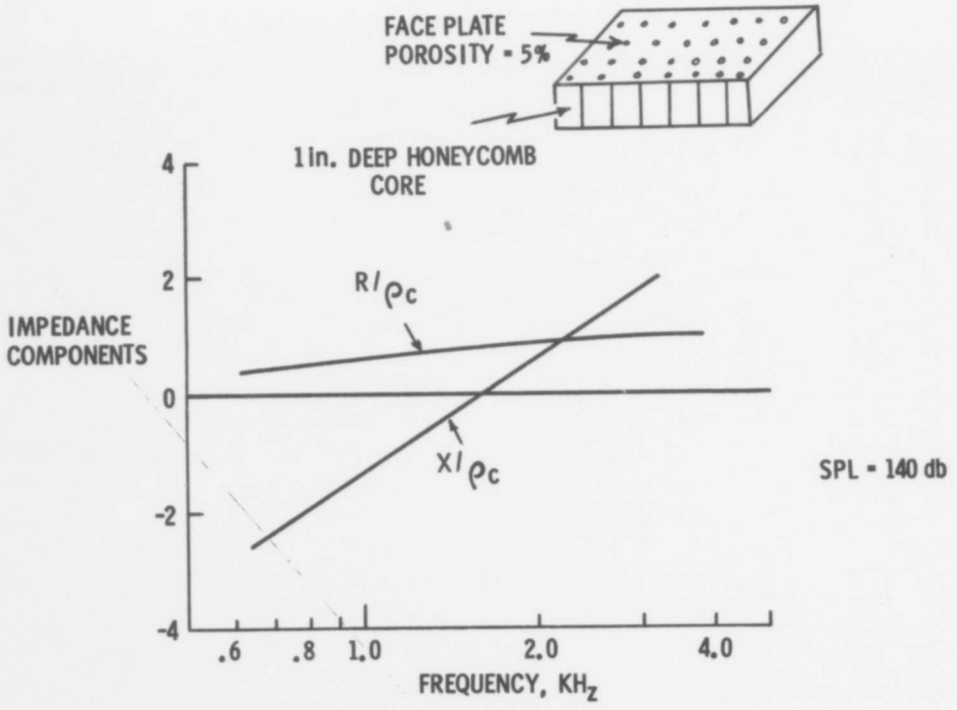

Figure 5 - Impedance Components of Single Layer Honeycomb with Porous Face Plate

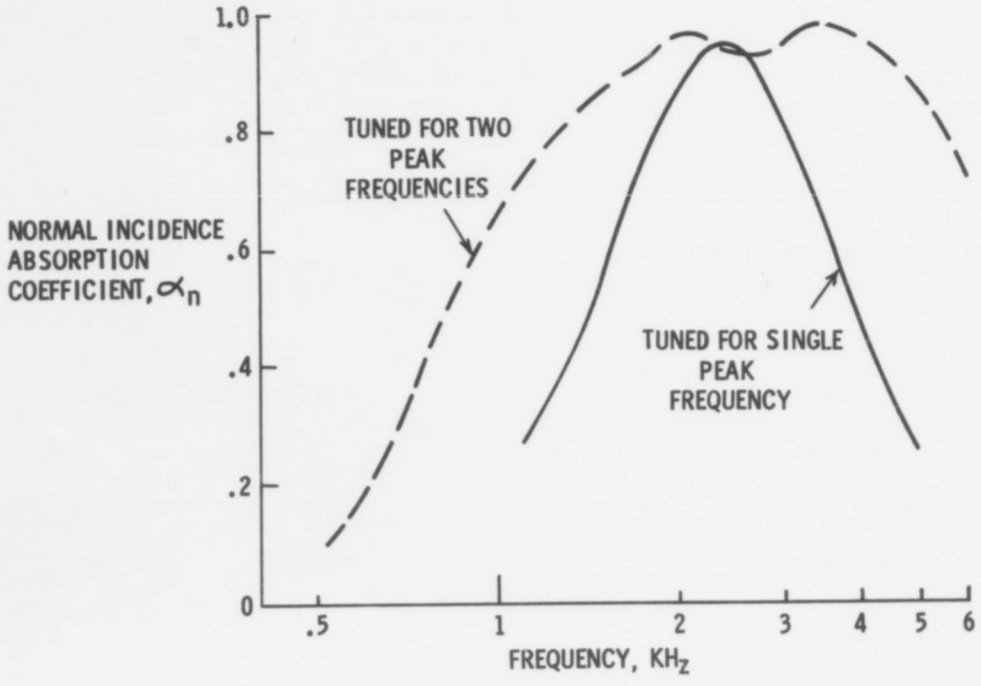

Figure 6 - Normal Incidence Absorption Characteristics for Two Different Treatment Designs

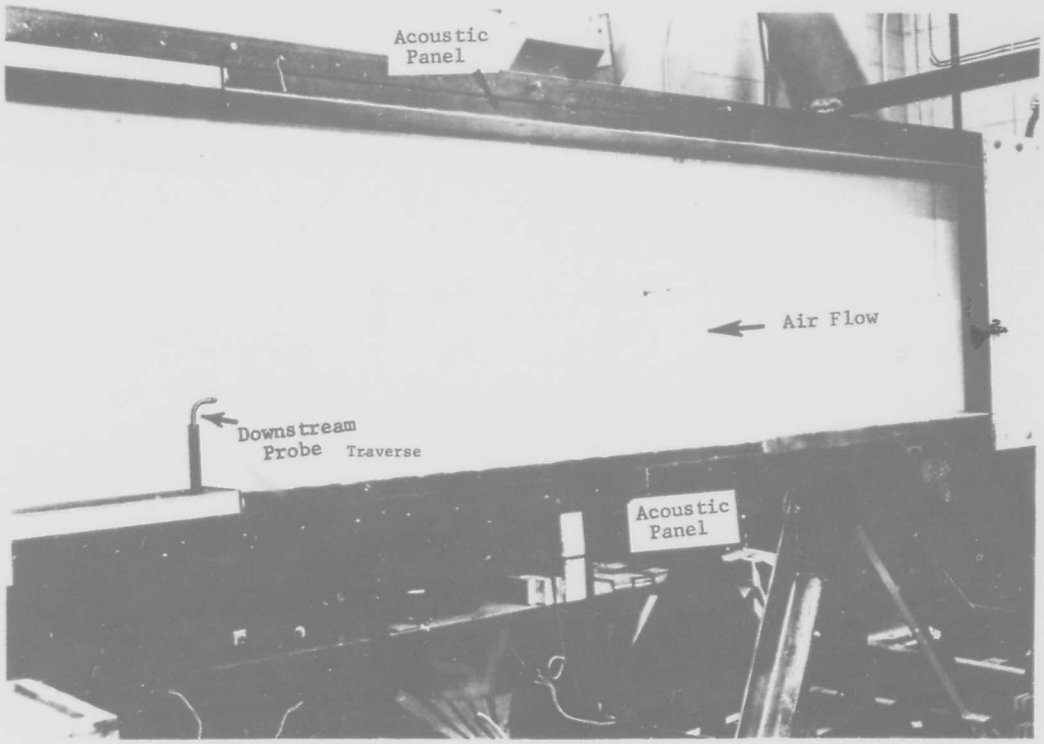

Figure 7 - Rectangular Duct Acoustic Treatment Transmission Loss Test Apparatus

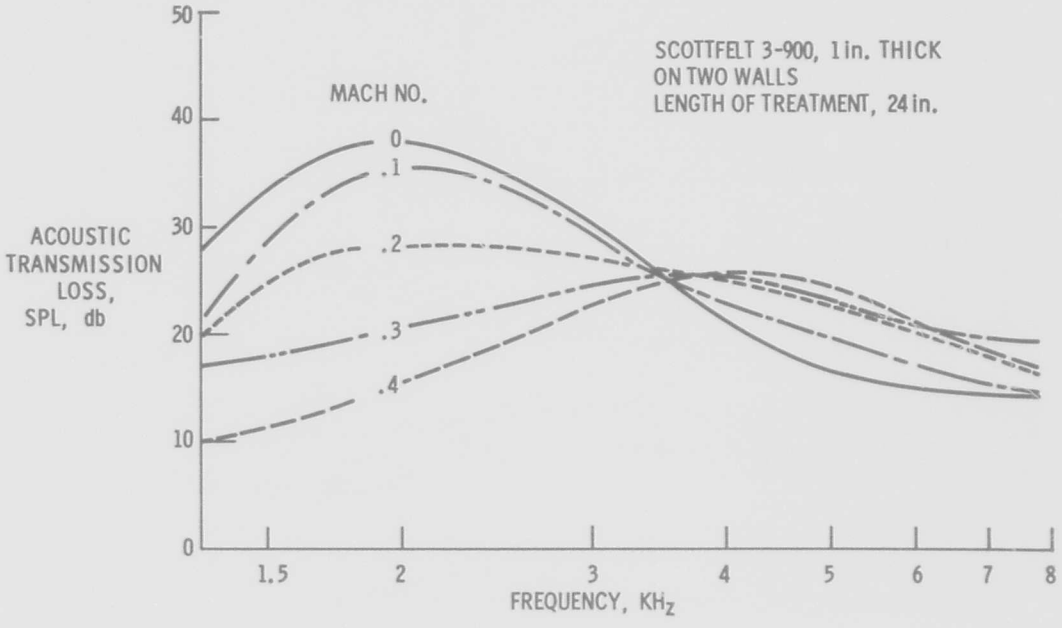

Figure 8 - Effects of Air Flow on the Acoustic Transmission Loss in a 4" by 17.5" Duct

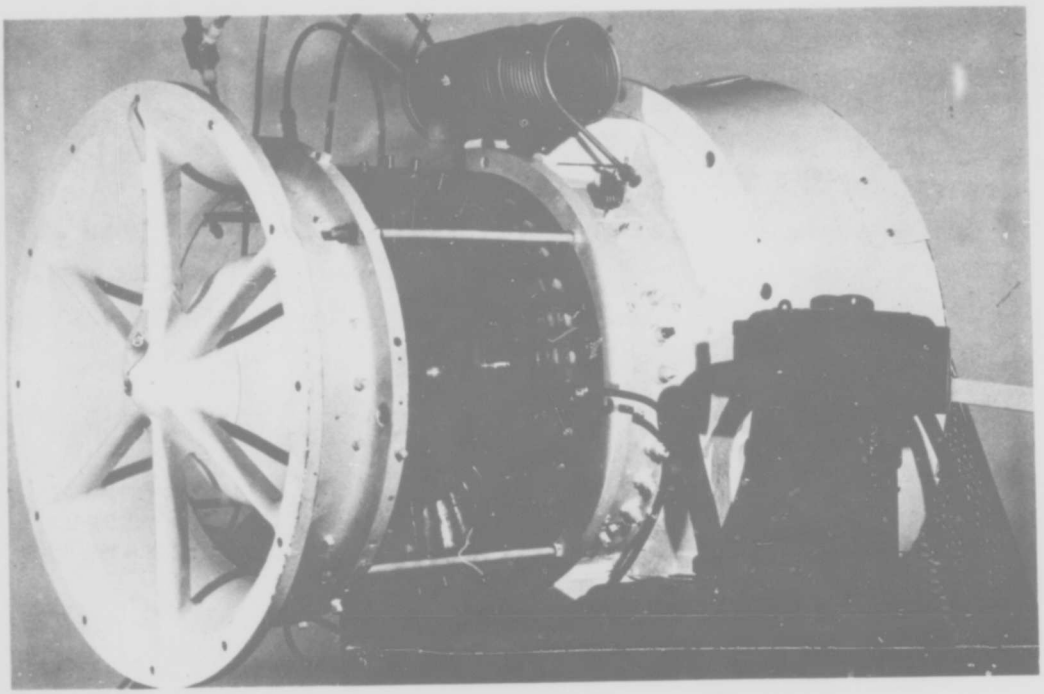

Figure 9 - 15" Laboratory Compressor with Acoustic Probe Ending in ρc Coil

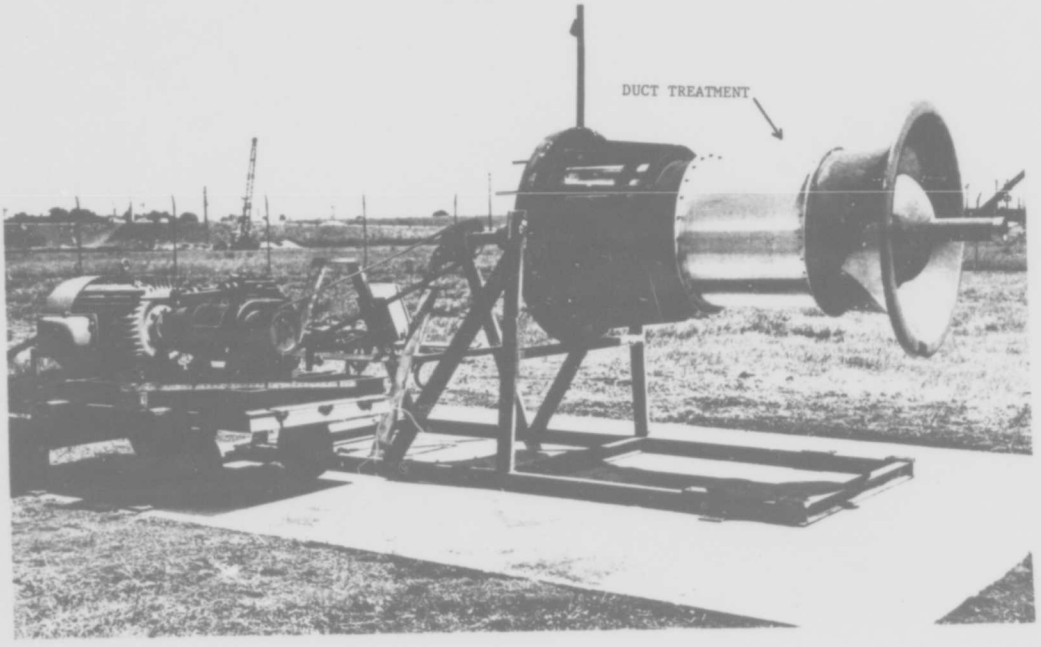

Figure 10 - 26" Acoustics Research Compressor, Duct Treatment Test Set-up

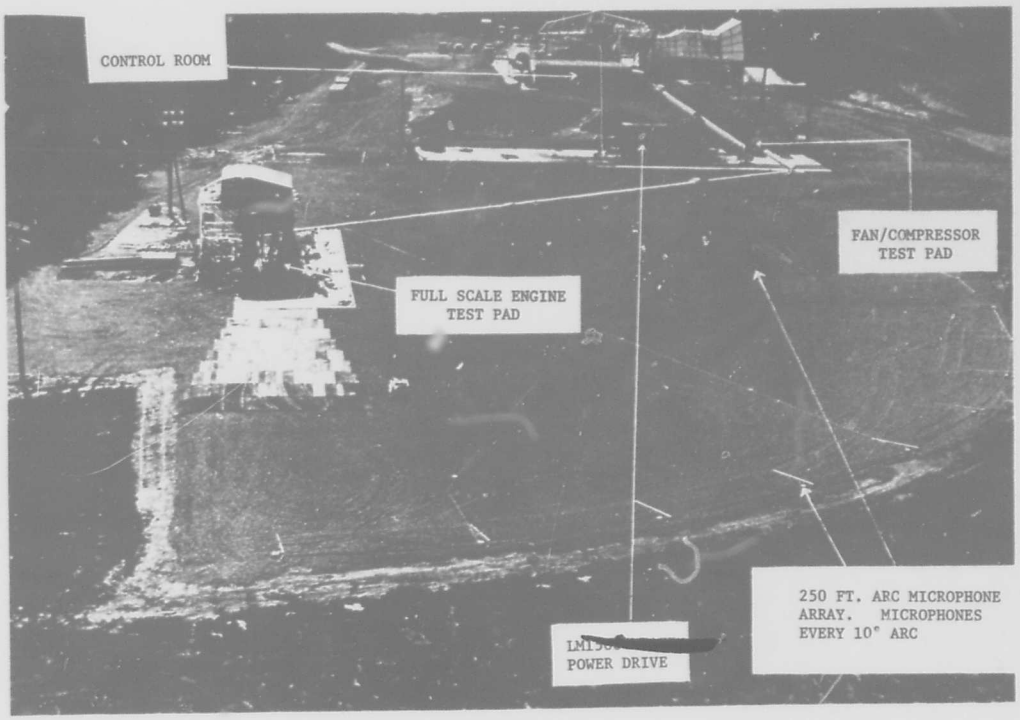

Figure 11 - Aerial View of Far Field Acoustic Test Facility (Peebles, Ohio)

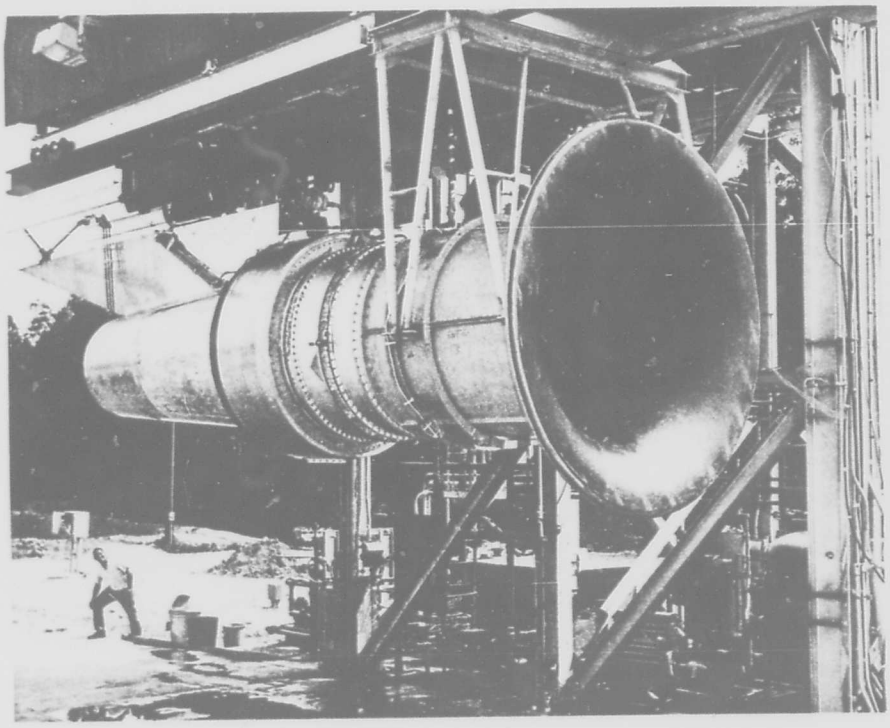

Figure 12 - Fan Engine Mounted in Full Scale Engine Acoustic Test Facility

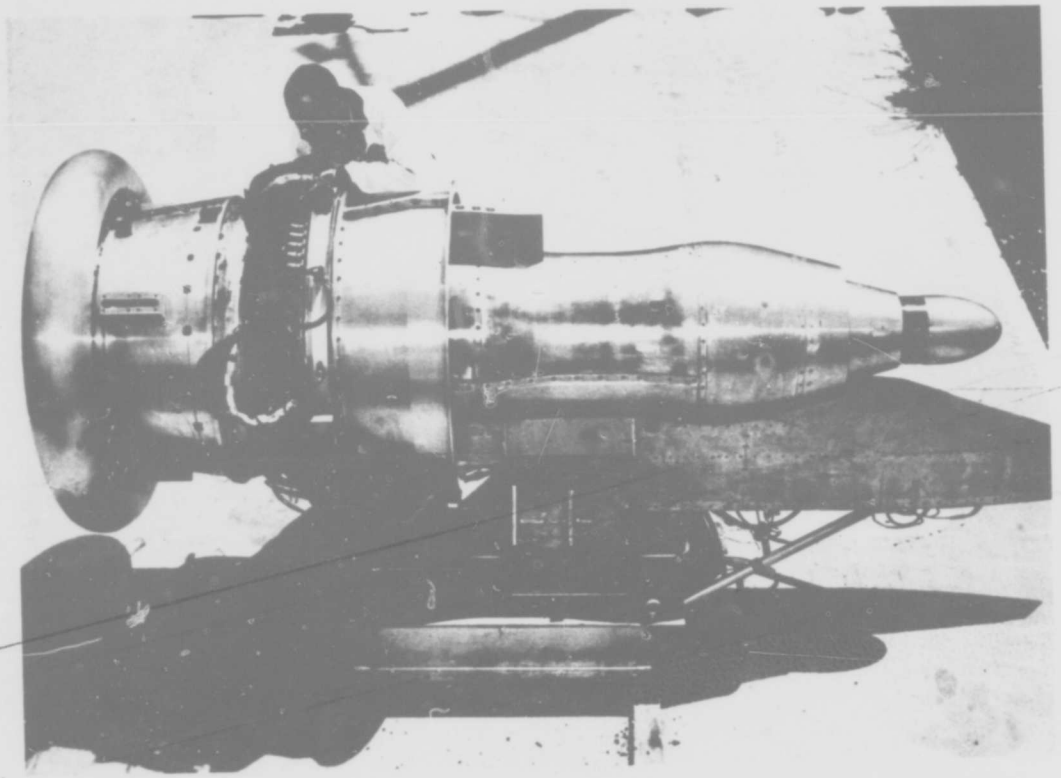

Figure 13 - 36" Acoustic Test Fan, Aft Cowl Duct Removed

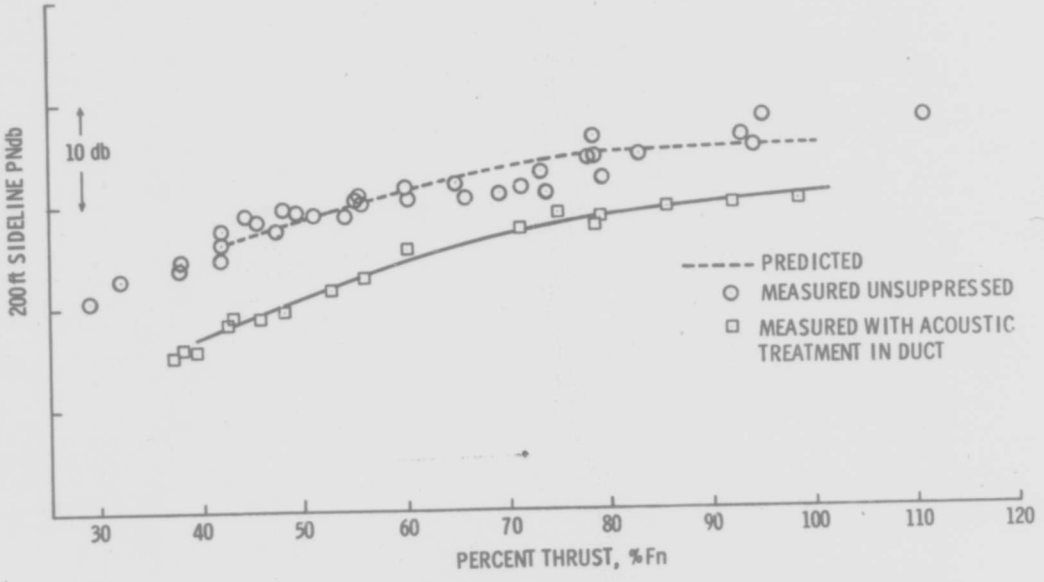

Figure 14 - Comparison of Predicted and Experimental Results for 36" Acoustic Test Fan

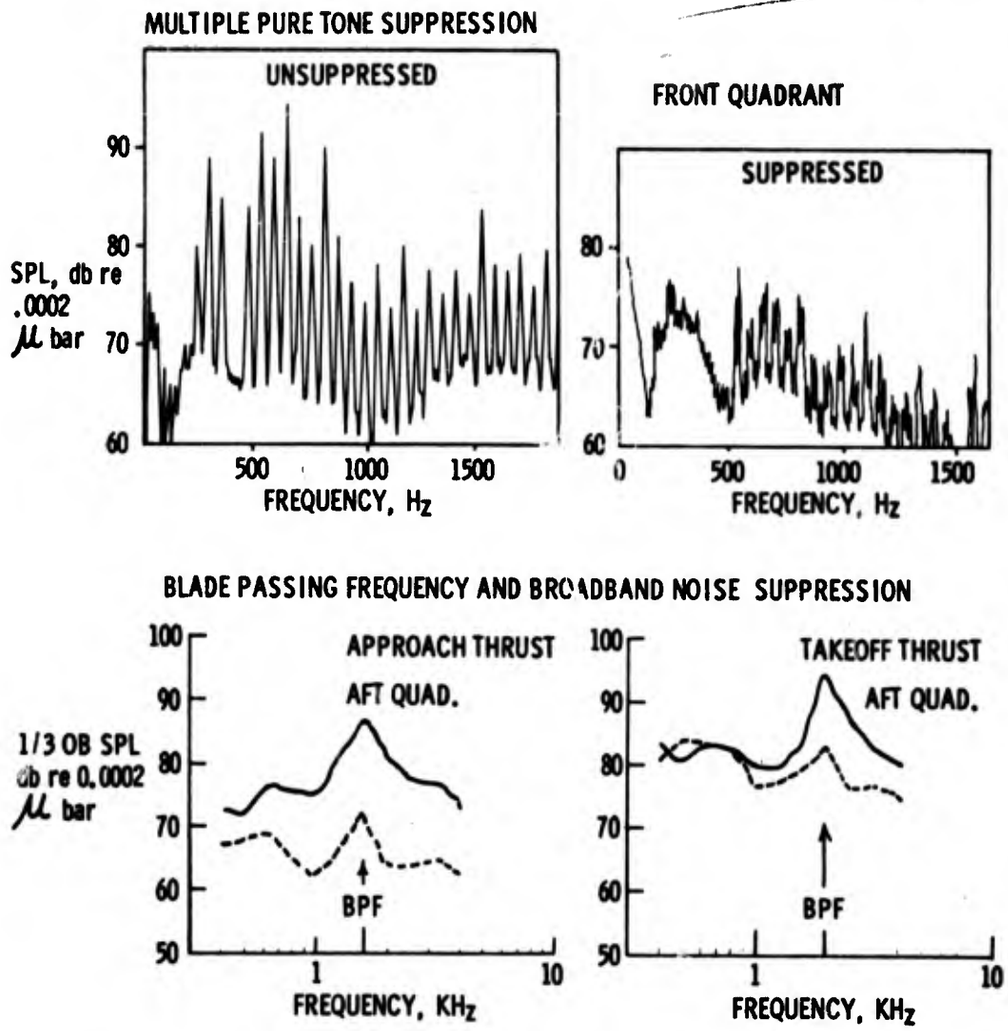

Figure 15 - Effectiveness of Acoustic Treatment in Reducing Component Noise

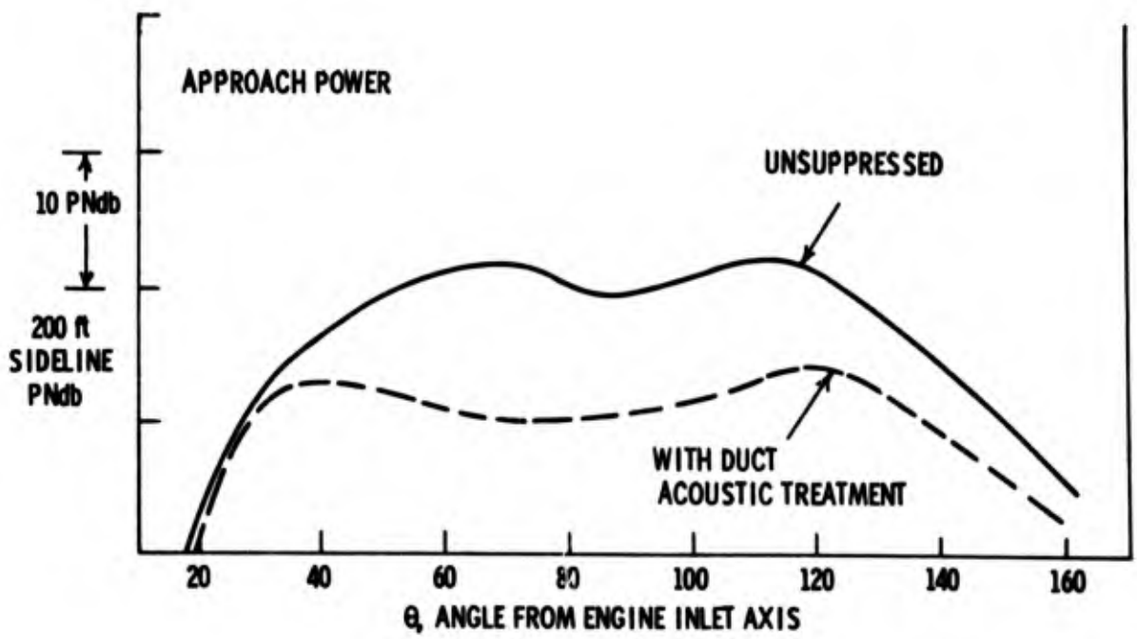

Figure 16 - Measured Directional Patterns of Suppressed and Unsuppressed Engine

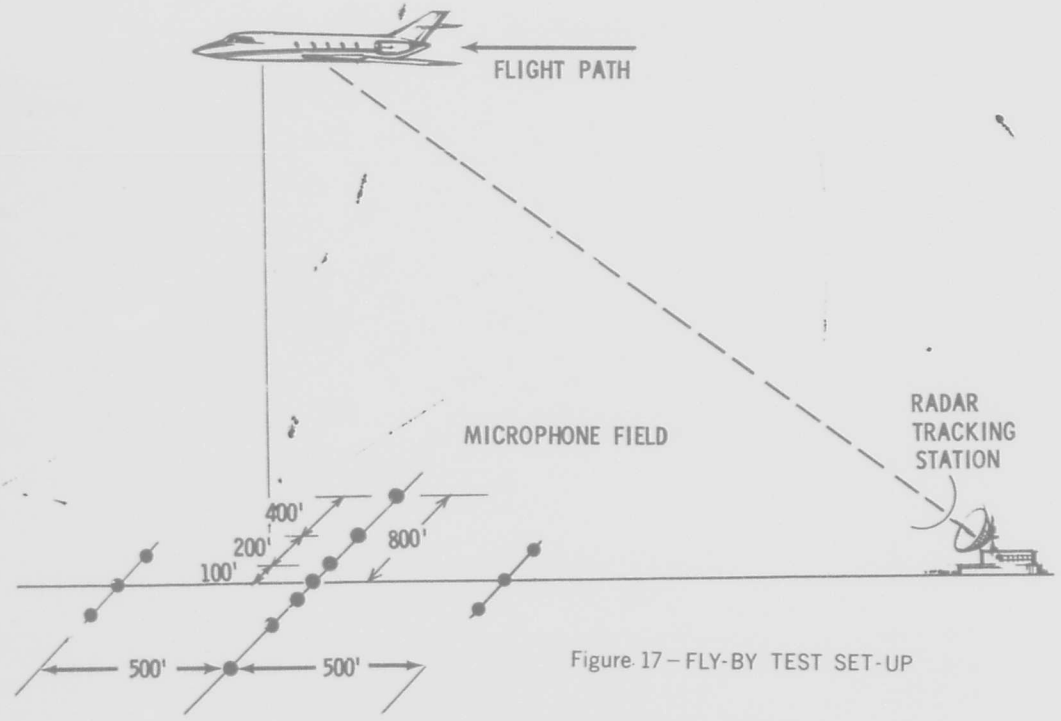

Figure 17 – FLY-BY TEST SET-UP

Figure 17 - Fly-by Test Set-up

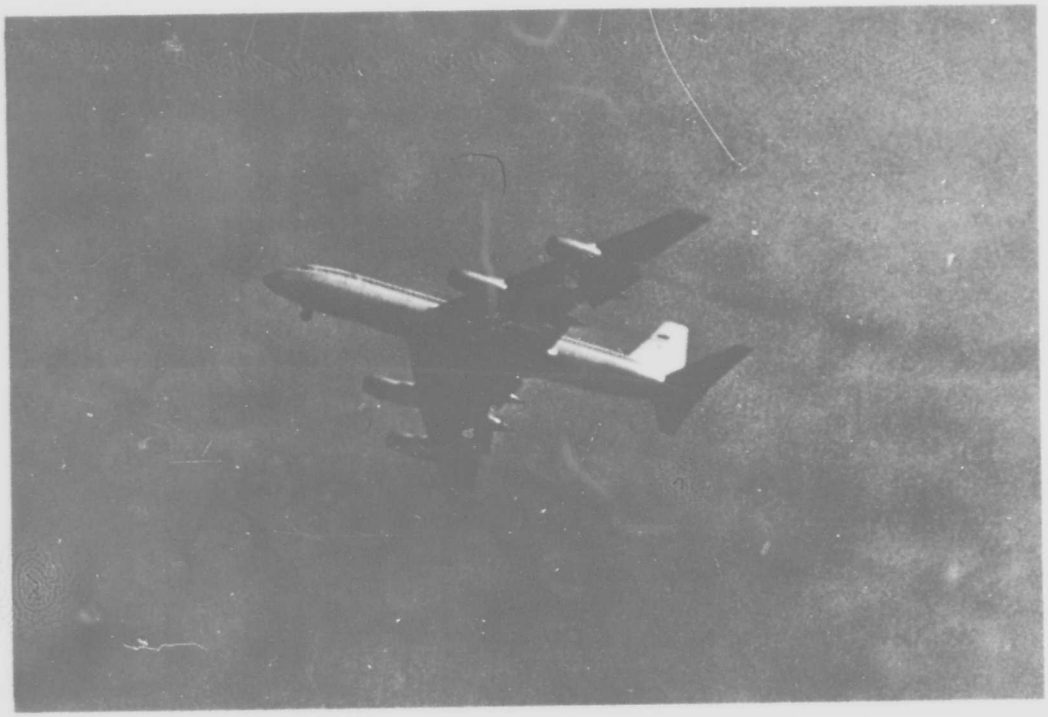

Figure 18 - Typical Convair 990 Fly-by Test Run

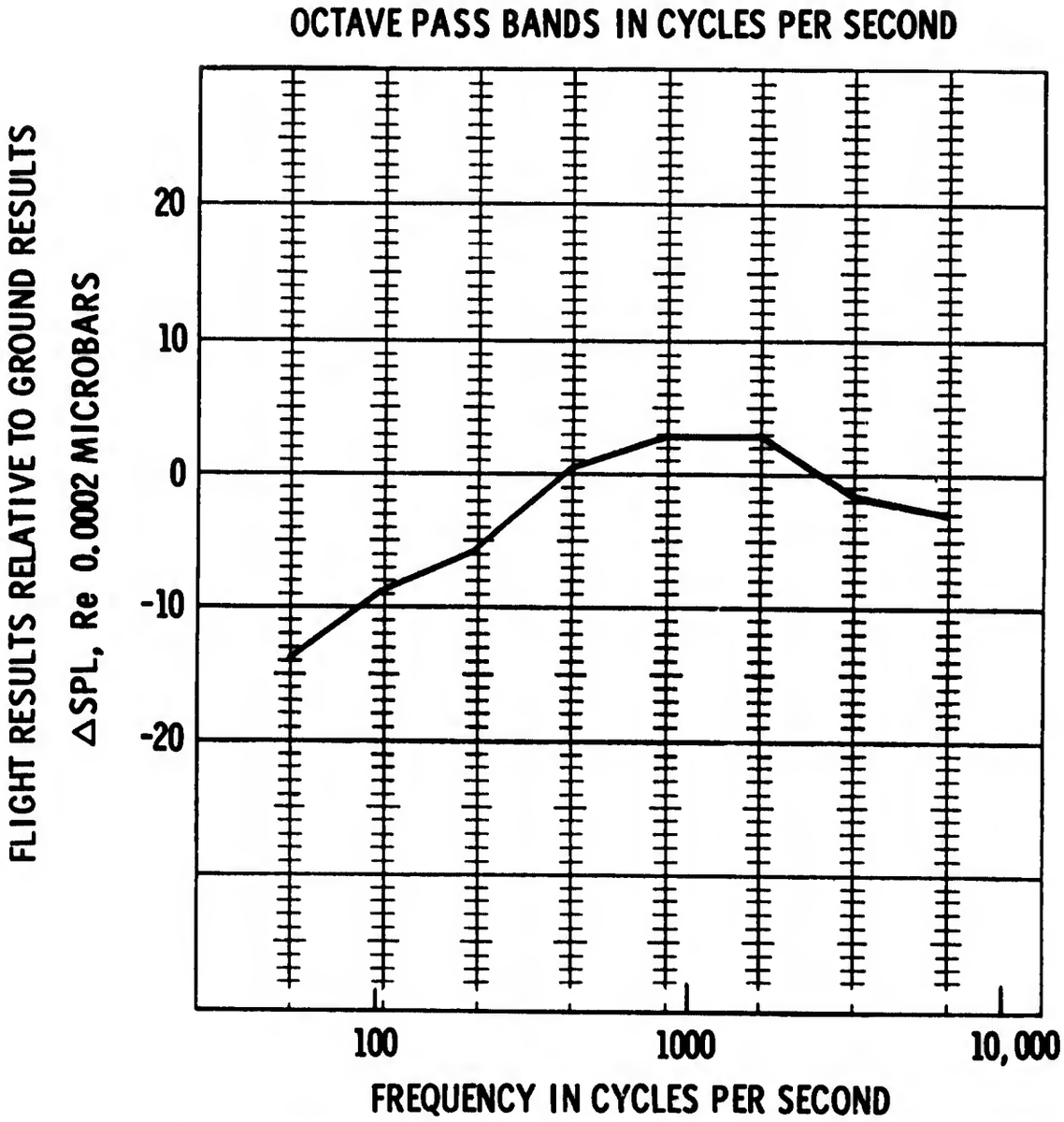

Figure 19 - Overall Flight and Ground Comparison for Convair 990/CJ805-23

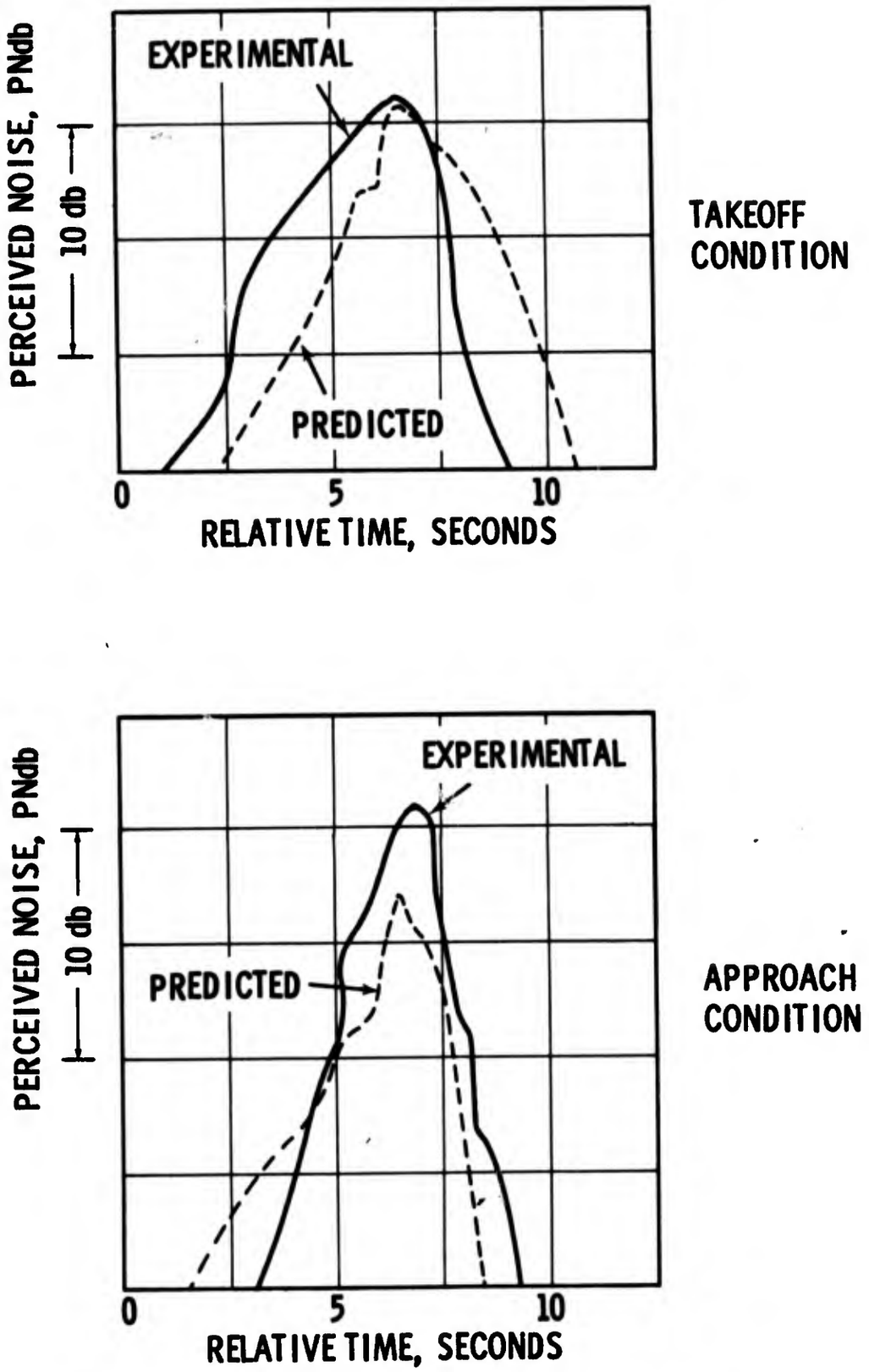

Figure 20 - Comparison of Prediction and Flyover Test Results

GENERATION AND SUPPRESSION OF COMBINATION TONE NOISE FROM TURBOFAN ENGINES

By
J. D. Kester
Senior Project Engineer
Acoustics
Pratt & Whitney Aircraft
East Hartford, Connecticut
USA

SUMMARY

Advanced acoustical design features have resulted in the elimination of several sources of noise from the JT9D high bypass ratio turbofan engine being developed by Pratt & Whitney Aircraft. With reductions in pure tone noise levels radiated out the inlet duct, combination tone noise has been uncovered as a principal remaining noise source at high powers where the fan blade tips are supersonic. Studies of the generation and propagation of this noise have been conducted on a variety of research rigs as well as on the full scale engine. Detailed mapping of the inlet duct noise field forward of a supersonic tip speed fan has provided a basic understanding of the properties of this noise source. Substantial reductions in the level of noise from this source have been demonstrated by the installation of sound absorbing liners in the inlet ducts of turbofan engines. Results of these studies are reviewed in this paper.

ALTHOUGH THE ADVENT of commercial high bypass ratio turbofan engines has resulted in lower noise levels, the importance of the fan noise component has increased. The lower level of jet noise achieved with these low jet velocity engines causes fan noises to be potentially even more dominant than those from current low bypass ratio turbofans. This trend, illustrated in Figure 1, is expected to persist into the future when even higher bypass ratio propulsion powerplants are developed, and for a wide variety of lift fan type engines now being studied for future transportation systems. The increasing importance of fan noise is attributable not only to increases in bypass ratio, but also to the strong trend toward advanced designs which incorporate much higher operating fan tip speeds than used for the high bypass engines now being developed. High fan tip speeds permit the engine designer to achieve light weight, compact engine designs not possible with lower fan speeds. Because of these trends, the achievement of quieter, high performance aircraft powerplants in the future depends strongly on the ability to develop quieter fans.

Research to date in fan noise has shown that at least three separate and distinct noise generating mechanisms are involved. One mechanism generates discrete tones of blade passing frequency. These tones from current low bypass ratio turbofans are generated by the periodic chopping of fan blades through wakes from upstream structure or vanes, and by the periodic impingement of fan blade wakes on downstream structure or vanes. These blade-vane wake interactions produce the shrill whine most noticeable during landing. An insight into the generation of this noise is provided by Reference (1). The noise generation principles derived in Reference (1) have been exploited in the design of the high bypass ratio JT9D engine now being developed for commercial service. As a result, this engine has lower levels of discrete tone noise than current low bypass ratio fans having inlet vanes.

A second source of noise inherent in all fans is broadband noise thought to be generated largely by the interaction of turbulence with fan blades and vanes. Details of the generation of this noise have not yet been described satisfactorily by theory. This noise can be expected to be a continuing problem for advanced installations, particularly installations such as wing mounted lift fans, in which aerodynamic constraints on the inlet design could result in highly turbulent flow into the fan.

The third source of fan noise, and the one to be discussed in this paper, is combination tone noise, sometimes called multiple pure tone noise. This noise becomes pronounced at supersonic blade tip speeds such as are used during take-off of most current turbofan engines and will be present from the commercial high bypass engines under development. All fan noise components are illustrated in Figure 2, which shows a typical narrow band inlet noise spectrum from a Pratt & Whitney Aircraft JT3D low bypass ratio turbofan engine at a take-off power fan tip speed. At all powers, interaction tones and broadband noise are produced by this engine. The presence of combination tone noise can be observed only at supersonic fan tip speeds such as are used for take-off.

Each fan noise component has a distinctive quality to a listener. A majority of listeners judge the shrill discrete tone noises generated by wake chopping interactions to be the most annoying component. Broadband noise generally is judged to be the least annoying. Combination tone noise has a most distinctive sound. Subjective judgments of this noise indicate it to be less annoying than pure tone noise, but more annoying than broadband noise. To a listener, the "apparent" frequency of this noise is judged to be at the engine rotational speed, or frequency, which is quite low. Most engines have rotational speeds in the 30 to 200 revolutions per second or cycles per second range depending on the engine size, larger engines having lower speeds. The quality of combination tone noise has been described by some as being similar to the noise from a buzz-saw in operation.

Because it was recognized that combination tone noise could be judged less annoying than a strong pure tone noise, attempts were made during the development of noise reduction features for low bypass ratio engines to produce combination tone noise with a subsonic rotor operated behind an inlet vane assembly. To achieve this, the blades in the rotor were irregularly spaced in the disk as shown in Figure 3. These rotors were tested behind inlet guide vane assemblies having uniform angular spacing between vanes. It should be noted that the frequencies of the interaction tones produced are determined entirely by the rotor blade spacing and not affected by either the number of inlet vanes, or by whether the inlet vanes are spaced in a non-uniform pattern. Tests of rotors such as the one shown in Figure 3, produced the measured noise spectra shown in Figure 4, and indicated that a large number of lower tones could be produced in place of one strong tone so that the desired combination tone noise quality was attained. A noise spectrum for a conventional rotor having uniformly spaced blades which produced one strong tone is shown for comparison. In achieving the irregular blade spacing, large variations in local gap chord ratio were required. This resulted in unacceptably high performance degradation for the modest improvement in measured noise level. For this reason, further work on subsonic rotors with irregular blade spacing was not pursued. As an interesting sidelight, the principle of irregular spacing to break up objectional tones has been applied successfully to the design of vehicle tires to eliminate objectionable highway noises and to the design of automobile cooling fans.

The importance of combination tone noise from single stage fans without inlet guide vanes became apparent in 1965 when several noise tests were conducted using the large diameter single stage fan demonstrator engine shown in Figure 5. This engine was used to evaluate and refine the advanced acoustical design features being introduced by Pratt & Whitney Aircraft in its JT9D engine which was then being designed. Omission of the inlet guide vanes from the single stage fan and large spacing between the fan blades and the exit guide vanes were JT9D engine design features intended to eliminate many sources of interaction tones. See Reference (2). A noise spectrum at an inlet angle measured during supersonic blade tip speed operation of the demonstrator engine is shown in Figure 6. Because the acoustical design features were effective, the interaction tone at blade passing frequency is low in level and does not protrude far above the level of the broadband noise. However, several discrete tones in the 300 to 1200 Hz frequency range (4th and 5th octaves) are apparent in the inlet noise spectra. Each of these tones is an integral multiple, or harmonic, of the rotational frequency of the engine, 50 revolutions per second (3000 rpm). Adjacent tones are separated in frequency by 50 cycles. This frequency separation produces the characteristic low pitched sound of combination tone noise.

Tests on the demonstrator engine provided an indication of several characteristics of combination tone noise. A plot of combination tone, broadband, and blade passing noise energy versus tip speed is shown in Figure 7. The amount of energy radiated as combination tone noise increased markedly as the rotor tip speed went through sonic giving an indication that the generation of this noise was related to shock wave formation at the fan blade tips. Plots of the radiation pattern of combination tone noise such as the one shown in Figure 8 indicated that the noise was radiated entirely out the inlet duct, and not out the fan discharge duct. The other fan noises, interaction tones and broadband noise, are radiated out both the inlet and fan discharge duct.

With combination tone noise identified as a major take-off power noise source from single stage fans which incorporate design features to reduce noise from other sources, emphasis was placed on understanding the generation of this noise. A program to investigate the generation of combination tone noise was initiated using the 28 inch diameter single stage fan rig shown in Figure 9. This rig, which incorporates the first stage rotor of a J52 engine, is capable of operating at tip speeds as high as 1250 feet per second, well into the supersonic region of interest. With the inlet duct opening into an anechoic (echo-free) room, noise measurements in the semi-far field of the inlet can be made. Although the size of the room is not adequate for true far field measurements, the noise directivity patterns measured at an 8 foot radius from the 28 inch rig were representative of noise directivity patterns measured in the far field of full scale engines. Also, changes in noise directivity pattern noted from modifications to the rig are useful in predicting changes in the far field noise for full scale engines when similar modifications are made.

One inherent disadvantage of most indoor fan noise test rigs is that the measurement of fan discharge noise is not possible. This, however, was not a major disadvantage in the study of combination tone noise which is radiated only from the inlet.

Shown in Figure 9 is the special inlet microphone probe traverse mechanism used to position accurately the microphone on the probe tip anywhere in the inlet duct. Traversing of the microphone in the radial axial, or circumferential directions is possible. This probe mechanism was used extensively to map out the noise field in the cylindrical inlet duct in front of a supersonic tip speed rotor. In order to measure accurately the time history of the supersonic blade passing wave form, it was necessary to use transducers and a measuring system having a frequency response up to at least 50 KHz for a blade passing frequency of about 5 KHz. Acoustical measuring systems which have acceptable frequency responses up to only 10 KHz are incapable of reproducing the steep pressure rise indicative of the passage of shock waves and thus would distort the time history of the wave form.

A typical near field rotor pressure field spectrum measured in the inlet duct near the outer wall about 1 inch forward from the 28 inch rotor blades operating at supersonic tip speeds is shown in Figure 10. The wave form pressure history having one pressure pulse per blade also is shown and is quite uniform. This was expected because the blades in the rotor were installed with equal spacing and the individual blades were manufactured to close dimensional tolerances which would suggest similar characteristics for each. The steep rise in the wave leading edge is indicative of the passage over the microphone of shock waves from the individual blades. As indicated by the noise spectrum, which is the Fourier analysis of the wave form at this location, the discrete tone at blade passing frequency is quite prominent in the rotor nearfield.

When the microphone was located 10 inches axially upstream of the rotor tips, a very dramatic change in the noise spectrum was noted. The spectrum at this location for the same rotor speed as for Figure 10 is shown in Figure 11, along with the wave form measured by the probe. The blade passing frequency tone decreased by about 20 decibels, whereas some combination tone components in the 500-1500KC region actually have increased in level by as much as 5 decibels. This spectrum compares qualitatively with the noise spectrum illustrated in Figure 12 measured by the "far field" microphones.

To determine what was happening to the noise from the supersonic rotor travelling upstream against the flow in the inlet duct, the probe was traversed axially and the wave form of the noise signal in the duct was displayed on a cathode ray oscilloscope and photographed every ½ inch of probe travel. An electrical impulse on the rig shaft was used to trigger each photograph to occur when the rotor passed through a given angular position. This series of wave forms is shown in Figure 13.

As the probe is traversed upstream, the character of the wave form is observed to change dramatically from the uniform wave form noted near the rotor to a series of pressure pulses having non-uniform spacing and non-uniform amplitudes farther forward of the rotor. This irregular wave pattern was observed to repeat each revolution of the rotor, indicating that the Mach wave from each individual blade is slightly different but highly repetitive. Because this irregular wave pattern is repeated each revolution of the rotor, the noise spectrum obtained from harmonic analysis is found to contain energy at all multiples of rotational frequency. Thus, a "transition zone" exists in the duct forward of the rotor where a marked decay in blade passing frequency noise level occurs and is accompanied by a marked increase in combination tone noise. This "transition zone" is illustrated in Figure 14, along with the overall noise decreases forward of the rotor as measured from an axial traverse of the inlet probe microphone. From analysis of data of the type shown in Figure 13, it was possible to reconstruct the spiral field of the wave fronts from adjacent blades in the duct forward of a supersonic rotor. This is illustrated in Figure 15 which compares the wave front locations measured with those that were predicted for that blade tip Mach number and axial flow condition.

As a result of these tests, it became apparent that combination tone noise would be generated by supersonic tip speed fan engines, and would contribute to community noise.

Although the design fan speed of the JT9D engine had been kept relatively low to minimize noise generation, the blade tips were supersonic during takeoff. Combination tone noise generation was expected to be produced at this condition so methods of suppressing this noise were required in order that the potentially quiet operation of the engine could be realized. Because combination tone noise resulted from the propagation of the Mach wave pattern created by fan blades at supersonic speeds, little could be done to prevent generation of this noise other than to restrict operation of the fan to subsonic tip speeds. However, if fan operation was limited to subsonic tip speeds, the resulting increase in engine size and weight would have been unacceptable. A method which was compatible with the other engine design requirements was required to control this noise.

Because the shock waves differed from blade to blade, some lack of uniformity within sets of blades produced to the same close tolerance must be involved. Closer control of blade tolerances was considered as a method of reducing this noise. Tests were conducted on rotors having a few blades installed with leading edge angles well outside of normal tolerance limits and other rotors were tested which had a few blades installed with blunter than normal leading edges. Tests of these rotors showed that combination tone levels could be increased by increasing the non-uniformities of the rotor. On the other hand, tests of blade sets carefully selected from large quantities of similar blades to have more uniform properties than would be expected from normal assembly procedures have shown only slightly lower levels of combination tone noise. Although the use of closer manufacturing tolerances on fan blades might provide some small reduction in this noise, it does not appear to be a practical method of reducing this noise. Close tolerances currently are used for these parts and greater accuracy would be quite difficult to achieve for production parts. The strong possibility also exists that a perfectly uniform rotor would, in place of combination tone noise, have a strong concentration of noise energy in more objectional blade passing frequency tones. Even if a rotor having a perfectly matched set of identical fan blades could be produced it would soon become non-uniform and generate combination tone noise in service because of non-uniformities resulting from normal repair procedures to blend out local nicks which result from ingestion of small foreign objects during taxi and ground operation.

The application of acoustical treatment to the walls of the inlet duct near the fan leading edge was considered to suppress combination tone noise. Treatment in this location where the "transition zone" occurs appeared quite attractive for several reasons. As only the outer portion of the fan blade operates at supersonic speeds, the blade attached shock waves are most intense near the outer duct wall, where the location of treatment presents no major structural or aerodynamic problems to the inlet designer. Near the rotor face, the noise energy is concentrated at blade passing frequency, which allows the treatment to be tuned for a relatively narrow band of frequencies. Well forward of the transition zone, the noise covers a wide range of frequencies and complicates greatly the problem of selecting an optimum tuning for an acoustical liner.

A series of acoustically treated inlet duct liners was fabricated and tested on the 28 inch diameter rig. Various lengths of liners having different types of treatment were evaluated. Several configurations showed substantial reduction of combination tone noise. One example is illustrated by Figure 16. It can be observed in Figure 17 that the combination tone noise in the case illustrated was reduced about 15 db with the short length of treatment shown. Although quite significant reductions were realized in combination tone noise, essentially no reduction in discrete tone noise was achieved. A probable reason for the lack of blade passing frequency tone suppression is that this noise is generated over the whole fan inlet annulus whereas combination tone noise is concentrated near the treated outer duct wall.

Results of tests on the 28 inch rig have provided insight into the generation of combination tone noise and have been used to guide the design of inlet liners for tests on JT9D engines. Similar levels of noise suppression have been achieved with these short lengths of inlet liners on full scale engines. Airplane installations of JT9D engines also have benefited from the results of this combination tone noise suppression work. Moderate lengths of very effective, light weight acoustical treatment have been incorporated in inlet duct walls with the result that combination tone noise in flight is suppressed at little loss in airplane performance. Although much work remains to be done before equally effective methods can be found to suppress the other sources of fan noise and jet noise, the successful investigation and subsequent reduction of combination tone noise represents an engineering achievement which will help to alleviate noise in communities near airports.

REFERENCES

1. J. M. Tyler and T. G. Sofrin, "Axial Flow Compressor Noise Studies." SAE Transactions, Vol. 70 (1962), pp. 309-332. Paper 345D.

2. J. D. Kester and T. G. Slaiby, "Designing the Low JT9D Engine to Meet Low Noise Requirements for Future Transports." SAE Preprint 670331, April 1967.

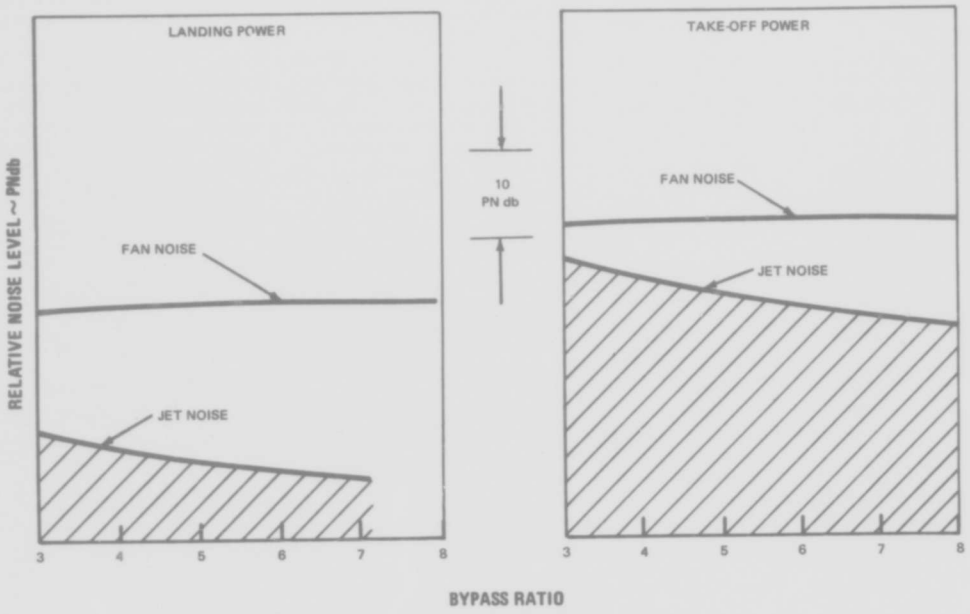

Figure 1 Comparison Of The Relative Loudness Of Jet Noise And Fan Noise As A Function Of Bypass Ratio.

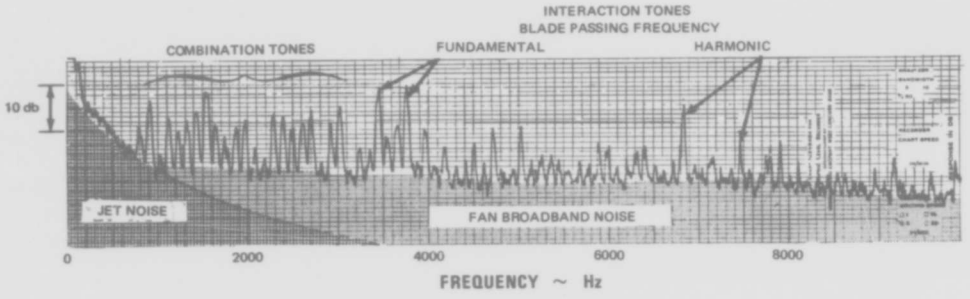

Figure 2 Narrow Band Noise Spectrum, Measured At An Inlet Angle From A JT3D Turbofan Engine At Take-Off Power. The JT3D Engine Powers 707 And DC-8 Jet Transports.

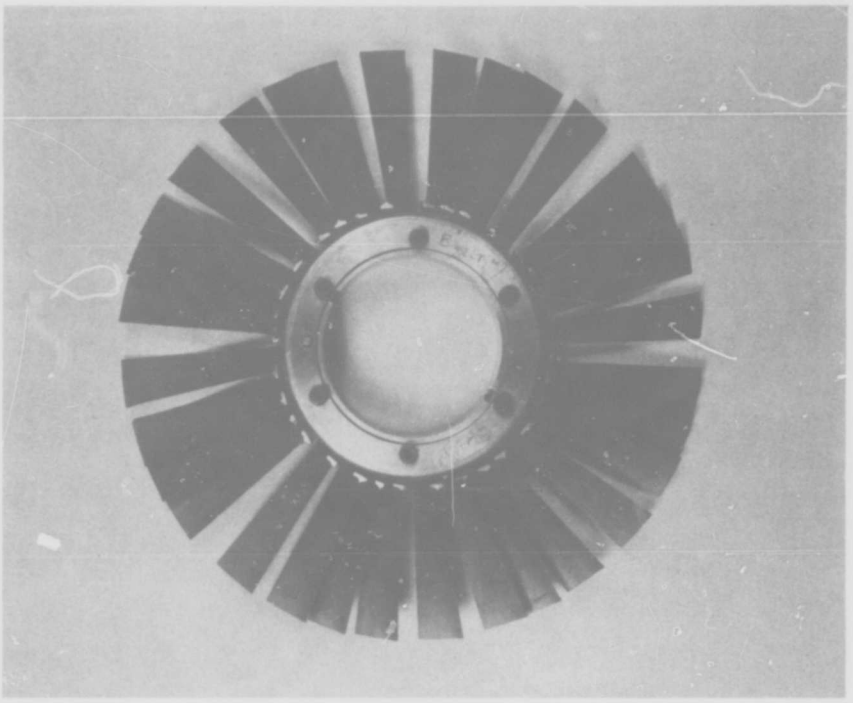

Figure 3 Ten Inch Diameter Test Rotor With 32 Irregularly Spaced Blades.

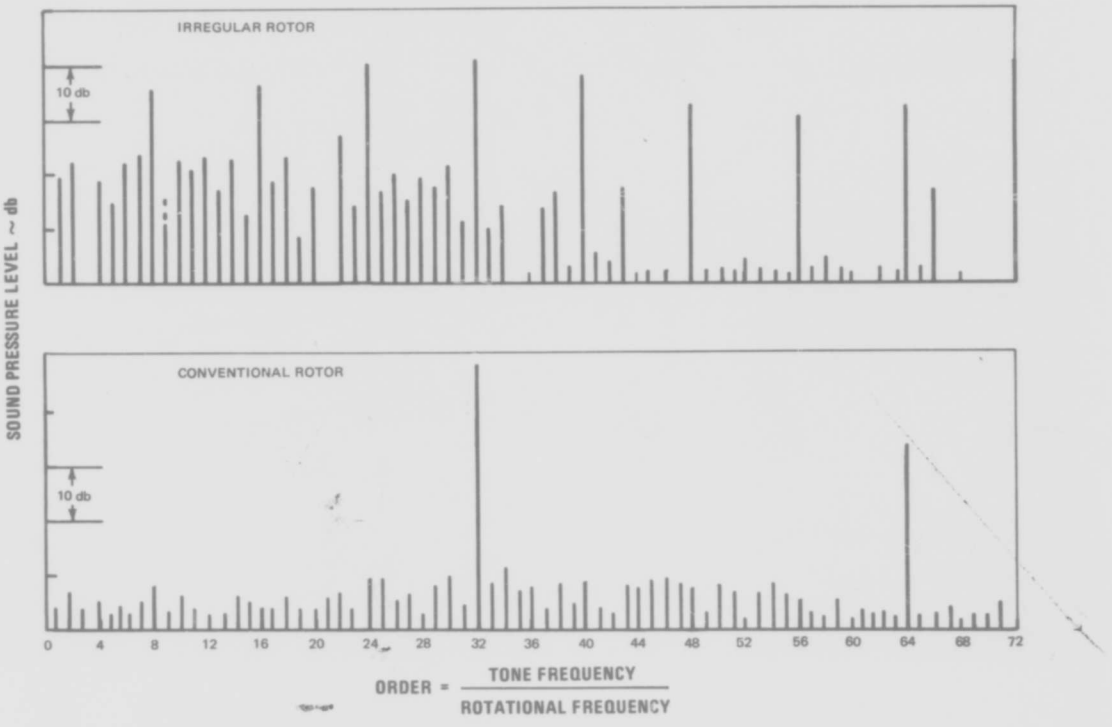

Figure 4 (Upper) Combination Tone Noise Spectrum Measured During Subsonic Operation Of Irregularly Spaced Rotor. (Lower) Typical Interaction Noise Spectrum Measured At The Same Condition With A Rotor Having 32 Equally Spaced Blades.

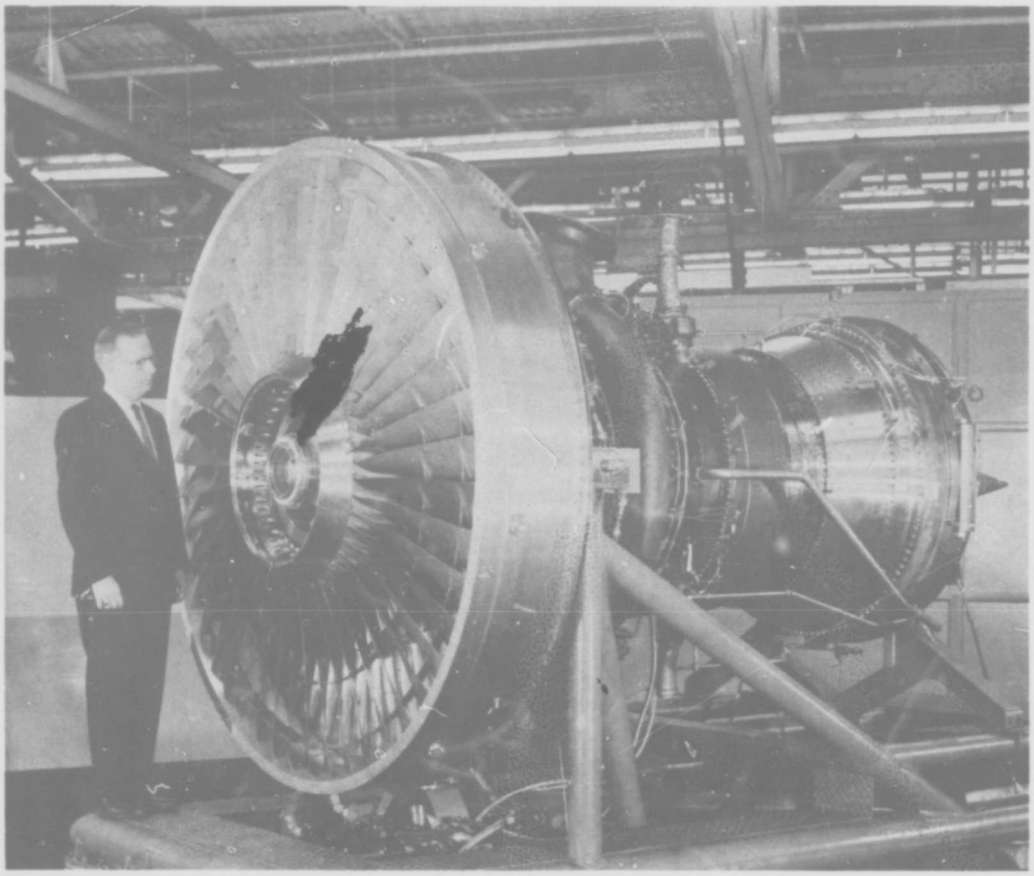

Figure 5 Single Stage 86 Inch Diameter Fan Demonstrator Engine.

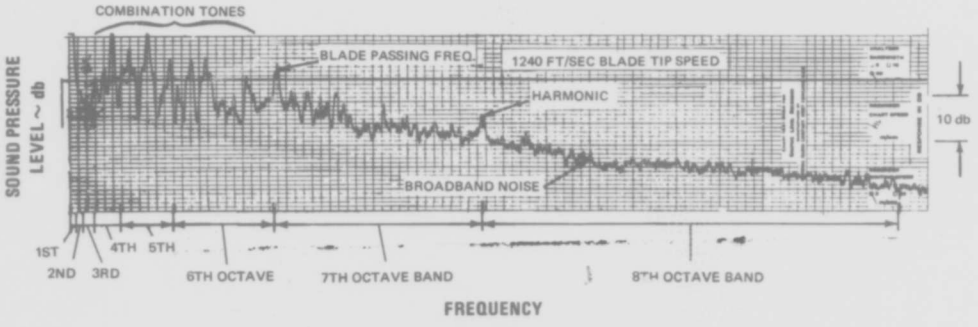

Figure 6 Narrow Band Inlet Noise Spectra Measured At Supersonic Tip Speed Operation Of Demonstrator Engine.

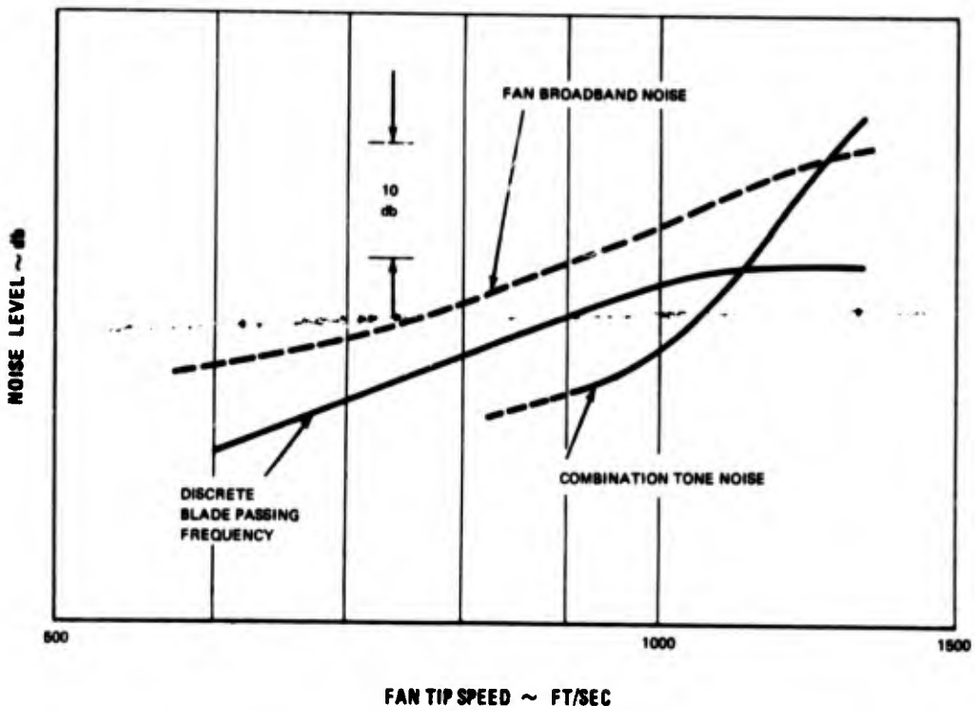

Figure 7 Variation Of Fan Noise Components With Fan Tip Speed.

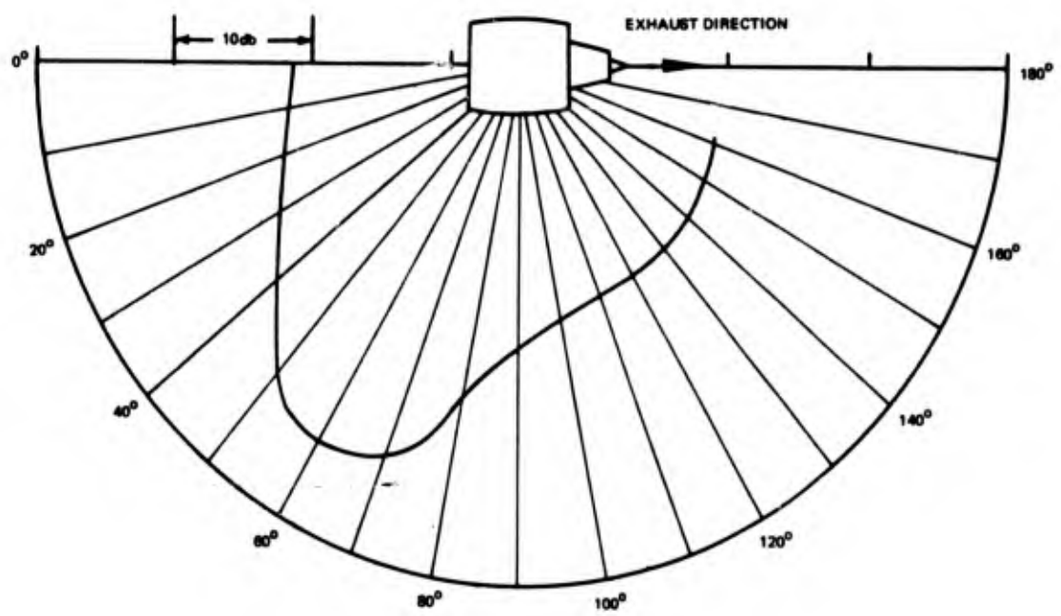

Figure 8 Combination Tone Noise Far Field Radiation Pattern.

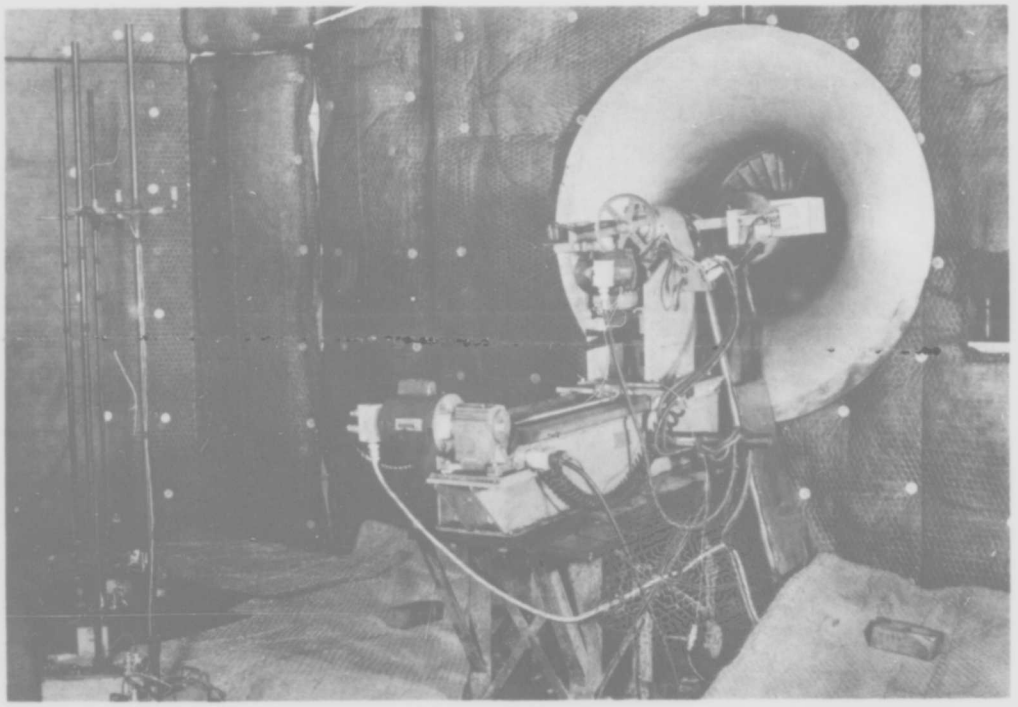

Figure 9 Inlet Of 28 Inch Diameter Single Stage Fan Noise Test Rig. In Front Of The Rig Is A Three Degree Of Freedom Inlet Duct Microphone Traverse Mechanism. "Far Field" Microphones Are Shown At Left.

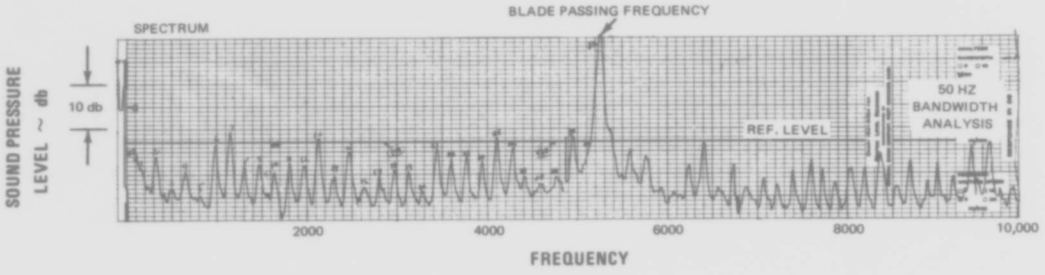

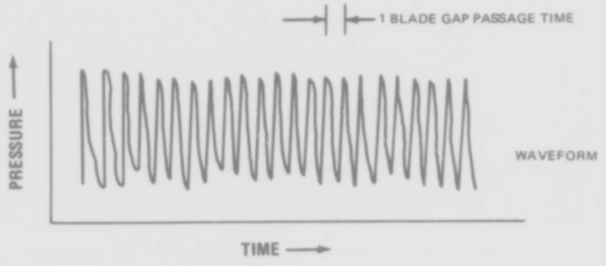

Figure 10 Waveform And Noise Spectrum Measured Using Probe Microphone 1 Inch Forward Of The 28 Inch Rig Blade Tips At A Supersonic Tip Speed.

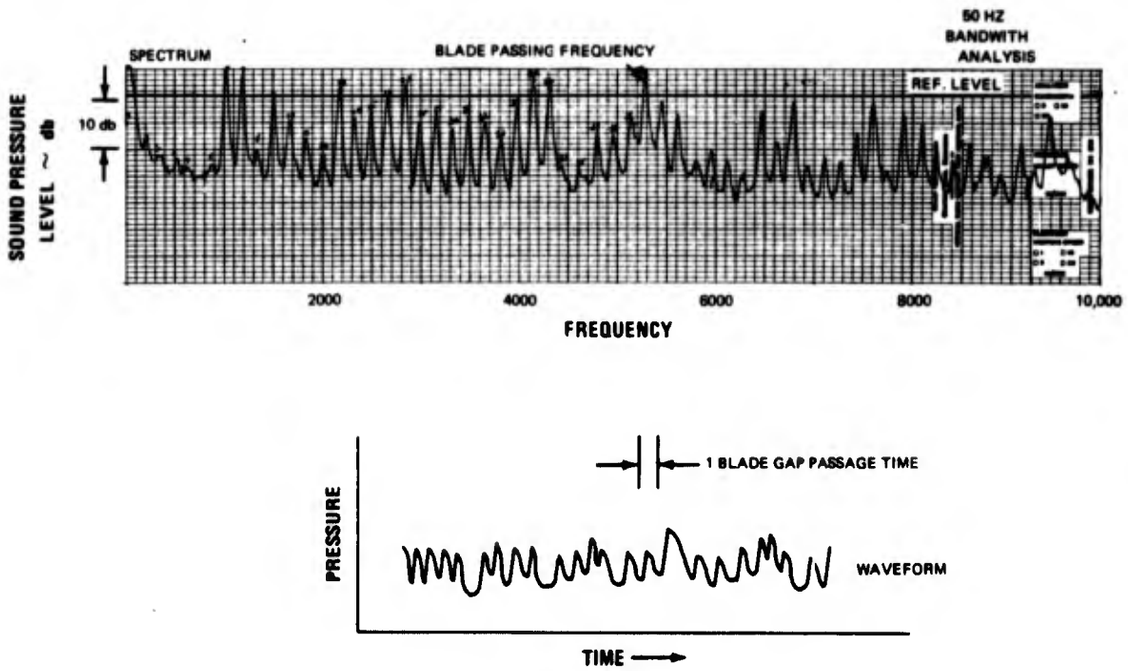

Figure 11 Waveform And Noise Spectrum Measured 8 Feet From The 28 Inch Rig Inlet When Operating At A Supersonic Tip Speed.

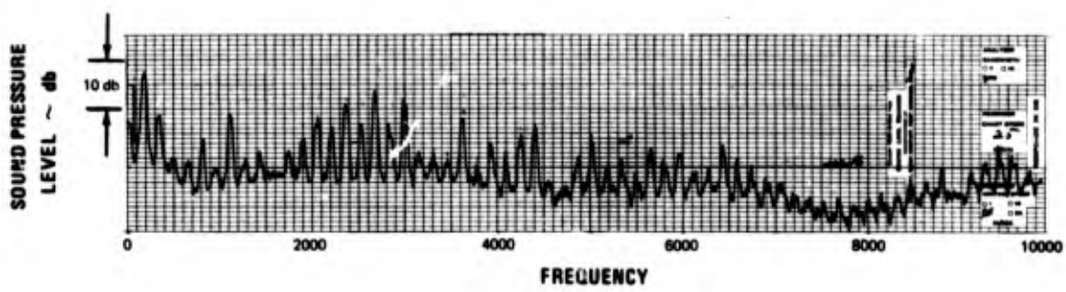

Figure 12 "Far Field" Spectrum Measured 8 Feet From The 28 Inch Rig Inlet When Operating At A Supersonic Tip Speed.

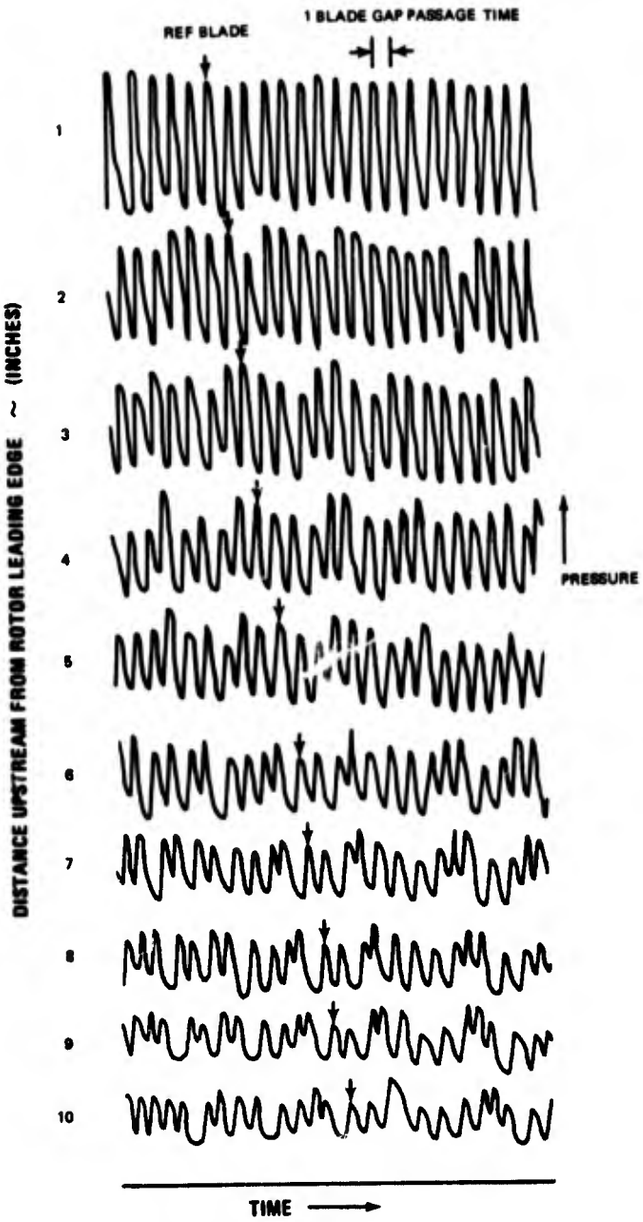

Figure 13 Sequence Of Wave Forms Measured With The Probe Microphone During An Axial Traverse In The Inlet Duct Forward Of The Rotor Operating At A Supersonic Tip Speed.

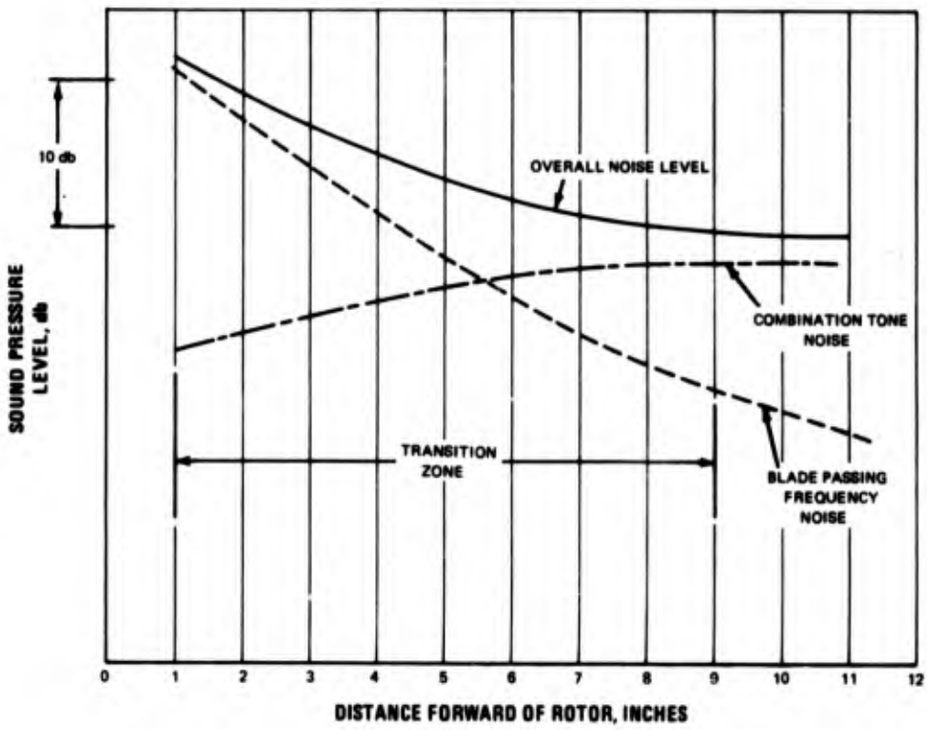

Figure 14 Relative Strengths Of Inlet Noise Spectral Components At A Supersonic Tip Speed Measured During An Axial Traverse Of The Microphone Probe. Note The Reduction In Blade Passing Frequency Noise And The Increase In Combination Tone Noise Forward Of The Rotor.

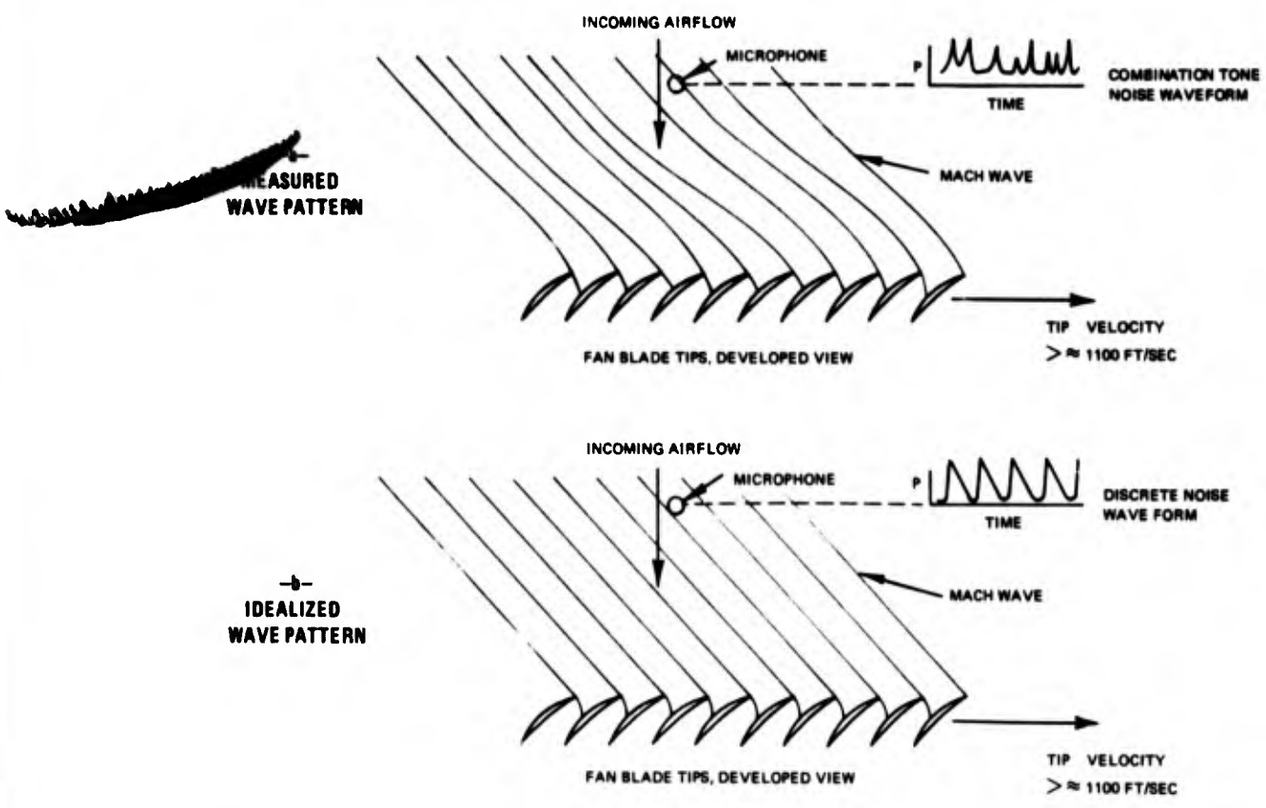

Figure 15 The Inlet Duct Pattern Shown In -a- Was Reconstructed From Axial Microphone Traverses Data Of The Type Shown In Figure 13. An Idealized Pattern Predicted For A Perfectly Uniform Rotor Is Shown In -b- For Reference.

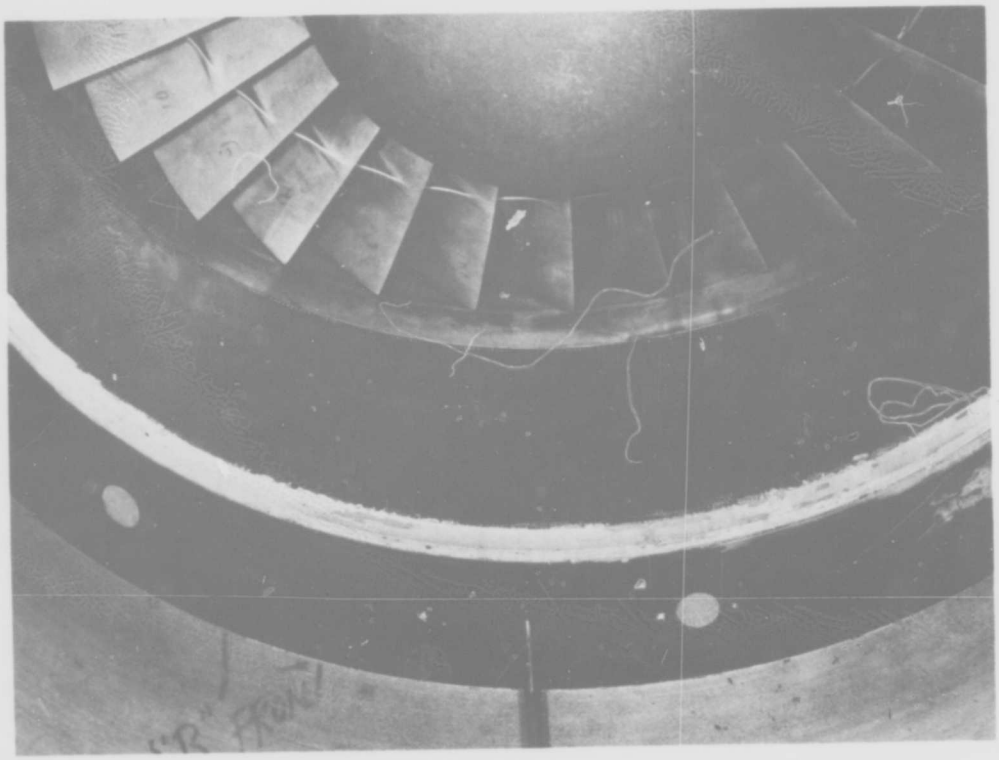

Figure 16 One Of Several Inlet Treatments Tested On The 28 Inch Rig.

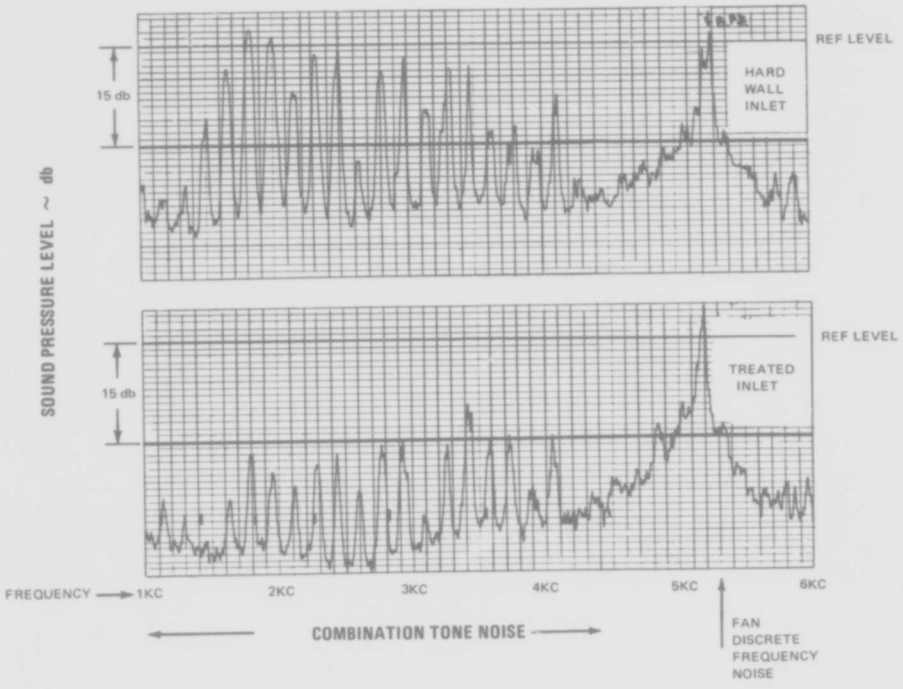

Figure 17 Noise Levels Measured From The 28 Inch Diameter Rig With And Without The Inlet Treatment Installed Indicated A Substantial Reduction From The Treatment.

METHODE D'ESTIMATION DU BRUIT D'UN TURBOREACTEUR A PARTIR DE SES GRANDEURS THERMOPROPULSIVES

par

R. Hoch et J.P. Duponchel

S.N.E.C.M.A.

Paris - France

SOMMAIRE

Par suite des contraintes qui résultent des limitations de bruit sur les aéroports et des projets de certification acoustique des avions, les méthodes d'estimation du bruit des turboréacteurs sont d'une grande importance, tant pour les constructeurs de moteurs et d'avions que pour les exploitants (compagnies aériennes, aéroports...).

La méthode proposée s'appuie en grande partie sur des méthodes de calcul détaillées, établies par la SNECMA. Elle permet, à la différence des méthodes usuelles, de faire une estimation très rapide du bruit, par simple lecture d'abaques.

Les paramètres thermodynamiques, généralement nécessaires à ces calculs, ont été remplacés par des grandeurs thermopropulsives caractérisant globalement le moteur (poussée nette, consommation spécifique, débit, rapport de dilution...) et qui sont directement accessibles dans une notice descriptive d'un turboréacteur.

L'estimation du bruit maximal (évalué en PNdB) produit par un avion, soit au point fixe, soit en vol ($M_o \leq 0,5$), peut être faite tant pour le compresseur que pour l'éjection, que le moteur soit simple flux ou double-flux.

On constate une bonne concordance entre les valeurs mesurées sur avions et les valeurs calculées à l'aide de cette méthode.

NOTATIONS

A_c	(m^2)	Aire efficace du col d'une tuyère convergente
b_i	(m)	Corde axiale au pied des aubes de la première roue mobile
C_s	(kg/daN.h)	Consommation spécifique
D_c	(m)	Diamètre du col d'une tuyère convergente
D_e	(m)	Diamètre extérieur de la première roue mobile
$F = \frac{Z_R N}{60}$	(Hz)	Fréquence de passage des aubes de la première roue mobile
F_n	(daN)	Poussée nette du turboréacteur
$h = r_e - r_i$	(m)	Hauteur radiale des aubes de la première roue mobile
l		Nombre d'étages de la soufflante d'un turboréacteur double-flux
L	(m)	Distance de l'observateur à la trajectoire d'un avion ou à l'axe d'un turboréacteur
m		Nombre de turboréacteurs équipant un avion
M_o		Nombre de Mach de vol de l'avion
N	(tr/mn)	Vitesse de rotation d'une soufflante ou d'un compresseur
N_L	(dB)	Niveau de pression sonore linéaire maximal à la distance L
N_{L_o}	(dB)	Niveau de pression sonore linéaire maximal de référence (L = 100 m, sans atténuation atmosphérique)
NP_L	(PNdB)	Niveau linéaire maximal de bruit perçu à la distance L
$\mathcal{J}_L$	(dB)	Terme de généralisation pour le bruit d'éjection (niveau de pression sonore linéaire maximal à la distance L pour une poussée de 1 daN)
q	(kg/s)	Débit-masse d'un turboréacteur
r_e	(m)	Rayon extérieur de la première roue mobile
r_i	(m)	Rayon intérieur de la première roue mobile
$U_e = \frac{\pi D_e N}{60}$	(m/s)	Vitesse d'entraînement de la première roue mobile
Z_R		Nombre d'aubes de la première roue mobile
λ		Rapport de dilution d'un turboréacteur double-flux
$\nu = r_i/r_e$		Rapport de moyeu
$\Delta\mathcal{F}$	(dB, PNdB)	Indice de convection
$\Delta N_{1 \text{ à } 5}$	(dB, PNdB)	Termes correctifs
Indices		
M_o		Conditions de vol à Mach M_o
p		Grandeurs primaires d'un turboréacteur double-flux
t		Grandeurs globales d'un turboréacteur double-flux

BLANK PAGE

LES METHODES D'ESTIMATION DU BRUIT D'UN TURBOREACTEUR font généralement appel à des calculs fort longs et nombreux par suite, d'une part de la complexité des interdépendances entre l'émission acoustique et les paramètres géométriques et aérothermodynamiques d'un moteur, d'autre part du caractère laborieux de l'évolution des niveaux en PNdB à partir des distributions spectrales de la pression acoustique. De ce fait, on a souvent tendance à considérer que l'estimation du bruit d'un turboréacteur est essentiellement du domaine du "spécialiste en acoustique".

De plus, la majorité de ces méthodes nécessitent la connaissance de nombreux paramètres caractéristiques du cycle ou du dimensionnement du moteur qui, très souvent, ne peuvent être fournis que par le motoriste.

La méthode,que nous proposons ci-après, permet d'estimer le bruit maximal produit par un turboréacteur,grâce à des abaques très simples qui font appel aux grandeurs thermopropulsives globales généralement publiées dans les fiches descriptives ou dans le dossier d'installation et de caractéristiques de ce turboréacteur.

CONDITIONS D'APPLICATION DE LA METHODE

Les abaques que nous présenterons permettent ainsi l'estimation du bruit d'éjection d'un turboréacteur (particulièrement élevé pour des moteurs simple flux) et celui des compresseurs et soufflantes (prédominant pour des moteurs double-flux à rapport de dilution élevé). Pour ces deux sources de bruit principales d'un turboréacteur, on pourra déterminer les niveaux de pression sonore (en dB) et les niveaux de bruit perçu (en PNdB) maximaux qu'elles produisent au niveau d'un observateur placé à une distance L de la trajectoire d'un avion ou de l'axe d'un turboréacteur au point fixe. La figure 1 schématise le problème. Nous avons choisi, pour la présentation des résultats, trois distances L dont l'usage est courant dans ce genre de calculs (L = 100, 300 et 450 mètres).

Les estimations pourront être faites pour un avion au point fixe ou pour un avion en vol, pourvu que son Mach de vol soit inférieur à 0,5. Dans ce dernier cas, nous admettrons, en première approximation, que l'axe des turboréacteurs est parallèle à la trajectoire de l'avion. Dans un souci de simplification, les éléments de calcul ont été établis pour des conditions atmosphériques standard :

- Pression : 760 mm Hg
- Température : 15°C
- Humidité relative : 70 %

Les niveaux de bruit que l'on pourra déterminer sont valables dans des conditions de champ libre (propagation des ondes acoustiques en atmosphère homogène au repos - pas de réflexions ni d'absorptions par le sol).

Signalons que pour la détermination des atténuations atmosphériques et pour l'évaluation des niveaux de bruit perçu (PNdB), nous avons retenu des méthodes d'usage courant (1), (2).

En outre, nous avons supposé que les turboréacteurs ne comportent pas de dispositifs réducteurs de bruit tels que des silencieux de jets, des traitements acoustiques dans les manches d'entrée ou dans les conduits d'éjection du flux secondaire...

BRUIT D'EJECTION

Dans cette première partie, nous présentons un certain nombre d'éléments qui permettent d'estimer le niveau de bruit maximal produit par l'éjection de turboréacteurs simple flux ou double-flux, que perçoit un observateur placé à une distance L de l'axe du moteur. Les abaques proposés ont été établis à partir de méthodes de prévision du bruit des jets développées par la SNECMA (3), (4). Ces méthodes, basées sur des résultats d'essais obtenus sur maquettes et sur turboréacteurs, se prêtent au calcul du champ sonore complet d'un jet (niveaux et spectres de pression acoustique) dans un domaine étendu de conditions d'éjection.

Nous examinerons ici la seule détermination du niveau de pression sonore linéaire maximal (en dB) et du niveau de bruit perçu correspondant (en PNdB) pour les deux types d'éjection suivants :

- Ejection de turboréacteurs simple flux ou double-flux à flux mélangés
- Ejection de turboréacteurs double-flux à flux séparés

Rappelons que l'angle d'émission sonore maximale d'un jet, repéré par rapport à l'axe du jet, est compris entre $\sim 25°$ et $\sim 55°$ suivant la valeur de la vitesse d'éjection.

La précision que l'on pourra espérer de ces estimations reste celle des versions intégrales des méthodes citées, à savoir approximativement $\pm$ 2 PNdB.

TURBOREACTEURS SIMPLE FLUX OU DOUBLE-FLUX MELANGES - Soit un tel réacteur, propulsant un avion à un Mach de vol M_o. Pour déterminer le niveau de bruit maximal, produit à une distance latérale L de l'axe du moteur, nous avons établi un certain nombre d'abaques qui nécessitent que l'on connaisse les quatre grandeurs suivantes :

- la poussée nette F_n (daN) du réacteur au Mach de vol M_o
- la consommation spécifique C_s (kg/daN.h)
- le débit-masse q (kg/s)
- le diamètre du col de la tuyère convergente D_c (m)

Nous avons retenu ces grandeurs, qui figurent généralement dans les dossiers de caractéristiques des moteurs, de préférence à des paramètres tels que la masse volumique du jet détendu qui interviennent dans la méthode originale (3).

Si le débit-masse en vol n'est pas connu, on peut le déterminer avec une approximation suffisante à l'aide de la figure 2, pourvu que l'on connaisse le débit au point fixe pour la même vitesse de rotation du compresseur. De même, la section A_c (donc le diamètre D_c) du col de la tuyère peut se déduire des figures 3a à 3e, lorsque la poussée nette F_n, le débit q et la consommation spécifique C_s du réacteur sont connus.

La détermination du niveau de pression sonore linéaire maximal à l'une des distances latérales L retenues (L = 100, 300 et 450 m) s'effectue comme suit :

On détermine d'abord (figure 4) un niveau de pression sonore de référence N_{L_o} à la distance L = 100 m

$$N_{L_o} \text{ (dB)} = \mathcal{N}_L + 10 \log_{10} F_n \qquad (1)$$

$\mathcal{N}_L$ étant un terme de généralisation, égal au niveau de pression sonore de référence, lorsque la poussée du réacteur est égale à 1 daN. L'abaque met parfaitement en évidence les influences séparées de la poussée spécifique F_n/q, de la consommation spécifique et de la poussée nette sur le niveau de pression sonore maximal produit par un jet. Toutefois, le niveau N_{L_o} ainsi déterminé ne tient pas compte de l'atténuation atmosphérique dont l'effet sur le niveau global dépend essentiellement de la forme et de la position du spectre sur l'échelle des fréquences. Les abaques de la figure 5 représentent, en fonction du diamètre D_c de la tuyère et de la poussée spécifique F_n/q, la correction ΔN_1 qu'il faut retrancher du niveau de référence N_{L_o} pour obtenir le niveau de pression sonore maximal N_L à l'une des trois distances L choisies

$$N_L \text{ (dB)} = N_{L_o} - \Delta N_1 \qquad (2)$$

Pour la distance L = 100 m, ΔN_1 représente le seul effet de l'atténuation atmosphérique, tandis qu'aux deux autres distances, il inclut l'effet de la divergence sphérique des ondes (loi en $1/L^2$). Le niveau de bruit perçu maximal en PNdB, à l'une des distances L, s'obtient en ajoutant au niveau de référence N_{L_o} un terme correctif ΔN_2

$$NP_L \text{ (PNdB)} = N_{L_o} + \Delta N_2 \qquad (3)$$

Ce terme correctif (figure 6) englobe l'atténuation atmosphérique, la divergence sphérique et les écarts entre les niveaux exprimés en PNdB et en dB car ces derniers dépendent des mêmes paramètres D_c et F_n/q que l'atténuation atmosphérique.

TURBOREACTEURS DOUBLE-FLUX A FLUX SEPARES - Supposons qu'à présent l'éjection se fasse par deux jets coaxiaux distincts. Une étude théorique (4) a montré que le bruit produit par une telle configuration d'éjection pouvait être considéré comme la somme du bruit que produirait le flux primaire seul, au cours de son mélange avec le milieu ambiant, et d'un terme additif ΔN_3 qui représente la contribution du flux secondaire au bruit total. Ce terme additif est une fonction du rapport des sections d'éjection secondaire et primaire, du rapport des vitesses d'éjection des deux flux et, dans une certaine mesure, de la distance entre les deux sections d'éjection. De nombreuses études expérimentales sur maquettes ont confirmé l'approche théorique citée qui montre en outre que la vitesse de vol, pourvu qu'elle soit faible, a une influence secondaire sur la quantité ΔN_3. Afin de ne point compliquer la méthode que nous présentons, nous avons supposé que, pour $M_o \leq 0{,}5$, le terme ΔN_3 était indépendant de la vitesse de vol. Dans un même souci de simplification, nous négligeons l'influence de la distance qui sépare les deux sections d'éjection.

Si nous considérons donc un turboréacteur double-flux à flux séparés, propulsant un avion à un Mach de vol M_o, nous calculerons d'abord le niveau de pression sonore de référence du flux primaire (figure 4) :

$$(N_{L_o})_p = \mathcal{N}_L + 10 \log (F_n)_p \qquad (4)$$

$\mathcal{N}_L$ étant déterminé par les grandeurs primaires $(F_n)_p/q_p$ et $(C_s)_p$ qui peuvent être calculées à partir des relations du tableau I, de même que la poussée primaire $(F_n)_p$.

TABLEAU I - Calcul des grandeurs primaires d'un turboréacteur double-flux

	1 = 1	1 = 2
$(C_s)_p$ (kg/daN.h)	$= \dfrac{C_{s_t} \dfrac{F_t}{q_t} - 3{,}3218 \dfrac{\lambda}{1+\lambda}}{\dfrac{F_t}{q_t} - \dfrac{\lambda}{1+\lambda}(25{,}724 - 34\,M_o)}$	$= \dfrac{C_{s_t} \dfrac{F_t}{q_t} - 6{,}533 \dfrac{\lambda}{1+\lambda}}{\dfrac{F_t}{q_t} - \dfrac{\lambda}{1+\lambda}(36{,}328 - 34\,M_o)}$
$\dfrac{F_p}{q_p}$ (daN/kg/s)	$= (1+\lambda)\dfrac{F_t}{q_t} - \lambda\,(25{,}724 - 34\,M_o)$	$= (1+\lambda)\dfrac{F_t}{q_t} - \lambda\,(36{,}328 - 34\,M_o)$
F_p (daN)	$= F_t - q_t \dfrac{\lambda}{1+\lambda}(25{,}724 - 34\,M_o)$	$= F_t - \dfrac{\lambda}{1+\lambda}(36{,}328 - 34\,M_o)\,q_t$

M_o	Mach de vol
1	Nombre d'étages de la soufflante
C_{s_t}	Consommation spécifique globale
F_t	Poussée nette globale
q_t	Débit-masse global
λ	Rapport de dilution
C_{s_p} F_p q_p	Grandeurs primaires

Afin de réduire le nombre de variables qui interviennent dans les calculs, diverses hypothèses ont été faites dans l'établissement de ces relations. Ainsi, nous avons supposé que le rapport de compression moyen des soufflantes est de 1,45 pour des soufflantes à un étage et de 2 pour des soufflantes à deux étages. De plus, nous avons pris un rendement polytropique de 0,87 et nous avons tenu compte de pertes de charge forfaitaires dans la manche d'entrée et dans le conduit d'éjection du flux secondaire.

Le niveau de pression sonore maximal produit à l'une des distances L par l'ensemble des deux flux peut alors s'écrire :

$$N_L \text{ (dB)} = N_{L_o} + \Delta N_3 - \Delta N_1 \qquad (5)$$

et le niveau de bruit perçu correspondant en PNdB :

$$NP_L \text{ (PNdB)} = N_{L_o} + \Delta N_3 + \Delta N_2 \qquad (6)$$

ΔN_3 est lu sur les figures 7a et 7b (suivant le nombre d'étages 1 de la soufflante) en fonction des grandeurs globales qui caractérisent le moteur au point fixe pour le même point de fonctionnement, à savoir, sa consommation spécifique, sa poussée spécifique et le rapport de dilution λ. Les grandeurs ΔN_1 et ΔN_2 sont lues sur les abaques des figures 5 et 6 en considérant la poussée spécifique globale du turboréacteur au Mach de vol M_o et un diamètre fictif D_c. Ce diamètre s'obtient à partir d'une aire A_c, déduite des figures 3a à 3e, à l'aide des caractéristiques globales du turboréacteur: $(F_n)_t$, $(F_n/q)_t$ et $(C_s)_t$ au Mach de vol M_o. Cette section fictive correspond à la section d'un réacteur double-flux à flux mélangés équivalent, ayant mêmes débit, poussée nette et enthalpie totale que le réacteur considéré.

BRUIT DES COMPRESSEURS ET DES SOUFFLANTES

Par suite de la grande complexité des mécanismes qui sont à l'origine du bruit des compresseurs et du nombre important de paramètres qui le déterminent, il est presque illusoire d'espérer aboutir à une méthode qui présente le même caractère de simplicité et le même degré de précision que celle que nous avons établie pour les jets. Parmi les méthodes de prévision qui existent à l'heure actuelle, de complexité d'ailleurs très variable, aucune ne prétend fournir des estimations dont la précision soit supérieure à ± 6 PNdB.

Dans le cadre de ce travail, nous avons par conséquent choisi la méthode qui, tout en faisant intervenir les paramètres principaux déterminant le bruit d'un compresseur ou d'une soufflante, se prêtait le mieux à la suppression des calculs intermédiaires, tout en conservant sa précision initiale. Sa validité a pu être vérifiée au cours d'essais que nous avons réalisés sur des compresseurs expérimentaux.

Pour effectuer l'estimation du bruit maximal, perçu à une distance latérale L de l'axe du moteur, la méthode retenue (5) nécessite la connaissance des trois grandeurs fondamentales suivantes :

- la vitesse de rotation de la première roue mobile de la soufflante ou du compresseur N (tr/mn)
- le diamètre extérieur de la première roue mobile D_e (m)
- le nombre d'aubes de la première roue mobile Z_R

Les compléments apportés à cette méthode nécessitent que l'on connaisse en outre :

- le débit-masse aspiré q (kg/s)
- le rapport de moyeu $\nu = r_i/r_e$

La vitesse de rotation et le débit sont généralement connus, le diamètre de la première roue mobile et son rapport de moyeu ν peuvent être déterminés à l'aide d'une coupe du moteur et le nombre d'aubes Z_R peut être obtenu (s'il n'est pas connu) avec une approximation suffisante à l'aide de la figure 8.

Grâce à la forme standard simplifiée du spectre de la pression sonore maximale, proposée dans la méthode choisie (5), nous avons pu établir les abaques des figures 9 et 10 qui offrent la même rigueur numérique que celle qui aurait été obtenue en utilisant la méthode originale. Ces abaques sont valables pour des compresseurs classiques de turboréacteurs simple flux ainsi que pour des soufflantes de turboréacteurs double-flux. Ils représentent respectivement, pour les trois distances latérales retenues (L = 100, 300 et 450 m), le niveau de pression sonore linéaire maximal (en dB), et le niveau de bruit perçu correspondant (en PNdB), en fonction de la vitesse de rotation N et du diamètre extérieur D_e de la première roue mobile du compresseur ou de la soufflante. Les courbes sont paramétrées en fonction de la fréquence centrale de la bande d'octave qui contient la raie spectrale correspondant à la fréquence fondamentale de passage des aubes de cette première roue :

$$F = \frac{Z_R \cdot N}{60} \quad (Hz) \qquad (7)$$

Le tableau II ci-dessous rappelle les fréquences de coupure des bandes d'octaves normalisées qui sont susceptibles, dans la majorité des cas pratiques, de contenir F.

TABLEAU II - Fréquences de coupure des bandes d'octaves normalisées

Octaves (Hz)	1 000	2 000	4 000	8 000
Fréquences de coupure (Hz)	700/1 400	1 400/2 800	2 800/5 600	5 600/11 200

POUR UN TURBOREACTEUR SIMPLE FLUX, il n'y a lieu de considérer que l'émission amont du bruit du compresseur, dont le niveau maximal est directement fourni par les abaques des figures 9 et 10. Ce niveau maximal est perçu dans une direction voisine de 70° par rapport à l'axe de la manche d'entrée.

POUR UN TURBOREACTEUR DOUBLE-FLUX, on sait que le bruit de la soufflante, qui domine généralement ceux des étages de compression suivants, se propage à la fois vers l'amont et vers l'aval du moteur (respectivement par la manche d'entrée et le conduit d'éjection du flux secondaire). Le maximum d'intensité de ces deux rayonnements est perçu dans des directions qui forment sensiblement des angles de 70° et 110° avec l'axe de la manche d'entrée.

Mais, par suite d'un phénomène de transport de l'énergie acoustique (convection) par l'écoulement d'air qui traverse la soufflante, l'émission aval est généralement beaucoup plus intense que l'émission amont. Il nous a donc paru intéressant d'établir un certain nombre d'abaques qui permettent, en

tenant compte de l'effet de cette convection, de déterminer le bruit maximal émis vers l'amont, connaissant celui qui est émis vers l'aval grâce aux figures 9 et 10.

Le calcul de l'indice de convection (6), (7) a été effectué en supposant que l'énergie acoustique émise est proportionnelle au débit et à la cinquième puissance de la vitesse relative à l'entrée de la roue mobile et qu'elle est soumise à la convection produite par cet écoulement relatif. On obtient alors, par intégration entre le pied et le sommet des aubes, les puissances qui se propagent respectivement vers l'amont et vers l'aval de la soufflante et qui permettent de déterminer, en fonction des vitesses relatives au pied et au sommet des aubes, les valeurs de l'indice de convection global. Les figures 11a à 11c représentent ces indices $\Delta\mathcal{F}$ (différence entre les niveaux maximaux émis vers l'aval et vers l'amont) pour des soufflantes modernes sans directrice d'entrée, en fonction de la vitesse d'entraînement $U_e = \Pi D_e N/60$, pour différentes valeurs de débit spécifique $q/\Pi r_e^2$ et pour des rapports de moyeu de 0,3, 0,4 et 0,5. Ayant déterminé le niveau maximal produit par l'émission aval de la soufflante à l'aide des figures 9 et 10, on obtient, en lui retranchant la valeur appropriée de l'indice de convection, une estimation du niveau maximal produit vers l'amont.

POINTS PARTICULIERS

L'INFLUENCE DU NOMBRE DE TURBOREACTEURS sur le bruit émis par un avion dépend essentiellement de la position de l'observateur par rapport à l'avion. Considérons un avion équipé de m turboréacteurs identiques qui fonctionnent au même régime. On admettra, en schématisant le problème (5), que :

- pour un observateur placé sous la trajectoire de l'avion, il convient d'ajouter aux niveaux calculés pour les différentes sources de l'un des moteurs, la quantité :

$$\Delta N_4 = 10 \log_{10} m \qquad (8)$$

- pour un observateur placé latéralement par rapport à la trajectoire, il convient, en tenant compte d'un certain effet de masque, d'ajouter la quantité :

$$\Delta N_4 = 5 \log_{10} m \qquad (9)$$

L'ABSORPTION PAR EFFET DU SOL peut modifier notablement les niveaux acoustiques lors des opérations au sol d'un avion (point fixe et roulage). Il est difficile, dans le cadre d'une méthode simplifiée, d'introduire de tels effets car l'atténuation globale que subissent les ondes sonores qui se propagent au voisinage du sol est essentiellement fonction de la nature du sol, du spectre acoustique considéré et des positions relatives de la source et de l'observateur. Nous nous contenterons de donner, à titre indicatif, des ordres de grandeur de cette atténuation pour les trois distances de référence choisies :

L = 100 m	ΔN_5 = 2 à 4 dB
L = 300 m	ΔN_5 = 3 à 7 dB
L = 450 m	ΔN_5 = 4 à 9 dB

LA REFLEXION DES ONDES SONORES par le sol conduit généralement, par un phénomène d'interférences acoustiques, à une perturbation profonde des spectres, variable avec l'impédence du sol et les positions respectives de la source et de l'observateur (8). De même que pour l'absorption, il est difficile d'introduire de tels calculs dans cette méthode. Signalons toutefois que l'augmentation du niveau global qui résulte de ce phénomène peut atteindre des valeurs de l'ordre de 1 à 3 dB, aussi bien pour un avion au sol que pour un avion en vol.

D'AUTRES EFFETS, tels que le mode d'installation des moteurs sur l'avion, les perturbations créées par le champ aérodynamique de l'avion sur la propagation initiale des ondes, peuvent altérer les valeurs des niveaux en champ libre qui permet de calculer cette méthode. Mais l'évaluation de ces effets reste encore difficilement accessible au calcul et fait davantage appel à des données empiriques.

LE NIVEAU DE BRUIT PERCU EFFECTIF d'un avion en vol constitue une approche pour juger l'effet subjectif total que produit le passage de cet avion. Il est évalué en PNdB effectifs (EPNdB) en ajoutant au niveau de bruit perçu maximal un terme correctif qui tient compte d'éventuelles irrégularités dans les spectres de pression acoustique (présence de raies par exemple) et une correction de durée (9). Son calcul fait donc intervenir l'évolution du bruit en fonction du temps, au point d'observation considéré, ainsi que la distribution spectrale de la pression acoustique en fonction de l'azimuth. De ce fait, un tel calcul sort du cadre de la méthode de prévision exposée. Néanmoins, pour les besoins pratiques, il nous a paru intéressant de proposer des valeurs approximatives de l'écart entre le niveau en EPNdB et le niveau de bruit perçu maximal. La figure 12 représente les résultats d'une tentative de corrélation de ces écarts en fonction de la seule distance L de l'observateur à la trajectoire, pour des Mach de vol qui correspondent sensiblement à l'approche et au décollage d'avions subsoniques. Malgré une grande dispersion (qui ne doit par surprendre) des résultats qui ont servi à l'établissement de cette courbe, les valeurs qu'elle fournit sont probablement représentatives, à ± 2 PNdB, de la tendance générale. Cette courbe permet donc, en première approximation, de chiffrer le niveau de bruit perçu effectif produit par le passage d'un avion sur une trajectoire de décollage

ou d'approche. Les écarts Δ entre les niveaux en EPNdB et les niveaux maximaux en PNdB que l'on pourra adopter pour les trois distances L choisies sont les suivants :

L = 100 m Δ ≃ - 4 PNdB
L = 300 m Δ ≃ 0 PNdB
L = 450 m Δ ≃ + 2 PNdB

COMPARAISONS MESURES - ESTIMATIONS

Dans cette dernière partie, nous examinons brièvement un certain nombre de comparaisons entre des mesures du bruit maximal d'un avion ou d'un turboréacteur au point fixe et les estimations faites avec la méthode proposée. Ces comparaisons, qui sont présentées par le tableau III, portent essentiellement sur le bruit d'éjection et sur le bruit de la soufflante,dont seule l'émission aval a été considérée. Quand il existait une incertitude sur l'importance relative des bruits d'éjection et de soufflante, l'estimation correspondant aux deux émissions a été effectuée. La valeur mesurée est comparée à la valeur maximale (repérée par un astérisque) de ces deux estimations.

Les mesures qui font l'objet de ces comparaisons sont tirées de rapports d'essais divers dont, par suite de leur nombre trop important, nous n'avons pu citer les références.

Signalons qu'il est à craindre que certains niveaux extraits de ces rapports aient été déterminés par association des niveaux maximaux atteints au cours du temps dans chacune des bandes d'analyse, conduisant ainsi à des valeurs en PNdB trop élevées. De plus, des perturbations multiples affectent généralement de telles mesures acoustiques (réflexions, atmosphère non homogène, effets d'installation des turboréacteurs, etc...).

Si l'on tient compte de l'ensemble de ces effets, il apparaît, au vu des écarts entre les mesures et les estimations, que la méthode exposée constitue une approche satisfaisante pour l'estimation du bruit des avions.

CONCLUSION

Par la méthode d'estimation du bruit des turboréacteurs que nous venons d'exposer, nous pensons mettre à la disposition du nombre toujours croissant de personnes, confrontées aux problèmes du bruit des avions, un moyen simple et rapide qui leur permettra de déterminer le bruit maximal produit au sol, lors du vol d'un avion.

Nombre de ces personnes n'étant pas nécessairement des spécialistes, soit en acoustique, soit en thermopropulsion, nous nous sommes efforcés, dans l'établissement de cette méthode, de substituer aux paramètres aéro-thermodynamiques caractéristiques du cycle du moteur et nécessaires au calcul du bruit, des grandeurs globales telles que le débit, la poussée, la consommation spécifique... qui sont familières à la plupart des techniciens. Dans un souci de simplification, nous avons également supprimé le maximum de calculs intermédiaires portant sur des grandeurs acoustiques, tout en conservant aux méthodes de base utilisées, leur précision originale. Les estimations que permet la méthode ont nécessairement un caractère d'approximation, notamment celles qui sont relatives au bruit des compresseurs et des soufflantes car elles font intervenir un nombre trop restreint de paramètres significatifs.

Nous pensons néanmoins qu'il sera possible de développer à l'avenir des méthodes qui, tout en répondant au même souci de simplification, tiendront compte du maximum de facteurs intervenant dans la génération du bruit des turboréacteurs et ravaleront les calculs du bruit d'un avion au niveau de calculs de routine.

TABLEAU III - Quelques comparaisons : mesures - estimations

Avion	Turboréacteur	Distance L (m)	Mesure (1) (PNdB)	Estimations (PNdB) (2)		Δ = (1)-(2)	Observations
				Jet	Soufflante (émission aval)		
Douglas DC.9	2 x JT8D-1	300	112,5	108,5	109 *	3,5	Décollage
Boeing 727	3 x JT8D-1	300	110	107,5	111 *	-1	Décollage
		120	112		113 *	-1	Approche
		120	114		117 *	-3	Survol à poussée réduite
Caravelle GE	2 x CJ 805-23	300	108,5	104,5	107 *	1,5	Décollage
		300	98		100,5 *	-2,5	Approche
		300	103,5		105 *	-1,5	Approche
Caravelle III	2 x RA 527	300	119	118 *		1	Décollage
Caravelle 6R	2 x Avon 29-6 533 R	300	122	120 *		2	Décollage
BAC 111	2 x RB.163-2	300	112	111 *		1	Décollage
Trident	3 x RB.163-1	300	113	113 *		0	Décollage
Boeing 707-120 B	4 x JT3D-1	300	118	114,5 *	114	3,5	Décollage
Douglas DC.8-50	4 x JT3D-1	300	115	114,5 *	114	0,5	Décollage
		120	114		117,5 *	-3,5	Approche
		200	110		108,5 *	1,5	Survol à poussée réduite
VC.10	4 x R Co 42	300	117	117 *	112	0	Décollage
Essai statique	Atar 09 C	100	136	134,5 *		1,5	Mesure au point fixe-Moteur maxi P.C
Mirage IV	2 x Atar 09 K	150	126	124 *		2	Point fixe - Plein gaz sec
			131	131 *		0	Survol M_o = 0,5 P.G. P.C.
Banc volant	Expérimental (simple flux)	325	121	122,5 *		-1,5	Survol M_o = 0,4 P.G. sec
		300	125	125 *		0	Survol M_o = 0,3 P.G. P.C.
		290	122	119 *		3	Survol M_o = 0,33
		285	113	110 *		3	Survol M_o = 0,3 Régime réduit
Essai statique	Expérimental (simple flux)	70	139	137 *		2	Mesure au point fixe

* Valeur estimée maximale

REFERENCES BIBLIOGRAPHIQUES

(1) Standard values of atmospheric absorption as a function of temperature and humidity for use in evaluating aircraft fly-over noise
S.A.E. ARP 866 - Août 1964

(2) K.D. KRYTER, K.S. PEARSONS
Modification of Noy tables
JASA Vol. 36 - Février 1964

(3) Méthode de prévision du bruit des jets des turboréacteurs
Document YLL.A N° 3 497 - SNECMA - Octobre 1967

(4) Estimation de la puissance sonore émise par deux jets coaxiaux
N.T. YLL.A N° 89 - SNECMA - Avril 1966

(5) Prediction of turbine-engine compressor or fan noise
S.A.E. proposed AIR 973

(6) M.J.T. SMITH, M.E. HOUSE
Internally Generated Noise from Gas Turbine Engines - Measurement and prediction
A.S.M.E. Paper N° 66 - GT/N.43 - Décembre 1965

(7) Calcul de l'indice de convection sonore dans un étage de compresseur ou de soufflante
F.T. YLL.A N° 164 - SNECMA - Septembre 1968

(8) R. HOCH, P. THOMAS
Influence des réflexions sur les spectres de pression acoustique des jets
1er Colloque d'Acoustique Aéronautique - Toulouse - Mars 1968

(9) Méthode de représentation du bruit des aéronefs au voisinage d'un aéroport
Révision de la recommandation ISO/R 507 - Septembre 1968

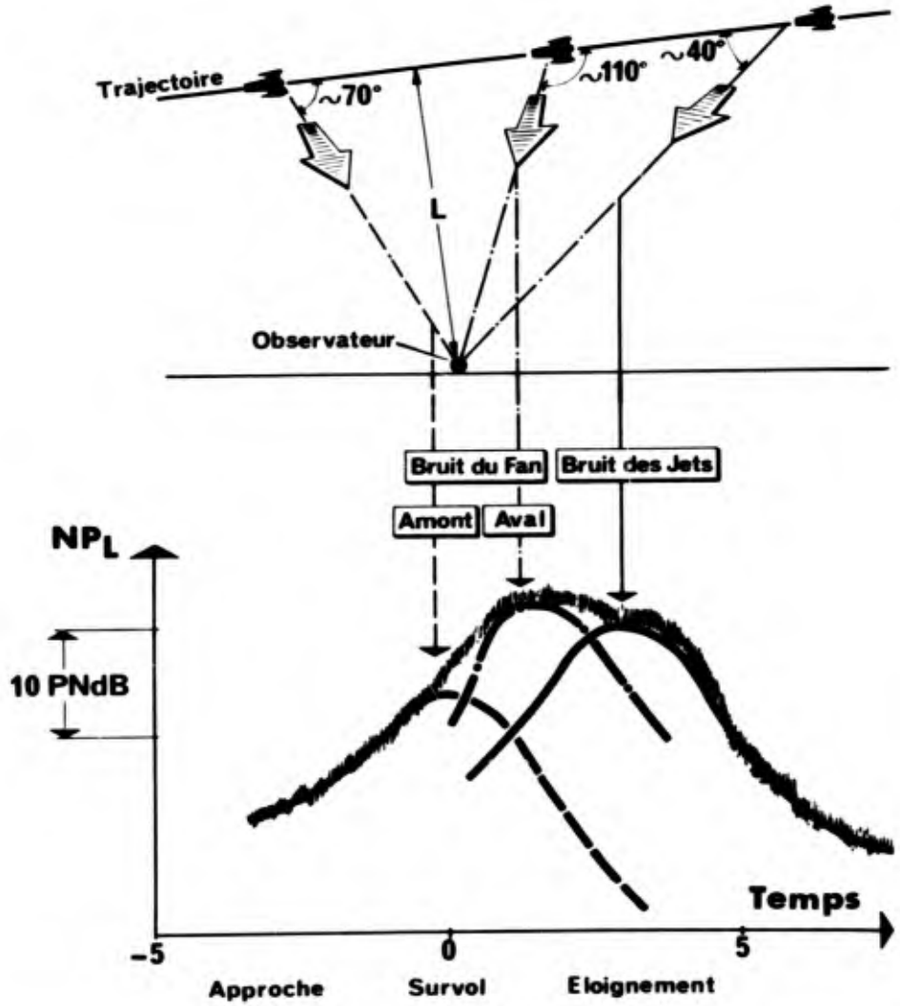

Fig.1 Illustration du problème

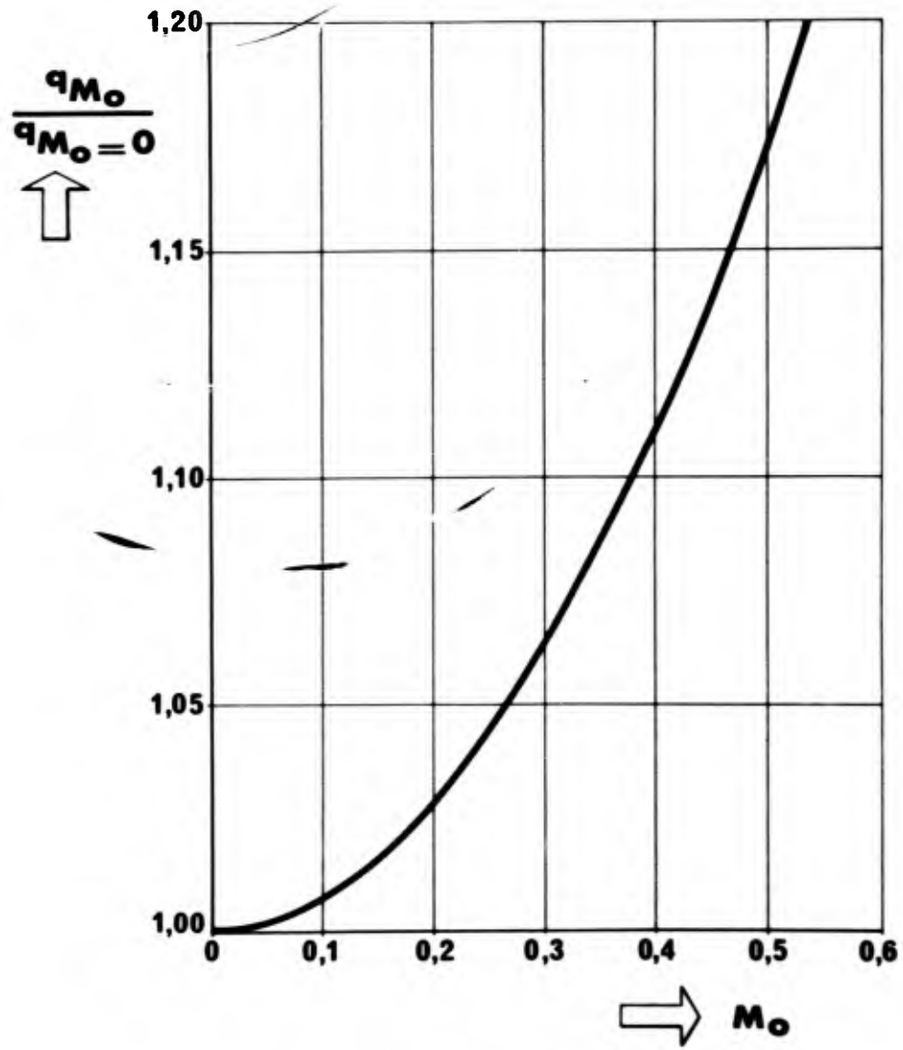

Fig.2 Débit-masse en vol

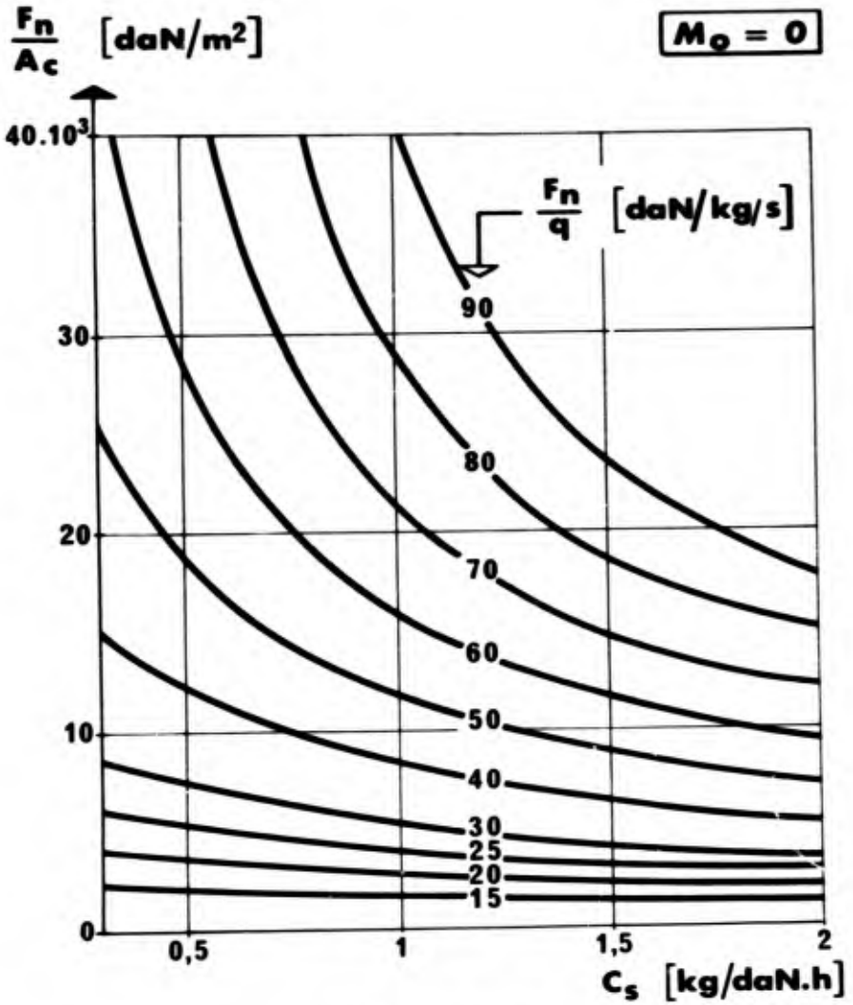

Fig.3(a) $M_o = 0$

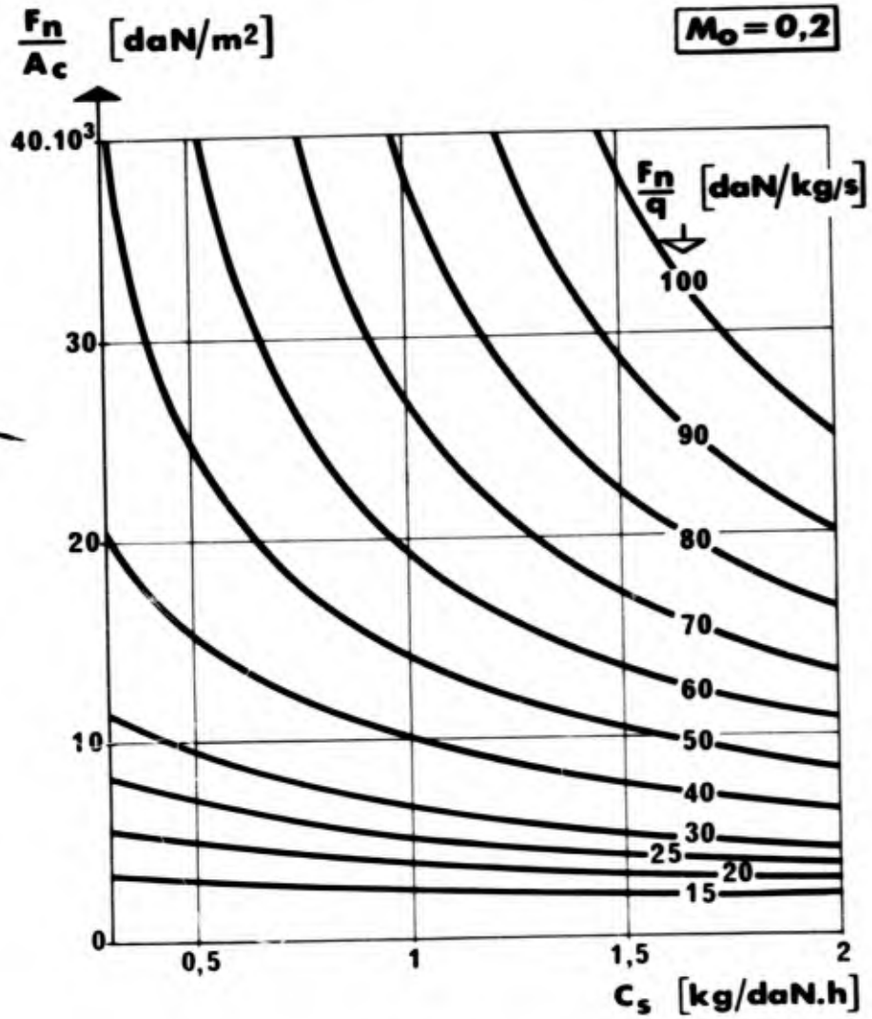

Fig.3(b) $M_o = 0.2$

Fig.3 Poussée par unité de section de tuyère en fonction du Mach de vol

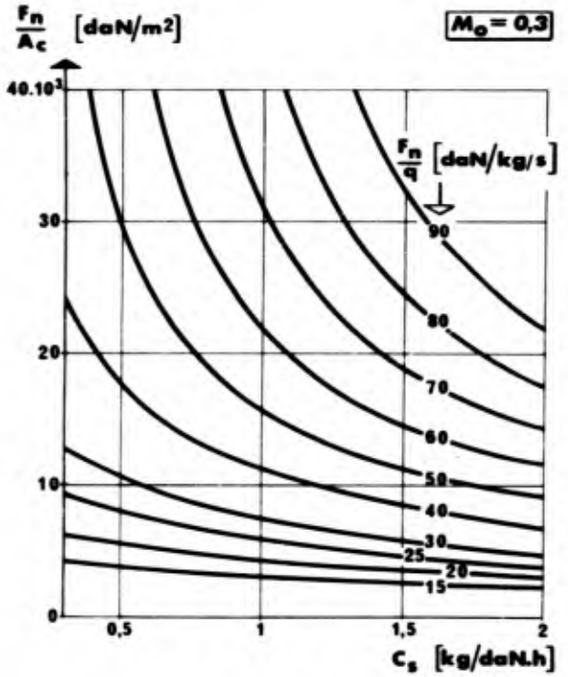

Fig.3(c) $M_o = 0,3$

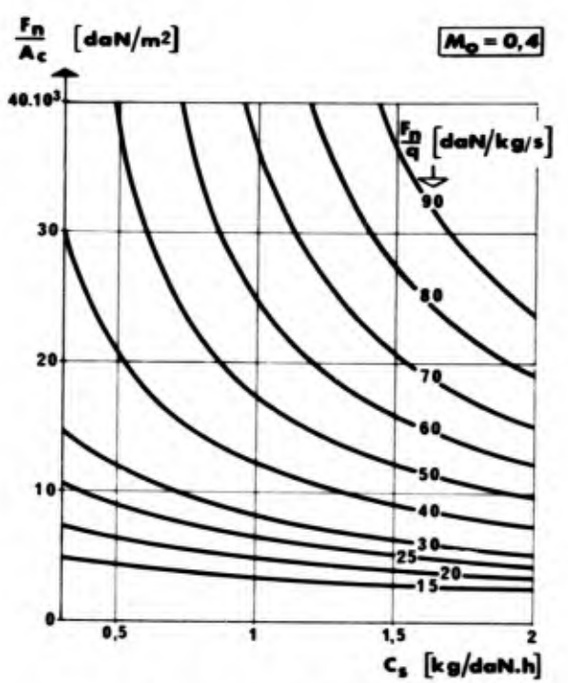

Fig.3(d) $M_o = 0,4$

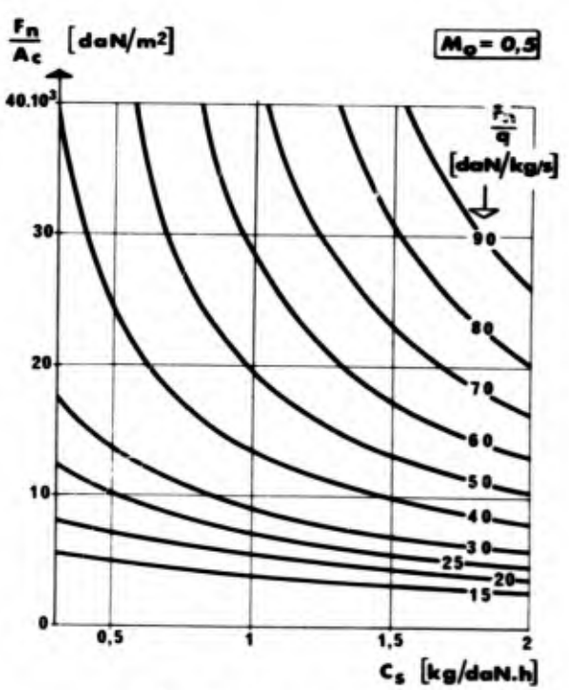

Fig.3(e) $M_o = 0,5$

Fig.3 Poussée par unité de section de tuyère en fonction du Mach de vol

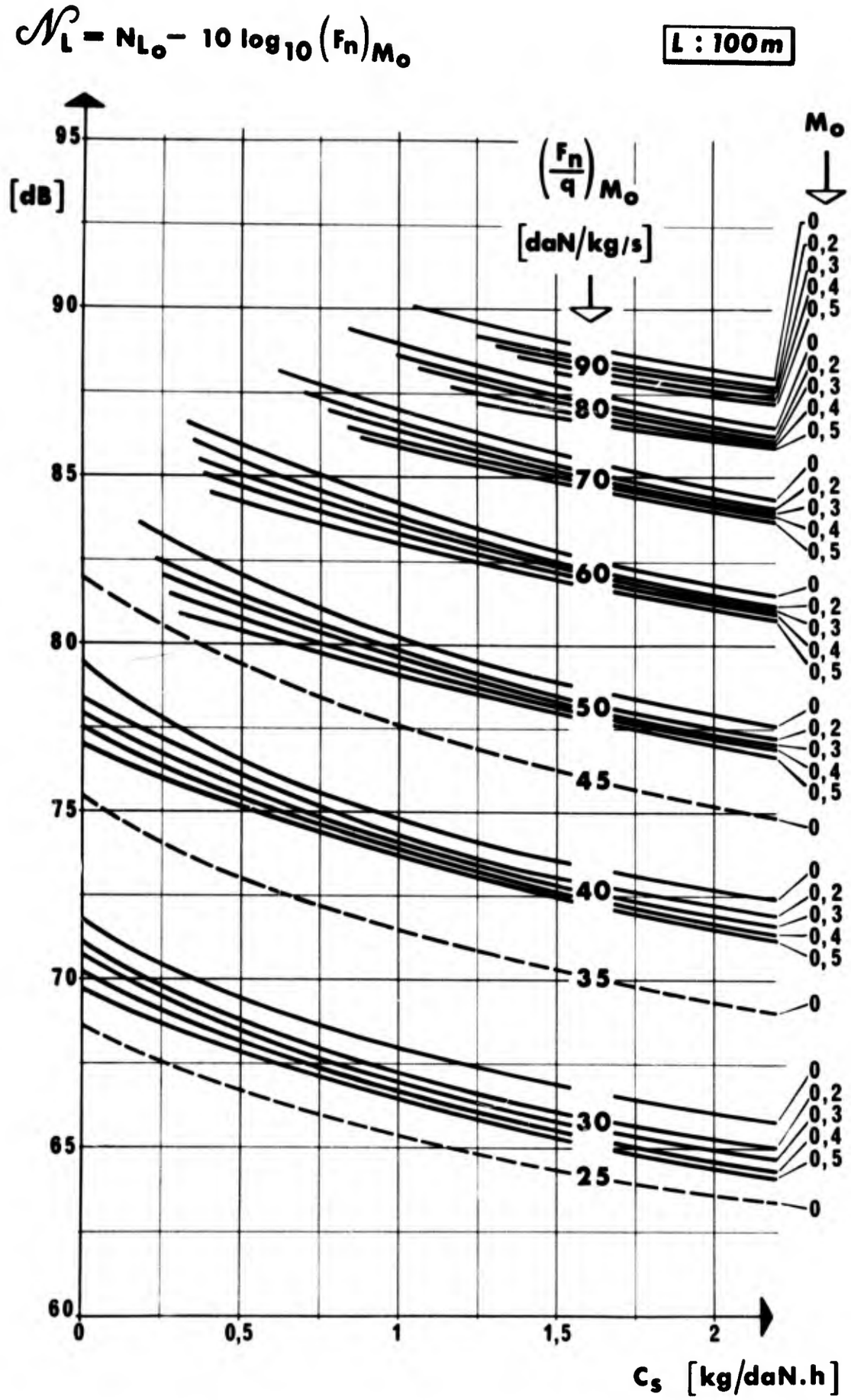

Fig.4 Bruit de jet: niveau de pression sonore linéaire maximal de référence
(L = 100 m - pas d'atténuation atmosphérique)

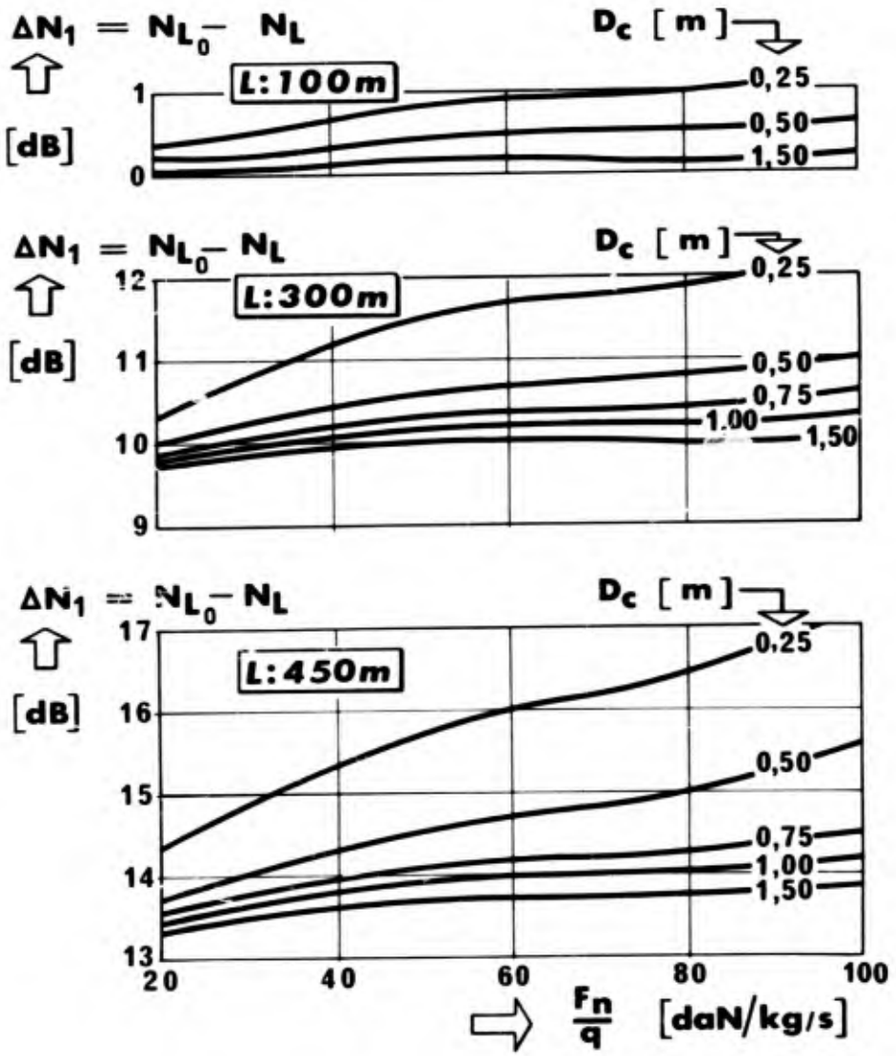

Fig.5 Correction d'atténuation atmosphérique et de divergence sphérique ($\Delta N_1 = N_{L_0} - N_L$)

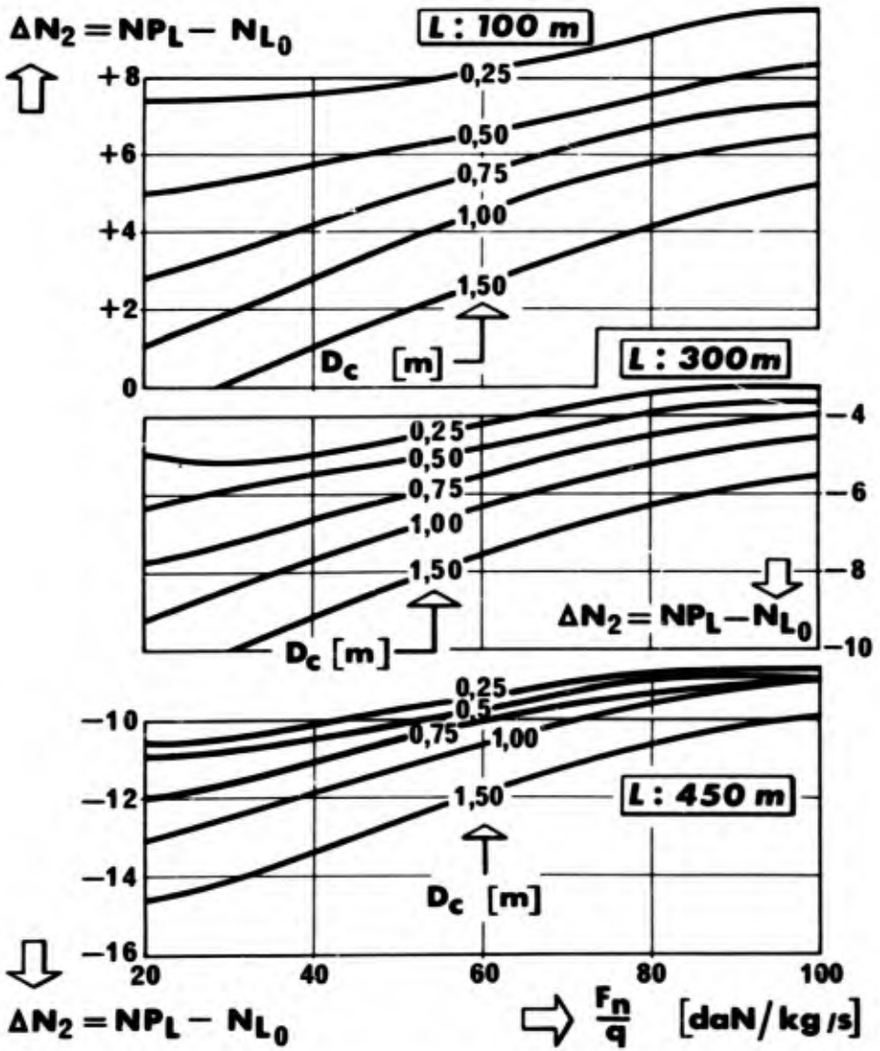

Fig.6 Différence entre le niveau en PNdB et le niveau de référence ($\Delta N_2 = NP_L - N_{L_0}$)

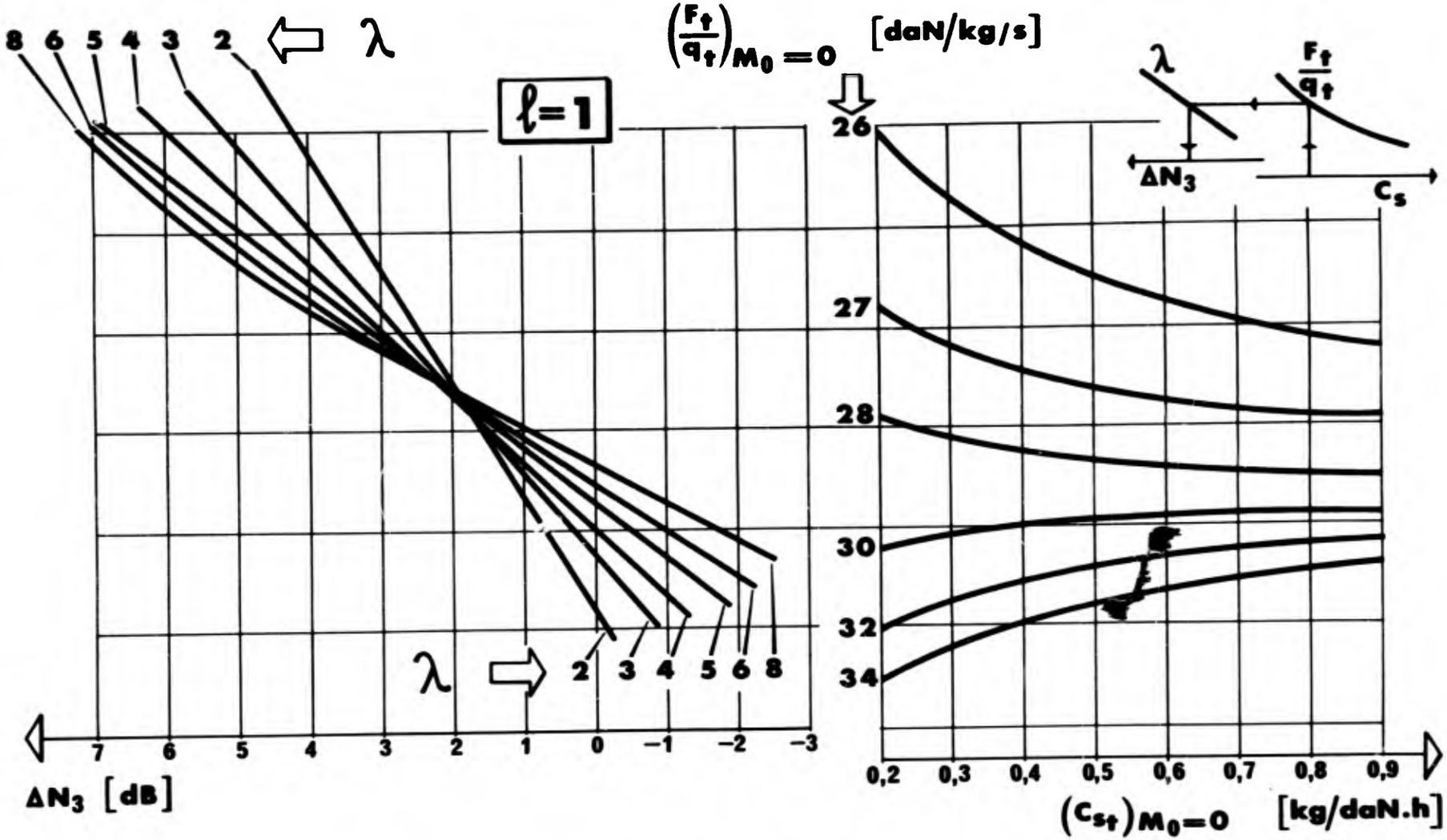

Fig.7(a) Contribution du flux secondaire au bruit global de deux jets coaxiaux - soufflante monoétage

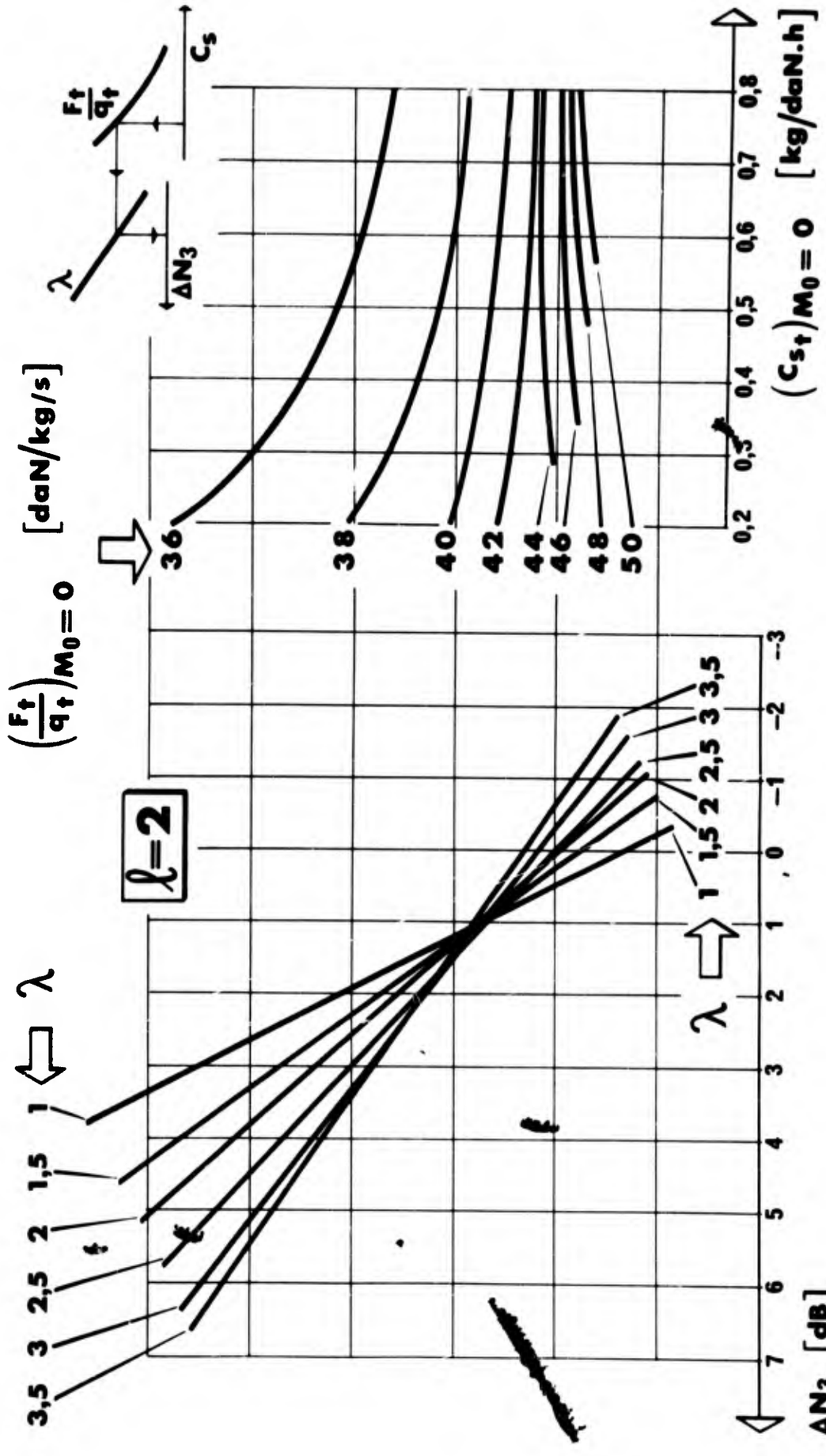

Fig.7(b) Contribution du flux secondaire au bruit global de deux jets coaxiaux - soufflante à deux étages

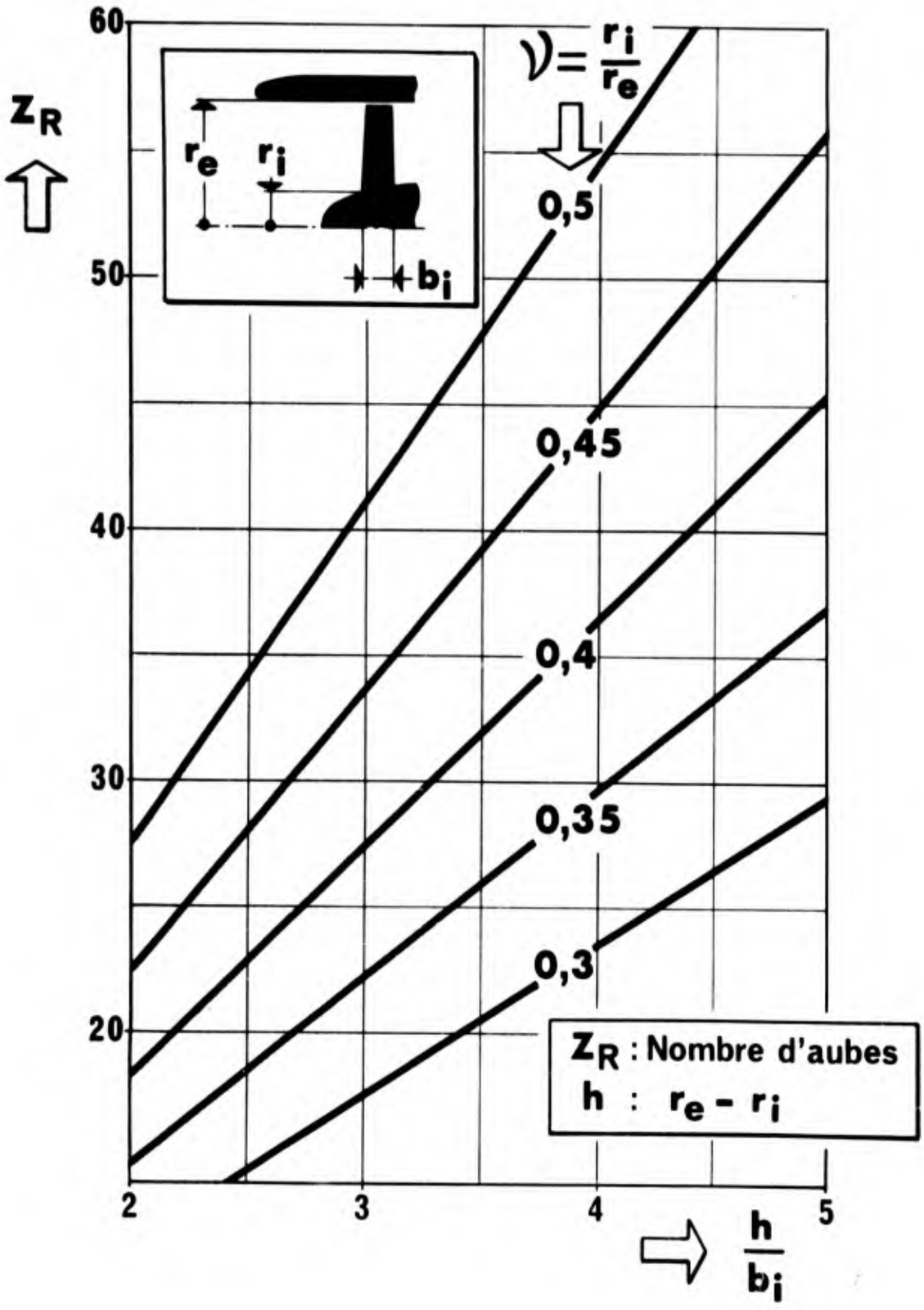

Fig.8 Détermination approchée du nombre d'aubes d'une roue mobile

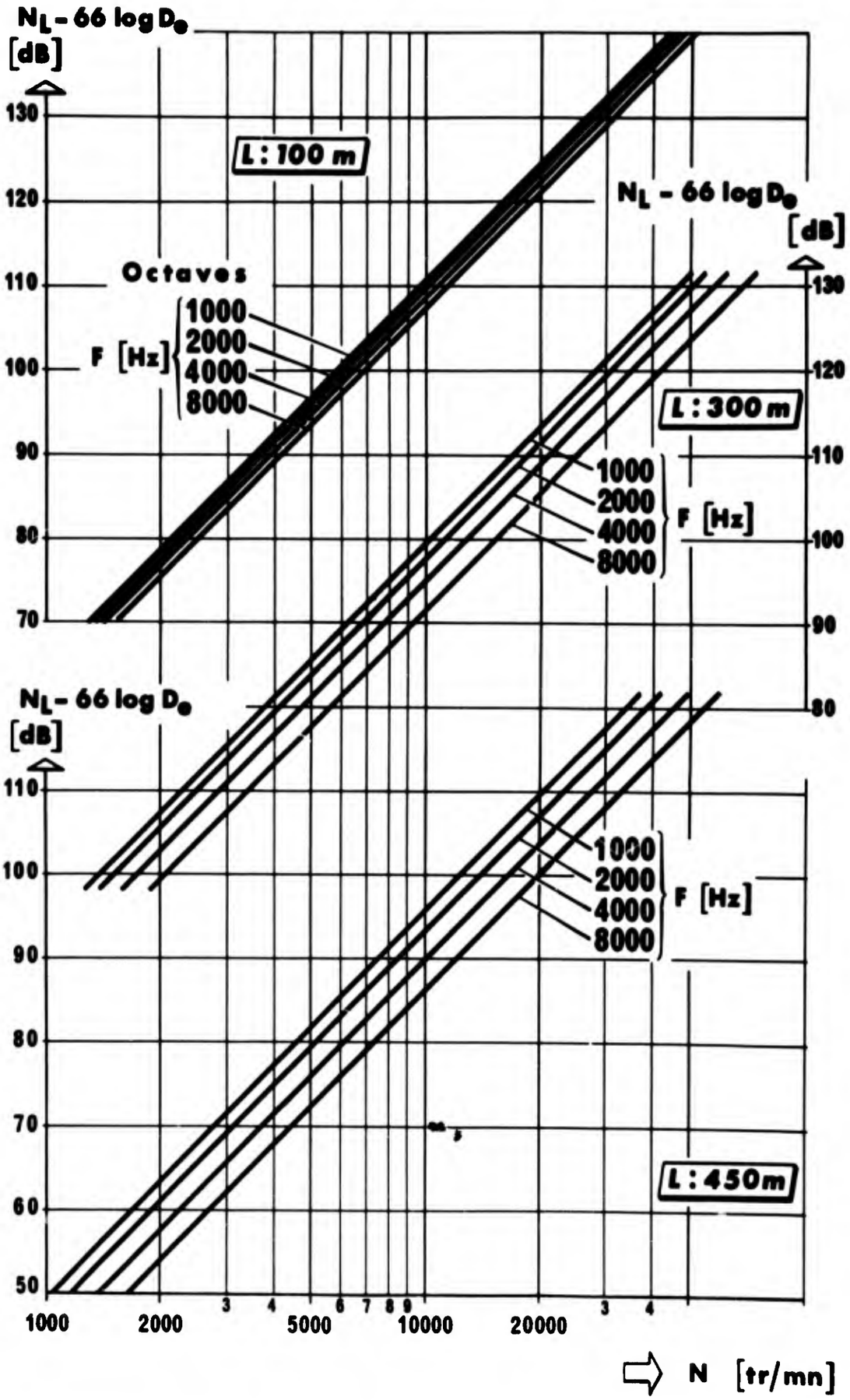

Fig.9 Niveau de pression sonore lineaire maximal de compresseurs ou de soufflantes (L = 100, 300 et 450 m)

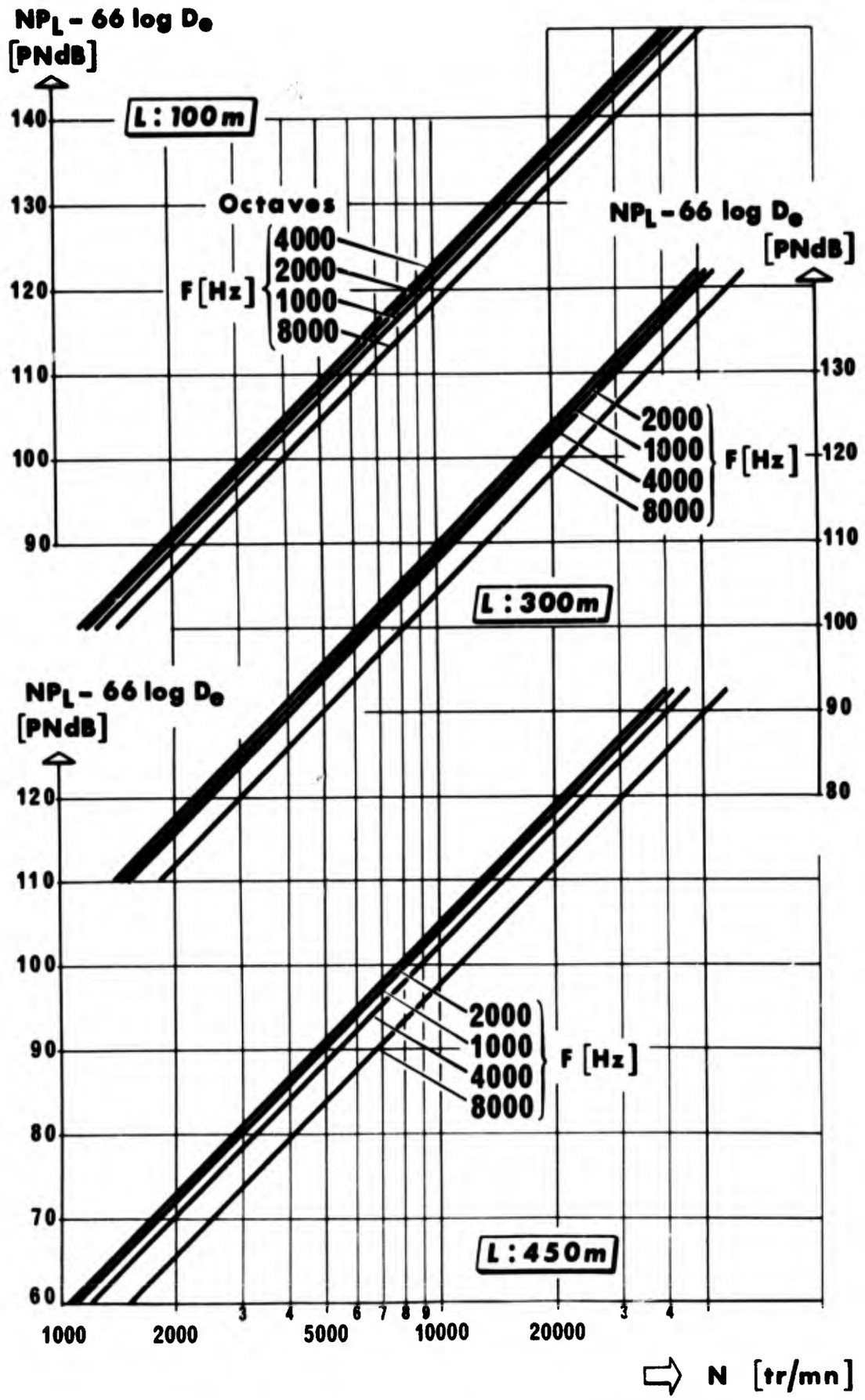

Fig. 10 Niveau de bruit perçu linéaire maximal de compresseurs ou de soufflantes (L = 100, 300 et 450 m)

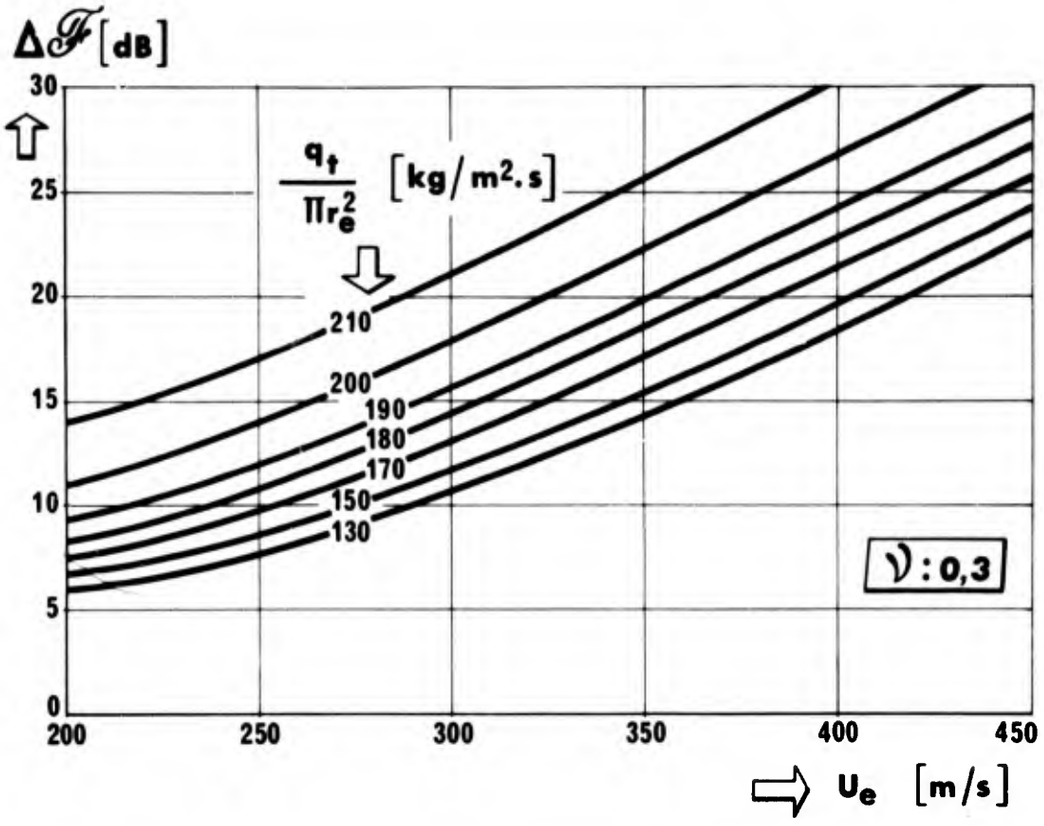

Fig.11(a) $\nu = 0,3$

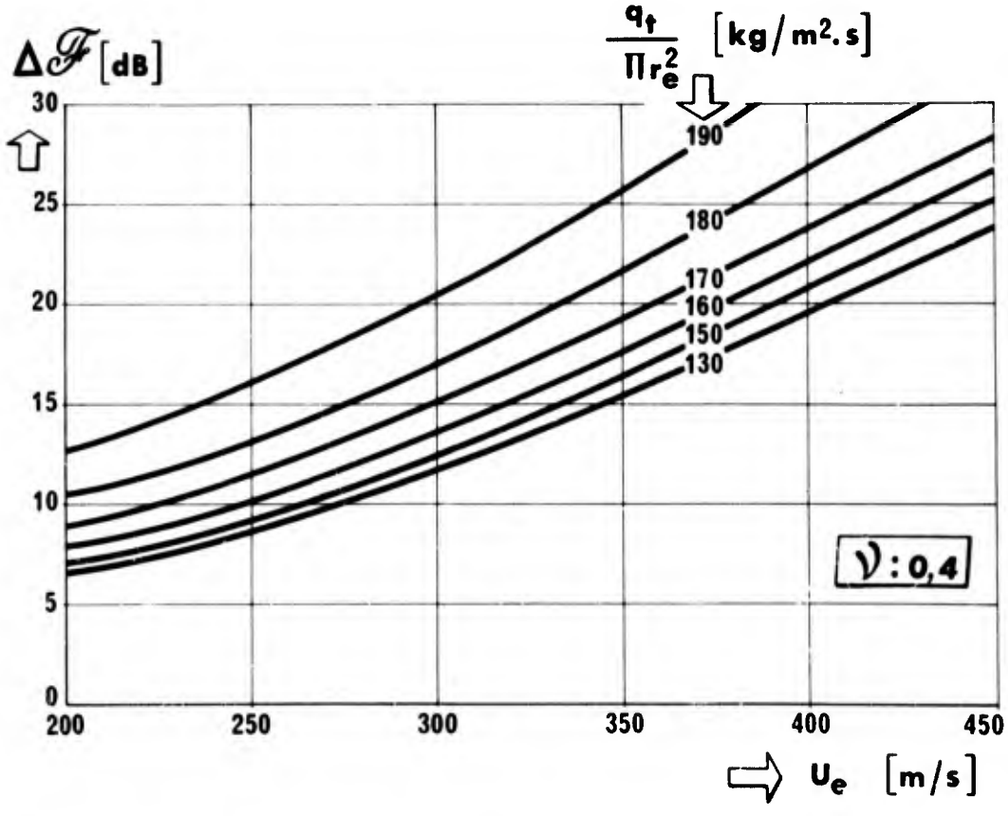

Fig.11(b) $\nu = 0,4$

Fig.11 Indice de convection

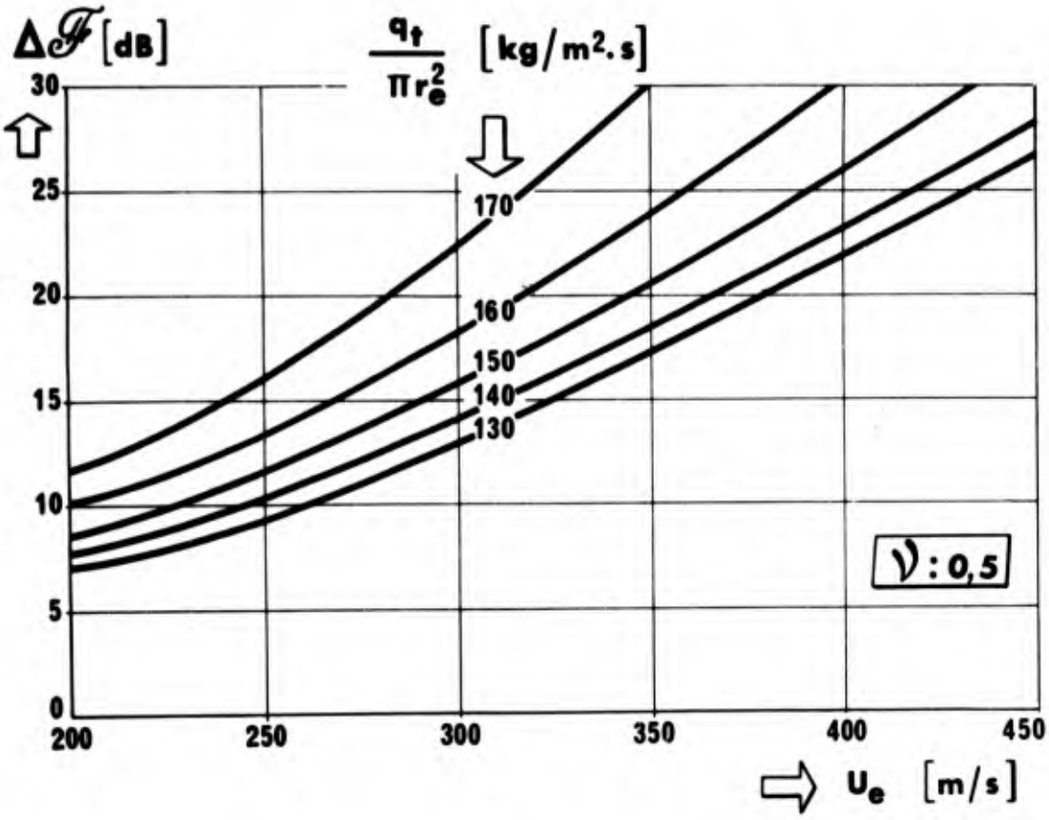

Fig.11(c) Indice de convection: $\nu = 0,5$

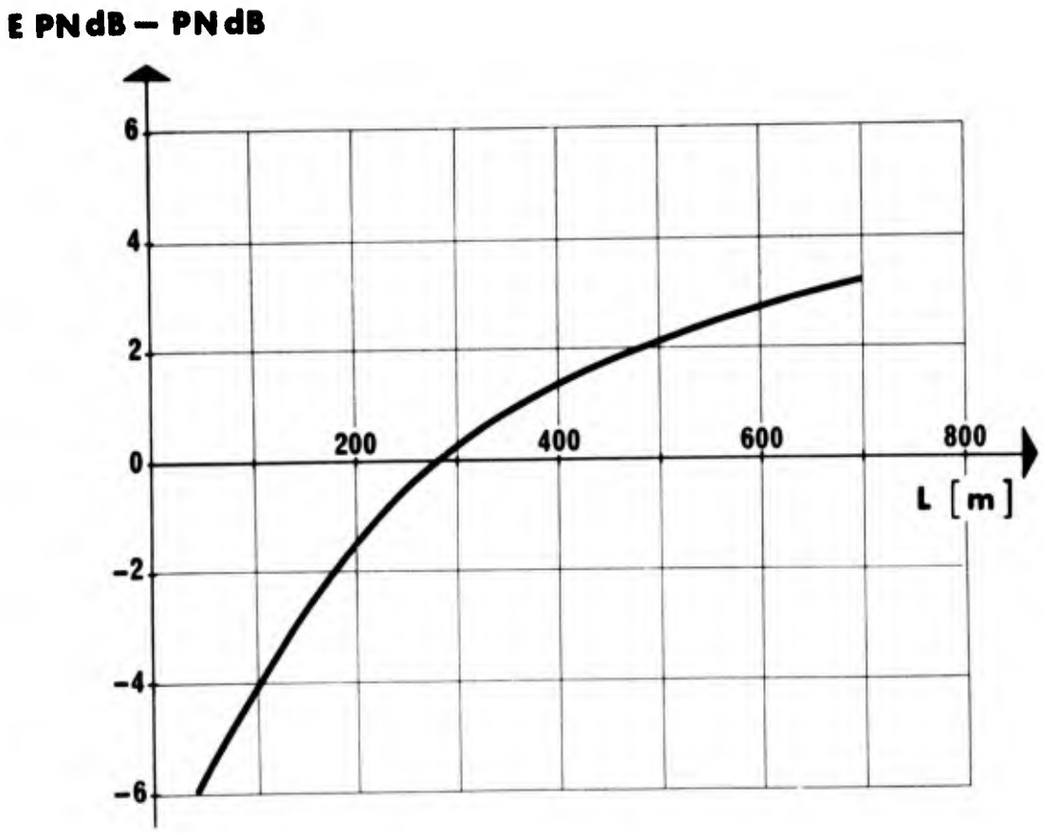

Fig.12 Différence: EPNdB - PNdB

METHODES DE DEPOUILLEMENT ET DE TRAITEMENT DE L'INFORMATION ACOUSTIQUE POUR L'ETUDE DU BRUIT DES MOTEURS D'AVION

par Jacques HAY

Office National d'Etudes et de Recherches Aérospatiales
29, avenue de la Division Leclerc
92 - CHATILLON-sous-BAGNEUX
(France)

0

0 0

SOMMAIRE

Après avoir brièvement rappelé le principe des analyseurs en temps réel utilisés pour l'étude des signaux acoustiques, on expose les techniques O.N.E.R.A. d'enregistrement et de dépouillement qui permettent actuellement d'accéder à l'analyse automatique d'un essai.

L'ETUDE DES BRUITS de moteur d'avion nécessite l'analyse d'un très important volume de signaux acoustiques. Des analyseurs de spectres en temps réel étant recemment apparus sur le marché, il convenait dès lors d'adapter les techniques d'enregistrement et de restitution pour accéder à un dépouillement rapide par l'automatisation d'un certain nombre d'opérations.

LE PRINCIPE DES ANALYSEURS EN TEMPS REEL UTILISES.

Ils sont de deux types : un analyseur tiers d'octave et un analyseur à bande fine.

L'ANALYSEUR TIERS D'OCTAVE* - Le principe de cet analyseur est rappelé dans le seul but de préciser le mode de sortie des spectres qu'il délivre et justifier la technique de dépouillement adoptée.

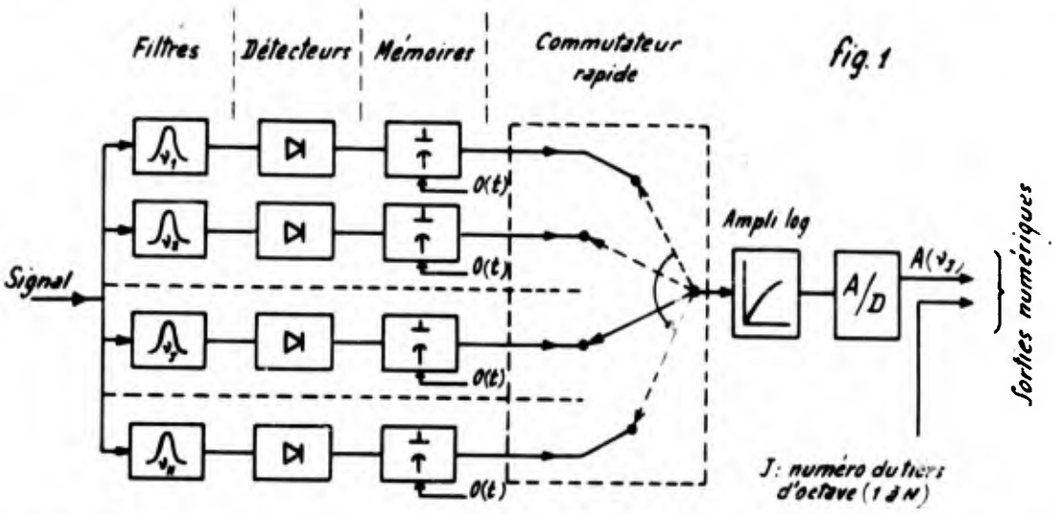

L'analyseur comprend N filtres tiers d'octave opérant en parallèle sur le signal. (fig.(1)). A chaque filtre sont associés un détecteur, de constante de temps** τ, et un circuit mémoire. Synchronisées par un même ordre $O(t)$ à l'instant t, toutes les mémoires figent à cet instant les valeurs de sortie des détecteurs. Un commutateur rapide lit successivement le contenu des N mémoires qui est transposé en décibels par un seul amplificateur logarithmique. Le spectre tiers d'octave, ainsi sérialisé, est numérisé. A la sortie numérique $A(\nu_j)$ est associé un signal identifiant le numéro de la composante (jème tiers d'octave). Les mémoires sont ensuite vidées puis, par un ordre $O(t')$ les mémoires figent les sorties des détecteurs et un nouveau cycle commence. La durée d'un cycle ($t'-t$) est de l'ordre de 25 ms.

REMARQUE : Même pour la constante de temps la plus faible (100 ms) on voit qu'un certain nombre de spectres successifs sont redondants (non statistiquement indépendants). Dans ce cas on obtiendra des spectres A_i et A_{i+1} "indépendants" pour $t_{i+1} - t_i$ de l'ordre de 200 ms, ce qui permet d'optimiser la propertion des spectres que l'on doit mémoriser.

L'ANALYSEUR A BANDE FINE*** - L'analyseur utilisé est du type hybride (analogique numérique) ; on accède à l'analyse d'une certaine gamme de fréquence en temps réel grâce à une compression du signal dans le temps (ou accélération) qui permet d'accélérer de la même façon la vitesse d'analyse. L'analyse se fait de manière analogique, par contre l'accélération du signal se fait grâce à des techniques numériques (registre à décalage ou ligne à retard acoustique). Pour l'exposé du principe de cet analyseur le mode d'accélération réel est remplacé par un mode d'accélération symbolique :

On suppose (fig. (2)) qu'une portion d'un signal $x(t)$ de durée Δt est enregistrée avec une vitesse de défilement v sur une boucle magnétique. On restitue ensuite le signal grâce à une tête de lecture montée sur un bras tournant ; par rapport à la boucle la vitesse du lecteur est $V = \alpha v$ $(\alpha >> 1)$. Le signal $x_a^i(t)$ lu pendant la ième révolution de la tête de lecture sera (à une translation près) le signal accéléré :

$$x_a^i(t) = x(\alpha t)$$

α est le rapport d'accélération

en posant $X(\nu) = T.F.[x(t)]$

$X_a^i(\nu) = T.F.[x_a^i(t)]$ (T.F. = Transformée de Fourier)

---

* Analyseur Hewlett-Packard 8054

** Suivant les signaux on peut choisir entre deux constantes de temps. L'une de l'ordre de 100 ms, l'autre de l'ordre de 1 s

*** L'analyseur actuellement utilisé est un UA7B de Federal Scientific Corporation

$$\left| X_a^i(\nu) \right| = \left| \int_0^{\Delta t/\alpha} x(\alpha t)\, e^{2j\pi\nu t}\, dt \right|$$

$$\left| X_a^i(\nu) \right| = \frac{1}{\alpha} \left| X(\nu/\alpha) \right|$$

On voit que l'étendue spectrale d'une période du signal accéléré et celle du signal initial sont dans le rapport α .

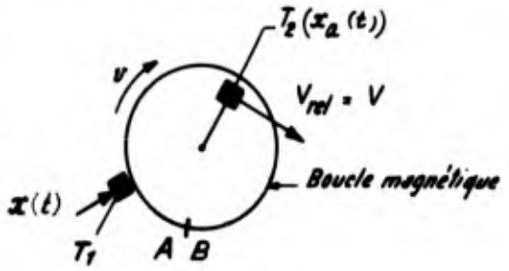

T_1 = tête d'enregistrement
T_2 = tête de lecture

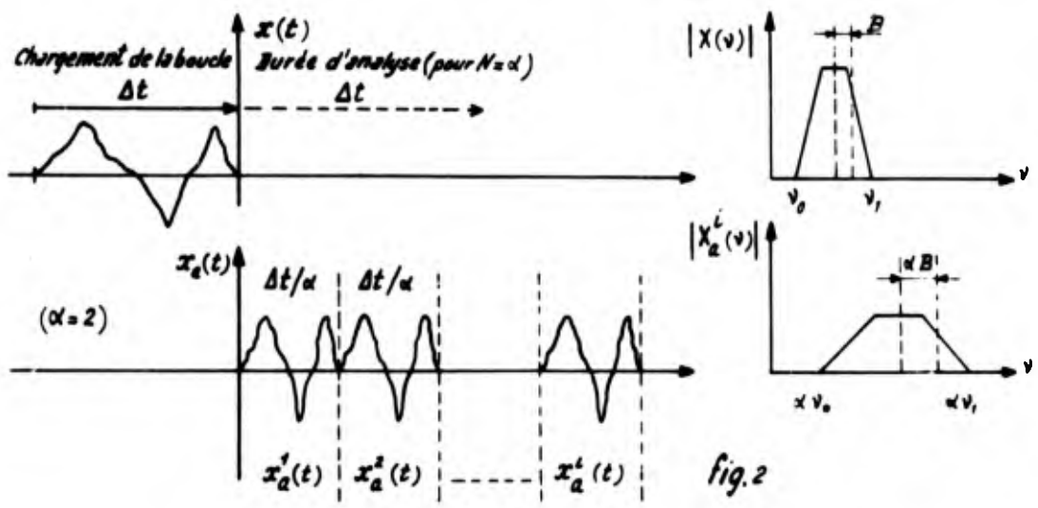

fig. 2

On veut connaître le spectre du signal $x(t)$ dans le domaine de fréquence (B, NB) par N points de filtrage équidistants et avec une résolution $B = \frac{1}{\Delta t}$ [M]. Il est équivalent (fig. (2)) d'analyser $x_a(t)$ avec un filtre de résolution α B.

Si d'autre part le filtre et le système de détection qui lui est associé ont un temps de réponse[MM] de $\frac{1}{\alpha B} = \frac{\Delta t}{\alpha}$, il suffit pour analyser le signal d'utiliser un filtre glissant $\mathcal{F}$ dont la fréquence centrale $\nu_{\mathcal{F}}$ prend successivement les valeurs $\alpha B, 2\alpha B, \ldots, N\alpha B$, aux instants $0, \frac{\Delta t}{\alpha}, \ldots, (N-1)\frac{\Delta t}{\alpha}$.

Compte tenu du temps de réponse propre au dernier point d'analyse, le temps total d'obtention d'un spectre est

$$T = (N-1)\frac{\Delta t}{\alpha} + \frac{1}{\alpha B} = \frac{N}{\alpha} \cdot \Delta t$$

Pour $\alpha = N$ on a

$T = \Delta t$: La durée de l'analyse est égale à la durée du signal.

Si l'on ne considère que l'entrée et la sortie de l'analyseur, tout se passe comme si le signal $x(t)$, de durée Δt , avait été analysé par N points de filtrage $\nu_j = iB\ (j = 1 \ldots N)$ le jème point étant obtenu à l'instant $t = j\frac{\Delta t}{N}$.

On suppose maintenant que :

1° - Après la $N^{ième}$ révolution de la tête de lecture ($i = N$) le filtre recommence une séquence d'analyse : pour $i = N+1$ $\nu_j = B$ etc ... pour $i = N+N$ $\nu_j = NB$.

M On peut montrer que la durée du signal réel $x(t)$ étant égal à Δt , son spectre ne comporte pas de pic dont la largeur est inférieure à $1/\Delta t$, il est par suite inutile de l'analyser avec un filtre à grande sélectivité.

MM Le temps de réponse d'un filtre est inversement proportionnel à sa bande passante.

En désignant par j le numéro de la composante spectrale $(j = 1 \grave{a} N)$

Pour le ième point de filtrage le filtre équivalent est tel que $\nu_j = jB$ avec $j = i - N\left[P.E.\left(\frac{i-1}{N}\right)\right]$
(P.E = partie entière).

2° - Au lieu de figer une portion Δt du signal sur la boucle, on enregistre en permanence $x(t)$. Ce qui revient à appliquer de manière continue le signal $x(t)$ à l'entrée de l'analyseur (fig. (3)).

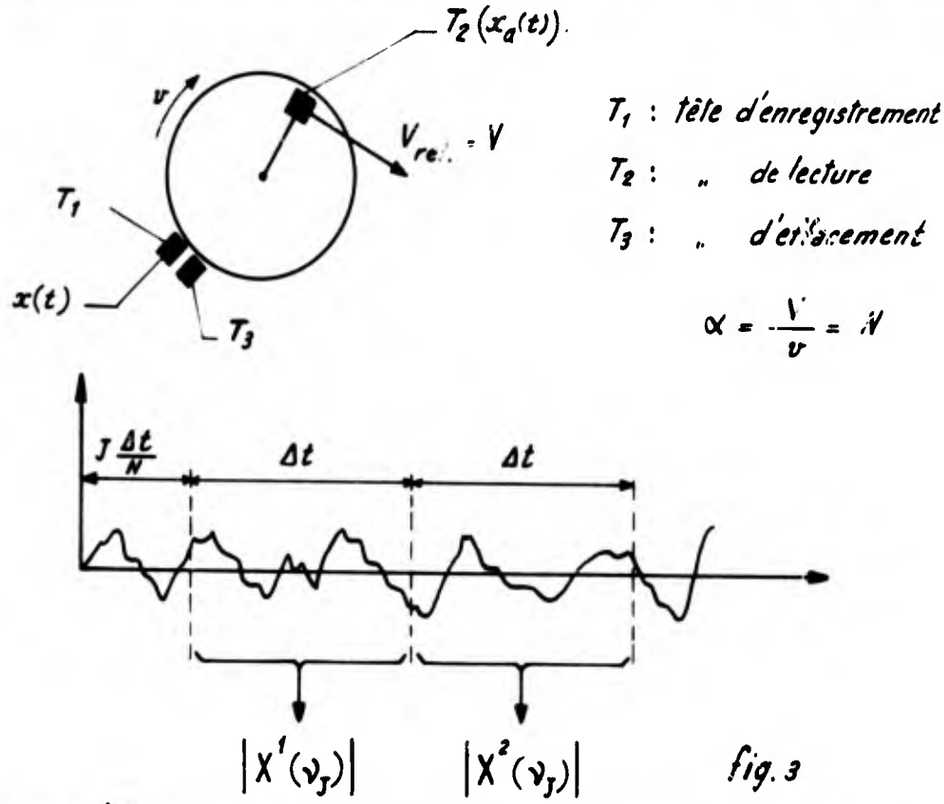

fig. 3

On appelle k^{ème} spectre élémentaire $|X^k(\nu_j)|\ (j = 1 \grave{a} N)$ le spectre obtenu au cours de la k^{ème} séquence d'analyse. On a évidemment $k = P.E.(i-1/N) + 1$. Pour un même point d'analyse ν_j on a représenté fig. (3) les portions du signal correspondant aux valeurs $k = 1$, $k = 2$.

A travers un circuit quadratique, les composantes $|X^k(\nu_j)|^2$ apparaissent en sortie de l'analyseur. Un moyenneur les numérise et en prend la moyenne arithmétique par bande de fréquence (fig. (4)).

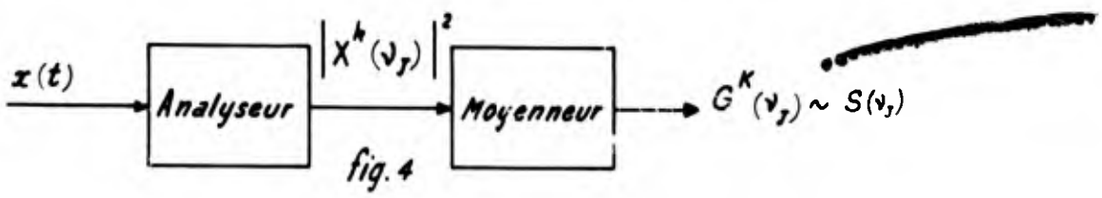

fig. 4

En réglant à K le nombre de spectres élémentaires pris en compte par le moyenneur, la fonction spectrale $G^K(\nu_j)$ qu'il délivre est liée aux $|X^k(\nu_j)|^2$ par

$$G^K(\nu_j) = \frac{1}{K} \sum_{k=1}^{k\,K} |X^k(\nu_j)|^2 \qquad 1 \leq j \leq N$$

On montre fig. (5) les portions de $x(t)$ relatives respectivement à $G^K(\nu_1)$ et $G^K(\nu_N)$

---

* Ce sont ces composantes spectrales $G^K(\nu_j)$ qui seront prises en compte par la chaîne d'acquisition c.f. chapitre suivant.

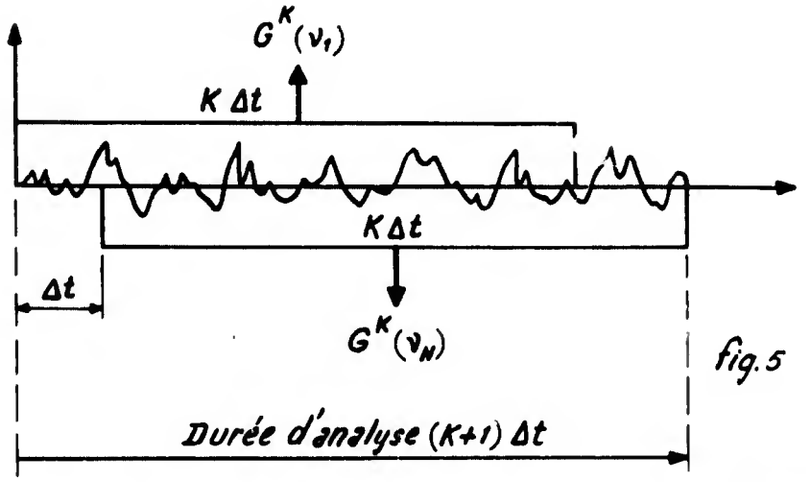

fig. 5

On voit que pour $K >> 1$ la durée d'analyse est égale à la portion du signal traité $((K+1)\Delta t \# K\Delta T)$ et que $G^K(\nu_j)$ correspond sensiblement à la même portion de signal quel que soit j.

λ désignant une constante d'étalonnage propre à l'appareil, $S(\nu)$ désignant la densité spectrale de puissance associée à $x(t)$ (échantillon d'une fonction aléatoire stationnaire ergodique) on sait que

$$S(\nu) = \lambda E\left[\left|X^k(\nu)\right|^2\right] \qquad (E = \text{Espérance mathématique})$$

Par suite, $\lambda G^K(\nu_j)$ est une estimation absolument correcte[**] de la densité spectrale de puissance $S(\nu_j)$.

En caractérisant la qualité de cette estimation par

$$\varepsilon = \frac{S(\nu_j)}{\text{Ecart type de } \lambda G^K(\nu_j)}$$

On trouve : $\varepsilon = \sqrt{K}$

On devra donc prendre K aussi grand que le permet la stationnarité réelle du signal acoustique $x(t)$ étudié.

CONCEPTION D'UNE METHODE D'ANALYSE RAPIDE ET AUTOMATISEE [***]

L'enregistrement analogique d'un champ sonore n..ire, au banc, ou l'enregistrement d'un bruit de survol sont appelés respectivement essai au banc ou essai de survol. Une même bande analogique comporte plusieurs essais en série, mais l'automatisme de l'analyse est actuellement restreint à l'essai, qui forme ainsi l'unité de dépouillement.

Il est à noter que la solution présentée ici se devait d'être compatible avec l'emploi d'enregistreurs monopiste à modulation directe (type NAGRA).

PRINCIPE DE LA METHODE - Un enregistreur analogique restitue l'essai à l'entrée d'un analyseur en temps réel ; des signaux annexes (R_3) ajoutés au signal acoustique lors de l'enregistrement, commandent au système d'acquisition la prise en compte des spectres sérialisés qui apparaissent à rythme constant à la sortie de l'analyseur. Ainsi les spectres mémorisés se trouvent datés dans une base de temps issue de l'expérience elle-même.

[**] A condition que $S(\nu)$ puisse être considérée comme constante dans chaque bande d'analyse B.

[***] Les appareils électroniques spécialement étudiés pour cette méthode d'analyse ont été réalisés grâce à une étroite collaboration entre la Division d'Acoustique et la Division d'Electronique et Mesures de l'O.N.E.R.A.

Pour compléter l'automatisme du dépouillement un signal R_1 en début d'essai initialise le système d'acquisition tandis qu'en fin d'essai un signal R_2 arrête la chaîne d'analyse et l'enregistreur magnétique (fig. 6).

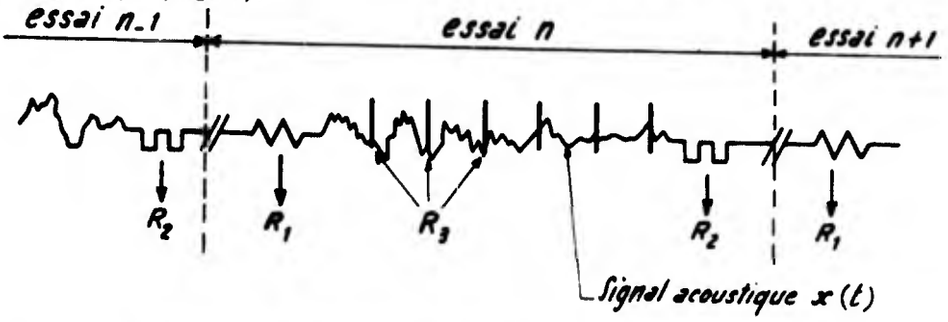

a) Image symbolique de la bande analogique.

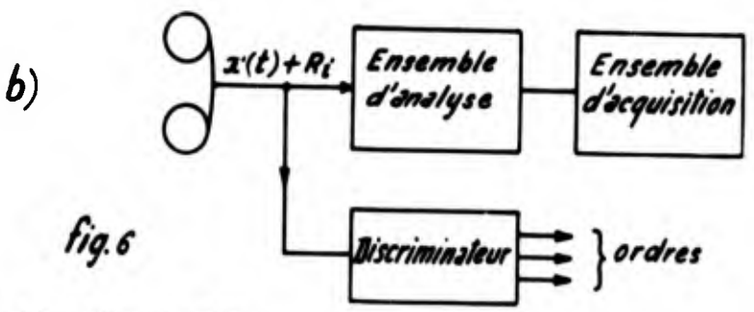

fig.6

TECHNIQUE D'ENREGISTREMENT.

A - CAS DES ESSAIS AU BANC - L'essai consiste à enregistrer le signal acoustique mesuré par un microphone décrivant un arc de cercle (c) autour du moteur (fig. 7).

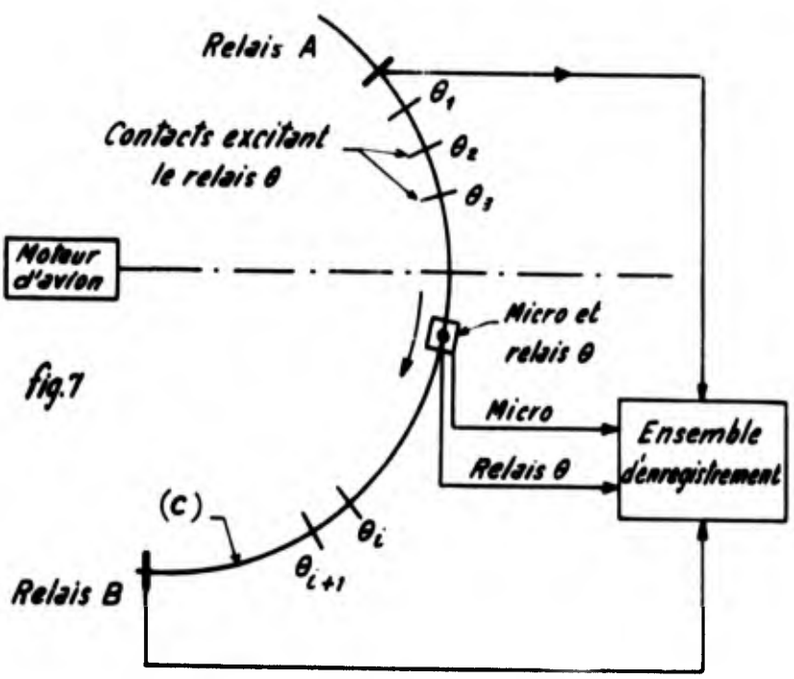

fig.7

Un relais θ solidaire du microphone est excité par les contacts θ_i ; ces "tops-relais" sont traduits par la chaîne en tops R_3 calibrés qui s'inscrivent sur la bande analogique. De même les relais A et B engendrent un top R_1 (début d'essai ou R_2 (fin d'essai) suivant le sens d'évolution du microphone sur (c) (fig. 8).

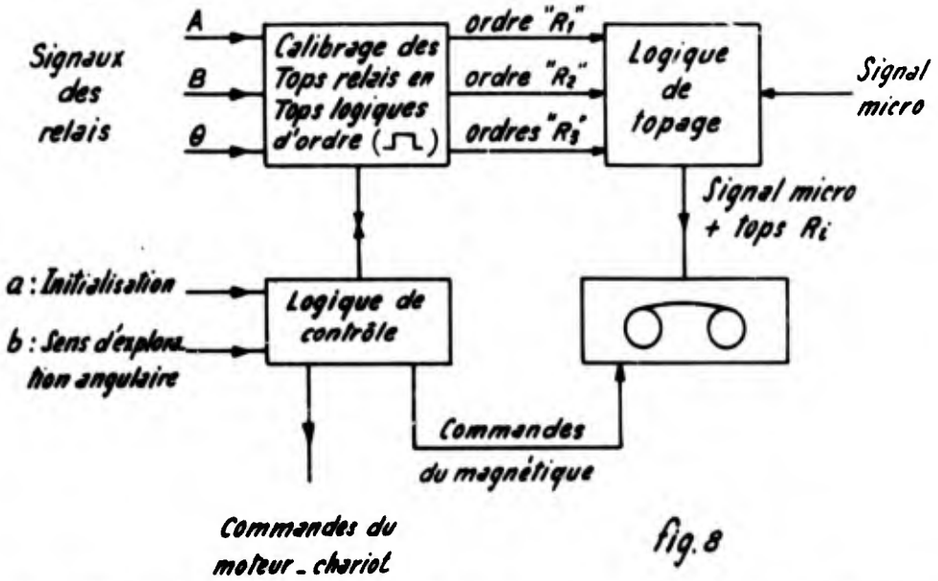

fig. 8

En fonctionnement automatique, a et b déclenchent toute la séquence d'enregistrement : démarrage de l'enregistreur, du chariot, tops Ri, puis arrêt du chariot et de l'enregistreur. Un pupitre, réplique de toutes les commandes et des tops, permet en fonctionnement manuel d'élaborer un enregistrement ayant la même structure que celui obtenu en séquence automatique. On peut ainsi donner à l'étalonnage par pistonphone -ou à l'étalonnage électrique- la même présentation qu'un essai normal et par suite automatiser l'analyse des essais d'étalonnage lors du dépouillement.

LA LOGIQQUE DE TOPAGE est schématisée fig. (9). Les circuits (α) représentent des fonctions logiques "ou". O_1, O_2, O_3 représentent trois oscillateurs qui délivrent respectivement les fréquences $f_1 = 2000$ Hz , $f_2 = 3900$ Hz , $f_3 = 5200$ Hz . Lorsque l'ordre R_1 se présente à l'entrée sous la forme d'un créneau de tension, il excite les circuits α_1 et α_2 qui pendant la durée du créneau ferment les commutateurs C_1 et C_2. En (2) sortie du sommateur on dispose alors de la somme des sinusoïdes f_1 et f_2. Grâce à (α_C) et au calibreur, le commutateur C_e substitue au signal acoustique le signal " $f_1 + f_2$ " pendant une durée calibrée de 10 ms ce qui constitue le top R_1. De manière analogue R_2 se compose de " $f_1 + f_3$ " et R_3 de " $f_2 + f_3$ ".

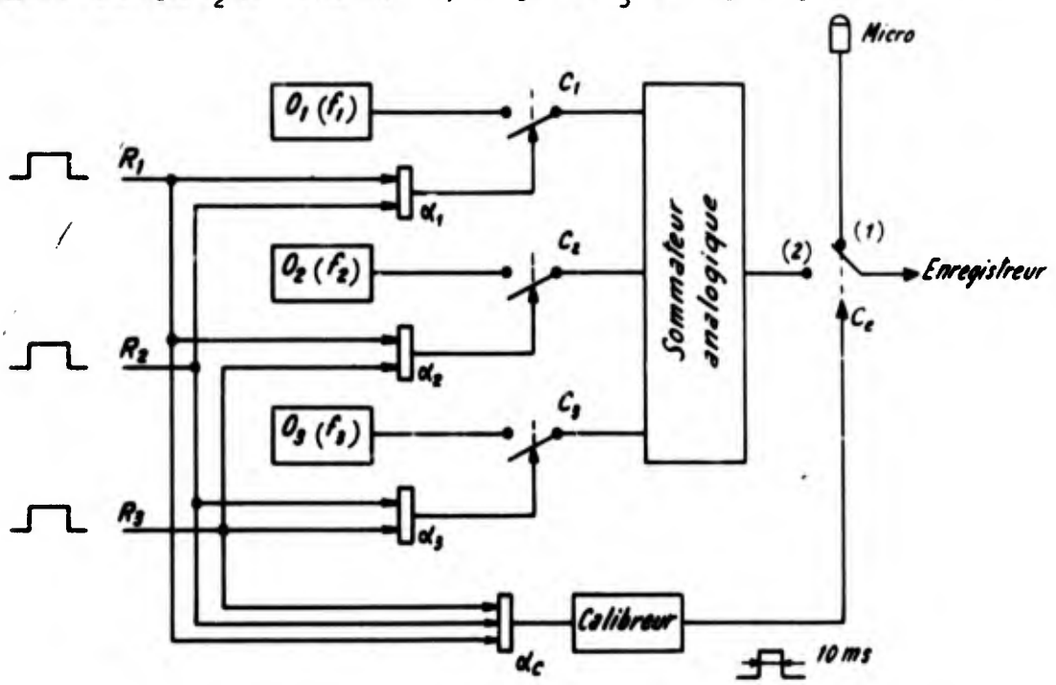

fig. 9 - Logique de topage des bancs d'essais

Le choix d'un topage à l'aide de deux fréquences permet de rendre très improbables des détections parasites par des fréquences pures contenues dans le signal acoustique. La durée des tops (10 ms) est optimisée pour leur permettre d'être détectée sans qu'ils modifient sensiblement l'analyse spectrale du signal acoustique..

B - LES ESSAIS DE SURVOL - Le principe de l'enregistrement est analogue au précédent. La logique de topage est identique, seule diffère l'origine des ordres : ils sont émis par une station pilote, qui les distribue par radio (ou liaison directe) aux différentes stations satellites d'enregistrement ainsi qu'au Centre de trajectographie (cinéthéodolite), fig. (10). En particulier les ordres R_3 sont synchronisées par une horloge et sont datés dans la base de temps du cinéthéodolite dont le dépouillement permettra de préciser la position de l'avion associée à chaque top R_3.

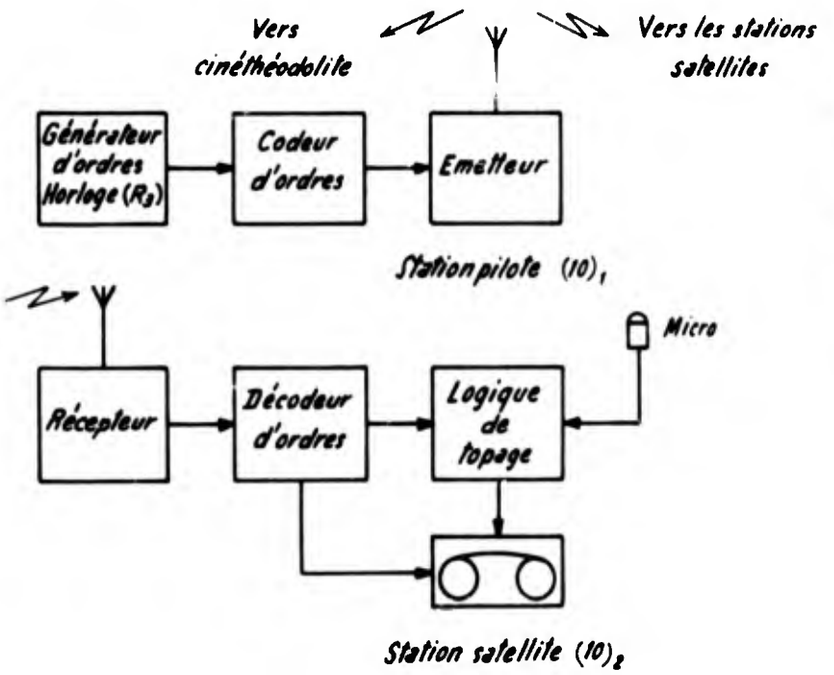

LA STATION PILOTE émet les les trois types d'ordres nécessaires : l'ordre "Marche", les ordres de top R_3 et l'ordre "Arrêt". Les ordres R_3 sont émis par l'horloge de topage, mais pour prévenir d'éventuels départs ou arrêts intempestifs des enregistreurs magnétiques les ordres "Marche" et "Arrêt" sont répétés à cadence régulière par le générateur d'ordres.

fig.10. Ensemble d'enregistrement des bruits de survols

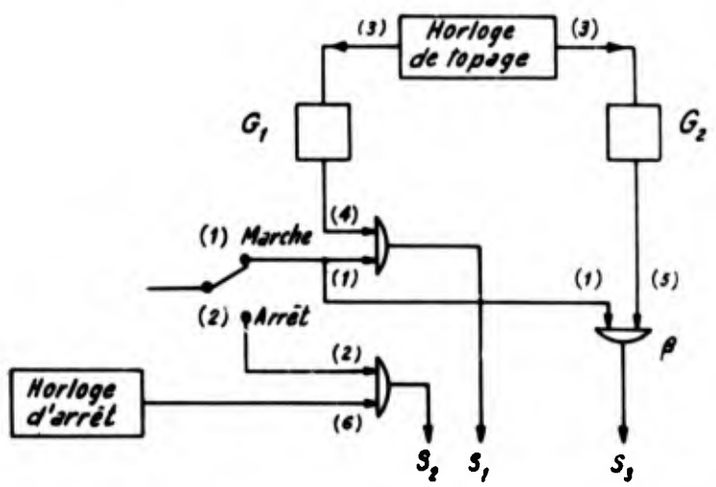

LE GENERATEUR D'ORDRES comprend une horloge de topage qui pilote deux générateurs de créneaux auxiliaires G_1 et G_2 ; G_1 est synchronisé sur les fronts positifs, G_2 sur les fronts négatifs des créneaux délivrés par l'horloge. Les circuits (β) représentent des fonctions logiques "et"

S_1 : Sortie des ordres "Marche" récurrents
S_2 : " "Arrêt" "
S_3 : " "R_3" "

fig. 11

Fig. 11 - Le générateur d'ordres

A titre d'exemple, on donne, (fig. 12) le fonctionnement du générateur d'ordres en représentant les états logiques des différents points du circuit.

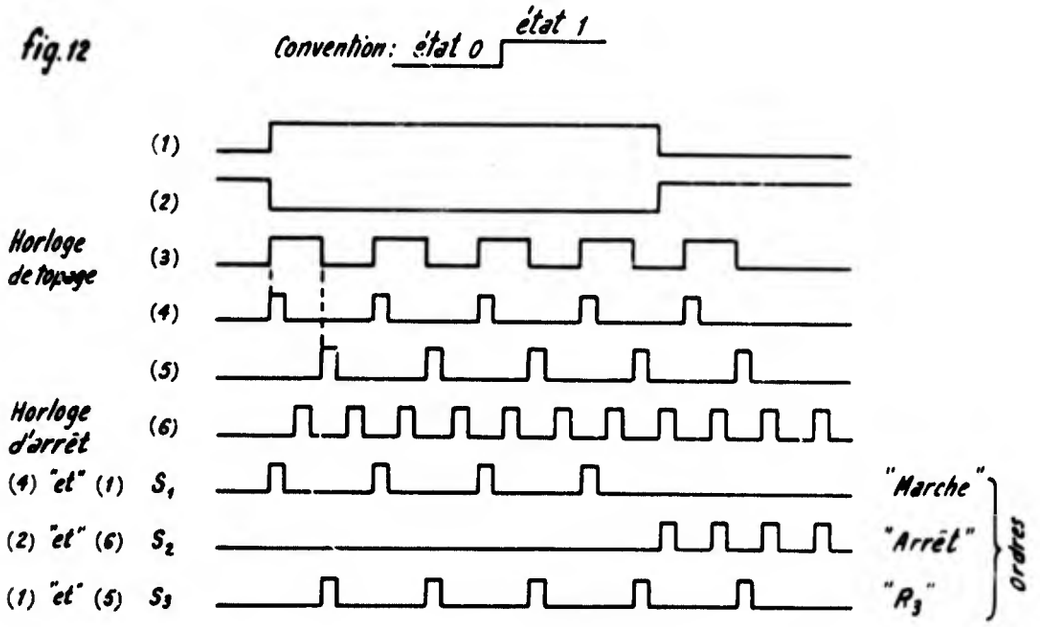

LE CODEUR D'ORDRES transforme ensuite les ordres "Marche", "Arrêt", "R_3" suivant un principe identique à celui de la logique de topage des bancs, (fig.9) : à chaque créneau d'ordre on associe la somme de deux sinusoïdes " f_i et f_j " de même durée que le créneau (fig. 13).

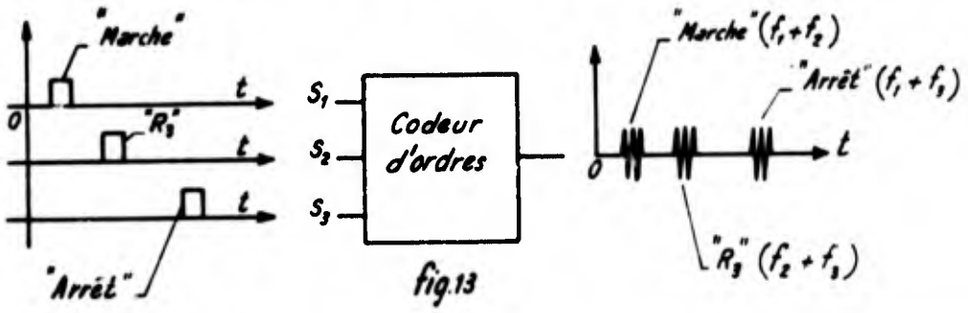

fig.13

LA STATION SATELLITE reçoit les tops (" $f_i + f_j$ ") le premier ordre "Marche" qu'elle détecte[m] démarre l'enregistreur puis avec un retard suffisant pour permettre la mise en vitesse de l'enregistreur il donne un ordre R_1 à la logique de topage, qui lui associe un top calibré R_1 sur la bande analogique.

Les ordres "Marche" suivants ne seraient pris en compte que si un ordre parasite "Arrêt" avait stoppé le système en cours d'essai. Les ordres "R_3" sont systématiquement transformés en tops calibrés R_3 sur la bande.

Enfin le premier ordre "Arrêt" que la station détecte donne un ordre R_2 à la logique de topage, donc un top calibré R_2 à la bande, puis arrête l'enregistreur. Les ordres "Arrêt" suivants ne seraient pris en compte que si un ordre parasite "Marche" avait démarré le système après la fin de l'essai.

TECHNIQUE DE DEPOUILLEMENT.

DEROULEMENT D'UNE SEQUENCE DE DEPOUILLEMENT - La mise en marche du lecteur magnétique est commandée manuellement, le top R_1 initialise la chaîne, les tops R_3 ordonnent l'acquisition (ou la synchronise par rapport au phénomène) le top R_2 arrête la chaîne et le lecteur. Le lecteur magnétique s'arrête après chaque essai, il est alors possible manuellement d'approprier à l'essai suivant les réglages de la chaîne d'analyse. Le premier essai de chaque bande est un signal de référence obtenu par un pistonphone dont le spectre est mémorisé par l'ensemble d'acquisition permettant ainsi un étalonnage absolu de tout le système (fig. 14).

---

m Le décodeur utilisé est analogue à celui décrit au paragraphe suivant (fig. 15).

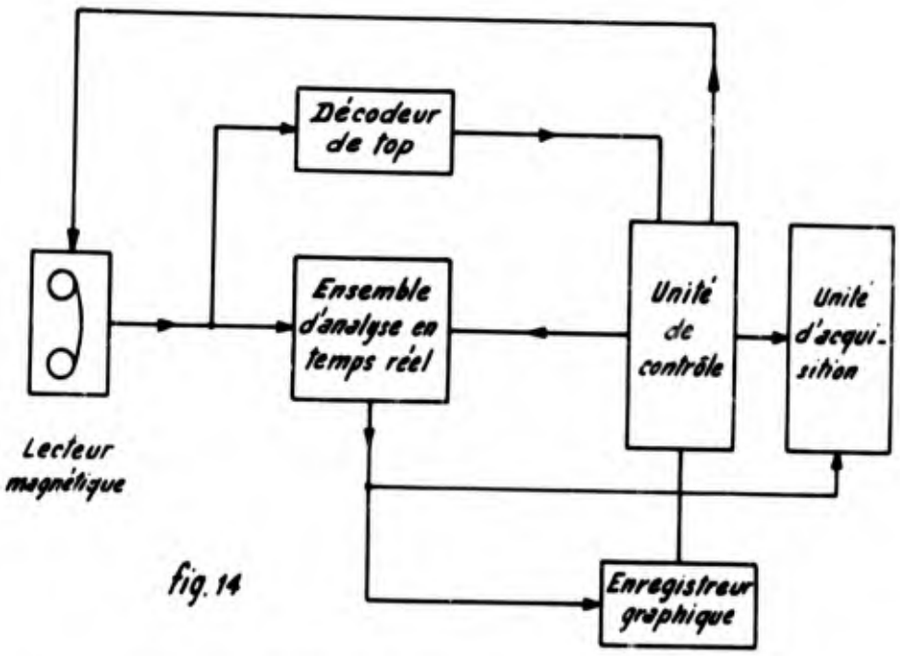

fig. 14

Le bon fonctionnement de l'ensemble est essentiellement lié au décodage correct des tops : tous les tops "R_i" doivent être détectés ; on doit rendre très improbables des détections parasites dues à des trains d'ondes sinusoïdales contenues dans le signal acoustique.

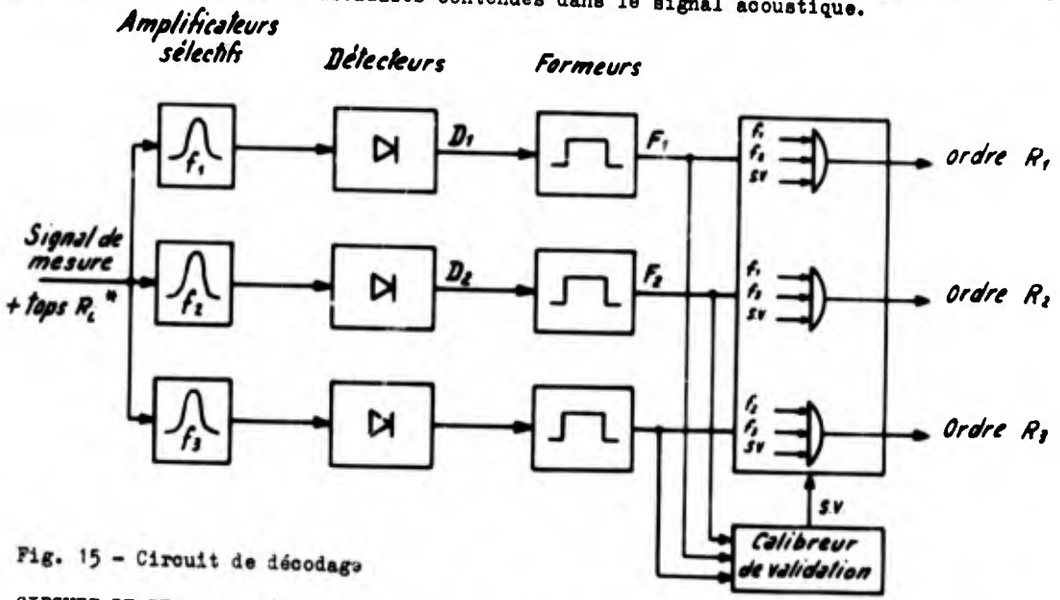

Fig. 15 - Circuit de décodage

CIRCUIT DE DECODAGE, (fig. 15) - Le calibreur de validation évite au décodeur de donner des ordres parasites R_i provenant de réponses transitoires des amplificateurs sélectifs. Par suite des déphasages entre les circuits, les fréquences f_i et f_j n'apparaissent pas exactement au même instant. Pour préciser le rôle du calibreur de validation, on considère l'exemple d'un top R_3 pour lequel f_1 précède légèrement f_2 .

On représente (fig. 16_1) les sorties du détecteur (D_i) et du formeur (F_i).

Le calibreur, après un retard τ_0 , associe au premier signal F_i (ici F_1) un signal logique d'une durée de 1 ms (signal de validation S.V.). Le signal S.V. appliqué aux circuits "et" du décodeur ne valide les signaux F_1 et F_2 que pendant 1 ms.

Pour un retard τ_0 suffisant (compte tenu de la sélectivité des amplificateurs qui définit leurs réponses aux transitoires) les réponses des circuits sélectifs d'entrée à un transitoire à l'instant $t = 0$ seront suffisamment amorties à l'instant $t = \tau_0$ pour que ce transitoire n'engendre pas un ordre parasite.

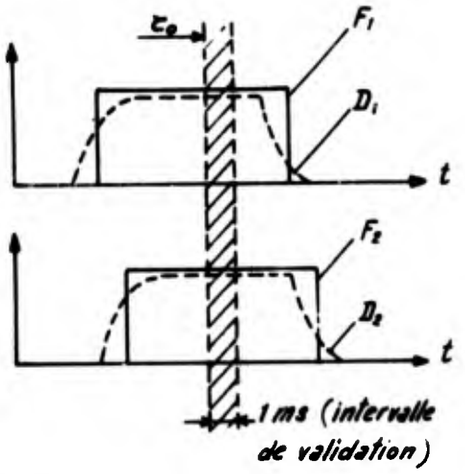

fig. 16_1)

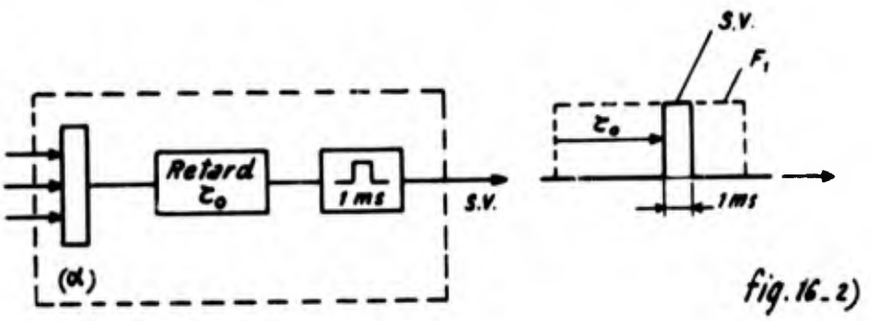

fig. 16_2)

fig.16_Calibreur de validation

L'ACQUISITION ET LE TRAITEMENT NUMERIQUE DES SPECTRES.

Trois types de dépouillements sont à distinguer :

Type I : les analyses fines d'essais au banc
Type II : les analyses "tiers d'octave" d'essais au banc
Type III : les analyses "tiers d'octave" d'essais de survol.

Deux raisons nécessitent cette distinction :

a - les tops R_3 des essais au banc sont liés à des repères géométriques fixes ; aussi, lors du dépouillement, permettent-ils en pilotant directement l'acquisition numérique d'associer à chaque spectre la position correspondante du microphone. Par contre, pour les essais de survol, le rythme d'acquisition des spectres est piloté par une horloge indépendante. Cette horloge date les tops R_3 qui ont été simultanément enregistrés lors du survol dans la base de temps du cinéthéodolite. Ainsi après calcul, chaque spectre est daté dans la base de temps du système de trajectographie.

b - L'analyseur à bande fine, en temps réel, est associé à un moyenneur qui permet d'approprier le temps d'intégration T au type de champ sonore étudié. De ce fait la chaîne d'acquisition prend en compte le même nombre de spectres que ce qu'exige la résolution angulaire choisie. L'analyseur tiers d'octave en temps réel ne dispose que de deux constantes de temps (100 ou 200 ms et 1 ou 2 s). Par suite, lorsque ni l'une ni l'autre ne convient à la résolution angulaire souhaitée, il faut acquérir un grand nombre de spectres numérisés que l'on regroupe ensuite par calcul en prenant la moyenne arithmétique des composantes de chaque tiers d'octave.

DEPOUILLEMENT DU TYPE I : Aux spectres $S(\nu)$ pris en compte par la chaîne d'acquisition, la figure (17) associe les angles $\Delta\theta$ correspondant aux portions de signal analysées. Le numéro i du spectre, également mémorisé, permet au programme de calcul d'associer à chaque spectre $S_i(\nu)$ son "adresse angulaire" η_i .

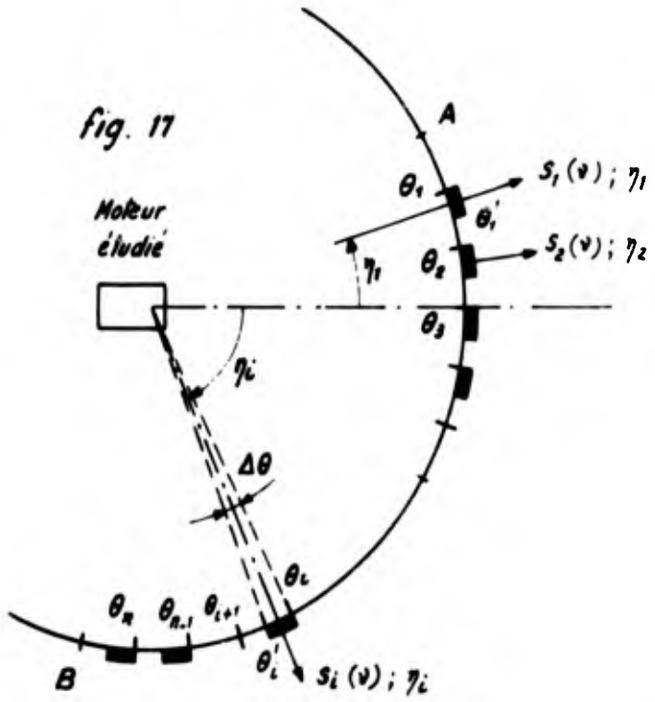

Fig. 17 - Analyses fines d'essais au banc

Si T désigne le temps d'intégration relatif aux spectres moyens $S_i(\nu)$

$$T = K \times \Delta t$$

si ces spectres se déduisent de la moyenne arithmétique de K spectres élémentaires.

Par suite $\Delta\theta = \Omega \cdot T$

Ω étant la vitesse angulaire du microphone décrivant A - B.

L'angle moyen associé au spectre moyen $S_i(\nu)$ est $\eta_i = \frac{1}{2}(\theta_i - \theta_i')$

DEPOUILLEMENT DES TYPES II et III : La figure (18) schématise le regroupement des spectres élémentaires mémorisés par la chaîne d'acquisition.

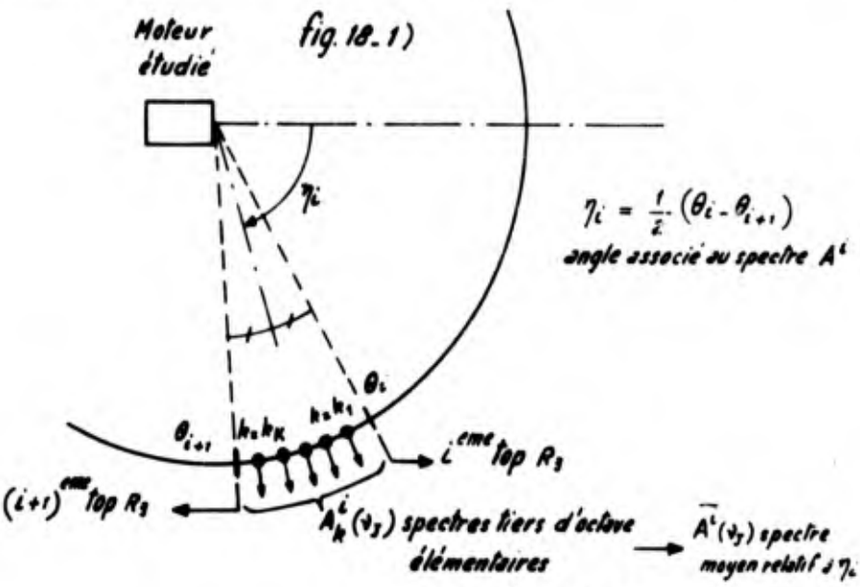

Fig. 18$_1$ - Regroupement des spectres tiers d'octave pour un essai au banc.

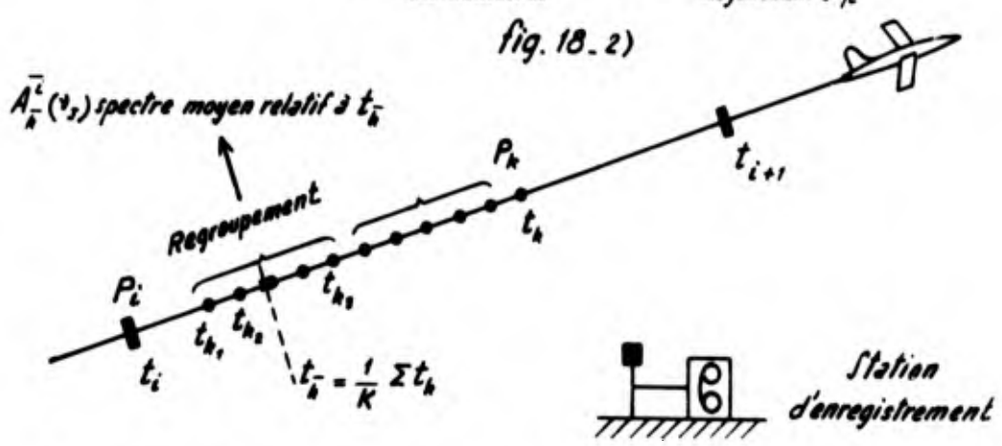

Fig. 18$_2$ - Regroupement des spectres tiers d'octave pour un enregistrement de bruit de survol

Pour les essais au banc - Fig. $(18)_1$ - le calcul donne $\overline{A^i}(\nu_j) = \frac{1}{K} \sum_k A_k(\nu_j)$ et grâce à un tableau de correspondance caractéristique de chaque banc d'essai le programme attribue au spectre $\overline{A^i}(\nu_j)$ l'angle moyen η_i

Pour les essais de survol, on a symbolisé fig. $(18)_2$ la position P_k de l'avion à l'instant t_k où le signal acoustique relatif au $k^{ème}$ spectre élémentaire est enregistré. (De même la position P_i est associée à l'instant t_i d'enregistrement du ième top R_3)

Au spectre moyen $\overline{A^i_k} = \frac{1}{K} \sum_{k=k_1}^{k=k_K} A^i_k(\nu_j)$, le calcul associe l'instant $t_K = \frac{1}{K} \sum_{k_1}^{k_K} t_k$.

Exemple : en mémorisant un spectre toutes les 100 ms, pour une constante de temps de l'analyseur de 200 ms on obtient en regroupant avec k = 5 un spectre toutes les 0,5 s.

Les différentes étapes du programme de calcul[m] qui à partir des spectres mémorisés termine l'analyse de l'essai peuvent se résumer par les opérations suivantes :

- Prise en compte de la sensibilité de la chaîne complète (mesure et analyse)
- Regroupement par paquets des spectres élémentaires
- Prise en compte des corrections de chaîne, définies par tiers d'octave
- Calcul de l'adresse angulaire (η_i) ou temporelle (t_k) associée à chaque spectre après calcul
- Calcul à partir des spectres du niveau global en fonction de l'angle ou du temps
- Pour les analyses des types II et II les résultats peuvent apparaître suivant deux rangements :

  a) un rangement identique à celui de l'acquisition : pour chaque valeur du paramètre (η ou t) le spectre $A(\nu_j)$ correspondant

  b) pour chaque tiers d'octave la fonction $A_j(\eta)$ ou $A_j(t)$

- Les résultats sont stockés sur bande magnétique numérique
- Des résultats d'essai -ou parties d'essai- peuvent être tracés par une table traçante numérique
- Un listing accompagne systématiquement chaque dépouillement. Il rappelle l'adresse de l'essai, les valeurs des paramètres liés au dépouillement et donne l'évolution du niveau global obtenu par calcul. La comparaison du niveau global obtenu par intégration des spectres et du niveau global mesuré directement permet de vérifier le bon fonctionnement du dépouillement.

CONCLUSION - La technique de dépouillement présentée permet un automatisme au niveau de l'essai. En tenant compte des opérations manuelles encore nécessaires avant le dépouillement en temps réel de l'essai suivant on peut admettre qu'actuellement le temps de dépouillement est de cinq fois à dix fois le temps réel d'enregistrement du phénomène. Par contre le futur laboratoire de dépouillement de l'O.N.E.R.A. permettra un automatisme complet au niveau de toute une bande magnétique analogique. Le rôle des tops "R_i" restera le même ; mais grâce à l'utilisation d'un ordinateur de pilotage et d'acquisition tous les réglages de la chaîne pour chaque essai seront faits automatiquement et "les calculs d'acquisition" seront faits en temps réel par l'ordinateur.

BIBLIOGRAPHIE.

[1] - BENDAT - PIERSOL
"Measurement and analysis of random data"
(Wiley and sons)

[2] - BLACKMAN - TUKEY
"The measurement of power spectra"
(Dover)

[3] - BLANC LAPIERRE - PICINBONO
"Propriétés statistiques du bruit de fond"
(Masson)

[4] - CRANDALL
"Random vibration"
Tomes I et II (Tech. Press)

[5] - STERN - DE BARBEYRAC - POGGI
"Méthodes pratiques d'étude des fonctions aléatoires"
(Dunod)

[6] - HAY J.
"Mesure et analyse des fonctions aléatoires stationnaires ergodiques"
(Revue Française de Mécanique) (à paraître)

m Le calcul se fait actuellement en temps différé au Centre de Calcul de l'O.N.E.R.A.

THE NEAR FIELD SOUND PRESSURES OF A CHOKED JET DURING A SCREECH CYCLE

by

R. Westley and J. H. Woolley

Structures Dept., National Aeronautical Establishment,
National Research Council of Canada, Ottawa

SUMMARY

An experimental investigation was completed of the distribution of the instantaneous near field sound pressures during the axisymmetric screech mode of a choked air jet.

The data supplements a previous report by the same authors on the near field sound pressure levels and spectra of a similar jet.

The investigation helps to clarify certain aspects of jet screech mechanism and provides data for predicting structural response in the near field.

SYMBOLS

x	axial distance from nozzle
y	radial distance from jet axis
t	time
t_o	time of trigger sound wave at reference microphone
$p(t,x,y)$	jet sound pressure at moving microphone
$p_{1/3}(t,x,y)$	screech sound pressure after $\frac{1}{3}$ octave filter
$p_{1/3max}(x)$	maximum screech sound pressure, (y = const., t = const.)
$p_{1/3min}(x)$	minimum screech sound pressure, (y = const., t = const.)
$p_o(t)$	jet sound pressure at reference microphone
f	screech frequency at reference microphone
$\phi/2\pi f$	time delay relative to reference microphone
n	integer

IT HAS BEEN NOTED that the sound spectra of choked jets display additional features to those of subsonic jets. These features include screech tones that can be enhanced or suppressed by the position of upstream sound reflectors, broad band peaks and a spreading of the bandwidth of the background noise.

Investigations of the screech tones of choked jets (1,2,3,4,5,6,7) were limited for some years to the study of model jets. A generally accepted explanation (1,2) of the screech mechanism was that a flow disturbance emitted a sound wave as it passed through a standing shock wave in the jet. The emitted sound wave then travelled upstream through the ambient air and released a new flow disturbance at the nozzel lip. This new disturbance was amplified as it travelled downstream with the mixing region flow and the feed back loop was completed when the disturbance reached the original shock wave. In the case of a jet with an upstream sound reflector it has been pointed out (8) that the feed back loop should include the additional time required for the sound wave to travel from the jet nozzle to the reflector and to return. These original model investigations included the measurement of the screech frequencies and comparison with the theoretical predictions, flow and sound visualisations, measurements of the root mean square sound pressure fluctuations near the jet boundary and identification of axisymmetric and spiralling modes of oscillation of the jet.

More recently screech frequencies and broad band peaks have been observed on full scale jet engines when operating under choked conditions at altitude. Reports of associated aircraft structural fatigue (9,10), interference with laminar boundary layer flow during flight tests (11) and the annoyance of crew or passengers within an aircraft suggest that studies of choked jet noise may have important applications. The fitting of fan engines to subsonic jet transport aircraft may free this type of aircraft from choked jet noise problems but, on the other hand, future supersonic transport aircraft will be fitted with engine nozzles that are choked with high pressure ratios.

The object of this investigation was to extend the near field scund pressure level data that was reported in ref. (12). In particular detailed information is required on the instantaneous sound pressure distributions near a choked jet during a screech cycle. This information is needed, firstly, to predict the response of a structure placed in the near field sound and, secondly, to obtain a better understanding of the details of the jet screech mechanism.

This report describes an experimental investigation of the pressure field cycle near a 2.25 in. diameter cold air jet, with nozzle pressure ratio of 3.1, when the jet was oscillating in the axisymmetric mode at a screech frequency of 3170 c/s.

EXPERIMENTAL APPARATUS

A block diagram of the equipment which was used to measure the sound pressure fields at various times during the jet screech cycle is shown in Fig. 1.

High pressure air was supplied through a 6 in. diam. pipe to a contraction section and to a parallel nozzle with internal diameter of 2.25 in. and length of 4.2 in. An 11 in. diam. pipe flange was situated 3.9 in. upstream of the nozzle lip.

A $\frac{1}{4}$ in. diam. condenser microphone could be motor driven at a speed of approximately 1 in. per sec., for a distance of up to 30 in., along a centre-line which was parallel to the axis of the jet. The axial distance, x, of the microphone from the nozzle was measured on a position potentiometer and was used as the input to the horizontal sweep of an oscilloscope. The jet sound pressure, $p(t,x)$, with t as time, was fed through a $\frac{1}{3}$ octave filter to give a screech pressure signal, $p_{1/3}(t,x)$, that was connected to the vertical deflection of the oscilloscope. Therefore the oscilloscope display consisted of a compressed trace of $p_{1/3}(t,x)$ versus x with the trace enclosed between the peak to peak envelope, $p_{1/3max}(x)$ and $p_{1/3min}(x)$.

The position on this display of the instantaneous axial distribution of screech pressure, for a selected time during the screech cycle, was obtained by trace intensity modulation at times $t = (t_o+\phi/2\pi f+n/f)$, where t_o was the time that a screech wave with zero pressure and positive slope passed a fixed reference microphone, ϕ was a selectable phase delay, f was the screech frequency and n was various integers. The reference microphone, which was used to trigger the trace intensity modulation, was located in the plane of the nozzle at a point 0.5 in. below the jet boundary. The reference sound pressure output, $p_o(t)$, was passed through a $\frac{1}{3}$ octave filter to yield the reference screech signal, $p_{o1/3}(t)$. The screech signal was converted by the stroboscope unit into timing spikes and delayed by a selectable phase delay, ϕ, to fire the oscilloscope intensity modulation at the required times. Thus the intensified curve $p_{1/3}(\phi/2\pi f,x)$ versus x appeared across the display of $p_{1/3}(t,x)$.

Interconnection of the timing pulses, with the spark control of a schlieren system, allowed photographs of sound and jet flow visualisation to be taken at the same selected time during the screech cycle.

The sound pressure level at the moving microphone was recorded on a trace recorder.

The translation of the axial traverse line of the microphone to a new radial distance, y, enabled one to plot the near field instantaneous screech pressure distribution, $p_{1/3}(\phi/2\pi f,x,y)$, over the whole of an axial plane of the jet and for various selected times during the screech cycle.

NEAR FIELD SOUND PRESSURE LEVELS

The root mean squares of the screech pressure over the cycle are plotted as sound pressure level contours in Fig. 3.

The distinctive features (12) are noted and include a series of standing wave type lobes that run almost perpendicular to the jet axis. The two strongest lobes are located opposite the 3rd and 4th shock cells with maxima sound pressure levels of above 165 db at the jet boundary. Three other maxima are found along the jet boundary at the downstream end of the 2nd cell, at the 1st shock wave and at a position slightly downstream from the nozzle with sound level pressures respectively of approximately 160, 155 and 150 db.

It will be noted that the lobe opposite the 1st shock wave extends only a short distance from the jet boundary. The standing wave pattern of sound reflections from the pipe flange become evident in the area between the nozzle and the flange. The sound pressure levels fall to about 130 to 140 db in regions 10 in. away from the axis or 20 in. downstream from the nozzle.

INSTANTANEOUS PRESSURE DISTRIBUTIONS NEAR JET BOUNDARY

Typical distributions of the instantaneous screech pressure along two axial traverses near the jet boundary at y = 2 in. and 3.75 in. are shown in Fig. 4 for reference microphone phase delays of ϕ = 0 and 90 deg. The traverse, (a), very close to the jet boundary illustrates the out of phase relation between sound pressures at the 3rd and 4th cells for ϕ = 0 deg., and the general movement of the whole sound wave distribution in a downstream direction as time increases from ϕ = 0 to 90 deg.

A noteworthy feature of the sound wave distribution along traverse, (b), at y = 3.75 in. is that the portion of the wave upstream of the 3rd shock wave appears to be travelling towards the flange while the portion of the wave downstream of this shock wave appears to be travelling in the downstream direction.

INSTANTANEOUS PRESSURE DISTRIBUTIONS OVER NEAR FIELD

Contours of sound pressure distributions for four typical near fields are plotted in Figs. 5, 6, 7 and 8 and correspond respectively to phase delays of ϕ = 0, 60, 120 and 180 deg. or a time sequence of t = 0, 53, 105 and 158 μsec. By examining the four fields in sequence, one can visualise the motion of the pressure field during the first half of the screech cycle. A photograph of a model of the pressure field for ϕ = 60 deg. is shown in Fig. 2.

A distinct feature, almost independent of time, is the zero pressure line that runs approximately from the point, (x = 10 in., y = 8 in.), to the point, (x = 6.5 in., y = 3.5 in.), and which continues, at certain times, to the edge of the third shock wave. This line occupies the position of the prominent trough that was seen between the two strongest lobes in the sound pressure level contours of Fig. 3. The line appears to radially bisect a series of roughly concentric waves which have opposite signs on opposite sides of the bisector.

The concentric waves appear to expand outwards from the surfaces of the 3rd and 4th cells and travel in the upstream, downstream and outward directions with their amplitude being modulated as they pass through the partial standing wave pattern shown in Fig. 3.

Very near to the jet and in a region bounded approximately by the jet boundary and a line drawn from the jet nozzle to the point, (x = 6.5 in., y = 3.5 in.), one notes that two pressure maxima and two pressure minima are being amplified and convected in a downstream direction. As the convected waves enter the area of the 3rd and 4th shock cells, it appears that the two main sources of the concentric waves undergo a reversal of pressure and the concentric wave system is displaced outwards by a half wavelength.

Many quantitative and qualitative details may be extracted from the instantaneous pressure fields for the complete cycle and the remainder of this paper will be limited to an examination of the time history of the "convected" and "radiated" wave distributions along the previously mentioned jet boundary traverse line, (a), and the near field traverse line, (b).

MOTION OF PRESSURE WAVES AT JET BOUNDARY, (y = 2 in.)

Details of the convection of the pressure waves distributed along the jet boundary at y = 2 in. are shown in Fig. 9. The curves show the time history of the axial displacements of the pressure maxima ($p_{1/3max}$), the pressure minima ($p_{1/3min}$), the zero pressures and the ± 3 × 7.7 mb. contours during three screech cycles.

One may trace the motion of the pressure maximum that appears to start from the flange at time, $\phi = 0.5\ \pi$. The maximum pressure passes through two standing wave anti-nodes, which are located between the flange and the nozzle and just downstream of the nozzle, at times $\phi = 1.5\ \pi$ and $2.5\ \pi$ respectively. The convection speed of the maximum pressure is reduced initially to about 0.52 of the speed of sound at approximately the middle of the 1st shock cell and the pressure peak passes the anti-node near the 1st shock wave, at time, $\phi = 3.67\ \pi$. Subsequently the pressure peak passes the anti-node in front of the 2nd shock wave at $\phi = 4.83\ \pi$, the anti-node between the 2nd and 3rd shock waves at $\phi = 6.00\ \pi$, the anti-node between the 3rd and 4th shock waves at $\phi = 7.17\ \pi$ and the next two anti-nodes at $\phi = 8.25\ \pi$ and $9.34\ \pi$ respectively.

The convection speed of the peak pressure increased to approximately 0.72 of the speed of sound in the region of the 3rd and 4th cells. It will be noted that, in the region of the jet between the nozzle and the 3rd cell, the peak pressure crosses anti-nodes at a time interval of approximately $\phi = 1.17\ \pi$.

The time position of the crossing points of adjacent maximum and minimum pressures with the anti-nodes have been joined by a broken line to show the time lags along the jet.

It will also be noted that a straight line can be drawn through the crossing points of the pressure maxima with the anti-nodes. This line has a slope equal to the speed of sound, it is directed in the upstream direction and, when drawn from the 3rd shock cell, will intersect the flange at time, $\phi = 10.5\ \pi$, which is exactly 5 screech cycles after the convected maximum pressure left the flange. This is in agreement with the predictions of ref. 8 although one could more generally point out from Fig. 9 that a feed-back loop chosen between any two anti-nodes would predict exactly the same frequency.

MOTION OF PRESSURE WAVES ALONG NEAR TRAVERSE, (y = 3.75 in.)

The motion of the axial pressure distribution along the line, y = 3.75 in., is shown in Fig. 10 during the period of three screech cycles. It shows the divergence of the upstream and the downstream radiations of pressure from the 3rd shock wave position. The mean speed of propagation of both sets of waves is approximately equal to the speed of sound. It will be noted that the maximum pressure peak of the upstream radiation reaches the flange at the time, $\phi = 10.5\ \pi$, and confirms the conjecture of the flange "feed-back loop" which was suggested by the jet boundary pressure distributions.

CONCLUSIONS

A relatively simple experimental technique has been developed to study the instantaneous pressure distributions of sound pressure in the near field of a choked jet during a screech cycle.

Measurements are given of the near field sound pressures of a 2.25 in. diam. jet when operating at a pressure ratio of 3.1 and screeching in the axisymmetric mode with a frequency of 3170 c/s.

A strong source of pressure radiation is found at the 3rd and 4th shock cells.

The radiation at the 3rd cell leads the 4th cell by approximately $1\frac{1}{6}\ \pi$.

The near field pressure consists of partial standing waves formed by the interaction of shock cell distributed sources, flange reflections and a convected pressure field associated with jet flow disturbances.

Flow disturbances appear to be released at the first cell by the standing wave pressure field formed by the flange.

The frequency of the screech is consistent with flange reflection feed-back theory although it is noted that more general feed-back loops, which include any pair of anti-nodes, would predict the same frequency.

In calculating feed-back loop times it should be recalled that the mean speed of disturbances within the jet appears to increase in the jet direction and that local acceleration and retardation of the disturbance may occur in each cell.

REFERENCES

1. Powell, A. — On the Mechanism of Choked Jet Noise. Proc. Phys. Soc. London, Sect. B, Vol. 66, 1953, pp. 1039-1056.

2. Powell, A. — On the Noise Emanating from a Two Dimensional Jet above the Critical Pressure. The Aeronautical Quarterly, Vol. IV, Part II, Feb. 1953, pp. 103-122.

3. Merle, M. — Ondes sonores émises par un jet d'air. Comptes Rendus de L'Académie des Sciences, Paris, Vol. 240, No. 21, 1955, pp. 2055-2057.

4. Lassiter, L.W. Hubbard, H.H. — The Near Noise Field of Static Jets and Some Model Studies of Devices for Noise Reduction. NACA Report 1261, National Advisory Committee for Aeronautics, Washington, 1956.

5. Lee, R. Kendall, R. et al. — Research Investigation of the Generation and Suppression of Jet Noises. Flight Propulsion Lab., General Electric Co., Cincinnatti, Ohio, 1961.

6. Hammitt, A.G. — Oscillation and Noise of an Overpressure Sonic Jet. J. Aerospace Sci., Vol. 28, No. 9, 1961, pp. 673-680.

7. Davies, M.G. Oldfield, D.E.S. — Tones from a Choked Axi-Symmetric Jet. ACUSTICA, Vol. 12, No. 4, 1962, pp. 257-277.

8. Poldervaart, L.J. Wijnands, A.P.J. Jongsma, F.H.M. — On the Production of Discrete Frequencies in the Noise Spectrum of a Supersonic Jet. Eindhoven University of Technology, Preliminary Report, A.R.C. Noise Sub-Committee Meeting, 26 Nov. 1968.

9. Clarkson, B.L. — The Development of a Design Procedure for Acoustic Fatigue. ISAV, Rept. 198, Institute of Sound and Vibration Research, University of Southampton, Sept. 1967.

10. McElhinney, D.M. — Designing to Combat Fatigue. Aircraft Engineering, Vol. 39, No. 10, 1967, p. 6.

11. Carmichael, R.F. Pelke, D.E. — In-Flight Measurements on the X-21A Laminar Flow Aircraft. Northrop Norair Report NOR-64-81, April 1964.

12. Westley, R. Woolley, J.H. — An Investigation of the Near Noise Fields of a Choked Axi-symmetric Air Jet. National Research Council, N.A.E. LR-506, June 1968.

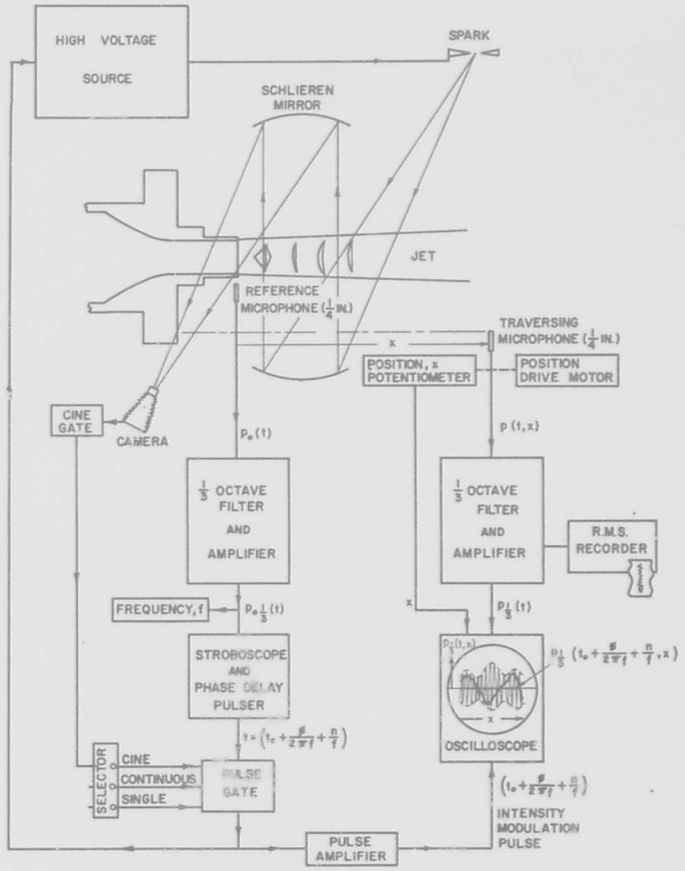

FIG. 1 MEASUREMENT OF NEAR FIELD INSTANTANEOUS SOUND PRESSURE

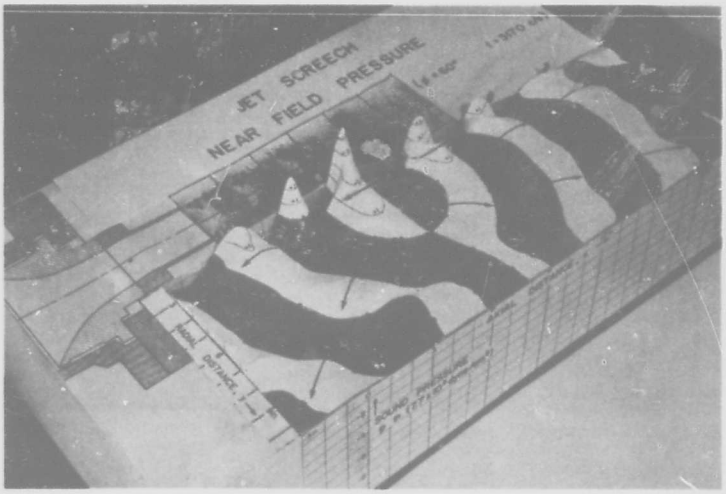

FIG. 2 NEAR FIELD PRESSURE DISTRIBUTION OF JET SCREECH

$\phi = 60°$ f = 3170 c/s

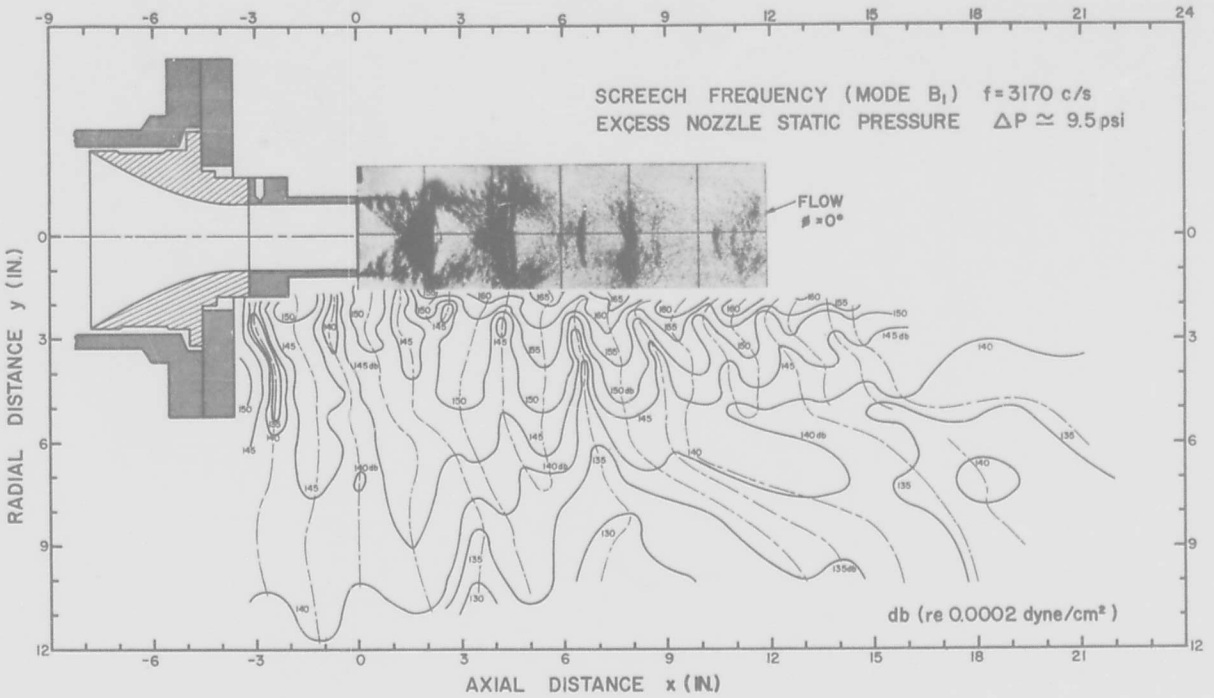

FIG. 3 SOUND PRESSURE LEVEL NEAR FIELD

S.P.L. $\frac{1}{3}$ OCT.

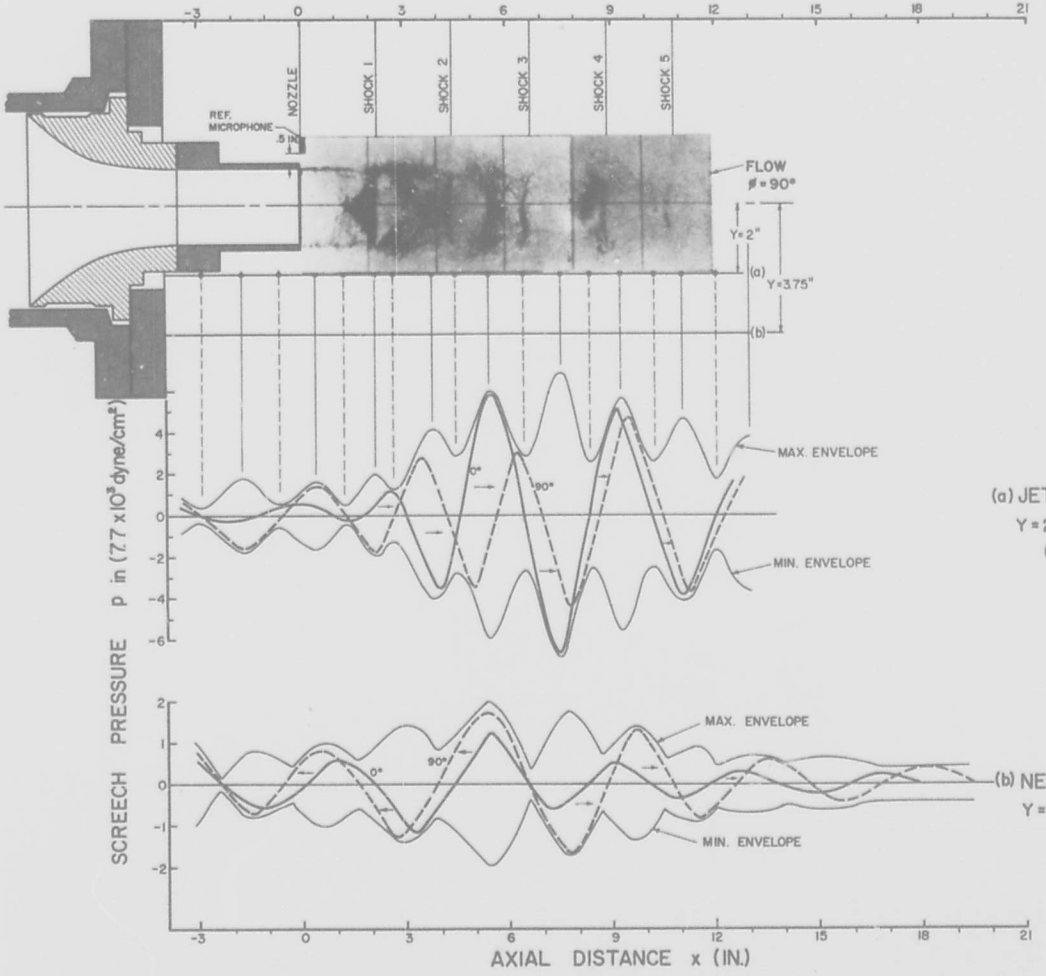

(a) JET BOUNDARY TRAVERSE
Y = 2", ϕ = 0°, 90°
(Δt = 0, 78 μ sec)

(b) NEAR FIELD TRAVERSE
Y = 3.75", ϕ = 0°, 90°
(Δt = 0, 78 μ sec)

FIG. 4 SCREECH PRESSURE DISTRIBUTION, (p – x)
(f = 3170 c/s , 1/3 OCTAVE FILTER)

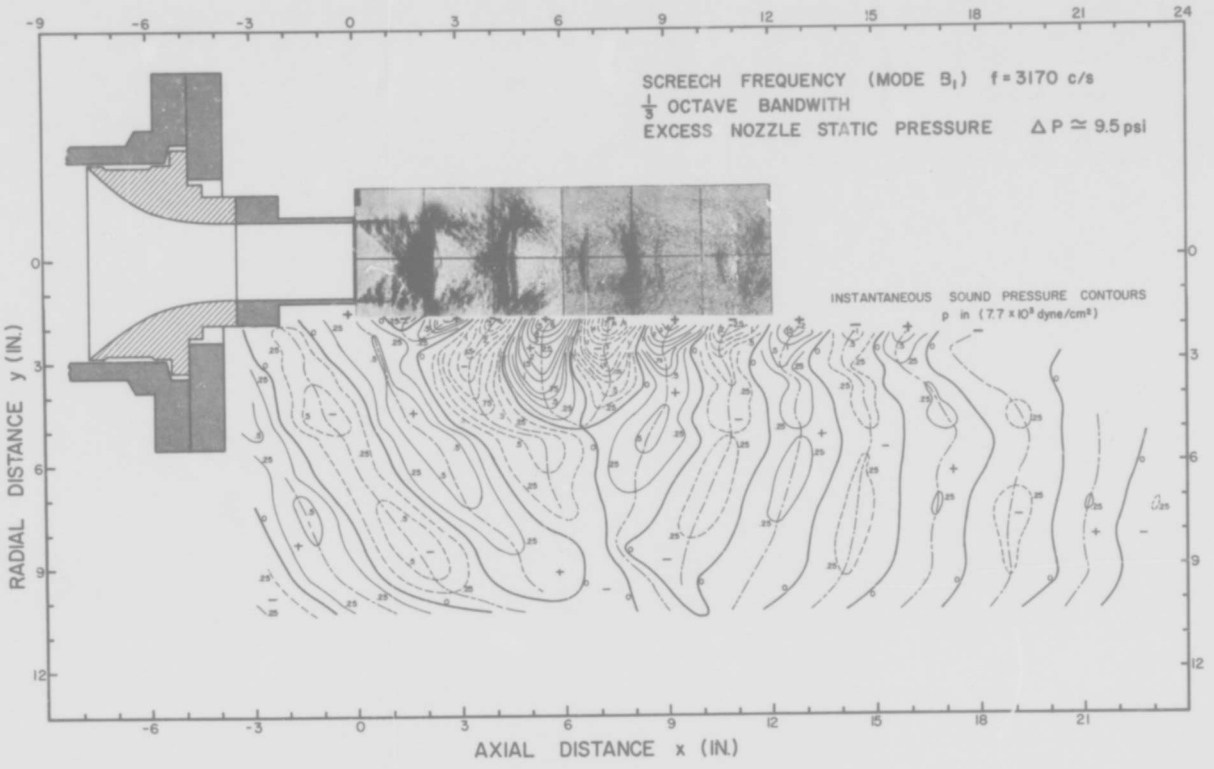

FIG. 5 SOUND PRESSURE DURING SCREECH CYCLE ($\phi = 0°$)

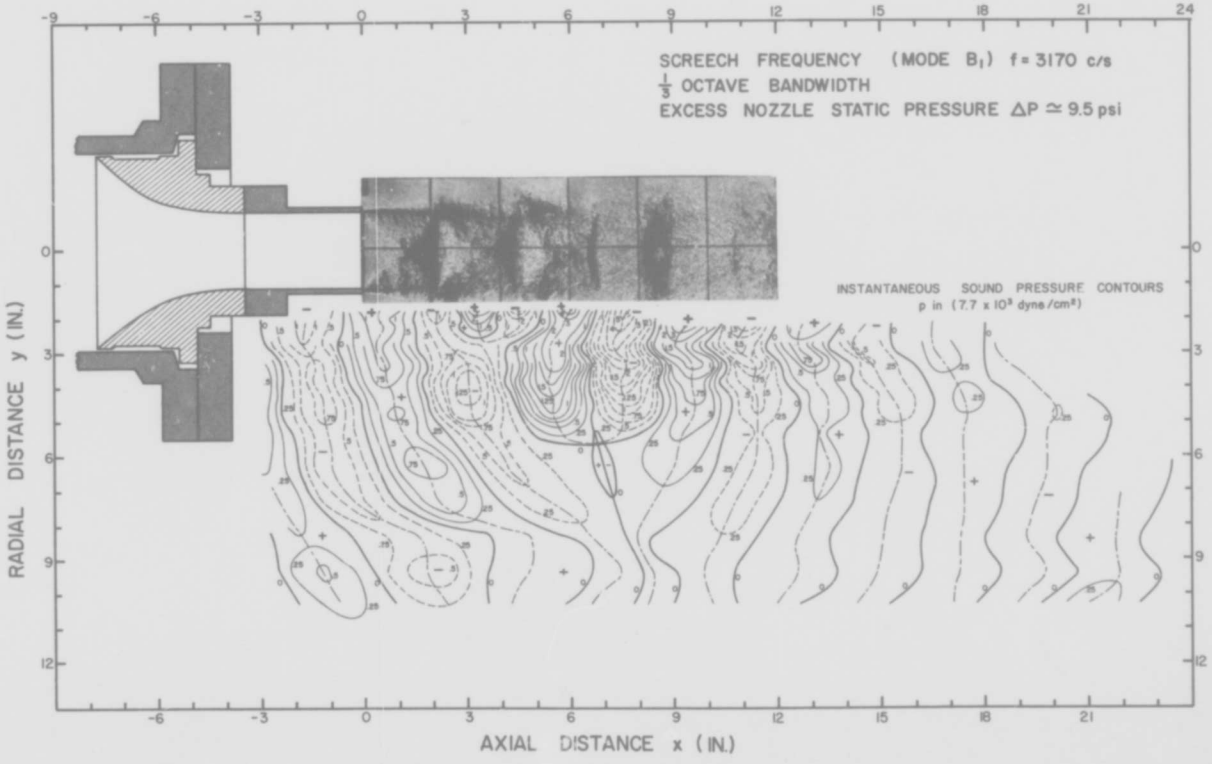

FIG. 6 SOUND PRESSURE DURING SCREECH CYCLE (ϕ = 60°)

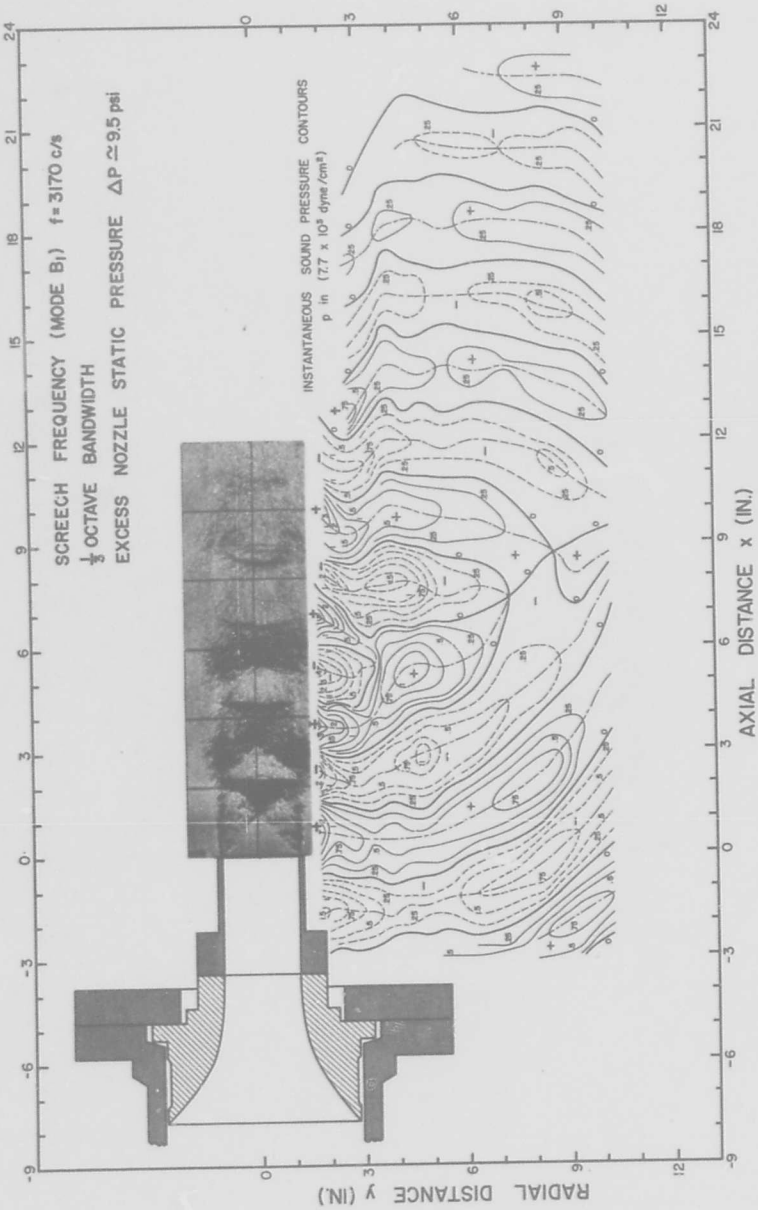

FIG. 7 SOUND PRESSURE DURING SCREECH CYCLE ($\phi = 120°$)

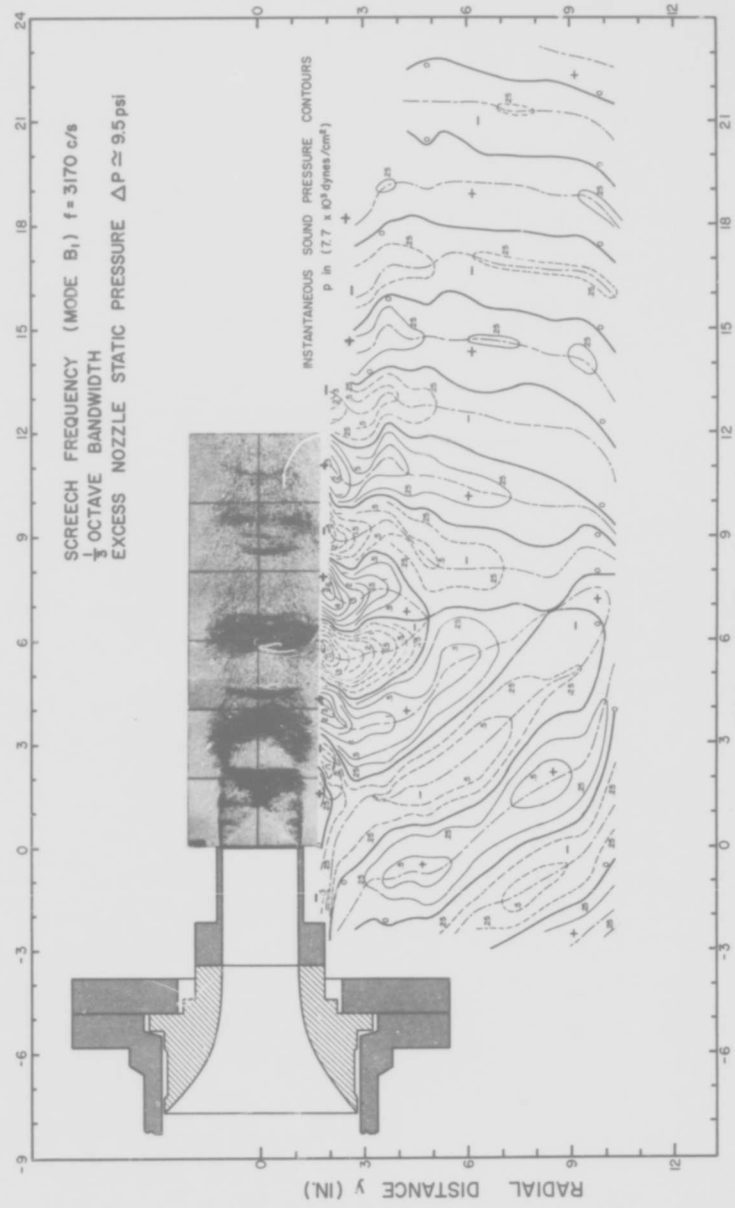

FIG. 8 SOUND PRESSURE DURING SCREECH CYCLE ($\phi = 180°$)

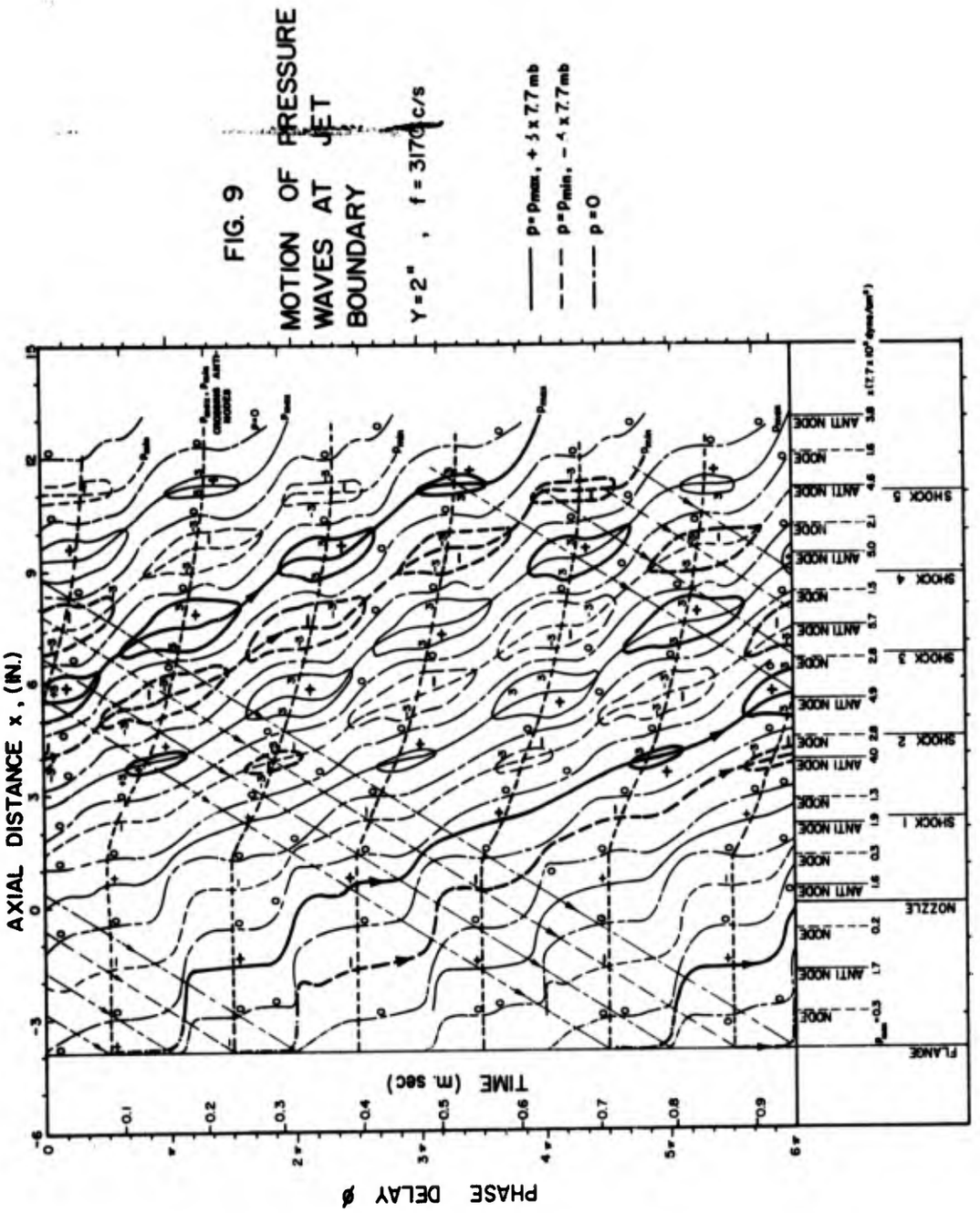
FIG. 9
MOTION OF PRESSURE WAVES AT JET BOUNDARY
Y = 2" , f = 3170 c/s
p = pmax. , + 3 x 7.7 mb
p = pmin. , - 4 x 7.7 mb
p = 0
AXIAL DISTANCE x , (IN.)
TIME (m. sec)
PHASE DELAY ø
PLANE
NOZZLE
SHOCK 1
SHOCK 2
SHOCK 3
SHOCK 4
SHOCK 5
ANTI NODE
NODE

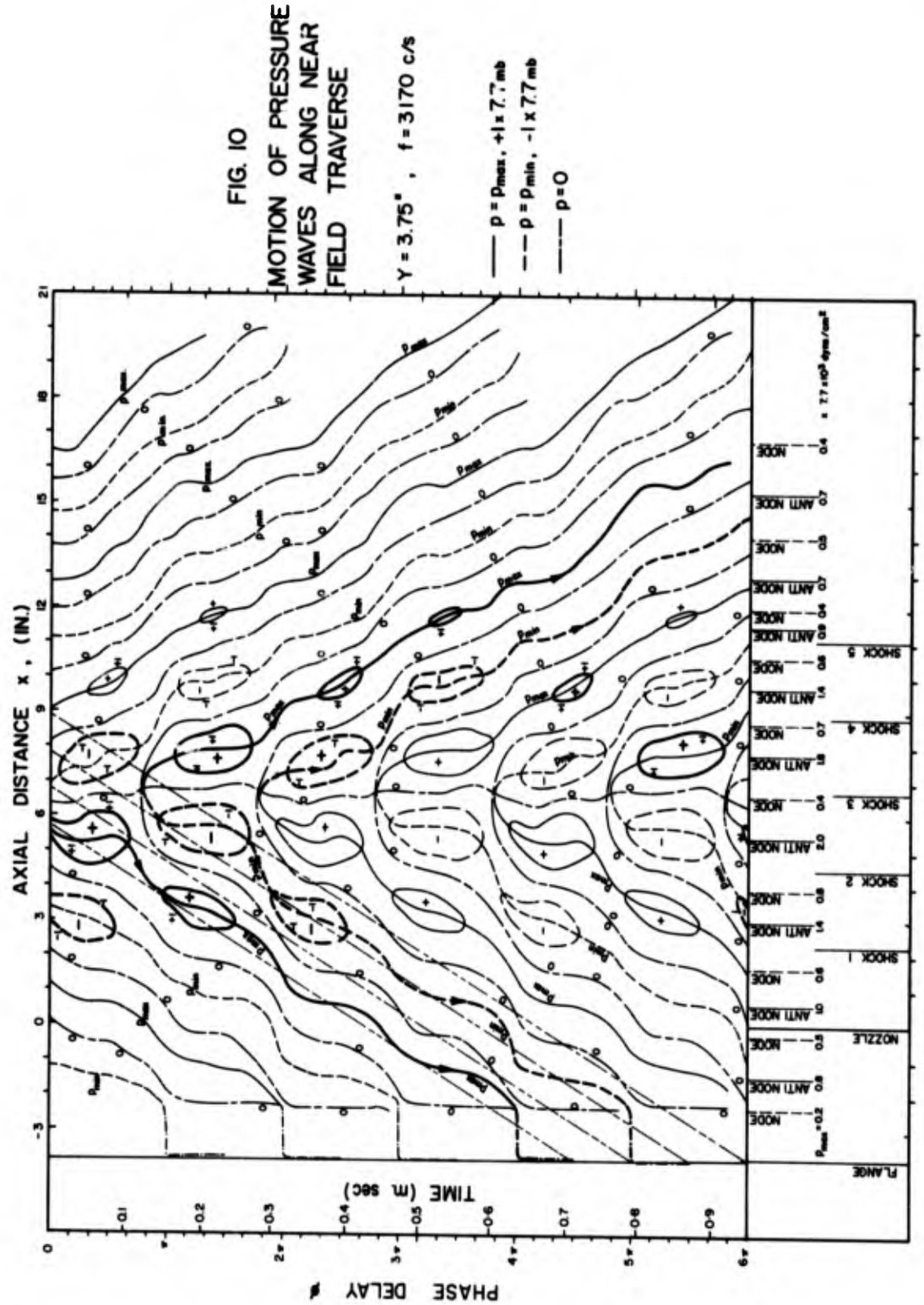
FIG. 10
MOTION OF PRESSURE WAVES ALONG NEAR FIELD TRAVERSE
Y = 3.75" , f = 3170 c/s
p = pmax, +1 x 7.7 mb
p = pmin, -1 x 7.7 mb
p = 0
AXIAL DISTANCE x , (IN.)
TIME (m sec)
PHASE DELAY ϕ
FLANGE
NOZZLE
SHOCK 1
SHOCK 2
SHOCK 3
SHOCK 4
SHOCK 5
NODE
ANTI NODE

ETUDE DU BRUIT DES AVIONS AU DECOLLAGE

par

I. P. A. PIANKO MARC

STAé - PARIS

S O M M A I R E

On étudie d'abord les trajectoires optimales pour minimiser le bruit d'un avion au décollage. La détermination de ces trajectoires met en valeur les paramètres de l'avion qui (à part la bruyance du moteur) déterminent le bruit au décollage. L'influence relative de chaque paramètre est calculée. On examine également dans quelle mesure les résultats sont modifiés par l'introduction des effectifs PNDB (correction de durée). Enfin on étudie l'influence de la technologie du moteur, ses contraintes et limitations sur les progrès futurs en matière de bruit au décollage.

NOTATIONS

Indice 0	:	point fixe au sol
Indice 1	:	en vol au régime de décollage
Indice 2	:	en vol après la réduction
Indice max ou m	:	maximum
Cx	:	coefficient de trainée
Cz	:	coefficient de portance
d	:	distance
D	:	débit en kg/s
F	:	poussée en daN (ou N)
g	:	accélération de la pesanteur en m/s2
g(θ) ou g(β)	:	champ sonore linéaire c'est à dire Nm - N en fonction de θ (ou de β)
h	:	distance du point de mesure à la trajectoire
L	:	longueur de décollage conventionnelle
log	:	logarithme décimal
Log	:	logarithme neperien
m	:	masse de l'avion
M	:	nombre de Mach
N ou $\mathcal{N}$	:	niveau de bruit en PNDB
S	:	surface de l'aile en m^2
s	:	section d'entrée du réacteur en m^2
t	:	temps en secondes
Ue	:	vitesse périphérique en bout d'aube du 1er étage compresseur en m/s
x	:	abscisse
z	:	altitude en mètres
α	:	angle de montée
β	:	angle du rayon sonore avec la trajectoire
γ	:	$\pi - \delta$
δ, ω	:	angles
θ	:	angle du rayon sonore avec l'horizontale
ξ	:	assiette de l'avion
λ	:	absorption atmosphérique par 1000 m en PNDB
φ	:	finesse de l'avion pendant la montée

<u>Unités acoustiques</u>

db	:	déçibel
PNdb	:	niveau de bruit perçu
EPNdb	:	niveau de bruit perçu effectif

ETUDE DU BRUIT DES AVIONS AU DECOLLAGE

I. P. A. PIANKO MARC

1.- TRAJECTOIRES OPTIMALES

1.1.- Introduction

Lorsqu'on aborde le problème du bruit crée par le trafic aérien autour des aéroports, la première réaction du grand public est d'incriminer le moteur.

Sans nier que la source du bruit est effectivement le moteur, nous devons dire tout de suite, en anticipant sur les conclusions de cette étude, qu'en fait la gêne que perçoit un observateur placé sous la trace de décollage, est une fonction complexe de divers paramètres dont certains spécifiquement aérodynamiques c'est à dire liés à la conception même des avions. Pendant longtemps la contrainte de bruit n'est pas intervenue au stade de la conception des avions. L'une des premières données propres aux avions sur lesquels on a travaillé pour diminuer le bruit au décollage fut une procédure dite "antibruit" qui n'est pas autre chose qu'une réduction de la poussée et par conséquent de la pente de montée.

1.2.- Recherche du point de réduction

1.2.1.- Position du problème

Nous allons donc commencer par la recherche d'une trajectoire optimisée par rapport au point de mesure . Le problème posé est le suivant. Un avion étant donné, ainsi qu'un point de mesure M fixé sous la trace, nous cherchons le point de réduction R qui permet d'enregistrer en M le niveau de bruit minimal. Sur la fig. 1 (planche n° 1), la trajectoire est schématisée par les angles α_1 et α_2. α_1 est déterminé par le régime de décollage du (ou des) moteur (s). Quand à l'angle α_2, sa valeur est arbitraire mais il est évident que pour minimiser le bruit en M, on a intérêt à prendre $\alpha_2 = 0$. Cependant, des règles de sécurité imposent une valeur minimale de α_2.

Avant de regarder ce qui se passe sur la trajectoire de décollage, examinons le bruit en M lorsque l'avion effectue un survol horizontal (voir fig. 2). Le bruit enregistré au point M à l'allure indiquée sur la fig. 3, en fonction de l'angle β formé par le rayon sonore et la trajectoire. Le maximum Nm est atteint pour une valeur β_m dont la valeur est en général comprise entre 130 et 150°. La courbe de la fig. 3, appelée champs sonore linéaire dépend de plusieurs paramètres qui sont essentiellement :

- le cycle moteur ou les conditions génératrices du jet (P, T)
- la vitesse de vol
- la distance h
- le mode d'installation des moteurs sur l'avion
- l'assiette de l'avion

La variation de Nm en fonction de la distance suit la loi en $20 \log \frac{1}{d}$, corrigée de l'absorption atmosphérique. En général, on peut représenter Nm en PNdb par $K \log \frac{1}{d}$, K dépendant du cycle et de la taille du moteur. Pour l'ensemble des moteurs, on peut dire que K varie entre 20 et 30.

Lorsque le bruit prédominant est le bruit de jet la valeur de K est

$$K = 20 + \frac{\lambda h}{435}$$

λ, l'attenuation atmosphérique en PNDB par 1000 m dépend essentiellement du diamètre de la tuyère et de la poussée spécifique en vol $\frac{F1}{D1}$. Les valeurs de λ sont données sur la planche n° 3.

Lorsque le bruit prédominant est le bruit de compresseur, K dépend de nombreux paramètres tels que diamètre du compresseur, vitesse périphérique, nombre d'aubes mais sa valeur est, en général, voisine de 27.

1.2.2.- Critère d'optimum

Si nous revenons à notre avion qui réduit au point R, il produira en M un bruit qui aura l'allure représentée sur la fig. 4 (planche n° 2), en fonction de l'angle θ. On distingue 2 tronçons de ligne. La première ligne (L1) est le champs sonore correspondant à la trajectoire initiale (angle α_1). Pour $\theta = \theta r$ où le niveau sonore atteint une valeur NR, la réduction produit une discontinuité. Puis on obtient la ligne (L2) qui est la portion de champ sonore correspondant aux conditions de vol après la réduction. Sur (L2) on obtient le maximum NT provenant de l'angle d'émission max β_m. Le premier maximum atteint NR, est inférieur à Nim, qu'on aurait atteint s'il n'y avait pas eu réduction.

Comme ce qui détermine le bruit en M, c'est le maximum du niveau sonore, il s'ensuit que le point de réduction cherché est celui qui entraine l'égalité de NR et NT.

En effet supposons qu'on ait trouvé un point R ($\theta = \theta r$) qui réalise l'égalité NR = NT. Si on avait réduit plus tôt, l'examen de la ligne (L1) montre que la première bosse serait diminuée, mais comme la distance MH_2 serait plus petite la deuxième bosse NT serait plus forte, donc le bruit M serait plus grand. Inversement, une réduction plus tardive augmenterait la valeur de la première bosse, donc le bruit en M serait également plus grand.

1.2.3.- Mise en équation

On peut écrire que le bruit $\mathcal{N}_1$ sur la ligne L1 peut être représenté par : $\mathcal{N}_1(\theta) = N1m - K1 \log \frac{h1}{ho} - g1(\beta)$. N1m est le bruit émis à l'angle d'émission maximum $\beta m1$, à la distance h_o de référence. K1 est la valeur de K correspondant au premier tronçon de la trajectoire. En choisissant h1 égale à ho, on simplifie le problème et $\mathcal{N}1(0) = N1m - g1(\beta)$. La fonction $g1(\beta)$ représente le champ sonore sur le premier tronçon de la trajectoire dont l'origine (0) serait placé pour $\mathcal{N} = N1m$.

De même sur la deuxième ligne (L2) le niveau de bruit peut être représenté par :

$$\mathcal{N}2 = N2m - K2 \log \frac{h2}{h1} - g2(\beta)$$

K2 n'est pas égal à K1 car sur le deuxième tronçon les paramètres du moteur ont changé (réduction). $g2(\beta)$ représente le champ sonore sur le deuxième tronçon de la trajectoire.

Sur la première ligne (L1), la bosse NR est obtenue pour θr. Comme $\beta r = \theta r + \alpha 1$, $NR = N_{1m} - g1(\theta r + \alpha 1)$.

Sur la 2ème ligne (L2), la bosse NT provient de $\beta 2m$ c'est à dire pour une valeur de β où $g2(\beta) = 0$.

Donc : $NT = N2m - K2 \log \frac{h2}{h1}$

L'égalité de NR et NT entraine donc :

$$N1m = N2m = -K2 \log \frac{h2}{h1} + g1(\theta r + \alpha 1)$$

1.2.4.- Résolution

Sur la fig. 1 bis on voit que $h1 = MR \sin(\theta r + \alpha 1)$
$h2 = MR \sin(\theta r + \alpha 2)$

soit $h2 = h1 \frac{\sin(\theta r + \alpha 2)}{\sin(\theta r + \alpha 1)}$

L'équation devient donc :

$$N_{1m} - N_{2m} = +K2 \log \frac{\sin(\theta r + \alpha 1)}{\sin(\theta r + \alpha 2)} + g1(\theta r + \alpha 1)$$

La résolution est possible par itérations. On résoud d'abord l'équation :

$N1m - N2m = g_1(\beta r1)$

Graphiquement, ainsi qu'indiqué sur la fig. 5, on obtient une première valeur $\beta r1$. Puis on cherche une meilleure approximation $\beta r2$ par l'équation $N1m - N2m - K2 \log \frac{\sin \beta r_2}{\sin(\theta r + \alpha 2)} = g_1(\beta r2)$ et ainsi de suite. Trois itérations suffisent en général pour donner la valeur βr cherchée.

Le niveau de bruit en M sera $N1m - g1(\beta r)$, alors que sans la réduction il aurait été N1m. Le gain obtenu grâce à la réduction est donc $g1(\beta r)$.

Remarque très importante

Il convient de remarquer que le champ sonore $g1(\beta)$ (fig. 5) correspondant au premier tronçon de la trajectoire est différent du champ sonore obtenu pendant un survol horizontal. En effet, pendant la montée, l'assiette de l'avion est différente de celle du survol en palier et ce fait modifie le champ sonore (déplacement de l'angle d'émission maximale et variation de la forme).

De même la valeur Nm, maximum du niveau sonore pendant un décollage sans réduction est différente du maximum pendant un vol en palier à la même distance toujours à cause du changement d'assiette. Si pendant le vol horizontal le niveau de bruit est représenté par $\mathcal{N}h(\beta) = Nm - g(\beta)$, pendant la montée (à la même distance et même vitesse) le niveau de bruit est donné par $\mathcal{N}v(\beta) = Nm - K1 \log \frac{\sin(\beta + \Delta\xi)}{\sin\beta} - g(\beta + \Delta\xi)$ où $\Delta\xi$ est la différence d'assiette.

Le maximum de $\mathcal{N}h$ est Nm; mais le maximum de $\mathcal{N}v$ est voisin de $Nm - K1 \log \frac{\sin(\beta m)}{\sin(\beta m - \Delta\xi)}$ > Nm car βm est de l'ordre de 130° à 150°. ($g(\beta m) = o$).

Remarque importante

L'angle β est l'angle correspondant au point où le bruit a été émis et non pas l'angle du point où se trouve l'avion au moment où l'on perçoit le niveau de bruit.

1.3.- Conséquences

1.3.1.- Importance du champ sonore

On remarque que pour déterminer le point de réduction optimum, il faut connaitre le champ sonore de l'avion en vol. Le gain augmente lorsque la courbe g1 (β) est pointue. Or le champ sonore dépend également de la géométrie de l'avion, du mode d'installation des réacteurs en particulier. C'est donc un domaine où l'avionneur peut agir pour diminuer le bruit de l'avion.

Toutefois l'importance d'un supplément de gain apportée par un "bon" champ sonore est faible. A titre d'exemple deux champs sonores extrêmes connus actuellement donnent l'un 9,5 et l'autre 8 PNdB de gain de réduction. La différence n'est pas négligeable en soi, mais relativement au gain total de 9 PNdB, elle est secondaire. L'intervention du champs sonore peut être primordiale pour le motif suivant. C'est le champ sonore qui détermine le point de réduction. Un champ sonore aplati conduit à réduire trop tôt. Or il peut arriver que l'avion se trouve alors à une altitude où des normes de sécurité interdisent toute réduction. L'avion ne pourra donc réduire que plus tard. Or on verra plus loin qu'une réduction tardive (plus haut que l'optimum) fait perdre une grande partie du gain potentiel. Cette situation peut se produire sur des avions peu motorisés, ou ayant une faible finesse lors du décollage.

1.3.2.- Niveau de bruit en M

Le niveau de bruit en M est $N2m - K_2 \log \frac{h2}{h1}$. Les deux facteurs qui le déterminent sont d'une part N2m, la bruyance propre aux moteurs pour maintenir la pente α_2 fixée, et d'autre part l'altitude h2 atteinte. D'où :

1ère conséquence évidente = Pendant la première phase de montée (avant réduction) il faut atteindre l'altitude la plus haute possible. Or cette altitude dépend presque entièrement de la conception et des performances aérodynamiques de l'avion. Les paramètres qui déterminent la longueur de piste, c'est à dire le taux de motorisation, la charge alaire, la trainée, et le Czmax. ainsi que les paramètres qui déterminent la pente de montée initiale c'est à dire taux de motorisation et finesse ont donc ure importance primordiale sur le niveau de bruit en M.

Deux autres paramètres qui interviennent sont la vitesse de montée choisie et la configuration des volets. Il est évident que pour monter avec le plus grand angle α_1, il faut choisir la plus petite vitesse. Les normes de sécurité imposent une vitesse minimum V_2 mais pratiquement la plupart des avions choisissent une vitesse économique plus forte (+ 10, + 15 ou même + 20 KTS). La configuration des volets n'est pas choisie pour rendre h2 maximal mais par d'autres considérations. En fait dans chaque cas particulier il y a lieu d'étudier la configuration optimale des volets pour minimiser le niveau de bruit au point de mesure choisi.

Le moteur intervient uniquement par la variation de la poussée en fonction de la vitesse.

2ème conséquence = C'est le niveau du bruit du moteur à régime réduit qui est déterminant. Tous les efforts pour réduire le bruit du moteur à plein régime sont inutiles s'ils n'ont pas d'effet sur le bruit du moteur à régime réduit (après réduction). Ils peuvent même devenir nuisibles s'ils dégradent les performances du décollage et de la montée. Cela est vrai uniquement pour le bruit sous la trace de décollage d'un avion utilisant une réduction. Il est évident que pour le bruit latéral c'est la bruyance à plein régime qui importe.

Nous touchons ici le problème clé des silencieux qui créent une perte de poussée au décollage donc dégradent les performances de décollage et de montée et dont l'éfficacité acoustique diminue en général à faible régime. Il s'ensuit que le gain obtenu grâce aux silencieux sur les avions est toujours limité, et, en deça de ce que donne les silencieux au point fixe.

1.3.3.- Niveau de bruit sous la trace :

Le problème traité aux paragraphes précédents permet de minimiser le bruit en un point donné M. Mais il est indispensable d'examiner comment évolue le bruit ailleurs, sous la trace, lorsque la réduction est effectuée pour le point M. Appelons $\mathcal{C}_M$, la courbe qui représente le niveau sonore en fonction de la distance au point "lâcher de freins", la trajectoire comportant une réduction optimisée pour M (cf. fig. 8, planche n° 4).

Il existe sous la trace un point C tel que CR fait avec le premier tronçon de la trajectoire, l'angle β_{1m} d'émission maximale (voir fig. 9). Pour tous les points situés avant C, la réduction n'a aucune influence sur le niveau sonore puisque celui-ci est déterminé par l'angle d'émission maximale, rencontré avant que la réduction n'ait eu lieu. La prolongation de la courbe $\mathcal{C}_M$ en pointillé (fig. 8), représente l'évolution du bruit, pour une trajectoire de décollage sans réduction. C'est donc la courbe C_{∞}. Le niveau sur C_{∞} varie comme $K1 \log \frac{1}{\text{distance au point } \Omega 1}$.

Le point C est déterminé par :

$$\frac{MC}{MH1} = \frac{1}{\sin \beta r} \left\{ \cos \theta r + \sin \theta r \cot g \left(\gamma 1m + \alpha 1 \right) \right\}$$

$$\text{ou} \quad \gamma 1m = \pi - \beta 1m$$
$$\beta r = \theta r + \alpha 1$$

Pour un point P quelconque situé entre C et M, le niveau de bruit est donné par la première bosse c'est à dire le niveau sonore émis en R, car la réduction est faite trop tard.

Soit N(P) le bruit en P. P' un point voisin de P, $\Delta N = N(P') - N(P) < 0$. La diminution du niveau sonore de P à P' parvient d'une part de l'augmentation de l'angle γ (passage de P à P") et d'autre part de l'augmentation de la distance du point à la droite $\Delta 1$ (passage de P" à P'). Soit $\Delta N = \frac{\partial N}{\partial \gamma} \Delta \gamma + \frac{\partial N}{\partial d} \Delta d$.

Comme en C, $\gamma = \gamma 1m$ (angle d'émission maximale) et que $\frac{\partial N}{\partial \gamma} (\gamma 1m) = 0$, la variation du niveau sonore au point C provient uniquement de la variation de la distance (comme K1 log 1/distance).

En d'autres termes la courbe $\mathcal{C}M$ est tangente à $\mathcal{C}oo$, ou bien on peut dire aussi que la tangente à $\mathcal{C}M$ varie de façon continue au point C. Au delà du voisinage de C, la pente est assez forte et provient essentiellement de la variation de θ .

Pour un point Q, situé après le point M, la réduction est faite trop tôt, donc le niveau de bruit est déterminé par l'angle d'émission maximale θ 2m (2ème bosse). Le niveau sonore sur cette partie de M varie comme $K_2 \log \frac{1}{\Omega 2 Q}$ c'est à dire plus faiblement que sur C .

Cette analyse montre qu'en M la pente de $\mathcal{C}M$ subit une <u>discontinuité</u>.

Sur la fig. 8, on voit comment se placent les différentes courbes $\mathcal{C}M$. La courbe $\mathcal{C}*$ représente le lieu des niveaux sonores minimisés (ce n'est pas une enveloppe à cause des points anguleux).

Le réseau des courbes M est fonction, pour un avion donné de :

- la température extérieure
- l'humidité de l'air
- la masse de l'avion au décollage

Ce dernier paramètre modifie profondément le réseau. La connaissance pour chaque avion de tous les réseaux des courbes $\mathcal{C}M$ permettrait d'exploiter, au mieux, les possibilités de la réduction et de les adapter aux zônes d'habitations propres à chaque aéroport.

Actuellement les avions possèdent une procédure antibruit standard qui est le plus souvent une réduction à une <u>altitude donnée</u>.

La connaissance complète des points de réduction optimisés permettrait une meilleur protection de la population en choisissant une procédure en fonction de la zône à protéger et également en fonction de conditions météorologiques et de la masse de l'avion au décollage. Rappelons encore qu'on peut également obtenir une réduction du bruit en optimisant la configuration de l'avion (volets).

Le problème dont nous parlons ici est different de celui traité dans les paragraphes précédents ou nous avons résolu un problème <u>local</u>, associé à un point unique. La protection d'une zone habitée est un problème global. La solution dépend non seulement de la configuration géométrique de la zone considérée mais également de la densité de population. Par ailleurs il y a une difficulté à la base c'est la définition même du bruit minimal au dessus d'une zone habitée. La solution dépend donc également de la définition choisie.

1.3.4.. Problèmes de mesures

L'examen rapide de la fig. 8 montre immédiatement qu'une réduction faite trop tôt (courbe $\mathcal{C}P$) donne en M un niveau sonore légèrement plus élevé que la "bonne "réduction. Mais si la réduction est faite trop tard (courbe $\mathcal{C}Q$) alors l'augmentation du niveau sonore en M est très importante. Ce qu'il y a de remarquable c'est que la différence de bruit produite par les 3 réductions voisines est faible partout sauf précisément au point M où l'on cherche à minimiser le bruit.

Si la réduction est faite trop tôt en R', le bruit en M est donné par la 2ème bosse, donc la variation $\Delta N' = N' - N$ est $\frac{K2}{2,3} \frac{\Delta h2}{h2}$ (2,3 = Log 10).

Mais si la réduction est faite trop tard en R", le bruit en M est déterminé par la 1ère bosse, soit l'émission faite en R". La variation provient alors de $\Delta\beta = \Delta\theta$ et l'on a $\Delta N" = N" - N = \frac{\partial N}{\partial \theta} \Delta\theta = \frac{dg1}{d\beta} \Delta\theta$. En fait le pilote réduit non pas à la vue de l'angle sous lequel il voit le point de mesure mais à une altitude imposée z.

Nous allons calculer $\Delta N'$ et $\Delta N"$ pour un $\frac{\Delta z}{z}$ donné.

En posant s = distance de R au sol, on a MH2 = h2 = h1 $\frac{\sin(\beta r - \alpha 1 + \alpha 2)}{\sin \beta r}$ soit

$\frac{\Delta h2}{h2} = \frac{(\alpha 1 - \alpha 2)\,\Delta\beta}{\sin\beta r \sin(\beta r - \alpha 1 + \alpha 2)}$. Comme $s = h1 \frac{\sin \theta r}{\sin \beta r} = h1 \frac{\sin(\beta r - \alpha 1)}{\sin \beta r}$.

$\frac{\Delta z}{s} = \frac{\alpha 1\ \Delta\beta}{\sin\beta r.\ \sin(\beta r - \alpha 1)}$. , on trouve alors :

Réduction trop tôt : $\Delta N' = \frac{K2}{2,3} \frac{\alpha 1 - \alpha 2}{\alpha 1} \frac{\sin(\beta r - \alpha 1)}{\sin(\beta r - \alpha 1 + \alpha 2)} \frac{\Delta z}{s}$

Réduction trop tard : $\Delta N'' = \frac{d g1}{d\beta} \frac{\sin(\beta r - \alpha 1)\sin\beta r}{\alpha 1} \frac{\Delta z}{s}$

ce qui donne : $\frac{\Delta N''}{\Delta N'} = \frac{d g1}{d\beta} \frac{2,3}{K2} \frac{\sin\beta r \sin(\beta r - \alpha 1 + \alpha 2)}{(\alpha 1 - \alpha 2)}$

Application à la Caravelle III : on trouve

$$\Delta N' = 7,45 \frac{\Delta z}{s}$$

$$\Delta N'' = 26,7 \frac{\Delta z}{s}$$

Soit pour une erreur d'altitude de 10 %

$\Delta N' \# 0,7$ PNDB
$\Delta N'' \# 2,7$ PNDB

La planche n° 5 montre le bruit enregistré lors d'un récent essai de la Caravelle. L'altitude optimale calculée de réduction est voisine de 2080 ft. On voit qu'un léger retard dans la réduction (erreur d'altitude de 20 ft) augmente le niveau de 2 DB alors qu'une réduction très prématurée (écart de 180 ft dans l'altitude) n'augmente le niveau sonore que de 1 Db.

Ce phénomène est une des raisons de la grande dispersion des mesures de bruit des avions au décollage. Il suffit que le pilote réduise légèrement trop tard pour que le résultat de la mesure soit décalé de beaucoup vers les niveaux élevés. En fait, ce décallage peut se produire pour d'autres raisons. On a vu que le point de réduction est déterminé par l'angle sous lequel on voit l'avion. Or lors des essais l'angle optimum peut être modifié par une rafale ou tout autre mouvement instationnaire qui modifie peu la trajectoire ou l'assiette de l'avion à l'instant de mesure, mais à une forte influence sur l'angle sous lequel on le voit. C'est la raison pour laquelle nous pensons que toute mesure faite lors d'un décollage avec réduction doit être controlée en un ou deux points de mesure situés immédiatement après le point de mesure (de l'ordre de 100 et 300 m en aval).

1.3.5.- Extension

On peut se demander si les résultats obtenus par une réduction ne peuvent être étendus par des trajectoires plus compliquées. Le problème le plus général serait de trouver une loi de réduction progressive. Mais il est évident qu'une telle solution serait inapplicable pour le pilote. Revenons à l'équation qui détermine βr : $N_{1m} - N_{2m} = K2 \log \frac{\sin(\theta r + \alpha 1)}{\sin(\theta r + \alpha 2)} + g1(\theta r + \alpha 1)$.

Dans cette équation le terme $K2 \log \frac{\sin \beta r}{\sin(\beta r - \alpha 1 + \alpha 2)}$ est un terme correctif pour tenir compte du fait qu'une réduction fait perdre de l'altitude à un avion.

Donc la recherche de la trajectoire la plus sophistiquée ne ferait gagner que cette quantité $K2 \log \frac{\sin \beta r}{\sin(\beta r - \alpha 1 + \alpha 2)}$.

Or cette quantité est en général petite vis à vis de $N_{1m} - N_{2m}$. On peut dire que $N_{1m} - N_{2m}$ est le gain potentiel maximum (de toutes les trajectoires possibles) et que le gain réel est diminué d'une quantité qui dépend de la trajectoire.

Remarque

Ceci est en défaut dans le cas rare suivant :
lorsque $N_{1m} - N_{2m}$ est très petit, la recherche d'une réduction optimisée conduit à $\beta r > 90°$ et dans le cas, le gain réel est supérieur à $N_{1m} - N_{2m}$ car alors h2 > h1.

Pour juger néanmoins de l'intérêt éventuel de trajectoires plus compliquées, nous avons étudié les possibilités d'une double réduction (planche n° 6).

Les inconnues sont alors : $\theta r1$, $\theta r2$ et $\alpha 2$.

Les mêmes raisonnements qu'en 1.2. donnent les équations suivantes :

$$N_{1m} - N_{2m} = K2 \frac{\sin(\theta r1 + \alpha 1)}{\sin(\theta r1 + \ 2)} + g1(\theta r1 + \alpha 1) - g2(\theta r2 + \alpha 2)$$

$$N_{2m} - N_{3m} = (K2 - K3) \log \frac{\sin(\theta r1 + \alpha 2)}{\sin(\theta r1 + \alpha 1)} + K3 \log \frac{\sin(\theta r2 + \alpha 2)}{\sin(\theta r2 + \alpha 3)} + g2(\theta r2 + \alpha 2)$$

Comme il y a deux équations et 3 inconnues, il faut se fixer une valeur de $\alpha 2$, résoudre les 2 équations par itération (calculer $\theta r1$ et $\theta r2$) puis faire varier $\alpha 2$ et choisir la valeur qui donne la plus grande valeur de $g1 (\theta r1 + \alpha 1)$, qui est le gain.

Dans le cas de la Caravelle, on obtient avec la double réduction un supplément de gain de 0,6 PNdB. La recherche des trajectoires de montée plus compliquées que la simple réduction peut présenter beaucoup plus d'intérêt dans le cas où le champ sonore est très aplati et où une simple réduction conduirait à perdre beaucoup d'altitude.

1.4.- Problèmes d'unité de mesure

Nous avons effectué la recherche du point de réduction dans le cas où l'unité de mesure est le PNdB. Il nous reste maintenant à examiner ce qui se passe si l'on travaille en effectifs PNDB (EPNDB). On sait qu'on obtient le niveau sonore en EPNDB en ajoutant algébriquement au niveau en PNdB, une correction de son pur et une correction de durée.

On peut incorporer la correction de son pur dans les niveaux de bruit et toutes les analyses faites restent valables.

La correction de durée proposée par l'ISO est $10 \log \frac{\Delta t}{To}$ où Δt est la durée pendant laquelle le niveau sonore est compris entre le niveau maximum et le niveau maximum - 10 PNdB (ou - 20) et To est une constante de temps égale à 15 secondes (ou 30 s si on prends - 20 PNdB).

Nous utilisons ici la formule approchée de la correction de durée dont la formulation exacte comportant une intégration se prête mal au calcul.

1.4.1.- Nous allons démontrer un premier résultat préliminaire. La correction de durée admet un maximum relatif lorsque la réduction est optimisée.
Nous ferons la démonstration graphiquement car c'est la méthode la plus claire et la plus rapide.

Sur la planche n° 7, on voit les deux tronçons de trajectoire, le point de réduction optimum R, le point de mesure M. Sur la partie inférieure est représenté le niveau sonore en face du point d'émission.

En particulier les 2 bosses égales proviennent d'une part de R et d'autre part du point T (angle d'émission maximale $\delta 2m$). En prenant - 10 PNdB au dessous des deux bosses, on trouve le trajet ARB correspondant au temps Δt cherché.

Si la réduction est faite trop tôt en R', la première bosse est diminuée de beaucoup et la seconde augmente peu. Le point T vient en T' et B en B' (conservation des angles).

Bien qu'on "voit" que A' R' B' < ARB nous allons le démontrer plus rigoureusement.

$AR = MH1 \ (\cot g \omega - \cot g \beta r)$

$RB = MH1 \ \frac{\sin (\beta r - \alpha 1 + \alpha 2)}{\sin \beta r} \left\{ (\cot g \delta + \cot g (\beta r - \alpha 1 + \alpha 2) \right\}$

Or $\alpha 1 - \alpha 2$ est une quantité petite (devant βr). On peut donc écrire :

$\sin (\beta r - \alpha 1 + \alpha 2) = \sin \beta r - (\alpha 1 - \alpha 2) \cos \beta r$

et

$\cot g (\beta r - \alpha 1 + \alpha 2) = \cot g \beta r + (\alpha 1 - \alpha 2) (1 + \cot g^2 \beta r)$

On obtient alors :

$ARB = AR + RB = MH1 \left\{ (\cot g \omega + \cot g \delta + (\alpha 1 - \alpha 2) (1 - \cot g \delta \cot g \beta r) \right\}$

Dans cette expression ω est déterminé par la condition :

Bruit provenant de A = Bruit max - 10 = Nim - g1 (ω)

Dans le cas de la réduction optimale le bruit max est Nim - g1 (βr)

Dans ce cas on a donc g1 (ω) = 10 + g1 (βr)

δ est déterminé par g2 (δ) = 10

Si on effectue une réduction prématurée en R', c'est la deuxième bosse N'2m qui donne le niveau sonore maximal donc $\delta' = \delta$ on a alors :

$\Delta (ARB) = MH1 \left\{ - (1 + \cot g 2 \omega) \Delta \omega + (\alpha 1 - \alpha 2) \cot g \delta \ (1 + \cot g 2 \beta r) \Delta \beta \right\}$; $\Delta \beta$ est négatif.

Quant à $\omega' = \omega + \Delta \omega$ il est déterminé comme on a vu par Nim - g1 (ω') = N'2m - 10

Comme $N'2m = N2m - K2 \log \frac{h'2}{h2}$

$g1 (\omega') = K2 \log \frac{h'2}{h2} + 10 + g1 (\beta r) = K2 \log \frac{h'2}{h2} + g1 (\omega)$

Comme $\frac{h'2}{h2} < 1$ (réduction prématurée)

$g1 (\omega') < g1 (\omega)$ donc $\Delta \omega < 0$

Il s'ensuit que $\Delta(ARB) < 0$ et l'on peut dire que la correction de durée diminue lors d'une réduction prématurée.

Si la réduction est faite trop tard en R", la première bosse est augmentée de beaucoup et la seconde diminue légèrement.

Le point T vient en T" (conservation de l'angle δ 2m). Mais l'angle δ n'est plus conservé car c'est la première bosse qui est le maximum. Le point B vient en B" avec δ " > δ . On voit encore que A"R"B" < ARB. Le calcul donne :

$$\Delta(ARB) = ME_1 \left\{ -(1 + \cotg 2\omega)\Delta\omega + (1 + \cotg 2\delta) \right\} \left\{ \alpha(1 - \alpha(2) \cotg \beta_r - 1 \right\} \Delta\delta + (\alpha(1 - \alpha(2) \cotg \delta (1 + \cotg 2 \beta_r) \Delta\beta$$

Dans cette expression $\Delta\omega > 0$ donc la contribution de $\Delta\omega$ diminue ARB.

$\Delta\delta > 0$ donc la contribution de $\Delta\delta$ diminue ARB car $(\alpha_1 - \alpha_2) \cotg \beta_r < 1$.

Seul le terme contenant $\Delta\beta$ augmente ARB mais son influence est négligeable à cause de $\alpha(1 - \alpha(2$ qui est petit.

Donc une réduction tardive fait également diminuer la correction de durée.

Nous avons bien démontré que la correction de durée passe par un maximum relatif dans le cas d'une réduction optimisée.

1.4.2.- Le problème se pose donc de savoir si le point de réduction optimisé avec les PNdB reste le même avec la correction de durée.

Etant donné la forte augmentation du niveau sonore lors d'une réduction tardive, le déplacement du point de réduction ne peut se produire que vers une réduction prématurée, auquel cas il est possible à priori que la diminution de la correction de durée compense l'augmentation du niveau sonore.

Nous examinerons sommairement ce cas en simplifiant l'expression $\dot{ARB} = h1 \left\{ \cotg \omega' + \cotg \delta + (\alpha(1 - \alpha(2) (1 - \cotg \delta \cotg \beta) \right\}$ dans laquelle nous négligerons le terme comprenant $(\alpha(1 - \alpha(2)$ qui est petit devant les deux autres. Comme la réduction est prématurée le niveau maximum du point de mesure M, provient de l'angle d'émission maximal (point T' de la planche n° 7). Ce niveau est $N_{2m} - K2 \log \frac{h'2}{h1}$. La correction de durée correspondante est $10 \log \frac{(A'R'B')}{VTo}$. Nous cherchons donc le maximum de la fonction.

$$y = N_{2m} - K2 \log \frac{h'2}{h1} + 10 \log (A'R'B') + C^{ste}$$

En dérivant par rapport à β on obtient :

$$\frac{dy}{d\beta} = -K2 \frac{d}{d\beta} \left\{ \log \frac{h'2}{h1} \right\} - \frac{10}{2,3} \frac{(1 + \cotg 2\omega')}{\cotg \omega' + \cotg \delta} \frac{d\omega'}{d\beta}$$

Or ω' est déterminé par la condition :

Bruit provenant de T' - bruit provenant de A' = 10 ce qui donne l'équation

$$g1(\omega') + N_{2m} - N_{1m} - K2 \log \frac{h'2}{h1} = 10$$

d'où

$$\frac{d\omega'}{d\beta} = K2 \frac{\frac{d}{d\beta} \left\{ \log \left(\frac{h'2}{h1}\right) \right\}}{\frac{dg1}{d\delta'}(\omega')}$$

Soit :

$$\frac{dy}{d\beta} = -\frac{d}{d\beta} \left\{ \log \frac{h'2}{h1} \right\} \left[1 + \frac{10}{2,3} \frac{(1 + \cotg 2\omega')}{\frac{dg1}{d\beta}(\omega') (\cotg \omega' + \cotg \delta)} \right]$$

En annulant le terme entre crochets où δ est connu on obtient l'équation qui détermine ω'. S'il existe une solution $\omega' > \omega$ (avec $g1(\omega) - g1(\beta r) = 10$) alors la réduction optimale en EPNDB sera fait plus tôt que celle en PNDB. L'existance de cette solution dépend du champ sonore et de βr. Il n'est pas dans notre propos d'examiner tous les cas possibles. Signalons toutefois à titre d'exemple que pour la Caravelle III, il n'eixste pas de solution, donc la réduction optimale en EPNDB est confondue avec celle en PNDB.

1.4.3.- Importance de la correction de durée

Un fait important sur lequel nous voulons insister est que le gain de la réduction en EPNDB est plus faible qu'en PNDB. En effet lorsque l'évolution du bruit en fonction du temps présente deux bosses, la correction de durée est plus grande que lorsqu'il y a une bosse unique. Le fait remarquable c'est que la différence entre "correction de durée avec réduction" et "correction de durée sans réduction" ne dépend quasiment pas du champ sonore mais seulement du gain de la réduction en PNDB. Nous avons calculé Δ N en EPNDB

en fonction de Δ M en PNDB pour les quatre champs sonores de la planche n° 24. Les résultats sont donnés sur la planche n° 8, et toutes les courbes sont à l'intérieur de la zone hachurée. La perte dûe à la correction de durée est très importante puisqu'elle représente environ un tiers du gain en PNDB.

2.- CALCUL DU GAIN DE LA REDUCTION

2.1.- Analyse des paramètres

Nous avons examiné dans la première partie comment déterminer le point de réduction optimum et certaines conséquences de la réduction. Nous nous proposons d'examiner quels sont les gains possibles qu'on peut obtenir grâce à la réduction.

Nous avons vu que le gain potentiel est $N_{1m} - N_{2m}$. C'est donc le bruit max du moteur au régime de décollage moins le bruit max du moteur à régime réduit. N_{1m} ne dépend que du moteur. Quant à N_{2m}, il dépend du moteur, de l'angle de montée résiduelle α_2, de la finesse de l'avion et de la motorisation. En toute rigueur la vitesse de l'avion intervient également mais pratiquement comme le bruit entre M = 0,2 et M = 0,3 ne varie qu'au plus de 0,3 PNdB et que d'autre part tous les avions ont des nombres de Mach de montée compris entre 0,21 et 0,25, en prenant M = 0,23, on fait une erreur tout à fait négligeable (inférieure à 0,1 PNdB).

Les paramètres qui entrent en ligne de compte sont :

côté moteur : cycle
côté avion : angle de montée résiduelle α_2
finesse pendant la montée
taux de motorisation

Pour pouvoir calculer N_{2m} il faut savoir comment varie le bruit du moteur en fonction de la poussée. Nous avons donc été conduits à étudier le bruit de jet, le bruit de compresseur et composer les deux bruits.

2.2.- Calcul du bruit de jet

2.2.1.- Bruit de jet au régime maxi

Pour le calcul du bruit de jet nous avons utilisé la méthode SNECMA (note technique : YLLA n° 169) qui donne le bruit de jet en fonction de la poussée spécifique (F/D), de la consommation spécifique C_s et du nombre de Mach de vol.

Nous avons simplifié de la manière suivante :

- nous avons pris le Mach de vol égal à 0,23
- nous avons pris la consommation spécifique fonction de Fo/Do. En effet si on trace pour tous les moteurs existants C_s en fonction de Fo/Do, (planche n° 9) on s'aperçoit qu'il existe une corrélation (assez mauvaise d'ailleurs).

Néanmoins en prenant une courbe moyenne les écarts par rapport aux points extrêmes sont les suivants :

Fo/Do	700	600	500	400
Ecarts PNdB	+ 0,5	+ 0,5	+ 0,4	+ 0,5
	- 0,4	- 0,5	- 0,4	- 0,4

On peut donc dire qu'en nous plaçant sur la ligne moyenne nous représentons le bruit du moteur moyen à $\pm$ 0,5 PNdB près. Notre étude garde donc toute sa valeur en tant qu'étude paramétrique. En conclusion on peut tracer les courbes représentées sur la planche n° 10, où Φ est le diamètre de la tuyère en m.

2.2.3.- Poussée et débit en vol

En général un réacteur est caractérisé par sa poussée au point fixe au sol Fo. Or on a besoin de connaitre sa poussée en vol. La planche n° 11 donne F/Fo en fonction du nombre de Mach et de Fo/Do. Le débit est donné par $\frac{D}{Do} = \left\{ 1 + \frac{\gamma - 1}{2} M2 \right\}^{\frac{\gamma+1}{2(\gamma-1)}}$ (conservation du débit réduit avec vitesse de rotation constante (planche n° 12).

2.2.4.- Bruit à régime réduit

Pour connaitre le bruit N_{2m}, il nous faut connaitre le débit du moteur en fonction de la poussée. En étudiant les caractéristiques de différents moteurs nous nous sommes apperçus que pour tous les moteurs $\frac{F}{D} / \frac{F1}{D1}$ en fonction de F/F1 suit une loi très voisine (mieux qu'à $\pm$ 3 % près) et que cette loi est pratiquement linéaire.

La planche n° 13 représente les lois de plusieurs moteurs, la planche n° 14, la loi moyenne retenue.

L'ensemble des données nous permet de calculer le bruit N_{2m} correspondant à la poussée F2. En effet $\frac{F2}{mg} = \alpha_2 + \frac{1}{\varphi}$ (φ = finesse).

En se fixant α_2 et φ on connait $\frac{F2}{mg}$; d'où $\frac{F2}{F1}$.

La planche n° 14 donne alors $\frac{F2}{D2} / \frac{F1}{D1}$. On calcule

$$\frac{F1}{D1} = \frac{F1}{Fo} \times \frac{Fo}{Do} \times \frac{Do}{D1}$$

F1/Fo est donnée par la planche n° 11
Fo/Do est un paramètre
D1/Do = $(1 + \frac{\gamma - 1}{2} * M2)^{\frac{\gamma}{\gamma-1}}$ (planche n° 12)

Connaissant $\frac{F2}{D2}$ et F2, on peut calculer N_{2m} par la planche 10.

2.3.- Bruit de compresseur

2.3.1.- Calcul du bruit de compresseur au régime maximum

Nous avons utilisé la méthode SAE AIR 973 modifiée par la SNECMA par l'introduction d'un facteur de convection (NT. YLLA N° 169) pour les moteurs double flux.

D'après cette méthode le niveau maximal linéaire à 300 m est donné par :

$$N(PNDB) = 20 \log \frac{\Phi}{P} + 46 \log \frac{60}{\pi} Ue - 75$$

Soit :

$$N - 10 \log F = -15 + 46 \log Ue - 10 \log \frac{D}{s} - 10 \log \frac{F}{D}$$

Pour représenter un moteur type nous avons pris Ue = 425 m/s et $\frac{D}{s}$ = 170 kg/m2. Ces valeurs représentent une bonne moyenne parmi les moteurs ainsi que le montre la planche n° 15. Le facteur de convection pour le bruit aval du compresseur est dans ces conditions de + 3 PNDB. On peut donc représenter N - 10 log F en fonction de $\frac{Fo}{Do}$ (planche n° 16). On voit que dès que $\frac{Fo}{Do}$ est inférieur à 490 m/s le bruit de compresseur aval est supérieur au bruit de jet.

Remarque

Etant donné la complexité du bruit de compresseur, qui dépend d'une multitude de paramètres (vitesse périphérique, nombre d'aubes, nombre d'étages, écartement rotor stator, présence de la roue directrice d'entrée) le résultat auquel nous arrivons doit être traité avec beaucoup de précautions. Il ne faut pas trop s'attacher aux valeurs absolues mais considérer plutôt les "tendances" et les "ordres de grandeurs".

Il n'est bien entendu pas possible de présenter par une seule courbe le bruit de compresseur de tous les moteurs. Les moteurs classiques (JT 8 D, JT 3 D) se placent cependant très bien sur notre courbe.

2.3.1.- Bruit de compresseur aux régimes réduits

L'examen de plusieurs moteurs (voir planche n° 17) montre qu'on peut prendre une loi moyenne de variation de la poussée en fonction du régime. On peut donc représenter la variation du niveau de bruit de compresseur en fonction de la poussée. (planche n° 18)

La variation du bruit du réacteur en vol en fonction de la poussée est représentée sur la planche n° 18. On remarque que pour un moteur très dilué ($\frac{Fo}{Do}$ = 300 soit un taux de dilution de l'ordre de 4 à 5) le bruit de jet varie d'une façon très voisine du bruit de compresseur. La planche n° 16 donne les maximum. On peut donc combiner les deux bruits et voir la variation du bruit total en fonction de la poussée.

2.4.- Résultats

Les planches n°s 19, 20 et 21 donnent le gain potentiel de la réduction (pour trois finesses différentes, et $\alpha 2 = 0,06$) en fonction du taux de motorisation. Examinons la planche n° 20 (finesse moyenne 10). On voit que pour un avion équipé de jets purs ($\frac{Fo}{Do} \gg 600$ où le bruit de compresseur est négligeable et pour lesquels le réacteur perd très peu de sa poussée en vol) le gain peut être très important, surtout pour des grands taux de motorisation. Pour des avions équipés de moteurs très dilués ($\frac{Fo}{Do}$ = 300 soit un taux de dilution de l'ordre de 4 à 5) le gain potentiel est beaucoup plus faible. La raison essentielle est la grande perte de la poussée en vol par rapport à la poussée statique. Pour ces avions, même si on arrivait à supprimer entièrement le bruit de compresseur, le gain serait sensiblement le même (nous avons vu que pour $\frac{Fo}{Do}$ = 300 la variation du bruit de compresseur en fonction de la poussée est presque identique à celle du bruit de jet).

Les avions équipés de moteurs moyennement dilués ($\frac{Fo}{Do}$ = 400 à 500 soit un taux de dilution de l'ordre de 1 à 2) ont un gain relativement faible, plus proche des moteurs très dilués que de jets purs. La raison en est que le bruit du compresseur intervient de façon importante et aplatit la courbe qui donne le niveau de bruit total en fonction de la poussée. Pour ces avions, le gain serait beaucoup plus important si on arrivait à supprimer le bruit de compresseur. En

particulier la courbe pour $\frac{Fo}{Do}$ = 500 serait presque confondue avec celle pour $\frac{Fo}{Do}$ = 600.

L'influence de la finesse peut être examinée mieux sur la planche n° 22 qui donne la variation du gain pour deux points de finesse (8 à 10 ou 10 à 12).

L'influence de l'angle de montée résiduelle α_2 est représentée sur la planche n° 23 qui donne la différence du gain entre $\alpha_2 = 0,04$ et $\alpha_2 = 0,06$. On remarque sur les planches 20, 22 et 23 que les influences du taux de motorisation, de la finesse et de la pente de montée sont beaucoup plus faibles dans le cas de réacteurs très dilués que pour les jets purs, ce qui veut dire que pour les avions futurs équipés de réacteurs très dilués les différences entre les avions seront très atténués. Pour nous situer rappelons que la finesse d'un biréacteur est voisine de 11 ($\frac{1}{\varphi} = 0,09$) celle d'un quadriréacteur proche de 8,3 ($\frac{1}{\varphi} = 0,12$). On peut faire le tableau de comparaison suivant :

Bimoteur actuel $\frac{Fo}{Do}$ = 500 à 600 $\frac{Fo}{mg}$ = 0,25 à 0,28 Gain = 5 à 10 PNDB	Quadrimoteur actuel $\frac{Fo}{Do}$ = 400 à 500 $\frac{Fo}{mg}$ = 0,2 à 0,22 Gain 0 PNdB
Bimoteur futur $\frac{Fo}{Do}$ = 300 $\frac{Fo}{mg}$ = 0,3 à 0,35 Gain = 4 à 6 PNdB	Quadrimoteur futur $\frac{Fo}{Do}$ = 300 $\frac{Fo}{mg}$ = 0,23 à 0,30 Gain 0 à 3 PNdB

Influence du champ sonore

Les valeurs du gain que nous avons donné sont des gains potentiels c'est à dire en faisant abstraction du champ sonore. Nous avons voulu examiner plus en détail quelle est l'influence du champ sonore. Nous avons pris pour chaque $\frac{Fo}{Do}$ un champ sonore différent (voir planche n° 24).

Sur la planche n° 25 on voit le gain potentiel Δ No et le gain réel Δ N.

Les différences sont surtout importantes en valeur relative pour le champ sonore très aplati. Le fait que le gain réel peut être supérieur au gain potentiel s'explique comme nous l'avons déjà vu par une réduction après le survol de l'observateur ($\beta_v > 90$).

3- BRUIT DES AVIONS AU DECOLLAGE

Dans les paragraphes précédents nous avons vu l'importance de quelques paramètres (tels que $\frac{Fo}{Do}$, $\frac{Fo}{mg}$) sur le gain de la réduction.

Nous allons examiner ici quelle est l'influence de ces paramètres sur le bruit au décollage. Nous nous limiterons ici au bruit sans réduction, puisque le gain de la réduction a été étudié.

3.1.- Influence du taux de motorisation

Pour évaluer l'influence du taux de motorisation nous avons été amenés à calculer la trajectoire de décollage.

Nous donnons ici le résultat pour 2 types d'avion, dont voici les caractéristiques qui interviennent dans le calcul de la longueur de décollage.

1er avion : Bimoteur, $\frac{M}{S}$ = 470, Cz max = 1,9, Cx = 0,065, Cs = 0,4, Moteurs : $\frac{Fo}{Do}$ = 600

2ème avion : Quadrimoteur $\frac{M}{S}$ = 530, Cz max = 2,2, Cs = 0,10, Cz = 0,8, Moteurs $\frac{Fo}{Do}$ = 300

La planche 26 donne l'évolution relative du niveau sonore en fonction du taux de motorisation. Il s'agit du bruit sans réduction à 6500 m du point de lâcher des freins. L'influence de la motorisation serait encore plus grande si on prenait en compte le gain de réduction.

Si on considère un bimoteur de $\frac{Fo}{mg}$ = 0,265 alors 10 % d'augmentation du taux de motorisation donnerait un gain de 2,8 PNdB. Pour un quadrimoteur 10 % d'augmentation du taux de motorisation (à partir de 0,23) donnerait également un gain de 2,8 PNdB. Avec le gain de la réduction ces valeurs deviendraient 3,6 et 4 PNdB.

L'influence du taux de motorisation est donc très importante. Le taux de motorisation est le paramètre fondamental dans la détermination du bruit au décollage.

C'est la différence des taux de motorisation entre les bi et quadriréacteurs qui explique en grande partie la difference de bruit du décollage.

3.2.- Influence du cycle du moteur

Nos moteurs ainsi que nous l'avons vu sont caractérisés par le paramètre $\frac{Fo}{Do}$. Pour les avions

équipés de moteurs simple flux ($\frac{Fo}{Do}$ 600) l'effet de F/D est donné approximativement sur la planche 16 (bruit de jet en fonction de $\frac{Fo}{Do}$) car pour les fortes poussées spécifiques, l'influence de $\frac{Fo}{Do}$ sur la longueur de décollage et sur la pente de montée est faible. Nous nous sommes intéressés plus particulièrement aux quadrimoteurs ayant des Fo/Do inférieurs à 500. En effet dans ce cas, une variation de Fo/Do doit entrainer une augmentation du taux de motorisation pour conserver la poussée en croisière. Nous avons donc pris le taux de motorisation variable avec Fo/Do. Pour cela nous avons choisi la variation de la poussée en croisière en fonction de Fo/Do, comme indiqué sur la planche 27. L'avion est un quadrimoteur défini au § 4.2., d'une masse de 150 000 kg. Le point de mesure est à 6500 m. Les bruits (sans réduction) sont donnés dans les tableaux ci-dessous où les flèches indiquent comment il faut lire l'influence de Fo/Do.

Bruit de jet (PNDB)

$\frac{Fo}{mg}$ \ $\frac{Fo}{Do}$	300	400	500
0,194			121,2
0,21		111,8	117,8
0,23	102,8	107,8	114,3
0,250	100,1	105,1	
0,273	97,8		

Bruit de compresseur aval (PNdb)

$\frac{Fo}{mg}$ \ $\frac{Fo}{Do}$	300	400	500
0,194			120,2
0,21		118,8	116,8
0,23	116,8	114,8	113,3
0,25	114,1	112,1	
0,273	111,8		

Les résultats sont donnés sur la planche n° 28.

Les quadrimoteurs actuels ont un $\frac{Fo}{Do}$ voisin de 400 (J T 3D - 3B) et un $\frac{Fo}{mg}$ de l'ordre de 0,21.

La valeur de 118,8 PNdB représente très bien leur niveau de bruit. Sur la fig. 28 on retrouve le fait que le remplacement des réacteurs actuels par des réacteurs très dilués n'apportera un très grand gain sur le niveau sonore qu'à condition que des progrès importants soient faits pour réduire le bruit du compresseur.

On peut espérer une diminution de l'ordre 15 PNDB si on atténue le bruit de compresseur de cette quantité. Une partie pourra être obtenue par des techniques étudiées depuis quelques années déjà et qui sont : suppression de la roue directrice d'entrée, écartement rotor-stator, diminution de la vitesse périphérique.

Toutefois il sera impossible par ces procédés d'obtenir des atténuations importantes.

Le supplément devra être cherché par des traitements acoustique des conduits (aval et amont) ou de manière générale par des silencieux de compresseur.

Des gains supplémentaires pourront être obtenus par la surmotorisation (3 PNdB pour 10 %, 5 PNdB pour 20 % de surmotorisation).

Enfin la technique de la réduction pourra donner encore 3 dB, dans le cas d'avions très motorisés.

Nous voudrions rappeler que des limitations dues au bruit de turbine risquent d'intervenir sur des réacteurs très dilués, de sorte que le thème du bruit des parties tournantes alimentera en grande partie les études de bruit à venir.

3.3.- Problèmes d'unité de mesure

Nous allons examiner quelles modifications apportent les EPNdB dans les conclusions des paragraphes précédents.

Nous avons vu que la durée à prendre en considération est $\Delta t = \frac{hi}{V} (\cot g \omega + \cot g \delta)$; hi est la distance du point de mesure à la trajectoire.

Or lorsque la motorisation croit, hi augmente donc la correction de durée augmente. En d'autres termes l'introduction de la correction de durée pénalise les avions motorisés. Cette pénalisation est très importante, ainsi que le montre la planche 29. Ceci revient à dire que l'influence de la motorisation que nous avons vu est beaucoup moins importante en EPNdB.

La planche n° 30 donne l'influence du taux de motorisation pour notre bi et quadriréacteur en PNdB et EPNdB. (sans réduction)

On voit que la correction de durée enlève environ 1/3 du gain apporté par la motorisation dans le cas du biréacteur et la moitié dans le cas du quadriréacteur.

Lorsqu'un avion utilise une réduction, les corrections de durées sont encore plus importantes car comme nous l'avons déjà vu la présence de 2 bosses augmente le temps d'exposition. Voici comment évolue la correction de durée avec réduction : (bimoteur)

Fo/mg	0,2	0,24	0,28	0,32	0,36
Correction de durée avec réduction dB	- 0,27	+ 3,12	+ 5,06	+ 6,5	+ 7,4
Correction de durée sans réduction dB	- 1,27	+ 0,82	+ 2,3	+ 3,5	+ 4,4

De ce fait la correction de durée enlève beaucoup de validité à la technique de la réduction. Le tableau ci-dessous rappelle les valeurs dans le cas de notre biréacteur type

Fo/mg	0,2	0,24	0,28	0,32	0,36
Gain de la réduction en PNdB	3,4	7	9,4	10,6	11,5
Gain de la réduction en EPNdB	2,4	4,7	6,7	7,6	8,5

D'une manière générale tous les efforts faits sur l'avion pour améliorer ses performances de montée seront systématiquement dégradées par la correction de durée (amélioration de la finesse, diminution de la trainée ...). C'est à dire plus un avion fait des progrès pour s'éloigner rapidement de la zone d'aéroport, plus la correction de durée qu'on lui appliquera sera forte ce qui est paradoxal.

La fonction de la correction de durée devrait être de discriminer les champs sonores des avions. Elle devrait inciter les constructeurs à faire des efforts pour améliorer (creuser) les champs sonores et ne pas les décourager de surmotoriser, d'affinner l'aérodynamique des avions ou de perfectionner des procédures de décollage anti bruit.

Nous pensons donc qu'il ne convient d'adopter la correction de durée que s'il s'avère qu'elle reflète parfaitement bien les réactions physiologiques de l'homme.

S'il n'en est pas ainsi l'introduction de la correction de durée aura pour effet le contraire de ce qu'on recherche.

Il est bien évident que la durée doit être prise en compte dans un critère de gêne due au bruit. Mais encore faut-il qu'elle soit prise à bon escient. Il nous semble qu'il serait plus judicieux de prendre en considération le temps uniquement pendant lequel le niveau sonore dépasse un seuil considéré comme gênant. De cette manière les effets néfastes et paradoxaux que nous avons vus

seraient supprimés.

Pour conclure, je voudrais dire en me résumant : l'unité de mesure pour caractériser le bruit des avions risque d'avoir des répercussions sur les caractéristiques des avions et peut avoir une influence sur les efforts techniques entrepris pour diminuer le bruit des avions. Il est donc d'une importance primordiale que cette unité reflète parfaitement bien la sensibilité de l'homme au bruit. Sinon l'unité de mesures peut avoir des résultats néfastes c'est à dire elle peut devenir un frein dans la voie de la diminution de la gêne dûe au bruit des avions.

REFERENCES

. J.W.LITTLE and J.E. MARBRY : Human reaction to aircraft engine noise (AIAA 4 th Propulsion joint specialist Conference)

. LATHAM COPELAND, David A.HILTON, Vera HUCKEL, Andrew C. DIBBLE, and Domenic J.MAGLIERI : Noise Measurement evaluations of various take-off climbout profiles. NASA TN D.3715

. SNECMA : Champs sonores linéaires en PNDB des jets en vol. Document n° 3808/YLLA

. R. HOCH et J.P. DUPONCHEL : Methode d'estimation du bruit d'un turboréacteur à partir de ses grandeurs thermopropulsives. SNECMA NT YLLA N° 169

. D.E. BISHOP : Frequency Spectrum and time duration descriptions of aircraft flyover noise signals FAA D5-67-6

. KRYTER, K.D. : Concepts of Perceived Noisiness J. Acoust.Soc. Amer. vol 43 n° 2 Feb. 1968

Fig. 1

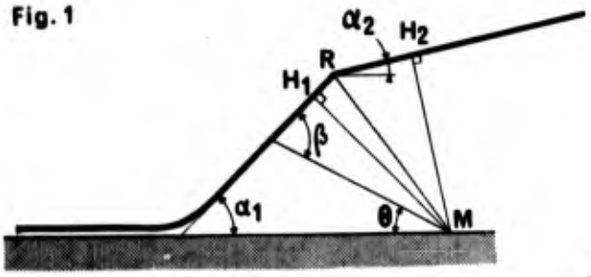

Fig. 2

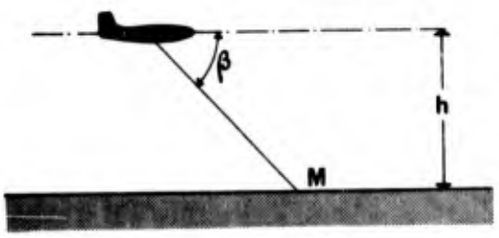

Fig. 3

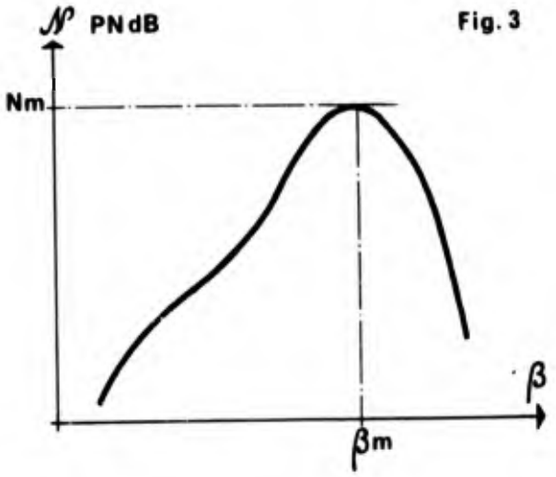

Planche 1 : **Recherche du point de réduction : position du problème**

$MH_1 = h_1 = MR \sin(\theta_r + \alpha_1)$
$MH_2 = h_2 = MR \sin(\theta_r + \alpha_1)$

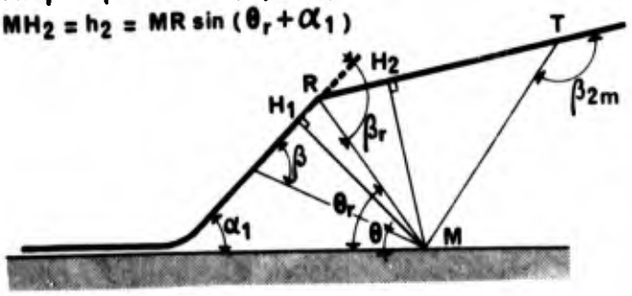

Fig. 1 bis

Fig. 5

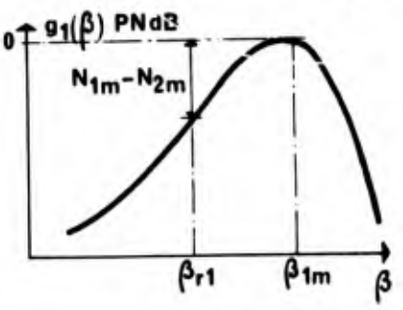

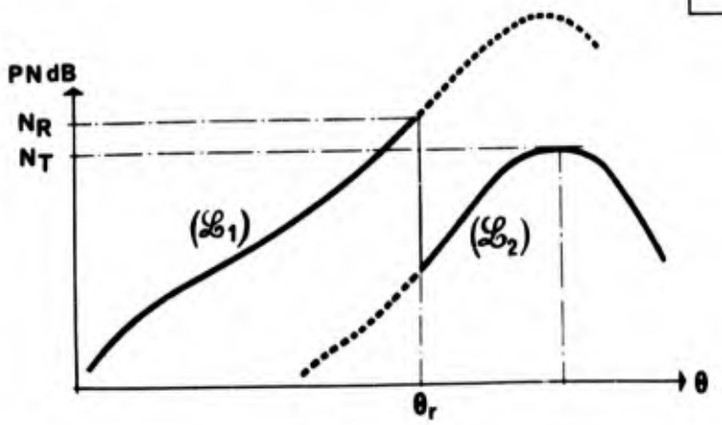

Fig. 4
NIVEAU DE BRUIT EN M

Planche 2 : **Recherche du point de réduction: critère d'optimum**

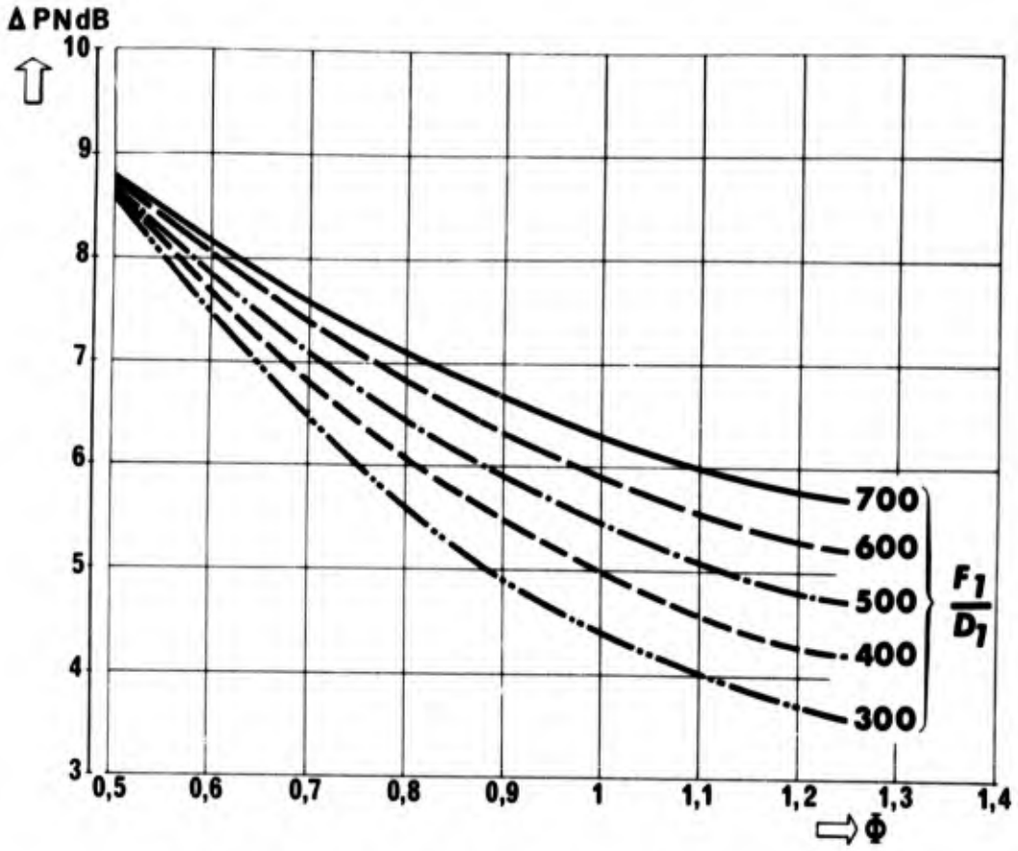

Planche 3 : Attenuation atmosphérique Δ N pour 1000μm PNdB

Fig. 8

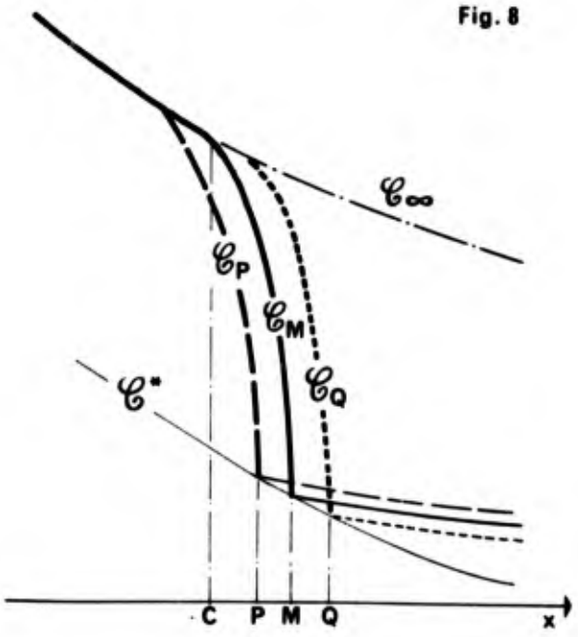

Fig. 9

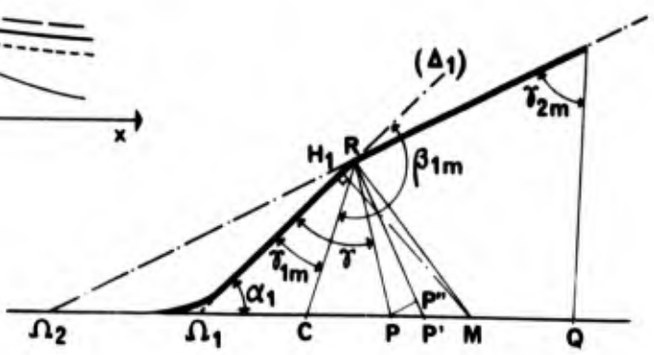

Planche 4 : Niveau de bruit sous la trace

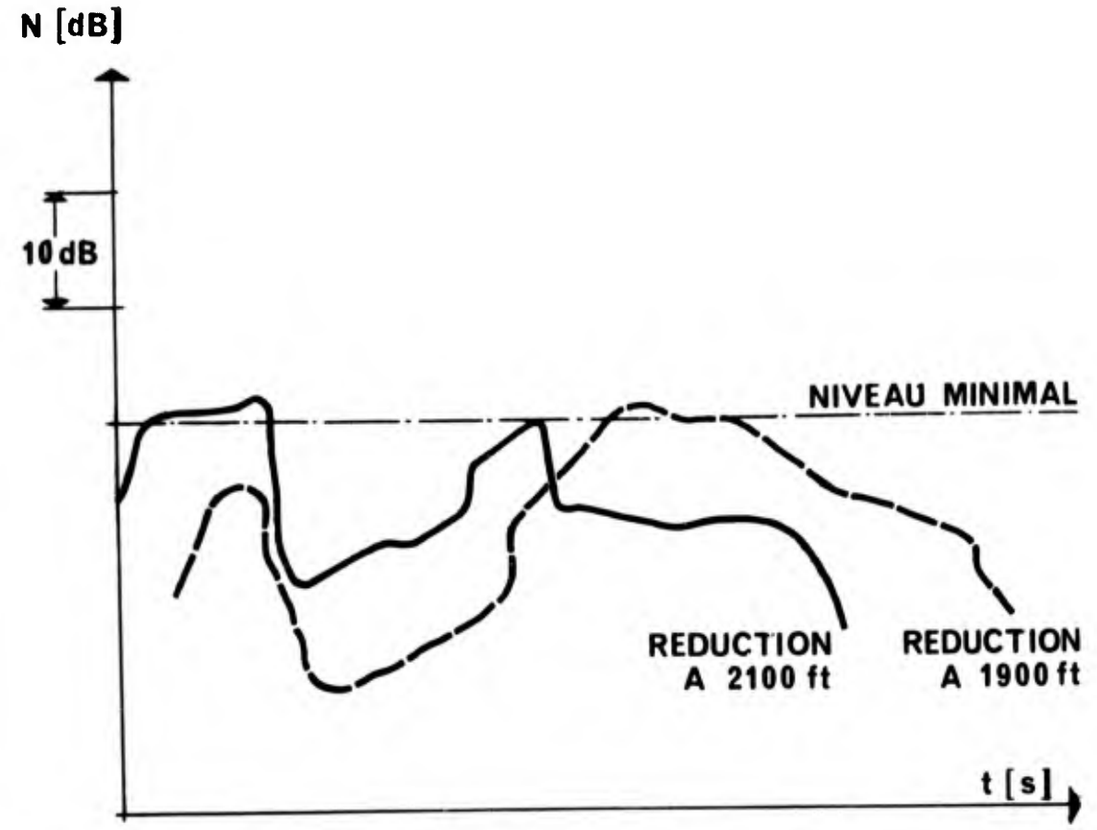

Planche 5 : Décollage de la Caravelle III

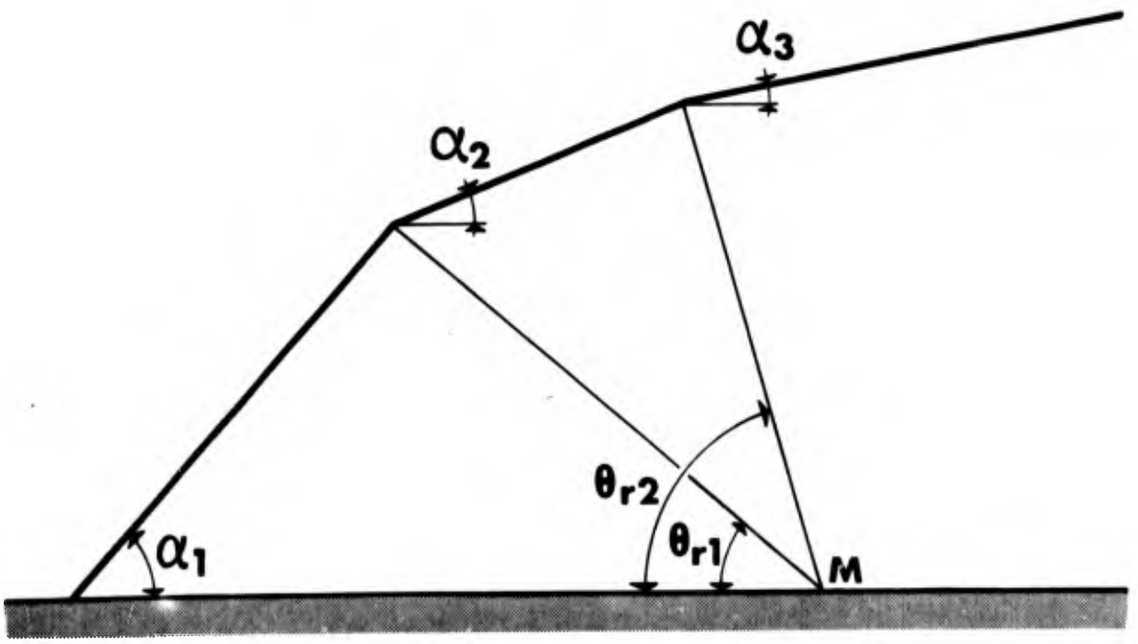

Planche 6 : Réduction double

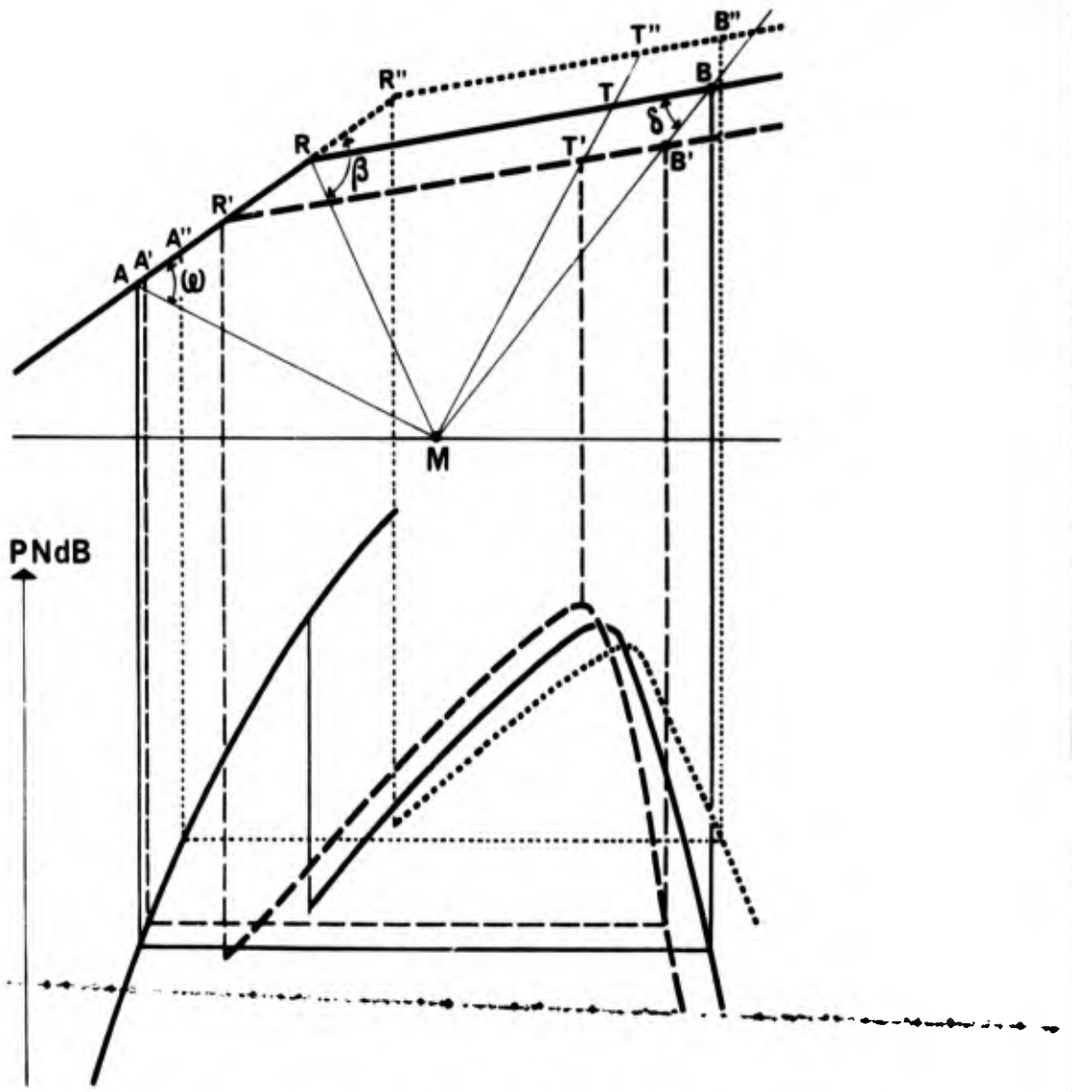

Planche 7 : **Correction de durée à la réduction optimale**

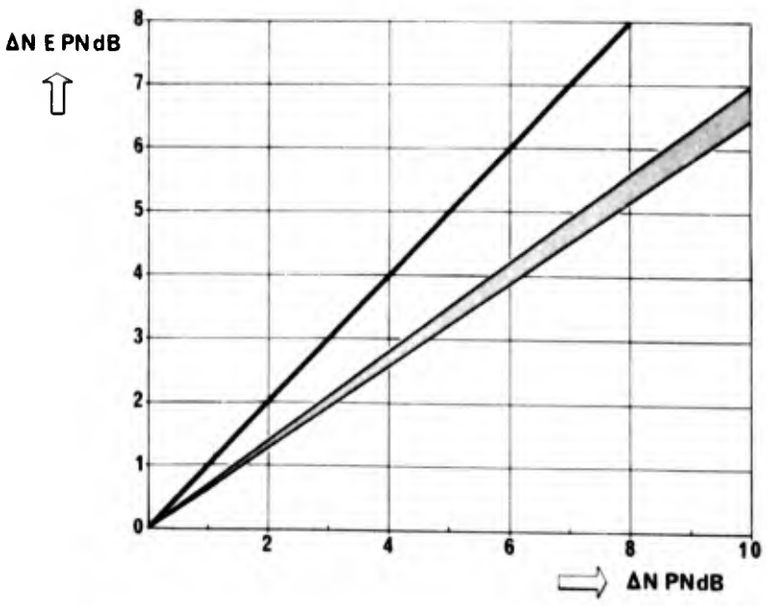

Planche 8 : **Influence de la correction de durée sur le gain de la réduction optimale**

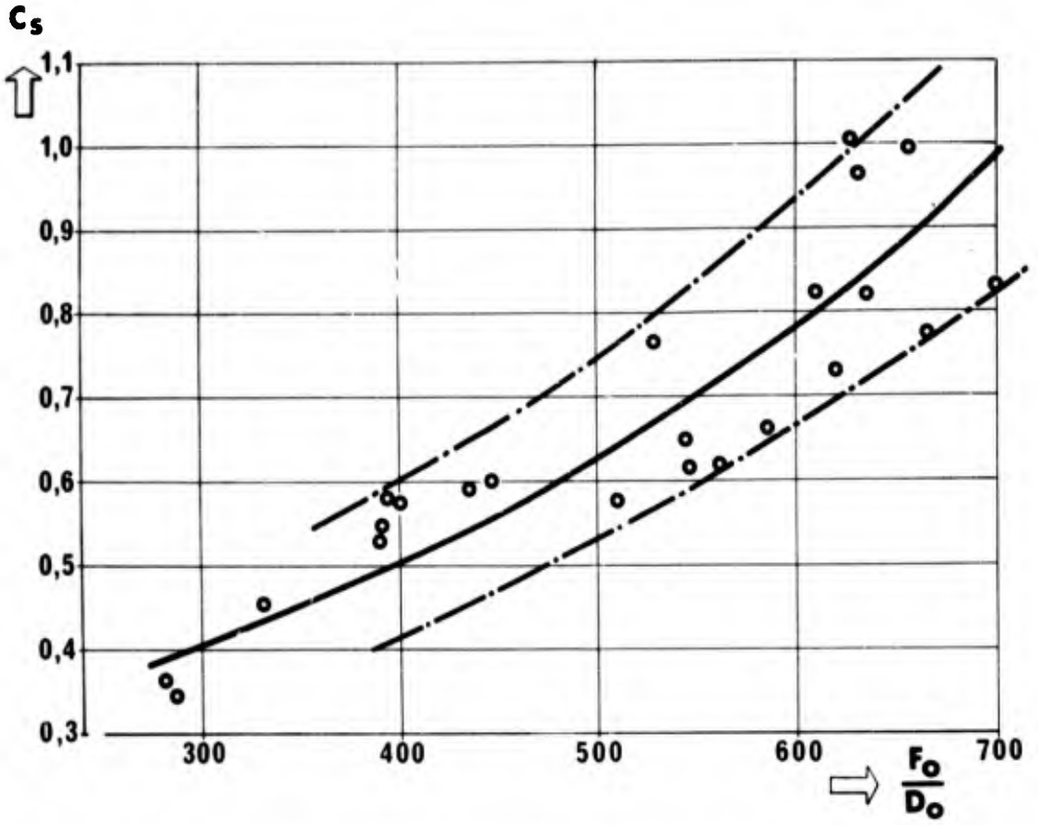

Planche 9 : **Relation entre la consommation spécifique et la poussée spécifique**

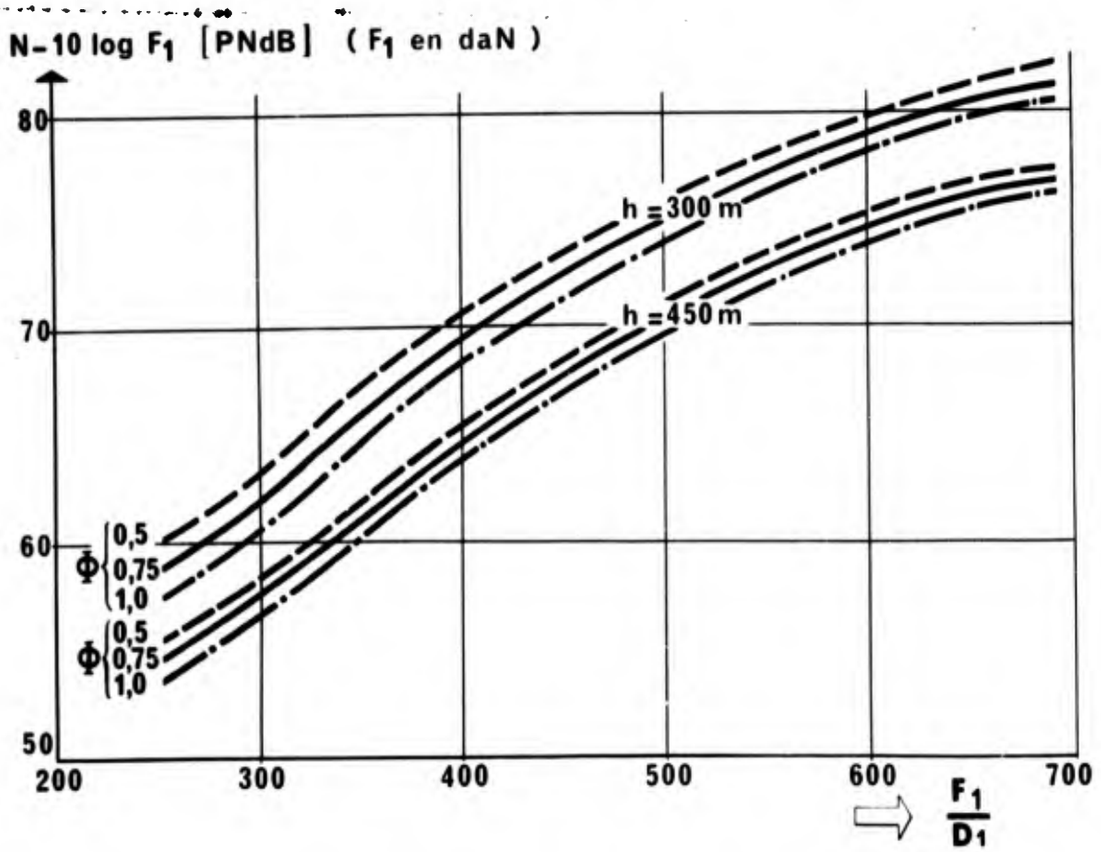

Planche 10 : **Bruit de jet en vol**

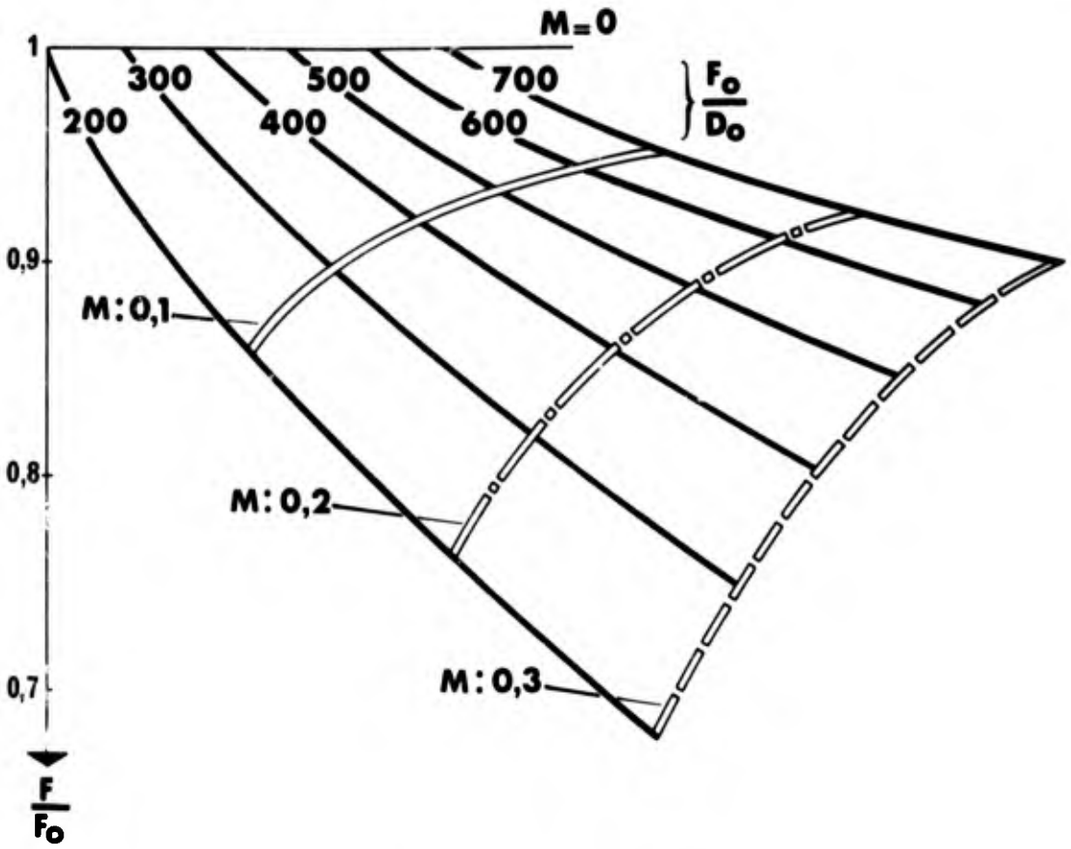

Planche 11 : Poussée en vol

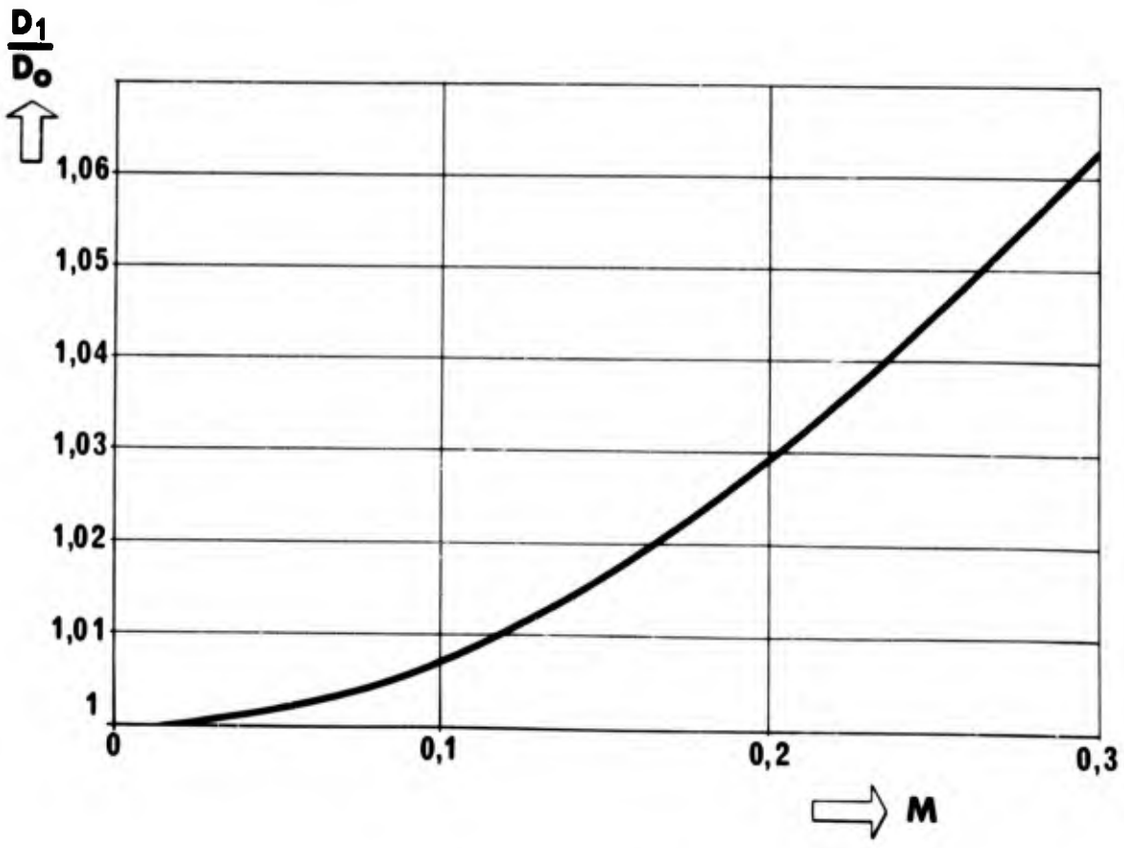

Planche 12 : Débit en vol

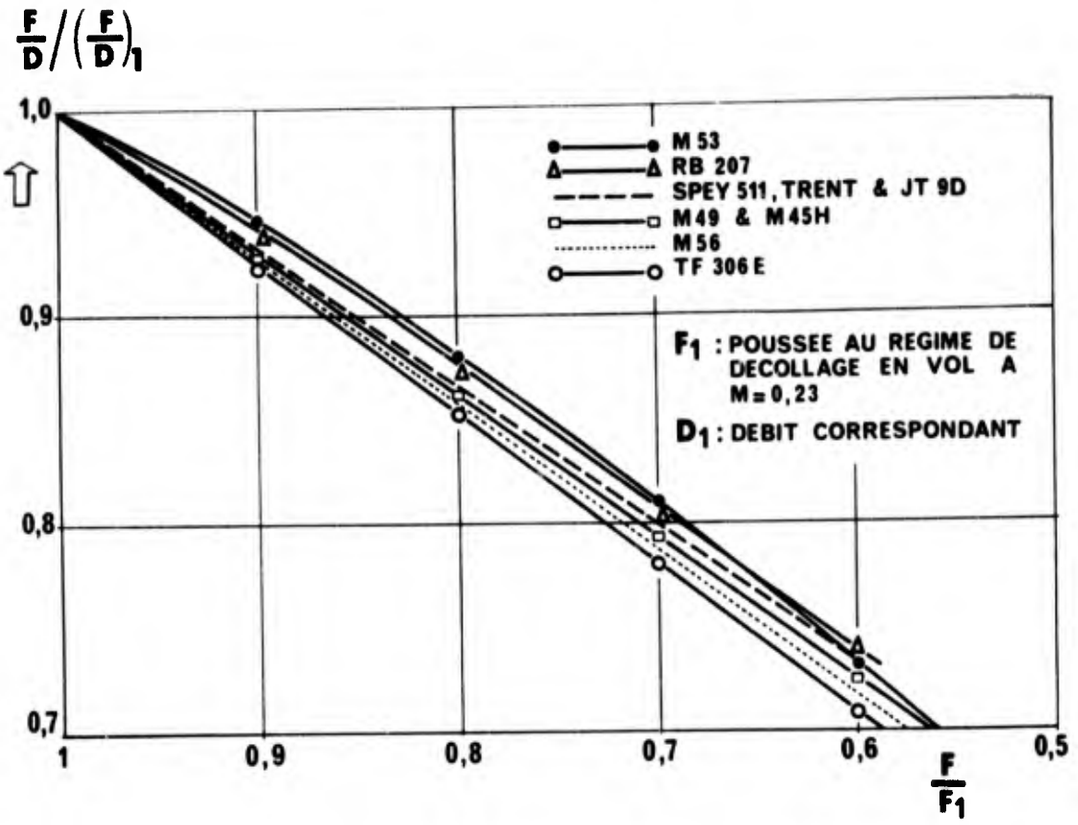

Planche 13 : **Poussée spécifique en fonction de la poussée (exemples)**

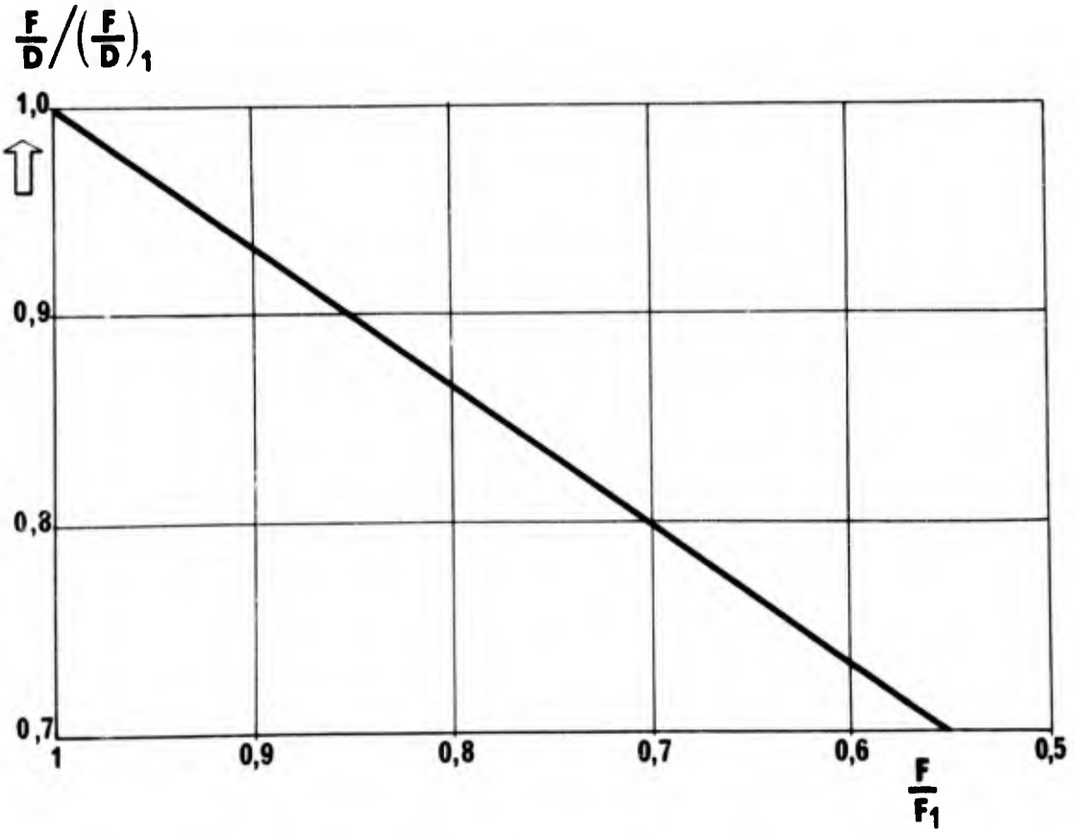

Planche 14 : **Poussée spécifique en fonction de la poussée (loi moyenne)**

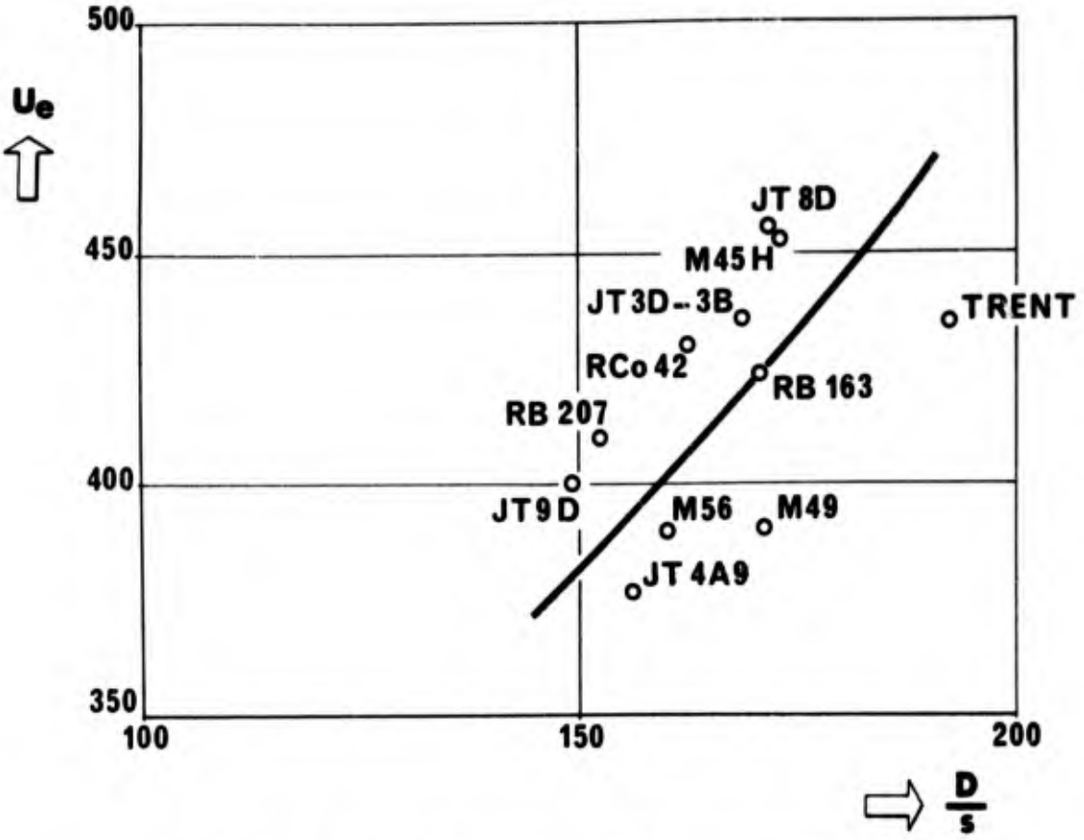

Planche 15 : Vitesse périphérique et débit spécifique des réacteurs

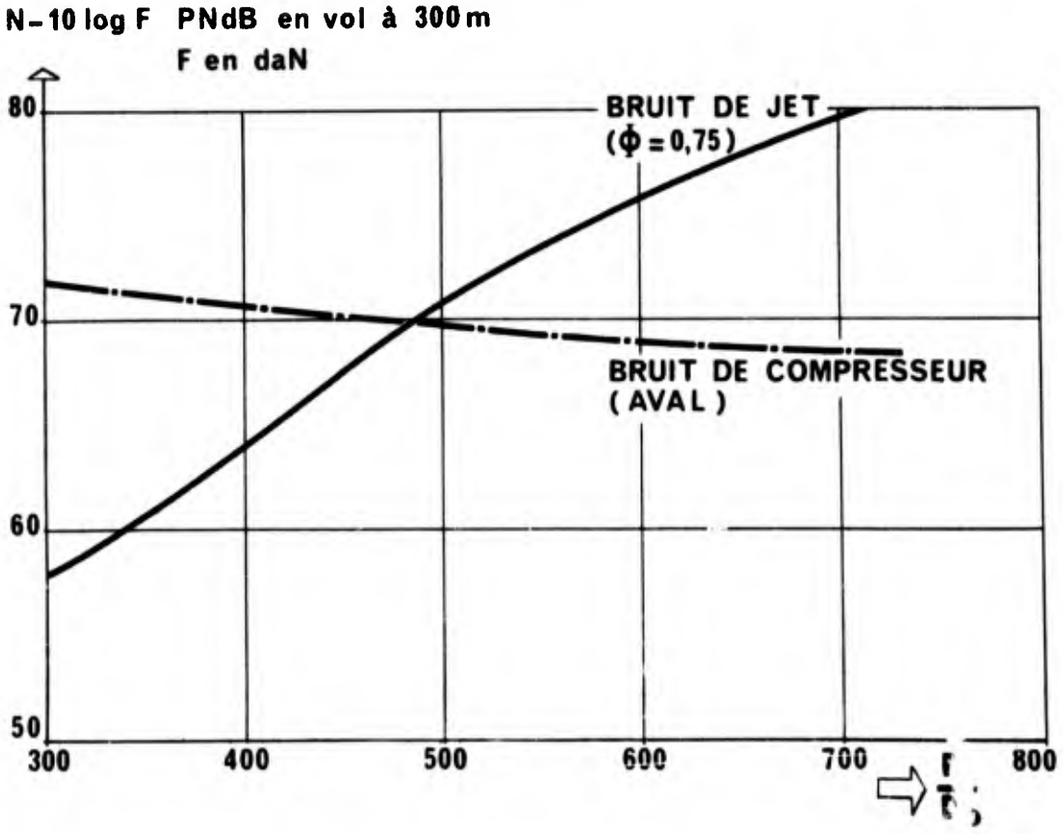

Planche 16 : Bruit d'un réacteur en vol au régime de décollage

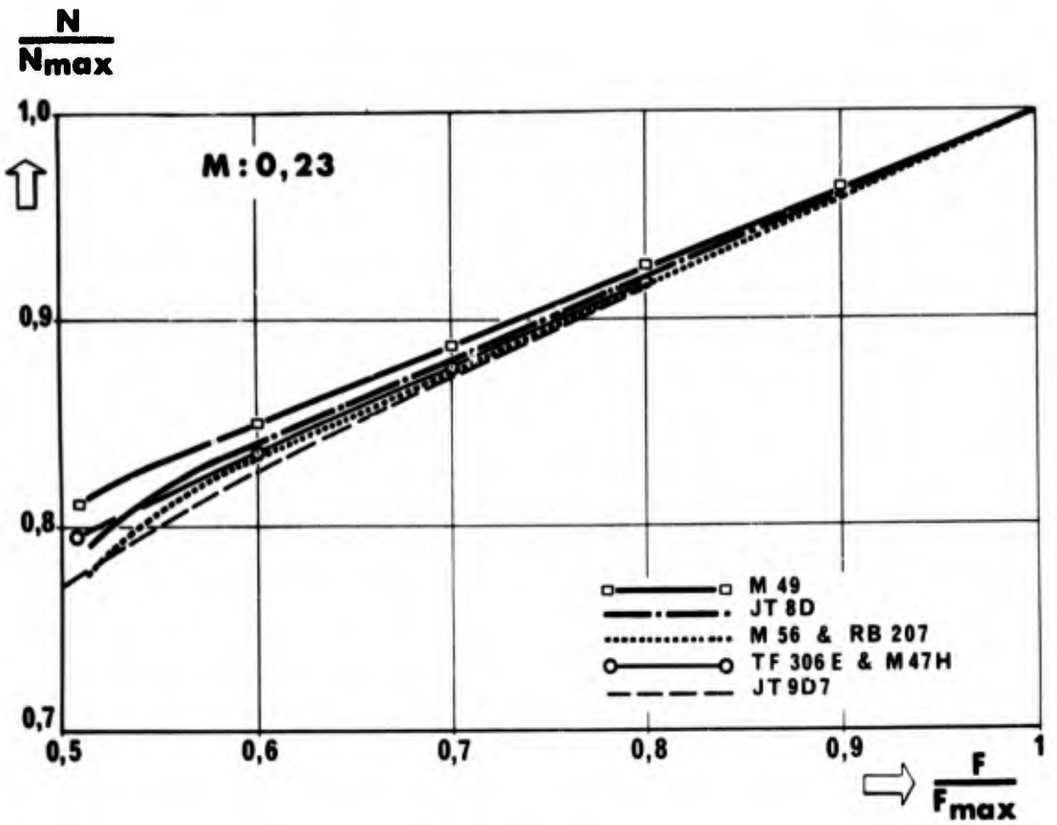

Planche 17 : Poussée en fonction de la vitesse de rotation

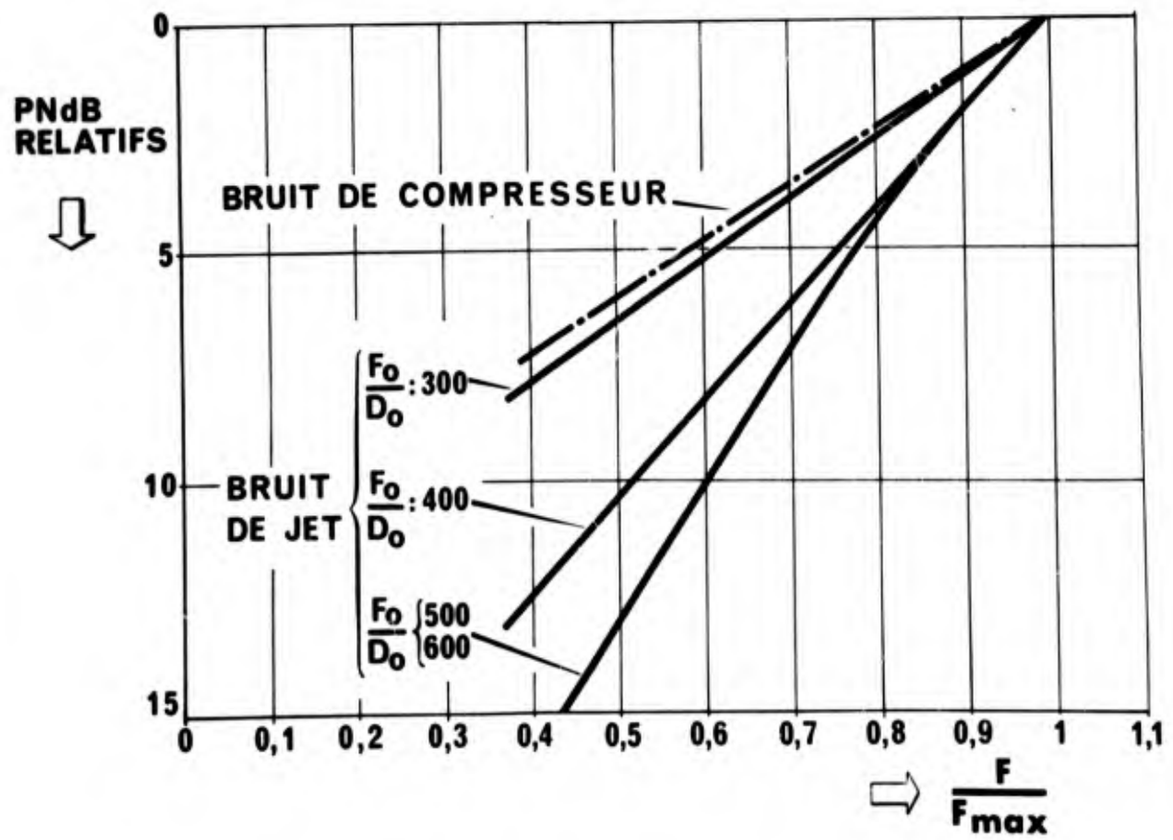

Planche 18 : Bruit d'un réacteur en vol en fonction de la poussée

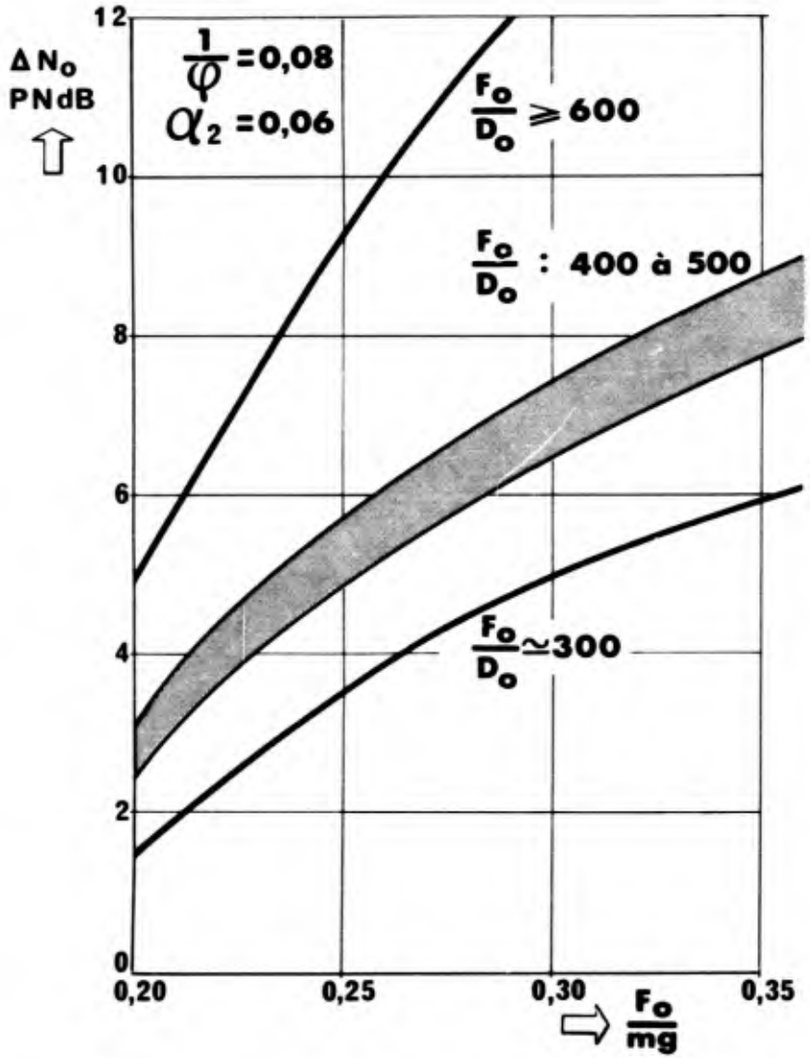

Planche 19 : **Gain potentiel de la réduction ($\frac{1}{\varphi}$ = 0,08)**

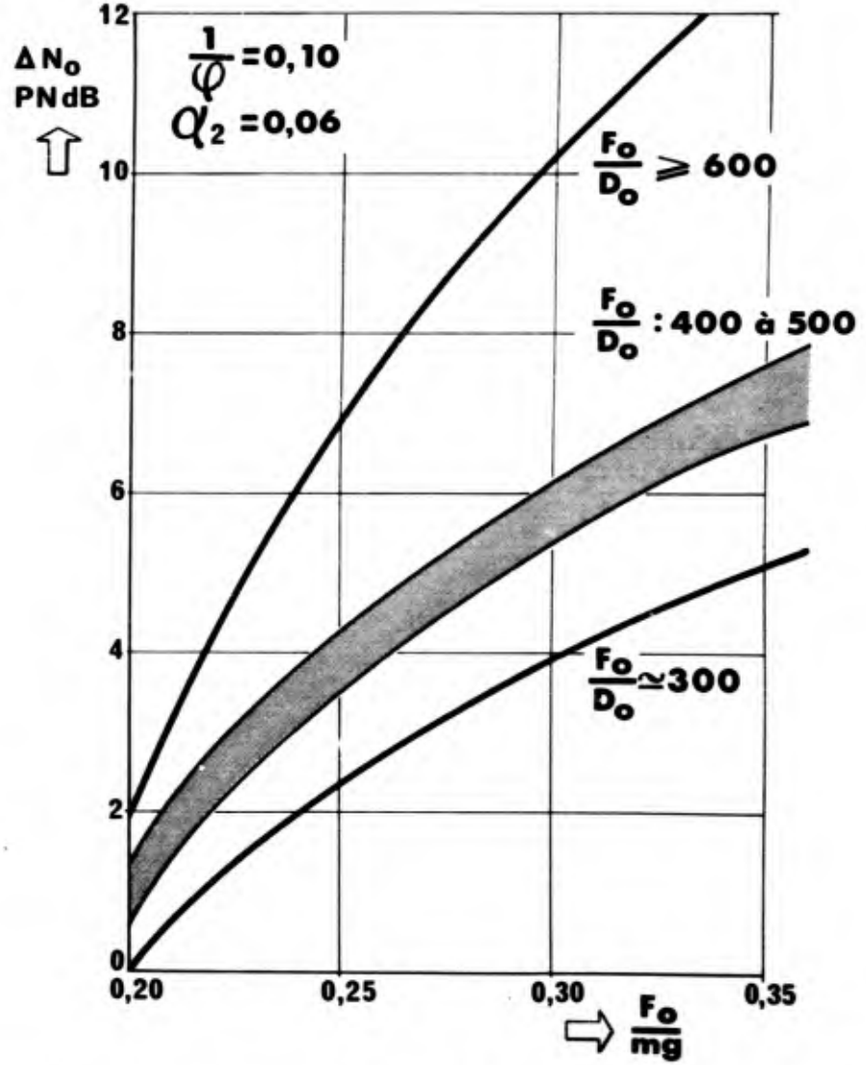

Planche 20 : **Gain potentiel de la réduction ($\frac{1}{\varphi}$ = 0,10)**

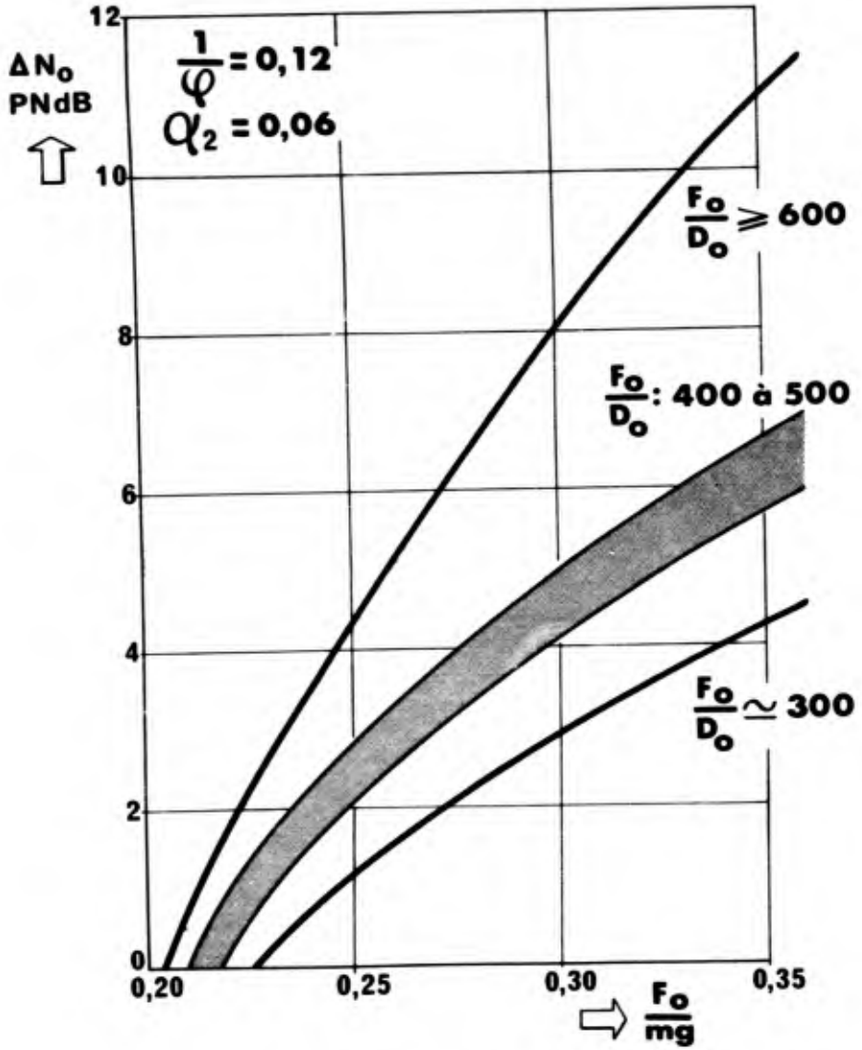

Planche 21 : **Gain potentiel de la réduction ($\frac{1}{\varphi}$ = 0,12)**

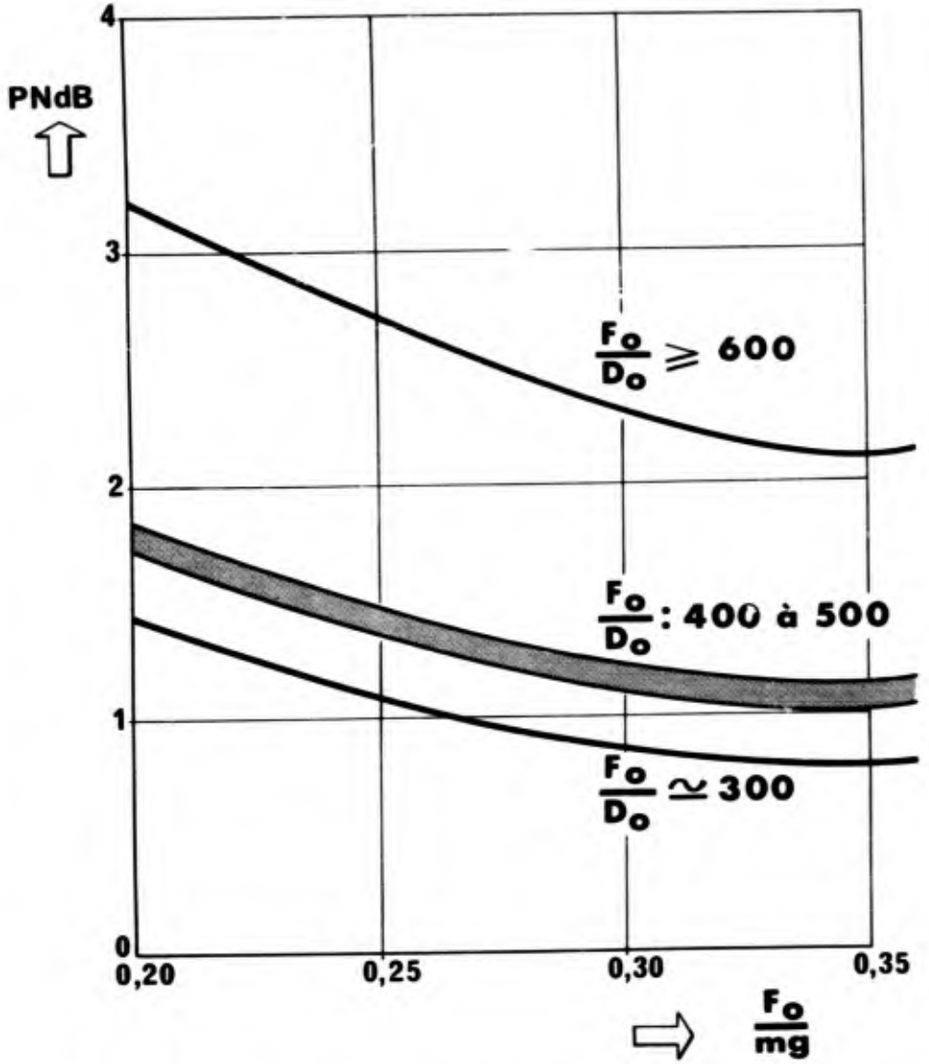

Planche 22 : **Influence de la finesse sur le gain de la réduction**

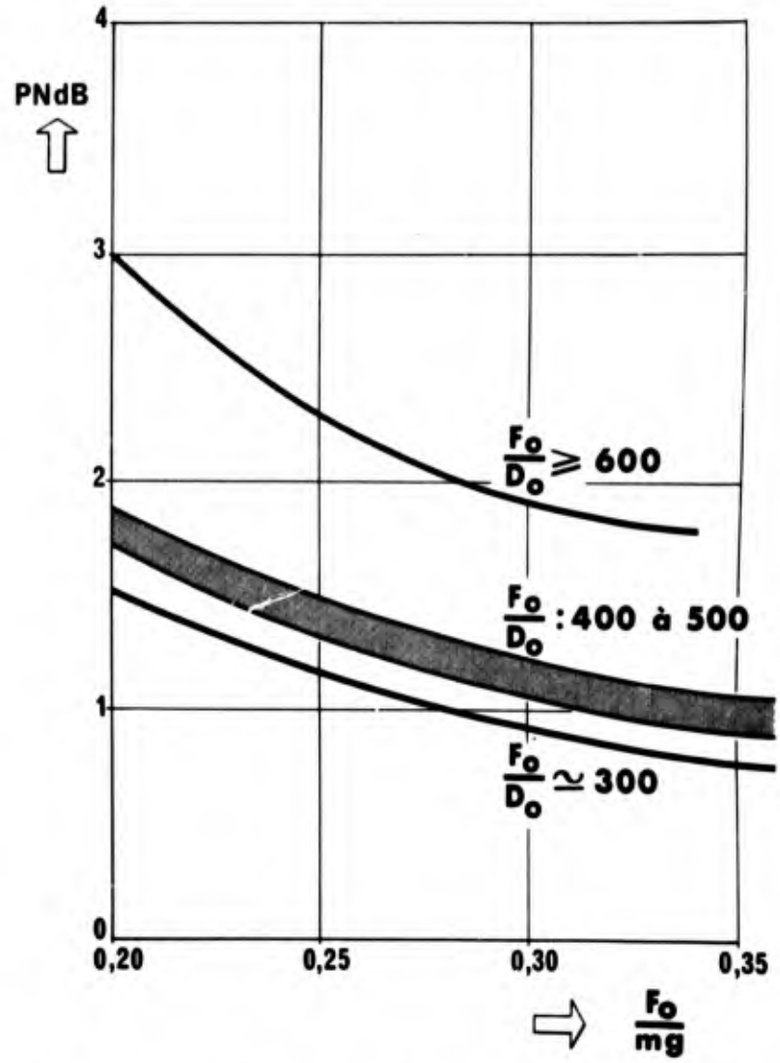

Planche 23 : **Influence de C_2 sur le gain de la réduction**

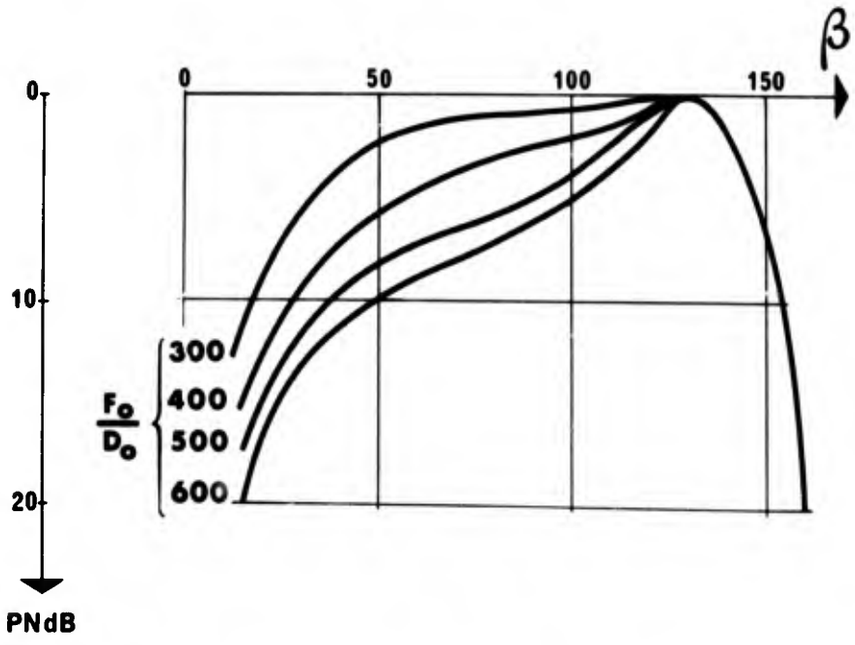

Planche 24 : **Champs sonores**

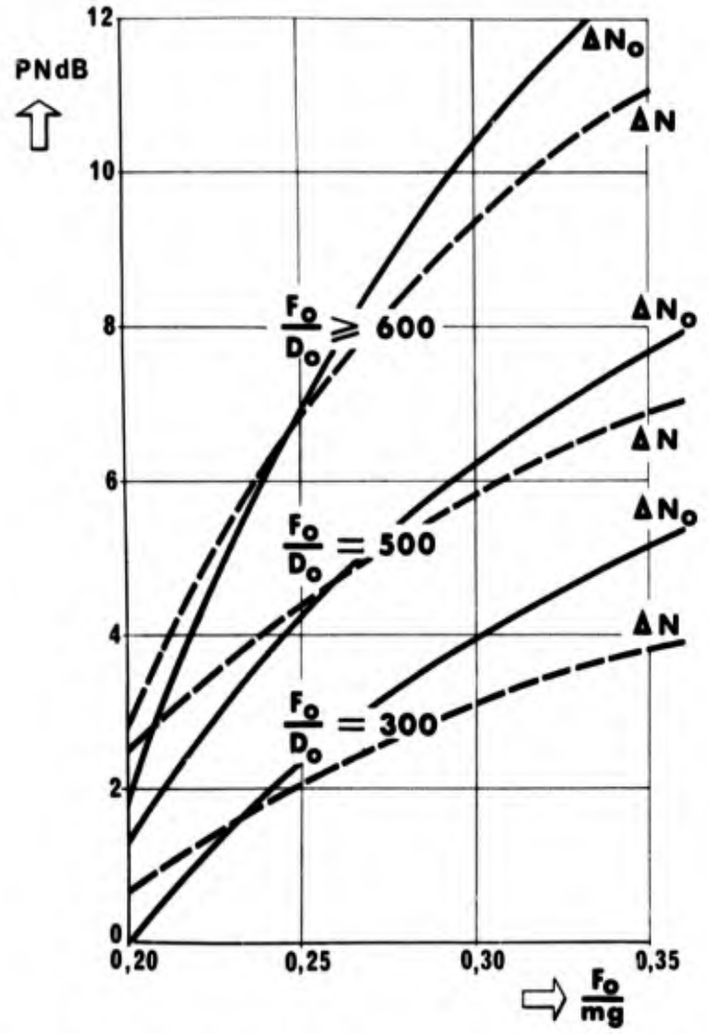

Planche 25 : **Influence du champ sonore sur le gain de la réduction**

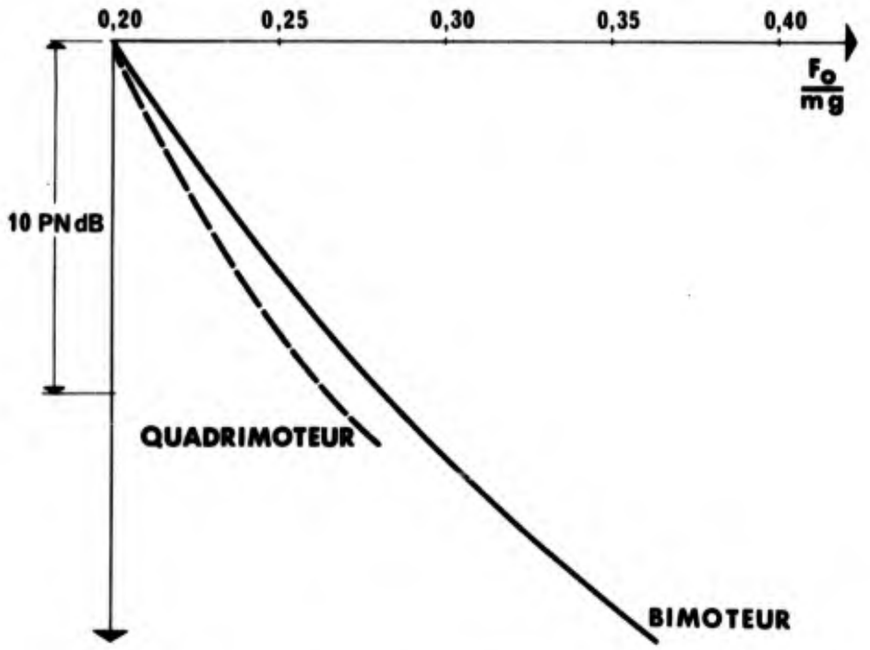

Planche 26 : **Influence de la motorisation sur le bruit au décollage**

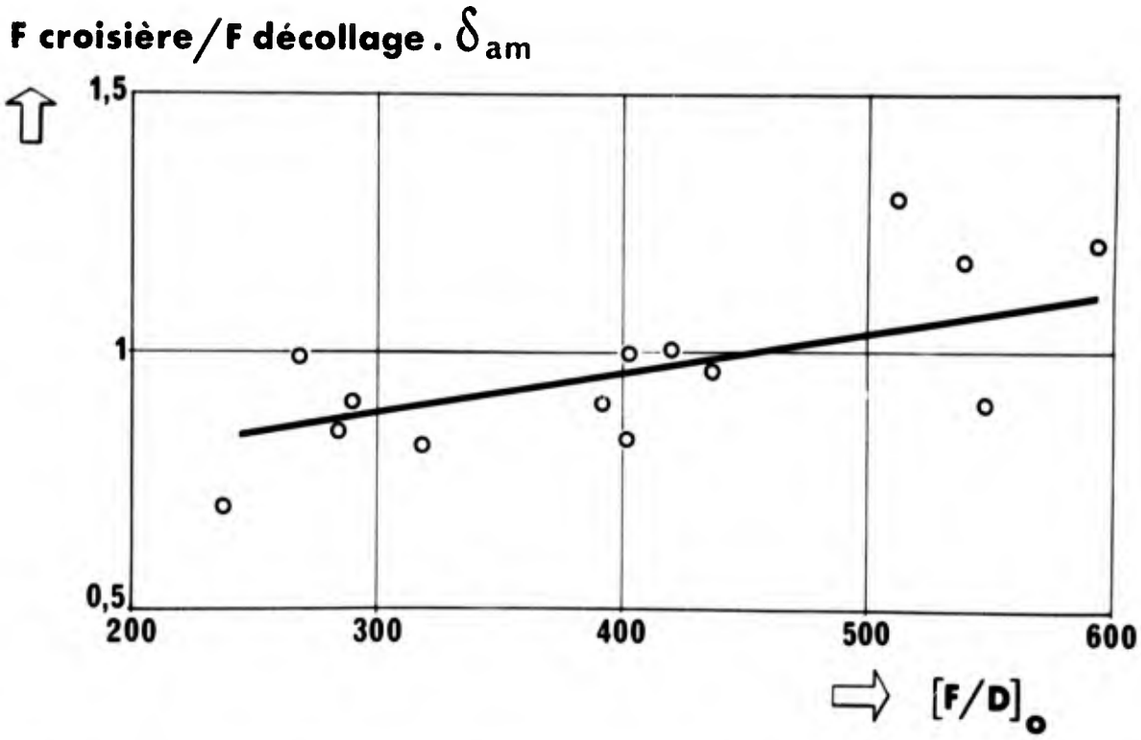

Planche 27 : **Variation de la poussée au décollage, en fonction de F/D à poussée en croisière constante**

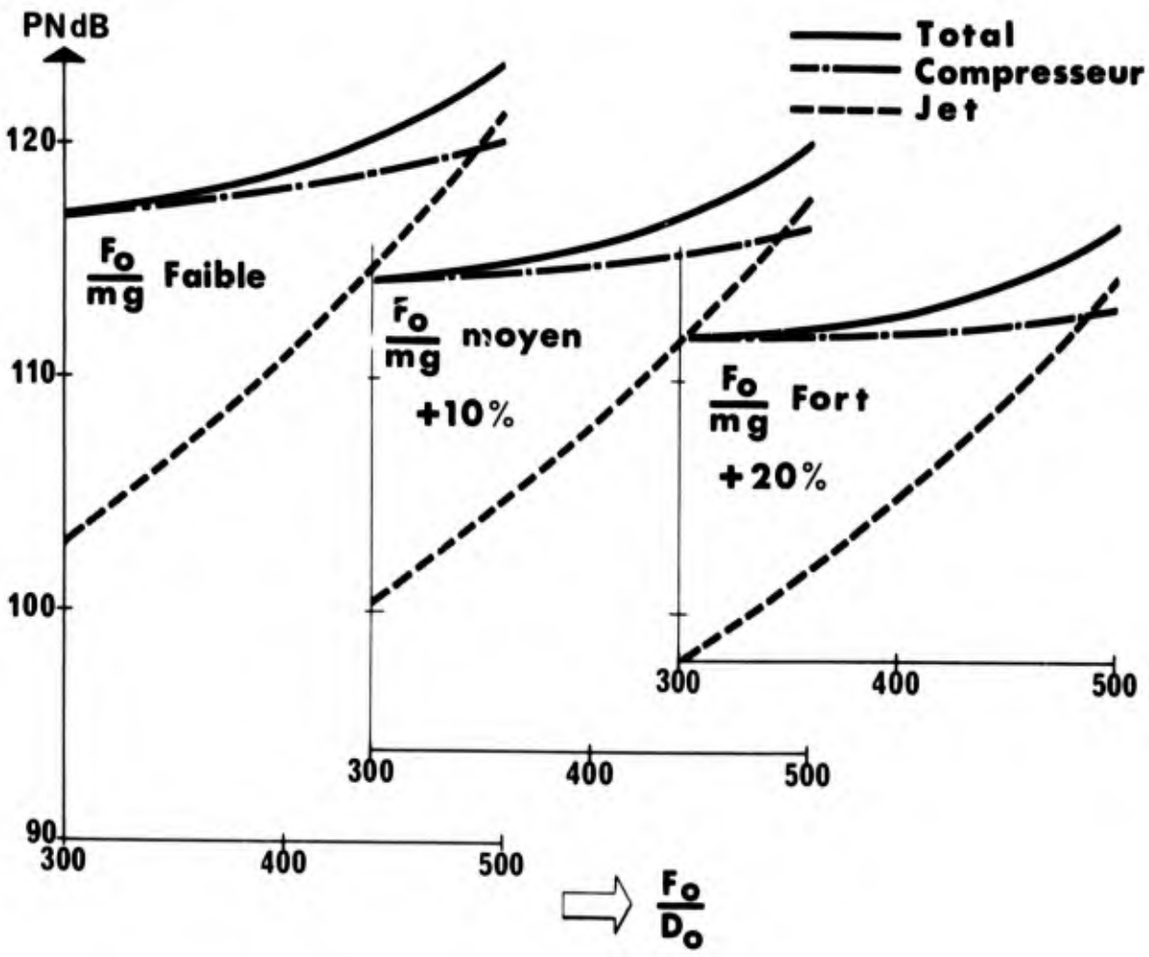

Planche 28 : **Bruit au décollage des quadrimoteurs**

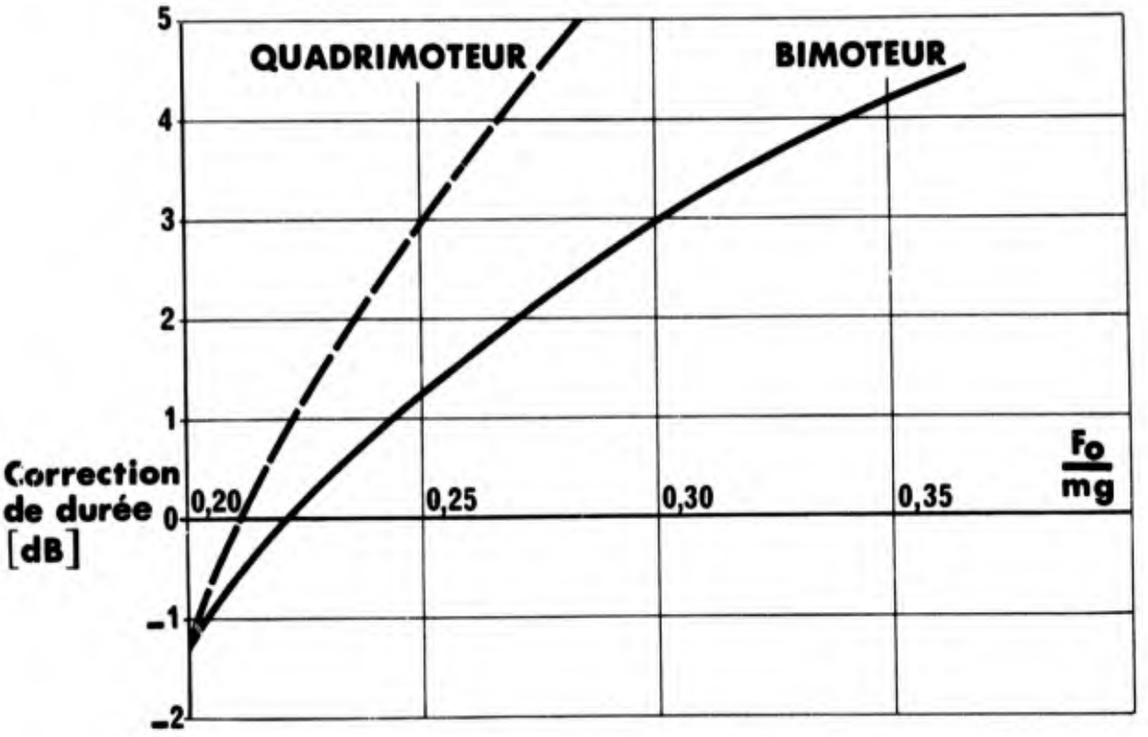

Planche 29 : **Correction de durée**

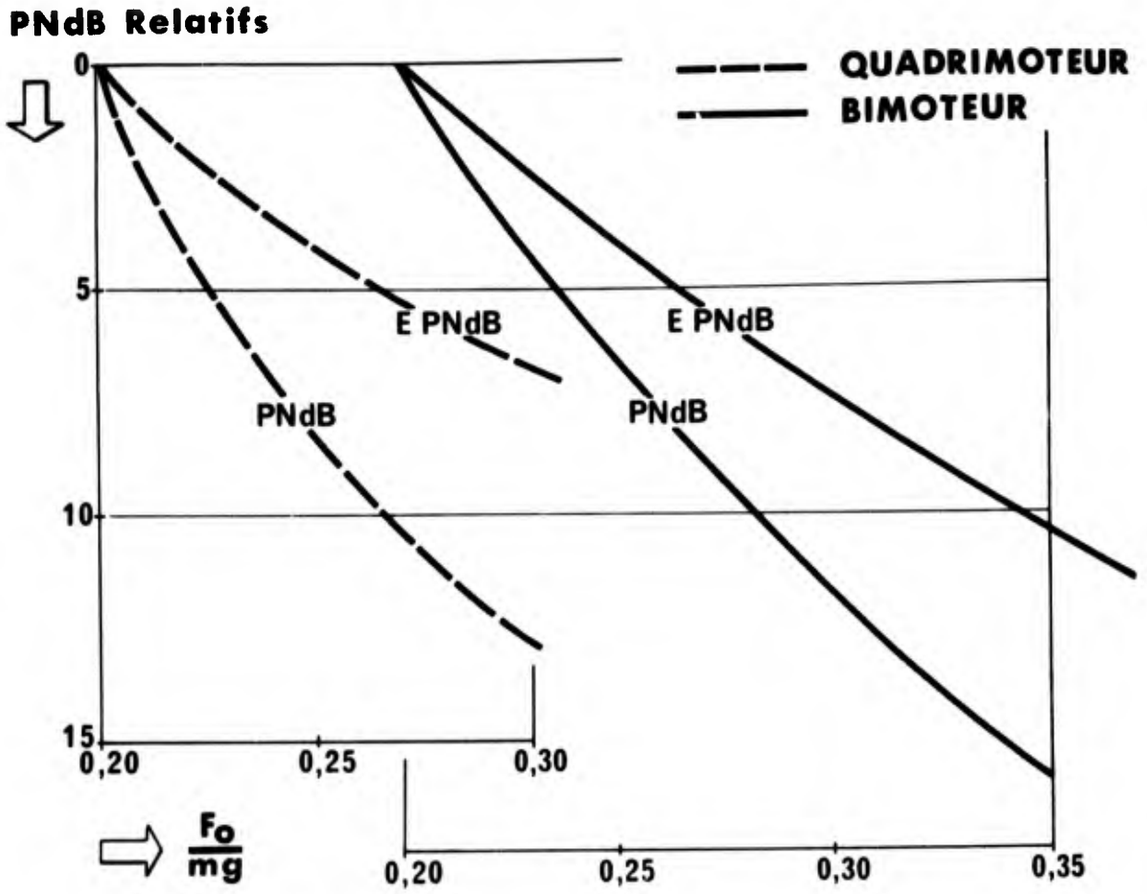

Planche 30 : **Influence de la motorisation sur le bruit au décollage**

GROUND CONFIGURATION EFFECTS ON SONIC BOOM

by

Dino Dini and Renzo Lazzeretti

Istituto di Macchine
Università di Pisa
PISA, ITALY

SUMMARY

The propagation of sonic boom generated in flight operation by a particular aircraft is most significantly affected by ground configuration, due to reflection and refraction in different distribution patterns.
The theory gives a reasonably clear explanation of the sound radiation fields as well as of the reflection laws depending on incidence angles and ground configuration; the relative surfaces will act as good reflectors to sound and shock generated and radiated from a very large distance.
More significant than the noise level affecting the community is the problem of the muntiplying effects of the reflected shock overpressure reaching/leaving the ground.

In the present paper, such effects are analysed for different ground geometries and possible overpressure values. More than twice until eight times the overpressure may be increased, but fortunately their damaging effects on man and light structures are in general sufficiently reduced.
Here the results of computations are presented in tabular form regarding the cases that may occur in practice.
The results of such analytical procedure are compared with known results obtained in other similar pressure-wave propagation.

SYMBOLS AND ABBREVIATIONS (following the order in the paper)

Δp	incremental pressure due to flow field of airplane, pounds/foot^2
V	flight velocity, feet/second
c	sound velocity, feet/second
M	Mach number of aircraft
L	length of the body, feet
y	distance normal to the body and its flight path, feet
w	airplane weight, pounds
B	bel, corresponding to the minimum audible sound of 10^{-16} watts per square centimeter
dB	one tenth of a bel
I	sound intensity, $I = p^2/\ c$ watts/sq.cm where: p is sound pressure in dynes/sq.cm.; is air density in gms/cu. cm; c is the speed of sound in cm/sec.
IL	intensity level in the dB scale. IL = 10 log I/I_r dB, where I_r is 10^{-16} watts/sq.cm.
SPL	sound pressure level as the intensity is proportional to the square of sound pressure, with reference pressure based on the lowest sound that can be detected by a healthy human ear. It is usual to use 0.0002 dynes/ /sq.cm. or 0.0002 microbars (where 10^6 microbars or one bar is approximately equal to normal atmospheric pressure). SPL = 20 log p/p_r dB where p_r is 0.0002 dynes/sq.cm.
PWL	sound power level used as a reference power. PWL = 10 log P/P_r dB, where: P is sound power in watts; P_r is 10^{-13} watts (10^{-12} in metric system)
PN dB	perceived noise decibel developed from tests that compare the annoyance level of sound with that of a known-sound pressure level centered on 1000 cps frequency. Measures in this scale take into account how human ear is affected by a particular energy. PNdB is used mainly for sounds measured outside the aircraft.
t	time in seconds
Δp_r	reflected overpressure, psf
p_o	atmospheric ambient pressure
Δp (t)	overpressure behind the shock front at the time t
I	impulse during the positive phase, psf. second
A_E	effective area distribution of airplane including effect of lift as well as volume
x	distance along the airplane body axis, feet
F	function found from Whitham's mathematical relationships dealing with the rate of growth of the effective area development
h	airplane altitude or lateral distance from model
l	airplane or model length
t_s	clearing time (time to clear face of reflection effect)
Δp_s	overpressure at time t_s
q (t_s)	dynamic pressure at time t_s
q (t)	dynamic pressure at time t
$\Delta p(t_s)$	overpressure at time t_s
S	shortest distance

v_o velocity of the shock front, ft/sec

Δp_b maximum overpressure on the back face

Δp_a side and to overpressure at $t = L/2\ v_o$

β angle of the incident shock on the ground

α_m average Mach cone angle

S' average distance from the center of a wall section to an open edge of the wall, representing the average distance which rarefaction waves must travel to reduce the reflected pressure to the stagnation pressure

K_R reflection factor, $\frac{p + p_r}{p}$

THE SUPERSONIC TRANSPORT AIRCRAFT will raise the problem of sonic boom in a much more acute form. Many countries will require the first generation of these transports to circumnavigate populated areas or to operate subsonically over them in order to avoid public reaction to their sonic booms. But, for the supersonic transport to be a real economical success, it may be necessary for later airplane generations to be capable of supersonic overland. Ground configuration effects on sonic boom need there fore to be explored too.

An aircraft flying at supersonic speed produces a complex system of shock waves. However, at a large distance from the aircraft, this wave system degenerates into a pair of shock waves, the so-called bow and tail waves. The propagation to the ground because of steady supersonic flight is similar, aside from amplitude considerations, to the shock wave pattern leaving the aircraft when it changes its velocity and the pressure discontinuity moves toward the ground. Fig. 1 illustrates how, in a diving maneuver at high altitude, the shock wave detaches from the nose of the aircraft. The two waves produce the sharp rises Δp in pressure separated by a region of gradual fall in pressure, which the ear receives as the characteristic "sonic boom".

For the steady flight boom in a idealized uniform atmosphere, the maximum pressure jump across the bow wave can be easily calculated for different shapes of the body, as a function of Mach number M, length of the body, aerodynamic characteristics, distance normal to the body and its flight path y, aeroplane weight w.
As an example, for a parabolic body of revolution, the magnitude of the shock decreases with the distance from the body proportional to $y^{-3/4}$, and the time delay between bow and tail wave is proportional to the body dimension and increases with $y^{1/4}$.
The strength of the steady flight sonic boom increases slowly with Mach number, once supersonic speed is reached, but increases rapidly with decreasing distance or altitude.
The dependence of the sonic boom overpressure on several parameters is schematically shown in Fig. 2. The condition of the ground, or the reflectivity can serve to absorb the incident shock wave or completely reflect it. If the wave is reflected, the intensity may reach twice the magnitude of the corresponding absorbed shock wave, and locally more in presence of multiple reflections.
The boom will be heard below, Fig. 3, and on either side of the flight path of the aircraft, Fig. 4 (Ref.1) for U.S. Standard Atmosphere 1962, for a distance which is a function of the speed and altitude of the aircraft and of the atmospheric conditions at the time. In view of the width of the belt in which the boom is audible, as much as 50 miles although with appreciable intensity fall off on either side of the flight path, a much grater number of people would be affected by supersonic flight over land than are now influenced by engine noise. The fact that booms might effect often in the future large parts of the same country will also make it difficult to avoid complaints from individuals and representative bodies particularly sensitive to their noise.

Sonic boom overpressure value of 1.5 psf will eventually prove to be tolerable; how ever it seems unlikely that such a value will prove to be acceptable on a routine basis. The experimental flying by supersonic military planes showed that there was strong public protest to sonic boom structure damages when the pressure jump was of the order of 3.5 ÷ 4 psf, due to focusing effects during acceleration or turns affecting limited areas. Current opinion is that the overpressure may have to be redu ced to values as low as 1 psf to be acceptable, as measured out-of-doors, whether the people are out-of-doors or indoors.

But, the pressure jumps to be expected from actually designed supersonic civil trans ports can normally be prevented from exceeding 2 psf so long as the aircraft is not allowed to fly supersonically until it has reached a height of about 40,000 ft. If the future goal is to reduce maximum overpressure to the above mentioned value of 1 psf, it is to be considered that:
- a 20 percent reduction in overpressure requires an 18 percent increase in altitude, which means obviously a substantial decrease in the payload;
- a cruising overpressure of current supersonic transports down to 1 psf level would necessitate aircraft 50 percent longer and lighter at the same time; changes that would require a large advance over present materials and structural technology.

That is to say that we cannot expect sizable reductions in the anticipated overpressure levels.
For a better understanding of the present design limitations, Fig. 5 (Ref. 2) shows airplane configuration effects on sonic boom overpressure levels. These curves are referred to planes weighing 400,000 pounds and 230 feet long.
Overpressures are necessary to carry the weight of the aircraft. Typical , a 700,000 pounds, 300 foot-long aircraft, flying at a Mach number of 3 and an altitude of 700,000 feet, has an overpressure level of 1.5 psf. But, other configurations are possible, Fig. 6 (Ref. 3), that would lead to substantially lower peak overpressures. Airplanes having lifting surfaces extended to the front of fuselage, and utilizing interference effects, can be effective in reducing maximum sonic boom overpressure, because they utilize near-field effects. To alleviate a portion of the boom due to the lift alone, it is possible to employ volume effects, as a given volume alone through the air at supersonic speeds might theoretically avoid any sonic boom production. Now we have considered factors concerning the source of the supersonic field, suitable to be controlled to varying degree; other factors, such as those associated

with atmospheric conditions and ground effects, cannot be controlled.

Supersonic flight at lower altitude may produce pressures on the ground high enough to break ordinary window glass and to result in building vibration being felt by its inhabitants and in possible small damage to buildings. From FAA sonic boom investigations conducted with fighter aircraft, qualitative indications were recently obtained about normal structural response of buildings varying considerably in design. In particular, the effects of repeated sonic boom, at White Sands, at a scheduled overpressure of 5 psf generated by B-58 and F-104 aircraft, produced no damage to previously undamaged material, and in general it was found that no structural damage occurred below 5 psf. Table I shows some shock noise phenomena reported in Ref. 4. Booms having an N-wave with a short rise time and sharp peak were reported as the most objectionable.

Table I

p pd/sq.ft.	p dB	Resulting physiological reaction	Associated physical phenomena
0.1 to 0.3	108 to 118	Not objectionable	Barely audible explosion
0.3 to 1.0	118 to 128	Tolerable	Distant explosion or thunder
1.0 to 3.0	128 to 138	Objectionable	Close-range thunder, some window damage
3.0 to 10.0	138 to 148		Damage to large plate-glass windows
10.0 to 30.0	148 to 158		Definite damage to small barracks-type windows

As it may be seen in Table I, and in order to evaluate sonic boom effects on people, the overpressure Δp is expressed in equivalent Intensity Level (IL) expressed in decibel (dB). Sound intensity levels cannot be measured directly and, since the human ear and most microphones are pressure-sensitive, sound levels are more usually obtained by measurement of sound pressures (S P L). As human response to any kind of aircraft noise does not correspond to physical measurement of sound level (dB), a "perceived noise" scale (PNdB) has been developed to deal with noise intensity and frequency spectrum. Measurement on this scale is corrected for the duration of the noise, and the frequency at which it occurs. Since the sonic boom only lasts a fraction of a second the "perceived noise" will be considerably less than the physical measurement in decibel. As an example, a piston-engined transport aircraft and a jet may both give readings of 104 dB on a sound-level meter but the jet will be judged to be noisier because it radiates a greater amount of high-frequency noise. Thus, on the PNdB scale, the jet may give a value of 116 PNdB while the piston-powered transport might indicate 102 PNdB.
By its real nature, the sonic boom cannot easily be compared with normal aircraft engine noise 112 PNdB at take-off is given as an acceptable noise limit. The 128 to 138 dB corresponding to a Δp of 1 to 3 psf appears to be on the borderline of acceptance. The ground overpressures directly beneath the Concorde flight track have been predicted, (Ref.6), as follows:
- cruising conditions: 1.3 to 1.6 psf; one or two booms sounding like close-range thunder will arrive in the region 130 to 320 miles from take-off;
- initial climb and acceleration: up to 2 psf; much louder bangs and minor damage could occur.

Sonic boom may arrive either through the air or through the ground over large areas. Modifications of initial overpressure and frequency values are to be expected more from ground configuration than from atmospheric conditions. Simple and multiple reflections from the ground may locally raise peak overpressures and wave frequency to unexpected values producing excitation and vibration of buildings and having significant effects on people in them. Fortunately, the energy amount transmitted from airplane to ground through the air is not big enough to impress substantial ground vibration influencing stability of a group of buildings as a whole. But, excitation induced from combination of air and ground paths on any part of a building may produce more than superficial damage of the structure.
Particularly where there are many reflecting surfaces, very close to each other with different orientations, energy concentration acts on some points, producing dangerous effects. An imaginary explanation of this fact could be given by the limiting case of pressure wave concentration at the center of a spherical cavity acting as normal reflecting wall of such waves. Damage from multiple reflections rarely occurs, as extensive tests have previously proved, only because it is quite difficult to have at the same time, and in the same small region, a coincidence between energy, or multiple reflection, concentration and weak materials. In that considering the small interested area, in general sufficiently thick to resist a relatively small force coming out from high overpressure. Different behaviour and severe damage could be produced on electronic equipment, or similar weak devices, by such condition of high pressure distributed on a small area (low force), Everybody has in mind domestic

current examples of overpressure action on doors and windows, in order to understand the more intense effect deriving from combination of inputs due to multiple reflection of the same phenomena.
A hand action in opening the main door at the street level of a building, much less in magnitude than 1 psf and longer in rise time and distributed over a small area, propagates overpressure upstairs in such a way as to be strongly appreciated by someone who is opening, almost at the same time, a door on the first floor. An ideal ized contemporary superimposition of similar impulses against the door could simulate the effect of multiple reflection as in a stronger manner could be determined by sonic boom.
Supersonic transport on a routine basis should have to avoid a close flight path by two airplanes flying in very different directions, to prevent having in any place on the ground a sonic boom superimposition.

The interaction of the air cavities and the structure of a building can be important in other response modes in cases where there are openings such as doors and windows. Pressure fluctuations inside the rooms occur with pressure transient markedly longer than outside, and the peak pressure value actually might exceed that of the outside exposure. It is known that this type of pressure environment may be important subjec- tively.
A person inside a building would be exposed to a rather complex series of stimuli, including auditory, visual, and vibratory inputs, owing to vibratory motions of the building it-self and the cavity resonances. The corresponding frequence range has the characteristic shape of the noise trace, associated with the rattling of structure, floor and furnishings.
In certain situations, these stimuli are significant.
People and animals outdoors are impinged directly by the sonic boom, sometimes with significant effects. Not rare have been the cases in which small animals have died because of sonic boom repeated reflection.

Damage to structures and people as above described may often happen, both with peak overpressure of 2, without reflection, or 1 psf with reflection. This means that effort in designing airplane configuration to reduce sonic boom effect on the ground has limitations. The results of some research to realize the "minimum boom" configu- ration show that the structural weight and cost of production are increased with respect to the "minimum drag" design. Further, a benefit in sonic boom during the climb (1.2 instead of 1.9 psf) brings a corresponding decrease in pay load (10 percent). From this it raises the question of whether or not to reduce overpressure appreciably through airplane configuration.
The problem remains; and it seems convenient to follow the way of suitable overland flight paths and airport locations.

TYPICAL INCIDENT OVERPRESSURE DIAGRAMS AT A FIXED LOCATION ON THE GROUND.

AN AIRCRAFT FLYING AT SUPERSONIC SPEED propagates a disturbance which moves in the atmosphere approximately as an acoustic wave system.
Weak but cumulative effects create shock waves, so that the overpressure distribution far way approaches an N-wave, Fig. 3. On the airplane "near field" the pressure sig- nature is complex, and both its shape and magnitude depend on the airplane configu- ration. At a sufficiently large distance, where the amplitude alone depends on the airplane shape, the characteristic "far field" N-wave is formed. Negligible errors will result if disturbances from all parts of the airplane, including those associated with lift, are assumed superimposed on the longitudinal axis.

In order to understand sonic boom loading on ground, we take as an example the im- pingement on a building, (Ref.7).In Fig. 6 the wave pattern, about 1000 feet in length and 0.3 seconds in time, generated by a supersonic transport sweeps over a sealed building applying complex transient vibrations.
Reading from left to right, the initial positive loading first forces the building outward; it is then forced inward from all directions then forced outward, and finally displaced laterally again because of the negative pressures acting on the back surface.
Some rather special effects may be present for a real building having openings such as doors and windows. As an example we see in Fig. 7b) (Ref.7) the results of tests conducted with aircraft flyovers of a cubic room having a window. It can be seen that: with window closed, the internal pressure transient has a relatively small amplitude and is damped out rather quickly; with window partially open, the duration of the inside pressure transient is quite longer and the peak overpressure exceeds that of the outside.

The behaviour of sonic boom on the ground is similar, even though much less in magni- tude and duration, to that established by blast overpressure at a fixed location on the ground. The variation of overpressure with time that would be observed at any location in the few seconds (for a large explosion in air) following the detonation is shown in Fig. 8. The number 1 represents the time of the explosion, and 2 indicates the time of arrival of the shock front. At the latter point, a strong wind commences to blow away from the explosion. This is often referred to as a "transient" wind be- cause its velocity decreases fairly rapidly with time. Following the arrival of the shock front, the pressure falls rapidly and at the time corresponding to the point 3 it is the same as that of the original (ambient) atmosphere. Although the over-

pressure is now zero, the wind will continue in the same direction for a short time. During the interval from 2 to 3 most of the destructive action of the air burst will be experienced. As the pressure in the blast wave continues to decrease, it sinks below that of surrounding atmosphere. In the time interval from 3 to 5 the negative (or suction) phase of the blast wave passes the given location. For most of this period, the transient wind blows in the direction toward the explosion. The maximum negative overpressure is always smaller than the peak overpressure at the shock front and quite minor in character. During the passage of the negative phase, the pressure at first decreases and then increases toward that of the ambient atmosphere which is reached at the time represented by the number 5. The dynamic pressure is very low in comparison to the shock overpressure, except for very strong blast wave. The experience gained in blast wave damage on the ground, very far from an atomic explosion, has indicated a peak overpressure of 70 psf to damage in some way every structure. But bigger overpressures, from 450 to 2000 psf, are necessary to damage severely or destroy any kind of structure from light steel-frame industrial buildings to reinforced concrete structures.

When the incident blast wave from an explosion in air strikes the ground surface, it is reflected.
On Fig. 9 we see four stages in the outward motion of the spherical blast originating from an air burst bomb. Shock front of stage 1 has not reached the ground; a reflected wave, indicated by the dotted line, has been produced in the third stage. The value of the pressure experienced at the surface is generally considered to be entirely a reflected overpressure, since reflection is formed instantaneously. In the region near ground zero, this total reflected overpressure Δp_r will be more than twice the value of the peak overpressure of the incident blast wave. The variation in overpressure with time on the point A, not too far from ground zero within the zone of regular reflection, is depicted in Fig. 9. At any location somewhat above the surface, point B in Figure, two separate shocks will be felt, the first due to the incident blast wave and the second to the reflected wave, which arrives a short time later. Especially in the case of a very short "positive phase" of the shock, this phenomenon is less appreciable and only regards a very small region close to the ground surface.
The process of incident and reflected wave interaction is called "Mach" or "irregular" reflection. At the successive stages represented by Fig. 10, the reflected shock near the ground has overtaken and fused with the incident shock to form a single shock front called "Mach stem". Triple points arise, as the reflected wave continues to overtake the incident wave, and the height of the Mach stem increases. The behaviour of this fused or Mach shock is the same as that described for shock fronts in general.
In the Mach region below the triple point path, the various blast wave characteristics at the shock front are uniquely related by the Pankine---Hugoniot equations. When the blast waves strike a surface head on, such as that of a structure, the instantaneous value of the reflected overpressure Δp_r is given by

$$\Delta p_r = 2\Delta p \left(\frac{7 p_o + 4\Delta p}{7 p_o + \Delta p} \right) \qquad (1)$$

It can be seen from this expression that the value of Δp_r approaches $8\Delta p$ for large values of the incident overpressure (strong shocks) and tends toward $2\Delta p$ for small overpressures (weak shocks). For many situations, the variation of the overpressure Δp (t) behind the shock front with time t at a given point (positive phase in Fig. 7) can be represented by the simple empirical equation

$$\Delta p \ (t) = \Delta p \ \left(1 - \frac{t}{t^*}\right) e^{-\alpha t/t^*} \qquad (2)$$

Where t^* is the duration of the positive phase of the blast wave. The average decay parameter may also be regarded as an adjustable factor which is selected so that a decay relation provides suitable values of blast impulse.
Another blast damage parameter is the impulse I which takes into account the duration of the positive phase, i.e. the total area under the overpressure time curve of Fig. 7,

$$I = \int_0^{t^*} \Delta p \ (t).dt \qquad (3)$$

As predicted for the sonic boom loading on sketch in Fig. 7, we may see in Fig. 11, in plan, a building which is being struck by an air blast wave moving in a horizontal direction. The shock front is seen approaching the structure perpendicularly, reaches the front face of the building, producing an overpressure up to at least twice (and generally several times) that in the incident front, proceeds and reaches the back. Here the pressure, earlier existing on the front face, is decreased and the blast wave diffracts around the structure. Finally when the shock front has passed, approximately equal air pressures are exerted on all the walls and roof of the structure. Lateral force could be produced if the structure is oriented at an angle to the blast wave.

For long structures the diffraction loading will operate for a consistent period of time, one-tenth of a second for a 75 feet length. For thin structures, like telegraph poles, the diffraction period is so short that the corresponding loading is negligible.

In the presence of openings, windows, panels, or doors which fail in a very short space of time, there will be a rapid equalization of pressure between the inside and outside of the structure, reducing markedly diffraction.

Coming back to the N-wave with two shocks separated by an expansion, typical of sonic boom as shown in Fig. 3 and 7, we start to compare its ground intersection, Fig. 12, with that coming out from air blast, Fig. 9.

The pressure field by an aircraft flying horizontally at supersonic speed steadily propagates through the volume limited by two cones. Bow and tail cones correspond to the two abrupt pressure rises wich are usually heard as a double boom on the ground. Because of the more and more space interested, the overpressure decreases with increasing propagation distance. Nevertheless, the shock waves mantain their characteristics for great distances.

The intersection with the ground has the shape of a parabolic band which sweeps on there at the same speed as the airplane.

This is easy to imagine if we consider the trace left by a horizontal plane cutting two cones having the same horizontal axis but tips separated by a distance of the order of the airplane length. At a certain instant the effect of the sonic boom is contained within this band: the overpressure of the shocks is greatest on the ground directly under the airplane (along the bisectrix of the band) and decreases, because of the increasing propagation distance, with increasing offset to either side of the path. Directly under the airplane, there is the greatest bow shock (point A) and the greatest tail shock (point B). The whole wave pattern (Fig.3) has gone; through the point B on the ground this is starting to pass through. At some distance to the side, two-three times the altitude of the airplane, the shocks have become so small that the abrupt jumps are vanishing. These points, called lateral cut-offs, Fig.4, define the lateral extents of the boom. Each fixed location on the ground interested by the bang, receives the impact of the entire wave pattern, like the effect of blast wave in Fig. 8. As a shadow on the ground the sonic boom band is following the airplane along its flight at supersonic speed. But, during propagation, the pressure signature and its location is often distorted by wind and atmospheric turbulence.

The pressure field by an air blast is propagating along spherical waves and its impact with the ground is starting from a point on the vertical intersection. From there the impingement with the ground is spreading along a circular area, interesting a large region depending on the blast intensity, until lateral cutoffs are reached. Beside different wave pattern and consequent effects, each point on the interested region is going across the typical pressure-time curve, with magnitude depending on decay due to distance.

For both the cases, sonic boom and explosion in air, the propagation velocity (at sufficiently large distance from the explosion) is about that corresponding to the quiet air sound speed. There is no difference in the mechanism of reflection on the ground; but the overpressures valued, in general considered for blast wave, are much more intense and therefore suitable of higher amplification in reflection. Less time duration of sonic boom at a fixed location on the ground focuses reflection effects only in a small area around any fixed location on the ground.

There is no significant difference in the subjective reactions of people to pressure jumps of a given value caused by aircraft and explosives, as measured out-of-doors, whether the observers were out-of-doors or indoors. This means that further experiments on people's reaction to sonic boom would be possible using explosives to produce the noise, a much more convenient method than using aircraft and one which can be applied locally to a small number of people with-out affecting a large area.

But, considering that the pressure diagram, Fig. 8, from an explosion has only an abrupt bow shock wave, the tail shock at the end of negative phase having almost disappeared, and this fact depending upon gradual and not sharp reaction to the quite rapid vanishing effect of the explosion waves system in the air, we may conclude that the sonic boom pattern on the ground is suitable to exert more vibration phenomena on buildings and people. Sharp rise time, both for positive and negative pressure jumps which are very close for short airplanes, may induce on people and buildings high frequency vibrations very dangerous at low altitude accelerated flight.

Now we have to analyse briefly how the "far---field" signature, Fig. 3, may be predicted for each airplane configuration. Each detailed shape is responsible of the "near---field" signature.

In Fig. 13, (Ref. 13), is illustrated the derivation of an equivalent body-area development for the flow field below a supersonic transport configuration.

The actual area A_E is essentially determined by the cross-sectional areas of the airplane and by the equivalent one due to the distribution of lift as determined from supersonic area-rule concepts, taking into account airplane boundary layer, engine airflow, control deflections, and shocks due to rapid chages of area.

Development of sonic boom prediction techniques is due to Whitham, Walkden, Carlson, and others, (Ref. 16 and 17), with procedures for performing the calculations efficiently and demonstrating the validity of the theory by comparison with wind tunnel and flight test results.

Whitham's method and in patticular a complex computing program like that in use at Langley Research Center, respectively in Fig. 14 and 15 from Ref. 13, permit the

definition of the pressure field, after an equivalent body (Fig. 13) is defined, through a function F representing the pressure signature very close to the body. The area development in Fig. 15 is obtained from the zero-lift-drag program, (Ref. 14), suitable for determining theoretical pressure signatures at any distance from given configuration, Mach number, altitude, and other flight conditions, and now in use by the aircraft industry. This method is verified through experimental wind-tunnel programs, using models as small as 1/2 + 4 inch of length and h/l ratios (lateral distance from model/model length) of the order of 4 + 32, for Mach number from 1.06 to 2.01, from 0° to 5° angle of attack, with reasonably good agreement of experiment and theory (Ref. 15). As illustrated in Fig. 16 (Ref.13) a considerable amount of correlation has also been done with flight test data extending from subsonic to supersonic speed taking into account, in predicting pressure signature, the atmospheric corrections. In Fig. 16 we see that the peak overpressure has gone from 100 psf, at 50 ft and M = 1.12, to less than 1 psf, at 48,000 feet and M = 1.93.

When impulse minimization by configuration modification is the goals, a compromise between drag and body shape for minimum far-field overpressure must be made; because, for example, a blunt body suitable for minimum impulse at all distances has shock losses near the body too high for practical applications.

Pressure builds up or superbooms on the ground can result from certain manoeuvers of an aircraft such as longitudinal, lateral or normal acceleration. The superboom areas on the ground are fixed and do not move with the aircraft. Their shape, size and location are readily predictable, as well as the multiple boom region, during known changes in acceleration rates, altitude, and airplane attitude.
In some cases, overpressure amplitude factors over 4.0, (Ref. 19), have been measured.

With regard to lateral spread of the sonic boom, already indicated in Fig. 13, we may see in Fig. 17, (Ref. 18), the bow shock wave ground intersection pattern, for fighter aircraft in steady level flight at 52,200 feet and M = 2.0, measured from an accurately calibrated and oriented array of matched microphones. It can be seen that the overpressures are maximum on the flight track and decrease with increasing lateral distance.

Pressure signatures measured along the ground track of an SR-71 airplane at various altitudes from below 50,000 feet to above 70,000 feet and Mach numbers to 3.0, are presented in Fig. 18. There, (Ref. 20), it appears that the peak-overpressure values decrease and the time durations increase as the altitude of the aicraft is increased, the Mach number effect being much less.

The propagation of shock waves through the atmosphere may be changed by the dynamics of the atmosphere itself as well as by refraction effects, with wide variation in wave shape and peak overpressure even at a distance of a few hundred feet on the ground, Fig. 19 (Ref. 13) regarding a fighter aircraft at 20,000 feet altitude and M = 1.7. In Fig. 20 (Ref. 13) variations of measured sonic boom pressure signature at ground are presented for small, medium and large aircraft.

Some characteristics of sonic boom influence the overall response of buildings, structural components or windows, others are effecting people out-of-doors or indoors. In Fig. 21 (Ref. 21), the traces represent, respectively: outdoor overpressure, overall pressure variation inside the building, audible portion of the signal and the vibratory signal resulting from floor accelerations.

REFLECTION ON THE GROUND

The shock front reaching the ground is reflected and, in some cases, as already shown on Fig. 9 and 10, the overpressure may be increased twice or more. When a horizontally moving shock front strikes a vertical wall (such as in the case of Mach stem formation, Fig. 10), or, more generally, a shock wave produced by sonic boom impinges normally a wall, the peak overpressure reaches the maximum reflected value given by Eq. (1). If the wall is inclined at an angle to the face of shock front, the reflected overpressure decreases as the angle increases.
From Eq.(1) we get, for very weak shock, $\Delta p_r = 2\Delta p$.

The reflected overpressure Δp_r on the front wall, Fig. 22, decays rapidly to a value Δp_s corresponding to the side on overpressure Δp (t_s) plus some proportion of the dynamic pressure q (t_s), in a time t_s called the clearing time. This is indicated schematically in Fig. 22, where Δp_r is acting at t = 0. The clearing time at a point on the front wall is a function of the shortest distance from the point on the structure to an edge where pressure can spill around the structure. The clearing time is

$$t_s = \frac{3}{v_o} \frac{S}{} \qquad (4)$$

where S is equal to H or to $\frac{1}{2}$ B whichever is less and v_o is the velocity of the shock front

$$v_o = 1{,}117 \sqrt{1 + \frac{6\Delta p}{7 \times 14{,}7}} \quad \text{ft/sec} \qquad (5)$$

The drag coefficient for the front face is unity, so that the drag pressure here is equal to dynamic pressure. The stagnation pressure is thus

$$\Delta p_s = \Delta p\ (t_s) + q\ (t_s) \qquad (6)$$

The dynamic pressure is obviously negligible for weak shocks like that of sonic boom. The pressure subsequently decays with time, so that

$$\text{Overpressure at time } t = \Delta p(t) + q(t) \qquad (7)$$

where t is any time between t_s and t^* (at the end of the positive phase). The average effective loading on the back face of the closed box-like structure of Fig. 22 is shown in Fig. 23. The shockn in Fig. 23. The shock front arrives at the back face at time L/v_o, but it requires an additional time $4S/v_o$, for the pressure to build up to the value Δp_b. Here, as before, S is equal to H or 1/2 B, whichever is the smaller. The drag coefficient on the back face is -1/2, and so the overpressure at any time after Δp_b is

$$\text{Pressure at time } t = \Delta p\left(t - \frac{L}{v_o}\right) - \frac{q}{2}\left(t - \frac{L}{v_o}\right) \qquad (8)$$

where t lies between $\frac{L + 4S}{v_o}$ and $t^* + \frac{L}{v_o}$.

The effective net translational force on the structure is the difference between the force on the front wall and that on the back wall.
In regard to the sides and top of the closed box-like structure of Fig. 22, although loading commences immediately after the sound wave strikes the front face at t = 0, they are not fully loaded until the wave has travelled the distance L, i.e. at time $t = \frac{L}{v_o}$. The average overpressure Δp_a at this time is considered to be the overpressure plus the drag loading at the distance L/2 from the front of the structure, so that,

$$\Delta p_a = \Delta p\left(\frac{L}{2v_o}\right) - \frac{q}{2}\left(\frac{L}{2v_o}\right) \qquad (9)$$

the drag coefficient on the sides and top of the structure being - 1/2. The loading thus increases from zero at t = 0 the value Δp_a at the time L/v_o, as shown in Fig. 24. After this time the pressure at any time t is given by

$$\text{Pressure at time } t = \Delta p\left(t - \frac{L}{2v_o}\right) - \frac{q}{2}\left(t - \frac{L}{2v_o}\right) \qquad (10)$$

where t lies between $\frac{L}{v_o}$ and $t^* + \frac{L}{2v_o}$. The overpressure and dynamic pressure, respectively, are the values at the time t -L/2 v_o.
Of course, dynamic pressure in equations from (6) to (10) may be disregarded for sonic boom.

Considering the ground band, Fig. 12 and 17, subjected at a time t to normal bow shock decreasing in each point from the initial value to zero in a time interval contained between 0.05 and 0.18 seconds (positive phase) for pressure signatures and airplane lengths normally predicted, Fig. 26, we see that the incident shock on the vertical plane, Fig. 25, reaches the horizontal ground not perpendicularly but with an angle β , and with a higher angle far away.
Flying at 40,000 ft altitude with M = 1.5, the angle β of the Mach cone is about 41°. The propagation of the Mach cone surface happens at more speed near the ground, about 1.15 times that at 40,000 ft, For that, the incident angle on the ground may be of the order of 40°, indicating also the slope of the ground receiving normal shock (the average angle of the cone from altitude to zero will be α_m = 45°). Peflection on the horizontal plane may be considered twice the incident shock, as it is until about β = 75° (1.65 times for β = 80°, 1.25 times for β = 85°).

At point A in Fig. 25, where the incident overpressure is decaying about linearly to zero in a time contained between 0.05 and 0.18 seconds, Fig. 26, the Mach stem (Fig. 10) is very weak and interests a small region A surface in A adequately oriented may be struck like the one in Fig. 22. As the velocity v_o of the shock front near the ground is, from Eq.(5), about 1,117 ft/sec (being very small the overpressure Δp), the initial value Δp = 2 psf in A, Fig. 26, will there be decayed to zero when the bow shock has arrived at B (dashed line in Fig. 26); AB = 1,117 . sin 45° . . 0.05 = 39.5 ft (AB = 1,117 . sin 45°. 0.18 = 142.20 ft). For M = 3 we have AB = = 1,117 sin 21° . 0.05 = 19.5° ft (AB = 70.4 ft). Normally to the flight track, the lateral spreading distances of the overpressure will be much larger, considering that the cone circle on the ground is as large as π . 40,000 = 125,600 ft.
This means that the clearing time, Fig. 22 must be evaluated in the same direction as the flight.
For $B = \frac{39.5}{3} = 13.15$ ft, in the case $t^* = 0.05$ sec ($B = \frac{142.2}{3} = 47.4$ ft for $t^* = 0.18$) we have

$$t_s = \frac{3S}{v_o} = \frac{3}{2}\cdot\frac{13.15}{v_o} = 0.018 \text{ sec for}$$

$t^* = 0.05$ sec ($t_s = 0.064$ for $t^* = 0.18$)

As in Fig. 22, it is $\Delta p_r = \frac{4.0 + 1.33}{2} = 2.66$ psf

at t = 0; $\Delta p_s = \frac{2.0 \cdot 0.018}{0.05} = 0.72$ psf

As we have shown above, the significant effect of sonic boom is limited to a very narrow belt. The same procedure could be applied for the negative phase of the pressure signature.

In Ref. 23 are presented mathematical methods for computing the pressure-time history of a sonic boom shock wave acting on any given exterior wall surface, using the theory of Keller and Blak (Ref. 24) to produce a series of pressure perturbation expressions for multiple wave reflections. From test data for the F-101 aircraft at flight Mach number, altitude and lateral distance from the flight, track, the bow to tail wave time intervals are estimated to be 0.135 seconds. Upon computing the incident to reflected wave time interval, Δt_r, the pressure history shown in Fig. 27 (Ref. 23) could be predicted; this wave shape is similar to that in Fig. 9.

A procedure like that exposed for the blast or sonic boom loading on a closed box-like structure, may be applied to a partially open box-like structure, We are intending a structure in which the front and back walls have about 30 percent of openings or window area. Because the wave can now enter the inside of the structure the loading--time curves must be considered for both the exterior and interior of the structure. For the front face; the outside loading is computed in the same manner as that used for a closed structure, using S' (list of symbols) instead of S; the inside pressure starts rising at zero time, because the wave immediately enters through the openings. The variations of the inside and the outside pressures with time are as represented in Fig. 28 a).
For the back face; the outside loading is the same as for a closed structure, with S' instead of S; the inside pressure, reflected from the inside of the back face, reaches the same value as the external overpressure at a time L/v_o; see Fig. 28 b). The net horizontal loading is obviously the difference of the net front and back loading.

Open frame structures present difficulty in computing the overpressure loading on each individual member during the diffraction process. The loading may be determined by multiplying the average member impulse by the number of the members. The resulting impulse may be separated into two impulses for front and back walls , as shown in Fig. 29; where the symbols A_{fw} and A_{bw} represent the areas of the front and back walls respectively which transmit loads before failure; and I_{fm} and I_{bm} are the overpressure loading impulse on front and back members, respectively.

These comparisons with explosion loading have been made because the sonic boom is, as is well known, an acoustic phenomenon not connected with the stationary emission of acoustic energy by the aircraft; it would exist even for noiseless aircraft.
It is an explosive type of noise and consists of two, three or even more pressure pulses separated by a time delay of 0.1 to 0.2 seconds, and it is generated by the shock wave pattern formed around the aircraft moving with supersonic speed.

A more critical situation may occur when the aircraft is flying in accelerated and decelerated flight, as in diving. In the first case the acceleration can have a crucial effect on the sonic boom; in fact the disturbances travel different distances as indicated in Fig. 30. It is then possible for pressure disturbances originating from several different aircraft positions to arrive simultaneously at one point on the ground. The sonic boom at this point is thus considerably reinforced. This situation may become worse if there is ground reflection too. Such focusing effects must be avoided at all cost.

Experimental simple reflection factor, $K_P = \frac{\Delta p + \Delta p_r}{\Delta p} = \frac{\Delta p_o}{\Delta p}$, were measured (Ref. 22) for fighter airplanes flying at very low altitudes; for a perfect reflecting surface K_P has a theoretical value of 2. The variation of ground reflectivity with shock wave Mach number is shown in Fig. 31 (Ref. 6).

To understand the phenomenon of a multiple reflection pressure wave and its amplitude factor, we may recall the progress of a sound wave in a closed room, as illustrated schematically by Fig. 32 (Ref. 26), where is represented a horizontal section of a room of 40 feet having walls reflecting plane sound; a sound source is located at S. In the four successive steps we see the wave front 1/200, 1/100, 1/50 and 1/17 second after it has left the source S, until the reflection pattern is quite complicated. In addition, there are other segments of the original wave front which have been reflected by the floor and ceiling.
There are two effects of this multiple reflection, to be generalized to all kinds of pressure waves.
A first effect is the increase of pressure caused by reflections. Depending on the duration of the perturbation emission, an observer in any part of the room will not only receive the pressure waves which come directly to his ear from the perturbation source but will also hear all the reflected waves. Thus the combined pressure of the direct and reflected perturbations on his ear will be greater than that of the direct perturbation alone. With low absorption coefficient, less than 5 percent as for example concrete or glass walls, the reflected pressure waves will lose little energy at each reflection and will build up the total pressure to a value far above that direct

perturbation alone.
A second effect of multiple reflections is reverberation, corresponding to the prolongation of the phenomenon after the original perturbation is stopped.
The example of Fig. 32 has to be well understood in order to avoid large interpretation mistakes. It is true that multiple reflections as the ones in Fig. 32 are increasing the original perturbation frequency, Fig. 21, inducing vibrations and audible noise. But it is also true that the emitted energy cannot be multiplied by reflections.
This latter consideration explains why the increased pressure produced by a pressure wave striking against a wall is only a local phenomenon on the wall itself, unless there is an energy concentration from a large front to a small area or volume. In such a way we may understand why pressure pulses incident in corners, from original large feeding fronts, may increase very much the pressure there to cause unpredicted damage. More impressive, though not regarding sonic boom or explosion propagation, is the example of Fig. 33 a), where many pressure disturbances are concentrating in one point from radial directions.
We may understand that a normal shock from a sonic boom, intersecting a wall is here increasing the pressure twice; whereas a very strong normal shock, from a blast wave, is able to increase the pressure on the wall until eight times.
Intuitively, we may see this big difference, in the reflection factor, considering the momentum changes and the speed impressed by the overpressures on the quiet air during their propagations.

In Fig. 33 a), b), c), d), e), f) and g) we have shown some examples of multiple reflections where the incident overpressure may be increased locally in the air more than twice. In such conditions the sonic boom too may produce dangerous effects. Fortunately these situations may happen only very close to the ground and in small regions.

EFFECTS ON STRUCTURES INDUCED BY SONIC BOOM

Ground configuration in populated areas is so much altered by the presence of buildings and other geometric distributions that their interdependence represents a particular aspect of the problem we are trying to analyse in this paper. On the other hand, it is well known that one of the more complex aspects of the sonic boom problem is that of reported damage to buildings. It is significant that the majority of such reports refers to superficial damage involving the secondary structures of buildings, and thus safety considerations are not important except for the special case of falling objects and glass fragments. No damage incidents in general occurred for overpressure exposure below about 0.8 psf. The number of damage incidents for a given type of structure increases obviously as the overpressure and induced vibration frequency increase. In the field of 1÷3 psf we may have 1÷3 percent of induced incidents per flight per million people. Higher values which occur only occasionally may be sufficient to trigger incipient damage in existing structures or to compromise secondary components of buildngs.
Residence-type structures suffer wave interaction in air cavity of the type indicated in Fig. 33. It could be seen, for floor vibrations, that a preferred phase relationship exists with the interior arrangment of the wall structures, because the panels between the vertical studs vibrate in a preferred manner.
Very high panel frequencies are also noted to exist and to be important. It could be seen that high-frequency responses, in a transient having about 0.5 to 1.0 second duration, are superimposed on lower frequency response modes; whereas the usual vibrations induced by engine noise are detectable for a time interval of 10÷20 seconds. Induced engine noise responses, in the range of about 150÷200 Hz, associate with the vibration of wall panels. More than 0.1 to 0.7 g acceleration amplitudes are observed from F-104, B-58 and XB-70 sonic boom tests.
In the previous chapter we have examined only the overpressure positive-phase impulse on buildings and ground, but we did not intend neglecting the negative-phase impulse. The two contrary impulses are responsible of induced vibrations on structures and ground.
Our experience as consultant engineers at the Centro Applicazioni Militari dell'Energia Nucleare, S.Piero a Grado (Pisa), Italy, have permitted the analysis of some structural damage on the ground and underground, produced by blast waves of different amplitudes. In many aspects this damage resembles that induced by sonic boom, previously unknown to us. In designing blast wave resistant multistore buildings we have considered loading diagrams such as those illustrated in the previous chapters, for the dynamic analysis through the methods of impulse and momentum changes on equivalent "mass".

SOME COMMENTS ON GROUND CONFIGURATION EFFECTS

From a general point of view, the ground configuration regarding large areas has no predominant effect on sonic boom. Some sort of multiple echoes on rough ground, building populated areas, concentration of different slope and orientation surfaces, mountain peaks and cavities, may amplify considerably the sonic boom effects on people and structures.
But, essentially, the ground configuration effects in their dangerous actions are concentrated in small regions, where is coming incident and reflected energy from

the surroundings; see examples in Fig. 33. In these small regions, the local overpressure may reach unpredicted values much more than twice the incident ones, some times followed by a certain vacuum degree due to the negative phase of the impulse signature. Besides, there is some focusing of booms due to atmospheric low altitude turbulence and topography. On certain occasions, the overpressure was quadrupled or more. Twice the normal overpressure was recorded fairly often.
The results of much research indicated that further experiments of people's reaction to sonic boom must be done; possibly using explosives to produce the noise, a much more convenient method than using aicraft and one which can be applied locally to a small number of people without effecting a large area.

The experiments seem to demonstrate that, over the limited range of boom intensity heard, there is not a single criterion to evaluate the reaction of the public who are sensitive to sonic bang by any means less than fullscale experiments. Damage can be caused to buildings, but little damage has apparently been experienced in the United States. The public reaction results seem to show that a small number of seriously annoyed citizens can render supersonic transport overflights of populated areas at supersonic speed a hazardous financial venture. For example, in Oklahoma City, the Government eventually paid out nearly 20,000dollars to some 300 who had complained. In summary, the sonic boom will probably remain the number one unsolved problem of the supersonic programs for some time to come.

From the above, and recalling the emphasizing echo effect of ground configuration on large areas, it follows that much care must be used in choosing flight paths in narrow belts and high altitude. The latter also to avoid giving up the economic transportation at supersonic velocity. On the other hand it is well known that such factors as atmospheric pressure at the altitude of the flight, the size and shape of the aircraft (minimum boom configuration), while not negligible, are secondary compared to those of altitude. The latter exerts a significant influence on the width of the belt across the surface of the earth in which the boom is audible. So a large number of people could be affected by sonic boom. Since people vary in their acceptance of sonic boom, the likelihood of a community outcry depends directly on the density of population.

Such dangerous influences built up by particular ground configurations in limited areas, as indicated in Fig. 33, and Mach stem effects on unattached light material, quarries and cement factories, may become intensively claimed during routine supersonic overland flights.
Nobody in the Bibliography has indicated some sort of possible accidents, such as feeding and spreading of already existing fires, blowout and flame cut-off power plants because of sonic boom overpressure inside the exhaust conducts. Everybody knows that the exhaust gas flow in thermoelectric plants is consequent of a very low Δp overpressure.
Secondary building components, not well attached, as well as voluminous and light packages lying in unstable equilibrium, old fashioned ornamental elements in ancient buildings, structures under construction, light and sailing boats, snow avalanches, resonance frequency and reflected overpressure in underground cavities, small animal chests, etc. may be claimed as frequently damaged.

Expecially in Europe where there are many precious ancient monuments, as well as old houses, supersonic flight paths could present crucial situations.

As we have seen, the sonic boom, with its correlation with ground configuration effect in populated areas, raises very complex problems especially in countries where the citizens are free and accustomed to speak in defence of their rights.

REFERENCES

1. Kane, E.J. and Palmer, T.Y.: Meteorological Aspects of the Sonic Boom. FAA SRDS Report RD 64-180, Sept. 1964.

2. Powers, J.O. and Power, K.: The Supersonic Transport - The Sonic Boom and You. FAA Department of Transportation, Washington-D.C., Nov. 1967.

3. Ferri, A. and Ismail, A.: Report on Sonic Boom. Part 1-Analysis of Configuration. New York University. NASA Contract NGR - 33 - 016 - 119.

4. Maglieri, D.J. and Carlson, H.W.: The Shock Wave Noise Problem of Supersonic Aircraft in Steady Flight. NASA Memorandum 3-4-59 L.

5. Maglieri, D.J. and Hubbard, H.H.: Ground Measurement of the Shock Wave Noise from supersonic Bomber Airplane-Altitude 30,000 to 50,000 f t NASA TND-880.

6. Parker, M.A.: The Sonic Boom Problem. Aircraft Engineering, August 1968.

7. Hubbard, H.H. and Mayes, W.H.: Sonic Boom Effects on People and Structures. Langley Research Center, NASA.

8. Glasstone, S. Editor: The effects of Nuclear Weapons. United States Atomic Energy Commission, June 1957.

9. Kinney, F.G.: Explosive Shocks in Air. The Mc. Millan Company, New York, 1962.

10. Dini, D.: Teoria ed effetti dell'onda d'urto dell'esplosione. Centro Applicazioni Militari Energia Nucleare, S.Piero a Grado, Pisa (Italy), 1957.

11. Dini, D.: Contributo alla ricerca di mezzi sensibili idonei alla misura delle caratteristiche delle onde di esplosione e di detonazione. Centro Applicazioni Militari Energia Nucleare. S.Piero a Grado, Pisa (Italy), 1962.

12. Thompson, J.P. and Parnell, J.E.: Sonic Boom and the SST. Lockheed Horizons California Company, fifth issue.

13. Carlson, H.W.: Experimental and Analytic Research on Sonic Boom Generation of NASA. Langley Research Center, NASA.

14. Carlson, H.W.; Mack, R.J. and Morris, O.A.: Sonic Boom Pressure-Field Estimation Techniques. Proceedings of the Sonic Boom Symposium. The Acoustical Society of America, St. Louis, Mo, November 3, 1965, pp. 510-518.

15. Carlson, H.W.: Correlation of sonic-Boom Theory With Wind-Tunnel and Flight Measurements. NASA TR R-213, 1964.

16. Whitham, G.B.: The flow Pattern of a Supersonic Projectile Communication Pure Applied Mathematics., vol.5, 1952, pp. 301-348.

17. Hicks, P.M. and Mendola, J.P.: Prediction of Aircraft Sonic Boom Characteristics from Experimental Near Field Results. NASA TM X-1477, 1967.

18. Maglieri, D.J.: Sonic Boom Flight Research - Some Effects of Airplane Operations and the Atmosphere on Sonic Boom Signatures. Langley Research Center, NASA.

19. Lansing, D.L. and Maglieri, D.J.: Comparison of Measured and Calculated Sonic Boom Ground Pattern Due to Several Different Aircraft Maneuvers. NASA TN D-2730, 1965.

20. Maglieri, D.J.: Sonic Boom Ground Pressure Measurements for Flights at Altitudes to Excess of 70,000 Feet and at Mach Numbers Up to 3.0. Langley Research Center, NASA.

21. Garrick, I.E. and Maglieri, D.J.: A Summary of Results on Sonic-Boom Pressure--Signature Variations Associated with Atmospheric Conditions. Langley Research Center-Langley Station Hampton, Va. NASA.

22. Maglieri, D.J.; Huckel, V. and Parret, T.L.: Ground Measurements of Shock-Wave Pressure for Fighter Airplanes Flying at Very Low Altitudes and Comments on Associated Response Phenomena. Langley Research Center - Langley Station, Hampton, Va., NASA.

23. Zumwalt, G.W.: Computation of the Pressure Time History of a Sonic Boom Shock Wave Acting on a Window Glass in a Building. Contract Andrews Associates, Inc. Oklahoma City, Oklahoma, NASA.

24. Keller, J.B. and Blank, A.: Diffraction and Reflection of Pulses by Wedges and Corners. Communication on Pure and Applied Mathematics, ser.4, N.1, June 1951.

25. Noise Final Report. Her Majesty's Stationery Office. Reprinted 1966, London.

26. Handbook of Noise Control. Edited by Harris, C.M., Mc Graw-Hill Book Company, 1957.

27. Shock and Vibration Handbook. Edited by Harris, C.M. and Crede, C.E. Mc Graw--Hill Book Company, 1961.

28. Von Gierke, H.E.: Effects of Sonic Boom on People. Review and Outlook . J. Acoust. Soc. Am., Vol. 39, part 2, May 1966.

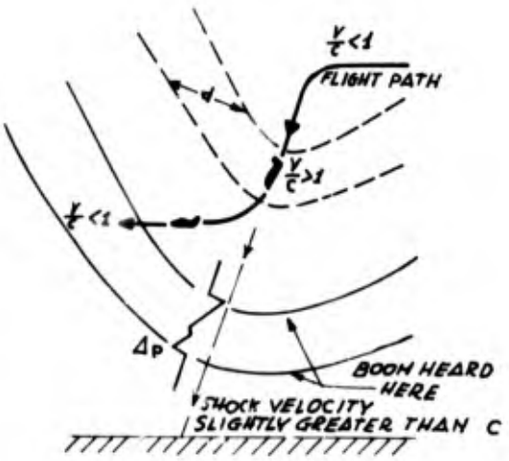
V/c<1
FLIGHT PATH
V/c>1
V<1
Δp
BOOM HEARD HERE
SHOCK VELOCITY SLIGHTLY GREATER THAN C

Fig. 1

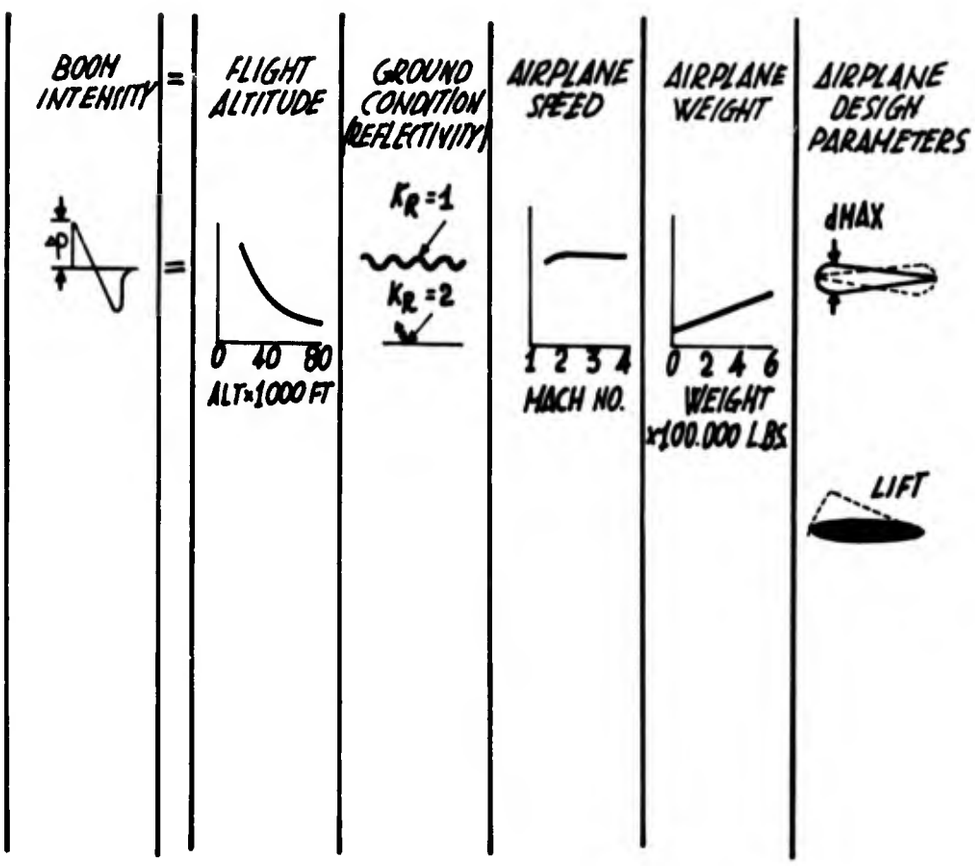
BOOM INTENSITY
=
Δp
=
FLIGHT ALTITUDE
0 40 80
ALT×1000 FT
GROUND CONDITION (REFLECTIVITY)
KR=1
KR=2
AIRPLANE SPEED
1 2 3 4
MACH NO.
AIRPLANE WEIGHT
0 2 4 6
WEIGHT ×100.000 LBS.
AIRPLANE DESIGN PARAMETERS
dMAX
LIFT

Fig. 2

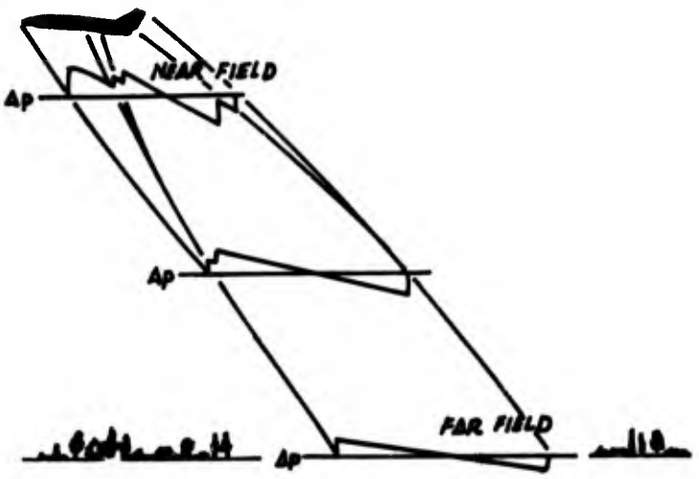

Fig.3

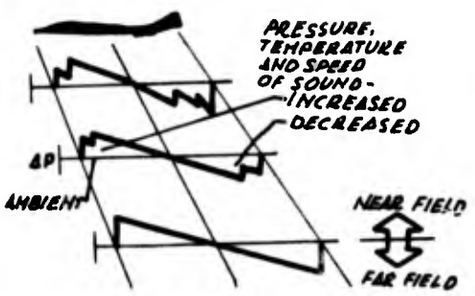

Fig.3-b Generation of the pressure field by an aircraft flying at supersonic speeds

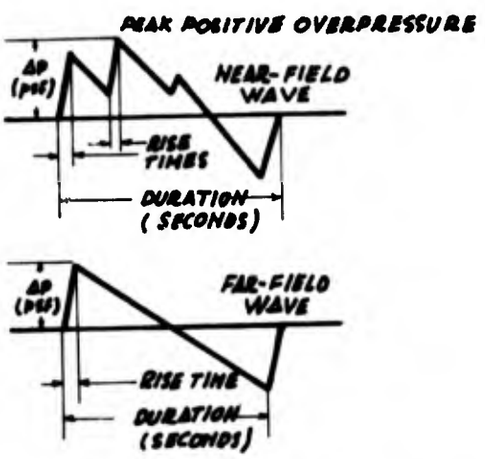

Fig.3-c Typical near-field and far-field pressure signatures showing significant dimensions

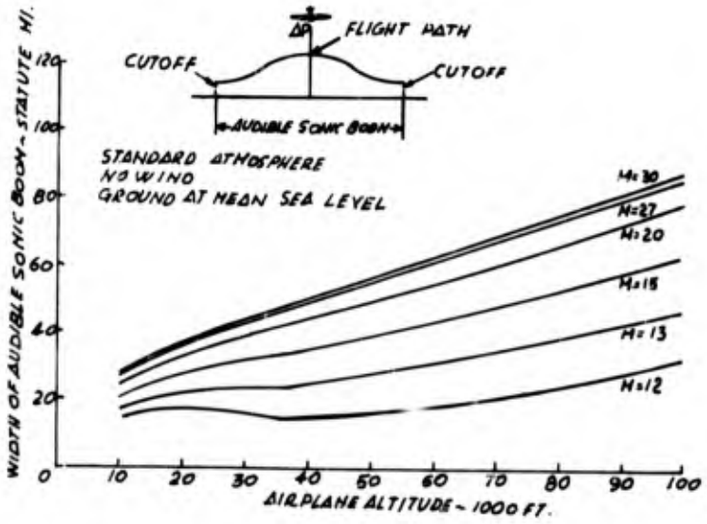

Fig.4

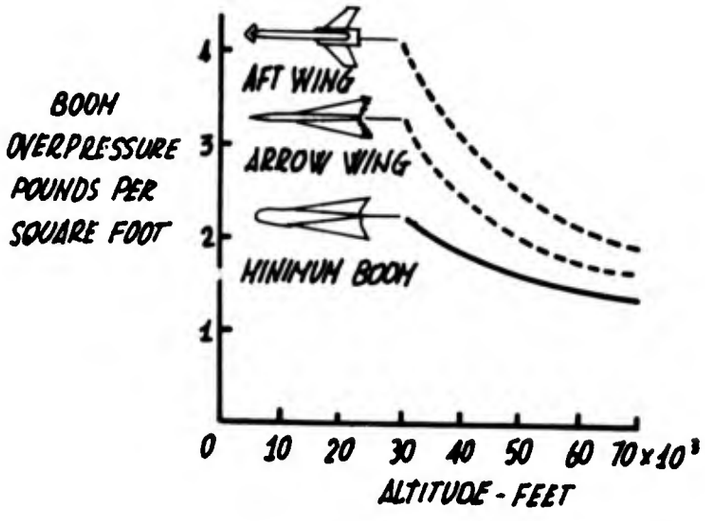

Fig.5

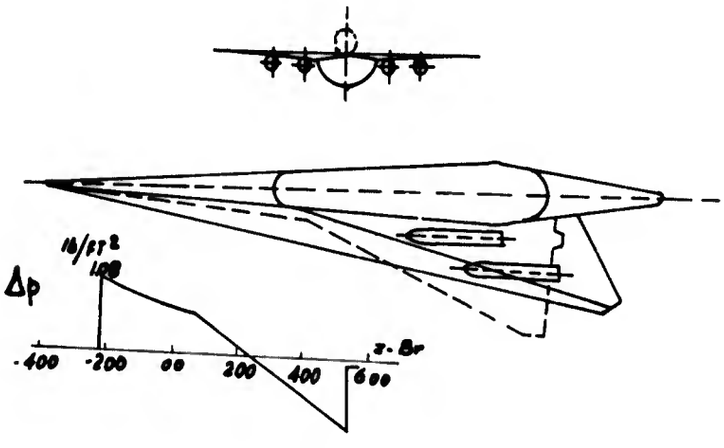

Fig.6

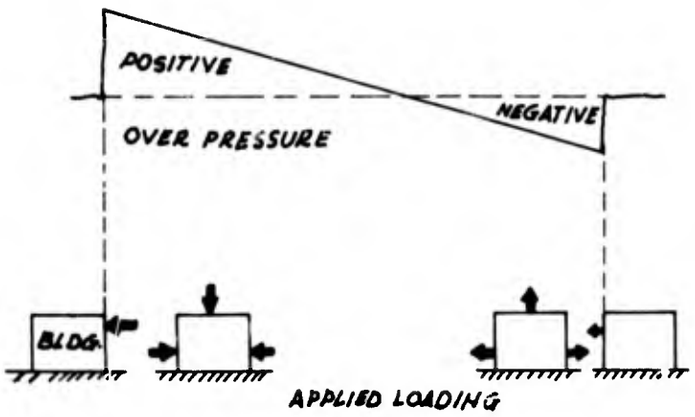

Fig.7 Sonic boom loading on buildings (from ref.1.)

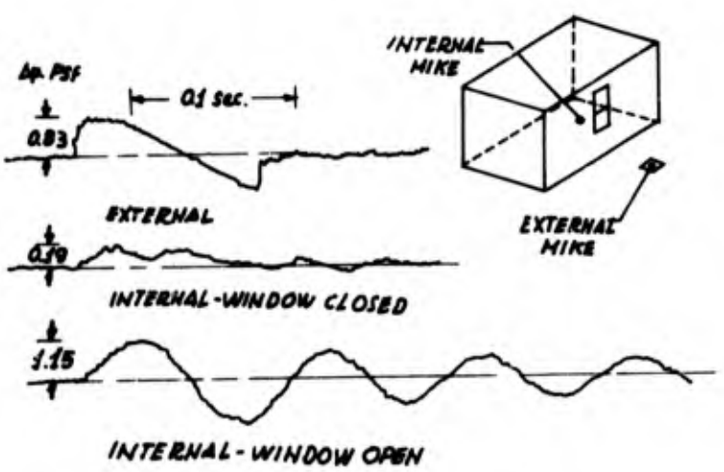

Fig.7 Internal room pressure time histories due to sonic booms for both window-closed and window-opened conditions


SHOCK FRONT
1
2
PRESSURE PHASE
3
4
SUCTION PHASE
5

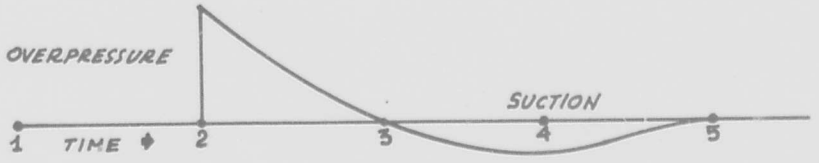
OVERPRESSURE
SUCTION
1
TIME
2
3
4
5

Fig. 8

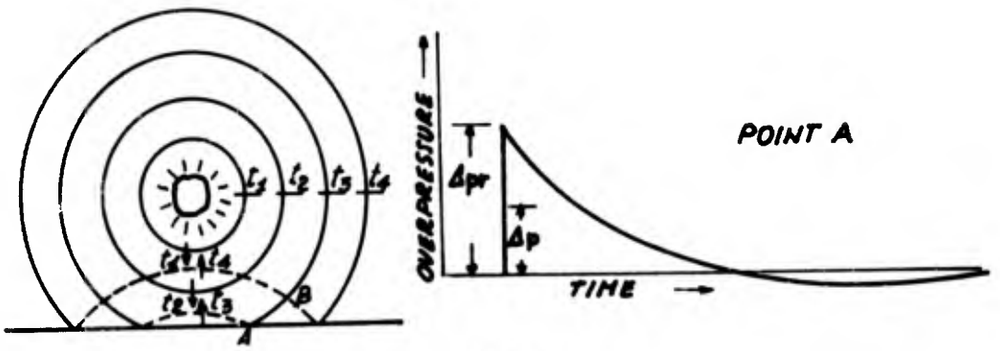

Fig. 9

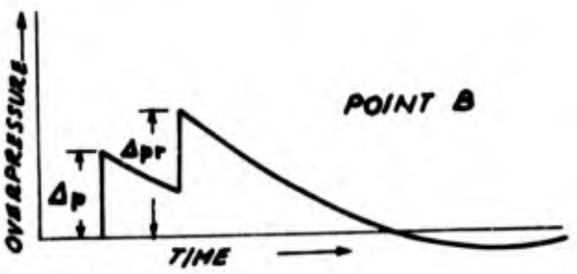

Fig. 9

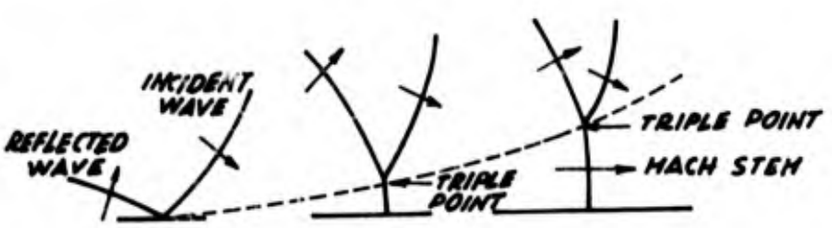

Fig. 10

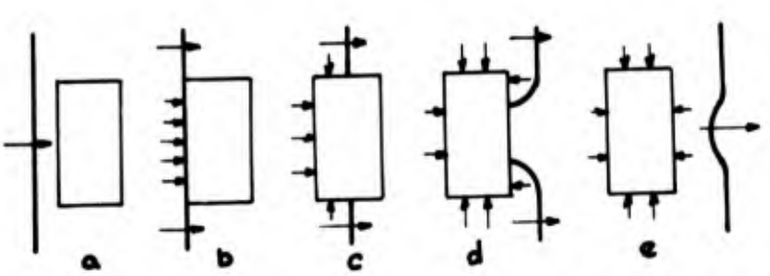

Fig. 11

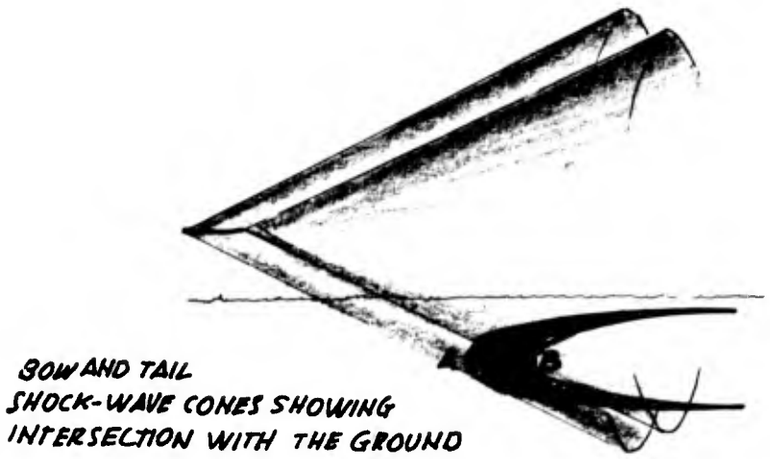
BOW AND TAIL
SHOCK-WAVE CONES SHOWING
INTERSECTION WITH THE GROUND

Fig. 12

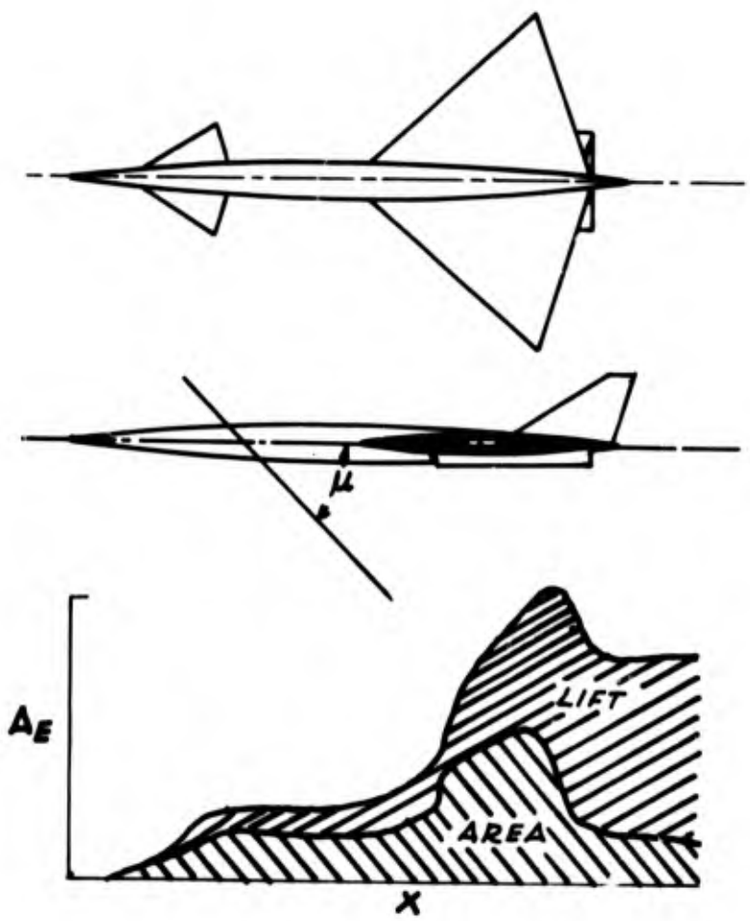
μ
A_E
LIFT
AREA
X

Fig. 13

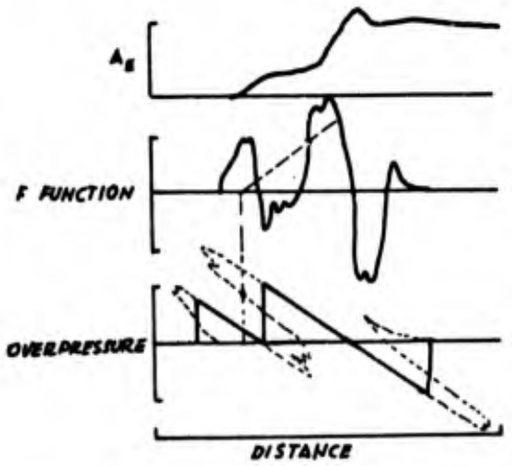

Fig. 14

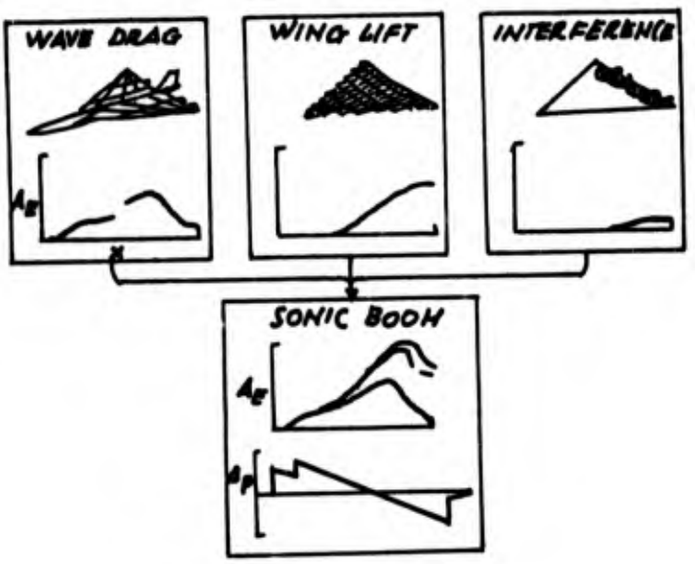

Fig. 15

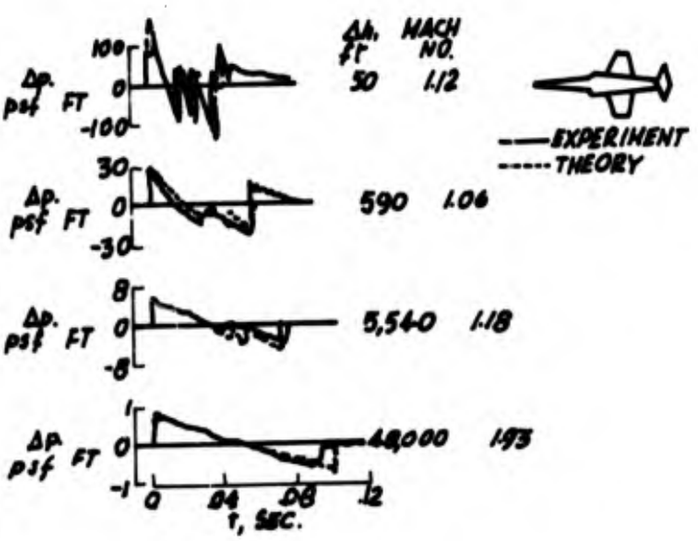

Fig. 16

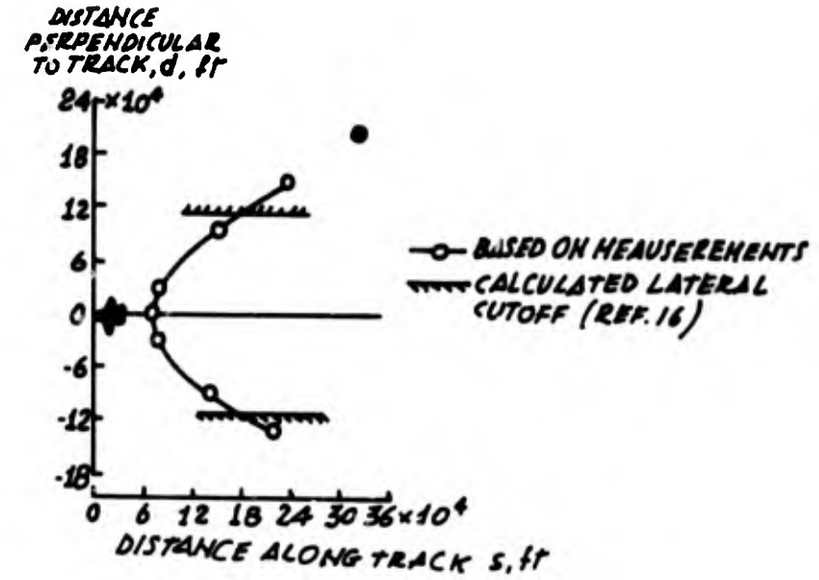
DISTANCE PERPENDICULAR TO TRACK, d, ft
24 ×10⁴
18
12
6
0
-6
-12
-18
0 6 12 18 24 30 36 ×10⁴
DISTANCE ALONG TRACK s, ft
BASED ON MEASUREMENTS
CALCULATED LATERAL CUTOFF (REF. 16)

Fig. 17

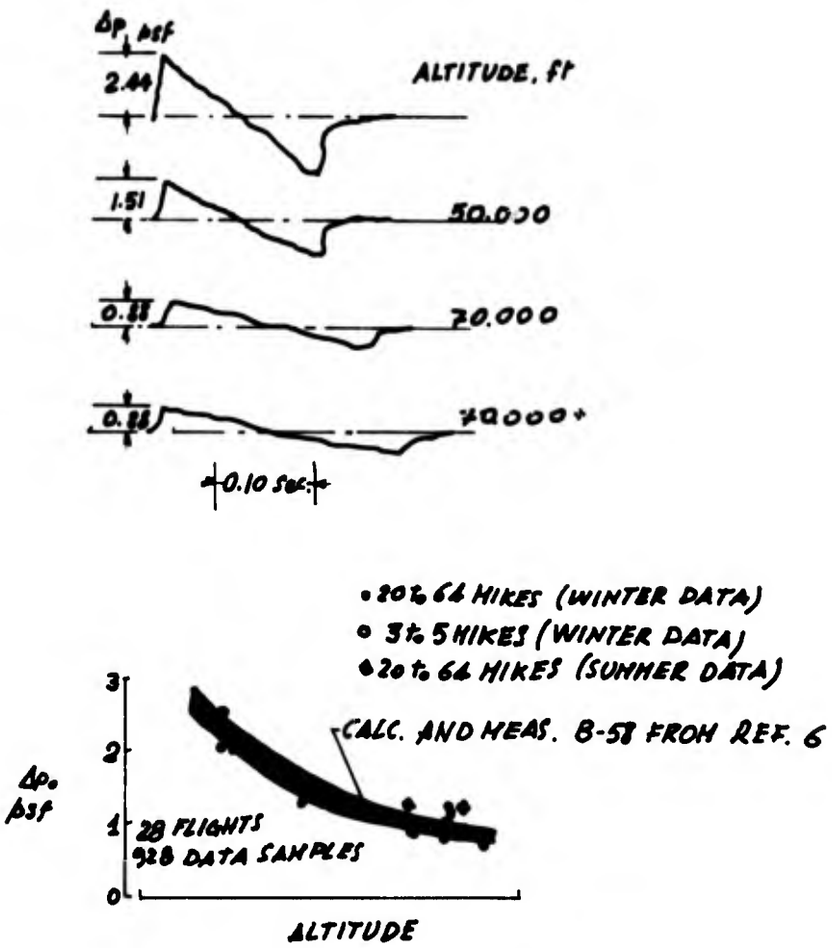
Δp, psf
2.44
1.51
0.88
0.88
ALTITUDE, ft
50,000
70,000
90,000+
0.10 sec
• 20 to 64 MILES (WINTER DATA)
○ 3 to 5 MILES (WINTER DATA)
◆ 20 to 64 MILES (SUMMER DATA)
CALC. AND MEAS. B-58 FROM REF. 6
Δp₀ psf
3
2
1
0
28 FLIGHTS
928 DATA SAMPLES
ALTITUDE

Fig. 18

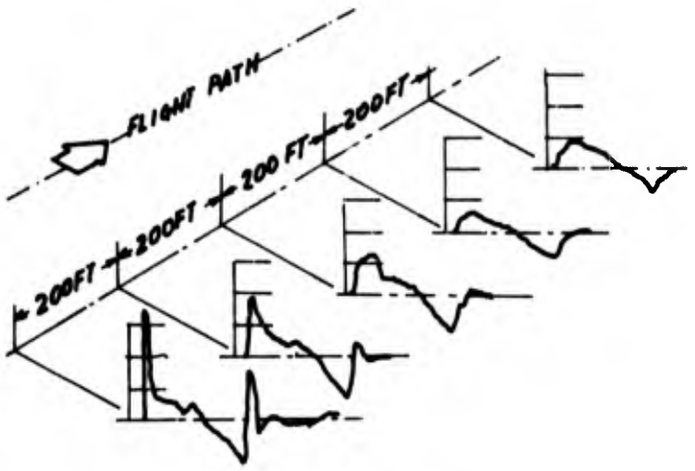

Fig. 19

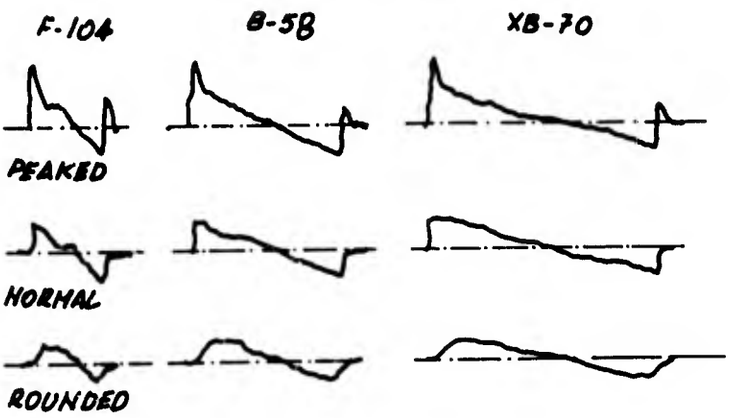

Fig. 20

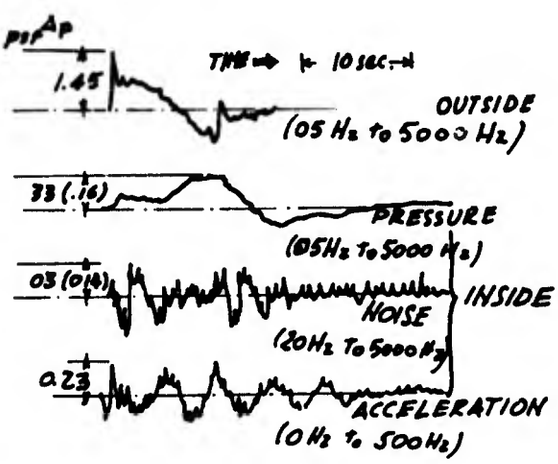

Fig. 21

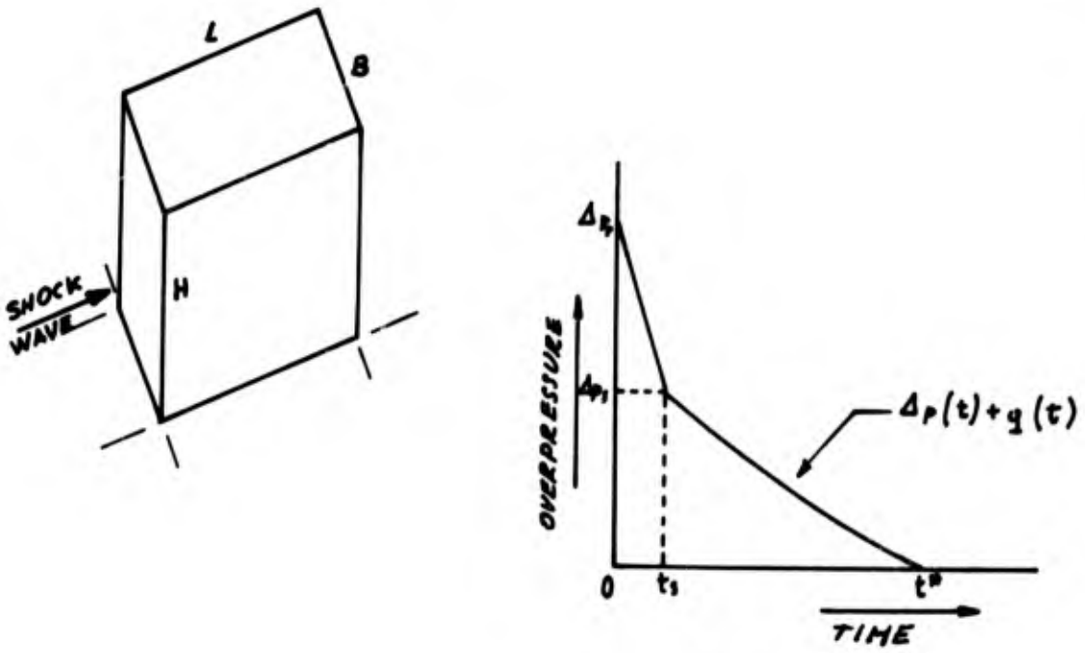

Fig. 22

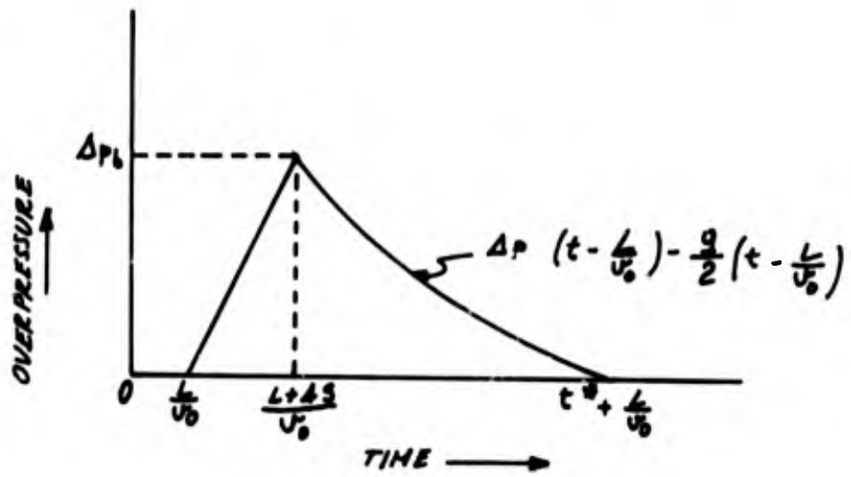

Fig. 23

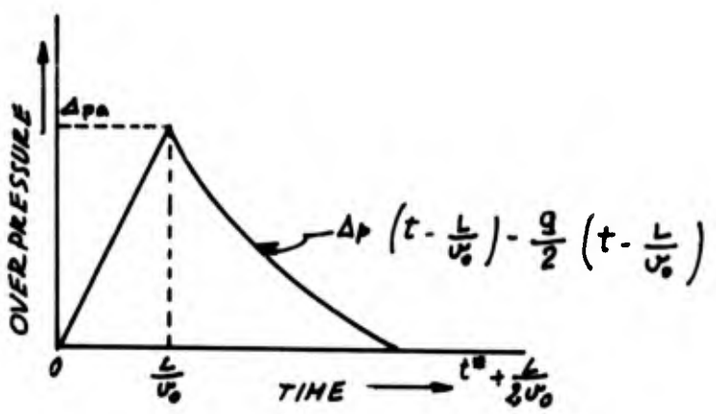

Fig. 24

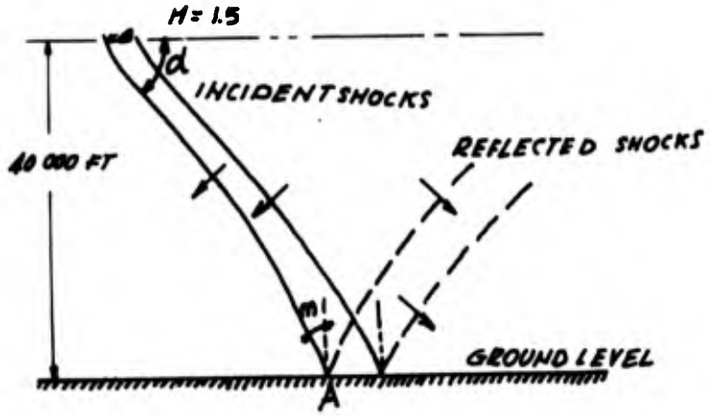
M = 1.5
d
INCIDENT SHOCKS
REFLECTED SHOCKS
40 000 FT
m1
GROUND LEVEL
A

Fig. 25

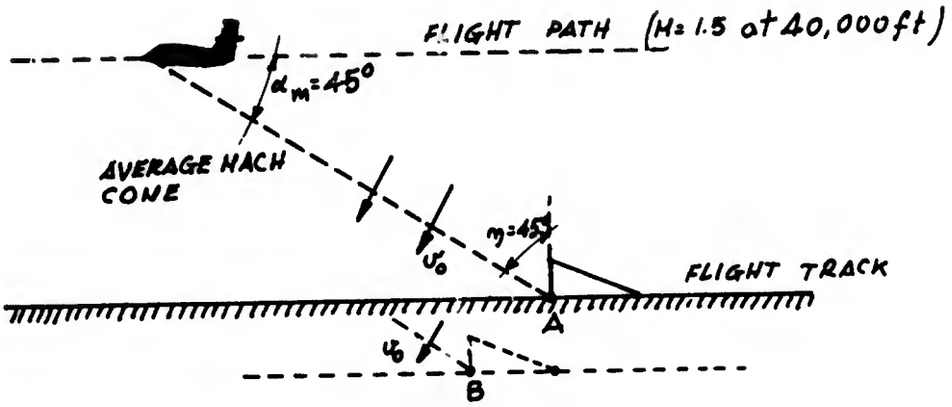
FLIGHT PATH (H = 1.5 at 40,000 ft)
$\alpha_m = 45°$
AVERAGE MACH CONE
$\eta = 45°$
u_0
FLIGHT TRACK
A
u_0
B

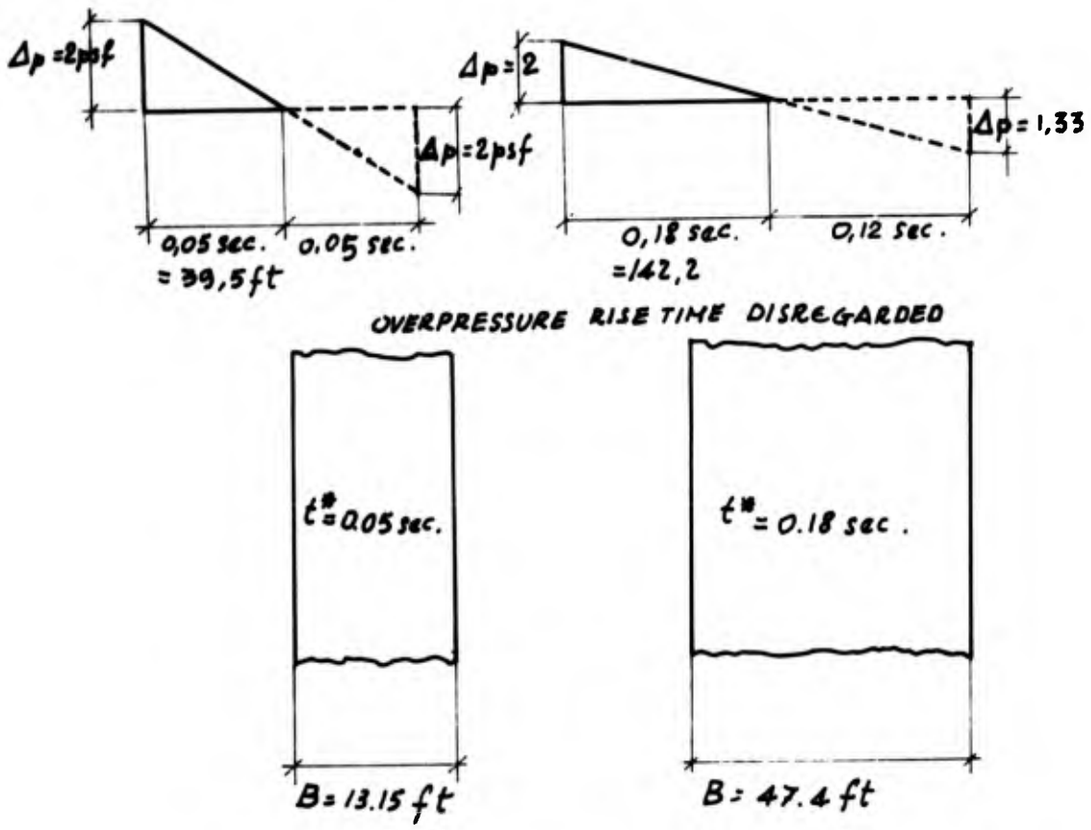
Δp = 2psf
Δp = 2psf
0,05 sec.
0,05 sec.
= 39,5 ft
Δp = 2
Δp = 1,33
0,18 sec.
0,12 sec.
= 142,2
OVERPRESSURE RISE TIME DISREGARDED
$t^* = 0.05$ sec.
$t^* = 0.18$ sec.
B = 13.15 ft
B = 47.4 ft

Fig. 26

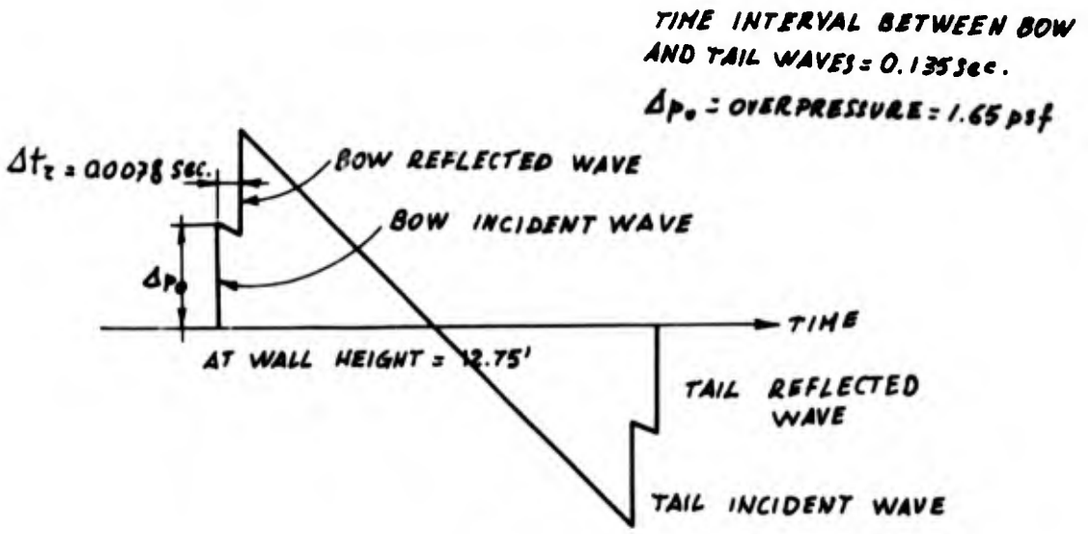

Fig. 27

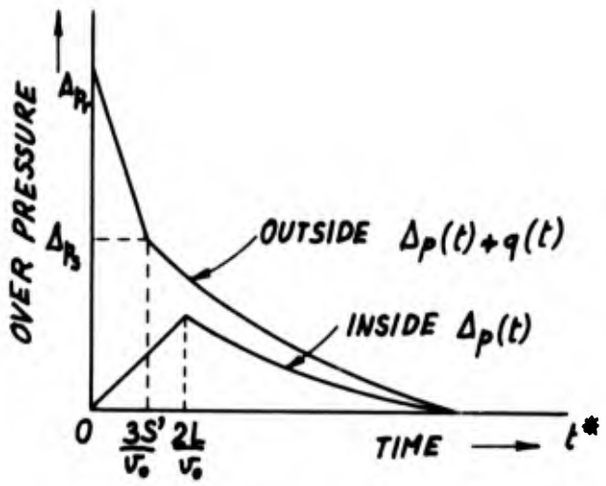

Fig. 28 (a)

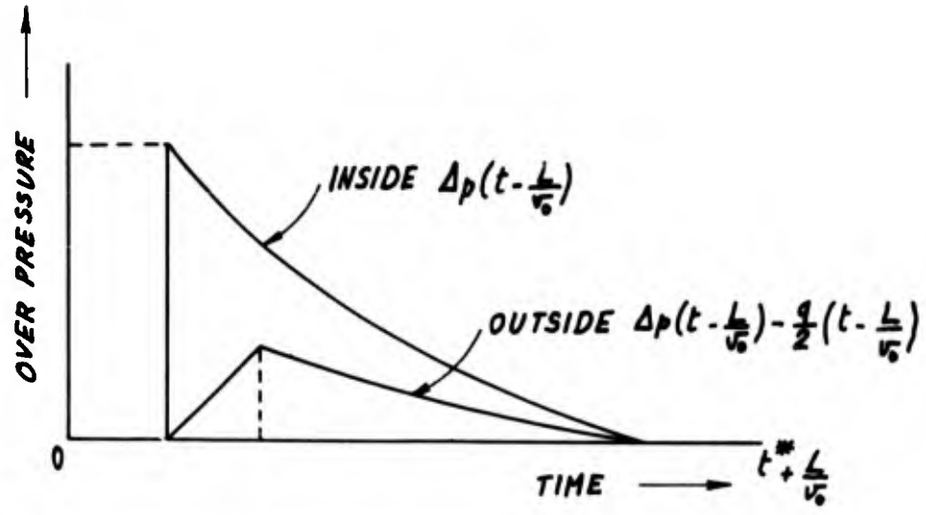

Fig. 28 (b)

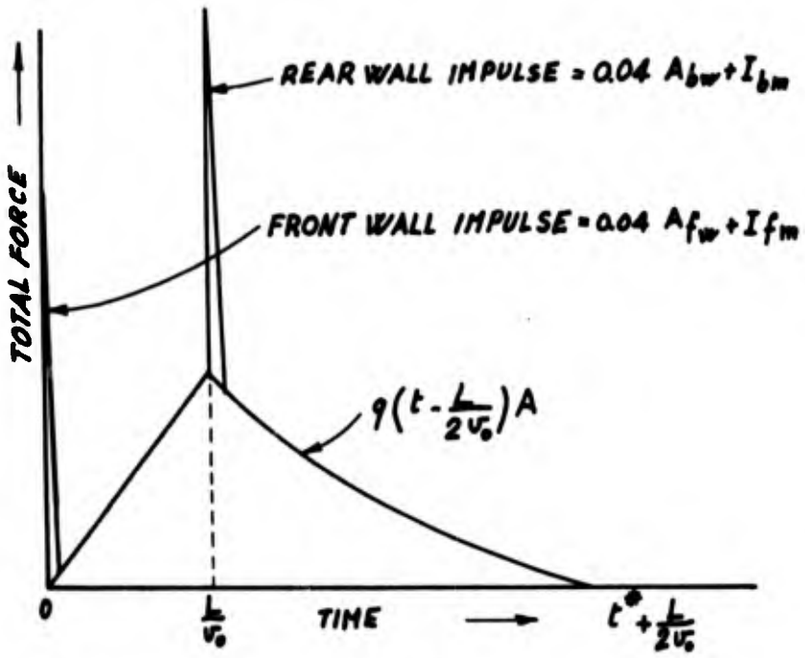

Fig. 29

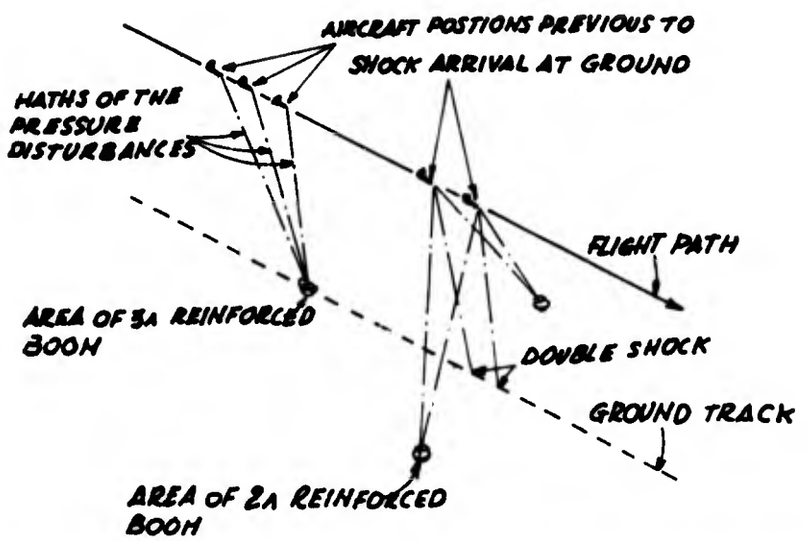

Fig. 30 Sonic boom reinforcement due to aircraft acceleration

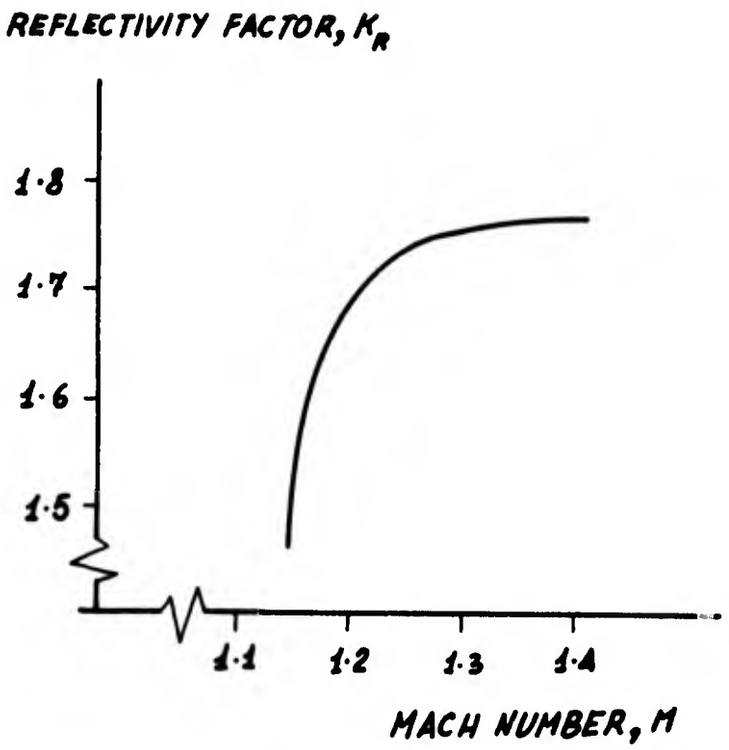
REFLECTIVITY FACTOR, K_R
1·8
1·7
1·6
1·5
1·1
1·2
1·3
1·4
MACH NUMBER, M

Fig. 31

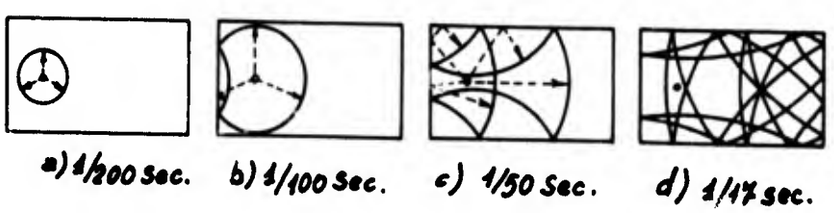
a) 1/200 sec.
b) 1/100 sec.
c) 1/50 sec.
d) 1/17 sec.

Fig. 32

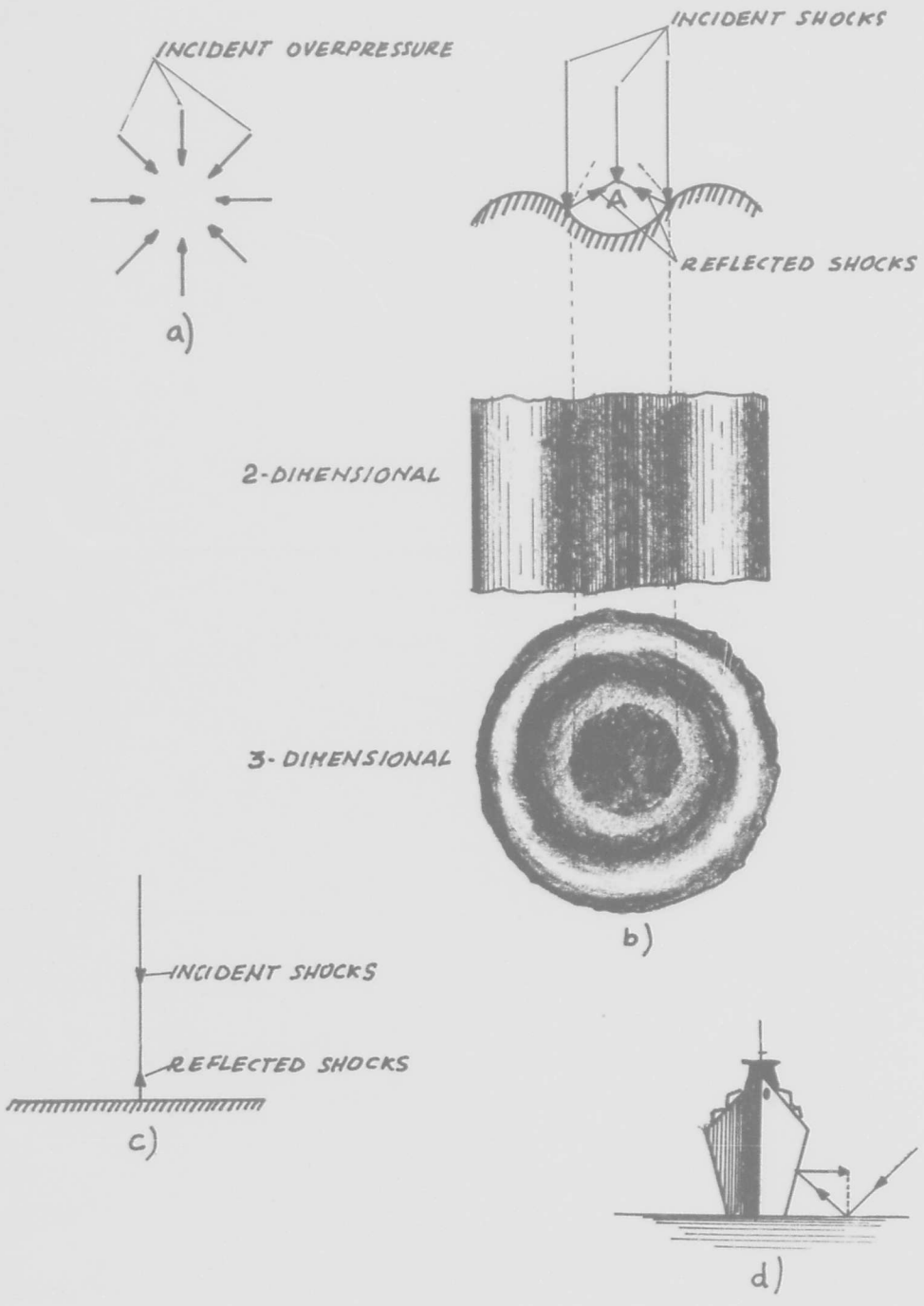
INCIDENT OVERPRESSURE
a)
INCIDENT SHOCKS
A
REFLECTED SHOCKS
2-DIMENSIONAL
3-DIMENSIONAL
b)
INCIDENT SHOCKS
REFLECTED SHOCKS
c)
d)

Fig. 33

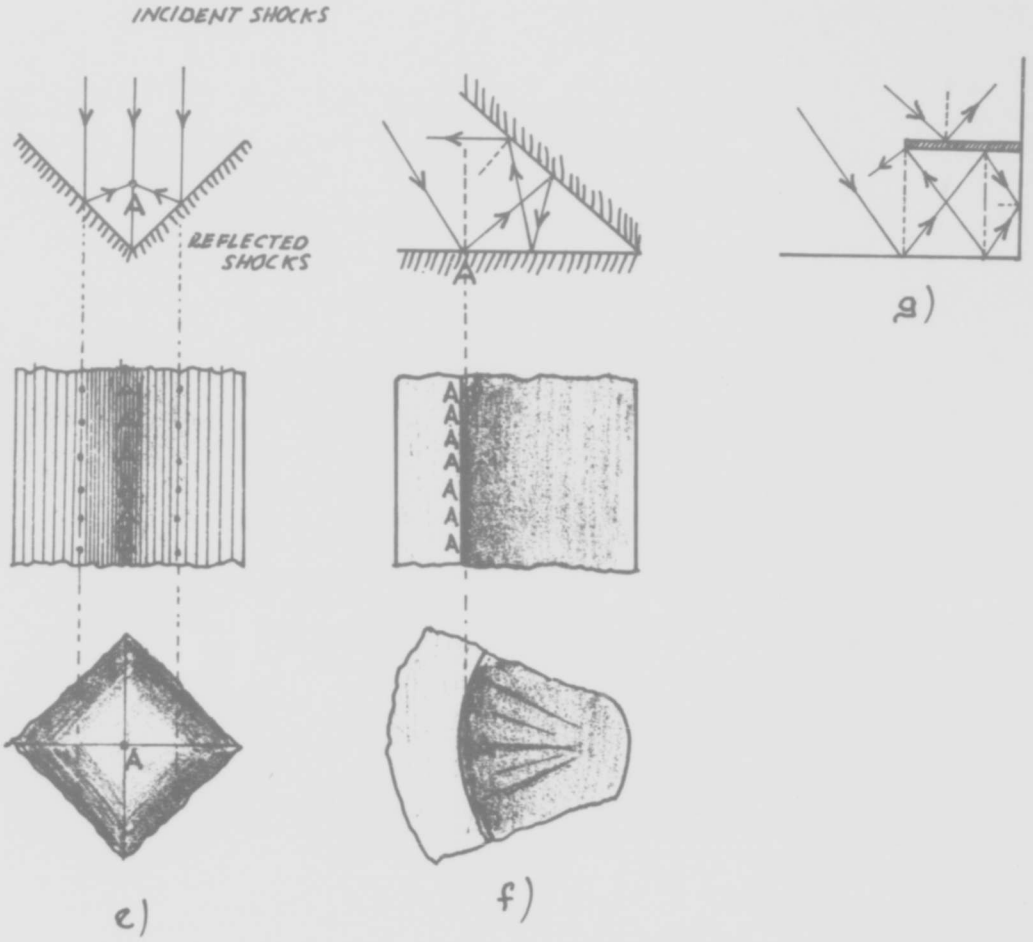

Fig. 33

BLANK PAGE

A preliminary study of atmospheric effects on the sonic boom

G.A. Herbert, W.A. Hass, and J.K. Angell

ESSA Research Laboratories
Silver Spring, Md.

Summary

Atmospheric effects on sonic booms generated by bomber and fighter aircraft are investigated through analysis of more than 4000 sonic-boom pressure traces obtained from a 40-microphone grid at Edwards Air Force Base, California, during the fall and winter of 1966-67. A computer program, which generates maximum overpressure values for a horizontally stratified real atmosphere, is tested against the mean observed overpressure on the grid and is shown to be in error by an average of ten percent when the maximum observed overpressure is derived from the positive impulse area. The pressure traces are grouped into 3 categories so that "spiked" signatures, which constitute the largest deviation from the mean, may be studied as a function of local weather conditions. This study shows a good correlation between the depth of the surface mixed layer and the percentage of spiked signatures. The variability of the maximum overpressure also increases with increase in low-level wind speed. Both these results suggest that turbulence in the planetary boundary layer is the main cause of spiked signatures and the associated large variation in maximum overpressure. There is some evidence that waves within an inversion contribute to overpressure variability on a larger scale.

1. Introduction.

With commercial supersonic transport (SST) operations in the offing, considerable emphasis is being placed upon the response of people and buildings to the sonic boom. The purpose of this paper is to provide additional evidence that the intensity of the sonic boom, and the variability thereof, is closely related to atmospheric structure, particularly the structure within the planetary boundary layer. This relation presumably will result in meteorologists of the future having to assume the responsibility of determining, both from a climatological and synoptic point of view, flight tracks with suitable atmospheric conditions for supersonic operations.

One of the interesting features of the sonic boom is the pronounced variation in the shape of its signature (the trace of the pressure deviation from the ambient level versus time) as a function of distance and time. The signature characteristically takes the form of a slightly rounded "N-wave" (top diagram of Fig. 1) but often "spikes" are observed near the leading edge of the wave (bottom diagram of Fig. 1). Large variations in sonic boom intensity in short distances due to the intermittent occurrences of these spikes were noted by Hubbard et al. (1964) and Hilton et al. (1964). The latter, for example, found a variation in maximum overpressure (maximum pressure deviation from the ambient) of 2 pounds per square foot (lb ft^{-2})[1] along a line of 6 microphones spaced at intervals of 61 m. A diurnal variation in the frequency of different types of pressure traces was reported by Maglieri (1966), with the morning signatures predominantly rounded whereas many spiked signatures were observed during the afternoon.

The importance of the planetary boundary layer in relation to the occurrence of spiked signatures was suggested by a blimp flight at Edwards Air Force Base, California, as reported by Maglieri et al. in Annex C of an interim report from the National Sonic Boom Evaluation Office (NSBEO, 1967). In this experiment, the overpressure trace at blimp altitude (600 m) showed little distortion whereas the signature at the surface was spiked. A reflected signature measured at the blimp was also spiked. In contradiction to this observation, Palmer (1964) had previously concluded, from theoretical considerations, that turbulent scattering from layers less than 1.5 km deep should have little effect on the pressure trace. The work of Parkin and Scholes (1954) concerning atmospheric attenuation rates for vertically directed sound waves suggests that sonic boom perturbations at the frequencies of the spikes (greater than 0.2 k Hz) would have to be amplified within the lowest few kilometers of the atmosphere if the disturbances are to be observed at the surface. The present paper implies that turbulence through a boundary-layer depth of at least 0.5 km is required to produce an appreciable percentage of spiked signatures at the surface.

2. Procedures.

The sonic boom data presented in this paper were obtained at Edwards Air Force Base, in the Mohave Desert of Southern California, between October 31, 1966, and January 16, 1967. The meteorological investigation was part of a much larger experiment involving studies of the response of structures and people to the sonic boom (NSBEO, 1967). The aircraft used to lay down sonic booms at Edwards AFB were F-104 fighters and B-58 and XB-70 bombers. The F-104's and B-58's flew at different heights on different days, but their average flight levels were about 8 and 12 km, respectively. The XB-70 flew at either 11 or 18 km. The speed of the F-104 and B-58 varied between Mach 1.3 and 1.7, while the XB-70 flew at Mach 1.5 at the lower height and Mach 1.8 to 2.5 at the greater height. The aircraft were operated at a constant speed in straight and level flight over the microphone arrays to be discussed below.

In previous studies of the sonic boom, the microphone array usually was cross-shaped or cruciform, with the microphones spaced at logarithmic intervals along both arms of the cruciform. It was deemed desirable in this experiment to establish a more-or-less square grid with equal spacing between microphones. Fig. 2 shows how a grid with a 61 m spacing was superimposed on the cruciform array with logarithmic spacing. This grid is known as the Site 9 grid, and hereafter will be so designated. In December the linear grid spacing at Site 9 was reduced to 15 m to ensure that any fine-scale overpressure variability would be satisfactorily documented. Making use of most of the Site 9 microphones, a 2.4 km "long-line" array, with microphones spaced generally at 61 m, was intermittently established about 15 km to the northeast of the Site 9 grid. The condenser-type microphones, installed within 0.1 m of the very flat surface of the dry-lake bed, were operated by the Langley Research Center and Flight Research Center of NASA, and by the Lockheed Aircraft Corporation. The frequency response of the microphone-recording systems ranged from 0.1 Hz to 10 k Hz. Details of the microphone installation have been presented by Hilton and Newman (1966).

Fig. 2 also shows the position of the 2 meteorological towers, upon which sensitive temperature and 3-dimensional wind ("vectorvane") instrumentation were mounted at heights of 4 and 28 m, respectively. A comparison between these measurements and the overpressure traces

[1] Because of convention, English units for the measurement of overpressure will be used throughout rather than the unfamiliar Newtons per square meter of the metric system (1 lb ft^{-2} = 47.9 N m^{-2}).

will be reported on in a later paper. During the experiment the Air Weather Service Detachment at Edwards AFB released, from a point 5 km north of Site 9, rawinsondes to probe the deep atmosphere, as well as slow-ascent radiosondes to provide temperature detail at low levels. A specially designed temperature sensor and recorder (with a time constant of 1 second and a measurement accuracy of 0.5°C) was placed in a Cessna 150 light aircraft in order to examine the hypothesis of Dr. Warren Johnson (1967) concerning the effect, on overpressure variability, of undulations or waves within an inversion. This aircraft flew a dog-leg pattern about 15 km southwest of Site 9. These differences in location should not be of great import owing to the general uniformity of the terrain.

3. Comparison between observed and computed overpressures.

Our ability to estimate the maximum overpressure to be expected from a given aircraft flying under given supersonic conditions was determined from the Friedman computer program (Friedman, Kane and Sigalla, 1963; Friedman, 1965) which uses a ray-tracing technique to follow an approximate near-field impulse through the observed temperature, pressure, and wind structure from the aircraft to the ground. It was recognized that in the case of the Friedman program the aircraft input data and the determination of near field structure was not as sophisticated as is possible, and consequently the program could not be expected to give exactly correct results; but it was the only program available to us. For this analysis, the 42 maximum observed overpressures obtained from the Site 9 grid were averaged for each of 62 sonic booms that occurred on nine different days. These average observed overpressures were then compared with the computer results derived from the use of real atmospheric data (obtained from the rawinsonde), as shown for the 3 different types of aircraft in Fig. 3. While a fair correlation of 0.70 is associated with the regression line determined for all the data in this diagram, it would appear that the Friedman program tends to overestimate the maximum overpressure from the F-104 and XB-70 and to underestimate the maximum overpressures from the B-58.

Since the Friedman program determines the maximum overpressure to be expected for a pure N-wave type of signature, whereas the maximum observed overpressures are very often those of spiked or rounded signatures, it was desirable to return to the original traces and derive a "nominal N-wave" overpressure through equilization (by planimeter) of the observed positive impulse area (see Fig. 1) and the impulse area associated with a pure N-wave. These impulse-derived overpressures were much more conservative, and yielded a correlation of 0.86 with the Friedman predictions, as shown in Fig. 4. It is emphasized that such a high correlation is obtained only because 42 observations of overpressure were averaged together. It will be shown later that, under many meteorological conditions, the variability between traces is such as to make a comparison between a numerical computation and an individual overpressure observation almost meaningless.

The question arises as to whether the use of the real atmosphere (as against a standard, no-wind atmosphere) in the Friedman program results in an improved relation between observation and computation. Edwards AFB is not an ideal location to test this since weather conditions deviate relatively little from the normal at this site. Nevertheless, Table 1 shows that use of the real atmosphere resulted in no improvement when maximum overpressure was considered, but did reduce the mean absolute difference between observation and computation from .25 to .21 lb ft^{-2} when positive impulse area was utilized to obtain a "nominal N-wave" overpressure. Since the average maximum observed overpressure was 2.1 lb ft^{-2}, for Mach numbers in excess of 1.3 the Friedman program is accurate to within 10 percent (in the mean) if the maximum overpressure is estimated from impulse area and an average overpressure is determined from many microphones.

4. Overpressure analysis.

An example of a spiked pressure trace was presented in Fig. 1. When these spikes occur intermittently, large differences in maximum overpressure are found within a few tens of meters. For example, Fig. 5 shows how the maximum overpressure varied from 4.1 to 2.9 lb ft^{-2} in a distance of 8 m owing, respectively, to the existence and absence of pressure spikes. Large temporal variations in maximum overpressure at a fixed location are also associated with spiked traces. Thus, Fig. 6 shows that at several microphone locations the maximum overpressure changed by a factor of two within 22 minutes, and for the whole grid the average overpressure changed from 2.9 to 2.3 lb ft^{-2}. This large spatial and temporal variability suggests that individual measurements of maximum overpressure may be quite unrepresentative, at least under certain meteorological conditions.

For this preliminary study of possible atmospheric effects on maximum overpressure and overpressure variability, the 1600 overpressure signatures obtained from the bomber flights (XB-70, B-58) were subjectively divided into rounded, N-shaped, and spiked categories (see Fig. 1). Only bomber data were used because near-field perturbations in the pressure signatures of the F-104 fighter aircraft often make classification difficult. Correlations were then determined between the number of signatures in each category and atmospheric parameters such as maximum wind speed, maximum wind shear, or thermal stability between the aircraft and the surface. None of these "deep-atmosphere" correlations was significant. On the other hand, a comparison with the thermal structure of the lower troposphere, as indicated by the depth of the mixed surface layer (the layer through which the lapse rate approaches the dry adiabatic),

gave more promising results. Grouping the data according to whether the mixing depth was less than 0.3 km, between 0.3 and 1.2 km, or greater than 1.2 km (approximately equal numbers of overpressure measurements in each group), the percentages of rounded, N-shaped, and spiked traces indicated in Fig. 7 were obtained. Also shown are the mean soundings representative of each group. It is seen that under essentially surface-inversion conditions there are no spiked traces and 92 percent of the traces are rounded. However, when there is a deep mixed layer, 23 percent of the traces are spiked and only 41 percent are rounded. Inasmuch as the intensity of turbulence is usually related to atmospheric stability, there is the implication here that turbulence in the planetary boundary layer is at least partially responsible for the spiked pressure traces. One might even go a step further and hypothesize that, since the depth of the mixed layer appears as a critical parameter, a certain size of eddy, compatible with this depth, is primarily responsible for the spiked signature. Alternatively, the scattering ultimately producing the spiked signature may originate in a shallow elevated layer, but a certain time (and distance) is required for coalescence into a spike.

Next investigated was the root mean square (rms) difference in maximum observed overpressure as a function of microphone separation. Since there was no evidence from the Site 9 grid data that the scale of overpressure variability was different in the along-track and cross-track flight directions, these rms differences were evaluated independently of direction. Four specific days (November 16, 21, and 23, and December 12) were selected for detailed analysis because the weather conditions were similar during the periods of supersonic flight on each day and because there were sufficient sonic booms on each day so that microphones could be "normalized" by comparing average daily readings for each microphone with the average daily reading for the whole grid. The microphone-recording-system uncertainty estimated thereby amounted to 0.1 lb ft^{-2}, in good agreement with the findings of Hubbard et al. (1964).

Fig. 8 shows the variation with distance of the rms overpressure-difference values on each of the 4 days (based, from top to bottom, on 10, 6, 5, and 5 sonic booms per day), together with information on the average depth of the mixed layer and the mean wind speed through this mixed layer. The limited sample suggests that the overpressure variability is a function of near-surface wind speed as well as depth of the mixed layer, with the variability half as large at a mean wind speed of 3 ms^{-1} as at a wind speed of 10 ms^{-1} even though the mixing depths are similar (cases of Nov. 23 and 16, respectively). This also implies a relation between intensity of turbulence and overpressure variability, inasmuch as at these levels the mechanical production of eddy kinetic energy is closely related to wind speed. The relative constancy of rms values for microphone separations ranging from 100 to 250 meters indicates a preferential tendency for periodic oscillations of maximum overpressure with such a length-scale since, for a periodic oscillation, the rms overpressure difference would be minimum at one wave length.

The overpressure variability at larger separation distances was estimated from F-104 flights over the 2.4 km line. On three of the five days on which this long array was used there was a pronounced change in boundary-layer stability between morning and afternoon. The average rms differences in overpressure as a function of microphone separation during the morning and afternoon of these 3 days, as well as the average vertical temperature profiles, are shown in Fig. 9. Each of the rms traces is based on 10 sonic booms. It is seen that the overpressure variability during the afternoon is at least half again as large as in the morning. Furthermore, particularly during the afternoon, there is evidence for a preferred overpressure wavelength of about 1.5 km, or an order of magnitude larger than that suggested by the (smaller) Site 9 grid data. It will be shown below that this larger wavelength may be associated with waves or undulations within the inversion capping the mixed layer, whereas we have already seen that the smaller wavelength is most likely associated with turbulence within the mixed layer itself.

5. Inversion waves.

The main reason for establishing the 2.4 km array was to test the hypothesis (Johnson, 1967) that waves within an inversion are responsible for periodic variations in overpressure because of variations in sonic boom refraction along the undulating surface. In this experiment the most striking evidence for the existence of such waves was obtained on December 16 (fig. 10). Note that at a height of 350 meters, or just above the inversion, there is a quasi-periodic variation in temperature (determined from the Cessna 150 aircraft) in the east-west direction but little variation in the north-south direction, strongly implying the presence of north-south-oriented wave-like oscillations. Near the base of the inversion, there is little evidence for periodic temperature variations in either direction. The maxima in the quasi-periodic temperature traces are indicated by arrows, and the average distance between these maxima is 1.6 km, quite close to the preferred length scale in overpressure variability estimated from Fig. 9. Unfortunately, overpressure measurements were not obtained on December 16, so that a direct comparison between length scales could not be made. On January 6 and 9, when the periodic nature of the temperature trace was not so pronounced, the preferred wave lengths of overpressure variability were 2.0 and 1.8 km (based on 2 and 5 sonic booms, respectively) while the temperature traces yielded preferred wave lengths of 2.5 and 2.0 km.

The results are encouraging, but more definitive data must be acquired before the hypothesis can be accepted. In particular, the problem is complicated by the fact that undulations within the inversion may well be caused by convective turbulence in the mixed layer

below, so that separation of causative effects is difficult. However, the nature of the Johnson mechanism suggests that the periodicity should reside in the positive impulse area rather than in the spiked overpressures presumably associated with turbulence. The search for such periodicities in positive impulse along the 2.4 km array has not been particularly successful, perhaps because of the uncertainties involved in evaluating impulse areas from the near-field signatures of the F-104's.

6. Conclusion.

There is good evidence that sonic boom intensity, and variability, is a function both of the depth of the mixed layer near the earth's surface and the strength of the wind near the earth's surface. This indicates that the "spiked" overpressure traces, which are normally associated with large intensities and variabilities, are caused by turbulence within the planetary boundary layer. Even though very few overpressure measurements have been made at night, this implies that night-time supersonic flights, because of the usually greater low-level stability, would generally result in less intense sonic booms with lesser variability than flights during the day. It may well be that in the future meteorologists will have to include in their routine forecasts estimates of the influence of the planetary boundary layer upon the intensity and range of variability of sonic booms.

REFERENCES

Friedman, M.P., 1965: A description of a computer program for the study of atmospheric effects on sonic booms. NASA Contractor Report 157, Washington, D.C., 69 pp.

Friedman, M.P., E.J. Kane and A. Sigalla, 1963: Effects of atmosphere and aircraft motion on the location and intensity of a sonic boom. AIAA J., 1, 1327-1335.

Hilton, D.A., V. Huckel, R. Steiner and D.J. Maglieri, 1964: Sonic-boom exposures during FAA community-response studies over a 6-month period in the Oklahoma City area. NASA Technical Note D-2539, 78 pp.

Hilton, D.A., and J.W. Newman, 1966: Instrumentation techniques for measurement of sonic-boom signatures, J. Acoust. Soc. Am., 39, S31-S35.

Hubbard, H.H., D.J. Maglieri, V. Huckel and D.A. Hilton, 1964: Ground measurements of sonic-boom pressures for the altitude range of 10,000 to 75,000 feet. NASA Technical Report R-198, 43 pp.

Johnson, W.B., 1967: The effect of inversion waves upon sonic-boom propagation. Technical Memorandum No. 2, Atmospheric Turbulence and Diffusion Laboratory, ESSA Research Laboratories, 17 pp.

Maglieri, D.J., 1966: Some effects of aircraft operations and the atmosphere on sonic-boom signatures, J. Acoust. Soc. Am., 39, S36-S42.

National Sonic Boom Evaluation Office, 1967: Sonic boom experiments at Edwards Air Force Base, Interim Report. NSBEO-1-67, Arlington, Va. (prepared under Contract AF 49(638)-1758 by Stanford Research Institute).

Palmer, T.Y., 1964: Effects of turbulence on the sonic boom. Paper presented at the Fifth Conference on Applied Meteorology of the American Meteorological Society, Atlantic City, New Jersey, 16 pp.

Parkin, P.K. and W.E. Scholes, 1954: Air-to-ground sound propagation. J. Acoust. Soc. Am., 26, 1021-1023.

Table 1. Mean absolute differences (lb ft^{-2}) between observed ($\overline{\Delta P}_o$) and impulse-derived ($\overline{\Delta P}_I$) overpressures, and overpressures computed from the Friedman program using observed temperatures, pressures, and winds (ΔP_{F_A}) and the standard atmosphere with no winds (ΔP_{F_S}).

$\overline{\left|\overline{\Delta P}_o - \Delta P_{F_A}\right|} = .34$ $\qquad$ $\overline{\left|\overline{\Delta P}_I - \Delta P_{F_A}\right|} = .21$

$\overline{\left|\overline{\Delta P}_o - \Delta P_{F_S}\right|} = .34$ $\qquad$ $\overline{\left|\overline{\Delta P}_I - \Delta P_{F_S}\right|} = .25$

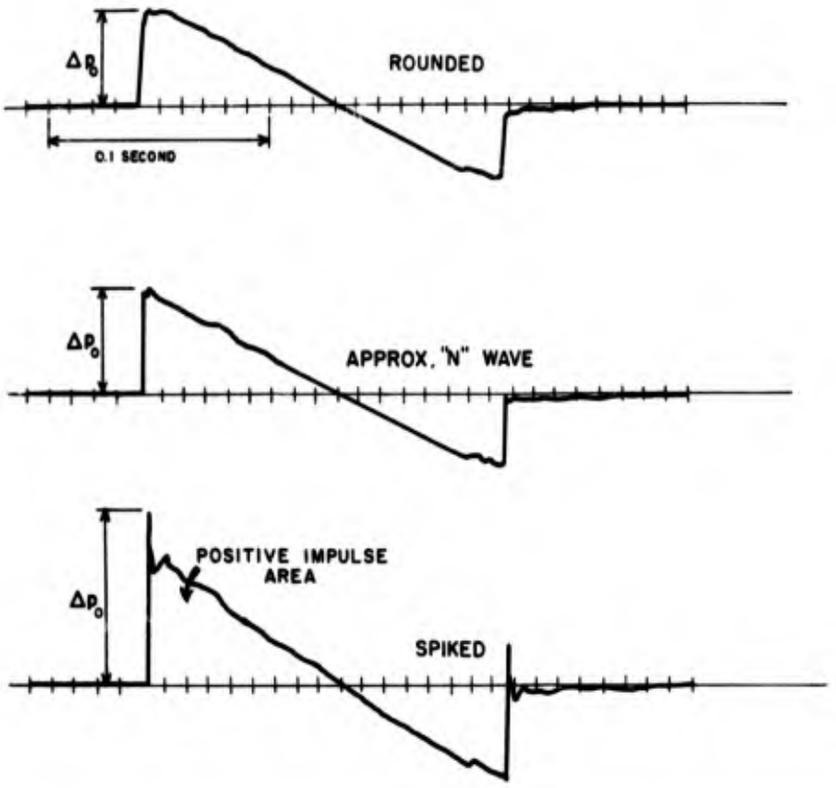

Fig. 1. Characteristic rounded, N-shaped, and spiked sonic boom pressure signatures (produced by a B-58 aircraft), and the general method of determination of maximum observed overpressure (ΔP_o). The positive impulse area is indicated at bottom.

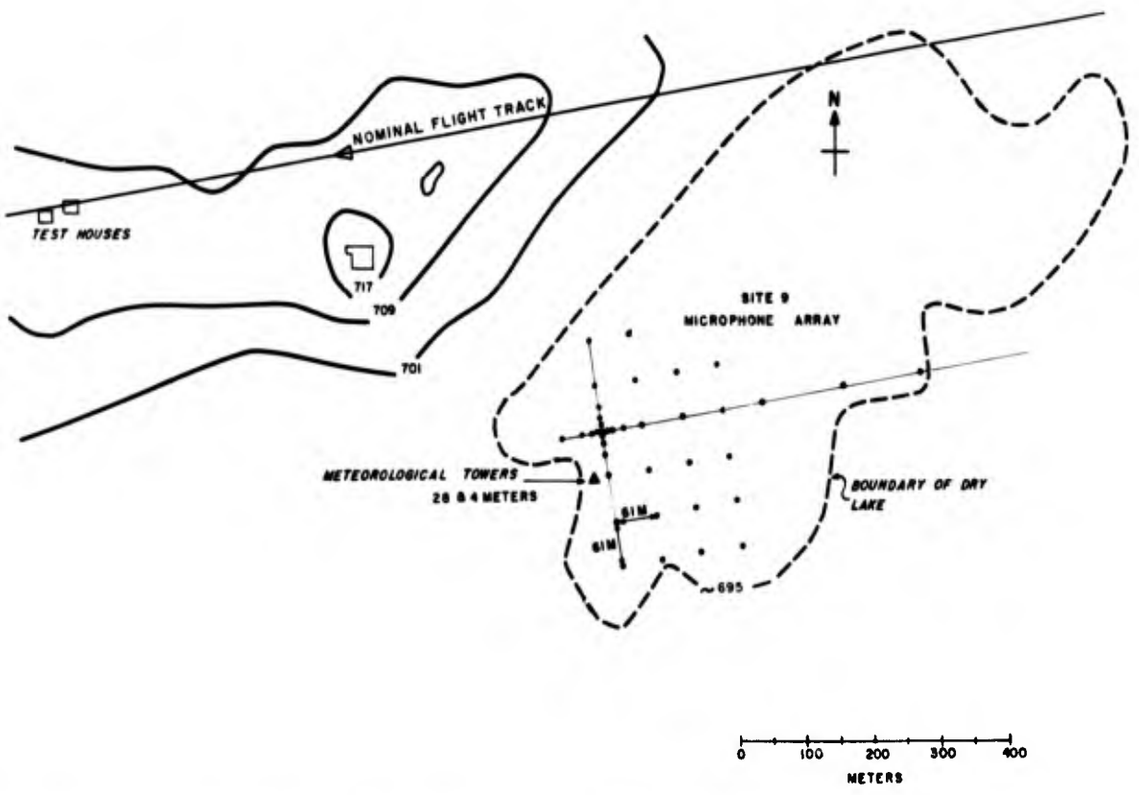

Fig. 2. Location of Site 9 microphone array (61 m spacing) at Edwards AFB in relation to the flight track of the aircraft and the positions of the meteorological towers and test houses. The solid and dashed isopleths indicate height, in meters, above sea level.

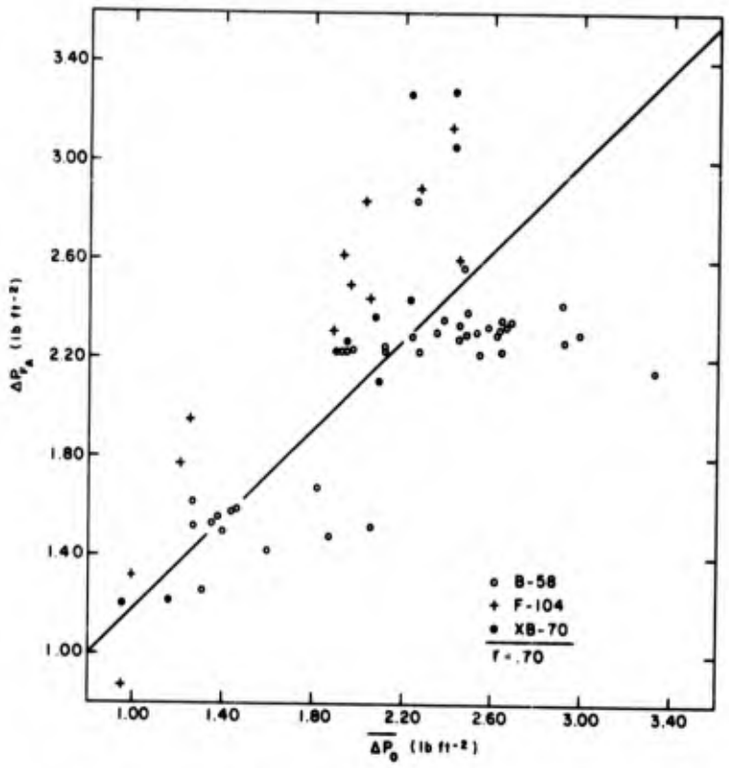

Fig. 3. Comparison between maximum observed overpressure determined from the average of the 42 microphones in the Site 9 grid (ΔP_O) and the maximum overpressure determined from the Friedman program using real atmospheric data (ΔP_{F_A}). The regression line and correlation coefficient, obtained by combining the data for the 3 different types of aircraft, are indicated.

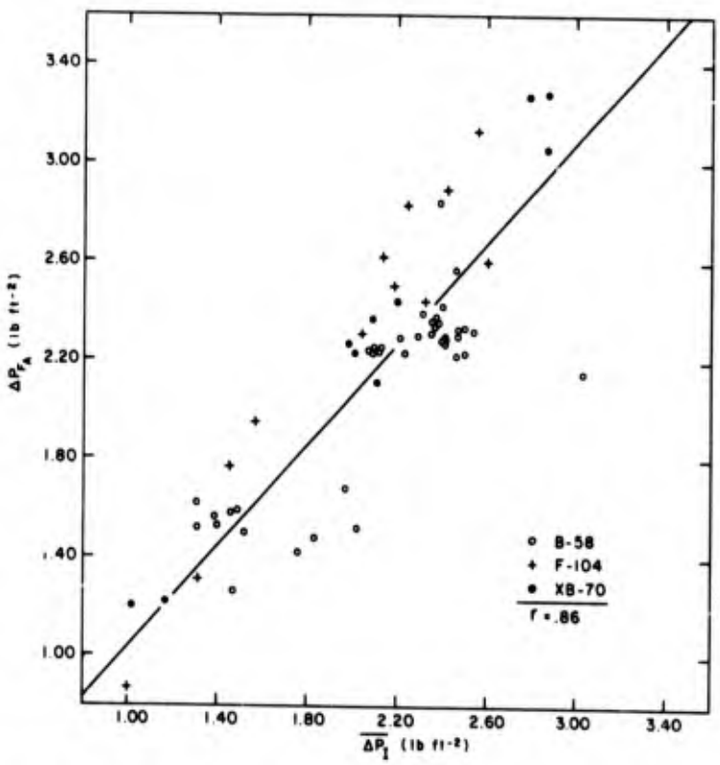

Fig. 4. Same as Fig. 3 except that the average maximum observed overpressure (ΔP_I) has been derived from the positive impulse area through the assumption of an N-wave signature (see text).

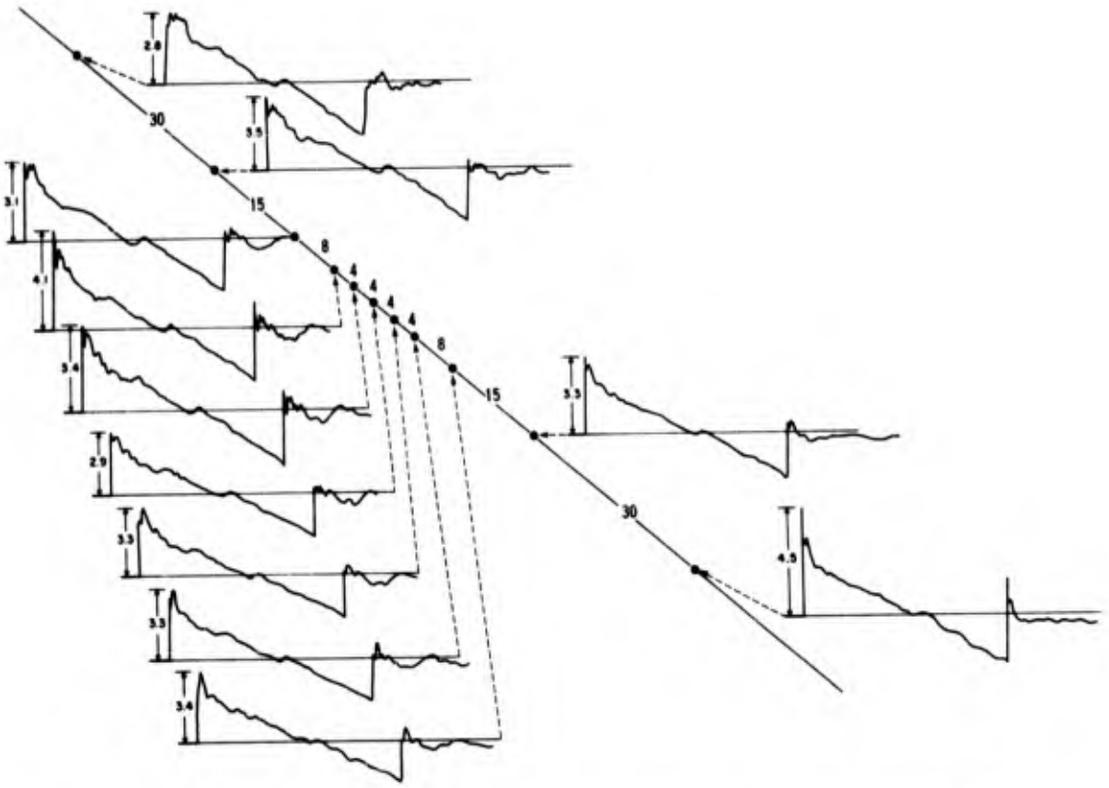

Fig. 5. Sonic boom pressure signatures along the flight track at 0859 PST on November 16, 1966. The distance between microphones is in meters and the maximum observed overpressure is in lb ft^{-2}.

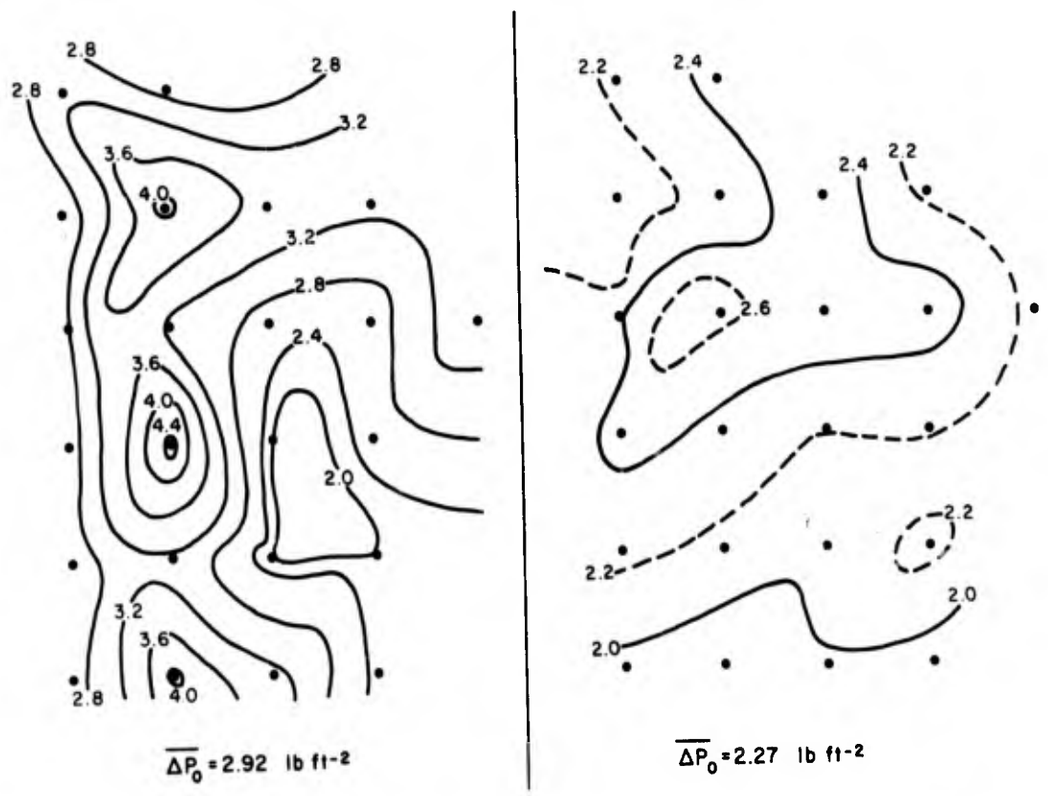

Fig. 6. Maximum observed overpressure, in lb ft^{-2}, on the Site 9 grid (61 m spacing) at 0955 PST (left) and 1017 PST (right) on November 17, 1966.

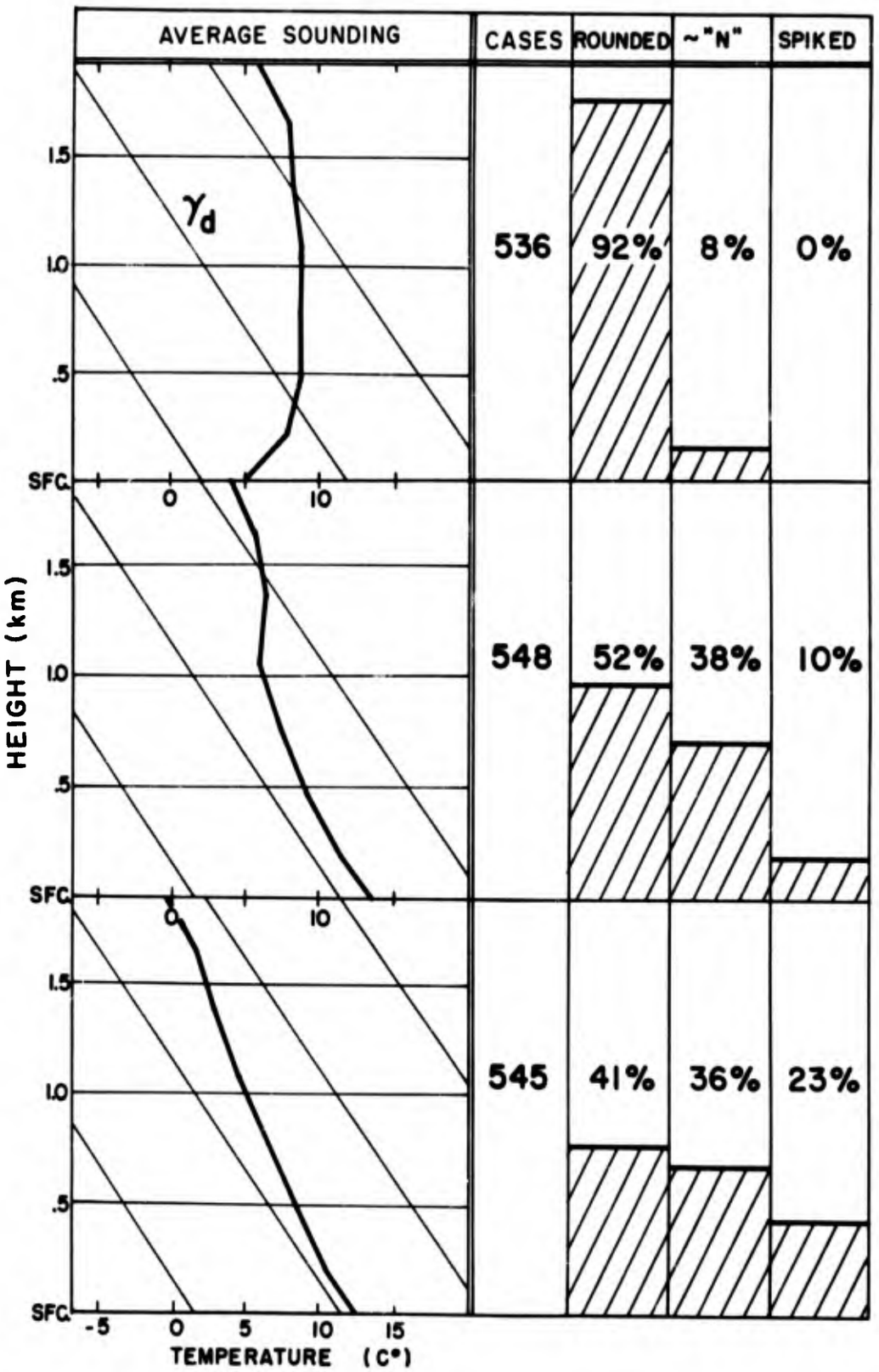

Fig. 7. Percentage of rounded, N-shaped, and spiked pressure signatures associated with the given average soundings. The slanting lines in the sounding diagrams represent dry adiabats.

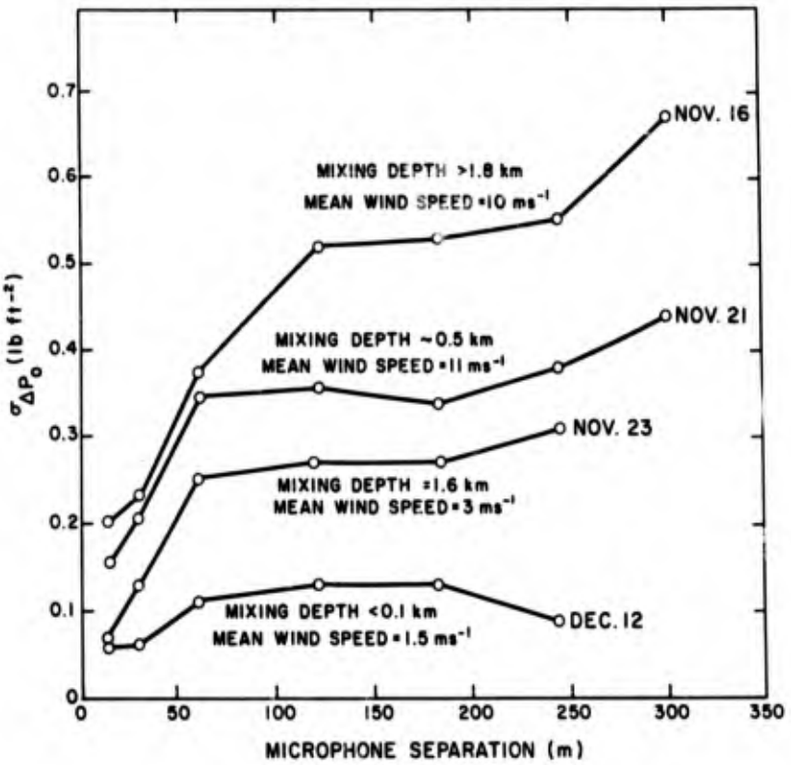

Fig. 8. Root mean square difference in maximum observed overpressure as a function of microphone separation at the Site 9 grid, based on 10, 6, and 5 sonic booms on November 16, 21, and 23, respectively, and 5 sonic booms on December 12, 1966. For each date the mean mixing depth, and mean wind speed in the mixed layer, during the time of the booms is indicated.

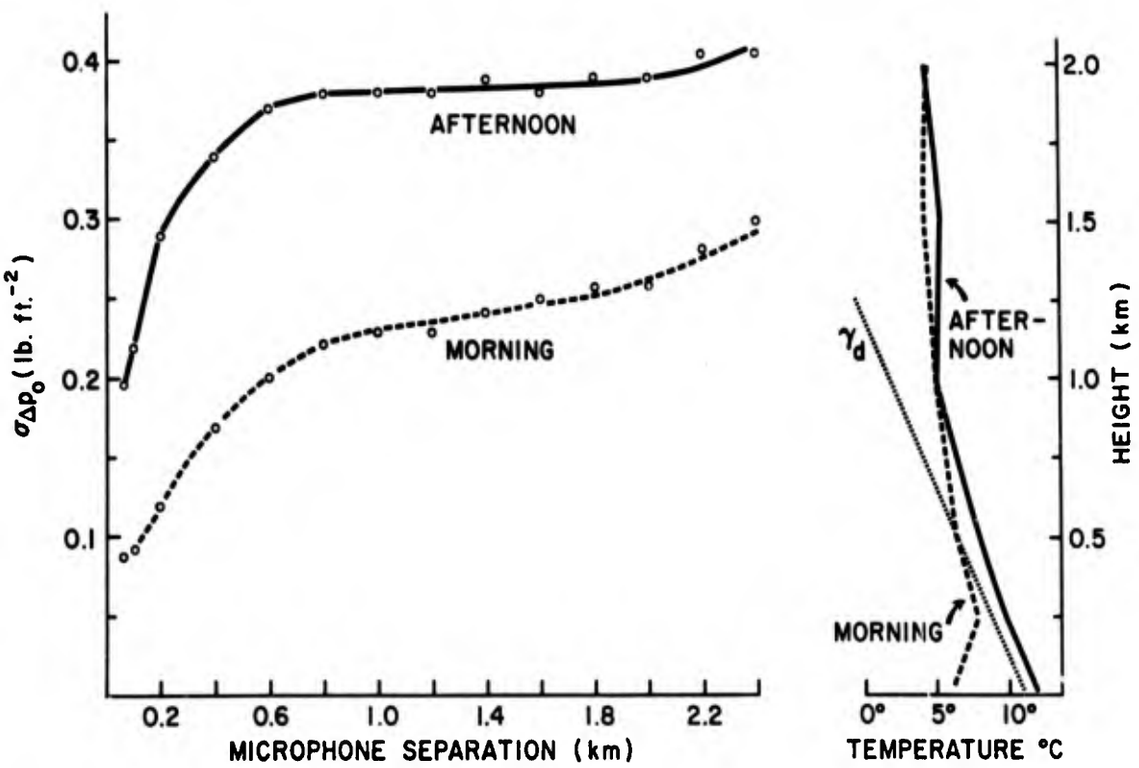

Fig. 9. Root mean square difference in maximum observed overpressure as a function of microphone separation along the 2.4 km long-line array, based on 10 sonic booms each in the morning and afternoon of 3 different days. The mean vertical temperature structure during these mornings and afternoons is shown at right.

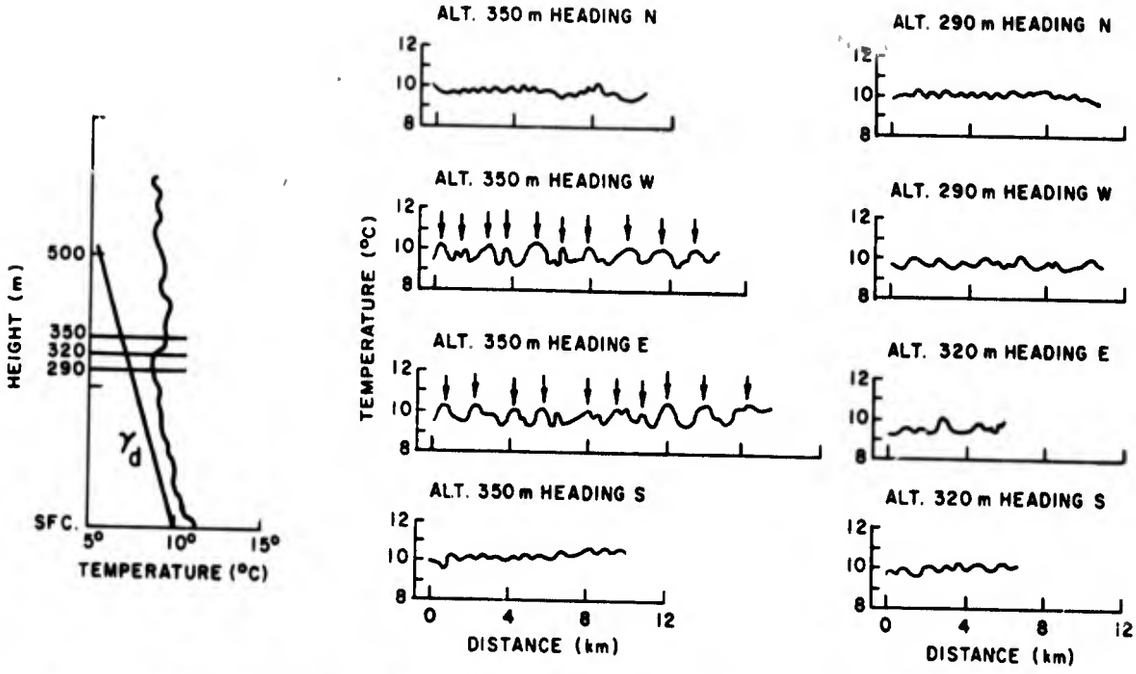

Fig. 10. Temperature oscillations derived from horizontal aircraft traverses in the given directions at the given mean heights, as obtained between 1145 PST and 1245 PST on December 16, 1966. The vertical arrows delineate temperature maxima. The vertical temperature structure at the time of the flight is shown at left.

BLANK PAGE

THE SIMULATION OF SONIC BANGS

by

C. H. E. Warren

Royal Aircraft Establishment

Farnborough, Hants

United Kingdom

SUMMARY

The various methods which have been developed in the United Kingdom for simulating sonic bangs are described. They range from explosive point charges, explosive line charges to shock-tube devices. The appropriate role of application, and its shortcomings, of each type of simulant is discussed. Some of the results that have been obtained in studies employing these devices are referred to briefly.

1. Introduction

The advent of supersonic aircraft has led to the phenomenon of the sonic bang. The possible effects of these sonic bangs are matters of current interest. One way of studying the effects is to do experiments in which actual sonic bangs are made by aircraft. Because the flying of supersonic aircraft is costly, this tends to be an expensive way of obtaining the desired information. Moreover, it is not practicable to make a sonic bang of precisely the desired intensity at precisely the desired time, as is usually required in experimental work. Accordingly studies employing actual sonic bangs tend to be somewhat 'hit-and-miss' experimentally. Further, as they cannot be confined to small target areas, they involve subjecting a much larger area to them than is required for experimental purposes. Therefore there is a need for ways of simulating sonic bangs.

This paper describes, in a chronological way, the methods that have been tried in the United Kingdom to simulate sonic bangs. It discusses what are considered to be the fields of application of the various methods, and gives some of the results that have been obtained.

2. Explosive point charges

The waveform of a typical sonic bang recorded outdoors near the ground in the open is shown in figure 1. It has what has become known as an N-waveform. In figure 2 is shown an oscillogram of the waveform of the bang from the explosion of a lumped, or 'point source', charge. It has what is usually known as a Friedlander waveform.

The bang from an explosive point charge differs from a sonic bang in two main respects. Firstly, it sounds different, in that one hears simply one actual bang from the rapid rise in pressure associated with the shock front, whereas with a sonic bang one usually hears two actual bangs from the two instants of rapid rise in pressure associated with the bow and stern shocks*. Secondly, there is clearly more 'energy' in a sonic bang than in an explosive bang of the same pressure rise across the shock, owing to its longer duration, and hence to its greater 'impulse'. The first of these objections makes a single explosive point charge a poor simulant from the subjective point-of-view, and the second a poor simulant from the point-of-view of effects on building structures.

However, the realism of an explosive point charge as a subjective simulant can be improved by simply arranging that in fact two charges are exploded, one delayed relative to the other by an interval of time equal to the interval between the two shocks of the sonic bang that one wishes to simulate. A simulant of this type was studied during the series of sonic bang experiments that formed part of the so-called Exercise Crackerjack[1] that was staged over the years 1961-1963. An example of the waveform produced is shown in figure 3.

As a simulant to be experienced outdoors it was found that basically an event consisting of a pair of explosive bangs is readily distinguishable from an aircraft sonic bang. However, when experienced indoors it was found to be indistinguishable, as is evidenced by the results given in the table overleaf, which lists the percentages, out of thirty people, who identified various bang events correctly.

---

* Our terminology here, although the common one, is clearly not without some confusion, for a 'sonic bang' consists of two actual bangs. It would be better if it were called, for example, 'a sonic bang event', and indeed this terminology is gaining favour in scientific circles where precision is required.

Event	Nature of bang	Percentage who identified it correctly	
		In total	Of those who had heard sufficient aircraft sonic bangs that they thought that they would be able to recognise them if they heard them under normal conditions outdoors
92	Explosive	57	56
93	Aircraft sonic	23	19
94	Explosive	47	50
95	Aircraft sonic	53	56
96	Explosive	47	44
97	Explosive	57	50
98	Aircraft sonic	40	38
99	Explosive	43	44
100	Aircraft sonic	37	38
101	Explosive	53	63
102	Explosive	60	56

It will be seen from the third column that, out of the thirty people, the percentages who identified an event correctly range around the 50% mark, which is what one would expect if the events were completely indistinguishable. Moreover, the figures lower in the table are not noticeably better than the earlier figures, so that there is little evidence of any 'learning'. It will be noticed that sixteen people who had heard sufficient aircraft sonic bangs that they thought that they would be able to recognise them as such generally did poorer than the party as a whole.

On the basis of this indistinguishability when experienced indoors, it was decided to use events consisting of a pair of explosive bangs as a sonic bang simulant for an investigation of the effects of bangs on the subjective reaction of a community[2]. A community of some 280 people was chosen, living roughly equidistant from the firing point of the explosive charges, as shown in figure 4. Actually it was found that if the charges were fired at ground level meteorological effects, such as wind shear, caused large variations in the intensity of the experienced events for the same nominal firing conditions. Accordingly it was necessary to suspend the explosive charges, from a balloon, at an altitude of about 135 m above the ground. With this arrangement a fairly controllable stimulus was obtained. Although the precise sonic bang waveform was not reproduced, subjectively the events were not atypical of sonic bangs, and there was the additional realism that the bangs were incident from above.

The main results of this study, made in 1963, are shown in figure 5, which plots the percentages annoyed, either at all or considerably, as the exercise progressed. The standard programme consisted of making twenty-four bangs on each of two days early in a week at random times between the hours of 0930 and 1530, and at a nominal pressure rise of 125 Pa. The community's reactions were retrieved towards the end of each week by means of a simple questionnaire. It will be seen that there is some evidence of adaptation to the bang environment. After five weeks of the standard programme variations were introduced, such as reducing the frequency of the bangs (week 6), increasing the frequency (week 10), reducing the intensity (week 12), increasing the intensity (week 14), making the bangs earlier in the day (week 7), and making them later in the day (week 11). The only variations that caused significant changes were the increases in frequency and in intensity, to both of which the community tended to react violently, as evidenced by the two pronounced peaks.

3. Explosive line charges

Although events resulting from the firing of a pair of explosive point charges, in the circumstances outlined in section 2, had been felt to give a good simulation of sonic bangs, there was a need for a better simulant, particularly for studying the effects on building structures. This problem was presented to the Explosives Research and Development Establishment[3] in late 1963, who decided to simulate the sonic bang waveform by using explosive line charges[4].

Whereas an explosive point charge gives the familiar Friedlander waveform, a uniform explosive line charge[5], when experienced end-on, gives a waveform consisting of single positive and negative pulses separated in time by an interval essentially equal to the length of time it takes for sound to travel the length of the charge, as shown in figure 6, which gives the calculated waveform, and figure 7, which gives a measured waveform. This is the basic fact, and forms the 'building brick' with which we can see intuitively how we can, by superposition, build up line charges to yield, in principle, roughly any desired waveform. By forming a charge consisting of a number of strands whose ends are successively offset relative to the others, as indicated in figure 8, we can see that it should be possible to construct a charge whose waveform approximates that of the desired sonic bang N-wave. The actual waveform from their so-called ERDE Mark I simulant, shown in figure 9, indicates the degree of success that the ERDE have had in developing this technique. It must be appreciated, of course, that one obtains this waveform only in positions end-on relative to the line charge. Although the waveform has the broad characteristics required, it has two main shortcomings; one is that the pressure rise rate of the second shock is not as great as that of the first shock; the other is that the waveform has some superimposed random noise.

In regard to the pressure rise rate of the second shock it was found that this could be improved by adding a small explosive point charge to the far end of the line charge. A faster pressure rise rate of the second shock was thereby achieved at the expense of introducing some pressure perturbations immediately after the second shock: it is not known how important these imperfections are.

In regard to the superimposed random noise figure 10 shows the energy spectrum of the waveform from an ERDE Mark I explosive line charge, curve BB, compared with that of the waveform from an ideal sonic bang, curve AA. It will be seen that the spectral energy of the simulant compares favourably with that of an ideal sonic bang up to a frequency of about 100 Hz: above this frequency there is an excess of energy, associated with the superimposed random noise. It is felt, however, that the simulant is adequate for application to targets in which the responses at frequencies below 100 Hz is of concern, such as building structures. Indeed, ERDE Mark I simulants (without the point charge addition) were used in a series of field experiments made by the Royal Aircraft Establishment in 1968 on the effects of sonic bangs on various elements of a building. Figure 11 shows a view of the test building. Various measurements were made, such as wall responses, window responses, etc. In many cases the measurements were compared with calculated values. A wide range of experimental conditions was investigated, embracing not only variations in bang intensity and duration, but also variations in the condition of the building, such as whether the doors were closed or open, etc. Figure 12 shows one of the window arrangements studied. From the arrangement on the right it was possible to compare the responses of a leaded light with those of a plain plate glass window of the same overall size. From the arrangement on the left it was possible to compare the responses of some shaped leaded lights with those of a simple diamond arrangement of leaded lights. A report on this work is in course of preparation. However, some of the results are shown in figure 13, which is a plot of the static deformation of a window after each bang in the programme. It shows that bangs of the order of 100 Pa pressure rise and 200 ms interval between shocks do not cause any creep in some typical leaded light installations, as evidenced by the fact that there is no overall drift in one direction or the other.

Now, owing to the excess of energy at high frequencies the ERDE Mark I simulant is not considered suitable for studying the effects on targets in which the responses at frequencies above 100 Hz is of concern. Such studies include, for example, the effects on human subjects. For such subjects it is known that the important parameters are the pressure rise and the pressure rise rate. We described in section 2 the quite good simulant consisting of a pair of explosive point charges that has been used for a study of the subjective reaction of a community. However that simulant suffered from the fact that, although the pressure rise rates were large, and typical of sonic bangs, the pressure fall rates were large too, this being not typical of sonic bangs. Now the shocks alone contribute subjectively significant energy to an actual sonic bang, at least as far as loudness is concerned, the remaining parts of the waveform being subjectively insignificant. Accordingly the Explosives Research and Development Establishment set themselves the design objective of reproducing the two shocks of the sonic bang waveform, and with the correct separation in time, but with very low pressure fall rates after each shock. Their resulting simulant, which they call the ERDE Mark II, is another explosive line charge arrangement which gives a waveform very like that of one of the pair of explosive point charges, but much elongated in time, as shown in figure 14. An essential feature of this simulant is the control that it gives the experimenter over the pressure rise rate, through the manner in which the charge is constructed. In practice, two of these explosive line charges would be used, the second being fired the required time interval after the first. The energy spectrum of the waveform from this simulant is shown as curve CC in figure 10 along with those from an ideal sonic bang, curve AA, and from an ERDE Mark I explosive line charge,

curve BB. It will be seen that the spectral energy of the simulant compares favourably with that of an ideal sonic bang above a frequency of about 10 Hz: below this frequency there is a deficiency of energy. So far this ERDE Mark II simulant has not been used in any response studies.

4. Shock tube device

When it became known in 1965 that the explosive line charge simulant had some superimposed random noise in its waveform, the Royal Aircraft Establishment began to consider a shock tube device for simulating sonic bangs, to which they gave the acronym Blunderbuss[6].

The basic principle behind the Blunderbuss depends upon the acoustical fact that, when a sphere of compressed air, as in a balloon, is released, an event having a N-waveform is radiated. In practice a rubber balloon tears, resulting in an N-wave having much superimposed random noise, but with a material that shatters, such as glass, very noise-free N-waves are obtained. The main unpracticability of the use of a sphere is that, in order to generate sonic bangs typical of civil supersonic aircraft, which have an interval between shocks of about 300 ms, the balloon would have to be about 100 m in diameter. However, one does not need to radiate the event over the whole of space, but only at a target. Accordingly, since the phenomenon of a bursting sphere is spherically symmetric, acoustically the same phenomenon can be generated in a conical tube whose apex corresponds to the centre of the sphere, and which has a diaphragm corresponding to the surface of the sphere, as shown in figure 15.

This, then, is the basic idea behind the Blunderbuss. In order to prove the idea a so-called pilot Blunderbuss has been constructed[7], with the diaphragm at various positions from about 0.1 to about 5.5 m from the apex, so that the interval between shocks of the resulting events ranged from about 0.6 to 35 ms. An example of the waveform that has been obtained is shown in figure 16, together with that from a typical sonic bang. It will be seen that a good N-wave is obtained, there being two clearly defined shocks of closely equal pressure rise, a high pressure rise rate, and very little superimposed random noise. Plans are now in hand to construct a larger Blunderbuss, capable of generating sonic bangs of up to 300 ms interval between shocks. This requires a driver section some 50 m long. The magnitude of the pressure rise at any station down the tube is governed by the pressure at which the diaphragm is burst: this is easily controlled by bringing the driver pressure to the required value, and then rupturing the diaphragm by 'firing' a built-in electrical heating element at the diaphragm station. An artist's impression of such a Blunderbuss is shown in figure 17.

It must be appreciated that one only gets the desired N-wave event in the tube of the Blunderbuss itself: it is not a 'gun' for 'shooting' simulated sonic bangs at targets outside it. Experimental work will be done in a so-called working section of some 3 m square. The main objects of study will be various elements of building structures, such as windows, portions of roofing, etc. Naturally the dimensions of such elements will not have to be large relative to the general dimensions of the working section, otherwise there will be the complications of appreciable reflection effects from the walls of the tube. However, it is envisaged that many experiments will be possible by mounting test specimens flush with the walls of the tube, thereby allowing the simulated sonic bangs to pass over them at grazing incidence. It is also envisaged that a room will be built on to the side of the working section, and separated from it by some typical sound-transmitting structure such as a window or a wooden partition. In this room studies could then be made of the effects of external bangs passing over this sound-transmitting structure on human or animal subjects in the internal conditions of the room.

Some experiments have already been performed in the pilot Blunderbuss. In particular studies have been made, on a reduced-scale model of the same experimental configuration of building as was used in the full-scale experiments using the ERDE Mark I simulant. The appropriateness of the facility for such studies has been demonstrated. Figure 18 shows a comparison between the measured and calculated responses of one of the walls of the model experimental building. Model work of this nature is particularly suited to checking out theoretical methods, because any discrepancies can usually fairly be attributed to shortcomings in the theory, owing to the high degree of precision that can be obtained in the experimental measurements.

5. Summing-up

It is appropriate in conclusion to compare the various simulants that have been described, and to discuss their roles of application.

The Blunderbuss, together with similar shock-tube devices, is seen as a tool for intensive experimental studies in the laboratory. It can be used for a wide range of

studies of a fundamental nature on human and animal subjects, and on elements of building structures.

The ERDE Mark I simulant is seen as a tool for field studies on real buildings, and the ERDE Mark II simulant as a tool for field studies on human and animal communities.

Finally the simulant consisting of a pair of explosive point charges is felt to have a role for field studies on human and animal communities. It is cheaper and more convenient to use than the ERDE Mark II simulant, and in many respects it is more realistic subjectively.

References

No.	Author	Title, etc.
1	C. H. E. Warren T. A. Holbeche	An investigation of the waveform characteristics and subjective effects of sonic and explosive bangs. RAE Technical Report 67167 (1967)
2	D. R. B. Webb C. H. E. Warren	An investigation of the effects of bangs on the subjective reaction of a community. J. Sound Vib., 6, No. 3, 375-385 (1967). RAE Technical Report 66072 (1966)
3	S. J. Hawkins J. A. Hicks	Some measurements on the sonic bangs produced at Exercise Westminster. ERDE Technical Memorandum 17/M/68 (1968)
4	S. J. Hawkins J. A. Hicks	A new explosives technique for synthesizing a wide range of pressure waveforms in air; Part 2: The application of linear explosive charges to the simulation of sonic bangs. ERDE Report 10/R/68 (1968)
5	S. J. Hawkins J. A. Hicks	A new explosives technique for synthesizing a wide range of pressure waveforms in air; Part 1: Approximate theory of air blast from extended explosive charges. ERDE Report 9/R/68 (1968)
6	C. H. E. Warren	Proposal for a shock-tube facility to simulate sonic bangs. RAE Technical Report 66344 (1966)
7	D. R. B. Webb R. J. Pallant	A device for simulating the sonic bang. Paper given at the Symposium d'Acoustique Aéronautique sponsored jointly by the Association Française des Ingénieurs et Techniciens de l'Aéronautique et de l'Espace, the Groupement des Acousticiens de Langue Française, and the British Acoustical Society, held in Toulouse in March 1968

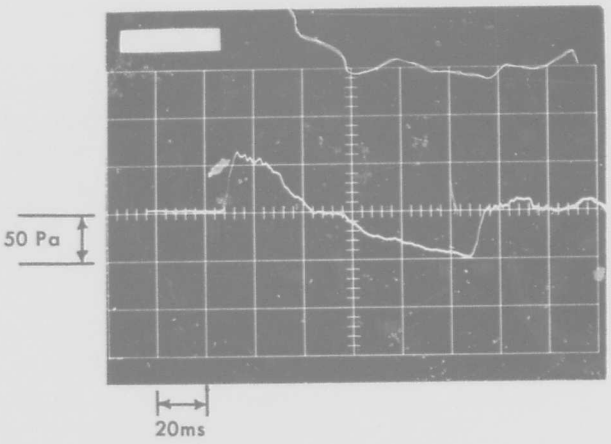

Fig.1. Typical sonic bang waveform

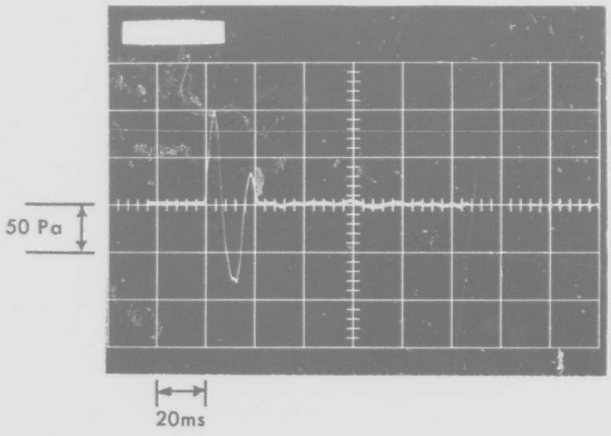

Fig.2. Waveform from an explosive point charge

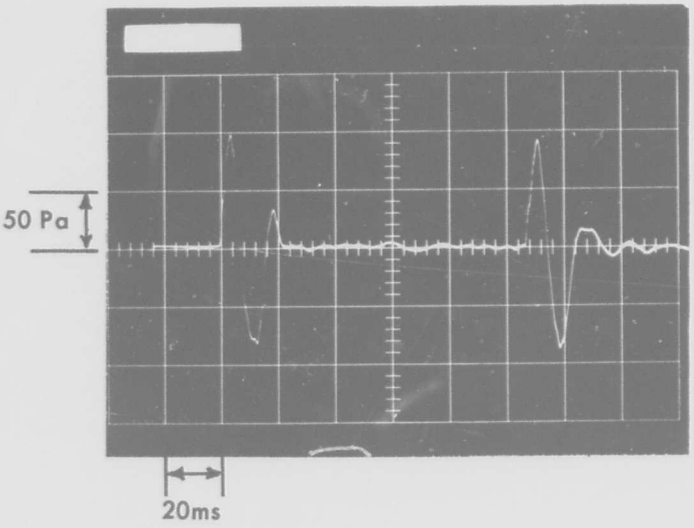

Fig.3. Waveform from a pair of explosive point charges

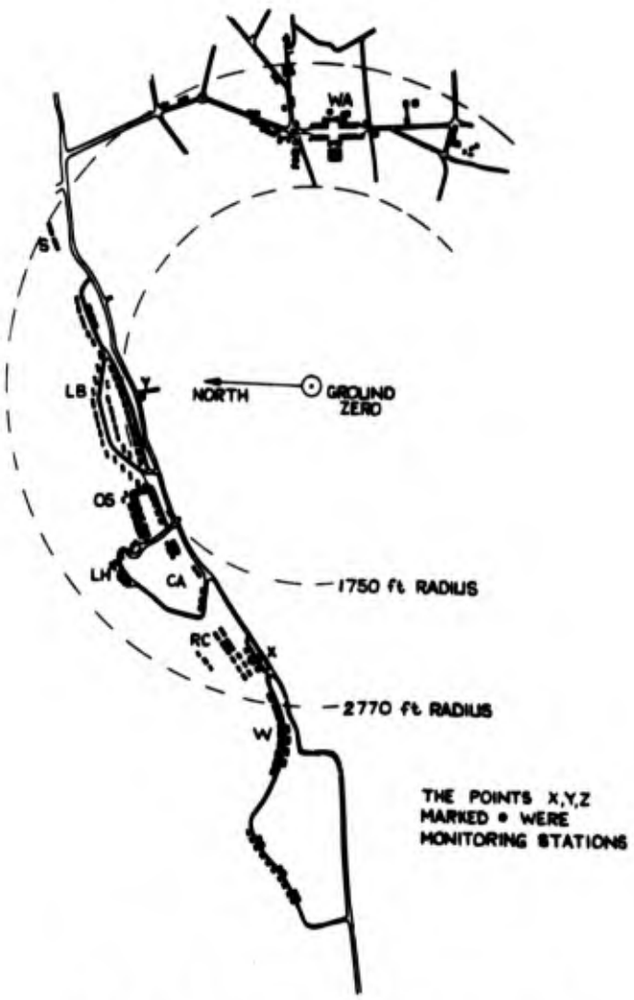

Fig.4. Site of community reaction experiment

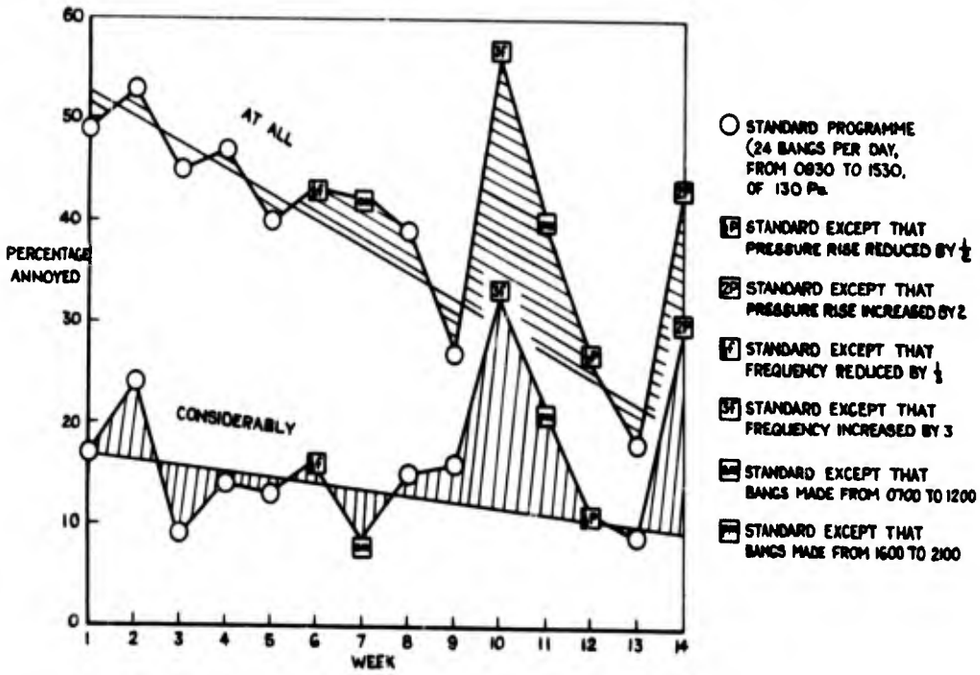

Fig.5. Results of community reaction experiment

Fig.6. Calculated waveform from a uniform explosive line charge

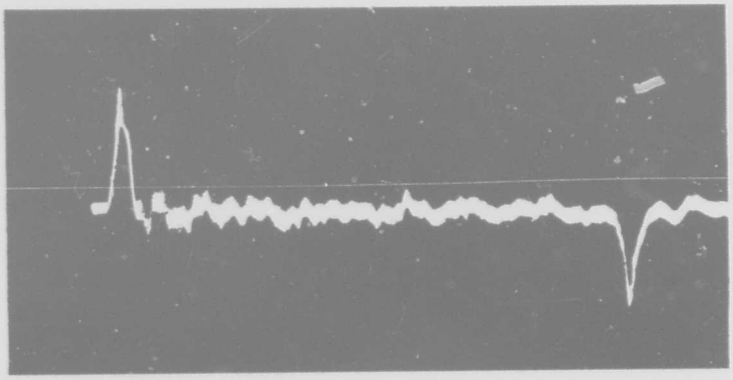

Fig.7. Measured waveform from a uniform explosive line charge

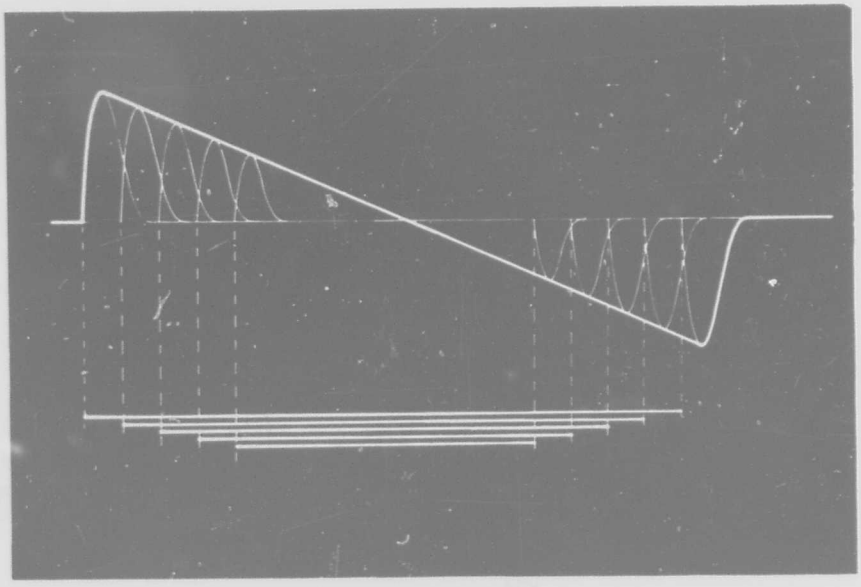

Fig.8. Construction of an explosive line charge to yield an N - waveform

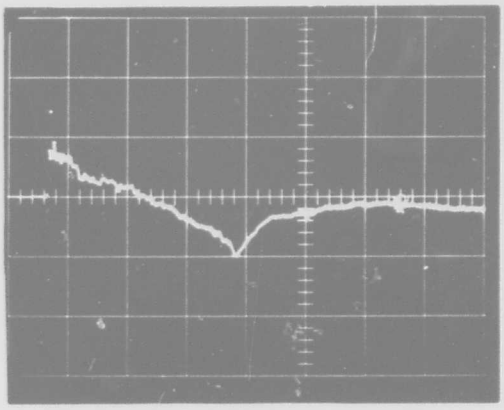

Fig.9. Waveform from an ERDE Mark 1 explosive line charge

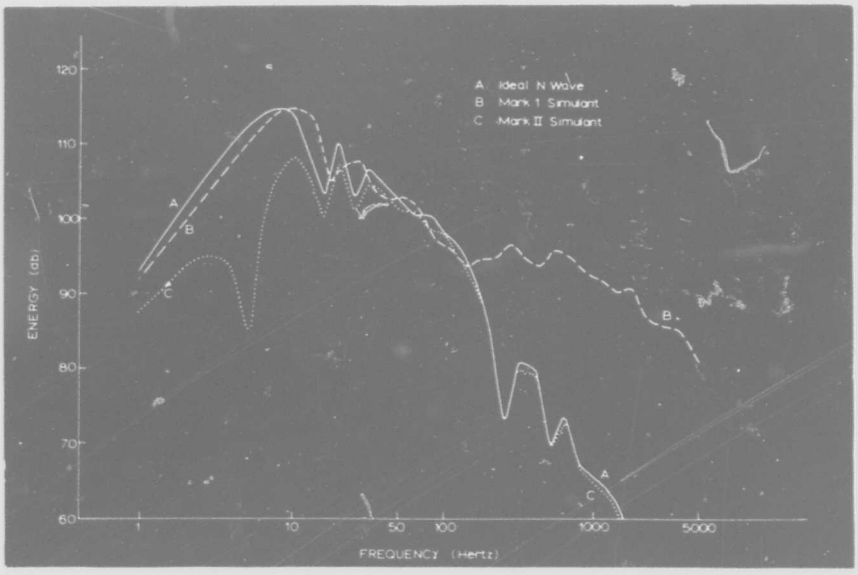

Fig.10. Energy spectra of the waveforms from an ERDE Mark 1 explosive line charge, an ERDE Mark 2 explosive line charge, and an ideal sonic bang

Fig.11. View of test building

Fig.12. View of window arrangements studied

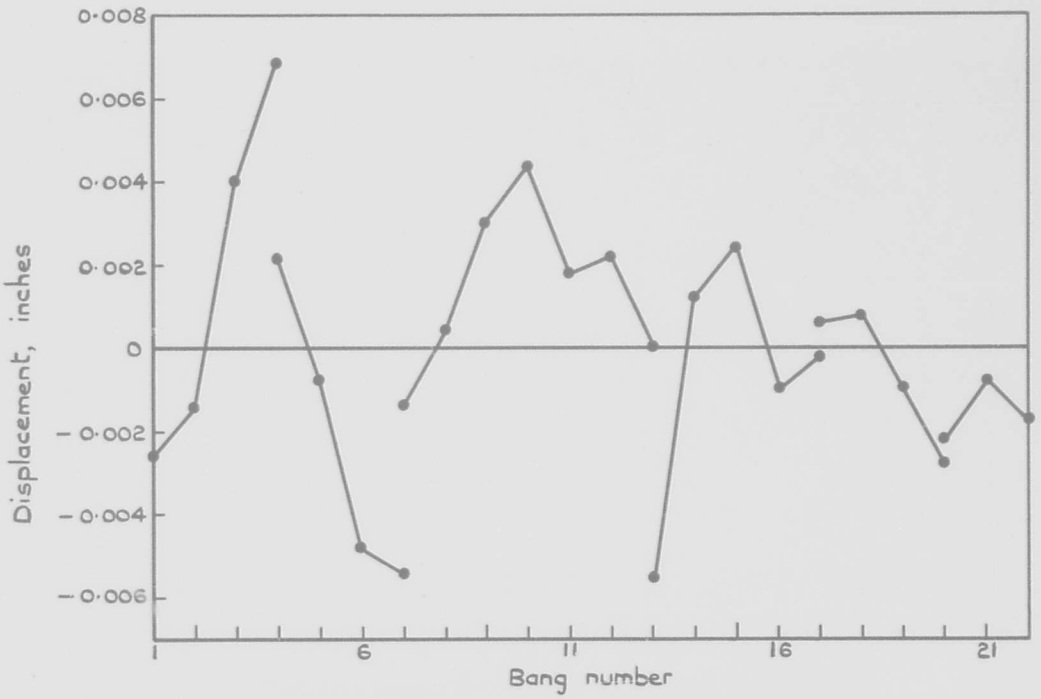

Fig.13 Creep measurements of leaded lights excited by simulated sonic bangs

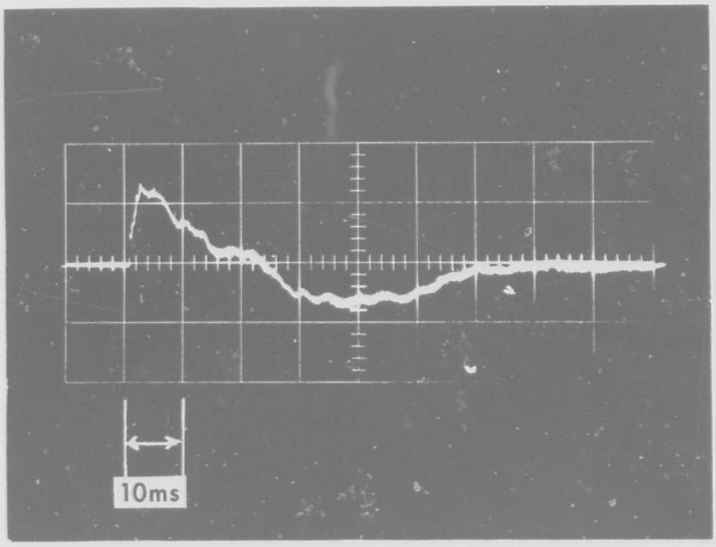

Fig.14. Waveform from an ERDE Mark 2 explosive line charge

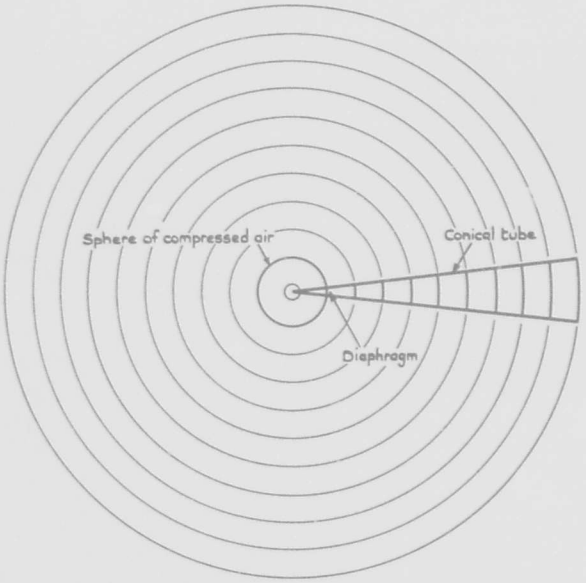

Fig. 15. Principle behind the Blunderbuss

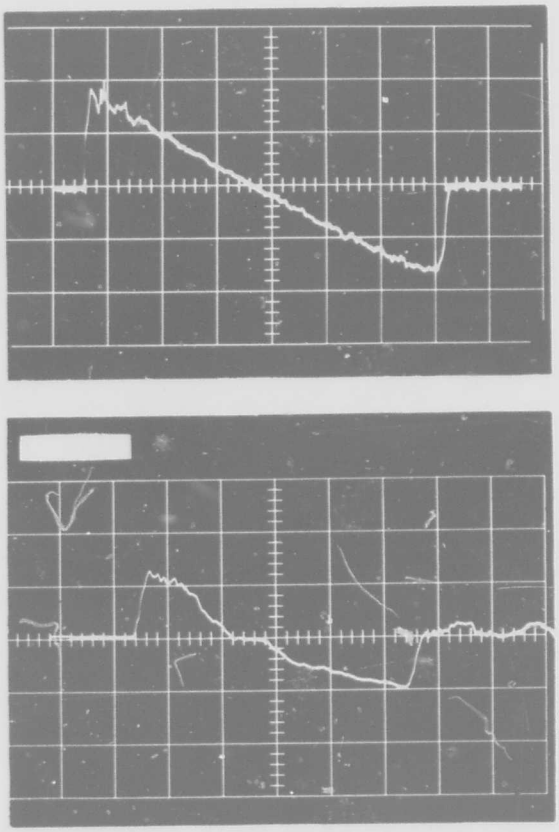

Fig.16. Comparison of the waveform in the Blunderbuss with a typical sonic bang waveform

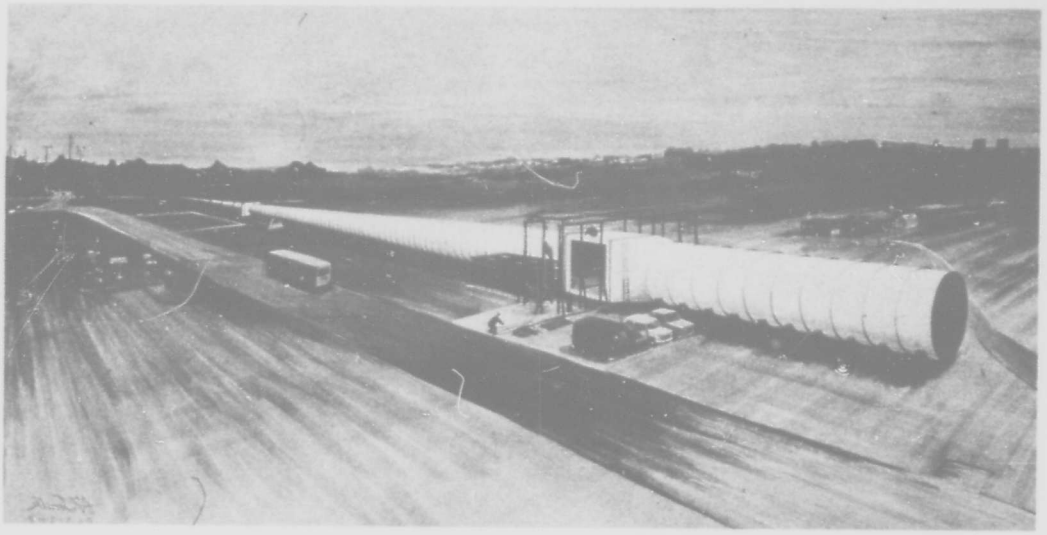

Fig.17. Artist's impression of the Blunderbuss

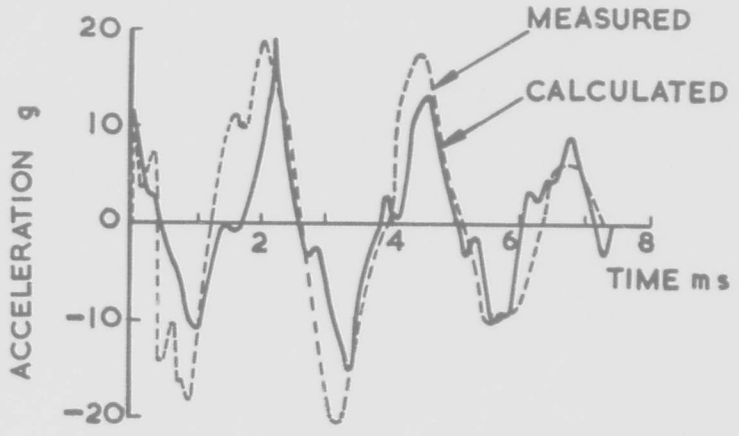

Fig. 18. Comparison between measured and calculated responses of a wall of a model building in the Blunderbuss

SONIC BOOM SIMULATION FACILITIES

by

Ira R.Schwartz

National Aeronautics and Space Administration,
Washington, D.C.

Summary

The requirements for experimental research to study the generation of sonic boom pressure fields, its propagation through a stratified atmosphere and its effect on humans and structures dictate the construction of unique sonic boom simulation facilities. A variety of sonic boom simulators have been built in an effort to meet the requirements of proper simulation. This paper discusses a broad spectrum of sonic boom simulator concepts with special emphasis on the NASA wind tunnel sonic boom techniques, the NASA Langley Low Frequency Noise Facility, the Ling Tempco Vought/NASA Shock Tube - Bursting Diaphram Facility and the General Applied Science Laboratories/NASA Quick Action-Valve Shock Tube Facility. In particular, this paper contains brief discussions of the overall design features of the facilities, their operating characteristics, their research capabilities and some research problems that are amenable to laboratory testing. The paper shows that substantial progress has been recently made in advancing the state of the art of sonic boom simulator development. Most of the requirements for sonic boom simulation and human and structural response can now be accommodated in a simple, inexpensive facility such as the GASL/NASA Quick Action-Valve Shock Tube Facility.

SONIC BOOM SIMULATION FACILITIES

Ira R. Schwartz
National Aeronautics and Space Administration
Washington, D. C.

Introduction

The generation of sonic boom by supersonic aircraft has established the need to conduct extensive investigations of this phenomenon and of its effect on people, structures, and animals. Further understanding of the effect of atmospheric conditions, of terrain, and of buildings on the propagation of the boom is needed to assess the boom potential and response.

Until very recently, most engineering research data on sonic boom was obtained by overflights of supersonic aircraft. Although these flight tests have contributed substantial qualitative information, this experimental method has serious limitations that are not conducive to a systematic research program of structural and human response to booms nor to conducting a basic research program on boom generation and propagation. Specifically, the flight testing technique is incapable to develop a specific boom signature, to conveniently modify the signature, and generally, to repeat a signature. Also, this full scale test procedure is very costly and time consuming thus limiting the scope of the programs that can be carried out and requiring the coordination of a large staff of people.

It is well known to researchers in this field that to obtain a better understanding of the various aspects of sonic boom phenomena, it is necessary to conduct a systematic investigation varying one parameter at a time. To accomplish this and since flight testing methods are not suitable for this type of program, studies must be conducted in sonic boom simulation facilities. Such a laboratory simulator should have the capability to reproduce the boom signatures of varying shapes with variable pressure amplitudes and duration. In addition, the simulator should be capable of varying these parameters in a predictable and simple manner. Other considerations for proper simulation would provide for the pressure wave representing the desired signature also be a traveling wave with a velocity corresponding to that expected to be incurred by the supersonic transport. Further, from an economical standpoint, the simulator should be inexpensive to operate on a per-shot basis so that numerous tests can be conducted economically if the problem requires statistical information. In addition it would be very desirable that the simulator have the capability to scale the signature wavelength, (time) so that particular tests can be conducted on scale models which would provide in many cases a significant cost reduction over full scale tests. A broad spectrum of sonic boom simulator designs have been built which satisfy some of the aforementioned requirements.

This paper contains brief descriptions of the main design features of the various facilities, discussions of their operating characteristics, their research capabilities, and of some research problems that are amenable to laboratory testing.

N-Wave Spectrum

To make an accurate determination of the required characteristics of sonic boom simulation facilities necessitates a thorough understanding of the physical properties of the waves, particularly, the spectral content of the waves. The basic features or variables of sonic boom pressure signatures that are believed to be important are shown in Figure 1. Illustrated are the overpressure Δp, the wave length T, the rise time τ, and the impulse functions, Ipos. All of these variables are important in the overall community response problem. With regard to the response of buildings, the important variables are believed to be the overpressure, the wavelength and the impulse [1-3]. It is apparent that the N-wave shape is idealized and may be altered to some extent by atmospheric effects and aircraft design considerations.

Also the factors affecting ground exposure have been discussed in the literature in great detail[4-7] and have been classified in three categories: (1) aircraft design, (2) aircraft operations and (3) atmospheric effects. Many of these factors can now be successfully programmed into sonic boom simulation experiments as a result of a computer program that was developed by the Aeronautical Research Associates of Princeton.[8,9] Much more research must be performed on problems such as: to determine the effects of atmospheric turbulence, non linear near field effects, diffraction into shadow zones, propagation of the N-wave near the caustic and topographical geometric shape effects. The availability of this information will allow the boom simulation experiments to improve upon the nature of ground exposure patterns.

Spectral Content of Wave

Knowledge of the spectral content of the wave is essential to understand the manner in which sonic boom exposures affect people and structures and hence result in a proper boom simulation in ground facilities. A typical spectral content of an idealized N-wave having a time duration of 0.1 sec., based on Fourier integral techniques[10] is illustrated in Figure 2. Relative amplitude on the vertical scale is plotted as a function of frequency, on the horizontal scale. The solid curve including several convolutions is essentially the spectrum of the wave. The dashed curve denotes the envelope of the spectrum of the wave at the high frequencies and is observed to drop off at the rate of 6dB/Oct. Also, it can be seen that the highest amplitudes are associated with the lower frequencies. The spectrum peaks at approximately 10 cps and then drops off rapidly above and below this frequency. An important feature to emphasize is that the spectrum extends from the higher frequencies which are in the audible or speech frequency range to the lower frequencies which are in the subaudible range. The lower frequencies are important for structural response whereas the higher frequencies are important for loudness effects.

Sonic Boom Simulation Techniques

A variety of boom simulators have been developed and built, each of which satisfies some of the requirements previously mentioned above. The various techniques employ wind tunnels, ballistic ranges, shock tubes with bursting diaphrams, piston-speaker systems, quick action valving shock tubes, and explosive arrays to produce the desired pressure waves. These simulator concepts, most of which will be described in this paper, are believed to represent the broad spectrum of sonic boom facilities which are in use today.

Wind Tunnel Techniques

The wind tunnel facility with scale models has been used successfully for many years to extend the basic understanding of sonic boom phenomena and to establish the sonic boom characteristics of specific airplane configurations. To accomplish this, both the NASA Ames and Langley Research Centers developed various wind tunnel testing techniques that were capable of overcoming such testing problems as: accurate construction of extremely small models, nonuniform and nonsteady tunnel test conditions, model and probe vibration, boundary layer effects, and complex near field signatures.[11, 12] For example, a typical arrangement of wind tunnel test apparatus located at the NASA Langley Research Center which produced satisfactory results in sonic boom research is illustrated in Figure 3. The model is sting supported by a remotely controlled actuator which allows longitudinal positioning of the model. The measuring probe and reference probe assembly is also on a remotely controlled actuator. To obtain the measurement of a particular signature, the probe position is fixed, which avoids the influence of tunnel flow nonuniformities. The model is moved to successive positions when a complete pressure signature is desired. At Langley, sonic boom wind tunnel tests have been performed with models ranging in size from ½ inch (.64 cm) to 4 inches (10.2 cm). Figure 4 shows a photograph of some of the one inch (2.54 cm) airplane models tested in the 4 x 4 foot (1.22 x 1.22 M) supersonic pressure tunnel. The choice of model size is determined by compromising between small models that permit an approach to far-field N-wave conditions for the measured signature and large models which provide more accurate airplane representation and more exact signature definition.

Direct comparisons of signatures measured in tunnel tests with those measured in flight are made possible by applying scaling laws.[11] Figure 5 shows an example of this comparison. A signature for one inch (2.54 cm) long model is compared with the measurements for a 100-foot (30.4 M) long bomber airplane. To obtain geometric similarity of airplane and model, the signature parameters account for the substantial differences in size, ambient pressure, distance or altitude and reflection factor. It is also necessary for direct comparison that the signatures be obtained, as shown in Figure 5, for similar lifting conditions. It can be noted that the tunnel data, when adjusted, agree well with flight measurements.

The application of the various test methods mentioned above (and described in greater detail in Reference 12) has made the wind tunnel a valuable sonic boom research tool which resulted in significant contributions toward the understanding of sonic boom generation and propagation. Although the wind tunnel facilities have demonstrated the capability of providing reasonably accurate data of the pressure fields of complete airplane models, these facilities cannot produce the traveling wave or time varying wave of the actual boom which is very important for response studies.

Shock Tube - Bursting Diaphram Technique

Another type of boom simulation facility developed by Ling Temco Vought under NASA sponsorship utilizes a system of shock tubes and acoustic horn to produce acoustic waves, but lacks the capability to satisfactorily reproduce the required boom signatures that are needed for various simulation conditions.[13] The simulator system shown on Figure 6 consists of two shock tube driver sections, each twelve feet (3.65 M) long coupled to an exponential horn, the mouth diameter of which is thirteen feet (3.96 M) and the length is thirteen feet (3.96 M). Its lower cut-off frequency is 50 HZ. A variable time delay circuit provides a controllable period between the bursting of the two diaphrams. The simulator can produce double blast

waves with a maximum peak pressure of 27 psf (15 6dB ref. 2×10^{-4} dynes/cm^2) at ten feet (3.04M) from the horn (on axis) using 30 psi static pressure. The boom duration can be varied from 10 to 600 msec. The pressure transients generated by this process have potential applications with studies of physiological and structural response to sonic boom overpressures. Detailed analysis of the generated waves is discussed in Reference 13. A typical pressure signature generated with the sonic boom simulator is shown on Figure 7. It represents the pressure - time history at a position ahead of the exponential horn. By proper adjustment of the initial static pressure in the driver tubes, it is possible to vary the amplitude of each boom.

The transfer function required to provide this wave signature from a perfect N-wave transient was established by analog simulation in the laboratory. Figure 8 shows that by insertion of a high pass filter with a lower cut off frequency of approximately 35 HZ, the ideal N-wave input signature can be transformed to a transient very similar to that shown in Figure 7. The simulator generates pressure amplitudes which are comparable in magnitude to those produced by a supersonic aircraft.

The frequency content or spectral analysis of the waves produced by the simulator can be derived from the pressure - time history by approximating the signature as an exponential blast wave of the form.

$$P(t) = \left(1 - \frac{to}{t}\right) e^{\frac{t}{to}}$$

Using a generalized transform the frequency content of this transient is developed as shown on Figure 9. As a result of the nonlinear nature of the problem, it is expected that the frequency content changes as a function of distance from the shock tube and approximates an exponential blast wave with constant period when the weak wave condition prevails.

Ballistic Range Technique

A third type of sonic boom simulator uses a ballistic range with a ballistic model for exploring atmospheric and topographical effects. This system produces a traveling wave and the wave shape can be varied by modifying the shape of the projectile. Preliminary reports, however, indicate that it is difficult to vary the shape, velocity amplitude, and rise time of the signature in a systematic manner in this facility concept. However it has been demonstrated that using a conventional one stage gun, projectiles can be accelerated up to Mach numbers of 5. The projectile generates a shock pattern that portrays the main characteristics of the sonic boom. Also, there are advantages for conducting simulation experiments of atmosphere dynamics effects and topographical effects on sonic boom waves in this type of facility, namely: (1) the simulated atmospheric dynamics, such as turbulence and temperature gradients can be prepared in a region before the projectile passes through this region; and (2) transient phenomena, such as reflection, refraction and scattering processes can be investigated directly under most complex conditions.

Piston Speaker-Technique

A fourth approach for a simulator facility is the piston - speaker type which uses a system of acoustic drivers to regulate the pressure in a chamber. This facility can reproduce the boom pressure variations very accurately. An example of this type of facility is the NASA Langley Low Frequency Noise Facility shown in the photograph of Figure 10. In addition to sonic boom research capabilities, this facility was designed to provide a research capability for large scale acoustic tests in the frequency range below 50 cycles per second. Descriptions of the facility are given in References 14 and 15. In Figure 11 a sketch of the facility's primary components and a room size test structure are illustrated. Also shown is a sketch of a man to illustrate the relative size of the structure.

The principal features of this facility are a cylindrical test chamber, a large piston in one end of the chamber, and a moveable wall which can be positioned to close the opposite end of the test chamber. The facility chamber may be open (Figure 10) or closed (Figure 11) while in operation by positioning the moveable wall to tune the chamber. The piston is hydraulically driven to generate sound pressures. The size of the facility is sufficient to accommodate a small building structure. The overall dimensions are 30 feet long (9.1M) by 27 feet (8.2M) in diameter. The cylindrical test chamber was designed to provide a stiff structure with the natural frequencies above the top operating frequency of 50 cps. The piston is 14 feet (4.3M) in diameter and made of aluminum honeycomb construction. The piston was designed for high stiffness with frequencies greater than the operating frequency. The piston shape is a double cone with a depth through the center of 2 (.6M) feet. The perimeter of the piston is lined with an adjustable teflon seal which provides close clearance (within 1/16 in. (0.16 cm) with the adjacent teflon wall surfaces.

In Figure 12 is a block diagram illustration of the electrohydraulic system used to drive the piston. The principal component of the hydraulic driver is a piston with an area of 8 in.^{2} (51.6 cm^2) and a maximum rated stroke of 9 in. (22.9 cm). The hydraulic pressure (maximum of 3500 psi (24MN/M^2) is electronically controlled by a system where the desired acoustic environment

is obtained by putting the necessary electric inputs into the system with a function generator such as a discrete frequency oscillator, the playback of a random signal recorded on tape, and the momentary closing of contacts. This signal is then conditioned and fed into a computer circuit which forms part of a servo-loop circuit controlling the operation of hydraulic valving at the driver. Thus, the hydraulic system operates on command of the electronic circuit. By this technique, desired acoustic output environments such as random, sinusoidal, or impulse types including the N-wave pressure - signature characteristic of sonic boom pressures can be obtained.

Regarding this facility's application to sonic boom research, it is important to note that useful ranges of the variables, overpressure, wave length, rise time, and the impulse, for N-wave type disturbances can be simulated by the facility. Further, this facility's capability is particularly suitable for studying the response of structural components. In Figure 11 the setup is such that the response of a single wall panel can be studied in detail. Various wall constructions, including several door and window installations, can be exposed to a broad range of N-wave type impulse loadings. Also this type of facility is amenable to a program of subjective studies relating to the indoor sonic boom exposure situation for which building vibrations are believed to be important. It cannot, however, simulate the traveling wave nature of the boom.

Quick Action Valve-Shock Tube Technique

The fifth sonic boom simulation facility that is described and discussed in this paper was recently designed and built by the General Applied Science Laboratory, Westbury, New York, under NASA sponsorship. It is believed that this facility concept has the capability to fulfill most of the basic requirements for an ideal sonic boom simulator as mentioned above.

The GASL/NASA facility can reproduce the important and essential aspects of the sonic boom, and will accomplish this in a repeatable manner. This device concept produces an accurate traveling pressure wave, and the wave can be either scaled or full scale wavelength, depending on the size and design of the device. The facility operates on a supply of stored compressed air rather than on a continuous steady state generator that is required for acoustic chamber type facilities. Thus, the energy associated with a single pulse can correspond to thousands of watts even though the source of this energy may be provided by a small motor (compressor).

A schematic of the pilot sonic boom simulator that was built at GASL,Inc. in early 1967 is shown in Figure 13. It was the purpose of this simulator to test the GASL,Inc. concept for the creation of sonic booms in the laboratory. The results of feasibility studies on this pilot facility warranted the construction of a new and larger facility which will be discussed later. The three basic elements of this pilot facility are the air supply operating at about 10 atm., a mass control valve and a conical duct. In this initial pilot facility, the duct was approximately 30 ft. (9.1M) long with a 4 foot (1.2M) wide opening.

The basic concept involved in the GASL/NASA simulator is that a pressure wave can be generated in the duct which is proportional to the rate of change of mass flow at the sonic throat located at the apex of the pyramid. Also, this mechanism for producing the pressure pulse is described by the following operating equation which relates the pressure produced as a function of time (sonic boom) to the rate of change of mass flow at the throat.

$$p(t) = K \frac{dQ}{dt} \qquad (t)$$

To prove this concept, a special valve was created so that this behavior could be clearly demonstrated. The basic valve design consisted of a throat made up of a long narrow slot through which the main air passed. In front of this slot, a plate with a cutout of prescribed shape was made to slide. Since the flow through the slot to a first order is proportional to the length of the slot, assuming it to be a one-dimensional nozzle, then the height of the cutout in the plate would represent the mass flow for any given position of the slot. Thus, to produce a square wave as is shown in Figure 14, a slide plate is needed which has a linear changing slot so that the mass flow then is linearly changing and hence the derivative of the mass flow becomes a step function of both positive and negative value. To produce the N-wave as shown in Figure 15, the slide must have a cutout where the mass flow or length of the opening is quadratic with respect to the axis of the slide. If the mass flow is quadratic, then the rate of change in mass flow will produce an N-wave as indicated in Figure 15.

The results obtained using these plate configurations of Figures 14 and 15 are shown at the bottom of Figures 14 and 15. The actual wave shapes measured in the pilot facility are shown here. The inversion of the pressure pulse occurs at the microphone signal and has no significance. The two waves illustrated in Figures 14 and 15 are approximately 3 milliseconds long with peak pressures on the order of 1 pound per square foot (5×10^{-4} dynes/cm^2). Note, that the square wave picture in Figure 14 is in backwards. The quality of these signatures for both the N-wave and the square wave provided confidence that the operating fundamentals of the sonic boom simulator were correct. Figure 16 shows a fast "N" wave produced in the GASL/NASA prototype sonic boom simulator with peak pressures corresponding to about 10 psf. Figure 17 indicates the various testing zones or regions inside the horn or duct where tests can be performed. Basically, the acoustic wave that travels down a tube is a spherical wave with its center essentially at the air

BLANK PAGE

control valve. Thus, a true traveling wave is generated in the simulator and can be used to show interaction with a model at normal incidence or the effect of Mach angle, i. e., speed of the aircraft can be simulated by placing a ramp in the facility inclined at angle theta, such theta equals the arc sign of one over the Mach number. Tests performed in this manner on the ramp can provide an exact simulation for any reasonable Mach number.

Based on the results obtained from the pilot facility and a comprehensive analysis of the physical parameters, a new and large sonic boom simulator was built at GASL under NASA sponsorship. A schematic of the final facility configuration is shown in Figure 18. A detailed description of the GASL/NASA sonic boom simulator and a semi-rigorous analysis of the phenomena associated with the simulator which provides a greater understanding of its fundamental operation is reported in Reference 16. The three main components of the full scale simulator are: the mass control valve, the conical duct and the cone termination (absorber).

The conical duct has been constructed of reinforced concrete walls about 8 inches (20.3 cm) thick. The basic dimensions of the duct are 100 feet (30.4 M) long and 8 feet (2.4 M) square at the terminale end. The fundamental construction of the conical duct was made to be extremely rigid so that there would be no loss of wave energy to the walls. To prevent separation of the flow, a 2½ degree half cone angle was selected.

Figure 19 shows a schematic of the plug valve used with the full scale GASL/NASA facility. Such design fulfills the requirements for large mass flow and suitably shaped nozzle to minimize jet noise. Although the slide valve mechanism used in the pilot facility produced the required mass flow profiles, the amount of mass that could be passed through such a valve is greatly limited because of its one dimensional character. In addition, the orifice produces a substantial amount of background noise.

The mass control feature of the plug valve in the full scale facility is provided by the shape of the plug on the end of the driving piston. The sonic throat is formed between the plenum and the transition to the conical duct and the tapered plug passes through this orifice to control the mass flow. The equivalent of 50 HP of instantaneous power is required to move the valve at the necessary speeds, although of course, this is on an impulse basis. A stored hydraulic system is used to furnish this power to the facility.

A large portion of this GASL/NASA research project on developing the sonic boom simulator was devoted to solving the problem of acoustic reflections from the open end of the conical duct. Although the adsorber is not required for very short wavelengths such as those utilized in scale model testing, it is apparent that for long wavelengths (full scale booms) the reflected signal from the open end of the duct will interfere with the outgoing pressure wave produced by the valve source. The interaction of reflected and outgoing waves produces a result which is not representative of the sonic boom signature.

By conducting an appropriate analysis of the wave propagation in and at the exit of the duct a unique solution was obtained which suggested the possibility of cancelling the reflected waves by means of a moving absorber. [16] A schematic of the actual moving absorber used in the facility is shown in Figure 20. The material selected for initial use in the facility was ½ inch (1.27 cm) thick fiberglas blanket.[3]

On Figure 21 are shown the results attained by using this moving porous piston technique. The upper picture illustrates an incident pressure wave and the subsequent reflections obtained when the exit of the conical duct is exhausting directly to the atmosphere. The lower picture illustrates the attenuation achieved with a similar input pressure wave after the adsorber was installed at the exit of the facility. It is apparent from this data that an order of magnitude reduction of reflected energy is obtained even with this initial untuned design.

Thus, the GASL/NASA facility described above has been demonstrated and does indeed simulate a sonic boom. Further, it incorporates features which make it a flexible device in varying the parameters over a broad range.

Applications of GASL/NASA Facility

This portion of the paper will first describe the capability of the GASL/NASA facility and then show how the facility should be utilized in performing sonic boom research studies.

The following table of values list the ranges of performance which should be available in the GASL/NASA facility, based on tests to date:

GASL/NASA Simulator Capability

Peak Pressure Level	up to 100 psf (48 x 10^3 dyns/cm^2)
Wavelength	½ ft - 500 ft (.08 M - 152 M)
Period	300μ sec - 0.5 sec
Rise Time (minimum)	1 millisecond
Repetition Rate (typical)	up to 60/hr
Model Scale	1:1 to 1000:1
Maximum Test Station Area	8 feet square (2.4 M square)

The typical repetition rate is a function of the air compressor supply capability. Actually, the figure of 60 booms per hour could readily be made 200 per hour, or similarly, multiple booms could be produced in rapid succession, separated by tenths of seconds. Also, in this facility tests can be made of both full scale and scale model phenomena where the scaling can be up to 1000:1 so that large topographical areas, for example on the order of 1 mile (1.6 KM) can be easily simulated.

It is significant to note that many applications of the GASL/NASA facility can be accommodated without any additions or modifications to the facility. For example, Figure 22 shows a test set up for measuring the dynamic response of large structural models. Here the physical model is placed inside the conical duct and proper instrumentation is provided so that the entire structural response can be measured if proper scaling has been performed. In a similar manner the effects of terrain on sonic boom signatures can also be studied with scaled terrain models.

Figure 23 shows a schematic of a cross section of the GASL/NASA concrete duct and a typical arrangement to test the effects of the sonic boom on the window and various window constructions. This would require minimum modification to the facility because knockout sections exist in the side walls of the facility which will permit such a setup to be made. In the present configuration windows up to 6 foot square (1.8M square) can easily be subjected to a complete range of sonic boom overpressures, signature shapes, and wave durations.

A test arrangement for conducting psychoacoustic and other studies utilizing the GASL/NASA facility is shown in Figure 24. A full scale room is attached to the horn and connected with a part corresponding to a window. This configuration realistically simulates that to be found in a large apartment house building where the sonic boom wave is incident to only one opening or part of the room.

Investigations of atmospheric effects on sonic boom in the GASL/NASA facility can be performed by producing thermal gradients and thermal turbulence using heaters mounted in the floor of the horn. Turbulent airstreams can be generated by introducing jets normal to the two verticle walls of the horn. This simulator has a unique capability to change the scale length of the N-wave so as to examine quantitatively the effects of wave length and turbulent scale size.

Thus, the GASL/NASA facility represents the most advanced state of the art in sonic boom simulation. It meets most of the requirements previously mentioned for performing basic and applied research on sonic boom phenomena including human and structural response. There is, however, room for improvement in this area of sonic boom simulation. With the advancement of knowledge of atmospheric and topographical effects on the sonic boom signatures, further progress will be required in developing new techniques or modifying the old ones to accommodate the requirements of practical sonic boom simulation facilities.

It can be concluded that substantial progress has recently been made in advancing the state of the art in sonic boom simulator technology and development. Most of the requirements for sonic boom simulation and human and structural response can now be accommodated in a single inexpensive facility such as the General Applied Science Laboratories/NASA Quick Action-Valve Shock Tube Facility. Further, from an economical standpoint, the GASL/NASA facility concept is inexpensive to operate on a per-shot basis so that numerous tests can now be conducted economically if the problem requires statistical information. The NASA wind tunnel techniques will continue to be valuable tools for extending the basic understanding of some boom phenomena and to establish the sonic boom characteristics of specific airplane configurations.

Finally, the availability of sophisticated analysis and computer methods of the propagation of sonic boom in a stratified atmosphere combined with the recent breakthroughs in sonic boom simulator designs permit the researcher to enter into a new dimension of understanding sonic boom phenomena, evaluating human and structural response, and hopefully, finding new methods for the minimization of sonic boom.

REFERENCES

1. Anon.: Structural Response to Sonic Booms, Federal Aviation Agency Report SST 65-1 Vol I (AD 610822), February 1965 (Prepared under Contract FA 64-AC-6-526 by Andrews Associates, Inc. and Hudgins, Thompson, Ball and Associates, Inc., Oklahoma City, Oklahoma)

2. Hilton, David A; Huckle, Vera; Steiner, Roy; and Maglieri, Domenic J.: Sonic Boom Exposures During FAA Community - Response Studies Over a 6- Month Period in the Oklahoma City Area, NASA TN D 2539, 1964

3. Maglieri, Domenic J; and Helton, David A: Signifance of the Atmosphere and Aircraft Operations on Sonic Boom Exposures, Paper Presented at NASA Conference on Aircraft Operating Problems, Langley Research Center, Hampton, Va. May 10-12, 1965 NASA SP-83, 1965

4. Maglieri, Domenic J.; and Carlson, H. W.: The Shock Wave Noise Problem of Supersonic Aircraft in Steady Flight, NASA Mem 3-4-59L (1959)

5. Hubbard, H. H.; and Maglieri, D. J.: Noise and Sonic Boom Considerations in the Operation of Supersonic Aircraft, Paper No. 64-548 Intern. Council Aeron. Sci. (Aug. 1964)

6. Anon.: Conference on Aircraft Operating Problems, NASA SP 83 (1965)

7. Hubbard, H. H.: Nature of the Sonic Boom Problem, Proceedings of the Sonic Boom Symposium Sponsored by the Acoustical Society of America, St. Louis, Mo. 3 Nov. 1965 pp 51-59

8. Hayes, Wallace D.; Haefeli, Rudolph C.; and Kulsrud, H. E.: Sonic Boom Propagation in a Stratified Atmosphere, with Computer Program, NASA CR - 1299, Prepared under Contract No NAS 1-7721 by Aeronautical Research Associates of Princeton, Inc.

9. Haefeli, Rudolph C.: Effects of Atmosphere, Wind and Aircraft Maneuvers on Sonic Boom Signatures Jan. 1969, ARAP Report 128 Prepared under Contract No. NAS 1-8490 by Aeronautical Research Associates of Princeton, Princeton, N. J. (To be published as NASA CR)

10. Taniguchi, H. H.: Instrumentation for Measurement of Sonic Boom, Noise Control 7, No. 2, 43-45, 1961

11. Carlson, Harry W.: Correlation of Sonic Boom Theroy with Wind Tunnel and Flight Measurements, NASA TR R-213, 1964

12. Carlson, Harry W.; and Morris, O. A.: Wind Tunnel Sonic Boom Testing Techniques, Paper presented at the AIAA Aerodynamic Testing Conference, Los Angeles, California, September 21 - 23, 1966

13. Dahlke, Hugo E.; Kantarges, George T.: Siddon, Thomas E., and Van Houten, John L.: The Shock Expansion Tube and Its Application as a Sonic Boom Simulator, NASA CR 1055, June 1968. (Prepared under Contract No. NAS 1-5652 by LTV Research Center)

14. Edge, Philip M. Jr.; Mayes, William H.: Description and Research Capabilities of the Langley Low-Frequency Noise Facility, Paper presented at the Sixty Ninth Meeting of the Acoustical Society of America

15. Edge, Phil M. Jr.; Mayes, William H.: Description of Langley Low Frequency Noise Facility and Study of Human Response to Noise Frequencies Below 50 CPS, NASA TN D-3204

16. Tomboulian, R: Research and Development of a Sonic Boom Simulation Device. (Prepared under Contract No. NAS 1-7985 by General Applied Science Laboratories, Inc. to be published)

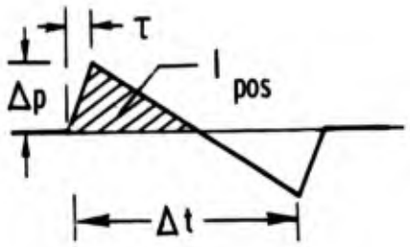

SIGNATURE VARIABLES IMPORTANT FOR:

COMMUNITY RESPONSE	STRUCTURAL RESPONSE
ΔP - OVERPRESSURE	ΔP - OVERPRESSURE
τ - RISE TIME	Δt - WAVE LENGTH
Δt - WAVE LENGTH	Ipos. IMPULSE FUNCTION
Ipos. IMPULSE FUNCTION	

FIGURE 1 - TRACING OF SONIC BOOM GROUND PRESSURE SIGNATURE

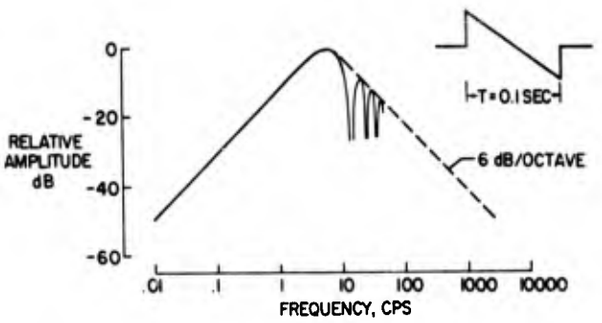

FIGURE 2 - CHARACTERISTIC FREQUENCY SPECTRA OF N-WAVES

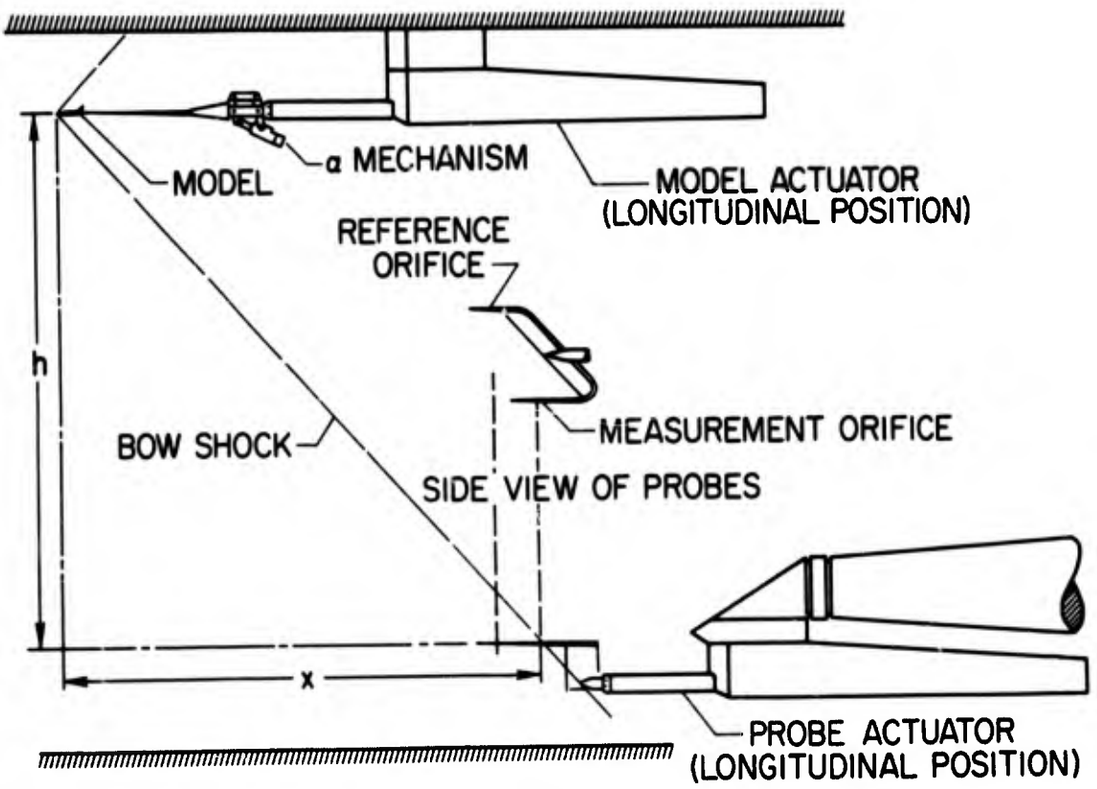

FIGURE 3 - NASA LANGLEY WIND-TUNNEL APPARATUS

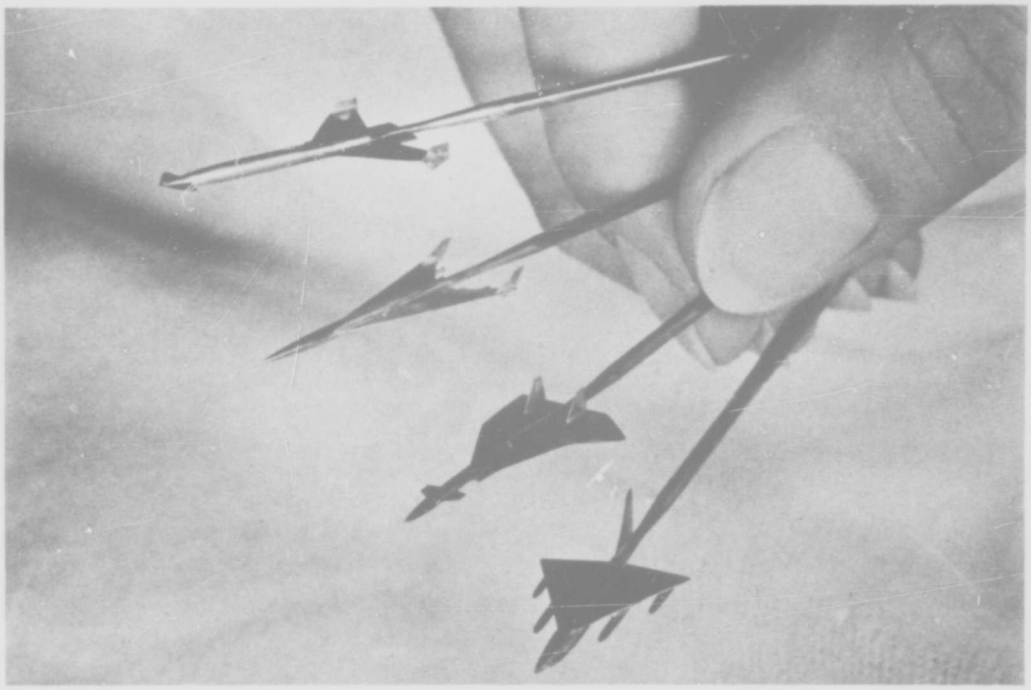

FIGURE 4 - TYPICAL NASA LANGLEY WIND TUNNEL MODELS FOR SONIC BOOM STUDIES

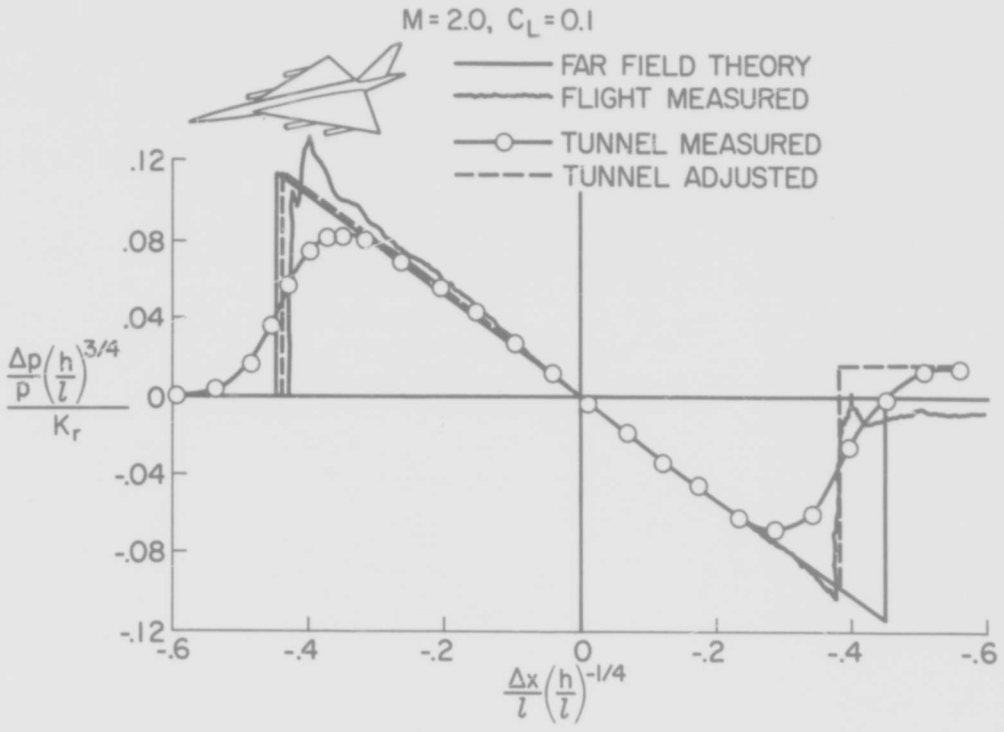

FIGURE 5 - CORRELATION OF NASA WIND-TUNNEL AND FLIGHT SIGNATURES

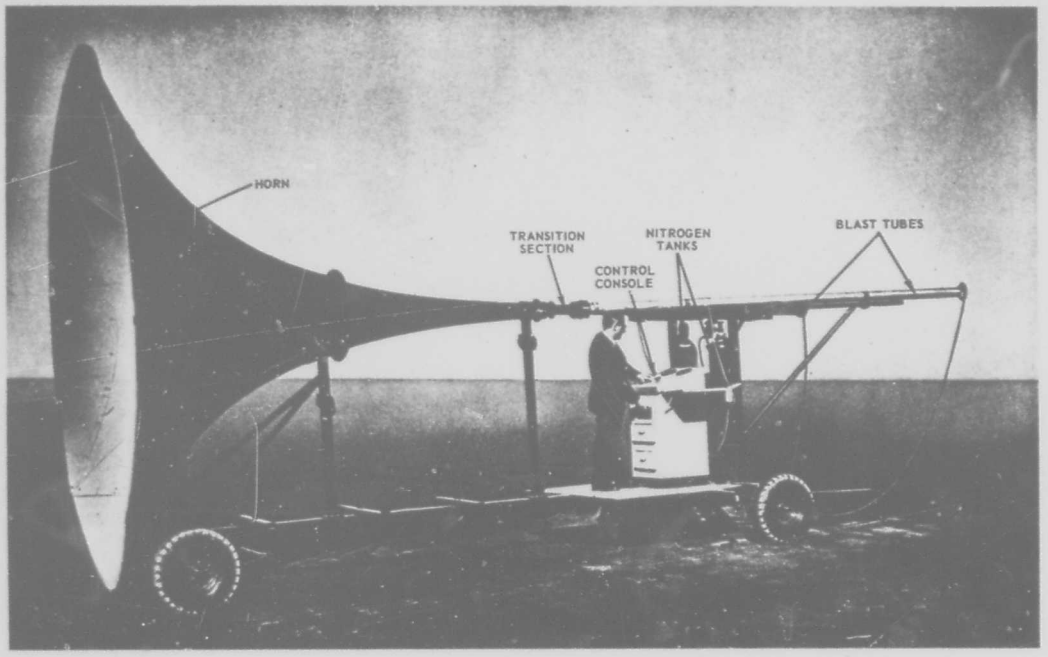

FIGURE 6 - LING TEMPCO VOUGHT SONIC BOOM SIMULATOR - SHOCK TUBE - BURSTING DIAPHGRAM

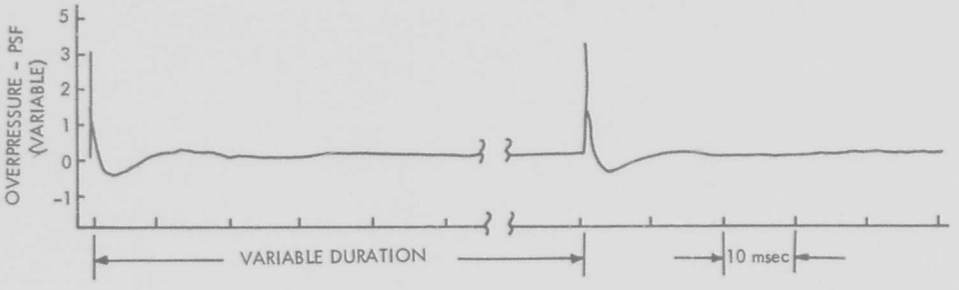

FIGURE 7 - PRESSURE SIGNATURES PRODUCED WITH THE LTV SONIC BOOM SIMULATOR

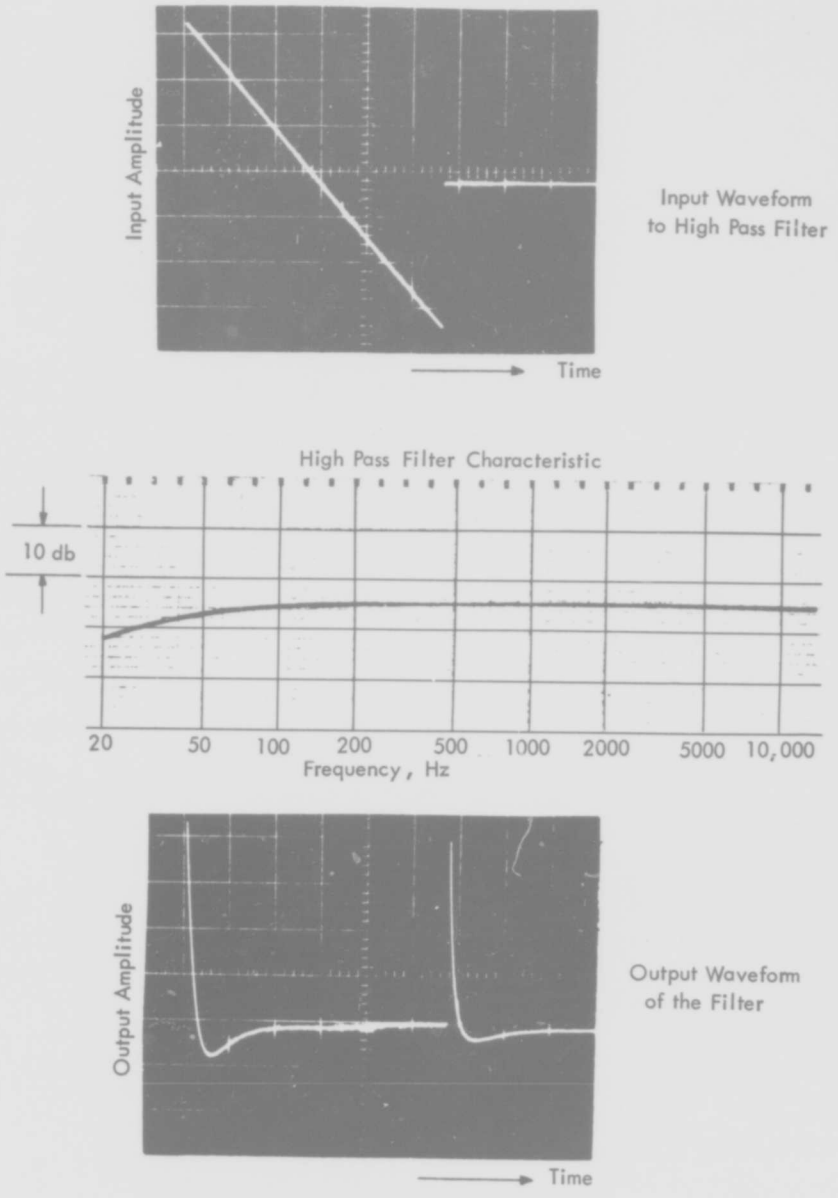

FIGURE 8 - LTV ANALOG STUDY - SUBJECTIVE SIMULATION OF SONIC BOOM PHENOMENA

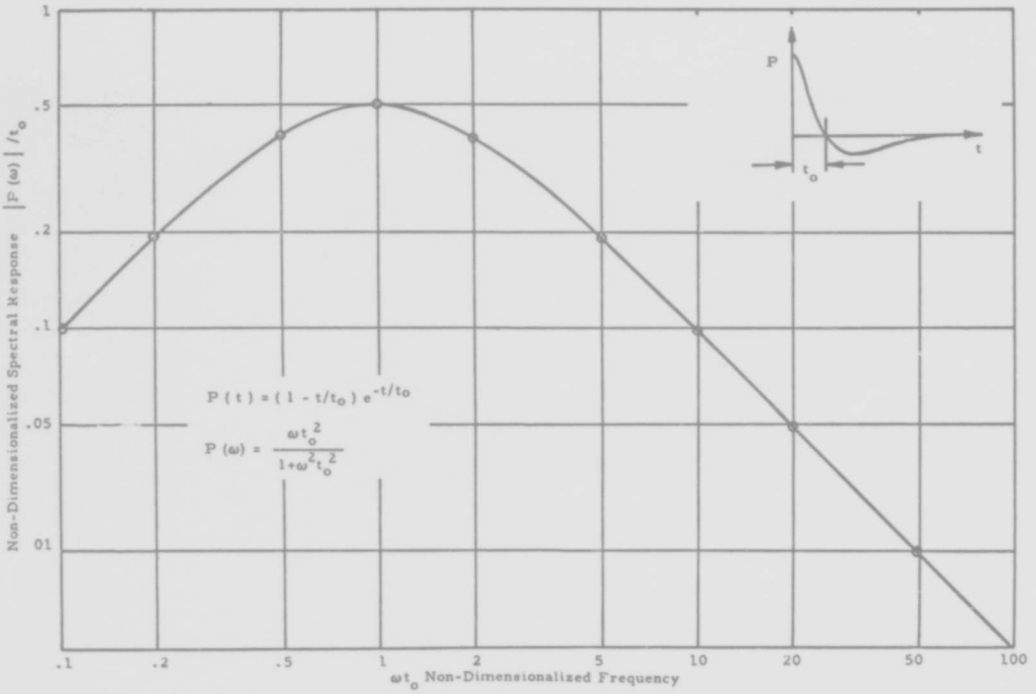

FIGURE 9 - SPECTRAL RESPONSE FOR AN EXPONENTIAL BLAST WAVE

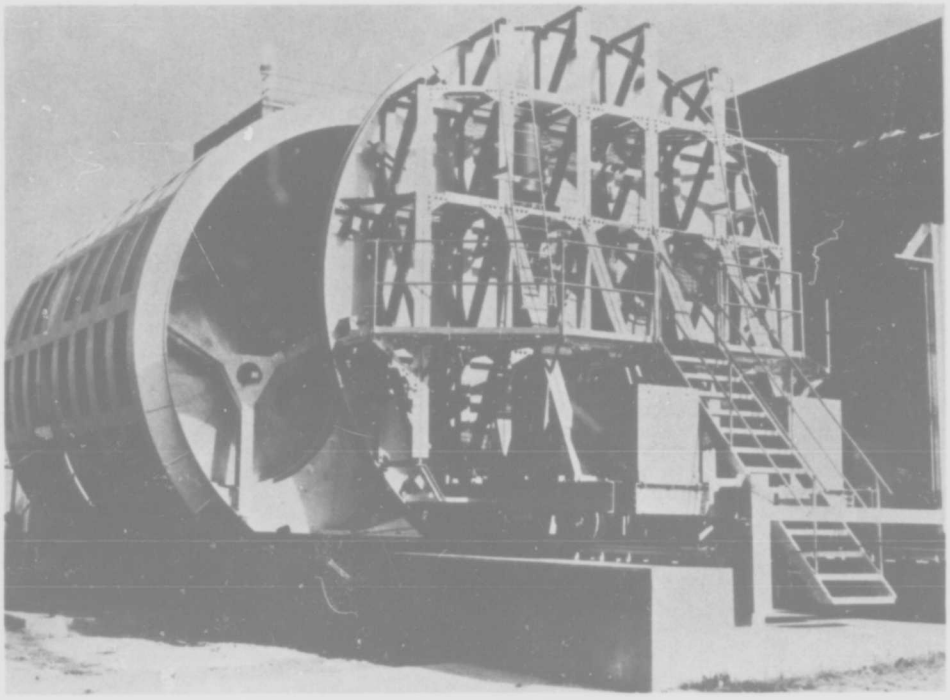

FIGURE 10 - NASA LANGLEY LOW FREQUENCY NOISE FACILITY - SONIC BOOM RESEARCH

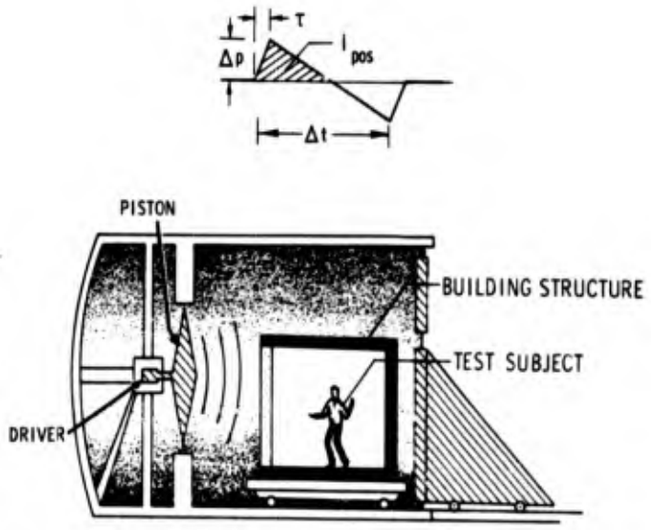

FIGURE 11- APPLICATION OF THE NASA LANGLEY LOW-FREQUENCY NOISE FACILITY TO THE PROBLEM OF SONIC-BOOM SIMULATION

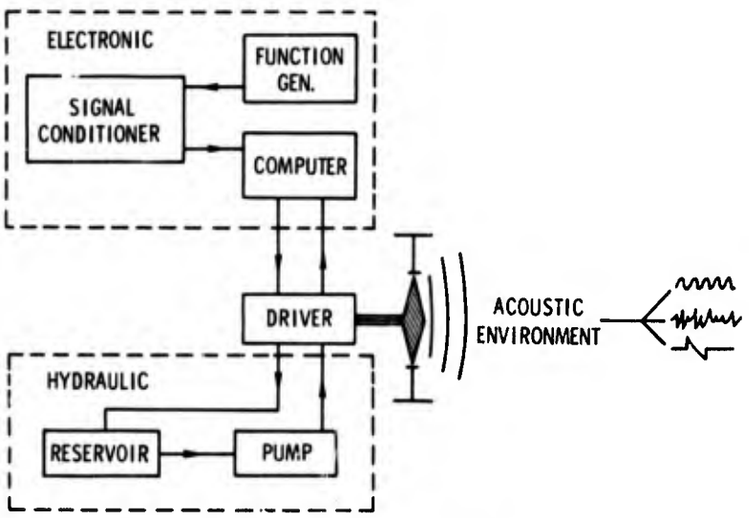

FIGURE 12- SCHEMATIC DIAGRAM OF THE ELECTROHYDRAULIC DRIVER SYSTEM FOR THE NASA LANGLEY LOW-FREQUENCY NOISE FACILITY

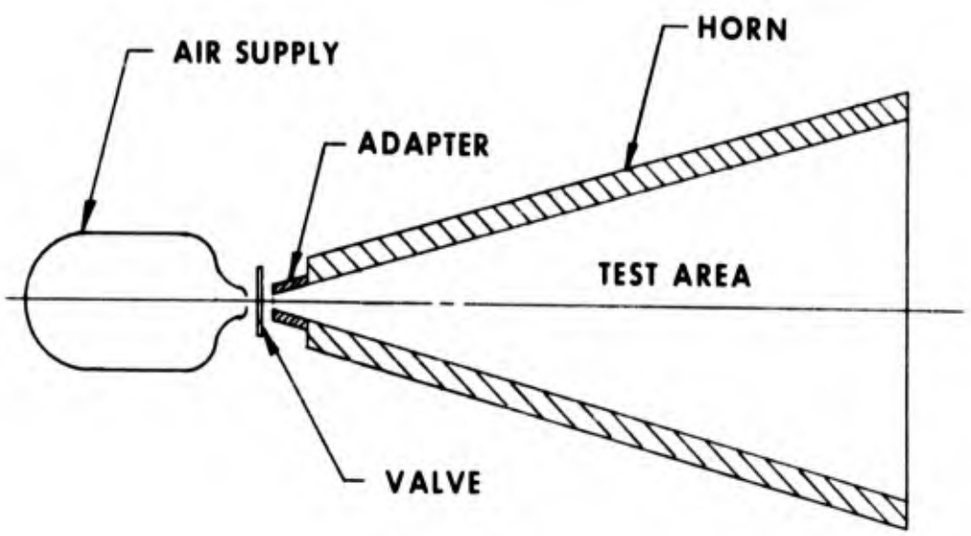

FIGURE 13- GENERAL APPLIED SCIENCE LABORATORIES PILOT (PROTOTYPE) SONIC BOOM SIMULATOR

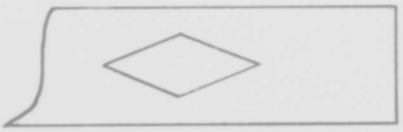

Square wave slide plate
for mass flow valve

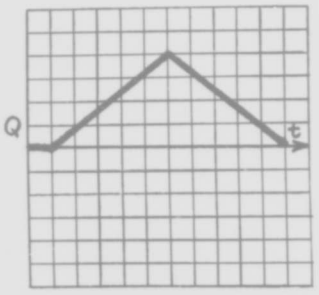

Mass Flow Q

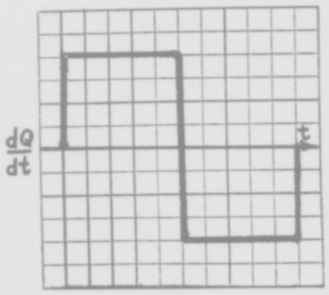

Rate of Change of Q

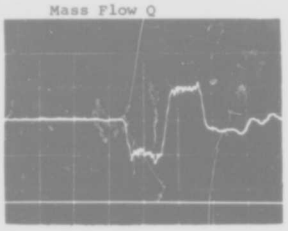

Trace for GASL prototype facility.

Sweep Speed: 1 millisecond per division

Amplitude corresponds to about 1 psf

FIGURE 14- SQUARE WAVE PLATE - [GASL PILOT (PROTOTYPE) SONIC BOOM SIMULATOR]

"N" wave slide plate
for mass flow valve

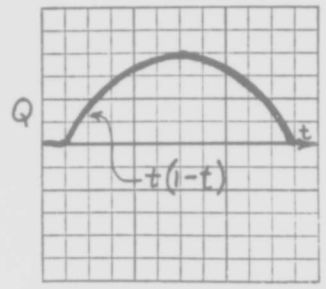

Mass Flow Q

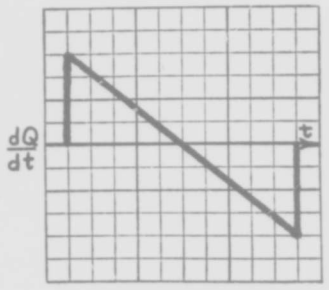

Rate of Change of Q

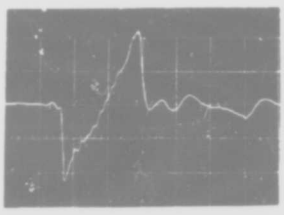

Trace from GASL prototype facility.

Sweep Speed: 1 millisecond per division

Amplitude corresponds to about 1 psf.

FIGURE 15- N-WAVE PLATE - [GASL PILOT (PROTOTYPE) SONIC BOOM SIMULATOR]

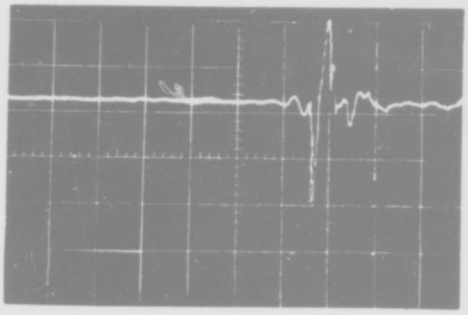

Sweep Speed:
1 millisecond
per division

FIGURE 16- FAST "N" WAVE PRODUCED IN THE GASL PROTOTYPE SONIC BOOM SIMULATOR. PEAK PRESSURES CORRESPOND TO ABOUT 10 psf.

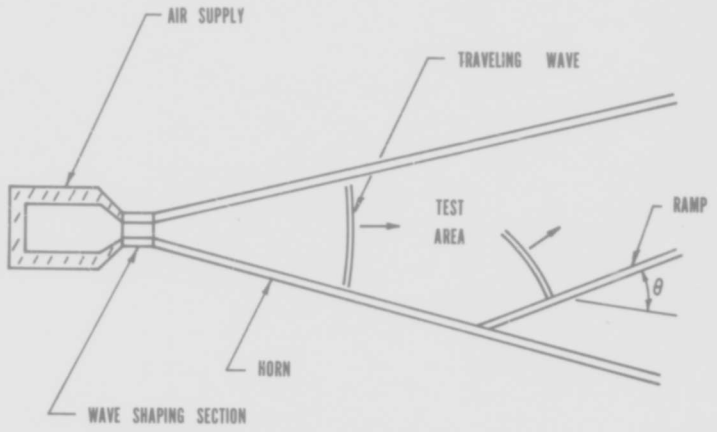

FIGURE 17- A SCHEMATIC OF THE GASL SONIC BOOM SIMULATOR FACILITY AND TEST AREA

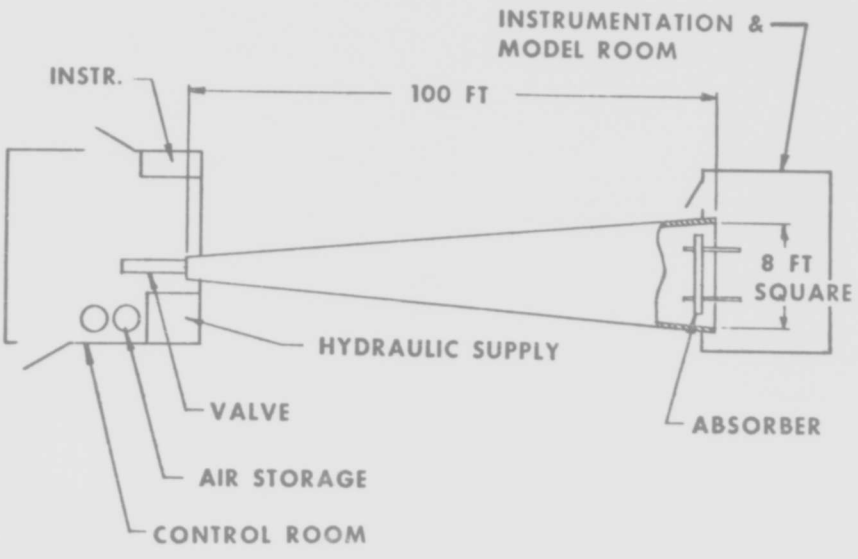

FIGURE 18- GASL/NASA SONIC BOOM TEST FACILITY LAYOUT SCHEMATIC

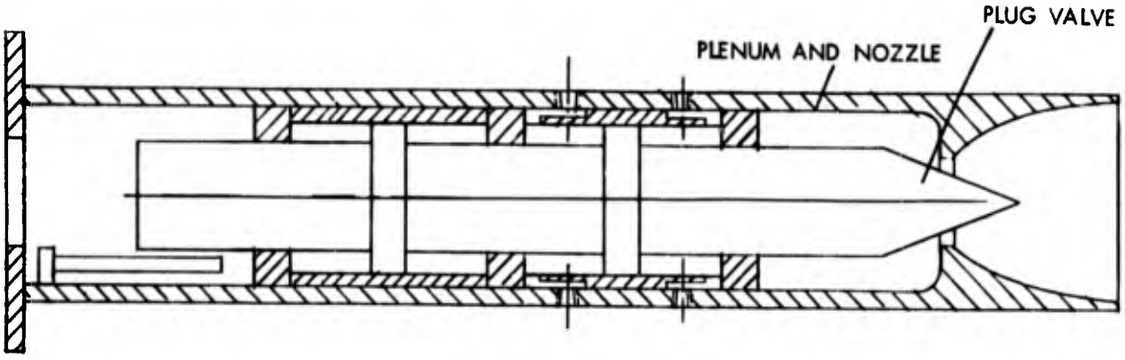

FIGURE 19- SCHEMATIC OF PLUG VALVE - GASL/NASA SONIC BOOM FACILITY

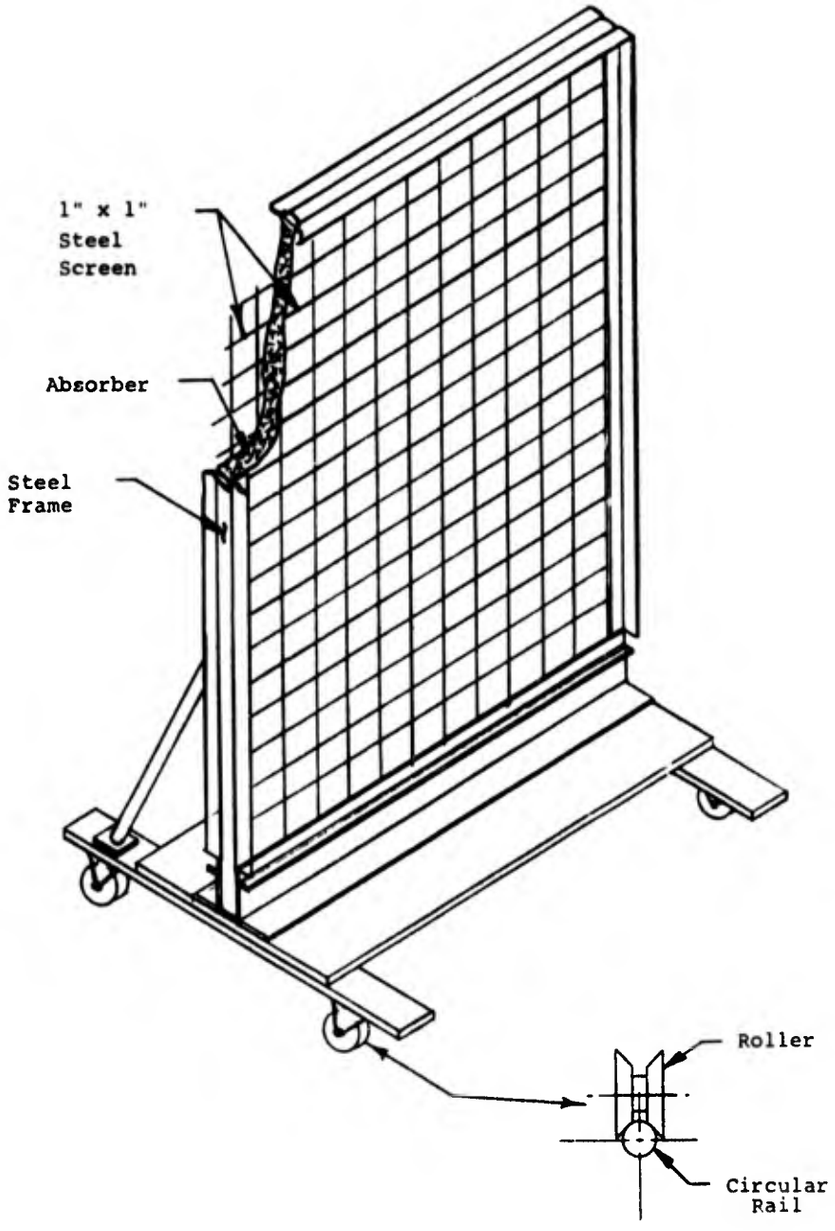

FIGURE 20- SCHEMATIC DRAWING OF MOVING ABSORBER - (GASL/NASA SONIC BOOM FACILITY)

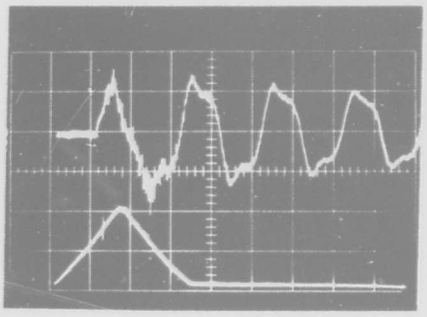

Without Absorber

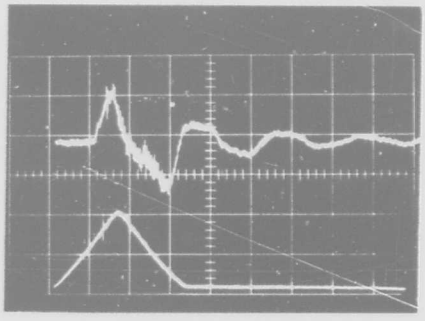

With Absorber

Each division equals 0.1 seconds. The moderate rise time is programmed by the mass flow control valve.

FIGURE 21 - DEMONSTRATION OF THE ABSORBER - (GASL/NASA SONIC BOOM FACILITY)

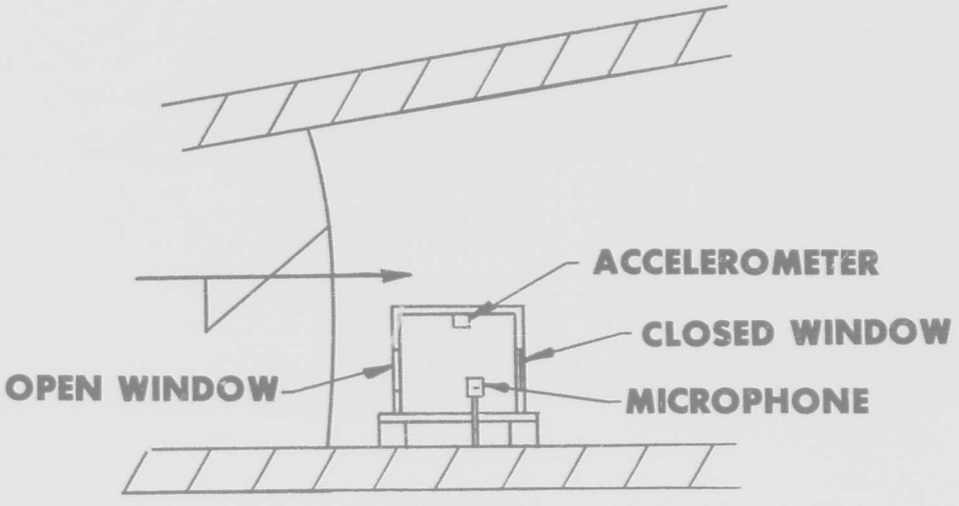

FIGURE 22 - MEASUREMENT OF DYNAMIC RESPONSE OF LARGE STRUCTURAL MODELS IN GASL/NASA SONIC BOOM FACILITY

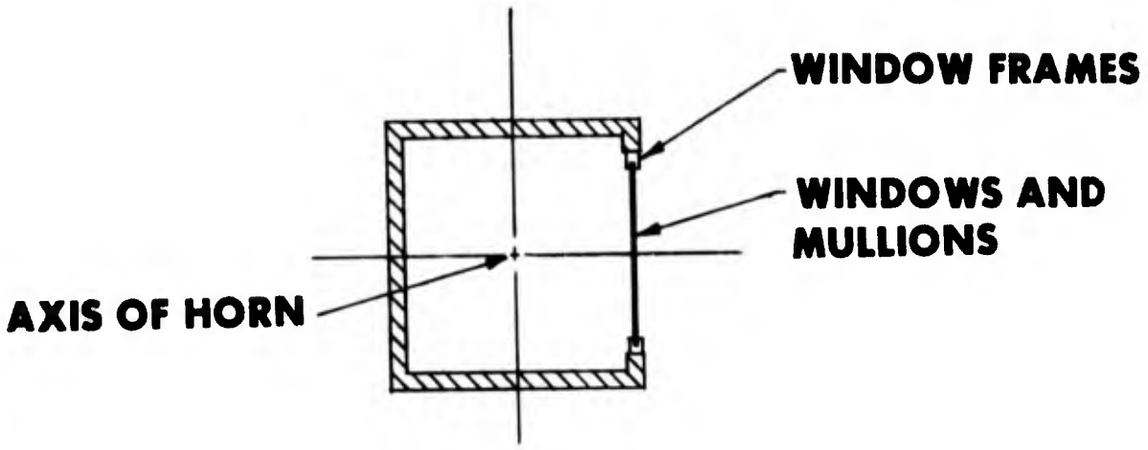

FIGURE 23 - TEST OF GLASS WINDOW CONSTRUCTION AND MATERIALS IN GASL/NASA SONIC BOOM

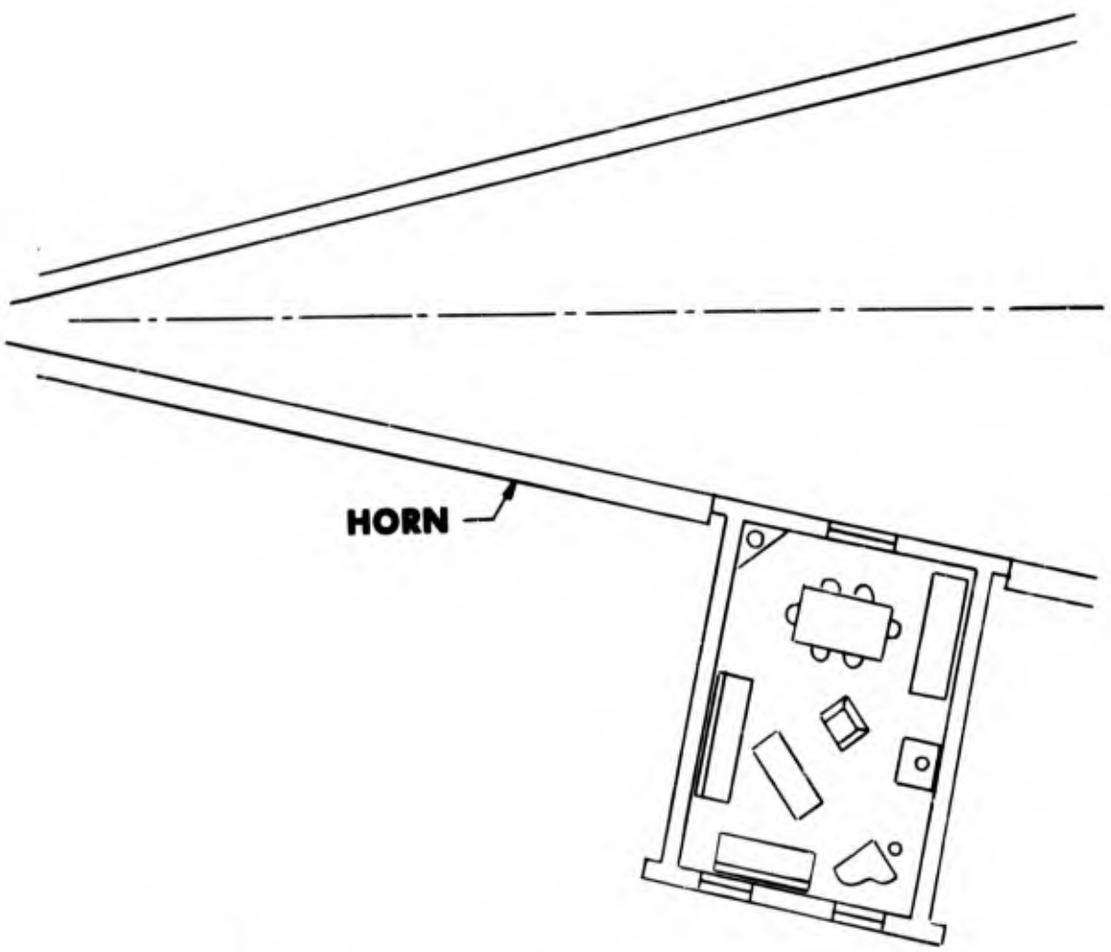

FIGURE 24 - PSYCHOACOUSTIC STUDIES IN GASL/NASA SONIC BOOM FACILITY

SONIC BOOM CONSIDERATIONS IN AIRCRAFT DESIGN

by Clarence S. Howell,[1] Armand Sigalla,[2]
and Edward J. Kane[3]
The Boeing Company

[1]Chief Engineer, Aerodynamics Technology Staff
[2]Assistant to Chief Engineer, Aerodynamics Technology Staff
[3]Aerodynamics Engineer, SST Aerodynamic Configuration Group

SUMMARY

Refined methods, based on modified linear aerodynamic theory, are available to calculate the detailed sonic boom characteristics of airplanes. The use of these methods has been justified through correlation with both wind tunnel and flight test data. The techniques for estimating sonic boom pressure signatures of an airplane are reviewed and the effects of different configuration variables are shown. In particular, configuration variables and novel concepts that could lead to potentially favorable sonic boom characteristics, such as low overpressure, long rise time, and noncoalescence of shocks, are examined. Numerical examples illustrate the magnitude for potential improvement in sonic boom and the resulting effects on other airplane performance parameters.

INTRODUCTION

One goal in design of supersonic airplanes is to minimize the objectionable aspects of sonic boom, within limits imposed by design and operational constraints. It is possible, through variations in configuration geometry, to develop airplanes with a wide diversity in their sonic boom characteristics. Unfortunately, only minimal guidance as to the undesirable features of sonic boom is provided by today's psychoacoustic knowledge. Furthermore, even though the designer might achieve an airplane with highly optimized sonic boom characteristics, the effects of atmospheric turbulence and/or transmission through the structure of a building (for indoor exposure) can mask the detailed features considered to be favorable. Thus, the advantages of design compromise for sonic boom reasons may well be nullified for the majority of those exposed to the boom. Aside from these considerations, it seems apparent that the less the overall pressure disturbances from ambient, the less the annoyance caused by sonic boom. For this reason, emphasis in most sonic boom work has been given to minimizing sonic boom overpressure (Refs. 30-1 to 30-4).

The purpose of this paper is to assess the known aerodynamic design methods for minimizing and modifying a sonic boom signature. The corresponding effects on aerodynamic efficiency (lift-drag ratio) are shown to illustrate the performance compromise for sonic boom. Mach number, altitude, and gross weight representative of a large supersonic commercial or military airplane during climb and acceleration are used for comparative purposes. Geometry typical of supersonic airplanes flying today is used as reference. To add perspective, it should be recalled that the magnitude of sonic boom also can be reduced by climbing and cruising at higher altitudes and through reductions in airplane gross weight made possible by improved propulsive and structural efficiency. The data in Figs. 30-1 and 30-2 illustrate the potential reductions through these means.

Figure 30-1, taken from Ref. 30-5, shows the wing area and engine size increases and resulting gross weight increases required to climb to altitudes higher than optimum for range in order to reduce sonic boom. Payload, range, and landing field length requirements were held constant for these data. It can be seen that sonic boom reductions greater than 15 to 20 percent are prohibitive.

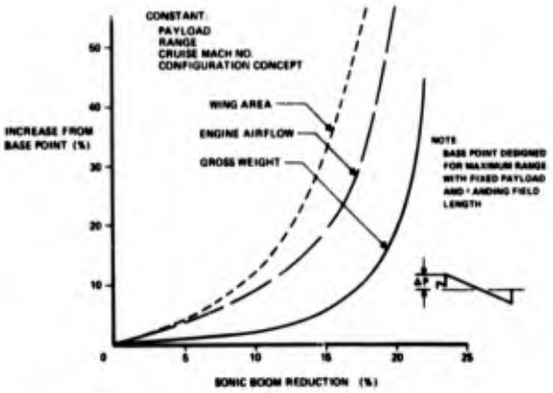

Fig. 30-1. Effect of Sonic Boom Overpressure on Airplane Design

The data in Fig. 30-2 illustrate the effect of gross weight on sonic boom. If it were to become possible, through future technology improvements in structures, propulsion, and aerodynamics, to reduce gross weight and decrease wing loading, relatively modest sonic boom reduction could be achieved.

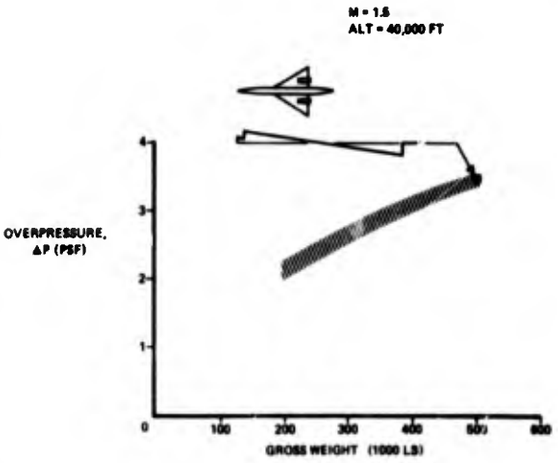

Fig. 30-2. Effect of Gross Weight

SONIC BOOM PRESSURE SIGNATURES

While a typical sonic boom pressure signature is an "N-wave" (shaped like the letter N), many variations are conceivable. Possible signatures shown in Fig. 30-3 are an asymptotic N-wave; signatures that include one or more intermediate shocks; and a signature with a finite rise time (i.e., without a fully developed front shock). These are the signatures one would expect to observe outdoors when the atmosphere is free of turbulence.

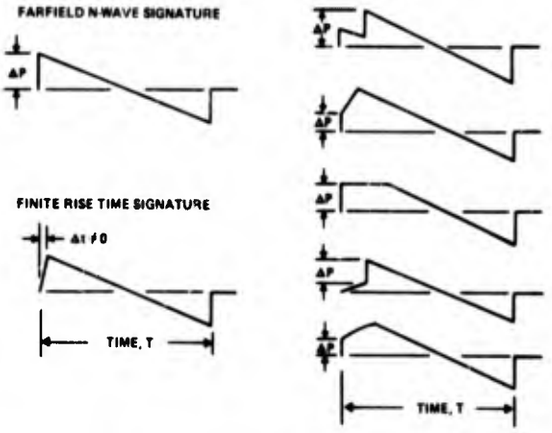

Fig. 30-3. Conceivable Pressure Signatures

As far as psychoacoustic reaction is concerned, there is no conclusive evidence that any of these is preferable to any other. Features, such as maximum pressure change, number of shock waves, or length of time between shock waves (especially for structural responses), may be significant. In general, it is known that rise times greater than about 10 milliseconds have a favorable effect, and it seems apparent that a sonic boom pressure signature with rise times greater than some value would be as imperceptible as the pressure field of a subsonic airplane. No supersonic airplane yet designed would produce such signatures.

EFFECT OF AIRPLANE LIFT AND VOLUME

It is convenient to separate the effects of airplane lift and volume when thinking about reduction of shock wave strength. The effect of lift is clearly related to the weight of the airplane,

and the effect of volume is related to its size and shape. Both effects have to be considered when calculating shock wave strength, but volume is dominant for low-altitude flight and lift for high-altitude flight (see Fig. 30-4).

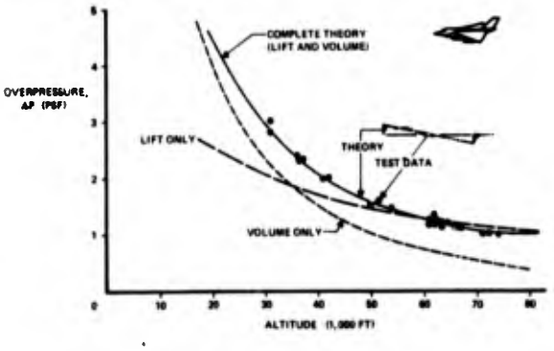

Fig. 30-4. Influence of Volume and Lift Contributions on Sonic Boom Overpressure

Lift and volume effects can be combined judiciously to minimize the total pressure jump, ΔP, when they are of the same order of magnitude. The characteristics of large supersonic airplanes are such that the sonic boom is lift dominated for most flight conditions.

WHITHAM'S SONIC BOOM THEORY

The sonic boom pressure signature of an airplane is calculated using Whitham's theory (Ref. 30-6). Each component of the airplane contributes to the signature (Fig. 30-5), and its contribution is determined from its area or (in the case of lift) equivalent-area distribution. Area, in this context, is in terms of the supersonic area rule of linearized aerodynamic theory. Each area distribution is related to a Whitham "F-function;" the pressure signature is obtained by analyzing superimposed F-functions. It is possible, in certain cases, to define airplane geometry, starting with a given signature. However, since the signature determined from an airplane's geometry is also a function of flight altitude, weight, and Mach number, this signature will be obtained for only one specific flight condition.

The development of a shock wave pattern is shown in Fig. 30-6. An example of the relationship of sonic boom pressure signatures to distributions of area is shown in Fig. 30-7. If it were to be established that one pressure signature is the most desirable, an effective area distribution could be found to produce that signature at some flight condition.

SONIC BOOM LOWER BOUNDS

It is possible to determine the least possible sonic boom for given airplane characteristics, such as lift, length, and volume, and given flight conditions. As shown in Fig. 30-8, a different lower bound results, according to the type of pressure signature that is assumed (Refs. 30-7, -8, and -9). The "airplane" for each lower bound pressure signature is defined in terms of F-functions and/or lift and area distributions, but there is no proof that a real airplane configuration can be found to correspond to the lower bound. The smallest lower-bound shock-wave strength in Fig. 30-8 is found by assuming a pressure signature that begins with a weak shock wave and continues with a very steep but not quite discontinuous pressure rise. The practical value of such an assumption has yet to be determined experimentally.

As noted before, for N-waves heard outdoors, annoyance is related to the time taken to reach the maximum overpressure, with finite rise times being less objectionable than discontinuous pressure changes (Ref. 30-10). It is possible, for a specific flight condition, to find a minimum-length airplane (including lift distribution) that will produce a pressure rise just short of discontinuous. The result of calculations, which are in accordance with the work of Ref. 30-11, is shown in Fig. 30-9 for the standard atmosphere; it can be seen that the airplane would have

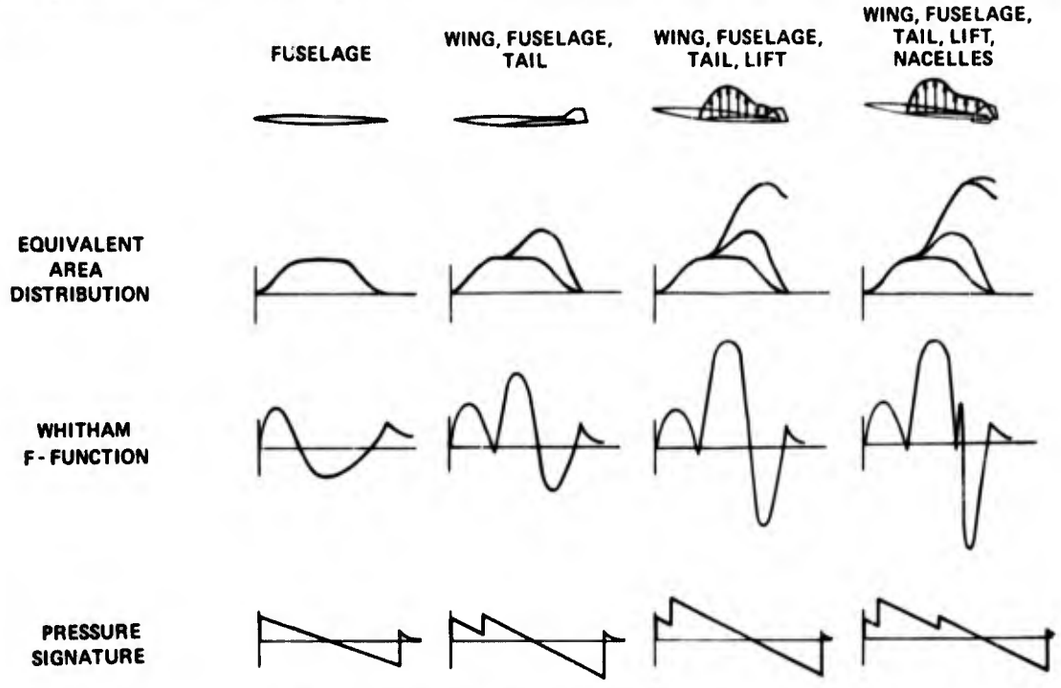

Fig. 30-5. Effect of Configuration Components on Pressure Signature

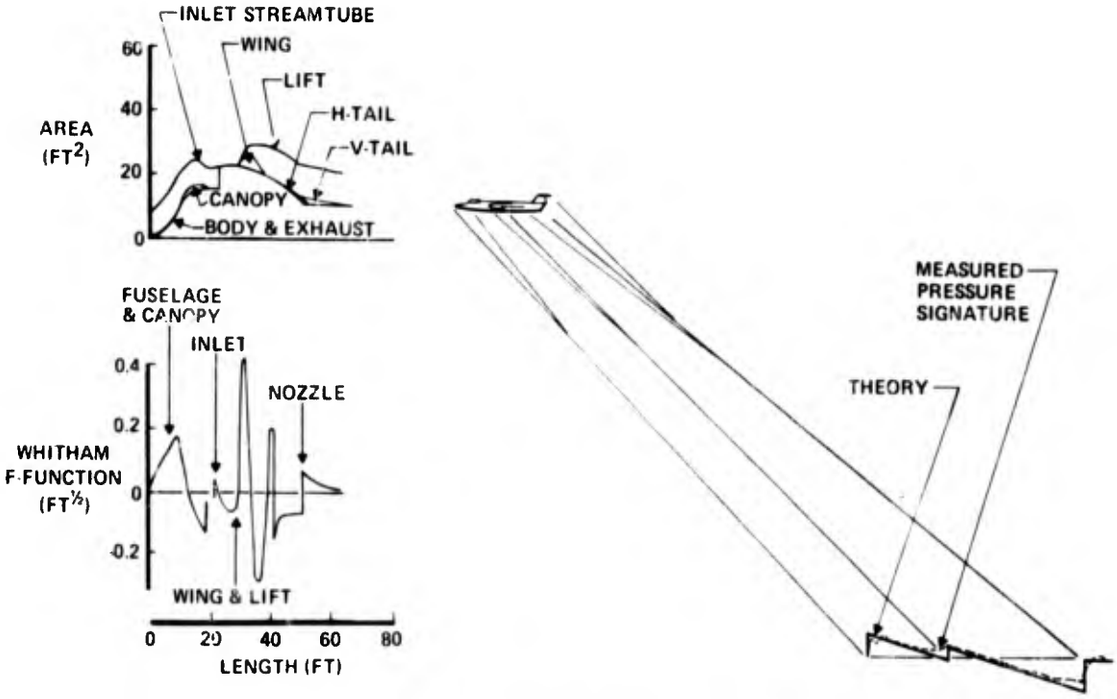

Fig. 30-6. Development of an Airplane's Sonic Boom Pressure Signature

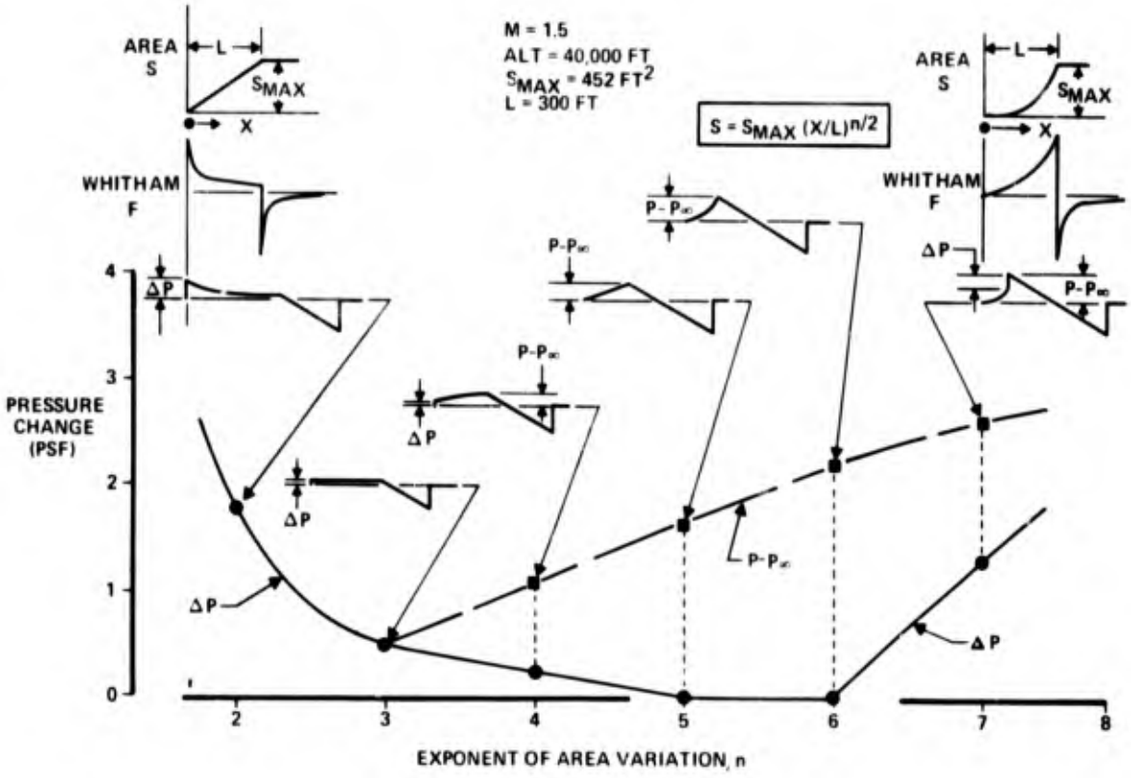

Fig. 30-7. Effect of Distribution of Area on Pressure Signature

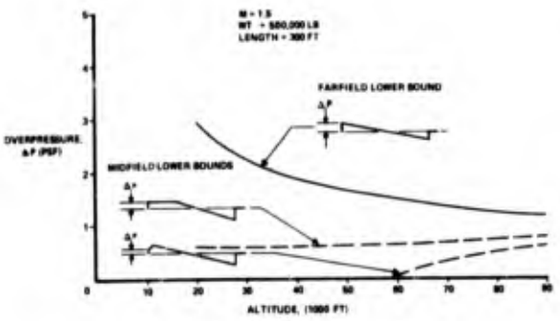

Fig. 30-8. Sonic Boom Lower Bounds

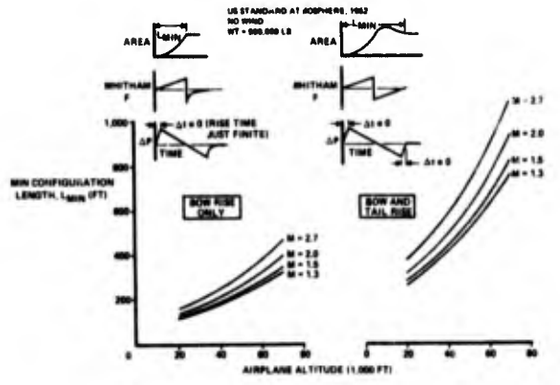

Fig. 30-9. Minimum Configuration Length for Finite Rise Time

to be very long indeed. To have a rise time of 10 milliseconds would require that the length be about 35 percent greater than that shown.

EFFECT OF CONFIGURATION MODIFICATIONS ON SONIC BOOM

WING

Since the sonic boom of heavy airplanes is lift dominated, it is natural to expect the wing to have a significant effect (Ref. 30-12). The influence of stretching the wing lift and volume distributions, holding span constant, is shown in Fig. 30-10. In this example, the maximum thickness of the wing was the same for all the planforms so that reduction of thickness ratio accompanied increased slenderness. It is seen that while the slenderness of the wing has a strong effect on sonic boom, it also has a significant effect on the maximum lift-drag ratio and structural weight of the airplane. Both reduced sonic boom and increased supersonic aerodynamic efficiency favor very slender planforms; in practice, slenderness is limited by structural weight and other design considerations.

The effects of variations of wing camber and twist are shown in Fig. 30-11. The effect on boom is much smaller than is the effect on airplane drag. For instance, concentrating most of the load at the trailing edge of the wing reduces the boom 9 percent in comparison to the flat wing, but increases the drag about 15 percent. A comparable result could be obtained by flying the airplane about 6,000 feet higher. Similarly, changes in wing dihedral have a small effect on sonic boom; small positive dihedral may reduce sonic boom a percent or so. It seems unlikely then that either camber and twist or dihedral would be determined by boom considerations.

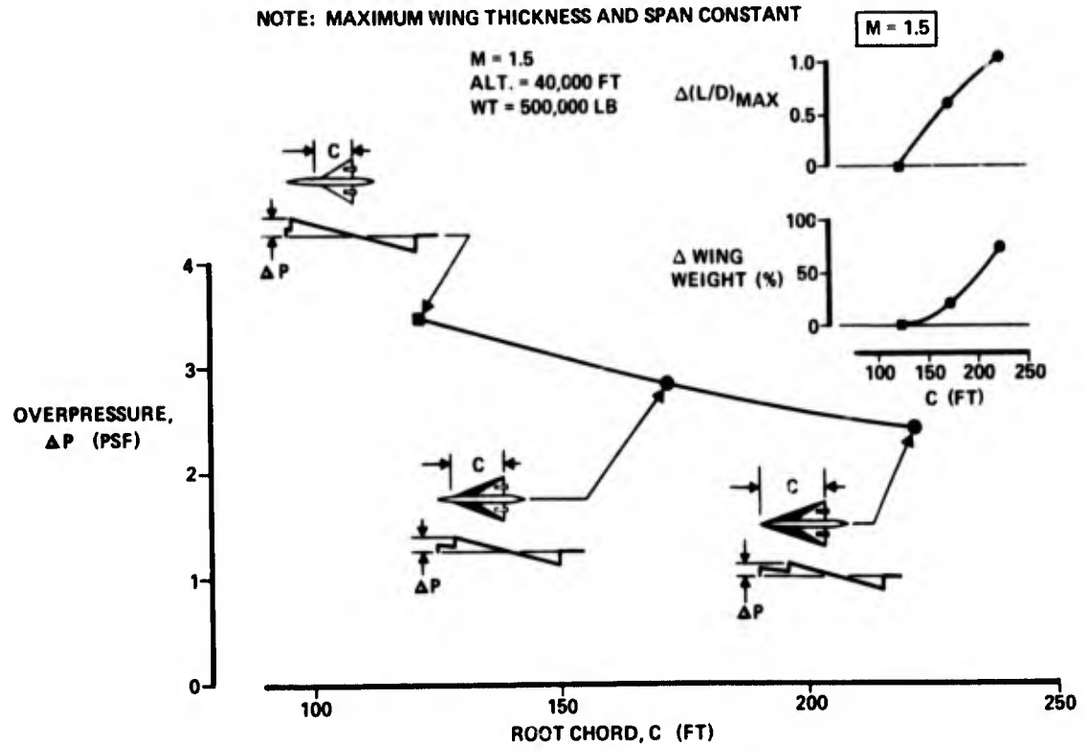

Fig. 30-10. Effect of Stretching Wing Lift and Volume

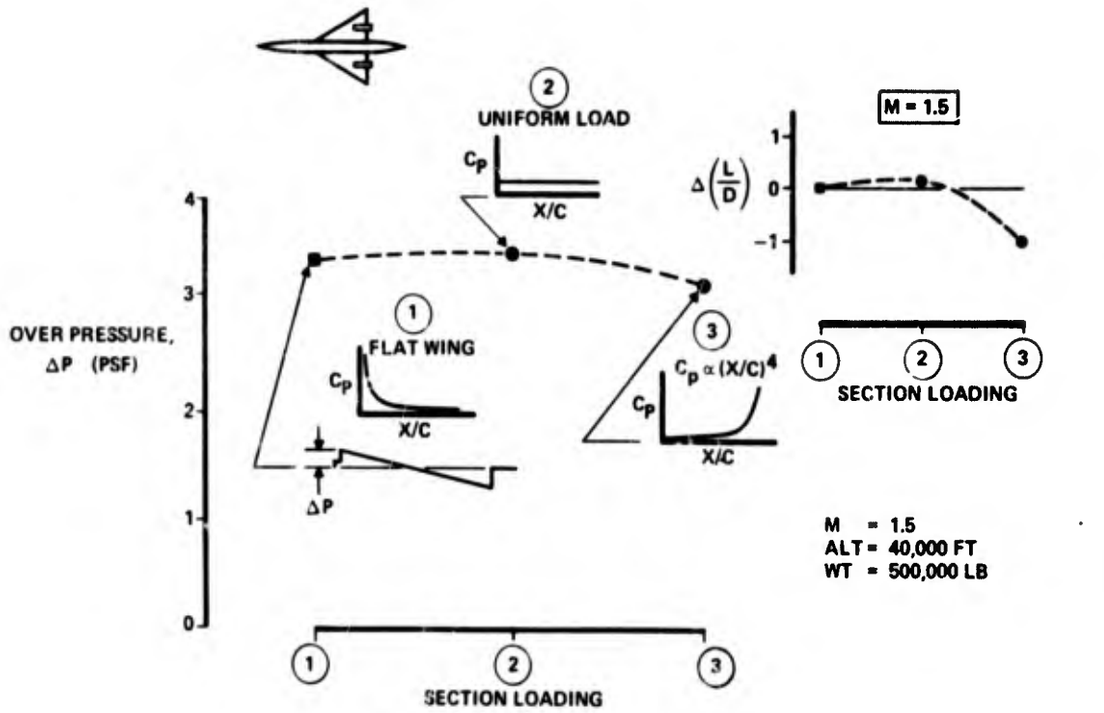

Fig. 30-11. Effect of Wing Camber and Twist

PROPULSION SYSTEM

The influence of the relative position of the propulsion system can be seen in Fig. 30-12 for an airplane with engines under the wing. If the engines are far enough aft, their shock wave is prevented from reinforcing that of the wing leading edge and that of the body. Aft engine location also has a favorable effect on the lift-drag ratio because of aerodynamic interference (Ref. 30-13); however, there is a best position. Overpressure diminishes continuously as the engines are moved back. Practical considerations suggest that the most rearward position of the engines be dictated by drag and structural feasibility rather than by sonic boom.

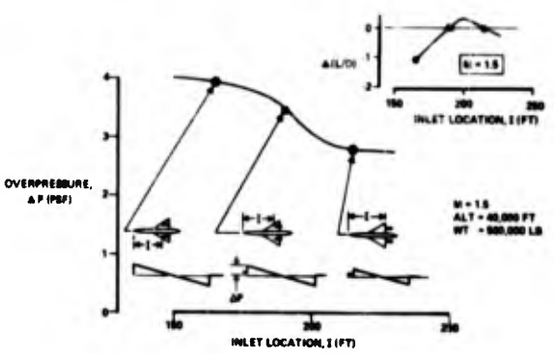

Fig. 30-12. Effect of Engine Location

The results shown in Fig. 30-12 were obtained assuming a nacelle shape characteristic of a modern airplane propulsion system. It is typical of these systems that the area of the engine intake is of about the same order of magnitude as the area of the nozzle, with the nozzle area somewhat greater. If a propulsion pod with a nozzle area considerably less than the intake area were possible, the effect on sonic boom would be beneficial because an expansion field would be created below the wing, tending to cancel the strong wing shock wave (Ref. 30-14). The results of detailed calculations are shown in Fig. 30-13. Starting with an intake area typical for the weight and size of the airplane considered, the nozzle area was reduced to zero. Obviously, this alone is not enough to have an important effect on sonic boom; the reduction obtained by complete elimination of the nozzle area is only about 4.5 percent. Further improvement can be achieved only by significant inlet area increases. The same 4.5 percent reduction could be obtained by flying 3,500 feet higher—with a drag increase of about 8 percent.

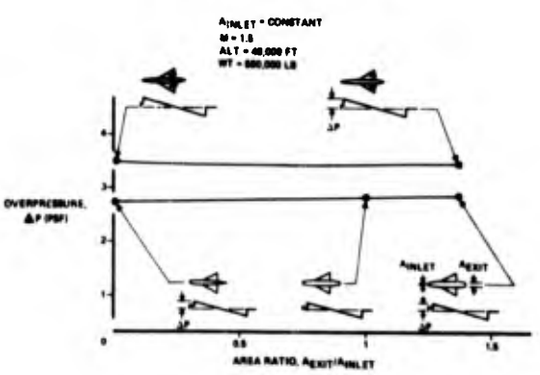

Fig. 30-13. Effect of Nozzle Area

Sonic boom can be reduced by thrust vectoring, as shown in Fig. 30-14. There is a reduction of shock wave strength because the wing is not required to produce as much lift, and for small angles there is a reduction of drag. However, excessive thrust deflection has an adverse effect on drag and also leads to complications in the design of the propulsion system. The rate of reduction of shock wave pressure with thrust angle at greater angles is much less than the rate of decrease of lift-drag ratio; it is, therefore, unlikely that thrust vectoring to reduce sonic boom would be allowed to compromise an airplane design.

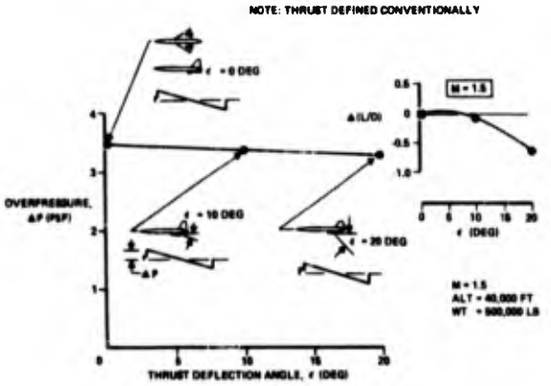

Fig. 30-14. Effect of Thrust Vectoring

FUSELAGE

Changes in the size of an airplane's fuselage affect the sonic boom pressure signature because expansion waves behind the nose decrease the strength of the wing shock wave. Where the effect of lift dominates, the influence of the fuselage in reducing the wing shock can be favorable (Fig. 30-15). To have any but a

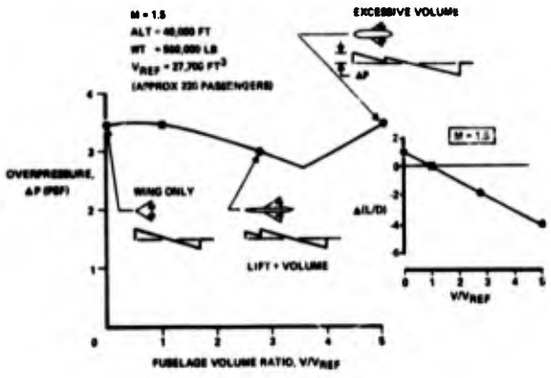

Fig. 30-15. Use of Volume to Reduce Boom

rather small effect, however, the volume of the fuselage has to be well in excess of that which is consistent with the basic size of the airplane and an efficient mission. To illustrate, consider the effect of doubling the fuselage volume, which, as shown, reduces the sonic boom by 7 percent at the expense of 18 percent increase in drag. This same reduction in boom could be achieved by flying 4,500 feet higher with a drag increase of only 12 percent. Nevertheless, fuselage shaping is important, and for a given capacity, the fuselage design can make a considerable reduction in drag without aggravating the sonic boom (Fig. 30-16). Lift on the fuselage forebody has a beneficial effect on

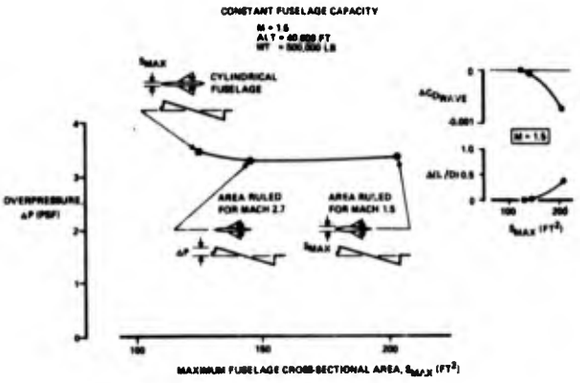

Fig. 30-16. Effect of Fuselage "Area-Ruling"

sonic boom, as shown in Fig. 30-17, but the amount of lift that a fuselage can carry efficiently is limited; forebody lift is merely a way of increasing the effective lifting length of the airplane.

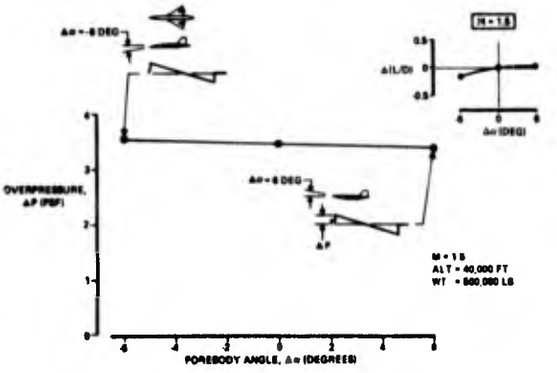

Fig. 30-17. Effect of Forebody Lift

It has been suggested (Ref. 30-15) that sonic boom pressure may be reduced by virtually lengthening the airplane through electrostatic fields or other electrical or magnetic phenomena. The effect of having a "phantom" forebody that does not carry lift has been examined, and the results are shown in Fig. 30-18.

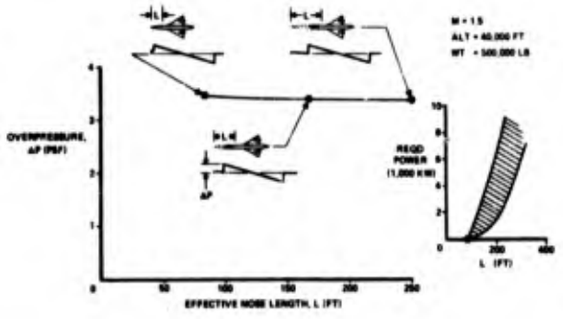

Fig. 30-18. Effect of "Phantom" Forebody

As can be seen, the change in sonic boom is negligible–about 2 percent despite an electrical power consumption equivalent to about 15 percent of the output of the airplane's engines. (See also Ref. 30-16.) The same reduction in overpressure could be obtained by flying 2,000 feet higher, at a cost of about 5 percent in drag.

CONCLUSION

It has been shown that aerodynamic design approaches are available to refine the sonic boom characteristics of an airplane. However, only relatively small changes in sonic boom are possible within the constraints imposed by requiring a useful, long-range, military or commercial mission. This is illustrated in Fig. 30-19, which shows the lower bounds from Fig. 30-8 together with the estimated level of sonic boom for airplanes flying today, the level that can be achieved for airplanes designed with today's technology, and the potential level sometime in the future following considerable technological improvement. For comparative purposes, these data have been normalized to the reference condition used throughout the paper.

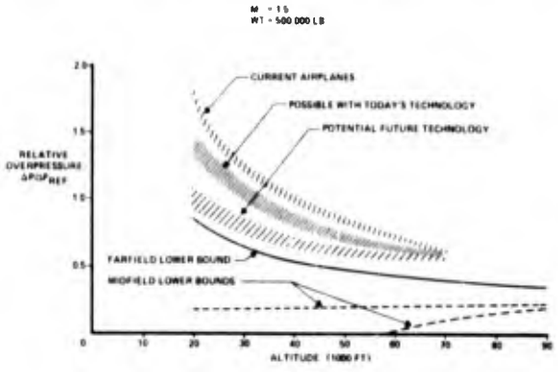

Fig. 30-19. Comparison of Sonic Boom Levels

Beyond the airplanes now built, improvement in sonic boom can result from careful attention to the lift distribution, area ruling of the fuselage, and location of the engines. By far the greatest configuration influences on sonic boom are wing planform and size, and it is through the wing that future improvement may occur, as paced by advances in structures and propulsion technology. The bound of projected future improvement shown in Fig. 30-19 is based on a considerable wing loading reduction from 60 to 45 pounds per square foot and an increase in wing slenderness causing a 40-percent increase in the streamwise length of the lift distribution. It may even be possible at some future time through wing design to eliminate sonic boom in the sense of eliminating objectionable rates of pressure change (including discrete shock waves); a lifting length about 10 times greater than that typical of today's airplanes would be necessary, which indeed does pose a challenge for future structural designers!

REFERENCES

30-1. H. W. Carlson, *The Lower Bound of Attainable Sonic Boom Overpressure and Design Methods of Approaching This Limit*, TN D-1494, NASA, October 1964

30-2. F. E. McLean, *Some Nonasymptotic Effects on the Sonic Boom of Large Airplanes*, TN D-2877, NASA, 1965

30-3. F. E. McLean, and B. L. Shrout, "Design Methods for Minimization of Sonic Boom Pressure Field Disturbances," *Journal of Acoustical Society of America*, Vol. 39, No. 5, Part 2, May 1966

30-4. F. E. McLean, *Configuration Design for Specified Pressure Signature Characteristics*, SP 180, NASA, May 1968

30-5. E. J. Kane and A. Sigalla, *Effect of Sonic Boom on Supersonic Transport Design and Performance*, D6-8614, The Boeing Company, February 1964

30-6. G. B. Whitham, "The Flow Pattern of a Supersonic Projectile," *Communications on Pure and Applied Mathematics*, Vol. V, pp. 301 to 348, 1952

30-7. L. B. Jones, "Lower Bounds for Sonic Bangs," *Journal Royal Aeronautical Society*, Vol. 65, No. 606, pp. 433 to 436, 1961

30-8. A. R. Seebass, "A Survey of Sonic Boom Theory," Annual Aviation and Space Division Conference, ASME, June 19, 1968

30-9. A. R. George, "Lower Bounds for Sonic Booms in the Midfield," (paper to be published in *AIAA Journal of Aircraft)*

30-10. E. E. Zepler and J. R. P. Harel, "The Loudness of Sonic Booms and Other Impulsive Sounds," *Journal of Sound and Vibration*, Vol. 2, No. 3, 1965

30-11. W. D. Hayes, *Geometric Acoustics and Wave Theory*, SP 180, NASA, May 1968

30-12. J. Morris, "An Investigation of Lifting Effects on the Intensity of Sonic Booms," *Journal Royal Aero. Soc.* Vol. 64, No. 598, 1960

30-13. A. Sigalla and T. H. Hallstaff, "Aerodynamics of Powerplant Installation on Supersonic Aircraft," *Journal of Aircraft*, Vol. 4, No. 4, July-August 1967

30-14. E. L. Resler Jr., *Reduction of Sonic Boom Attributed to Lift*, SP 180, NASA, May 1968

30-15. M. S. Cahn and G. M. Andrew, "Electro-Aerodynamics in Supersonic Flow," preprint 68-24, AIAA Sixth Annual Meeting, January 1968

30-16. S. Cheng and A. Goldberg, "An Analysis of the Possibility of Reduction of Sonic Boom by Electro-Aerodynamic Devices," preprint 69-38, AIAA Seventh Aerospace Sciences Meeting, January 1969

AN APPLICATION OF QUADRUPOLE THEORY TO CORRELATE THE DIRECTIVITY AND SPECTRA OF HIGH SPEED JET NOISE

J.D. VOCE
Rolls-Royce Limited (Bristol Engine Division)

P.A. LUSH
Institute of Sound and Vibration Research,
University of Southampton

SUMMARY

A considerable amount of experimental data has been obtained from model jets running at a wide range of velocities and temperatures at Rolls-Royce Limited (Bristol Engine Division). The purpose of this paper is to outline efforts being made to correlate this data, using Lighthill's quadrupole theory of jet noise generation with modifications due to Ffowcs Williams for high speed flow. The early part of this work showed that a theoretical model based on a distribution of randomly orientated quadrupole sources predicts the emission angle of peak intensity and the directivity of the radiation with reasonable success, but it does not predict the spectrum behaviour. Since it can be shown that the mixing region of a jet generates lateral quadrupoles with lobes aligned at 45° to the jet axis, a more complicated model can therefore be devised consisting of a distribution of lateral quadrupolessuperimposed upon the randomly orientated quadrupole distribution. This type of model can be used to improve the prediction of spectrum behaviour and also give a better prediction of the peak intensity emission angle. However, certain discrepancies cannot be explained in terms of this model and possible reasons for this are discussed and suggestions for improvements, currently being investigated, are given.

LIST OF SYMBOLS

c_α	speed of sound under ambient conditions
D	nozzle exit diameter
e	anisotropy factor ℓ_2/ℓ_1
F	modified Doppler factor $\left[(1-M_c\cos\theta)^2+\alpha_1^2 M_c^2(\cos^2\theta+e^2\sin^2\theta)\right]^{1/2}$
f	frequency of observed sound
$H(\omega)$	power spectral density of turbulence fluctuations, $\rho u'u'$
$K(\omega)$	power spectral density of turbulence fluctuations, $p'+\rho u'u'$
ℓ	isotropic integral length scale of turbulence
ℓ_1, ℓ_2	integral length scales in longitudinal and lateral directions respectively
M_c	acoustic Mach number of convection velocity $= V_c/c_\alpha$
M_J	acoustic Mach number of jet velocity, $= V_J/c_\alpha$
Q	ratio of strengths of lateral to random quadrupoles in directivity factor
Q'	ratio of strengths of lateral to random quadrupoles in frequency spectrum factor
p, p'	pressure and pressure fluctuation
U_i, U	mean velocity components
u_i', u'	fluctuating velocity components
V_c	convection velocity of eddies in jet
V_J	fully expanded jet velocity
$W(f)$	power spectral density of observed sound
x_i	space co-ordinate
α	ratio of turbulence frequency in moving frame attached to eddy to that in fixed frame, $\omega_0\ell/V_c$
α_1	similar to α but for anisotropic eddies, $\omega_0\ell_1/V_c$
θ	angle between direction of emission and jet axis in downstream direction
θ_{peak}	emission angle of peak intensity
ρ	fluid density
ω	radian frequency of turbulence as measured in moving reference frame
ω_0	typical radian frequency of turbulence as measured in moving reference frame, equivalent to the inverse of the integral time scale of the moving frame autocorrelation.

IN ORDER TO PREDICT THE NOISE RADIATION FROM JET ENGINES, Rolls-Royce (Bristol Engine Division) has carried out a comprehensive series of measurements of the acoustic radiation from model jets. The correlation of this data is desirable so that a universal prediction method can be devised and reliable extrapolations can be made. This paper reports attempts to correlate the experimental data using Lighthill's theory of jet noise generation by acoustic quadrupoles. Since the data involved high speed jets, it was necessary to use the extensions of this theory due to Ffowcs Williams, which allow for the supersonic convection of turbulence. The paper considers the directivity of the intensity and the frequency spectra of the jet noise but it does not attempt to predict the absolute levels of the sound radiation. The directivity factor derived from the theory is compared with the measured field shapes, and, in the case of spectra, the theory is used to derive correlation parameters to collapse the measured spectra on to a general curve.

In the simplest form of the high speed theory, the noise is radiated from a distribution of randomly oriented quadrupoles and the directivity is due entirely to convection of the quadrupoles. When this theory is applied to the experimental data, it is found that the directivity is predicted fairly well, especially near the peak intensity but the angle of peak emission is not estimated well over the whole speed range. In correlating the spectra, it is necessary to correct the observed frequency with a modified Doppler factor, based on the eddy convection velocity and including a term which accounts for the radiated wavelength being comparable with the eddy size. When this is done the observed frequency is converted into the frequency of the turbulence as viewed in a reference frame attached to the eddy. It is found that the spectra can be correlated for different jet velocities and temperatures but only if a separate correlation is made at each emission angle. It was noticed that there appeared to be two basic spectra with peak frequencies separated by about three octaves.

This can be satisfactorily explained by reverting to Lighthill's original model for jet noise. He showed that the shear region of the jet would radiate predominantly a lateral quadrupole orientated at 45° to the jet axis. A more complex model can now be devised by combining these lateral quadrupoles with the distribution of randomly orientated quadrupoles. It can be shown that this model has two separate spectra and a considerable improvement can now be made in collapsing the spectra on to a single curve which is independent of the emission angle. In addition the angle of peak noise emission is predicted better especially at the lower jet velocities.

THE JET NOISE EXPERIMENTAL DATA. Measurements of the acoustic output from model jet nozzles have been obtained by Rolls-Royce (Bristol Engine Division) from their jet noise facility (see Fig. 1). The rig, which is mounted in an anechoic test chamber, is mounted freely on an air bearing. During running, thrust can be measured by the air pressure required on a thrust capsule to bring the rig back to a null position. Primary and secondary air supply pressures, which can be varied independantly up to 100 p.s.i. absolute, are obtained from an external compressor facility. The normal air delivery temperature to the rig is about 300°K, but by the use of a combustion chamber the primary nozzle temperature can be continuously varied between 450 and 1250°K. The primary flow exhausts through a 3 in. diameter conical convergent nozzle at fully expanded Mach numbers up to about 1.8 and at fully expanded jet velocities up to about 3000 ft/sec.. The measuring apparatus is standard B & K microphones and spectral analysers and the measurements are recorded on magnetic tape for later analysis. The microphones are traversed on a 10 ft. radius (40 nozzle diameters) centred on the jet exit between angles of 15° and 105° to the jet axis.

A typical set of data consists of 1/3 octave S.P.L. at angular increments of 7½° between 15° and 105° to the jet axis, and at a particular pressure ratio and total temperature. The whole set consists of runs at about ten separate pressure ratios between about 1.5 and 6.0, each carried out at four separate jet total temperatures between 288°K and 1250°K.

THE THEORETICAL MODEL USED

SUMMARY OF JET NOISE THEORY. The theory of aerodynamically generated sound, as initiated by Lighthill (1), consists essentially of rewriting the equations of fluid motion in the form of a wave equation for fluid density with all the residual terms collected together as a source term. In physical terms, the flow in which the sound is generated is replaced by fluid at rest acted on by an externally applied stress system. The source term represents the difference between the usual stresses in the fluid due to pressure, viscosity and momentum flux and the stress consisting of sound pressure fluctuations, which would exist in the fluid at rest. The stresses of the source term are acoustically equivalent to a distribution of quadrupole sources radiating into a uniform fluid at rest.

Assuming that the source term given by the stresses is known, then the wave equation can be solved and an expression for the density fluctuations in the far field can be obtained. Since fluid velocities in high speed jets are of the same order as the speed of sound, a full allowance for the effect of retarded times must be made. This solution was first obtained by Ffowcs Williams (2).

The stress system of the source term is in practice not known but some progress can be made if viscous stresses and temperature differences are neglected. The residual term, which is the momentum flux, has recently been analysed by Jones (3). It may be separated into two parts, one of which is a quadrupole source and the other is a higher order source, i.e. octupole. Since the octupole source is less efficient than the quadrupole then it is negligible at least at convection velocities lower than the velocity of sound. The quadrupole source may also be split into several parts when the velocities are written as the sum of a mean and a fluctuating part. The two most important sources are the self noise term, which is a turbulence-turbulence contribution and the shear noise term; which is a turbulence-mean shear contribution.

The above theory has been fully worked out and now requires detailed checking using experimental data from high speed jets.

PHYSICAL DESCRIPTION OF THE THEORETICAL MODEL. It has been established that jet flows consist of turbulent eddies or correlation volumes which are convected downstream at some speed less than the centreline jet velocity. An eddy may be regarded as radiating sound like a quadrupole source and since it is convected, some modification to the directional pattern of the radiation will occur. If the turbulent velocity fluctuations within a particular eddy are regarded as isotropic and if the eddy is not in a region of large velocity gradients, the eddy will contribute to the self noise and the associated quadrupole will have a random orientation. A distribution of such eddies will produce a spherical directivity pattern. If the eddy is in a region of a large velocity gradient, such as the mixing region of a jet, then it contributes to the shear noise and radiates as an orientated quadrupole. An eddy in the mixing region of a jet produces a lateral quadrupole oriented at 45^0 to the jet axis. Since all the eddies in a given region are affected in the same way, the directivity of a distribution of such sources will be the same as one source. Since these sources are being convected there will be some distortion of the basic quadrupole field shapes. Mathematically this distortion is given by some power of the Doppler factor for a moving source. Since the random and lateral quadrupoles each involve a different number of time differentiations, the power of the Doppler factor is different in each case, being 5 for the random quadrupole and 3 for the lateral quadrupole. The Doppler factor itself must be modified when the source is convected at speeds near that of sound. Since the motion of the source reduces the wavelength of sound radiated in the direction of motion it becomes comparable with the source size near sonic speeds. The correction takes the form of an extra term which avoids the singularity that would otherwise occur. This term arises naturally if full account is taken of the retarded time in the theory.

This paper reports some attempts to correlate jet noise directivity and spectra at first on the assumption that the radiation is due entirely to a distribution of random quadrupoles. When this model was found to be inadequate, especially in attempting to correlate spectra, the directivity and spectra of the radiation from a combination of random quadrupoles and lateral quadrupoles were investigated and compared with the experimental data.

THE DIRECTIVITY OF JET NOISE

THE THEORETICAL DIRECTIVITY. Expressions for the directivities of both randomly oriented quadrupoles and lateral quadrupoles oriented at 45^0 to the jet axis can be obtained from the theory. The directivity of the intensity of sound radiated from randomly orientated quadrupoles is derived entirely from the distortion of the spherical field shape caused by source convection. For the low speed theory, where convection Mach numbers are less than unity, the directivity factor is $(1-M_c \cos\theta)^{-5}$ where M_c is the eddy convection velocity divided by the speed of sound in the radiation field and θ is the angle between the jet axis and the direction of emission. For high speed convection this factor becomes

$$\left[(1-M_c\cos\theta)^2 + \alpha_1^2 M_c^2 (\cos^2\theta + e^2 \sin^2\theta) \right]^{-5/2}$$

where α_1 and e are turbulence parameters given by $\alpha_1 = \omega_e \ell_1 / V_c$ and $e = \ell_2/\ell_1$. In these equations, ω_e is the inverse of the integral time scale in the moving frame of reference attached to an eddy, ℓ_1 and ℓ_2 are the integral length scales in the longitudinal and lateral directions respectively and V_c is the convection velocity. Physically α_1 may be interpreted as the ratio of the time taken by the eddy to pass a fixed point in the fluid to the decay time of the eddy and e is the anisotropy factor.

The directivity factor for a lateral quadrupole orientated at 45^0 to the jet axis is given by $4\cos^2\theta \sin^2\theta$ and for low speed convection this factor must be modified to $4\cos^2\theta\sin^2\theta/(1-M_c\cos\theta)^3$. The different power of the factor $(1-M_c\cos\theta)$ in this case is due to the different time dependence of the shear noise source term. For high speed convection, the directivity becomes $4\cos^2\theta\sin^2\theta/[(1-M_c\cos\theta)^2 + \alpha_1^2 M_c^2 (\cos^2\theta + e^2\sin^2\theta)]^{5/2}$

The overall directivity of a model combining the two types of quadrupole is obtained by adding together the separate expressions for the directivities. The overall directivity is therefore $1/F^5 + Q\sin^2 2\theta/F^3$ where $F = [(1-Mc\cos\theta)^2 + \alpha_1^2 Mc^2(\cos^2\theta + e^2\sin^2\theta)]^{1/2}$ and Q is the ratio of the strength of the lateral to the random quadrupole distributions. The theoretical directivity can now be calculated provided values of the turbulence parameters α_1 and e, the relationship between the convection velocity and jet velocity, and the ratio of the strengths of the two types of quadrupole are all known. In practice none of these quantities is known precisely, but for subsonic jets the approximate values have been found to be $\alpha_1 = 0.2 - 0.4$ and $e = 0.3$ and the convection velocity is about $0.65\ V_J$ (4). When the original calculations for this theory were done, the value of α_1 for supersonic flow was thought to be a little higher at 0.6 and the convection velocity a little lower at about $0.5\ V_J$

COMPARISON OF THEORY WITH EXPERIMENTAL DATA. For a quick assessment of the theoretical model, it is sufficient to compare the theoretical and experimental variations of the emission angle of peak intensity with jet velocity. If the random quadrupole alone is considered it can be shown that the peak emission angle is given by $\cos^{-1}\ 1/Mc\,[1+(1-e^2)\alpha_1^2]$. From this expression it can be seen that the peak lies along the jet axis for sufficiently low jet velocities. When the jet velocity rises above about 1.5 times the speed of sound, C_∞, the peak swings away from the axis. This behaviour is not very similar to the experimental data but a good fit can be obtained between jet velocities of 1.3 C_∞ and 2.4 C_∞ if the convection velocity V_c is assumed to vary as $V_c = aC_\infty + bV_J$ instead of being a constant fraction of V_J, where suitable values of a and b are .37 and .29 respectively (see Fig. 2).

However the addition of the lateral quadrupole considerably improves the prediction of peak emission angle in the low speed range, although an overestimation still occurs at the high speed end. It was found that the value of Q, the ratio of the strengths of the lateral to the random quadrupole, had a significant effect on the result and the best fit was obtained with $Q = 2$ (see Fig. 3). Above jet velocities of about 2 C_∞ the experimental variation of the peak angle flattens off and becomes approximately constant at about 45°. This effect could again be achieved by decreasing the ratio V_c/V_J.

If the whole directivity is now considered, it is found that the overall shape of the random quadrupoles is very similar to that of the combination of two types of quadrupole in the directions between 0 and 90°. However between 90° and 180°, it is quite different since secondary peaks appear in the latter case. Comparing the experimental data with the theoretical predictions obtained from the model with two types of quadrupole (see Fig. 4), it can be seen that the general fit near the peak is quite good, once the peaks have been correctly predicted. However errors can be seen at angles to the jet axis, below about 30° for the lower jet velocities and at angles above about 60° for the higher jet velocities.

Improvements in the fit at these points could possibly be made by suitably adjusting the various parameters α_1, V_c/V_J and Q and in addition it may be necessary to introduce the variation of some or all of these parameters with jet velocity.

THE FREQUENCY SPECTRUM OF JET NOISE

CORRELATION OF SPECTRA USING RANDOM QUADRUPOLE THEORY. A reasonable collapse of spectra at different jet velocities and total temperatures can be obtained if separate correlations are made at each emission angle. The 1/3 octave sound pressure level is normalised with respect to the overall S.P.L. and the frequency is corrected by the modified Doppler factor and normalised as a Strouhal number. In this way the observed frequencies are converted into the frequencies as measured in a reference frame attached to the convected eddy. The frequency normalising parameter used in this case was $fD/V_J \cdot [(1-Mc\cos\theta)^2 + \alpha^2 Mc^2]^{1/2}$ and the modified Doppler factor used here differs from that mentioned previously since the anisotropy factor has been put equal to unity. In this expression, α is equal to $\omega_0 l/V_c$ where l is the length scale of the eddy, assumed isotropic. It is found that, in order to obtain good correlation, the value of α should decrease with jet velocity (see Fig. 5). It is probable that had a more realistic anisotropy factor been used, the value of α would tend to remain constant at least over part of the velocity range. The collapse of data can be improved further by correlating results not at the same emission angle but at the same angle relative to the peak emission angle.

A close scrutiny of these results show that there are two basic spectra with peak frequencies separated by about three octaves. (See Fig. 6) The lower frequency spectrum dominates between emission angles of 0° and 60° and the higher frequency spectrum at emission angles greater than 60°. This behaviour can be resolved by adding the contribution of a lateral quadrupole to that of the random quadrupoles. This more complex model accounts for the spectral variation with emission angle and will probably allow the spectra to be collapsed on to a single curve.

THE THEORETICAL FREQUENCY SPECTRA. The power spectral density of the acoustic radiation from convected quadrupoles has been studied by Ffowcs Williams (2), and he derives an expression which involves the radiated frequency and the spectrum of the source strength stress tensor. For a distribution of randomly orientated quadrupoles, the spectral density has the form $(2\pi f)^4 . H(\omega)$ where f is the radiated frequency, ω is the radian frequency associated with the turbulent eddy and H is the spectrum of $\rho u'u'$, and where u' is the isotropic turbulent velocity fluctuation. The frequency ω may be interpreted as the frequency of the source fluctuation since it is that viewed in a frame of reference attached to the eddy. The frequencies ω and f are related by the modified Doppler factor, i.e. $\omega = 2\pi fF$

The spectral density of the radiation from orientated lateral quadrupoles will have the form $(2\pi f)^2 \sin^2 2\theta \ (\partial \bar{u}_1/\partial x_2)^2 K(\omega)$, where $\partial \bar{u}_1/\partial x_2$ is the mean rate of strain and $K(\omega)$ is the spectrum of $p' + \rho u'u'$ and where p' is the pressure fluctuation.

For this simple evaluation of the theory $\partial \bar{u}_1/\partial x_2$ is replaced by V_J/D , the jet velocity divided by the nozzle diameter, and p' is assumed to be negligible compared with $\rho u'u'$ so that $K(\omega)$ becomes identical with $H(\omega)$. Therefore the spectral density of the radiation from a combination of random and lateral quadrupoles has the form $(fD/V_J)^2 \times [(fD/V_J)^2 + Q' \sin^2 2\theta] H(\omega)$ where Q' is the ratio of the strength of the lateral to the random quadrupoles and the 2π factors have been absorbed by Q' . The value of Q' will not be numerically equal to Q because of the 2π factors and because the mean rate of strain is not exactly equal to V_J/D . This expression can now be used to convert the observed acoustic spectrum into a spectrum associated with the turbulent fluctuations in the flow.

CORRELATION OF SPECTRA USING MORE COMPLEX MODEL. For the initial assessment of this theoretical expression the fact that the experimental measurements of the spectra are the S.P.L. in a band proportional to the frequency (i.e. 1/3 octave) rather than the spectral density is ignored. In addition, the Doppler correction to the frequency ω is omitted, and the value of Q' is taken to be unity. The measured spectra at various emission angles for a given V_J and D are divided by the factor $(fD/V_J)^2 \left[(fD/V_J)^2 + \sin^2 2\theta\right]$ in order to convert them into the turbulence spectrum $H(\omega)$, and the resulting spectra are then compared.

The measured spectra for a given jet velocity show a marked variation with emission angle, θ (see Fig. 7). It can be seen that the main changes occur at frequencies less than that given by V_J/D . Above this frequency the spectra are more or less the same shape. The application of the theoretical expression to the data considerably reduces this variation so that the resulting spectra almost collapse on to a single curve (see Fig. 8). There is however, some discrepancy at the low frequencies below about $0.1\ V_J/D$. Examination of the theoretical expression shows that at angles removed from 0^0 and 90^0 if the frequency is less than V_J/D then the observed spectrum is that of a lateral quadrupole, i.e. $f^2 H(\omega)$. If the frequency is greater than V_J/D then the random quadrupole dominates and the spectrum has the form $f^4 H(\omega)$. At emission angles close to 0^0 and 90^0 the spectrum becomes $f^4 H(\omega)$ and the random quadrupole dominates at all frequencies. This behaviour is closely followed by the measured spectra.

If the corrections for the use of 1/3 octave spectra and the Doppler factor are applied, the S.P.L. in a 1/3 octave band has the form $(fD/V_J)^2 \left[(fD/V_J)^2 + Q' \sin^2 2\theta\right] H(2\pi fF)/f$ where $H(2\pi fF)$ is the 1/3 octave spectrum and not the spectral density. When this expression is applied to the data, the collapse appears to get worse (see Fig. 9). However, this correction is necessary and helps to account for the observed difference between spectra at emission angles symmetrical about 45^0. Consideration of the theoretical expression without this correction shows that the spectra at say 30^0 and 60^0 should be identical and this is not observed experimentally. This approach is promising and the examination of more data may resolve the difficulty. Adjustment of the value of Q' may also effect some improvement. In addition the original assumption that the spectra $H(\omega)$ and $K(\omega)$ are equivalent may not be correct especially if $K(\omega)$ is dominated by the spectrum of the pressure fluctuations. It is possible that the pressure fluctuation is directly proportional to the velocity fluctuation, i.e. $p' \sim \rho U u'$. In this case the spectra $H(\omega)$ and $K(\omega)$ may have the same form but $H(\omega)$ will generally be an octave higher than $K(\omega)$.

DISCUSSION AND CONCLUSIONS

From the preliminary evaluations reported in this paper it is apparent that the theoretical model comprising both randomly oriented quadrupoles and lateral quadrupoles oriented at 45^0 to the jet axis is a considerable improvement over the model with random quadrupoles only. Since the experimental results show that the angle of peak noise emission is largely a function of jet velocity and more or less independent of jet temperature, the variation of peak noise angle is predicted qualitatively by both theoretical models. However the model using two types of quadrupole predicts the peak angle more closely at the lower jet velocities below about $1.5\ C_\infty$. Also the random quadrupole model requires a reduction of the convection speed factor (V_c/V_J) with jet velocity whereas the other model will adequately predict the peak noise angle for jet velocities up to about $2.0\ C_\infty$ with a constant value of the convection speed factor. However a reduction of this factor with jet velocity is required at jet velocities above

about 2.0 c_∞ if the peak noise angle is to be predicted correctly. This is justifiable possibly on the grounds that the convection velocity chosen represents some average value and if the structure of the jet significantly changes at the higher speeds, the average convection velocity will also be changed.

The overall shape of the directivity is similar for both models except in the direction between 90° and 180° to the jet axis downstream of the nozzle, where the addition of the lateral quadrupole increases the intensity so that it becomes almost constant between 90° and 135°. This compares favourably with the general shape of experimental results at these angles. The agreement between theory and experimental data for the general shape between emission angles 0° and 90° is best near the peak. There are discrepancies at angles between 0° and 30° for the lower jet velocities below about 2.0 c_∞ where the levels are overestimated by the theory. Again the theory underestimates the intensity at angles greater than about 60° for the higher jet velocities above about 2.0 c_∞ . It is possible that the discrepancy at small angles to the axis is due to refraction of the sound by the shear layers, which is not allowed for completely by the theoretical model. At rights angles to the jet, it is possible that a contribution from shock-turbulence interaction, in particular shock cell tones, which again is not completely accounted for by the theory, increases the intensity in this direction. It may also be possible to resolve the discrepancies by adjusting the strength of the lateral quadrupole relative to the random quadrupoles and the value of the turbulence parameter, α_1 . In addition, it may be necessary to vary these quantities with jet velocity, and this may be justified again on the grounds that they represent averages taken over the jet as a whole and may therefore vary with jet velocity. Regarding the adjustment of the values of Q and α_1, it has been noticed that an increase in α_1 will decrease the difference between the peak intensity and that at 90° to the jet, so that it agrees more closely with observations. Physically an increase in α_1 means that the eddy structure is decaying more rapidly. Whether this is correct for a hot supersonic jet is not known unless it can be argued that the shock structure induces a more rapid break up of the eddies.

The jet noise spectra can be correlated quite well using the random quadrupole model provided separate correlations are made at each emission angle. However the spectral behaviour is accounted for remarkably well by the more complex model using two types of quadrupole and this offers a good prospect for collapsing the results on to a single curve. Although the shapes of the spectra at different emission angles are made similar using this model, they do not all coincide and further work is required to resolve this difficulty. It is possible that adjusting the strength of the lateral quadrupole relative to the random quadrupole and allowing it to vary with frequency will improve the match between theory and experiment.

Comparison of the experimental data and theoretical predictions shows that the quadrupole theory as a whole represents the acoustic radiation from jets, and in particular that a more complex model based on two types of quadrupole improves the description of the jet noise considerably. However some of the details are not in agreement and this may partly be attributed to the lack of information concerning the turbulence structure of hot supersonic jets. It is possible that suitable adjustment and variation of these turbulence parameters may improve the agreement between theory and experiment.

ACKNOWLEDGEMENTS

The authors are grateful to Mr. P.E. Doak and Dr. J.E. Ffowcs Williams for many stimulating discussions concerning this work and to the Noise Department of Rolls-Royce Ltd., (Bristol Engine Division), for providing the experimental data. They also wish to acknowledge the financial assistance of the Ministry of Technology.

REFERENCES

(1) M.J. Lighthill On Sound Generated Aerodynamically I & II.
Proc. Roy. Soc. A, (1952), 211, 564-587 and (1954), 222, 1-32.

(2) J.E. Ffowcs Williams The Noise from Turbulence Convected at High Speed.
Phil. Trans. Roy. Soc. A (1963), 255, 469-503.

(3) I.S.F. Jones Aerodynamic Noise Dependent on Mean Shear.
J. Fluid Mech. (1968), 33, 65-72.

(4) P.O.A.L. Davies, M.J. Fisher and M.J. Barratt
The Characteristics of the Turbulence in the Mixing Region of a Round Jet.
J. Fluid Mech. (1963), 15, 337-367.

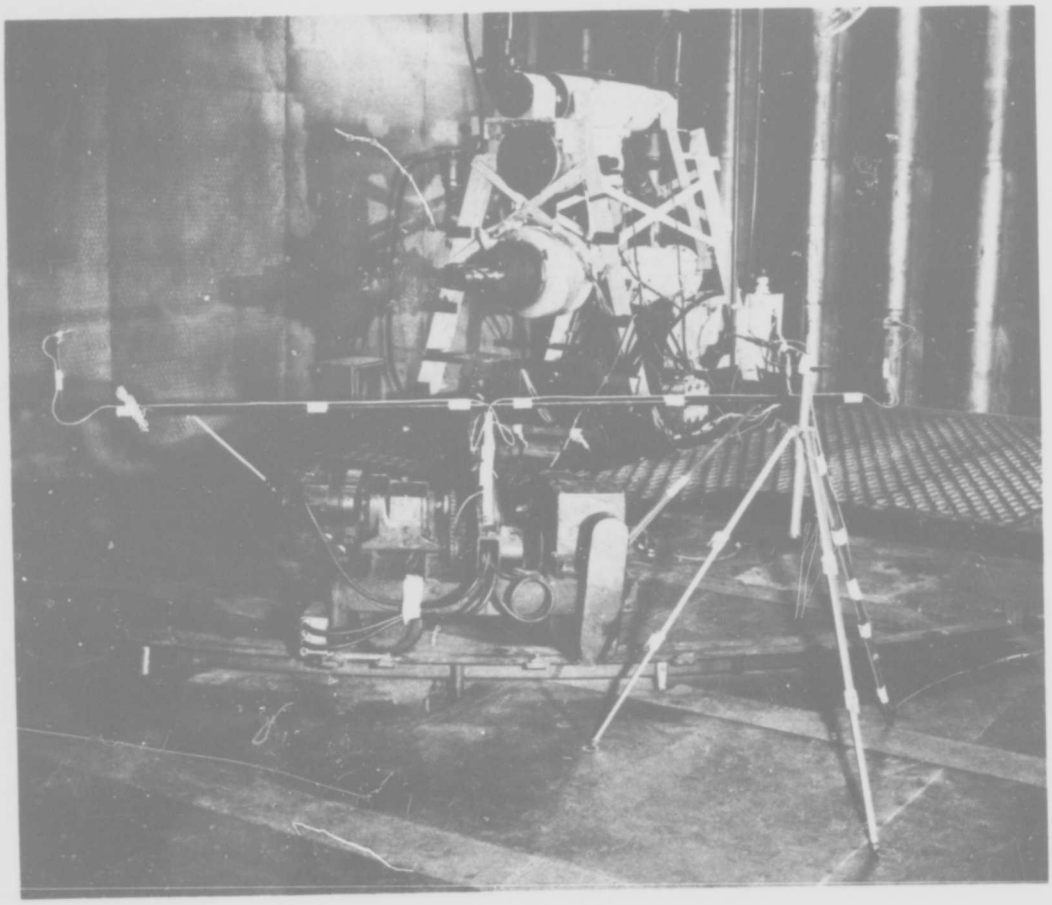

Fig.1 General view of jet noise rig.

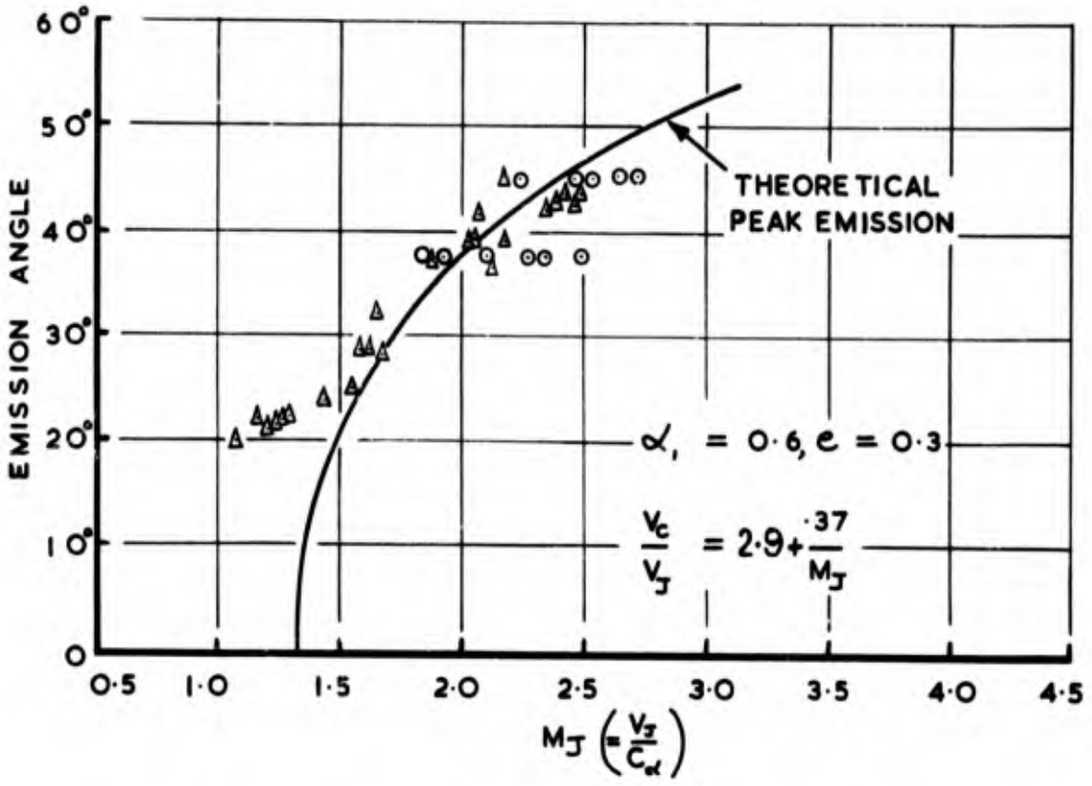

Fig. 2 Peak noise emission angle compared with random quadrupole theory.

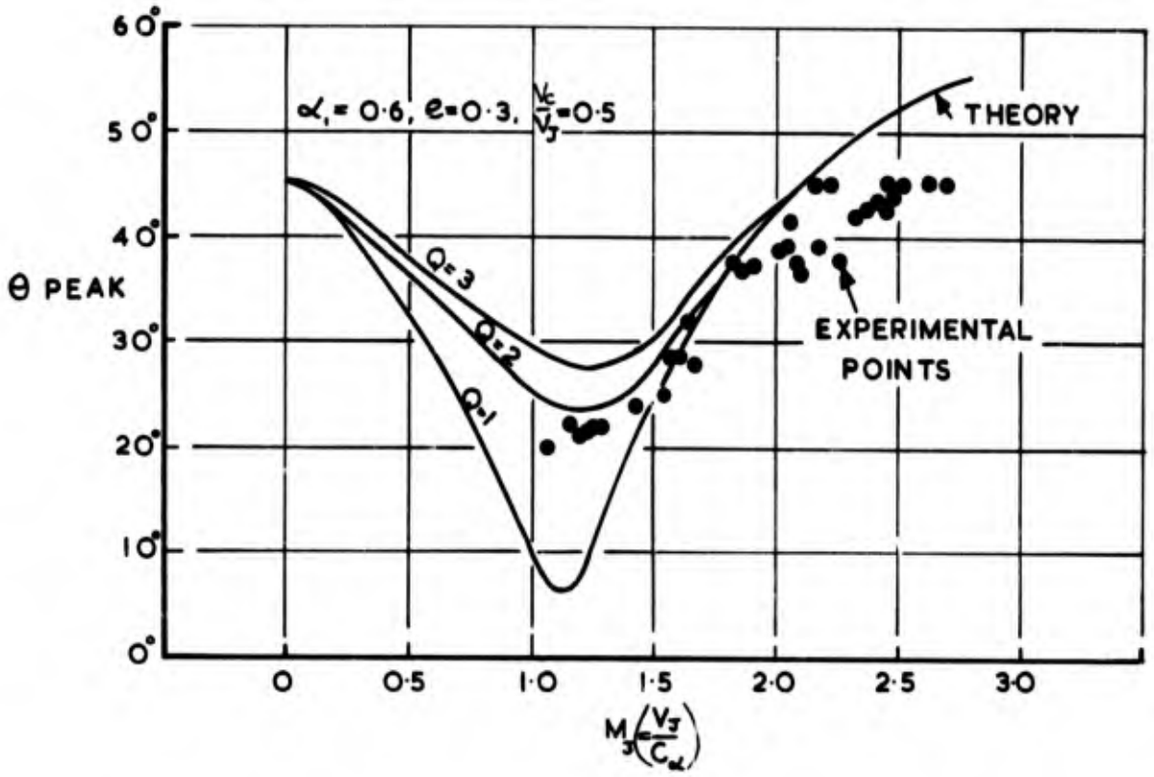

Fig. 3 Comparison of theoretical and experimental peak noise emission angle.

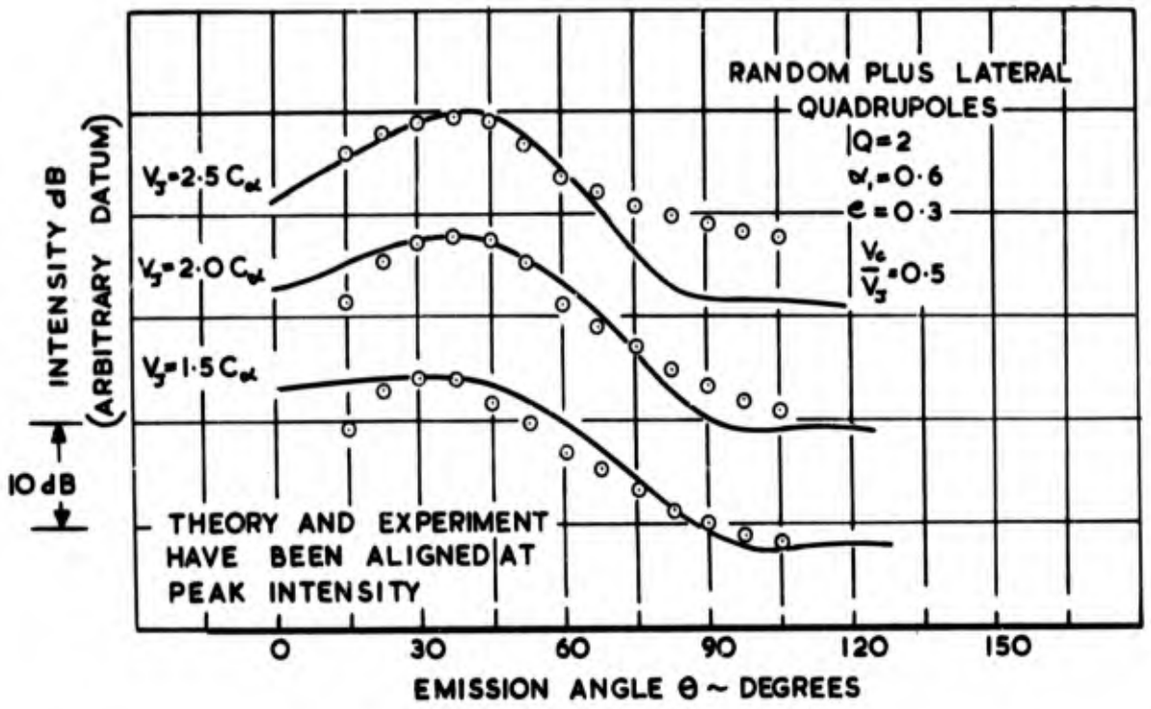

Fig. 4 Comparison between theoretical and experimental directivity.

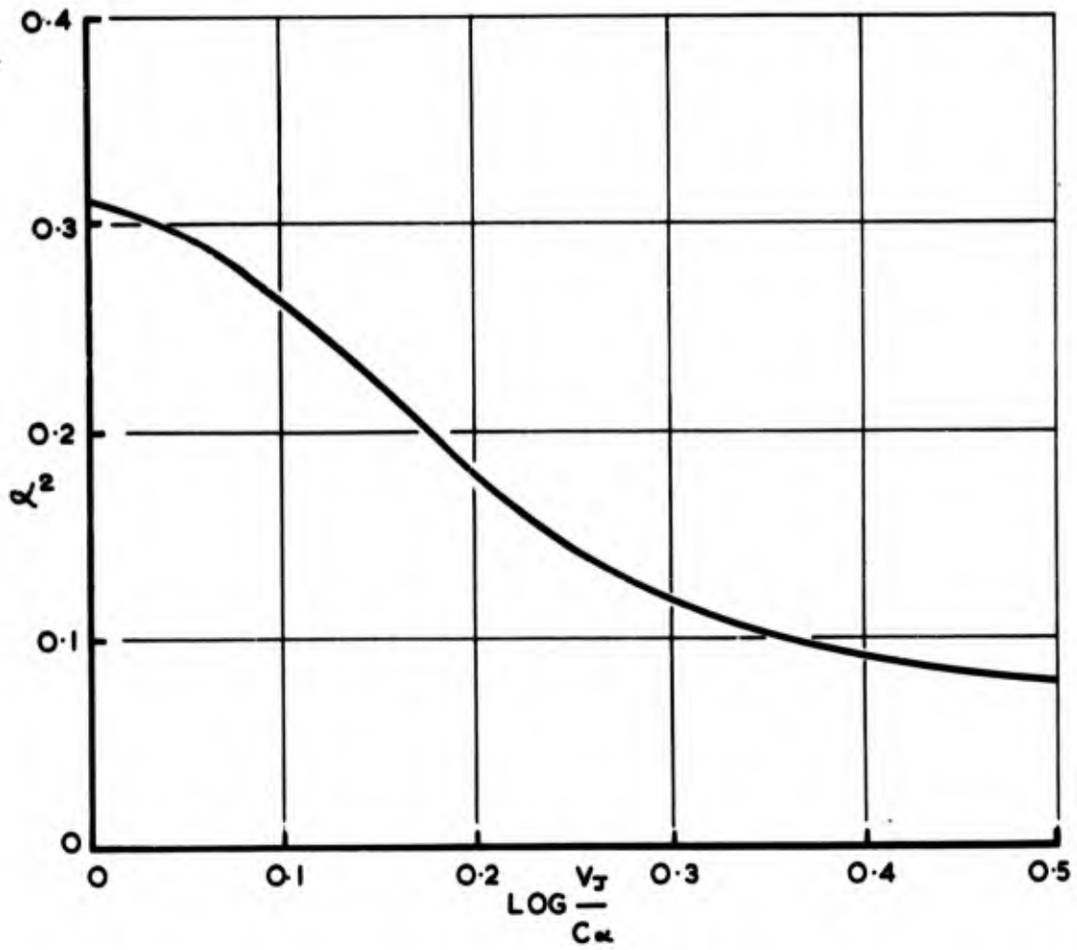

Fig. 5 Variation of correlation factor α^2 with $V_J/C\alpha$

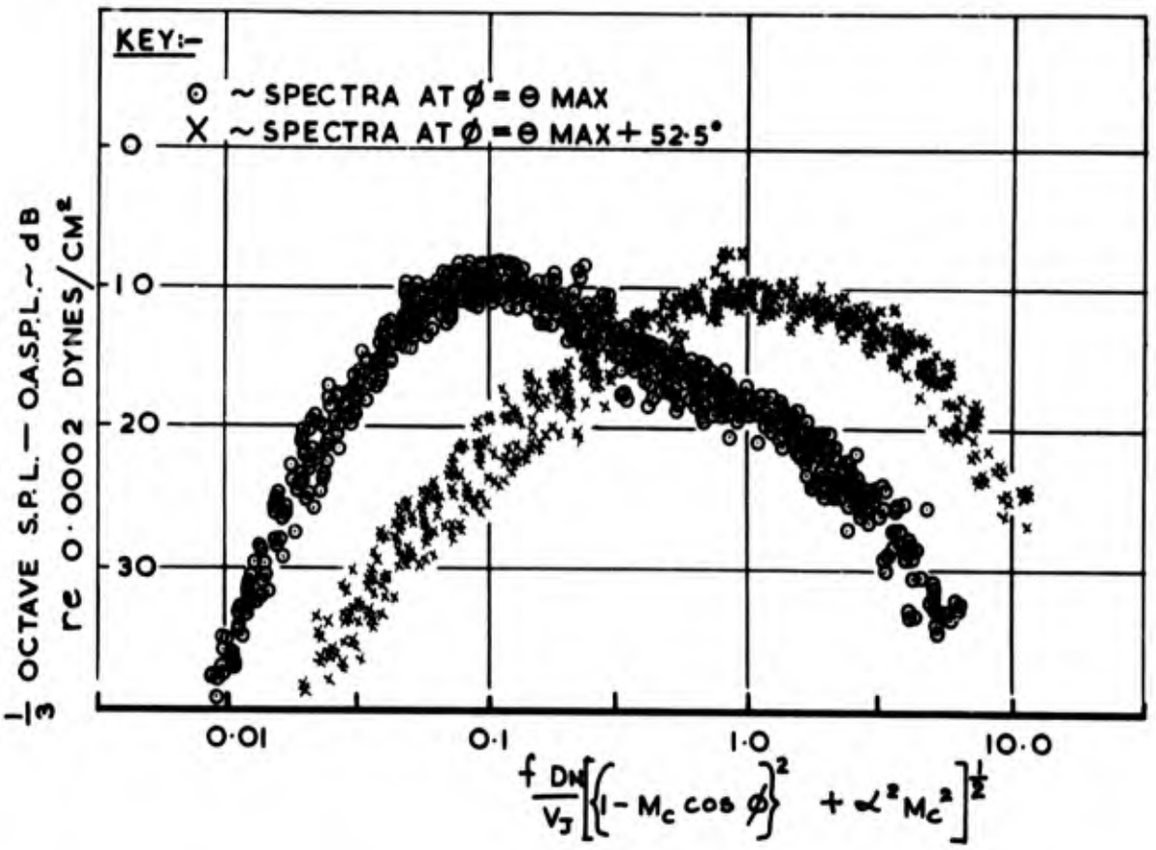

Fig.6 The two types of frequency spectrum shown on normalised plot.

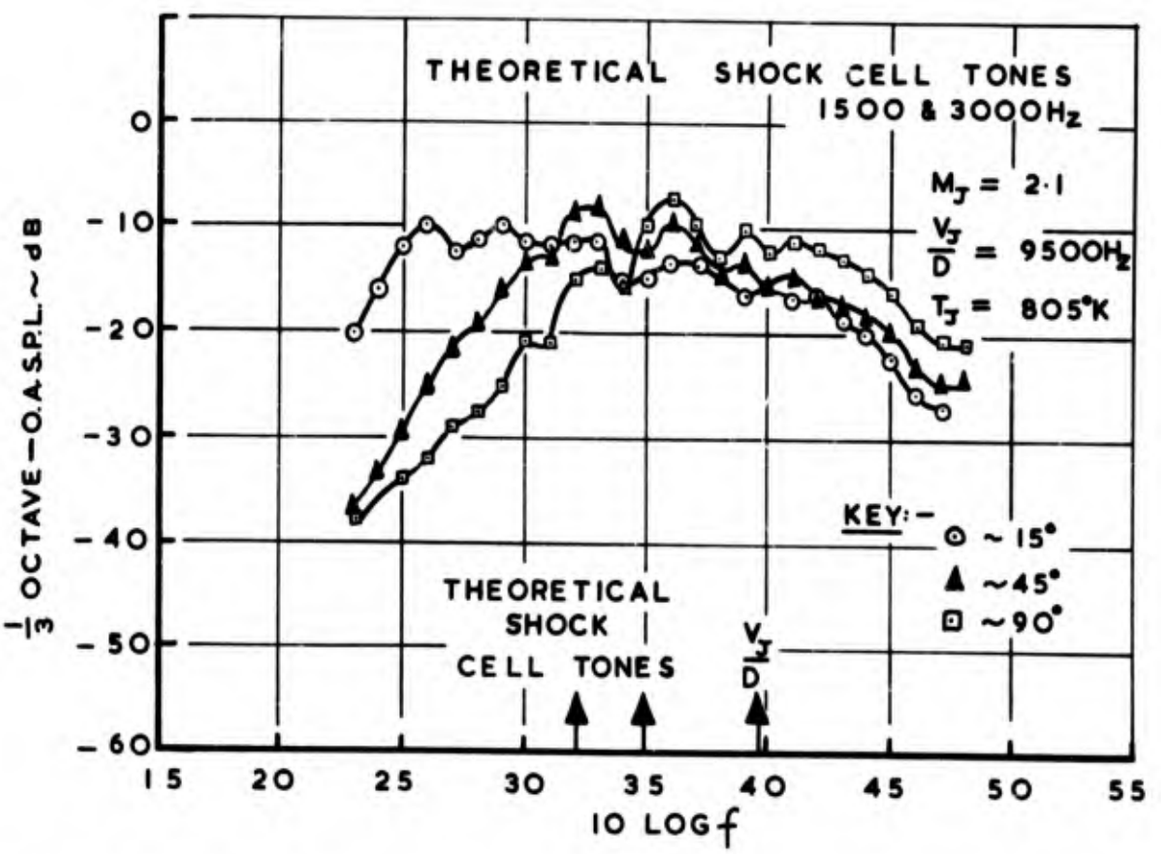

Fig.7 1/3 octave S.P.L. frequency spectra for various emission angles.

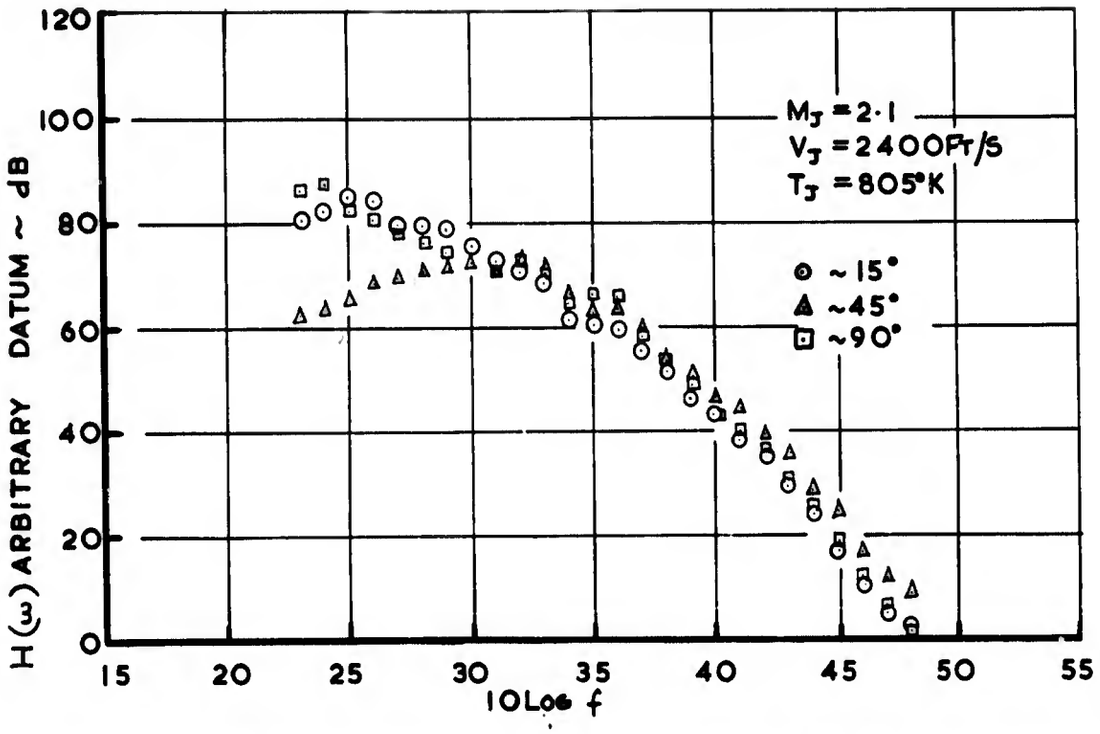

Fig.8 Estimate of the spectrum $H(\omega)$ for various emission angles.

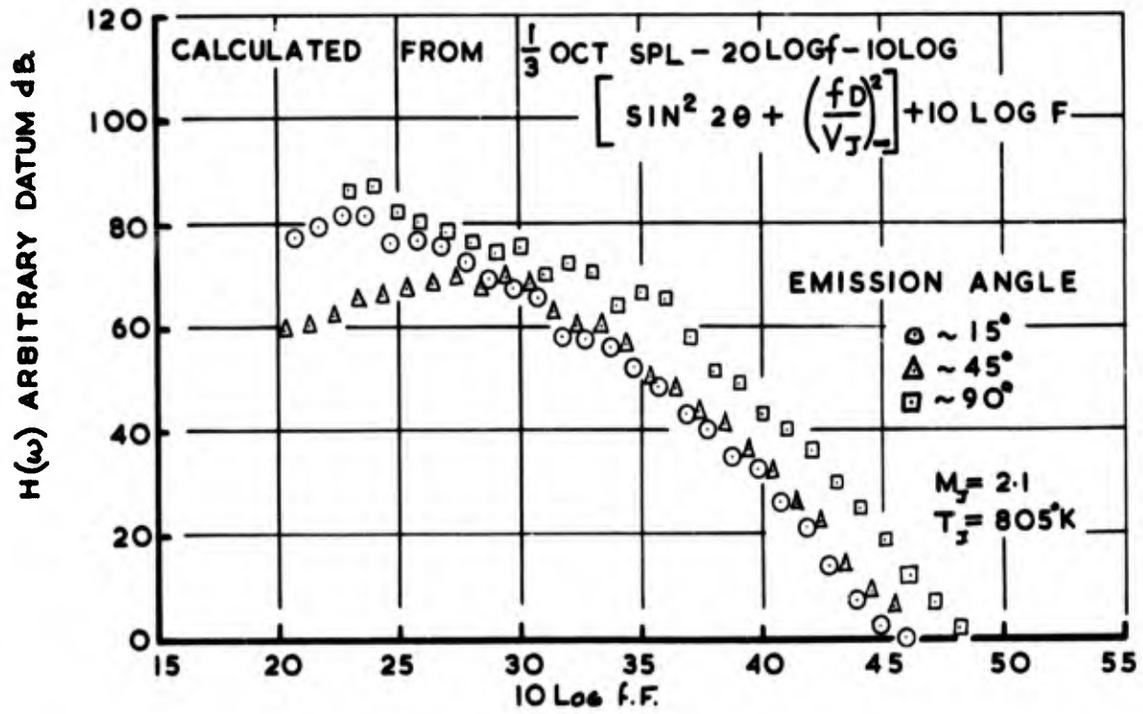

Fig.9 The spectrum $H(\omega)$ for various emission angles.

ENGINE QUIETING - ENGINE DESIGNS

by

NELSON F. REKOS

HEADQUARTERS
NATIONAL AERONAUTICS AND SPACE ADMINISTRATION
WASHINGTON, D.C., U.S.A.

SUMMARY

This paper describes a major research and development effort called the Quiet Engine program which is being undertaken by the National Aeronautics and Space Administration. The Quiet Engine program is aimed at the development and establishment of the technology required for the design and development of a subsonic aircraft engine which produces a minimum of noise through basic changes in engine design. The results of the preliminary work conducted to date on the Quiet Engine program indicate that noise reductions of about 20 PNdB below the noise levels of current commercial subsonic turbofan engines, are feasible.

Aviation's widening horizons can be attributed to a great extent to the successful development of extremely reliable and efficient gas turbine engines for the highly successful subsonic jet transports. The introduction of the newest series of these transports, the airbuses and jumbojets, is expected to have a significant effect on aircraft operations and economics. However, considering the fact that the present aircraft noise environment in airport neighborhoods is unacceptable to the general public, it becomes increasingly apparent that the growth of commercial aviation could be severely impacted if appropriate steps are not taken soon to alleviate the problem.

Figure 1, can be regarded as a roadmap for the presentation of this paper beginning with an assessment of the aircraft noise problem followed by a description of possible solutions to the problem. The Quiet Engine program will then be described beginning with the work conducted in the definition phase of the program followed by a review of the significant findings resulting from the various tasks studied in the definition phase. Finally, a description of the design constraints which were chosen for the request for proposals to industry to develop the Quiet Engine will be presented.

Figure 2, illustrates the engine noise sources in both turbojet and turbofan engines. Jet transports, when they were first introduced into commercial service were plagued by exhaust noise which was extremely difficult to attenuate without seriously compromising engine performance. This is due primarily because the bulk of the jet noise is generated some 5 to 20 jet diameters downstream of the exhaust nozzle. Basic studies of jet exhaust noise generation indicated that the intensity of jet noise is proportional to the eighth power of the exhaust velocity particularly in the range of the exhaust velocities encountered with turbojet engines. Although a great deal of research and development time was expended to resolve the jet exhaust noise problem, only limited success was noted. It was not until the turbofan engine was introduced that the engine designer, more or less, accidentally discovered a useful design tool with which he could begin to alleviate the jet exhaust noise problem. In the turbofan process energy is extracted from the gas generator flow to drive a fan located in front of a turbojet compressor. The energy used by the gas generator turbine to drive the fan has the effect of reducing the gas generator exhaust velocity and, of course, this results in lower jet noise output. However, as jet noise decreased with decreasing average jet velocity, it was discovered that fan noise became increasingly more disturbing. Fortunately, fan noise is of a different character from gas generator jet noise in that part of the fan noise is concentrated in relatively narrow frequency band giving rise to discrete tones and a siren-like whine. Also, unlike the jet noise, fan noise appears to be generated inside the fan portion of the engine and as a result it is possible to exert control over the noise generation through proper design of the fan-engine components and over the noise radiation through the use of acoustic absorbent liners in the fan engine inlet and discharge ducts.

The National Aeronautics and Space Administration (NASA) has responded to the aircraft noise problem by initiating two major research and development efforts. The first effort is a nacelle acoustic treatment program aimed at the reduction of fan noise through the use of acoustically absorptive materials in the fan-inlet and fan-discharge ducts of the Pratt and Whitney JT3D turbofan engine which powers most of the current fan-engine commercial jet aircraft. The Nacelle Acoustic Treatment program is managed by the NASA Langley Research Center. The second effort is referred to as the Quiet Engine program which is aimed at the development and establishment of the technology required for the design and development of a subsonic aircraft engine which produces a minimum of noise through basic changes in engine design. The Quiet Engine program which is managed by the NASA Lewis Research Center is the major subject of this paper.

Figure 3, illustrates the noise measurement reference points to be referred to in the following discussions. The take-off reference point being 3 statute miles from brake release, with the approach reference point being 1 statute mile from touchdown on a 3^{o} glide slope approach. Perceived noise level in decibels will also be used throughout this paper.

Figure 4, shows a schematic of the Pratt and Whitney JT3D turbofan engine which powers the Boeing 707 and Douglas DC-8 4-engine transports. The noise outputs related to each of the noise generating stations shown in the sketch are used as the baseline standard from which comparisons will be made later with Quiet Engine noise objectives. As you can see, during approach conditions the maximum noise at the ground reference station, 118 PNdB, is from the fan inlet and discharge ducts. During take-off, maximum noise at the ground reference station is 121 PNdB from the fan discharge duct. The jet noise floor of the JT3D engine, 100 PNdB, occurs during approach conditions which make the JT3D engine a likely candidate for noise suppression by use of acoustically absorbent materials, particularly during approach conditions.

In late 1966 the NASA Lewis Research Center conducted studies to determine the effects of turbofan cycle characteristics on engine noise levels, engine size, and engine performance. The initial cycle studies provided a field of interesting cycle points around a bypass ratio of 5.0. More detailed studies to define the Quiet Engine were then initiated with two major gas turbine engine manufacturers beginning in June 1967 and concluded in September 1968. These detailed studies by the gas turbine engine manufacturers was referred to as The Quiet Engine Definition Program, and consisted of three major tasks, as shown in Figure 5. The first task was a parametric cycle study involving about 480 different engine cycle combinations to determine the effects of varying the cycle design on noise, performance, engine weight, and engine dimensions. Based on important trends revealed in the Task I results, the most promising cycles were then selected for further detailed cycle analysis in Task II. Task II also evaluated variations in engine configuration arrangements. In Task III, the design configurations were narrowed to one engine design and a complete detailed design of the engine was made.

Figure 6 illustrates the range of engine cycle characteristics examined in Task I. The cruise thrust level of 4900 pounds was selected because the cruise thrust of the JT3D baseline reference engine is 4400 pounds and since it was conceivable that the Quiet Engine could be used as a replacement engine for the JT3D, it was estimated the larger diameter and greater drag of the Quiet Engine would require about 10% greater cruise thrust than the JT3D engine. The other parameters reflect the attempt to keep the study within the limits of current technology. Task I was also predicated on experimental evidence which indicated that the single most important parameter in determining fan noise output is the relative flow velocity at the fan tip.

Typical Task I results are shown with the following two figures (Figures 7 and 8). Figure 7 shows the effect of turbine inlet temperatures on engine weight, and thrust specific fuel consumption over a range of bypass ratio. In general, the higher temperature showed lighter engine weights and higher fuel consumption with a tendency to level off at a bypass ratio of 5 or 6. Figure 8 shows the effect of fan pressure ratio and engine pressure ratio on cruise specific fuel consumption. There is a sharp increase in fuel consumption at fan pressure ratios below 1.4 and decreasing cycle pressure ratio below 18 also increased fuel consumption.

The conclusions reached in Task I are shown in Figure 9 and indicate that: fan noise is the predominant noise source in the turbofan engines studied; variations in cycle parameters in the range of interest do not significantly influence total noise, although turbine inlet temperature had an effect on jet noise; fan tip speed should be kept below sonic tip speeds. Low noise levels occur with fan bypass ratio and fan pressure ratio combinations associated with lower cruise specific fuel consumption. Also, engines with the lowest noise levels tend to be large and heavy. No clear choice for a quiet engine cycle could be made from Task I.

The candidate Quiet Engine characteristics examined during Task II are shown in Table I. All of the engine designs provided for good acoustical design procedures such as, spacing between rotor and stator blade rows equal to at least two rotor blade chords, the number of stator blades should be greater than twice the number of rotor blades, and elimination of fan inlet guide vanes. As can be seen the engine designs covered a range of bypass ratio (3, 5 and 8) and fan pressure ratio which when coupled together with low fan tip speed necessitated examining various combinations of engine configurations having 2 or 3 engine spools and/or 1 or 2 fan stages. The characteristics of the JT3D baseline engine are also shown in this figure for comparison.

Figure 10 summarizes the results obtained during Task II. Engine designs with bypass ratios below 5.0 were too noisy. Designs with bypass ratios about 6.0 were considered too large for optimum aircraft installation, while the potential noise reductions from a low tip speed two-stage fan were not adequate, at least 3 PNdB higher noise levels were predicted for two stages. In addition, there is a weight penalty associated with a two-stage fan compared to a single-stage fan. Finally, the results showed that the design cycle variables should be selected so that the jet noise level is well below the fan noise level to allow margin for acoustic treatment of fan inlet and fan exhaust ducts.

Two configurations were selected for the final Quiet Engine design to be studied in Task III; one by each contractor. These Task III configurations embody all the background experience and knowledge derived from Task I and Task II and are shown in the following two figures.

Figure 11 is a schematic of a 5.5 bypass ratio Quiet Engine design which is a 3-spool design with a 5 stage low pressure turbine driving the single-stage fan on one spool. A separate single-stage turbine drives the 8-stage intermediate pressure and high pressure compressors on separate spools.

Figure 12 is a schematic of a two-spool 5.4 bypass ratio Quiet Engine design. A 5-stage low pressure turbine drives the single-stage fan on one spool. While a 2-stage high pressure turbine drives a 12-stage high pressure compressor on the other spool. The performance and physical characteristics of both designs are shown in Table II.

In Figure 13, a comparison is made between the noise outputs estimated for the Quiet Engine and that measured with the JT3D baseline engine. The jet exhaust noise can be reduced by 24 PNdB during take off and 16 PNdB during approach conditions. The 17 PNdB and 15 PNdB reductions in fan exhaust duct noise during take off and landing, plus similar reductions in fan inlet duct noise, are especially signficiant because the noise reductions shown are those to be achieved by engine design alone and do not include the use of acoustic absorbent material. Current experimental work indicates that further noise reductions of 10 PNdB in the fan inlet and exhaust duct are feasible. It can be concluded that significant noise reductions approaching the limit set by the jet noise floor are possible with the Quiet Engine.

With these attractive noise reduction goals in mind the National Aeronautical and Space Administration decided to initiate the development of an experimental flight-prototypical Quiet Engine that essentially embodies the design constraints and characteristics resulting from the Task III study and shown in Figure 14.

It is anticipated that considerable information will be forthcoming from numerous fan research programs underway or planned for in the next few years. Since fan noise dominates the noise output of the Quiet Engine, it is desirable to be able to incorporate the advanced fan technology in the Quiet Engine as it is developed. Therefore, the Quiet Engine fan was specified to be mounted on a shaft by itself so that changes in fan configuration and speed could be achieved with the least impact on the rest of the engine. A limit of 12.5 was set as the maximum pressure ratio per compressor in order to avoid any problems associated with an advanced technology high pressure ratio compressors. A minimum cycle pressure ratio for good fuel economy was determined to be 18. In addition, the maximum design turbine inlet temperature was set at 1775^{o}F in order to assure that jet noise levels will be sufficiently below fan noise to allow efficient use of acoustic absorbent material in the fan ducts. The design turbine inlet temperature limit of 1775^{o}F corresponds to a take off turbine inlet temperature of 2000^{o}F.

The Pratt and Whitney Aircraft Division of the United Aircraft Corporation and the General Electric Company have each been selected for the award of separate fixed price contracts to design, fabricate and test experimental quiet jet engines. There will be two phases to each contract. The first phase provides for detailed engine design and procurement of selected engine components. At the conclusion of the engine design portion of the first phase, six months after the award, NASA will have the option of instructing the contractor to proceed with the construction of two engines and to conduct a test program providing for a total of at least 250 hours of engine operation. Each contractor will then refurbish and deliver one of the engines to the NASA Lewis Research Center for additional testing. The second phase is expected to take about 30 months.

ACKNOWLEDGEMENT:

The author is grateful to the assistance given to him by Mr. James J. Kramer, Quiet Engine Program Manager, NASA Lewis Research Center, Cleveland, Ohio, during the preparation of this paper.

ASSESSMENT OF AIRCRAFT NOISE PROBLEM

ENGINE NOISE SOURCES

QUIET ENGINE DEFINITION PHASE

SUMMARY OF RESULTS

QUIET ENGINE DESIGN CONSTRAINTS

Figure 1 Introduction to the Quiet Engine Program

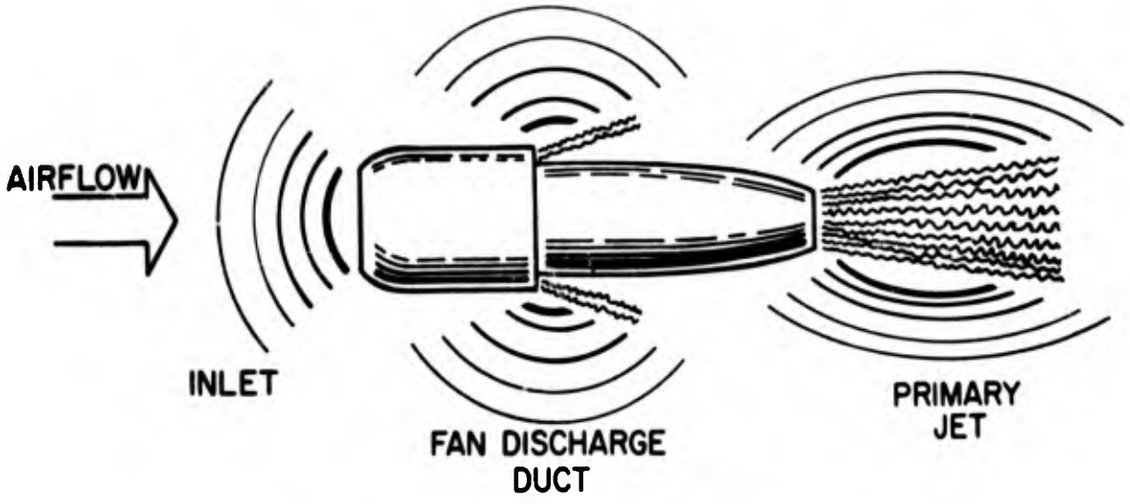

Figure 2 Engine Noise Sources

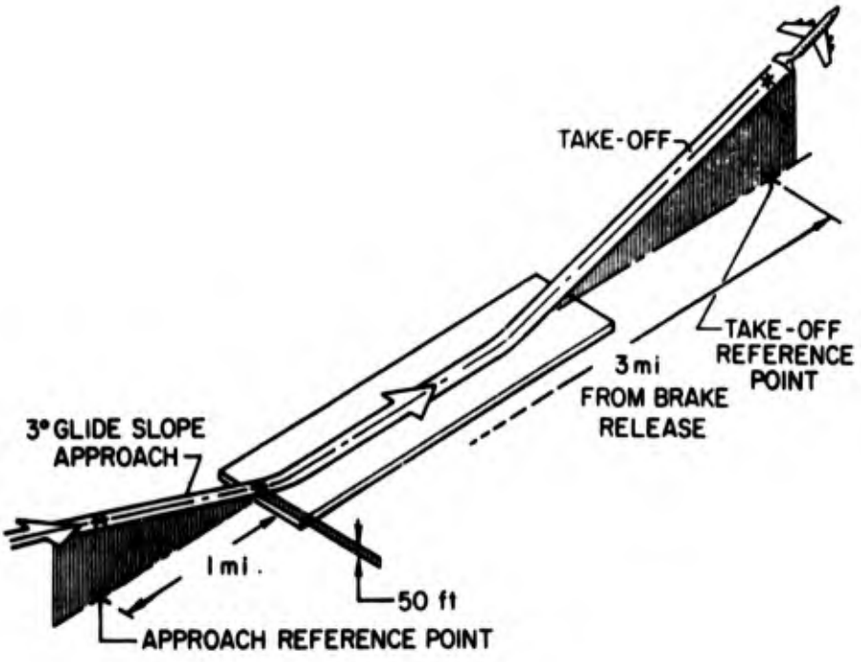

Figure 3 Noise Reference Points

BOEING 707/DOUGLAS DC-8

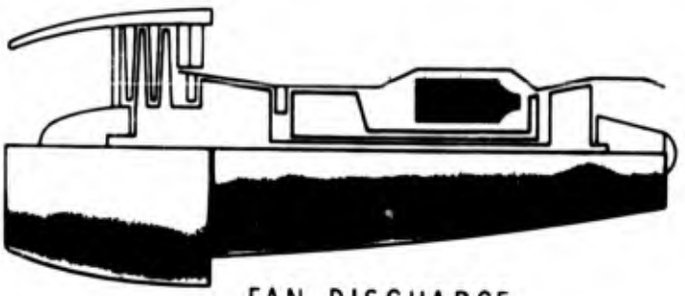

Figure 4 JT3D Engine

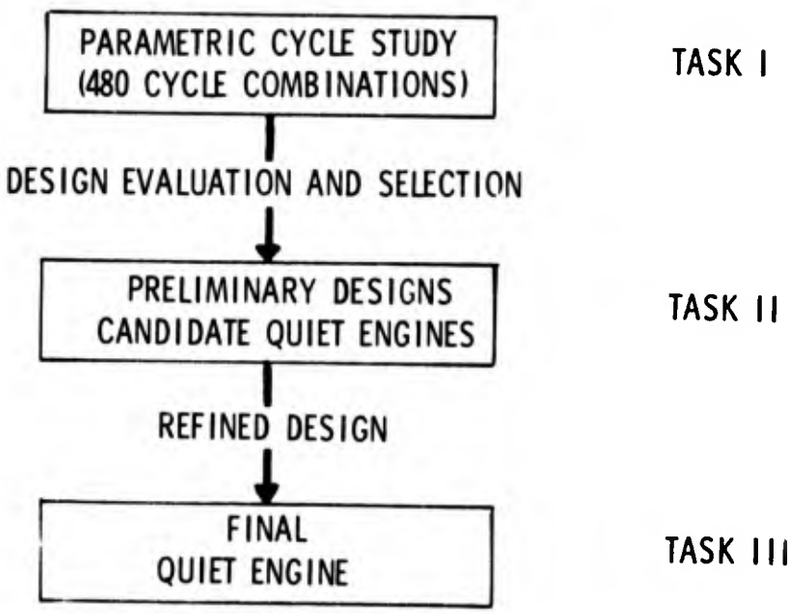

Figure 5 Quiet Engine Definition Program

CRUISE THRUST	4900 LB
TAKEOFF THRUST	20,000 - 25,000 LB
BYPASS RATIO	3 - 8
FAN PRESSURE RATIO	1.3 - 1.7
COMPRESSOR PRESSURE RATIO	15 - 30
TURBINE INLET TEMP, CRUISE	1600^0 - 2100^0 F
TURBINE INLET TEMP, TAKEOFF	1600^0 - 2300^0 F

Figure 6 Range of Cycle Parameters

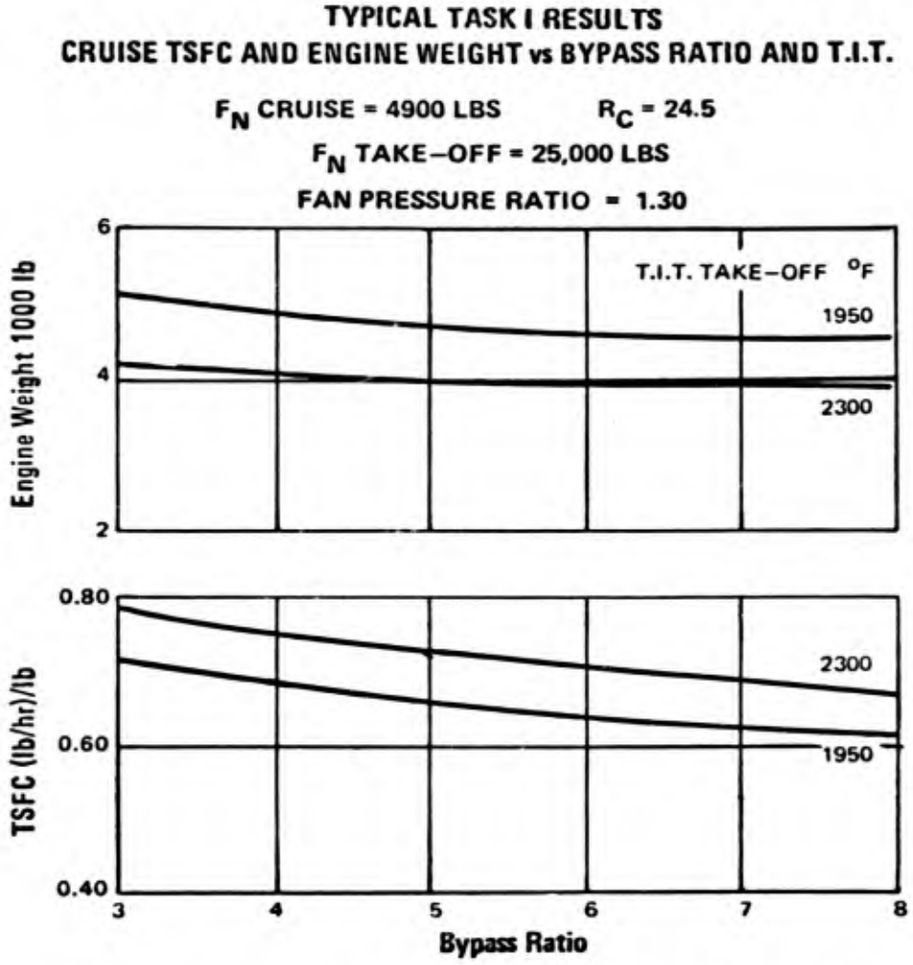

Figure 7 Turbine Inlet Temperature VS Engine Weight and Bypass Ratio

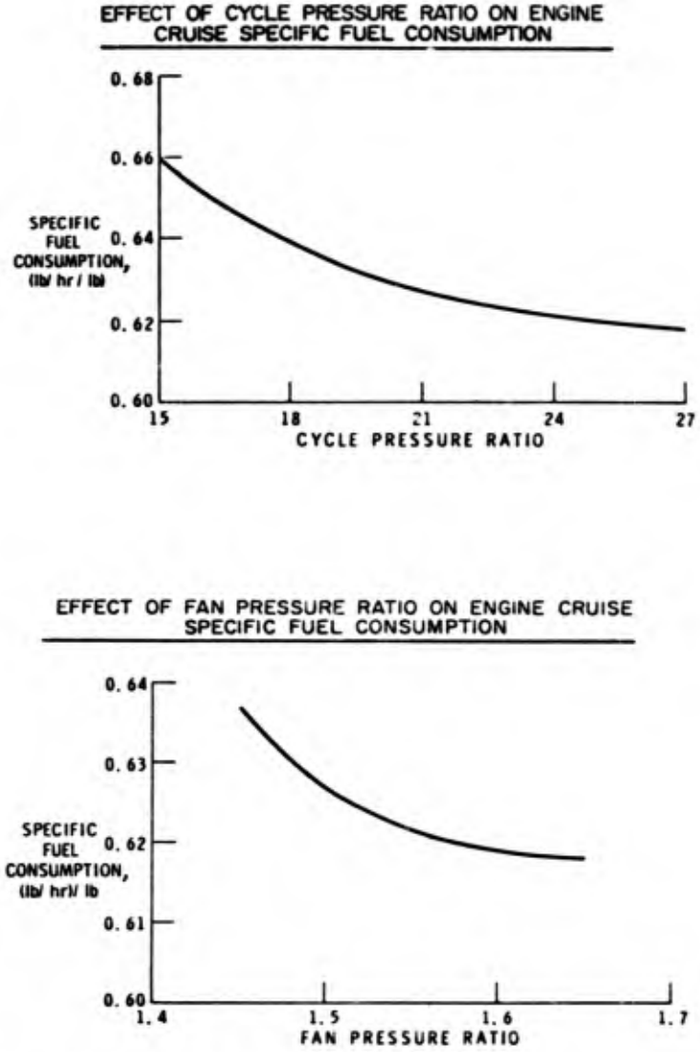

Figure 8 Turbine Inlet Temperatures VS Fuel Consumption and Bypass Ratio

PREDOMINANT NOISE SOURCE	∿	FAN
CYCLE VARIATIONS	∿	LITTLE NOISE INFLUENCE
LOW NOISE	∿	LOW FAN TIP SPEED
LOW NOISE	∿	FAN BPR AND PR WITH LOW SFC
LOW NOISE	∿	LARGE, HEAVY ENGINES

Figure 9 Conclusions - Task I

FAN BYPASS RATIO	<	5 JET NOISE TOO HIGH
FAN BYPASS RATIO	>	6 TOO LARGE
2-STAGE FAN	∿	HEAVY AND APPEARS NOISY

JET NOISE LEVEL BELOW FAN NOISE LEVEL

Figure 10 Task II Results

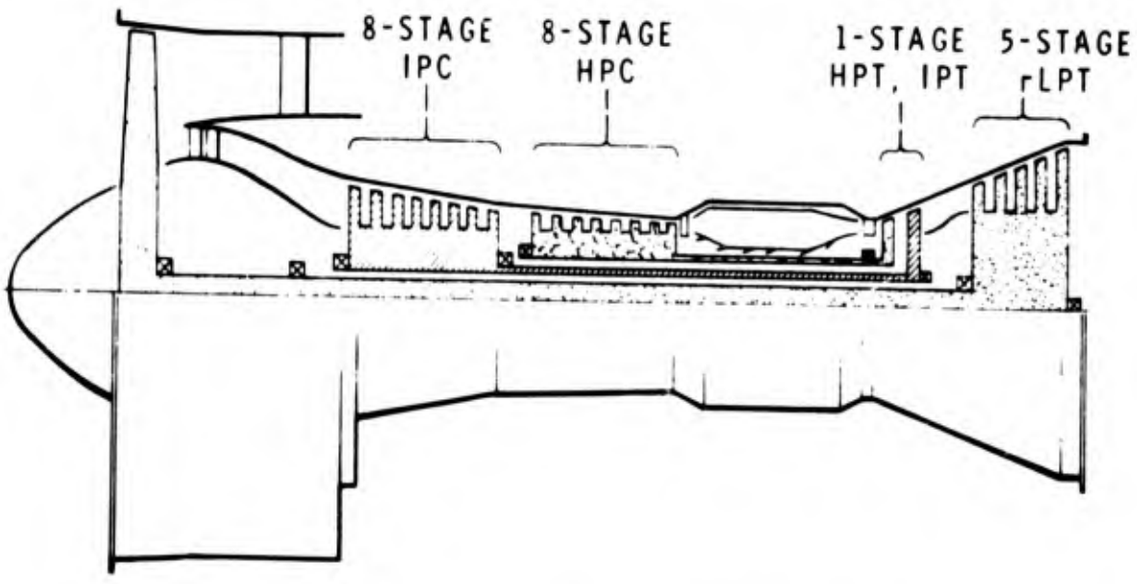

Figure 11 5.5 Bypass Ratio Quiet Engine

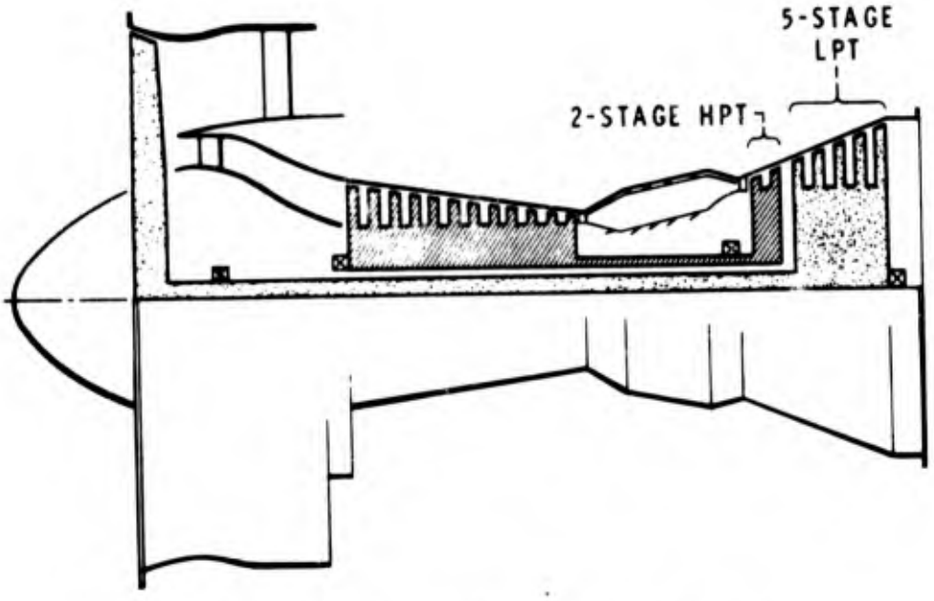

Figure 12 5.4 Bypass Ratio Quiet Engine

QUIET ENGINE VS JT3D

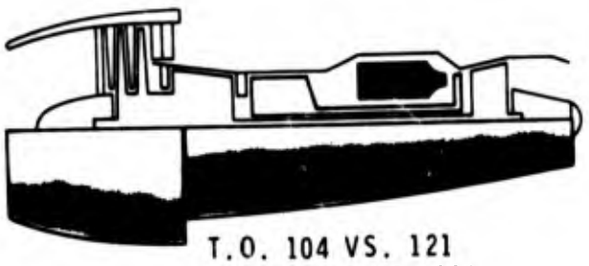

Figure 13 Quiet Engine Noise Output Comparison

ENGINE		
	BYPASS RATIO	5 - 6
	CRUISE THRUST	4900 LB
	TAKEOFF THRUST	22 000 LB
FAN		
	INLET GUIDE VANES	NONE
	SPACING BETWEEN ROTOR AND STATORS	2 ROTOR CHORDS
	TIP SPEED, TAKEOFF	1030 FT/SEC
	PRESSURE RATIO, CRUISE	1.5 - 1.6
	ON SPOOL WITH NO COMPRESSOR STAGES	
COMPRESSOR		
	ROTORS	1 OR 2
TURBINE		
	INLET TEMPERATURE, TAKEOFF	2000° F
	INLET TEMPERATURE, CRUISE	1775° F

Figure 14 Quiet Engine Design Characteristics

Table I Candidate Quiet Engine Characteristics

							JT3D
BYPASS RATIO	3.0	5.0	5.0	8.0	5.0	5.0	1.40
FAN PRESSURE RATIO	1.71	1.60	1.60	1.35	1.50	1.50	1.7
NUMBER OF ENGINE SPOOLS	2	3	3	2	3	3	2
NUMBER OF FAN STAGES	2	2	2	1	1	2	2
FAN TIP SPEED AT TAKEOFF, ft/sec.	990	990	985	1030	1110	780	1470

Table II Preliminary Characteristics - Quiet Engine Design

Cruise (35,000; M=0.82)		
Bypass Ratio	5.5	5.4
Cycle Pressure Ratio	24.1	18.4
Fan Pressure Ratio (Tip)	1.50	1.60
Turbine Temperature	1750°F	1770°F
Thrust	4900 lb.	4900 lb.
Specific Fuel Consumption	0.61	0.633
Corrected Air Flow	940.8	870
Takeoff (Sea-level, Standard Day)		
Turbine Temperature	1900°F	2000°F
Thrust	23,000 lb.	23,000 lb.
Fan Tip Speed	1026 ft/sec	1000 ft/sec
Relative Tip Mach Number	1.05	1.0
Dimensions		
Fan Tip Diameter	74.6"	70.0"
Fan Hub-to-Tip Ratio	0.465	0.45
Weight	4750 lb.	5200 lb.

BLANK PAGE

NOISE CHARACTERISTICS OF THE C-5A HEAVY LOGISTICS TRANSPORT

James A. Bair
C-5A System Project Office
Aeronautical Systems Division
Air Force Systems Command
United States Air Force

SUMMARY

The latest available community noise data from the C-5A Heavy Logistics System noise measurement program are presented. Noise measured at ground stations duri akeoff and landing is presented and compared to predictions. Limited comparison of meas nd predicted noise levels to community standards is included. The remaining portions of the C-5 noise measurement program are outlined.

SYMBOLS

PNdB - Perceived Noise Level in Decibels

DBA - "A" Weighted Overall Sound Pressure Level in Decibels

This paper presents the currently available data on the community noise characteristics of the C-5A "Galaxy" heavy logistics transport. Predicted values, extrapolation of engine test stand measurements, and some fly-over measurements are included. These data are limited and must be considered preliminary. A complete noise survey covering all aspects of community noise will be made in the near future.

The C-5A "Galaxy" is being manufactured for the United States Air Force by the Lockheed-Georgia Company of Marietta, Georgia. The wing span is 223 feet and the aircraft is 248 feet in overall length. The basic flight design gross weight is 728,000 pounds while the maximum design gross weight for operation at reduced load factor is 769,000 pounds. The airplane is designed to carry 220,000 pounds of payload normally or up to 265,000 pounds under emergency conditions. The aircraft is not volume limited, having a 19 foot wide, 13.5 foot high, 145 foot long cargo compartment. The large internal volume stemmed from a requirement to carry outsized military equipment.

Power for the "Galaxy" is supplied by 4 General Electric TF-39 high bypass ratio turbofan engines. The TF-39's supply 41,000 pounds of thrust per engine. The engine utilizes an 8 to 1 bypass ratio and an 8 foot diameter intake. Fan air discharges through an annular duct surrounding the core engine. The fan exhaust duct is about 2 and 1/2 feet long while the intake duct is approximately 4 feet long. The total fan cowl length is 9 and 1/2 feet. Engine length from intake to core engine exhaust is 20 feet.

The noise prediction and measurement program required by the C-5A contract is primarily directed toward the problem areas of sonic fatigue of structure and interior noise level control rather than community noise characteristics. Acoustic models were used to map noise level contours over the surface of the aircraft for the low frequency or jet noise portion of the C-5A sonic environment. The effect of fan noise was estimated by extrapolating TF-33P7 engine data (C-141 aircraft). Near field sound measurements from test stand engine operations have been used to supplement these data. During a portion of the flight test program, an extensive skin sound pressure level and strain survey will be conducted. These measurements will provide final verification of the design data.

The problem of community noise around military and civil airfields has received increasing attention during the development cycle of the C-5A. Air Force interest in this problem has been encouraged both in the hope of improving Air Force-community relations and by the possibility of civil airline use of the C-5A. For this purpose, a limited prediction and measurement program has been conducted.

At the time the contract for this aircraft was written, the most commonly envisioned civil airline certification criteria consisted of a 112 PNdB limit at a point 1 statute mile prior to touchdown and 3 statute miles from brake release on takeoff. Figure 1 shows a September 1964 prediction of perceived noise level (PNdB) versus distance for takeoff and figure 2 presents a similar plot for approach (1). The takeoff prediction is for maximum gross weight and a 1.2 times stall velocity climbout. The approach prediction consists of a roughly 6 PNdB wide band intended to provide for variations in power and pilot technique. The takeoff values exceed 112 PNdB by 6 to 7 PNdB at 3 miles while the approach values are from 1 to 7 PNdB high at 1 mile.

At the time of a general update of C-5A noise predictions (2), the community noise values were also revised as shown in figures 3 and 4. Figure 3 shows that the C-5A will exceed the 112 PNdB criteria at all gross weights over 550,000 pounds. The 700,000 pound airplane exceeds the criteria by 8.5 PNdB whereas the original estimate was 6 to 7 PNdB at maximum gross weight. The approach values have also increased by about 6 PNdB.

During late 1967, the first engine test stand measured TF-39 noise data became available. Because of engine and landscape limitations, these data were for 95% fan speed measured along a 30 foot sideline. No significantly better data were to be available prior to flight test. Therefore, these data were scaled up in rpm and extrapolated to the far field. These data were then used to produce a final set of community noise predictions as seen in figure 5 and figure 6 (3). Again, increases in perceived noise levels are indicated.

A preliminary fly-over noise measurement program was conducted by the Lockheed-Georgia Company in conjunction with some of the early flights of the C-5A (4). By this time, civil aircraft noise certification criteria in the United States was beginning to solidify in the form of effective perceived noise levels as stated in Federal Aviation Agency Proposed Standards (5). The Lockheed measurements were designed to verify the perceived noise level predictions and to get a feel for the effective perceived noise level characteristics of the C-5A airplane.

Figure 7 presents a typical perceived noise level versus time plot for a C-5A takeoff flyover. The PNdB values are calculated at half second intervals. These data are for a 516,800 pound airplane 655 feet above the observer. This altitude has been determined to correspond to 7300 feet from brake release. The maximum perceived noise level is 126 PNdB. The February 1968 value (figure 5) for a 500,000 pound aircraft at 7300 feet from brake release is 128 PNdB. The corresponding prediction from March 1966 (figure 3) is 122 PNdB. An effective perceived noise level of 125 PNdB was calculated for this case by the method of reference 5.

Figure 8 presents a similar plot for a 512,500 pound airplane 228 feet above the observer during approach. This corresponds to 4343 feet from runway threshold. The maximum perceived noise level is 131 PNdB as compared to the February 1968 prediction of 130 PNdB (figure 6), March 1966 values of

123 to 126 PNdB (figure 4), and September 1964 prediction of 114 to 120 PNdB. The calculated effective perceived noise level is 127 PNdB.

Figure 9 shows a roll-by of the C-5A at takeoff power. The microphone was 800 feet from the runway. A maximum perceived noise level of 117 PNdB results. At this time, these data have not been extrapolated to provide effective perceived noise levels at the measurement points specified in the FAA noise standards (5).

In addition to the data previously discussed, 4 additional takeoff and 2 more landing measurements have been made. As compared to figure 5, the measured perceived noise levels for takeoff varied from 1 to 7 PNdB lower than predicted. Approach measurements were from 1/2 to 2 PNdB higher than predicted (figure 6). Effective perceived noise levels have not been calculated for these measurements.

Presented in figure 10 is a comparison of the C-5A takeoff time history of figure 7 with several other fan engine aircraft (5 and 6) at near similar conditions. Note that the increase of noise to the maximum perceived noise level is generally similar for all the aircraft but that C-5A noise falls off much more rapidly than the others. This effect is discernible to the ear in such a way that it sounds like engine power is reduced after the airplane passes the observer. Due to this short duration and possibly to a favorable relationship of fan noise frequencies, persons exposed to C-5A noise consider it less noisy than other large Air Force and commercial aircraft.

The relationship between perceived noise levels of this aircraft and "A" weighted (DBA) overall sound pressure levels is shown in figure 11. The perceived noise level variations of figures 7 and 8 are repeated (top curves) in PNdB with accompanying plots of "A" weighted overall SPL in dB (lower curves). The two sets of curves are very similar. For the takeoff case, the DBA and PNdB curves are different by an almost constant 13 dB. On approach, the peak values are 13 dB apart while the average time history difference is about 11 dB. The reason for this is illustrated in figure 12, which presents a typical C-5A flyover octave band spectrum. The high frequency end of this spectrum compares closely to the frequency response of the "A" weighting characteristics. The dominance of the higher frequency fan noise over the lower frequency exhaust noise is also evident. The aircraft was 700 feet overhead when this measurement was made.

The data currently available as outlined in this paper provide a preliminary look at C-5A community noise characteristics. In the near future, further test programs are planned which will provide a complete picture of C-5A noise. The United States Air Force Aerospace Medical Research Laboratory will conduct a far field noise survey at Edwards Air Force Base, California. This site provides sufficiently open areas so that terrain interference is not a problem. Data will be taken on a 200 meter semicircle around the airplane and along radial lines. These data will be used to generate equal sound pressure level, perceived noise level, and speech interference level contours for base planning use. The Lockheed-Georgia Company will conduct additional fly-over noise measurements. These measurements will be taken at points further from brake release on takeoff and runway threshold on landing including, if possible, the FAA measurement points. Also, as more flight test data on height above terrain, power settings, and other parameters become available, it will be possible to extrapolate available data accurately.

REFERENCES

1. J. R. Ballentine, H. W. Bartel, J. R. Carroll, CX-HLS Vibration, Acoustics and Sonic Fatigue Analyses, ER-7375, Lockheed-Georgia Company, Marietta, Georgia, September 8, 1964.

2. J. R. Reese, W. H. Guinn, C-5A Preliminary Exterior and Interior Noise Analysis, LGIS38-1-1, Lockheed-Georgia Company, Marietta, Georgia, March 31, 1966.

3. T. R. Ives, G. Swift, J. W. Vogel, C-5A Final Exterior and Interior Noise Analysis, LGIUS58-1-1, Lockheed-Georgia Company, Marietta, Georgia, February 15, 1968.

4. John S. Gibson, Lockheed-Georgia Company, Noise Measurements on the World's Largest Aircraft, Paper X9, Meeting of the Acoustical Society of America, Cleveland, Ohio, November 21, 1968.

5. Anon, Aircraft Development Service Proposal for FAA Noise Certification Criteria, revised February 1, 1968.

6. D. E. Bishop, Descriptions of Flyover Noise Signatures Produced by Various Jet Transport Aircraft, FAA DS-67-18 DOT-FAA Washington, D. C., August 1967.

FIGURE 1

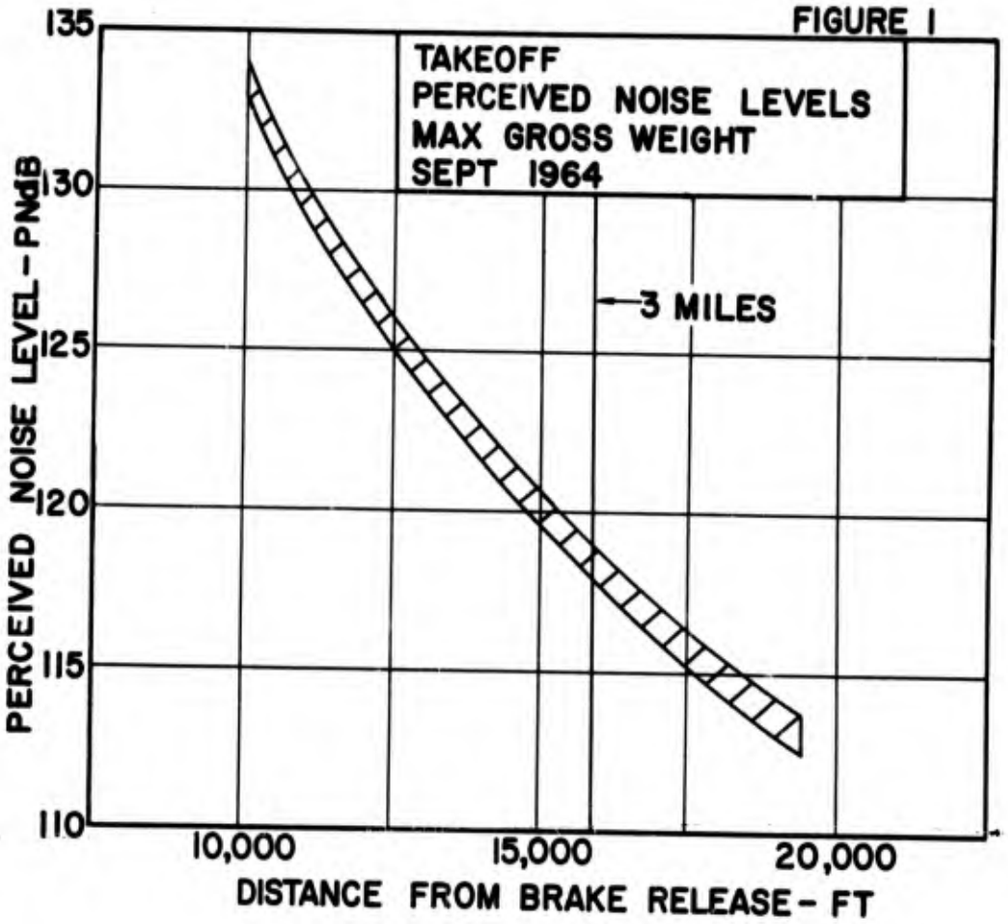

FIGURE 2

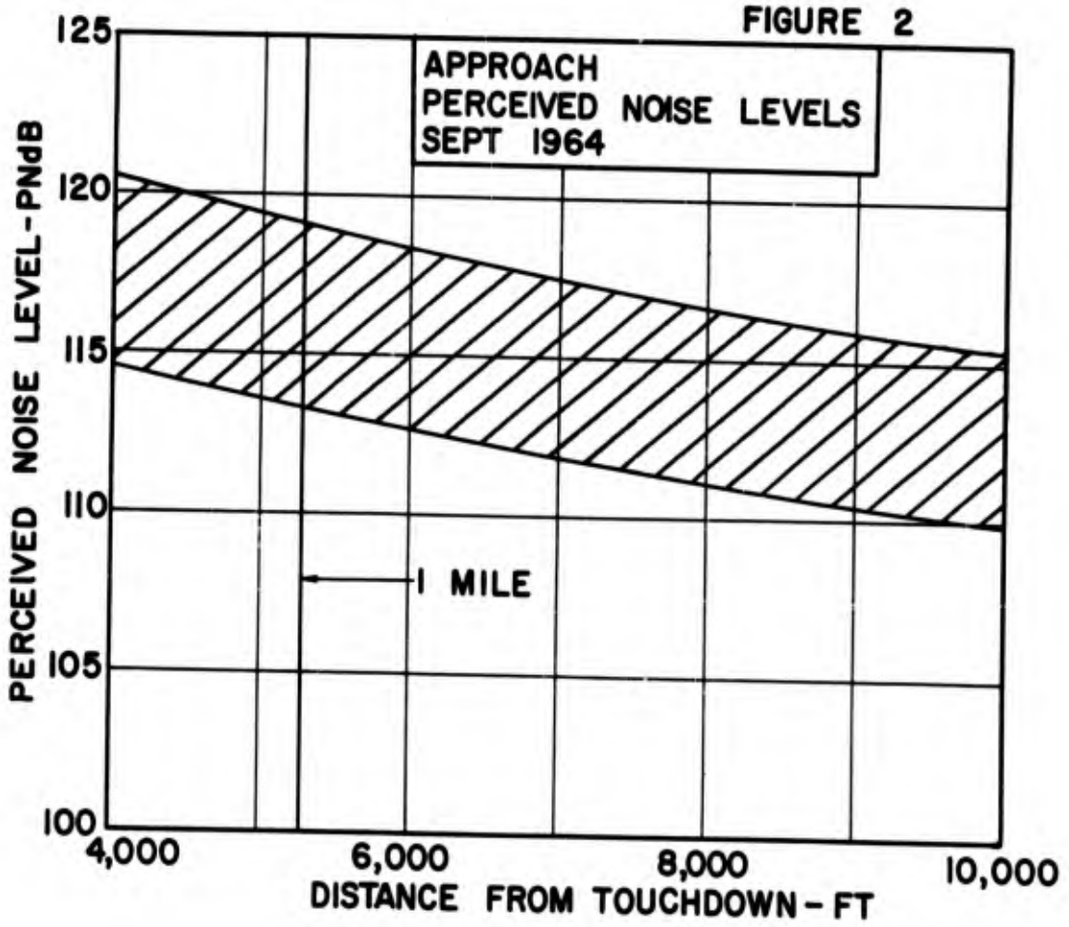

FIGURE 3

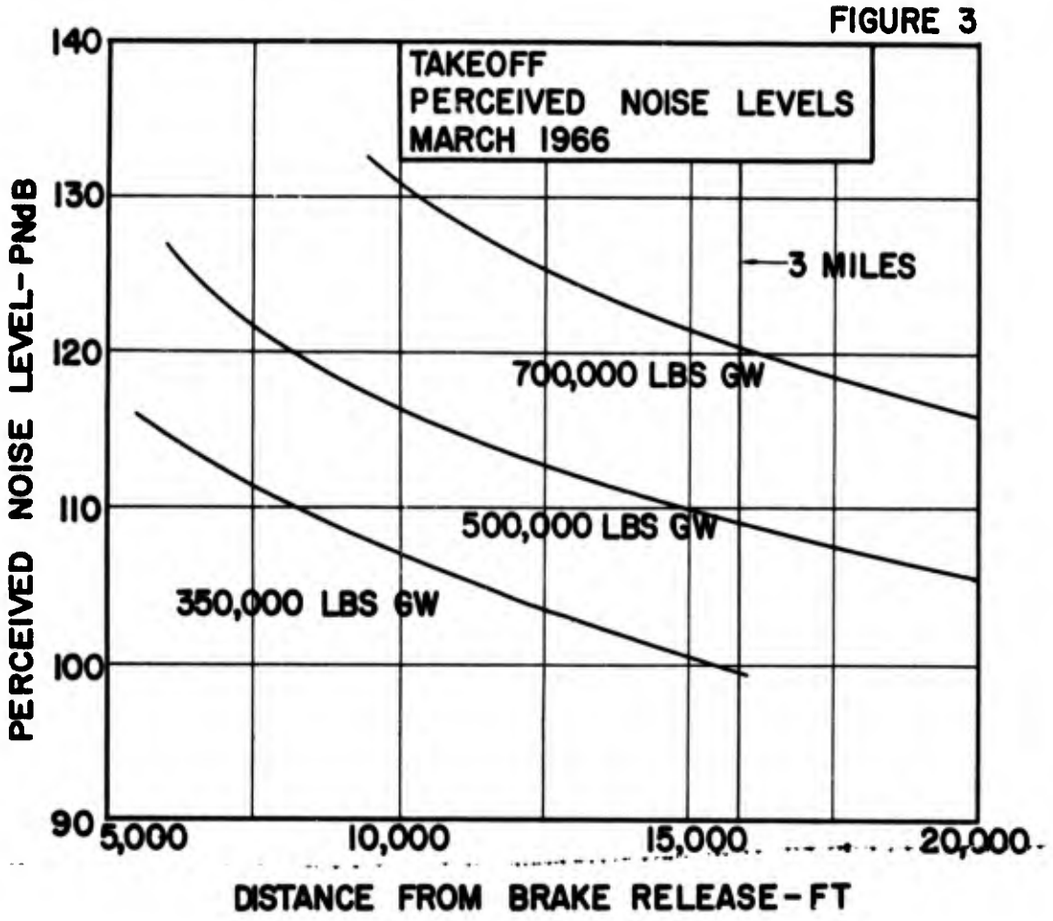

FIGURE 4

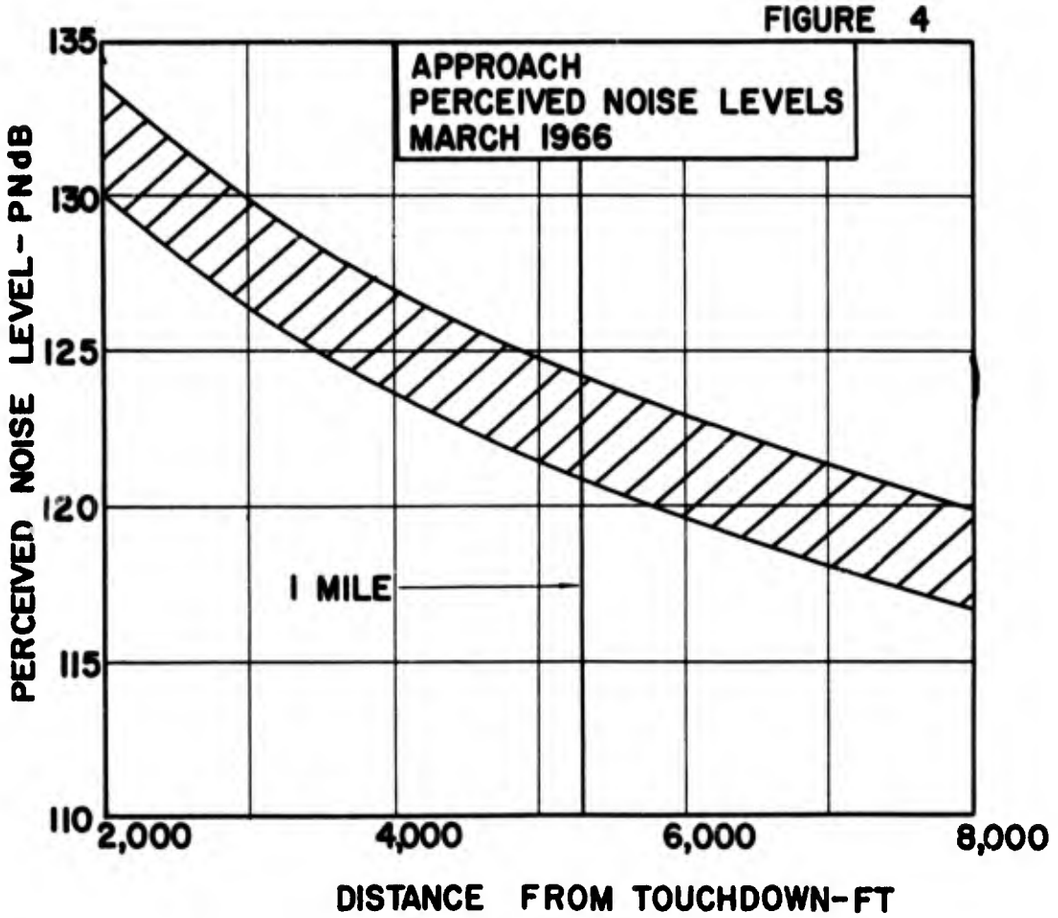

FIGURE 5

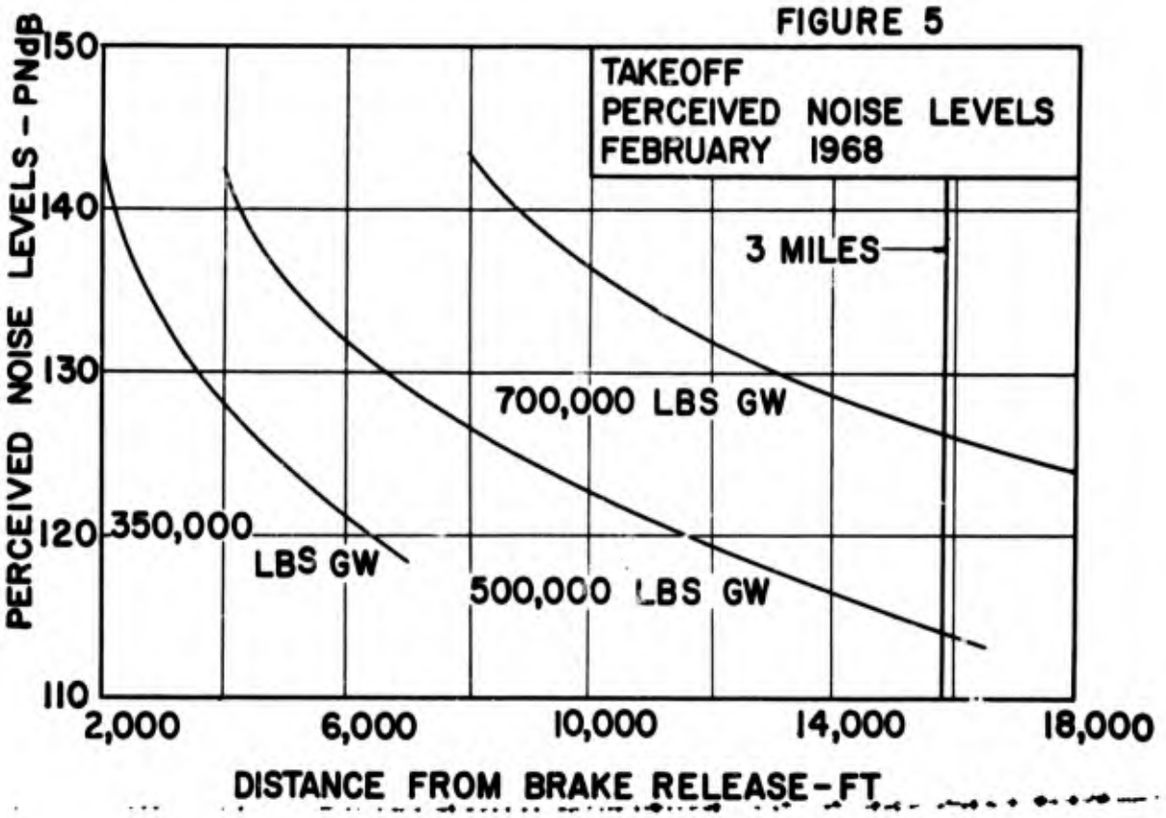

FIGURE 6

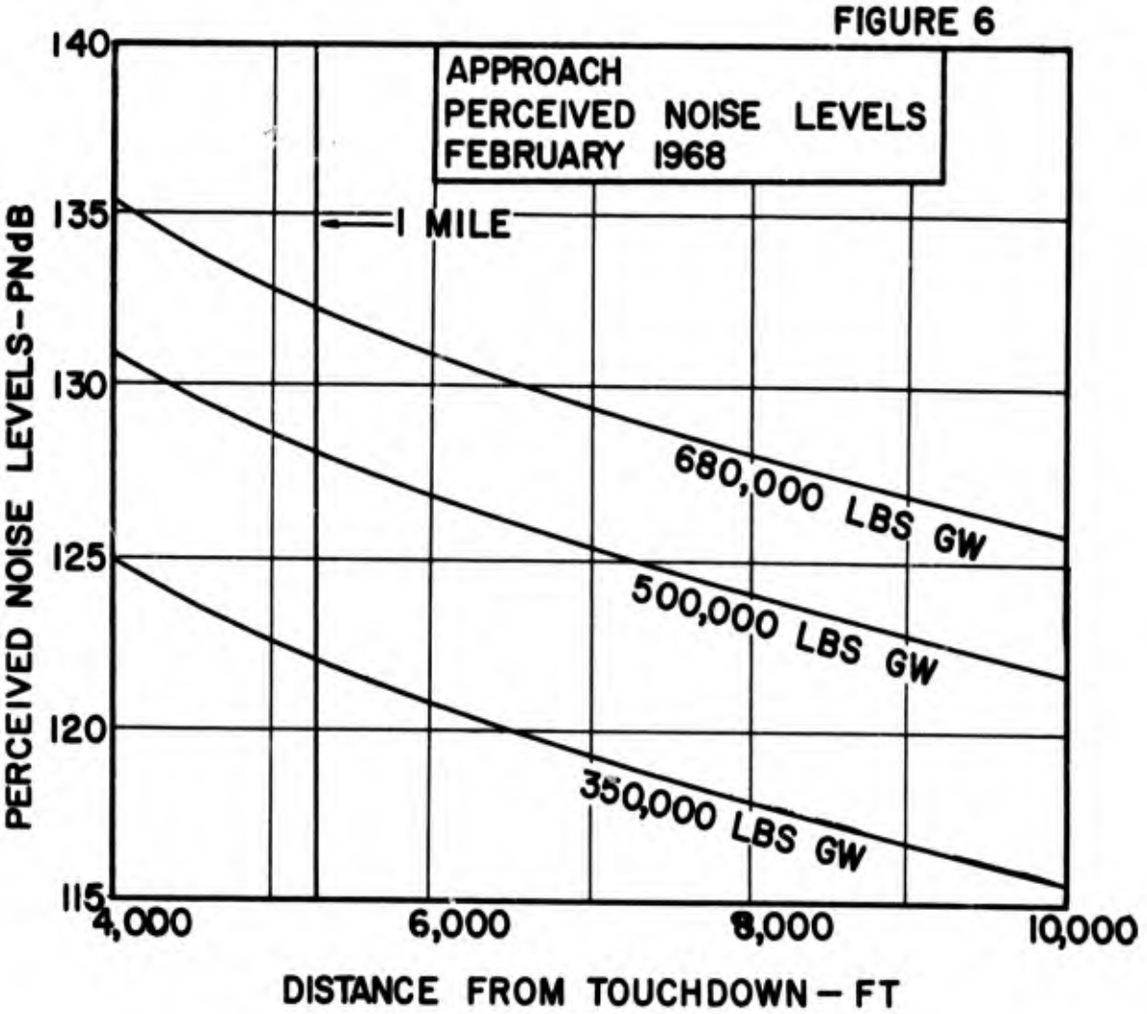

TIME HISTORY

FIGURE 7
TAKEOFF
516,000 LBS GROSS WEIGHT
655 FT ALTITUDE

FIGURE 8
APPROACH
512,000 LBS GROSS WEIGHT
228 FT ALTITUDE

FIGURE 9
ROLL BY
800 FT FROM RUNWAY

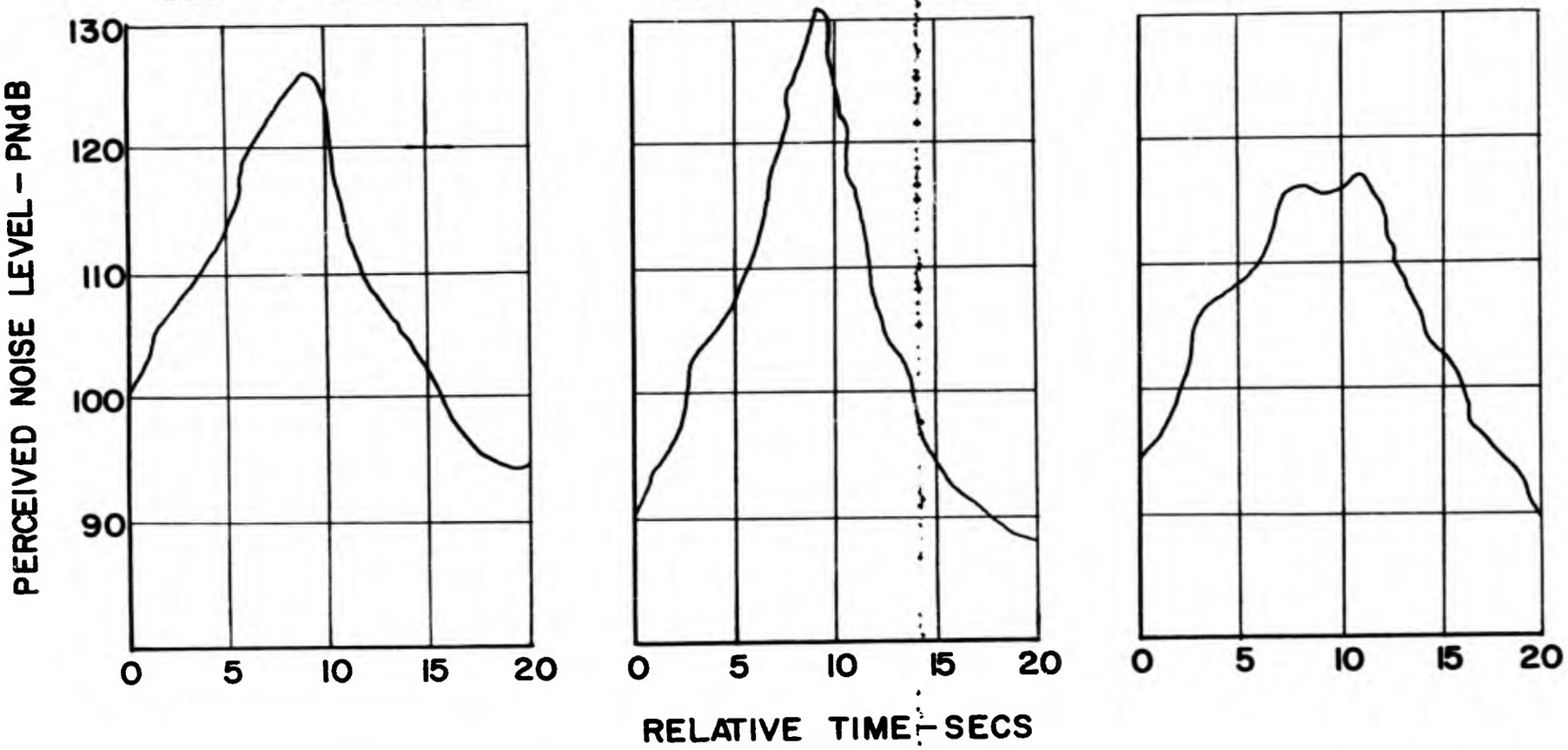

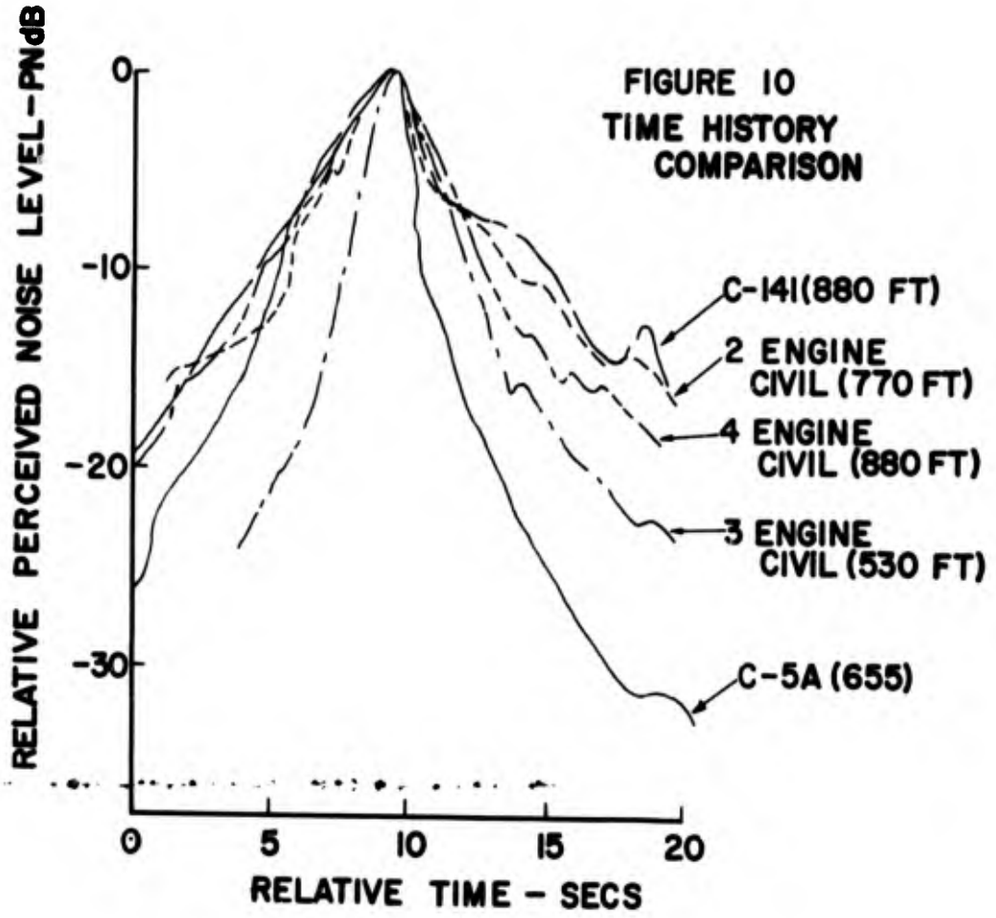

FIGURE 10
TIME HISTORY COMPARISON

PERCEIVED NOISE - "A" WEIGHT COMPARISON

FIGURE 11

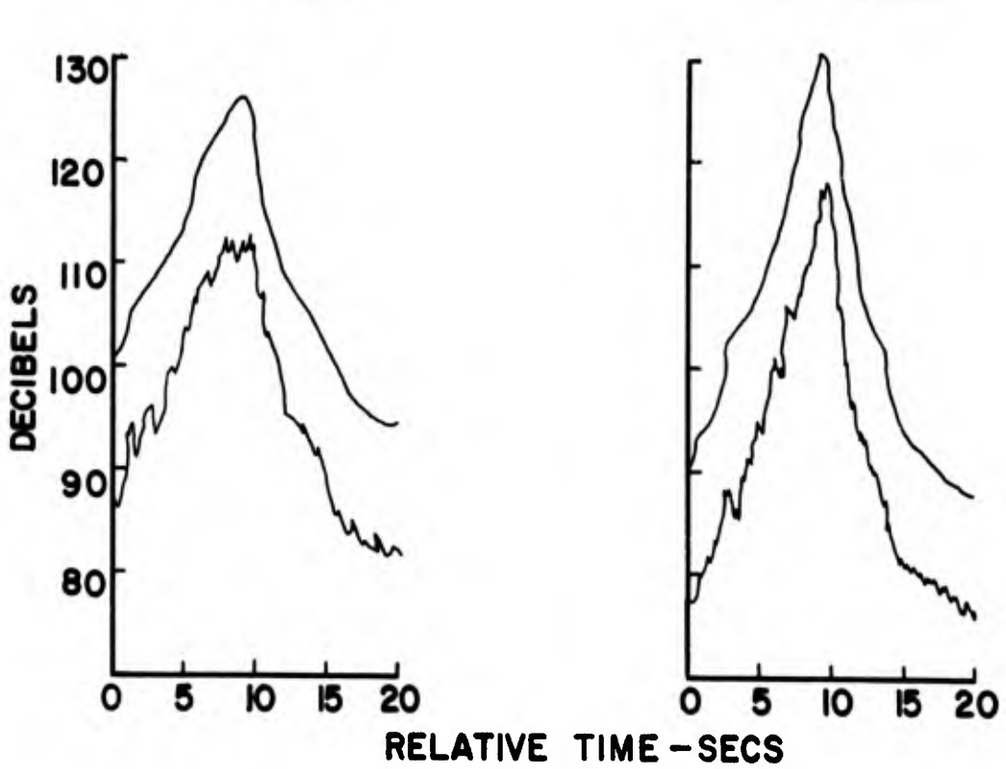

OCTAVE BAND SPECTRUM

FIGURE 12

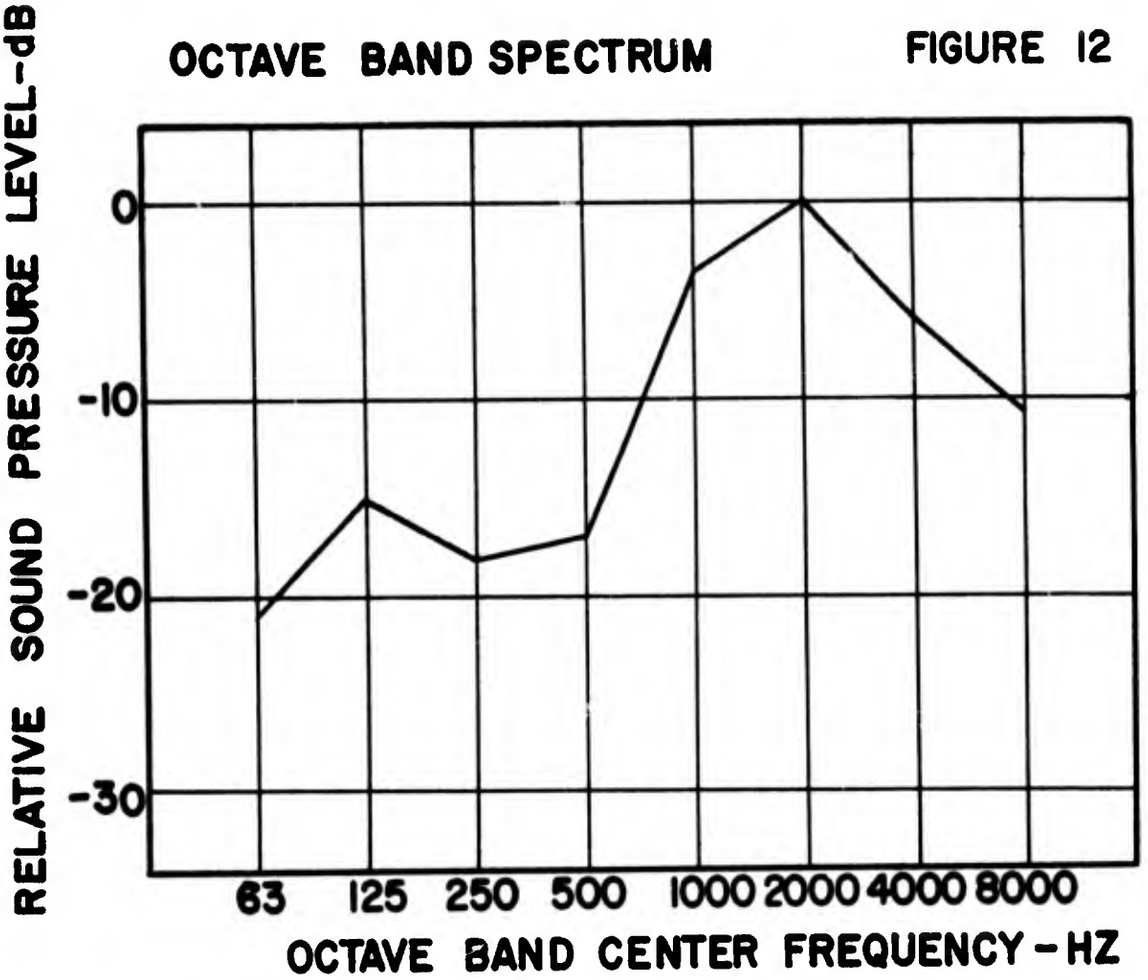

ENGINE QUIETING - NACELLE ACOUSTIC TREATMENT

by

NELSON F. REKOS

HEADQUARTERS
NATIONAL AERONAUTICS AND SPACE ADMINISTRATION
WASHINGTON, D.C., U.S.A.

SUMMARY

This paper describes a major research and development program directed towards reducing the fan noise radiated from the turbofan engines used in current Boeing and McDonnell-Douglas four-engine commercial transports. The reduction in fan noise is expected to be achieved by the modification of the engine nacelles and by the judicious application of acoustically absorptive materials in the fan inlet and discharge ducts. The results of ground tests conducted with full scale acoustically treated nacelles indicate that fan noise reductions on the order of 12 PNdB to 15 PNdB below the noise levels of the current subsonic turbofan engine installations are feasible.

The presentation of this paper will follow the outline shown on Figure 1, beginning with an assessment of the aircraft noise problem followed by a description of the possible solutions to the problem and an outline of the objectives of the National Aeronautics and Space Administration (NASA) Nacelle Acoustic Treatment program. The Nacelle Acoustic Treatment program will then be described beginning with the technology associated with duct-lining materials and nacelle design concepts, followed by a discussion of the application of duct-lining materials to engine nacelles and a presentation of results of full scale ground tests, and flight tests of turbofan engine nacelles. Finally, a brief assessment of the performance penalties of retrofitting current subsonic turbofan transports with acoustically treated nacelles will be noted.

The principal engine noise sources in both turbojet and turbofan engines are illustrated in Figure 2. Jet transports, when they were first introduced into commercial service were plagued by exhaust noise which was extremely difficult to attentuate without seriously compromising engine performance. This is primarily because the bulk of the jet noise is generated some 5 to 20 jet diameters downstream of the exhaust nozzle. Basic studies of jet noise generation indicate that the intensity of jet noise is proportional to the eighth power of the exhaust velocity in the range of the exhaust velocities encountered with present non-afterburning turbojet engines. Although a great deal of research and development time was expended in attempts to solve the jet exhaust noise problem, only very limited success was achieved. It was not until the turbofan engine was introduced that the engine designer more or less accidentally discovered a useful design tool with which he could begin to alleviate jet exhaust noise. In the turbofan process, energy is extracted from the gas generator flow to drive a fan located in front of a turbojet compressor. The energy absorbed by turbine to drive the fan has the effect of reducing the gas generator exhaust velocity and, of course, this results in a lower jet noise output. However, as jet noise decreased with decreasing average jet velocity, it was discovered that fan noise became increasingly more disturbing. Fortunately, fan noise is of a different character from jet noise in that part of the fan noise is concentrated in relatively narrow frequency bands giving rise to discrete tones and a siren-like whine. Unlike the jet noise, fan noise is generated inside the engine nacelle and as a result it is possible to exert control over the noise radiation through the use of acoustic absorbent liners in the fan engine inlet and discharge ducts. Also, it is possible to control some of the noise that is generated in the fan section through design of the fan components.

The National Aeronautics and Space Administration has responded to the aircraft noise problem by initiating two major research and development noise reduction efforts. One program referred to as the Quiet Engine program (managed by the NASA Lewis Research Center), is aimed at the development of the technology required for the design of subsonic aircraft engines, with substantially less noise than engines in current use through engine design. The other program is a Nacelle Acoustic Treatment program aimed at the reduction of fan noise through the use of acoustically absorptive materials in the fan-inlet and fan-discharge ducts of the nacelles of DC-8 and 707 aircraft using the Pratt and Whitney JT3D turbofan engine. This Nacelle Acoustic Treatment program, managed by the NASA Langley Research Center, is the subject of the present paper.

A schematic diagram of the Pratt and Whitney aircraft JT3D turbofan engine which powers the Boeing 707 and McDonnell-Douglas DC-8 four-engine transports is shown in Figure 3. The noise output from each of the noise generating stations within the engine are shown in the sketch for take-off and landing approach conditions. The take-off reference point used is 3 statute miles from brake release, while approach noise is measured 1 statute mile from touchdown (a 3^{o} glide slope approach is used for the approach estimates).

During approach conditions, the maximum noise output, 118 PNdB, is from the fan inlet and discharge ducts. During take-off, maximum noise level is 121 PNdB and it emanates fan discharge duct, and is 4 PNdB higher than the jet exhaust noise during take-off. The jet noise floor, 100 PNdB, occurs during approach conditions.

The difference of 18 PNdB between the noise emissions for landing approach conditions from the fan inlet and discharge ducts and the jet noise, led the NASA to conclude that the JT3D turbofan engine and nacelles could be used to demonstrate the effectiveness of nacelle modifications as a means of reducing fan noise. Therefore, in May 1967, the Nacelle Acoustic Treatment program outlined in Figure 4, was initiated with the award of separate contracts to the McDonnell-Douglas Corporation and to the Boeing Company. The overall objective of these two contracts is to identify turbofan-nacelle modifications capable of reducing aircraft noise during approach conditions without adversely affecting take-off noise or compromising flight safety and still maintain an economically viable airplane.

The approach followed by both contractors was somewhat dictated by the present nacelle designs used in the DC-8 and 707 aircraft. As a result McDonnell-Douglas directed its efforts to acoustically treated inlets and acoustically treated "short" fan discharge ducts (48 inches long) with the goal of 7 to 10 PNdB reduction on approach noise. Boeing directed its initial efforts to investigating acoustically treated "long" fan discharge ducts which are nearly coplanar with the primary nozzle and to the development of sonic or near sonic inlets as a means of reducing noise emanating from the inlet as an alternative to the techniques of absorbing the noise with absorbent materials. The overall objective of the Boeing program was a 15 PNdB reduction in fan noise. However, results obtained during the early part of the McDonnell-Douglas program showed that the use of noise aborbing materials in the fan inlet duct was so effective in attenuating the fan noise emanating from the inlet that the Boeing program was redirected to accomplish the goal of 15 PNdB suppression with a treated inlet in combination with the "long" duct. At the outset of the program the NASA felt that 7 to 10 PNdB was the maximum that could be obtained by acoustic treatment of the inlet and that this inlet would have to be choked to achieve additional fan inlet suppression.

The initial effort of both contractors was focused on the evaluation and selection of acoustically absorbent materials suitable for incorporation in engine nacelles. Three basic lining design concepts, Figure 5, were examined. The narrow band resonator shown at the top consists of a perforated plate bonded to a honeycomb backing chamber. This concept relies on the Helmholtz resonator principle, or air spring. The broadband homogeneous absorber, shown in the middle, consists of a blanket of felt or fiberglass material. Noise is absorbed in the blanket through friction. The broadband resistive resonator, shown at the bottom, consists of a porous layer bonded to a honeycomb backing chamber similar to the concept shown at the top and incorporates the basic principles of the other two.

The noise attenuation characteristics of the lining concepts shown on the previous figure are shown in Figure 6. The peaked solid curve in the top plot shows the sharply tuned resonator effect. The perforated plate concept could provide broader bandwidth of attentuation, as shown by the dotted curve, by the addition of a fine wire screen or by varying the size of the perforations and/or the depth of the honeycomb backing chamber. Although the homogenous absorber blanket concept provides broad bandwidth attentuation (as shown in the middle plot) the materials available such as felt and fiberglass, are not suitable because of their structural brittleness or because of their tendency to absorb or retain fluids. The broadband resistive resonator shown in the bottom plot, is similar to the perforated plate concept except that a porous layer such as felt metal or polyimide material, is used instead of a perforated plate or screen. This last concept (the porous layer and honeycomb) was selected as the lining concept best suited because of its broadband attentuation characteristics and its suitability in an engine environment. The candidate materials examined during the program are listed in Figure 7. In the McDonnell-Douglas design, felt wire fibers were used for the porous surface with a fiber glass honeycomb. Boeing selected a polyimide resin impregnated fiber glass for the porous surface and honeycomb.

Typical results obtained during flow duct tests of the porous surface and honeycomb concept are shown in the next four charts. The peak attenuation, Figure 8, of an acoustic lining configuration varies with airflow velocity in the duct and the flow resistance (Rayls) of the material. As flow velocity is increased, the nominal flow resistance must be adjusted to maintain a high level of attenuation. Therefore, it is necessary to design duct treatment for the flow regime in which it will be used. One of the most important parameters to be considered in the design of acoustic duct linings is that of duct height, Figure 9. Large changes in attenuation can result from variation of duct height or separation between treated surfaces. In the example shown, decreasing the duct height from 12 inches to 6 inches resulted in a decrease of 15 dB in peak attenuation It can be expected, Figure 10, that in a fixed length of duct lining, increasing the area of treated surface will increase the attenuation However, the treatment of a second and opposite side of a duct produces a substantial increase in attenuation tion. The small increase in attenuation shown by treating sides C & D is due to the smaller area of these sides and the greater distance between them. Also for a given duct height, increasing the treated length, Figure 11, increases the attenuation. The initial portion of the treatment is more effective because there are many more acoustic modes at the duct entrance which can be attenuated than for the remainder of the propagating modes which exist further along the duct.

Some of the inlet treatment configurations studied in the nacelle program are shown in Figure 12. The inlet configurations range from a lightbulb type of center body to various combinations of concentric rings, vanes and struts. Each of the concepts shown, results from attempts to maximize the acoustic treatment area. Acoustic treatment is applied to areas shown by the dark bands; the inner

surface of the nacelle shell, both sides of the vanes and rings, and on the outer surface of the inlet center body.

Although the radial strut concepts increased the treated area, it was dropped from consideration early in the program because the wakes from the struts created new noise sources. The lightbulb design provided a substantial area for treatment, about 27 square feet more than the two-ring inlet configuration; however, the lightbulb inlet required an increase in cowl length because of aerodynamic performance considerations with the net result the incremental increase in nacelle weight over the basic untreated nacelle was twice that of the two-ring inlet. The limited available lining area of the retractable lining design and the complex cowl structure limited the usefulness of this concept.

The noise reductions achieved with some of the more promising inlet concepts during full scale tests are shown in Figure 13. The data was taken at 150 feet, at a 60° angle position, from the forward centerline, with a landing power setting. A fan-exhaust noise suppression enclosure was installed so that only the inlet noise would be measured. The results show that the improvement in noise reduction in the critical fundamental blade passing frequency region where intense combination tones are encountered, is quite significant going from the no-ring inlet to the one-ring and then to the two-ring inlet. This improvement is due primarily to the increase in treated area and the favorable height or distance between the treated surfaces. However, the results do not indicate any significant additional attenuation from the increased treated area (27 square feet) of the lightbulb inlet over the two-ring inlet. The lightbulb and two-ring inlets provided noise reductions, in terms of PNdB, of about 12 to 15 PNdB. The noise reduction with the one-ring inlet was about 10 PNdB.

On the basis of these results the ring inlet concept was chosen for further study; the two-ring inlet for the Boeing long discharge duct, and the one-ring inlet for the McDonnell-Douglas short discharge duct nacelle. The attenuation of the fan noise from the two-ring inlet was expected to match the 13 - 16 PNdB of attenuation estimated by Boeing with the long treated fan exhaust duct and the one-ring inlet the 10-12 PNdB attenuation of the short duct.

Schematic diagrams of the two modified test nacelle configurations are shown, Figure 14. The McDonnell-Douglas configuration at the top is designed with a co-annular single ring inlet having a total of 64 square feet of treated inlet area (shown by the heavy lines), and a 48-inch treated fan discharge duct having a total of 70 square feet of treated duct area. The Boeing configuration at the bottom is designed with a two-ring treated inlet (87 square feet of treatment area) and a long treated fan discharge duct having a total of 267 square feet of treated duct area. The treated areas in both designs include the inlet cowl wall, both sides of the ring, the surface of the nose dome, the inside and outside walls of the fan discharge ducts, and both sides of several splitters in the discharge duct. The acoustical performance as determined from ground tests of the original and modified nacelles, measured at 150 feet at 110° from the forward center line is compared in Figure 15, for the approach landing power setting. About 9 - 11 PNdB of suppression was noted. This attenuation indicated that a good match was achieved between the acoustical performance of a one-ring treated inlet and a 48 inch treated fan exhaust duct. Estimates show that if the DC-8 aircraft were to be equipped with nacelles treated in the same manner as the ground test nacelles, the noise reduction objectives of 7 to 10 PNdB during approach conditions would be met.

Ground test results from the Boeing two-ring treated inlet were not available at the time of writing this paper; however, Figure 16, ground test results with the Boeing long treated duct nacelle were obtained without any inlet treatment. The data shown were recorded at 370 feet for the approach landing power setting at 5000 rpm and measured at the 110°. Noise reductions of 9 to 16 PNdB with the treated duct over the existing duct were noted. In view of the success achieved by McDonnell-Douglas with a fully treated ground test nacelle, it is felt that the noise reduction goal of 15 PNdB set for the Boeing 707 aircraft will be met with the two-ring inlet coupled with the long treated discharge duct.

The advantages and disadvantages of incorporating modified nacelles in current four-engine transport aircraft have been estimated and are listed in Figure 17. The expected noise reduction would be approximately 10 and 15 PNdB during landing for the short duct (48 inches) nacelle (DC-8 type) and the long duct nacelle (707 type) respectively. The weight increase is estimated to be 332 pounds for the short duct nacelle and 3360 pounds for the long duct nacelle. The cruise speed would not be affected for either modification and the range penalty is not significant for the DC-8 but the 707 would suffer a range loss of 180 nautical miles in maximum range. It should be noted that the higher weight and range loss for the long duct nacelle is accompanied by a greater noise reduction - all of which is due to the additional acoustic treatment with the Boeing nacelle. These

estimated noise reductions with nacelle modifications were based on the results of ground tests with full-scale engines. Both contractors are proceeding to equip a DC-8 and a 707 aircraft with flight rated nacelles to validate the estimated noise reductions and check performance estimates and operational constraints through a series of flight tests.

In conclusion, although the results from ground tests of the treated nacelles are encouraging, the studies of economic impact of these nacelle modifications on existing aircraft have not yet been completed and the final evaluation of the success of the Nacelle Acoustic Treatment program must await the completion of the flight tests.

ACKNOWLEDGEMENT:

The author is grateful to the assistance given to him by Mr. John G. Lowry, NASA Langley Research Center, Hampton, Virginia, during the preparation of this paper.

ASSESSMENT OF AIRCRAFT NOISE PROBLEM

OBJECTIVES OF THE NACELLE ACOUSTIC TREATMENT PROGRAM

TECHNOLOGY OF DUCT-LINING MATERIALS AND CONCEPTS

APPLICATION OF TECHNOLOGY TO FULL SCALE NACELLES

SUMMARY OF RESULTS

Figure 1 - Introduction to the Nacelle Acoustic Treatment Program

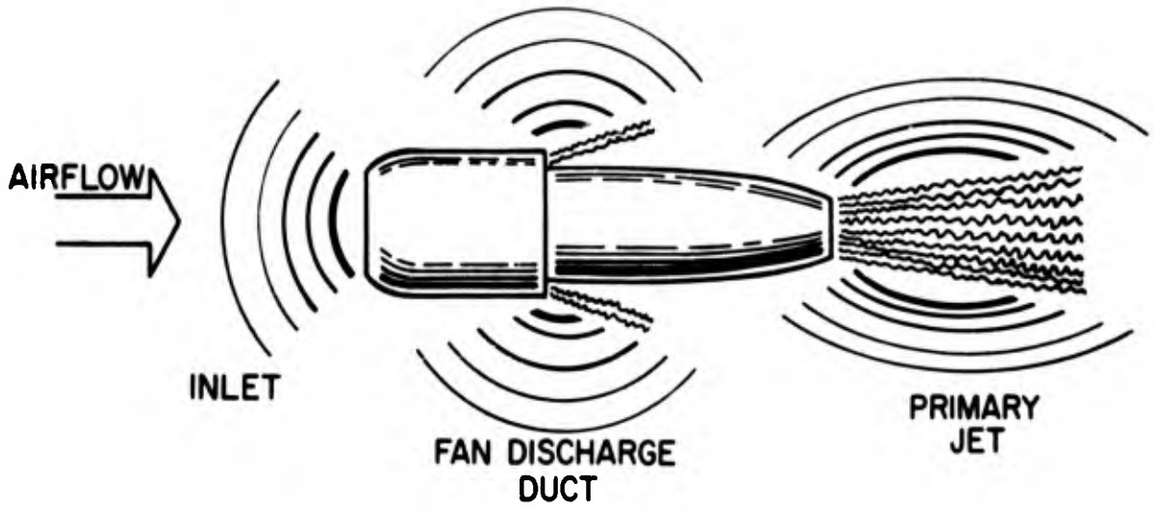

Figure 2 - Engine Noise Sources

BOEING 707/DOUGLAS DC-8

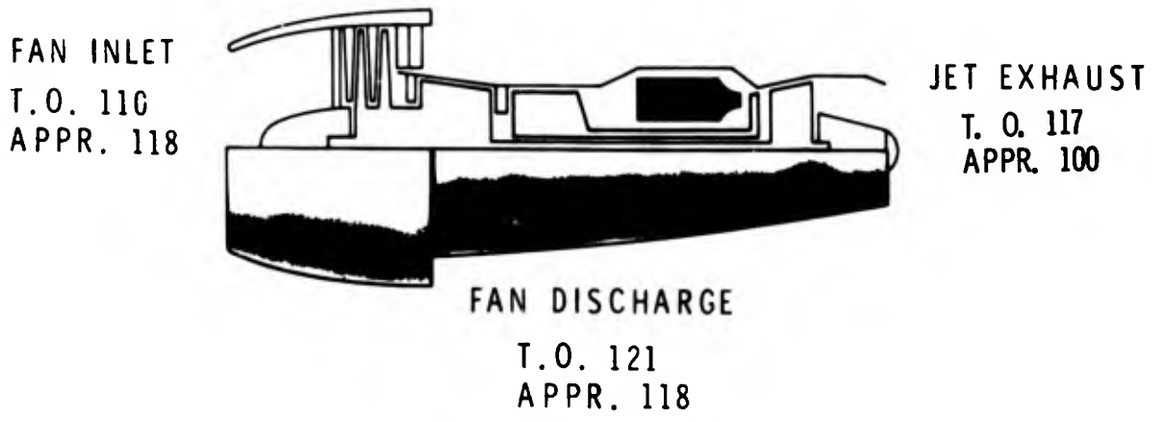

Figure 3 - JT3D Engine

IDENTIFY NACELLE MODIFICATIONS CAPABLE
OF REDUCING LANDING NOISE BY 15 PNdB

EVALUATION OF SUPPRESSION CONCEPT

FLIGHT EVALUATION OF FINAL CONCEPTS

EVALUATION OF ECONOMIC FACTORS

Figure 4 - Nacelle Acoustic Treatment Program Objectives

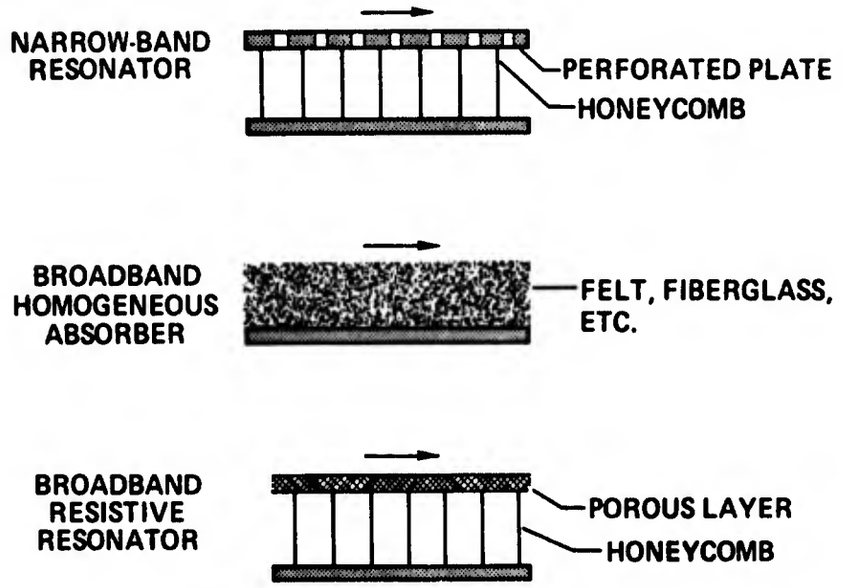

Figure 5 - Acoustic Lining Concepts

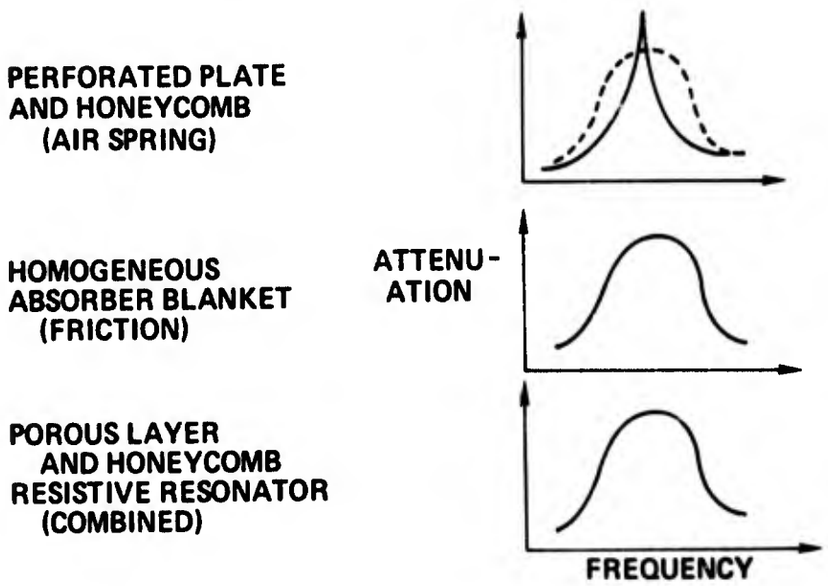

Figure 6 - Lining Mechanisms

POROUS SURFACE MATERIALS

Metallic
- Felted wire fibers - sintered
- Layers of woven-wire screen - sintered
- Sintered powders
- Perforated plate

Nonmetallic
- Layers of woven fiber-glass cloth - resin or rubber impregnated

HONEYCOMB-SUPPORT STRUCTURES

Metallic
- Stainless steel or aluminum - welded or brazed

Nonmetallic
- Heat-resistant phenolic-resin-impregnated fiber-glass cloth (bonded)
- Phenolic-resin-impregnated nylon-coated paper
- Polyimide-resin-impregnated fiber-glass cloth (bonded)

Figure 7 - Candidate Material

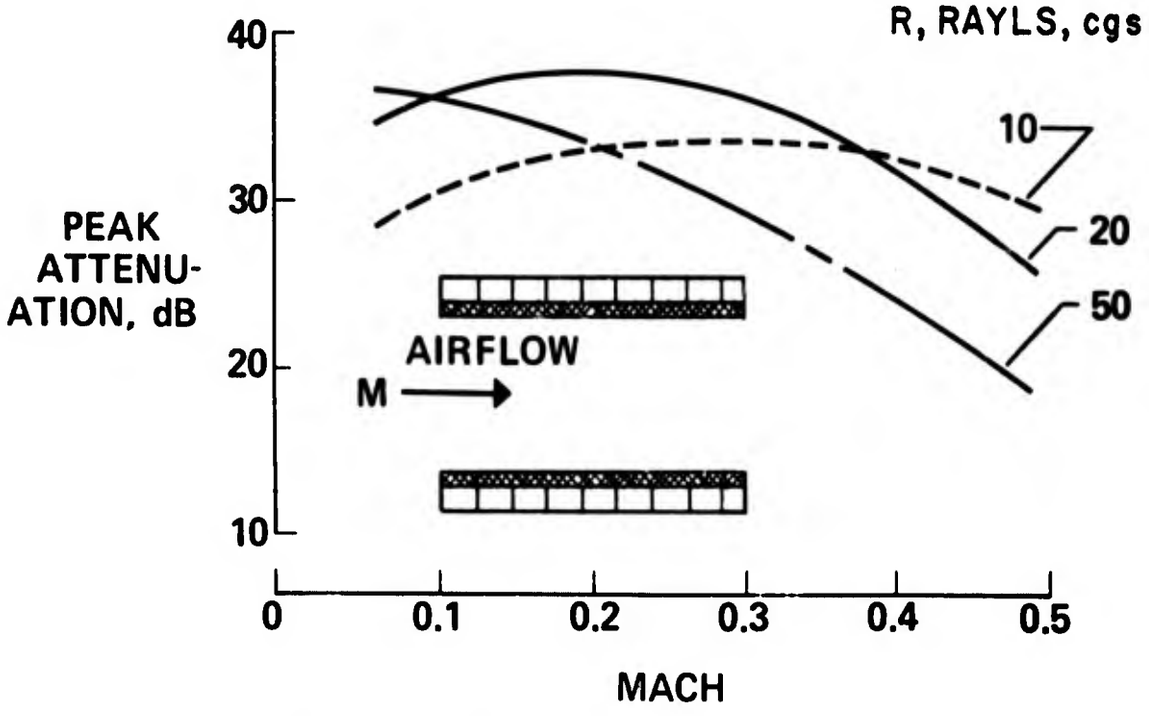

Figure 8 - Effect of Flow Velocity

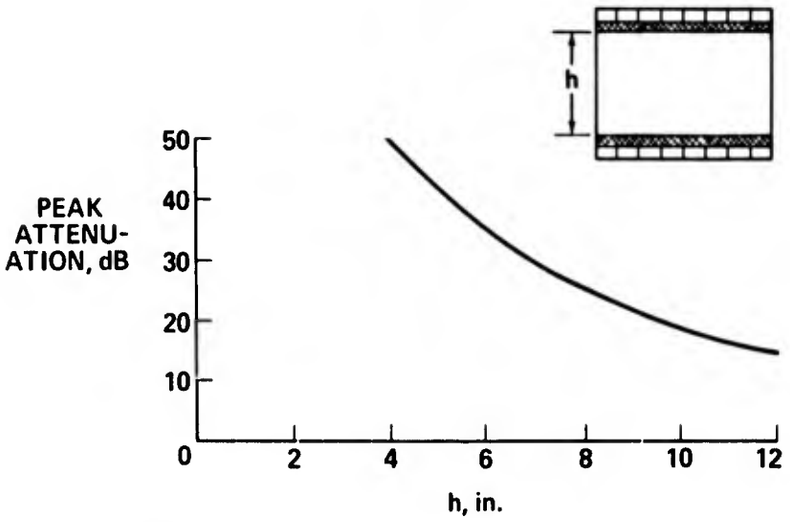

Figure 9 - Effect of Duct Height

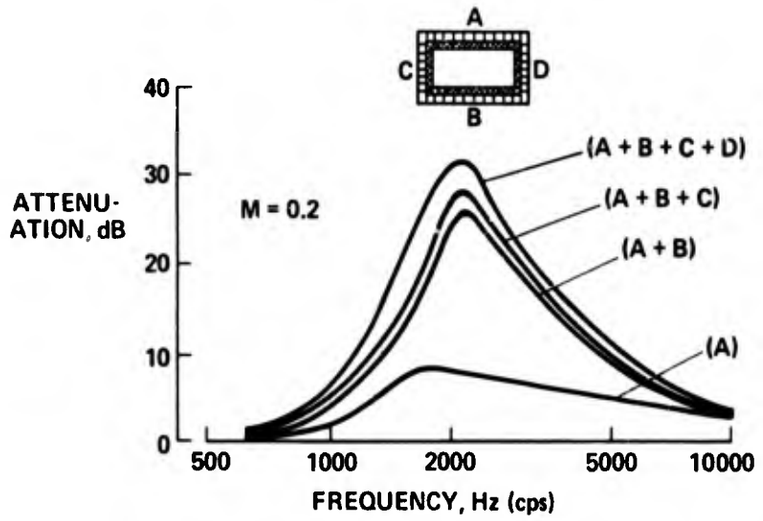

Figure 10 - Effect of Treated Area

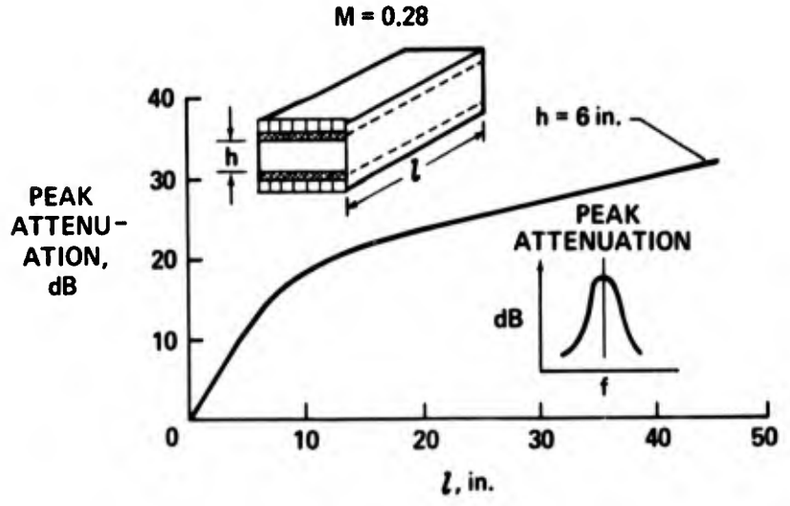

Figure 11 - Effect of Treatment Length

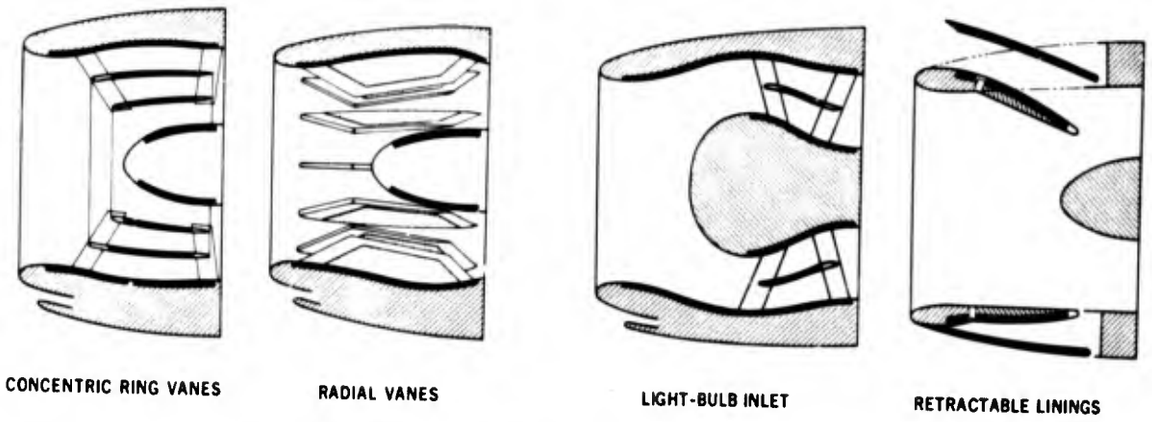

Figure 12 - Inlet Configurations Studied

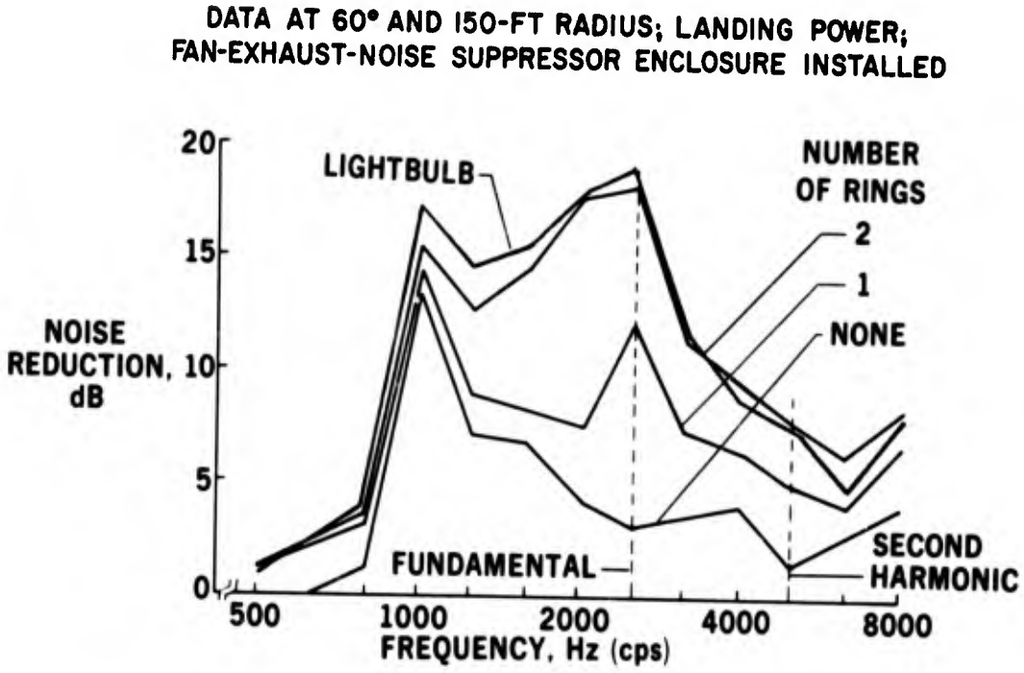

Figure 13 - Summary of Inlet Noise Reductions

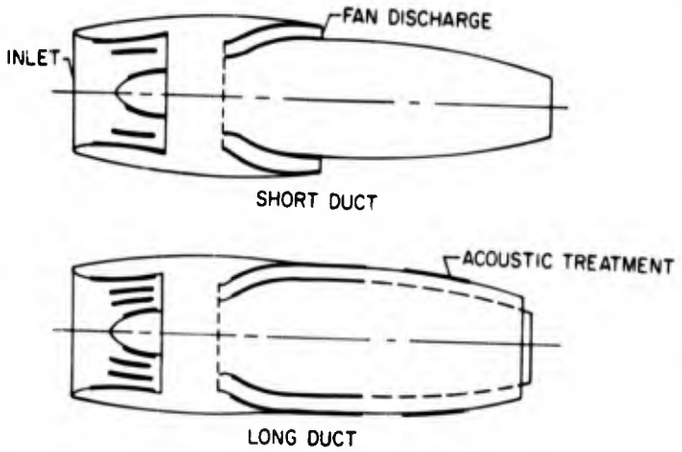

Figure 14 - Schematics of DC-8 and 707 Flight Test Nacelles

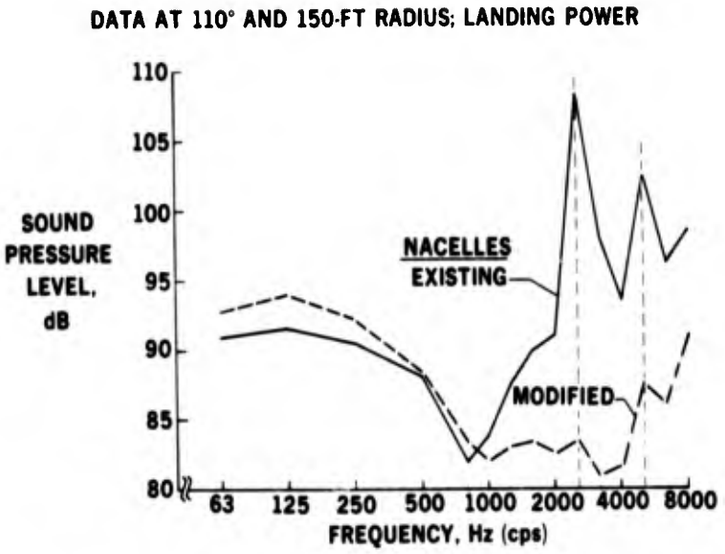

Figure 15 - Noise Levels with DC-8 Treated Nacelle

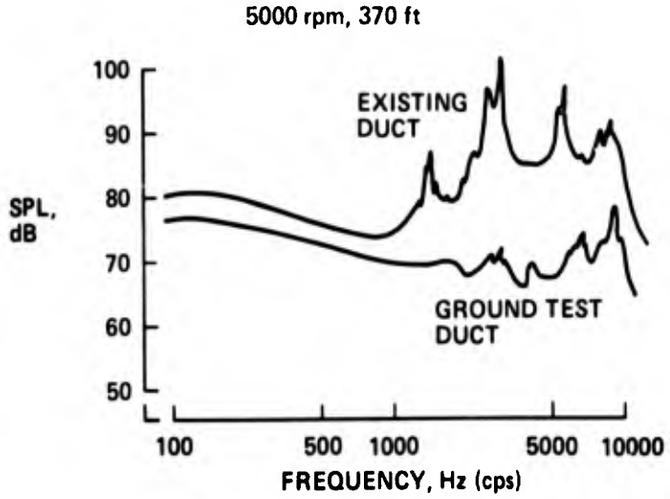

Figure 16 - Noise Levels with 707 Treated Nacelle

	SHORT DUCT NACELLES (DC-8)	LONG DUCT NACELLES (707)
PNdB REDUCTION – LANDING	9 TO 11	13 TO 16
WEIGHT INCREASE PER AIRCRAFT	332 lbs.	3,360 lbs.
CRUISE SPEED CHANGE	0	0
RANGE PENALTY	NOT SIGNIFICANT	180 N. MILES

Figure 17 - Nacelle Acoustic Treatment Program Results

APPENDIX I

DISCUSSIONS

This appendix contains the discussions which followed the presentation of the papers at the Joint FDP/PEP meeting on "Aircraft Engine Noise and Sonic Boom" held at the Institut Franco-Allemand de Recherches de Saint-Louis, 12, rue de l'Industrie, Saint-Louis, France.

These discussions are transcribed from forms completed by the authors and questioners during the meeting and are keyed (by reference number) to the papers contained in this AGARD Conference Proceedings.

Le présent appendice constitue un recueil de discussions qui ont suivi la présentation des exposés à l'occasion de la Réunion tenue conjointement par le Groupe de Travail de la Dynamique des Fluides et le Groupe de Travail de la Propulsion et de l'Energétique concernant le bruit engendré par les avions et les bangs soniques, à l'Institut Franco-Allemand de Recherches de Saint-Louis, 12, rue de l'Industrie, Saint-Louis, France.

Ce recueil de discussions a été transcrit d'après les formulaires remplis respectivement par les auteurs et les questionneurs au cours de la Réunion dont les numéros de référence correspondent à ceux des exposés figurant dans cet Conference Proceedings de l'AGARD.

LIST OF SPEAKERS AND DISCUSSORS

Angell, J.K.	ESSA GRAMAX, Silver Spring, Silver Spring Md., USA
Auriol, A.	I.S.L., Saint-Louis, 68, France
Cox, R.N.	The City University, London, UK
Douwes Dekker, F.E.	Schiphol Airport, Schiphol, Netherlands
Duponchel, J.P.	SNECMA, Centre d'Essais de Villaroche, France
Drell, H.	Lockheed California Cy, Burbank, California, USA
Ferri, A.	New York University, Bronx, New York, USA
Ffowcs-Williams, John E.	Imperial College of Science and Technology, London, UK
Gordon, G.	Bolt, Beranek and Newman Inc., Van Nuys, California, USA
Guiraud, J.P.	ONERA, Châtillon/Bagneux, France
Gruschka, H.D.	University of Tennessee, Tullahoma, Tennessee, USA
Hay, J.	ONERA, Châtillon/Bagneux, France
Hayes, W.D.	Princeton University, Princeton, New Jersey, USA
Hoch, R.	SNECMA, Centre d'Essais de Villaroche, France
Kane, E.J.	Boeing Company, Renton, Washington, USA
Kester, J.D.	Pratt & Whitney Aircraft Division, East Hartford, Conn., USA
Kobrynski, M.	ONERA, Châtillon/Bagneux, France
Lilley, G.M.	University of Southampton, Southampton, UK
de Maistre, A.	Ministère de l'Air, Paris, 15ème, France
Martlew, D.L.	P.L. & N. Department, NGTE, Farnborough, Hants, UK
McPike, A.L.	Douglas Aircraft Co., Longbeach California, USA
Morgan, William B.	General Electric Company, Cincinnati, Ohio, USA
Nixon, C.W.	Wright-Patterson AFB, Ohio, USA
Oswatitsch, K.	DVL - Aachen, Aachen, Germany
Powers, J.O.	Federal Aviation Administr., Washington, USA
Schwartz, I.	NASA Headquarters, Washington, USA
Sears, W.R.	c/o Graduate School of Aerospace Engineering, Cornell University, Ithaca, New York 14850, USA
Seebass, A.R.	Cornell University, Ithaca, New York, USA
Sirignano, W.A.	Guggenheim Laboratories, Princeton, New Jersey, USA
Stuff, R.	DFVLR Institut Aachen, Aachen, Germany
Suciu, S.N.	General Electric Company, Cincinnati, Ohio, USA
Théry, C.	I.S.L., Saint-Louis, 68, France
Thevenin, J.C.	SNECMA, Centre d'Essais de Villaroche, France
Thomas, P.	SNECMA, Centre d'Essais de Villaroche, France
Wanner, J.C.	Serv. de l'Aéronautique /EG, Paris, 15ème, France
Warren, C.H.E.	R.A.E., Farnborough, UK
Webber, C.J.	Rolls Royce, Ltd., Aero Engine Division, Hucknall, Notts, UK
Wecken, F.	I.S.L., Saint-Louis, 68, France
Westley, R.	Structures and Materials Lab., M14, NAE/NRC, Ottawa, Ontario, Canada

Discussion on the Paper
AIRPORT DESIGN AND OPERATION FOR MINIMUM NOISE EXPOSURE
(Paper 3)
presented by
J.O.Powers, USA

A.Ferri

Figure 2 indicates that if people do not accept noise then something can be done about it, and it is up to us to do something. I should like to ask two questions:

(i) Shall we need "police" to enforce the procedures established? Surely not.

(ii) Why does the acceptable noise level vary with weight? Is this due to technical considerations of aircraft design?

J.O.Powers

(i) The FAA does not monitor airport noise at the present time. We feel that our objectives can be accomplished through certification and by operational procedures which are monitored.

(ii) Our noise regulation must be consistent with technical practicability and economic reasonability, which imply a variation of the upper allowable limit with weight. We do, however, expect that each class of aircraft shall make a maximum contribution toward achieving lower noise levels.

H.Drell

I am concerned that the shaded area in Figure 3 shows that present aircraft can be reduced in noise to 101 EPNdB and yet the FAA proposed rule allows maximum noise of 106 EPNdB, say, for a 300,000 lb new aircraft. The public will thus question the validity of the FAA proposed rule and why it is not lower. I question the validity of the 101 EPNdB as being possible on the present aircraft.

J.O.Powers

While the present rule allows maximum noise levels as indicated on the figure, the rule also requires that the noise be reduced as much below that level as is economically viable and technically feasible. Accordingly, within the bounds of safety, the FAA will push for continually reduced noise levels for all aircraft. The question of the validity of 101 EPNdB as a possible noise level for forecast aircraft is contingent on the current NASA acoustic treatment programme, which we consider to be very promising.

C.J.Webber

What are the considerations which led the FAA to prescribe 6% as the climb gradient after take-off which gives minimum noise annoyance,

Such a high gradient gives, in fact, an increase in the maximum perceived level compared with a lower, and equally safe, gradient.

J.O.Powers

In all noise abatement considerations safety is the primary consideration. The choice of the 6% gradient is, however, also considered to minimise the area contained in a given NEF contour and hence hopefully to minimise annoyance. The lower gradient, while reducing the level at the cutback front, tends to carry that lower level to greater distances from the airport, and hence the area in a specific NEF contour is increased. The larger climb gradients tend to increase the noise exposed area by an increase in lateral spread of the noise.

G.M.Lilley

I would like to draw attention to the difficulties in making noise estimates of new aircraft and in noise measurements generally. Even in the case of known noise characteristics from an engine under static conditions it has been shown impossible to predict within, say, about ±7 EPNdB the aircraft noise under the take-off path or on the approach. This is the result of engine-airframe noise interference and the effect of aircraft motion. Thus the difficulty in working towards precise certification limits may prove to be impossible in the future. In the field of noise measurement we note that noise is not a steady measurement when we observe that all noise propagated from an aircraft is distorted by its passage through the atmosphere, and in particular through turbulence. The accurate measurement of the mean noise from an aircraft may involve many flights. I would like to hear how the authors believe these two features of the aircraft noise problem can be dealt with adequately under Noise Certification.

J.O.Powers

The FAA is aware of the difficulties of aircraft noise prediction, particularly from a paper aircraft to an in-flight aircraft. Accordingly our NPRM currently contains an allowance for prediction accuracies. In addition the FAA is currently sponsoring several programmes directed at the improvement of aircraft noise prediction and probably will sponsor such programmes for some years in the future. Any problem of working towards precise certification limits is difficult but I do not believe this to be impossible. The subject of unsteady atmospheric conditions on noise measurements currently is being approached by limiting conditions under which the measurements are made. Inaccuracies do come into the measurements by virtue of inaccuracies in the measurement of atmospheric conditions and the use of these measurements to reduce the data to standard conditions. It is also apparent that a sufficient number of measurements must be taken to have a high degree of statistical confidence in the certificated values.

F.E.Douwes Dekker

The definition of noise *exposure* (NNI,CNR,etc.) presupposes a continuous relationship between annoyance and noise exposure. Such simplicity seems not to exist. In fact annoyance *is aroused* by: frequency of occurrence, peaking factor, duration, spectrum. Annoyance *is eased* by: unavoidability, time of day, economic links. As soon as annoyance is aroused, any aircraft in an approach peak becomes irritating regardless of actual noise *level*. Therefore the operation for minimum noise exposure should not be based only on certification and noise abatement procedures but also on the following factors:

(i) Reduction of *avoidable* noise: training flights, accelerated climbs, stabilised approaches, free turn-outs, minimum overflying altitude.

(ii) Psychological *acceptability* of noise exposure by: financial benefits, economic links with civil aviation, help to move out; reduce protest stimulus, public relations.

(iii) Reduction of *affected areas:* specific noise corridors, strict air traffic control, concentration of noise exposure, minimum number of tracks for approach or take-off, open corridors for night flying and SST-operation. FAA policy seems therefore to be too much limited to economic and political feasibility of restrictions to civil aviation, and not enough to direct reduction of number of complaints.

J.O.Powers

I am inclined to agree with most of your suggestions and will not elaborate on them except to say that the primary consideration when applying noise abatement techniques must necessarily be safety. I do feel that there is a bit of misunderstanding about the NEF concept and the FAA policy. The NEF's, as such, give only an acoustic exposure and do in fact take into account such factors as frequency of occurrence, duration, spectrum, etc. There is no implication of a simple relationship between exposure and annoyance. These relationships are necessarily very complete and are currently under continuing study. The comment on FAA policy is quite an over-simplification and I would prefer to say that we attempt to base our noise abatement policy on the principle of "equity" rather than economic and political expediency.

Discussion on the Paper
HUMAN RESPONSE TO SONIC BOOM
(Paper 5)
presented by
C.W.Nixon, USA

E.J.Kane

The results shown in this paper are based only on "N" wave type signatures. Would the author care to comment on the influence of pressure signature shape on psychoacoustic responses? That is the influence of variations such as occur due to atmospheric variations or those which might be produced by configuration design, such as flat-top waves or signatures with general shock waves.

C.W.Nixon

The question, I believe, concerns the influence of pressure signature variations on psychoacoustic responses, specifically the so-called flat-top waves and those with spikes or peak characteristics. The flat-top waves, with both the positive and negative pressure components flattened, essentially have had their peak over-pressures reduced and, in keeping with what was said earlier, would be more acceptable than an equivalent signature that had not been flattened. If only the positive portion of the signature is flattened, and the negative portion has been unaltered, there would be little difference in subjective judgement of the boom due to the flattening. The presence of a spike or peaks on a sonic boom signature is discussed in the written version of the paper and is shown to essentially increase the peak over-pressure, and consequently the loudness or annoyance. An example is given there which shows an increase in loudness or annoyance of 4 to 8 dB of a sonic boom when a peak component is added to the impulse. If the question refers to the high frequency energy which rides on the N-wave signature as many shock waves (as in a near-field boom) instead of a single spike, this carries greater energy in the audio frequency range and is judged to be louder than the same boom without the multiple shock waves.

It is my understanding that atmospheric effects on signature variations are substantially beyond our control and that aircraft configuration design changes to minimize undesirable components in the shock wave signature are not really feasible at this time.

W.D.Hayes

Does improvement in acceptability resulting from change in wave shape apply only to outdoor subjects or to those inside buildings as well?

C.W.Nixon

A sonic boom experience indoors is less acceptable than the same sonic boom heard outdoors. A change in wave shape or signature of the sonic boom which increases the acceptability of the outdoor boom, i.e. lower overpressure level, absence of any peak components, slower rise time, would also be expected to increase the acceptability of the indoor boom exposure. I can recall no specific data at this time which would allow me to estimate the quantity or amount of change that might be expected. The indoor versus outdoor relationship would remain, with the indoor boom from the changed wave shape still less acceptable than the same outdoor boom with changed wave shape.

J.O.Powers

In reference to Professor Haye's question about the important parameters with respect to structural response I would like to comment that it is probable that total influence is probably dominant. His comment considers the implications of finite rise time signatures and the ability of indoor listeners to derive any benefit from such signatures. Such potential benefit is no doubt related to the structural transfer function of the house. I feel it would be very interesting to measure the indoor pressure variation in response to finite rise time signatures for representative structures and to use them in human response tests, particularly as related to sleep studies.

Discussion on the Paper
TURBOFAN ENGINE NOISE
(Paper 6)
presented by
Colin G. Gordon, USA

J.E.Ffowcs Williams

Could you please comment on the apparent simple source induced sound you reported in an early publication on this problem? Evidently that is no longer found. Could you give an explanation of the conditions governing the present experiments that differ from those in the early tests?

C.G.Gordon

In the paper referred to by Dr Ffowcs Williams (Ref.(a)), the measured data indicated dependence of the radiated sound intensity, from the obstructed jet at low flow velocity, upon the fourth power of flow velocity. This was interpreted in the paper as evidence of aerodynamic monopole radiation from the system. No such evidence (of monopole radiation)

has been observed in the current series of experiments, however. It is a pertinent question to ask "why"?

Monopole radiation requires a net fluctuation of the volume flow across the exit plane of the jet pipe. In the absence of fluctuating volume flow into the system (from the supply compressor) a monopole source can only be generated if the system itself is capable of storing and releasing flow periodically within it. Since compressibility effects in subsonic air are small, then the ability of the system to support monopole radiation will depend strongly upon its geometry. The extent of geometric discontinuity provided in the experiment described in Reference (a) was much more severe than that provided in the current study. It is felt that herein lies the reason for the difference in data.

G.M.Lilley

In Figure 3 you show that the acoustic power output changes from V^6 to V^8 as the speed increases. Have you checked by measurements in the mixing region that the flow is similar with change in jet exit speed? Only if the flow is similar would you expect a law such as V^8 with the index independent of speed change. Thus changes in the power law index will indicate different sources of noise in different speed régimes. Is it not possible that there are changes in the flow in the mixing region with exit speed, arising from changes in the exit boundary layers with Reynolds number, and in the mixing region development that could account for the change from V^6 to V^8 within the speed range of the experiment? This is not to say that lip induced noise is not important, but have you any evidence that this effect was present at the low speeds of your experiment?

C.G.Gordon

Professor Lilley refers to the observed change in velocity exponent for the plain unobstructed jet as the exit velocity is increased. He suggests that the noise tentatively identified as lip noise may, in fact, derive within the free jet and that the change in the velocity exponent may be the result of velocity-dependent changes in the free-jet turbulence.

In the study in our paper we did not measure the extent or form of the turbulence in the free jet. Such measurements are complicated to perform and still harder to interpret. Also, our observations on the unobstructed jet pipe were secondary to the main purpose of this study, which was to examine the noise radiation from pipe located obstructions.

This notwithstanding, we feel that the evidence is fairly firm that the unobstructed pipe in our experiment was dominated at the lowest flow velocities by lip noise. First of all, we have shown in our experiments that a sixth power of velocity can be associated with noise of dipole origin. Ffowcs Williams and others have shown theoretically that the exit lip of a jet pipe forms a source for such dipole sound. Further, the approximate velocity below which lip noise should dominate jet noise has been calculated and this shows good agreement with the transition velocity in our experiments. There seems no reason at the present time to doubt the existence of lip noise or to doubt its dominance over jet noise at low speeds. The weight of evidence in our mind supports the argument presented in this paper.

Reference (a). Ffowcs William, J.E. Gordon, C.G. *Noise of Highly Turbulent Jets at Low Exhaust Speeds.* AIAA Journal, Vol.3, 1965, pp.791-793.

Discussion on the Paper
NOISE ASSOCIATED WITH SHOCK WAVES
(Paper 7)
presented by
D.L.Martlew, UK

J.E.Ffowcs Williams

Why should the onset frequency of a continuous spectrum shock noise be associated with the Powell frequency, which is a discreet frequency prediction?

D.L.Martlew

The frequency at which the broad band noise associated with the shock waves first appears is not directly associated with the frequency of the discrete tones. It appears to be related simply to the rate at which any single disturbance passes the shocks, whereas the oscillation condition requires that disturbances are spread such that a feedback loop can be established.

R.Westley

Could you please amplify on, firstly, the method you used to separate the broad band peak noise from the screech tones and, secondly, the method used to determine the frequency at which the "step-up" of the broad band noise occurs. In research on cold jets, which have more pronounced screech tones, we found it difficult with 1/10 octave filters to separate the two types of noise when the "step-up" occurred near the screech frequency.

D.L.Martlew

The discrete tones were generally sufficiently narrow on the 5% bandwidth spectra that the level of the broad band noise could be inferred from nearby bands with reasonable certainty. Naturally this method is not perfect and some of the scatter in the results may be due to this.

The frequency at which shock-associated broad band noise comes in is not easy to determine. The rise in the spectrum is fairly sudden and the frequency of the peak level was read off instead. This peak frequency is relevant in that it represents that at which most acoustic energy is radiated.

J.O.Powers

The conical plug nozzle appears to produce jet noise reduction and I therefore would like to ask if you have experience with rectangular or two-dimensional plug nozzles and if so what type of noise reduction would be expected?

D.L.Martlew

We have not made noise measurements on rectangular or two-dimensional plug nozzles at NGTE, so I cannot give an answer.

Discussion on the Paper
JET NOISE FROM MOVING AIRCRAFT
(Paper 8)
presented by
J.E.Ffowcs Williams, UK

G.M.Lilley

I was interested to see your results from the water table analogy. Could you tell us what index for the power law was obtained at low jet Mach numbers? If this was V^3, could this be explained as a mass fluctuation?

In the comparison of your formula for jet noise with experiment you show that good agreement is obtained if the convection Mach number is assumed constant. Are there cases where improvement between theory and experiment would be obtained if an acceleration of the source were to be included or, alternatively, if allowance for the variation of convection speed across the field of turbulence were to be included?

J.E.Ffowcs Williams

In answer to your first question, we observe both a V^3 and a V^5 dependence, indicating the presence of both monopole and dipole sources at the nozzle exit.

In answer to your second question, I would think there are cases where the variation of convection speed is important. This is probably so near the shock wave at the end of a cell in a choked jet system. Eddy deceleration would then radiate *bremsstrahlung*. Also there are indications of the increase in eddy convection speed relative to the absolute speed as jet speed is increased. This must also be important.

Discussion on the Paper
DETERMINATION DU CHAMP SONORE PRODUIT PAR L'EVOLUTION DES AVIONS A REACTION
(Paper 9)
presented by
M.Kobrynski, France

J.E.Ffowcs Williams

I should like to comment on the manner in which theoretical models are applied in this subject. A possible approach is to develop strictly the definite consequences of a model and to test it against experiment. If the model fails, the inference is that the correct mechanism has not been covered by the model. This failure can, in fact, teach us a great deal.

A second approach is to start with a model as a near fit to experimental data and to modify the formulae empirically for best fit. Such an approach is obviously very valuable in developing prediction schemes but not so valuable in indicating the correctness of the source model initially postulated.

There appear to be two failures of the model in this paper. The first concerns the choice of a convection factor raised to the power γ, rather than 5/2 as the model predicts. The second is in the spectral shift due to the Doppler factor. Eddies, which are the

assumed sources of sound, travel in the opposite direction to the aircraft so that the Doppler factor assumed in the paper is in the opposite direction to that of the basic model. If this is, in fact, a correct fit to the data there is a very interesting failure of the convected quadrupole model which ought to be studied more closely.

M. Kobrynski

Je souscris bien volontiers à vos considérations de caractère général. Ceci dit, j'ai montré que le modèle théorique, actuellement proposé, devrait être modifié afin d'aboutir à une meilleure correlation avec les données expérimentales; c'est pourquoi j'ai été amené à remplacer l'exposant fixe du facteur de convection par l'exposant variable avec M_v , γ , retenu d'ailleurs uniquement pour les conditions spécifiées au bas de l'équation (32). D'autre part, le facteur Doppler considéré n'intervient pas au sens que vous voulez bien lui attribuer, car je me suis attaché à mettre en évidence (équations (15) et (25)) la modification du spectre acoustique local consécutive au nombre de Mach de vol, le spectre de base étant celui du jet stationnaire.

W. R. Sears

Do I understand correctly that this work is based on modifications of earlier theories than the Ffowcs Williams theory of Paper No.8, and that the newer theory of Paper No.8 could be applied to calculate the same cases for comparison with the same experiments?

(The answer given by Dr Ffowcs-Williams is affirmative but he is not aware of the existence of an adequate body of experimental data.)

M. Kobrynski

Il serait en effet intéressant de procéder aux vérifications expérimentales mentionnées par le Professeur Sears.

Discussion on the Paper
ETUDE DES INTERFERENCE ACOUSTIQUE PAR REFLEXION;
APPLICATION AUX SPECTRES DE PRESSION ACOUSTIQUE DES JETS
(Paper 10)
presented by
P. Thomas, France

W. B. Morgan

The Session Chairman asked what account US engine manufacturers took of the phenomena described in the paper. The reply was that it is necessary to make these corrections particularly for jet noise measurements (low frequency dominant noise source). These corrections are not, however, as important for higher frequencies such as may be dominant for measurements, since correction goes plus and minus frequently in the higher octave bands. The plus and minus corrections tend to balance out.

P. Thomas

Ainsi que je l'ai precisé au dèbut de l'exposé, la mèthode de correction proposée concerne uniquement les analyses spectrales de bruit de jet. Bien que nous n'ayons pas encore abordé le problème des analyses spectrales de bruit de fan, je pense que les remarques de M. Morgan sont intéressantes et je le remercie des précisions qu'il vient d'apporter.

Discussion on the Paper
SONIC BOOM OF BODIES OF REVOLUTION
(Paper 11)
presented by
K.Oswatitsch, Germany

Errata

Equation (7) should read

$$\frac{\partial y}{\partial \eta} = \operatorname{tg}(\alpha + \theta)\,\frac{\partial x}{\partial \eta}; \qquad \frac{\partial y}{\partial \xi} = \operatorname{tg}(-\alpha + \theta)\,\frac{\partial x}{\partial \xi}.$$

Equation (9) should read

$$\frac{\Delta p}{p_0} = \sqrt{(1 - \operatorname{tg}\epsilon \cot \alpha_\infty \cos\beta)}\left(\frac{\Delta p}{p_0}\right)_{\epsilon=0}.$$

Page 11-3, Section 4, Par.1, 12th line:

Figure 4 shows the ratio of the pressure jump Δp in the shock over the local, high dependent static pressure p_0.

Page 11-4, Par.2:

Figure 8 shows R. Stuff's computation of the front and tail shock for a declerated sharp-nosed body of revolution of a thickness ratio $\tau = 0.0488$. The disturbances entering the shock shown in Figure 8 were produced by the body, when it flew at Mach Number 1.5.

Page 11-4, Par.3, second line:

The disturbances forming the bow waves left the body, when it flew at Mach number 1.5.

G.M.Lilley

(a) Is it correct that R.Stuff has extended his calculations from those as presented for propagation in an isothermal atmosphere to those of a more general atmosphere?

(b) In the case of accelerated motion you indicated that it was not possible to find calculations near a point of focus. Could you discuss therefore how it is possible to calculate the strength of the shock waves at all positions as the cusped waves develop, and in particular the strength of the following quasi-vertical waves.

K.Oswatitsch

(a) We are going to extend our calculations from the isothermal atmosphere to a more general atmosphere with a gradient in the speed of sound.

(b) (This replies also to the comment below by Guiraud.)

The method presented does not exclude the point of focus and the rotation is valid in the whole field. The location of the disturbance is determined by integration along the characteristics and shocks are given by overlapping. In order to get an analytical formula for the shock, I assumed for simplicity the flow to be undisturbed on one side of the shock. This assumption leads to wrong results near the point of focus and yields

an integrable singularity at this point. But integrating through this singularity I obtained the shock strength behind the cusp. By excluding the assumption, it would be possible to calculate the shock near the point of focus.

J.P.Guiraud

Je peux peut être apporter une contribution à cette question au passage de la focalisation. La théorie du Professeur Oswatitsch est une théorie linéaire dans le plan des caractéristiques, les phénomènes non linéaires apparaissent dans le retour au plan physique. Or il se trouve que le passage par la focalisation n'échappe pas à cette règle: il est essentiellement linéaire, les effets non linéaires n'intervenant que pour placer les chocs. Compte tenu de ces remarques il ne me paraît pas étonnant que la théorie du Professeur Oswatitsch puisse permettre de prévoir les chocs après leur rebroussement sur la coustique.

K.Oswatitsch

See (b) above.

Discussion on the Paper
FOCALISATION DANS LES ONDES COURTES NON LINEAIRES.
APPLICATION AU BRUIT BALISTIQUE DE FOCALISATION
(Paper 12)
presented by
J.P.Guiraud, France

W.D.Hayes

To obtain the maximum pressure on a caustic, a non-linear theory is needed if a shock is present, because the linear theory gives infinite pressure.

J.P.Guiraud

Je suis d'accord sur ce point. En revanche l'essentiel de l'écoulement peut être obtenu par une théorie linéaire à la différence de ce qui se passe pour l'onde en N hors focalisation.

Discussion on the Paper
REFRACTION ATMOSPHERIQUE ET REFLEXION AU SOL DES BANGS
(Paper 13)
presented by
C. Théry, France

F. Wecken (Remarques concernant la théorie du "superbang")

(i) La Figure 1 montre l'allure d'un rayon sonore au voisinage de la caustique et explique les coordonnées locales x_1, x_3, la distance σ et le rayon de courbure relative R dans le cas général. La Figure 2 se rapporte au cas spécial de la caustique plane dans une atmosphère stratifiée au repos, cas qui d'après Guiraud est équivalent au cas général. Les rayons sonores sont des paraboles. L'angle ϕ est l'angle défini par Théry. La Figure 3 montre le même domaine tel qu'il apparaît à un observateur se deplaçant avec les fronts d'onde comme un écoulement parallèle plan permanent transsonique. Les fronts d'ondes ou lignes de Mach dans l'écoulement non perturbé sont des paraboles sémicubiques; le nombre de Mach augmente linéairement avec x_3. Les grandeurs de perturbation δu_1 etc. dues à l'onde en N modifient M et distordent la limite sonique et les lignes de Mach; la Figure 3 n'en tient pas encore compte, le choc incident étant supposé faible. Le saut $-\Delta M$ provoqué par un choc est identique à la grandeur y de Théry. Les formules suivantes indiquent la variation de l'intensité d'un choc faible suivant l'approximation acoustique d'après Théry (1) en atmosphère isobare et en atmosphère arbitrairement stratifiée, au voisinage de la caustique ($\phi \ll 1$); les lois de puissance correspondantes (2) en fonction de σ et de x_3 sont également indiquées. La constante sans dimension k a un sens physique simple (3) dans le cas isobare, mais elle est généralement une caractéristique du phénomène. Il est cependant plus aisé d'utiliser la grandeur η proportionnelle à k d'après (4) qui par la suite sera maintenue comme seule caractéristique essentielle sans dimension de la focalisation de chocs. Avec η la loi acoustique de l'intensité près de la caustique (1) (2) prend la forme (5). Au voisinage immédiat du point de focalisation cependant (marqué dans la Figure 3 par un rectangle étroit) l'approximation acoustique tombe en défaut, et le calcul de Théry se termine, à l'instant où la limite sonique est atteinte derrière le choc, avec l'intensité critique (6). La même formule indique la distance critique de la caustique. La formule (7) pour l'intensité de focalisation (d'après Guiraud, 1965) présente une analogie étroite avec (6) si l'on utilise la notation de Théry soit y. Elle comprend une constante universelle purement mathématique mais non connue numériquement, dont nous parlerons plus tard.

(ii) La Figure 4 montre le petit rectangle de la Figure 3 agrandi, et à côté figure (d'après Guiraud) une transformation normalisante (8) appliquant le plan x_1, x_3, d'une façon nondimensionnelle et affine sur le plan ξ, ζ (Fig. 5) et dépendant essentiellement de η. Dans les nouvelles coordonnées ξ, ζ, on obtient pour la nouvelle grandeur de perturbation U l'équation aux dérivées partielles (10) non linéaire avec la condition aux limites à l'infini (11). On cherche une solution avec des lignes de discontinuité (chocs); pour ces dernières la condition (12) doit être remplie; $\bar{U}$ est la valeur moyenne des valeurs U de part et d'autre de la discontinuité. (13) détermine l'intensité et la position du choc incident. Nous ne considérons qu'un seul choc isolé et devons pour cela soumettre la longueur l de l'onde de pression à une condition (9) qui en général est suffisamment remplie. La grandeur normalisée de perturbation $U = U(\xi,\zeta)$ est définie par (10) à (13) comme fonction universelle purement mathématique. L'état non perturbé $U = 0$ remplit (10) à (12) mais non (13). U est borné mais non $\ll 1$ dans un domaine fini; U ne peut donc pas être traité comme perturbation au sens usuel du mot. L'allure exacte des chocs n'est pas connue; (13) indique simplement le comportement asymptotique. Il n'est pas possible à première vue de préciser si la perturbation réflechie (Fig. 5) est également un choc. La limite sonique n'est plus la ligne $\xi = 0$. Il n'existe plus de point de focalisation ($x_1 = x_3 = 0$) mais plutôt un champ de focalisation. Il n'existe pas de domaine non perturbé devant le choc incident. La variation de $U(\xi,\zeta)$ ne peut guère être déterminée autrement que par intégration numérique de (10). Alors seulement la position et la valeur de U_{max} et de ΔU_{max} peuvent être indiquées

et l'on pourrait dans (7) la valeur constante de Guiraud déterminer la limite sonique et les caractéristiques qui sont données par (14).

(iii) (15) montre comment on parvient de (10) à l'équation bien connue du potentiel transsonique par une transformation simple. Les méthodes théoriques des écoulements transsoniques sont donc applicables en principe. En particulier on peut obtenir l'équation de Tricomi par une transformation de Legendre en partant de l'équation du potentiel mais ceci ne présente pas une grande utilité lorsque l'on est en présence de chocs. Par contre une linéarisation de (10) donne directement l'équation de Tricomi (16). Mais c'est seulement avec la condition indiquée que le membre non linéaire de (10) peut être négligé, et cette condition n'est certainement pas remplie dans toute l'étendue du plan. Maintenant nous écrivons u au lieu de U du fait qu'il s'agit d'une fonction différente. Guiraud a résolu en 1965 l'équation de Tricomi avec les conditions (11), (13) par une formule homogène (17). La solution satisfait (13) non seulement de façon asymptotique pour $\xi \to \infty$ mais rigoureusement jusqu'à $\xi = 0$; ici on a donc $\Delta u \to \infty$. Une singularité logarithmique (18) apparaît comme onde réfléchie; le long de cette courbe u a des valeurs arbitrairement élevées. Ici au moins la condition dans (16) est fortement violée; la linéarisation est inadmissible et la solution (17) inutilisable comme approximation pour U dans le domaine correspondant (hachuré dans la Figure 6). Néanmoins la solution de Tricomi donne quelques renseignements généraux. Les caractéristiques, qui peuvent en même temps être des chocs, sont des paraboles semicubiques exactes (19). Le long de celles-ci des perturbations se propagent dans le domaine hyperbolique ($\zeta > 0$). La perturbation réfléchie doit satisfaire à la même loi de puissance que l'onde incidente (13). En outre on peut évaluer dans le plan entier l'ordre de grandeur de U par (20), la perturbation de la pression donc par (21). Vers le bas (pour $x_3 \to -\infty$), (21) n'est valable que pour le choc isolé; la perturbation provenant d'une onde en N décroit beaucoup plus rapidement par suite d'une interférence des phases de surpression et de sous-pression.

(iv) Le paradoxe de la singularité logarithmique apparaissant lors de la réflexion d'un choc faible sur la limite sonique causé par une linéarisation inadmissible a déjà été discuté en 1947 dans cet Institut[1] lors d'un problème beaucoup plus simple, à savoir la réflexion totale acoustique sur une surface séparatrice de deux milieux. Le cas linéaire peut être décrit mathématiquement par l'équation (22) qui a été étudiée par des auteurs russes[2] et qui se réduit dans le demi-plan supérieur à l'équation ordinaire des ondes dans le demi-plan inférieur à l'équation de Laplace. La Figure 7 montre des familles de caractéristiques correspondant à (22).

(v) Si l'onde réfléchie présentait à l'endroit à (Fig.8) une pointe aigüe pour U (Fig.9a) suivant la singularité logarithmique, une distorsion affine, production d'un choc et dégradation de la pointe suivrait immédiatement en aval à cause de la propagation non linéaire (en b, Fig.8 et 9b). Dans la Figure 8 on a schématisé chocs, incidents et réfléchis ainsi que les caractéristiques. En outre la déformation de la limite sonique est essentielle pour le comportement de la solution $U(\xi,\zeta)$. D'après Théry l'intensité du choc augmente lorsque l'on s'approche de la caustique jusqu'au point critique, où on a $M = 1$ derrière le choc. La limite sonique subit donc un saut et présente l'allure indiquée par la Figure 10. Il est vrai que deux hypothèses de Théry ne sont pas remplies exactement, à savoir l'hypothèse de l'état non perturbé devant de choc et la condition de Whitham derrière le choc. Son résultat qualitatif serait malgré tout exact. Or il n'est pas clair, si au point critique C un choc réfléchi prend naissance immédiatement ou si celui-ci se forme par la suite. En tout cas l'intensité du choc incident doit diminuer de C vers le bas et disparaître d'une façon continue à la limite sonique. Le saut de pression maximal doit se trouver au voisinage immédiat de C. Il y a lieu de supposer qu'un point triple se forme (Fig.11) et que le choc réfléchi n'est pas plus intense que le choc incident. Dans ce cas on aurait encore $M > 1$ en T derrière le choc incident, le point critique ne serait donc pas encore atteint. Le saut de pression maximal serait représenté par le choc de Mach tout

---

Référence 1. Rapport LRSL – 29/47.

Référence 2. Bizadse, W.A. *Zum Problem der Gleichungen vom gemischten Typus.* VEB Verlag der Wissenschaften, Berlin, 1957.

près, au-dessous de T, avec l'intensité du choc incident étant presque doublée. Ainsi ont été obtenus les résultats indiqués.

(vi) Les considérations qualitatives ci-dessus masquent le défaut d'un calcul rigoureux de $U(\xi,\zeta)$. Ce dernier serait en principe possible sur un ordinateur assez puissant le mieux étant, sans doute, de procéder à l'intégration des équations non-stationnaires. En ajoutant une variable temporelle le problème mixte est, comme on sait, rendu purement hyperbolique. En raison des chocs, dont l'emplacement n'est pas connu on utilisera la viscosité artificielle introduite par von Neumann et Richtmeyer.

Fig. 1

$$\frac{1}{R} = \frac{1}{R_{\mathcal{R}}} - \frac{1}{R_{\mathcal{C}}} \qquad \left(\frac{1}{R_{\mathcal{R}}}, \frac{1}{R_{\mathcal{C}}} \gtrless 0\right)$$

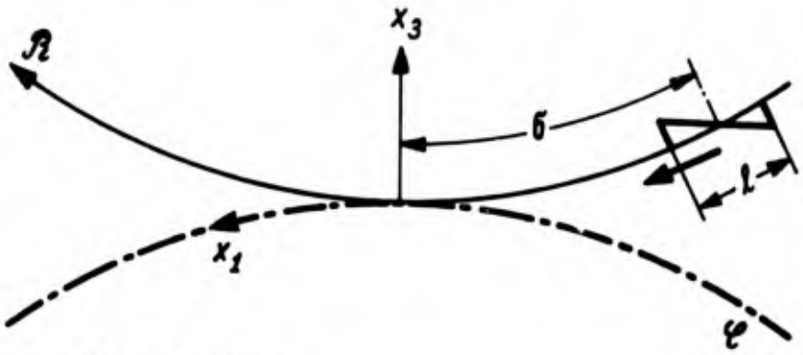

Rayon sonore

$$\mathcal{R} : x_3 = \frac{x_1^2}{2R}$$

Caustique

$$\mathcal{C} : x_3 = 0$$

Fig. 2

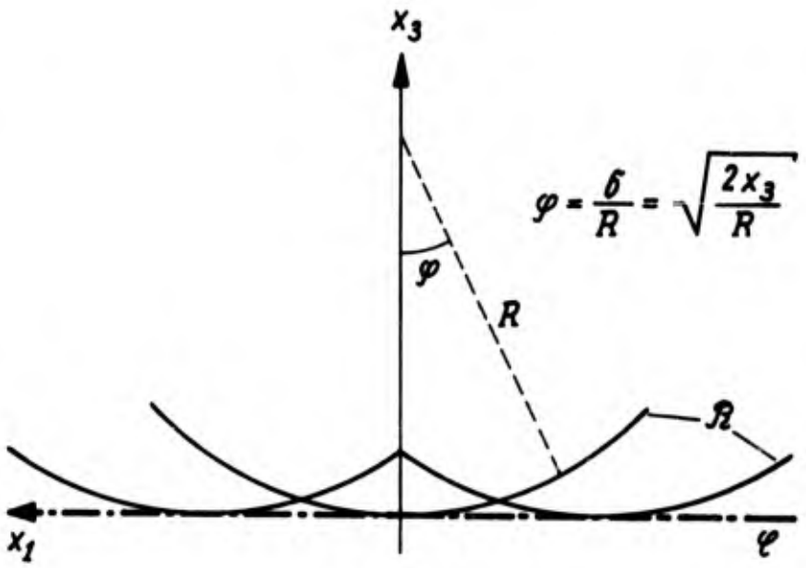

$$\mathcal{R} : \frac{x_1}{R} = \pm\sqrt{\frac{2x_3}{R}} + C^{te}$$

Fig. 3

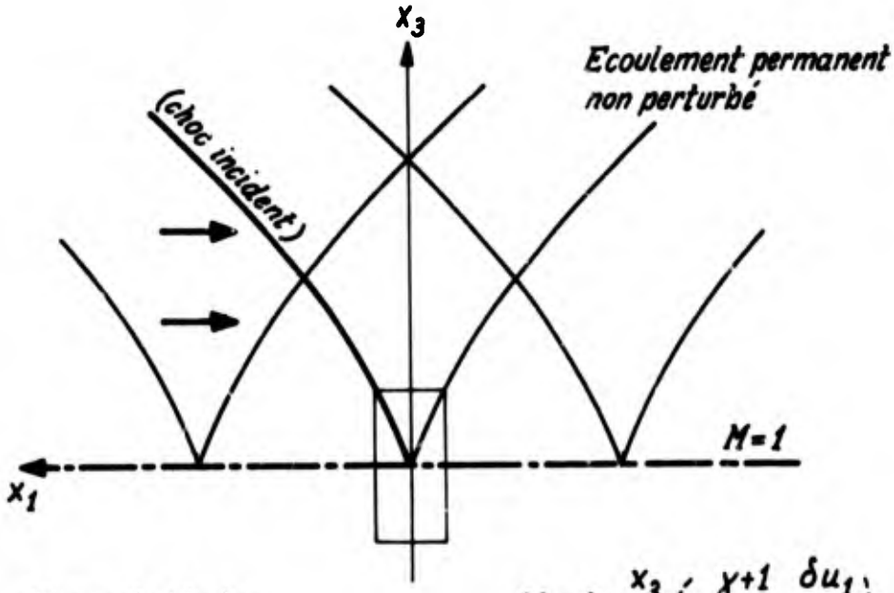

lignes de Mach

$$\frac{x_1}{R} = \pm \frac{1}{3}\left(\frac{2x_3}{R}\right)^{3/2} + C^{te}$$

$$M = 1 + \frac{x_3}{R}\left(-\frac{\gamma+1}{2}\frac{\delta u_1}{a_0}\right)$$

$$-\delta M = \frac{\gamma+1}{2}\frac{\delta u_1}{a_0} = \frac{\gamma+1}{2\gamma}\frac{\delta p}{p_0} \; (= y)$$

(1) $$\frac{\Delta p}{p_0} \underset{(ac.)}{=} \frac{k}{\sqrt{\sin 2\varphi}} \quad (p_0 = C^{te}) = \frac{k}{\sqrt{2\varphi}} \quad (\varphi \ll 1)$$

(2) $$\frac{\Delta p}{p_0} \sim \sigma^{-\frac{1}{2}} \sim x_3^{-\frac{1}{4}}$$

(3) $$k \hat{=} \left(\frac{\Delta p}{p_0}\right)_{min} \quad (\ll 1)$$

(4) $$\eta = \frac{\gamma+1}{\gamma\sqrt{2}}\, k$$

(5) $$y \underset{(ac.)}{=} \frac{\eta}{2\sqrt{\varphi}} \quad (\ll 1)$$

(6) $$y_{cr} = \frac{x_{3,cr}}{R} = \frac{1}{2}\left(\frac{25}{18}\right)^{3/5} \cdot \eta^{4/5}$$

(7) $$y^* = C^{te} \cdot \eta^{4/5}$$

Fig. 4

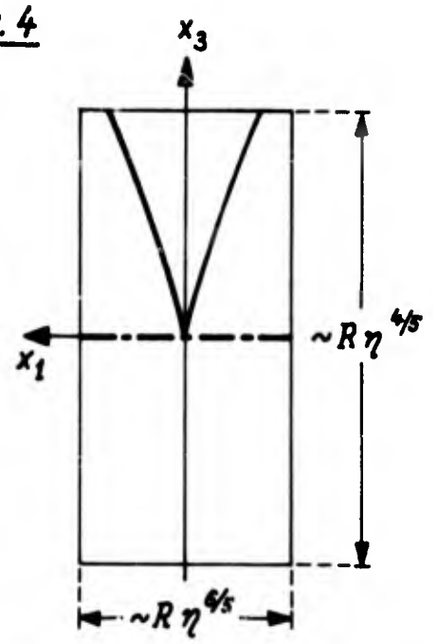

$$\text{(8)}\quad \begin{cases} \dfrac{x_1}{R} = 2^{-4/5}\eta^{6/5}\xi \\ \dfrac{x_3}{R} = 2^{-13/15}\eta^{4/5}\zeta \\ \dfrac{\gamma+1}{2}\dfrac{\delta u_1}{a_0} = 2^{-13/15}\eta^{4/5}U \end{cases}$$

longueur d'onde

$$\text{(9)}\quad \ell \gg R\eta^{6/5}$$

(choc isolé)

$$\text{(10)}\quad \frac{\partial^2 U}{\partial \zeta^2} - \frac{\partial}{\partial \xi}\left[(\zeta - U)\frac{\partial U}{\partial \xi}\right] = 0$$

$$\text{(11)}\quad U \to 0 \text{ pour } |\xi| + |\zeta| \to \infty$$

$$\text{(12)}\quad \left(\frac{d\xi}{d\zeta}\right)_{choc} = \pm\sqrt{\zeta - \bar{U}}$$

Fig. 5

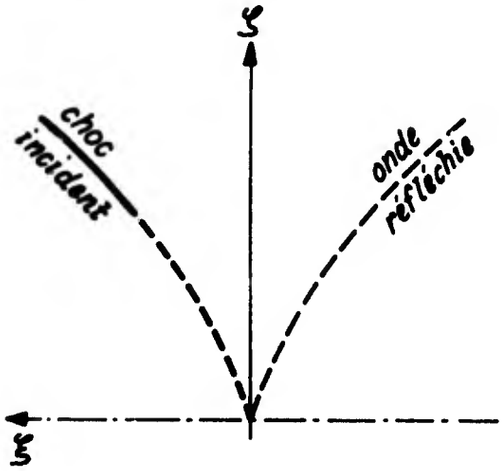

choc incident :

$$\text{(13)}\quad \begin{cases} \Delta U \approx 2^{-1/6}\zeta^{-1/4} \\ \xi \approx \dfrac{2}{3}\zeta^{3/2} \\ (\zeta \to \infty) \end{cases}$$

(14) $$\begin{cases} M \gtrless 1 \Longleftrightarrow \varsigma - U \gtrless 0 \\ \left(\frac{d\xi}{d\varsigma}\right)_{car.} = \pm\sqrt{\varsigma - U} \end{cases}$$

(15) $$\varsigma - U = \frac{\partial \psi}{\partial \xi} \Rightarrow \psi_{\varsigma\varsigma} - \psi_\xi \psi_{\xi\xi} = 0 \Rightarrow \text{Tricomi}$$

(16) $$\begin{cases} \text{linéarisation} : |U| \ll |\varsigma| \ , \ U \approx u \ , \\ u_{\varsigma\varsigma} - \varsigma u_{\xi\xi} = 0 \ (\text{Tricomi}) \end{cases}$$

(17) $$u(\xi,\varsigma) = |\varsigma|^{-1/4} \phi\left(\xi\,|\varsigma|^{-3/2}, \ \operatorname{sgn}\varsigma\right)$$

(18) $$\phi \sim \ln \frac{1}{\left|\xi\,\varsigma^{-3/2} + \frac{2}{3}\right|} \quad \left(\xi\,\varsigma^{-3/2} \approx -\frac{2}{3}\right) \quad \text{(paradoxe !)}$$

caractéristiques , chocs :

(19) $$\xi = \pm\frac{2}{3}\varsigma^{3/2} + C^{te}$$

Fig. 6

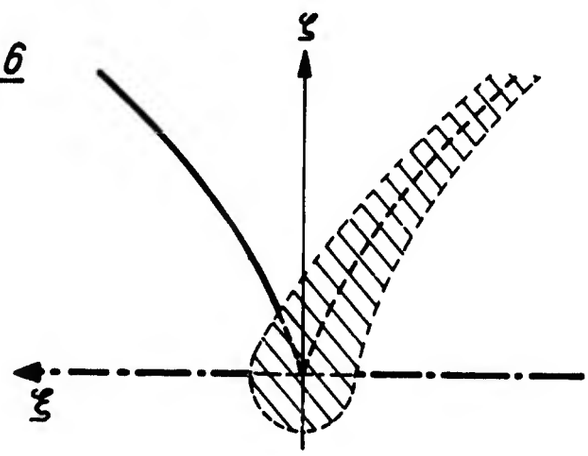

(20) $$U \lesssim \frac{1}{1 + |\xi|^{1/6} + |\varsigma|^{1/4}}$$

(21) $$\frac{\delta p}{p_0} \lesssim \frac{\eta}{\eta^{1/5} + \left|\frac{x_1}{R}\right|^{1/6} + \left|\frac{x_3}{R}\right|^{1/4}}$$

Fig. 7

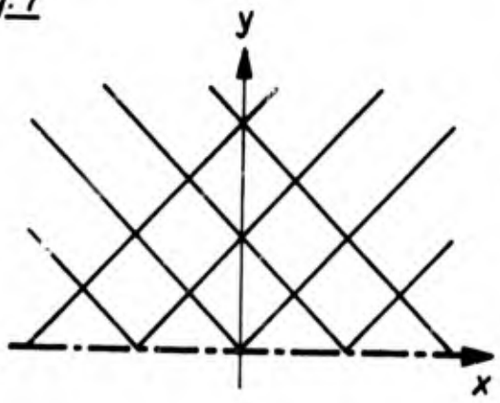

(22) $u_{yy} - \operatorname{sgn} y \cdot u_{xx} = 0$

Bizadse 1953

Fig. 8

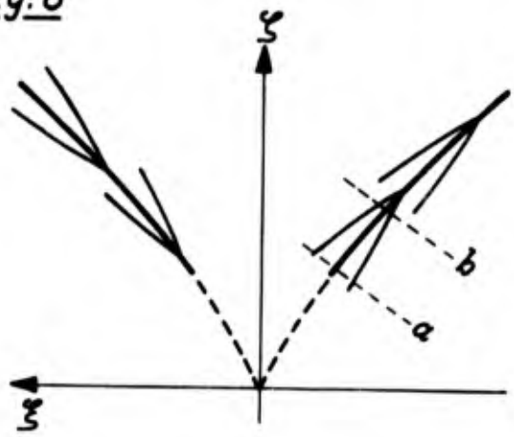

Fig. 9

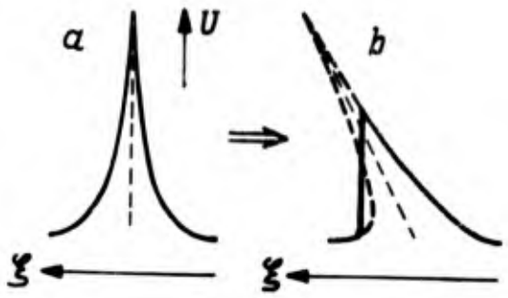

Fig. 10

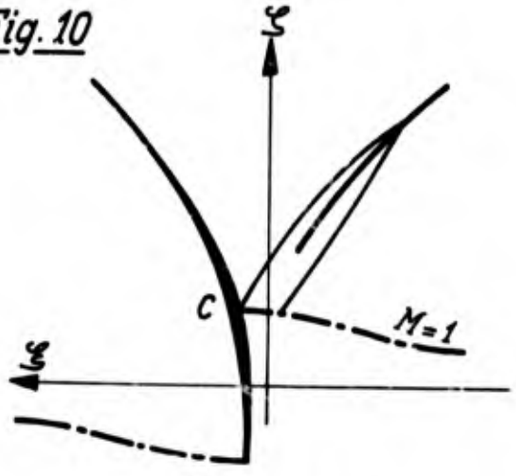

$\Delta p_{max} \lesssim \Delta p_{cr}$

Fig. 11

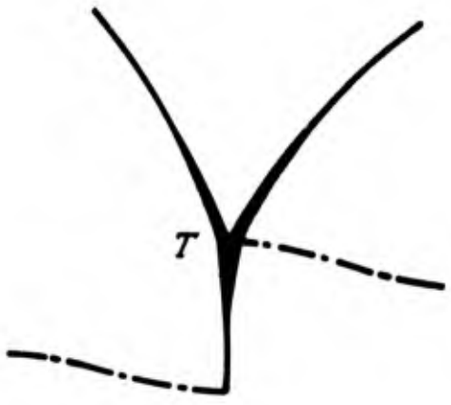

$\Delta p_{max} \lesssim 2\Delta p_{cr}$

A. de Maistre

M. Théry a fait allusion à des distorsions prévisibles sur la forme de l'onde au voisinage de la caustique. Est-il possible d'avoir des précisions sur la forme de ces distorsions?

C. Théry

En ce qui concerne les distorsions dues à la réfraction, il est à noter que la forme du signal réfracté ne varie que peu au cours de la réfraction dans le domaine accessible au calcul. On note cependant une légère tendance à la formation d'un pic de pression immédiatement derrière le choc avant à mesure que l'on se rapproche de la zone de focalisation. Cela est peu accentué mais le calcul du signal complet s'arrête assez loin du point critique, la zone accessible au calcul étant limitée à la caractéristique remontante issue du point critique. Si il y a déformation prononcée du signal, c'est en-dessous de cette zone qu'elle se produit. Une autre cause possible de distorsion du signal perçu peut être due à la réflexion au sol. L'une des diapositives projetées, l'analyse du phénomène, montre que dans les cas instationnaires l'effet du renforcement d'intensité dû à la réflexion est surtout sensible au pied de l'onde et c'est à cette cause possible de distorsion qu'il a été fait allusion au cours de l'exposé.

W. D. Hayes

Y a-t-il des indications à propos des erreurs qui se trouvent dans cette méthode approximative?

C. Théry

La méthode qui conduit à l'obtention d'une relation différentielle décrivant le comportement d'un choc au cours de sa réfraction admet l'existence d'une relation caractéristique immédiatement derrière le choc. Elle est donc effectivement approchée. Mais la comparaison entre ce que fournit cette méthode approchée et le calcul complet (numériquement précis) utilisant les deux systèmes de caractéristiques (Fig.1b et Fig.6) montre que cette approximation est excellente. Cela dans le cas bidimensionnel. Pour ce qui concerne le phénomène tridimensionnel (ou bidimensionnel de symétrie de révolution) le calcul (complet) mené fournit des résultats qui ne diffèrent pas qualitativement et peu quantitativement de ceux obtenus en bidimensionnel. Les formules de comportement asymptotique et de similitude se retrouvent être vérifiées tout au moins si l'on prend soin de tenir compte de l'effet d'expansion tridimensionnel. La méthode basée sur les propriétés caractéristiques ne permet pas effectivement d'atteindre le point où l'écoulement devant le choc devient sonique mais en ce point le choc est nécessairement evanescent. Cela ne paraît donc pas très grave. Le calcul s'arrête à l'altitude critique (écoulement sonique derrière le choc) très voisine en fait de l'altitude sonique. Dans la région comprise entre ces altitudes on en est réduit à une description un peu hypothétique de ce qui se passe: existence du choc réfléchi sur la caustique dont le point triple se situerait en fait un peu au-dessus du point critique (configuration en Y) ou existence d'un faisceau de compression qui ne se fondrait en un véritable choc réfléchi qu'à une certaine distance du choc incident ainsi que Mr Wecken l'a indiqué dans son intervention (Figs.10 et 11). Par suite les surpressions critiques que nous avons calculées ne devraient constituer qu'une borne inférieure de la surpression maximale de focalisation mais une borne qui devrait en être très proche. Il est également certain que la méthode utilisée ne tient aucun compte de l'existence d'un champ de perturbations possible en avant du front de l'onde. Or ce champ existe dans le cas de focalisation en palier accéléré et aussi dans le cas de focalisation en altitude à vitesse constante. Pour rendre le procédé utilisé satisfaisant il faut supprimer la connexion qui existe de part et d'autre de l'onde par l'intermédiaire de la zone d'écoulement subsonique, donc placer la réflexion au sol à l'altitude sonique par

exemple, sinon à une altitude telle que la réflexion qui s'y produise soit régulière de sorte que l'onde réfléchie ne vienne pas perturber le phénomène de réfraction: on voit donc que l'extrapolation du résultat obtenu dans les conditions restrictives que l'on vient de définir au cas de focalisation à vitesse constante mais en altitude, n'est pas à faire sans réserves. (On ne sait pas quelles corrections numériques cela entraînerait mais peut-être cela peut être connu à partir du travail de M. Guiraud qui traite du problème précurseur.) Si elle est licite numériquement et puisqu'il ne semble pas qu'il y ait d'objections à formuler à l'encontre de la loi de similitude établie par Guiraud, il semble possible de traiter du cas plus général et d'intérêt pratique de la focalisation par palier accéléré et les résultats de calcul mentionnés au cours de l'exposé obtenus par comparaison des courbures relatives des rayons sonores et de la caustique indiquent que le rôle joué par l'accélération de l'avion pour des valeurs réalistes de celle-ci devant être mineur, le bon accord quantitatif des résultats fournis par ce travail avec ceux des essais en vol menés à Istres par le CEV est encourageant.

C.H.E. Warren

Concerning Figure 4, which gives the amplification due to reflection in the pressure rise across the shock, I wonder whether M. Théry can give any indication of the amplification that would occur in the "impulse" (integral of the overpressure during the positive phase) especially near the critical limiting condition.

C. Théry

Il est malaisé de fournir une réponse quantitativement précise à cette question. Il est vraisemblable que la réflexion sur un sol rigide d'une onde N stationnaire sans incidence limite entraînera sensiblement un triplement de l'impulsion, le même phénomène ayant lieu pour les ondes de compression. Cela pourrait peut-être être contrôlé expérimentalement. Quoiqu'il en soit, le passage par l'incidence limite a lieu au cours d'une phase instationnaire du vol et cela pourrait être une cause pour laquelle l'effet sur l'impulsion pourrait être bien moins sensible. Cela dépend de la rapidité de l'évolution de l'incidence comparée à la longueur d'onde. Mais ainsi qu'on le signalait précédemment l'évolution de la pression derrière l'onde réfléchie est très rapide dans les cas instationnaires et il semble qu'en pratique l'impulsion sera bien moins affectée que la surpression de crête. Cela se traduira par une forte distorsion du signal.

J.P. Guiraud

Je voudrais reprendre ici la question soulevée par le Professeur Hayes.

En premier lieu, je ne suis pas tellement étonné que, en ce qui concerne l'analyse dimensionnelle, il y ait concordance entre la théorie de M. Théry et la mienne. En effet, la théorie de M. Théry est fondée sur l'application de l'approximation de Whitham à la propagation de l'onde de choc. Cela signifie que, dans les équations du phénomène, M. Théry en retient assez pour que la similitude soit nécessairement respectée.

En revanche je partage l'inquétude du Professeur Hayes en ce qui concerne le coefficient numérique. Je sais bien que l'étude par voie numérique à l'aide de la méthode des caractéristiques apporte une confirmation aux résultats obtenus à partir de la méthode approchée. Toutefois, dans le voisinage de la focalisation le phénomène est fondamentalement transsonique ce qui signifie qu'il échappe à la méthode des caractéristiques.

C. Théry

Effectivement le calcul ne permet pas d'atteindre la zone très réduite d'ecoulement subsonique.

Discussion on the Paper
THEORY CALCULATION AND EXPERIMENTAL RESULTS
(Paper 15)
presented by
J.O.Powers, USA

J.C.Wanner

Vous avez obtenu, au cours des essais NASA sur la focalisation, une mesure du coefficient d'amplification nettement inférieur à celui obtenu au cours de l'opération Jéricho. Ne pensez-vous pas que la différence provient du fait que les points de mesure de l'expérimentation NASA n'étaient pas suffisamment rapprochés et qu'en fait vous n'avez pas observé la focalisation elle-même?

J.O.Powers

While your suggestion of the difference in amplification factors may be the key to the discrepancies I could not substantiate this for sure. I feel that the problem of the linear acceleration super boom is one which should be investigated in more detail, and in fact the United States is imminently planning such investigations in connection with the present ESSA Pendelton tests.

G.M.Lilley

In the NASA experiments on the focused boom it is noted that the rise times near a point of focus are greater than were observed in the experiments of M. Wanner, although the Mach number of the tests was different. Could this be the effect of different atmospheric conditions, with the NASA tests being associated with heavier turbulence at low altitudes. With the larger rise times one might expect a lower peak pressure.

J.O.Powers

Truly rise time is an indication of atmospheric turbulence but I doubt that the differences between the two test programmes can be explained on the basis of their single parameter. In general, during the Edwards programmes when this type of phenomena was being investigated, the overflights were made during the early morning hours when the atmosphere was stable. Again I would like to suggest that these differences should be the subject of further investigations.

J.C.Wanner

Je m'élève vigoureusement contre l'interprétation de la comparison entre nuisance du bang et nuisance du bruit. Pourquoi ne pas comparer avec la nuisance due au froid aux pieds? C'est une plaisanterie bien entendu mais elle fait bien ressentir la difficulté de la comparaison. Quel est votre avis sur ce point?

J.O.Powers

Many investigations have expressed similar reservations. Some have suggested that the paired comparison technique should be used only for sounds which are just perceptibly different and the boom and noise do not fall into this category. One might, however, accept these comparisons on the basis that the results are qualitative and do in fact represent the emphasis of the sonic boom with a more familiar noise.

A. Auriol

Pensez-vous qu'il y ait un facteur d'amplification du bang associé à chaque sorte de manoeuvre ou bien une sorte de facteur limite, nombre "magique" pratiquement applicable dans tous dans tous les cas, pour le calcul de la pression.

J.O. Powers

The determination of specific amplification factors is a matter of continued research. Amplified operational sonic boom will, in my opinion, be controlled by the establishment of limitation on flight manoeuvres. The linear acceleration amplification will be probably the most difficult to control in magnitude but I believe it will be controlled by pre-determination of the location of touch down and hence acceleration; long strips can be set aside for that purpose.

Discussion on the Paper DEVELOPMENT OF ACOUSTIC ABSORBERS FOR TURBOFAN ENGINES (Paper 17) presented by C.J. Webber, UK

W.A. Sirignamo

In addition to the steady-state flow, the oscillatory portion of the velocity is important. The flow through the orifice is driven by the stagnation pressure; therefore, both the static pressure and the velocity oscillations have their effects on the resistance and reactance.

C.J. Webber

Agreed, both must be determined in order to give a complete definition of the environmental conditions.

Discussion on the Paper
AIRCRAFT ENGINE NOISE MEASUREMENT TECHNIQUES, FACILITIES, AND TEST RESULTS
(Paper 18)
presented by
W.R.Morgan and S.N.Suciu, USA

J.O.Powers

(i) Could you comment on the ability of the designer to design for a given spread of frequencies and the accuracy of tuning for a specific frequency, as indicated in Figure 6?

(ii) Is the prediction method indicated in Figure 14 advanced to an extent where the designer can predict the full scale engine characteristics with a high degree of confidence?

W.R.Morgan

(i) Figure 6 is a plot of *normal incident* absorption coefficient for treatment material *without fluid flow.* The ability of the designer to predict and "tune" certain types of treatment materials for given frequencies can, in fact, be accomplished with rather good precision, insofar as normal incident absorption coefficients without fluid flow are concerned. However, this is only one factor involved in the design of treatment material and is, in itself, normally insufficient. Other more subtle factors that should be accounted for are the change in impedance of the absorption material at the boundary layer between the fluid flow and the treatment material, and the change of absorption characteristics as affected by the flow being in the direction of or against the direction of sound propagation. The effect of fluid flow on one type of treatment is illustrated by Figure 8.

(ii) As indicated by Figure 14, the spread of data about the prediction line is of the order of ±3 dB. This discrepancy is most likely caused by both inaccuracy in the prediction method and scatter in the experimental data. The prediction method should be exercised on additional fans (preferably different design types) before placing a confidence level on the accuracy of prediction.

H.Drell

(i) Answering Dr Powers, the scatter shown is still ±3 dB and ground to flight includes addition uncertainties.

(ii) Concerning ground measurements and reflection from the ground, and possible impact on accuracy of using such data to predict in-flight data, what type of ground surface is used in the G.E. facility and have you examined the effect of different surfaces?

W.R.Morgan

(i) With regard to Figure 20, and for the take-off case, the experimental flyover data did check the prediction at the peak noise value rather precisely. However, there is approximately a three-second delay in the rise and fall of the predicted noise curve relative to the experimental data. This discrepancy cannot fully be explained at this time and could be a result of experimental data scatter or possibly computer representation. With regard to the approach case, there is a discrepancy of approximately 4 PNdB between the experimental peak flyover noise level and predicted peak noise level. Again, this might be attributed to experimental data scatter and/or computer representation (including such factors as precise aircraft course, angle of attack, etc.). It was the intent in presenting these curves to show results of a digital computer technique wherein static

ground test data is programmed in the computer, the computer representation "flown", and predicted noise levels obtained. These predicted noise levels were then compared with the actual experimental flyover test data (Fig.20). The figure represents only two cases attempted to date. More cases should be tried before assigning an accuracy value to the technique, including cases for different engines. The results to date are, however, encouraging and only future evaluation of the technique will prove it to be, or not to be, a useful prediction method.

(ii) The ground surface at the Peebles, Ohio, Test Facility is a coarse crushed rock surface. This surface exhibits an absorption phenomenon in the vicinity of 300 Hz and a moderate amount of reflection at frequencies below 1000 Hz. For moderate to high bypass fan engines, where the spectrum is normally dominated by noise levels in the higher frequency bands, neglecting the ground absorption introduces, for all practical purposes, little or no error in perceived noise. At this facility a constant sound source (artificial narrow band source) is utilised to obtain information on reflection and ground absorption throughout the desired frequency range. These tests also include tests with microphones at different heights to obtain cancellation and reinforcement reflection data. At the General Electric Edwards California Flight Test Facility, static noise tests have been performed over hard sandy surfaces and concrete surfaces. This type surface does not appear to exhibit the low frequency absorption phenomenon but does seem to exhibit the reflection phenomenon.

J.C.Thevenin

The agreement between experimental results and predictions presented on Figure 3 seems very good. I should be glad of any information or references to your prediction method.

W.R.Morgan

Two references that are applicable are:

Benzakein, M.J.
Kazin, S.B.
A Theoretical Prediction of Aerodynamically Generated Noise in Fans and Compressors. Presented at the November 1968 Meeting of the Acoustical Society of America.

Benzakein, M.J.
Kazin, S.B.
Fan Compressor Noise Prediction. American Society of Mechanical Engineers, Paper 69-GT-9.

A.L.McPike

(i) Do the static to flight noise level differences presented in Figure 19 represent the differences at the angle of peak noise or do they apply to all angles?

(ii) A question addressed to authors of theoretical papers treating both static and "in motion" jet noise generation is "Do the data presented in Figure 19 appear to be consistent with what you would expect from your studies?".

W.R.Morgan

(i) The flight to ground comparison of Figure 19 is on the basis of comparison of octave maximum SPL values at a constant distance. The maximum SPL for each octave was determined from ground test measurements and adjusted by SAE procedures to a fixed, constant sideline distance. The maximum SPL for each octave was then also determined from the flight tests and adjusted to the same sideline distance from the source. Comparison of these numbers for each octave resulted in the plot of Figure 19.

(ii) During the conduct of the programme, some analysis was performed relative to the ground plane cancellation and reinforcement effect as well as the jet relative velocity effect. This analysis did indicate that the majority of the differences in the first, second, and third octave bands of Figure 19 could be accounted for by taking into account the jet relative velocity due to the aircraft motion. In addition, the cancellation and reinforcement analysis showed that there should be a periodic positive and negative effect present. The positive and negative values in the fifth, sixth, seventh, and eighth octave bands of Figure 19 are attributed, at least in part, to this effect.

G.M.Lilley

Could you please explain the basis for the predicted curves in Figure 20? Is the prediction associated with the static engine measurements with the engine isolated from the airframe or with the engines installed in the airframe? Also does the prediction method allow for the flight speed? Can we take the differences between the experimental and predicted curves as being a function of engine-airframe noise interference?

W.R.Morgan

The ground static measurements used as input data to the computer were taken from an aircraft wing nacelle mounted engine. The prediction method does contain elements that should take into account the flight speed of the aircraft. However, the fan engine used to obtain the data was an untreated, high bypass fan engine and, using recognised methods, the corrections due to aircraft flight speed should be small compared to the differences shown by Figure 20. For this particular fan engine, far field noise data have been recorded for both the wing nacelle mounted condition and without the nacelle. Again, it doesn't appear that the differences in the experimental data for these two conditions would account for the differences between the predicted and experimental data in Figure 20. A possible explanation for the differences might be the assumptions used in the computer representation as to the precession of the aircraft angle of attack, flight path, etc.

Discussion on the Paper
GENERATION AND SUPPRESSION OF COMBINATION TONE NOISE FROM TURBOFAN ENGINES
(Paper 19)
presented by
J.D.Kester, USA

J.O.Powers

If the treatment does not tend to reduce the PNdB, does it not in effect reduce the EPNdB?

J.D.Kester

The effect of EPNdB also will be small and could be measured either as an increase or a decrease. A noise increase would result if the levels in 1/3 octave bands near the blade passing tone were lowered, resulting in a larger correction for the tone. The decrease could result if the 1/3 bands controlled by the combination tone noise were lowered enough to contribute to the overall noise sum used in the PNdB calculation.

C.J.Webber

Figure 14 shows that as a probe microphone is brought nearer to the front face of the fan the fundamental tone level rises. Is this due to increased *generation* of tone, because of the wake from the probe and its supports, rather than due to the mechanism of "transition" proposed by the author?

J.D.Kester

I do not believe the presence of the probe increases the generation of discrete tone noise. What is observed is the discrete tone which exists in the very "near field" of the rotor which results from the lift field around each blade.

Discussion on the Paper
METHODE D'ESTIMATION DU BRUIT....
(Paper 21)
presented by
R. Hoch and J.P.Duponchel, France

C.J.Webber

Figure 7(a) shows the effect on jet noise of the addition of a coaxial secondary flow at different bypass ratios. The relationship between the temperatures in the primary and secondary streams will vary with bypass ratio and with thrust in actual engines. Did your theoretical and experimental work which resulted in Figure 7(a) include the effects of temperature variations?

J.P.Duponchel

Cette étude est basée sur une méthode de prévision du bruit d'éjection que nous avons établi à la SNECNA. Cette méthode de prévision repose sur une exploitation (recherches de corrélation) de mesures effectuées tant sur maquettes que sur réacteurs.

Pour les réacteurs simple flux ou double flux mélangés (mélange parfait), la méthode de prévision, qui consistait en une relation de la forme

$$N_{Lo} = g[U_e - U_0 , \rho_j , A_c]$$

a été transformé, dans le cadre de cette étude, en une relation de la forme

$$N_{Lo} = h[M_0 , F_n , q , C_s] .$$

Pour les réacteurs double flux séparés (tant en tuyerès coplanaires e = 0 qu'en tuyère primaire émergente e) le point de départ est l'etude réalisée par Monsieur F.B.Greatrex, *By-pass Engine Noise* (Society of Automotive Engineers, 1961).

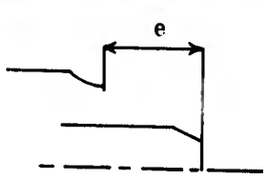

A l'aide de cette étude, nous avons effectué quelques calculs:

$$(N_{LO})_{2\ flux} = (N_{LO})_{primaire} + \Delta N_3 \ , \qquad (1)$$

avec

$$\Delta N_3 = g\left(\underbrace{M_0 \ , e \ , \frac{A_s}{A_p}}_{\text{configuration}} \ , \frac{T_s}{T_p} \ , \frac{P_s}{P_p}\right).$$

Nous avons calculé, dans certains cas de vol, et pour certaines configurations d'éjection, la relation

$$\Delta N_3 = g\left(\frac{A_s}{A_p} \ , \frac{u_s}{u_p}\right). \qquad (2)$$

(Hypothèse: les masses volumiques ρ_p et ρ_s ont été supposées très voisines).

Des essais en chambre sourde ont été effectués afin de vérifier ce resultat théorique - Un ensemble de maquettes double flux a permis les montages suivants:

- e variant de 0 à 4 D_p
- 7 valeurs de A_s/A_p (0,5 - 1,0 - 1,5 - 2 - 3 - 3,85 - 4,75).

Les mesures ont confirmé les résultats obtenus par des considérations théoriques (1) et (2) (pour $M_0 = 0$). Les essais furent effectués avec une température primaire constante $T_p = 330^oK$, 700^oK et 1100^oK.

Les figures 7(a) et 7(b) sont une transposition du champ (2), les quantités A_s/A_p et u_s/u_p étant remplacés par λ, C_s, F_n/q_t et e. Les 2 planches sont valables pour des tuyères coplanaires. Les hypothèses effectuées alors sont les suivantes:

planche 7(a) = soufflante monoétage - rapport de compression $p_{tF}/p_{t2} = 1,45$,

planche 7(b) = soufflante à 2 étages - rapport de compression $p_{tF}/p_{t2} = 2$, rendement polytropique du fan: 0,85,

par suite, ces planches ne sont valables que lors du décollage.

Des mesures en chambre sourde, au Centre d'Essais des Propulseurs, sont en cours: le programme d'essais est conçu, non plus en vue d'études théoriques (températures constantes, ou vitesse constante...) mais en tenant compte des évolutions réelles des grandeurs sur un réacteur. En effet,

$$H_7 = H_5 - (H_4 - H_2) - \lambda \Delta H_2^F$$

pour des conditions de vol ($M_0 = 0$ par exemple),
une température entreé turbine,
un rapport de compression global primaire,
une certaine répartition de rendements polytropiques η,

donc à température primaire donnée), pour un montage (e) donné, correspond

$$\Delta H_2^F = \frac{k}{\lambda}.$$

$$\frac{P_p}{P_a} = g_1(\lambda)$$

$$\frac{A_s}{A_p} = g_2(\lambda)$$

et indirectement, pour les valeurs A_s/A_p des maquettes, il est possible de calculer la relation

$$\Delta H_2^F = h_1(T_p) = h_2(\lambda) ,$$

et par suite de mesurer $(\Delta N_3)_{dB}$ pour chacune de ces conditions génératrices.

Le résultat est $(M_0 = 0)$:

$$(\Delta N_3)_{dB} = g(\lambda , H_5 , H_4 - H_2 , e , \eta) .$$

La taille du réacteur (ou le régime) n'intervient pas car on exprime ΔN_3 en décibels. Le régime du réacteur est inclu dans H_5, $H_4 - H_2$, η et λ.

Discussion on the Paper
METHODES DE DEPOUILLEMENT ET DE TRAITEMENT DE L'INFORMATION ACOUSTIQUE POUR L'ETUDE DU BRUIT DES MOTEURS D'AVION
(Paper 22)
presented by
J. Hay, France

C. J. Webber

Your paper describes an elegant but rather complex system of control during data acquisition. Have you considered the advantages of multi-track recording in allowing the use of a simpler system?

J. Hay

Conservant un principe identique la méthode ferait intervenir une électronique beaucoup plus simple en réservant aux signaux annexes une ou plusieurs pistes d'un enregistreur magnétique multi-pistes.

En fait le topage logique que nous avons étudié devait être compatible avec des enregistreurs-monopiste car différents coopérants aux études de bruit d'avions sont équipés de NAGRA III assez bien adaptés aux enregistrements de bruits de survol grâce à leur dynamique étendue et leur faible poids.

Discussion on the Paper
A PRELIMINARY STUDY OF ATMOSPHERIC EFFECTS
ON THE SONIC BOOM
(Paper 26)
presented by
K. Angell, USA

J. O. Powers

I would like to point out that the microphones at Pendelton are hydrophones not the frequently used condensor microphones. Currently other questions of mounting, surface reflection, surface characteristics, etc. are soon to be studied in a sonic boom generator.

K. Angell

No comment.

G. M. Lilley

(a) Could the author indicate whether the results of overpressure which he reported for the SR-71 were peak pressure or that deduced from the measurements of impulse?

(b) Also, have the measurements of the rise time been correlated with different weather conditions and in particular can they be placed in categories such as for the rounded, peak and N-wave forms?

K. Angell

(a) The overpressures reported for the SR-71 were peak pressures.

(b) The rise times have not previously been correlated with weather conditions by ESSA. Such a study is just now beginning, and one of the interesting features noted is a correlation between rise time and time duration of the peaks superimposed on the N-wave.

K. Oswatitsch

My question concerns the method of measuring the pressure in the boom waves with the microphone. Is it absolutely sure that one gets the real pressure distribution in the wave in this way? What are the assumptions needed in order to obtain, from the test, the pressure distribution in the wave? Is there a difference in the placement of the microphone in the USA and in France?

K. Angell

To our knowledge, a detailed comparison, between microphone and other wide band pressure transducers, has not been conducted to establish sonic boom recording fidelity. In terms of the relative pressure distribution within a signature or between an ensemble of signatures, all recordings are susceptible to any back ground noise present at the time of the boom. Thus local aircraft noise or wind noise can contaminate the signal. One must assume that the microphone and recording system have a uniform frequency response and that the microphone's reflecting environment is sufficiently uniform so as not to introduce distortions in the reflected wave. Furthermore it is necessary to assume that environmental pressure

changes are small for the period of the sonic boom. The microphone exposure used during the Edwards Air Force Base sonic boom experiments is explained by Hilton and Newmann (1965). The microphones were supported at ground level, over a hole, by a reflection board. From photographs of the French test it appears that the microphones were mounted on concrete slabs. There does seem, therefore, to be a slight difference in exposure.

C.H.E. Warren

The question of the method of measurement of sonic bangs is an important one. The matter is currently being considered by the appropriate Technical Committee of the International Standards Organisation, and a standard for measurement is being prepared. Having attended the committee discussions, I think I can state that the French and United States measurement procedures are essentially the same, to the extent that any differences in their results are almost certainly not associated with the measurement procedures.

K. Angell

No comment.

A. Auriol

Je peux indiquer que, lors des expériences françaises, des appareils de mesure avaient été placés par l'ISL entre les capteurs employés par le CEV pour les mesures courantes. Les appareils de l'ISL étaient particulièrement sensibles, de types différents, et montés de différentes façons, de manière à pouvoir juger de l'influence du type de capteur et du mode de montage sur le résultat de mesure. Les détails peuvent être trouvés dans les rapports* de mesure. Les résultats ont montré une bonne coincidence entre les résultats des appareils de mesure couramment utilisés et ceux des appareils de mesure d'étalonnage.

K. Angell

No comment.

**Rapports ISL de Mr Frobose sur les mesures de bangs:*

N 30/64 : Ondes de choc de tête d'un Mirage III – Vols complémentaires à "Jéricho Marina".
T 30/64 : Mirage III: Résultats et remarques des essais "Jéricho Marina" à Istres.
N 5/65 : Bangs supersoniques produits par F-104 G – Essais à Meffen.
T 38/66 : Mirage III: Jéricho Instrumentation à Istres.
T 23/67 : Proposition en vue de la normalisation des techniques de mesure de la pression pour l'étude des bangs.
N 11/63 : Ondes de choc de tête d'un Mirage IV – Brétigny.
T 30/67 : Bangs produits par un Mirage III B en vol accéléré: Jéricho – Focalisation – Istres 1966.

Discussion on the Paper
THE SIMULATION OF SONIC BANGS
(Paper 28)
presented by
C.H.E.Warren, UK

G.M.Lilley

The simulation of waveform with respect to duration and peak pressure has been shown by your measurements to be very good in certain cases. Is it possible to reproduce a given rise time in either the line charge or laboratory simulation facilities, and in addition to represent some of the atmospheric turbulence interference characteristics of live sonic booms, including, say, the effect of spikes? Could you also say what your views are on the need to simulate the waveform associated with focused booms and whether this could be achieved in both the line charge and laboratory simulation facilities.

C.H.E.Warren

With the ERDE simulants it is possible to control the rise time, but as the Mach 1 simulant is poor at high frequencies anyway it is doubtful whether it is purposeful to attempt to simulate the rise times with this simulant. With the Blunderbuss it will be recalled that we are able to attain very short rise times, and we consider that it should be a simple matter to introduce some form of acoustic absorbers to increase these rise times as necessary.

In regard to the attainment of other waveforms, for the reasons that I have given in regard to rise times, I do not think that it would be a very purposeful thing to attempt with the ERDE Mach 1 simulant. With the Blunderbuss I do not think that the variation of waveform can be done simply. As I see it, its role *vis-à-vis* other simulators, is the generation of N-waves of good N-waveforms, to facilitate comparison of experimental measurements with theoretical predictions.

R.N.Cox

To what extent do you have to take precautions in Blunderbuss against waves travelling along the metal structure and arriving before the air shock at the measuring station?

C.H.E.Warren

None: because we have found that no waves of significant magnitude travel along the metal structure, as is evidenced by the waveforms that we measure.

A.R.Seebass

I would like to ask Mr Warren whether or not he feels that for indoor subjective response the very useful simulation of a sonic boom by two point charges still obtains at the higher impulses we expect from SST over flights? Another way of asking the same question is at what levels of impulse does this simulation begin to fail?

C.H.E.Warren

Although the two point charges were found to yield a good simulant of the sonic bang of a fighter-type aircraft, having a time between shocks of 100 ms, there was of course

the unresolved question of precisely what pressure rise of the simulant corresponded to a given pressure rise of the sonic bang being simulated, and accordingly the results of our study were relative only, and not absolute. To be sure I agree with you that for sonic bangs of time between shock of 300 ms, typical of civil supersonic aircraft, not only would the simulant be one that it would be difficult to relate to the actual sonic bang quantitatively, but also it might become a less satisfactory simulant qualitatively, owing to its inability to excite buildings in the way that the long-period 300 ms sonic bang would.

Discussion on the Paper
SONIC BOOM CONSIDERATIONS IN AIRCRAFT DESIGN
(Paper 30)
presented by
E.J.Kane, USA

A.R.Seebass

I would like to point out that you seem to have depicted the mid-field lower bounds for the front shock alone (last figure). As a consequence you have, perhaps, not done the airplane designers full justice. When both the front and rear shock strengths are minimised together, then the mid-field minima are not so optimistic (see, e.g., *Nature*, Vol.221, No.5181, 1969).

E.J.Kane

The lower bounds referred to (see Dr Seebass's reference) are indeed higher, but the lower bounds shown in the paper were only used to provide reference levels. Dr Seebass's comment is correct and makes me, as an aerodynamic designer, feel very modest. Thank you.

H.D.Gruschka

In the case where the engines were considered to be incorporated into the wing, was this a jet-flap-type arrangement? If not, can you see any potentials or favourable effects (on sonic boom reduction) due to this principle?

E.J.Kane

A jet-flap concept, specifically, was not studied, but the results for such a method of reducing the boom would be very similar to that shown in Figure 30-14; i.e., a small favourable effect for boom and drag for small angles.

APPENDIX II

ROUND TABLE DISCUSSION ON SONIC BOOM PROBLEMS

edited by

C.Théry

Institut Franco-Allemand de Recherches, St. Louis, France

Board:	Affiliation:
Prof. W.R.Sears (Chairman)	Cornell Univ., Ithaca, N.Y., USA
Prof. W.D.Hayes	Princeton Univ., USA
Prof. A.R.Seebass	Cornell Univ., Ithaca, N.Y., USA
Mr J.Vallee	Centre d'Essais en Vol, Istres, France
Mr C.H.E.Warren	R.A.E., Farnborough, UK
Participation:	
Prof. K.Oswatitsch	D.V.L., Aachen, Germany
Mr E.J.Kane	Boeing Co., Renton, USA

ROUND TABLE DISCUSSION ON SONIC BOOM PROBLEMS

Professor Sears

The objection has been raised that this table is not round. However, it is topologically the same as a round table. It could even be obtained from a round table by conformable mapping, I believe. First let me remind you of the purpose of this round table, namely that at the end of this interesting and somewhat lengthy meeting it would be well to get some thoughtful people together to summarize, to consider what we have learned and what we have not learned during the week and where we stand on the subject of the sonic boom. For those of you who are more interested in a matter of engine noise, I can only apologize and point out that the distinguished panel chairman of the PEP panel had to leave this morning – I think he had a somewhat diminished interest in having a round table on his subject. So, anyway, we shall have a round table concerning the sonic boom. Let me introduce the participants: On the extreme left is M.Vallée Ingenieur naviguant d'essais and chef adjoint du service methodes of the CEV, Istres. Next to him my good friend Professor W.D.Hayes of Princeton University, whose work most of you know and whose work has been referred to several times during the week and whom we have heard asking questions and making a few comments. On my right, Mr C.H.E.Warren of Farnborough from whom we heard an interesting paper this morning, and to the right of him my colleague Richard Seebass who is especially a professor of aerospace engineering at Cornell and incidently Acting Director of the Center for Applied Mathematics at Cornell and who has worked extensively in this field.

Now what I thought we would do to get the things started, is to ask each of these gentlemen to make a short statement, as controversial as possible, on some aspect of the sonic boom, a field that is of particular interest to him and, particularly with a focus towards the questions I have asked you before: Where do we stand, what we have learned, what we have not learned, where do we go from here? In connection with this, what I think is undoubtedly the central question, can we eliminate or attenuate or alleviate this unpleasant phenomenon that is called the sonic boom, sonic bang, "band sonique". So I would like to begin by calling on Professor Hayes to make a few remarks in a particular area of our ability, to understand and to predict the sonic-boom phenomenon.

Professor Hayes

I thank you. In predicting the sonic boom signal or bang signal, we must start with an F-function from the aeroplane. This is a function of Mach number and azimuthal angle, and of lift coefficient. It is, in general, linear in the lift coefficient. For a careful prediction of details of a signal, it is necessary also to worry about, for example, what the elevators are doing. Essentially I think that the problem of prediction of the F-function is in an excellent state. We must first calculate lift distributions on the aircraft, and this is quite well understood. And once we have that, then we can calculate the equivalent body of revolution and obtain the F-function by quadrature. So I think there is no problem here. If we have an atmosphere without turbulence and do not have diffraction effects, we have straightforward propagation of sonic boom. It seems quite clear that the straightforward application of geometric acoustics together with the calculation of the non-linear distortion is a sound procedure, and is also well understood. There are no basic difficulties here. We can also calculate from the geometric acoustics where a focusing should appear, and I also think that there is essentially no problem in determining where to expect a focusing. I am of the opinion that eventually, and particularly if there is any supersonic flight overland, there will have to be designed into aircraft onboard computers for computing where the focus will appear, to ensure that the focus will not appear strongly on the ground. In a normal supersonic flight the focus first appears very close to the aircraft and, hence, with positive altitude. In steady level flight the focus is essentially at infinity and, hence, at infinite negative altitude. In a descent, there is never any real focusing. So the important part of the focusing problem should normally appear in the fact

that somewhere between the point at which the aircraft becomes supersonic and the point at which the aircraft is in level flight at supersonic speed, the focal point must go from positive altitude above the ground to negative altitude below the ground. A small onboard computer can tell you where the focus is. The important thing is that there should be a transition manoeuvre in which the focus is thrown as suddenly as possible from a sufficiently large positive altitude to a sufficiently large negative altitude. This, I think is something that we may have to worry about in the future, and is something that can be easily accomplished.

When we come to diffraction effects, we find that diffraction effects are in not a very good state as far as prediction is concerned. But, fortunately, most diffraction effects are not very important. Exactly what the sonic boom signal looks like in a shadow zone, is a very interesting mathematical problem but it is not very interesting for the engineer. The answer that he is interested in is that the signal is very weak in a shadow zone, and immediately his interest disappears. The diffraction effect that is most important, of course, is the one which appears because of a focusing, and this effect normally appears in the form of a caustic. The caustic is something for which we must have a definition; so let me define it.

A ray is to be considered not as a line in space but as a point trajectory in space-time. We should think of propagation in terms of a four-dimensional space plus time. A caustic is a three-dimensional hypersurface in this four-dimensional space which is an envelope of these trajectories which are the rays. So the fact that the caustic has this mathematical nature has to be kept in mind in order to treat it. I have looked at the caustic problem to some extent theoretically, and so has M. Guiraud, and I think we are essentially in agreement. The status there is that if we know the kinematics of a caustic (i.e. its form as a three-dimensional hypersurface in space-time) then we can calculate directly with no particular difficulties what happens in the vicinity of a caustic from a linear point of view.

The linear solution presents no fundamental difficulties. The difficulty appears when we have a shock. So, if we have a bangless boom, a signal with no shocks in it, the solution would be essentially complete to a high degree of accuracy on the basis of a linear theory, locally. If we have a shock present, then the linear theory presents the difficulty that it tells you that the pressures are infinite. This means that in the immediate vicinity of the shock, it is essential to have a non-linear theory. M. Théry and M. Auriol have obtained approximate solutions for this particular type of problem. I think the difficulty here is that we have no way, except in the special cases where the solutions are exact, of knowing what the errors are. What we essentially must do is to obtain, by the solution of appropriate partial differential equations, quantitative non-linear solutions that will resolve the shock strength problem. Then, I believe, this can be combined with the linear solution using the similitude of Guiraud to obtain realistic solutions in the vicinity of a caustic. If we are interested in the propagation of the signal past the caustic, then I think we are again in good state. I believe that in this case we can take the linear solution ignoring the singular behavior near the caustic, simply carried through the caustic. The signal propagated on the other side of the caustic will have a logarithmic infinity, but this logarithmic infinity will be immediately erased by the non-linear folding and shock producing process that we calculate in the normal shock propagation. The essential point is that we must make a transformation of a signal shape, from whatever it is immediately before the caustic, to a mathematically related shape immediately after the caustic. This relation may be given, for example, if we consider the shape before the caustic as represented by the real part of an analytic function of a complex variable on the real line. The shape on the other side of the caustic will be the imaginary part of the same analytic function. It is a straightforward calculation. One difficulty remains, however, which is related to the fact that the caustic is a three-dimensional hypersurface. There is a basic dimensional parameter in a caustic which, to use a description that is not quite precise but most easily understood, can be considered to be the relative curvature between the caustic considered as a surface and the ray which is tangent to the caustic surface. This relative curvature gives us a dimensional parameter which must be known in any case in order to obtain solutions for the

caustic problem. This is easily calculated for caustics which appear in level flight at constant speed. It is considerably less easy to calculate with an aircraft flying a general manoeuvre. Some mention has been made of a super-superbang. This already appears as concept in geometrical optics, where it is a cusp in a caustic, a caustic cusp, and is referred to in geometrical optics as an "arête". I think this is probably the appropriate term for us to use also. In this case, I think, almost nothing has been done. I think if we solve the caustic problem, we shall have done quite a bit. On the question of turbulence, I am afraid, I myself can say very little. It is not a field in which I am at home. I think that generally the large scale turbulence gives a statistical spread in the pressure signals obtained on the ground while the small scale turbulence tends generally to smooth the signal. Turbulence in general leads to finite rise-times. It does occasionally, on a statistical basis, give rise to the spikes. If we have bangless booms, or sonic boom signals without shocks, the spikes should not appear. This would be so because the spikes appear to be inherently associated with the fact that the basic signal has a shock. I believe the people involved in the turbulence problems are hopeful that they can consider the prediction problem there essentially solved, on a statisical basis, of course. Thank you.

Professor Sears

Thank you, Professor Hayes.

Incidently, may I notice that one of the things Professor Hayes has done in addressing himself to the question what can we do about alleviating the sonic boom, has been to discuss the focusing in a caustic, which is essentially a problem that the people who worry about sonic boom have not yet worried about. I think it is a good thing that we have somebody out ahead.

I would like now to ask Professor Seebass to say something about configuration effects and minimum-boom signatures and things like that.

Professor Seebass

With regard to the sonic boom minimization, my topic for this afternoon, most of what I want to say will be in some sense reiterating what Mr Kane said earlier today. As you all know, the classical far-field theory tells us that the overpressure is composed to two parts. One is due to the volume of the aircraft, and one is due to the lift, or weight of the aircraft. The volume contribution decays like one over the altitude to the one-half power times the square root of the pressure at the altitude divided by the pressure at the ground. The lift contribution decays like one over the square root of the altitude itself. Furthermore, the volume contribution decays like the length of the aircraft to the three quarters power, while the lift contribution decays like the length of the aircraft to the one quarter power. When you combine these facts with the estimated length, weight, and altitude of operation of SST's, you conclude that the dominant contribution to the overpressure is that due to the lift or weight. When we talk about minimization we can say something about each of these components. The volume can be handled easily. In principle, the volume contribution can be eliminated à la Busemann, for if we design the Busemann ring-wing then there is no contribution to the boom from the volume. Then the question of how we minimize the lift or weight contribution remains. Now we know that the lift or weight contribution is essentially inescapable and is related in a very subtle way to the support of the aircraft by the ground. The pressures on the ground are very large compared to the pressures you really need to support the aircraft there. When you integrate them, if you do it precisely enough, you find that the aircraft is supported by the ground. Now, when it comes to minimizing the lift or weight contribution, let me remind you that the equivalent body of revolution for lift alone is a slender body of revolution that never closes. That is, if you are below the aircraft, the equivalent slender body of revolution extends to infinity downstream with a finite base area, the base area being directly

proportional to the lift or weight of the aircraft. So what you want to do here is to determine what is the minimum overpressure, shock pressure rise or impulse for this lift.

I am going to divide my remarks into two parts. First, I want to say something about exotic configurations. By exotic configurations I mean those that embody fluxes of energy, momentum and mass to or from the flow in order to increase the effective length over which the lift is distributed. We heard about one such scheme from Mr Goldberg and some discussion of other schemes from Mr Kane. Next I want to make some remarks about the aerodynamic approach where we consider that the Bernoulli constant is fixed throughout the flow and we do not rely on exotic approaches. Then we have to ask what is the best we can do in minimizing various features of the overpressure signature. Before I do that, let me reiterate a warning that came from Mr Kane today; you cannot brook much compromise in the efficiency of the aircraft if you want to minimize the boom, because some of the most effective ways to reduce the boom are to increase the altitude of operation, increase the lift to drag ratio, decrease the specific fuel consumption, increase the length without adding structural weight and to increase the structural efficiency. Neither exotic nor aerodynamic approaches can tolerate much of a compromise in these areas.

Let me now say something about exotic configurations. As I mentioned just a minute ago, the equivalent body of revolution due to lift never closes; it effectively extends downstream to infinity. However, we all know that aircraft engines modify the Bernoulli constant of the flow that passes through them and it is not entirely unreasonable to think of aircraft in which a reduction of the engine stream tube area is used to compensate for the growth of the equivalent body of revolution due to the lift. By using this idea, it is hypothetically possible to totally eliminate the boom due to lift. Naturally the second law of thermodynamics requires that infinitely far downstream the engine stream tube area must be larger than the entering stream tube area, and it is this plumming of the engine exhaust which takes many aircraft lengths to occur that gives rise to a weak pressure turbulence on the ground. A portion of this disturbance accounts for the support of the aircraft by the pressure field there. Because this pressure disturbance is spread over such a large longitudinal distance, it is reasonable to assume that no significant steepening of the pressure signal into shock waves occurs. Professor Resler at Cornell who first had this idea, has carried out a detailed engine cycle analysis. In my view his results indicate how very difficult it is to make gains by this route with reasonable restrictions on turbine inlet temperature. Furthermore, Professor Hayes has pointed out in an earlier conference that you suffer a severe drag penalty when you do this and, as Mr Kane pointed out this morning, total elimination of the exhaust stream on present SST configurations would only reduce the overpressures by about 5%. However, should it eventually prove feasible and practical to design aircraft with engines whose stream tube capture area is a significant fraction of the base area of the equivalent body due to the lift, then some gains may be expected by this route.

Let me conclude, then, with some discussion of what we might achieve through aerodynamic means with the Bernoulli constant of the flow fixed. When I do this I tread dangerous ground, and I feel a retort from my fellow panel members is likely. Our understanding of these features of the overpressure signature that are most annoying is far from complete. If shock waves are absent from the pressure signature and rise times are on the order of a hundredth of a second, then, as was pointed out earlier in the conference, there is little acoustical energy in the audible range. The most annoying feature of a sonic boom, at least as it is experienced outdoors, lies in the shock waves themselves. On the other hand, the low frequencies which are inaudible outdoors contain the majority of the acoustical energy and cause structures to vibrate, windows to rattle and bric-à-brac to fall. As a consequence, overpressure signatures without shock waves may not be much less annoying indoors than their fully steepened counterparts. Let me leave the unanswered question of which features of the overpressure signature are the most critical ones with the ad-hoc assumption that one of the most annoying features of the sonic boom is due to the presence of shock waves in the pressure signature, and turn to the technical and answerable question of what minimum shock pressure rises and overpressure levels may be achieved. Several years ago at NASA Langley, McLean noticed that it takes several hundred aircraft lengths for the

overpressure signature to reach its asymptotic form in a homogeneous atmosphere. This led him to examine the required aircraft length and weight, for a fixed altitude and Mach number, to achieve signatures with finite rise times. At first glance, his results seem fairly pessimistic: To achieve one one-hundredth of a second rise time instead of front and rear shocks, a 600.000 pound aircraft would need to be nearly a thousand feet long. I am sure nobody knows how to build a 600.000 pound aircraft that is a thousand feet long. However, McLean assumed that the only effect of the atmosphere was that it changed the level of the pressure. But as Professor Hayes recently reminded us, the increasing acoustic impedance below the aircraft causes the midfield to extend to infinity. There is a fairly convenient way to state this principle, that we may call the principle of Hayes, that is essentially this: The signature shape that exists at a distance of $\frac{\pi}{2}H$ from the aircraft in a homogeneous atmosphere is the shape that is obtained asymptotically in an isothermal atmosphere with scale height H. You can take advantage of this effect to freeze the midfield and makes it extend to infinity. By taking advantage of that fact you compute what is the best one may do in minimizing the shock pressure rise or overpressure. When you do that, you have to decide if you want to worry about both the front and rear shock waves or only the front shock wave. From my point-of-view there is no question; you have to do the same thing to both shock waves and there is a dramatic difference in the aircraft lengths required if you minimize both the front and rear shock wave strengths simultaneously rather than the front shock wave strength alone. I would like to show you one or two slides which show this difference.

FRONT AND REAR SHOCK PRESSURE RISE VERSUS AIRCRAFT LENGTH
W = 600,000 LBS, M = 2.7, h = 60,000 FT
Atmospheric Scale Height = 20,000 FT

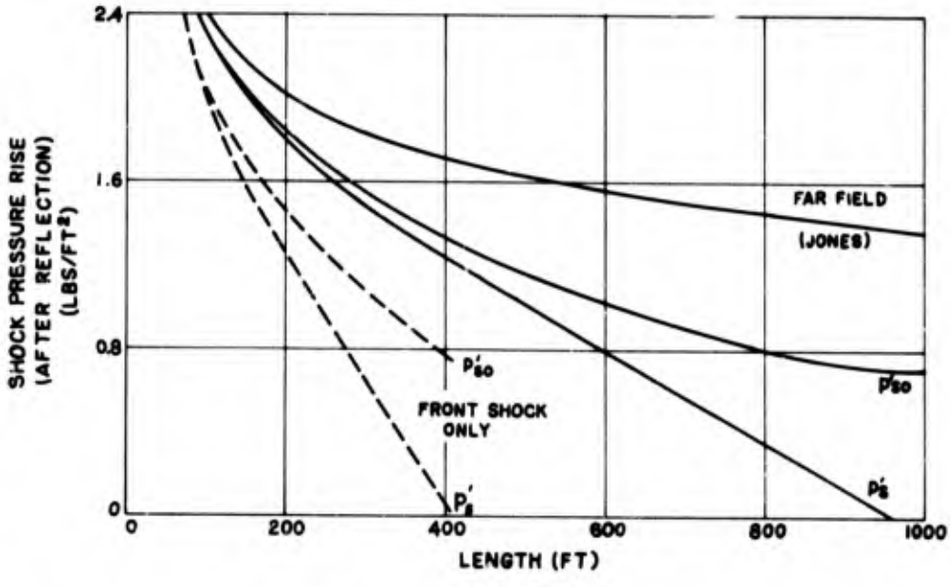

The first slide is simply a plot of the shock pressure rise after reflection for a 600.000 pound aircraft flying at Mach 2.7 at 60.000 ft. in a isothermal atmosphere with a scale height of 20.000 feet. The "Jones" curves are the far-field minimums; the others result from taking advantage of the atmosphere. In effect, you find the length required to achieve these overpressures. If we insist on considering both shocks, you can see that the length required for a given overpressure has increased considerably. It takes about 408 feet to totally eliminate the front shock while something more like 2.36 times 408 is needed to eliminate both shocks. Now may I have the next slide, which shows what the numbers look like for two weights that are typical of a domestic SST. This is a small

SHOCK PRESSURE RISE VERSUS AIRCRAFT LENGTH
ALTITUDE = 60,000 FT, MACH NUMBER = 2.7
Atmospheric Scale Height = 20,000 FT

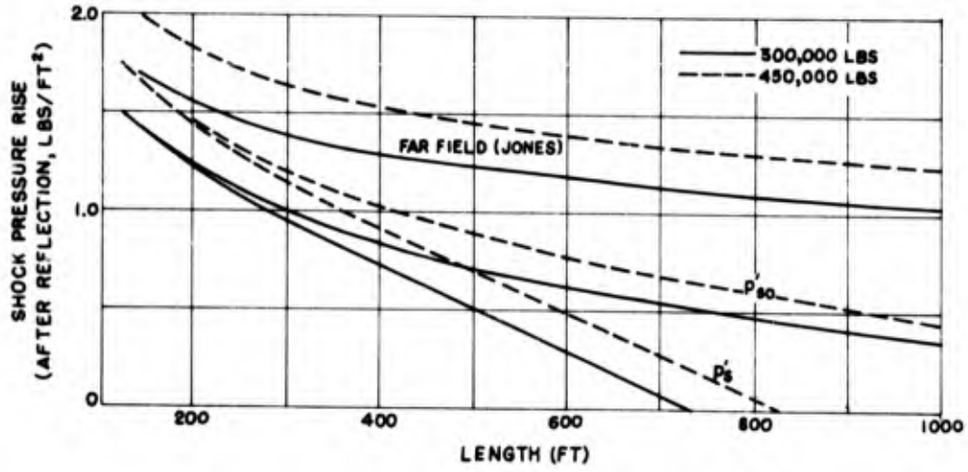

aircraft with a small fuel load, because the range requirements are down. As you can see, it looks like no matter how clever we are with aerodynamic techniques, we are going to have overpressures of about one pound per square foot.

In conclusion, it seems that we can safely prognosticate a continual evolution of SST designs with greatly improved sonic boom characteristics. While gains may be expected from improvements in the overall efficiency of such aircraft and careful aerodynamic design, I do not foresee any revolutionary concept that will totally eliminate the sonic boom. Recent research efforts seem to be pointing the way to the design of a domestic SST with cruise overpressures of less than one pound per square foot. Whether or not these evolutionary gains will be sufficient to make a domestic SST an economically viable concept is as yet unknown. We cannot hope to provide the answer until we know what features of the overpressure signature are the most annoying ones, and what integrated overpressure loadings are likely to prove to be acceptable.

Professor Sears

Now I would like to call on Mr Vallee.

Mr Vallee

Je voudrais vous rappeler essentiellement quelques résultats qui vous ont été donnés par l'Ingénieur en Chef Wanner concernant les essais de focalisation et vous donner quelques précisions à ce sujet. Nous avons orienté, en France, nos études expérimentales sur le domaine des focalisations, parce que c'est un domaine relativement limité et peu expérimenté. A noter qu'on a pu faire les travaux que l'on a fait parce que l'on a réussi à constituer une petite équipe de théoriciens et de praticiens qui a une cohésion suffisante pour mener à bien de tels essais, et qui est bien décidée à traiter ces problèmes de manière objective. Je vous rappelle que nous avons effectué deux expériences de focalisation différentes. La première qui s'appelait "Jéricho focalisation" conduite avec un Mirage III à 600 m d'altitude et avec l'accélération rectiligne de 3 m/s^2; et une deuxième expérimentation "Jéricho Virage", menée avec un Mirage IV à 11 000 m d'altitude, qui comportait des virages, avec un facteur de charge de 2, et des accélérations rectilignes à 1 m/s^2. Vous voyez donc que ces deux expérimentations ont été menées dans des conditions

très différentes. Nous avons trouvé dans les deux expériences, avec les restrictions que vous a exposées l'Ingénieur en Chef Wanner, un coefficient d'amplification du Δp d'une valeur de l'ordre de 4 à 5. Je ne veux pas dire pour autant que cette valeur de 5 peut être considérée comme une valeur magique dans une focalisation quelconque, loin de moi cette pensée. C'est pour cela que nous avons dès maintenant prévu l'expérience "Jéricho Carton" qui doit nous donner des résultats expérimentaux complémentaires sur l'influence des paramètres intervenant dans la focalisation, et qui doit également nous permettre d'étudier cette superfocalisation ou super-superbang dû à un phénomène très particulier, celui de la mise en virage d'un avion.

Ce rappel étant fait, je voudrais éviter que les résultats de nos essais vous fassent considérer la focalisation comme un phénomène épouvantable... Pour cela, je veux attirer votre attention sur le fait que nos essais ont un caractère très discret, très particularisé, et que nos résultats ne peuvent pas, a priori, être extrapolés facilement.

Tout d'abord, le facteur d'amplification de 5 est un facteur maximal que nous avons rencontré et qui est mesuré par rapport au Mach de focalisation. Je précise ceci pour éviter la procédure erronée de calcul qui consisterait à multiplier par 5 le Δp dû à l'avion en vol de croisière pour obtenir le Δp de focalisation. Un avion opérationnel, qui fait son accélération au voisinage de la tropopause, focalise vers Mach 1,20 auquel correspond un Δp nominal qui est plus faible en général que le Δp de croisière, sauf peut-être si l'avion vole à des altitudes extrêmement élevées en croisière. C'est donc cette valeur nominale correspondant à Mach 1,20 qu'il conviendrait de multiplier par 5 pour avoir le niveau de la focalisation, c'est-à-dire le Δp de la focalisation.

Deuxièmement, les focalisations que nous avons enregistrées intéressaient une surface très limitée. Il s'agit d'un phénomène "crête" dont la largeur, Mr Wanner vous l'a dit, est de l'ordre de, peut-être, 20 à 50 m. Sa longueur est par contre celle de la ligne de focalisation qui est évidemment beaucoup plus grande, mais la focalisation est tout compte fait un phénomène qui est très limité sur le terrain. D'autre part, je pense qu'on peut actuellement conclure que nous pouvons effectivement calculer l'emplacement de cette zone de focalisation par rapport à la trajectoire de l'avion. Et il n'est pas du tout impensable, comme nous le disions tout à l'heure, qu'un calculateur embarqué permette de placer la focalisation en accélération d'un avion à quelques kilomètres près par rapport à la trajectoire supposée connue. Il est évident que les erreurs de trajectoire s'ajouteraient. Nous avons en effet, dans nos essais, abouti à la conclusion que la précision de la localisation d'une focalisation par accélération rectiligne était de l'ordre de quelques kilomètres, avec un calcul en atmosphère standard. Je ne pense pas que le calcul en atmosphère réelle avec le vent et la température améliore considérablement cette précision. Ce calcul introduit même des risques d'erreurs supplémentaires dans le cas d'une mauvaise connaissance de l'atmosphère. Donc je pense qu'on peut être optimiste sur la façon dont on peut placer la focalisation produite par l'accélération rectiligne de l'avion.

Troisièmement, nos résultats d'essai ont pour base des enregistrements magnétiques analogiques de pression, mais nous n'avons fait apparaître dans nos conclusions que l'étude du Δp et de son coefficient d'amplification. Nous n'avons pas étudié en détail, notamment, l'évolution de l'impulsion, c'est-à-dire l'intégrale positive du bang, et bien qu'une telle étude puisse se faire à partir de nos enregistrements. Aussi je ne suis pas en mesure de vous dire, actuellement, quel est le "coefficient d'amplification" de l'effet produit par une focalisation, par exemple vis-à-vis des structures. Nous avons vu ce matin que le signal focalisé a une allure très particulière, le pic est très élevé, mais la surface de l'onde n'est pas multipliée par le même coefficient, c'est certain. Je pense que ce facteur est très important, et une étude est à mener dans ce domaine vis-à-vis des effets sur les structures. Ceci n'a pas été fait actuellement.

C'étaient les trois rappels que je voulais faire.

Professor Sears

And finally, in alphabetical order, Mr Warren.

Mr Warren

You did say at the beginning that you wished us to make our contributions brief. I noticed that we have used up nearly three-quarters of the time set aside for this round table. My colleagues, of course, have not been up on this stage before, so I guess they wanted to talk a little bit at length, but I have been up here, so I really am going to try to be brief, if that is all right with you. You also asked us to be provocative. Now, I don't think Professor Hayes was, for I agree with pretty well everything he said. He gave us a most definitive statement of the problem. Except for one point, where I think he said that the state of the art of calculating the F-function was pretty well buttoned up. I think I would take a little bit of issue there because I am not happy that we do absolutely the right thing necessarily in calculating the F-function for an aeroplane with its engine flow. You have really got to work out the equivalent area for the aeroplane that exists plus the incoming and outgoing streamtubes to the engine, which really means in principle you have got to know the shape of the streamtubes. I really wonder if we do know them that well. I mean, how, from the practical point of view, do we handle this problem. We have talked a bit about the focus, the cusp and the caustic. My attitude on this is that the real problem with the sonic bang is the cruise problem. I have always, myself, taken the attitude that the focus in any case is something which will have to be planted in a place where it does not matter, and as we have heard in many of the papers, it is a very limited domain. Equally we have heard, it can be planted accurately too. So this is the way I think that the problem will be handled. Just a final point I want to make. I was very interested in the two papers this morning by Goldberg and by Kane on the possibilities for minimizing, reducing or alleviating the boom. But thinking of it from the point of view of the aircraft designer, I just want to make the point that some of these things we have heard will increase the drag. Now let's get it quite clear. One percent on drag is a lot. I know from my colleague John Hay of the British Aircraft Corporation that if the drag goes up by 1%, this is really what the people in the design offices of firms worry about. One percent in drag can make just the difference between a viable aeroplane and a non-viable aeroplane. If the drag is greater by more than one percent when an aeroplane flies, compared with what has been estimated then that's the sort of thing that sends one back into the windtunnel to try out fairings or things like that. It is really important, one percent on drag. So I don't think that a small reduction in boom which would cost 1% of d g is a solution. On the other hand, 10% on the pressure rise of sonic bang is peanuts. And the final point I want to make is that we must be very careful as Professor Seebass said, that in this minimization we minimize the right quantity. Very naturally a lot of the work we talk has been about minimizing the peak overpressure or pressure rise, but some of these schemes I have seen suggested actually increase the impulse. Now I think that the sonic bang, as a problem, is primarily an indoors problem. People sleep indoors. The surgeon does his operations indoors etc... The indoor situation, I say, is more important than the outdoor one. Following on from that, I always remember a report by, I think it was Domenic McGlieri, in which he showed that the intensity of the boom indoors, which he measured in some sort of acoustical way in decibels, correlated well with the impulse outdoors. In other words, I think that the impulse is probably what one has got to minimize if one wants to alleviate the most important situations. Some of the procedures for reducing the peak overpressure entail increasing the impulse. Accordingly I get worried as to whether one is optimizing the right thing.

Professor Sears

Thank you Mr Warren. Now the chairman can have a word. I want to say also to Professor Hayes, about the happy state of calculating the lift distribution on the wings at supersonic speeds: If Professor Ferri were here he might tell us that he is not happy

at all: Nobody can calculate the lift distribution on these wings! He is talking about the fact that there are difficult non-linear effects right on the wings; I mean before you know the lift distribution you get some tough aerodynamic problems here.

I was very happy to hear Mr Vallee who told us that the focus problem is not so terrible as has been predicted. But Professor Hayes said he thought it would be nice if we could carry out a quick maneuver to bring that focus point from above the ground to well under the ground in a hurry, so it would not annoy anybody, but I wonder if anybody is going to carry out anything "quickly" at a Mach number of 1.2 with a real airplane!

One of the things we need to know is, what are the unacceptable features of the signature? We want the public-relations people, psychoacousticians, or civil engineers to tell us, what do you want? This feature or that feature? It reminds me that through these years we have been concerned with these phenomena, they are just as unhappy with us! They say, they keep saying, what can we do, what can we study, what can we say, because those damned aerodynamicists will not tell us what the signature is really going to be? We think that we really tell them what the signature will be, but when they say no, you do not, because you say, you admit, that it will be dependent on the weather, on atmospheric turbulence and such things. What I mean is that, from our standpoint, we see that those fellows are being unreasonable. But they think we are the ones who are unreasonable.

We are able to compute the signature with very impressive accuracy in a real, quiescent atmosphere and for real configurations. We understand clearly, whether they do or not, that the effects of atmospheric turbulence has got to be handled in some way by statistics, some kind of experience, and Dr Angell is hard at work along this line. Now is there a possibility that we are being unreasonable with them when we say, why don't these fellows tell us what is acceptable and what is not acceptable to the public? May there be also some kind of unanswerable question in this, the answer to which would only come after years of experience?

Well, let us ask if any of the round-table participants has a quick question, or remark, or rebuttal to make before we turn to the audience.

Professor Seebass

I want to reply to Mr Warren. He said that he thinks that it is important to minimize the impulse. We have known how to minimize the impulse for a long time. Certainly, we aerodynamicists have not done anything of much value in minimizing shock pressure rise and overpressure if those are not important quantities. I quite concur with that view that impulse is important and was surprised this morning when Mr Warren said that for indoor simulation two bangs with little impulse are as annoying as an N-wave with a large impulse. Now it is not clear to me how important the impulse is to indoor annoyance. Mr Warren, could you respond to that?

Mr Warren

Yes, I have responded to this in the written reply that I have given to your question on my paper. The point here is this. You are referring to the way I simulated bangs of an appreciable duration. To be sure, I agree with you. The simulant of the two point charges compared with the sonic bang appreciable duration was a good one, we felt, in the sense that people could not distinguish the one from the other. But as I pointed out, and elaborated in the written reply that I have given, we recognize that it was not possible to relate the two quantitatively. Then you went on to say that this might be all right when comparing this simulant with a short duration sonic bang typical of a fighter but, would it be as good a simulant with the longer duration bang of a SST. As I have said this morning, and as I have amplified in my reply, it would become a worse simulant.

Professor Hayes

With respect to the calculation of the F-function and the distinction between what was in good shape and what was not in good shape, I was making the distinction more between what is fairly well understood theoretically and what is not so well understood theoretically. The distinction was more with respect to what is clear we can do and what it is not so clear that we can do, rather than what is already available in computer programs and developed algorithms and what is not yet available in this way. So, e.g., the F-function is easier to calculate in principle than perhaps it is at this moment in practice. The same is certainly true for linear solutions in caustics. Nobody has a computer program or an algorithm for obtaining even the linear solution in caustics. It is just that the fundamental parameters are known, the basic functions that are needed are hypergeometric functions. They are in principle easily calculable.

I would like to mention that I certainly agree completely with Mr Wanner when he complains against the expression of the strength of sonic booms signals in db. It is clear that it is important for the psychoacoustician to have a measure of acceptibility or non acceptibility. It is, however, unappropriate to measure sonic booms in terms of db or pndb. I also would like to object to the focalisation ratio, on the basis that it is inappropriate. The pressure signal measured on the ground which (I am full of admiration for what has been done in the Jericho program) is the pressure above the line in this ratio is clear; but the pressure below the line is arbitrary to quite a degree. You must decide what the reference pressure is and there is a certain arbitrariness in determining what the reference value is. Thus I believe that this ratio is not really an appropriate measure. It is also clear that if you increase the acceleration or increase the manoeuvre curvature of an airplane that you could drive this ratio up, however it is defined, to well above five to ten, or that if you have a well planned manoeuvre which is aimed at destroying a particular microphone you can get up to a hundred. Thank you.

Professor Sears

Well I think what I would like to do is to accept questions or discussions or arguments from the floor, with only the request that we try to keep in mind the proposed theme of this round-table, which is, as I said, where do we stand with regard to the elimination or alleviation of this unpleasant phenomenon. Professor Oswatitsch.

Professor Oswatitsch

The near field solution seems to me to be a little underestimated for the whole solution because the near field solution goes nearly up to the ground. It is not exactly a near field solution, it is some medium solution. In any case, I think, we know now that the asymptotic solution is not on the ground, and if one checks the calculations, one finds out that e.g. the lower the drag is, the higher the sonic boom is, in theoretical results. Therefore, it seems to me that it is of some importance how the combination of shock waves from the wings, from the bodies accumulate to a rotational one and we try to calculate these things and I would be very glad to get some encouragements that this is of some value what we do. The theory is not so difficult but in any case it makes work. Thank you.

Professor Sears

I want to make sure to understand you. Are you suggesting that you think that the approximation of the Whitham theory, the concept of the equivalent body of revolution and such things, lead us to an underestimation in the near-field?

Professor Oswatitsch

Not so much the Whitham theory as to calculate with a simple, equivalent body of revolution. I think, because you see, if you have quite weak shock waves from the trailing edge, from the wings and so on, weaker the shock wave are larger is the way to combine a shock wave of revolution and this is, I think, quite a long distance of the body but if we calculate right, a thing one gets I mean underestimation of the sonic boom higher, I mean, an underestimation of the influence. I think the sonic boom is lower and one gets e.g. the theory with equivalent body of revolution.

Professor Seebass

I want to make some reply. I think that it is important to know the answer to Dr Oswatitsch's question and I know of no one doing such theoretical calculations except Mr Lomax of NASA-AMES. However, a number of very careful experiments of very asymmetric bodies were conducted by NASA Langley, and those experiments have been reviewed in NASA SP 147 and SP 180. It is remarkable how rapid this azimuthal redistribution of the pressure is; it happens very rapidly.

Professor Sears

Unfortunately we are a little late, Mr Kane.

Mr Kane

I have two very brief comments to perhaps clarify some points made by the panel members. First of all, I believe that Mr Warren remarked that it would be desirable to include the effects of engine stream tube in the calculation of the sonic boom signature. This effect has been included in calculations done in the US for the past two or three years.

Mr Warren

You do?

Mr Kane

Yes, we do. Specifically, calculations made both by NASA and by Boeing include these effects.

Secondly there was a remark made, again I believe by Mr Warren, about the significance of impulse. This distresses me a little because of the emphasis placed on a single parameter, such as impulse, to characterize the effect of the wave form. For instance, tests to determine the effect of shock waves generated by various airplanes on glass breakage indicate that not only is the impulse significant, but also the number of shock waves constituting the wave form. The data I am thinking of is from a test conducted by NASA where windows were exposed to various levels of maximum overpressure (NASA TND-3443). Two airplanes were used; one was the F-104 which produces a very irregular wave form shape with many shock waves in it, and the other was a F-106 which at the same altitude had approximately the same overpressure, that is, the same maximum pressure change but a much more regular signature shape. The impulse of the pressure waves for both these planes was about the same but the 104 created considerably less damage. I conclude that there are more factors involved than just the impulse or overpressure when evaluating either structural or psychoacoustic responses.

Professor Sears

I would like to thank the interpreters for their wonderful work during this week.